Geological Survey of Canada
Commission géologique du Canada

PAPER
ÉTUDE 84-1B

This document was produced
by scanning the original publication.

Ce document est le produit d'une
numérisation par balayage
de la publication originale.

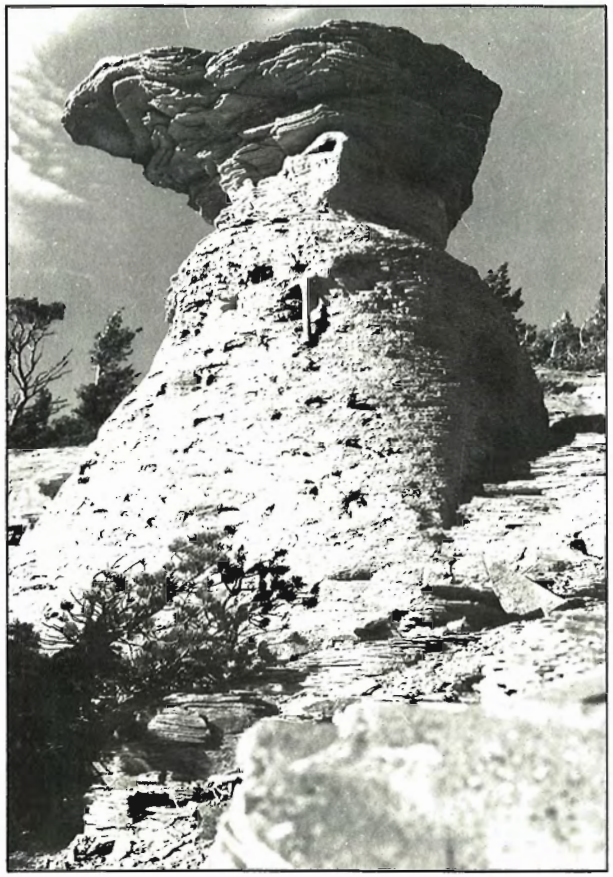

CURRENT RESEARCH

RECHERCHES EN COURS

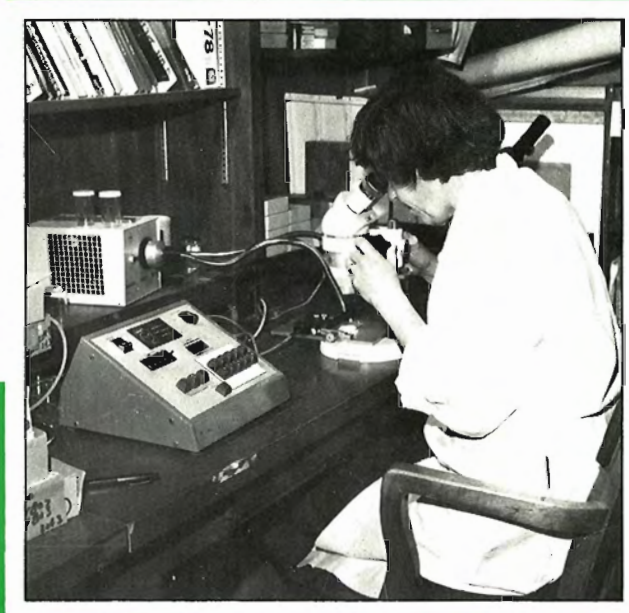

PART
PARTIE B

1984

Canada

Notice to Librarians and Indexers

The Geological Survey's twice-yearly *Current Research* series contains many reports comparable in scope and subject matter to those appearing in scientific journals and other serials. All contributions to the Scientific and Technical Report section of *Current Research* include an abstract and bibliographic citation. It is hoped that these will assist you in cataloguing and indexing these reports and that this will result in a still wider dissemination of the results of the Geological Survey's research activities.

Avis aux bibliothécaires et préparateurs d'index

La série Recherches en cours *de la Commission géologique paraît deux fois par année; elle contient plusieurs rapports dont la portée et la nature sont comparables à ceux qui paraissent dans les revues scientifiques et autres périodiques. Tous les articles publiés dans la section des rapports scientifiques et techniques de la publication* Recherches en cours *sont accompagnés d'un résumé et d'une bibliographie, ce qui vous permettra, nous l'espérons, de cataloguer et d'indexer ces rapports, d'où une meilleure diffusion des résultats de recherche de la Commission géologique.*

Technical editing and compilation
Rédaction et compilation techniques

R.G. Blackadar
W.C. Morgan
H. Dumych
P.J. Griffin
N.C. Ollerenshaw
M.-F. Dufour
L.E. Vincent

Production editing and layout
Préparation et mise en page

M.J. Kiel
Debby Busby

Typed and checked
Dactylographie et vérification

Jacinthe Caron-Blais
Susan Gagnon
Janet Gilliland
Shirley Kostiew
Janet Legere
Sharon Parnham
Murielle Pelletier
Diane Winsor

GEOLOGICAL SURVEY
PAPER 84-1B

COMMISION GÉOLOGIQUE
ÉTUDE 84-1B

CURRENT RESEARCH

PART B

RECHERCHES EN COURS

PARTIE B

1984

© Minister of Supply and Services Canada 1984

Available in Canada through

authorized bookstore agents and other bookstores

or by mail from

Canadian Government Publishing Centre
Supply and Services Canada
Ottawa, Canada K1A 0S9

and from

Geological Survey of Canada offices:

601 Booth Street
Ottawa, Canada K1A 0E8

3303-33rd Street N.W.,
Calgary, Alberta T2L 2A7

100 West Pender Street
Vancouver, British Columbia V6B 1R8
(mainly B.C. and Yukon)

A deposit copy of this publication is also available
for reference in public libraries across Canada

Cat. No. M44-84/1BE Canada: $12.00
ISBN 0-660-11651-0 Other countries: $14.40

Price subject to change without notice

Geological Survey of Canada – ***Commission géologique du Canada***

R.A. PRICE
Director General
Directeur général

J.G. FYLES
Chief Geologist
Géologue en chef

M.J. KEEN
Director, Atlantic Geoscience Centre, Dartmouth, Nova Scotia
Directeur du Centre géoscientifique de l'Atlantique, Dartmouth (Nouvelle-Ecosse)

R.G. BLACKADAR
Director, Geological Information Division
Directeur de la Division de l'information géologique

W.W. NASSICHUK
Director, Institute of Sedimentary and Petroleum Geology, Calgary, Alberta
Directeur de l'Institut de géologie sédimentaire et pétrolière, Calgary (Alberta)

J.C. McGLYNN
Director, Precambrian Geology Division
Directeur de la Division de la géologie du Précambrien

A.G. DARNLEY
Director, Resource Geophysics and Geochemistry Division
Directeur de la Division de la géophysique et de la géochimie appliquées

J.S. SCOTT
Director, Terrain Sciences Division
Directeur de la Division de la science des terrains

D.C. FINDLAY
Director, Economic Geology and Mineralogy Division
Directeur de la Division de la géologie économique et de la minéralogie

R.B. CAMPBELL
Director, Cordilleran Geology Division, Vancouver, British Columbia
Directeur de la Division de la géologie de la Cordillère, Vancouver (Colombie-Britannique)

Separates

A limited number of separates of the papers that appear in this volume are available by direct request to the individual authors. The addresses of the Geological Survey of Canada offices follow:

601 Booth Street,
OTTAWA, Ontario
K1A 0E8

Institute of Sedimentary and Petroleum Geology,
3303-33rd Street N.W.,
CALGARY, Alberta
T2L 2A7

Cordilleran Geology Division
100 West Pender Street,
VANCOUVER, B.C.
V6B 1R8

Atlantic Geoscience Centre,
Bedford Institute of Oceanography,
P.O. Box 1006,
DARTMOUTH, N.S.
B2Y 4A2

When no location accompanies an author's name in the title of a paper, the Ottawa address should be used.

Tirés à part

On peut obtenir un nombre limité de "tirés à part" des articles qui paraissent dans cette publication en s'adressant directement à chaque auteur. Les adresses des différents bureaux de la Commission géologique du Canada sont les suivantes:

601, rue Booth
OTTAWA, Ontario
K1A 0E8

Institut de géologie sédimentaire et pétrolière
3303-33rd, St. N.W.,
CALGARY, Alberta
T2L 2A7

Division de la géologie de la Cordillère
100 West Pender Street
VANCOUVER, Colombie-Britannique
V6B 1R8

Centre géoscientifique de l'Atlantique
Institut océanographique de Bedford
B.P. 1006
DARTMOUTH, Nouvelle-Ecosse
B2Y 4A2

Lorsque l'adresse de l'auteur ne figure pas sous le titre d'un document, on doit alors utiliser l'adresse d'Ottawa.

SCIENTIFIC AND TECHNICAL REPORTS
RAPPORTS SCIENTIFIQUES ET TECHNIQUES

ECONOMIC GEOLOGY/GÉOLOGIE ÉCONOMIQUE

S.S. GANDHI: Galena-sphalerite-chalcopyrite veins in Aphebian dolomite and Archean basement at Artillery Lake, Northwest Territories 33

R. THORSTEINSSON: A sulphide deposit containing galena, in the lower Devonian Disappointment Bay Formation on Baillie Hamilton Island, Canadian Arctic Archipelago 269

GEOCHEMISTRY/GÉOCHIMIE

W. DYCK and Q. BRISTOW: Quantitative determination of ^{210}Po in geochemical samples 41

P.J. ROGERS and M.A. MACDONALD: Stream sediment sampling, orientation studies and geochemical associations from selected deposits on Cape Breton Island, Nova Scotia 65

GEOPHYSICS/GÉOPHYSIQUE

Q. BRISTOW and J.G. CONAWAY: Temperature gradient measurements in boreholes using low noise high resolution digital techniques 101

MARINE GEOSCIENCE/ÉTUDES GÉOSCIENTIFIQUES DU MILIEU MARIN

D.L. FORBES: Coastal geomorphology and sediments of Newfoundland 11

R.B. TAYLOR and D. FROBEL: Coastal surveys, Jones Sound, District of Franklin 25

D.E. HEFFLER: RALPH – an instrument to monitor seabed sediments 47

J.A. WRIGHT, C.E. KEEN, and M.J. KEEN: Marine heat flow along the northeast coast of Newfoundland 93

PALEONTOLOGY/PALÉONTOLOGIE

M.J. ORCHARD: Pennsylvanian, Permian and Triassic conodonts from the Cache Creek Group, Cache Creek, southern British Columbia 197

M.J. ORCHARD: Early Permian conodonts from the Harper Ranch beds, Kamloops area, southern British Columbia 207

H.J. HOFMANN: Organic-walled microfossils from the latest Proterozoic and earliest Cambrian of the Wernecke Mountains, Yukon 285

A.E.H. PEDDER: **Dehiscens** Zone corals from the Lower Devonian of Yukon Territory 315

QUATERNARY GEOLOGY/GÉOLOGIE DU QUATERNAIRE

Inventory Mapping and Stratigraphic Studies/Inventaire cartographique et stratigraphique

P.J. KURFURST, K. MORAN, and F.M. NIXON: Drilling and sampling in frozen seabottom sediments, southern Beaufort Sea 193

Paleoecology and Geochronology/Paléoécologie et géochronologie

R.A. HEWITT and J.E. DALE: Growth increments of modern **Mya Truncata** L. from the Canadian Arctic, Greenland, and Scotland 179

Sedimentology and Geomorphology/Sédimentologie et géomorphologie

J.R. MACKAY: Lake bottom heave in permafrost; Illisarvik drained lake site, Richards Island, Northwest Territories 173

J.A. HEGINBOTTOM: The bursting of a snow dam, Tingmisut Lake, Melville Island, Northwest Territories 187

W.W. SHILTS: Esker sedimentation models, Deep Rose Lake map area, District of Keewatin 217

S.G. EVANS and D.R. LISTER: The geomorphic effects of the July 1983 rainstorms in the southern Cordillera and their impact on transportation facilities 223

T.W.D. EDWARDS and R.A. KLASSEN: Preliminary isotopic and chemical characterization of natural gas in sediments of Lac Harrington, Quebec, and Golden Lake, Ontario 237

REGIONAL GEOLOGY/GÉOLOGIE RÉGIONALE

Arctic Islands/Archipel Arctique

B.F.G. FISCHER: Stratigraphy and structural geology of the region surrounding Bunde and Bukken fiords, Axel Heiberg Island, Canadian Arctic 309

Cordilleran Region/Région de la Cordillère

B. BLAISE et E. MERCIER: La sédimentation au Précambrien supérieur et au Paléozoique inférieur sur la marge de la plate-forme du Mackenzie (monts Ogilvie, Territoire du Yukon) 85

Precambrian Shield/Bouclier précambrien

A. CIESIELSKI: Pétrologie des gneiss du domaine du lac Bienville, sous-province archéenne d'Ungava, Québec: rapport d'étape 1

M.J. JACKSON, J.G. PIANOSI, and J.A. DONALDSON: Eolian dunes in early Proterozoic Thelon Formation near Schultz Lake, central Keewatin 53

D.C. KAMINENI, G.F. McCRANK, D. STONE, R.B. EJECKAM, R. FLINDALL, and R. SIKORSKY: Geology of the central plateau of the East Bull Lake pluton, northeastern Ontario 75

S.K. HANMER: Structure of the junction of three tectonic slices; Ontario gneiss segment, Grenville Province 109

S.K. HANMER and A. CIESIELSKI: A structural reconnaissance of the northwest boundary of the Central Metasedimentary Belt, Grenville Province, Ontario and Quebec 121

R.A. STERN: Geochemistry of Archean granitic rocks in the Perching Gull Lakes area, northwestern Ontario 143

A.N. LeCHEMINANT, M.J. JACKSON, A.G. GALLEY, S.L. SMITH, and J.A. DONALDSON: Early Proterozoic Amer Group, Beverly Lake map area, District of Keewatin 159

STRATIGRAPHY/STRATIGRAPHIE

W.H. FRITZ: Uppermost Precambrian and Lower Cambrian strata, northern Omineca Mountains, north-central British Columbia 245

A.F. EMBRY: Stratigraphic subdivision of the Roche Point, Hoyle Bay and Barrow formations (Schei Point Group), western Sverdrup Basin, Arctic Islands 275

A.F. EMBRY: The Wilkie Point Group (Lower-Upper Jurassic), Sverdrup Basin, Arctic Islands 299

A.F. EMBRY: The Schei Point and Blaa Mountain groups (Middle-Upper Triassic), Sverdrup Basin, Canadian Arctic Archipelago 327

N.C. MEIJER DREES and H.H.J. GELDSETZER: Correlation between Upper Devonian surface and subsurface map units in west-central Alberta 337

STRUCTURAL GEOLOGY/GÉOLOGIE STRUCTURALE

S.K. HANMER: The potential use of planar and elliptical structures as indicators of strain regime and kinematics of tectonic flow 133

I.W. MOFFAT and R.M. BUSTIN: Superposed folding in the northern Groundhog Coalfield; evidence for polyphase deformation in the northeastern corner of the Bowser Basin 255

T. JERZYKIEWICZ and D.R. VAN HELDEN: Preliminary observations on pock marks and fractured pebbles in the upper Cretaceous and Paleocene of the central Alberta Foothills near Hinton 263

SCIENTIFIC AND TECHNICAL NOTES
NOTES SCIENTIFIQUES ET TECHNIQUES

C.F. CHUNG and R.G. GARRETT: Note on optimal composite sample size selection 351

E. FROESE: Geology of the Weldon Bay – Fay Lake area, Manitoba 355

M.R. DAWSON, R.M. WEST, and L.J. HICKEY: Paleontological evidence relating to the distribution and paleoenvironments of the Eureka Sound and Beaufort formations, northeastern Banks Island, Arctic Canada 359

J.A. HEGINBOTTOM: Continued headwall retreat of a retrogressive thaw flow slide, eastern Melville Island, Northwest Territories 363

F.J.E. WAGNER: Regional distribution of marine Mollusca (gastropods and pelecypods) in Eastern Canada 367

K.L. CURRIE: A note on the solubility of quartz in supercritical water 369

P.G. KILLEEN, G.R. BERNIUS, L. SCHOCK, and C.J. MWENIFUMBO: New developments in the GSC borehole geophysics test area and calibration facilities 373

D. TESKEY and J. BROOME: Computer programs for production of shaded relief and stereo shaded relief maps 375

DISCUSSIONS AND COMMUNICATIONS

DISCUSSIONS ET COMMUNICATIONS

J-M. DUBOIS, A. LAROCQUE, P. BOISSONNAULT, C. DUBÉ, A. POULIN, Q.H.J. GWYN, G. LAROQUE, et A. MORISSETTE: Discussion de "Notes on the deglaciation of southeastern Quebec" 391

M. PARENT: Notes on the deglaciation of southeastern Quebec: discussion 395

N.R. GADD: Notes on the deglaciation of southeastern Quebec: reply 399

J.D. AITKEN: Strata and trace fossils near the Precambrian-Cambrian boundary, Mackenzie, Selwyn and Wernecke mountains, Yukon and Northwest Territories: discussion 401

W.H. FRITZ, G.M. NARBONNE, and S.P. GORDEY: Strata and trace fossils near the Precambrian-Cambrian boundary, Mackenzie, Selwyn and Wernecke mountains, Yukon and Northwest Territories: reply 409

CANADA – NEWFOUNDLAND CO-OPERATIVE MINERAL PROGRAM 1981-84 / CANADA – TERRE-NEUVE: PROGRAMME COOPÉRATIF SUR LES MINÉRAUX 1981-84 . . 414

Author Index/Index des auteurs 427

1.

PÉTROLOGIE DES GNEISS DU DOMAINE DU LAC BIENVILLE, SOUS-PROVINCE ARCHÉENNE D'UNGAVA, QUÉBEC: RAPPORT D'ÉTAPE

Project 800005

A. Ciesielski
Division de la géologie du Précambrien

Ciesielski, A., Pétrologie des gneiss du domaine du lac Bienville, sous-province archéenne d'Ungava, Québec: rapport d'étape; dans Recherches en cours, partie B, Commission géologique du Canada, Étude 84-1B, p. 1-10, 1984.

Résumé

Le domaine du lac Bienville constitue un des sous-ensembles de l'Archéen du Québec; ce domaine est essentiellement gneissique, de composition granodioritique et présente une grande homogénéité pétrographique. Les analyses font ressortir trois suites différentes, soit granitique, granodioritique et tonalitique, ces deux dernières constituant le <<mélange>> initial dont sont issus les granites s.s. par fusion in situ. Le domaine du lac Bienville constitue un terme inférieur de la croûte continentale archéenne et son terme tonalitique aurait pu être généré à partir d'une croûte basaltique primaire.

Abstract

The lac Bienville Domain is one of the Archean domains of Quebec; essentially gneissic, it consists of granodiorite and is petrographically homogeneous. Analysis has identified three different sequences, granitic, granodioritic and tonalitic. The latter two constitute the initial "melange" from which the granites s.s. have originated as a result of in situ fusion. The lac Bienville Domain is a lower member of the Archean continental crust and its tonalitic sequence could have been produced from a primary basaltic crust.

Introduction

L'Archéen du Québec a été divisé en trois sous-provinces litho-tectoniques, lesquelles contiennent à leur tour différents domaines ou zones dont la distinction est basée sur des critères lithologiques et structuraux (Ciesielski, 1983). Les travaux de terrain menés de 1980 à 1982 ont permis une cartographie détaillée des gneiss de la région de Poste-de-la-Baleine, une révision de la géologie le long de la Grande Rivière (Ciesielski, 1984) ainsi qu'une reconnaissance géologique le long de la côte de la baie James, entre Chissassibi et la pointe Louis-XIV. Outre les travaux de l'auteur, on dispose pour la région des travaux de Eade (1966), Sharma (1977), Shumacher et Fouque (1978), Marchand (1981) et Mercier et Ciesielski (1983) qui sont des travaux de reconnaissance ou d'exploration détaillée.

La sous-province d'Ungava est essentiellement gneissique, principalement de composition granodioritique à enclaves multiples et de nature variée et contient, pour la moitié, des domaines riches en roche du faciès des granulites, soit au nord le domaine de Minto et à l'est le domaine de Caniapiscau (voir la carte dans Ciesielski, 1983; Stevenson, 1968; Herd, 1978).

Géologie

Bien que tout le domaine du lac Bienville n'ait pas été cartographié en détail, les observations directes et indirectes recueillies montrent une grande homogénéité lithologique dans le quadrilatère délimité par Poste-de-la-Baleine, le golfe de Richmond, le lac à l'Eau Claire et le lac Bienville (fig. 1.1). Généralement, il s'agit d'un granitoïde (p. ex. tonalite à granite s.s.) à granulométrie moyenne, de couleur gris-rose, exhibant des foliations à intensité très variable, des structures de fluage et d'assimilation d'enclaves (schlieren), ainsi que des plis multiples à dimension, forme, orientation et plongement très variables. On note une grande variété d'enclaves dont:

des diorites et granodiorites à amphibole et pyroxène,

des métagabbros,

des métasédiments au faciès des amphibolites et des granulites,

des ultrabasites foliées ou massives,

des amphibolites ou métabasites à amphibole et pyroxène et,

des dykes anté-tectoniques plus ou moins assimilés.

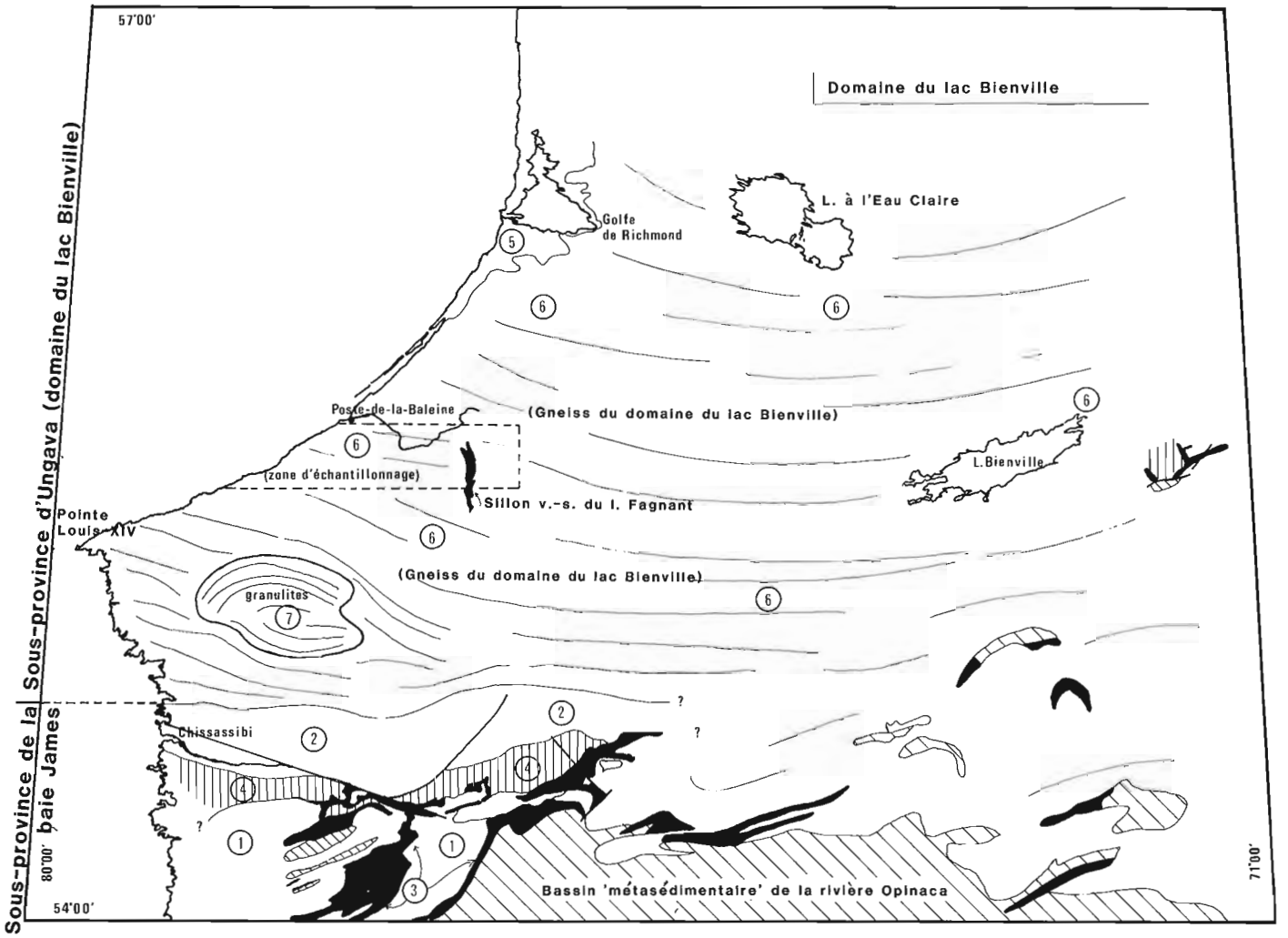

Figure 1.1. *Carte géologique montrant l'attitude des foliations du domaine du lac Bienville ainsi que la limite entre les sous-provinces archéennes d'Ungava et de la baie James, caractérisée par la présence de granodiorites à phénocristaux.*

1 - complexes plutoniques syn et tardi-tectoniques associés aux ceintures vertes
2 - granodiorites à phénocristaux tardi-tectoniques
3 - sillons volcano-sédimentaires, faciès des schistes verts et des amphibolites
4 - gneiss anté-kénoréens, probablement anté-volcaniques
5 - couverture sédimentaire protérozoïque
6 - gneiss granodioritiques du domaine du lac Bienville, faciès des amphibolites
7 - gneiss granulitiques très déformés

Les pegmatites ont deux origines: elles sont soit générées à partir d'une réaction entre les granodiorites fraîchement mises en place (protolites des gneiss du domaine du lac Bienville) et les enclaves basiques qu'elles sont en voie d'assimiler, ou soit le résultat d'une phase tardive de granitisation donnant naissance à des veines ou à des amas de pegmatites et d'aplites discordants sur la phase principale de déformation et n'ayant aucune orientation privilégiée.

Plus au sud, en allant vers la Grande Rivière, on remarque une augmentation de la déformation et du taux d'enclaves dans la roche.

Déformation

Les gneiss du domaine du lac Bienville sont caractérisés par une grande variation de l'intensité de la déformation. On note souvent sur un même affleurement des roches dont l'aspect passe de presque massif à très déformé et qui montrent des signes évidents de fluage magmatique ou métamorphique et d'assimilation avancée d'enclaves d'amphibolites. Outre la déformation qu'ont subie les enclaves (reliquats de couverture ou restites) antérieurement à la mise en place des granodiorites, on a reconnu au moins deux phases de foliation; la première est orientée à N280° et représente la déformation majeure du sud de la sous-province d'Ungava, tandis que la seconde est grossièrement orientée vers le nord en concordance avec l'orientation du petit sillon volcano-sédimentaire du lac Fagnant (Mercier, 1981, fig. 1) et la déformation principale relevée dans le domaine de Minto, au nord de la sous-province d'Ungava (Stevenson, 1968). Les déformations ont donné naissance à une gneissosité ou foliation marquée de façon différente dans les roches où, étant donné leurs natures plutoniques, des paramètres comme la viscosité, la disponibilité de l'eau et

l'assimilation de roches de compétences différentes ont joué un rôle important. On peut noter des textures massives et proto-mylonitiques se côtoyant. Les foliations se manifestent plus nettement aux endroits caractérisés par un taux élevé d'amphibole et de biotite primaires. On remarque en outre une absence de marqueur ou d'horizon cartographiable si ce ne sont quelques dykes anté-tectoniques de petite taille qui sont spacialement liés à des plis asymétriques de grande envergure. Ces dykes ont subi les effets d'une différenciation minérale, caractérisée par un <<litage>> d'amphiboles de couleurs différentes, d'origine probablement métamorphique et parallèlle aux murs du dyke à angle avec la foliation principale. La présence d'enclaves bréchiques a pour effet de diminuer l'intensité de la déformation, et on notera souvent l'aspect massif de la matrice alors que l'entourage peut être fortement gneissifié. En outre, il existe une relation évidente entre la déformation et la présence de matériel granitique qui se présente en amas ou en veinules intimement liés à la gneissification et qui est interprétée comme une orthomigmatisation généralisée des granodiorites survenue à la même époque que la déformation principale.

Pétrographie

L'étude des lames minces révèle la présence de grains de dimension moyenne, une texture grossièrement équigranulaire malgré la forte recristallisation et le fait que l'altération a joué de façon très irrégulière. Les contacts entre les grains de plagioclase semblent indiquer une automorphie ancienne; les quartz sont systématiquement recristallisés avec diminution de la taille des grains et contacts finements interlobés exhibant des myrmékites. Les feldspaths potassiques, eux, sont presque toujours mâclés microcline et leurs formes suggèrent qu'ils sont dus à une cristallisation tardive. On note aussi la présence de biotites vertes et brunes et d'amphiboles dans des proportions allant jusqu'à 10 %. L'altération touche principalement les ferromagnésiens et les plagioclases produisant de la chlorite, de l'épidote, de la muscovite et de la séricite. Les minéraux accessoires sont l'apatite, le spène, l'allanite et le zircon. La roche montre des textures évidentes de recristallisation et de rétromorphose de type hydrothermal qui ne s'est pas manifestée selon une orientation préférentielle. La biotite et l'amphibole montrent des signes d'abrasion évidents ainsi qu'une association symplectique très fine au quartz.

Le métamorphisme se situe au niveau du faciès des amphibolites supérieur, éventuellement début de celui des granulites, avec une rétromorhose isotrope dans le champ des schistes verts. Les enclaves basiques et métasédimentaires exhibent des assemblages du faciès des amphibolite mais se caractérisent cependant par la présence d'ortho- et de clinopyroxène (transition probable au faciès des amphibolites supérieur ou à celui des granulite).

Géochimie

Les échantillons ont été prélevés immédiatement au sud de Poste-de-la-Baleine à l'intérieur d'un quadrilatère de 25 sur 100 km comprenant trois lignes d'échantillonnage orientées est-ouest et distantes de 10 km, avec des arrêts d'hélicoptère à tous les 2 km (fig. 1.1).

Les roches à analyser ont été sélectionnées sur chacune des lignes en fonction de leur homogénéité et de leur ressemblance entre elles. Le personnel des laboratoires de la CGC ont analysé les échantillons selon les méthodes habituelles, afin d'identifier les éléments majeurs et à l'état de traces et les résultats ont été soumis au calcul mésonormatif comprenant la biotite et l'amphibole (tab. 1.1). Les résultats ont été transposés dans une projection An-Ab-Or et classés selon les critères de Barker, 1979 (fig. 1.2). On note la présence de trois familles distinctes: granite (sensu stricto), granodiorite et tonalite. La première se situe sous la projection de la ligne cotectique séparant les champs des deux feldspaths (Winkler et coll., 1975). On note aussi une nette distinction entre les moyennes des gneiss gris archéens (les cercles de la figure 1.2, d'après Martin et coll., 1983) et les gneiss du domaine du lac Bienville, ces derniers étant en général plus tonalitiques que trondjhémitiques (c'est-à-dire un rapport Ab/An plus faible). On note exactement les mêmes tendances dans la figure 1.3, où se dégagent très nettement les granites en fin de tendance calco-alcaline ainsi que deux tendances plus floues, soit la tendance calco-alcaline des granodiorites (centre du diagramme) et la tendance tonalito-trondjhémitique (enrichissement relatif en Na_2O, partie centre gauche du diagramme). Bien qu'en général les données de terrain ne révèlent pas l'existence d'entités cartographiables de composition particulière, quelques affleurements situés immédiatement au sud de la zone d'échantillonnage (fig. 1.4) et la nature orthomigmatitique de presque toutes les roches semblent indiquer que les gneiss du domaine du lac Bienville proviennent de sources caractérisées par au moins deux compositions différentes, c'est-à-dire la tonalite et la granodiorite; le membre granitique, pour sa part, est en partie issu de la fusion partielle in situ du mélange formé survenue pendant la déformation. La projection Qz-Pl-Or montre aussi (fig. 1.5) les deux tendances calco-alcaline (C-A, rapport Qz/Or constant) et tonalitique (G-T, rapport Pl/Or constant de Ermanovics et coll., 1979), ainsi qu'une concentration de points près du minimum, laquelle correspond à la production du matériel granitique par fusion partielle tardive.

Les roches à tendance tonalitique correspondent à la partie sud de la zone d'échantillonage; on peut y voir une relation certaine avec la présence d'une très grande formation de gneiss granulitiques entre Poste-de-la-Baleine et la Grande Rivière (fig. 1.1) se manifestant par une influence du genre métamorphisme de contact et donnant naissance dans les enclaves de paragneiss et d'amphibolites à deux pyroxènes. Les deux diagrammes AFM et Jensen (fig. 1.6) exhibent les deux séries calco-alcalines classiques avec un rapport Fe/Mg remarquablement constant où se distinguent, en fonction de l'alumine ou des alcalins, deux familles: l'une plutôt granodioritique, l'autre tonalitique. Sur la figure 1.7, on observe une relation inverse entre le calcium et la silice. On y a reporté les suites classiques I et S (Chappel, 1978; Hine et coll., 1978), et on remarque une certaine incompatibilité entre les suites des gneiss du domaine du lac Bienville et les autres suites plus réçentes, qu'elles soient d'origine ignée ou sédimentaire. On en déduit que si les suites tonalito-granodioritiques du domaine du lac Bienville montrent un certain parallèllisme avec les suites ignées, la suite granitique pour sa part, bien que d'origine ignée elle aussi, est en parfaite contradiction avec le modèle proposé. S'il est possible de prédire la tendance de contamination de certaines suites plutoniques d'après des critères chimiques (rapport Al/Na+K+Ca/2, voir Pitcher, 1983) et les types d'enclaves qu'elles comportent, la situation est tout à fait autre dans le cas des gneiss en question; ces derniers comportent presque tous les types d'enclaves imaginables (sauf les calcaires), n'ont pas un volume circonscrit dans l'espace, ne sont pas reliés spacialement à une tectonique particulière et bien que groupées, leurs compositions chimiques s'étalent de façon régulière entre le granite et la tonalite. Il faut donc invoquer un modèle non-uniformitariste qui comporte des variantes satisfaisant à chaque contexte archéen (Barker et coll., 1981; Collerson et coll., 1981) et qui tienne compte du volume énorme de roches produites sur une aussi grande surface à partir d'une croûte primaire tholéiitique ou tonalitique.

Tableau 1.1. Analyse des éléments majeurs

ID	SIO2	AL203	FE203	FEO	MGO	CAO	NA2O	K2O	TIO2	P2O5	MNO	S	CR203	CO2	H2O	ZR	SR	RB	ZN	NI	BA	K/RB	OTZ	COR	OR	AB	AN	MGBI	FEBI
300	70.00	13.60	.90	2.80	1.91	1.37	2.40	3.72	.43	.13	.04	0.00	.01	.60	1.30	.016	.034	.010	.005	.005	.116	309	39.62	6.10	14.99	22.37	.68	7.30	5.21
305	68.10	15.80	.50	2.00	1.62	2.39	3.40	2.56	.35	.15	.02	0.00	.01	.50	1.20	.018	.056	.005	.002	.004	.106	425	33.89	5.69	9.37	31.49	6.70	6.15	3.81
306	70.90	15.20	.50	1.60	.96	2.62	3.40	2.38	.32	.13	.03	0.00	0.00	.20	.90	.022	.046	.005	.004	.004	.073	395	35.79	3.87	10.32	31.40	10.04	3.63	2.99
307	69.00	15.30	1.20	1.40	.91	2.50	3.40	3.35	.30	.12	.05	0.00	0.00	.20	.60	.015	.051	.010	.005	.002	.126	278	30.76	3.01	17.05	31.52	9.61	3.46	1.94
309	73.30	14.10	.20	1.00	.96	.54	2.30	6.21	.19	.07	.01	0.00	.01	.10	.70	.019	.015	.018	.000	.003	.131	286	33.73	3.63	34.04	21.11	.95	3.61	1.93
313	72.30	14.00	.90	1.00	.54	1.62	2.80	3.97	.21	.07	.02	0.00	.01	.20	.60	.014	.043	.009	.004	.003	.139	366	36.85	3.46	22.27	26.14	5.80	2.07	1.31
315	71.60	14.20	1.00	1.50	.86	2.43	2.90	2.97	.28	.09	.03	0.00	.01	.10	.50	.017	.043	.010	.005	.003	.139	246	37.40	2.95	14.71	27.03	10.23	3.28	2.31
317	70.20	14.30	1.10	1.50	1.31	2.61	3.10	3.24	.30	.15	.04	0.00	.01	.10	.60	.020	.057	.009	.006	.003	.131	299	33.60	2.17	15.27	28.76	10.63	4.98	2.22
319	71.50	14.50	1.00	1.40	1.29	1.19	2.90	4.62	.28	.08	.03	0.00	.01	0.00	1.00	.016	.032	.008	.003	.004	.158	479	33.05	3.48	23.61	26.66	4.51	4.86	2.06
321	67.80	14.40	2.30	1.50	2.16	1.50	2.30	4.15	.39	.18	.05	0.00	.01	.10	1.40	.020	.036	.010	.007	.010	.139	344	35.40	5.22	19.82	21.68	4.49	8.34	1.11
323	68.30	14.20	2.00	2.20	1.74	3.27	2.80	2.34	.53	.20	.06	.05	.01	.10	.80	.022	.044	.013	.011	.005	.065	149	36.01	2.85	8.49	26.20	12.96	6.67	2.80
344A	68.10	16.30	.60	1.90	1.14	2.63	4.10	2.04	.32	.13	.04	0.00	0.00	.20	1.00	.019	.047	.011	.007	.002	.076	154	30.45	4.21	7.48	37.85	10.09	4.31	3.55
336	72.90	14.00	.80	.80	.69	1.45	3.30	4.17	.21	.09	.04	0.00	.01	.30	.50	.013	.043	.019	.004	.005	.095	182	33.97	2.90	22.93	30.28	4.06	2.59	1.00
340	73.10	13.20	.70	.90	.73	.78	2.40	5.31	.18	.07	.02	.04	0.00	0.00	.70	.014	.028	.017	.004	.002	.107	259	36.22	2.83	30.21	22.48	2.90	2.80	1.21
341	74.20	12.80	.60	1.00	.51	1.15	2.30	5.66	.35	.06	.02	0.00	.01	.10	.50	.021	.036	.018	.001	.003	.097	261	35.76	1.83	32.30	21.31	3.57	1.94	1.59
344	70.50	15.70	1.00	.90	.79	1.64	4.50	2.74	.24	.06	.03	0.00	.01	.10	.70	.018	.026	.009	.003	.003	.062	253	29.21	3.37	14.01	41.15	6.39	2.96	1.00
347	66.80	14.70	1.20	2.20	1.26	3.30	3.10	2.58	.47	.16	.05	.03	.01	.10	.80	.025	.066	.010	.007	.003	.125	214	33.51	2.29	10.55	28.85	13.53	4.80	3.58
350	67.50	14.90	1.50	2.20	1.66	3.43	3.20	2.46	.50	.18	.07	0.00	0.00	.20	1.10	.018	.049	.008	.010	.005	.087	255	32.19	2.56	8.96	29.76	13.29	6.33	3.41
401	71.20	13.40	.10	1.90	1.52	.49	2.10	5.21	.35	.09	.02	0.00	.01	.20	1.30	.013	.017	.008	.000	.004	.153	540	37.88	4.94	26.34	19.81	0.00	5.87	3.70
403	65.60	15.40	.80	3.20	2.12	1.28	2.80	4.06	.52	.19	.05	0.00	.01	.70	1.80	.019	.041	.012	.009	.004	.109	281	32.42	7.27	16.40	26.16	0.00	8.12	5.58
405	69.70	13.60	1.50	1.80	1.26	2.67	2.90	3.66	.42	.10	.07	0.00	.01	.20	.70	.015	.035	.008	.005	.003	.085	380	32.93	1.42	17.83	27.02	10.23	4.81	2.55
408	67.00	15.10	.80	3.10	2.94	.45	2.30	3.86	.55	.15	.02	.02	.01	.10	2.30	.016	.011	.008	.002	.004	.174	400	37.62	8.17	13.57	21.66	0.00	11.35	5.20
410	72.40	14.80	.60	1.20	.85	2.28	3.60	1.86	.19	.08	.02	0.00	.01	0.00	.70	.024	.047	.007	.004	.003	.049	220	38.11	3.55	8.07	33.38	10.45	3.23	2.02
413	71.60	15.10	0.00	1.30	.43	2.39	3.70	3.32	.14	.03	.02	0.00	.01	0.00	.50	.012	.055	.010	.001	.000	.117	275	30.85	1.48	17.37	34.09	11.46	1.62	2.79
419	71.40	14.40	1.20	1.40	1.27	1.48	3.10	3.66	.37	.12	.05	0.00	.01	.20	.90	.022	.030	.017	.008	.004	.084	179	35.51	4.33	17.99	28.56	4.11	4.79	1.92
427	70.90	14.40	1.30	1.70	.98	2.88	4.00	2.37	.40	.13	.05	0.00	.01	.40	.70	.025	.033	.009	.005	.004	.047	218	32.07	1.95	10.38	36.40	9.64	3.65	2.43
429	61.80	18.00	1.30	2.30	2.18	3.97	4.10	3.19	.43	.23	.06	0.00	.01	.50	1.30	.022	.057	.009	.007	.002	.073	294	18.37	3.14	11.69	37.28	13.70	8.12	3.70
432	66.90	13.90	1.90	2.60	2.39	3.13	2.90	2.07	.52	.14	.08	0.00	.01	.30	1.60	.025	.049	.006	.010	.005	.072	286	35.96	3.31	4.59	27.31	11.43	9.22	3.95
434	65.20	16.40	2.00	2.20	1.81	4.54	3.50	1.58	.56	.21	.05	0.00	.01	.40	1.00	.028	.063	.007	.007	.004	.057	187	29.61	3.16	3.52	32.22	17.09	6.83	2.85
441	65.80	15.40	1.40	2.90	1.77	3.19	4.30	1.96	.42	.30	.07	.20	.01	.30	1.00	.034	.039	.009	.006	.007	.022	181	26.94	2.63	4.89	39.48	10.74	6.66	4.46
449	75.10	12.30	.70	.70	.30	.95	2.30	5.32	.16	.07	.01	.01	.01	.10	.40	.014	.028	.019	.003	.003	.086	232	38.49	1.86	31.48	21.49	3.19	1.15	.82
450	69.20	14.20	1.30	1.50	1.03	1.81	3.00	4.77	.36	.17	.04	0.00	.01	.40	.90	.020	.051	.014	.006	.004	.147	283	30.12	2.94	25.40	27.83	4.22	3.92	2.03
455	66.00	14.20	1.90	2.90	2.32	3.99	2.70	2.81	.55	.13	.08	0.00	.01	.10	.80	.016	.056	.008	.010	.005	.117	291	30.91	.80	8.87	25.24	17.06	8.89	4.56
456	62.00	15.80	2.10	3.50	2.68	4.97	3.50	2.39	.54	.22	.11	.01	.02	.40	1.10	.020	.044	.007	.007	.002	.070	283	22.74	.63	4.65	32.18	19.26	10.10	5.60
500	63.70	15.50	2.10	2.60	2.89	3.55	3.00	2.26	.60	.20	.06	0.00	.01	.90	1.60	.016	.061	.008	.007	.006	.064	234	32.08	5.64	4.65	27.87	8.82	11.00	3.66
502	59.40	16.40	2.70	4.40	2.97	5.97	2.80	1.79	.74	.25	.11	.01	.01	.10	1.00	.022	.056	.006	.007	.003	.065	248	23.80	.88	0.00	26.16	25.77	10.86	6.73
504	65.20	15.30	2.10	2.80	1.93	3.10	3.30	3.27	.55	.15	.08	0.00	.01	.50	1.00	.019	.039	.013	.007	.003	.070	209	27.65	3.27	12.72	30.44	9.57	7.29	4.10
506	63.20	16.10	2.80	2.90	2.56	3.94	3.50	1.92	.71	.26	.09	0.00	.01	.20	1.60	.023	.066	.007	.006	.004	.079	228	27.53	3.47	3.32	32.35	14.52	9.69	3.67
509	63.00	16.00	1.70	3.70	2.28	4.81	3.30	1.69	.62	.22	.09	.03	.01	0.00	1.10	.019	.068	.006	.008	.010	.077	234	27.06	1.49	.91	30.78	21.05	8.71	6.41
510	69.20	13.70	1.50	2.20	1.64	2.96	1.60	3.89	.49	.11	.06	.01	.01	0.00	.80	.016	.049	.006	.008	.008	.214	538	38.44	2.72	18.12	15.15	12.92	6.36	3.42
514	66.30	15.00	1.70	3.10	2.16	3.81	3.20	2.22	.54	.22	.07	.03	.01	0.00	1.00	.017	.053	.008	.008	.010	.083	230	30.62	1.82	5.25	29.62	16.06	8.19	5.04
517	70.70	15.70	1.70	0.00	.86	2.94	4.50	1.28	.31	.06	.02	.01	0.00	.20	.50	.015	.061	.008	.005	.002	.020	133	32.41	2.86	5.70	41.24	12.09	3.23	0.00
521	62.50	15.10	2.70	3.30	2.50	4.54	3.40	1.64	.59	.18	.10	0.00	.01	.20	1.30	.015	.065	.007	.007	.002	.045	194	27.36	1.28	1.17	31.95	18.86	9.63	4.72
523	60.10	16.60	2.30	4.10	2.76	5.92	4.00	1.70	.78	.25	.10	.02	.02	.30	.90	.021	.061	.008	.007	.004	.038	176	18.49	0.00	0.00	36.47	22.65	9.96	6.35
525	59.00	15.50	2.80	4.70	3.69	5.82	2.90	1.72	.79	.31	.13	0.00	.02	.60	1.60	.022	.054	.007	.007	.005	.041	204	23.26	1.61	0.00	26.91	20.97	10.89	5.90
529	64.10	14.70	3.30	2.10	2.66	5.23	3.30	1.44	.61	.18	.10	.01	.02	.70	.80	.020	.057	.006	.006	.006	.048	199	29.58	1.16	1.53	30.46	18.72	10.06	1.48
531	64.10	15.20	2.10	2.40	2.37	3.33	3.30	2.14	.59	.22	.06	0.00	.01	.80	1.60	.017	.059	.007	.007	.003	.103	254	31.72	5.16	5.46	30.90	8.31	9.09	3.25
533	68.90	15.20	.70	2.10	1.79	2.42	3.70	1.72	.47	.15	.04	0.00	.01	.10	1.30	.018	.032	.005	.007	.003	.035	285	35.17	4.57	3.82	34.40	9.06	6.82	3.89
535	71.90	15.40	.70	1.20	.73	2.79	4.10	2.00	.29	.09	.02	0.00	.01	.20	.60	.015	.037	.007	.005	.003	.070	237	33.23	2.72	9.08	37.25	11.11	2.72	1.88
538	74.20	14.10	.20	1.20	.73	2.68	3.80	1.23	.10	.05	.02	0.00	0.00	.50	.80	.008	.029	.004	.001	.009	.029	255	40.90	3.40	4.22	34.85	9.66	2.74	2.38
540	69.20	16.30	.40	1.50	.90	3.64	5.00	.62	.27	.08	.04	0.00	.01	.10	.80	.009	.050	.004	.005	.007	.034	129	28.81	1.73	0.00	45.70	16.24	3.23	2.73
542	58.60	16.10	3.10	4.00	3.46	6.14	3.00	1.60	.71	.22	.12	.01	.01	.10	1.40	.018	.064	.007	.010	.008	.074	190	21.26	0.00	0.00	28.07	26.81	10.94	4.81
546	70.80	14.40	1.30	2.40	1.36	3.67	3.50	1.17	.46	.08	.04	0.00	0.00	.10	.70	.009	.039	.003	.008	.010	.046	324	36.94	1.91	1.42	32.18	15.81	5.12	3.92
549	60.90	17.60	2.50	3.50	2.40	5.18	3.70	1.80	.72	.32	.07	0.00	.01	.30	.70	.024	.072	.009	.008	.002	.066	166	22.29	2.81	1.99	33.79	19.52	8.98	5.13
552	67.30	14.00	1.50	2.40	1.81	3.47	3.00	2.78	.44	.15	.08	0.00	.01	.30	1.40	.016	.051	.009	.009	.005	.107	256	32.21	1.55	10.35	28.08	13.35	6.94	3.88
558	74.20	12.60	.90	.80	.69	.97	2.60	4.72	.23	.08	.02	0.00	.01	.30	.70	.013	.035	.020	.003	.002	.096	196	38.56	2.98	26.70	24.20	1.65	2.63	.88
559	75.70	12.40	1.20	1.00	.83	.95	2.40	4.67	.32	.09	.03	0.00	.01	.20	.80	.012	.034	.016	.003	.004	.084	242	40.66	3.08	25.64	22.06	1.79	3.13	1.03
560	67.90	14.30	1.90	1.70	1.06	2.08	2.70	4.96	.89	.26	.04	.03	.01	.30	.80	.042	.058	.022	.007	.003	.125	187	29.76	3.58	26.71	25.14	3.76	4.04	1.81
562	69.60	14.70	1.20	1.80	.92	2.75	3.20	2.73	.38	.12	.04	0.00	.01	.20	.80	.020	.057	.008	.008	.002	.110	283	34.47	3.08	12.81	29.84	10.66	3.52	2.78
564	65.20	15.60	1.90	2.30	1.69	4.07	3.70	1.66	.44	.14	.06	0.00	.01	.40	1.20	.013	.055	.009	.007	.003	.057	153	29.24	2.42	4.13	34.46	15.78	6.45	3.22
565	69.50	16.00	1.20	1.40	.98	2.48	3.80	3.40	.29	.12	.04	0.00	0.00	.20	.60	.015	.049	.009	.007	.002	.123	313	28.26	2.96	16.85	34.49	9.34	3.64	1.88

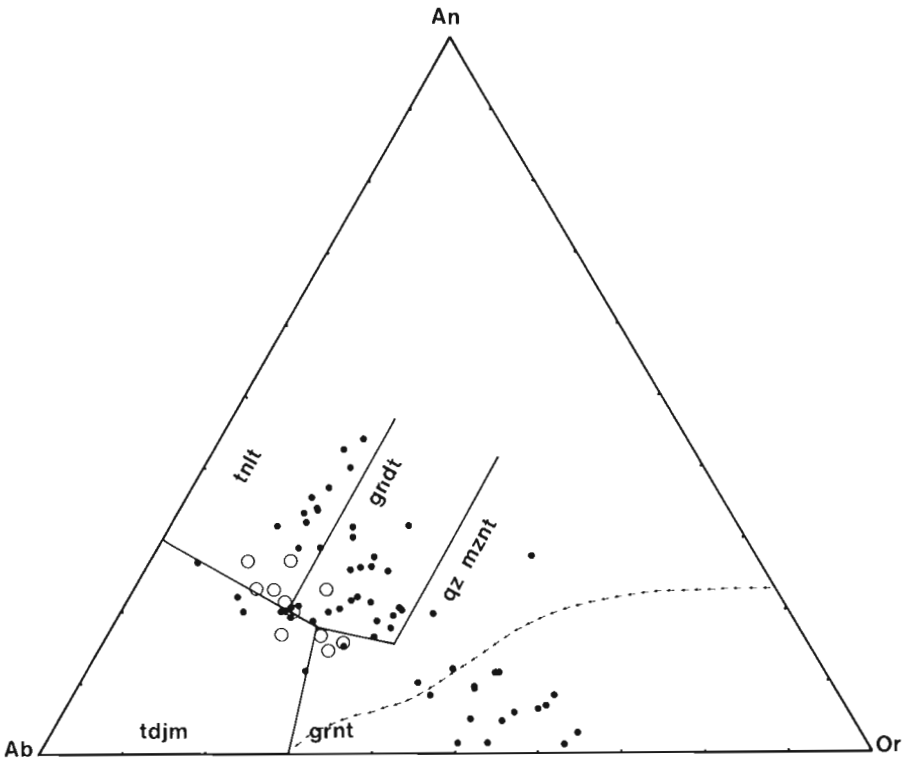

Figure 1.2

Projection des analyses (points noirs) dans le diagramme An-Ab-Or, à partir du tétrahèdre des granites, selon la classification de Barker (1979). La projection de la ligne cotectique séparant les champs des deux feldspaths est calculée pour pH_2O = 5kb d'après Winkler et coll. (1975). Les cercles représentent les moyennes des gneiss gris archéens de Martin et coll. (1983).

TNLT – Tonalites
GNDT – Granodiorites
GRNT – Granites
TDJM – Trondjhémites
MZNT – Monzonites

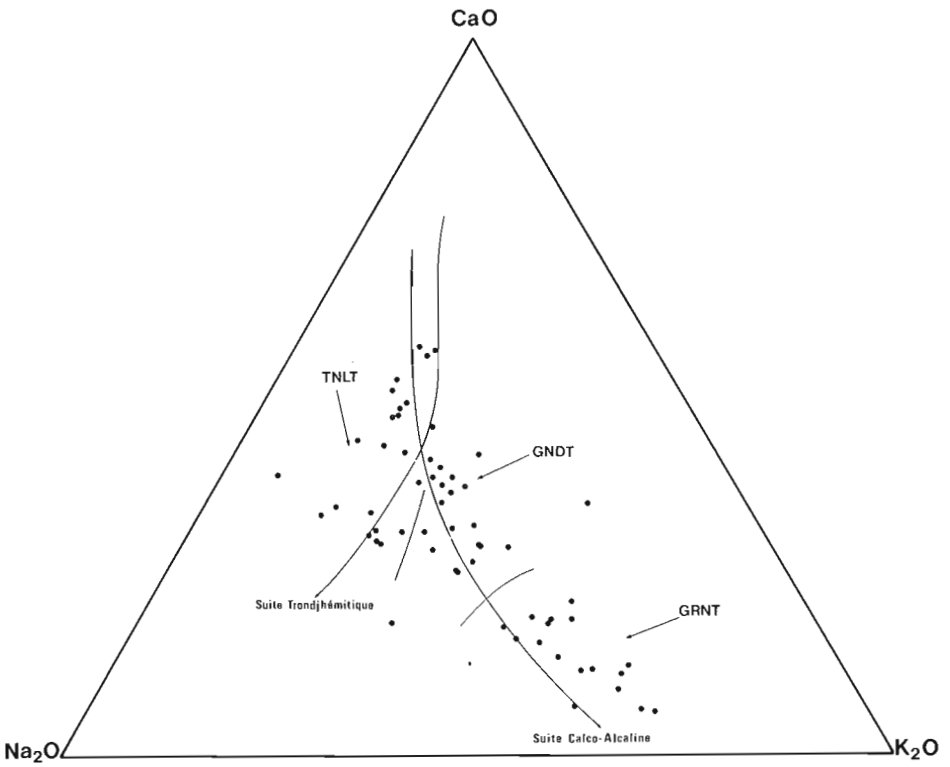

Figure 1.3

Projection des analyses dans le diagramme $CaO-Na_2O-K_2O$ (% W) montrant les suites trondjhémitiques et calco-alcalines. Les traits courts séparent ces deux dernières tendances ainsi qu'un terme granitique.

Figure 1.4. *Deux types de gneiss qui se distinguent sur l'affleurement: tonalitique et granodioritique. Les flèches indiquent le contact tectonique.*

Une analyse rapide des éléments majeurs du tableau 1.1, montre qu'il existe un rapport direct entre SiO_2 et K_2O et entre Al_2O_3 et Na_2O, ainsi qu'un rapport inverse entre SiO_2 et Al_2O_3.

Les éléments à l'état de traces ont été reportés dans un diagramme Ba-Rb-Sr (fig. 1.8) où on note un rapport Rb/Sr relativement constant et où seul Rb a une valeur absolue faible mais constante, soit 80 à 100 ppm (tab. 1.1). La tendance de différenciation des analyses concorde de façon relative avec celle de El Bouseily (1975) et on en déduit une filiation chimique (rapport Rb/Sr constant, augmentation de Ba) entre les tonalites et la granodiorite, alors que la genèse des granites par orthomigmatisation s'est effectuée avec une légère augmentation du taux de Rb. Pris deux par deux, ces trois éléments n'ont pas de rapport de variation directe ou inverse entre eux, seul Sr varie directement avec CaO et inversément avec SiO_2; le rapport K/Rb pour sa part ne varie pas de façon évidente en fonction du taux de potassium dans la roche (tab. 1.1). Dans la figure 1.9, les rapports Rb/Sr montrent un groupement des analyses dont la valeur moyenne est de 0,25, et une position sur les isobathes de Condie (1976) qui correspond à une plus grande <<profondeur>> par rapport aux séries volcaniques archéennes représentées par des traits courts. Il appert en effet que l'épaisseur réelle des ceintures volcano-sédimentaires archéennes ne dépasse pas 8 à 10 km et les systèmes des ceintures volcano-plutoniques et bassins <<métasédimentaires>> représentent un niveau relativement peu profond de la croûte archéenne (passage du faciès des schistes-verts à celui des amphibolites, amphibolites moyen), alors que des gneiss comme ceux du domaine du lac Bienville représentent une partie beaucoup plus basse de la croûte (passage de la fin du faciès des amphibolites à celui des granulites) où les caractères rhéologiques plus prononcés ont donné naissance à des mélanges pouvant être homogènes sur de très grandes profondeurs.

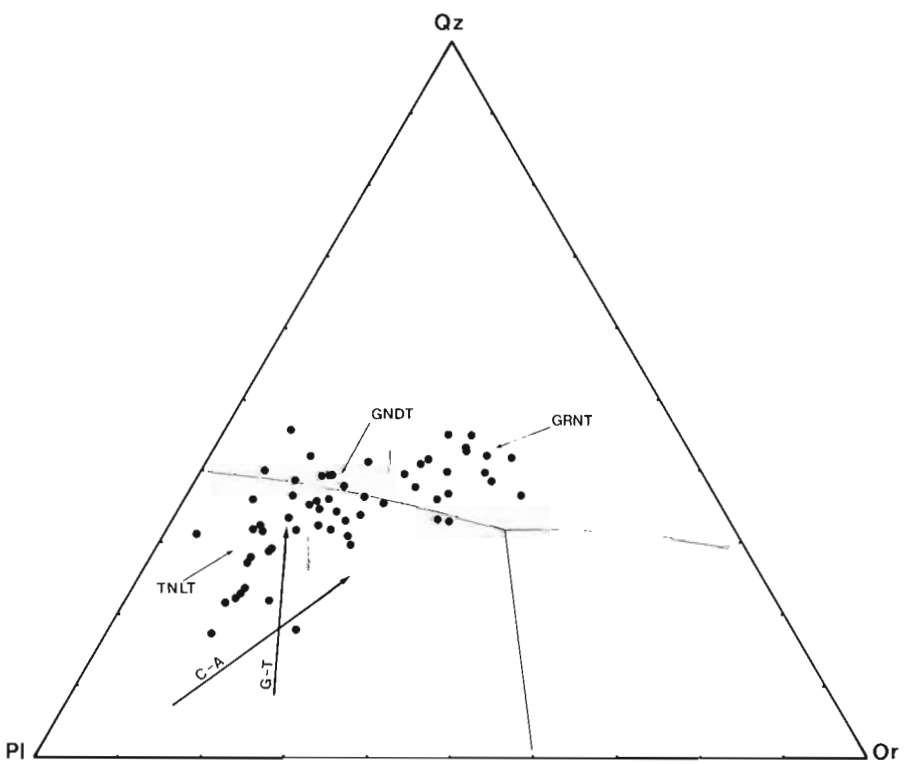

Figure 1.5

Positions des analyses dans la projection Qz-Pl-Or où se dégagent les trois groupes, soit les tonalites, les granodiorites et les granites. Les deux tendances calco-alcaline et gabbro-trondjhémitique sont tirées de Ermanovics (1979). Les lignes cotectiques sont valables pour pH_2O*=5kb.*

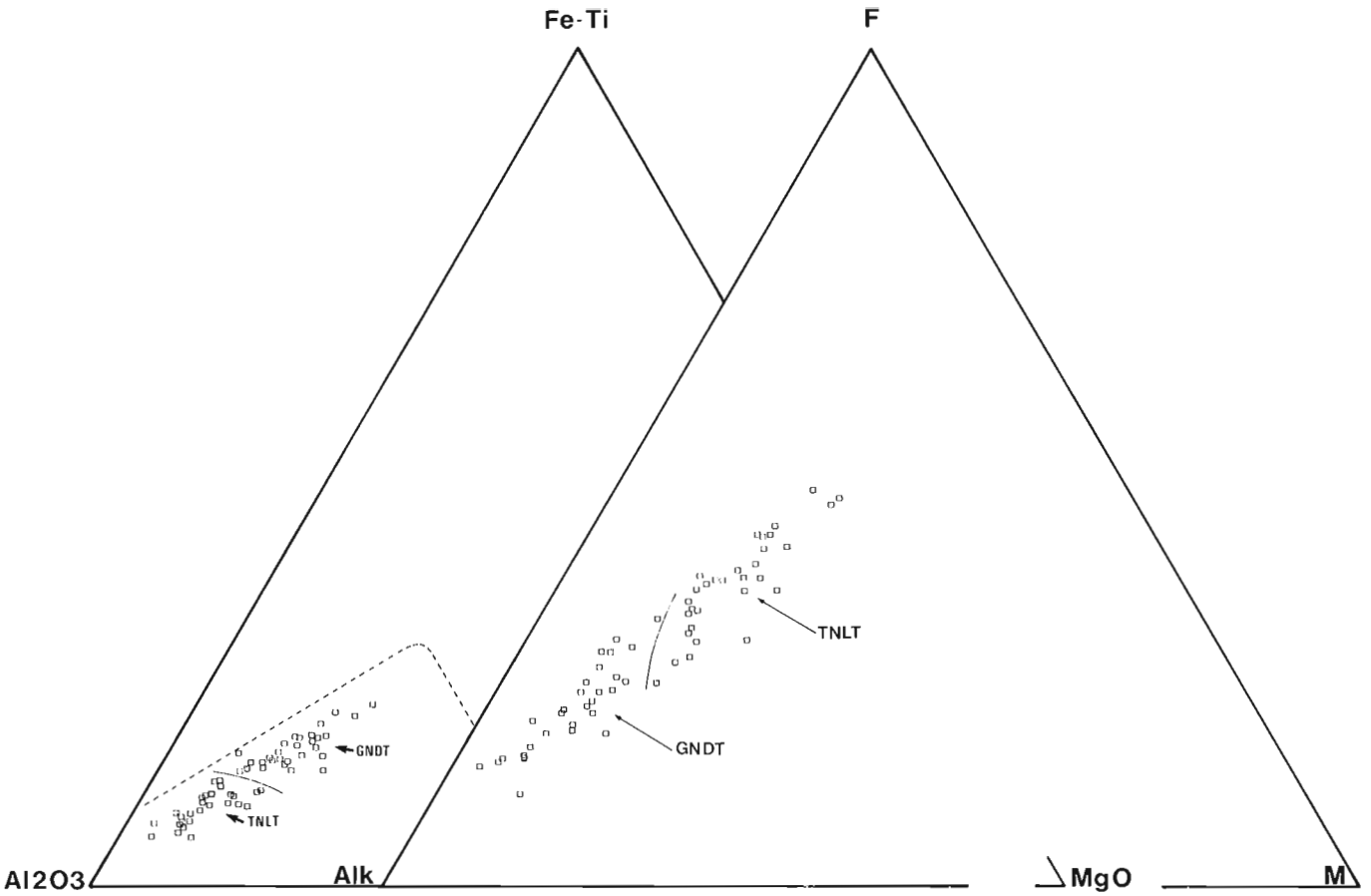

Figure 1.6. *Deux projections AFM et Jensen (% W) montrant des suites calco-alcalines classiques, avec un rapport Fe/Mg constant et où on ne distingue que la suite tonalitique et le granodiorite-granite, en fonction d'un enrichissement en alumine ou en alcalin.*

Discussions

Étant donné l'homogénéisation atteinte par les gneiss en question, il devient très difficile d'effectuer des analyses structurales en raison de l'aspect très variable, sur un même affleurement, de la morphologie et de l'attitude des plis, et vu qu'ils ne sont pas reliés à des zones de déformation particulière. Étant donné également la rhéologie et les fluages syn-cinématiques du matériau, il devient impossible d'évaluer la position de quelque contrainte que ce soit ou de comprendre vraiment le sens des mouvements du fait que les linéations sont totalement absentes dans la roche. En outre, la région se prête difficilement à l'élaboration du modèle d'une tectonique en dômes ou en écailles comme elle s'y prête ailleurs dans les terrains archéens et grenvilliens.

La géochimie démontre que les gneiss du domaine du lac Bienville constituent une série calco-alcaline en regard des alcalins et de l'alumine, et deux séries calco-alcalines et tonalito-trondjhémitiques en regard de l'enrichissement en calcium et en potassium. La filiation des deux membres chimiques, c'est-à-dire la granodiorite et le granite, aux tonalites supposées primaires, est déduite de leur cohérence à la suite calco-alcaline de la figure 1.3, de rapports Fe/Mg et Rb/Sr particulièrement constants ainsi que du caractère orthomigmatitique de la portion granitique des gneiss.

On en arrive donc à conclure à un <<mélange>> magmato-cinématique de plusieurs compositions ayant pris naissance à partir d'une croûte initiale probablement basique (tholéiitique) ou de manière in situ par orthomigmatisation. La figure 1.10 montre une échelle relative en fonction de la température et du temps qui sert à établir le modèle de l'évolution des précurseurs et protolites des gneiss du domaine du lac Bienville. L'origine des tonalites à partir de matériel tholéiitique a déjà été amplement décrite par Tuthill-Helz (1976) et de nombreux modèles y font référence (voir Condie et coll., 1982; Barker, 1979; Martin et coll., 1983). Il est impossible de prédire le nombre d'évènements magmatiques ou de mises en place de grande envergure ayant donné naissance aux tonalites et granodiorites, puisqu'aucune enclave n'a montré de caractère de restite et encore moins de restite de composition différente. La granitisation in situ a débuté après le déclenchement de la déformation cata- et mésozonale et a été rendue possible par une disponibilité de l'eau jusque-là absente, probablement à partir du lessivage des ferromagnésiens hydratés. Des compositions proches du minimum granitique sont atteintes lors d'une augmentation de la pression partielle d'eau et de la fugacité d'oxygène et d'un abaissement de la température. Vient ensuite une phase d'extension (dykes de diabases anté-kénoréens), qui nécessite une augmentation de la compétence de la roche et une diminution de la température, le tout accompagné d'une rétromorphose s'étalant jusqu'à la fin de la déformation polyphasée. Tardivement, une pulsion magmatique minimum à la faveur d'une autre phase de fracturation isotrope a donné naissance à des filons aplitiques et pegmatitiques. Le tout se termine par une ou plusieurs phases d'extension post-kénoréenne donnant des dykes de diabase d'âge indéterminé.

Le niveau actuel d'érosion du domaine du lac Bienville a été atteint il y a environ 2 Ma comme en font foi les sédiments protérozoïques de la fosse du Labrador et de l'arc de Nastapoka exempts de déformation et reposant en discordance sur le socle. Afin de concilier des niveaux d'érosion différents de part et d'autre des sous-provinces de la baie James et d'Ungava, on se doit d'invoquer une remontée beaucoup plus importante du secteur d'Ungava, et

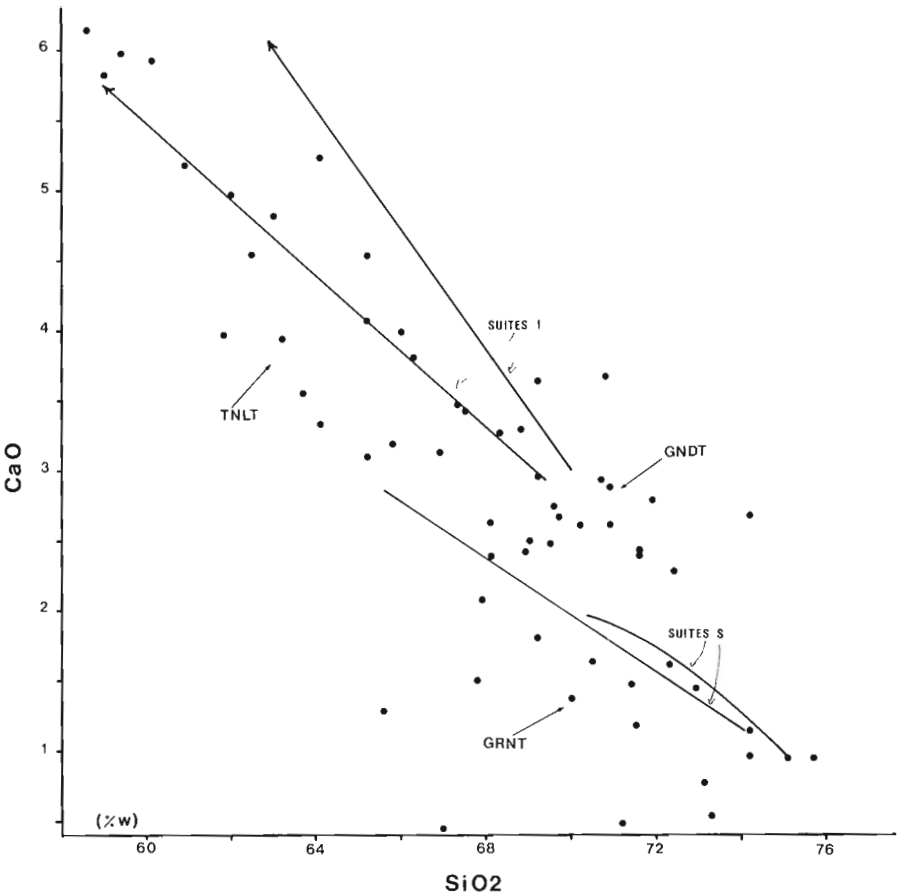

Figure 1.7

On observe un certain parallèllisme entre les suites I et les gneiss du domaine du lac Bienville dans le diagramme CaO/SiO_2, d'après Hine et coll. (1978) et Chappel (1978). On note une incompatibilité entre les granites d'origine ignée et les suites S.

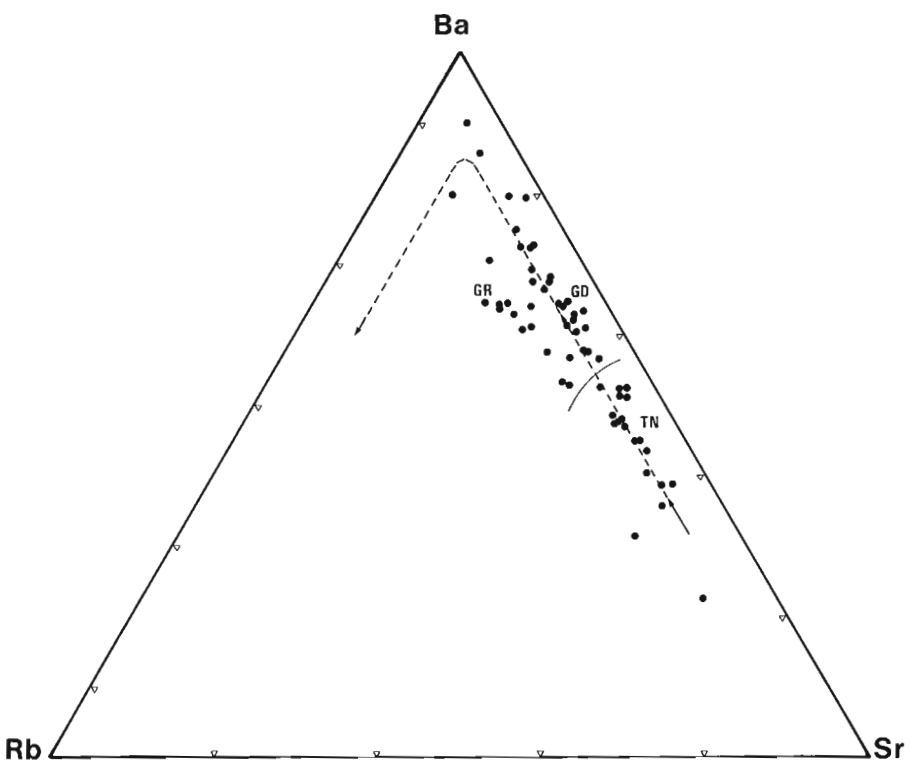

Figure 1.8

Suite des gneiss du domaine du lac Bienville dans le diagramme Ba-Rb-Sr utilisant la tendance de différenciation de El Bouseily et coll. (1975). On note une filiation entre les tonalites (TN) et les granodiorites (GD). Les granites (GR) se distinguent par une variation du taux de Rb.

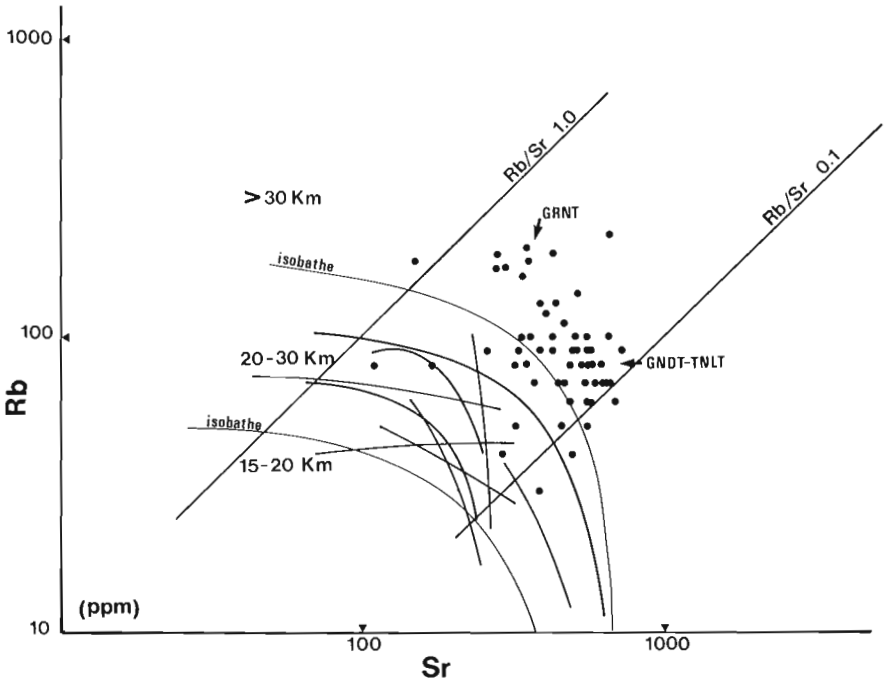

Figure 1.9

Diagramme Rb/Sr montrant un groupement des analyses de composition granodioritique et tonalitique avec une légère différenciation des compositions granitiques. Les traits courts correspondent aux séries volcaniques archéennes de Condie (1976), Rb/Sr=0,25.

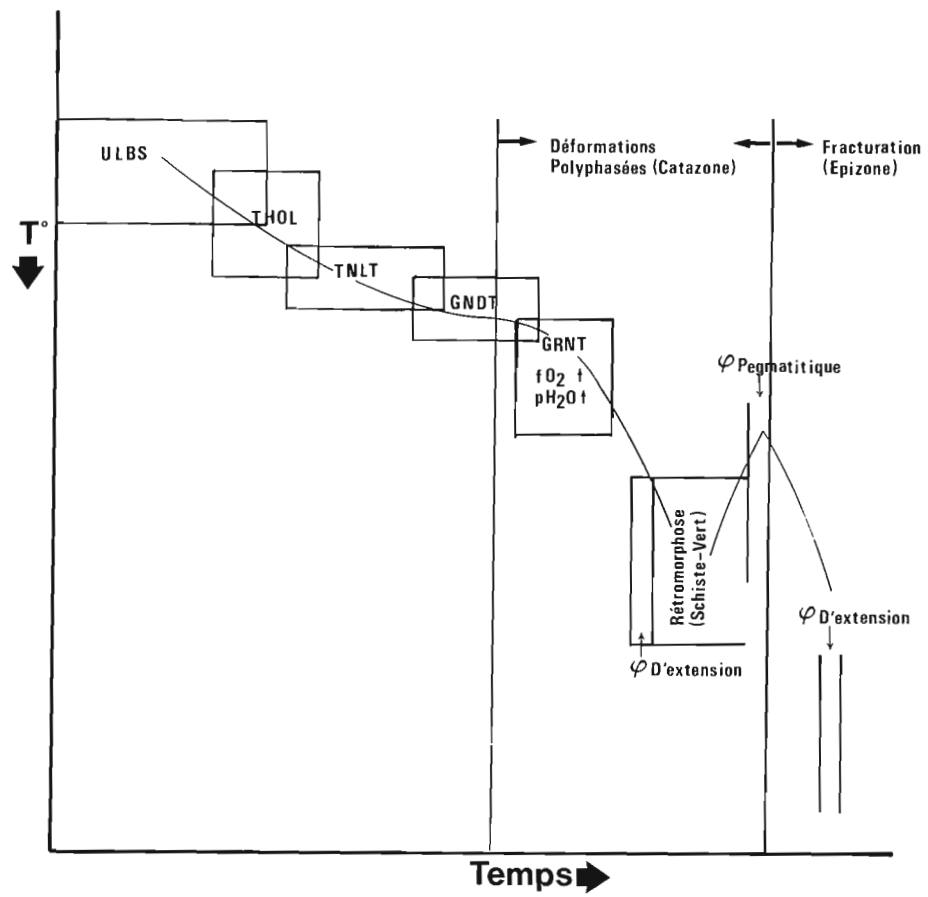

Figure 1.10

Diagramme en fonction de la température et du temps schématisant l'évolution des gneiss du domaine du lac Bienville, plus particulièrement la genèse des tonalites à partir de basaltes, celle des granodiorites à partir des tonalites, puis la genèse des granites par orthomigmatisation du <<mélange>> pendant la déformation. La ligne continue montre les changements présumés de la température dans le temps.

ULBS – Ultrabasites
THOL – Tholéiites

ceci à la faveur d'une grande fracture du socle dont le rôle exact demeure inconnu; il s'agit d'une fracture située à la limite des deux sous-provinces et qui se serait probablement produite à la faveur de la mise en place tardive des granodiorites à phénocristaux à la limite des deux sous-provinces. La différence verticale de remontée entre ces dernières peut être de l'ordre de 10 km et un mécanisme causal responsable, comme par exemple la <<sous-cratonisation>>, n'est pas apparent sur les cartes des anomalies gravimétriques dont on dispose. Il semble qu'une remontée du socle due à la création de matériel nouvellement différencié et exerçant des poussées verticales est plus conforme, encore que cette idée pose le problème de la cause d'une telle différenciation rajeunissant la base de la croûte ainsi que de sa nature exacte et de son âge.

Des travaux en cours permettront d'augmenter la réprésentativité des analyses chimiques des gneiss et des enclaves du domaine du lac Bienville et, probablement, de répondre aux problèmes que posent la nature des enclaves et leurs implications dans les modèles génétiques de façon à faciliter la modélisation d'une pétrogénèse comparative plus élaborée.

Remerciements

Ce travail a bénéficié des idées proposées par M. I. Ermanovics (CGC) lors de discussions, et d'une lecture critique de M. M. St-Onge (CGC).

Références

Barker, F.
1979: Trondjhemites: definition, environment and hypotheses of origin; dans Trondjhemites, Dacites and Related Rocks, ed. F. Barker, Elsevier, Amsterdam.

Barker, F., Arth, J.G., and Hudson, T.
1981: Tonalites in Crustal Evolution; Royal Society of London, Philosophical Transactions, v. 301, no. 1461, p. 293-303.

Chappel, B.W.
1978: Granitoids from the Moonbi District, New England Batholith, Eastern Australia; Journal of the Geological Society of Australia, v. 25, p. 267-283.

Ciesielski, A.
1983: Cartographie d'une partie de la sous-province archéenne d'Ungava à la hauteur de Poste-de-la-Baleine, Québec; dans Recherches en cours, partie B, Commission géologique du Canada, Étude 83-1B, p. 109-119.

1984: Géologie de la Grande Rivière (Chissassibi-LG-3), sous-province archéenne de la baie James, Québec (1/250 000); Commission géologique du Canada, Dossier public 979.

Collerson, K.D., Kerr, A., and Compston, W.
1981: Geochronology and evolution of late archaean gneisses in Northern Labrador: an example of reworked sialic crust; Geological Society of Australia, Special Publication no. 7.

Condie, K.C.
1976: Plate Tectonics and Crustal Evolution; (first edition) Pergamon Press.

Condie, K.C. and McCrink, T.P.
1982: Geochemistry of Proterozoic volcanic and granitic rocks from the Gold Hill-Wheeler Peak area, Northern Mexico; Precambrian Research, v. 19, p. 141-166.

Eade, K.E.
1966: Fort George River and Kaniapiskau River (west half) map-areas, New Quebec; Geological Survey of Canada, Memoir 339, 83 p.

El Bouseily, A.M. and El Sokkary, A.A.
1975: The Relation between Rb, Ba and Sr in Granitic Rocks; Geology, v. 16, p. 207-219.

Ermanovics, I.F., McRitchie, W.D., and Houston, W.N.
1979: Petrochemistry and tectonic setting of plutonic rocks of the Superior Province in Manitoba; dans Trondjhemites, Dacites and Related Rocks, F. Barker (ed.), Elsevier, Amsterdam.

Herd, R.K.
1978: Notes on metamorphism in New Québec; dans Metamorphism in the Canadian Shield, Geological Survey of Canada, Paper 78-10, p. 79-83.

Hine, R., Williams, I.S., Chappel, B.W., and White, A.J.R.
1978: Contrasts between I- and S-type granitoids of the Kosciusko Batholith; Journal of the Geological Society of Australia, v. 25, p. 219-234.

Marchand, P.
1981: Rapport géologique de synthèse, 1978 à 1980 pour la région Duncan LG-2. Baie James, Québec, SDBJ (Société de Développement de la Baie James.).

Martin, H., Chauvel, C., and Jahn, B.M.
1983: Major and trace element geochemistry and crustal evolution of Archaean granodioritic rocks from Eastern Finland; Precambrian Research 21, p. 159-180.

Mercier, E.
1981: Métavolcanites et métasédiments archéens du N E de la province du lac Supérieur (Bouclier canadien) Québec, Canada; Mémoire de D.E.A. inédit, Université des Sciences et Techniques de Lille, 59 p.

Mercier, E. et Ciesielski, A.
1983: Un reliquat de zone volcano-sédimentaire dans la sous-province archéenne d'Ungava, Québec; Recherches en cours, partie B, Commission géologique du Canada, Étude 83-1B, p. 165-175.

Pitcher, W.S.
1983: Granite type and tectonic environment; dans Mountain Building Processes, K. Hsu (ed.), Academic Press, London.

Schumacher, F. et Fouque, J.P.
1978: Carte géologique au 1/250 000 du Permis S.E.S., SERU Nucléaire, Eldorado Nucléaire, SDBJ (Société de Développement de la Baie James).

Sharma, K.N.M.
1977: Région de la Grande Rivière; ministère des Richesses naturelles du Québec, Rapport géologique 184.

Stevenson, I.M.
1968: A geological reconnaissance of Leaf River map-area, New Quebec and Northwest Territories; Geological Survey of Canada, Memoir 356, 112 p.

Tuthill-Helz, R.
1976: Phase relations of basalts in their melting ranges at PH_2O=5kb. Part II. Melt compositions; Journal of Petrology, v. 17, no. 2, p. 139-193.

Winkler, H.G.F., Boese, M., and Marcopoulos, T.
1975: Low temperature granitic melts; Neues Jahrbuch für Mineralogie, Monatshefte, H 6, p. 245-268.

2. COASTAL GEOMORPHOLOGY AND SEDIMENTS OF NEWFOUNDLAND

Project 810036

D.L. Forbes
Atlantic Geoscience Centre, Dartmouth

Forbes, D.L., Coastal geomorphology and sediments of Newfoundland; in Current Research, Part B, Geological Survey of Canada, Paper 84-1B, p. 11-24, 1984.

Abstract

Coastal surveys initiated in Newfoundland in 1981 have yielded a large data set for analysis of geomorphological features and sediments in the coastal zone. Mesotidal conditions, winter ice development, and seasonal storm-wave events are important controls on coastal development in the region. Other major factors influencing the evolution of the coast include bedrock lithology and structure, late Cenozoic glacial erosion and sedimentation, postglacial changes in relative sea level, paraglacial sediment supply, substrate control, and shorezone compartmentalization. Erosion of cliffs in glacial and proglacial deposits constitutes the major source of sediment to the coastal zone. Major coastal features on the island include rock outcrop, rock platforms, cliffs in rock and unconsolidated sediments, fiords, estuaries and associated tidal flats, lagoons, tidal inlet systems, barriers, beaches, and locally well-developed coastal dunes. Salt-marsh deposits are rare. Ice-related boulder cluster and barricade features occur at some sites. Storm surges, storm waves, and tsunamis represent significant hazards to development in the coastal zone.

Résumé

Des levés littoraux entrepris à Terre-Neuve en 1981 ont donné un vaste ensemble de données pour l'analyse des entités géomorphologiques et des sédiments dans la zone littorale. Les conditions mésotidales, la formation de la glace d'hiver et les phénomènes de vagues de tempêtes saisonnières constituent des régulateurs importants dans l'évolution régionale du relief littoral. Au nombre des autres grands facteurs susceptibles d'influer sur l'évolution du littoral, on considère la lithologie du socle et sa structure, l'érosion et la sédimentation glaciaire de la fin du Cénozoique, certains changements postglaciaires dans le niveau relatif de la mer, les apports en sédiments paraglaciaires, le contrôle du substratum ainsi que la compartimentalisation de la zone littorale. L'érosion des falaises dans les dépôts glaciaires et proglaciaires constitue la source principale des sédiments dans la zone littorale. Les principales formes de relief côtières dans l'île comprennent les affleurements rocheux, les plates-formes rocheuses, les falaises découpées dans la roche et les sédiments non consolidés, les fjords, les estuaires et les zones d'estran connexes, les lagunes, les réseaux de passes maréales, les barrières, les plages et les dunes littorales bien formées par endroits. Les dépôts de marais salins sont plutôt rares. Il arrive de rencontrer des amas et des barricades de gros blocs. Les ondes de tempête, les vagues de tempête et les tsunamis représentent des dangers importants pour la mise en valeur de la zone littorale.

Introduction

This report presents a general outline and some preliminary results of a coastal survey project initiated by the Atlantic Geoscience Centre (AGC) in 1981. Although AGC had carried out earlier coastal surveys in Labrador (McLaren, 1980; Reinson et al., 1979; Reinson and Rosen, 1982; Rosen, 1979, 1980), little work had been done on the island of Newfoundland. Brief descriptions of modern and relict coastal features had been provided by Flint (1940), Henderson (1972), Brookes (1974) and Grant (1980), among others; reconnaissance mapping of onshore coastal features on the northeast and southeast coasts had been undertaken by Environment Canada (Hiscock, 1981; Hiscock and Maloney, 1983); and brief descriptions of selected beaches used or contemplated as sources of aggregate had been obtained by the provincial government (e.g. McKillop, 1955; Northcott, 1963). The present project was designed to complement these efforts by completing reconnaissance-level classification of physical shore-zone characteristics for the entire island, by establishing a network of sites representing the full spectrum of coastal environments for detailed surveys of geomorphology, sedimentology, and stability through time, and by extending surveys in selected areas onto the shoreface and inner shelf to develop an understanding of the coastal zone as a complete system.

Data collection

The project has made extensive use of existing airphoto and bathymetric information. New data were acquired in the course of five road tours, an extensive helicopter reconnaissance, and **CSS Dawson** cruise 83-014. In addition to work carried out from **CSS Dawson**, nearshore surveys were undertaken using inflatable boats and a small chartered fishing vessel.

Results of the helicopter survey include low-level 35 mm oblique colour photography of the shorezone from Trinity Bay around the Avalon Peninsula and west along the south coast to 58°40'W (Fig. 2.1). Ship and boat data include bathymetric, sidescan, and seismic surveys, and bottom-grab, piston-core, and vibracore sampling in selected basin and shoreface locations. In addition, detailed studies (including surveyed shore profiles and sediment sampling) have been undertaken at 79 representative sites (Fig. 2.2, 2.3). Of these, 54 are monumented for resurvey, 23 have been resurveyed one or more times (some sites as many as four times) to investigate coastal stability, storm response, and seasonal variability, and 23 include multiple survey lines for assessment of alongshore variability. The site network covers a wide variety of nearshore, beach, barrier, lagoon, estuarine, tidal flat, and cliff locations.

Nevertheless, there remain some significant gaps in our survey coverage, notably along the east coast of the Northern Peninsula and in the Strait of Belle Isle; and coverage of inner-shelf and nearshore parts of the coastal zone is very limited. It is still too early in the project to undertake a complete synthesis for the entire island. Instead, what is offered here is a brief summary of coastal features in Newfoundland, with examples of detailed data obtained at a few sites.

Geological and oceanographic setting

The development and present configuration of the coast are strongly affected by several environmental and paleo-environmental factors. These include bedrock lithology and tectonics, effects of glaciation (including glacial erosion; glacial, proglacial, and paraglacial sedimentation; and post-glacial changes in relative sea level), and characteristics of the modern oceanographic environment (including tidal range, wave regime, and ice conditions).

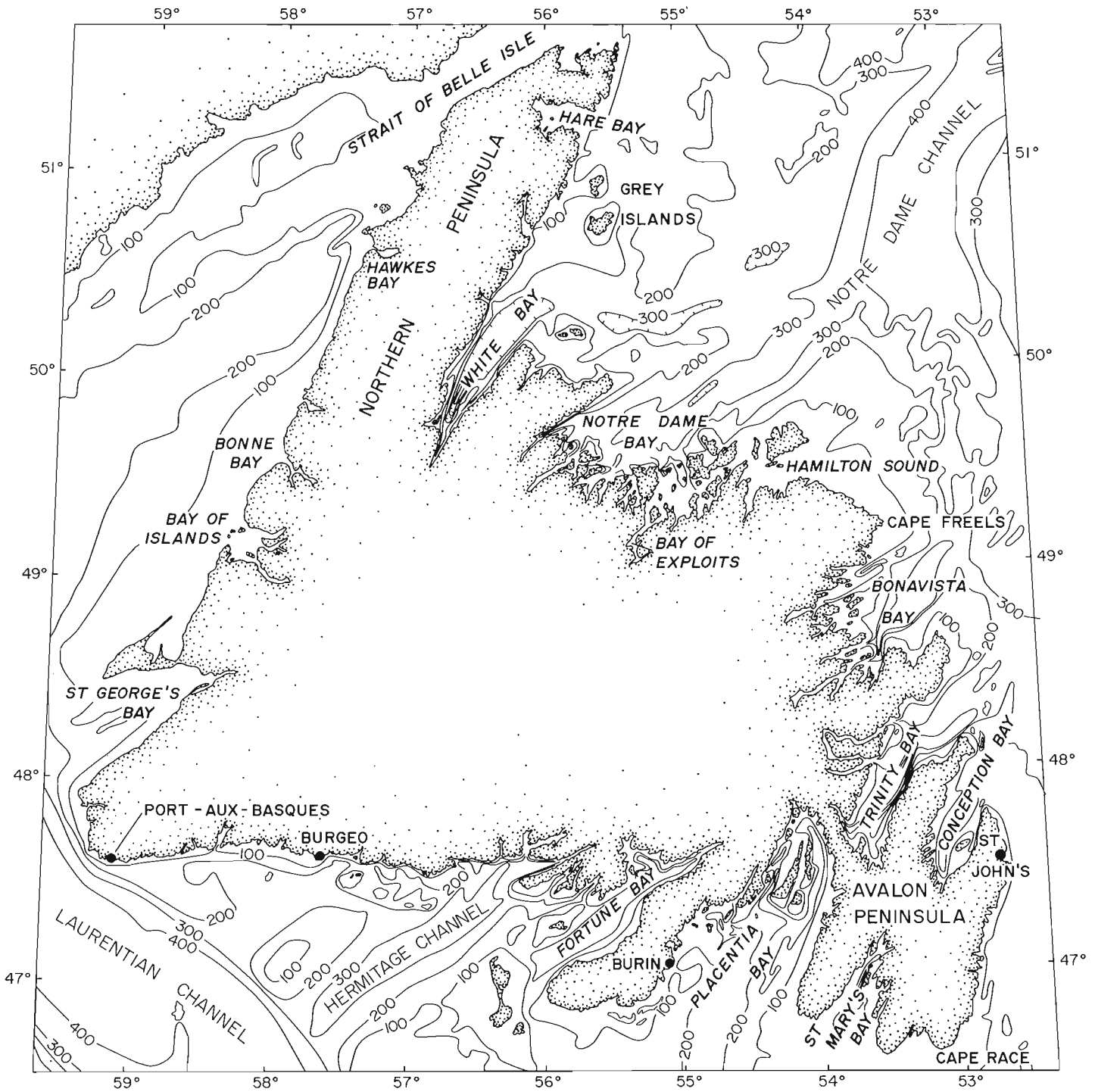

Figure 2.1. *Major geographical features, Newfoundland, and locations referred to in the text.*

Newfoundland forms the northernmost segment of the Canadian Appalachians. Of five major zones recognized in the Appalachian orogen (Williams, 1979), four (Humber, Dunnage, Gander, and Avalon) are represented in Newfoundland. Major rock types (Williams, 1979, fig. 1) include: (1) crystalline basement rocks, clastic sediments and volcanics, an extensive carbonate sequence, and easterly-derived sediments and ophiolites in the Humber Zone (west coast, Northern Peninsula, White Bay); (2) marine volcanics and sediments overlying oceanic crust in the Dunnage Zone (Notre Dame Bay to Hamilton Sound); (3) sialic basement, metamorphosed cover rocks, and clastic sediments in the Gander Zone (south coast and northeast coast between Hamilton Sound and Bonavista Bay); (4) essentially unmetamorphosed clastic sediments and volcanics, with minor carbonate in the Avalon Zone (east of a line from Hermitage Channel to northern Bonavista Bay); and (5) a number of large intrusions of granitic to dioritic and gabbroic rocks (Stockwell et al., 1968; Williams, 1979). The most extensive exposures of intrusive rocks at the modern coast occur between Bonavista Bay and Hamilton Sound and on the central south coast. Major faults (Stockwell et al., 1968)

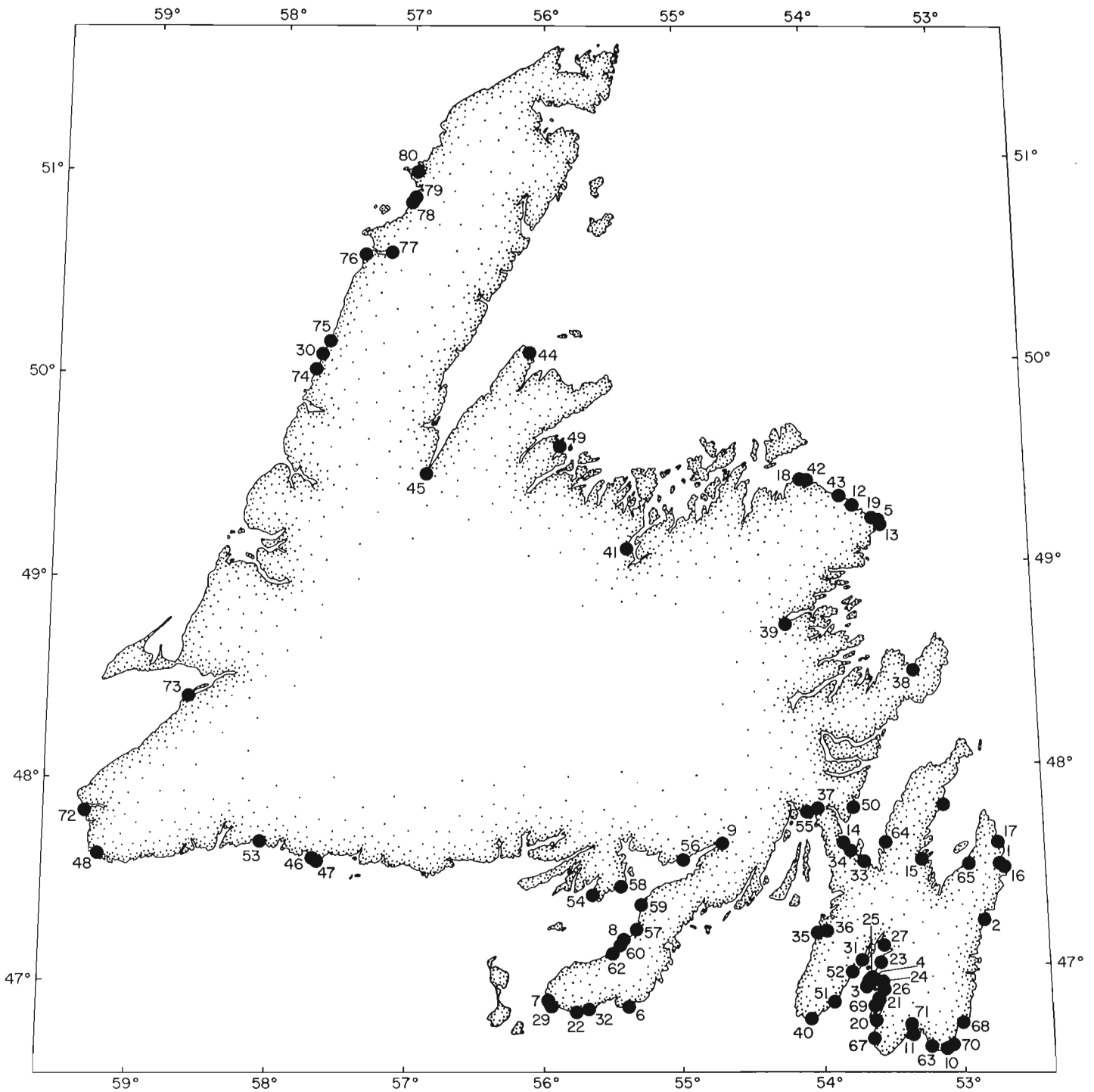

Figure 2.2. *Locations of detailed study sites established on the Newfoundland coast.*

control the alignment of the coast on the west side of White Bay and north along the east coast of the Northern Peninsula, in western Notre Dame Bay, and in Placentia, Trinity, Conception, and St. Mary's bays.

Late Cenozoic glaciation has exerted a major influence on the development of the Newfoundland coast. Although the stratigraphy and distribution of glacial deposits on the island have received considerable attention over the years (see reviews by Grant, 1977; Brookes, 1982), the limits of late Wisconsinan glaciation remain controversial. Marine geological data suggest extensive mid and early late Wisconsinan glaciation of the shelf (Fader et al., 1980; Mudie and Guibault, 1982; G.B. Fader and D.J.W. Piper, personal communications, 1984); onshore data indicate much more restricted later late Wisconsinan limits (Grant, 1977; Tucker and McCann, 1980). The glacial legacy to the coast is clearly visible in the widespread development of fiords, including overdeepening of major bays and shelf channels, the extensive occurrence of tills and outwash deposits that constitute the major sources of sediment to coastal systems, and the ongoing Holocene marine transgression.

Postglacial changes in relative sea level are less well documented in Newfoundland than in many other parts of the country. Published data for the northwest coast and St. George's Bay were summarized by Quinlan and Beaumont (1981): these reveal, in the Strait of Belle Isle area, a pattern of continuously falling relative sea level from about 12 ka BP, with some evidence of a stillstand or minor resubmergence at the present time (D.R. Grant, personal communication, 1983); and, in the St. George's Bay area, a period of initial drop in relative sea level followed by an inferred stillstand and renewed transgression since ca 6 ka BP. Quinlan and Beaumont (1982) have sketched four zones of idealized relative sea level history related to northwestward migration of an ice-marginal lithospheric forebulge: these range from a pattern of falling relative sea level throughout postglacial time in the northwest, through various patterns of initial uplift and falling relative sea level followed by marine transgression in intermediate zones, to a history of continuously rising relative sea level in the southeast. The distribution of these zones in Newfoundland remains conjectural but they nevertheless provide a useful conceptual model for interpretation of coastal development.

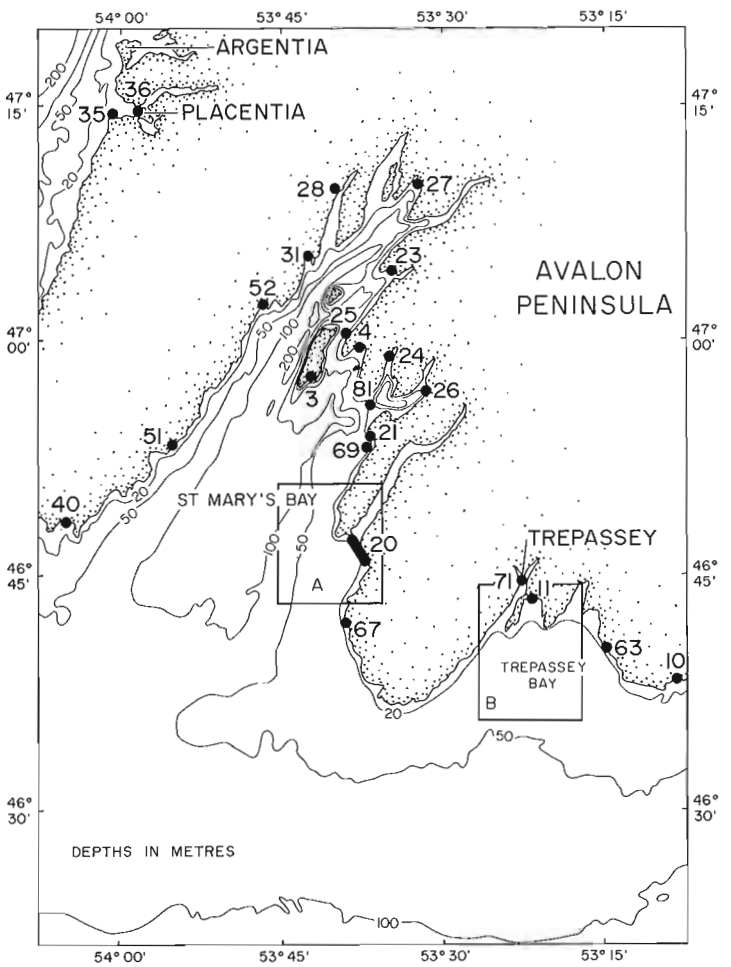

Figure 2.3. *Map of St. Mary's Bay and Trepassey Bay, showing locations of detailed study sites in this part of the southern Avalon Peninsula, overdeepened basin in St. Mary's Bay with depths in excess of 200 m, silled basins in St. Mary's Harbour (site 81) and Holyrood Pond (site 20), and locations of Figures 2.5A (box A) and 2.9 (box B).*

Historical tide data provide information on recent trends in relative sea level. Records on file with Marine Environmental Data Service (Fisheries and Oceans Canada) date back to the mid-1930s at two sites, Port-aux-Basques and St. John's. Data for the period of substantially continuous records at St. John's (1957-1983) reveal no statistically significant trend; however, mean sea level appears to have risen by roughly 0.1 m between 1936 and the mid-1950s. At Port-aux-Basques, on the southwest coast, the tidal data show a consistent rising trend over the past 50 years, with a statistically significant mean rate of +5.5 ± 0.2 mm/a for the interval 1959-1981. The tidal trends corroborate geological evidence of contemporary submergence throughout the island.

The range of large tides around the coast of Newfoundland varies from 0.7 to 2.7 m (Canadian Hydrographic Service, Tide and Current Tables). Coastal dynamics are dominated by local storm waves generated by extra-tropical cyclonic disturbances in late autumn and winter. Occasional severe storms may occur in any season, including very rare penetration of tropical storms to the Newfoundland coast during the late summer hurricane season. The 1-, 10-, and 100-year significant wave heights in deep water off the east coast of Newfoundland are approximately 8, 11, and 15 m, respectively (Neu, 1982). Annual wave heights of 5 to 7 m have been estimated for sites on the west coast of the island (Woodward-Clyde Consultants and Western Canada Hydraulic Laboratories Ltd, 1982). The wave regime at the coast is highly variable, due not only to long-term fluctuations in sea state (Neu, 1982), but also to varying exposure and variable rates of energy dissipation on the shoreface. Fetch limitation by sea ice is another important control, and this too shows strong year-to-year variability. Landfast ice develops in sheltered embayments and has a mean duration of up to 14 weeks at some sites (Hiscock and Maloney, 1983). On the Atlantic coast, the drift ice season ranges from an average of 17 weeks (15 years out of 15) off the Strait of Belle Isle in the north to about 2 to 3 weeks (10 years out of 15) in Trinity Bay (Hiscock and Maloney, 1983). In the Gulf of St. Lawrence, heavy ice may be present along the southern west coast for an average of 12 weeks of the year (Markham, 1980). On the south coast, Gulf ice penetrates east from Port-aux-Basques and occasional east-coast ice moves south around Cape Race, especially late in the season.

Coastal development in Newfoundland

Much of the coast of Newfoundland presents high cliffs to the waters of the North Atlantic. Yet there is a wide range of coastal features to be found on the island. The most important of these are listed in Table 2.1, where they are classified into groups of predominantly erosional, depositional, and ice-related features.

Table 2.1. Coastal features in Newfoundland

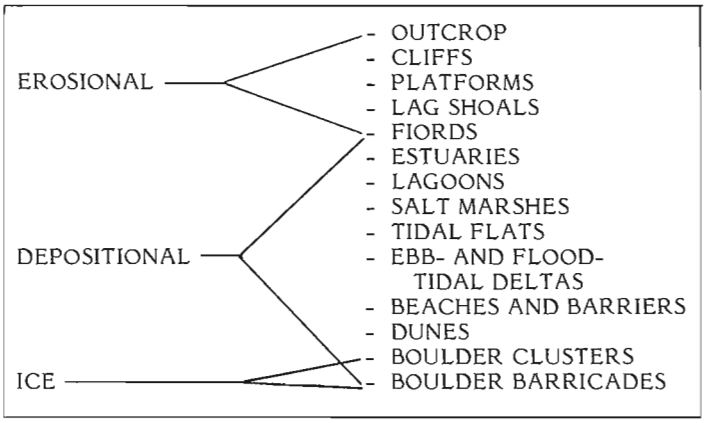

Erosional features

Most sections of the coast are sediment-starved, except where abundant glacial deposits provide local sources. In such areas, erosional features including cliffs and lag shoals may be developed in tills or outwash gravels. On the other hand, a high proportion of the total length of coastline on the island is formed in rock. The character of rocky shoreline depends to a large extent on local topographic relief, but also in part on the rock type and on the degree of exposure of the shore.

In some exposed coastal areas, marine transgression across low-relief terrain with thin or discontinuous unconsolidated cover has produced a distinctive wave-washed rock or skerry topography. Examples occur on the south coast east of Port-aux-Basques and on the northeast coast near Cape Freels. In the latter area, small coves bounded by low peat cliffs, wave-washed granite outcrop, and isolated glacial erratics, dominate the shore zone for some distance south of the cape.

In areas of higher relief, various outcrop, ramp, and cliff forms ocur, sometimes in association with a modern or relict rock platform at the base (Fig. 2.4A). The detailed morphology of rock-controlled shore segments such as this is largely determined by bedrock lithology and structure. Exhumed bedding planes in sedimentary strata may form large sloping ramps with intervening vertical cliffs (Fig. 2.4B). Exposures of vertically dipping beds yield quite a different cliff morphology (Fig. 2.4C). Where intrusive rocks occur at the coast in areas of high relief, as along parts of the south coast, smooth curvilinear cliff forms are common, both on fiord walls (Fig. 2.4D) and on the open coast. Cliff heights up to 300 m or more occur along the south coast and heights in excess of 250 m are found elsewhere: e.g. on the northeast shore of Conception Bay (Henderson, 1972) and on the west side of White Bay.

Erosional shore platforms are common in many parts of the island. These include both actively developing rock platforms and relict examples dating from various episodes in late Cenozoic time, the most widely recognized being a well-developed feature attributed to the Sangamon interglacial (Henderson, 1972; Grant, 1980; Tucker et al., 1982). The morphology of the platforms is strongly affected by rock type and structure, including angle of dip, and by elapsed time since initiation of platform development (Fig. 2.4A, E). The presence of wide platforms in both exposed and sheltered locations (as on the open-Atlantic coast near Cape Race and conversely near the head of St. Mary's Bay) suggests that both frost-shattering and wave erosion may be important processes of platform genesis in the Newfoundland coastal environment (cf. Guilcher, 1954, 1981; Trenhaile, 1983).

Prominent coastal cliffs up to 45 m high occur in glacial and proglacial deposits. Examples include parts of the shores of St. George's Bay (MacClintock and Twenhofel, 1940; Brookes, 1974), sites on the south side of Fortune Bay (Tucker and McCann, 1980), and cliffs in Holyrood Bay (site 20) on the east side of St. Mary's Bay (Rogerson and Tucker, 1972; Eyles and Slatt, 1977). Measurements taken from a line of markers established along the cliff top south of Holyrood Pond (Fig. 2.4F, 2.5) indicate a mean recession of 0.3 ± 0.1 m/a over a 20-month interval (1982-08-23 – 1984-04-18). The cliffs at this site are up to 25 m high. Assuming parallel retreat of the cliff face, these limited data suggest a potential sediment contribution of the order of 10^3-10^4 m^3/a. Some of the largest coastal depositional systems (see below) occur adjacent to large cliff sources such as this.

Depositional features

Despite their origin as erosional products, fiords play an important role in the coastal system as basins for accumulation of fine grained sediments. Spectacular fiords are common on the west coast, the south coast (Fig. 2.4D), in Bonavista Bay, Trinity Bay, and Placentia Bay; less prominent examples occur on the northeast coast and in St. Mary's Bay, where deposits in the silled basins of St. Mary's Harbour (site 81, Fig. 2.3) and Holyrood Pond (site 20, Fig. 2.3, 2.4F, 2.5) have been investigated under this project. In addition, most of the major Newfoundland bays were overdeepened by late Cenozoic glacier ice and can be considered fiords in the broad sense (cf. Piper et al., 1983); and the major channels on the south and northeast Newfoundland shelves, including Laurentian, Hermitage, and Notre Dame Channels, were modified in the same way (Fader et al., 1980).

Estuaries occur at river-mouth locations, often in fiords or river valleys flooded by rising relative sea level during Holocene time. They serve as partial traps for fluvial sediment discharged to the coast. In Newfoundland, the largest rivers are the Exploits, Humber, and Gander, which drain respectively to the Bay of Exploits, Bay of Islands, and Gander Bay in Hamilton Sound. Both the Humber and the Gander have significant lake storage. Other estuaries of note occur, for example, at the heads of St. George's, Fortune, Placentia, and White bays. The large fiord-estuary at Placentia (site 36) and three small river-mouth systems on the west coast have been described in studies commissioned by Small Craft Harbours Directorate (Woodward-Clyde Consultants, 1982; Woodward-Clyde Consultants and Western Canada Hydraulic Laboratories Ltd, 1982). As part of the present project, tidal-flat surveys have been carried out in estuaries at Hawkes Bay (site 77, Fig. 2.6A) and at Come-by-Chance (site 37, Fig. 2.6B, C, D). Salt-marsh facies rarely form large components of estuarine systems in Newfoundland.

Lagoons and tidal inlets occur in association with barrier beach systems. The Newfoundland coast exhibits a wide variety of such systems (Fig. 2.4F, 2.6 E, F, 2.7, 2.8). Some barriers have quasi-permanent tidal inlets draining the back-barrier lagoon; some have intermittent inlets that open during major runoff events (or are opened artificially) but cannot be maintained against the transport of sediment by waves; and others have no tidal inlets at all. Factors controlling the development and stability of tidal inlets in gravels may be somewhat different from those operating in sandy systems: in the Newfoundland context, the ratio of freshwater runoff to lagoon storage volume and the permeability of gravel barriers may be important controls. Although well-developed tidal inlet systems with large ebb- and flood-tidal deltas are not common in Newfoundland, extensive coalesced flood-delta deposits occur in lagoons

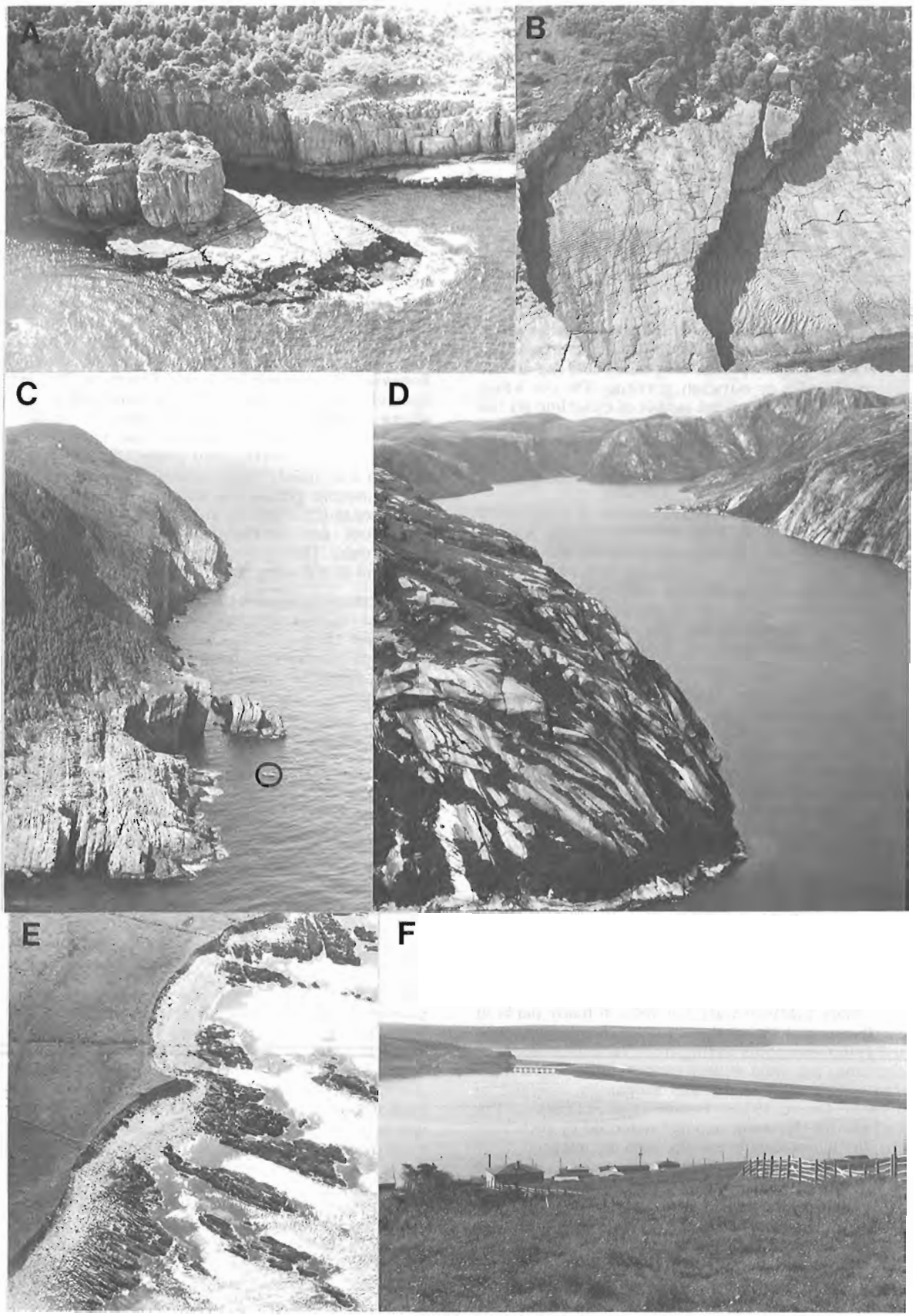
A
B
C
D
E
F

Figure 2.4

A: Cliff and relict shore platform in late Precambrian clastic sedimentary rock at Long Point, on east coast of Avalon Peninsula south of St. John's, 1981-08-01 (FZ8417);

B: Steeply sloping ramps developed on exhumed bedding planes of late Precambrian clastic sequence at Cape Ballard, north of site 68, east coast of Avalon Peninsula, 1981-08-01 (FZ8215);

C: Boat working cod-trap off cliffs developed in vertically-dipping late Precambrian clastics at Cape Broyle, east coast of Avalon Peninsula midway between sites 2 and 68, 1981-08-01 (FZ8308);

D: Fiord-wall cliffs in Devonian granite, La Hune Bay, south coast east of Burgeo, 1981-08-09 (FZ2825);

E: Low till cliffs, thin gravel beach wedge, and intertidal platform developed on steeply-dipping late Precambrian clastics at Coldeast Point, east coast of Avalon Peninsula south of Cape Broyle (Fig. 2.4C), 1981-08-01 (FZ8300);

F: View seaward across Holyrood Pond (site 20), St. Mary's Bay, showing gravel barrier, tidal inlet (at bridge), and cliffs cut in Wisconsinan till and glaciofluvial deposits (beyond bridge).

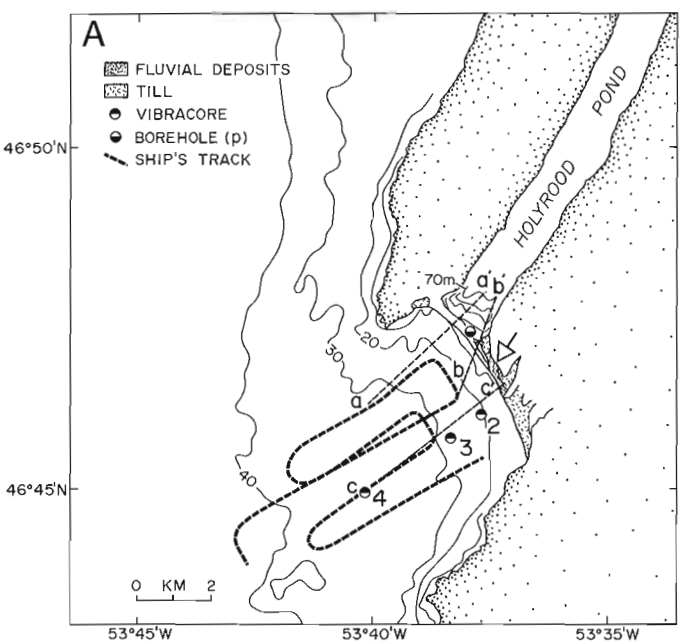

Figure 2.5A. *Map of Holyrood Bay and Pond (site 20), showing distribution of Wisconsinan till and glaciofluvial deposits (after Rogerson and Tucker, 1972), ship's track (**CSS Dawson** 83-014; bathymetry, sidescan, and seismic profiling), locations of vibracores obtained from **CSS Dawson**, of borehole (Geocon, 1965), and of profile sections plotted in Figure 2.5B; arrow indicates location of cliff recession measurements in the area of glaciofluvial deposits south of Holyrood Pond.*

along the southeast coast of Fortune Bay (in the vicinity of site 62, Fig. 2.7A) and at a few other locations (e.g. site 26, Fig. 2.3) and significant ebb-tidal deltas occur in some sheltered embayments (e.g. site 24, Fig. 2.7B).

In addition to the barrier deposits, which vary greatly in volume, width, and crest elevation (Fig. 2.8), beaches also occur as bayhead or pocket accumulations, as cliff-base wedges, or as thin transgressive units on a rock substrate. The spectrum of beach sediments ranges from muddy angular gravels bordering sheltered waters such as the Bay of Exploits (site 41), through the clean sands of beaches such as Big Barachois (site 48, Fig. 2.6E) or Cape Cove, Cape Freels (site 13), to the well-rounded cobbles and boulders of Freshwater Bay barrier near St. John's (site 1, Fig. 2.6F) or the upper-foreshore boulders of an unnamed west-coast beach (site 30). Beachface sediment samples analyzed to date show a range of mean grain size from 0.14 mm (2.8 phi) at site 77 to 290 mm (-8.2 phi) at site 30.

Beach storage volumes reflect a number of factors that control the sediment budget and geomorphological evolution of beach systems. These include changes in relative sea level, incident wave energy, compartmentalization, sediment supply, and substrate control. On many parts of the Newfoundland coast, mobile sediments form very thin veneers on the shoreface and beaches are fed primarily from coastal cliff sources. Rocky headlands restrict longshore transport of sand and gravel, breaking the coastal sediment system into small isolated compartments. Beach development under these conditions is strongly dependent on local sediment supply within the compartment.

At Holyrood Bay (site 20), seismic and vibracore data reveal thin sand and gravel cover over till in depths of 20 to 40 m (Fig. 2.5). Borehole data obtained onshore (Geocon Ltd., 1965) show that the barrier itself rests on till over rock forming the sill of Holyrood Pond fiord (Fig. 2.4F, 2.5). The high rate of sediment supply from cliff sources south of the pond (see above) has contributed to the large volume of sediment in the beach at this site (Fig. 2.8), helping to maintain the barrier (which supports an important road link)

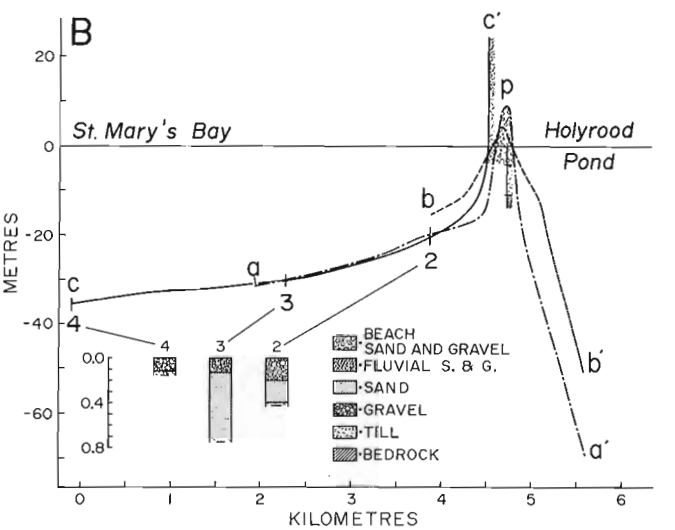

Figure 2.5B. *Profiles along three lines plotted in Figure 2.5A, showing vibracore and borehole stratigraphy; note position of barrier on fiord sill, sediment source in cliffs, and thin sand and gravel over till on the shoreface.*

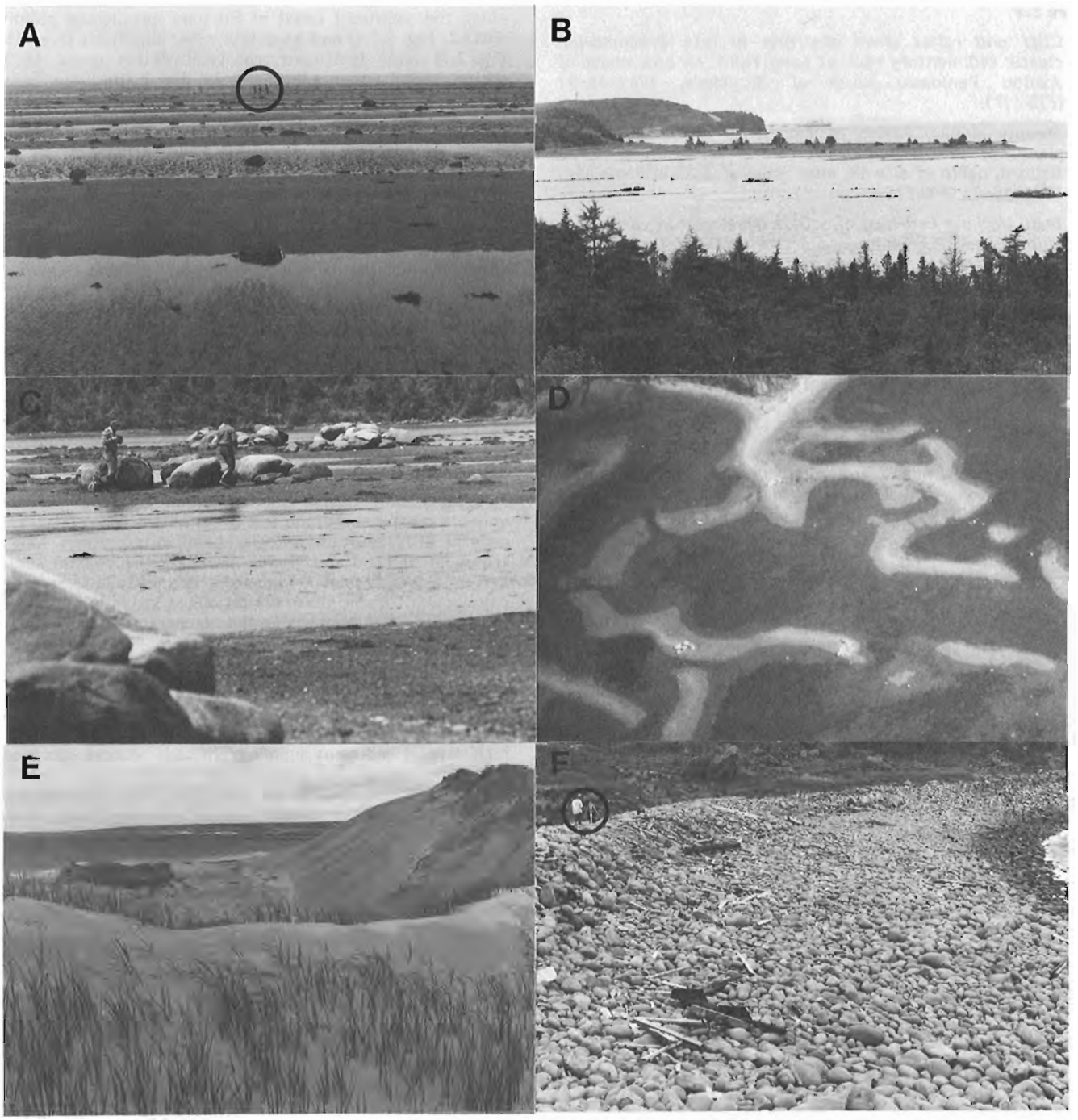

Figure 2.6

A: View seaward across multiple-bar system developed in sands on cobble- and boulder-strewn tidal flat at Hawkes Bay (site 77), 1982-09-06; note figures in distance for scale;

B: View seaward across Come-by-Chance estuary, showing boulder clusters on partly-submerged tidal flat, with barrier beyond and refinery dock in far distance, 1983-06-24;

C: Close-up view of boulder clusters on Come-by-Chance tidal flat at low tide, 1983-06-24;

D: Oblique airphoto of Come-by-Chance tidal flat, showing boulder clusters on crests of low muddy-gravel ridges, low tide, 1981-08-02 (FZ2221);

E: Sandy foreshore and dunes at Big Barachois (site 48), 1983-07-03;

F: Well-rounded cobbles and boulders forming barrier at Freshwater Bay (site 1), east coast of Avalon Peninsula south of St. John's, 1983-06-22; note figure and tripod for scale.

in the face of continued washover transport of sediment into the deep basin landward of the sill. In contrast, the shingle barrier in Mutton Bay (site 11, Fig. 2.3, 2.9) lies within a small compartment with very limited sediment supply. Anecdotal and airphoto data suggest that this barrier has migrated landward at least 50 m over the past 50 years; in this case, washover transport exceeds the supply of new material to the beachface. The shoreface is characterized by a thin gravel lag over till, except in the inner part of the bay where thin patches of sand occur. The quantity of sedimnt stored in this barrier is a small fraction of the volume at Holyrood Pond (Fig. 2.8).

Prograded beach systems are rare in Newfoundland, reflecting the scarcity of sediment and the history of marine transgression. Major prograded deposits deserving further attention have been recognized at Doting Cove (site 43), at Frenchman's Cove (site 8), and at Placentia (site 36). Multiple beach ridges, recording Holocene progradation, also occur at several sites in St. Mary's Bay (4, 23, 27) and at Come-by-Chance (site 37, Fig. 2.10).

Wind-blown coastal dunes are absent or poorly developed on most parts of the Newfoundland coast, largely because of the limited quantities of sand available in the beaches. The well-developed dune ridge forming the barrier crest at site 52 on the western shore of St. Mary's Bay is an unusual feature for the area. Well-developed dunes occur at Bellevue Beach, Trinity Bay (site 34), and on the northeast coast (sites 12 and 13). However, the largest dune systems observed on the island are on the west coast, where crest elevations up to 12 m above mean sea level have been surveyed at Big Barachois north of Port-aux-Basques (site 48, Fig. 2.6E) and up to 16 m at Portland Creek (site 75).

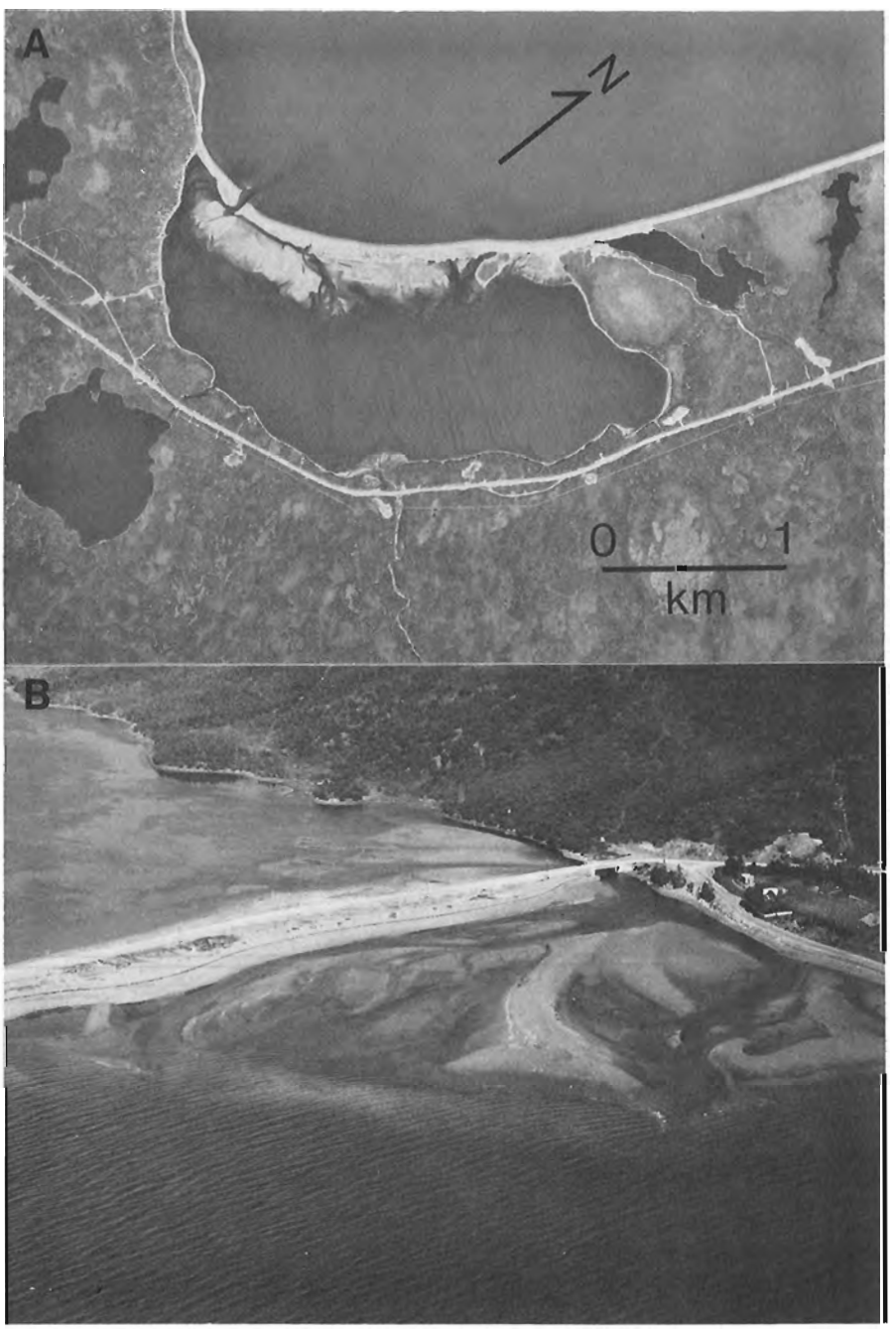

Figure 2.7

A: Sand-gravel barrier with extensive coalesced flood-tidal delta deposits in lagoon at Grand Beach (site 62) on the Burin Peninsula coast, southern Fortune Bay (part of photo no. NFA24563-124, Newfoundland and Labrador Department of Forest Resources and Lands, 1976-07-23);

B: Sandy-gravel barrier deposit with flood-tidal delta in lagoon (background) and large ebb-tidal delta (foreground), Mall Bay (site 24), 1981-08-01 (FZ0521).

Ice-related features

Boulder-strewn tidal flats and boulder barricades are common features in many areas of the eastern Canadian seaboard (see Rosen, 1979; Guilcher, 1981; McCann et al., 1981; and other reports cited by Drake and McCann, 1982), although Newfoundland examples have not been described previously in the literature. Three sites surveyed under the present project (37, 39, and 77, Fig. 2.2) were characterized by large concentrations of boulders in the intertidal zone.

At site 77 in Hawkes Bay (Fig. 2.6A), boulders and cobbles are randomly distributed over a wide intertidal surface dominated by a wave-formed multiple bar system in the sands. Although winter ice may effect some redistribution of the larger clasts, no organized accumulations of cobbles or boulders occur. In contrast, well-formed boulder barricades are a prominent feature of the shore-zone in the upper reaches of Freshwater Bay near Gambo (site 39) and large boulder clusters dominate the tidal flats of the Come-by-Chance estuary (site 37).

The boulder barricades at Gambo have widths in the order of 5 m and mean relief of 0.5 to 1 m, incorporate boulders of b-axis dimension 1.5 m or more, and front bouldery tidal flats up to 200 m wide. These and comparable features in the St. Lawrence Estuary near Rimouski (Guilcher, 1981) are among the most southerly well-developed barricades described in eastern North America.

Boulder deposits of a different kind occur on intertidal flats in the Come-by-Chance estuary (Fig. 2.6B, C, D). There are five major boulder clusters, each consisting of about 10 to 30 boulders; the largest clasts have b-axis dimensions exceeding 1.3 m. The survey transect in Figure 2.10 passes through one such cluster. The clusters lie on the crests of low mud-sand-pebble ridges that form a crude polygonal network on the flats. Some of the boulders are partially embedded in the muddy-gravel substrate. Boulder clusters on tidal flats in Frobisher Bay (Baffin Island) have been described by McCann et al. (1981), who suggested that ice grounding on large boulders and overturning or pushing by ice may be important processes in their formation. However, the extreme concentration of large clasts in a small number of clusters, as observed at Come-by-Chance, is not a feature of the Frobisher flats. Ice transport of boulders is believed to be important in the Come-by-Chance estuary, but the detailed mechanism responsible for the concentration of large clasts at a small number of point locations on the ridge crests remains to be established and is a focus of continuing research.

Coastal hazards

Hazards to development in the Newfoundland coastal zone include rapid cliff recession (see above), storm waves, storm surges, and earthquake-generated tsunamis.

High waves superimposed on very high tides in December 1983 were reported (Canadian Press, 1983) to have washed beach rocks onto a highway north of St. John's, to have flooded the waterfront apron in St. John's Harbour, and to have caused extensive flooding in Placentia (site 36). Another storm in early January 1982 generated a surge 0.57 m above predicted high water at Argentia (Fig. 2.3), 1.3 m at Lamaline (site 22, Fig. 2.2) and 1.3 m in Trepassey Harbour (site 71, Fig. 2.3). Flooding associated with this surge is reported to have caused $750 000 damage in Placentia (Canadian Press, 1983).

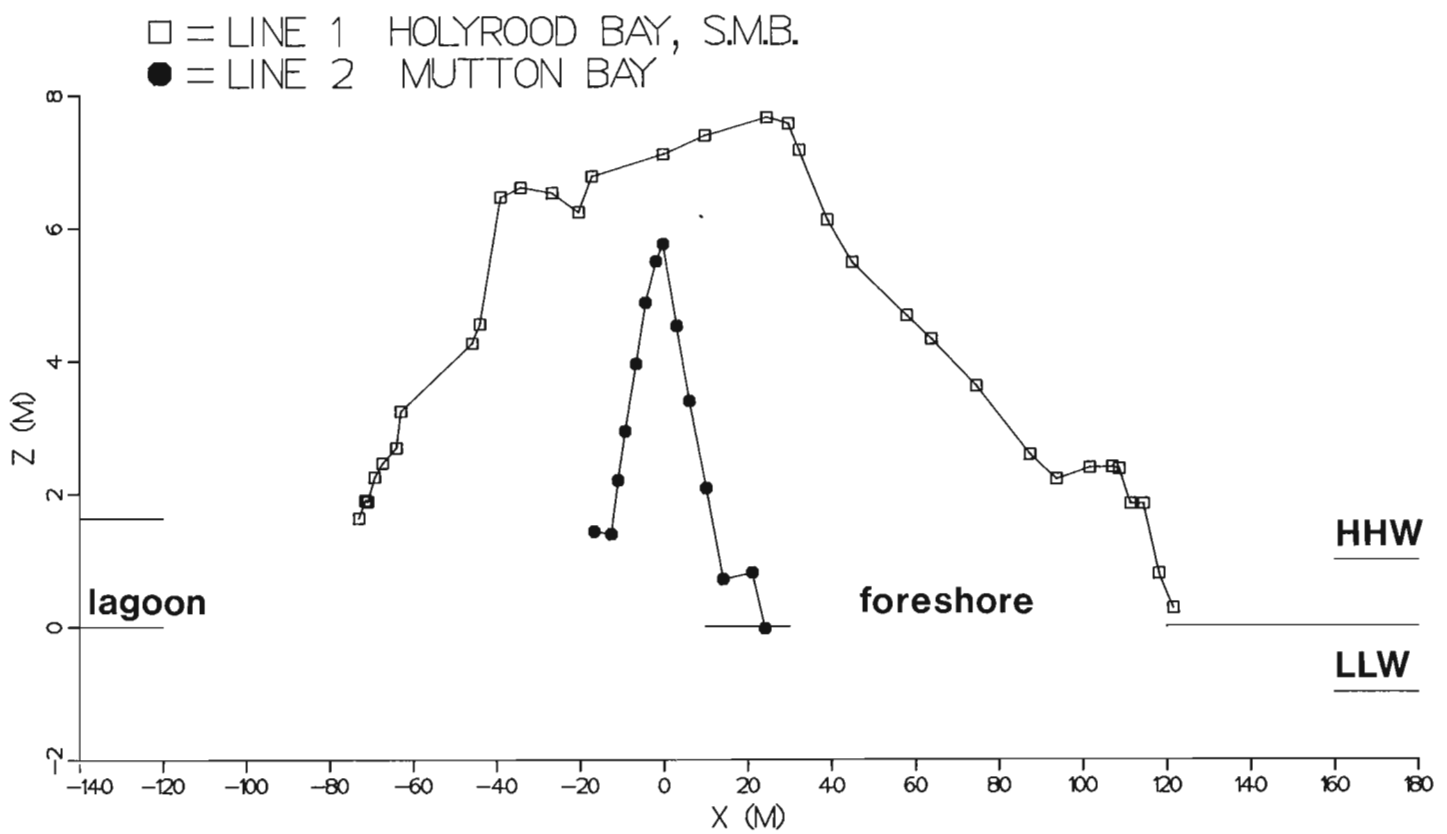

Figure 2.8. *Surveyed profiles across gravel barriers at Holyrood Pond (site 20, Fig. 2.5A, on line a-a') and Mutton Bay (site 11, Fig. 2.9), showing contrast in sediment storage volume, barrier width and crest elevation; three horizontal lines at right indicate mean sea level, higher high water (HHW) and lower low water (LLW) at large tides.*

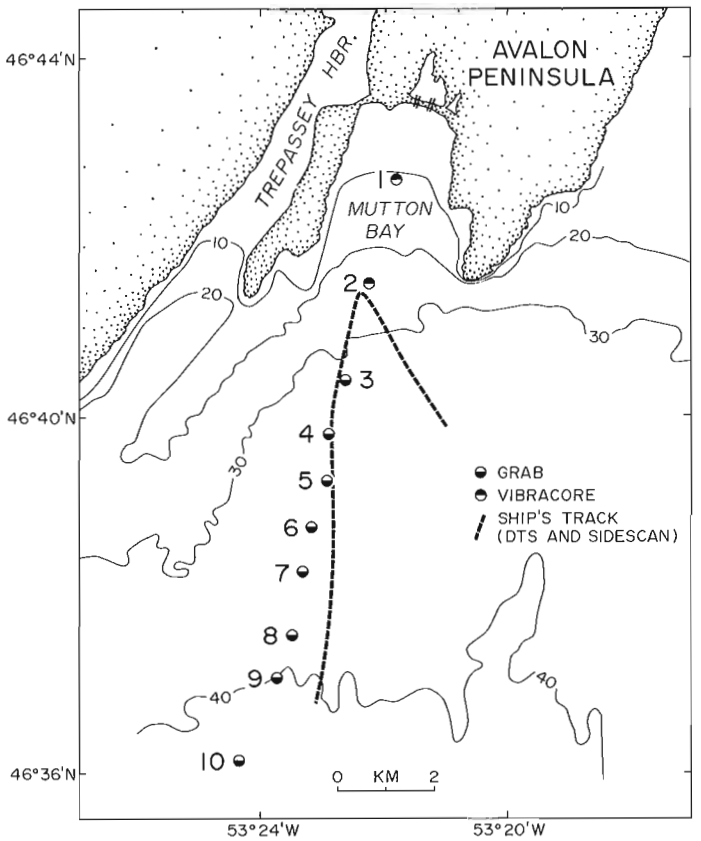

Figure 2.9. *Map of Mutton Bay, Trepassey Bay (site 11), showing ship's track (**CSS Dawson** 83-014; bathymetric, sidescan, and seismic [Huntec DTS] profiling), and locations of vibracores and grab samples; bottom sediments are thin lag gravels over till or rock, except in the inner bay (station 1), where some thin patchy sand occurs; short lines across barrier indicate locations of surveyed profiles.*

The Canadian Forces METOC wave chart for the January 1982 storm (1982-01-10; 1200 GMT) shows significant wave heights exceeding 6 m superimposed on the storm surge in Trepassey Bay and outer St. Mary's Bay. Wave overtopping and erosion of the barrier crest at Holyrood Pond (site 20, Fig. 2.5, 2.8), at levels over 6 m above higher high water large tide (HHWLT), took out the road and caused substantial washover transport of sediment into Holyrood Pond: local residents reported that it was the worst storm in approximately 30 years. At Mutton Bay (site 11, Fig. 2.8, 2.9), a washover channel 0.5 m deep was cut across the coarse-shingle barrier crest at 4.5 m above HHWLT; 16 m to the west, shingle eroded from the beachface was deposited on the crest and backshore slope of the barrier. Because the Mutton Bay barrier has a lower crest elevation than the deposit at Holyrood Pond, the former is subject to more frequent overwash. Our surveys show that another storm in June 1982 reworked the crest of the Mutton Bay barrier although it did not affect the upper beachface at Holyrood Pond.

Earthquake-generated tsunamis constitute another coastal flood hazard. The 1929 Grand Banks earthquake (magnitude 7.2) caused slumping of some 5×10^{10} m^3 of sediment from the upper continental slope off Laurentian Channel and deposition of debris-flow and turbidite units on the slope and abyssal plain (Piper and Normark, 1982). The resulting tsunami, superimposed on spring tides, caused the loss of some 27 lives (Hollet, 1929) and extensive damage to homes and fishing equipment from Lamaline (site 22, Fig. 2.2) east and northeast to the vicinity of Burin. Wave heights reported were 5 m at Burin (Hollett, 1929) and up to 12 m at St. Lawrence (Giovannini, 1929); other unconfirmed accounts suggest that runup may have been much higher locally along the coast. The probability of events comparable to the 1929 tsunami is difficult to assess at present. One earthquake source model for the outer Laurentian Channel area yields an estimated recurrence interval of about 300 years (Basham et al., 1983); however, marine geological evidence suggests that magnitude-7 events are in fact much rarer,

Figure 2.10. *Surveyed profile across tidal flat and barrier at Come-by-Chance (site 37, Fig. 2.6B), 1983-06-24; note ridge and boulder-cluster relief on tidal flat and multiple beach ridges on prograded barrier deposit.*

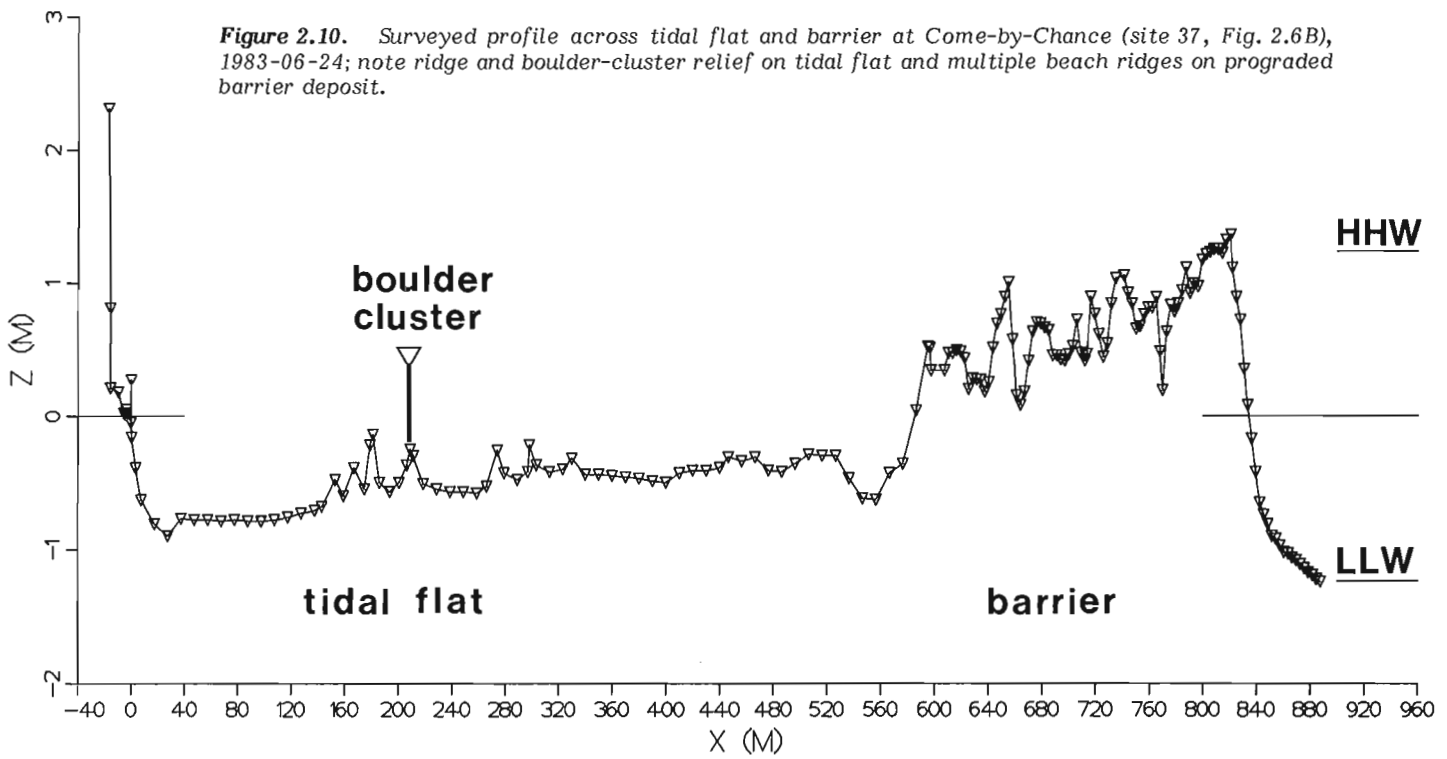

with recurrence intervals in the order of 10^4 years or more (Piper and Normark, 1982; D.J.W. Piper, personal communication, 1984). An alternative model, in which potential earthquake sources are assumed to be uniformly distributed along the entire eastern Canadian margin (Basham et al., 1983) suggests that the recurrence interval for magnitude-7.2 events may be as little as 100 years. Unfortunately, we have little basis for estimating the recurrence frequency of tsunamis, even assuming a known probability distribution for earthquakes.

Summary

Since initiation of a coastal reconnaissance program in Newfoundland in 1981, we have developed a broad overview of physical shorezone characteristics in many parts of the island. This has been supplemented by detailed studies at 79 sites, of which 54 are monumented to allow repetitive surveys for assessment of coastal stability over time. Shorezone morphology and sediments have been investigated at all sites; and bathymetric, sidescan, seismic, bottom-grab, and bottom-core data have been obtained in basin and shoreface locations at a number of the sites.

Major coastal features documented in Newfoundland include: extensive rock outcrop; widespread modern and relict shore platforms; cliffs up to 300 m in rock and 45 m in unconsolidated sediments; minor lag shoals; numerous major fiords and a large number of smaller fiord-like embayments; estuaries and lagoons, with very limited salt-marsh development; tidal inlet systems, including ebb- and flood-tidal delta complexes in sands and gravels; beach and barrier systems in sediments ranging from muddy gravels and sands to well-sorted pebble, cobble, and boulder material; locally well-developed coastal sand dunes; and ice-generated boulder barricades and clusters.

The Atlantic coast is dominated by winter storms; the Gulf coast by autumn and early winter events before development of extensive ice cover. Storm surge anomalies of 1.3 m have been documented on the southeast coast. Large storm waves superimposed on such surges may rework barrier crest deposits at elevations greater than 6 m above HHWLT at intervals of 10-50 years, whereas barriers up to 4.5 m above HHWLT are overtopped much more frequently. Tsunami waves with amplitudes of 12 m or more are known to have devastated part of the south coast following the 1929 Grand Banks earthquake: estimates of the recurrence interval for such an event range from 100 to 100 000 years.

Acknowledgments

I am grateful to David Frobel, Robert Murphy, Michael Gorveatt, Aubrey Fricker, Mona Botros, David Mosher, Aubrey Newcombe (all of AGC), Hugh Miller (Memorial University of Newfoundland), Bernard Pennell (Trepassey), John MacDonald (Versatile Helicopters), John Mein, officers and crew of **CSS Dawson**, and many others for assistance in collection of the data; to Donald Clattenburg and Sherry Wittmann for grain-size analyses; to Valerie Conrod, Andrew Kendall, and Mark King for data analysis; to Darrell Beaver, Roy Sparkes, and Keith White for production of track plots; and to Art Cosgrove and colleagues for drafting services. Eric Hiscock (Environment Canada) and David Aggett (Newfoundland and Labrador Department of Fisheries) kindly furnished unpublished data early in the project; Mobil Oil Canada Ltd and Petro-Canada Exploration Inc. have generously made proprietary coastal video and other data available for viewing; and P.D. Lester (Chief Bridge Engineer, Newfoundland and Labrador Department of Transportation) made available the Holyrood Pond borehole data. I have benefitted from discussions with C.L. Amos, G.B. Fader, D.R. Grant, D.J.W. Piper, R.J. Rogerson, D.G. Vanderveer, and others including many residents of coastal communities. I thank R.B. Taylor, D. Frobel, and D.J.W. Piper for reading the manuscript and suggesting a number of improvements.

References

Brookes, I.A.
1974: Late-Wisconsin glaciation of southwestern Newfoundland (with special reference to the Stephenville map-area); Geological Survey of Canada, Paper 73-40, 31 p.

1982: Ice marks in Newfoundland: a history of ideas; Géographie physique et Quaternaire, v. 36, p. 139-163.

Basham, P.W., Adams, J., and Anglin, F.M.
1983: Earthquake source models for estimating seismic risk on the eastern Canadian continental margin; in Proceedings, Fourth Canadian Conference, Earthquake Engineering; The University of British Columbia, Vancouver; p. 495-508.

Canadian Press
1983: Big tides flood [Avalon] peninsula; The Mail Star, Halifax, 1983-12-23.

Drake, J.J. and McCann, S.B.
1982: The movement of isolated boulders on tidal flats by ice floes; Canadian Journal of Earth Sciences, v. 19, p. 748-754.

Eyles, N. and Slatt, R.M.
1977: Ice-marginal sedimentary, glacitectonic, and morphologic features of Pleistocene drift: an example from Newfoundland; Quaternary Research, v. 8, p. 267-281.

Fader, G.B., King, L.H., and Josenhans, H.L.
1980: Surficial geology south of Newfoundland with emphasis on the glacial and post-glacial history; Geological Association of Canada, Program with Abstracts, v. 5, p. 52.

Flint, R.F.
1940: Late Quaternary changes of level in western and southern Newfoundland; Geological Society of America, Bulletin, v. 51, p. 1757-1780.

Geocon Ltd.
1965: Proposed Holyrood Pond bridge: soil stratigraphy; Drawing no. M3153-1; in unpublished sub-contractor report to Foundation of Canada Engineering Corporation Ltd; Newfoundland and Labrador Department of Transportation, St. John's.

Giovannini, A.A.
1929: Interview in The Evening Telegram, St. John's, 1929-11-25, p. 6.

Grant, D.R.
1977: Glacial style and ice limits, the Quaternary stratigraphic record, and changes of land and ocean level in the Atlantic Provinces, Canada; Géographie physique et Quaternaire, v. 31, p. 247-260.

1980: Quaternary sea-level change in Atlantic Canada as an indication of crustal delevelling; in Earth Rheology, Isostasy and Eustasy, ed. N.-A. Mörner, John Wiley and Sons, London; p. 201-214.

Guilcher, A.
1954: Morphologie littorale et sous-marine; Presses universitaires de France, Paris; 216 p.

1981: Cryoplanation littorale et cordons glaciels de basses mer dans la région de Rimouski, côte sud de l'estuaire du Saint-Laurent, Québec; Géographie physique et Quaternaire, v. 35, p. 155-169.

Henderson, E.P.
1972: Surficial geology of Avalon Peninsula, Newfoundland; Geological Survey of Canada, Memoir 368, 121 p.

Hiscock, E.H.J.
1981: The coastal zone of the Avalon and Burin Peninsulas, Newfoundland: an ecological land survey; Lands Directorate, Environment Canada, Dartmouth, 83 p.

Hiscock, E.H.J. and Maloney, D.A.
1983: The northeast coast of Newfoundland: an ecological land survey; Lands and Integrated Programs Directorate, Environment Canada, Dartmouth; 176 p.

Hollett, Magistrate
1929: Wireless from SS PORTIA to Prime Minister, St. John's, via Cape Race; The Evening Telegram, St. John's, 1929-11-21, p. 6.

McCann, S.B., Dale, J.E., and Hale, P.B.
1981: Subarctic tidal flats in areas of large tidal range, southern Baffin Island, eastern Canada; Géographie physique et Quaternaire, v. 35, p. 183-204.

MacClintock, P. and Twenhofel, W.H.
1940: Wisconsin glaciation of Newfoundland; Geological Society of America, Bulletin, v. 51, p. 1729-1756.

McLaren, P.
1980: The coastal morphology and sedimentology of Labrador: a study of shoreline sensitivity to a potential oil spill; Geological Survey of Canada, Paper 79-28, 41 p.

McKillop, J.H.
1955: Beaches in eastern Newfoundland: preliminary report; Geological Survey of Newfoundland (now Newfoundland and Labrador Department of Mines and Energy), Open File no. Nfld 87, 116 p.

Markham, W.E.
1980: Ice atlas: eastern Canadian seaboard; Atmospheric Environment Service, Environment Canada, Toronto; 96 p.

Mudie, P.J. and Guilbault, J.-P.
1982: Ecostratigraphic and paleomagnetic studies of late Quaternary sediments on the northeast Newfoundland shelf; in Current Research, Part B, Geological Survey of Canada, Paper 82-1B, p. 107-116.

Neu, H.J.A.
1982: 11-year deep-water wave climate of Canadian Atlantic waters; Canadian Technical Report of Hydrography and Ocean Sciences no. 13, Fisheries and Oceans Canada, Dartmouth; 41 p.

Northcott, T.
1963: Beaches of Newfoundland excluding the Avalon Peninsula; Newfoundland and Labrador Department of Mines and Energy, Open File no. Nfld 404, 84 p.

Piper, D.J.W. and Normark, W.R.
1982: Effects of the 1929 Grand Banks earthquake on the continental slope off eastern Canada; in Current Research, Part B, Geological Survey of Canada, Paper 82-1B, p. 147-151.

Piper, D.J.W., Letson, J.R.J., DeIure, A.M., and Barrie, C.Q.
1983: Sediment accumulation in low-sedimentation, wave-dominated, glaciated inlets; Sedimentary Geology, v. 36, p. 195-215.

Quinlan, G. and Beaumont, C.
1981: A comparison of observed and theoretical postglacial relative sea level in Atlantic Canada; Canadian Journal of Earth Sciences, v. 18, p. 1146-1163.

1982: The deglaciation of Atlantic Canada as reconstructed from the postglacial relative sea-level record; Canadian Journal of Earth Sciences, v. 19, p. 2232-2246.

Reinson, G.E. and Rosen, P.S.
1982: Preservation of ice-formed features in a subarctic sandy beach sequence: geologic implications; Journal of Sedimentary Petrology, v. 52, p. 463-471.

Reinson, G.E., Frobel, D., and Rosen, P.S.
1979: Coastal geologic mapping in the Groswater Bay-Lake Melville region, central Labrador; in Proceedings, Symposium on Research in the Labrador Coastal and Offshore Region; Memorial University of Newfoundland, St. John's; p. 14.

Rogerson, R.J. and Tucker, C.M.
1972: Observations on the glacial history of the Avalon Peninsula; Maritime Sediments, v. 8, p. 25-31.

Rosen, P.S.
1979: Boulder barricades in central Labrador; Journal of Sedimentary Petrology, v. 49, p. 1113-1124.

1980: Coastal environments of the Makkovik region, Labrador; in The Coastline of Canada, ed. S.B. McCann; Geological Survey of Canada, Paper 80-10, p. 267-280.

Stockwell, C.H. et al.
1968: Tectonic Map of Canada; Geological Survey of Canada, Map 1251A.

Trenhaile, A.S.
1983: The development of shore platforms in high latitudes; in Shorelines and Isostasy, ed. D.E. Smith and A.G. Dawson; Institute of British Geographers, Special Publication no. 16; Academic Press, London; p. 77-93.

Tucker, C.M. and McCann, S.B.
1980: Quaternary events on the Burin Peninsula, Newfoundland, and the islands of St. Pierre and Miquelon, France; Canadian Journal of Earth Sciences, v. 17, p. 1462-1479.

Tucker, C.M., Leckie, D.A., and McCann, S.B.
1982: Raised shoreline phenomena and postglacial emergence in south-central Newfoundland; Géographic physique et Quaternaire, v. 36, p. 165-174.

Williams, H.
1979: Appalachian orogen in Canada; Canadian Journal of Earth Sciences, v. 16, p. 792-807.

Woodward-Clyde Consultants
1982: Hydraulic and physical character of Placentia in relation to the fishing industry; unpublished report prepared for Small Craft Harbours Directorate, Fisheries and Oceans Canada, St. John's, 50 p.

Woodward-Clyde Consultants and Western Canada Hydraulic Laboratories Ltd.
1982: A study of the accessibility of three small craft harbours – western Newfoundland; unpublished report prepared for Fisheries and Oceans Canada, St. John's, 100 p.

3. COASTAL SURVEYS, JONES SOUND, DISTRICT OF FRANKLIN

Project 820043

R.B. Taylor and D. Frobel
Atlantic Geoscience Centre, Dartmouth

Taylor, R.B. and Frobel, D., Coastal surveys, Jones Sound, District of Franklin; in Current Research, Part B, Geological Survey of Canada, Paper 84-1B, p. 25-32, 1984.

Abstract

In 1983, low-altitude video tapes were made of the coast of Jones Sound; launch surveys were completed off five tidewater glaciers along the northeast coast of Devon Island. Large submarine glacial deposits off northeast Devon Island suggest that some of the valley glaciers once stood 2 to 7 km offshore for a considerable time before rapidly retreating to near their present position. Today, the proglacial tidewater environments in bays resemble those of the slowly retreating shallow-water glaciers in Glacier Bay, Alaska. Most of the Devon Island tidewater glaciers are grounded and are fringed by an ice-proximal shelf. Ice-front thickness is commonly 55 to 76 m but at the face of larger glaciers, it exceeds 100 m. Sediment gravity flows, observed across the ice-proximal shelf foreslope, are an important agent in the transfer and deposition of sediment in the proglacial basins.

Résumé

En 1983, des rubans vidéos ont été pris à faible altitude le long de la côte du détroit de Jones; on a également effectué des relevés à bord de chaloupes au large de cinq glaciers en eau tidale le long de la côte nord-est de l'île de Devon. De vastes dépôts glaciaires sous-marins situés au large de la partie nord-est de l'île de Devon semblent indiquer que certains glaciers de vallée se sont jadis avancés jusqu'à 2 ou 7 km au large pendant une période assez longue avant de reculer rapidement jusqu'aux environs de leur position actuelle. A l'époque actuelle, les milieux d'eau tidale proglaciaire dans les baies resemblent à ceux des glaciers au mouvement de recul lent trouvés dans les eaux peu profondes de la baie des Glaciers (Alaska). La plupart des glaciers en eau tidale reposent sur le fond et sont entourés par une plate-forme gisant à proximité des glaces. L'épaisseur de la glace atteint généralement 55 à 76 m, mais au front des plus gros glaciers, elle dépasse 100 m. Les coulées de sédiments par gravité, dont on a noté la présence à travers l'avant-pente de la plate-forme gisant à proximité des glaces, constituent un agent important dans le transfert et la mise en place des sédiments dans les bassins proglaciaires.

Introduction

A coastal geology survey of Jones Sound was initiated in August 1983 as part of a larger marine geology-geophysics and hydrographic survey of the seabed of Jones Sound (MacLean et al., 1984). During the first phase of the coastal program aerial oblique, colour video tapes were made of the coastline. During the second phase, selected representative coastal environments were visited using a launch or helicopter deployed from **CSS Baffin**, our base of operations. However, extensive fog and coastal sea ice restricted our shore work to one site on Coburg Island and three others on southern Ellesmere Island (Fig. 3.1). At each of the shore stations, a bench mark was established and a beach profile was surveyed with sediment samples collected along it. In addition, the thickness of active layer, the effects of sea ice-shoreline interaction, and the character of raised beaches were noted. Launch surveys were limited to the tidewater glacier environment of northeast Devon Island. Only the aerial photographic program and observations of several tidewater glacier environments off northeast Devon Island are discussed in this report.

Coastal video photography

On 13 and 14 August 1983, a videotape of 935 km of coastline along Jones Sound including Coburg Island (Fig. 3.1) was made using a fixed-wing aircraft. An additional 200 km of coastline was photographed on 9 September, along North Kent Island and Colin Archer Peninsula, Devon Island using a helicopter. Coastal fog obscured the northern Devon Island coast between Sverdrup Inlet and Brae Bay. The videotapes were shot from aircraft flying less than a kilometre offshore at an elevation of 150 to 180 m. A Sony DXC-1800K colour video camera and VO-4800 video cassette recorder were used with 20 minute, 3/4" Sony U-matic Type S tapes. Commentary on the physical shore-zone character and coastal sea-ice conditions was added simultaneously to the tapes. The average length of coast covered per tape was 72 km. Videotapes provide a valuable reference for a multitude of users. We use them primarily to describe the coast, to locate specific coastal or shore-ice features and to identify shoreline changes since the last air photo coverage in the late 1950s. Detailed coastal geology maps can also be produced from this data base.

Tidewater glacier coastal environment, northeast Devon Island

It is estimated that 30 per cent of the shoreline between Brae Bay and Raper Point on Devon Island, is lined by tidewater glaciers (Fig. 3.2). They descend to the coast from the ice cap that covers most of eastern Devon Island through steep sided valleys cut mainly in Precambrian gneisses (Frisch, 1983). Bold talus-banked rock cliffs of 300 to over 480 m elevation make up the coastline between the valley glaciers (Fig. 3.3). For the most part, these coastal slopes are too steep to permit the accumulation of much unconsolidated sediment and the formation of depositional shore features. Beach development is restricted to a low

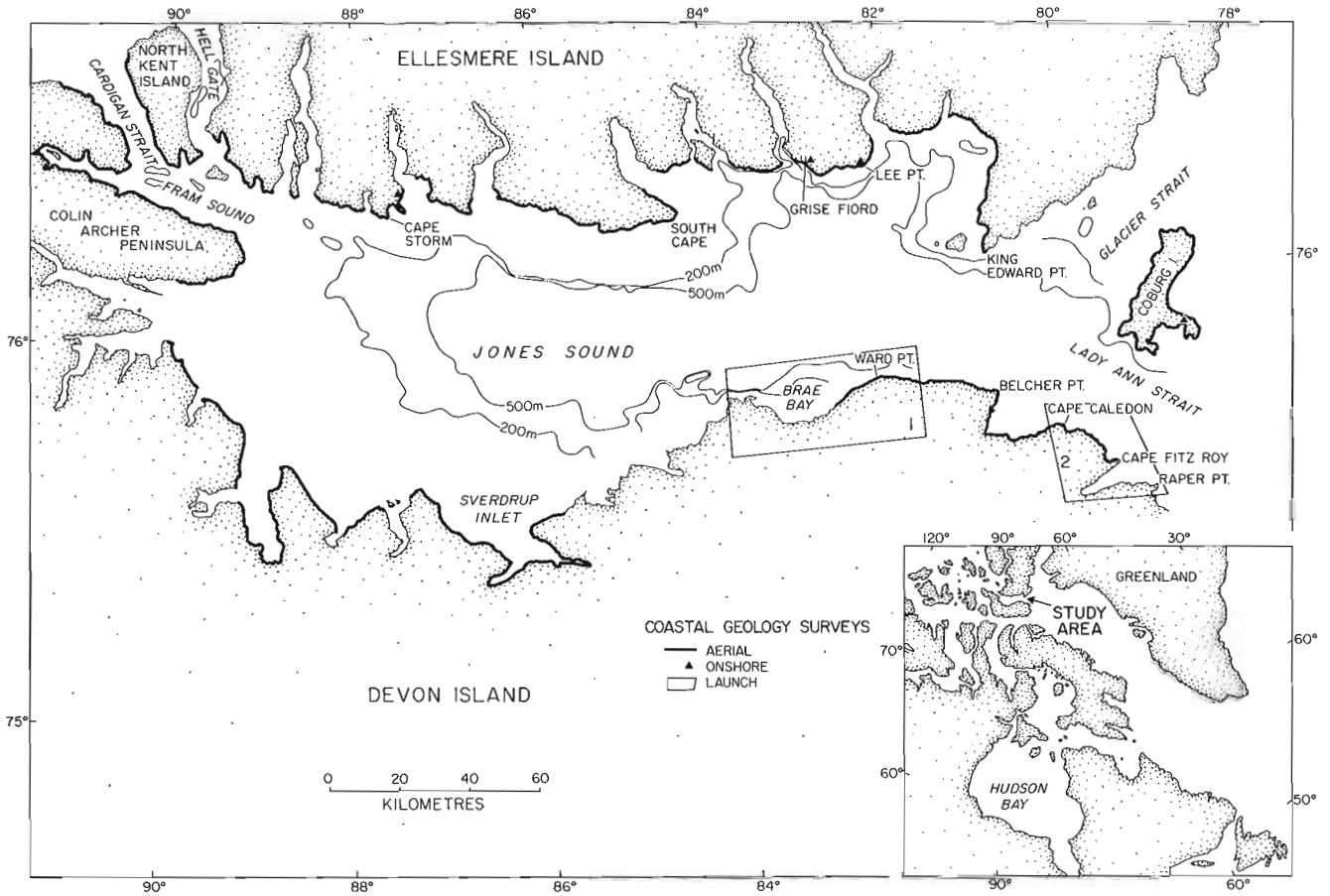

Figure 3.1. *Index map of 1983 coastal geology surveys in Jones Sound. Detailed charts of launch surveys along northeast Devon Island are presented in Figure 3.4.*

Figure 3.2. *Tidewater glaciers, such as Sverdrup Glacier shown here, descend to the coast from the east Devon Island ice cap through steep sided valleys. This view of the eastern face of Sverdrup Glacier illustrates its low, crevassed ice front and the termination of survey line A_3-A_4 (Fig. 3.4a).*

coastal platform west of Ward Point where waves have reworked glacial outwash sediment and other colluvial deposits into discontinuous beach ridges.

There is no published hydrographic or marine geologic information for the pro-tidewater glacier settings of northeast Devon Island. In an attempt to gain a better understanding of these environments, launch surveys were carried out on 16 and 19 August 1983 off five tidewater glaciers and off one non-tidewater glacier (Fig. 3.4a, b). The objective of the survey was to obtain information on bottom morphology and sediment characteristics so that preliminary conclusions could be drawn about recent glacier activity, i.e. retreat or advance, and modern proglacial sedimentation processes. Samples of the top centimetre of bottom sediment were collected for C. Schafer, Paleoecology Section, Atlantic Geoscience Centre, to provide data for the development of a comprehensive foraminiferal assemblage model for ice margin environments.

The survey launch was equipped with a 30 kHz Elac echosounder, a 500 joule Huntec Hydrosonde 2a sparker system and a Petite Ponar sediment grab sampler. Navigational control was limited to radar fixes on distinct shore features and the face of each glacier investigated. Aerial videotape coverage of the coastline from Brae Bay to Cape Fitz Roy complements the launch surveys which were restricted to Brae Bay and to the coastline between Cape Caledon and Raper Point.

Figure 3.3. *Bold talus-banked rock cliffs with semi-permanent snow patches exist between the tidewater glaciers of northeast Devon Island. Where talus has been removed by waves, the base of the snow patch is commonly exposed as an 'icefoot' feature. This view of the shoreline is between Capes Caledon and Fitz Roy.*

Brae Bay

Sverdrup Glacier at the head of Brae Bay is a comparatively wide tidewater glacier (Fig. 3.5) with a front that rises from a few metres to an estimated vertical face of 20 m above sea level along its western end. The front presently lies in water depths of 35 to 68 m. The shallower depths occur along a narrow (<100 m wide) shelf along the western portion of the glacier front (A_1-A_2 – Fig. 3.6). Despite the fact that Sverdrup Glacier is presently free of supraglacial debris, Brae Bay contains glacial deposits for a distance of over 7 km from the present ice front. These deposits form two small islands which rise an estimated 6 to 8 m above sea level, in the northeastern part of the bay (Fig. 3.4a, 3.5). They reflect a major terminal moraine that ranges from 3 km to in excess of 5 km offshore from the present ice front in that part of the bay (A_3-A_4, Fig. 3.6). A second bank of sediment lying 6 to 7 km offshore on the western survey line (A_1-A_2), may indicate an even earlier ice still-stand position. The two moraines are separated by hummocky topography that resembles ice-melt deposits. The moraines are composed of sand and gravel, and are mantled by a cobble-boulder lag.

It is evident from the echo sounding survey lines (Fig. 3.6) that the bottom topography varies considerably in areas that are immediately adjacent to the present ice front. Off the western ice front, the narrow ice-proximal shelf is fringed by a 160 m deep basin which has been infilled by a minimum of 10 m of acoustically-transparent sediment. This cover of fine sediment (Sample L101, Fig. 3.6), pinches out upslope on the landward side of the large moraine in water depths of 50 m and disappears completely in water depths shallower than 16 m (Samples L103, 104). In contrast, off the eastern face of Sverdrup Glacier there is no sign of a deep proglacial basin; the bottom topography is very irregular and becomes progressively shallower offshore. Bottom sediment sampled within a kilometre of the eastern ice front (L107-109) is mainly an olive-green silt of variable cohesiveness with traces of sand in samples collected farther offshore.

Along the eastern shore of Brae Bay, the valley glaciers do not reach tidewater. They terminate on a low coastal (rock?) platform that extends a kilometre offshore from the high plateau slope. Today the valley glacier fronts are covered by ablation till and outlined by terminal moraines located just above the present shoreline. For comparative purposes, a survey line was run inshore to one of these non-tidewater glaciers (Fig. 3.4 to 3.6 – Section B_1-B_2). A nearshore platform mantled by glacial debris extends several hundred metres offshore to depths of 6 m. Seaward of this platform, the bottom slopes gradually to 70 m water depth where a ridge, possibly a moraine, exists at about 3.5 km offshore.

Ward Point to Cape Fitz Roy

Tidewater glaciers cover just over 40 per cent of this segment of coastline. Lateral moraines extend farther offshore than the present ice fronts which suggests that most of the glaciers are in a recessional stage. Nevertheless, there is a tidewater glacier west of Cape Caledon that has a floating (?) ice tongue that extends a substantial distance beyond the main ice front and its associated lateral moraines. The only extensive ice-free coastal area is at Belcher Point where the rugged rock shoreline rises to over 200 m.

In 1983, launch surveys were completed off two tidewater glaciers east of Cape Caledon (lines C_1-C_2 and D_1 to D_3 – Fig. 3.4b, 3.7). At the first glacier (line C_1-C_2), the seabed drops sharply across narrow rock ledges to depths greater than 400 m. The only indication of unconsolidated sediment is a ridge (moraine?) at 100-120 m water depth, approximately 500 m from the glacier front. A continuation of the survey line closer inshore was prevented by sea ice.

At the second tidewater glacier (Fig. 3.8), two survey lines (D_1-D_2 – D_3) and three bottom sediment samples were obtained. The ice front, grounded in 20 to 30 m of water, is fringed by a narrow shelf covered by silt and gravel. Shells, sea urchins, starfish and shell fragments are abundant. Off the western portion of the ice front, the seabed drops sharply (line D_1-D_2) from the ice-proximal shelf, whereas off the centre of the glacier (line D_2-D_3) two submarine ridges occur. The seaward ridge has a hummocky topography with hollows that are infilled by at least 2 m of acoustically transparent material. Between the two ridges, at least 10 m of fine sediment has been deposited. A sub or englacial stream flows from the large arch cut in the central face of the glacier (Fig. 3.8) and is thought to be related to the abundant sediment and sea fauna observed off this glacier.

A third glacier was surveyed at the head of the small bight west of Cape Fitz Roy (Fig. 3.4b). Here, a 76 m thick ice front is fringed by an ice-proximal shelf covered by silt and pebbles (line E_1-E_2, Fig. 3.7). The shelf foreslope extends to a depth of 230 m before the bottom rises again at a sill near the entrance to the bight. Although, the composition of the sill could not be determined, sparker records suggest that it is mantled by unconsolidated sediment. At the base of the ice-proximal shelf slope and across the inner part of the bight, the seabed is infilled by a minimum of 3-4 m of overlapping layers of acoustically transparent sediment that resemble slump deposits. The bottom profile across the bight (parallel to the ice face) is a classic u-shape (line E_3-E_4, Fig. 3.7).

Cape Fitz Roy to Raper Point

Fourteen valley glaciers, mostly tidewater, descend from the Devon Island ice cap into the unnamed inlet between Cape Fitz Roy and Raper Point (Fig. 3.4b). The largest tidewater glacier fills the head of the inlet. As no published bathymetric information is available for this inlet, a survey line was run along its length (approximately 0.6 km from the north shore) to the head of the inlet.

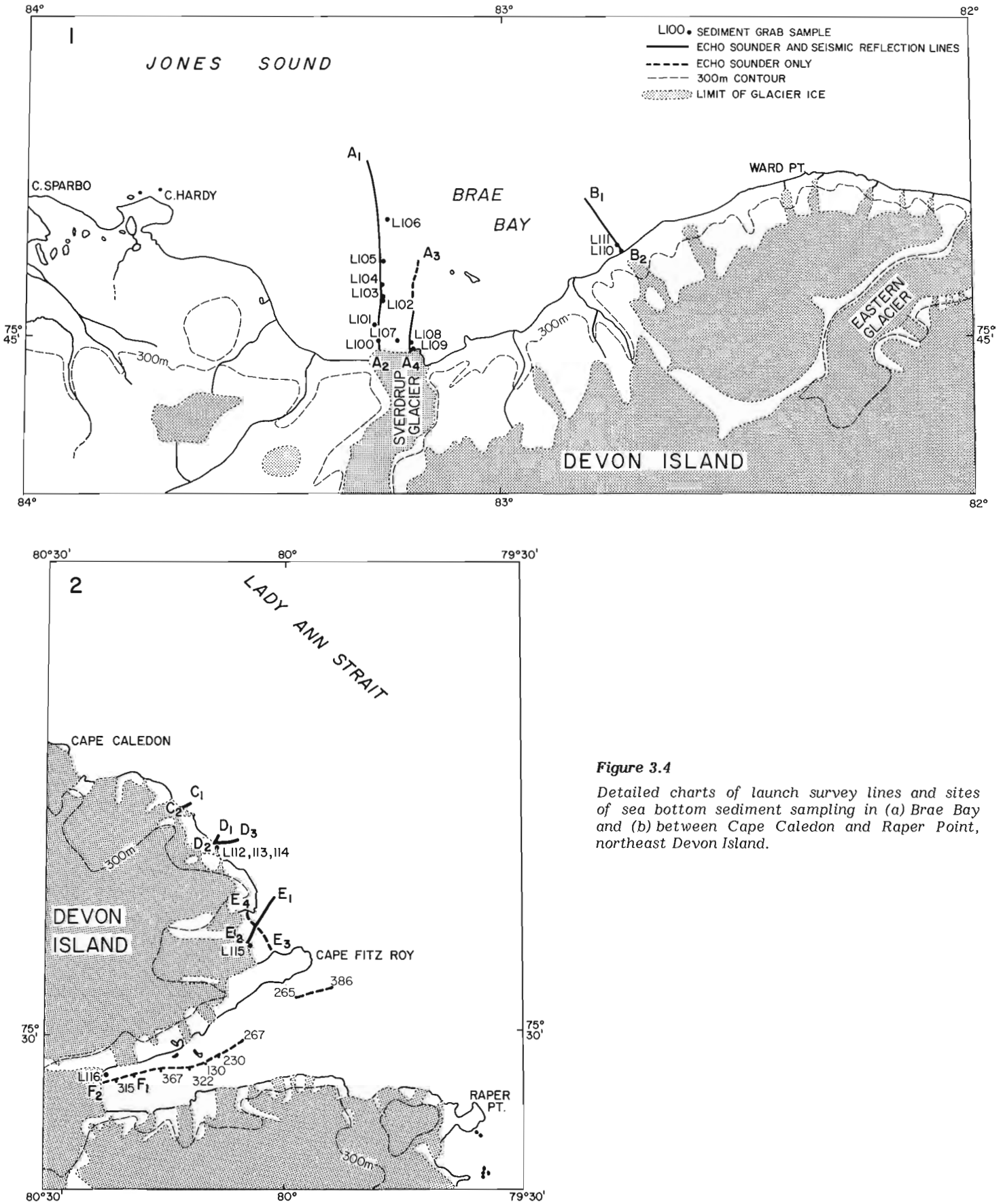

Figure 3.4

Detailed charts of launch survey lines and sites of sea bottom sediment sampling in (a) Brae Bay and (b) between Cape Caledon and Raper Point, northeast Devon Island.

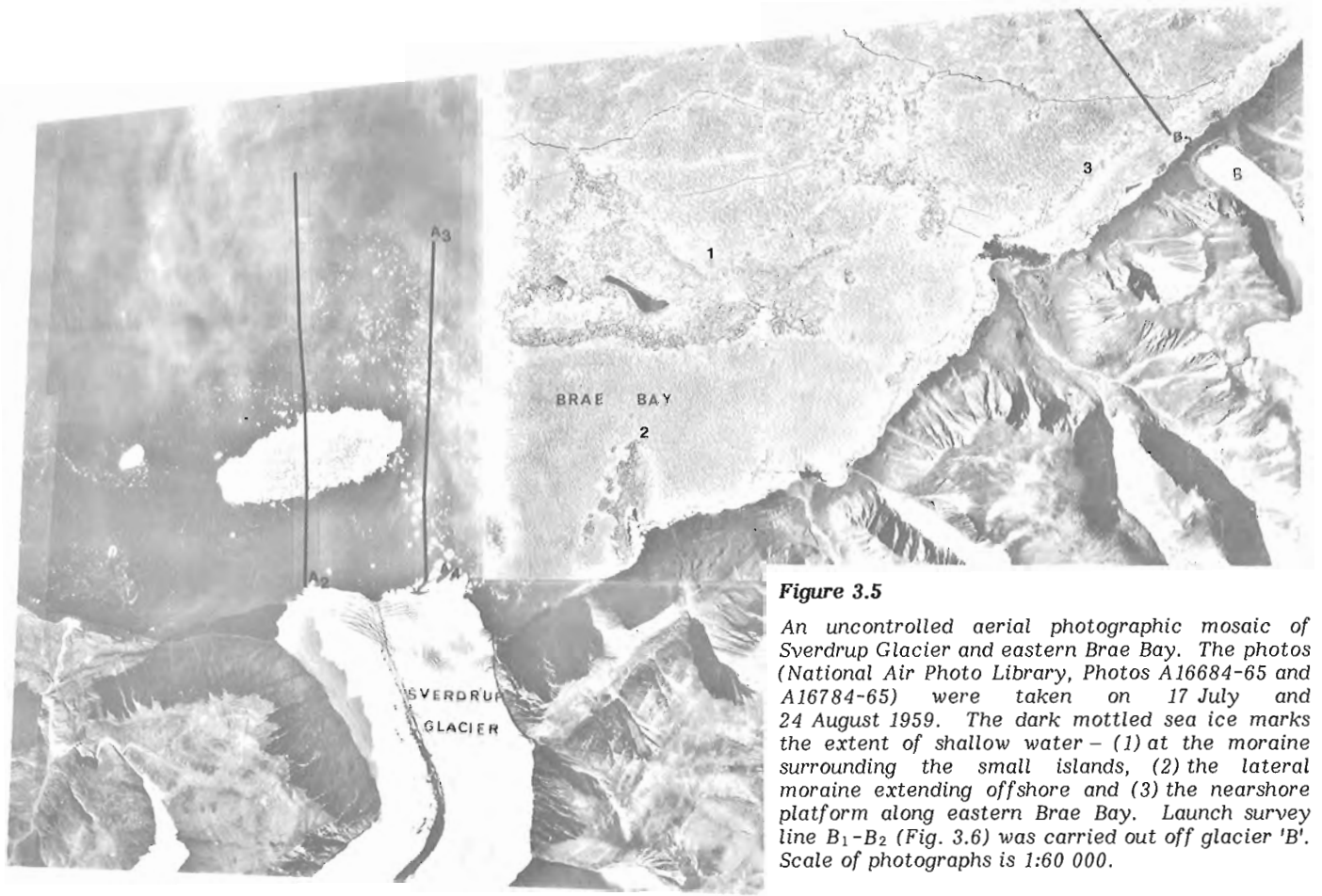

Figure 3.5

An uncontrolled aerial photographic mosaic of Sverdrup Glacier and eastern Brae Bay. The photos (National Air Photo Library, Photos A16684-65 and A16784-65) were taken on 17 July and 24 August 1959. The dark mottled sea ice marks the extent of shallow water – (1) at the moraine surrounding the small islands, (2) the lateral moraine extending offshore and (3) the nearshore platform along eastern Brae Bay. Launch survey line B_1-B_2 (Fig. 3.6) was carried out off glacier 'B'. Scale of photographs is 1:60 000.

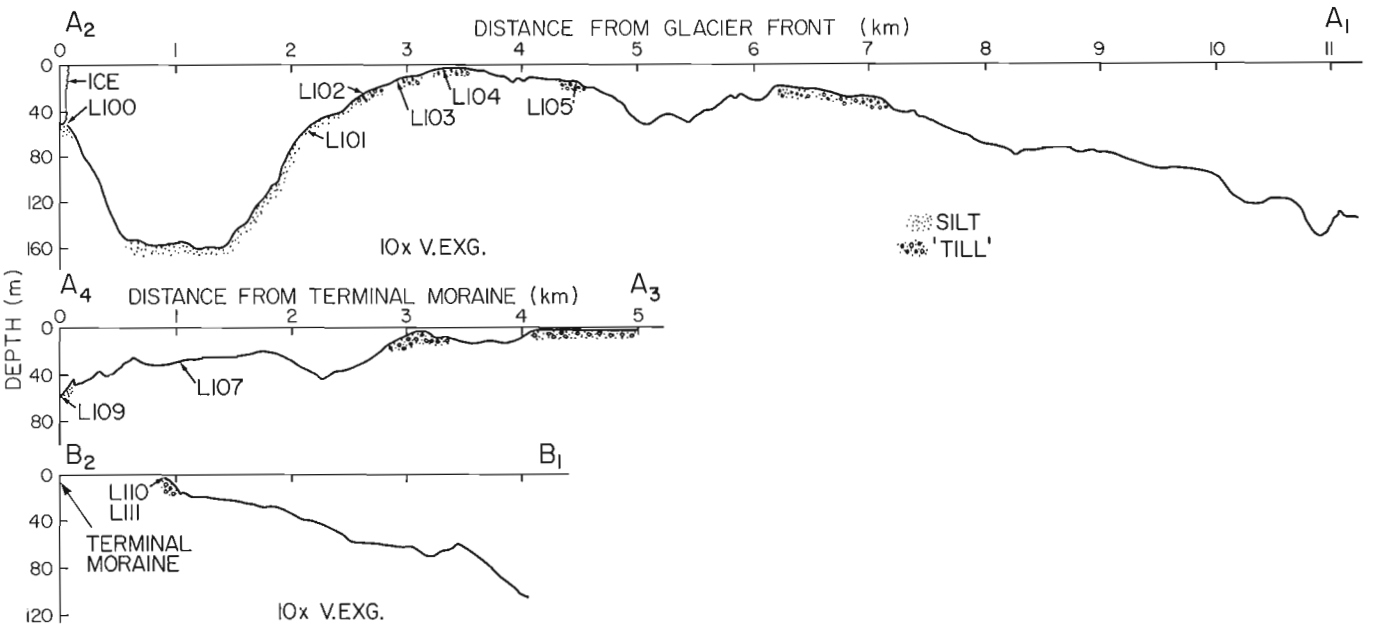

Figure 3.6. *Cross-sectional profiles of the nearshore bottom off Sverdrup Glacier (A_1-A_2 – western face and A_3-A_4 – eastern face) and off a smaller non-tidewater glacier (B_1-B_2) located along eastern Brae Bay. See Figure 3.4a for the location of survey lines.*

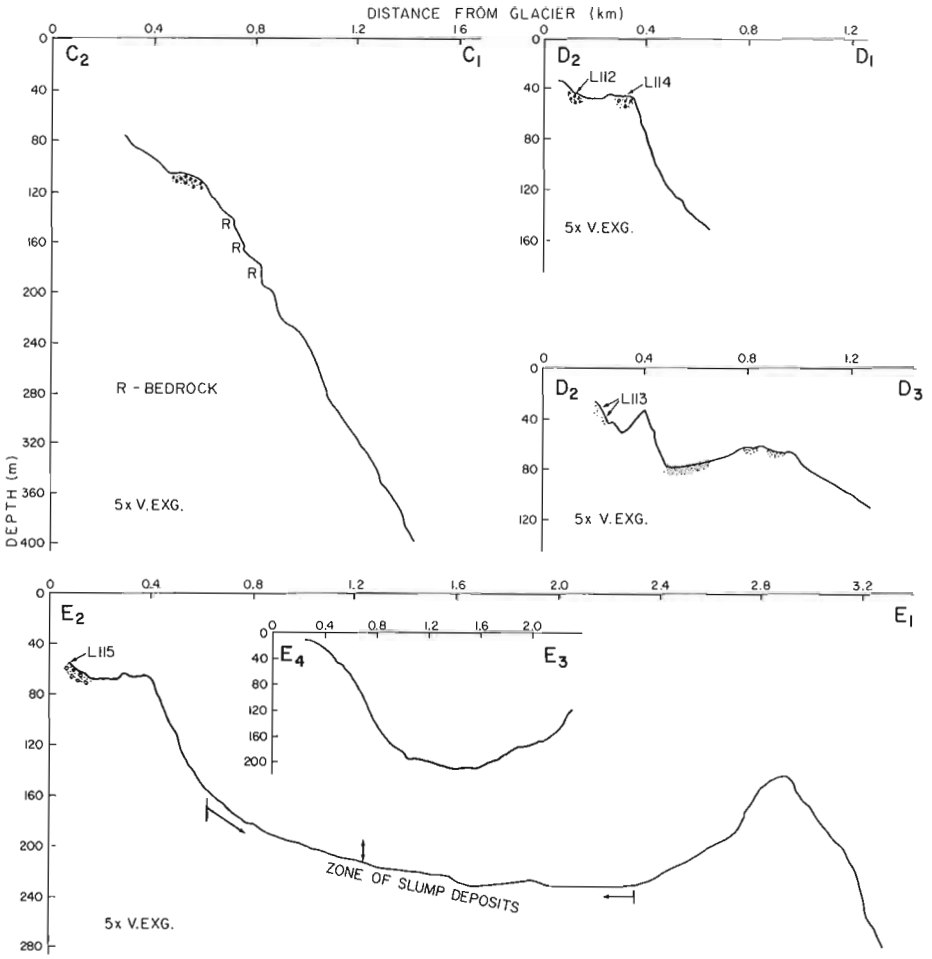

Figure 3.7

Cross-sectional profiles of the nearshore bottom off the tidewater glaciers surveyed between Capes Caledon and Fitz Roy. See Figure 3.4b for the location of survey lines.

Figure 3.8. *At the second tidewater glacier surveyed east of Cape Caledon (Fig. 3.4b), the proglacial sediments are thought to be primarily derived from the sub or englacial stream which flows through a large arch in the central ice front. The subaerial ice front thickness is estimated to be 32-40 m.*

Unfortunately, problems with the echo sounder and sparker system prohibited the plotting of a continuous bottom profile. The range of depths encountered is marked in Figure 3.4b. The submarine topography of the inlet is very irregular. Changes in relief of 30 to 100 m occur commonly because of glacial debris deposited by side entrance glaciers. Shallowest water depths of 120 m were recorded near the small rock islands that are situated near the central part of the inlet. Toward the entrance of the inlet, several ridges exist in water depths nearing 200 m. A shallow sill was not observed. Off the tidewater glacier at the head of the inlet, a landward dipping shelf exists in water depths of 180-200 m (Fig. 3.9). The landward limit of this shelf and the possibility of another shelf closer to the present ice front could not be determined because the survey line terminated within 0.5 km of the ice face, for safety reasons. Bottom sediments resembling slump deposits cover the lower shelf foreslope and a large submarine ridge (moraine?) exists approximately 2 km offshore of the present ice front in water depths of about 290 m.

Discussion

Along northeast Devon Island, the tidewater glaciers examined were grounded and most had a total ice-front thickness of 55-76 m. Others such as the large tidewater glacier at the head of the unnamed inlet east of Cape Fitz Roy, had an ice thickness greater than 100 m. The proglacial environment in bays along northeast Devon Island resembles that described by Powell (1980) for the slowly retreating shallow water glaciers in Glacier Bay, Alaska. The Devon glaciers are

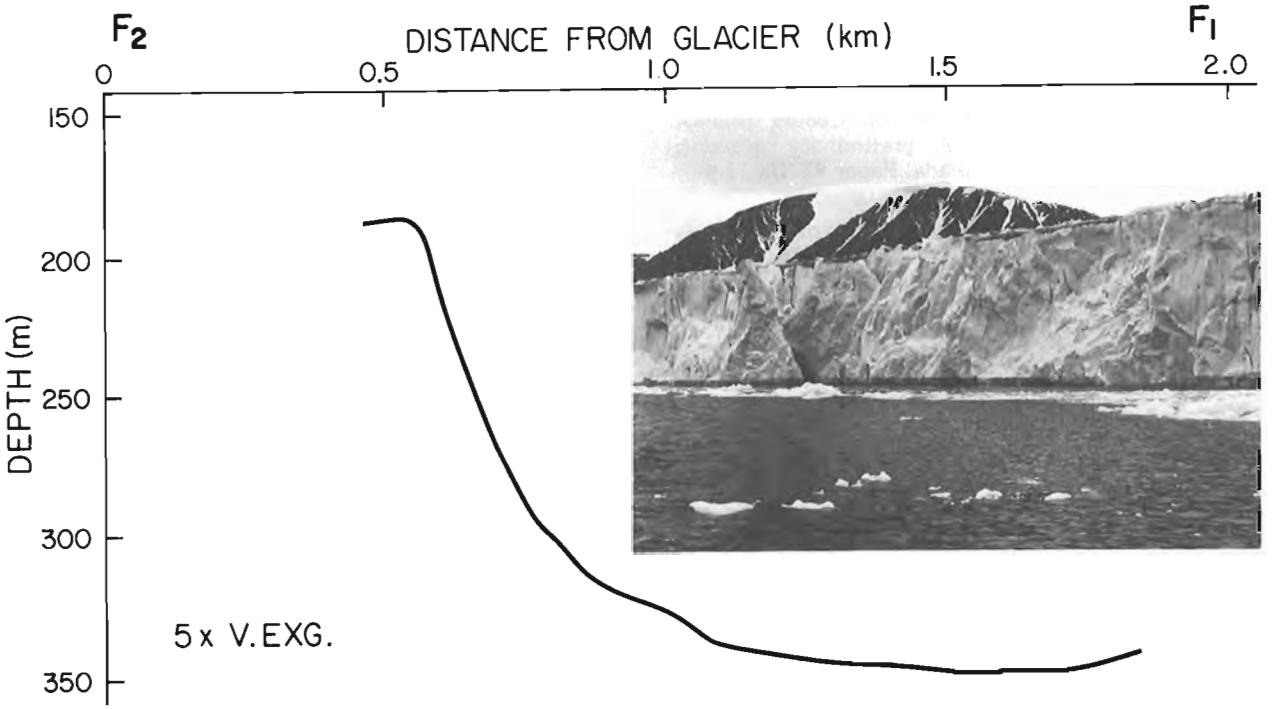

Figure 3.9. *Proglacial bottom morphology and photo of ice front at the head of the unnamed inlet between Cape Fitz Roy and Raper Point. Subaerial ice front thickness is approximately 37 m. Note the tidal line cut in the base of the ice face and the layer of supraglacial debris at the top of the ice face. Location of section F_1-F_2 is shown in Figure 3.4b.*

fringed by an ice-proximal shelf that is covered by silts and coarser clasts derived from melting of the ice and from the dumping of supraglacial debris. The shelf foreslope extends to depths of 160 to 340 m where proglacial basins have been infilled by at least 10 m (limit of penetration by instrument) of acoustically transparent sediment. Seismic records show that subaqueous sediment gravity flows do occur down the shelf foreslope and that this process is responsible for a large proportion of the sediment deposited in the proglacial basins. On their seaward side, the basins are outlined by morainal banks or sills which are mantled by cobble-boulder lag deposits. Shoaling waves and grounding sea ice are responsible for the winnowing of the fines from the shallow morainal banks. Similarly, off the non-tidewater glacier in eastern Brae Bay, the nearshore bottom is composed of wave-reworked glacial debris which is devoid of finer sediment.

Geomorphological evidence suggests that most but not all of the tidewater glaciers along northeast Devon Island are receding. Submarine glacial deposits in the shallow bay environments indicate that valley glaciers once extended at least 2 to 7 km farther offshore than today. However, along the outer coast of Devon Island where water depths exceed 400 m, no evidence of valley-glacier ice-front positions was found. The apparent deposits of till observed farther offshore (MacLean et al., 1984) are thought to be related to more regionally extensive Pleistocene glaciations. The best field evidence of valley-glacier activity was collected during the launch surveys off Sverdrup Glacier. The extensive bank of sediment 3 to 7 km offshore in Brae Bay provides evidence that Sverdrup glacier remained at that distance offshore for a considerable time. The double ridge observed on line A_1-A_2 (Fig. 3.6) suggests that more than one ice still stand may have occurred in this part of the bay. Moreover, the absence of submarine ridges, i.e. moraines, closer inshore suggests that Sverdrup Glacier rapidly retreated to near its present position following the still stand. Today Sverdrup Glacier is near the head of the bay and it is fringed by an ice proximal shelf which may indicate that its retreat has slowed down again. Some calving presently takes place at the ice front; however, melting appears to be a more important mechanism of retreat. Slight variations in the location and morphology of proglacial submarine features were observed along the other tidewater glaciers of northeast Devon Island; the geomorphological and sedimentological evidence collected, however, supports the conclusions drawn from glacier activity in Brae Bay.

Future research will focus on the analysis of the bottom sediment samples collected at the glacier fronts, particularly in regard to the characteristics of their contained foraminiferal assemblages at various distances from the ice face.

Acknowledgments

Arctic field work cannot be conducted without the assistance of many people; these surveys were no exception. We acknowledge the continued logistics support from Polar Continental Shelf Project, the crew of **CSS Baffin**, and M.G. Swim, Chief Hydrographer on board. G. Fenn, B. Chapman and M. Ruxton assisted on the launch. P. Girouard assisted with the shore work and P. Rask, D. Sinclair and T. Schmidt piloted the aircraft for the aerial surveys. Financial support of this program by the office of Energy Research and Development, Department of Energy, Mines and Resources is gratefully acknowledged. Thanks also to C. Schafer and B. MacLean for their constructive review of the manuscript.

References

Frisch, T.
1983: Reconnaissance geology of the Precambrian Shield of Ellesmere, Devon and Coburg Islands, Arctic Archipelago: A preliminary account; Geological Survey of Canada, Paper 82-10, 11 p.

MacLean, B., Woodside, J.M., and Girouard, P.
1984: Geological and geophysical investigations in Jones Sound, District of Franklin; in Current Research, Part A, Geological Survey of Canada, Paper 84-1A, p. 359-365.

Powell, R.D.
1980: Holocene glaciomarine sediment deposition by tidewater glaciers in Glacier Bay, Alaska; Ph.D. Thesis, Ohio State University, 420 p.

4. GALENA-SPHALERITE-CHALCOPYRITE VEINS IN APHEBIAN DOLOMITE AND ARCHEAN BASEMENT AT ARTILLERY LAKE, NORTHWEST TERRITORIES

Project 770024

S.S. Gandhi
Economic Geology and Mineralogy Division

Gandhi, S.S., Galena-sphalerite-chalcopyrite veins in Aphebian dolomite and Archean basement at Artillery Lake, Northwest Territories; in Current Research, Part B, Geological Survey of Canada, Paper 84-1B, p. 33-40, 1984.

Abstract

Quartz-carbonate veins with abundant galena, sphalerite, chalcopyrite and pyrite were discovered during 1983 at 11 widely separated localities within a 40 x 7 km area of Aphebian dolomite and subjacent Archean rocks at Artillery Lake, and define a metallogenic district.

The dolomite includes quartz pebbly and gritty lenses, and some stromatolitic and argillitic beds. It is gently folded and locally highly brecciated. The breccia is probably sedimentary and/or due to solution collapse. The veins carrying Pb, Zn and Cu sulphides are epigenetic and post-date brecciation. It is postulated that the metals were leached from the basement by meteoric waters, reacted with sulphur probably derived from H_2S entrapped in the dolomite, and were precipitated at low temperature in open fractures and cavities. The dolomite was later truncated on its southeast side by a northeast-trending fault related to the McDonald Fault system, and is cut by north-northwest-trending Mackenzie diabase dykes of Helikian age.

Résumé

On a découvert en 1983 des veines de quartz et de carbonate contenant beaucoup de galène, de sphalérite, de chalcopyrite et de pyrite dans 11 endroits très espacés, à l'intérieur d'un secteur de 40 sur 7 km constitué de dolomie aphébienne reposant sur des roches archéennes dans le lac Artillery; on a défini ce secteur comme étant un district métallogénique.

La dolomie contient des lentilles grèseuses et caillouteuses renfermant du quartz, et quelques couches à stromatolites et d'argilite. Elle est légèrement plissée et fortement brèchique par endroits. La brèche est probablement d'origine sédimentaire ou produite à la suite d'un effrondrement de dissolution, ou les deux. Les veines contenant des sulphures de Pb, de Zn et de Cu sont épigénétiques et sont postérieures à la bréchification. On suppose que les métaux ont été lessivés du socle par les eaux météoriques, ont réagi avec le soufre provenant probablement du H_2S piégé dans la dolomie et ont précipité à de faibles températures dans des fractures ouvertes et dans des cavités. La dolomie a été tronquée plus tard sur le côté sud-est par une faille de direction nord-est liée au système de failles de McDonald; elle est traversée par des dykes de diabase de Mackenzie de direction nord nord-ouest et d'âge hélikien.

Introduction

A brief reconnaissance survey of the Artillery Lake area was undertaken by the writer during 1983 in conjunction with mineral resource assessment of a proposed National Park to extend northeasterly 270 km from the East Arm of Great Slave Lake to Artillery Lake region, and which is 13 to 30 km wide. In the Artillery Lake sector of the proposed park, only one chalcopyrite occurrence was documented prior to the present survey (Folinsbee, 1952), and a sphalerite occurrence was verbally reported to have been found in early 1950s by Inco Limited, but no data on it were published or available in the assessment files. The proposed park area has been withdrawn from staking since 1971, and this may in part explain the dearth of mineral occurrences reported prior to the present survey.

The ten-day survey revealed the presence of abundant coarse galena, sphalerite and chalcopyrite in quartz-carbonate veins at 11 localities (Fig. 4.1). The previously reported sphalerite occurrence is believed to be at showing A-1 (Fig. 4.1). The chalcopyrite occurrence (Folinsbee, 1952) at showing A-4 was mapped in detail and the mapping revealed the presence of previously unreported veins carrying coarse galena and sphalerite in the vicinity of the chalcopyrite-bearing veins (Fig. 4.2). The latter are prominently exposed but do not contain galena and sphalerite; this is probably the reason why these minerals were not found earlier.

The discoveries are widely distributed in an area approximately 40 x 7 km underlain largely by an Aphebian dolomite that unconformably overlies the Archean rocks. Most of the veins are in the dolomite but some occur in the Archean basement in the vicinity of dolomite. They collectively define a metallogenic district on which this paper is a preliminary report.

General geology and isotopic dates

Artillery Lake is situated near the southeastern margin of the Archean Slave Structural Province. The Archean rocks are unconformably overlain by predominantly dolomitic beds that are preserved in geographically restricted area of Artillery Lake (Folinsbee, 1952; Wright, 1952, 1957, 1967). These beds are informally regarded here as 'Artillery Lake formation'. The formation is gently folded and is truncated on its southeastern side by an east-northeast-trending fault, interpreted as part of the McDonald Fault system trending in

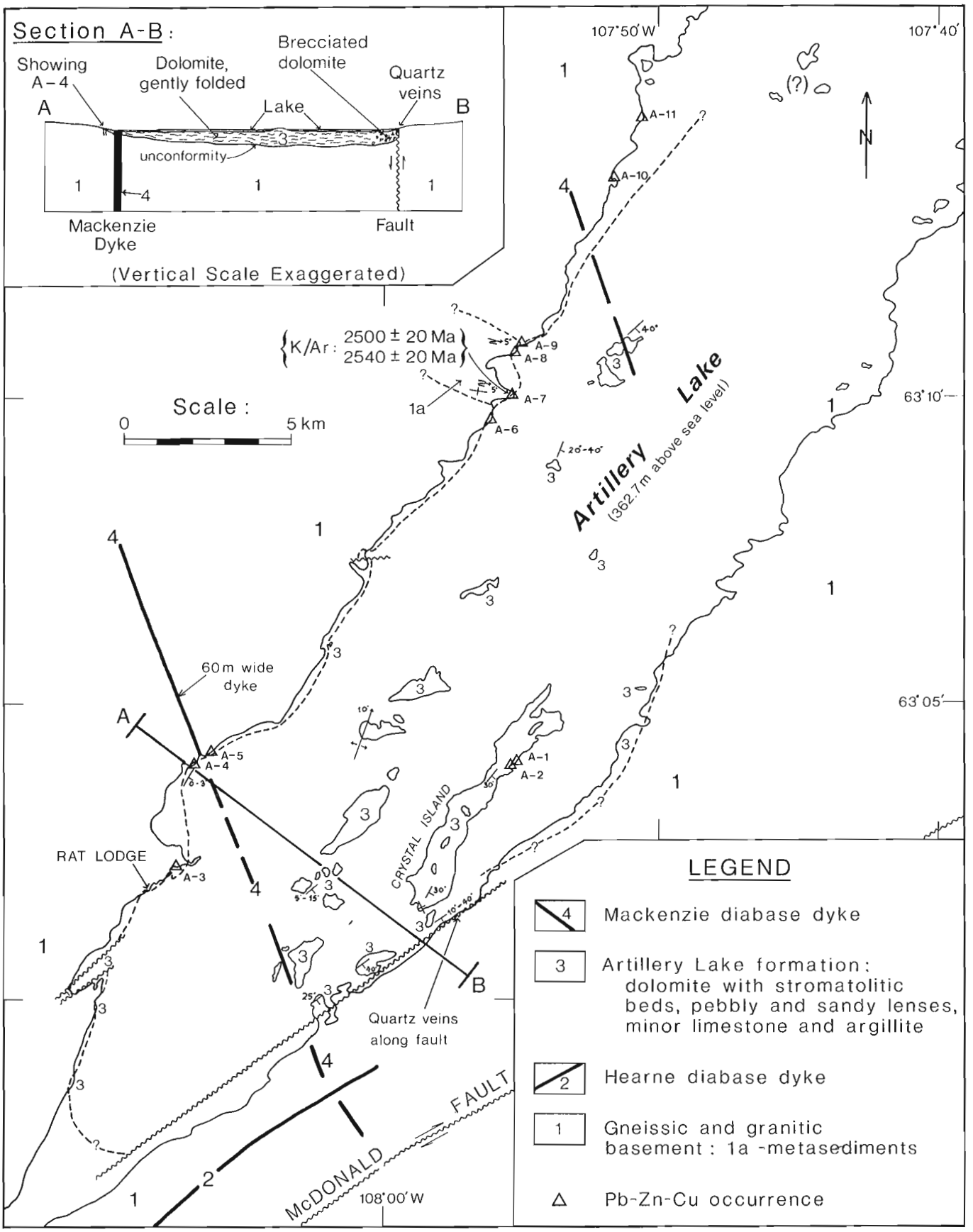

Figure 4.1. *Geology and Pb-Zn-Cu occurrences of Artillery Lake area, District of Mackenzie. (Modified after Folinsbee, 1952 and Wright, 1952, 1957, 1967).*

the same direction. Most of the movements along the fault system occurred during the late Aphebian (Hoffman et al., 1977; Gandhi and Loveridge, 1982). Diabase dykes trending in two directions occur in the study area: a northeast trending Aphebian Hearne dyke south of the lake (Hoffman et al., 1977), and several north-northwest trending dykes of the Mackenzie swarm. The latter cut the dolomite and were intruded about 1300 Ma (Wanless et al., 1965, p. 49-50).

Along the northwestern shore of Artillery Lake, the predominant basement rock is a feldspar porphyritic granite-granodiorite, with minor metasedimentary and metavolcanic rocks and numerous pegmatite dykes. The metasediments at showing A-7 contain coarse muscovite-rich pockets in the vicinity of pegmatite lenses. K-Ar age determinations on two muscovite samples, approximately 30 m apart, at showing A-7 yielded dates of 2500 ± 20 Ma and 2545 ± 20 Ma (unpublished data Geological Survey of Canada, 1984, samples GFA-83-571 and 568 respectively). These metasediments are possibly an eastern extension of the belt of Archean metasedimentary and metavolcanic rocks, mapped by Folinsbee (1952) in the Walmsley Lake map sheet, that occur within 7 km northwest of showing A-7.

Along the southeastern shore of Artillery Lake, the basement rocks are mafic banded gneisses, leucocratic quartz-feldspar gneisses, granite gneiss, intrusive granite and pegmatites. They were regarded as Aphebian by Wright (1967), based on a K-Ar date on a sample located outside of the area of Figure 4.1.

Minimum age of the Artillery Lake formation is indicated by lead isotopic data on galenas from the newly discovered veins. Calculated dates of vein formation from collinear $^{207}/^{204}$Pb:$^{206}/^{204}$Pb compositions of 3 samples are in the range of 1890 and 1990 Ma according to Roscoe (1984). An additional collinear analysis obtained subsequently changes the indicated ^{207}Pb/^{206}Pb ratio to 0.301 from 0.312 and the probable age range to 1890 to 1850 Ma based on assumed source radioactive mineral ages in the range 2590 to 2620 Ma (S.M. Roscoe, personal communication, 1984).

Artillery Lake formation

Lithology. Rocks included in the Artillery Lake formation are massive and thinly bedded dolomite, siliceous dolomite and limestone, lenses of quartz pebbles and gritty sandstone, some of which contain dolomitic fragments and argillaceous dolomitic pebbles, some stromatolitic beds and minor dark grey argillite and argillaceous dolomite. The formation is brecciated along the east side of Crystal Island and to the south of the island.

Massive and thinly bedded dolomites are predominant. On the fresh surface, they range from buff white to pale pink. Their weathered surfaces are either buff white or tan to reddish brown. At many places, the colour boundary is sharp and jagged, indicating brecciation or veining, although this is not evident on the unweathered surface. Some of thinly bedded greyish white beds appear to be limestone.

Pebbly and gritty lenses with dolomite cement are present near the unconformity on the northwestern shore and also on Crystal Island and in its vicinity. They are up to 30 cm thick and several metres long. The pebbles are mostly of well rounded quartz up to 3 cm long, but in some lenses subangular fragments of quartz and/or dolomite are also present. The coarse to fine sandy grains are also predominantly of well rounded quartz. Flat lensoid pebbles of dark grey argillaceous dolomite are present in some lenses. Graded bedding is observed in some of the lenses. In the southern part of Crystal Island, a lens of well sorted medium grained quartz sandstone rests on a bed of stromatolite-like calcareous mounds up to 35 cm in diameter that have convex upwards, concentric internal structure. Some concentric layers have sheaf-like carbonate aggregates perpendicular to layering, with coarser crystals upwards. Similar structure on a smaller scale is seen in some thin beds at the south end of Crystal Island where quartz aggregates with pyrobitumen globules occur at the core of the domal structure. Beds of columnar stromatolite occur in dolomite on an island south of Crystal Island and on a peninsula 1.5 km to its southwest. They have convex upwards internal structure and are approximately 2 cm in diameter. They are silicified to varying degrees.

The presence of argillaceous dolomite was reported by Folinsbee (1952) in the southwestern part of Artillery Lake. Dark grey argillite and thinly bedded argillaceous dolomite beds up to 2 m thick were found by the writer south of Crystal Island (at the fault boundary) and on an island east of showing A-9 where a Mackenzie diabase dyke is exposed (Fig. 4.1).

Veins. Numerous veins cut the Artillery Lake formation. These can be grouped into 4 types: (i) dolomitic veins, (ii) barren chert and quartz veins, (iii) pyrite veins and irregular pods, and (iv) galena-sphalerite-chalcopyrite-pyrite-quartz-carbonate veins. There may be more than one generation of each type and they may overlap in time, except for the fourth group which is apparently the youngest and is described further under galena-sphalerite-chalcopyrite occurrences.

Dolomite veins are common in the dolomite, as well as in the basement on the northwest shore of Artillery Lake, reflecting proximity of these basement rocks to the dolomite, now stripped away. The veins are commonly 5 to 10 cm wide and several metres long. They are commonly horizontal or gently dipping in the basement and subparallel to foliation, whereas they are randomly oriented in the Artillery Lake formation. Their fresh surface is commonly pale pink, and the weathered surface is buff white.

Barren chert and quartz veins are abundant. They lace the dolomite beds and range from fine cherty to coarse grained. They stand out on differentially weathered dolomite surfaces. The veins are of various sizes, ranging from narrow stringers to true veins that are up to a metre wide and several tens of metres long. Most common however are 1 to 3 cm wide, cherty veins that are either subparallel to each other or form a stockwork. In addition, cherty layers and siliceous patches are common in domal stromatolite-like structures. Larger quartz veins are commonly progressively coarser towards the centre with vuggy cores lined with well terminated quartz crystals up to 2 cm in diameter. Crystal Island was so named because of the presence of clusters of small clear quartz in such veins and geodes (Tyrrel, 1901, p. 18). Locally cores of the veins are filled with calcite. Some of the coarse quartz veins cut the brecciated dolomite. Vitreous black globular pyrobitumen is seen in a few quartz veins at the south end of Crystal Island.

Pyrite veins and pods up to half a metre thick are present in dolomite as well as in the basement, and were observed at most of the showings. They are composed of coarse aggregates of pyrite crystals or grains, up to a few millimetres long, or spherulitic pyrite up to 2 cm in diameter with radiating crystals. Other commonly associated minerals are quartz and carbonates. Pyrobitumen occurs with them in several places. It commonly forms globular or oval patches with smooth outlines up to 3 cm long, as seen at showings A-1 and A-2.

Unconformity. The basal unconformity of the Artillery Lake formation is exposed at several localities along the northwestern shore of the lake. It is characterized by pebbly and gritty basal beds and saprolitic character of the

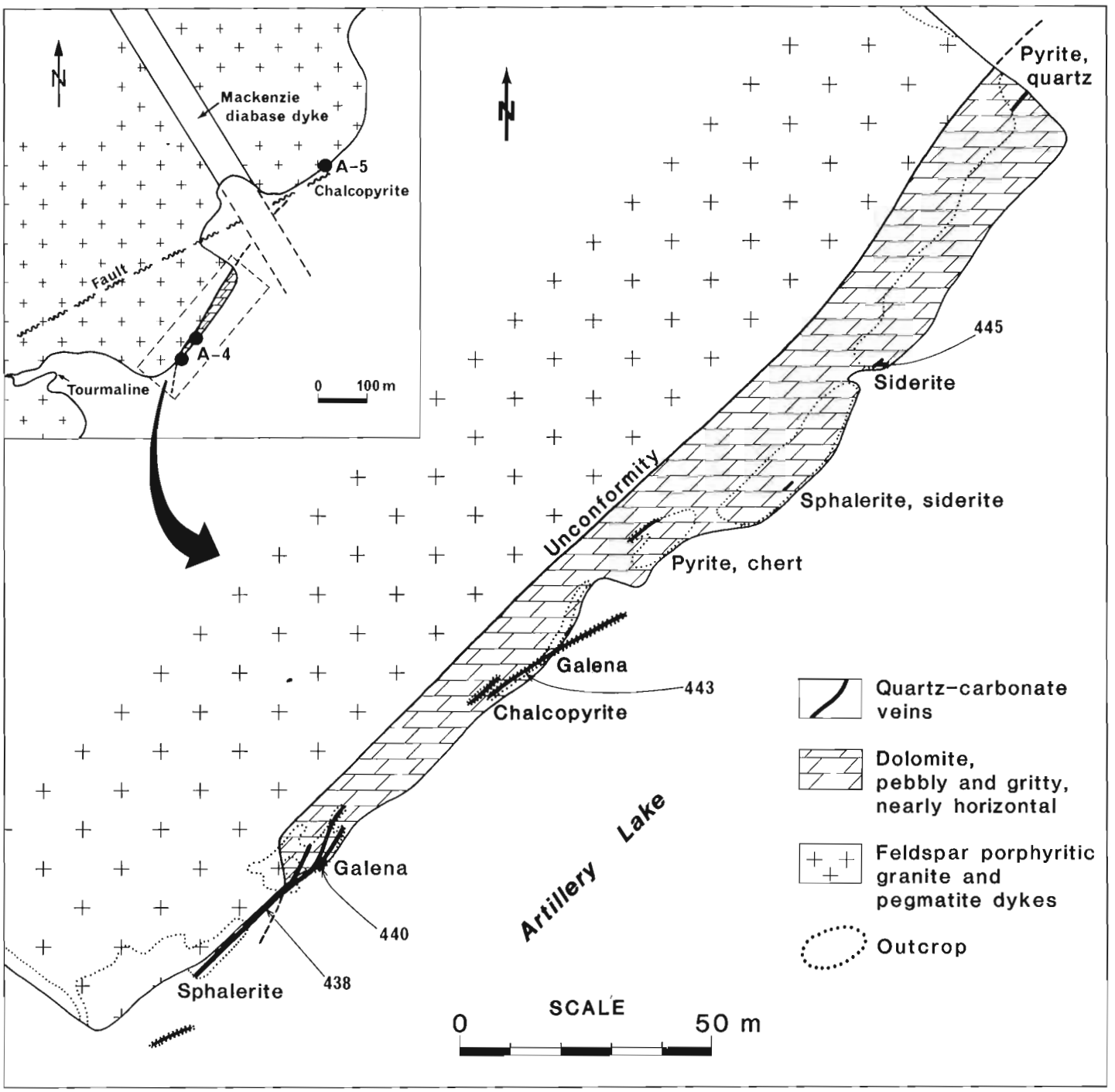

Figure 4.2. *Plan of showing A-4, Artillery Lake, District of Mackenzie (63°03'44"N; 108°06'38"W).*

basement granite. Folinsbee (1952) described the dolomitic exposures at showing A-4 to be in fault contact with the basement granite. He also mentioned a zone of brecciated and carbonate granodiorite and brecciated dolomite, presumably at showing A-4. He described the showing as copper-bearing quartz veins in the fault zone along the contact between granite and dolomite. Detailed mapping by the writer, on the other hand, revealed that nearly horizontal beds of buff coloured dolomite with gritty and pebbly lenses rest unconformably on the granodiorite-granite basement with pegmatite dykes (Fig. 4.2). The granitic rocks at the unconformity are friable for a few metres below it. They contain dolomitic material interstitially, and are cut by numerous dolomitic veins which are up to 25 cm thick and subhorizontal, nearly parallel to crudely defined foliation in the granitic rocks. The dolomitic veins cut the steeply dipping pegmatite veins and are in turn cut by cherty and vuggy coarse quartz veins that are commonly localized along the margins of dolomitic veins. The dolomite and quartz veins also cut the dolomite beds. The abundance of veins may have given an impression of the fault zone mentioned by Folinsbee.

Southwest of showing A-4, shore outcrops of basement granite have some joints and open fractures filled by silty and sandy dolomitic material that has nearly horizontal stratification, indicating their proximity to the unconformity.

Structure. The available structural data indicate that the Artillery Lake formation is nearly horizontal on the northwestern shore of the lake, dips gently to moderately to the southeast with minor open folds on the islands, and is highly variable in attitude in the brecciated zone along the southeastern boundary, as illustrated in cross-section of Figure 4.1. Preserved thickness of the formation is probably in the order of 150 m. The brecciated zone is 1 to 2 km wide and is exposed on Crystal Island, on the islands to the southwest, and also on the southeastern shore of Artillery Lake. The brecciated blocks vary from a few centimetres to several metres in length, and variations in attitude of bedding at many places indicate the presence of much larger blocks in a megabreccia.

South of Crystal Island, a fault trending northeast truncates the Artillery Lake formation. The granitic basement on the southeast side of the fault is predominantly pegmatitic. The fault is marked by an abundance of quartz veins trending parallel to it, and containing fragments of granite, pegmatite and dolomite. Granitic rocks adjacent to the veins have some hematitic red colouration. The fault is parallel to the northeast-trending McDonald Fault system on the East Arm of Great Slave Lake and is therefore interpreted as part of the system (Reinhardt, 1969; Hoffman et al., 1977; Gandhi and Loveridge, 1982). Topographically the most prominent fault (over 300 km long) of the system is located 5 km to the southeast of the fault that truncates the Artillery Lake formation (Fig. 4.1).

Galena-sphalerite-chalcopyrite occurrences

Showings A-1 to A-11

A-1. A quartz vein on the east shore of Crystal Island is up to 30 cm wide and over 5 m long, and contains abundant coarse honey-coloured sphalerite, pyrite and minor galena, chalcopyrite and calcite. Fragments of dolomite occur in the vein. The vein is steep and trends northeast. Subsidiary veins in the vicinity are rich in galena. Approximately 50 m to the southwest along the shore there is a pod approximately 0.5 x 0.5 m in area, that contains quartz, spherulitic pyrite up to 3 cm in diameter with fibrous radiating crystals, and aggregates of black vitreous pyrobitumen. The host dolomite is brecciated on a large scale with fragments over a metre long. A galena and a sphalerite sample from this showing contained 360 and 67 ppm silver respectively. In comparison, seven other samples of these minerals from showings A-2, A-4, A-6, A-7 and A-11 contained between 28 and 92 ppm silver.

A-2. This showing is at the end of a small bay 150 m from A-1; the two may represent parts of a larger vein system. Irregular veins up to 15 cm thick at showing A-2 contain large clusters of coarse galena, quartz, minor sphalerite pyrite, calcite, and traces of chalcopyrite. The veins are commonly steep, and up to several metres long. They have a general northeasterly trend, but are at low angles to each other and at places they coalesce. The host dolomite is buff- and tan-weathering with beds and lenses that are sandy and pebbly, containing quartz and dark grey argillaceous lensoid pebbles. Bedding is variable in attitude due to brecciation. Dolomitic dykes and pyrite-rich veins and pods are common in the host rock. The latter are up to 25 cm wide and contain spherulitic pyrite up to 2 cm in diameter, with radiating fibrous crystals, and also black vitreous pyrobitumen aggregates up to 3 cm long and a centimetre wide. The galena-bearing veins cut them.

South-southwest of showings A-1 and A-2 on Crystal Island there are a few minor occurrences of galena and chalcopyrite in bedrock and of sphalerite with pyrobitumen in locally derived rubble.

A-3. A chalcopyrite aggregate 5 x 3 cm on surface, occurs in a coarse quartz vein which is part of a stockwork of cherty to coarse quartz veins in buff-and tan-weathering dolomite. Some pyrite and calcite are present. A few chalcopyrite grains and aggregates occur elsewhere in the stockwork and in rubble.

A-4. This is the largest of the occurrences reported here, and was mapped in detail (Fig. 4.2). The veins are steep, en echelon, sinuous and up to 1 m wide. Galena, sphalerite and chalcopyrite vary in relative abundance along strike of the veins. At the southwest end of the showing area, a coarse quartz vein carries aggregates of very coarse dark brownish grey sphalerite, up to 4 cm long, for most of its 45 m strike length. Near its northeast end, where it bifurcates (sample locality 440, Fig. 4.2) it contains scattered crystals of galena approximately 1 cm to a side. The dolomite wallrock here is altered to a medium grained aggregate of carbonate and quartz for a few centimetres from the vein. Near the centre of the showing area (sample locality 443) two chalcopyrite-pyrite-quartz veins are prominently exposed for about 10 m strike length. Folinsbee (1952) described them as two parallel quartz veins 0.3 m wide and 2.3 m apart and traceable for 107 m, with chalcopyrite in vugs of banded comb-quartz veins. He, however, did not report the presence of galena and sphalerite bearing veins that occur in their vicinity. For example, the southeastern of the two chalcopyrite-rich veins contains some galena crystals to the northeast (sample locality 443) and extends farther northeast for over 30 m below the lake. Quartz-pyrite veins are common to the northeast for 150 m, as described by Folinsbee. They include a rare vein of red chert grading to white quartz, and cut by a dolomite vein. In addition, there are a few veins containing aggregates of coarse siderite cystals up to 2 cm long with minor dark grey sphalerite, pyrite and chalcopyrite. Siderite is brownish white on fresh surface and weathers to dark red-brown.

The showing thus has a system of veins whose mineralogical variation reflects a complex history of formation and conditions favouring some lateral and probably vertical zoning, at the unconformity between granitic basement and dolomitic beds.

A-5. A coarse quartz vein approximately 15 cm wide and exposed for 5 m strike length contains coarse aggreates of chalcopyrite and pyrite up to 8 cm wide. It is vertical and trends northeast and is located on strike with the chalcopyrite-rich veins of showing A-4 approximately 300 m to the southwest (Fig. 4.2 inset). Subsidiary veinlets are present in its vicinity. Younger, barren coarser quartz veins cut the chalcopyrite-bearing veins. The veins are surrounded by boulders and thin overburden on the lake shore, and their wall-rock is differentially eroded away at the exposure.

A-6. Coarse galena-rich quartz veins up to 2 cm thick, and also coarse sphalerite-rich quartz veins occur in dolomite and dolomite sandstone with abundant rusty weathering pyritic pods. Galena cubes are up to 1 cm to a side. Minor pyrite and calcite are associated with them. The veins are irregular, generally steep, and are exposed over a 25 m long northeast trending zone.

A-7. Coarse galena aggregates with quartz and minor pyrite, sphalerite, chalcopyrite and calcite occur in veins that are a few centimetres wide. The veins are in tightly folded easterly trending Archean metasediments that are cut by pegmatites, and overlain by remnants of gritty dolomite. They are irregular with a general northeasterly trend and are exposed in a 15 m long zone. The metasediments and pegmatites are also cut by nearly horizontal dolomitic veins. The galena-rich veins are younger than the dolomitic veins and patches.

A-8. Sphalerite-bearing quartz veins are sparsely distributed at two localities 220 m apart, in highly folded, easterly trending Archean metasediments that are cut by dolomitic veins. The sphalerite-bearing veins are a few centimetres wide and several metres long, and contain variable amounts of coarse, resinous yellow to brown sphalerite. Quartz ranges from thinly laminated agate to coarse crystals. Pyrite and calcite are present in small amounts. The veins are younger than the dolomitic veins as well as the massive pyrite-quartz veins and aggregates that cut them. They are irregular with general northeasterly trends.

A-9. Veins here are generally similar to those at showing A-8 located 550 m to the southwest, except for the presence of galena crystals up to 4 mm to a side that occur locally in the veins. The host rocks are similar to those at showing A-8.

A-10. Nearly horizontal veins of thinly laminated agate, with layers of fine to medium grained pyrite and sphalerite occur in basement granite with local gneiss zones. The basement rocks are cut by dolomite veins that indicate proximity to dolomite of the overlying Artillery Lake formation. One dolomitic vein is up to 2 m wide, vertical, and trends northeast.

The sphalerite-bearing veins are up to 25 cm thick and several metres long. Their nearly horizontal layering reflects repeated successive deposition of thinly laminated agate, sphalerite and pyrite. Some fragments of an earlier sequence are covered by a later sequence. The agate laminae are a fraction of a millimetre to a millimetre or so thick and are grey, light grey and white. They are continuous even in some layers showing irregular folds or domal structures up to a centimetre in diameter. Thin sections show fine grained, acicular quartz crystals, parallel and perpendicular to lamination in alternate layers. Medium to coarse grained sphalerite occurs in layers and in aggregate at irregularities of agate layers. Pyrite forms more continuous layers up to 2 mm thick adjacent to the sphalerite aggregates and layers. Pyrite also occurs as irregular aggregates and as abundant disseminations in a few cherty layers. Coarse quartz occurs between some pyrite layers and also as irregular patches and veins with fragments of layered material.

A-11. A vein here is similar in character to those at showing A-10. It is nearly horizontal, up to 25 cm thick and several metres long and occurs in medium grained hornblende granite. The layered veins of showings A-10 and A-11 do not contain visible galena but samples from them contained 726 and 2090 ppm lead, and a small quantity of galena was separated in laboratory from the sample of showing A-11.

Discussion

Association of galena and sphalerite with platform carbonate rocks is common, and the occurrences at Artillery Lake define such a metallogenic district. The occurrences are of vein-type and differ morphologically from the well known Mississippi Valley-type deposits that are stratigraphically controlled e.g. the Pine Point deposits in Devonian strata located approximately 400 km southwest of Artillery Lake. The latter deposits are epigenetic, precipitated from low temperature hydrothermal solutions in open spaces with some replacement of host rocks in structurally passive regions (Jackson and Beales, 1967; Ohle, 1980; Anderson and Macqueen, 1982). The ground preparation for these deposits was by solution along fractures and by karsting, further modified by ingress of mineralizing solutions. The vein-type occurrences of Artillery Lake display some textures that are similar to those common in the Mississippi Valley-type deposits. Thus in general they are comparable to the latter from the stand point of deposition of metals from solutions. On the other hand, the location of most of them at and below an unconformity with crystalline basement implies a different set of constraints. In terms of their geological setting, the Artillery Lake occurrences closely resemble galena-sphalerite-barite veins associated with the Helikian Sibley Group in Ontario (Franklin and Mitchell, 1977), and the Artillery Lake formation is similar to the lower part of Aphebian Mistassini Group in Quebec, which also hosts small occurrences of galena and sphalerite (Chown and Caty, 1973; Franklin et al., 1983, p. 31).

Paleoweathering and alteration of basement below the Artillery Lake formation were observed at showing A-4 as described earlier and also at a few other places. The regolithic zone resembles, although it is not as well developed or exposed, the Aphebian Mistassini regolith developed on Archean basement and characterized by dolomitization, and also by veins of dolomite, chert and anthraxolite-quartz-calcite-pyrite, which are controlled by rectangular vertical and horizontal joints (Chown and Caty, 1983). The Mistassini regolith, according to Chown and Caty (1983), was altered during trangressive intertidal to supratidal carbonate formation. They interpreted the carbonate deposition to have occurred in a sabkha environment in evaporitic conditions, which evolved from more temperate climate prevalent at the time of regolith formation. At Artillery Lake, similar conditions appear to have prevailed. Some local transportation and redeposition of the Aphebian regolith occurred, as reflected by sandy and pebbly lenses in basal beds of the Artillery Lake formation. The orthoquartzite lenses elsewhere in the formation however represent mature sediments derived from predominantly granitic Archean terrane of low relief.

The pyrite-quartz(+pyrobitumen) veins and pods, dolomite veins, and numerous barren quartz veins are believed to have developed during various stages of diagenesis of the Artillery Lake formation. The younger

galena-sphalerite-chalcopyrite-bearing veins occupy tensional fractures formed probably by gentle warping along northeast-trending axes and by opening and reactivation of basement fractures and faults due to minor structural adjustments in the basin. The galena-sphalerite-bearing veins on Crystal Island post-date brecciation of the Artillery Lake formation. The large-scale brecciation along the east shore of the island and to the southwest is younger than the veins regarded as diagenetic, and differs from the 'synsedimentary' brecciation and redeposition of dolomitic fragments in some beds and lenses of the formation.

Origin of the larger scale breccia is not known with certainty at present. The breccia may be sedimentary and/or of solution collapse type. It lacks evidence for shearing and compression. This absence of compressive stress is also indicated by the character of pyrobitumen from showing A-2. It has low atomic H/C ratio (0.20) typical of 'anthraxolite' rank but its reflectance values put it in much lower 'impsonite' rank (below 'shungite'), according to a study undertaken at the Institute of Sedimentary and Petroleum Geology in Calgary (L.R. Snowdon and F. Goodzari, personal communication, 1984). These features indicate a considerable thermal effect, but also suggest the absence of any significant shear or compressive stress which would normally tend to align the molecular 'sheets' of fused aromatic carbon atoms. The pyrobitumen is clearly indigenous to the Artillery Lake formation. This implies that the brecciation did not involve shear or compressive stress. The possibility of protection of pyrobitumen from the effects of such a stress, because of its position in quartz-lined vugs, cannot be ruled out but it seems highly unlikely that the applied stress was not transmitted to the pyrobitumen and associated spherulitic pyrite, given the irregularities of the aggregates.

Further studies of pyrobitumen and of fluid inclusions in vein minerals from Artillery Lake are planned to determine the temperatures attained. It may be noted in this regard that the temperature range of formation of Mississippi Valley-type deposits is 80 to 200°C (Anderson and Macqueen, 1982), and in the case of pyrobitumen associated with the Pine Point deposits, Macqueen and Powell (1983) proposed that the thermal effects are due to hydrothermal solutions that formed the deposits, rather than due to burial. For the Artillery Lake occurrences, mineralization temperature was clearly too low to affect the K/Ar isotopic equilibrium in the host Archean metasediments and pegmatites, as is the case with occurrences associated with the Sibley Group (Franklin and Mitchell, 1977).

Two possible sources of metals in the veins are the basement rocks and the shales in the Artillery Lake formation. Galenas from the veins show variations in radiogenic lead component that may reflect the Archean basement source. (Roscoe, 1984, and personal communication, 1984). Furthermore most of the occurrences are localized at and near the unconformity, and are found in the formation as well as in the basement. For the Mississippi Valley-type deposits most workers favour shales deposited in the deeper parts of the basin as sources of the metals, such as proposed by Jackson and Beales (1967) for the Pine Point deposits. Some shale beds do occur in the Artillery Lake formation. It is probable that more shales were deposited in the Artillery basin, most likely to the southeast, and are now largely eroded due to uplift. The shale source however is speculative in contrast to the basement source for the reasons given above. The source of sulphur on the other hand must be sought in the Artillery Lake formation, because low solubilities of Pb and Zn in the presence of reduced sulphur (H_2S or HS^-) do not permit their transport together in significant quantities in ore-forming solutions. This chemical constraint has led most workers to invoke an endogenous source of sulphur for the Mississippi Valley-type deposits (Anderson and Macqueen, 1982). It is believed to have filtered in as H_2S derived from nearby evaporites where it was produced by sulphate-reducing bacteria, possibly in the presence of petroleum.

On the basis of the above discussion it is postulated here that heated meteoric waters rising from depth leached metals from the basement, and deposited them in open fractures and cavities at and near the unconformity by reaction with H_2S entrapped in the Artillery Lake formation.

Guides to exploration

The newly discovered occurrences at Artillery Lake illustrate the type of exploration target that may be present in this type of Slave Province terrane. In the particular case of the Artillery Lake sector, the occurrences described here define a new metallogenic district, and its characteristics may have application in similar terranes outside the proposed park area. Guides to exploration include the common northeast trend of the vein zones and the proximity to the unconformity. Host fracture systems, significant sulphide-rich occurrences and associated barren pyrite-rich veins and pods should be readily detectable by geophysical methods. Most of the prospective area is covered by the lake, but the lake is generally shallow and hence amenable to exploration. In particular, lake sediment geochemical approaches may be valuable in target definition. The possibility of stratabound deposits typical of the Mississippi Valley-type deposits must also be considered because vein-type occurrences are associated with them in some districts.

Conclusions

New discoveries of galena-sphalerite-chalcopyrite-bearing veins at 11 widely separated localities in 40 x 7 km area define a metallogenic district in an Aphebian platform carbonate environment. The occurrences are localized in tensional fractures and cavities at an unconformity with the predominantly granitic Archean basement and in a breccia zone formed by solution collapse. They were deposited by low temperature hydrothermal solutions of meteoric origin that leached metals from the basement and reacted with H_2S entrapped in the Aphebian sediments. The district presents interesting exploration possibilities.

Acknowledgments

The writer was ably assisted in mapping and prospecting by Dave Broughton. Interest and encouragement provided by S.M. Roscoe and F.W. Chandler of the Geological Survey of Canada is greatly appreciated. Discussions with a number of other members of the Geological Survey of Canada have been valuable, however the opinions expressed here are the writer's own.

The manuscript was critically read by D.F. Sangster and S.M. Roscoe of the Geological Survey of Canada.

References

Anderson, G.M. and Macqueen, R.W.
1982: Ore deposit models – 6. Mississippi Valley-type lead-zinc deposits; Geoscience Canada, v. 9, no. 2, p. 108-117.

Chown, E.H. and Caty, J.L.
1973: Stratigraphy, petrography and paleocurrent analysis of the Aphebian clastic formations of the Mistassini-Otish basin; Geological Association of Canada, Special Paper 12, p. 51-71.

1983: Diagenesis of the Aphebian Mistassini regolith, Quebec, Canada; Precambrian Research, v. 19, p. 285-299.

Franklin, J.M. and Mitchell, R. H.
1977: Lead-zinc-barite veins of the Dorion area, Thunder Bay District, Ontario; Canadian Journal of Earth Sciences, v. 14, no. 9, p. 1963-1979.

Franklin, J.M., Roscoe, S.M., Loveridge, W.D., and Sangster, D.F.
1983: Lead isotope studies in Superior and Southern Provinces; Geological Survey of Canada, Bulletin 351, 60 p.

Folinsbee, R.E.
1952: Walmsley Lake, District of Mackenzie, Northwest Territories; Geological Survey of Canada Map 1013A, with descriptive notes, scale 1 inch to 4 miles.

Gandhi, S.S. and Loveridge, W.D.
1982: A Rb-Sr study of the Et-Then Group basalts, Great Slave Lake, District of Mackenzie; in Rb-Sr and U-Pb Age Studies, Report 5; in Current Research, Part C, Geological Survey of Canada, Paper 82-1C, p. 155-160.

Hoffman, P.F., Bell, I.R., Hildebrand, R.S., and Thorstad, L.
1977: Geology of the Athapuscow Aulacogen, East Arm of Great Slave Lake, District of Mackenzie; in Report of Activities, Part A, Geological Survey of Canada, Paper 77-1A, p. 117-129.

Jackson, S.A. and Beales, F.W.
1967: An aspect of sedimentary basin evolution: The concentration of Mississippi Valley-type ores during late stages of diagenesis; Canadian Petroleum Geology Bulletin, v. 15, p. 383-433.

Macqueen, R.W. and Powell, T.G.
1983: Organic geochemistry of the Pine Point lead-zinc ore field and region, Northwest Territories, Canada; Economic Geology, v. 78, no. 1, p. 1-25.

Ohle, E.L.
1980: Some considerations in determining the origin of ore deposits of the Mississippi Valley-type: Part II; Economic Geology, v. 75, p. 161-172.

Reinhardt, E.H.
1969: Geology of the Precambrian rocks of Thubun Lakes map-area in relationship to the McDonald Fault system, District of Mackenzie; Geological Survey of Canada, Paper 69-21, 29 p.

Roscoe, S.M.
1984: Lead-isotope dating of galena-bearing veins in dolomite at Artillery Lake, Northwest Territories and Mistassini Lake, Quebec; Geological Association of Canada – Mineralogical Association of Canada, Program with abstracts, v. 9, p. 101.

Tyrrel, J.W.
1901: Report on an exploratory survey between Great Slave Lake and Hudson Bay, Districts of Mackenzie and Keewatin; Department of the Interior, Canada, Bulletin 12, 329 p.

Wanless, R.K., Stevens, R.D., Lachance, G.R., and Rimsaite, R.Y.H.
1965: Age determinations and geological studies, Part I Isotopic ages, Report 5; Geological Survey of Canada, Paper 64-17, 126 p.

Wright, G.M.
1952: Reliance, District of Mackenzie, Northwest Territories (map and descriptive notes); Geological Survey of Canada, Paper 51-26.

1957: Geological notes on eastern District of Mackenzie; Geological Survey of Canada, Paper 56-10.

1967: Geology of the southeastern barren grounds, parts of the District of Mackenzie and Keewatin (Operations Keewatin, Baker, Thelon); Geological Survey of Canada, Memoir 350, 91 p.

5. QUANTITATIVE DETERMINATION OF ^{210}Po IN GEOCHEMICAL SAMPLES

Project 780015

W. Dyck and Q. Bristow
Resource Geophysics and Geochemistry Division

Dyck, W. and Bristow, Q., Quantitative determination of ^{210}Po in geochemical samples; in Current Research, Part B, Geological Survey of Canada, Paper 84-1B, p. 41-46, 1984.

Abstract

To test the usefulness of ^{210}Po in soils as a means of detecting buried U mineralization, methods for the determination of ^{210}Po were investigated and adapted for routine production of ^{210}Po data from geochemical samples.

A number of conditions affecting autodeposition and detection of ^{210}Po were investigated. The optimum area of deposition with a 450 mm^2 solid state detector was found to be 300 mm^2. Convenience dictated room temperature overnight deposition times, although increased temperature increased speed and efficiency of deposition. A clear inverse relationship was observed between volume of solution and deposition efficiency with stirring times of less than 2 hours.

For routine analysis, soil and rock powders were dissolved by leaching 1 g samples in teflon beakers successively with conc. HNO_3, HF, and HNO_3-$HClO_4$, evaporating the solution to dryness between leaches, and taking the residue up in 20 mL 0.5 M HCl. The ^{210}Po was deposited on 19 mm diameter Ni discs and counted with an alpha spectrometer system employing 450 mm^2 ruggedized surface barrier detectors.

The method achieved 90% recovery of ^{210}Po from solution and a detection efficiency of 30%. With a counting time of 3 hours, the method is capable of detecting 0.2 pCi of ^{210}Po per gram of sample.

Résumé

Afin de vérifier si l'on peut utiliser le ^{210}Po dans les sols pour détecter une minéralisation d'U profonde, on a étudié des méthodes de détermination du ^{210}Po que l'on a adaptées à la production courante de données sur le ^{210}Po à partir d'échantillons géochimiques.

On a étudié un certain nombre de conditions influant sur la mise en place spontanée et la détection du ^{210}Po. Des essais effectués à l'aide d'un détecteur à semiconducteurs de 450 mm^2 ont établi que la surface optimale de mise en place était de 300 mm^2. La température de la pièce et les temps de sédimentation pendant la nuit ont été fixés en se basant sur des raisons d'ordre pratique, bien que des températures plus élevées entraînent un accroissement de la vitesse et de l'efficacité de mise en place. Les résultats ont établi une nette relation inversement proportionnelle entre le volume de la solution et l'efficacité de sédimentation suite à des périodes d'agitation inférieures à 2 heures.

Dans les analyses de routine, on a dissous des poudres de sol et de roche en lessivant successivement des échantillones de 1 g dans des béchers en téflon dans du HNO_3 conc., du HF, et du HNO_3-$HClO_4$, avec évaporation à sec de la solution entre chaque lavage, et en reprenant le résidu dans 20 mL de HCl 0,5 M. Le ^{210}Po s'est déposé sur des disques de Ni de 19 mm de diamètre. Un spectromètre alpha doté de détecteurs à barrière de surface résistants de 450 mm^2 a servi pour le comptage.

Le recours à cette méthode a permi la récupération de 90 % du ^{210}Po de la solution, avec une efficacité de détection de 30 %. Avec un temps de comptage de 3 heures, la méthode permet de détecter 0,2 pCi de ^{210}Po par gramme d'échantillon.

Introduction

^{210}Po is the last radioactive decay product of the ^{238}U series. Its apparent usefulness as a pathfinder for U mineralization has prompted several commercial laboratories to add ^{210}Po determinations to their list of services for U prospecting. The argument for such a method is based on the fact that ^{210}Po, in theory, can provide an integrated signal of the gaseous, and hence more mobile, decay product ^{222}Rn. The long half-lives of ^{210}Pb and ^{210}Po (22a and 138d, respectively) relative to their gaseous parent, ^{222}Rn (3.8d), ensure that the variations in the Rn flux, due to diurnal and annual-environmental disturbances in the soil, are not reflected in the concentrations of ^{210}Pb and ^{210}Po.

Both Pb and Po are adsorbed strongly in soils and hence are not widely dispersed as a result of chemical weathering. Consequently, there is a slow buildup of these isotopes to equilibrium concentrations with Rn in the soil, the effective equilibration time being about 100 years and, unless weathering patterns change markedly during that time, a stable ^{210}Pb and ^{210}Po signal, independent of diurnal and

seasonal changes, should be observed at any one site. The reason for determining ^{210}Po rather than ^{210}Pb is simple; ^{210}Po is much easier to determine. It plates spontaneously onto metallic discs from solutions, and its 5.4 Mev alpha particle emission can be counted with relative ease with a solid state detector. The determination of ^{210}Pb, on the other hand, requires chemical separation and purification steps, and sensitive beta particle detectors.

Millard (1963) described a method for the quantitative determination of ^{210}Po in minerals, and Smithson et al. (1978) gave procedures for the determination of ^{210}Po in soils, rocks and natural water samples. However, both reports describe procedures involving Ag discs and complex electroplating units which make the procedures expensive and slow. In the Radiochemistry Laboratory of Carleton University, Ottawa, (R.D. Wiles and I.G. de Jonge, personal communiation, 1984) stainless steel discs, coated on one side with an acrylic were tested but pure uncoated Ni discs proved to be more effective for precise analyses. The coating prevents the deposition of ^{210}Po on one side, hence only one side needs to be counted. This latter method was thought to offer a faster less expensive procedure for mass production of ^{210}Po data and was therefore investigated in more detail. Poor ^{210}Po yields and poor analytical precision in preliminary trials led to a more systematic investigation of the factors that were causing these irregularities. The results of these investigations and a quantitative method of analyzing geochemical samples for ^{210}Po are described below.

Apparatus and procedures

In general, methods of determination of ^{210}Po involve bringing the sample into solution, electrodeposition of ^{210}Po onto a metallic disc, and alpha-particle spectrometer counting of the activity with a solid state detector. Analytical precision and accuracy are ultimately determined by the efficiency with which the three above steps are carried out. The counting system, sample preparation procedure, and factors which were found to influence the deposition of ^{210}Po in our experiments are described below.

Alpha spectrometer system

The size of the alpha-particle detector (area, sensitivity, and energy resolution of the active portion of the detector) determines the optimum size of the disc for ^{210}Po deposition, which, in turn, determines to some extent the apparatus and procedures for the dissolution of samples. For this work four 450 mm^2 ruggedized surface barrier detectors inside two ORTEC 576 alpha spectrometer modules were chosen. Each module provides two completely independent channels and each channel includes a vacuum chamber, a detector voltage source, a preamplifier, a biased amplifier, a test pulser, and a discriminator. The vacuum chamber accommodates a surface barrier detector and a sample holder. During counting, a pressure of 0.2 mm Hg or less is maintained with a pump and a cold trap between pump and chamber. Signals from the four detectors are fed to a 1024 channel pulse height analyzer consisting of a Nuclear Data model ND 570 analogue to digital converter interfaced to a Texas Instruments model 960-B mini computer. A four channel router (D.S. Davidson Co. model 904 A) is interfaced to the analogue to digital converter so that signals from the four detectors are acquired as four separate 256 channel spectra in the computer memory. Multichannel analysis software developed for the system (Bristow, 1975) allows the spectra to be processed in such a way as to provide an accurate measure of the ^{210}Po activity in terms of the count rate in the 5.30 Mev peak of the alpha particle emission.

The only other spectral peak likely to interfere with this measurement would be one at 5.34 Mev due to alpha emission from ^{228}Th. Its position is shown in Figure 5.1. However, the comparatively high resolution of the system (30 kev @ 5 Mev), the weak intensity of the 5.34 Mev emission, and the achievement of a high degree of separation of ^{210}Po from virtually all other trace elements in the plating process, all combine to reduce potential interference from ^{228}Th to negligible levels.

The energy discrimination of the solid state detectors is illustrated in Figure 5.1. The ^{226}Ra and ^{210}Po peaks were obtained from a 36 year old National Bureau of Standards standard ^{226}Ra solution. 200 pCi of ^{226}Ra and its decay products were baked onto a Ni disc by evaporating 0.10 mL of a 2000 pCi/mL ^{226}Ra solution and counted immediately. In addition to the large separation of ^{210}Po from ^{226}Ra, it is noteworthy that the areas under the peaks of these two nuclides reflect fairly well the age of the solution, considering the dependence of the growth of ^{210}Po on the growth of the 22 year half life ^{210}Pb. If ^{210}Pb had had enough time to equilibrate with its long lived parent ^{226}Ra, its daughter, ^{210}Po, would have given the same activity as ^{226}Ra.

The ^{241}Am peak shown in Figure 5.1 and the counting efficiency of the solid state detectors was determined with a thin calibrated ^{241}Am source. The efficiency was found to be 29.6%, varying slightly from detector to detector and with time. The calibrated ^{241}Am source, was positioned 4 mm from the detector surface for the determination of the counting efficiency. All subsequent measurements were carried out at the same detector-sample distance and the counting efficiency for the discs with ^{210}Po was therefore also assumed to be 29.6%, because the energies of the alpha particles from these two elements are similar. The counting efficiency, the recovery of ^{210}Po from solution, and the background and sample counts determine the detection limit of the method. Background counts of the detectors were of

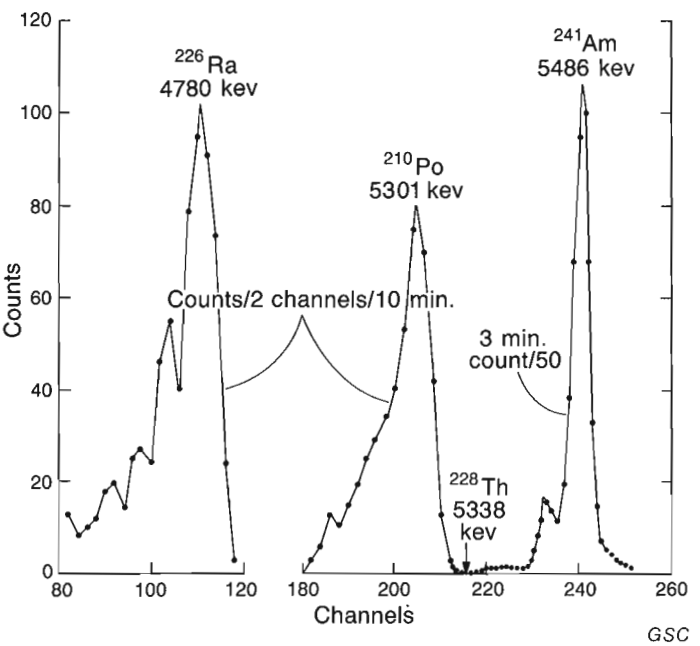

Figure 5.1. Energy discrimination of the alpha particle detectors.

the order of 1 count per hour but would occasionally rise to 6 or 10 counts per hour after a highly radioactive sample had been in the chamber. Apparently some radioactive atoms were able to jump the 4 mm gap between sample disc and detector, perhaps as a result of alpha recoil, and be retained there. However, cleaning the detector surface with soap, water and alcohol removed most of this contamination. In practice the detection limit is determined by the available counting time. For example, a sample with 1 pCi/g of ^{210}Po would give rise to about 0.6 cpm in the system described here. To accumulate 100 counts for a measurement uncertainty of 10% would therefore require a counting time of 3 hours. To just detect 1 pCi of ^{210}Po with a 30% certainty would require a 15 minute count.

Factors affecting the recovery of ^{210}Po from solution

The choice of leaching agents, conditions of electrodeposition, and counting efficiency and stability of the counting system all affect precision and accuracy. Published accounts of investigations of various factors (Millard, 1963; Smithson et al., 1978) show that ^{210}Po deposits spontaneously from a weak HCl solution onto metallic discs such as Ag, Ni, Pt, and stainless steel. This fact makes the separation of ^{210}Po easy but also necessitates special care in handling the solution during dissolution of the sample. Samples should not be dissolved in Pt ware because some ^{210}Po will plate onto it. Teflon or styrene containers are preferred for handling solutions. Large amounts of Fe interfere with the autodeposition of ^{210}Po, but its interference can be minimized by reducing Fe^{3+} to Fe^{2+} with ascorbic acid or hydrazine dihydrochloride. In this study, tests with ascorbic acid did not affect the analytical precision, but the presence of HNO_3 gave more erratic results. As described below, the method and reagents used for leaching and deposition of ^{210}Po had a marked effect on the recovery of ^{210}Po.

Initial experiments with stainless steel discs coated on one side with acrylic indicated rather slow and incomplete deposition of ^{210}Po. Obviously a more thorough investigation was needed to determine a more reproducible method of deposition. A number of experiments were therefore carried out with 40 pCi aliquots of ^{210}Po to determine the efficiency of autodeposition from solution under different conditions. The results are plotted in Figure 5.2 as the ratio of observed to expected counts, allowing for the counting efficiency of the detectors. The conditions of deposition for each curve are summarized in the figure legend.

Curve 3 in Figure 5.2A was obtained with conditions finally chosen for routine analysis for ^{210}Po, i.e. 300 mm^2 uncoated Ni discs shaken overnight at room temperature in 20 mL 0.5 M HCl. Evidently 100 mm^2 discs achieve similar results but are more difficult to prepare; discs were prepared from sheet metal, 316 stainless steel or Ni 200, using a standard chassis punch. Increasing the temperature also improved plating efficiency and cut down plating time, but was not found to be practical. Hot plates with magnetic stirrers served well for individual samples but are not designed for large batches of samples. As the results in Figure 5.2B and 5.2C show, the acrylic coating not only slowed down the deposition of ^{210}Po but also cut down on the efficiency of deposition. The reason for this is not clear. One possibility is that some of the coating dissolved and formed a stable complex with ^{210}Po. The difference between stainless steel and Ni discs is hardly noticeable, although all the tests combined suggested that Ni gave somewhat better reproducability. The retarding effect of the acrylic coating is even more evident in curves C1 and C2 and curves D1 and D2 (Fig. 5.2). These results indicate that for the highest yield, and hence best precision and accuracy, the deposition of ^{210}Po should be carried out in as small a volume as possible at a temperature as high as possible.

Even under optimum conditions, as determined from the investigations of the factors affecting the efficiency of deposition of ^{210}Po, analytical precision was still somewhat lower than predicted from the random nature of radioactive decay. The authors believe that temperature was the main cause of this uncertainty. As curve D2 in Figure 5.2 indicates, considerable increase in yield is observed when the temperature rises from room temperature, 22°C, to above 30°C. Since such temperature fluctuations were observed in the laboratory in the summer, it is conceivable that the greater than random fluctuations in yield were in fact due to these temperature variations. Also, as noted above, the metallic surfaces displayed some passivity when parts of the disc were coated with acrylic. Another source of error could therefore be due to variations in active sites on the discs as a result of improper cleaning methods. Finally, the fact that exceedingly small quantities of ^{210}Po were used, may also, in an indirect way, have led to imprecision. 40 pCi of ^{210}Po is only about 10^{-14} g or 10^6 atoms of ^{210}Po. Any variations in electrolyte, type and cleanliness of discs and containers, could affect the distribution of ^{210}Po between container walls, solution, and disc. The strong time and temperature dependence of the deposition process suggests that it takes a fairly long time for a ^{210}Po atom to reach the surface of a disc and diffuse through the diffusion layer of the electrolyte associated with solid-liquid interfaces (Glasstone, 1946, p. 1026).

Recommended analytical procedure

Dissolve 1 g of powdered sample in a 100 mL teflon beaker by means of the following six cycles of acid addition and evaporation to dryness: 5 mL of conc. HNO_3 (two cycles); 5 mL of HF (two cycles); 5 mL of a 3:2 mixture of conc. HNO_3 and conc. $HCLO_4$. To the residue add 5 mL of 0.5 M HCl, warm, and transfer the solution to a 45 mL clear styrene vial (#14 vial, 60 mm by 30 mm diameter with snap-on lid). Rinse the teflon beaker three times with 5 mL aliquots of 0.5 M HCl and add rinses to the sample solution for a final total volume of 20 mL. Add a clean 19 mm stainless steel or Ni disc to the sample solution, snap the lid on the vial, put the vial on a mechanical shaker, and shake overnight. The discs used for the tests described here were prepared from 0.46 mm thick (0.018 inch) sheet metal using a chassis punch commonly found in electronic shops. Prior to plating, the discs were cleaned with a strong soap solution in an ultrasonic bath and rinsed with distilled water. By placing the side of the disc with the protrusion in the centre (left there by the punch) on the bottom of the vial, the disc was free to rock and thus permit plating on the underside also without having to suspend the disc in the solution.

The above method lends itself to the preparation of many samples simultaneously, limiting factors being the number of teflon beakers, size of hot plate, and size of shaker available.

After the deposition of ^{210}Po the discs are rinsed with water, dried in a vacuum dessicator, and counted on both sides, when convenient, in the alpha spectrometer system described above. Large differences were consistently observed between the counts from one side of each disc and the other. Obviously some assymetry exists between the plating efficiency of the two sides although the reason for this is not understood. However, the sums of counts from both sides of replicate samples did not differ significantly, and the asymmetry was therefore not investigated further.

For routine, semiquantitative data the leaching procedure can be simplified to one 10 mL hot 6 M HCl leach. Depending on the type of material, this procedure leaves a small fraction of ^{210}Po in the sample, but is considerably faster. Tests such as the ones shown in Table 5.1 show that

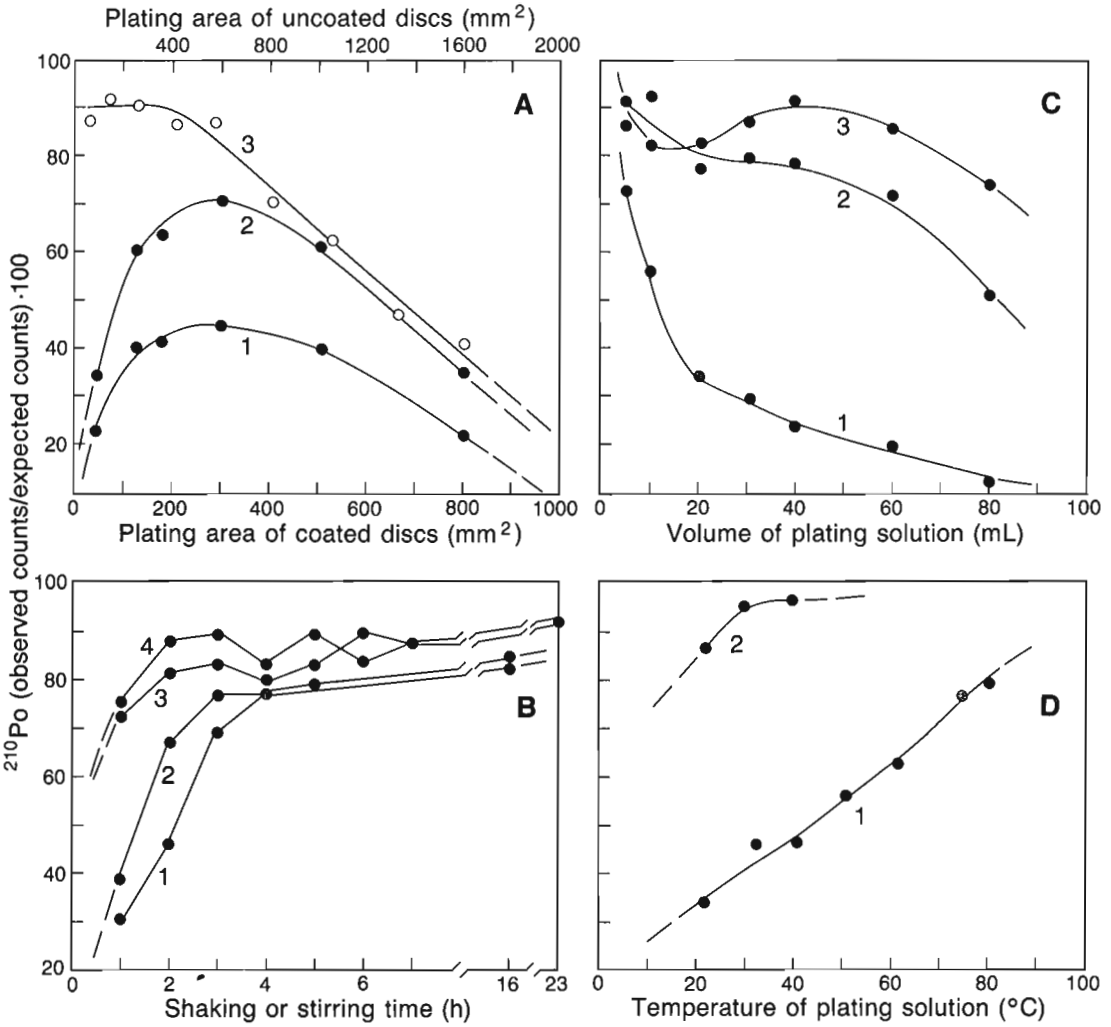

A. *Effect of plating area on plating efficiency:*

1. *Stainless steel discs coated with acrylic, room temperature, stirring time = one hour.*
2. *Same as (1) except that the temperature = 55°C.*
3. *Ni discs, no coating, shaking = 17 hours, room temperature.*

B. *Effect of shaking time on plating efficiency:*

1 and 2. Stainless steel and Ni discs, respectively, coated with acrylic, plating solution = 20 mL, room temperature.

3 and 4. Same as (1) and (2) except that uncoated discs were used.

C. *Effect of volume of plating solution on plating efficiency:*

1. *Stainless steel discs, coated with acrylic, room temperature, shaking time = one hour.*
2. *Ni discs, uncoated, room temperature, shaking time = one hour.*
3. *Same as (2) except shaking time = 18 hours.*

D. *Effect of temperature on plating efficiency:*

1. *Coated stainless steel discs, plating solution = 20 mL, shaking time = one hour.*
2. *Uncoated Ni discs, plating solution = 20 mL, shaking time = one hour.*

Figure 5.2. *The effect of plating conditions on the efficiency of spontaneous deposition of ^{210}Po onto metallic discs.*

Table 5.1. ^{210}Po content of soil samples in pCi/g using two different leaching methods

Soil horizon	N	Hot 6 M HCl leach					Hot conc. HNO_3, HF, and $HClO_4$ leaches				
		Median	Mean	S. Dev.	Min.	Max.	Median	Mean	S. Dev.	Min.	Max.
Forest litter	9	15.7	15.8	4.9	9.6	24.0	24.5	24.0	5.8	16.0	32.0
Ah	9	4.6	5.5	3.8	1.4	12.3	11.0	11.2	5.6	3.9	22.0
Ae	9	0.1	0.4	0.6	0.1	1.7	0.6	0.8	0.8	0.1	2.6
Bf	9	0.3	0.7	1.2	0.1	3.7	0.4	1.0	1.3	0.1	3.9
C	9	0.4	1.7	2.9	0.1	8.1	0.5	2.3	3.8	0.1	11.0

*To convert to Bq/g multiply pCi/g by 0.03657

this percentage is fairly consistent and that good correlation (r = 0.96) is obtained with the more elaborate sample separation techniques. However, the counting step is the slowest step in the whole procedure because of the long counting times required to ascertain background levels of ^{210}Po.

Calibration of method

The overall method is calibrated using a standardized ^{210}Pb/^{210}Po solution or a weak U ore sample with a well known U concentration and known to be in radioactive equilibrium. In the case of the standard solution, different aliquots are added to 1 g samples of silica sand containing negligible amounts of radioactivity and treated in the same manner as the unknown samples so that any bias in the sample preparation is cancelled out. A graph of activity in Bequerels versus counts per minute (Bq vs cpm) is constructed from the standard solutions and used to read off the ^{210}Po content using the net cpm of unknowns. Three such graphs are shown in Figure 5.3. The uppermost graph was obtained with aliquots of a standard ^{210}Pb/^{210}Po solution without silica sand, while the middle graph was obtained with silica sand in the leaching process. This solution was purchased from Amersham Corporation, Oakville, Ontario, a subsidiary of the Radiochemical Centre. An 8% loss in sensitivity is evident on the average; the sensitivity of eight aliquots of the Amersham standard alone was averaging 15.79 ± 0.15 cpm/Bq and with silica sand 14.50 ± 0.27 cpm/Bq. Loss of sensitivity also increases as the ^{210}Po content of the samples decreases. The lowest graph of Figure 5.3 was obtained using two reference U ore samples believed to be in radioactive equilibrium. The apparent loss of sensitivity at very low ^{210}Po concentrations is probably due to the loss of a significant fraction of ^{210}Po by adsorption on walls of the containers in which the sample solutions are handled. The reason for believing that the U ore reference samples are in equilibrium is based on experiments carried out by Grasty and Dyck (1984) with four related U reference ores. These four ores, their measured ^{210}Po content, and true ^{210}Po content, calculated from the accepted chemically certified U content, assuming radioactive equilibrium, are listed in Table 5.2. The measured ^{210}Po content was obtained from the average of eight determinations using the recommended procedure described above and the calibration graph obtained with the Amersham reference solution wth silica sand.

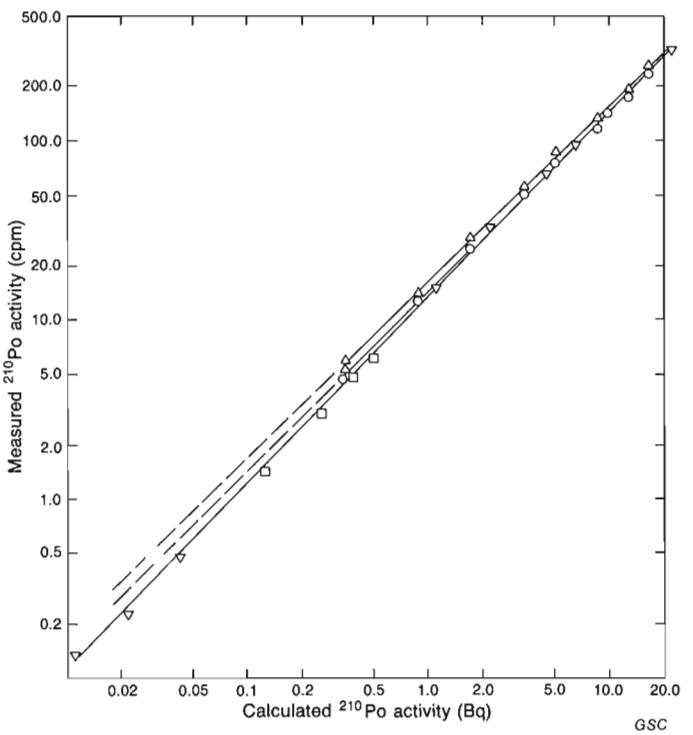

△ - *standard ^{210}Po solution only*

○ - *standard ^{210}Po solution added to 1 g silica*

▽ - *U reference ore DH-1*

□ - *U reference ore DL-1*

Figure 5.3. *Calculated vs measured ^{210}Po activities of an Amersham standardized ^{210}Pb/^{210}Po solution and standard U ore samples.*

Table 5.2. Measured and calculated ^{210}Po concentrations of four certified U reference ores

Ore	Measured activities using the Amersham 210Pb/210Po solution		Calculated activities assuming radioactive equilibrium	
	Bq/g*	pCi/g	Bq/g	pCi/g
DL-1A	1.395 ± 0.037	38.18 ± 1.01	1.432	39.19
BL-2	16.15 ± 0.35	442.0 ± 9.6	15.41	421.8
DH-1A	31.33 ± 0.77	857.5 ± 21.1	32.46	888.4
BL-5	906.8 ± 22.4	24919 ± 613	875.4	23950

*To convert to pCi/g multiply Bq/g by 27.34
To convert to ppm eU (uranium equivalent) multiply Bq/g by 81.011

To illustrate the effect of the two leaching methods described above, the results of analyses of 45 soil samples by the two methods are shown in Table 5.1. In each horizon, where the ^{210}Po concentration is significantly above the detection limit of 0.2 pCi/g, the more severe leaching technique gives significantly higher ^{210}Po values. The significance of the vertical distribution of ^{210}Po in the soil horizons is explained in detail by Dyck (1984). The very high concentration in the uppermost soil layer essentially reflects the fact that most of the gaseous parent of ^{210}Po, ^{222}Rn, escapes into the air before decaying to ^{210}Pb and ^{210}Po. These decay products are then washed out of the atmosphere by rain and snow and are returned to the ground, where they are readily adsorbed onto the particles forming the soil.

Acknowledgments

The authors thank Mr. J.C. Pelchat, Geochemistry Subdivision, Geological Survey of Canada, for carrying out many intricate experiments, and contributing extensively with observations and suggestions to the success of this work.

References

Bristow, Q.
1975: Gamma-ray spectrometry instrumentation; in Report of Activities, Part C, Geological Survey of Canada, Paper 75-1C, p. 213-219.

Dyck, W.
1984: Evaluation of the ^{210}Po method at the Midwest uranium deposit, northern Saskatchewan, Canada; Journal of Geochemical Exploration, v. 20.

Glasstone, S.
1946: Physical Chemistry, 2nd edition, 9th printing; D. van Nostrand Company, Inc., 1320 p.

Grasty, R.L. and Dyck, W.
1984: Radioactive equilibrium in four Canadian uranium ores; in Current Research, Part A, Geological Survey of Canada, Paper 84-1A, p. 53-56.

Millard, H.T. Jr.
1963: Quantitative radiochemical procedure for analysis of polonium-210 and lead-212 in minerals; Analytical Chemistry, v. 35, no. 8, p. 1017-1023.

Smithson, G.L., Dalton, J.L., and Mason, G.L.
1978: The determination of polonium-210; in Radiochemical Procedures for Determination of Selected Members of the Uranium and Thorium Series; CANMET Report 78-22, Energy, Mines and Resources Canada, p. 23-28.

6. RALPH – AN INSTRUMENT TO MONITOR SEABED SEDIMENTS

Project 790036

D.E. Heffler
Atlantic Geoscience Centre, Dartmouth

Heffler, D.E., RALPH – an instrument to monitor seabed sediments; in Current Research, Part B, Geological Survey of Canada, Paper 84-1B, p. 47-52, 1984.

Abstract

RALPH is an instrument designed at the Atlantic Geoscience Centre to study the dynamics of seabed sediments in nearshore and continental shelf waters. The sensors include current meters, a depth gauge and an optical transmissometer. A time-lapse camera takes photographs of the seabed in synchronism with the sensor samples. All the data are logged internally and the system can operate autonomously for more than one month.

RALPH was deployed on the shoreface at Martinique Beach, Nova Scotia, in June 1983 to study a summer-accreting beach. The combination of photographs of the bed and logged data from the sensors offer insight into the formation and stability of various bedforms.

RALPH is being extensively used for nearshore studies and in continental shelf areas of interest to petroleum exploration.

Résumé

RALPH est un appareil conçu au Centre géoscientifique de l'Atlantique pour étudier la dynamique des sédiments sous-marins dans les eaux littorales et celles de la plate-forme continentale. Les capteurs comprennent des courantomètres, une jauge de profondeur et un transmissomètre optique. Une caméra conçue pour les prises de vue accélérées prend des photographies du fond de la mer en synchronisme avec les prélèvements des capteurs. Toutes les données sont enregistrées à l'intérieur et le système peut fonctionner de façon autonome pendant plus d'un mois.

RALPH a été déployé sur l'avant-côte de la plage Martinique (N.-É.) en juin 1983 afin d'étudier l'accroissement par alluvionnement d'une plage en été. La combinaison des photographies du lit et des données enregistrées à partir des capteurs jette un peu de lumière sur la formation du lit et sur la stabilité de ses configurations.

On continue d'avoir recours à RALPH pour les études du littoral et dans les zones de la plate-forme continentale susceptibles de se prêter à l'exploration pétrolière.

Introduction

Development of a unified instrument to study the dynamics of marine sediments was initiated in 1978 at the Atlantic Geoscience Centre. Study of sediment-transport processes required an instrument that could measure multiple oceanographic and sedimentologic variables near the seabed for at least one month. This need resulted in RALPH, an instrument that was ready for field testing by October 1979 (Heffler, 1979). Following significant redesign and addition of sensors, RALPH is today an operational instrument with extensive field use. However, the capabilities of RALPH are still being extended. This paper describes the present configuration of the instrument and illustrates the capabilities of the system with samples of data obtained at Martinique Beach, Nova Scotia.

Overview

RALPH was designed to study, as a single independent instrument, the processes of seabed sediment transport. It is essential that measurements be taken at the same location and synchronized in time. Storm effects are very significant and it is imperative that RALPH be able to continue operation through a strom event as well as tidal cycles. Hence RALPH was designed for long term deployments as a totally autonomous instrument requiring no connection to the shore or a surface vessel. Its area of application ranges from just outside the surf zone to the edge of the continental shelf.

RALPH includes a special purpose low-power computer to control the sensors and handle the data. The computer offers the possibility of preprocessing some of the data and of conditional data logging.

RALPH Sensors

RALPH's sensors include two Marsh McBirney electromagnetic current probes (model 512 OEM) mounted 100 cm and 30 cm above the seabed. Each sensor measures 2 perpendicular components of horizontal current with a time response less than 0.25 second. A Vitran Model 218-12 strain gauge pressure transducer is used to measure water depth, including waves and tidal information. Two units are available, one for shallow water use, and one for deep water. A Sea Tech optical transmissometer with a 25 cm beam is mounted horizontally 50 cm above the seabed. This gives an estimate of sediment suspended in the water column 0.5 m above the bed.

The capabilities of the sensors are summarized in Table 6.1.

The data logger accepts 120 000 16 bit words. Since the error rate has proven to be rather high, the data are stored with redundant formatting. At present about 15 000 samples of the 4 velocity components, pressure, transmission, and time can be stored.

Table 6.1. Summary of sensor capabilities of RALPH

Sensor	Range	Accuracy	Resolution	Noise
Current	± 312 cm/s	1%	0.2 cm/s	0.5 cm/s
Pressure (shallow)	0-25 m	1%	1 cm	2 cm
(deep)	0-200 m (0-300 psia)	1%	6 cm	10 cm
Trans-mission	0-100%	< 1%	< 1%	1%

Photographs of the seabed are taken by a Super-8 (8 mm) movie camera used in the single step mode. A 50 J flash is mounted near the bed for illumination.

The data tape is replayed on a special tape reader which sends the data either to a personal computer or to the Cyber 171 computer at the Bedford Institute of Oceanography. Programs have been written on the Cyber to convert the data to proper units and to generate plots.

Physical structure

RALPH is a tripod-mounted structure which is stable in the presence of horizontal currents and has minimum effect on near-bear flows and sediment transport. A main pressure case, containing the computer, data logging electronics, power supply and camera is mounted 1.5 m above the bed. A flash for the camera is mounted near the bed to give oblique illumination for the photographs. An acoustic relocation pinger and battery pack for the flash are mounted next to the main pressure case. Figure 6.1 illustrates RALPH ready for deployment.

The tripod is constructed of 10 cm aluminum pipe and can be disassembled for shipment. Assesmbled, RALPH stands almost 3 m high, with 3.3 m spacing between its feet. The weight is 100 kg in air and 50 kg in water. Lead ballast weights are inserted into sockets on the feet and add 350 kg of extra weight. These weights can be installed or removed y divers to facilitate handling RALPH from small boats.

The main pressure case is made from 25 cm diameter 0 in. schd. 40) aluminum pipe 75 cm long, with 2 cm thick ıd caps. A 14 cm diameter port on the bottom provides a ımera window. Three 10 cm ports are welded on the top. ıe is a spare; the others provide access for the current eter and pressure gauge connections. All other electrical nnections are on one end cap.

Figure 6.2 shows the inside frame of RALPH. The wer control board includes voltage regulators, sensor itches and connectors for component parts. A special ısing has been constructed to mount the circuit boards for 2 current meters. This is located so the connections are cessible through one of the top ports when the frame is in pressure case.

The data logger in RALPH is a Datel LPS-16 low power ital cassette recorder with a built in 16 channel, 12 bit .logue to digital converter (A/D). The analogue to digital ıverter and recorder sections have been separated by difying the circuit board and both sections are interfaced arately to the computer. The data storage capacity is kbytes and represents one of the major limitations of LPH.

The camera is a Minolta model XL-401 Super-8 movie camera used in the single step mode. This gives 3600 frames on one film cartridge. The image quality is sufficient to determine bedform size, shape and movement. The lens is set to 8.5 mm focal length. The image size is approximately 1 by 1.5 m on the seabed. The camera is mounted at 33 degrees from the vertical but refraction at the window – water interface bends this to 20 degree incidence at the bed. This angle gives a little highlighting to seabed features but does not seriously distort the field of view. The camera shutter speed is 1/50 s and an aperture of f8 is used with ASA 160 Ektachrome film. A 50 J flash is mounted less than 1 m from the bed at an angle of 50 degrees from the vertical.

The power for RALPH is provided by 54 akaline "D" cells cemented to swing-out plates on either side of the camera. These will operate RALPH for 3 months in standby mode and more than one month in full operation. An additional power supply of 21 "D" cells in a separate pressure case operates the light source for more than 5000 flashes.

RALPH contains a custom-built computer featuring low power consumption and rugged construction. Hinged wire wrap boards allow easy access for testing and further development. The processor is an RCA 1802 microprocessor. This processor and all the other electronics are CMOS (Complementary Metal Oxide Semicondutor) components which consume very little electrical power. The entire computer is constructed on three wire wrap boards which contain 2 UART's (Universal Asynchronous Receiver Transmitter or serial port), a dual 8-bit port, 2 hardware multiply/divide chips, a real-time clock, a 2 line by 16 character LCD monitor and 6 byte wide interfaces to the A/D tape recorder unit. The memory includes 10 kbytes of CMOS PROM (Programmable Read Only Memory) and 18 kbytes of CMOS RAM (Random Access Memory). The entire computer requires only 4 mA of electrical currrent.

The computer is connected to a standard terminal through a connector on the end cap. Before deployment, an operator can check various parameters, test all the sensors, and start the program which controls data acquisition. A continuous display of status (time and data logging in progress) is visible on the LCD monitor in the camera window. This can be inspected by SCUBA divers while RALPH is on the bottom.

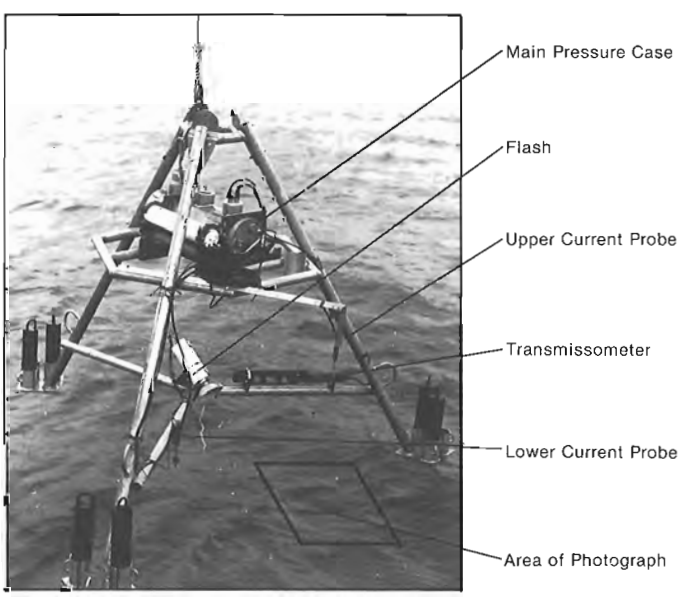

Figure 6.1. *RALPH ready to be deployed.*

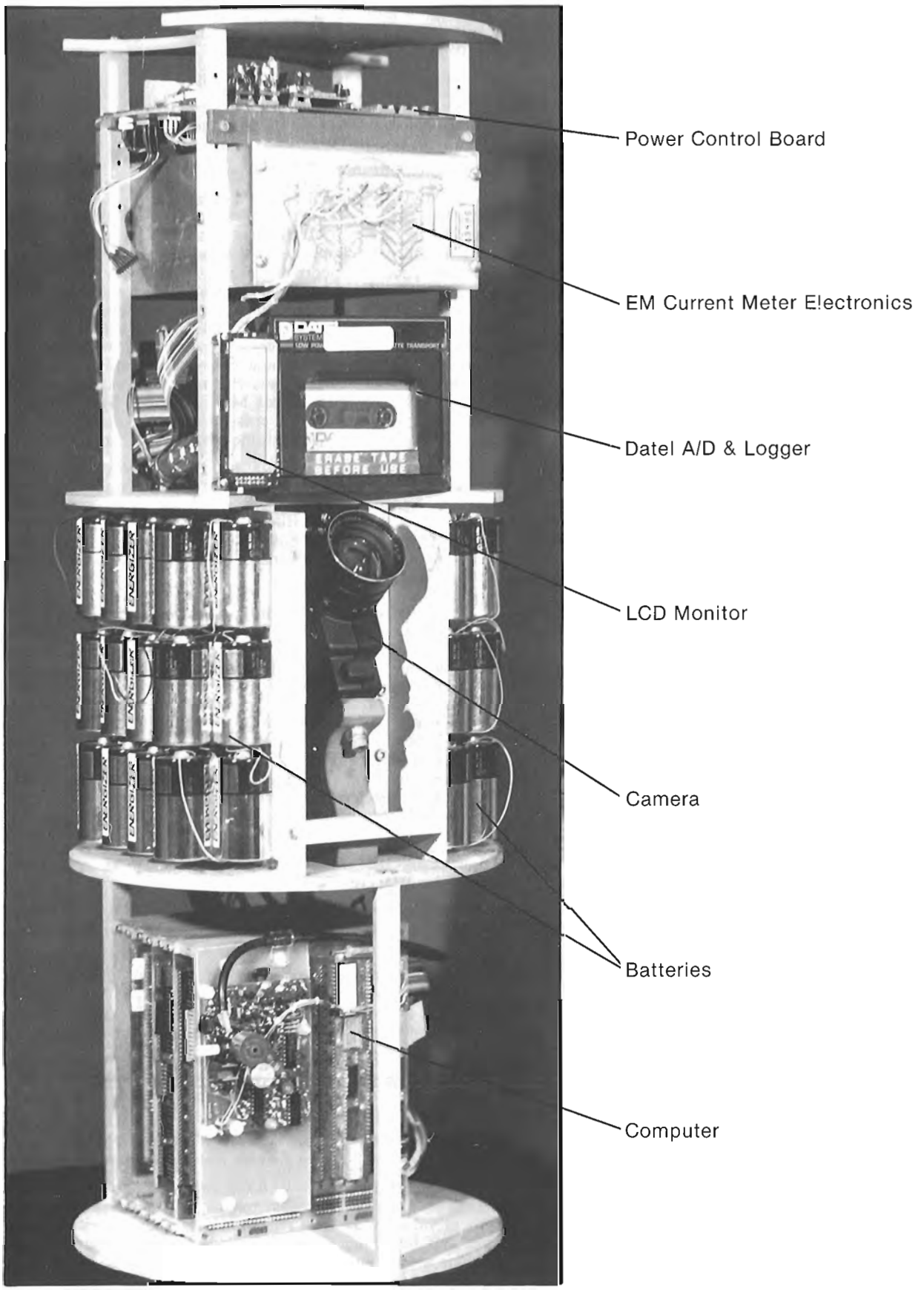

Figure 6.2. *The inside frame of RALPH showing the electronics, camera, batteries and data logger.*

The programs in RALPH have all been written in assembly language. The programs are in 3 parts:

1. Utilities – subroutines which control (a) communication through the terminal, (b) data acquisition and storage hardware, (c) the clock, and (d) the sensors.
2. ARTE (Almost Real Time Executive) – a set of subroutines which control the execution of tasks. ARTE maintains queues of tasks waiting to be executed at fixed times or contiionally on certain events. ARTE allows the tasks to schedule other tasks or declare events. A complicated data logging scenario which may run for 2 months can be developed in a day and fully tested in a few hours.
3. Tasks – the set of programs which gather data during a specific drop. A typical task might be to turn on all sensors, wait for a warm up period, store a time series of data in memory, preprocess the data and write it on tape. Before relinquishing control to ARTE, it could then reschedule itself to repeat 6 hours later.

Handling RALPH

RALPH is a large open tripod designed for minimum perturbation of the bed and near bed currents. Hence it is awkward to handle at sea. On a ship with cranes, it is handled like any oceanogrpahic equipment. It is usually moored with a ground line to a back up anchor and surface float. A surface float or subsurface float with acoustic release is secured to RALPH itself.

In nearshore waters, where ships with cranes cannot operate, other techniques have been employed. A float made from a farm tractor inner tube, inflated with a SCUBA tank and secured to a plywood pannel, is placed under the main platform of RALPH. The instrument can then be towed to the launch site with a small boat and then lowered by deflating the tube. The weights are placed in the feet by SCUBA divers. The inner tube is then removed for the duration of the experiment. Recovery with diver assistance can be performed in the reverse order. On one occasion, with only a rubber boat available, RALPH was recovered by divers, towed through 1 m breaking surf and carried up the beach.

In another deployment, RALPH was launched by slinging from a helicopter, lowering on site, and releasing a floating surface line. Recovery in this case was by ship.

Data logging scenario

The computer controlling RALPH affords great versatility in data logging. The data logging scenario currently used is as follows:

1. At 0600 and 1800 each day, measure a time series of 512 one second readings of current, transmission and pressure; then store all the data on tape. Photograph the seabed every 5 seconds for the first half of the time series.
2. At every odd hour, perform the same time series readings, calculate the means and mean deviations of each variable, and then record only these means and mean deviations on tape. No photographs are taken. Mean deviation is calculated using:

$$\text{mean deviation} = (1/N)\sum_{i=1}^{N} (x_i - \bar{x})$$

where: N is the number of samples

x_i are the sample values

and $\bar{x}$ is the sample mean.

Given the simple arithmetical capabilities of RALPH, the mean deviation is easier to calculate than the standard deviation.

3. Photograph the bed every 30 minutes.
4. Every midnight, photograph several frames without the flash to place daily markers on the film.

A deployment example

RALPH was deployed at Martinique Beach, Nova Scotia, in June 1983 to study summer conditions on the shoreface. The RALPH site was in 11 m of water approximately 0.5 km seaward from this exposed, wave-dominated, summer-accreting beach. The 17 day deployment included 3 moderate summer storms (rms wave height of 0.5 to 1.2 m) and a 5 day calm period. Serveral distinct bedform types were observed in the photographs and were related to the measured waves and nearbed current regimes. Figure 6.3 shows the mean and mean deviations of the data for the entire deployment and Figure 6.4 shows part of one time series. The analysis has been described by Boyd et al. (1983) and Forbes et al. (in press). Several aspects of this analysis demonstrate the usefulness of RALPH.

The standard deviations and mean deviations of the signals during all the time series which were recorded on tape were calculated and compared. Their high correlation ($r^2 = 0.99$) gives us confidence in deriving the standard deviation from the mean deviation of the records stored every two hours. The standard deviation is equal to 1.25 X (mean deviation).

Mean deviation of depth (wave height) and of current (wave component of bottom current) showed a negative correlation with the mean transmission values. This shows that sediment entrainment to 50 cm above the bed is caused by wave-generated bottom currents. High values of mean deviation of transmission observed during the storms demonstrate that the sediment is being locally entrained. The time series data show several events where a wave group is followed (several seconds later) by a dramatic reduction of transmission. One such event is shown in Figure 6.4. This shows that sediment is advected to 50 cm within a few seconds of the passage of a large wave and stays in suspension for a few tens of seconds.

During the 17-day experiment, four distinct bedform types were observed:

1. Long-wavelength, well defined ripples. These exhibited almost no movement. The wavelength was amost equal to the nearbed orbital diameter.
2. Short-wavelength, well defined ripples. These often showed migration (almost always shoreward) and occurred during periods of large orbital diameters of the wave component of bottom current.
3. Bifurcated ripples showed no consistent migration but exhibited a pattern change with time. These seemed to be a transition stage between type 2 and longer wavelength patterns.
4. Long wavelength forms with short interrupted crests. These formed a stable pattern under calm conditions.

Bedform migration velocities can be determined from the time-lapse photographs taken at 30 minute intervals. Typical values were about 1 cm/h. The pictures taken every 5 seconds for 4 minutes during the time series shows no fast motions which could be aliased on the 30 minute pictures.

The bedform migration during this experiment was almost always onshore, in agreement with observed summer accretion of the beach. The small mean currents were

almost below the threshold of sensitivity and were generally offshore. This suggests that bedform migration is not a simple function of near bed flors. A winter experiment is planned to investigate why the more intense winter storms cause beach erosion.

RALPH history

The following is a short history of the deployment and use of RALPH to date.

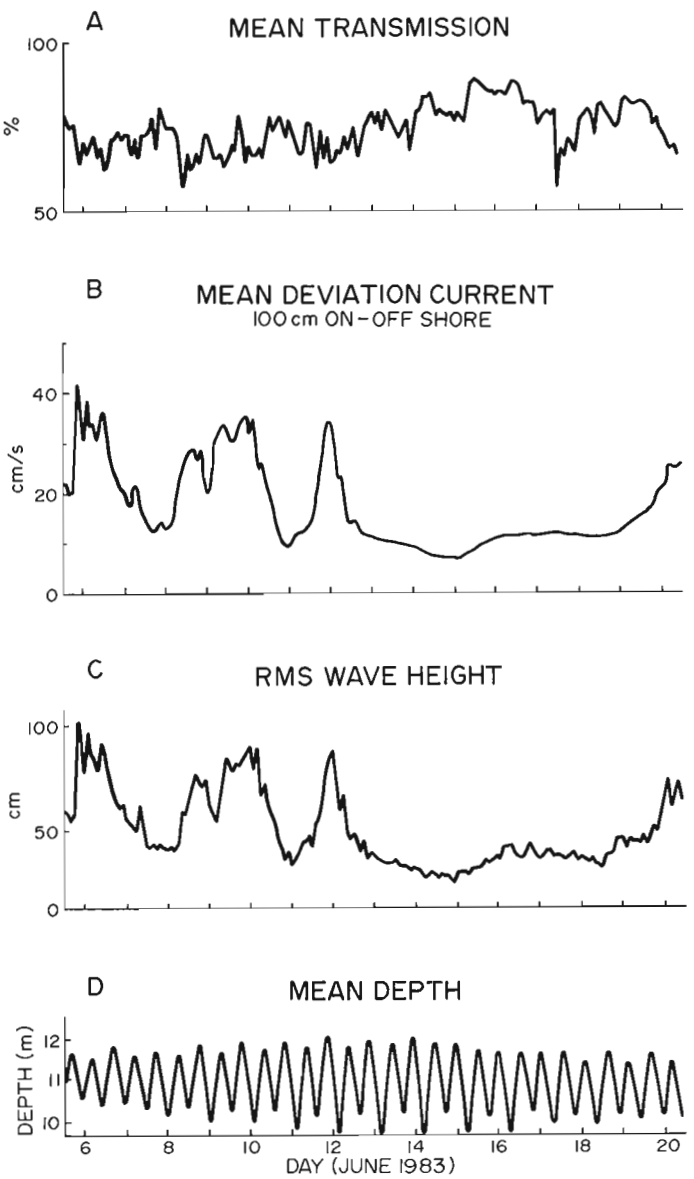

Figure 6.3. *Light transmission, current, waves and tide at Martinique Beach N.S., 6 to 20 June, 1983. All data are from internally calcualted means and mean deviations of time series (512 one second samples) taken every 2 hours. (a) Mean transmission showing increased light transmission (decreased suspended sediment concentration) during clam period 14-19 June. (b) Mean deviation of onshore-offshore current 100 cm above bed. Shows 3 storm events with mean deviation of current 30 cm/s (rms 37.5 cm/s). (c) Mean deviation of depth (wave height) note excellent correlation with (b). (d) Mean depth showing tides.*

1978	Summer	- Conceived design and began construction.
1979	Summer	- Unsuccessful tests in Labrador Sea.
	Fall	- First successful test in Halifax Harbour Harbour (see Heffler, 1979).
1980	Spring	- Test in Halifax Harbour, Lost. New RALPH built.
1981	Summer	- Tests in Bedford Basin.
	Fall	- 2 drops in Aspy Bay, Nova Scotia. Excellent photographs, some good data. Revised sampling scheme. Following this experiment, the tripod was redesigned to reduce the effects of scour of the seabed.
1982	March	- Halifax Harbour. Good data. Camera failed (see Delure, 1983).
	April-May	- Sable Island area. RALPH tipped due to unsuitable mooring technique. Some interesting photographs of tidal and wave generated bedforms were obtained.
	June	- Extensive dockside testing.
	September	- Beaufort Sea. Some poor data, low visibility precluded photographs.

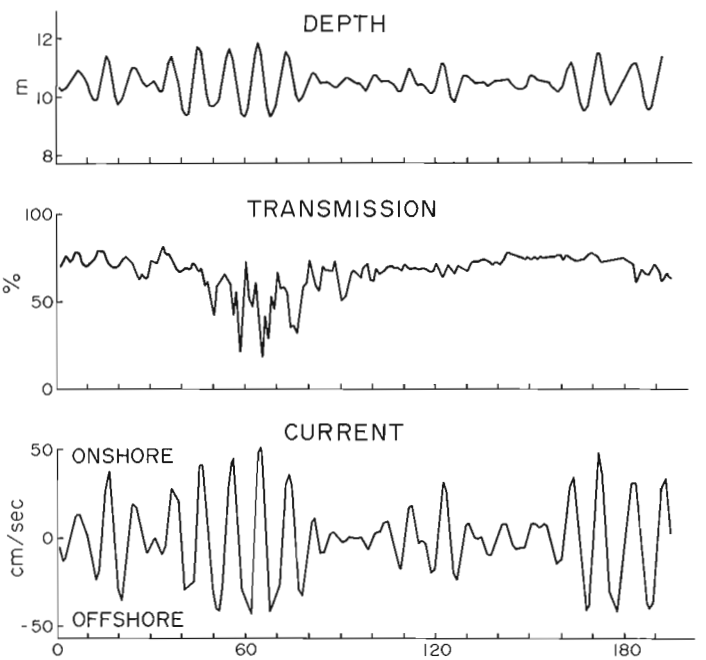

Figure 6.4. *A portion of the time series on 12 June. (a) Depth, showing passage of a large wave group at 40-80 seconds (b) Transmission – note sudden reduction (increased suspended sediment) shortly after passage of wave group. (c) Onshore-offshore current 30 cm above bed.*

1983	May	- Cole Harbour, N.S. Good photographs, data drifted due to low batteries.
	June	- Martinique Beach. Excellent data and photographs (see Forbes et al., 1984).
	July-August	- Halifax Harbour.
	September	- Unsuccessful attempt to deploy in Beaufort Sea due to heavy sea ice.
	October-November	- Two deployments at the Canadian Coastal Sediment Study, Pte. Sapin, New Brunswick. Good data.
1984	February	- Deployed at Hibernia on the Grand Bank in 80 m depth. Three earlier attempts in the winters of 1981, 82, 83 had been aborted due to weather, ice and the sinking of the Ocean Ranger.

Future plans

RALPH will continue to be used for nearshore studies on the Atlantic coast and in continental shelf areas of special interest such as Hibernia, Sable Island and the Beaufort Sea. A continuous upgrading of internal programming, data playback and analysis, and internal preprocessing are planned.

Planned additional components include:

1. Stereo Cameras – to provide better definition of ripple scale bedforms, including ripple height.
2. Peizometers – To measure seabed pore pressure and its effect on thresholds for sediment entrainment.
3. More EM current meters – to determine near-bed velocity profiles.
4. Conductivity and temperature sensors – to document density and viscosity and to define water mass movement, particularly in estuarine environments.
5. An Acoustic Suspended Sediment Profiler (ASSP) – to measure the profile of suspended sediment in the bottom metre of the water column. This should make possible accurate bedform measurements even in turbid water.
6. Massive Underwater Data Logger (MUDL) – to increase the data logging capabilities of RALPH to 20 Mbytes. This will be ready for testing in June 1984.

Conclusions

RALPH is an operational instrument that now gathers data important in the study of the processes of seabed sediment transport. RALPH measures near-bed currents, suspended sediment and depth (for wave and tides) and concurrently photographs the bed. Its internal data preprocessing capability condenses information for digital data logging and enables conditional data logging. RALPH can be deployed from large research vessels or, with the aid of divers, from small vessels in the nearshore zone. RALPH development is still an acitve project at the Atlantic Geoscience Centre. Additional sensors and increased data capacity are planned in the immediate future. We are presently developing better methods of anlayzing and interpreting the data.

RALPH is being used presently to study sediment dispersal on high-energy, sandy beaches and at sites near the edge of the continental shelf. The data obtained have already provided valuable insights into the mechanisms of sediment dispersal at various sites on the Atlantic Coast.

References

Boyd, R., Forbes, D.L., and Heffler, D.E.
1983: Fairweather sediment dispersal on the shoreface of the Nova Scotia Atlantic Coast (abstract); EOS, Transactions, American Geophysical Union 64, p. 1102.

DeIure, A.
1983: Storm effects in Halifax Harbour; M.Sc. Thesis, Dalhousie University, Halifax.

Forbes, D.L., Heffler, D.E., and Boyd, R.
– RALPH observations of shoreface sedimentation processes at Martinique Beach, Eastern Shore of Nova Scotia (abstract); Maritime Sediments and Atlantic Geology. (in press)

Heffler, D.E.
1979: RALPH a Sediment Dynamics Monitor; in Workshop on Instrumentation for Currents and Sediments in the Nearshore Zone; Associate Committee for Research on Shoreline Erosion and Sedimentation, National Research Council of Canada Ottawa, p. 163-174.

7.

AEOLIAN DUNES IN EARLY PROTEROZOIC THELON FORMATION NEAR SCHULTZ LAKE, CENTRAL KEEWATIN

Project 820004

M.J. Jackson[1], J.G. Pianosi[2], and J.A. Donaldson[2]

Jackson, M.J., Pianosi, J.G., and Donaldson, J.A., Aeolian dunes in early Proterozoic Thelon Formation near Schultz Lake, central Keewatin; in Current Research, Part B, Geological Survey of Canada, Paper 84-1B, p. 53-63, 1984.

Abstract

To identify the depositional setting and evolution of an unusual crossbedded sandstone facies of the early Proterozoic Thelon Formation in central Keewatin, a small area (approx. 1 km^2) north of Schultz Lake was mapped in detail. It comprises overlapping festoons, commonly tens of metres in size, which contain steeply dipping (20-39 degrees) arcuate cross-strata deposited by persistent westerly-directed paleocurrents. The original sedimentary textures and structures in these siliciclastic strata have been largely obliterated by extensive silicification, but slabbing and X-ray photography has revealed reverse-graded crosslaminae which may have been formed by migrating wind ripples. Based on comparison with modern large-scale sandy bedforms, the festoon facies is interpreted as a lithified dune field similar to those present in the western Sahara today. Aeolian environments have also been documented in possibly correlative strata of the Hornby Bay Group suggesting such environments were widespread at this time in northern Canada.

Résumé

Pour identifier le cadre de la mise en place et l'évolution d'un faciès inhabituel de grès entrecroisé du début de la formation protérozoïque de Thelon, dans le centre du Keewatin, on a dressé la carte détaillée d'une petite zone (environ 1 km^2) au nord du lac Schultz. Elle comprend des festons chevauchants dont les dimensions atteignent fréquemment des dizaines de mètres et que caractérisent des strates croisées de forme arquée et à fort pendage (20 à 30°) mises en place par des paléocourants persistants de direction ouest. Les textures sédimentaires d'origine et les structures dans les strates silicoclastiques ont été nettement oblitérées par une vaste silicification, mais le tranchange et la photographie aux rayons-X ont révélé une intercalation fine et croisée à sédimentation graduée inverse dont la formation peut être due au déplacement des ondulations sous l'effet du vent. En la comparant aux dépôts sableux à grande échelle contemporains, on peut interpréter le faciès festonné comme un champ de dunes pétrifiées semblable à ceux que l'on trouve actuellement dans le Sahara occidental. Des milieux modelés par le vent ont été aussi étudiés dans les strates correspondantes du groupe de Hornby Bay qui a peut-être la même origine, et les résultats suggèrent que de tels milieux étaient répandus alors dans le nord du Canada.

Introduction

During regional reconnaissance mapping of central Keewatin in the 1960s (Donaldson, 1965, 1969) a facies of very large scale (metres to tens of metres) crossbedded sandstone was recognized in the early Proterozoic Thelon Formation, and a possible aeolian origin was suggested (Donaldson, 1967, p. 51). On the basis of more detailed study of this facies in 1982 by Chiarenzelli and Donaldson, the suggestion of possible aeolian origin was strengthened. Based mainly on character and size of crossbedding, fine grain size and unimodal west-southwest paleocurrents, they tentatively interpreted an area north of Schultz Lake as an exhumed barchan dune field (LeCheminant et al., 1983). In addition, similar large scale crossbedding was recognized in the Pitz Formation which comprises porphyritic acid lavas and intercalated epiclastic and pyroclastic rocks; the overlying Thelon Formation is mostly composed of quartz arenites of fluvial origin.

Studies of modern aeolian deposits (e.g. McKee, 1966; Bigarella, 1972; Wilson, 1972a, b; Hunter, 1977a, b) and of ancient sequences of possible aeolian origin (e.g. Walker and Harms, 1972; Brookfield, 1977; Mader, 1982; Hunter, 1981; Kocurek and Dott, 1981; Rubin and Hunter, 1982; Ross, 1983) have greatly enhanced our ability to confidently differentiate aeolian from subaqueous sands in the geological record. These studies have also provided valuable information on the processes involved in aeolian bedform formation and genesis of sand seas.

During the final week of July 1983, we revisited the small well-exposed area north of Schultz Lake (Fig. 7.1, 7.2) described by LeCheminant et al. (op. cit.) to search for features indicative of aeolian origin, and to assess the validity of their tentative interpretation of a barchanoid origin for the crossbedded strata. To enable comparison with features described in the geological literature, the area was mapped in detail (Fig. 7.3) and a cross-section was measured (Fig. 7.5). Eighty paleocurrents and about 250 crossbedding attitudes were measured (Fig. 7.3, 7.16). In addition, a representative suite of 30 hand specimens was collected for slabing, petrographic study and X-ray photography. The study area is near a small unnamed lake at 64°56'N, 97°40'W, which hereafter is informally referred to as 'Dune Lake' (inset, Fig. 7.5).

An area near Marjorie Lake where similar possible aeolian dunes occur in the Pitz Formation, (LeCheminant et al., op. cit.) was not revisited, but an additional locality in the Thelon Formation that contains an identical facies was discovered late in the field season and was briefly examined; the characteristics and palaeocurrents in this area (approximately 40 km northwest of 'Dune Lake') are indistinguishable from those studied in detail at 'Dune Lake', and so are not described further. Although the facies of large-scale crossbeds appears to be relatively thin (see later) it is probably widespread in the northeastern part of the Thelon Basin.

[1] Bureau of Mineral Resources, Geology and Geophysics, P.O. Box 378, Canberra City, Australia 2601; fieldwork done while on a one-year exchange with the Geological Survey of Canada, Ottawa

[2] Department of Geology, Carleton University, Ottawa, Ontario K1S 5B6

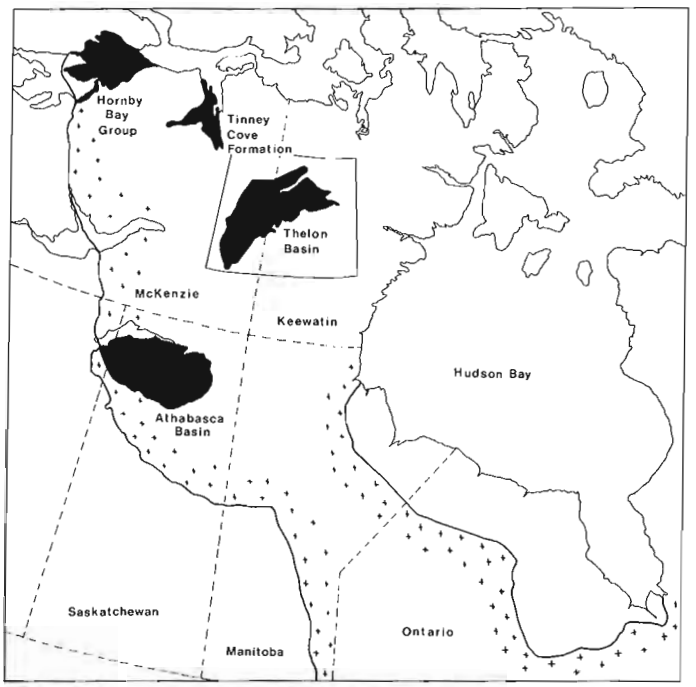

Figure 7.1. Thelon Basin and possible correlative early Proterozoic sequences/basins on the Canadian Shield. Area covered by Figure 7.2 outlined.

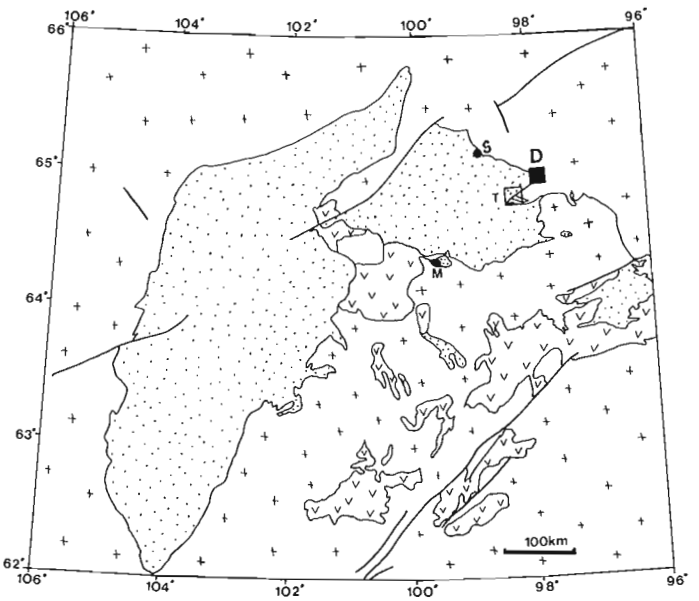

Figure 7.2. Regional geology (simplified) Thelon Basin. Location of 'Dune Lake' (D) and other areas containing festoon facies (M – Marjorie Lake, and S – Sand Lake). Thelon Formation-fine stipple; older Dubawnt Group-v symbol; basement-+ symbol. Lakes omitted for clarity. Area mapped by Tella and Thompson 1983 (T).

Regional setting

The Thelon Formation is a flat-lying sequence of early Proterozoic siliciclastic strata with a maximum thickness that may exceed 1000 m. It unconformably overlies a diverse assemblage of rocks including Archean granite and gneiss, Aphebian metasedimentary and metavolcanic rocks and late Aphebian-Paleohelikian sedimentary and volcanic rocks of the Dubawnt Group in the central and western parts of Keewatin and adjacent Mackenzie (Fig. 7.1). The Thelon Formation has a minimum age of ~ 1660 Ma (Miller, 1983). The formation outcrops extensively west and north of Dubawnt Lake in an area some 500 km by 200 km that has generally been referred to as the Thelon Basin (Fig. 7.1, 7.2). Similar clastic sequences of early to middle Proterozoic age occur in the Athabasca Basin of northern Saskatchewan (Ramaekers, 1981), the Bathurst Inlet area (Campbell and Cecile, 1981), and the Coppermine Homocline (Hornby Bay Group, Kerans et al., 1981) (Fig. 7.1). Within these basins quartz-rich arenites of the same approximate age as the Thelon Formation have been deposited in a variety of continental environments including braided fluvial, alluvial fan, and shallow lakes, commonly in areas that were undergoing syndepositional faulting. Kerans et al. (op. cit.) and Ross (1983) have convincingly documented evidence for aeolian deposition in sinuous-crested transverse dunes in the Coppermine Homocline.

Sedimentological studies of the Thelon Formation have shown that the sequence is divisible into a number of distinct and mappable facies dominated by various types of quartz and felspathic sandstones. Early studies on a regional scale (Donaldson, 1969; Cecile, 1973) identified four main facies. The presence of features such as conglomerates, channels, planar and trough cross-stratification, fining-up sequences, desiccation cracks, and asymmetric ripples indicate deposition in mainly alluvial fan and braided fluvial environments (Fig. 7.7). In addition, nearshore marine environments were also suggested (Cecile, 1973) in the uppermost part of the Thelon Formation. Chiarenzelli (1983) has documented a number of regoliths beneath and within the lower part of the Thelon Formation.

In the area immediately southwest of 'Dune Lake' which was mapped at 1:50 000 scale in 1982 (Fig. 7.2) by Tella and Thompson (in LeCheminant et al., 1983) the Thelon Formation is subdivided into three facies: a basal polymict conglomerate which is commonly ferruginous and in parts regolithic; a pebbly coarse-grained sandstone facies; and a fine- to medium-grained sandstone facies. The latter two contain large-scale (actual measurements not stated) trough and planar crossbedding, channels, ripples and desiccated mudstone intercalations.

The 'Dune Lake' area is near the northeastern extremity of the Thelon Basin, about 12 km northeast of the area mapped by Tella and Thompson. At 'Dune Lake' the Thelon Formation is flat-lying to gently-dipping and unconformably overlies, or is in fault contact with, the basement complex. A major northeast-trending fault with associated subparallel shear zones forms its southern limit (inset, Fig. 7.5). The sedimentary facies are similar to those described by LeCheminant et al. (op. cit.), with the addition of the large-scale crossbedded facies that is the subject of this report.

The sequence is flat lying and almost continuously exposed in an area of subdued topography. Except in the southeast, the area has not been dissected to any extent, and consequently most of the outcrops provide near-horizontal sections through a series of overlapping curved cross-strata (Fig. 7.8). In the southeast, however, a total of about 30 m of section is exposed in numerous small cliffs that provide vertical faces up to 2 m high where a small creek has incised through the Thelon Formation. Here the large-scale trough crossbedded facies is about 25 m thick. It is overlain and underlain by poorly sorted, fine to very coarse grained pebbly sandstone with decimetre-scale wedge-planar and

trough crossbedding. The contacts between the two facies are relatively sharp, but conformable. The presence of asymmetric (current) ripples, up to 3 cm high and with ripple indices around 4, together with coarser lags along the lower bounding surfaces of 10-30 cm thick trough cross-sets, provide evidence of a fluvial origin for these enclosing facies. A few paleocurrent measurements from asymmetric ripples and crossbed foresets indicate dominantly west-flowing fluvial systems. As discussed later, this is similar to paleocurrents in the large-scale crossbedded facies.

Field Methods

Geological map

A small area of semicontinuous outcrop (600 m by 500 m) flanking the north shore of 'Dune Lake' was mapped at 1:500 scale (Fig. 7.3, 7.4, inset on 7.5). To provide appropriate topographic control the area was subdivided into a 100-m square grid using a tape and prismatic compass. Rock cairns were built to mark the corners of the 100 m-square cells. These were then subdivided into 50 m and 25 m squares (where justified by complexity) using less permanent markers. The outcrop distribution, topography and bedding features were then sketched into these small squares taking particular note of the shape and size of the arcuate crossbeds, lateral variations of these surfaces, and erosional relationships between these and other intersecting surfaces. Cumulative errors arising from this crude surveying method were kept to a minimum by a process of looping back to the central cairn of four adjacent 100-m cells. Distance measurements in this subdued terrain proved to be fairly accurate, and in most cells the 400 m loops were accurate to within about 4 m (i.e. about 1 per cent). Errors in azimuth measurements with the prismatic compass were determined to be less than 2 degrees, and over distances of a few hundred metres such crude control is more than adequate. Twenty-three 100 m-square cells were surveyed, geologically mapped and later compiled into a single map at 1:500 scale. This map was reduced to approximately 1:10 000 scale, slightly simplified, and is reproduced here as Figure 7.3. This 'factual' map forms the basis for the interpretive map, Figure 7.4, in which areas of no outcrop have been interpreted and the major sets and bounding surfaces have been emphasized.

Cross section

As noted earlier, the area on the southeast shore of 'Dune Lake' is slightly more dissected than that to the north. In addition to horizontal sections of the outcrop, this southern area also contains numerous vertical faces up to 2 m high. To supplement the plan view of the foresets obtained from the map, a section along A-D (inset Fig. 7.5) was measured to provide information for the third dimension. The section was measured at 1:200 scale by means of pacing for distance control and a Brunton compass for elevation control along a line trending 135 degrees true, which is almost normal to the dominant paleocurrents determined for the area. The attitudes of the crossbeds were measured at regular intervals along the traverse, and major discontinuity

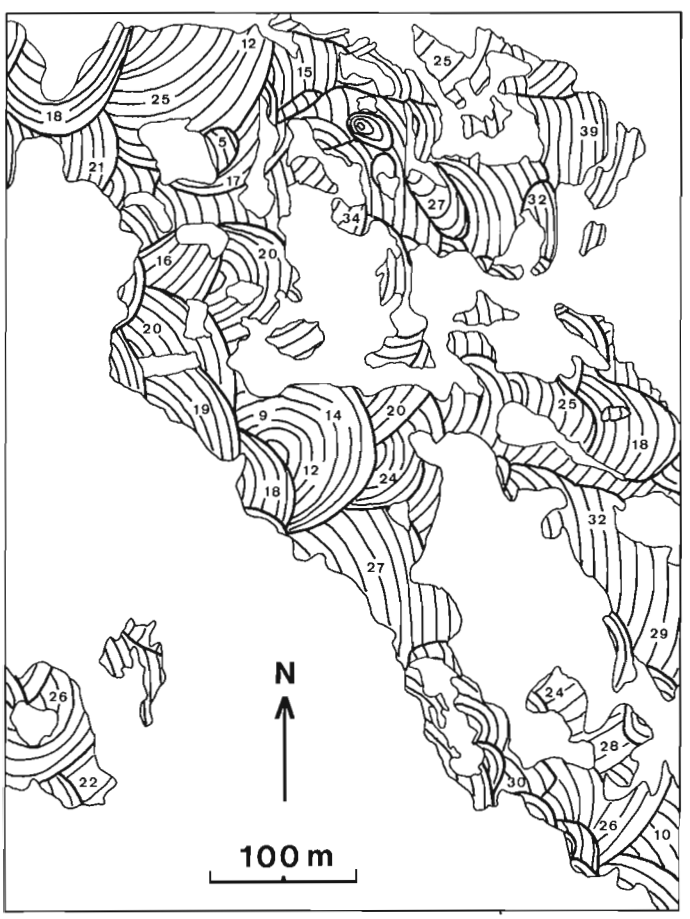

Figure 7.3. Objective field data map showing surface traces of crossbeds, lower bounding surfaces to sets, crossbed inclinations and areas of no outcrop. For detailed location see inset accompanying cross-section.

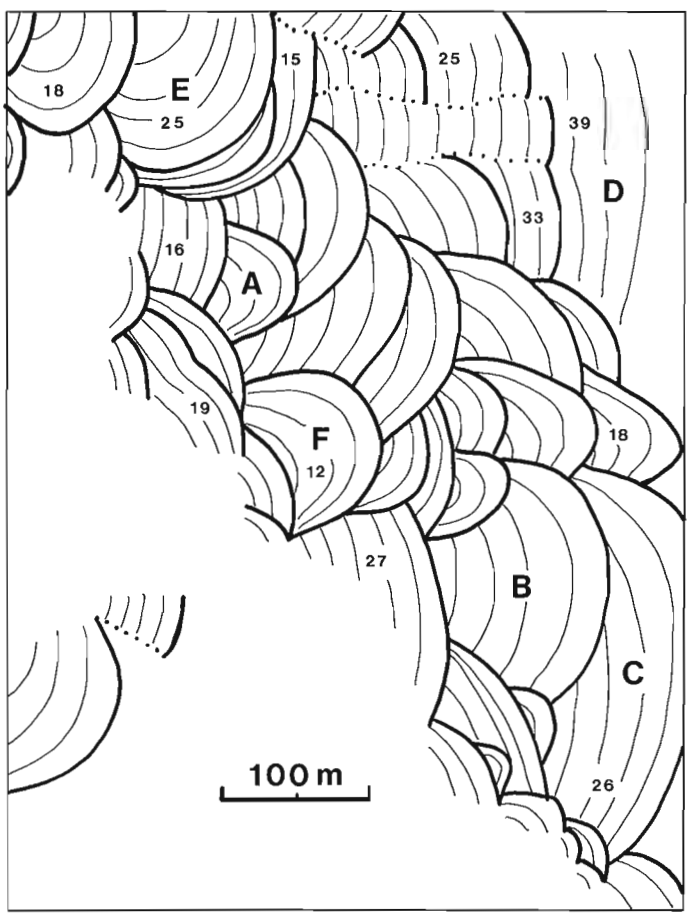

Figure 7.4. Interpretive map based on field data map. Main festoons highlighted, representative crossbed dips included. Small festoons omitted for clarity. Letters refer to comments in text.

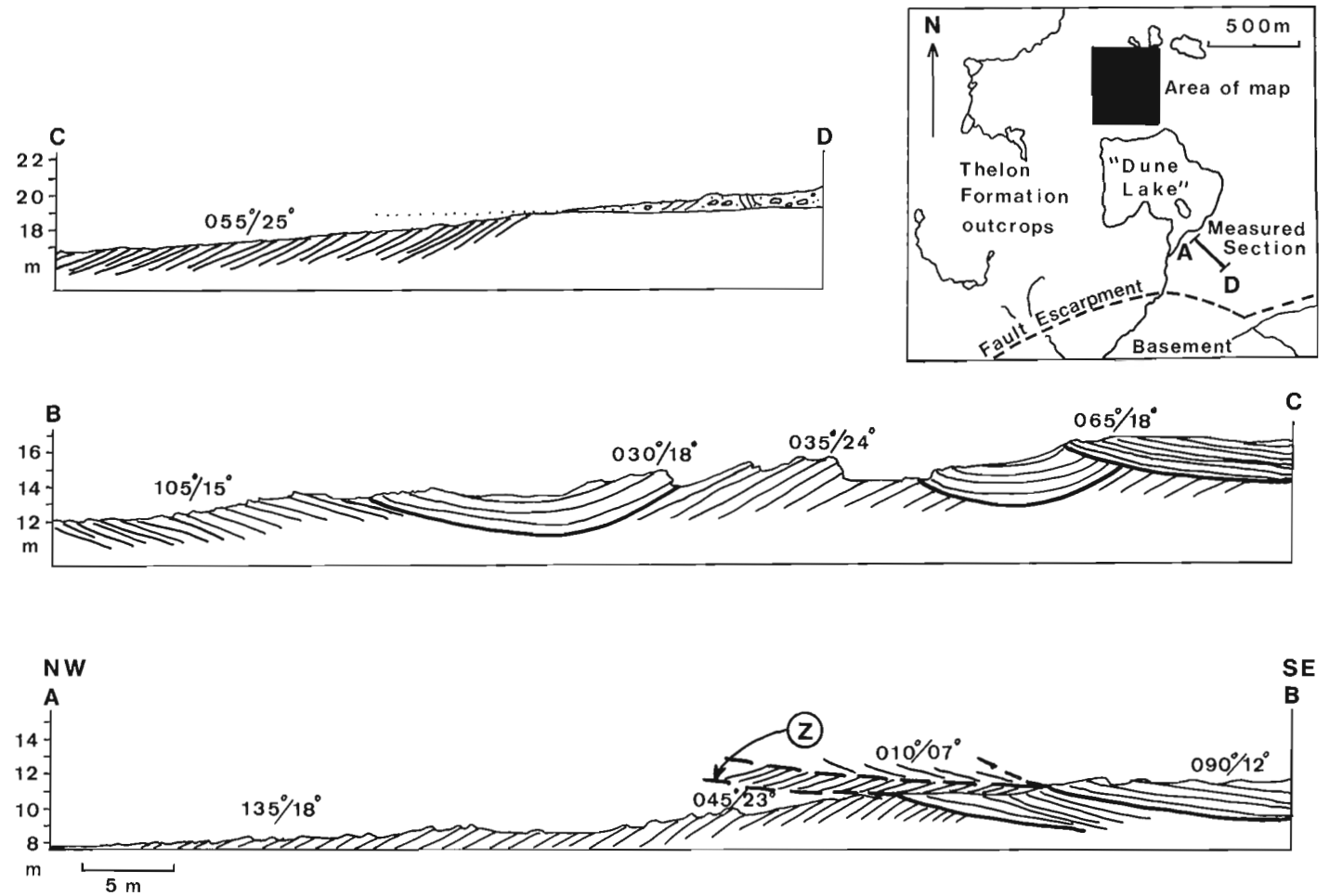

Figure 7.5. *Crossbedding (in section) along line A-D on inset map. Set bounding surfaces – heavy lines; cross-stratification – fine lines. Point A is 90 m from shore of lake at elevation +7.5 m.*

surfaces were marked. At a few points along the line, information from a few metres on both sides of the line was projected onto the section. The field data were compiled at 1:200 scale and then reduced (Fig. 7.5). A generalized and interpretive section at a much reduced scale is shown in Figure 7.6.

Results

General form of structures

The general morphology of the cross-sets that compose this facies of the Thelon Formation at 'Dune Lake' is readily comprehended by referring to Figures 7.4, 7.5, 7.6. The area comprises overlapping sets of arcuate crossbeds (Fig. 7.8, 7.9, 7.10). Both in plan and section there is remarkable parallelism between the lower bounding surface and the overlying cross-strata in individual sets. Only in a few places can asymptotic relationships between cross-strata and bounding surfaces be seen (e.g. Z, Fig. 7.5). This type of stratification is classical festoon crossbedding. Interestingly, the definition of festoon crossbedding in the AGI Glossary (1980, p. 228) is based on examples from dune sequences in Wyoming that were originally thought to be of subaqueous origin (Knight, 1929) but which are now considered aeolian (Steidtmann, 1974). A review of the literature on aeolian sands has provided only three examples showing closely comparable cross-stratification (see Interpretation). At 'Dune Lake' the festoons 'open' mainly towards the west, with a subsiduary swing towards the northwest in the northwest corner of the area. Persistent truncation of the cross-sets on the west side of the festoons indicates that the earliest festoons are in the east and that the deposit formed by gradual westward augmentation by, and advance of, these large sets.

Preserved size of bedforms

Measurements indicate that the perserved widths of individual festoons range from about 50 m (e.g. festoon A, Fig. 7.4) up to about 180 m (festoons B and C, Fig. 7.4). Truncation of the flanks of these festoons show that they originally were slightly larger. The effects of erosion are probably of even more consequence to estimates of original festoon length as many of the festoons show considerable down-current erosion. In the largest festoons (C, D, E), lengths approach 150 m, but these obviously represent minimum sizes. A similar impression of festoon size is indicated in the cross-section: at the northwest end of the measured section, an uninterupted 80 m of regularily dipping foresets is preserved in one festoon cut parallel to its axis and in the middle part of the section, several troughs cut normal to their axes, are 5 to 20 metres thick. In plan view, the radii of curvature of foreset surfaces and lower bounding surfaces are commonly regular and even; radii of curvature range from about 20 m to 300 m; some show tightening of

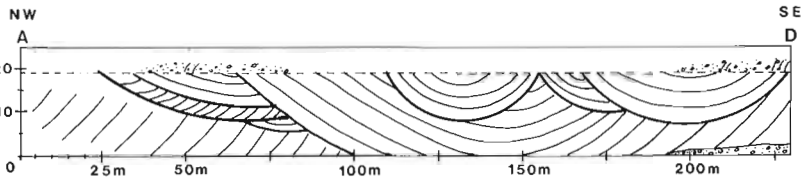

Figure 7.6

Reduced and generalized interpretation of style of cross-stratification based on measured section A-D.

curvature on festoon flanks. Examples of festoons with a wavy surface were seen, but are rare. With wavelengths of only a few metres, these are visible in the field (Fig. 7.11), but because of their size and subtle nature are not portrayed on the map.

Foreset attitude

Cross-stratification is displayed as foreset surfaces with a spacing of 1 to 30 cm, but most foresets are in the 5-15 cm range (Fig. 7.12). Thinner laminations between these main bedding surfaces are marked by subtle grain size variations. Subsequent studies of slabs and thin sections have revealed internal grain size variations in some of the massive-looking beds (Pianosi, 1984). At the southeast end of section A-D, flaggy and fissile sandstones occur in gently dipping crossbeds at the top of the aeolian facies, immediately beneath the base of the overlying fluvial sandstones.

Foreset dips range from 6 to 39 degrees (the latter exceeds the maximum angle of repose for sand, usually quoted as 34 degrees for dry sand). The preservation of such a high angle of repose for some of the foresets implies that little compaction could have occurred before or subsequent to lithification which seems surprising in view of the age and intense authigenic alteration evident in thin section (Fig. 7.16). Intuitively, we had expected to find some evidence of compaction, similar to that cited by Walker and Harms (1972) for the Permian Lyons Sandstone of Colorado. They reported the steepest crossbed dip in an aeolian facies to be 28 degrees, attributing the apparent absence of higher foreset dips in part to post-depositional compaction and intrastratal alteration. This does not appear to have happened in the 'Dune Lake' area.

The mean value of 250 foreset dip angles within the 'Dune Lake' map area is 19 degrees. Some festoons are characterised by steep dips (e.g. festoon C, dips 24-33 degrees) whereas others are characterized by gentle dips (e.g. festoon F, dips 6-14 degrees). Because these festoons appear to be otherwise identical this apparent variation is probably due mainly to exposure at different levels in the original bedforms rather than to differences in types of bedforms. Some festoons contain a wider range of dips, in these the steepest dips occur in the axial regions (Fig. 7.12) and shallower dips are prevalent on the flanks (Fig. 7.13). In most of the larger festoons cross-strata can be traced laterally over horizontal distances of tens of metres without interruption or significant change of dip; in a few foresets, gradual shallowing of dips occurs as the flanks are approached (Fig. 7.13). The character of the down-dip continuity of foresets is difficult to determine due to the lack of vertical relief. In almost all cases, however, the foresets are regular and of constant dip, although rare downdip shallowing attributed to asymptotic-shaped lower foresets is present.

LeCheminant et al. (1983) described the 'Dune Lake' crossbeds as being up to 5 m thick, and the wedge-planar sets from the Pitz Formation near Marjorie Lake as up to 9 m thick. Our work shows that the 'Dune Lake' sets are much thicker. Calculations of set thicknesses (using measured outcrop length along festoon axes, foreset dip angles, and reasonable foreset curvatures) indicate that some of the festoons are 20 m thick, with a few of the largest approaching 40-50 m. Because there has been an unknown amount of erosion from the downcurrent ends of all festoons these values represent only minimum figures for original bedform depositional thicknesses.

Palaeocurrent measurements

The axes of all festoons in the map area (about 50) together with additional measurements from throughout the 'Dune Lake' area are shown in Figure 7.16, and compared with measurements from studies made in 1982. Inferred paleowinds with a distinct mode to the west-southwest are evident.

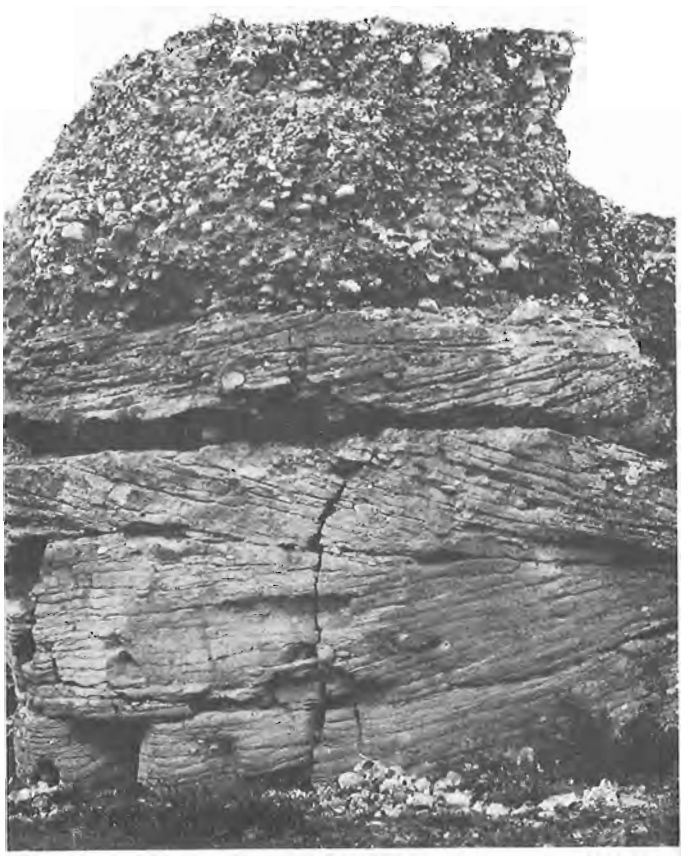

Figure 7.7. *Trough crossbedded pebbly sandstone overlain by quartz pebble conglomerate, typical fluvial facies of Thelon Formation. Outcrop is about 3 m high. (GSC 204114 R)*

Interpretation

As noted earlier Chiarenzelli and Donaldson's 1982 study tentatively interpreted this area as an exhumed near-horizontal section through a field of aeolian barchan dunes. In the light of our more detailed study how realistic is this interpretation?

Aeolian origin

A number of authors (e.g. Hunter, 1977a, b; Hunter, 1981; Kocurek, 1981; Kocurek, Dott, 1981) have commented that past interpretations of aeolian environments and/or processes have often been based on questionable or unreliable criteria, amongst which they would include features such as large-scale of cross-stratification, excellence of sorting, presence of frosted grains, presence of raindrop and other terrestrial impressions (e.g. dinosaur tracks). Recently, more reliable criteria for distinguishing between aeolian and subaqueous sands have been established, and one of the most important of these is the type of small scale stratification present. Hunter (1977b) has described the three basic types of stratification in modern aeolian dunes as having formed by the three main processes operating in dunes: grains avalanching, grains falling from suspension, and migration of wind ripples. Although some of these basic types of stratification present in dry windblown sands can also form in waterlaid sands, there are significant differences in detail. Hunter (1977b) suggested that some of the strata formed by avalanching (his "sandflow cross-strata"), and strata formed by one variety of climbing wind-ripples (his "subcritically climbing translatent strata") in aeolian dunes are distinctly different from their subaqueous counterparts (the size, shape and reverse grading of the aeolian stratification being especially distinctive). In addition, a rare type of wind-ripple cross-stratification ("supercritically climbing translatent strata") does not have a subaqueous counterpart.

Figure 7.8. *Oblique aerial view of northwestern part of detailed map area showing gentle topography and outcrop of overlapping large festoon. Dark areas are wet, sandy soil. Bar is about 20 m long. (GSC 204114 D)*

Figure 7.9. *View looking southwest (down paleowind) over curved foreset surfaces. Measured section A-D runs from right to left across foreground. The fault escarpment separating Thelon Formation (high ground) on right, from basement (low ground) on left is just visible in top right hand corner of photograph. Base of cliff highlighted by snow bank. Note figure in foreground for scale. (GSC 204114 L)*

Figure 7.10. *Gently rising ground in northwest part of map area exposing section through festoons, parallel to paleocurrent axis. Foresets dip to right in foreground, to left in middle ground (behind figure from hips to head level), and into photograph in background (top right corner above level of head of geologist). (GSC 204114 F)*

Figure 7.11. *Scoop-shaped festoon looking upwind, gentle undulation on surface of stratification visible. Ink line traces out pattern of a single crossbed surface (hidden on right of photo). Distance to 'head' of scoop about 30 m. (GSC 204114 J)*

Despite a deliberate and careful search for these structures in the sandstones at 'Dune Lake' none were found. Two poor examples of very small scale ripples (few millimetres in height, a few centimetres in wavelength) were observed on low dipping foresets at the flanks of two festoons, but they were not sufficiently well preserved for their features to be determined with any accuracy. Follow-up laboratory studies on a representative suite of samples from throughout the 'Dune Lake' area (Pianosi, 1984) suggests, however, that some of the small scale aeolian stratification described by Hunter (1977a, b) may in fact be present. Polished slabs of large hand specimens revealed parallel, subparallel and slightly discordant internal laminations defined by slight grain size variations; the latter are interpreted as low angle crosslamination. Reverse grading, which according to Hunter (1977a, b) is very characteristic of wind ripples, was identified in a few samples, but it is not very distinctive and therefore cannot be considered as conclusive evidence of aeolian origin.

Figure 7.12. *Steeply-dipping (30 degrees) crossbed surfaces spaced about 20 cm apart. Stratigraphic bedding is approximately horizontal. (GSC 204114 E)*

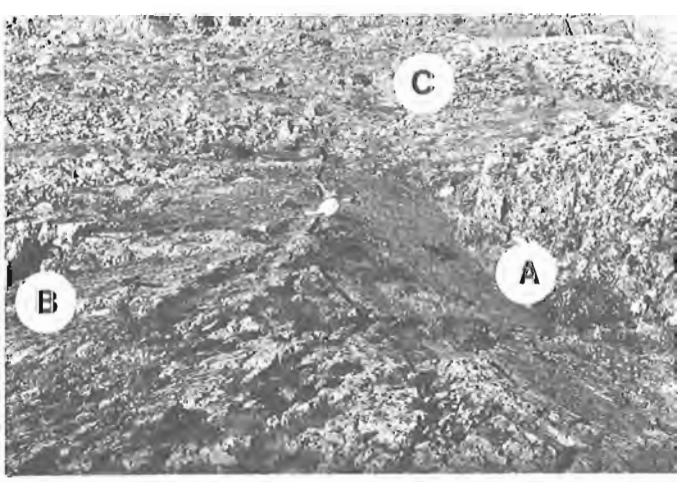

Figure 7.13. *Intersecting foreset surfaces at flanks of festoon. Cap on contact (broken line). Forsets A dip 10 degrees to northwest, Forsets B dip 5 degrees to southwest, these are overlain by C dipping away from viewer. (GSC 204114 G)*

Studies of thin sections from the whole area (Pianosi, 1984) have shown that the Thelon Formation has here undergone a complex history of silica cementation. In many thin sections authigenic changes are so extensive that little remains of the original texture (Fig. 7.15). The difficulty in defining stratification types in the field may be due to this pervasive secondary silicification which has effectively obliterated subtle grain size variations and textures that typically define aeolian stratification types. The subtle nature of these small-scale structures is well illustrated by Fryberger and Schenk (1981) who had to use layers of hand-sprinkled magnetite grains to define these stratification types in wind sedimentation tunnel experiments. In the case of the Thelon Formation at 'Dune Lake', much of the outcrop appears to comprise steeply-dipping crossbeds which would have been lee slip-faces of the original dunes. Hunter (1977b) pointed out that on modern dunes steep lee-faces are dominated by sandflow cross-strata. Because these are commonly internally massive, and their recognition is based mainly on external morphology, we believe that these would be particularly difficult to identify in the 'Dune Lake' area due to the lack of downdip exposure of cross-sets. Further, Hunter (1977b, p. 379) remarked that "on dunes whose original heights were probably greater than 2 or 3 m, as judged from the large horizontal extent of the sets and large plan-view radius of curvature of the cross-stratification"... and that is the case here, ..."the sandflow cross-strata are commonly in contact with one another and therefore the individual cross-strata commonly are indistinguishable."

Unfortunately, therefore, we seem to be in a similar situation to pre-1970 where we lack clear and conclusive evidence of the small-scale stratification and structures diagnostic of aeolian dunes.

Stratigraphic setting

Fortunately, the stratigraphic setting of the Thelon Formation at 'Dune Lake' indicates that an aeolian environments is the most likely setting for this facies of large scale crossbedded sandstones. As described earlier, the festoon facies is about 25 m thick and is sandwiched between smaller scale crossbedded pebbly sandstones which elsewhere have been interpreted convincingly as of fluvial origin (Donaldson, 1965, 1967; Cecile, 1973). Giant bedforms have been reported from deep fluvial channels (Coleman, 1969)

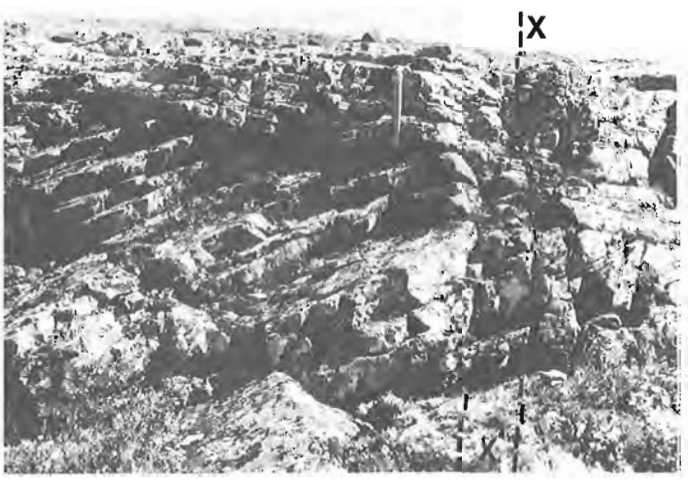

Figure 7.14. *Section through festoon facies southeast of 'Dune Lake' showing relationship between crossbedding, lower bounding surface and underlying set. Geological pick for scale. X-X' small normal fault. (GSC 204114 I)*

and perhaps the festoon facies represents such a deeper subfacies of the fluvial Thelon Formation? This is considered highly unlikely, however, because at 'Dune Lake' the facies contacts are both sharp and conformable, and the change from fluvial to festoon facies involves not only a major increase in bedform size but also a complete loss of pebbles, loss of feldspar, and an increase in sorting and roundness of the framework grains. Furthermore, although sinuous crested sand waves or dunes in rivers give rise to large-scale trough crossbedded sequences (e.g. Conaghan and Jones, 1975) such deposits should contain at least some of the following: fining-up cycles, a spectrum of bedform types and sizes, channel lags, and possibly also vertical accretion deposits. None of these has been observed at 'Dune Lake'.

The only other known situation where very large scale sandy bedforms occur is in the tidal marine environment. In fact, it was the recognition in the 1960s of such large scale bedforms in tidal shelf seas that led to the questioning of the validity of using large scale crossbedding to characterize aeolian sequences (Walker and Middleton, 1979). Although some tidal sand ridges are up to 40 m high and consist of well-sorted crossbedded sands, they are dominantly linear features parallel to the strongest tidal current, and hence are not analogous to the Thelon festoons. Tidal sand waves, although curved, are much smaller than tidal ridges (maximum size about 5 m; Reading, 1978) and therefore are not analogous to the larger Thelon bedforms. Again the stratigraphic context argues strongly against any setting other than continental: tidal sand waves and ridges are associated with tide-dominated deltas and estuaries, and there is no evidence of such facies in the Thelon Formation in the vicinity of 'Dune Lake', or, in fact, in the Thelon Basin as a whole (Cecile, 1973).

The stratigraphic context of the large scale cross-stratified sandstones in the slightly older Pitz Formation near Marjorie Lake is pertinent to this discussion. These sandstones overly a regolith developed on deeply weathered basement and are overlain concordantly by extrusive rhyolitic lavas and welded tuffs which in turn are overlain by pebbly crossbedded fluvial Thelon Formation. This too represents a distinctly continental setting.

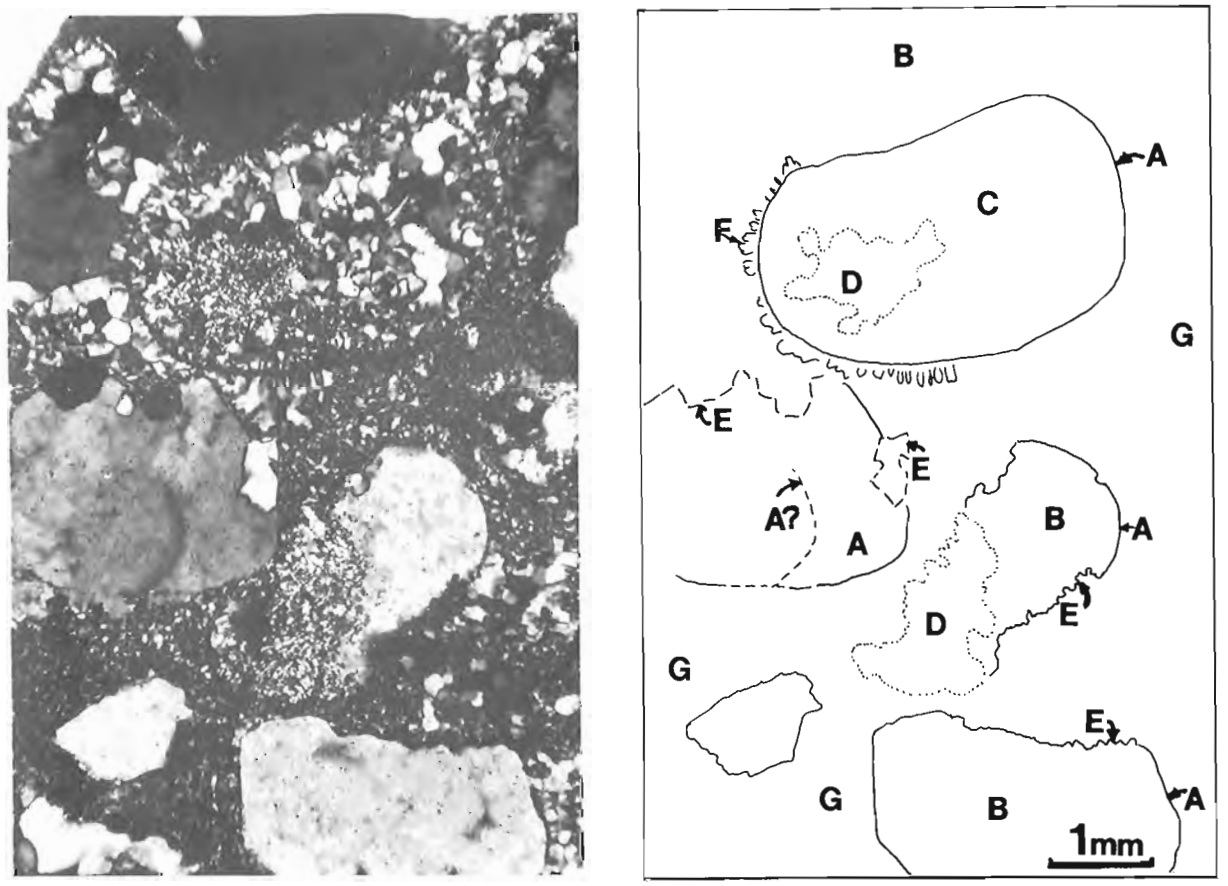

A - original grain boundaries (few preserved);

B - original monocrystalline (strained) quartz grain;

C - polycrystalline quartz grain;

D - incipient and irregular replacement of B and C by very fine grained quartz microlites;

E - irregular, embayed grain margins due to pressure solution;

F - 'molar-tooth' quartz crystals rimming grain C indicating growth into pore spaces;

G - cherty pore infilling material "pseudomatrix". Bar is 1mm long.

Figure 7.15. *Photomicrograph (X-nicols) and line sketch of silicified aeolian arenite from 'Dune Lake'.*

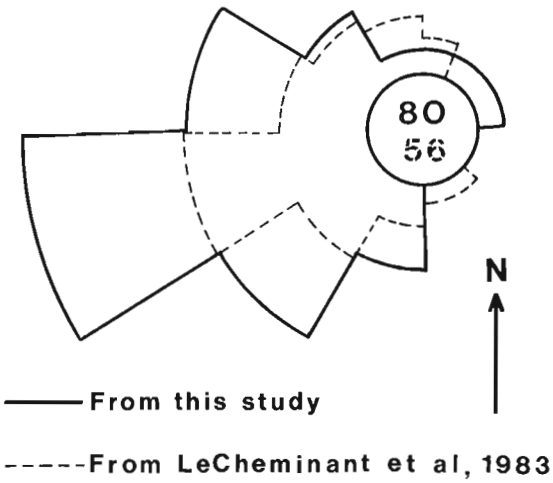

Figure 7.16. *Rose diagrams of axes of festoons from this and earlier studies. Southwest paleocurrents dominant.*

In summary, it seems that continental environments prevailed at this time in the northeastern part of the Thelon Basin and that, based on gross structure and facies associations, the previous suggestions of aeolian origin for the very large scale crossbedded facies at 'Dune Lake' were justified.

Dune type

In modern deserts, aeolian dunes and draas ('draas' are a large form of dune, see Wilson, 1971) take on a variety of forms. Based mainly on shape and orientation relative to the winds that form them, a number of different aeolian bedform types have been defined (Collinson and Thompson, 1982; McKee, 1966). Hunter (1981) noted that interpretation of dune type must be based in part on determination of 'dune plan-view morphology', and that in fossil sequences this is largely determined by curvature of individual crossbeds and distribution of crossbed dip directions. The dominance of curved cross-strata at 'Dune Lake' therefore indicate that the dunes in which they were deposited must have had regularly curved depositional surfaces. Of modern dunes only the barchan, parabolic, and aklé variety contain such surfaces in abundance. Most other dune types (e.g. transverse, dome, star, seif) are characterized by extensive planar surfaces which will produce dominantly planar cross-stratification, or they are characterized by depositional surfaces that dip in various directions, and hence are not applicable to the Thelon Formation at 'Dune Lake'. Of the three possible modern analogous dune forms, parabolic dunes have horns or flanks pointing upwind (opposite to that seen in the dunes at 'Dune Lake') and their formation is ascribed largely to fixation of the bulk of the dune by vegetation; hence these can be eliminated as a possible analogy for the 'Dune Lake' bedforms. From our more detailed study the plan view morphology of the festoons resembles classical barchan shapes (e.g. Finkel, 1959). Representatives of the steep upper slip face, more gently dipping lower lee face, and lateral horns all appear to be present at 'Dune Lake'. In fact the field appearance of these bevelled Thelon foresets is identical to published illustrations of barchan dunes, viz., 1) 'interdune corridor of truncated barchan dunes' (McKee, 1966); 2) 'planed-off festoons of a Cenozoic barchan, east of Abu Dhabi' (Glennie, 1970, Fig. 84); and 3) 'horizontal erosion surfaces through recent coastal barchan dunes in Brazil' (Bigarella, 1972, Fig. 10). From these comparisons, the interpretation by LeCheminant et al. of this area as a barchan dune field seems reasonable.

However, a more detailed analysis of the features of modern barchan dunes (McKee, 1966; Bigarella, 1972, Hunter, 1977b) indicates that the interpretation may not be this straightforward. Tabular planar and wedge planar cross-stratification are the main types of stratification preserved in the isolated small barchans studied by these authors, with trough cross-stratification being relatively rare. In addition, bounding surfaces between the sets are commonly planar and extensive, and are similar to those described by Brookfield (1977) who erected a three-fold hierarchy to subdivide aeolian bounding surfaces based on a study of Permian aeolian deposits from Scotland. The classification is based on the extent, regularity and interrelationships of these bounding surfaces and he attributed their formation to the migration of various sizes of climbing bedforms. This hierarchy appears to be widely applicable to aeolian deposits, and has been applied by various authors to other ancient sequences formed by migrating (climbing) transverse or barchan dunes.

A direct application of Brookfield's three-fold classification (and by implication an interpretation of bedform genesis) to the Thelon Formation at 'Dune Lake' is not possible due to the non-planar nature of the lower surfaces of the festoons. However, the contacts with the enclosing fluvial facies could represent 1st-order surfaces, and the scoop-like lower bounding surfaces to the festoons could be the equivalent of Brookfield's 2nd-order surfaces. According to Brookfield (op. cit.) first order surfaces are the most extensive and are attributed to the passage of the largest aeolian bedforms – drass – across an area. Such an interpretation is reasonable in this situation if the festoon facies as a whole is considered as a large draa complex. First order sufaces cut across second order surfaces, which according to Brookfield, are gently to moderately dipping surfaces bounding sets of cross-strata. In his example, second order surfaces are attributed to the passage of dunes across drass, or to longitudinal dunes migrating across the lower lee slopes of draas. At 'Dune Lake' the second order surfaces are scoop-like hollows of limited extent which are infilled by sets of more-or-less concordant cross-strata. Lower hierarchies of bounding surfaces equivalent to Brookfield's 3rd order surfaces were not seen in the Thelon festoon facies.

Brookfield (op. cit.) recognized that his proposed classification does not fit some ancient aeolian sandstones and suggested that sequences of overlapping trough cross-stratified units could be produced by migrating series of aklé dunes or draas. These bedforms consist of sinuous ridges, transverse to the wind, made up of crescentic sections alternately facing into, and away from, the wind (Cooke and Warren, 1973). The alternating barchanoid and linguoid elements enclose hollows which during migration form the loci for deposition of trough or scoop-like cross-stratified units. In a situation where there were low angles of climb of the bedforms, planar surfaces could be detroyed by the migration of the hollows, resulting in deposits of overlapping festoon cross-stratified units, lacking planar bounding surfaces. This type of mechanism might produce the festoon facies at 'Dune Lake'. The original bedforms thus may have been aklé, rather than barchan, dunes.

The main difference between barchan and aklé dunes appears to be that barchans develop as isolated forms on hard desert surfaces in response to unidirectional winds and a sparse sand supply, whereas aklé dunes develop under similar unidirectional winds where there is a considerable quantity of sand. Cooke and Warren (1973) noted that in modern deserts, the simplest pattern of bedforms, both in dune and draa-sizes, is the network of sinuous ridges of linguoid and barchanoid elements called aklé in the Sahara. Perhaps the exhumed eolian facies at 'Dune Lake' represents accretion of aklé dune forms, extensively eroded concurrently with deposition, so that the characteristic sinuous traces in plan view have been consistently destroyed.

References

Bigarella, J.J.
1972: Eolian environments, their characteristics, recognition and importance; in Recognition of Ancient Sedimentary Environments, ed. J.K. Rigby and W.K. Hamblin; Society of Economic Paleontologists and Mineralogists, Special Publication no. 16, p. 12-62.

Brookfield, M.E.
1977: The origin of bounding surfaces in ancient aeolian sandstones; Sedimentology, v. 24, p. 303-332.

Campbell, F.H.A. and Cecile, M.P.
1981: Evolution of the Early Proterozoic Kilohigok Basin, Bathurst Inlet-Victoria Island, Northwest Territories; in Proterozoic Basins of Canada, ed. F.H.A. Campbell; Geological Survey of Canada, Paper 81-10, p. 103-131.

Cecile, M.P.
1973: Lithofacies analysis of the Proterozoic Thelon Formation, Northwest Territories (including computer analysis of field data); unpublished M.Sc. thesis, Carleton University, Ottawa, 119 p.

Chiarenzelli, J.
1983: Mid-Proterozoic chemical weathering, regolith, and silcrete in the Thelon Basin, Northwest Territories; unpublished M.Sc. thesis, Carleton University, Ottawa, 197 p.

Coleman, J.M.
1969: Brahmaputra River: channel processes and sedimentation; Sedimentary Geology, v.3, p. 129-239.

Collinson, J.D. and Thompson, D.B.
1982: Sedimentary structures; Allen & Unwin, London, 194 p.

Conaghan, P.J. and Jones, J.G.
1975: The Hawkesbury Sandstone and the Brahmaputra: a depositional model for continental sheet sandstones; Geological Society of Australia Journal, v. 22, no. 3, p. 275-283.

Cooke, R.U. and Warren, A.
1973: Geomorphology in Deserts; Batsford, London, 375 p.

Donaldson, J.A.
1965: The Dubawnt Group, District of Keewatin and Mackenzie; Geological Survey of Canada, Paper 64-20.

1967: Two Proterozoic clastic sequences: a sedimentological comparison; Geological Association of Canada, Proceedings, v. 18, p. 33-54.

1969: Descriptive notes (with particular reference to the Late Proterozoic Dubawnt Group) to accompany a geological map of central Thelon Plain, Districts of Keewatin and Mackenzie; Geological Survey of Canada, Paper 68-49.

Finkel, H.J.
1959: Barchans of southern Peru; Journal of Geology, v. 67 (6); p. 614-647.

Fryberger, S.G. and Schenk, C.
1981: Wind sedimentation tunnel experiments on the origins of aeolian strata; Sedimentology, v. 28, no. 6, p. 805-821.

Glennie, K.W.
1970: Desert Sedimentary Environments; Developments in Sedimentology 14; Elsevier, Amsterdam, 222 p.

Hunter, R.E.
1977a: Terminology of cross-stratified sedimentary layers and climbing ripple structures; Journal of Sedimentary Petrology, v. 47, p. 697-706.

1977b: Basic types of stratification in small eolian dunes; Sedimentology, v. 24, p. 361-387.

1981: Stratificiation styles in eolian sandstones: some Pennsylvanian to Jurassic examples from the Western Interior U.S.A.; in Society of Economic Paleontologists and Mineralogists, Special Publication no. 31, p. 315-329.

Kerans, C., Ross, G.M., Donaldson, J.A., and Geldsetzer, H.J.
1981: Tectonism and depositional history of the Helikian Hornby Bay and Dismal Lakes Groups, District of Mackenzie; in Proterozoic Basins of Canada, ed. F.H.A. Campbell; Geological Survey of Canada, Paper 81-10, p. 157-182.

Knight,
1929: The Fountain and the Casper formations of the Laramie Basin; a study on genesis of sediments; University of Wyoming, Publications in Science, Geology, v. 1, pt. 1, p. 1-82.

Kocurek, G.
1981: Significance of interdune deposits and bounding surfaces in aeolian dune sands; Sedimentology, v. 28, p. 753-780.

Kocurek, G. and Dott, R.H., Jr.
1981: Distinctions and uses of stratification types in the interpretation of eolian sand; Journal of Sedimentary Petrology, v. 51, p. 579-595.

LeCheminant, A.N., Ashton, K.E., Chiarenzelli, J.,
Donaldson, J.A., Best, M.A., Tella, S., and Thompson, D.L.
1983: Geology of Aberdeen Lake map area, District of Keewatin: preliminary report; in Current Research, Part A, Geological Survey of Canada, Paper 83-1A, p. 437-448.

Mader, D.
1982: Aeolian sands in continental Red Beds of the Middle Buntsandstein (Lower Triassic) at the Western Margin of the German Basin; Sedimentary Geology, v. 31, p. 191-230.

McKee, E.D.
1966: Structures of dunes at White Sands National Monument, New Mexico (and a comparison with structures of dunes from other selected areas); Sedimentology, v. 7, 69 p.

Miller, A.R.
1983: A progress report: Uranium-phosphorous association in the Helikian Thelon Formation and sub-Thelon saprolite, central District of Keewatin; in Current Research, Part A, Geological Survey of Canada, Paper 83-1A, p. 449-456.

Pianosi, J.G.
1984: Interpretation and classification of dune forms in the Thelon Formation, northwest of Schultz Lake, N.W.T., Canada; unpublished B.Sc. thesis Carleton University, Ottawa, Canada, 40 p.

Ramaekers, P.
1981: Hudsonian and Helikian basins of the Athabasca region, northern Saskatchewan; in Proterozoic Basins of Canada, ed. F.H.A. Campbell; Geological Survey of Canada, Paper 81-10, p. 219-233.

Reading, H.G. (editor)
1978: Sedimentary Environments and Facies; Blackwell, Oxford, 557 p.

Ross, G.M.
1983: Proterozoic aeolian quartz arenites from the Hornby Bay Group, Northwest Territories, Canada: implications for Precambrian aeolian processes; Precambrian Research, v. 20, p. 149-160.

Rubin, D.M. and Hunter, R.G.
1982: Climbing of large-scale bedforms in theory and in nature; Sedimentology, v. 29, p. 121-138.

Steidtmann, J.R.
1974: Evidence for eolian origin of cross-stratification in sandstones of the Casper formation, southernmost Laramie Basin, Wyoming; Geological Society of America Bulletin, v. 85, p. 1835-1842.

Walker, R.G. and Harms, J.C.
1972: Eolian origin of flagstone beds, Lyons Sandstone (Permian), type area, Boulder County, Colorado; Mountain Geology, v. 9, p. 279-288.

Walker, R.G. and Middleton, G.V.
1979: Eolian Sands; in Facies Models, ed. R.G. Walker; Geoscience Canada Reprint Series 1, p. 33-41.

Wilson, I.G.
1972a: Universal Discontinuities in bedforms produced by the wind; Journal of Sedimentary Petrology, v. 42 (3), p. 667-669.

1972b: Aeolian bedforms – their development and origins; Sedimentology, v. 19, p. 173-210.

8. STREAM SEDIMENT SAMPLING, ORIENTATION STUDIES AND GEOCHEMICAL ASSOCIATIONS FROM SELECTED DEPOSITS ON CAPE BRETON ISLAND, NOVA SCOTIA[1]

Project 820025

P.J. Rogers[2] and M.A. MacDonald[3]

Rogers, P.J. and MacDonald, M.A., Stream sediment sampling, orientation studies and geochemical associations from selected deposits on Cape Breton Island, Nova Scotia; in Current Research, Part B, Geological Survey of Canada, Paper 84-1B, p. 65-74, 1984.

Abstract

Stream sediment samples were collected in orientation surveys at the Meat Cove and Coxheath deposits, Nova Scotia. Using non-parametric statistics it is possible to identify significant correlations at the deposit, local lithology and regional survey levels. Each deposit exhibits a characteristic geochemical association or fingerprint of various elements. Some of these elements are not significant in absolute terms in the regional threshold value but are present in the multi-element patterns. The recalculation of threshold levels with respect to principal catchment area lithologies is recommended for Nova Scotia surveys.

A stream sediment survey using field sieving and a linear sample spacing of 2 km on first, second or third order streams is able to detect deposits like Meat Cove and Coxheath. New analytical technology, the Inductively Coupled Plasma, with 'total' acid extraction yields larger element suites and is a method well suited to follow-up studies to locate mineralized areas. The use of partial acid extraction and Atomic Absorption Spectroscopy is still suitable for regional-type surveys.

Résumé

On a recueilli des échantillons de sédiments fluviaux lors de levés d'orientation dans les gisements de Meat Cove et de Coxheath (Nouvelle-Écosse). En se servant de méthodes statistiques non paramétriques, il est possible de définir des corrélations importantes à l'échelle du gisement, de la lithologie locale et de la région. Dans chaque gisement, il existe une association géochimique caractéristique ou empreinte de divers éléments. Certains de ces éléments ne sont pas importants en termes absolus en ce qui concerne la valeur seuil régionale, mais ils sont présents dans les profils multi-éléments. On recommande de recalculer les niveaux seuil en fonction des lithologies des principaux bassins pour les levés en Nouvelle-Écosse.

Il est possible de déceler des gisements comme ceux de Coxheath et de Meat Cove en tamisant des sédiments fluviaux à tous les 2 km sur des cours d'eau de premier, deuxième ou troisième ordre. Les grandes séries d'éléments fournies par la nouvelle technique analytique du plasma à couplage par induction ainsi que par l'extraction totale à l'acide, conviennent bien aux études subséquentes de localisation des zones minéralisées. L'extraction partielle à l'acide et la spectroscopie par absorption atomique conviennent encore pour les études régionales.

Introduction

During 1982 and 1983 a regional stream sediment survey was conducted throughout northern Nova Scotia. The project was funded by the Geological Suvey of Canada under the Canada-Nova Scotia Cooperative Mineral Program 1981-84. The regional survey complemented concurrent sample collection programs for lake sediments, lake and stream waters and heavy minerals (Fig. 8.1) (Rogers and MacDonald, 1983). The main aim of the exercise is to provide geochemical information to aid in locating unknown mineralized areas and enhance our knowledge of the resource potential of Nova Scotia.

Stream sediment surveys are applied to mineral exploration worldwide (Levinson et al., 1980) and are an extremely cost-effective exploratory tool (Meyer et al., 1979). The main exploration characteristic of a stream sediment is due to the variability of composition, grain-size, sorting and colour induced by the differing geological properties in the drainage catchment area (Rose, 1975). The determination of the variability in the sediment medium due solely to the presence of mineralization involves a plexus of independent variables such as lithology, climate, topography, humus, vegetation type and water-sediment interface reactions.

The orientation surveys reported here were conducted concurrently with the regional phase due to time and budgetary constraints. Past Nova Scotian surveys by both government agencies and private companies have confirmed the applicability of utilizing the -80 mesh material as the analytical fraction (MacNabb et al., 1976). Consequently most effort was directed towards verifying regional sampling design for adequate spacing, the application of field sieving techniques and to obtaining geochemical "fingerprints" of different deposit types in Nova Scotia. A wide variety of metallogenic provinces and resultant mineralization styles can be found in Nova Scotia (Chatterjee, 1983a). Extensive and ubiquitous glacial deposits are found within contrasting physiographic units (Grant, 1972). The two deposits selected for orientation surveys to reflect this diversity of input process to the regional geochemistry are Meat Cove and Coxheath. They also had the advantage of being relatively undisturbed by mining activities. All samples collected were analyzed jointly by Atomic Absorption Spectrometry (AAS) and Inductively Coupled Plasma – Atomic Emmission

[1] Contribution to the Canada-Nova Scotia Co-operative Mineral Program 1981-84.
Project carried by Geological Survey of Canada and Nova Scotia Department of Mines and Energy.

[2] Nova Scotia Department of Mines and Energy, P.O. Box 1087, Halifax, Nova Scotia B3J 2X1
[3] R.R.7, Williams Point, Antigonish County, Nova Scotia B2G 2L4

Spectroscopy (ICP-AES). The application of ICP-AES technology (Thompson, 1983) to exploration could thus be tested against the "traditional" AAS method.

General geology and physiography

Meat Cove deposit

The Meat Cove deposit is situated about 5 km east of the village of Meat Cove, Cape Breton Island (Fig. 8.1). The deposit is a magnesian skarn with disseminated and massive sphalerite with lesser amounts of pyrite, pyrrhotite, chalcopyrite, galena and magnetite (Chatterjee, 1979). The host rocks include interbedded siliceous dolomitic limestone and garnetiferous quartz-feldspar-biotite schist and were interpreted by Neale (1964) as the roof-pendant of a syenite body. From lithogeochemical traverses across the orebody, Chatterjee (1979) concluded that there had been a net introduction of Zn, Cu, Pb, Fe and Hg into the wall rocks and concentration of Cd, As and Ni in the ore zone.

The Meat Cove deposit is located at the northern extremity of the Cape Breton Highlands Block (Fig. 8.1). This physiographic region consists of an elevated, deeply incised plateau (about 450 m in elevation) and is underlain by crystalline rocks of Precambrian age. The area has a characteristically thin till cover on land forms composed of saprolite (McKeague, 1983). French Brook originates adjacent to and down slope from the deposit and descends from the plateau to a rolling lowland underlain by sediments of Carboniferous age and finally to the Atlantic Ocean in a distance of 4.5 km.

Coxheath deposit

The Coxheath copper deposit is situated approximately 10 km southwest of Sydney (Fig. 8.1). The deposit consists primarily of chalcopyrite in shear zones near a contact between felsic and mafic volcanics and a quartz diorite body. Chatterjee (1983b) classified the deposit within the Cu-Mo association of "typically I-type polyphase granitoid complexes." The ore zone contains elevated levels of B, Sc, Co, Ni, Cr, Cu and Zn.

Physiographically the area differs greatly from the upland plateau area of the Meat Cove deposit. The lowland areas have a thick till cover characterized by hummocky and drumlinized topography (Grant, 1972). Maximum elevations in the area rarely exceed 200 m. Grantmire Brook flows across the deposit, descending from 160 m to 80 m along a linear distance of 1 km onto a broad plain. The Coxheath area thus has a much lower hydraulic gradient and also a higher input of sediment from glacially transported sources than does Meat Cove. Iron and manganese mineral coatings on pebbles and boulders are common at Coxheath and absent at Meat Cove.

Sampling and analysis

Stream sediment samples were taken at linear intervals of 350 m in both areas. Material was collected by wet-sieving onsite to pass through a 1 mm nylon screen, placed in Kraft paper bags and air dried. Samples were then dry sieved to collect the -80 mesh material for analysis. Each analytical batch of 20 contains one standard, one field duplicate pair and one blind duplicate pair (Garrett et al., 1980). Samples were sent to a commercial laboratory for analysis by AAS using partial extraction by $HCl-HNO_3$ and by ICP-AES using 'total' extraction by $HF-HClO_4$.

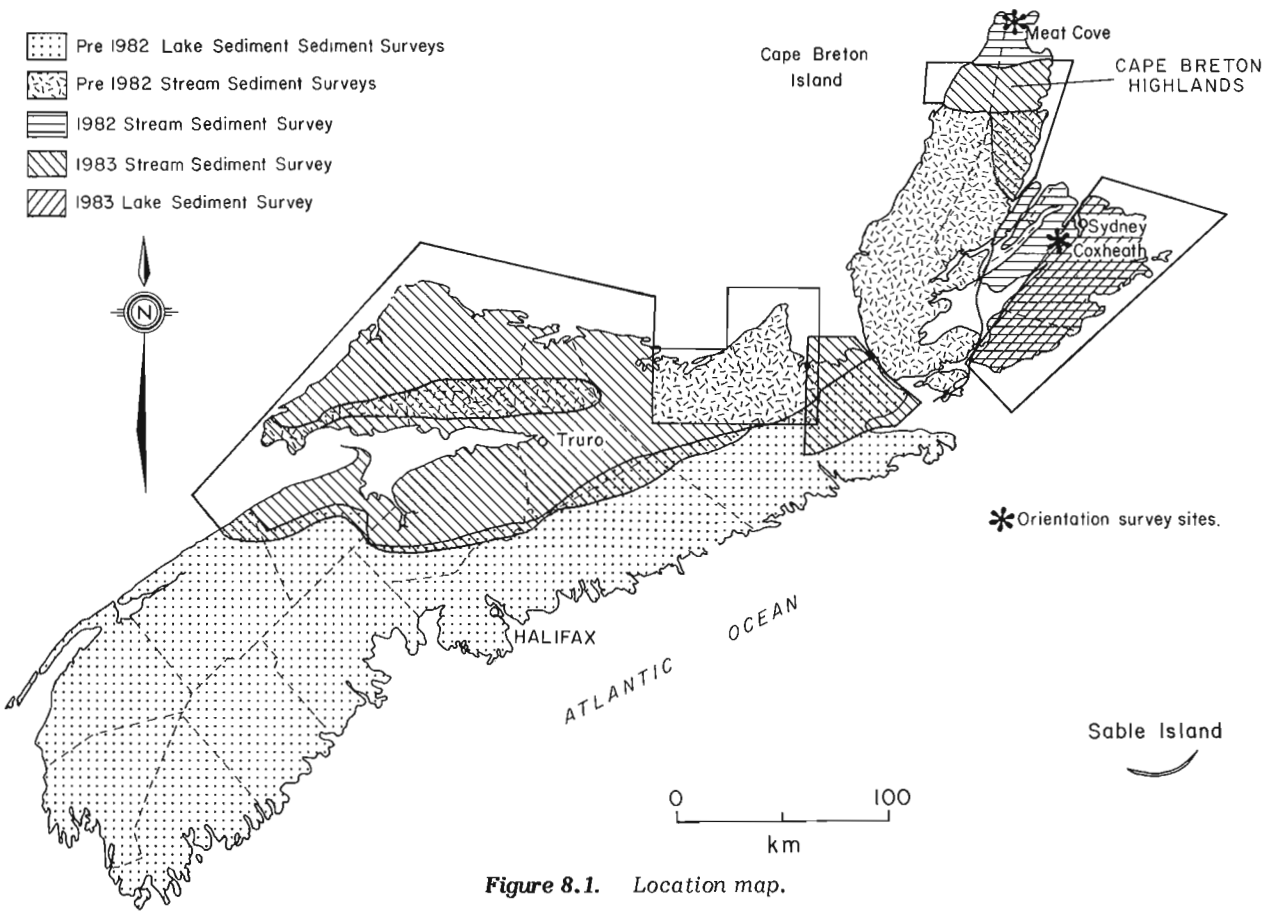

Figure 8.1. *Location map.*

Results

Sampling design

The regional and orientation surveys had identical sample collection and analytical (by AAS) procedures. Spacing for the regional survey was normally at 2 km intervals to sample most first, second and third order streams. To evaluate the significance of differences between the two survey levels a number of data subsets were used. The first data subset includes all regional data from the surrounding area of at least 200 km^2. This subset contains data from areas underlain by several lithologies and includes representative data from the regional orientation deposits. The second subset contains stream sediment data from areas underlain by lithologies similar to or associated with the mineralization. The third subset contains the deposits themselves.

Apart from basic statistics, thresholds for the individual elements were calculated following Hawkes and Webb (1962) using:

$T = \bar{x} + 2s$ where T = Threshold
$\bar{x}$ = Arithmetic Mean
s = Standard Deviation

Threshold values thus calculated appear in Table 8.1.

To characterize the geochemical expression of the deposits in the secondary environment, the regional and local subsets were assessed using non-parametric ranking statistics. This method enables the comparison of different populations of similar elements from the two survey levels (Rogers et al., in press). To estimate these regional and local effects Spearman rank correlation coefficients were obtained for each subset. Generally correlations greater than 0.5 were considered important. Thus for each data subset a number of significant correlations is derived for regional stream sediment data, local lithologies and the deposit itself. By identifying and then subtracting the regional and local effects a net inter-element "fingerprint" for the deposit is obtained. In this way the recognition of the more subtle geochemical expression of the deposit types in their local and regional context will assist in the detection of less pronounced geochemical anomalies.

Meat Cove zinc deposit

Basic statistics for the Meat Cove deposit are presented in Table 8.2. Downstream from the deposit the stream sediments are enriched in Zn, Pb, Ag and As and depleted in Cu, Ni, Co, Mn, Mo, Fe and U when compared to the regional background and local area data from granitoid lithologies (alkali granites and syenites). Hg is enriched with respect to the regional data and depleted when compared to the granitoid lithologies.

Thresholds and the corresponding number of anomalous samples are in Table 8.1. Utilizing the regional thresholds, stream sediments from the Meat Cove area are anomalous in Zn, Ag, Pb and As for distances of 4, 3.5, 1.5 and 1.2 km respectively from the deposit; for dispersion trains for Zn and Ag see Figures 8.2a, b. Recalculation of thresholds from the local granitoid lithologies enhances the As anomaly and diminishes the Pb and Ag anomalies. Mo becomes anomalous in two samples.

In Table 8.3 correlations are denoted by R for regional and G for granitoid lithologies. Table 8.3 includes a graphical representation of the "net effect" for the Meat Cove zinc deposit. Note the robust Ag-Cu, Ag-As, Ag-Pb and Cu-As correlations (i.e. Spearman correlation coefficients >0.90). Also worthy of note is the strong participation of Hg, Fe, Mn and U as prominent elements with as many as or more than

Table 8.1. Thresholds with numbers of anomalous samples, regional and local lithologies

GROUP/ELEMENT	MEAT COVE AREA	ALKALI GRANITOIDS SYENITES MEAT COVE	COXHEATH AREA	GRANITOID ROCKS COXHEATH
Zn	475/16	459/16	390/0	346/0
Cu	61/0	66/0	42/10	35/12
Pb	125/6	218/4	120/0	116/0
Ni	68/0	39/0	49/0	41/0
Co	29/0	30/0	94/0	78/2
Ag	0.24/20	0.35/15	0.2/10	1.8/2
Mn	9440/0	5830/0	33,940/0	27,089/0
As	9.6/5	4.3/11	42/1	22/2
Mo	5/0	2/2	13/0	5/9
Fe	5.78%/0	4.90%/0	5.14%/1	4.81%/1
Hg	142/0	267/0	174/2	206/2
U	19/0	24/0	9/0	14/0
	N = 203	N = 32	N = 473	N = 157

Key: 475/16 — Threshold value, ppm; Number of anomalous samples

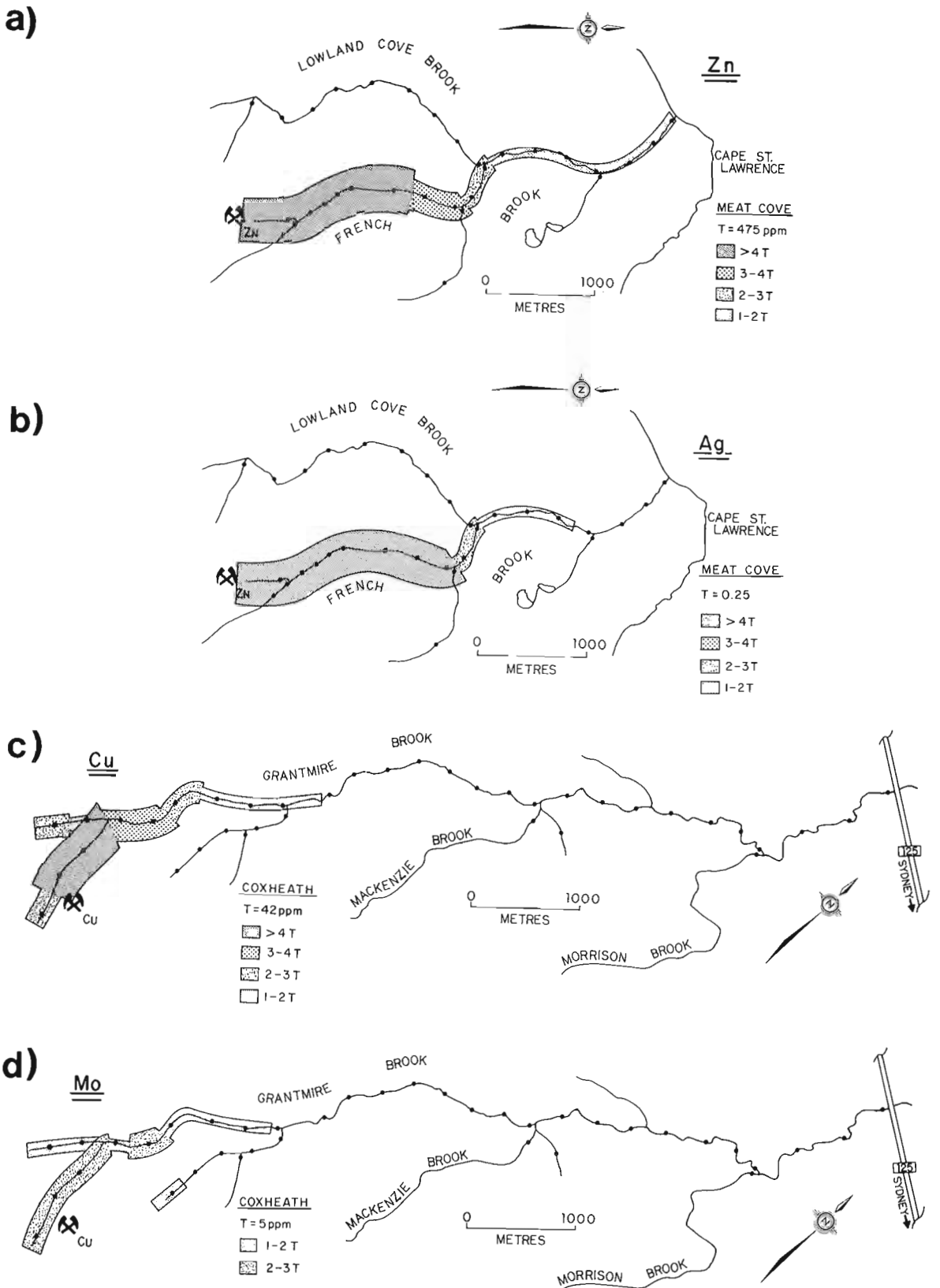

Figure 8.2. *Dispersion trains for Zn (a) and Ag (b) at Meat Cove and Cu (c) and Mo (d) at Coxheath.*

Table 8.2. Basic statistics for streams draining the orientation deposits, regional survey area and principal lithologies

		Zn	Cu	Pb	Ni	Co	Ag	Mn	As	Mo	Fe	Hg	U
MEAT COVE DEPOSIT													
N = 21	$\bar{x}$	1525	13	121	10	11	1.5	761	8.0		2.47	57	4.4
	S.D.	1285	6	135	2	3	1.8	184	8.3		0.49	29	1.6
	C.V.	84	49	112	20	30	123	24	103	N.D.	20	50	37
	RG.	138-4500	5-30	23-500	6-14	7-18	0.1-166	490-1100	1.5-31.5		1.85-3.90	20-120	2.0-8.4
Regional	$\bar{x}$	190	24	28	24	16	0.1	1994	3.0	1	3.08	50	6.3
N = 203	S.D.	143	18	49	22	7	0.1	3724	3.3	2	1.35	46	6.4
	C.V.	75	76	174	91	44	50	187	108	117	44	92	102
	RG.	20-1280	4-152	4-485	3-210	2-48	0.1-0.7	140-29000	0.5-27.5	1-22	0.25-11.60	20-530	1.6-39.2
Syenite and	$\bar{x}$	216	26	48	20	16	0.1	1840	2.1	1	2.90	78	7.8
Alkali	S.D.	122	20	85	10	7	0.1	1998	1.1	0.5	1.00	94	8.3
Granites	C.V.	56	78	179	50	43	83	109	55	34	36	121	107
N = 32	RG.	80-660	6-107	5-485	6-42	5-32	0.1-0.7	590-11550	0.5-5.0	1-2	1.55-5.35	30-530	1.6-39.2
COXHEATH DEPOSIT													
N = 22	$\bar{x}$	96	155	21	14	21	0.6	1380	9.8	4	2.60	81	3.2
	S.D.	24	336	12	2	21	1.6	683	14.3	4	0.84	67	0.4
	C.V.	25	217	57	14	100	273	49	146	82	32	83	13
	RG.	64-162	7-130	11-58	11-18	9-89	0.1-7.3	670-3900	2.0-67.5	1-12	1.70-5.10	30-280	2.5-4.1
Regional	$\bar{x}$	122	14	36	20	23	0.1	5806	9.1	3	2.54	69	3.2
N = 473	S.D.	134	14	42	14	35	0.1	14066	16.6	5	1.30	52	3.1
	C.V.	110	100	117	72	254	52	242	182	190	51	75	97
	RG.	3-1650	1-171	2-385	2-131	1-360	0.1-0.8	38$\geq$100000	0.5-195	1-42	0.25-10.60	20-500	0.5-47.3
Granitoid	$\bar{x}$	135	17	37	19	21	0.1	4639	5.6	4	2.71	77	4.3
Rocks	S.D.	106	9	39	11	28	0.8	11225	8.1	1	1.05	64	4.8
N = 157	C.V.	78	56	104	56	132	67	242	144	172	38	84	114
	RG.	38-740	3-68	5-230	6-74	4-200	0.1-0.8	150-85000	0.5-825	1-42	1.10-6.90	20-500	0.5-47.3

Key to Symbols: $\bar{x}$ = Arithmetic Mean
S.D. = Standard Deviation
C.V. = Coefficient of Variation ($CV\% = \frac{100 \times S.D.}{\bar{x}}$)
RG. = Range
N.D. = Not Detected

All values in p.p.m.; except Fe (% in percent) and Hg (ppb).

four inter-element correlations; yet in absolute terms no element is anomalous compared to background values. Zinc, which is the main anomalous element at Meat Cove, does not significantly correlate with other elements. Uranium displays strong negative correlations with Cu, Mn, As, Hg and Ag. Selected scattergrams are presented in Figure 8.3a to illustrate the strong correlations between the principal elements.

Coxheath copper deposit

Basic statistics for the Coxheath are presented in Table 8.2. Stream sediments at Coxheath are enriched in Cu, Ag, As and Hg and depleted in Zn, Pb, Ni and Mn compared to data from the regional and granitoid subsets. U is depleted when compared to granitoid data.

On a regional basis (Table 8.1) Coxheath stream sediments display pronounced Cu and Ag anomalies with anomalous dispersion trains up to 3 km in length. As, Hg and Fe anomalies are restricted to the deposit area. However if thresholds are recalculated using data from local granitoid lithologies, the Ag anomally is drastically reduced and Mo becomes anomalous up to 3 km away from the deposit. Dispersion trains for Cu and Mo at Coxheath are shown in Figures 8.2c, d.

Spearman rank calculations are presented in Table 8.4 and, as for Meat Cove, regional and lithological inter-element correlations $\geq$0.50 are included (also denoted by R for regional and G for granitoid). The net inter-element correlation effects are represented together with the correlation matrix in Table 8.4. With the exception of Cu-Mo, Cu-Mn and Cu-Zn, all correlations are $\geq$0.90. Hg, As and, to a lesser extent, Co are integral components of the inter-element "fingerprint" at Coxheath. However, they are only slighly anomalous in total concentration compared to the regional data. Representative scattergrams of some of the principal correlations are presented in Figure 8.3b.

Table 8.3. Spearman rank correlation coefficients for Meat Cove zinc deposit. R denotes significant regional correlation; G denotes significant correlation for granitoid rocks

Zn	Cu	Pb	Ni	Co	Ag	Mn	As	Mo	Fe	Hg	U	
1.00	.62	.82 G	-.02	.80	.80	.48	.79 G		.59	.71	-.56	Zn
	1.00	.88	-.65 R	.59 R	.91	.85	.94		.83 R, G	.79 G	-.83	Cu
		1.00	-.41	.79 G	.95	.67	.96 G		.73 G	.75	-.72 G	Pb
			1.00	.05 R	-.45	-.53	-.48		-.52	-.28	.54	Ni
				1.00	.71	.50	.73		.61 R	.74	-.52 R	Co
					1.00	.69	.97		.72	.76	-.76	Ag
						1.00	.76		.82	.88	-.85	Mn
							1.00		.78	.87	-.82	As
								1.00				Mo
									1.00	.80	-.72 R, G	Fe
										1.00	-.82	Hg
											1.00	U

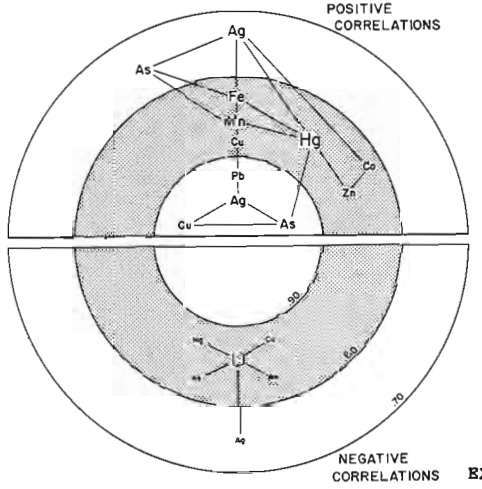

EXPLANATION

Circles correspond to Spearman rank correlation coefficients intervals.

Size of element symbols are proportional to number of correlations.

Tie lines crossing intervals signify correlations below interval value.

Table 8.4. Spearman rank correlation coefficients for Coxheath copper deposit. R denotes significant regional correlation; G denotes significant correlation for granitoid rocks

Zn	Cu	Pb	Ni	Co	Ag	Mn	As	Mo	Fe	Hg	U	
1.00	.89	.49	.23	.93 R	.06	.72 R	.91 R	.92 R	.92 R	.92 R	.46	Zn
	1.00	.36	.07 G	.97 R	.20	.76	.95	.93	.85 R	.95	.40	Cu
		1.00	-.16	.42 G	.25	.35 G	.45	.48	.39	.49 G	-.01	Pb
			1.00	.11 R	-.23	-.26	.13	.04	.38	.06	.34	Ni
				1.00	.19	.81 R, G	.97 R	.93 G	.89 R, G	.95	.34	Co
					1.00	.18	.20	.21	.12	.15	-.52	Ag
						1.00	.80 R	.73 R, G	.74 R, G	.73 R, G	.30	Mn
							1.00	.91	.88 R, G	.94	.41	As
								1.00	.84 R, G	.90	.43	Mo
									1.00	.87 R, G	.45	Fe
										1.00	.37	Hg
											1.00	U

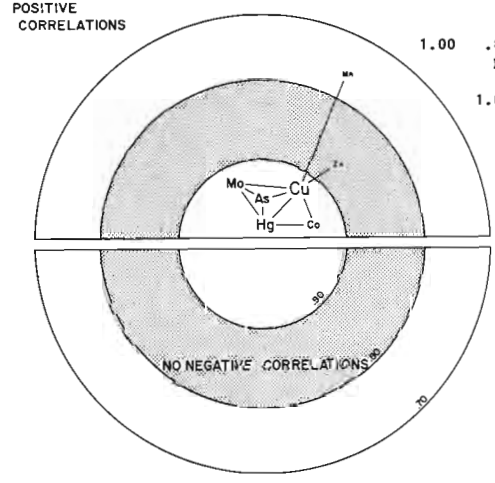

EXPLANATION

Circles correspond to Spearman rank correlation coefficients intervals.

Size of element symbols are proportional to number of correlations.

Tie lines crossing intervals signify correlations below interval value.

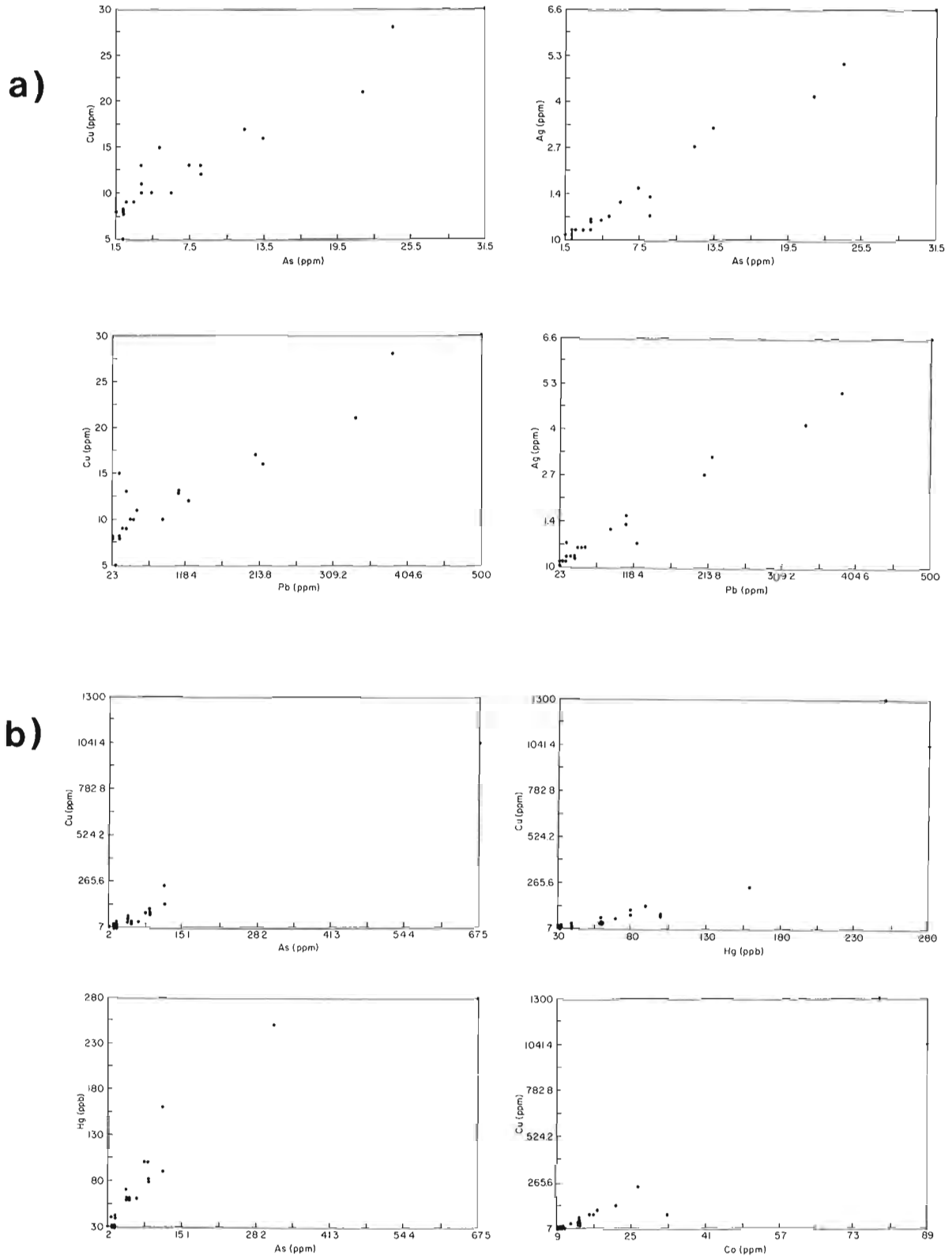

Figure 8.3. *Scattergrams for selected elements at Meat Cove (a) and Coxheath (b).*

ICP-AES in exploration

Analytical results (AAS and ICP-AES) for common elements from Coxheath and Meat Cove stream sediments were compared using Kruskal-Wallis one way analysis of variance. Results are given in Table 8.5. Most elements, except Co, display significant differences between the two techniques at either Meat Cove or Coxheath. No significant difference is detected for Cu, Mn and Mo at Coxheath and Zn and Pb at Meat Cove; all of these elements are anomalous at each location.

The statistical analysis indicates no significant difference between elements found at elevated concentrations in both deposits. The significant differences noted are probably due to analytical variance at or near the detection limit rather than between the analytical methods themselves (Fletcher, 1981).

Bar diagrams for selected elements at Meat Cove and Coxheath (Fig. 8.4) show a noticeably higher anomaly/background contrast for AAS when compared to ICP-AES. This undoubtedly represents the effects of the partial leach of $HCl-HNO_3$ used for AAS against the 'total' $HF-HClO_4$ dissolution used for the ICP-AES. Scott and Kokot (1975) found ICP-AES to give lower results than AAS for Cu, Pb, Zn, Co and Ni, probably due to interferences in the flame. This study used an identical digestion with a nitric-perchloric extraction. Although the present study indicates AAS to be more suitable when partial extractions are used to detect hydromorphic or chemical anomalies the ICP-AES is still useful. The much larger element suite offered by ICP-AES identified a much larger anomalous suite for the Meat Cove and Coxheath deposits (Fig. 8.5). In particular depletions in K, P, Ti, Na and Sr in the stream sediments draining the Meat Cove skarn are of interest. These can be considered as "negative anomalies". Those of Sr and P were detected up to 1 km downstream of the deposit. The ICP-AES could profitably be employed during detailed 'follow up' studies once an anomalous area is recognized. The increased data content from the samples would merit consideration at this point. The 'negative anomalies' for skarn deposits like Meat Cove supports the use of ICP-AES as a useful exploration tool.

Conclusions

Results from the two orientation surveys indicate that the regional sample spacing utilized in the stream sediment survey (i.e. 1 sample per 2 linear km) is sufficient to locate any undiscovered "Meat Cove" or "Coxheath" type mineralization which is exposed in a well drained area.

Further enhancement and evaluation of anomalies in stream sediments and the establishment of new anomalous elements may be achieved by recalculating thresholds with respect to major catchment area lithologies.

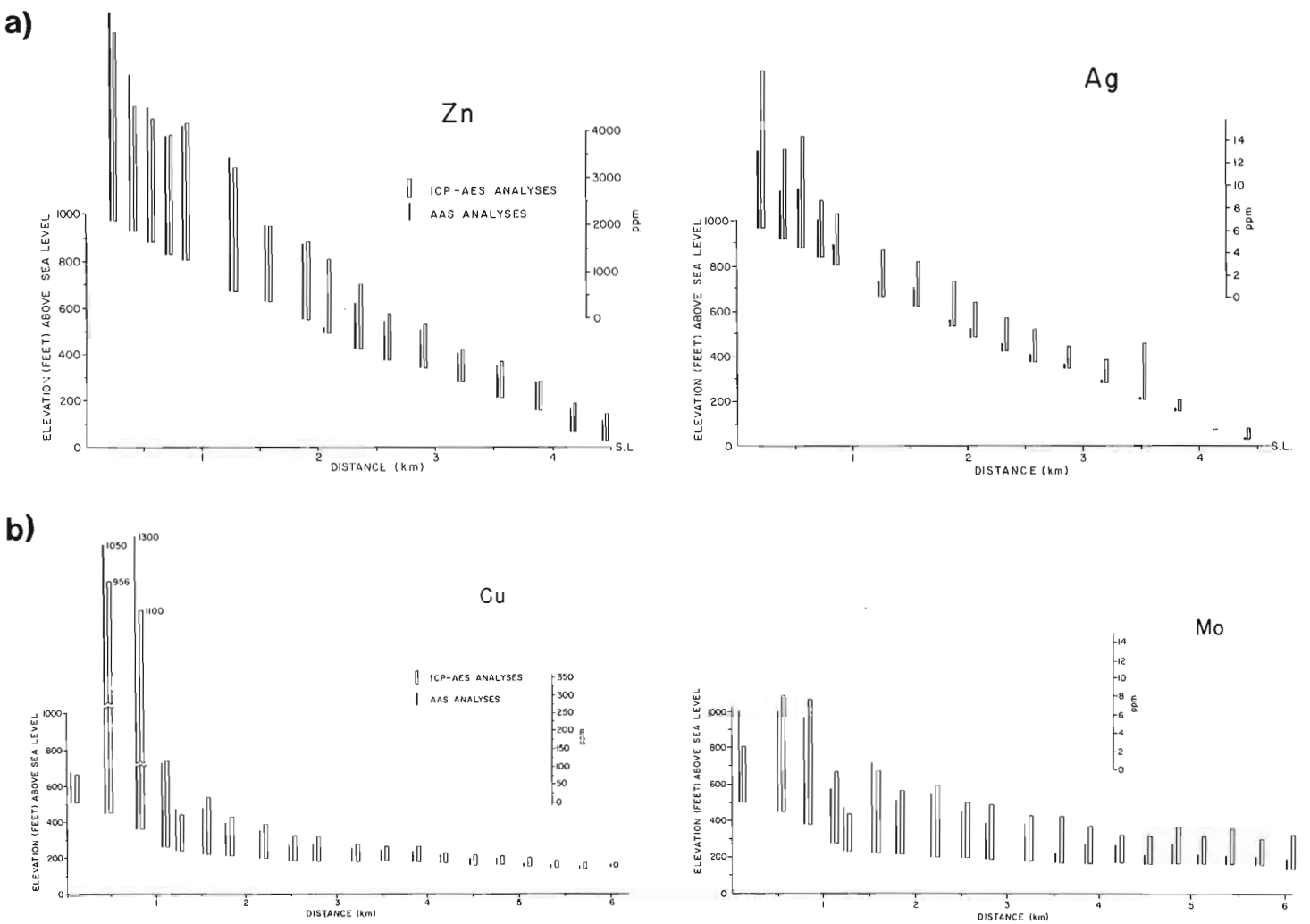

Figure 8.4. *Bar diagrams for AAS and ICP-AES for Meat Cove (a) and Coxheath (b).*

Table 8.5. Kruskal-Wallis one way analysis of variance for analytical results of stream sediments by AAS vs. ICP-AES

	Zn	Cu	Pb	Ni	Co	Ag	Mo	Fe
Coxheath Copper Deposit N = 41	17.29 .000 ***	3.19 .074 N.S.	28.44 .000 ***	30.99 .000 ***	5.30 0.21 N.S.	54.49 .000 ***	6.40 .011 N.S.	43.90 .000 ***
Meat Cove Zinc Deposit N = 31	0.80 .371 N.S.	12.19 .000 ***	4.52 .033 N.S.	19.17 .000 ***	0.06 .804 N.S.	9.20 .002 **	44.78 .000 ***	43.90 .000 ***

Explanation:
16.41 ——— Chi-Square Ratio
.000 XXX ——— Significance
Significance value
N.S. ——— Not Significant
* ——— Probability of significant difference between 95 and 99%
** ——— Probability of significant difference between 99 and 99.9%
*** ——— Probability of significant difference >99.9%

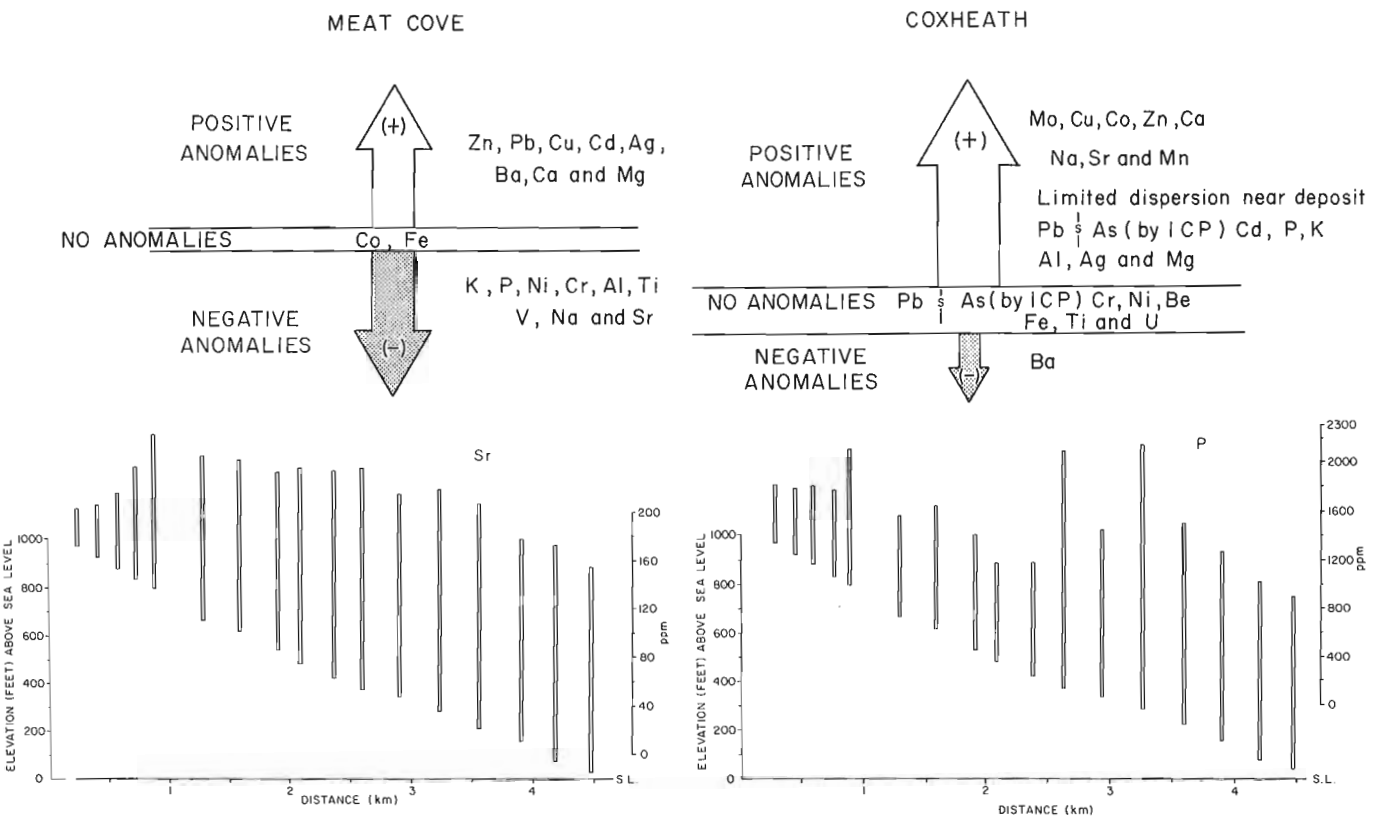

Figure 8.5. *Orientation deposits and anomalies defined by AAS and ICP-AES. Bar diagrams to illustrate negative anomalies.*

Spearman rank, non-parametric correlation calculation for inter-element relationships serves to "fingerprint" the individual mineral deposits. Coxheath displays strong Cu-Mo, Cu-As, As-Mo, Cu-Co, Hg-Co, Mo-Hg, Hg-As and Hg-Cu and weak Cu-Zn and Cu-Mn correlations. Meat Cove displays strong Ag-Cu, Ag-As, Ag-Pb, Cu-As and weak Hg-As, Pb-Cu, Cu-Mn, Mn-Fe, Hg-Fe, Hg-Mn, Hg-Zn, Zn-Co positive correlations and moderate U-Hg, U-Cu, U-As, U-Mn and weak U-Ag negative correlations. The ICP-AES method is recommended for detailed 'follow up' of defined anomalies.

The present study has demonstrated that any regional geochemical survey in Nova Scotia must take cognisance of the contrasting lithologies, metallogeny and physiography of the catchment drainage area. The Meat Cove deposit has a marked multi-element 'fingerprint' compared to the much reduced pattern at Coxheath. Although most of this could be a function of mineralization type, the flat hydraulic gradient and probable dilution by glacial outwash deposits at Coxheath also probably contributed to this process.

The distinction of subtle inter-element correlations, e.g. with Hg, which are not evident by considering absolute value alone, merits consideration. These subtly expressed 'pathfinder' elements could be identified on a regional scale by using ratio plots. Establishment of these "net inter-element correlations" may be useful in classifying and interpreting subtle geochemical anomalies from buried or weakly exposed mineralization.

AAS coupled with partial extraction sample digestion produces higher anomaly/background contrasts than for the 'total' HF digestion suite ICP-AES. However ICP-AES provides an inexpensive way of analyzing for a large number of elements not normally used in regional surveys due to high costs of analysis.

Acknowledgments

We would like to thank our field crew, E. Amirault, D. Cooke, M. Drohan, S. Edmonds, T. LaPierre, and B. McLeod for their dedication and hard work in collecting the samples; Don Bernasconi, Carol McKinnon and the draughting section staff for their able assistance with the diagrams; and our colleagues at the Nova Scotia Department of Mines and Energy for advice and encouragement. Finally, thanks to Janice Glenn for the draft typing of the manuscript.

References

Chatterjee, A.K.
1979: Geology of the Meat Cove zinc deposit, Cape Breton Island, Nova Scotia; Nova Scotia Department of Mines and Energy, Paper 79-3, 27 p.

1983a: Metallogenic map of the province of Nova Scotia; Nova Scotia Department of Mines and Energy, 1:500 000.

1983b: Contrasting granophile (Sn:W:Mo:Cu:U) deposits of Nova Scotia; Nova Scotia Department of Mines and Energy, Report 83-1.

Fletcher, W.K.
1981: Analytical methods in geochemical prospecting; in Handbook of Exploration Geochemistry; vol. 1, ed. G.J.S. Govett, Elsevier, Amsterdam, 255 p.

Garrett, R.G., Kane, V.E., and Zeigler, R.K.
1980: The management, analysis and display of regional geochemical data; Journal of Geochemical Exploration, v. 13, p. 115-152.

Grant, D.R.
1972: Surficial geology of southeastern Cape Breton Island, Nova Scotia; in Report of Activities, Part A; Geological Survey of Canada, Paper 72-1A, p. 160-163.

Hawkes, H.E. and Webb, J.S.
1962: Geochemistry in Mineral Exploration; Harper and Row, New York.

Levinson, A.A., McCammon, R.B., and Hitchon, B.
1980: Introduction to Exploration Geochemistry, 2nd edition; Applied Publishing Co., 924 p.

MacNabb, B.E., Fowler, J.H., and Covert, T.G.N.
1976: Geology, geochemistry and mineral occurrences of the Northeast Margaree River drainage basin in parts of Inverness and Victoria Counties, Cape Breton, Nova Scotia; Nova Scotia Department of Mines and Energy, Paper 76-4, 30 p.

McKeague, J.A.
1983: Properties and genesis of a soil and the underlying gibbsite-bearing saprolite, Cape Breton Island, Canada; Canadian Journal of Earth Sciences, v. 20, no. 1, p. 37-48.

Meyer, W.T., Theobald, P.K., Jr., and Bloom, H.
1979: Stream sediment geochemistry; in Geophysics and Geochemistry in the Search for Metallic Ores, ed. P.J. Hood; Geological Survey of Canada, Economic Geology Report 31, p. 411-434.

Neale, E.R.W.
1964: Pleasant Bay, Nova Scotia; Geological Survey of Canada, Map 1159A.

Rogers, P.J. and MacDonald, M.A.
1983: Regional geochemical surveys; in Program and Summaries, Nova Scotia Department of Mines and Energy seventh annual open house and review of activities; Nova Scotia Department of Mines and Energy, Information Series No. 6, p. 33-35.

Rogers, P.J., Stea, R.R., and MacDonald, M.A.
– A statistical investigation of the geochemical reflection of gold mineralization in the tills and lake sediments of the Eastern Shore Region, Nova Scotia; in Prospecting in Areas of Glaciated Terrain; Institution of Mining and Metallurgy, London.

Rose, A.E.
1975: The mode of occurrence of trace elements in soils and stream sediments applied to geochemical exploration; in Geochemical Exploration 1974, ed. I.L. Elliott and W.K. Fletcher; Elsevier, Amsterdam, p. 691-705.

Scott, R.H. and Kokot, M.L.
1975: Application of inductively coupled plasmas to the analysis of geochemical samples; Analitica Chimica Acta, v. 75, p. 257-270.

Thompson, M.W.
1983: Handbook of Inductively Coupled Plasma Spectrometry; Chapman and Hall, New York, 273 p.

9.

GEOLOGY OF THE CENTRAL PLATEAU OF THE EAST BULL LAKE PLUTON, NORTHEASTERN ONTARIO

D.C. Kamineni, G.F. McCrank, D. Stone, R.B. Ejeckam, R. Flindall and R. Sikorsky
Atomic Energy of Canada Limited, Ottawa

Kamineni, D.C., McCrank, G.F., Stone, D., Ejeckam, R.B., Flindall, R., and Sikorsky, R., Geology of the central plateau of the East Bull Lake pluton, northeastern Ontario; in Current Research, Part B, Geological Survey of Canada, Paper 84-1B, p. 75-83, 1984.

Abstract

The central plateau of the East Bull Lake pluton is divided into 12 map units based on mineralogy and magmatic structures. The basal anorthositic section of the pluton grades to a rhythmically layered gabbro unit that in turn grades to a troctolite-norite sequence. Above this, units differing in mineral content and textures include dendritic, pegmatitic, crescumulate, and massive gabbros.

Numerous mafic dykes intrude the pluton and include amphibolite, diabase, feldspar porphyry, hornblende porphyry and aphanitic-glassy dykes.

All gabbro units are affected by alteration, which includes alteration rims around pyroxene, replacement of primary minerals, and alteration along microfractures. Fractures in the pluton are filled with high-temperature fillings, a mixture of fillings in and near major fault zones, and low-temperature fillings.

Core logs prepared from two boreholes show that most of the units at surface are correlative with those in the subsurface. The depth of the pluton is about 800 m, and it is underlain by a gneissic granite.

Résumé

On divise le plateau central du pluton de East Bull Lake en 12 unités cartographiques basées sur des structures minéralogiques et magmatiques. La section basale anorthositique du pluton passe progressivement à un gabbro, présentant des lits rythmiques, qui passe à son tour à une séquence de troctolite et de norite. A cette dernière succèdent des unités à teneur minéralogique et textures différentes: gabbros dentritiques, pegmatitiques, massifs et à cristaux à angle droit.

Le pluton est traversé par de nombreux dykes mafiques qui sont constitués d'amphibolite, de diabase, de porphyre feldspathique, de porphyre à hornblende et de grains fins à vitreux.

Tous les gabbros ont subi des altérations dont les bordures d'altération autour du pyroxène, le remplacement des minéraux primaires et l'altération le long des microfractures. Les fractures du pluton sont remplies de matériaux de haute température, mélanges de matériaux de remplissage dans les principales zones faillées et près de ces dernières, et des matériaux de basse température.

Les diagrammes des carottes préparés à partir de sondage montrent que la plupart des unités de surface corrèlent avec celles de profondeur. Le pluton, profond d'environ 800 m, repose sur un granite gneissique.

Introduction

The East Bull Lake pluton is about 30 km north-northwest of Massey, Ontario. Previous work on the intrusion include study by Born (1978), Born and James (1978), Brown and Kamineni (1981), McCrank et al. (1983), and James et al. (1983).

Detailed geological mapping was carried out in the central region (plateau) of the East Bull Lake pluton, during the summer of 1983 (Fig. 9.1). The study involved mainly subdivision of the rocks of the plateau, mapping of dykes, measurement of strike and dip of layering, and sample collection for an ongoing petrological and geochemical investigation. The plateau was mapped at 1:2500 scale, based on an enlargement of a 1:15 840 aerial photograph. The shape and extent of the outcrops were located on the photograph by using north-south grid lines, spaced at 200 m, and cut for this project.

The map of the plateau (Fig. 9.1) provided prerequisite information for siting four boreholes.

Geology

The central region of the East Bull Lake pluton was subdivided on the basis of mineral content, texture and structure, variation in styles of layering, and similar criteria. Twelve units were mapped: (1) anorthosite layered unit, (2) rhythmically layered gabbro, (3) troctolite, olivine gabbro, and norite layered unit, (4) nonregularly layered gabbro, (5) irregularly layered gabbro, (6) dendritic layered gabbro, (7) coarse grained and pegmatitic layered gabbro, (8) massive gabbro, (9) crescumulate gabbro, (10) K-feldspar-bearing gabbro, (11) stockwork gabbro and (12) granophyre dykes. In addition, a mafic volcanic unit and mafic and aplitic dykes are also present.

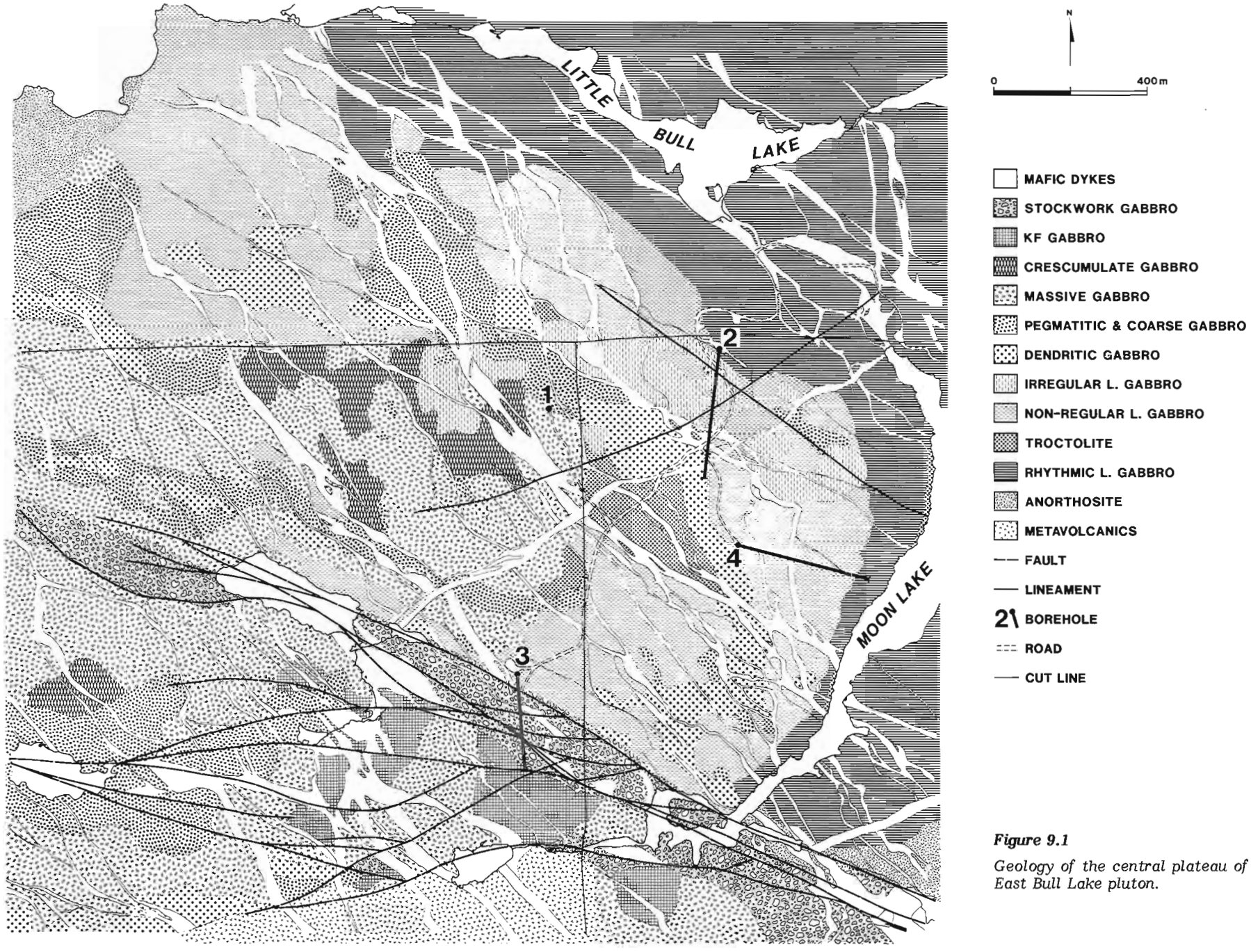

Figure 9.1

Geology of the central plateau of the East Bull Lake pluton.

Mafic volcanic unit

This unit occurs along the southern margin of the map area. The volcanics show pillow structures and are metamorphosed to chlorite-, epidote- and actinolite-bearing assemblages. These mineral assemblages suggest that they were metamorphosed under epidote-amphibolite conditions (Winkler, 1974; Turner, 1981). The volcanics have a general foliation striking about 320 degrees and dipping 70 degrees to the northeast.

Anorthositic layered unit

This unit occurs in the northwest and southeast corners of the map area. The anorthosite is rich in plagioclase feldspar (An ~ 70) and generally contains 1 to 10 per cent clinopyroxene, which in some cases may show spheroidal and orbicular forms. Layers with high pyroxene content and segregations of pyroxene crystals within anorthosite layers are common. The pyroxene content in such zones may be as great as 50 per cent and, therefore, locally the unit is gabbro or gabbroic anorthosite. The pyroxene crystals are invariably large, ranging from 1 to 10 cm. A thin alteration rim of amphibole mantles all the pyroxene crystals. Contacts between layers in this unit are sharp, and may show slump structures (Fig. 9.2).

Rhythmically layered unit

This unit occurs mostly on the eastern side of Moon Lake and on the northern part of the plateau, and is characterized by regular layers of alternating anorthosite and gabbro (Fig. 9.3). Generally, the anorthosite layers (15-25 cm thick) are thinner than the gabbroic layers (1 m thick). Certain gabbro layers may be considerably thicker than 1 m, if so the rhythmic layering is not evident but 'igneous lamination', where feldspar and pyroxene crystals are strongly oriented parallel to the layering, is conspicuous (Hess, 1960). This type of gabbro is well exposed on the southeastern shore of Moon Lake and extends outward in the same direction.

The contacts between anorthosite and gabbro layers are sharp. Some gabbroic layers may show cumulation of pyroxenes and size gradations or mineral grains. Some layers have a high enough pyroxene content to be pyroxenite.

One notable feature of this unit is a set of fractures oriented perpendicular to layering that are concentrated in the anorthositic layers (Fig. 9.4) but dissipated in adjacent gabbroic layers. These fractures are well healed with clinoamphibole (actinolite), epidote and chlorite fillings.

Troctolite, olivine gabbro and norite layered unit

This unit, exposed as discontinuous areas of outcrop along the western shore of Moon Lake, comprises interlayered troctolite, olivine gabbro, and norite. Troctolite, which always occurs at the base, is characterized by an abundance of olivine and calcic plagioclase, with subordinate amounts of orthopyroxene. A decrease in olivine and an increase in pyroxene content in certain layers modify the troctolite to olivine gabbro. Some layers contain little or no olivine, but contain abundant orthopyroxene, and form norite.

All three rock types contain high concentrations of magnetite.

Serpentine crystals, oriented perpendicular to fracture walls, are a common fracture filling material in this unit. Chlorite associated with serpentine occurs as slickensides.

Nonregularly layered gabbro

This unit, which occurs mainly in the northern and eastern parts of the plateau, consists of a number of subunits that are distinct in texture and contain subtle differences in layering.

One of the abundant subunits is the fine- and coarse-grained layered gabbro. The layers in this subunit alternate rhythmically from coarse- to fine-grained gabbro. Thickness of the layers is variable and ranges from a few centimetres to about 1 metre. Generally, the coarse-grained gabbro forms thicker layers, which show subophitic texture and which may also display mineral grading (Fig. 9.5) and crossbedding (Fig. 9.6). The arrangement of layers and the general appearance of this subunit are somewhat similar to the rhythmically layered unit, but, in contrast, the anorthosite layers are absent.

Gabbro, with well-developed ophitic texture, is another major subunit. Layering is not common, but where present, ophitic gabbro with differing grain size defines the layering (Fig. 9.7). Sulphide mineral grains are common.

Gabbro containing pyroxene-rich layers forms a minor subunit within the nonregularly layered gabbro unit. Three or four pyroxene-rich layers (1 to 2 cm thick) occur in groups that are spaced at approximately 5 to 10 cm intervals.

Irregularly layered gabbro

Gabbro containing fine layering giving rise to colloform and corrugated structures (Wager and Brown, 1968), occurs as patches within the nonregularly layered gabbro. These structures are more prominent in horizontal than in steep cross sections, a feature also noted by Wager and Brown (1968) in the Skaergaard Intrusion.

Grain size in the irregularly layered gabbro unit varies from fine to medium, with the size differences defining the layering. An important characteristic of this unit is that it contains xenoliths of both gabbroic and anorthositic composition (Fig. 9.8). Some xenoliths display stretching. A rim of coarse grained material is common around the xenoliths and presumably represents a reaction rim between the xenolith and the host gabbro.

Dendritic layered gabbro unit

Dendritic or comb-structure layered gabbro is located in the central region of the plateau and occurs as linear bands in the central and southern regions of the area. Slender curvilinear crystals of clinopyroxene ranging from 1 to 50 cm in length are variably altered to clinoamphibole. These crystals often radiate out from a nucleus and give rise to a 'fan-like' shape (Fig. 9.9). The long axes of pyroxene crystals in the dendritic gabbro are oriented both parallel or, more commonly, perpendicular to the layering. The interstices between pyroxenes are generally filled with medium grained plagioclase and, in some cases, with K-feldspar and quartz.

Pegmatitic and coarse-grained gabbro

Gabbro with pegmatitic grain sizes occurs as layers, and usually associated with dendritic-layered gabbro. Mineralogically, the unit comprises large crystals of pyroxene and plagioclase and, occasionally, minor amounts of K-feldspar and quartz. Large concentrations of magnetite are present in some outcrops. The pyroxenes in this unit are as large as the pyroxenes in the dendritic layered unit, but in contrast their long axes are straight rather than curved.

The pegmatoidal layering is only an expression of grain size caused by local differences in either growth rate or concentration of volatile components and is thus independent of modal variation.

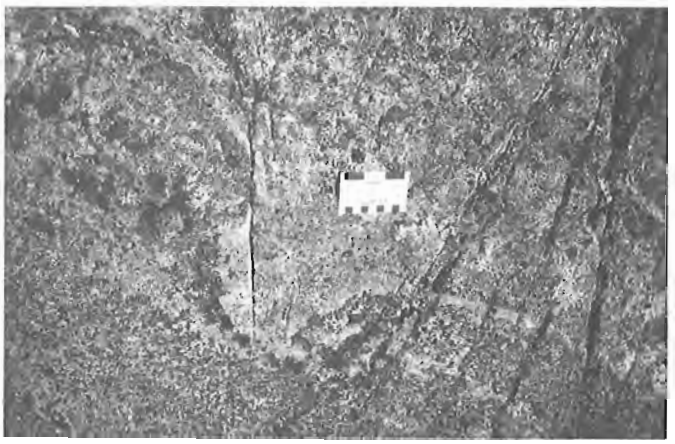

Figure 9.2. *Slump structure between anorthosite layer and pyroxene-rich layer. (203671-P)*

Figure 9.3. *Alternating rhythmic layers of anorthosite and gabbro. (203671-M)*

Figure 9.4. *Concentration of fractures in anorthositic layers in the rhythmic layered unit. (203671-I)*

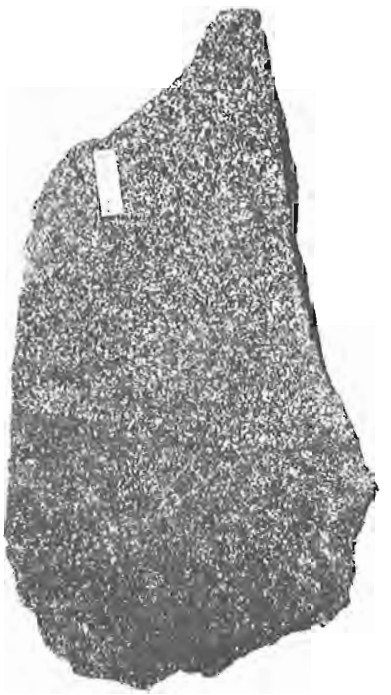

Figure 9.5. *Layered coarse- and fine-grained gabbro of the nonregularly layered unit. Note the subophitic texture and mineral grain gradation in the coarse-grained layer. (203555-U)*

Figure 9.6. *Cross bedding in the nonregularly layered gabbro unit. (203671-S)*

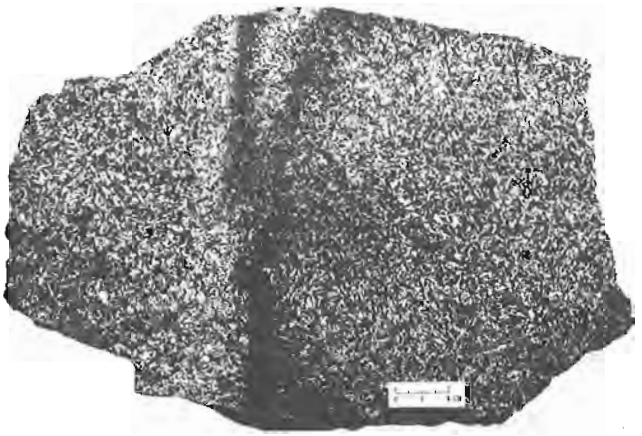

Figure 9.7. *Layered ophitic-textured gabbro. Note the difference in grain size between the two layered and crossbedding. (203616-U)*

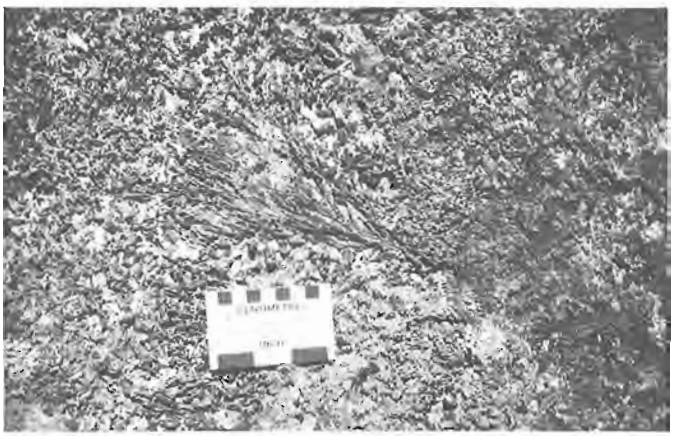

Figure 9.9. *Dendritic layered gabbro showing fan-like shape. (203671-J)*

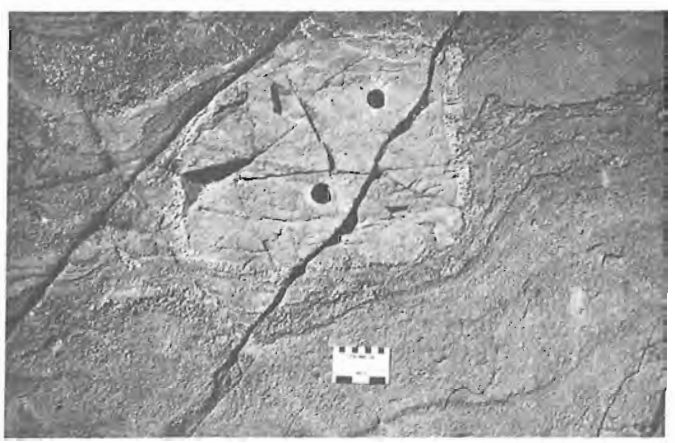

Figure 9.8. *Irregular layered gabbro unit. Note xenoliths with reaction rim. (203671-L)*

Figure 9.10. *Stockwork gabbro showing network of quartz and feldspar veins. (203671-O)*

Coarse-grained gabbro with equigranular texture is abundant in some parts of the area. In the present study, no attempt was made to separate this unit from that of the pegmatitic gabbro. The area outlined south of 'Folson Lake Fault' is composed of this rock type.

The coarse-grained gabbro is mainly plagioclase and clinopyroxene. The clinopyroxene is altered to blue-green amphibole and contains minor amounts of iron oxides and sphene. Fine- to medium-grained gabbro layers are richer in ferromagnesian minerals and are interlayered with coarse-grained gabbro in some outcrops.

Massive gabbro

This unit is concentrated in the central part of the area, and comprises medium- to fine-grained gabbro with subophitic texture. It contains 2-5 per cent modal quartz and may represent one of the late differentiates of the East Bull Lake pluton.

Clinopyroxene, noted as relicts in the massive gabbro, is mostly converted to clinoamphibole; plagioclase is partly altered to epidote and calcic amphibole. Fractures containing epidote and chlorite are common and characteristically contain a thick zone (≈2 cm) of wall rock alteration. Because of the extensive alteration, this unit is termed metagabbro.

Crescumulate gabbro

This unit is also concentrated in the central and western regions of the area and is very similar to massive gabbro, except that it has a characteristic planar orientation of elongated crystals. Prisms of plagioclase and altered pyroxene show strong preferred orientation, generally perpendicular to the layering, which gives rise to 'crescumulate layering' (Wager, Brown and Wadsworth, 1960). In some instances, the oriented crystals are elongated within layers and may represent igneous laminations (Hess, 1960).

Pyroxene crystals in the crescumulate gabbro are thoroughly altered to amphiboles. Two types of amphiboles are recognized under microscope: (1) blue-green amphibole, rimming pyroxene and (2) colourless-calcic amphibole, occupying cores of pyroxene. Plagioclase grains show moderate alteration to epidote and calcic amphibole. In view of the high degree of alteration, the crescumulate gabbro is also termed metagabbro.

Stockwork gabbro

This unit extends as a narrow zone along the northwest-trending 'Folson Lake Fault' (McCrank et al., 1983). It is characterized by an intricate network of quartz and feldspar veins comprising 20 to 30 volume per cent of the rock (Fig. 9.10). There are at least two generations of quartz veins. Feldspar veins are mainly plagioclase and the low temperature K-feldspar polymorph adularia.

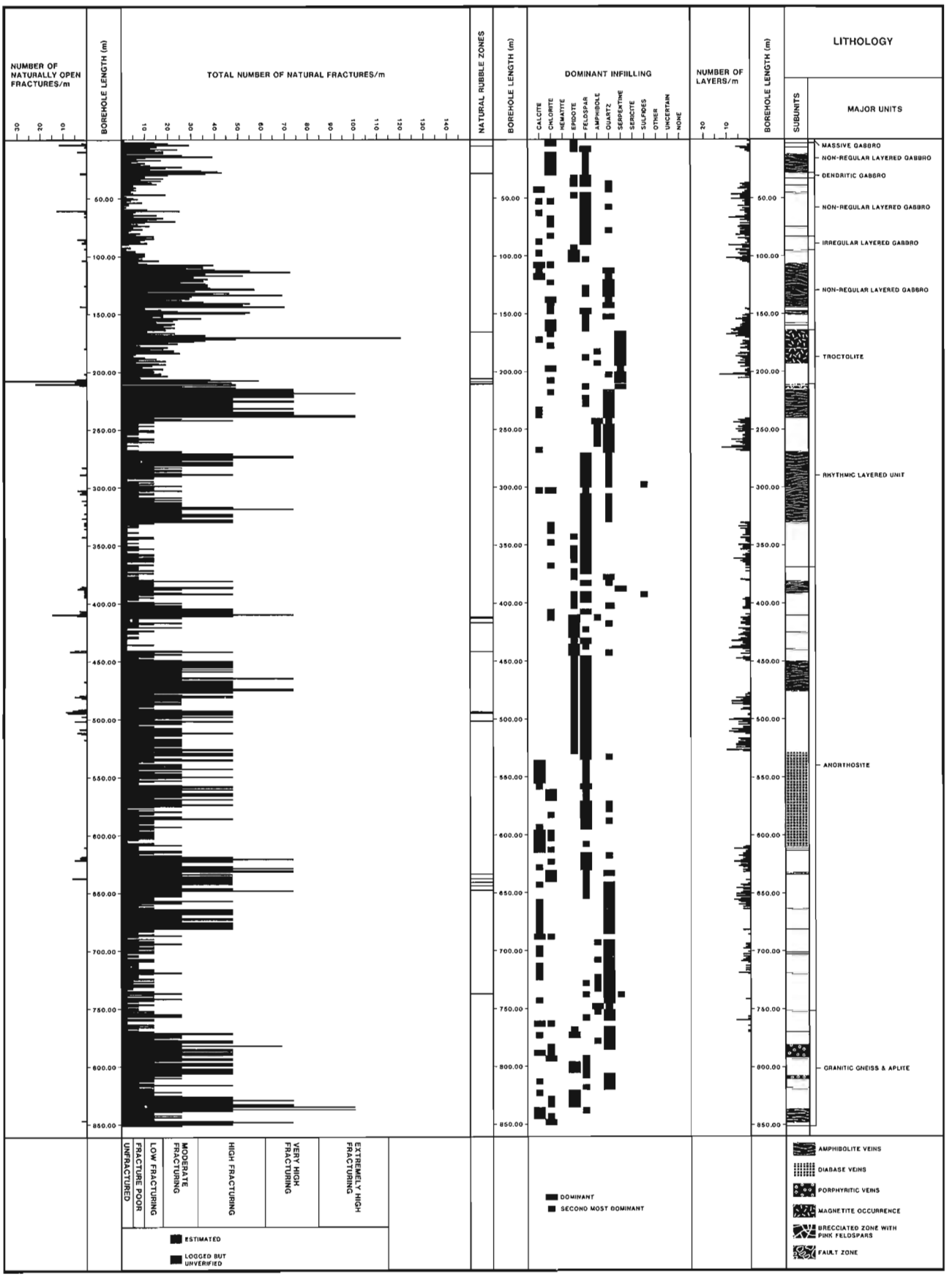

Figure 9.11. *Generalized core log of borehole EBL-1.*

Another distinct feature of the stockwork gabbro is the presence of K-feldspar in the rock matrix. K-feldspar commonly occurs along minor fractures and extends into the surrounding rock matrix by replacing plagioclase. Pyroxenes are altered to calcic amphibole and generally exhibit microscopic kink folds. This unit is related to the 'Folson Lake Fault Zone'. Rocks comprising the stockwork gabbro have been affected by the fault and rock alteration to such an extent that correlation to unaffected rock units is somewhat difficult.

K-feldspar-bearing gabbro

This unit, occurring in the southern part of the map area (Fig. 9.1), is similar to the massive gabbro unit, except that it also contains K-feldspar in microfractures and the rock matrix. In the rock matrix, K-feldspar replaces plagioclase and the pyroxenes are altered to amphibole. It differs from the stockwork gabbro by the absence of a network of quartz and feldspar veins.

Granophyre dykes

Dykes ranging from 10 to 40 cm in thickness and a few metres to tens of metres in length transgress the layering in the gabbro. The dykes are composed of plagioclase, quartz, K-feldspar and acicular blue green amphibole. Minor amounts of sphene, epidote, biotite, apatite and magnetite are present. Graphic and symplectite intergrowths of quartz and feldspars are abundant.

Mafic dykes

Most mafic dykes trend 300 to 320 degrees. The exception is two dykes which trend northeast-southwest. The dips of most dykes range from 90 to 70 degrees northeast.

Although all dykes are mafic, they differ in texture and mineralogy, which allows five subdivisions.

1. Amphibolite dykes are medium to fine grained and comprise randomly oriented actionlitic hornblende, plagioclase, epidote, and iron oxides.
2. Diabase dykes are medium grained. They contain two pyroxenes, plagioclase, magnetite and sphene. Olivine may be present in some and sulphides commonly fill fractures.
3. Feldspar porphyry dykes contain phenocrysts of plagioclase (commonly sassaurritized) in a fine- to medium-grained matrix of pyroxenes and plagioclase. In some dykes, the pyroxenes are altered to actinolitic hornblende.
4. Hornblende porphyry dykes up to 1 m thick contain phenocrysts of hornblende with preferred orientation in a fine grained matrix. The orientation is more predominant at the margins.
5. Aphanitic glassy dykes average about 10 cm thick, and are generally associated with fault zones and lineaments. They are oriented at right angles to these structures.

Rock alteration

The East Bull Lake pluton displays considerable alteration in the rock matrix and along fractures. The rock matrix is affected by hydrothermal metamorphism, where hydrous minerals such as amphibole, epidote, serpentine and chlorite are commonly developed.

The alteration products in the rock matrix show three modes of occurrence:

1. Rims around primary crystals: blue-green amphibole, commonly mantling clinopyroxene, is visible in hand specimens of anorthosite having segregations of large pyroxene crystals. Biotite rimming magnetite is another variety that belongs to this category.
2. Replacement of primary minerals: secondary hydrous minerals completely replace and pseudomorph the primary minerals. Three types of pseudomorphism are common: calcic amphibole replaces clinopyroxene and epidote replaces plagioclase; Mg-Fe amphiboles (anthophyllite and cummingtonite) and serpentine replace olivine and orthopyroxene, which is predominant in the troctolite layered zone; biotite; sphene, blue-green amphibole and leucoxene replace magnetite.
3. Alteration along microfractures: microfractures, transecting pyroxene and plagioclase, and filled with blue-green amphibole and epidote, are common in the anorthositic layered and rhythmic layered units. In the troctolite zone, the microfractures contain serpentine, chlorite and iron oxides. Iron oxide appears to be a by-product released during serpentinization of olivine and orthopyroxene.

Fracture infillings

The fractures in the East Bull Lake pluton are filled with a variety of minerals. Three groups of fracture fillings (veins) can be categorized according to their genesis:

1. High temperature fracture fillings: The group of fracture fillings, formed during the hydrothermal cooling stage that occur throughout the pluton includes blue-green amphibole, epidote, quartz, sulphides, chlorite, serpentine, carbonate and feldspars. Among these, sulphide fillings are confined to the anorthosite zone and serpentine is restricted to the troctolite zone.
2. Fracture fillings in and near major fault zones: A number of major fault zones are characterized by a high density of fractures that are filled with some high-temperature fillings, and other fillings that are developed exclusively in this zone. The high-temperature fillings are epidote and chlorite. Quartz is abundant in these fractures and generally contains rutile needles. Two types of K-feldspar fillings, microcline and a low-temperature polymorph-adularia, occur exclusively in this environment. Additional fillings include psuedotachylite and a cherty-type quartz which may also have originated as a type of "glassy matter" (Weiss and Wenk, 1983).
3. Low-temperature fracture fillings: Some fractures contain low temperature minerals such as kaolinite, hydrous iron oxides, and carbonate.

Field observations suggest that most fractures containing low-temperature fillings are a consequence of continued evolution of high-temperature fillings and fault-related fractures rather than a result of actual growth of new fractures. For example, various proportions of kaolinite are commonly found in fractures containing K-feldspar; some of these may be 100 per cent kaolinite and some amorphous variety of clay minerals. Therefore, it is interpreted that the formation of kaolinite is an in situ process involving degradation of K-feldspar by the following reaction:

$$KalSi_3O_8 + 2H + 9H_2O \rightarrow 2K + 4H_4SiO_4 + A_2Si_2O_5(OH)_4$$

Microcline — Silicic acid — Kaolinite

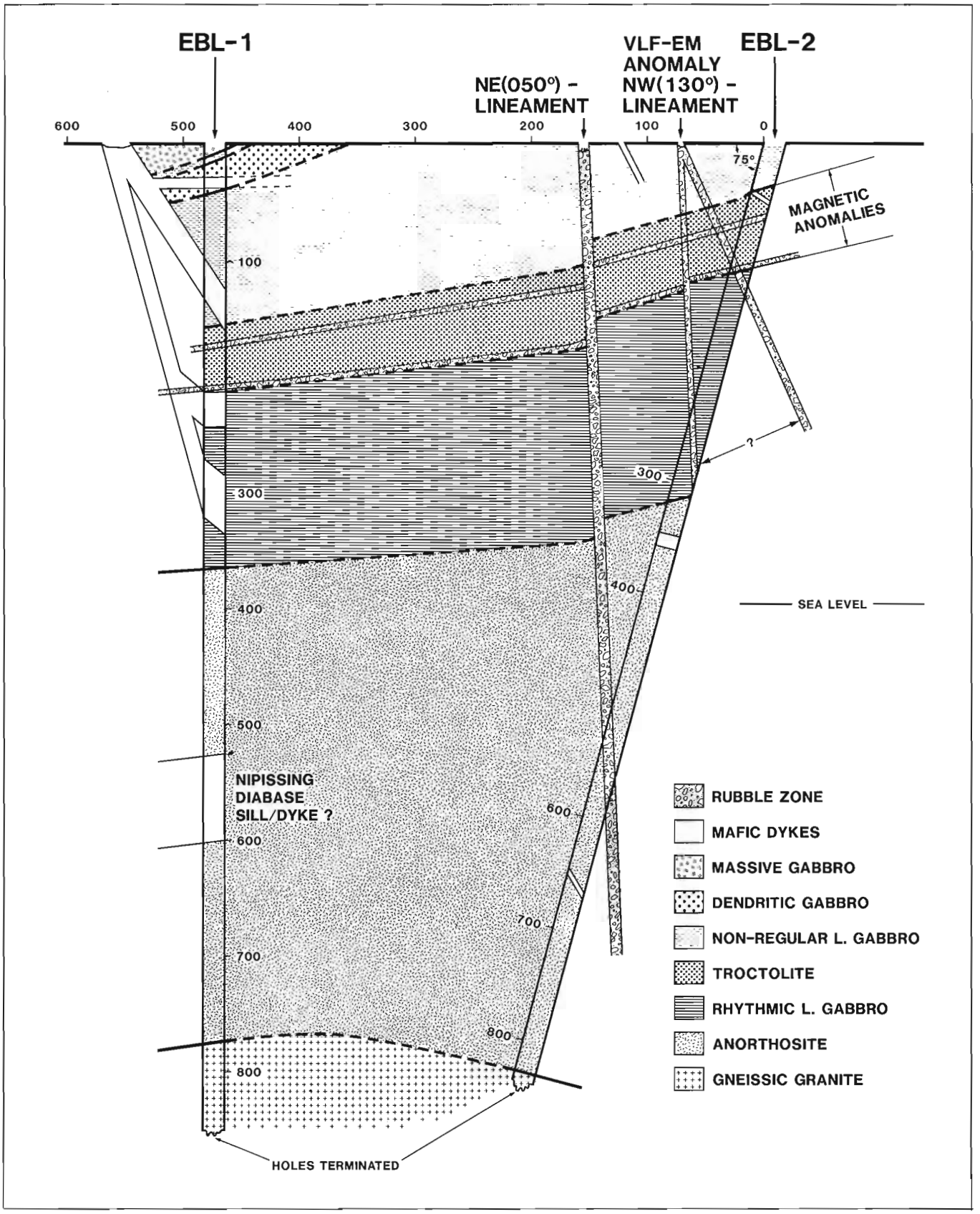

Figure 9.12. *Schematic cross section displaying the geology between boreholes EBL-1 and EBL-2.*

Kaolinite is also found in the anorthosite layered zone on outcrops with steep cross sections, where fractures with low dips (≤20°) form kaolinite by degradation of plagioclase, presumably by the following reaction:

$$CaAl_2Si_2O_8 + 3H_2O \rightarrow Ca^{2+} + 2OH^- + Al_2SiO_2O_5(OH)_4$$

Anorthite — Kaolinite

Similar rock-water reactions can be written for the origin of iron oxides and carbonate.

Subsurface geology

Four boreholes (see Fig. 9.1) were sited to investigate specific geophysical and geological features of the plateau. Borehole 1 is a vertical borehole intended to outline the extent of 'magmatic layering' and test a gravity model predicting depth of the pluton. Borehole 2, trending 190° and plunging 75°, was aimed to intersect two lineaments trending 130° and 050° (Fig. 9.1). Borehole 3 (trending 160°/plunging 60°) was located to obtain a cross section beneath the 'Folson Lake fault zone'. Borehole 4 (trending 100°/plunging 70°) is planned to obtain a stratigraphic cross section of the plateau towards Moon Lake. Boreholes 1 and 2 have been completed and boreholes 3 is in progress (April 1984).

The generalized core log of borehole 1 (EBL-1) comprises stratigraphic sequence, fracture frequency, fracture infillings and location of rubble zones representing possible open fractures (Fig. 9.11). The log shows lithologic units that are correlatable with those shown in Figure 9.1 and indicates that the pluton is 773 m thick here. The troctolite-olivine gabbro-norite horizon, which is exposed along the western shore of Moon Lake (Fig. 9.1), is intersected by the borehole at 164 m. Extension of this unit from this depth to the surface at Moon Lake indicates that it dips towards the borehole at 12 degrees. The troctolite-olivine gabbro-norite zone is highly magnetic at surface and subsurface, except in zones where it is highly serpentinized, and may be the cause of a number of magnetic anomalies recorded in this area.

Borehole 2 (EBL-2) intersects most major map units intersected by EBL-1. Because of its location and orientation, EBL-2 intersects only the lower map units present in EBL-1. The borehole broke through the basal anorthosite unit into gneissic granite at 799 m (borehole length is 827 m). The most obvious difference between the two borehole is the paucity of mafic dyke material in EBL-2.

The troctolite-olivine gabbro-norite map unit, a good marker horizon, first appears around 51 m and extends to 122 m. A major part of this unit is brecciated and contains serpentine and chlorite-filled fractures and is crosscut by aphanitic glassy dykes. Some of these characteristics are also seen in the 130 degree trending lineament and suggests possible correlation with the 130 degree lineament (Fig. 9.1). A VLF-EM anomaly associated with the lineament may be due to the presence of abundant serpentine and chlorite. Down-dip projection of the lineament at 70 degree dip to the northeast, intersects the borehole at about 100-120 m, with the brecciated troctolite zone. A similar projection of the lineament at 90 degree dip intersects the borehole at 300 m depth in a zone with similar character (Fig. 9.12).

A major 'rubble zone' is present in EBL-2 around 555 m. This occurs within the anorthositic layered unit. The true thickness of this zone is about 48 m. The top 8 m of the 'rubble zone' is silicified. Numerous offset feldspar-filled fractures are commonly present below the silicified zone. The grains in the anorthositic rock matrix are fragmented and brecciated. Veinlets of psuedotachylyte are dispersed around feldspar fragments. Projection of this 'rubble zone' at a dip of 90° to the surface correlates with the 050 degree trending lineament (Fig. 9.1), but surface measurements of the fractures in the lineament dip at 55 to 65 degrees. Therefore, this zone must dip independently of its component fractures or else must be displaced, with depth, in an en echelon pattern.

Lithologic layering and the associated textures of some map units appear to be correlatable over hundreds of metres in the subsurface (Fig. 9.12).

Acknowledgments

The authors are grateful to Dr. Ingo Ermanovics for providing advice and encouragment. Grateful thanks are also due to R. Buchanan for valuable assistance and to John Dugal for organizing the drilling project.

References

Born, P.
1978: Geology of the East Bull Lake mafic intrusion, District of Algoma, Ontario; Unpublished M.Sc. thesis, Laurentian University, Sudbury, Ontario.

Born, P. and James, R.S.
1978: Geology of the East Bull Lake layered anorthosite intrusions, District of Algoma, Ontario; in Current Research, Part A, Geological Survey of Canada, Paper 78-1A, p. 91-95.

Brown, A. and Kamineni, D.C.
1981: Preliminary report on the fractures sets at East Bull Lake pluton, Ontario; Canada, Department of Energy, Mines and Resources, Internal Report, 128 p.

Hess, H.H.
1960: Stillwater complex; Geological Society of America Memoir 80, 368 p.

James, R.S., Born, P., and Bigauskas, J.
1983: Geology of the East Bull lake layered complex, District of Algoma, Ontario; in Current Research, Part B, Geological Survey of Canada, Paper 83-1B, p. 1-11.

McCrank, G.F.D., Stone, D., Kamineni, D.C., Zayachkivsky, B., and Vincent, G.
1983: Regional geology of the East Bull Lake area, Ontario; in Current Research, Part A; Geological Survey of Canada, Paper 83-1A, p. 457-464.

Turner, F.J.
1981: Metamorphic petrology (second edition); Mineralogical, Field and Tectonic Aspects; McGraw Hill, Washington, New York and London, 524 p.

Wager, L.R. and Brown, G.M.
1968: Layered Igneous Rocks; Oliver and Boyd, Edinburgh.

Wager, L.R., Brown, G.M., and Wadsworth, W.J.
1960: Types of igneous cumulates; Journal of Petrology, v. 1, p. 73-85.

Weiss, L.E. and Wenk, H.R.
1983: Experimentally produced psuedotachylite-like veins in gabbro; Tectonophysics, v. 96, p. 299-310.

Winkler, H.G.F.
1974: Petrogenesis of metamorphic rocks (Third edition); Springer-Verlag, New York, 450 p.

10.

LA SÉDIMENTATION AU PRÉCAMBRIEN SUPÉRIEUR ET AU PALÉOZOÏQUE INFÉRIEUR SUR LA MARGE DE LA PLATE-FORME DU MACKENZIE (MONTS OGILVIE, TERRITOIRE DU YUKON)

Projet 800022

B. Blaise[1] et E. Mercier[1]
Division des sciences de la Terre

Blaise, B. et Mercier, E., La sédimentation au Précambrien supérieur et au Paléozoïque inférieur sur la marge de la plate-forme du Mackenzie (monts Ogilvie, Territoire du Yukon); dans Recherches en cours, partie B, Commission géologique du Canada, Étude 84-1B, p. 85-92, 1984.

Résumé

Un ensemble sédimentaire de la région de Dawson (carte 116B, C) datant du milieu et de la fin du Protérozoïque, comprend environ 4 km de roches carbonatées et détritiques mises en place en milieu littoral. Au cours de la fin du Protérozoïque, ou tout au début du Paléozoïque, divers faciès orientés d'est en ouest se sont développés de façon à créer deux zones parfaitement distinctes, soit une zone de faciès à forte composante détritique et volcanique, au sud, et une zone de faciès à roches carbonatées gisant au nord. La limite entre les deux faciès s'est maintenue jusque vers le milieu ou la fin de la période ordovicienne; par la suite, la transgression des schistes argileux sur le terrain occupé par les roches carbonatées a occasionné le déplacement de la limite de ce faciès vers le nord, au-delà de la région à l'étude.

On estime que la dolomitisation et la silicification des roches carbonatées d'origine protérozoïque ont eu lieu au tout début du processus de diagenèse; l'enfouissement et les hautes températures survenus ultérieurement ont été à l'origine de la production d'illite, de phengite et de talc fortement cristallins au sein des unités riches en argile. Les conglomérats contenus dans l'unité 9 de la séquence datant de la fin du Protérozoïque renferment des grains de quartz à facettes dont la présence pourrait bien être due à l'action des glaciers.

Abstract

Middle and Upper Proterozoic strata in Dawson map area (116B, C) comprise approximately 4 km of carbonate and clastic rocks of shallow water aspect. During latest Proterozoic or earliest Paleozoic time, an east-west trending facies boundary developed, separating dominantly clastic and volcanic facies on the south from shallow water carbonate on the north. The boundary persisted until mid-to-late Ordovician time when shales transgressed the carbonate, displacing the facies boundary northward beyond the map area.

Dolomitization and silicification of Proterozoic carbonates is regarded as early diagenetic; subsequent burial and heating were sufficient to produce high crystallinity illite, phengite and talc within clay rich units. Conglomerates within unit 9 of the Upper Proterozoic succession contain faceted quartz grains suggesting a glacial influence.

Introduction

La carte 116B, C de Dawson (Green, 1972) au nord de la Cordillère canadienne permet d'observer le contact de deux zones paléogéographiques appartenant à la marge du craton Nord-américain dont la différentiation daterait du Paléozoïque inférieur et moyen (Tempelman-Kluit, 1981; fig. 10.1). Il s'agit, au nord, de la plate-forme du Mackenzie et, au sud, du bassin de Selwyn. La première est caractérisée par des dépôts carbonatés dont la mise en place a eu lieu en eau peu profonde, et la seconde, par des dépôts clastiques et volcaniques.

Immédiatement au nord de la limite de ces zones, un affleurement (30 000 km^2) de sédiments d'origine protérozoïque, selon Green (1972), est connu sous le nom de <<Coal Creek Dome>>. Les travaux préliminaires de Thompson et Roots (1982) avaient, entre autres résultats, permis l'établissement d'une stratigraphie provisoire de l'affleurement en 12 unités dans cette région. Ces auteurs avaient émis l'hypothèse d'une séparation majeure entre les unités 1, 2 et 3, corrélables avec le supergroupe de Wernecke du Protérozoïque moyen (séquence A de Young et coll., 1979), et les terrains sus-jacents (4 à 12), en partie paléozoïques.

Des études en cours sur la moitié est de <<Coal Creek Dome>> (Mercier, en préparation), d'ordre cartographique (1/50 000), structural et portant sur la diagenèse des séries, confirment la séparation entre les unités 1, 2 et 3 qui seront appellées <<socle>> et les unités supérieures auxquelles on donnera le nom de <<couverture>>. En outre, ces unités supérieures, objet du présent article et pour lesquelles la nomenclature originale a en grande partie été conservée, sont considérées comme étant concordantes les unes sur les autres et constituant un ensemble continu du Protérozoïque au Paléozoïque, sans que la limite puisse être précisée pour le moment.

Cet ensemble supérieur affleure essentiellement au sud de la zone étudiée (moitié est de <<Coal Creek Dome>>), c'est-à-dire immédiatement au nord de la limite paléogéographique évoquée précédemment.

Stratigraphie

Remarques préliminaires

1. Des études passées ou en cours (Blaise, 1983; Mercier, en préparation) ont permis de dégager des microfossiles dans différentes unités de la série étudiée. Certaines formes semblent assimilables à celles du Protérozoïque supérieur illustrées dans Chauvel et Mansuy (1981) ou Allison et Moorman (1973). Aucune utilisation pratique en biostratigraphie n'a, pour l'instant, pu être faite. Les rares macrofossiles qui ont été trouvés et dont l'étude est

[1] Géologie structurale, Sciences de la Terre – Université de Lille I – 59655 Villeneuve d'Ascq Cedex, France

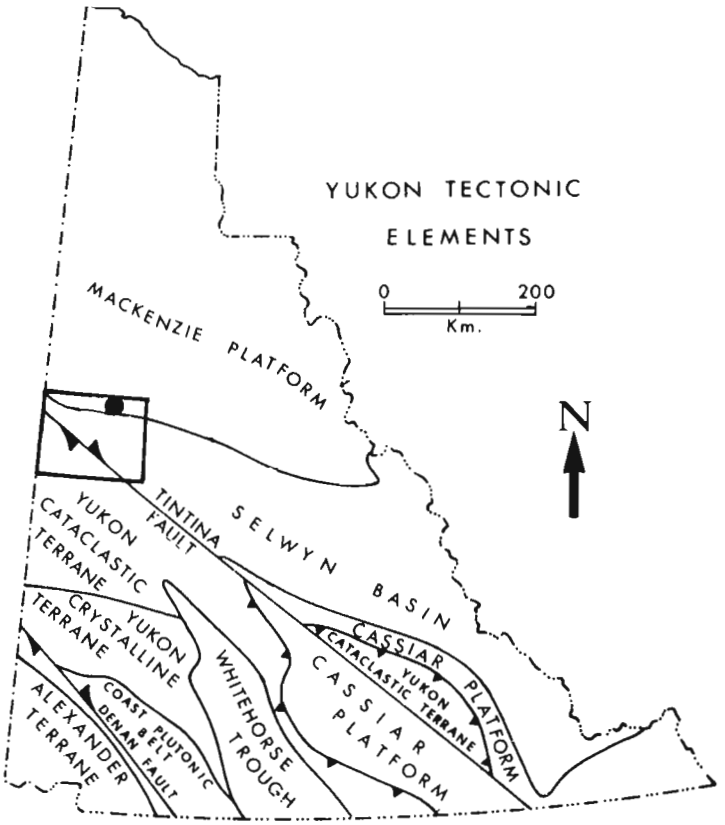

Figure 10.1. *Carte structurale du territoire du Yukon (Tempelman-Kluit, 1981). Cadre à trait gras: carte 116 B, C de Dawson; point noir: localisation du secteur étudié.*

en cours ne proviennent que du sommet de la série (unité 11). Ainsi, pour la quasi-totalité de la série, aucun contrôle paléontologique ne vient confirmer les corrélations entre les différentes coupes.

2. La série a subi des contraintes d'âge sans doute mésozoïque et une partie a dû être charriée vers le nord, différenciant ainsi un ensemble chevauchant et un ensemble chevauché.
3. Tous les niveaux décrits sont concordants les uns sur les autres. On peut observer pour chacun d'entre eux, sur presque toutes les coupes, un passage graduel de faciès avec l'unité sus-jacente. Des exceptions sont à signaler: les contacts brutaux de la formation de Road River sur l'unité 11 et, localement (au nord-est), de cette dernière sur l'unité 9.
4. La stratigraphie est décrite à la figure 10.3. On remarque l'importance des unités dolomitiques essentiellement constituées de dolomies grises, massives, et mal stratifiées, souvent riches en accidents siliceux bleutés ou noirs à bord diffus, présentant parfois des structures algo-laminaires, des niveaux de brèches intraformationnelles monogéniques et, localement, des oolites, des pisolites et plus rarement des oncholites. Ce faciès ubiquiste sera désigné par la suite par le terme <<faciès dolomitique massif>>.

Description sommaire des unités

Unité 4. Sur la colonne A et sur la colonne F (fig. 10.3), la base est constituée d'au moins 600 m de dolomie en bancs minces (5 à 30 cm) souvent gréseuse et d'une couleur variant du gris à l'orangé clair. On y observe des niveaux de brèches intraformationnelles mais jamais de chert. Le sommet est constitué par le faciès dolomitique massif sur 350 m (respectivement faciès 4a et 4b des fig. 10.2 et 10.3).

Il faut également signaler la présence, juste au nord de la coupe C, sur près de 10 m d'épaisseur de quelques intercalations décimétriques à métriques d'un conglomérat sédimentaire lité à matrice argilo-silteuse et à éléments dolomitiques associés à des galets mous d'argile silteuse, à des quartz d'origine rhyolitique(?) et à des microgalets constitués de lattes désordonnées de muscovite provenant de l'altération de roches magmatiques ou métamorphiques.

Unité 5. Il s'agit d'une unité détritique de 200 m d'épaisseur. À l'ouest, elle se compose essentiellement de matériaux argileux et dolomitiques (colonnes A et B, fig. 10.3). Vers l'est (colonnes D, F, fig. 10.3), elle devient progressivement plus gréseuse avec notamment des faciès rouge-lie-de-vin et, à la base, des passées conglomératiques.

Unité 6. Cette unité, épaisse de 2000 à 2500 m, est presque exclusivement constituée du faciès dolomitique massif. Moins de 2 % de l'épaisseur totale est représentée par des niveaux métriques d'argilites noires ou de grès. Très massive, cette unité se distingue morphologiquement par ses grandes falaises et du fait qu'elle présente les plus hauts sommets de la zone étudiée.

Unité 7. Il s'agit d'une série peu épaisse (60 à 150 m) essentiellement argilo-silteuse avec quelques bancs dolomitiques et quelques niveaux de grès sombre, riche en oxydes métalliques.

Unité 8. À l'ouest, la base est constituée de 300 m de dolomie calcareuse noir anthracite, riche en matières organiques. Elle est mal stratifiée et présente quelques accidents silicifiés diffus, des brèches intraformationnelles et quelques niveaux argileux. Ce faciès diminue d'épaisseur vers l'est et disparaît un peu à l'est de la colonne E (fig. 10.2 et 10.3). Au-dessus, on observe 500 m de dolomies massives légèrement plus sombres que le faciès dolomitique massif typique, sans oolite ni pisolite, avec des niveaux à stromatolites et des niveaux bioclastiques à bioclastes calcaires.

À l'est, la totalité de la série (800 m) est constituée par le <<faciès dolomitique massif>> qui présente néanmoins des accidents siliceux toujours très sombres (colonne F).

Unité 9 (200 m à plus de 400 m). Les variations de faciès sont très importantes: quatre faciès principaux peuvent être distingués (le détail de leur extension est donné à la figure 10.4).

La faciès 9a est constitué de grès, de silt et d'argilite lie-de-vin avec des intercalations centimétriques à métriques de microconglomérats, souvent granoclassés, à ciment gréseux lie-de-vin ou ocre. On y observe, notamment sur la colonne D, des <<ripples marks>> symétriques, des <<muds cracks>> et de nombreux exemples de stratification oblique.

Le faciès 9b est constitué d'argilites et de silts noirs avec localement des niveaux plus gréseux ou dolomitiques.

Le faciès 9c est constitué de conglomérats ocres à ciment dolomitique renfermant des clastes dolomitiques et siliceux (cherts) pluricentimétriques parfois disposés en séquences rhytmiques positives épaisses de 0,10 à 1 m, ainsi que de grès dolomitiques et de dolomies sableuses parfois conglomératiques.

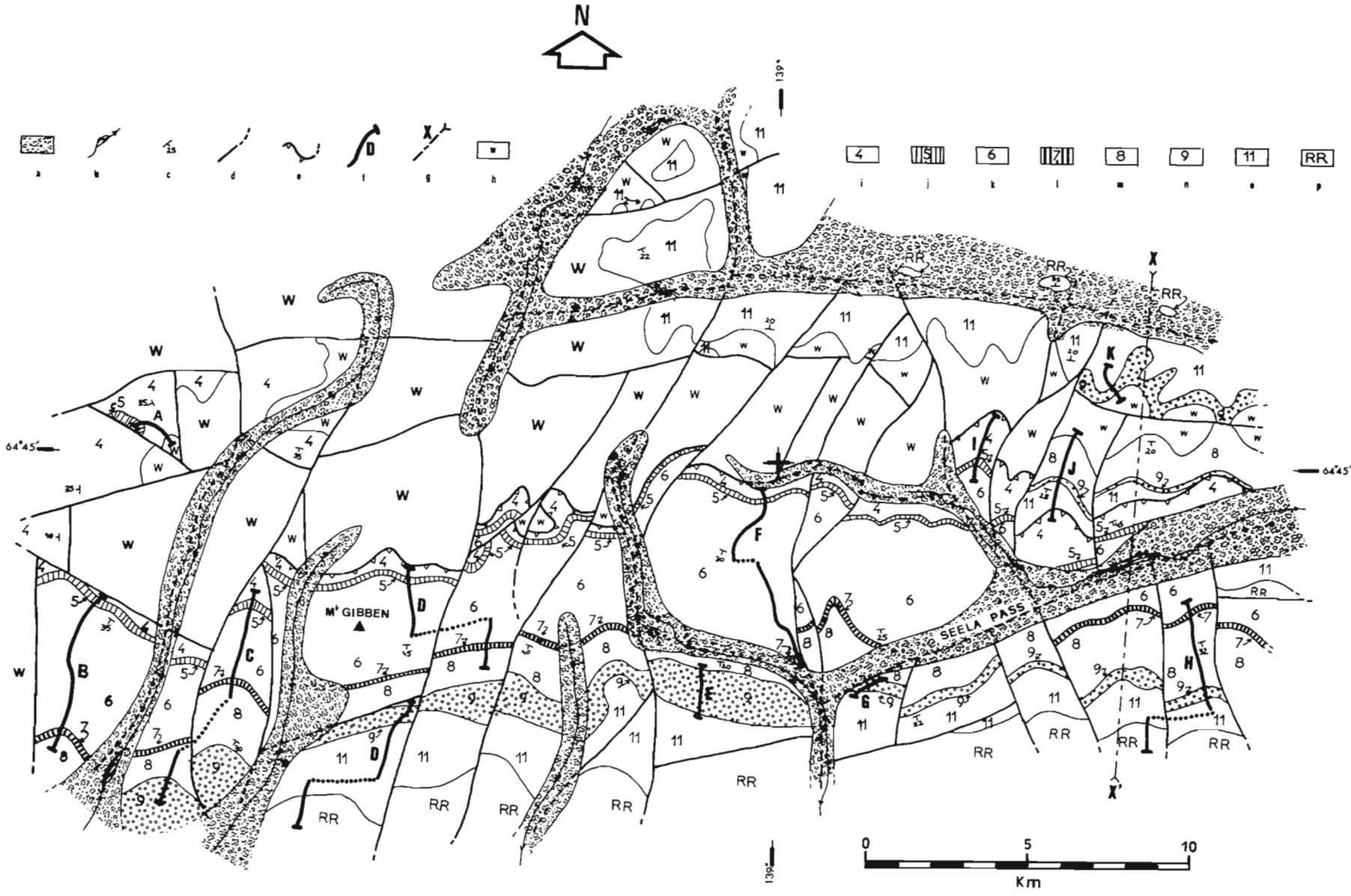

Figure 10.2. *Carte géologique du sud-est de <<Coal Creek Dome>>; a: alluvions; b: rivière; c: pendage; d: faille; e: chevauchement; f: colonnes lithostratigraphiques des figures 10.2 et 10.3; g: coupe structurale des figures 10.2 et 10.4; h: supergroupe Wernecke indifférencié (Protérozoïque moyen); i: unité 4, dolomies; j: unité 5, argilites et grès; k: unité 6, dolomies; l: unité 7, grès et argilites; m: unité 8, dolomies; n: unité 9, conglomérats, grès et argilites; o: unité 11, dolomie; p: formation de Road River, argilites et cherts.*

(unité 4 à 11: Protérozoïque supérieur – Paléozoïque inférieur, limite inconnue; et base de la formation de Road River: Ordovicien supérieur – Silurien inférieur).

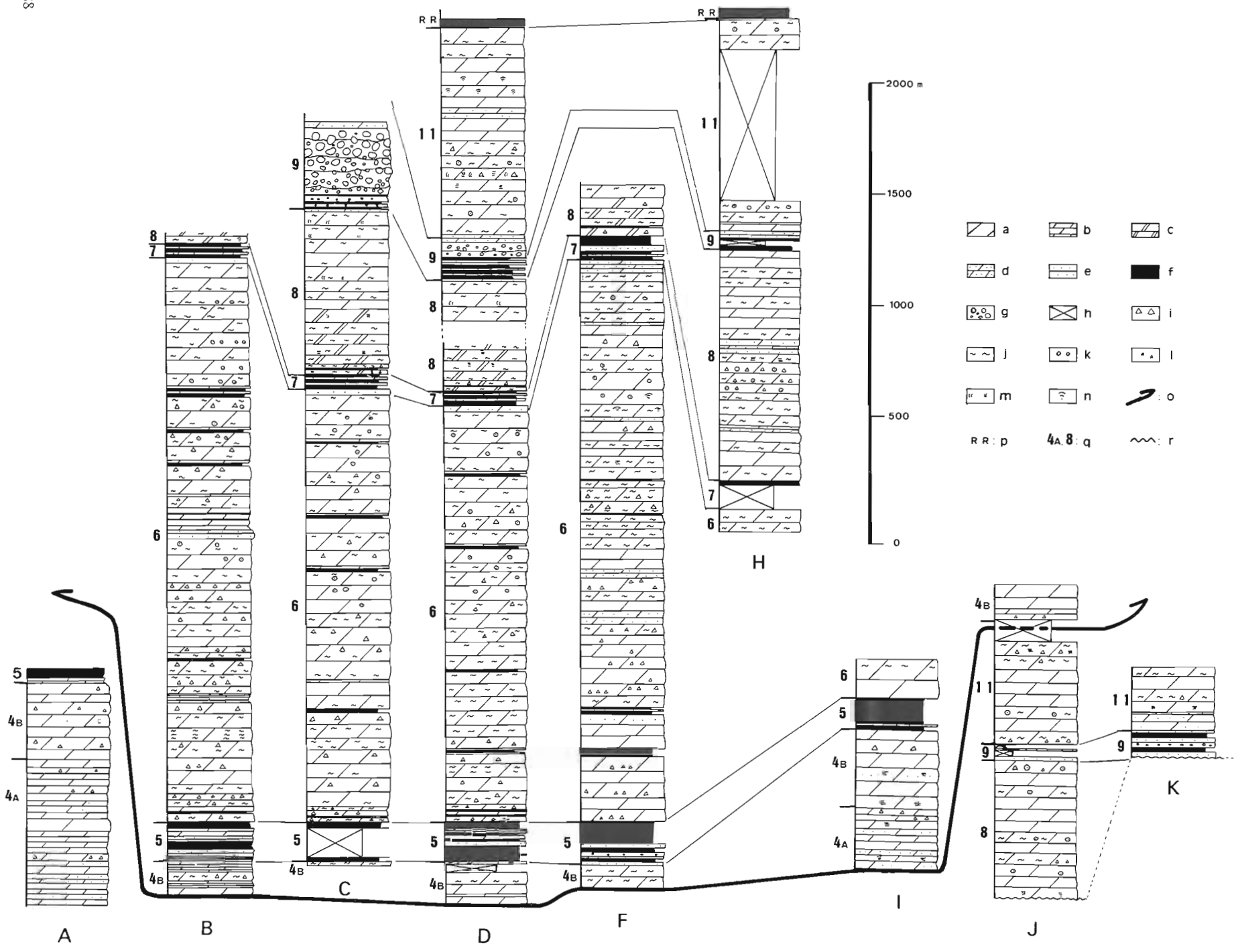
2000 m
1500
1000
500
0
a
b
c
d
e
f
g
h
i
j
k
l
m
n
o
RR : p
4A.8 : q
r
A
B
C
D
F
H
I
J
K

Le faciès 9d est constitué d'un conglomérat grossier, non classé, à galets roulés de taille centimétrique à métrique, à ciment calcaro-sableux. Parfois à la base de ce faciès, on peut distinguer des bancs conglomératiques métriques à décimétriques, soulignés par des horizons centimétriques argilo-silteux de couleur lie-de-vin. Près de 90 % des clastes proviennent des unités décrites préalablement et le reste, des unités du Protérozoïque moyen non décrites ici. On observe également quelque galets d'argilites lie-de-vin et des niveaux siliceux rouge-vermillon.

Unité 10. Cette unité,citée pour mémoire, affleure 15 km à l'ouest de la zone étudiée. Elle est constituée d'un ensemble volcanique dont Roots (1983) a montré qu'il s'agissait en fait d'un niveau intercalé dans l'unité 9.

Unité 11. Il s'agit d'une unité de près de 1000 m d'épaisseur, constituée essentiellement par le faciès dolomitique massif; on procède actuellement à l'étude des échantillons de macrofaune qu'elle a livrée. Elle regroupe les unités 11 et 12 de Thompson et Roots (1982) à valeur trop locale et correspond en partie à l'unité 8 de Green (1972) qui la considérait d'origine ordovicienne d'après des données recueillies 100 km plus à l'est. Mais 45 km à l'ouest du secteur à l'étude, Thompson (comm. pers.) a pu dater un niveau médian du Cambrien inférieur en raison de la présence d'Archéocyathidés; la présence d'un diachronisme à l'échelle du terrain n'est donc pas à exclure.

La formation de Road River

Elle se compose d'argilites et de niveaux siliceux noirs dont l'âge de la base a été établi grâce à la présence, dans le sud-ouest du terrain, de graptolites datant de la période allant de l'Ordovicien inférieur (?) au Silurien inférieur (Degardin dans Blaise, 1983). Au sud, le contact basal, bien que brutal, semble stratigraphique, conclusion concordant avec les observations de Thompson (comm. pers.) et Roots (1983) en d'autres points de la carte de Dawson, mais contraire à la carte de Green (1972) qui admet l'existence d'un chevauchement au sud de <<Coal Creek Dome>>, soit la faille de Dawson.

Environnement sédimentologique et évolution diagénétique précoce

La présente section portera, dans un premier temps, sur le <<faciès dolomitique massif>> qui regroupe les membres 4, 6, 8 et 11 puis, dans un deuxième temps, traitera individuellement des membres à faciès détritiques.

Figure 10.3. *Colonnes lithostratigraphiques localisées sur la figure 10.2. Les colonnes E, G sont représentées sur la figure 10.4*

a: dolomie massive; b: dolomie en bancs minces; c: dolomie calcareuse noire; d: dolomie sableuse; e: grès; f: argilite, silt; g: conglomérat; h: lacune; i: horizon de brèches intraformationelles; j: horizon à niveau silicifié; k: horizon à oolites, pisolites; l: horizon à laminations alguaires; m: horizon à bioclastes calcaires; n: horizon à stromatolites; o: position du chevauchement; p: formation de Road River; q: membre lithostratigraphique; r: discordance.

Formation de Road River: Ordovicien supérieur – Silurien inférieur à la base.

Unités 4 à 11: Protérozoique supérieur – Paléozoique inférieur, position de la limite inconnue.

Le <<faciès dolomitique massif>>

Une sédimentation de plate-forme semble être indiquée par trois faciès remarquables: des niveaux oolitiques et pisolitiques, des brèches intraformationnelles et des structures laminaires parfois bréchiques. Les auteurs estiment, suivant les interprétations de Moussine-Pouchkine et Bertrand-Sarfati (1980), que les faciès bréchiques soient dus à des dessications successives en zone intertidale. L'examen de lames minces permet d'observer une dolomitisation en microsparite ou en micrite de sédiments originels fins. Cette dolomitisation, d'après Lucas et coll. (1976), asociée aux faciès bréchiques, peut être interprétée comme résultant d'une dolomitisation précoce pénécontemporaine de la sédimentation.

Les observations faites sur les nombreux niveaux silicifiés montrent des horizons onduleux fracturés, des amas siliceux parfois diffus et, en lame mince, une interdigitation entre les cristaux de quartz, calcédoine le plus souvent, et les cristaux très fins de dolomie. Ce type de faciès a été interprété par Knauth (1979) et Geeslin et Chafetz (1982) comme étant le résultat d'une silicification et d'une dolomitisation synchrone avec interaction entre une zone d'eau météorique et une zone d'eau marine.

Unité 5. À l'est, la sédimentation est très détritique (conglomérats, grès et argilites). À l'ouest, les dépôts plus dolomitiques contiennent des niveaux stromatolitiques broyés renfermant des horizons à structures recristallisées rappelant des <<bird eyes>>.

Unité 9. Les relations entre les différents faciès sont indiquées sur la figure 10.4.

Dans les argillites lie-de-vin (faciès 9a) on observe des <<muds cracks>>, des <<ripple marks>> et de nombreux exemples de stratification oblique.

Le faciès conglomératique très grossier ne présente pas de granoclasement. La taille des éléments est souvent métrique à plurimétrique. Les premiers éléments d'une étude des grains de quartz de la matrice de ce conglomérat ont montré un façonnement d'origine, semble-t-il, glaciaire (Blaise, 1983).

Les relations très étroites existant entre le faciès lie-de-vin mis en place sous une faible tranche d'eau atteignant parfois l'émersion et le faciès conglomératique grossier semble écarter l'hypothèse d'une mise en place en profondeur pour le deuxième. La première interprétation ci-présentée attribue un caractère continental à ce dépôt conglomératique, avec une origine glaciaire directe ou une reprise de dépôt glaciaire grâce au rejeu de certaines failles (voir la section traitant de la tectonique).

La formation de Road River

Les auteurs admettent que cette formation présente des faciès de bassin.

Ces quelques éléments indiquent, pour les unités 4 à 11, une bathymétrie de dépôt faible (atteignant parfois l'émersion). Les faciès dolomitiques ont subi une dolomitisation et une silification précoce.

Évolution diagénétique profonde: apport de la minéralogie des argiles

Des diagrammes de diffraction des rayons X ont été faits sur 16 échantillons et indiquent la présence:

- d'une très forte teneur en illite (90 % en moyenne de la fraction argileuse) fortement cristalline;

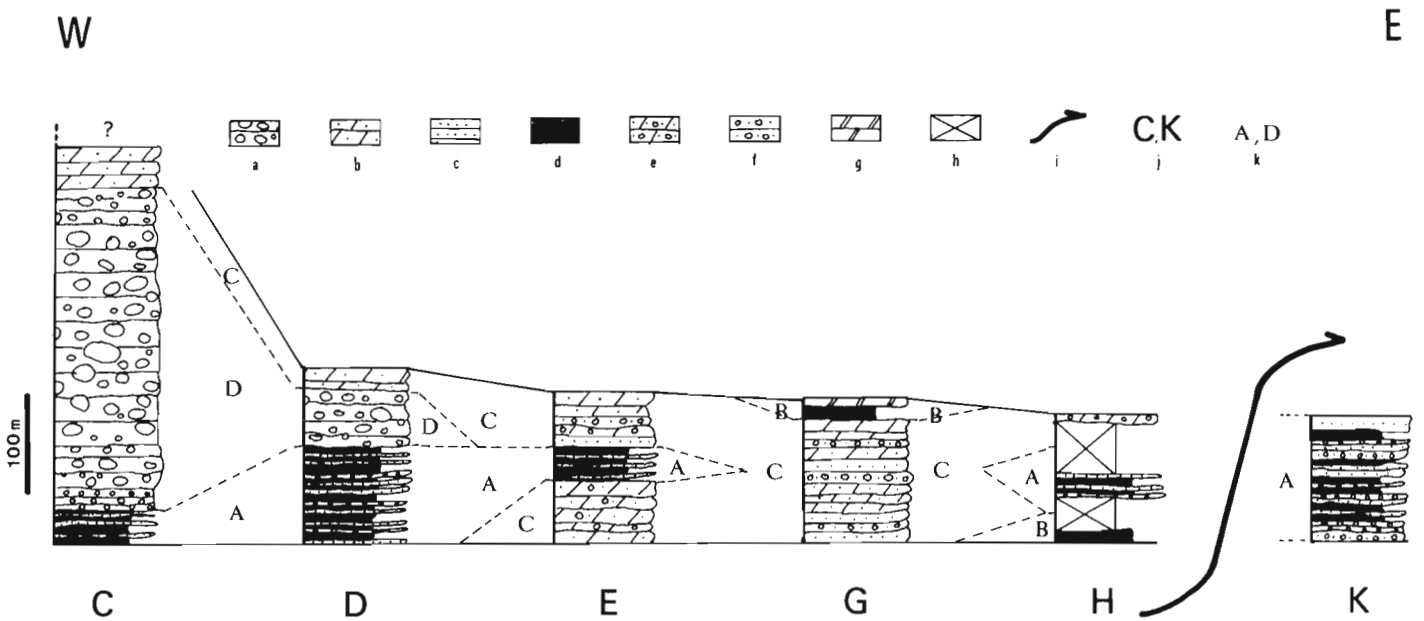

a: conglomérats; b: dolomies sableuses; c: grès; d: argilites et silts; e: grès dolomitiques et dolomies conglomératiques; f: grès et conglomérats; g: dolomies calcareuses noires; h: lacune d'observation; i: chevauchement; j: unité 9 des colonnes lithostratigraphiques localisées sur la figure 10.2; k: faciès décrits dans le texte.

Figure 10.4. *Schéma des variations de faciès de l'unité 9.*

- d'une teneur relativement faible en chlorite (inférieure à 5 % en général);
- d'interstratifiés irréguliers de type illite-smectite, illite-vermiculite, vermiculite-smectite, chlorite-vermiculite et chlorite-smectite (entre 5 et 10 % de la fraction argileuse quand ils sont présents); et
- de phengites en faible quantité associées à de l'illite et souvent avec de la chlorite.

De plus, dans un échantillon de dolomie sombre (unité 8), on trouve:

- de la smectite (20 % de la fraction argileuse) associée à du talc. Cette smectite, de type magnésienne (réflexion à 1,54 A de la raie 060), est remarquablement cristallisée.

Les cristallinités élevées de l'illite, la présence de phengite et de talc montrent que les argiles étudiées ont subi de sévères contraintes thermodynamiques (Dunoyer de Segonzac, 1969), non révélées auparavant, en raison de l'absence d'une schistosité. Cela peut s'expliquer par l'épaisseur de la série et des terrains sus-jacents. La présence encore faible de chlorite est à noter ainsi que le fait que de petites quantités de minéraux interstratifiés subsistent. Ce phénomène indiquerait un domaine de diagenèse profonde proche de l'anchimétamorphisme. La présence d'une quantité relativement importante de smectite est inhabituelle dans le contexte présent. Une étude a été entreprise sur ce minéral (Blaise, en préparation) mettant en évidence des caractères spécifiques compatibles avec une genèse in situ semblable à celle décrite plus haut.

Tectonique cassante et tectonique synsédimentaire

La région étudiée est découpée par des failles transversales (nord-sud) et directionnelles (est-ouest) sensiblement verticales.

Les failles transversales qui se prolongent vers le nord dans le Protérozoïque moyen y provoquent des rejets différents (plus importants ou opposés) à ceux observables dans la couverture. Ces failles résultent donc de la réactivation de failles du socle. Il semble que cette réactivation ne comporte pas de composante taugentielle comme le montre la cartographie des dykes basiques verticaux, présents uniquement dans le socle, qui ne sont pas décalés par ces failles.

Les auteurs font remarquer que, dans la région de la passe de Sella, certaines failles directionnelles viennent s'interrompre contre des failles transversales. Par ailleurs et d'une manière générale, il semble que le rejet final des failles transversales, à l'exclusion de celles qui sont limitées par des failles directionnelles où le résultat est alors inverse, correspond à un effondrement du compartiment est. Le rejet final des failles directionnelles correspond à un effondrement du compartiment sud. Un cas d'intérêt particulier est celui de la faille située à 5 km à l'est du mont Gibben, remarquable pour son mouvement en ciseau dans le sens inverse des aiguilles d'une montre autour d'un axe situé au milieu des affleurements de l'unité 6.

Ainsi, une tectonique cassante, différenciant des compartiments d'ordre kilométrique limités par des failles et dont la chronologie de mise en place est d'ordre pluri-phasé, caractérise la zone.

Au nord-est de la passe de Sella, la carte (fig. 10.2) montre l'existence de failles dont certaines ont fonctionné avant la mise en place de l'unité 8, d'autres avant celle de l'unité 9 et d'autres encore avant celle de l'unité 11 (fig. 10.5). Au niveau de la colonne C (fig. 10.3), des petites failles à rejet décamétrique touchent les premiers niveaux gréseux de l'unité 7 mais sont scellées par les dépôts silteux non touchés. Ces mouvements qui provoquent des lacunes de sédimentation ou d'érosion dans certains compartiments, sont sans doute assez brutaux et ne semblent s'être développés qu'à quelques moments particuliers et contemporains de la sédimentation des unités détritiques. Une illustration spectaculaire de ce phénomène est le conglomérat grossier (faciès 9d) qui a été alimenté à 90 % par les unités sur lesquelles il repose en concordance.

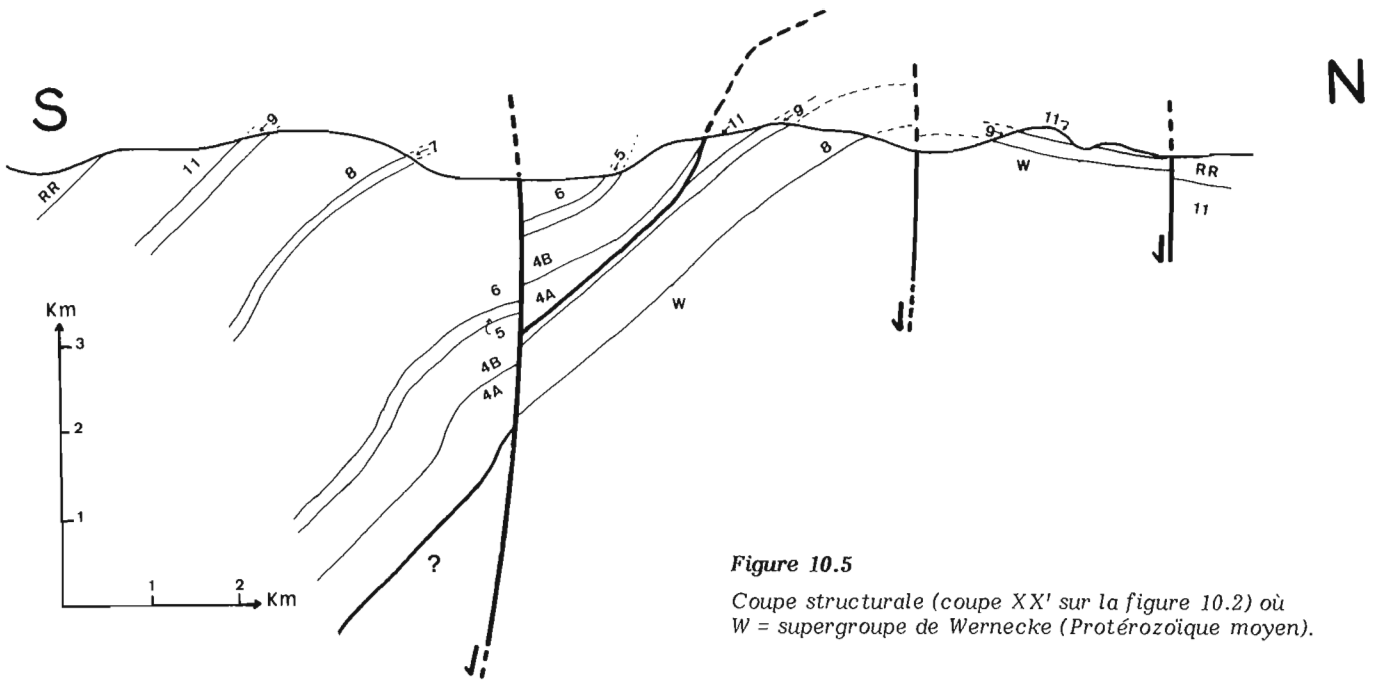

Figure 10.5

Coupe structurale (coupe XX' sur la figure 10.2) où W = supergroupe de Wernecke (Protérozoïque moyen).

Mais il faut aussi envisager l'existence d'une tectonique synsédimentaire à manifestation moins cartographique et relevée par la subsidence de compartiments faillés. La comparaison des colonnes B, C et F montre des différences d'épaisseur de plus de 500 m dans l'unité 6 qui se produisent brutalement dans des zones masquées par des alluvions mais où la cartographie met en évidence l'existence de failles. Dans le contexte précédemment exposé, on ne peut pas exclure l'existence d'une érosion au sommet de la coupe C. Il faut également remarquer la présence d'abondantes brèches intraformationnelles dans l'unité 6 des coupes B et F; certaines d'entre elles y sont spécifiques et se caractérisent par des bancs de 0,50 à 1 m présentant un granoclassement d'éléments figurés de dolomies de différentes couleurs (grise, blanche, orangé clair, etc.). L'interprétation de ces observations semble devoir s'inscrire dans le cadre d'un milieu tectonique synchrone de la sédimentation avec des dépôts de brèches allochtones dans le compartiment subsident. Une tectonique synsédimentaire, dont aucune manifestation antérieure à la mise en place de l'unité 6 n'est connue, a donc touché la zone étudiée. Néanmoins, une grande part des rejets finaux observables sont issus de phases cassantes tardives, datant au moins du post-Silurien inférieur et, d'après le contexte général (Tempelman-Kluit, 1981), d'origine mississipienne ou mésozoïque, ou les deux.

Tectonique compressive (Mésozoïque ?)

Dans les rares niveaux incompétents (argilites), des déformations ont été observées localement. Il s'agit de schistosité de fracture frustre, de plis décimétriques déversés, de stries, de plissements et plus rarement de petits chevauchements à rejet métrique. L'étude de ces déformations indique un déplacement du sud vers le nord.

À l'est de la zone, le monoclinal repose sur des terrains plus récents par l'intermédiaire d'un chevauchement (fig. 10.5); en progressant vers l'ouest, ces terrains récents disparaissent à la faveux d'une faille précoce. Le monoclinal repose alors sur des terrains plus anciens du Protérozoïque moyen. Mais on constate que ce contact se fait à des niveaux stratigraphiques différents de l'unité 4, laquelle va jusqu'à disparaître à l'ouest de la colonne F; la base du monoclinal est alors constituée par l'unité 5 dans laquelle on n'observe pas la partie supérieure argilo-silteuse à l'instar de la colonne F, 2 km plus au nord. Cette absence est interprétée en termes de laminage.

Immédiatement à l'ouest, on voit l'unité 4 réapparaître progressivement en plusieurs localités et l'on constate que le contact est marqué par des brèches tectoniques: les éléments dolomitiques anguleux parfois esquilleux, parfois cassés avec une cassure franche, sont séparés par quelques millimètres de matrice. La matrice calcareuse, de couleur ocre, est très recristallisée (contrairement à celle des brèches intraformationnelles abondantes dans la série). À l'extrémité ouest du terrain, ce contact n'apparaît pas du fait du jeu d'une faille directionnelle tardive.

Ces observations semblent indiquer que la base du monoclinal correspond à un chevauchement à vergence nord qui, dans le contexte général (Tempelman-Kluit, 1979, 1981), doit dater du Mésozoïque.

On remarque sur la carte (fig. 10.2) que le tracé des failles synsédimentaires du compartiment chevauchant correspond, après charriage, au tracé des failles du socle (à la précision de la carte près, le tracé exact étant masqué par les alluvions), phénomène qui indiquerait, en première approximation, une distance de charriage faible.

Néanmoins, comme une tectonique cassante (synsédimentaire) a eu lieu avant le chevauchement et à moins d'admettre qu'une phase supplémentaire a annulé exactement les rejets initiaux, on peut croire que le décollement initiateur du chevauchement s'est produit à des altitudes différentes selon les compartiments. Selon cette hypothèse, au moment du charriage, il aurait existé des <<rails>> qui auraient induit la direction du charriage et empêché une dérive latérale du tracé des failles. Si cette conception est bonne, on pourrait envisager une allochtonie d'assez grande ampleur.

Références

Allison, C.W. and Moorman, M.A.
1973: Microbiota from the late Proterozoic Tindir Group, Alaska; dans Geology, vol. 6, p. 65-68.

Blaise, B.
1983: Géologie de la région du Mont Gibben (Montagnes Ogilvie, Territoires du Yukon); D.E.A., Université Lille I, 56 p.

Chauvel, J.J. et Mansuy, C.
1981: Paleocryptidium cayeuxi: une cyanophyscée du Précambrien du Massif Armoricain; Bulletin de la Société géologique de France, t. XXIII, n° 5, p. 449-458.

Dunoyer de Segonzac, G.
1969: Les minéraux argileux dans la diagenèse. Passage au métamorphisme; thèse d'État, Strasbourg, 317 p.

Geeslin, J.H. and Chafetz, H.S.
1982: Ordovician aleman ribbon cherts: An example of silicification prior to carbonate lithification; Journal of Sedimentary Petrology, vol. 52, n°4, p. 1283-1293.

Green, L.H.
1972: Geology of Nash Creek, Larsen Creek and Dawson map-areas, Yukon Territory; Geological Survey of Canada, Memoir 364, 157 p.

Knauth, L.P.
1979: A model for the origin of chert in limestone; Geology, vol. 7, p. 274-277.

Lucas, G., Cros, P., et Lang, J.
1976: Les roches sédimentaires – 2 – Étude microscopique des roches meubles et consolidées; Doin éd., 503 p.

Moussine-Pouchkine, A. et Bertrand-Safarti, J.
1980: Séquences sédimentaires algo-laminaires littorales: les dolomies de Sarnyéré du Protérozoïque supérieur (Vendien, Gourma-Mali); Revue de Géologie dynamique et de Géographie physique, vol. 22, fasc. 2, p. 89-99.

Roots, C.F.
1983: Mount Harper Complex, Yukon; Early paleozoic volcanism at the margin of the Mackenzie Platform; Recherches en cours, Partie A, Commission géologique du Canada, Étude 83-1A, p. 423-427.

Tempelman-Kluit, D.J.
1979: Transported cataclasite, ophiolite and granodiorite in Yukon: – evidence of arc continent collision; Geological Survey of Canada, Paper 79-14, 27 p.
1981: Geology and mineral deposits of southern Yukon; dans Geology and exploration 1979-80, ed. ministère des Affaires indiennes et du Nord canadien, p. 7-31.

Thompson, R.I. and Roots, C.F.
1982: Ogilvie mountains, Yukon; Part A: A new regional mapping program, part B: volcanic rocks in north-central Dawson map area; dans Recherches en cours, Partie A, Commission géologique du Canada, Étude 82-1A, p. 403-414.

Young, G.M., Jefferson, C.W., Delaney, G.D., and Yeo, G.M.
1979: Middle and late Proterozoic evolution of the northern Canadian Cordillera and Shield; Geology, vol. 7, p. 127-128.

11. MARINE HEAT FLOW ALONG THE NORTHEAST COAST OF NEWFOUNDLAND

Project 800040

J.A. Wright[1], C.E. Keen, and M.J. Keen
Atlantic Geoscience Centre, Dartmouth

Wright, J.A., Keen, C.E., and Keen, M.J., Marine heat flow along the northeast coast of Newfoundland; in Current Research, Part B, Geological Survey of Canada, Paper 84-1B, p. 93-100, 1984.

Abstract

Marine geothermal heat flow techniques are described for measurements in four silled fiords along the northeast coast of Newfoundland. The results indicate that standard deep ocean basin methods can produce useful results in some cases in shallow fiords and bays along a coastline. Measurements were attempted in four fiords, Conception Bay, Trinity Bay, Ship Run and Hall's Bay, but only those in Conception Bay and Ship Run provided interpretable geothermal gradients. Corrections for bottom water exchange in the fiord, for sedimentation history and for topographic and refraction effects are applied. The individual corrections reach maximum values of 10% with large (> ± 10%) uncertainties, especially in the sedimentation correction. The bottom water temperature variations cause a dominantly annual perturbation to the gradient. With 3 to 5 m of sediment penetration, the uncertainty in the temperature transient correction can be almost eliminated. The final results of four measurements in each of the bays yield average heat flows of 47 mW m^{-2} in Conception Bay and 44 mW m^{-2} in Ship Run. These are consistent with nearby conventional land-based measurements in the same geological environments in Newfoundland.

Résumé

Des techniques de flux géothermiques marins sont décrites pour des mesures prises dans quatre fjords à circulation d'eau restreinte le long de la côte nord-est de Terre-Neuve. Les résultats indiquent que des méthodes normales s'appliquant aux bassins en océan profond peuvent produire des résultats utiles dans le cas de certains fjords et baies peu profonds le long d'un littoral. On a essayé de prendre des mesures dans quatre fjords, soit la baie de Conception, la baie de la Trinité, la baie Ship Run et la baie de Hall, mais seules celles qui ont été prises dans la baie de la Conception et dans la baie Ship Run ont fourni des gradients géothermiques pouvant être interprétés. Des corrections ont été faites pour tenir compte de l'échange de l'eau de fond dans le fjord, de l'évolution de la sédimentation et des effets du relief et de la réfraction. Les corrections individuelles atteignent des valeurs maximales de 10 % avec un facteur d'incertitude élevé (> ± 10 %) particulièrement en ce qui a trait à la correction appliquée à la sédimentation. Les variations thermiques de l'eau de fond donnent lieu à une perturbation annuelle dominante du gradient. Avec une pénétration des sédiments de 3 à 5 m, l'incertitude dans la correction transitoire de la température peut être éliminée ou presque. Les résultats définitifs des quatre mesures prises dans chacune des baies donnent des flux thermiques moyens de 47 mW m^{-2} dans la baie de la Conception et de 44 mW m^{-2} dans la baie Ship Run. Il s'agit là de résultats compatibles avec les mesures presque classiques relevées à terre dans les mêmes milieux géologiques à Terre-Neuve.

Introduction

This paper describes the first marine heat flow measurements made in fiords and bays offshore eastern Canada. The study was undertaken partly to determine the circumstances under which measurements of heat flow can be reliably obtained in these environments. Consequently, we illustrate some of the problems which were encountered and which are likely to influence future studies of this kind. The measurements were obtained from **CSS Dawson** in the fall of 1980 in four fiords along the northeast coast of Newfoundland (Fig. 11.1). This region has the attribute that heat flow in all of the main geological zones (Williams, 1979) within the northern part of the Appalachians can be sampled by selecting an appropriate suite of fiords. Therefore, a second objective of this paper is to compare the results of the marine heat flow measurements with land based heat flow values in Newfoundland (Wright et al., 1980) and relate these to their geological setting.

For the past two decades, heat flow measurements have been made routinely in the deep ocean basins. The most important condition which allows reliable measurements there is that the bottom water temperature is relatively constant and temperature variations do not seriously perturb the geothermal gradient (e.g. see Lubimova et al., 1965). This condition may not be satisfied in general in the shallow waters of the continental shelves, and it is only recently that the bottom water temperatures of certain lakes and fiords have been shown to be sufficiently stable to permit a reliable measurement of heat flow (Rankin and Hyndman, 1971; Von Herzen et al., 1974; Hyndman, 1976). These measurements in shallow water environments can make an important contribution to continental heat flow in coatal regions. They eliminate the need for deep boreholes on land, which are expensive and are usually drilled for other purposes in locations which are not always optimal for solving geological problems.

[1] Department of Earth Sciences, Memorial University of Newfoundland
St. John's, Newfoundland A1B 3X7

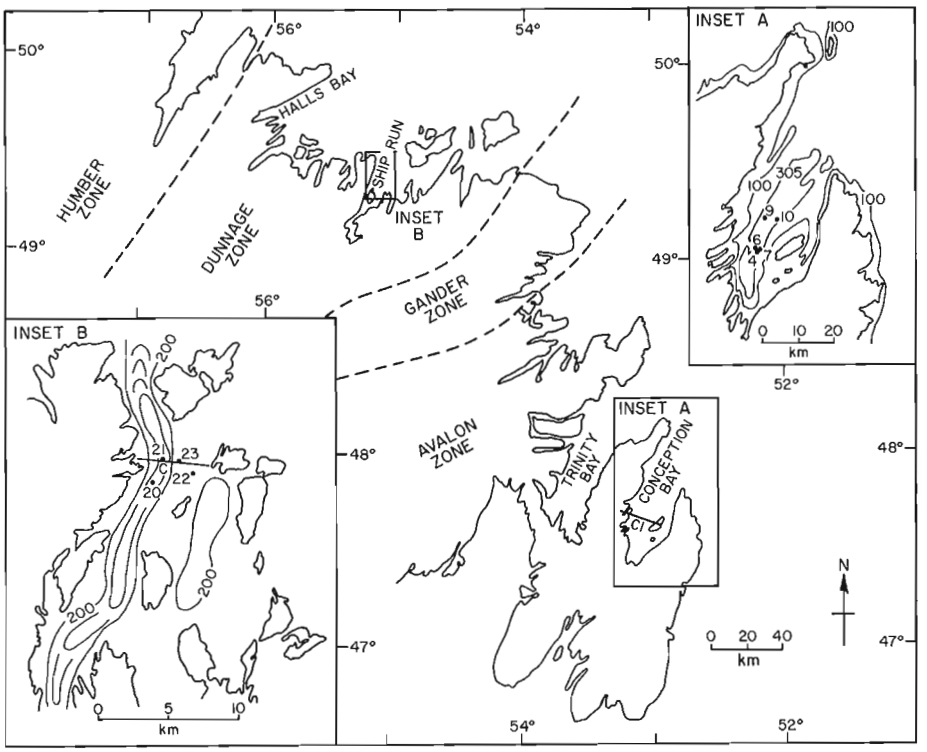

Figure 11.1

Location map of the northeast coast of Newfoundland showing successful heat flow sites and the tectonic zonation of the northern Appalachians (Williams, 1979).

The fiords and bays along the northeast coast of Newfoundland provide a good opportunity to employ these techniques. The geological setting and zonation of the northern Appalachians is reviewed by Williams (1979). The heat flow measurements in Conception Bay and Trinity Bay are in the Avalon zone, which is a Precambrian displaced terrain and forms the easternmost zone of the Appalachian orogen in Newfoundland (Fig. 11.1). The measurements in the Ship Run and Hall's Bay lie within the Dunnage zone, which contains vestiges of the proto-Atlantic Ocean and island arc sequences which are built on this oceanic crust. In general, the basement rock types range from more acidic in the Avalon zone, to the mafic and ultramafic rocks of the Dunnage zone. Hence, the heat flow may tend to lower values in the Dunnage zone, due to the low radiogenic heat production in these mafic/ultramafic rocks. It should be noted that the measurements are at least 200 km from the present continental margin, and hence will not be influenced by Mesozoic rifting and opening of the southern Labrador Sea which produced this margin.

Measurement techniques and results

The heat flow stations are located in the deepest parts of the inlets. Where conditions permitted, several stations were occupied on lines perpendicular to the morphological trends of the inlets so that the effect of refraction of heat by irregular topography could be assessed. Seismic reflection measurements allowed us to select sites which appeared to have a suitable upper layer of soft sediment. These data also provide sediment thicknesses beneath the heat flow stations. Sediment cores from which the thermal conductivity was measured were obtained at or near each heat flow station. The cores also provide preliminary estimates of sedimentation rates over the past 8000-10 000 years. Navigation during the cruise was provided by radar ranging, with the estimated accuracy of the site locations ± 200 m.

The thermal gradient is measured using a 5 m 'Bullard' type probe (Applied Microsystems Ltd., TR-12). The sensor string has fourteen thermistors spaced along its length with the temperature data for each thermistor stored internally. The recorded data must be extrapolated to infinite time from penetration to correct for the frictional heating effect. The instrument is a single penetration type and must be brought on deck after each drop. This does not involve excessive additional time in the shallow water depths of the bays. The greatest problem encountered was that of obtaining penetration into certain sediment types. Twenty-seven stations were occupied with complete or partial penetration at sixteen of these. Table 11.1 presents the location, water depth, depth of penetration and the uncorrected gradient for each station. A typical temperature profile for a site in each of the bays is shown in Figure 11.2.

The probe is not capable of measuring a value of thermal conductivity in situ. Thermal conductivities are calculated using both the needle probe method (Von Herzen and Maxwell, 1959) and the water content method (Ratcliffe, 1960) on the core samples. Where there appeared to be obvious variation in sediment texture or type down the core, specimens were selected so as to sample the full length. Many of the cores began to de-gas as soon as they were brought on deck. The presence of gas bubbles makes the application of the needle probe technique somewhat questionable. Table 11.2 shows the samples selected for conductivity measurements and the conductivities measured using both the needle probe and water content techniques. It is noted that there are often significant differences between the two methods, with a bias toward lower values for the needle probe measurements. This is the anticipated effect of gas bubbles in the sediment. The conductivity values for sites within each bay show no significant systematic variations. Therefore, in the calculation of the heat flow at each site, the harmonic mean of the water content

Table 11.1. Location of heat flow stations and uncorrected gradients

Station no.	Location	Lat.	Long.	Water Depth (m)	Penetration (m)	Uncorrected Gradient (mK m^{-1})	Rating*
4	CBY	47°38.02'	53°05.80'	264	3.5	53	Fair
6	CBY	47°38.18'	53°06.52'	280	4.0	56	Fair
7	CBY	47°38.10'	53°05.30'	268	3.0	55	Fair
9	CBY	47°42.80'	53°03.36'	260	2.5	--	Not usable
10	CBY	47°42.10'	53°01.30'	250	4.0	58	Good
11	TBY	47°59.42'	53°24.15'	559	1.0	--	Not usable
12	TBY	47°59.47'	53°23.60'	558	2.0	--	Not usable
13	TBY	47°59.53'	53°23.88'	558	3.0	24	Poor
14	TBY	47°56.40'	53°26.50'	538	1.0	--	Not usable
15	TBY	48°03.16'	53°21.80'	567	2.0	--	Not usable
16	TBY	48°05.24'	53°20.00'	556	2.0	26	Poor
20	SHR	49°27.78'	55°05.45'	596	5.0	68	Good
21	SHR	49°28.24'	55°05.65	610	4.5	60	Good
22	SHR	49°29.05'	55°06.42'	615	4.5	65	Good
23	SHR	49°29.52'	55°06.83'	614	3.5	49	Fair
26	HBY	49°35.10'	55°49.00'	450	4.5	--	Not usable

* The overall rating is a subjective estimate of the validity of the measurement taking into account the depth of penetration and the consistency of the temperature data.

CBY = Conception Bay: TBY = Trinity Bay: SHR = Ship Run: HBY = Hall's Bay

conductivity values for each bay is used with the corresponding gradient. An uncertainty of ± 15% is associated with the mean conductivity value.

The uncorrected gradients (Fig. 11.2) show significant departures from linearity. These departures are primarily due to bottom water temperature variations. The least disturbed gradients were obtained in Ship Run where the gradient exhibits good linearity below about 1.5 m within the sediment. In Conception Bay, the disturbance is much greater in the upper 2 m of sediment, but the gradient becomes almost linear below that depth. In the following section, we show that in these areas, an estimate of the true geothermal gradient can be recovered by correcting for temperature variations at the seafloor. In Trinity Bay and Hall's Bay, however, the gradients are sufficiently disturbed that no reliable recovery of the geothermal gradient is possible. These sites are not discussed further. It is of interest to note that deep inlets with shallow sill depths at their entrances do not consistently provide the best temperature data for geothermal studies. Conception Bay is a relatively shallow, exposed inlet in which better temperature gradients were obtained than in either Hall's Bay or Trinity Bay, which more closely satisfy the above criteria.

Corrections to the measured values

The effects of the following factors are assessed in this section: annual bottom water temperature variations; sedimentation; lateral heat transport by topographic refraction; variation in land and seafloor temperatures (warm rim effect) and by the thermal conductivity contrast between bedrock and the unconsolidated sediments; and glaciation. Corrections to the geothermal gradient are considered for each of these factors.

Annual temperature variations at the seafloor

The shape of the temperature profile in the mud for the locations shown in Figure 11.2 is reminiscent of that resulting from a sinsoidal surface variation diffusing into a half-space (Carslaw and Jaeger, 1959, p. 81). This effect has also been noted by Lewis (1983) in studies of the heat flow in two inlets in British Columbia. Using the observed wavelength of the

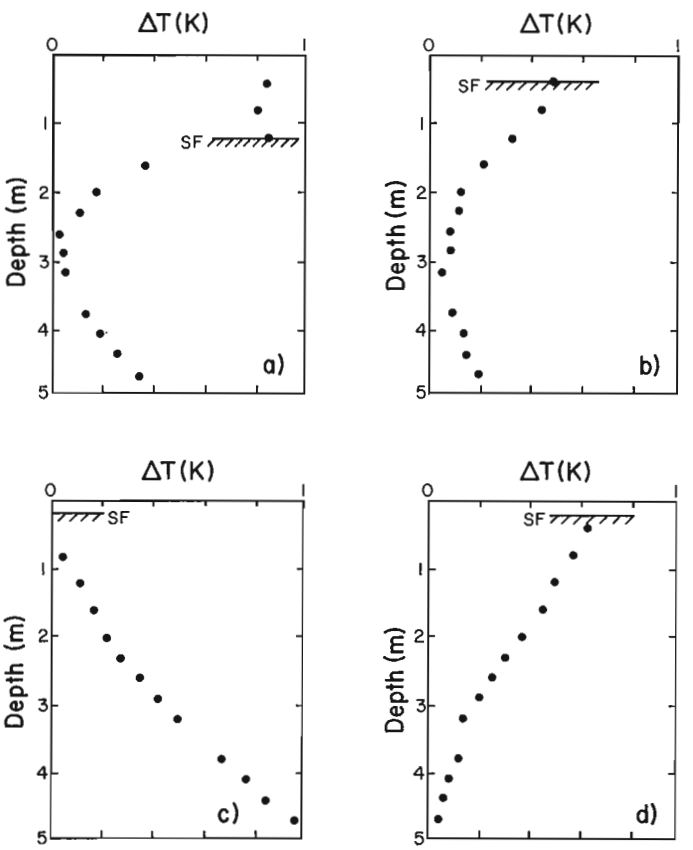

a) Conception Bay (STN. 10)

b) Trinity Bay (STN. 13)

c) Ship Run (STN. 20)

d) Hall's Bay (STN. 26)

(SF = inferred seafloor). Depth scale is relative to the top of the probe.

Figure 11.2. *Observed temperature profiles*

transient, it is seen that the dominant period of the effect perturbing the gradient is annual. In order to study the perturbation more quantitatively, a simple model of an annual-sinusoidal seafloor temperature variation is investigated. The phase and amplitude of the model transient and a superimposed linear gradient are adjusted to achieve the best possible fit to the observed data. The fitting procedure weights more heavily the temperatures deeper in the sediment as these exhibit a more linear behaviour and are not as influenced by shorter period events (i.e. storm surges). The superimposed gradient is representative of the true geothermal gradient. A typical result for station 4 showing the observed temperatures and the model data is shown in Figure 11.3.

The validity of the modelling procedure follows from an understanding of the physical oceanography of the region. The exchange of water in fiords with sills is governed by several factors (Gade and Edwards, 1980). Conception Bay has a 170 m sill and opens directly onto the continental shelf. It is probable that the temperature variations at sill depth external to the fiord reflect variations in the wind field over the shelf, which are known to be seasonal. It is known as well that the Labrador Current has an annual surge which reaches the Avalon Peninsula in autumn and could lead to cold water influx into Newfoundland fiords (Hay, personal communication, 1984). The amplitude of the annual water temperature fluctuation at 170 m depth in this region is on the order of 0.5 to 1.0 K (Keeley, 1981). Its time of occurrence is highly variable but is often in late fall. On the order of a 1 K amplitude is required in the model study for the geothermal case. The phase of sinusoid that best models the transient effect is such that the bottom water temperature is maximum in December. These results are consistent with the oceanographic data. It is recognized that the temporal dependence of the cold water influx is not sinusoidal, but it is certain that the annual compoent is dominant with the higher frequency components having little effect on the temperatures at depths greater than 1 m below the seafloor. Lewis (1983) considered the sediment gradient perturbations induced by both sinusoidal sea-bottom transients and sea-bottom transients consisting of ramps and steps with a one year periodicity. Lewis (1983) concluded that a sinusoidal annual variation models the short-term transient as well as any of the other models investigated. It is recognized that a step change in seafloor temperature that is not annual and may have occurred recently (i.e. within the past 1-10 years) could also perturb the gradient (see Lewis, 1983; Fig. 11.4).

Table 11.2. Thermal Conductivity Values

Site	Location*	Core Number	Thermal conductivity ($W\ m^{-1}\ K^{-1}$) Needle Probe	Water content
4	CBY	PC-2-2	0.60	0.71
4	CBY	PC-2-3	0.44	0.71
4	CBY	PC-2-5	0.64	0.75
7	CBY	PC-4-1	0.62	1.00
7	CBY	PC-4-2	0.95	1.00
11	TBY	PC-10-2	0.54	0.75
11	TBY	PC-10-3	0.80	0.75
11	TBY	PC-10-5	0.64	0.71
20	SHR	PC-17-1	0.68	0.68
20	SHR	PC-17-2	0.80	0.70
26	HBY	PC-27-1	0.80	0.76
26	HBY	PC-27-2	0.82	0.76
26	HBY	PC-27-4	0.69	0.92
26	HBY	PC-27-6	0.98	0.97

*Location codes as in Table 11.1

The results from MEDS station 27 (Keeley, 1981) do not indicate any large step discontinuities in seafloor temperature over the past ten years. Any changes prior to that would have negligible effect on the gradients at 3-4 m depth in the sediments.

This analysis allows the observed data to be corrected for the bottom water temperature variations, thus permitting estimation of the true geothermal gradient. The gradients so deduced for each station are given in Table 11.3.

Sedimentation rate corrections

Corrections for the reduction of the geothermal gradient by deposition of sediment are made using simple theoretical models for both a constant sedimentation rate over a specific time interval and for instantaneous deposition of a given thickness of sediments. Both of these models are described by Von Herzen and Uyeda (1963).

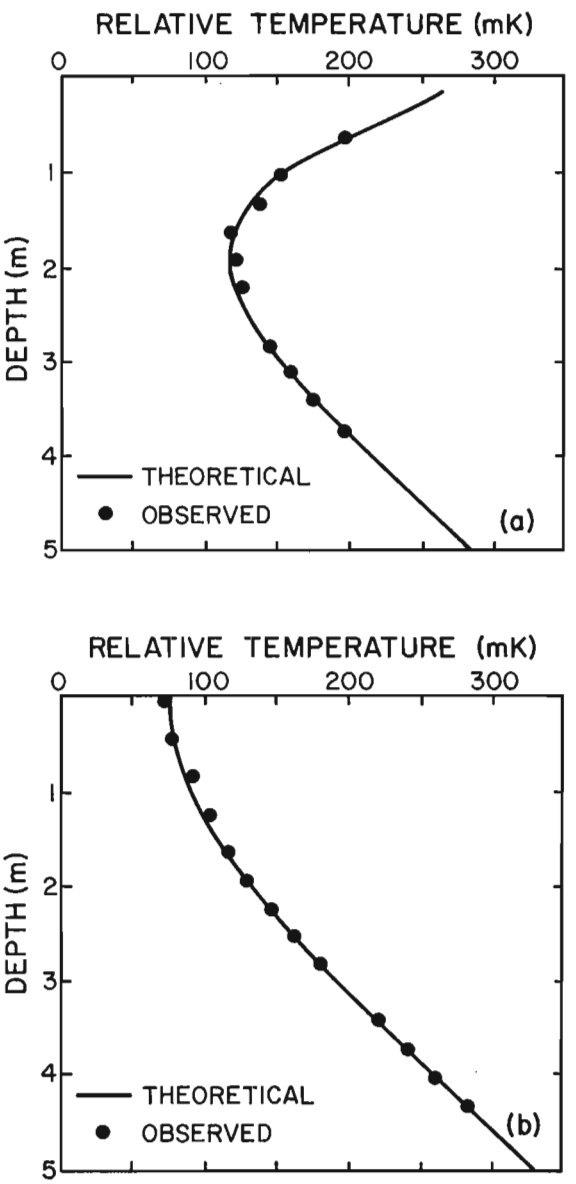

Figure 11.3. *Modelled temperature profile with observed data (a) station 10 ΔT (peak-to-peak) = 300 mK; $k = 1.80 \times 10^{-7}\ m^2 s^{-1}$, $\Delta T/\Delta z = 58\ mK\ m^{-1}$ (b) station 20 ΔT (peak-to-peak) = 75 mK; $k = 1.80 \times 10^{-7}\ m^2\ s^{-1}$, $\Delta T/\Delta z = 66\ mK\ m^{-1}$.*

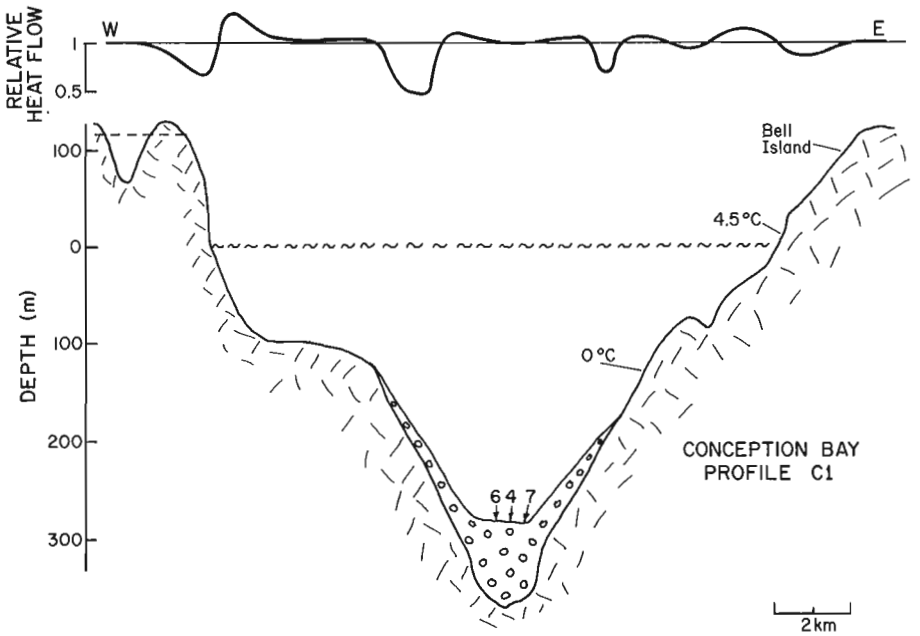

Figure 11.4

Cross-section along profile C1 in Conception Bay showing the relative heat flow disturbance for sedimentation and topographic effects.

The sedimentation rates for Conception Bay have been estimated from biostratigraphic data of cores, combined with seismic reflection data which provide estimates of the total thickness of sediments. The total sediment thickness in the central basin is about 90 m along transect C1 and about 35 m at site 10 (Fig. 11.1, 11.4). The sediments comprise an uppermost unit, about 10 m thick which was deposited during the past 15 000 years. The estimated sedimentation rate for this unit is 0.66 mm/yr (Mudie, personal communication, 1984), from correlation of core data with seismic reflections. The age of the sediments underlying this unit is unknown, but the youngest estimate is 15 000-20 000 years. This implies that about 25-80 m of sediments were deposited during the last glaciation and that these sediments may comprise tills and glacial outwash. Alternatively, the lowermost sediments may represent older Pleistocene deposits. Computations were made on the basis of three assumptions:

i) Sediments deposited during the past 15 000 years contribute a significant correction. Older sediments were deposited sufficiently long ago that their contribution is negligible. Using the estimated sedimentation rate of 0.66 mm/yr, a correction of +6% is obtained for all stations:

ii) The major effect on heat flow was very rapid (instantaneous) deposition of sediments during the glacial maximum about 20 000 years ago. An estimated 80 m was deposited beneath stations 4, 6, and 7, and 20 m beneath station 10, resulting in correction of +12 and +3% respectively:

iii) The total thickness of sediments observed was deposited at a continuous rate during the past 20 000 years. The corrections are +40% for stations 4, 6 and 7 and +20% for station 10.

Of three models, the first two are more consistent with current geological hypothesis, therefore we apply a correction of 6% to the heat flow values. This correction, derived from the first model, does not differ greatly from the results of the second. For the models assuming continuous sedimentation, the value of thermal diffusivity is taken as 6.0×10^{-7} m^2 s^{-1}, intermediate between that of sediment and bedrock. For the model of instantaneous deposition a sediment diffusivity (2.0×10^{-7} m^2 s^{-1}) is used (see Von Herzen and Uyeda, 1963).

A similar analysis was performed for the stations in Ship Run. However, less is known of the sedimentation rates. Seismic data show a total sediment thickness of about 200 m (Fig. 11.5). Since this is more than twice the total thickness in Conception Bay at stations 4, 6 and 7, we assume that the sedimentation rate is double that of Conception Bay. Using the same three sets of assumptions, a correction of +11% is required on the basis of the first assumption. Instantaneous deposition of 180 m of sediment 20 000 years ago yields a correction of +28%, while continuous deposition of 180 m over the past 20 000 years gives +69%. We have applied a correction of +11% to the heat flow values, recognizing that this may be in error by as much as 18%.

Topography, conductivity contrasts and warm rim corrections

Figures 11.4 and 11.5 show cross-sections of Conception Bay and Ship Run respectively. It is clear that heat flow may be perturbed from the regional value due to the topographic variations, the conductivity contrasts between the low conductivity sediments and high conductivity basement rocks, and the fact that surface temperatures will vary from low values at the seafloor within the basins to high values on the nearby land. All three corrections were assessed by obtaining a two-dimensional numerical solution to the steady state equation of conductive heat transport using a finite-difference approximatation. This method has been discussed by Sclater et al. (1970), and applied to heat flow measurements in lakes by Von Herzen et al. (1974). For each heat flow value, a cross-section of the inlet which included land topography, inlet bathymetry and sediment thickness was constructed. The assumption of two-dimensionality is reasonable, given the shape of the inlets. The sinuous nature of Ship Run suggests some departure from two-dimensionality (Fig. 11.1), but it is unlikely to seriously affect the results.

Table 11.3. Correction to the observed gradient

Station	Observed gradient	Corrections to the gradient			Final gradient
		Bottom water	Sedimentation rate	Topography	
	mKm^{-1}		$mK\ m^{-1}$		$mK\ m^{-1}$
4	53	-3	+4	+3	57
6	56	-3	+3	+4	60
7	55	-3	+3	+1	56
10	58	-3	+3	+3	59
20	68	-2	+6	-2	71
21	60	-1	+7	-1	65
22	65	-1	+7	-1	70
23	49	-2	+5	-3	49

The method used follows that described by Von Herzen et al. (1974) and is not to be repeated here. The only difference is that we have chosen to compute the effects across the entire width of these features, unlike that previous study where only half the width of the basin was modelled. The mean annual temperature of the land (4.5°C) was obtained from tabulated data (Anon, 1958) for St. John's and Fogo, the two stations nearest the heat flow sites. Below 150 m water depth the temperature at the seafloor is assumed to be 0°C. The sediment conductivity is chosen to be 0.84 $Wm^{-1}\ K^{-1}$, slightly higher than values measured in near surface sediments (0.75 $W\ m^{-1}\ K^{-1}$) to allow for lesser water content in the deeper sediments. Basement conductivities are 2.93 $W\ m^{-1}\ K^{-1}$ and 3.35 $W\ m^{-1}\ K^{-1}$ for Conception Bay and Ship Run respectively. The slightly higher value for Ship Run reflects the presence of outcrop of Devonian granite around this inlet, while Conception Bay is surrounded by Paleozoic clastic sediments and volcanic rocks. A value of 2.93 $W\ m^{-1}\ K^{-1}$ is compatible with measurements on the Harbour Main volcanics.

Calculations were performed for both cross-sections along which heat flow measurements were made. First, results were obtained for section C1 in Conception Bay, along which three heat flow stations were occupied. Here, the correction varies from +7% in the central region to about 0% at the edge of the deep central basin (Fig. 11.4). Because the total width of the basin is much greater than its depth, the warm rim effect is negligible, and the heat flow values are only affected by the central 14 km of the cross-section illustrated in Figure 11.4. Therefore, the warm rim effect and the onshore topography are neglected in calculations for sites 9 and 10. Along this profile, both topography and sediment thickness are less. The correction at heat flow site 10 is +2%.

In Ship Run four sections, along each of which one heat flow station was occupied in the deep central basin, were constructed and corrections computed. Here topographic and sediment variations are more pronounced (Fig. 11.5). The warm rim effect is important because of the proximity of land to the deep part of the inlet. Corrections for stations 20, 21, 22 and 23 are -3, -2, -2, and -7% respectively. The correction is slightly more at the last station, probably because of the steeper topography there. Otherwise, the different shapes of the cross-sections appear to make little difference to the results, supporting the assumption of two-dimensionality.

There is probably about 1% numerical noise introduced in the computations. Scatter in computed heat flow occurs due to the finite step size implicit in the finite difference approximation. The computed heat flow results (Fig. 11.4, and 11.5) have been smoothed to remove the noise introduced

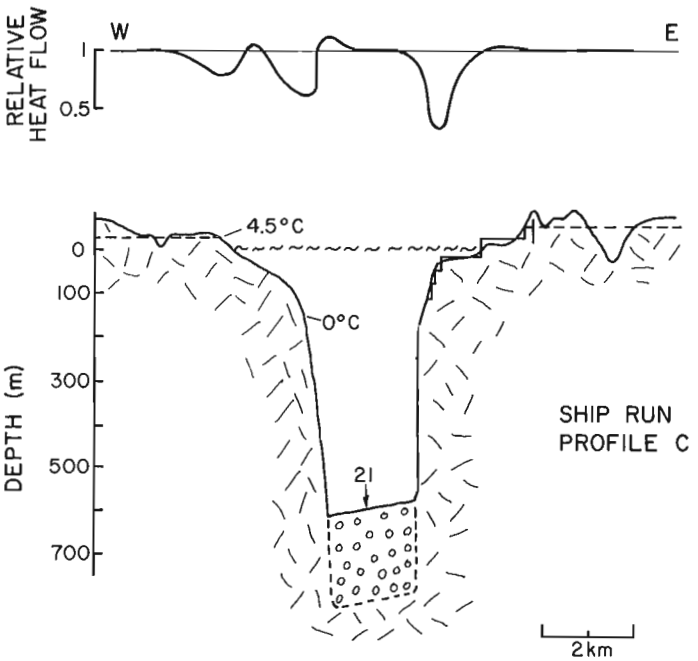

Figure 11.5. Cross-section along profile C in Ship Run showing the relative heat flow disturbance for sedimentation and topographic effects.

by the finite difference approximation. Vertical and horizontal step sizes of 10 and 125 m and 25 and 100 m were used to approximate the Conception Bay cross-sections and Ship Run cross-sections respectively. The total width of the cross-sections necessary to satisfy the boundary conditions were 12-14 km in both cases. The problem of accurately assessing these effects for steep-sided inlets such as Ship Run is important; approximations such as those suggested by Jeffreys (1940) and used by Hyndman (1976) in correcting heat flow values for lateral heat conduction are not accurate. This is illustrated in Figure 11.5 where the relative heat flow is shown. It is clear that there is significant lateral heat transport, due mainly to rapid changes in surface temperature, and that vertical extrapolation of surface temperature down to a horizontal plane is not a valid assumption.

Glaciation

If the temperature at the bottom of the inlets were significantly lower than present due to their occupation by grounded ice cover during the Wisconsian glaciation,

Table 11.4. Heat flow values

Station	Heat flow mW m^{-2}	Uncertainty
4	46	
6	49	
7	45	
10	48	
Conception Bay average	47	± 25%
20	49	
21	45	
22	48	
23	34	
Ship Run average	44	± 25%

a correction must be applied. It is assumed here that this correction is negligible for two reasons. First, the present bottom water temperature in the inlets is close to 0°C, the temperature likely to have prevailed at the base of the ice, so little change in bottom temperature has occurred. Second, even if the temperature at the ice base was somewhat lower, for example -4°C, the glacial maximum occurred about 18 000-20 000 years ago, a sufficient time for the effect to have diffused and the disturbance to have become constant within the upper 4 m of sediment (Rankin and Hyndman, 1971; Von Herzen et al., 1974).

Discussion

The corrected heat flow values (Table 11.4) are deduced from the final gradient values (Table 11.3) and the thermal conductivity values (Table 11.2). The average value for the measurements in Conception Bay is 47 mW m^{-2} while that for Ship Run is 44 mW m^{-2}. The average for Ship Run is biased to a relatively lower value by the low gradient recorded for station 23. If this value is discounted, the average for Ship Run is 47 mW m^{-2}. These two values for Ship Run are not significantly different at the level of confidence of the measurements. Table 11.4 shows that the overall level of confidence for the final values is ±25%. This estimated error is influenced primarily by the lack of good penetration of the probe into the mud and the resulting correction for the temperature transient and by the large corrections for sedimentation rate.

These heat flow values are compared to those on land in Newfoundland (Wright et al., 1980). The Conception Bay results are in the Avalon zone of Williams (1979). The only land-based value in the Avalon zone is at St. Lawrence (82 mW m^{-2}) where the value is anomalously high because of the high radioactivity level in the St. Lawrence granite. It is probable that elsewhere in this Precambrian terrain that a value of 50 mW m^{-2} is more respective. The average value of 44 mW m^{-2} for the Ship Run measurements is consistent with those readings in the Dunnage zone on land (Buchans, 45 mW m^{-2}; Victoria, 54 mW m^{-2}). The Ship Run measurements are close to a large Devonian granitic intrusion (Long Island granite). The gravity signature of the Long Island gravity low (Weaver, 1967) indicates that it is batholithic in nature. The apparent absence of a high heat flow associated with the granite is suggestive of a low K content for the intrusion.

These results demonstrate that reasonable heat flow values can be obtained in the shallow fiords along a coastline. However, they point to several difficulties associated with the measurements. The problems due to temperature transients in the bottom water can be greatly lessened by using heavier probes with deeper penetration. The model studies indicate that a depth of penetration of 3-5 m is adequate to suppress the dominant annual effect. The problem of sedimentation rate correction is more severe and difficult to attack. Without a detailed knowledge of the sedimentation history for the fiord, this source of error will probably dominate the overall error in the measurement. The topographic effect modelling shows that the simple approximations for correction (Jeffreys, 1940) are not accurate and that a more extensive analysis of this correction is required.

Acknowledgments

We thank the Officers and crew of **CSS Dawson** for their help during the cruise. Alex Hay, Roy Hyndman and Peta Mudie are thanked for many useful and stimulating discussions. The work was supported by an EMR Canada Research Agreement to JAW.

References

Anonymous
1958: Tables of temperature, relative humidity and precipitation for the world. Part I; Her Majesty's Stationary Office, London.

Carslaw, H.S. and Jaeger, J.C.
1959: Conduction of Heat in Solids; 2nd edition, Oxford University Press, London.

Gade, H.G. and Edwards, A.
1980: Deep water renewal in fjords; in Fjord Oceanography, ed. H.G. Freeland, D.M. Farmer, and C.D. Levings; Plenum, New York, p. 453-490.

Hyndman, R.D.
1976: Heat flow measurements in the inlets of southwestern British Columbia; Journal of Geophysical Research, v. 81, p. 337-349.

Jeffreys, H.
1940: The disturbance of the temperature gradients in the earth's crust by inequalities of height; Monthly Notices of the Royal Astronomical Society, Geophysical Supplement, v. 4, p. 309-312.

Keeley, J.R.
1981: Temperature, Salinity and Sigma-t at Station 27 (47°33'N, 52°35'W). An Analysis of Historical Data; Technical Report No. 8, Marine Environmental Data Service, Department of Fisheries and Oceans, Canada.

Lewis, T.
1983: Bottom water temperature variations as observed, and as recorded in the bottom sediment, Alice Arm and Douglas Channel, British Columbia; in Hydrography and Ocean Science, v. 18, p. 138-161.

Lubimova, E.A., Von Herzen, R.P., and Vdintsev, G.B.
1965: On heat transfer through the ocean floor; in Terrestrial Heat Flow, ed. W.H.K. Lee; American Geophysical Union, Geophysical Monograph Series no. 8, Washington, p. 78-86.

Rankin, D.A. and Hyndman, R.D.
1971: Shallow water heat flow measurements in Bras D'Or Lake, Nova Scotia; Canadian Journal of Earth Sciences, v. 8, p. 96-101.

Ratcliffe, E.H.
1960: The thermal conductivities of ocean sediments; Journal of Geophysical Research, v. 65, p. 1535-1541.

Sclater, J.G., Vacquier, V., and Rohrhirsch, J.H.
1970: Terrestrial heat flow measurements on Lake Titicaca; Earth and Planetary Science Letters, v. 8, p. 45-54.

Von Herzen, R.P. and Maxwell, A.E.
1959: The measurement of thermal conductivity of deep-sea sediment by a needle probe method; Journal of Geophysical Research, v. 64, p. 1557-1563.

Von Herzen, R.P. and Uyeda, S.
1963: Heat flow through the eastern Pacific Ocean floor; Journal of Geophysical Research, v. 68, p. 4219-4250.

Von Herzen, R.P., Finckh, P., and Hsu, K.G.
1974: Heat flow measurements in Swiss lakes; Journal of Geophysics, v. 40, p. 141-172.

Weaver, D.F.
1967: A geological interpretation of the Bouguer anomaly field of Newfoundland; Publications of the Dominion Observatory, Ottawa, Ontario, v. 35, p. 223-251.

Williams, H.
1979: Appalachian orogen in Canada; Canadian Journal of Earth Sciences, v. 16, p. 792-807.

Wright, J.A., Jessop, A.M., Judge, A.S., and Lewis, T.J.
1980: Geothermal measurements in Newfoundland; Canadian Journal of Earth Sciences, v. 17, p. 1370-1376.

12.

TEMPERATURE GRADIENT MEASUREMENTS IN BOREHOLES USING LOW NOISE HIGH RESOLUTION DIGITAL TECHNIQUES

Project 810008

Q. Bristow and J.G. Conaway [1]
Resource Geophysics and Geochemistry Division

Bristow, Q. and Conaway, J.G., Temperature gradient measurements in boreholes using low noise high resolution digital techniques; in Current Research, Part B, Geological Survey of Canada, Paper 84-1B, p. 101-108, 1984

Abstract

Continuous temperature logging equipment, developed at the Geological Survey of Canada, takes advantage of modern technology by using an integrated circuit voltage-to-frequency converter in the temperature probe to accomplish the analog-to-digital conversion with a sensitivity of 2 KHz/K. By measuring the length of time to accumulate 8192 pulses, against a 10 MHz crystal clock at the surface, continuous measurements can be made with a resolution of almost 10^{-5} K at intervals of less than 0.4 seconds.

Initial experiments in a thermally stable borehole with a well documented temperature profile indicate that the thermal equivalent noise of the measurement system is of the order of 0.1 mK (millidegrees Kelvin). This permits temperature gradients to be determined with a precision of 5 mK/m (millidegrees Kelvin per metre) over a depth interval as small as 2 cm. A small amount of smoothing can reduce noise to a very low level. Typical gradients in undisturbed boreholes are from 10 to 30 mK/m and variations of the order of 5 to 10 mK/m over a few centimetres may, under favourable conditions, indicate changes in lithology.

Résumé

La Commission géologique du Canada a tiré avantage des techniques modernes pour mettre au point un matériel d'enregistrement continu de la température comportant dans la sonde de température un convertisseur tension-fréquence à circuit intégré qui permet une conversion analogique-numérique avec une sensibilité de 2 kHz/K. En mesurant le temps nécessaire pour accumuler 8192 impulsions, avec un cristal étalon de 10 MHz, on peut mesurer la température de façon continue avec une résolution de presque 10^{-5}°K à des intervalles de temps inférieurs à 0,4 secondes.

Les premières expériences dans un trou de sonde à caractère thermique stable et doté d'un profil de température bien connu, montrent que le bruit thermique équivalent du système de mesure est de l'ordre de 0,1 mK (millidegrés Kelvin). Cela permet de mesurer les gradients thermiques avec une précision de 5 mK/m sur un intervalle de profondeur aussi faible que 2 cm. Un léger lissage peut réduire le bruit à un niveau très faible. Dans des trous de sonde non perturbés, les gradients caractéristiques varient de 10 à 30 mK/m et des variations de l'ordre de 5 à 10 mK/m sur quelques centimètres peuvent, dans des conditions favorables, indiquer des variations lithologiques.

Background

Temperature gradient profiles in boreholes provide essential information in establishing terrestrial heat flow patterns. They also provide useful information concerning groundwater flow and can be used, in some cases, as an aid in stratigraphic correlation. The oil industry makes routine use of temperature and temperature gradient logs for applying corrections to electrical resistivity logs, and for detection of gas leaks (Kappelmeyer and Haenel, 1974; Bryant, 1960). For many years borehole temperature measurements have been made by more or less classical methods using thermistors in bridge circuits as the starting point, and these have been well documented in the literature (Beck, 1965; Simmons, 1965). In recent years sophisticated digital resistance meters have been used along with thermistor probes and uphole digital resistance instrumentation (e.g. Conaway and Beck, 1977a) to produce high resolution temperature gradient logs. When hundreds or thousands of metres of cable are involved, the problems of eliminating the effects of conductor resistance, insulation leakage resistance and induced noise become formidable. Early attempts to overcome these problems were made by including the temperature sensing element as one component of an oscillator, causing the frequency to become a function of the temperature. This frequency was measured by surface equipment and was essentially independent of the cable effects mentioned above.

Recent advances in integrated circuit (I.C.) technology have resulted in the availability of highly stable voltage-to-frequency (V/F) converters packaged as standard 14 pin dual-in-line integrated circuits. We constructed an experimental temperature probe consisting of a thermistor sensor and such a V/F converter to digitize the signal. This probe was connected via 1000 m of cable to a minicomputer-based data acquisition system in a logging truck.

[1] Now at Seismograph Service Corp., Tulsa, Oklahoma, U.S.A.

The principle of operation is shown diagrammatically in Figure 12.1. Data were collected from a hole with a well documented stable temperature profile in order to assess the instrumental noise level attainable with this system. These and other logs have shown that, under favourable conditions, temperature gradient data are reproducible as well as being sensitive indicators of lithology. In cases where water flows are present, these are generally indicated by perturbations in the gradient logs.

Analog/digital conversion of the sensor signal

The advantages of digitizing sensor signals before transmission over long lines rather than afterwards are universally recognized and are particularly relevant to borehole logging operations. The use of a V/F converter to produce a pulse train whose frequency is proportional to the analog sensor signal is the cheapest and most elegant method. This is only applicable, however, if the highest analog signal frequencies are less than half that of the frequency being generated by the V/F converter. In the case of borehole temperature measurements the signal is essentially a slowly varying D.C. level, so that V/F conversion is an eminently suitable solution.

An obvious alternative to the technique described above is to use a successive approximation type analog-to-digital (A/D) converter to sample the sensor signal at predetermined time intervals and a parallel-to-serial converter to transmist the digital result as an RS232C signal or similar protocol. This would require a minimum of two fairly complex and power-hungry I.C.s and some additional support chips in the probe. The measurement resolution would be limited by the A/D converter (for example a 12 bit device has a resolution of 1 part in 4096) and additional sample-and-hold circuitry would be required to provide the A/D converter with stable samples of the signal for conversion to a digital representation. Some form of two-way "handshaking" between the probe electronics and the surface equipment might also be required.

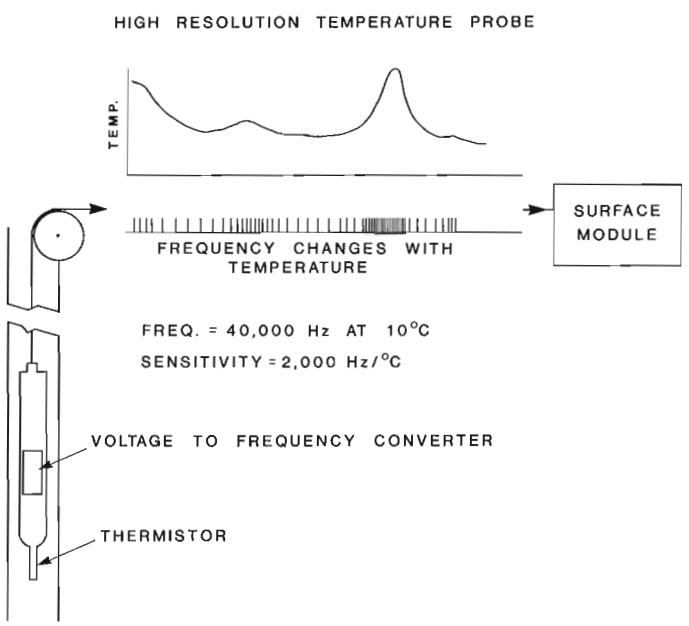

Figure 12.1. *Principle of voltage-to-frequency conversion.*

Table 12.1. AD 537 V/F Converter Data Summary

Power supply:	4.5 - 36 V
Frequency range:	0 to 150 kHz
Useable temp. range:	0 to + 70°C
On-chip reference voltage data	
Voltage:	1.00 V +/- 5%
Stability vs temp.:	50 ppm/K
Stability vs. power supply:	+/- 0.03% of supply

The V/F conversion technique by contrast requires only a single relatively inexpensive I.C. in the probe, with the measurement resolution being limited only by the sophistication of the surface equipment. A further advantage is that the sensor signal is automatically averaged (without any additional in-probe circuitry) over whatever time interval is set for measurement of the frequency by the surface equipment. Finally, two-way "handshaking" between the probe electronics and the surface equipment is not required.

Experimental probe

The temperature sensor used was a thermistor assembly made to a U.S. Geological Survey specification by Fenwal Electronics. It consists of a thin-walled metal tube approximately 4 mm diameter by 15 cm long, containing a number of individual thermistor beads wired in a series-parallel combination to give a nominal resistance of 10 000 ohms at 20°C. The transfer function is given by the manufacturer as a function of the resistances R_1 and R_2 measured at two temperatures Θ_1 and Θ_2:

$$R_1 = R_2 \exp \{\beta (1/\Theta_1 - 1/\Theta_2)\} \quad (1)$$

where β is a constant which is dependent on the thermistor material. For any given resistance, R, at a temperature, Θ, equation (1) resolves to the basic relationship:

$$R \propto \exp (\beta/\Theta) \quad (2)$$

The V/F converter used is the Analog Devices Inc., model AD537. A summary of the data supplied by the manufacturer is shown in Table 12.1. The I.C. includes a 1.0 volt reference source which has sufficiently good stability to be used as the energizing voltage for the thermistor.

Figure 12.2 shows the relatively simple circuit arrangement which was used to accomplish conversion of the thermistor signal to a frequency in the probe, and also the circuitry used to convert the pulse train to useable logic signals for frequency measurement in the surface equipment. The V/F converter is actually a current-to-frequency converter and takes as its signal the current driven through the thermistor by the one volt source (approximately 100 micro amps at 20°C). Power for the device is supplied from the surface via one of the two conductors of a shielded twisted pair cable used for the logging operation.

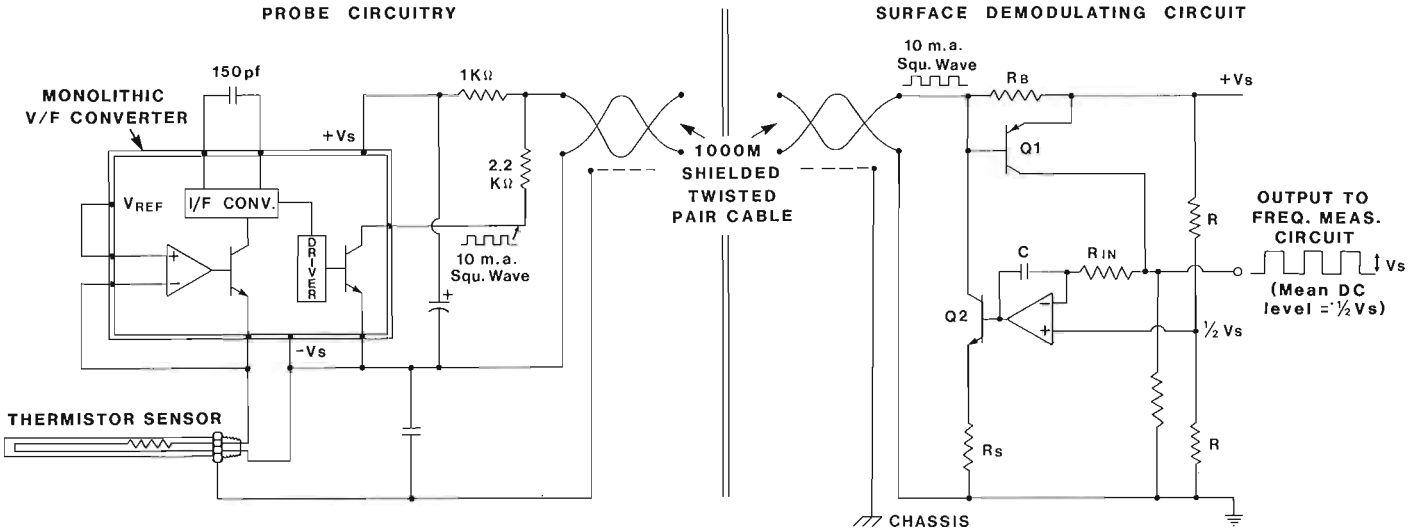

Figure 12.2. *Probe and surface demodulation circuits. Current for the probe circuitry is supplied via one of the two conductors. The frequency signal is superimposed on this D.C. level as a 10 m.a. square wave. The demodulation circuit employs a novel automatic bias arrangement to ensure that Q1 responds to the signal.*

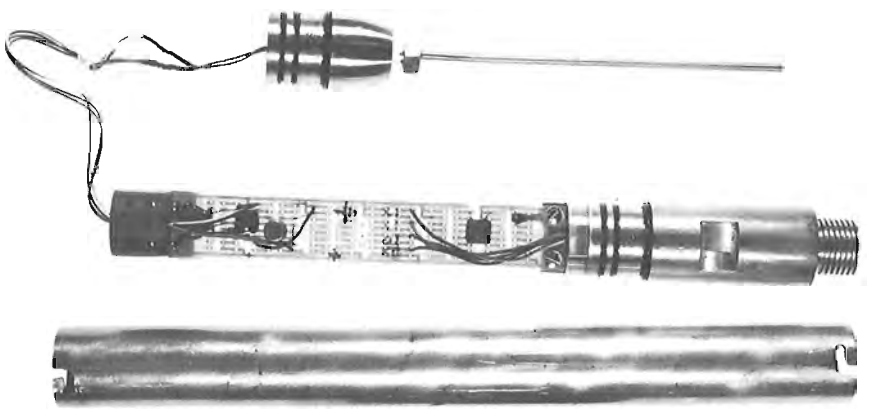

Figure 12.3

The complete temperature probe disassembled.

Top: *Thermistor element mounted in nosepiece.*

Middle: *Circuit board attached to bulkhead which mates with G.O.I. cablehead connector.*

Lower: *32 mm O.D. stainless steel housing. It is secured to nosepiece and bulkhead with bayonet locks to simplify disassembly.*

The cable has a polyurethane jacket and a KEVLAR fibre strand which gives it a breaking strength of 450 g. One thousand metres was used for these experiments. The main reason for the choice of this type of cable over the industry standard 4HO steel armoured cable is the relatively light weight (approximately 33 g/1000 m). This makes it attractive for portable logging systems which are desirable for mineral exploration in relatively inaccessible terrain.

The output signal from the V/F converter is a current square wave with a 50% duty cycle at a frequency determined by the thermistor temperature. It is superimposed on the current which powers the device from the surface, and which passes through the resistor R_B in the surface demodulation circuit of Figure 12.2. The transistor Q1 is biased automatically so that it is switched on and off by the square wave component of the current through R_B. The D.C. component of this current is augmented and controlled by Q2 and the operational amplifier integrator in a feedback loop, so that a symmetrical square wave, with an average D.C. level of one-half the supply voltage, is maintained at the point marked "output". This scheme avoids the necessity for critical adjustment of the value of R_B to achieve the correct bias for Q1 to respond to the square wave component of the current generated by the V/F converter. This setting would otherwise depend on the ambient temperature of Q1 and the average current being drawn by the probe circuitry.

The sonde pressure housing consists of a 32 mm O.D. stainless steel tube fitted at one end with a nose piece and at the other with a Gearheart Industries standard 4-pin male connector body. Both of these pieces are sealed with "O" rings and are retained in the tube section by simple bayonet locks. The thermistor unit is fitted at one end with a "1/8-NPT" pipe thread which engages with threads in the nose piece to produce a pressure-tight seal. A photograph of the disassembled probe is shown in Figure 12.3

Surface equipment

The data acquisition system and cable winch are mounted in a four-wheel-drive vehicle. It has been in use as a research logging system by the GSC since 1978 for acquiring natural gamma spectral data from boreholes. More recently it has been adapted to acquire complete Induced Polarization waveforms transmitted digitally from a borehole probe. The system, which has been described in detail elsewhere, (Bristow and Killeen, 1978; Bristow, 1979) consists of a Data General NOVA minicomputer and a nine track magnetic tape drive together with a six channel strip chart recorder, an alphanumeric display with limited graphics

capability, and a small hard copy terminal with full keyboard for data entry and a permanent record of such entries. Probe depth is measured by an optical shaft encoder on the well-head pulley. The encoder generates one pulse for each millimetre (nominally) of cable travel, and provides a logic level indication of logging direction as well. This signal is used in a hardware servo loop which controls the winch motor to maintain constant cable speed. It is also used by the NOVA for displaying depth on the chart recorder as a one metre sawtooth, and for recording depth on tape along with data from the probe being used. Probe velocity is also calculated and displayed on the CRT display along with other data.

The NOVA minicomputer has provision for custom interface circuitry to be installed on its standard 15" square input/output boards. The necessary circuitry to measure frequency was built on to one such board, and the main software operating system was modified to compute, display and record temperature.

Measurement resolution

When an analog sensor signal is digitized, the overall measurement resolution becomes a function of two parameters: (i) the signal-to-noise ratio of the sensor, and (ii) the quantity defined by a single increment in the digital representation chosen, often referred to as the measurement precision. Temperature gradients in undisturbed boreholes are typically between 10 and 30 mK/m depending on the thermal conductivities of the major lithological features in the area. In some applications better spatial resolution is desirable and readings should be made at depth intervals of 0.1 m or shorter. The temperature differences over such intervals are then of the order of 2 mK for an average gradient of 20 mK/m. For this system an overall measurement resolution of 10^{-4} K was set as a design goal, giving a corresponding temperature gradient resolution of 1 mK/m for depth sampling intervals of 0.1 m. This capability would represent a substantial improvement over borehole temperature measurement equipment described to date and allow fine structure to be observed in gradient data with better spatial resolution than had previously been possible.

The temperature measurement precision attainable with this system is a function of the resolution with which the frequency can be measured. In general the longer the time interval over which the frequency measurement is made, the better the precision will be. The absolute accuracy is a separate consideration and depends on the accuracy of the timing standard used and the stability of the sensor and associated electronics.

The V/F converter frequency as generated by the circuit arrangement of Figure 12.2 is inversely proportional to the thermistor resistance. Some simple calculations using the known value of the constant β, the resistance of the thermistor at 10°C, and the known parameters of the V/F converter, showed that a frequency change of approximately 2.0 kHz/K would be observed in the region of 10°C. In order to determine the frequency with a precision commensurate with a resolution of 0.1 mK, a sampling time of 5 seconds would thus be required. This constraint however is unacceptable if a reasonable logging speed (5-10 m/min) is to be maintained with the temperature being sampled at say 0.1 m intervals.

The time for a frequency determination can be reduced while maintaining the resolution either by multiplying the base frequency using a phase-locked loop and frequency divider arrangement, or by measuring the time for a fixed number of cycles against a high frequency time standard. The latter approach was chosen for this system. The circuitry built onto the NOVA interface board counts the number of pulses from a crystal controlled 10 MHz clock over the time interval taken to accumulate 8192 cycles from the V/F converter in the temperature probe. Synchronization circuitry was incorporated to ensure that each measurement interval started at a coincidence between the clock and V/F converter pulse trains, thereby eliminating the uncertainty of +/- 1 that would otherwise be present in the clock count. Block diagrams illustrating the advantages of measuring period rather than frequency are shown in Figure 12.4.

The relation between the V/F converter frequency, f, and the number, N, of 10 MHz clock pulses accumulated in 8192 cycles of f is given by

$$f = 8192/(N \times 10^{-7})$$

Since f is inversely proportional to the thermistor resistance and also to N, a simple overall relation between N and the temperature θ (°K) can be written as:

$$N = \exp(C).\exp(\beta/\theta),$$

$$\text{or: } \beta/\theta = \log(N) - C \qquad (3)$$

where C is a constant of proportionality.

The constants C and β can be determined by a direct experimental calibration.

The measurement resolution is now the rate of change of N with θ, (whether in °C or °K) and from equation (3) this is seen to be:

$$dN/d\theta = -\beta/\theta^2.\exp(C).\exp(B/\theta) \qquad (4)$$

An experimental calibration in a controlled temperature bath produced values for the constants β and C of 3360 and 2.588 respectively, which when applied to equation (4) give a value of $dN/d\theta$ of 0.8×10^5 clock pulses/degree at 10°C. That is to say temperature differences in the order of 0.01 mK could be resolved in the absence of noise.

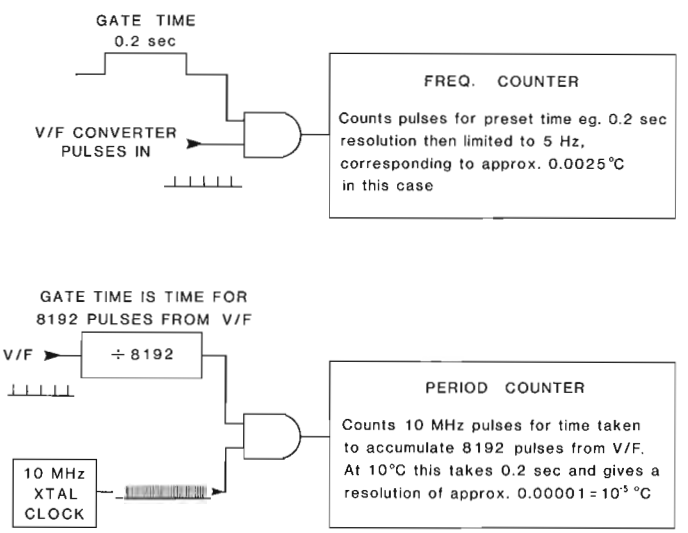

Figure 12.4. *Advantage of period measurement as opposed to frequency measurement.*

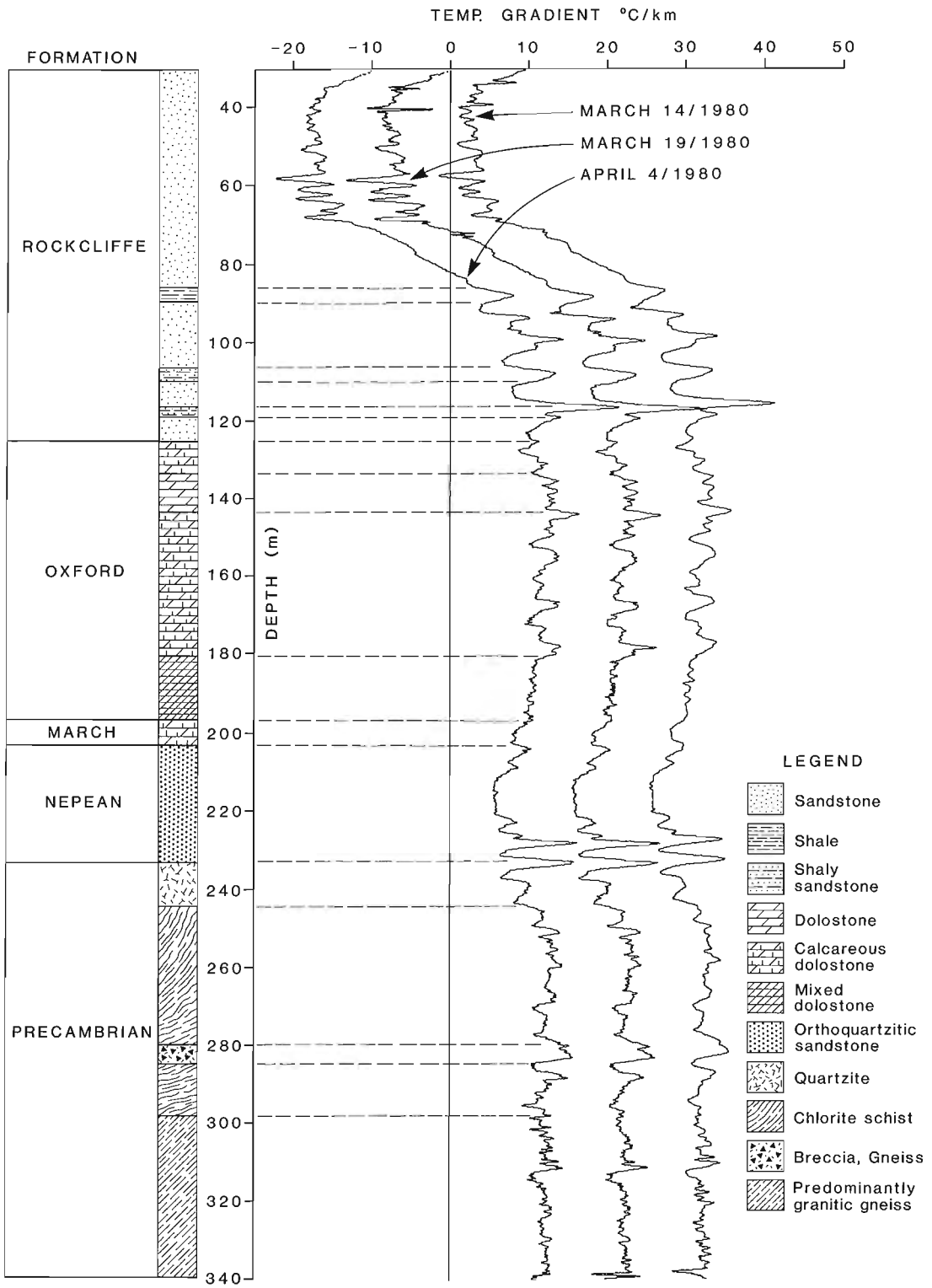

Figure 12.5. *Three temperature gradient logs processed from temperature logs recorded by the high-resolution temperature probe. The borehole is at the Ottawa site of the Earth Physics Branch of the Department of Energy, Mines and Resources. The log marked April 4th, 1980 is correctly positioned with respect to the gradient scale. The other two are offset for clarity by 10 and 20 mK/m respectively.*

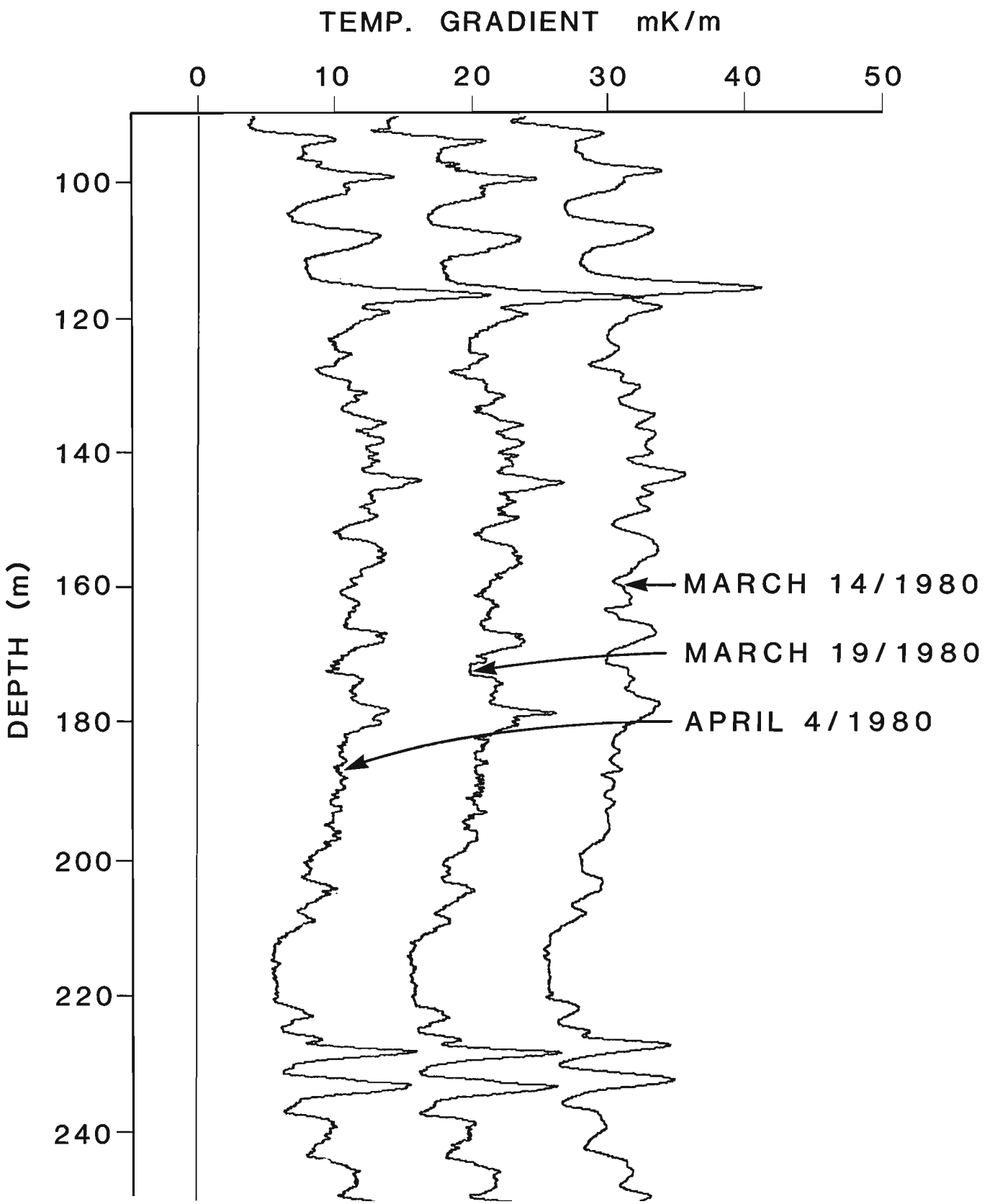

Figure 12.6. *The section of Figure 12.5 between 90 and 250 m is shown here at an expanded scale to illustrate reproducibility of detail in the three logs.*

The accumulation time for 8192 cycles of the V/F converter frequency decreases with increasing temperature. At 0°C, the minimum likely to be encountered, this time is approximately 0.4 seconds, which thus becomes the longest possible sample time needed to record a measurement.

An improved inverse filter

The thermal sensor used in these experiments has a nearly exponential time response to a step change in temperature. If the thermal time constant, τ, is defined in the usual way as the time to reach (1-1/e) of the applied step amplitude, then the sensor's impulse response f(t) is given by

$$f(t) = \exp(-t/\tau)$$

An approximate inverse filter has been derived (Costain, 1970; Conaway, 1977) which is designed to remove the smearing effect of the thermal time constant; this is especially important for high resolution continuous temperature gradient logging. In situations where $\tau >> \Delta t$, (Δt is the sampling interval), this inverse filter gives good results. When τ is not at least several times larger than Δt, some improvement in the processed log can be achieved by using an exact inverse filter of the type described by Treitel and Robinson (1964). Such a filter was described by Conaway (1980) for the exponential ratemeter of a gamma-ray logging system. This same inverse filter can be applied to temperature logging without modification. This filter has two coefficients, given by:

$$\frac{1}{1 - e^{-\Delta z/v\tau}} \quad , \quad \frac{e^{-\Delta z/v\tau}}{1 - e^{-\Delta z/v\tau}}$$

(where v is the logging speed and Δz is the sample depth interval). The inverse filter can be combined with a 3-point derivative operator (Conaway, 1977) and a suitable smoothing filter. The combined operator can then be used to give a smoothed, deconvolved temperature gradient log in a single pass. The improvement offered by this filter over the approximate filter will be especially noticeable if the raw log has high precision and low noise.

Results and discussion

The purpose of this work was to use the best technology available to assemble a borehole temperature measurement system which would have a significantly lower instrumental noise level than any system previously developed. Such a system would allow temperature gradient logs to be derived from the basic temperature data without fine detail being masked in instrumental noise which is always amplified in the process of applying a derivative operator to obtain a gradient. High quality temperature gradient logs may provide detailed information on the lithology intersected by the borehole in a similar manner to electrical logs, (Beck, 1976; Conaway and Beck, 1977b). No particular emphasis was placed on determining the absolute accuracy or long term stability of the system for precision temperature measurement. Although good performance in these aspects is necessary for measurements related to heat flow studies, they do not significantly affect temperature gradient measurements. For this reason an initial calibration using a controlled temperature bath and a secondary standard was made to an absolute accuracy of a few tenths of a degree only, to establish the values of the constants C and β in equation (3).

Figure 12.5 shows three temperature gradient logs processed from temperature logs recorded on different dates in a borehole at the Ottawa site of the Earth Physics Branch of the Department of Energy, Mines and Resources. This borehole was drilled for use in research programs and has a nearly stable fluid column. The reproducibility of the fine detail is clearly evident in Figure 12.6, which shows the section in Figure 12.5 from 90 to 250 m on an expanded scale. The data were recorded during descent of the probe at a speed of approximately 6 m/minute and a sampling interval of 0.4 seconds, so that each measurement represented the average value over a 4 cm depth. The most noise-free portions of the logs occur at the minimum temperature where the gradient crosses the zero axis. A listing of recorded temperature values over these portions showed, in each case, that changes for more than ten consecutive readings were less than 10^{-4} K as the minimum level was crossed. These data suggest that the instrumental noise level was at least below 10^{-4} K which was the design goal. It may well be that the natural thermal noise level in the borehole fluid will prove to be the limiting factor.

The geological log of this hole shows that most of the rock unit boundaries are delineated by the temperature gradient logs. This log (compiled many years ago), was not described in the detail that would be necessary to account for all of the temperature gradient anomalies, and it seems probable that a re-examination of the core with these temperature gradient logs as a guide might well reveal lithological detail that was previously overlooked. While such a postmortem is not possible in this case, the idea of using a temperature gradient log as a guide in the compilation of a geological log might prove beneficial in drawing attention to particular sections of core.

Conclusion

A tool has been described which is relatively inexpensive to produce when compared to other geophysical borehole logging tools, but which is capable of acquiring temperature logs with a noise level sufficiently low that detailed and reproducible temperature gradient logs can be derived from them. Applications are anticipated in heat flow studies, radioactive waste management studies, hydrogeological work and recognition of lithological discontinuities as an aid in mineral exploration.

Acknowledgments

The authors are indebted to J. Parker and Y. Blanchard for patience and skill in assembly and testing of the electronics involved, and the W. Hyatt for care and attention to detail in acquiring the test logs.

References

Bristow, Q.
1979: Airborne and vehicle mounted geophysical data acquisition systems controlled by NOVA minicomputers; in Proceedings of the 6th Annual Data General Corporation Users Group meeting, New Orleans, December 4-7.

Bristow, Q. and Killeen, P.G.
1978: A new computer-based gamma ray spectral logging system; Presented at the 48th Annual International Society of Exploration Geophysicists meeting, San Francisco, November 1st.

Beck, A.E.
1965: Techniques of measuring heat flow on land; in Terrestrial Heat Flow, ed. W.H.K. Lee; American Geophysical Union, Monograph no. 8, Washington, p. 24-57.

1976: The use of thermal resistivity logs in stratigraphic correlation; Geophysics, v. 41, no. 2, p. 300-309.

Bryant, H.L.
1960: Production well logging techniques; Geophysics, v. 25, p. 905-927.

Conaway, J.G.
1977: Deconvolution of temperature gradient logs; Geophysics, v. 42, no. 4, p. 823-837.

Conaway, J.G. (cont.)
1980: Exact inverse filters for the deconvolution of gamma-ray logs; Geoexploration, v. 18, p. 1-14.

Conaway, J.G. and Beck, A.E.
1977a: Continuous logging of temperature gradients; Tectonophysics, v. 41, p. 1-7.

1977b: Fine scale correlation between temperature gradient logs and lithology; Geophysics, v. 42, p. 1401-1410.

Costain, J.K.
1970: Probe response and continuous temperature measurements; Journal of Geophysical Research, v. 75, p. 3968-3975.

Kappelmeyer, O. and Haenel, R.
1974: Geothermics; Gebruder Borntraeger, Berlin.

Simmons, G.
1965: Continuous temperature logging equipment; Journal of Geophysical Research, v. 70, p. 1349-1352.

Treitel, S. and Robinson, E.A.
1964: The stability of digital filters; I.E.E.E. Transactions on Geoscience Electronics; v. GE-2, p. 6-18.

13.

STRUCTURE OF THE JUNCTION OF THREE TECTONIC SLICES; ONTARIO GNEISS SEGMENT, GRENVILLE PROVINCE

Project 830009

S.K. Hanmer
Precambrian Geology Division

Hanmer, S.K., Structure of the junction of three tectonic slices; Ontario gneiss segment, Grenville Province; in Current Research, Part B, Geological Survey of Canada, Paper 84-1B, p. 109-120, 1984.

Abstract

Contacts between domains and subdomains in the Moon Bay area contain mesh structures and show cross-cutting relationships. Thus as previously suggested by Davidson and others they are tectonic. Small scale and large scale structural considerations suggest a complex kinematic picture.

Résumé

Les contacts qui existent entre certains domaines et sous-domaines de la région de la baie Moon contiennent des structures en mailles et présentent des liens en travers-banc. Par conséquent, il s'agirait de contacts d'origine tectonique comme l'ont avancé Davidson et d'autres auteurs. Certaines considérations d'ordre structural à petite et à grande échelle permettent de croire à une image cinématique complexe.

Introduction

Recent fieldwork in southwest Grenville Province, Ontario (Davidson and Morgan, 1981; Davidson et al., 1982) has established the existence of lithologically, structurally and metamorphically distinct domains and subdomains (Fig. 13.1, inset). From both structural trends (foliation and layering) and outcrop observations, these authors proposed that the domains and subdomains were juxtaposed by deep crustal thrusting toward the northwest during a major Himalayan-type deformation (Grenvillian Orogeny).

During the 1982 field season, one month was spent on the coast of Georgian Bay, Ontario, studying in detail the structure of the junction between Parry Sound domain, Moon River and Go Home subdomains. Chris Hamblin provided field assistance.

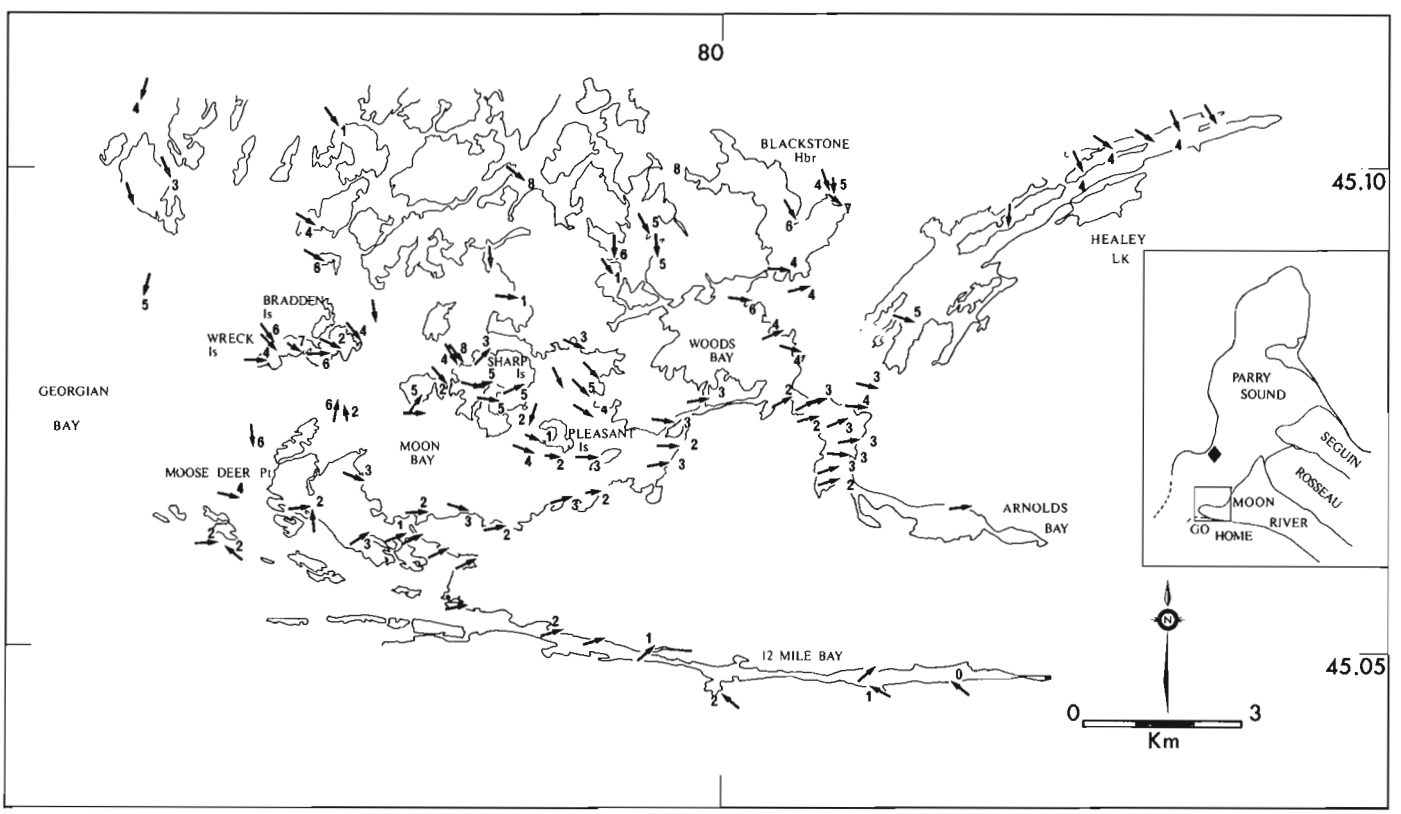

Figure 13.1. *Map of localities and finite extension lineation. Plunges given in 10-degree classes. Inset: outline map of domains subdomains with study area indicated. Diamond is Parry Sound town.*

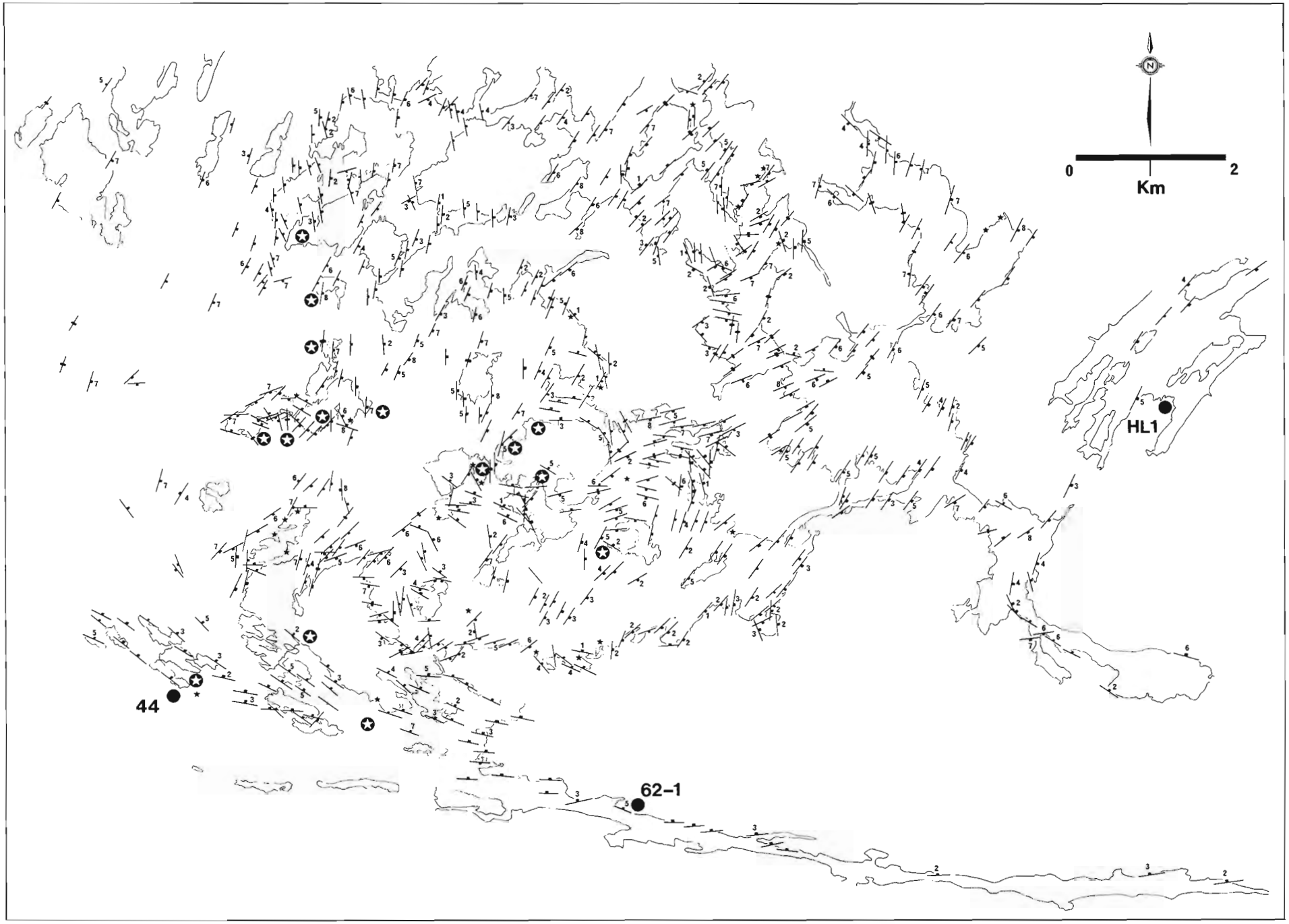

Figure 13.2. *Orientation of foliation and layering. Dips given in 10-degree classes. Small black stars: horizontal foliation. White stars: Hypersthene. Solid dots: quartz petrofabric sample localities.*

To recapitulate the principal lithological and geometrical findings of Davidson et al.: Parry Sound domain contains abundant mafic rocks and widespread granulite facies mineral assemblages; Moon River subdomain is composed of amphibolite facies straight-layered, migmatitic gneisses; Go Home subdomain is composed of orthogeneiss, metasedimentary gneiss (including "meta-arkose") and well layered migmatitic gneiss. Stacking geometry is: Go Home under Parry Sound under Moon River. The geometrical aspects of the Davidson et al. model are supported by recent gravity study in the area (Lindia et al., 1983).

Map scale structure

The penetrative regional foliation and/or tectonic layering has been mapped in some detail (Fig. 13.2) and a foliation trajectory map constructed (Fig. 13.3). The trajectory map shows a natural four-fold division (zones A-D) based upon geometry and degree of strain heterogeneity. The geometrical distinction of zones A, C and D is self evident from comparison of Figures 13.2, 13.3. Zone B, however, is distinguished by its heterogeneity of foliation orientation. The interpreted configuration (Fig. 13.3) is that of an horizon of disc-like pods both under and overlain by the regional foliation (Fig. 13.2). This relationship varies even about a given pod, indicating that the zone B structures are not simple domes and/or basins. The core regions of pods are commonly characterized by (i) crosscutting pegmatite and fine grained granitoid sheets, (ii) open folding of the gneissic structure, with or without associated axial planar foliation, (iii) irregular, thick (several metres) amphibolite layers and non-tabular boudins of the same, visibly derived by flattening of mafic vein networks, and (iv) grain size and textural variations within a given layer. The cores contrast with the more highly strained, predominantly quartzofeldspathic gneisses, in which pre-existing heterogeneities have been transposed into a regular, 10 cm scale continuous gneissic layering, exemplified by the concordant disposition of relict pegmatites, and tabular amphibolite layers and lenses with local development of sheath folds (Quinquis et al., 1978). The transposed gneisses are not finer grained than the core rocks (500-1000 μ) in spite of greater ductile strain.

The four-fold division of the foliation trajectory map is also reflected in the azimuthal distribution of mineral stretching lineations and rodding (Fig. 13.1). Uncertainty concerning the kinematic significance of the stretching lineation at some localities (see below) precludes any blanket interpretation of the lineation pattern. Note, however, that the greatest azimuthal variation coincides with the podded structure of zone B.

Granulite facies mineral assemblages have been identified in zone A, northern zone B and the western part of zone D (Fig. 13.2). In other words, they occur in Parry Sound domain rocks, are absent in Moon River subdomain rocks and occur irregularly in the contact zones (B and D) which delimit the domains and subdomains.

The domainal and zonal subdivision of the area is evident in the magnetic field (Geological Survey of Canada 1953, 1965). Parry Sound domain shows a high magnetic relief in contrast to the flat field of Moon River and Go Home subdomains. Zone B is readily distinguished at the boundary of the two fields as a northeast trending magnetic high (> 2000 gammas; see Fig. 13.3). The magnetic expression of zone D clearly truncates that of Parry Sound domain. Twelve Mile Bay itself is marked by a relatively steep slope in the magnetic field within zone D.

Outcrop scale structure

Outcrop scale structure is complex and highly variable from place to place. The greatest complexity and variability is seen within the pod structures in zone B. Generalized descriptions of the structure now follow for each of the four zones.

Zone A

Lithological homogeneity leads to relatively simple structures. Buff granitoid and amphibolite are flattened to produce a planar banded gneiss (Fig. 13.4A). This layering is usually boudinaged and the boudinage is commonly folded. Boudinage is generally asymmetrical. Where boudin asymmetry changes sense across fold axial planes,

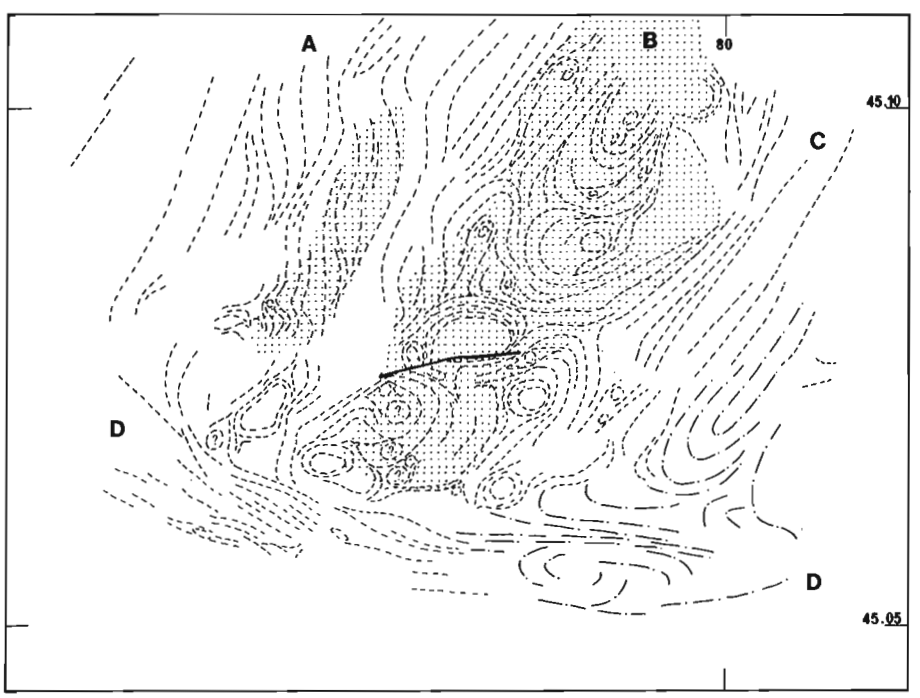

Figure 13.3

Foliation trajectory map. Traces only. Solid line: interpolated fault. Dot-dash line: airphoto interpretation only. Shading: area enclosed by 2000 gamma isomagnetic line. '?': interpolated circular foliation structure under water. A-D: zones discussed in text.

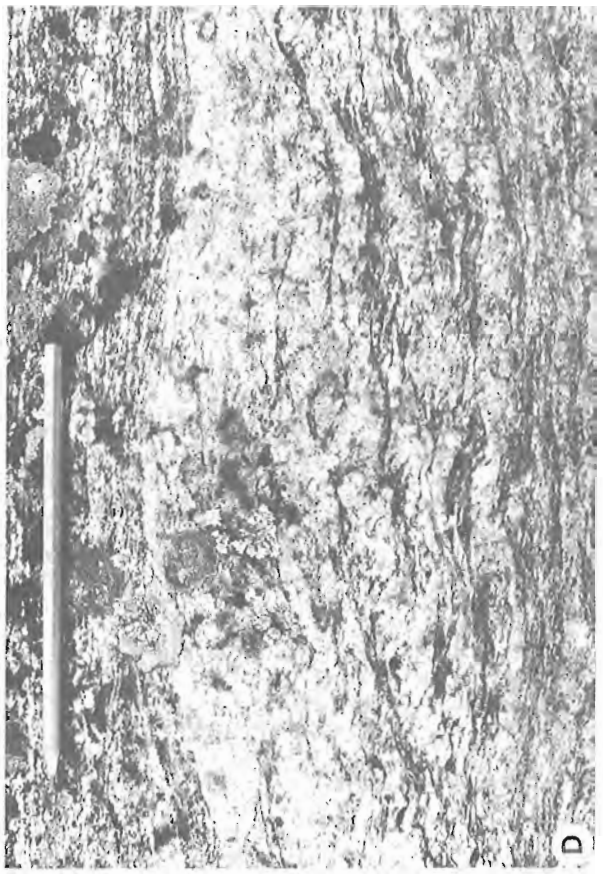
D

E

A

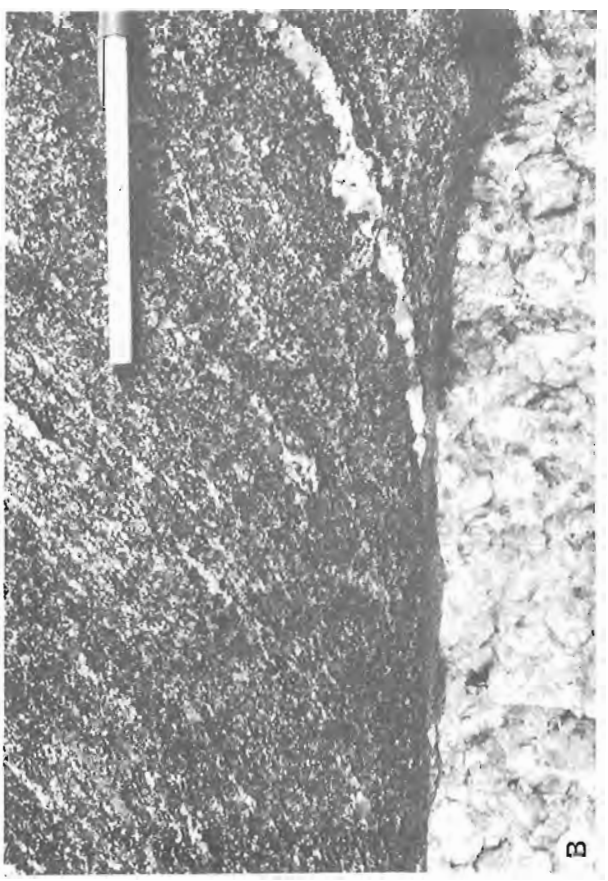
B

Figure 13.4

A – Boudinaged mafic layers in often quartz-poor quartzofeldspathic gneiss. Note possible 'dextral' rotation of one block and general asymmetric shape of boudins. Note also isoclinal fold (centre right). Zone A, east of Frying Pan Island (GSC 203942-R)

B – Amphibole-rich layer at sheared contact between amphibolite and isotropic pegmatite. Note deflection of new internal foliation in amphibolite. Zone B, south Wreck Island (GSC 204085-C)

C – Dextral 'C' (white arrow) and 'S' (black arrow) planes where 'S' is axial planar to minor folds of gneissic banding. Zone A, Bradden Island (GSC 203942-X)

D – Deformed pegmatite in metre-width shear zone. Discrete mylonitic 'C' planes parallel to pencil. Penetrative grain fabric sits clockwise with respect to 'C'. Shear bands slope top right to bottom left. Zone B, south Wreck Island (GSC 204085-D)

E – Rotated winged feldspar within sinistral metre-width shear zone cutting and deflecting pre-existing external layering/foliation. Note very similar grain size of grey homogeneous layers both within and without the shear zone. Zone A, east of Frying Pan Island. (GSC 204085-E)

F – Deformed hornblende-quartz-feldspar pegmatite and relict pegmatite (trains of winged feldspar porphyroclasts) in fine dark mylonite in discrete shear zone. Note sinistral rotation of feldspars (centre left). Zone B, south Wreck Island. (GSC 203942-Y)

Figure 13.5

A – Discrete metric-sized shear zone cuts and deflects earlier external layering of already transposed gneiss. Note lack of grain size reduction within shear zone. Compare apparent dextral offset with sinistral rotation of winged feldspar within shear zone. Zone B, south east Moon Bay. (GSC 203942-Z)

B – 10 m scale pods in mesh structure (see text). Zone B, south Wreck Island. (GSC 203942-W)

C – Interior of pod in mesh structure. Note visible large folds not transposed. Quartzofeldspathic gneiss/amphibolite contacts not straight. Note thick intrusive quartz-feldspar vein in foreground. Zone D, Martin Island, south of Moose Deer Point. (GSC 203942-S)

D – Transposed equivalent of 13.5C in mesh structure. Note flat layering in centre distance as transposed gneisses wrap around a pod. Note mafic pod edge (left foreground). Zone D, Martin Island (GSC 203942-V)

E – Steep dipping sinistral metric-sized shear zone. Extension lineation down dip in deformed pegmatite in shear zone centre. Note ambiguity of fold asymmetry as a kinematic indicator. Zone A, Bradden Island (GSC 203942-T)

F – Fish shaped shear bounded pod dipping to southeast. Highway 69 at Moon River bridge (GSC 203942-N)

the asymmetry may be attributed to local fold mechanics. While folds in outcrop cannot be related simply to major mapping scale structures, some outcrop areas of variable size contain folds that show a constant sense of asymmetry. Fold axes are usually parallel to the stretching lineation, irrespective of fold tightness.

Gneissic structure comprises compositional layering and a variably developed mineral alignment foliation, and locally contains dark mylonitic laminae up to several millimetres thick which anastomose on a fine scale. Similar laminae composed of fine hornblende may line amphibolite – granitoid contacts (Fig. 13.4B). Though rare, composite fabrics with elements identical in geometry and behaviour to 'C' and 'S' planes and shear bands (Berthé et al., 1979a, 1979b; White et al., 1980) are apparent. They show that the penetrative grain alignment foliation is 'S' and the mylonitic laminae comprise 'C' planes and shear bands (Fig. 13.4C, 13.4D).

The main gneissic banding is locally cut by shear zones of the order of one metre wide (Fig. 13.4E). Whereas the orientation of these shears is variable, they invariably show displacements compatible with extension along the main layering. Some shears contain fine- to medium-grained, homogeneous, dark rock. This is mylonite in the sense of Bell and Etheridge (1973). In thin section average grain sizes are 500 μ (feldspar) to 1 mm (hornblende). In some cases it is clear that finer grain sizes (< 100 μ) are preserved in bands where a second phase impedes grain boundary migration in the first phase (e.g. biotite pinning quartz). Many of these shears contain pegmatites and/or relicts of pegmatite (Davidson et al., 1982). Such relicts may now comprise K-feldspar or plagioclase porphyroclasts exhibiting core-and-mantle structure, either isolated or linked by polycrystalline tails in foliation-parallel trains (Fig. 13.4F). Others comprise long lenses of polycrystalline, internally unstrained feldspar derived from coarse single parent grains. In yet other examples the shear zones contain a medium grained, visibly crystalline rock. In some rocks no grain size reduction is detectable across the shear zone boundaries (Fig. 13.4E, 13.5A). The shear zone is therefore distinguished by the deflection, straightening and thinning of gneissic layering across the zone boundaries. Average matrix grain sizes up to 1 mm are common.

Zone B

The structural heterogeneity of this zone may in part reflect the presence of thick layers of competent amphibolite intercalated with the softer quartzofeldspathic rocks. The pod northeast of Moose Deer Point, for example, is cored by a large body of agmatitic to massive amphibolite, as is the western quarter of Wreck Island. Such obvious lithological control does not, however, apply to some other pod structures, e.g. Sharp Island and south-central Moon Bay. Here the ratio of amphibolite to quartzofeldspathic gneisses is not detectably higher in the pod cores than in the enclosing transposed gneisses. Furthermore, the first examples lie outside of the magnetic anomaly underlain by the latter examples. This suggests that the detailed magnetic pattern is not a simple reflection of the proportion of mafic lithologies. In part, the magnetic pattern may reflect low strain state within the pod cores (Wintsch, 1981). The podded structure in either case can be visibly attributed to deformation of the layering, folding and crosscutting veins (commonly of pegmatite), now preserved in the pod cores, into an intervening network of anastomosing high strain zones (Fig. 13.5B). This corresponds to Sibson's (1979) "mesh structure". The mesh size varies from several tens of metres to several kilometres. The transposed gneisses, characterized by regular, straight, continuous layering, are themselves cut by oblique metre-wide shear zones identical to those described for zone A. Locally, the shear zones which contain mylonite are seen to cut across decametric pods of the mesh structure (e.g. southern Wreck Island).

Zone C

Simplicity of structure as in zone A appears to reflect, in part, lithological homogeneity. Gneisses of this zone are mostly banded on a decimetric to centimetric scale. The layering is regular and continuous and is locally seen to result from the progressive transposition of a more coarsely layered, folded gneiss cut by pegmatite. This homogeneity is locally perturbed by large metre-sized boudins of amphibolite or very coarse isotropic pegmatite (e.g. western Arnold's Bay). Long (hundreds of metres), narrow (tens of metres) sheets or lenses of anorthosite with inclusions of metagabbro and metaleucogabbro do not perturb the zone structure (Healey Lake, western Arnold's Bay). Rather, the regularity and continuity of centimetre-sized amphibolite bands in the anorthosite would suggest homogeneous, stable ductile flow. As in zones A and B, this zone is affected by oblique shears whose width is measureable in metres. None of the shears in this zone, however, contain mylonite.

Zone D

The dominant structure in this zone varies from simple and planar in the east to a planar mesh structure in the west. This mesh structure (Figs. 13.5C, 13.5D) coincides spatially with the presence of hypersthene in amphibolite sheets and masses at the mouth of Twelve Mile Bay. Moreover, oblique shears with widths measureable in metres which cut the principal layering and resemble those already described, locally contain mylonite in the western part of the zone (e.g. Martin Island). Coarsely recrystallized,

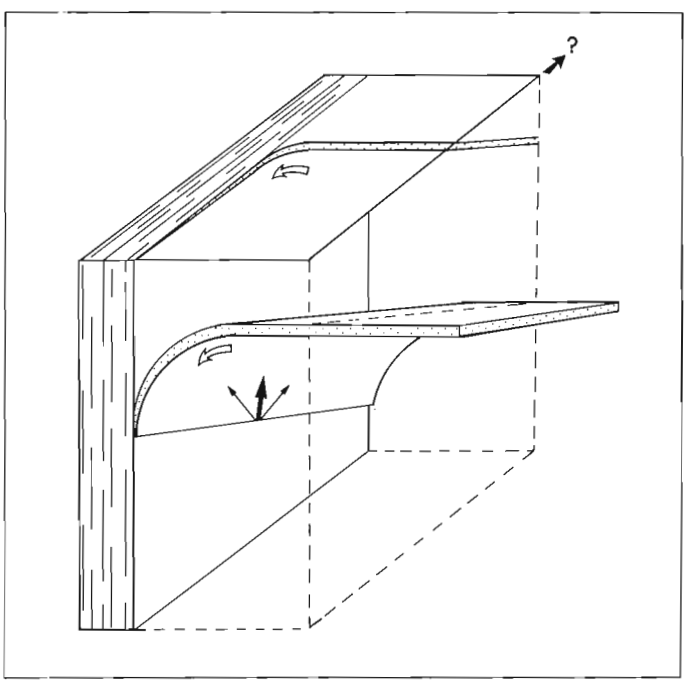

Figure 13.6. *Schematic representation of the relationship between deflection observed, in the horizontal plane, of a pre-existing planar structure, the possible true movement vectors (three possible vectors – arrows – shown for clarity) within the shear zone and the real resolved component of shear in the plane of observation. The latter, indicated by the queried arrow, would be dextral for the left-most true movement vector but sinistral for the other two. See text.*

clean anorthosite occurs along the north shore of eastern Twelve Mile Bay as sheets similar to those in zone C. Their ductile behaviour during deformation apparently contrasts with that of small, angular, misoriented blocks of anorthosite in migmatitic quartz-feldspar-biotite gneiss on the south shore.

Kinematics

The interpretation of structural observations in terms of movement is dependent upon the assumed model boundary conditions. Most studies assume an ideal simple shear model when analyzing non-coaxial strains. This model predicts a simple relationship between the flow direction and the maximum finite extension direction which, at high strains, are subparallel (Ramsay and Graham, 1970). A few studies, however, have demonstrated that other models may pertain to natural flow, e.g. the maximum finite extension direction may be perpendicular (Lister and Price, 1979). These models allow for a major component of pure shear combined with the simple shear strain component (see also Ghosh and Ramberg, 1976). Still other models imply simultaneous operation of two mutually perpendicular simple shear couples (Brun and Burg, 1982).

Apart from the 'C' and 'S' planes, shear bands and deflected layering, three other field structures have been considered by the author as potential kinematic indicators (in this area): oblique, boudinaged pegmatites; winged feldspar porphyroclasts ("sigmoidal feldspars" of Davidson et al., 1982); asymmetric boudinage of concordant amphibolite layers. Asymmetric folding has not been used as a principal kinematic indicated (see Ramsay et al., 1983).

Sense of flow along the layering has been deduced at several scales: at the larger scale of the transposed gneisses of the mesh structure and of the regional layering (Fig. 13.4D) and at the smaller scale of the metre-width oblique shear zones (Fig. 13.4C, 13.4E). Flow sense is given as a resolved component of motion in the horizontal plane unless otherwise stated.

Larger scale

From asymmetric boudinage and oblique pegmatites, the western side of zone A has been affected by sinistral shear, while dextral shear has affected the eastern part. The extension lineations plunge south and southeastward at about 45 degrees on steep foliation planes. Without topographic relief, the relationship of flow direction to lineation is therefore equivocal in the field. In zone B the orientation of foliation and lineation is highly variable. Both sinistral and dextral slip along the layering are deduced from asymmetric boudinage in the transposed gneisses. An example of kinematic complexity is furnished by northwestern Bradden Island (north of Wreck Island) where the following observations in well layered but not transposed gneisses clearly indicate the operation of two mutually perpendicular shear couples. Because of difference in scale of the resulting structures, their time relations cannot be determined.

(i) Foliation dips steeply northwestward; lineation is dip parallel.

(ii) Asymmetric boudinage, rotated amphibolite blocks, planar pegmatitic segregations observed on horizontal surfaces indicate dextral shear perpendicular to the bulk finite extension direction.

(iii) 'C' planes, 'S' planes and shear bands seen on vertical surfaces indicate 'northwest side up' shear along the bulk finite extension direction.

In zone C flow along layering was remarkably homogeneous. Locally heterogeneous flow is evidenced by boudinaged amphibolite and pegmatite (e.g. between Arnold's Bay and Wood's Bay). Here boudinaged oblique pegmatite and winged feldspar porphyroclast relicts from sheared pegmatite indicated sinistral shear along the east plunging lineation. However, these outcrops sit within a major inflection of the regional strike of the Moon River structure and may relate to local boundary conditions. In zone D flow was again very homogeneous in the eastern part. In the mesh structure to the west, however, 'C' planes, 'S' planes and shear bands, rotated winged feldspars and asymmetric boudinage all indicate a dextral sense of slip, along the northeasterly plunging lineation. Note that, locally, two mutually perpendicular lineations are developed, though spatially mutually exclusive (Fig. 13.1). The northwesterly plunging lineation lies parallel to the rotation axis of the non-coaxial deformation.

Smaller scale

Layering in all four zones is deflected and transposed into metre-width oblique shear zones (see above). Except for the special case where the layering intersects the shear zone parallel or perpendicular to the flow direction, the deflection of pre-existing external layering itself does not yield an unequivocal shear direction (D. De Paor and P. Ryan, personal communication). It follows that where the intersection is not normal to the plane of observation, the deflection seen does not yield an unequivocal shear sense. This problem is all the more acute the smaller the angle the line of intersection makes with the plane of observation

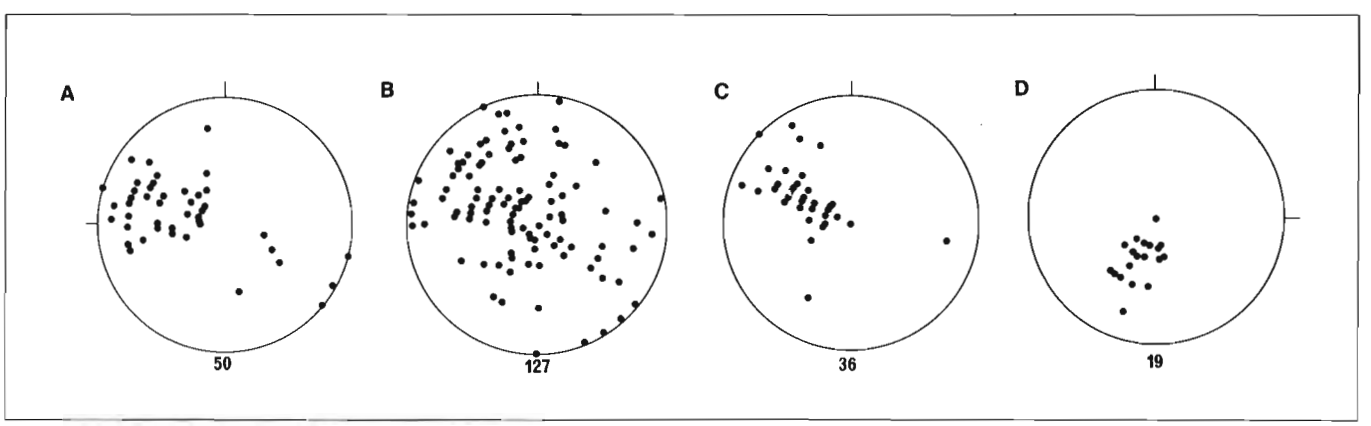

Figure 13.7. *Poles to foliation/layering in Zones A-D. Dips given in 10-degree classes.*

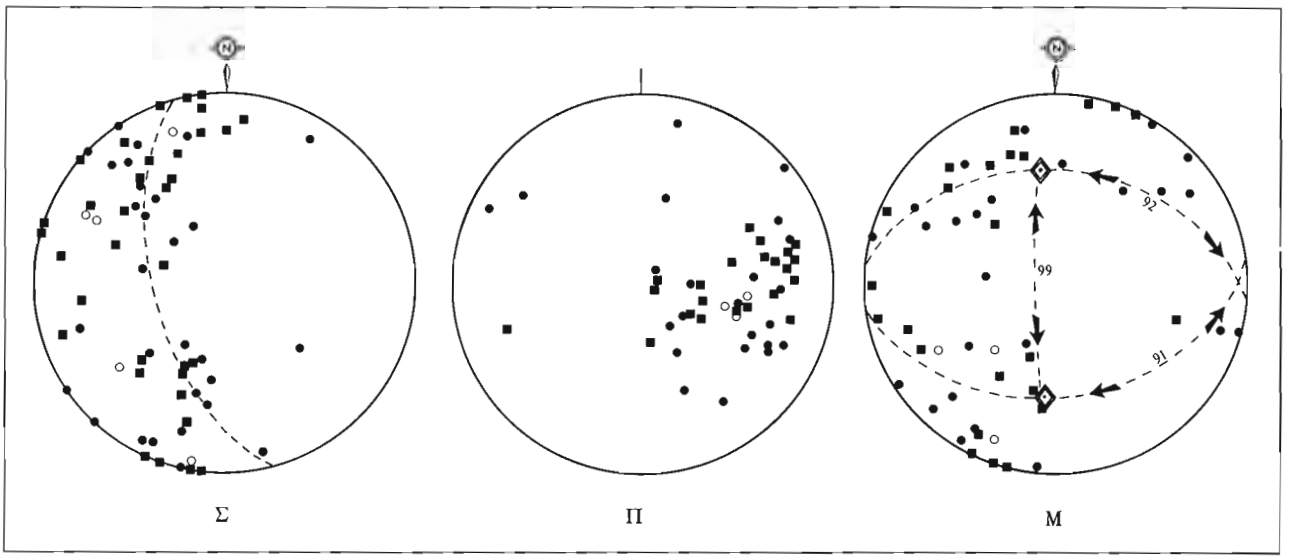

Figure 13.8. *Elements of kinematic analysis of discrete shear zones (Arthaud, 1969). Σ: poles to shear planes. Π: slip directions. M: poles to constructed movement planes (containing Σ and Π) for individual shear zones. Squares: dextral. Dots: sinistral. Circles: uncertain. Intersection of great circles in M: principal finite extension direction (E1). Diamonds: poles to great circles = E2 and E3 (E1 > E2 > E3). Mixed populations in both great circles suggest E2 ≈ E3. The bulk finite strain is therefore of the constrictional type with east-west extension.*

(Fig. 13.6). However, even without independent evidence for the kinematic significance of the stretching lineation, sections through shear zones perpendicular to the extension lineation which show important deflection of external layering must indicate that the deformation within the shear zone deviates significantly from ideal simple shear. This is especially so where the intersection is parallel to the stretching lineation. Such is the case for a number of metre-width shears in all zones (Fig. 13.5E). Mindful of these cautions, it is still possible, where the intersection direction is known and where independent criteria of shear direction and sense (e.g. winged feldspars, shear bands) are available, to determine the kinematics of a given shear zone. Note that those shear zones containing mylonite invariably approximate the ideal simple shear model.

Given the random distribution of layering on a synoptic plot combining all four zones (Fig. 13.7), a kinematic analysis of the population of shears having dimensions measureable in metres was attempted (Arthaud, 1969). At outcrop scale, the individual shears generally dip towards the eastern quadrants (Fig. 13.8) and show a 'normal fault' sense of slip. However, some of the mylonitic shears in zone A and part of zone B show unambiguous 'reverse fault' sense. If the plot of movement planes (Fig. 13.8) has any significance, it suggests that the shears were generated during regional east-west extension and that only minor penetrative strain has occurred since. The paucity of westward dipping shears coupled with the three-dimensional nature of the strain suggest that the shears bound asymmetric model octahedral volumes (Reches, 1978; Reches and Dietrich, 1983), corresponding to the abundant east dipping 'fish', bounded by easterly dipping shears, noted at various scales (e.g. Fig. 13.5F).

Petrofabrics

A pilot universal stage analysis of five specimens has been undertaken to test for the presence of crystallographic preferred orientations. All specimens come from zones C and D. Four are quarzofeldspathic gneisses and one is a quartzite. The fabric patterns (Fig. 13.9) contain consistently oriented elements. One specimen (MB44-2) clearly shows a very close approximation to a type I cross girdle pattern (Lister, 1977). When viewed in the 'Y/Z' plane (Lister and Price, 1978), the leading edge of the girdle is oblique (anticlockwise) with respect to the normal to the principal gneissic layering and suggests the operation of a 'top-side-to-northwest' flow plan oblique to the layering. Berthé et al. (1979b) described a similar fabric girdle obliquity in gneisses affected by shear bands. Accordingly, the fabric pattern would indicate overthrusting to the northwest. The other patterns either show a single girdle or point maxima oblique to the normal to layering. They all show subsidiary elements in the top right and bottom left quadrants. By analogy with MB 44-2, all of the patterns suggest 'top-side-over' to the north along the principal layering, irrespective of whether the layering dips north or south (see, however, Passchier, 1983). Further investigation is required and is being undertaken.

Discussion

Any overall interpretation of kinematic evidence must consider the questions of scale and timing. From regional mapping and geophysical study (Davidson and Morgan, 1981; Davidson et al., 1982; Culshaw et al., 1983; Lindia et al., 1983), it is known that Parry Sound domain has an axial keel, the floor of which is deepest in two places – just northwest of the synformal Moon River and the Seguin subdomains. This geometry is consistent with gravitational sinking of the dense Parry Sound rocks (Lindia et al, 1983). Furthermore, (i) Parry Sound rocks extend under the overlying subdomains yet do not outcrop along their contacts with the Rosseau subdomain (Fig. 13.1). (ii) If the supra-Parry Sound rocks were autochthonous, their synformal geometry should reflect the keel structure of the underlying domain; it does not. (iii) The pattern of flow lines in a sinking slab with two sink maxima will result in a constriction between the maxima (Ramberg, 1981, p. 316), in this case approximately northwest of Rosseau subdomain.

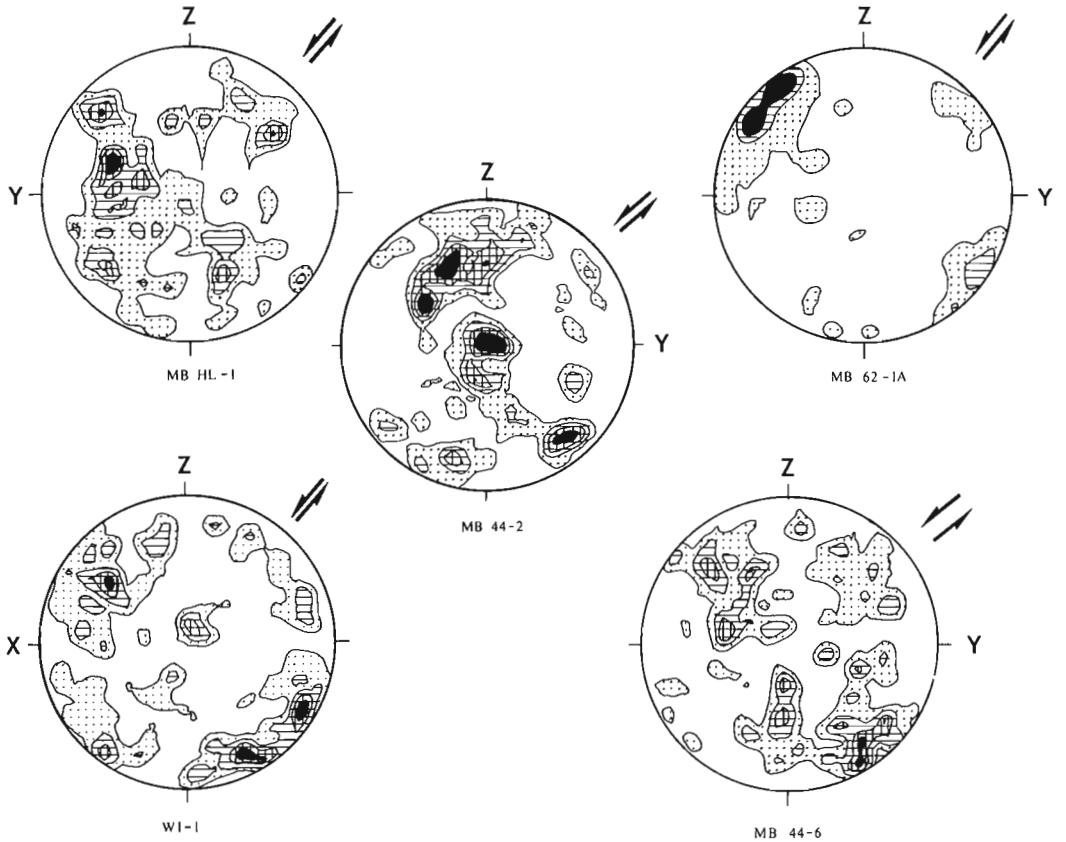

Figure 13.9. *Quartz 'C'-axis crystallographic preferred orientation diagrams. Projections in Y/Z plane exception for WI-1. Discussed in text. Circa 200 points per diagram. Contoured by Starkeys's (1969) method at 1, 2, 3, 4, and 5 points per 0.5% area except 1, 5, and 10 points per 0.5% area in 62-1A.*

The foregoing points suggest that gravitational sinking occurred in Parry Sound domain prior to the emplacement of the overlying rocks. Given the absence of an unconformity and the presence of major zones of intense ductile deformation delimiting the contacts (Davidson et al., 1982), this emplacement must have been tectonic. Kinematic indicators of the type described here occur throughout the Ontario Gneiss Segment and give a regional northwesterly direction of overthrusting (Davidson et al., 1982; Culshaw et al., 1983).

At the more local scale, the magnetic field pattern and the distribution of granulite facies assemblages suggest that Parry Sound rocks are incorporated into the mesh structures of zones B and D and that zone B is the structural boundary between Parry Sound domain and Moon River subdomain. The foliation trajectory map shows that zone D truncates this boundary.

Gneissic layering bounding the zone B pod structures has a statistical southeast regional dip, yet describes concentric map patterns. It follows that layering wraps around the pods which therefore cannot be simple boudin structures. There being no evidence for a tube-like geometry, the structures are therefore enclosed discoids. This implies that the pods have rolled. Rolling pod cores ccommodating an overall regional overthrusting to the northwest would result in 'top-side-down' slip along southeast dipping planes at the pod margins. However, kinematic indicators in zone B do not give an unique sense of slip along the gneissic layering, perhaps implying a major component of pure shear at some stage of the deformation. Zone A structure is compatible with several strain models, e.g. pure shear, folded simple shear, etc. Zone C is not well endowed with kinematic indicators. Zone D is discussed below.

The oblique shears with widths measureable in metres that cut the layering in zones A-C give 'top-side-down' slip on easterly dipping planes. The relationship of small-scale slip to large-scale movement depends upon the behaviour of the shear-bounded volumes. If they actively rotate and so generate the bounding shears, as hypothesized for the pod cores of the zone B mesh zone, then the shears accommodate regional westward overthrusting. However, if the bound volumes simply rotate in response to the activity on the shears then, by analogy with shear band structures, they accomodate regional 'top-side-down' slip to the east.

Observations in zone D are also in apparent kinematic contradiction with the regional overthrusting model. However, the Go Home – Moon River subdomain boundary is more complex than previously thought:

(i) Lineation plunge and sense of shear switch across Twelve Mile Bay (Fig. 13.1 and A. Davidson, personal communication).

(ii) This, combined with the local gradient in the magnetic field, suggests the presence of a discrete discontinuity under Twelve Mile Bay.

(iii) Much of the visible structure in zone D post-dates the juxtaposition of Parry Sound and Moon River rocks across the zone B mesh structure. The observed kinematic indicators are therefore post regional overthrusting.

Zone D is therefore the result of younger movement on the Moon River – Go Home boundary which reactivated the even older Parry Sound – Go Home contact. Outcrops along the

Twelve Mile Bay road and Highway 69 show clear evidence of sinistral movement parallel to a subhorizontal lineation, along the Moon River – Go Home boundary, compatible with northwestward transport of Moon River subdomain (Davidson et al., 1982, Fig. 13.3B). This could pre-date the dextral zone D movement deduced here.

Conclusions

1. Tectonic mesh structures are present at the boundaries between domains and subdomains in the Moon Bay area. The boundaries are therefore shear zones.
2. The internal structure of Parry Sound domain is older than the tectonic emplacement of Moon River subdomain.
3. Part of the deformation in the Go Home/Parry Sound boundary represents a late deflection (reversal ?) of the movement pattern during the ductile aftermath of northwestward overthrusting.
4. Bulk finite extension direction is variable in space and time. Initially oriented north-south in the north and east-west in the south, it changes to east-west during the operation of the discrete shear zones, perhaps in response to down-stream obstruction of the northwestward overthrusting. Latest strain increments resolved by quartz crystallographic fabrics suggest continued late northwestward overthrusting and east-west bulk extension.

References

Arthaud, F.
1969: Méthode de la détermination graphique des directions d'allongement, de raccuorcissement et intermediaire d'une population de failles; Bulletin de la Societé géologique de France, v. 11, 729-737.

Bell, T.H. and Etheridge, M.A.
1973: Microstructures of mylonites and their descriptive terminology; Lithos, v. 6, p. 337-348.

Berthé, D., Choukroune, P., and Jegouzo, P.
1979a: Orthogneiss, mylonite and non-coaxial deformation of granites: the example of the South Armorican shear zone; Journal of Structural Geology, v. 1, p. 31-42.

Berthé, D., Choukroune, P., and Gapais, D.
1979b: Orientations préférentielles du quartz et orthogneissification progressive en régime cisaillant; l'example du cisaillement sud-armoricain; Bulletin de Minéralogie, v. 102, p. 265-272.

Brun, J.P. and Burg, J.P.
1982: Combined thrusting and wrenching in the Ibero-Amorican arc: a corner effect during continental collision; Earth and Planetary Science Letters, v. 61. p. 319-332.

Culshaw, N.G., Davidson, A., and Nadeau, L.
1983: Structural subdivisions of the Grenville Province in the Parry Sound – Algonquin region, Ontario; in Current Research, Part B, Geological Survey of Canada, Paper 83-1B, p. 243-252.

Davidson, A. and Morgan, W.C.
1981: Preliminary notes on the geology east of Georgian Bay, Grenville Structural Province, Ontario; in Current Research, Part A, Geological Survey of Canada, Paper 81-1A, p. 291-298.

Davidson, A., Culshaw, N.G., and Nadeau, L.
1982: A tectono-metamorphic framework for part of the Grenville Province, Parry Sound region, Ontario; in Current Research, Part A, Geological Survey of Canada, Paper 82-1A, p. 175-190.

Geological Survey of Canada
1953: Lake Joseph, Muskoka and Parry Sound Districts, Ontario; Aeromagnetic Map 126G.

1965: Sans Souci, Ontario; Aeromagnetic Map 1495G.

Ghosh, S.K. and Ramberg, H.
1976: Reorientation of inclusions by combination of pure shear and simple shear; Tectonophysics, v. 34, p. 1-70.

Lindia, F.M., Thomas, M.D., and Davidson, A.
1983: Geological significance of Bouguer gravity anomalies in the region of Parry Sound domain, Grenville Province, Ontario; in Current Research, Part B, Geological Survey of Canada, Paper 83-1B, p. 261-266.

Lister, G.S.
1977: Discussion: Crossed girdle C-axis fabrics in quartzites plastically deformed by plane strain and progressive simple shear; Tectonophysics, v. 39, p. 51-54.

Lister, G.S. and Price, G.P.
1978: Fabric development in a quarz-feldspar mylonite; Tectonophysics, v. 49, p. 37-78.

Passchier, C.W.
1983: The reliability of asymmetric C-axis fabrics of quartz to determine sense of vorticity; Tectonophysics, v. 99, T9-T18.

Quinquis, H., Audren, Cl., Brun, J.P., and Cobbold, P.R.
1978: Intense progressive shear in Ile de Groix blueschists and compatibility with subduction or obduction; Nature, v. 273, p. 43-45.

Ramberg, H.
1981: Gravity, deformation and the earth's crust; Academic Press, 2nd edition, 454 p.

Ramsay, J.G. and Graham, R.H.
1970: Strain variation in shear belts; Canadian Journal of Earth Sciences, v. 7, p. 786-813.

Ramsay, J.G., Casey, M., and Kligfield, R
1983: Role of shear in development of the Helvetic fold-thrust belt of Switzerland; Geology, v. 11, p. 439-442.

Reches, A.
1978: Analysis of faulting in a three dimensional strain field; Tectonophysics, v. 47, p. 109-129.

Reches, A. and Dieterich, J.H.
1983: Faulting of rocks in three dimensional strain fields: I. Failure of rocks in polyaxial, servo controlled experiments; Tectonophysics, v. 95, p. 111-132.

Sibson, R.H.
1979: Fault rocks and structure as indicators of shallow earthquake source processes; in United States Geological Survey, Open File Report 70-1239, p. 276-304.

White, S.H., Burrows, S.E., Carreras, J., Shaw, N.D., and Humphreys, F.J.
1980: On mylonites in ductile shear zones; Journal of Structural Geology, v. 2, p. 175-187.

Wintsch, R.P.
1981: Syntectonic oxidation; American Journal of Science, v. 281, p. 1223-1239.

14. A STRUCTURAL RECONNAISSANCE OF THE NORTHWEST BOUNDARY OF THE CENTRAL METASEDIMENTARY BELT, GRENVILLE PROVINCE, ONTARIO AND QUEBEC

Project 830009

S.K. Hanmer and André Ciesielski
Precambrian Geology Division

Hanmer, S.K. and Ciesielski, A., A structural reconnaissance of the northwest boundary of the Central Metasedimentary Belt, Grenville Province, Ontario and Quebec; in Current Research, Part B, Geological Survey of Canada, Paper 84-1B, p. 121-131, 1984.

Abstract

Ductile deformation in the northwestern boundary zone of the Central Metasedimentary Belt is associated with a component of northwestward overthrusting. The overlying marbles represent the matrix to a large scale tectonic mélange. The boundary zone is a distinct tectonic structure in Ontario where high strain non-carbonate gneisses immediately underlie, and interdigitate with, the marble mélange. In Quebec, the boundary is structurally indistinct but lithologically abrupt. This along strike variation in the structure of the boundary zone may reflect the variation in carbonate/silicate gneiss interdigitation and the mechanical importance of the marbles during deformation.

Résumé

Une déformation ductile dans la zone frontière du nord-ouest de la ceinture métasédimentaire Centrale est associée à une composante de chevauchement orientée vers le nord-ouest. Les marbres sus-jacents, représentent la matrice d'un mélange tectonique à grande échelle. Le mélange de marbres de la zone frontière, structure tectonique distincte en Ontario, repose immédiatement sur, s'entrecroise même avec, des gneiss non carbonatés ayant subi de fortes contraintes. Au Québec, la frontière est structurellement indistincte, mais lithologiquement abrupte. Cette variation en direction longitudinale dans la structure de la zone frontière peut refléter la variation dans l'entrecroisement de gneiss carbonatés et de gneiss silicatés et l'importance mécanique des marbres pendant la déformation.

Introduction

Recent work in the Grenville Province in Ontario has resulted in a major advance in concepts of the structural setting of the Ontario Gneiss Segment (Davidson and Morgan, 1981; Davidson et al., 1982; Culshaw et al., 1983). These workers have identified five lithologically, metamorphically and structurally distinct domains whose boundaries are the sites of high strain tectonites. Local details of the deformation in the bounding tectonites can be complex (Hanmer, 1984a). However, the local superposition of higher grade on approximately contemporaneous lower grade metamorphic rocks, in combination with regionally consistent small scale kinematic indicators, allowed Davidson and co-workers to show that the domains were juxtaposed by ductile overthrusting towards the northwest during the Grenville Orogeny.

This new interpretation of the Ontario Gneiss Segment structure highlights the question of the structural context of the Central Metasedimentary Belt (CMB; Wynne-Edwards, 1972) and, more especially, of its northwest boundary zone (Culshaw et al., 1983), henceforth referred to as 'the boundary' (Fig. 14.1). Recently Schwerdtner and Lumbers (1980) and Lumbers (1982) proposed that the base of the CMB in Ontario is marked by a southeast dipping 'Coarse Clastic Sequence' which rests unconformably upon the Ontario Gneiss Segment (see also Appleyard, 1974). An alternative interpretation of the 'Coarse Clastic Sequence' lithologies is that they are tectonites derived by deformation of coarse igneous and metamorphic rocks (Barlow, 1899; Adams and Barlow, 1910; Davidson and Morgan, 1981). The latter authors suggested that the CMB may have been thrust over the Ontario Gneiss Segment.

Our field work in 1983 comprised a structural reconnaissance along the northwest boundary of the CMB in Ontario and Quebec from Minden to Baskatong Reservoir (Fig. 14.1, 14.2). Our observations were made principally on roadside outcrops and all results are to be considered preliminary indications requiring confirmation through systematic mapping. Principal findings are: (1) a regional kinematic pattern of overthrusting to the northwest as suggested by Davidson and Morgan (1981) and Culshaw et al. (1983) characterises the length of the boundary; (2) the northwest margin of the Grenville marbles is a tectonic mélange which has played an important mechanical role in the tectonics of the boundary zone; (3) in Ontario the margin of the marbles is a zone of interdigitation with underlying non-carbonate gneisses; in Quebec the boundary is abrupt. The underlying non-carbonate gneisses in Ontario present a distinct zone of high strain tectonites. While similar tectonites exist in Quebec, they do not constitute a distinct zone.

Tectonites

Davidson and Morgan (1981) and Davidson et al. (1982) have described a suite of silicate (as opposed to carbonate) gneiss types in the Ontario Gneiss Segment which they show to be high strain tectonites. We have observed similar lithologies which we now describe briefly. While we differ slightly in terminology, our understanding of the significance of these gneiss types is essentially that of Davidson and co-workers.

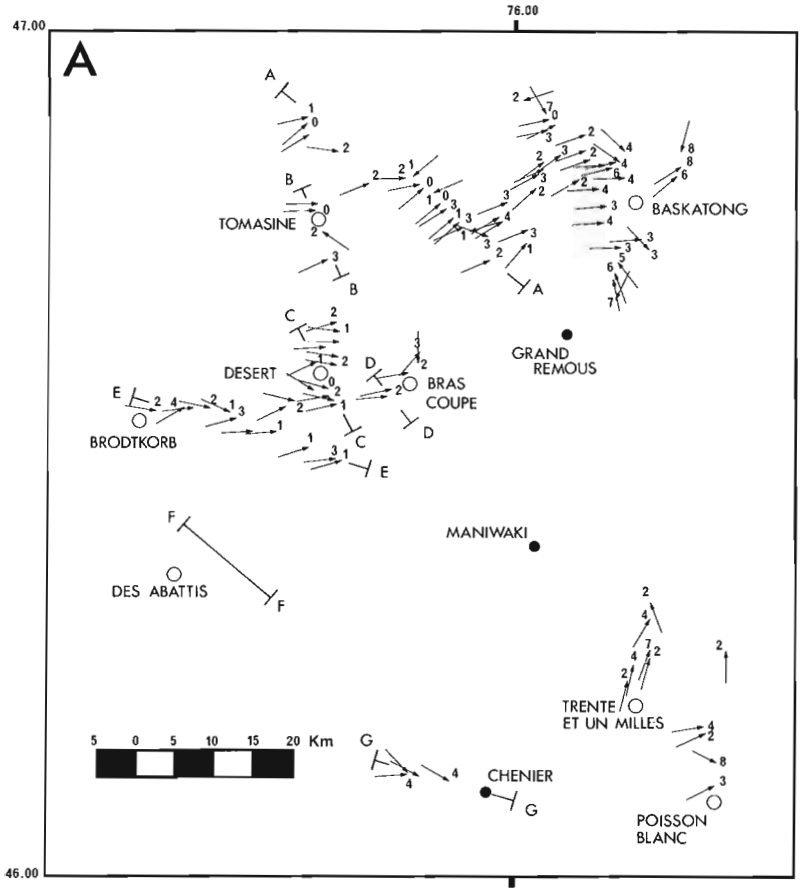

Figure 14.1

A – Recorded finite extension directions/ lineations in the Central Metasedimentary Belt boundary zone, north of the Ottawa Valley in Quebec. Open circles are lakes. Dots are settlements. Positions of cartoon sections in Figure 14.2 are marked.

B – Same description as Figure 14.1A but for an area south of the Ottawa Valley in Ontario. Inset: location map. G – Georgian Bay, Lake Huron; O – Lake Ontario; GFTZ – Grenville Front Tectonic Zone; OGS – Ontario Gneiss Segment; CMB – Central Metasedimentary Belt. Sections of boundary zone pertinent to 1A and 1B are indicated.

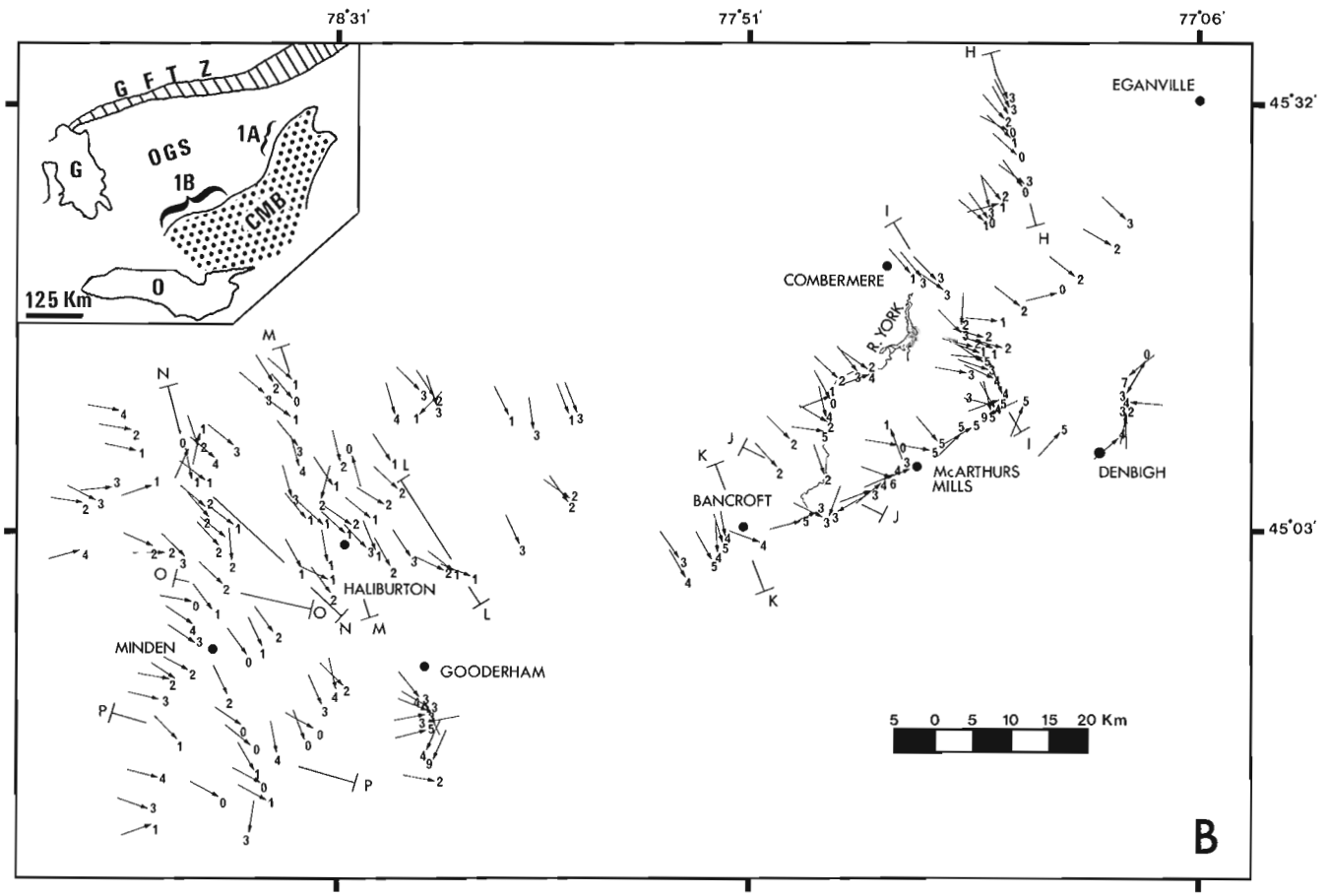

'Transposed gneiss'

This lithology is identical to the layered 'straight gneiss' of Davidson et al. (1982, plate 30.1E). It consists of continuous (tens of metres), parallel sided, centimetre-thick layers of leucocratic granitoid and amphibolite gneiss with layers of more intermediate composition (Fig. 14.3A). Locally these gneisses are seen to result from the transposition and attenuation with strain of (a) granitic or mafic vein networks emplaced into pre-existing background gneisses (Fig. 14.3B); (b) mafic inclusions in granitoid orthogneiss; (c) folded gneissic layering; (d) combinations of a and c. In thin section this gneiss is well recrystallized with few internally strained grains. Grain size is between 500 and 1000 μm.

'Porphyroclastic gneiss'

This lithology is identical to 'tectonoclastic gneiss' of Davidson et al. (1982). It comprises a background gneiss of variable composition (quartzofeldspathic to amphibolitic to aluminous with sillimanite) containing isolated K-feldspar and plagioclase inclusions, feldspar aggregates and streaks aligned in the foliation. The more discrete inclusions are clearly coarse grained quartz-feldspar pegmatite relics. Locally, within a single outcrop, all states of mechanical and mineralogical disaggregation from discrete isotropic pegmatite to isolated feldspar inclusions are seen to be a function of the strain state of the pegmatite (Fig. 14.3C). The isolated feldspars are therefore considered as porphyroclasts. In thin section the gneiss is well recrystallized with a 500 to 1000 μm grain size.

'Straight gneiss'

This useful field term is used to designate a well layered gneiss whose layering, while not as rectilinear as that of transposed gneiss, is nevertheless remarkable for the absence of discordant features typical of nondescript irregular layered gneiss (e.g., cross-cutting veins, fold axial planes oblique to layering). Transposed gneiss is therefore a special case of straight gneiss. Straight gneiss is also distinct from homogeneous poorly layered tonalitic gneiss whose foliation is planar on account of the homogeneity of the deformed material. Typical examples can be seen northwest and southwest of Haliburton where its general character and association suggest that straight gneiss represents an intermediate strain state between irregular layered and transposed gneiss.

'Block gneiss'

This lithology is identical to 'Block Tectonite' of Davidson et al. (1982). It is the result of heterogeneous extension in amphibolite layers in a less competent quartzofeldspathic matrix plus the introduction of pegmatitic material of generally granitic composition.

This classification is to some degree arbitrary in the sense that it only reflects the present aspect of the gneiss. Block gneisses are, at least in part, lithologically controlled. A folded transposed or straight gneiss into which veins are intruded becomes irregular. Therefore, this tectonite classification is not necessarily a simple and direct reflection of accumulated strain. Carbonate tectonites are described below.

Central Metasedimentary Belt Boundary Zone

Ontario

A relatively simple structural geometry is presented by the boundary between Minden and Eganville. Regionally, foliation and layering dip to the southeast at less than 40 degrees (Fig. 14.2). An extension lineation is variably developed in the foliation as a preferred mineral alignment or elongate mineral aggregates (streaks and rods). It is also marked by the bisectors of sheath folds (Quinquis et al., 1978; Cobbold and Quinquis, 1980) and by simple tight to isoclinal fold axes. Extensional structures (shear band foliation of White et al., 1980) intersect the main foliation at approximately 90 degrees to the lineation. These observations serve to demonstrate that the lineation is indeed parallel to the bulk finite extension direction.

The cartoon sections across the boundary zone illustrate the spatial relationships of the various lithologies (Fig. 14.2). Here we will highlight the structure of the marbles which we consider to have been of great mechanical significance during deformation at the CMB boundary. The marbles are generally breccias (Adams and Barlow, 1910) riddled with inclusions of granitoid and paragneiss (Fig. 14.3E). From the cartoon sections: (a) Marble breccia occurs to the south and east. (b) Transposed, porphyroclastic and straight gneisses occur to the north and west. (c) Some spatial overlap or interdigitation occurs between carbonate and silicate high strain tectonites at the southern limit of the latter. We cannot speculate on the existence or nature of a northern limit to the high strain silicate gneisses. (d) Discrete blocks and/or slabs of less strained irregular gneiss, homogeneous tonalitic gneiss, syenite and syenitic gneiss, granite, anorthosite, and sillimanite paragneiss are intercalated with the high strain tectonites and marbles. Some are bound above and below by marble breccia, e.g., the Glamorgan Gneiss between Gull Lake and Birchbark Lake (cartoon P); the Dysart Gneiss about Drag Lake between highways 519 and 121 (cartoons L and M); the anorthosite at Kashagawigamog Lake (cartoon D); the syenitic gneiss north of Bancroft (cartoons J and K); the Raglan Hills-Mallard Lake Gabbro near Hardwood Lake (cartoon I); the Wingle 'Granite' (sic: tonalite) (cartoon I). In all cases, regional foliation in the marble breccia and in the major gneiss inclusions is concordant with major lithological contacts and dips moderately to gently southeast. The general picture is that of slabs of a variety of compositions 'floating' in a marble tectonite. This implies important movement of material within the marble. We now examine some details of the relationship between marble and inclusions.

South of Minden at Miners Bay (Fig. 14.3D), splendid roadcuts expose pink granite intruded into and cross-cutting the gross layering of a coarse chaotic marble breccia. Many chaotically misoriented, dispersed, folded and rolled-up included blocks and slabs are compositionally identical to the intrusive granite. We interpret these observations to indicate synkinematic emplacement, tectonic erosion and incorporation of an igneous mass within an highly ductile, flowing marble tectonite. In other places folded and boudinaged branching granite and syenite veins also appear to represent syntectonic magmatic sheets. Elsewhere, thin slices of foliated granitoid or gneiss are visibly pried off from thicker slabs and incorporated in the breccia. This is ideally illustrated on Highway 62 at York River, north of Bancroft (cartoon K), where a thick slab of pink granitoid is underlain by chaotic marble breccia. The granitoid slab is penetrated along its foliation by several 1 m thick sheets of marble breccia containing small, well rounded, tectonically eroded fragments of wall rock (Fig. 14.3E). One of the marble sheets ends blindly within the outcrop. It is clear that the marble sheet has forcibly intruded into intact unfaulted granitoid.

We interpret the marbles of the CMB boundary zone as the highly ductile matrix to a major tectonic 'mélange' containing inclusions from tens of kilometres in length to centimetre-sized debris. At outcrop scale it is evident that the chaotic or laminar nature of the flow in the mélange is principally a function of inclusion shape, i.e., as long thin

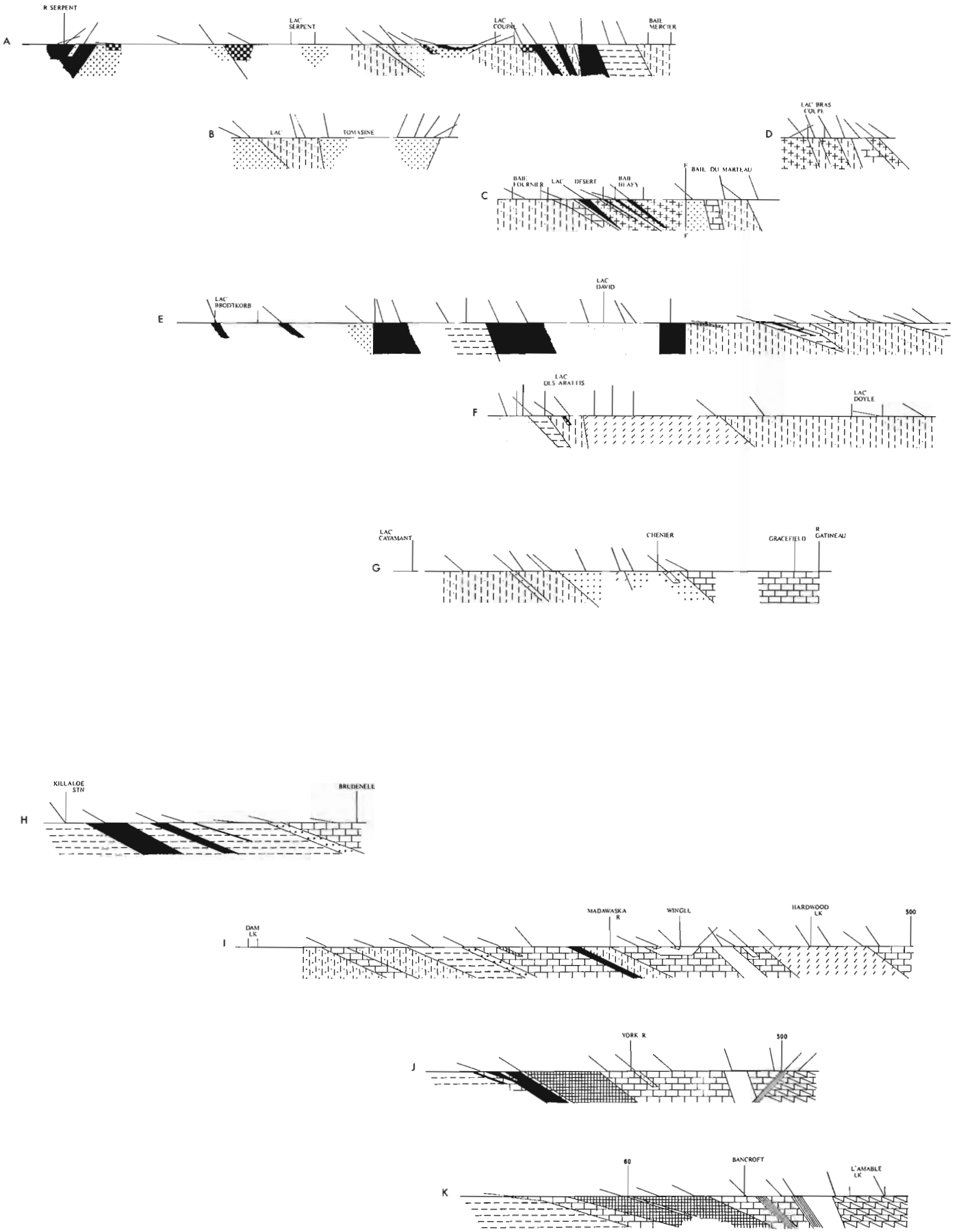
A
R SERPENT
LAC SERPENT
LAC COUPAL
BAIE MERCIER
B
LAC
TOMASINE
C
BAIE FOURNIER
LAC DESERT
BAIE HEAFY
BAIE DU MARTEAU
D
LAC BRAS COUPE
E
LAC BRODTKORB
LAC DAVID
F
LAC DES ABATTIS
LAC DOYLE
G
LAC CAYAMANT
CHENIER
GRACEFIELD
R GATINEAU
H
KILLALOE STN
BRUDENELL
I
DAM LK
MADAWASKA R
WINGLL
HARDWOOD LK
500
J
YORK R
500
K
60
BANCROFT
L'AMABLE LK

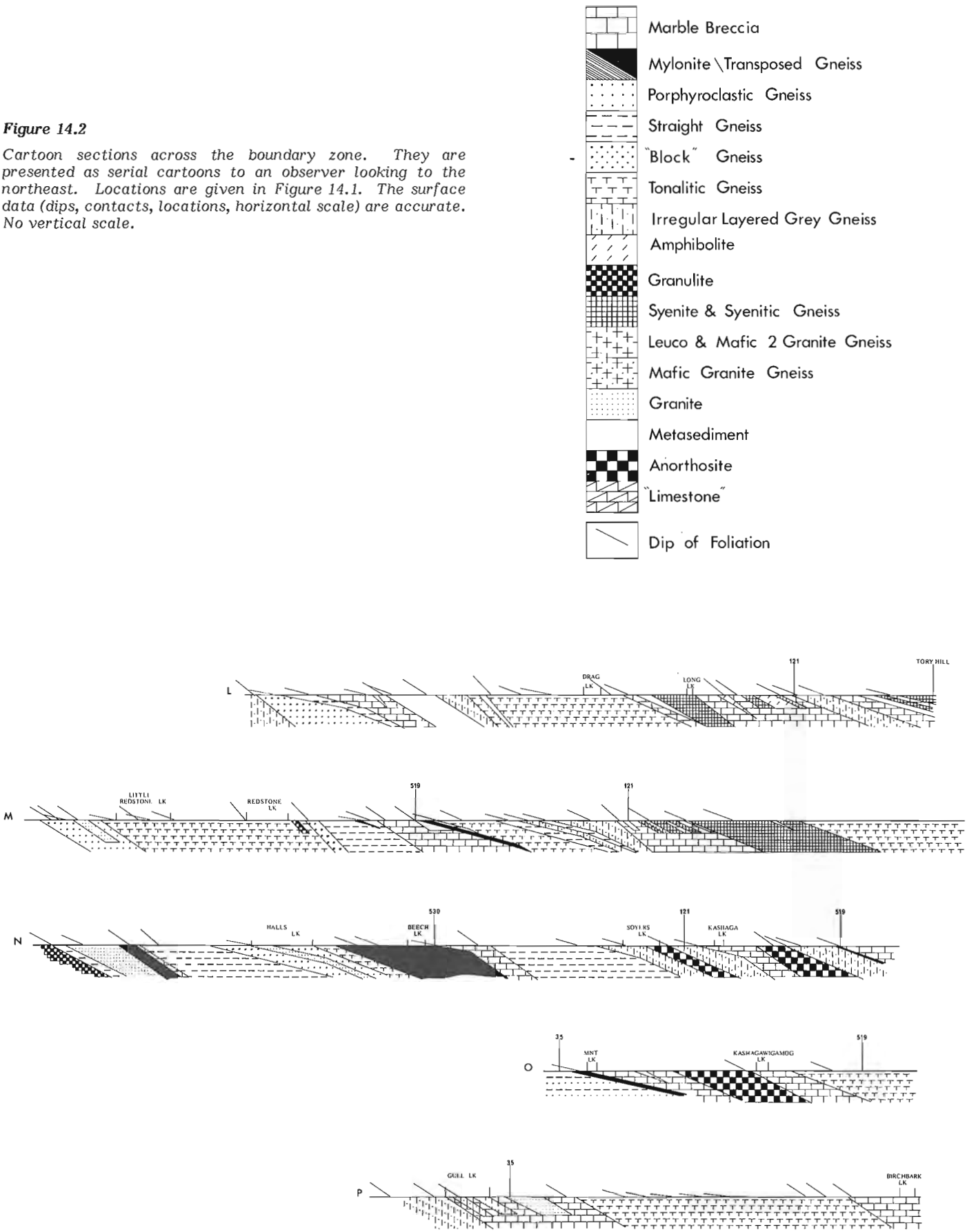

Figure 14.2

Cartoon sections across the boundary zone. They are presented as serial cartoons to an observer looking to the northeast. Locations are given in Figure 14.1. The surface data (dips, contacts, locations, horizontal scale) are accurate. No vertical scale.

Figure 14.3

A – Sub-horizontal transposed gneiss Highway 35, north of Minden (GSC 204128-E)

B – Branching network of granitic veins oblique to, yet transposing into, foliation of amphibolite gneiss. Highway 118, west of Haliburton. Lineation in picture plane. (GSC 204128-F)

C – Porphyroclastic gneiss layer derived by deformation of discrete (see contact) extremely coarse quartz-feldspar pegmatite. East of Chenier. Looking northeast. Lineation in picture plane. (GSC 204128-I)

D – Semi-chaotic marble breccia with inclusions of granitoid. A crude layering dips to left. Highway 35 Miners Bay, south of Minden. Looking south. Lineation in picture plane. (GSC 204128-H)

E – Injected sheet of marble emplaced along foliation of homogeneous granitoid gneiss. Abundant rounded fragments of wall rock in marble. Sheet ends blind to left. Highway 62, north of Bancroft. Looking east. Lineation in picture plane. (GSC 204178-U)

F – Parallel sided sheet of isotropic syenite fractured and rolled up into 'Z' shape. Highway 117, northeast of Grand Remous. Looking southwest. No lineation. (GSC 204128-T)

sheets break up, so the flow passes from laminar to chaotic. If the large scale inclusions are really sheet-like, as implied in the cartoon sections, then large scale flow in the marble mélange was probably laminar.

Analogous discrete kilometre scale inclusions of lower strain gneiss are intercalated with the high strain gneisses underneath and to the northwest of the marble mélange; the principal difference being that the bounding tectonites in this case could, in part, be developed at the expense of the inclusions. In the Haliburton-Minden area, a major slab of homogeneous tonalitic gneiss is bounded above and below by porphyroclastic gneiss in the vicinity of Redstone Lake (cartoon M). This slab appears to attenuate to a thin sliver caught between transposed and porphyroclastic gneiss to the west (cartoon N).

Of particular interest, because of their rare occurrence along the boundary in both Ontario and Quebec, are mylonites which occur (a) along the line through Bancroft-McArthurs Mills, (b) along the York River to the east and north of Bancroft, and (c) southwest of Bancroft towards Paudash. These are petrographically classical mylonites in the sense of Higgins (1971) and also correspond to the definition of Bell and Etheridge (1973). Grain size is in the order of 50 µm. The York River mylonites are mostly carbonate and contain stable clinopyroxene (diopside ?). At outcrop scale they contain abundant distorted inclusions of syenitic gneiss and quartzofeldspathic mylonite. The other mylonites are quartzofeldspathic with neoblasts of biotite. They are locally interlayered with amphibolite schist.

Quebec

The boundary in Quebec is more difficult to define structurally than in Ontario (Fig. 14.1, 14.2). The western limit of the marbles is unequivocal and runs north-south through Chenier to Baskatong Reservoir (Baer et al., 1977). It is bounded to the west, abruptly and without significant interdigitation, by irregular, often migmatitic gneiss. As illustrated in the cartoon sections, high strain gneiss (transposed, porphyroclastic and regular) occurs within the irregular gneiss. In contrast to the Ontario section: (a) foliation and lithological contacts have irregular, often vertical dips; (b) the extension lineation (see Ontario section for criteria) azimuth is extremely variable; (c) the high strain tectonites do not immediately underlie the marbles, nor are they spatially arranged so as to constitue a distinct zone. In brief, while there is a discrete lithological boundary to the CMB, there is no obvious involvement of the underlying rocks in structurally delimiting the CMB in Quebec (however, see cartoon G).

Marbles only occur locally (cartoons C and D) to the west of the western limit of the marble outcrop. The marbles of the marble belt were examined principally along Gatineau River valley and in the roadcuts northwest of Grand Remous. Here they contain decametre-scale slabs and blocks of syenite and other granitoid lithologies and spectacularly show very similar structures to those noted in the marble mélange in Ontario (Fig. 14.3F). A single carbonate mylonitic outcrop occurs south of Grand Remous.

Kinematic indicators

Throughout the boundary zone, 'C and S' fabrics (Berthé et al., 1979a) are of limited importance. Shear band foliations (Berthé et al., 1979b; Platt and Vissers, 1980; White et al., 1980) are more common and occur at the centimetre to metre scale (Figs. 14.4A, B). The asymmetry of minor folds is not considered to be a kinematic indicator (e.g., Hanmer, 1984a). However, very locally the sense of displacement along attenuated lower limbs of recumbent folds in 3D outcrop is significant if observed in near profile sections (De Paor and Ryan, personal communication, 1984; Fig. 14.4C). The most common movement indicators are a variety of rotated objects of variable composition, material properties, shape and initial orientation. We emphasize here that the kinematic significance attributed to a given asymmetric or rotated structure is dependent upon the mechanical model proposed to account for the observed geometry. A detailed discussion of the mechanical models we envisage to account for the kinematic indicators we use is not appropriate here, but is presented elsewhere (Hanmer, 1984b).

'Simple inclusions'

These are sub-equant to mildly elliptical competent inclusions without, or with only minor, tail-like appendages. The example of garnet with 'dragged' plagioclase pressure shadows observed in a plane perpendicular to foliation and parallel to lineation is kinematically self evident (Fig. 14.4D). Similarly the 'rolled-up' parallel sided syenite sheet (vein ?) in marble mélange (Fig. 14.3F). However, the rolled amphibolite block with its stubby appendages set in quartzo-feldspathic gneiss (Fig. 14.4F) is deceptively simple and highlights a complicating factor in the structural geology of the boundary in Quebec. Although the block has clearly rotated clockwise, the axis of rotation is parallel to the bulk finite extension direction of the deformation (Fig. 14.4E). This implies that a 'rolling dough' strain model (Lister and Price, 1978) is more applicable here than an approximation to ideal simple shear (Ramsay and Graham, 1970). The point to retain here is that the onus is on the observer to justify (a) interpreting the field lineation as the finite extension direction and (b) any assumption of a special relationship between the field lineation and the direction of tectonic flow, e.g., ideal simple shear.

'Planar inclusions'

Coarse, often isotropic (unstrained ?) quartz-feldspar ±biotite pegmatites occur at angles of up to 45 degrees to the layering of the host gneiss. They may occur within pre-existing minor shear zones which have clearly influenced their emplacement. Alternatively they occur independently of any visible fault or shear. With strain the pegmatites develop an initially symmetrical pinch-and-swell structure and rotate to decrease the angle they make with the layering. Although conjugate sets are present, veins dipping to the southeast predominate numerically (Hanmer, 1984b).

Competent winged inclusions of various kinds share a number of geometrical features similar to the 'sigmoidal feldspars' used by Davidson et al. (1982) and Culshaw et al. (1983) as kinematic indicators. Although we do not yet have quantitative statistics, the long axes of a significant proportion of the winged inclusions observed by us and by Davidson and co-workers in high strain tectonites make an angle of 135 degrees with the flow plane (foliation) normal (Hanmer, 1984b, Fig. 14.5). This configuration is not accounted for by the ideal simple shear model (Hanmer, 1984b).

'Surf and turf' and 'foliation fish'

Pull-apart structures are very common. These pull-apart structures are frequently disposed en-echelon in the layering (Hanmer, 1984b). The empirical observations are: (a) 'turfs' (informal name; Hanmer, 1984b, Fig. 14.8) develop from symmetrical blocky boudins by synthetic rotational strains developed in the leading-top and the trailing-bottom corners of the boudins; (b) 'surfs' (informal name; Hanmer, 1984b, Fig. 14.6) develop by the antithetic rotation

A

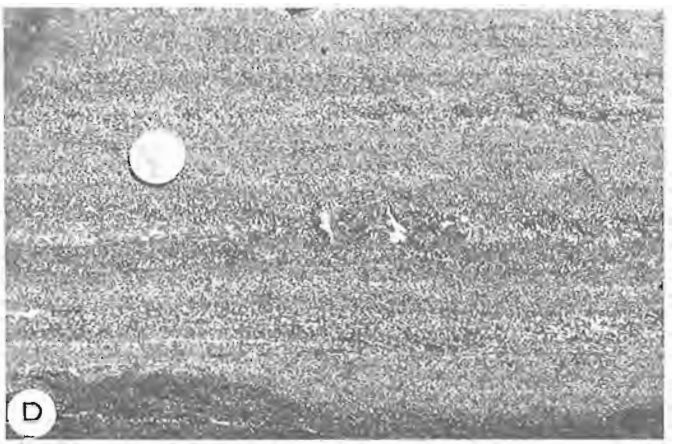
D

B

E

C

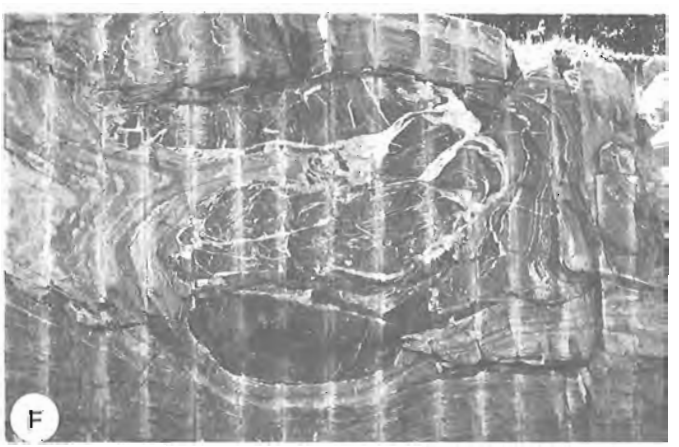
F

Figure 14.5

A – 'Foliation fish.' A distinct elliptical 'packet' defined only by the 10 degree angle its internal foliation makes with the external, very straight foliation. Highway 500, southeast of Combermere. Looking northeast. Lineation in picture plane. (GSC 204128-L)

B – 'Foliation fish.' Elliptical 'packets' of amphibolite-granite gneiss whose internal foliation is systematically 10 degrees oblique with respect to the external layering. Highway 512, west of Eganville. Looking northeast. Lineation in picture plane. (GSC 204128-K)

of initially symmetrical swell structures; (c) 'foliation fish' (informal name; Fig. 14.5A, B; Hanmer, 1984b, Fig. 14.8) are structures related to 'surfs', comprising elliptical packets of antithetically rotated foliation which do not detectably differ in viscosity from the enveloping rocks.

Figure 14.4

A – Sinistral shear band foliation. Highway 500, southwest of McArthurs Mills. Looking down. Lineation in picture plane. (GSC 204128-R)

B – Metre wide shear cutting regional foliation. One of a number of shears constituting an array analogous to large scale shear band structures. Highway 41, north of Denbigh. Looking south. Lineation plunges toward camera. (GSC 204128-P)

C – Narrow mylonite zone (between arrows) cuts of lower limb of recumbent northwest facing fold. Highway 512, west of Eganville. Looking east. Lineation in picture plane. (GSC 204128-N)

D – Rotated garnet in amphibolite. Note sinistral drag of plagioclase pressure shadows. Highway 41, north of Denbigh. Looking down. Lineation in picture plane. (GSC 204128-Q)

E – Sheath fold in buff layer visible to left in F. Looking southwest. Indicates bulk extension direction is southwest-northeast oriented. Highway 117, northeast of Grand Remous. Lineation normal to picture. (GSC 204128-O)

F – Amphibolite block with stubby tails rotated clockwise. Bulk extension direction (see E) is parallel to rotation areas. Highway 117, northeast of Grand Remous. Looking southwest. Lineation normal to picture. (GSC 204128-M)

Large scale movement pattern

Minor structures show a regionally consistent pattern of ductile overthrusting towards the northwest all along the CMB boundary zone. This pattern is seen in the silicate gneisses and in the marble mélange where flow was not too chaotic. We emphasise that the pattern of differential movement is constant and, in Quebec, independent of the local finite extension direction. This movement picture is complicated in Quebec by a component of dextral transcurrent shear along the northeast plunging extension direction, ideally exposed on Baskatong Reservoir. We have seen no evidence to separate the northwest overthrusting (Fig. 14.3F, 14.4F) and the dextral transcurrent components (Hanmer, 1984b, Fig. 14.4F, 14.5A) in time. Theoretically the two components could be contemporaneous (Brun and Burg, 1982); they are mechanically compatible and occur at the northeast end of the CMB. This complex interplay of deformation components, if confirmed, bears a strong resemblance to lateral 'tip strains' described from fold and thrust belts (Coward and Kim, 1981; Coward and Potts, 1983).

An analogous feature of opposite symmetry complicates the movement pattern in Ontario. The corridor of upright northeast striking foliation passing through McArthurs Mills (McArthurs Mills Line or Fault; Hewitt and James, 1955) shows evidence for sinistral transcurrent motion (Fig. 14.4A) along the moderate to steeply northeast plunging extension direction. This represents a downthrow on the southeast side. Given the presence of mylonites, we propose calling this structure the McArthur Mills Shear Zone. Three other structures of north-south trend have components of sinistral transcurrent motion compatible with the regional overthrusting to the northwest: (a) A corridor of upright concordant foliation with a moderately northward plunging extension lineation extending north from Denbigh (Fig. 14.4B, D). (b) The York River marble mylonites to the north and east of Bancroft which underlie the Raglan Hills-Mallard Lake Gabbro to the northeast (cartoons I and J; Hanmer, 1984b, Fig. 14.5). While the strike of mylonite foliation swings from north-south to northeast passing around

the margin of the gabbro, the extension lineation remains southeast plunging (Fig. 14.1B). In the north-south section, the northwest overthrusting seen in the mylonites is, therefore, an oblique slip with a sinistral component. (c) A similar description applies to the major bend in the main CMB boundary north of Haliburton-Minden. The possible significance of these north-south structural zones, and others clearly visible on a recently published map (Lumbers, 1982), in terms of thrust tectonics warrant further detailed investigation.

Finally, we note that locally kinematic indicators clearly show that some of the penetrative ductile deformation is associated with 'top-side-down' movement along southeast dipping planes (e.g., east of Bancroft and northwest of Grand Remous).

Concluding remarks

We have discussed the structure of the CMB boundary zone in terms of a single regional event with local spatial, and perhaps temporal, complications. This is a working hypothesis which we justify, in the absence of geochronological or field data to the contrary, by the coherence of the regional movement pattern. Further, structurally constrained, geochronological work would enable this hypothesis to be tested.

Acknowledgments

We are indebted to Bob Thivierge (Ottawa) and Brian Brock (Carleton) for generously sharing ideas and outcrops in their field areas between Bancroft and Combermere. During the course of the summer we were ably assisted by Carol Coté. This paper was critically read by Tony Davidson.

References

Adams, F.D. and Barlow, A.E.
1910: Geology of the Haliburton and Bancroft Areas: Province of Ontario; Geological Survey of Canada, Memoir 6, 419 p.

Appleyard, E.C.
1974: Basement/cover relationships within the Grenville Province in Eastern Ontario; Canadian Journal of Earth Science, 11, p. 369-379.

Baer, A.J., Poole, W.H., and Sanford, B.V.
1977: Rivière Gatineau, Geological Survey of Canada, Map 1334A.

Barlow, A.E.
1899: The origin of some Archean conglomerates; Ottawa Naturalist, v. 12, p. 205-217.

Bell, T.H. and Etheidge, M.A.
1973: Microstructures of mylonites and their descriptive terminology; Lithos, v. 6, p. 337-348.

Berthé, D., Choukroune, P., and Jegouzo, P.
1979a: Orthogneiss, mylonite and non-coaxial deformation of granites: the example of the South Amorican shear zone; Journal of Structural Geology, v. 1, p. 31-42.

Berthé, D., Choukroune, P., and Gapais, D.
1979b: Orientations préférentielles du quartz et orthogneissification progressive en régime cisaillant, example du cisaillement sud-armoricain; Bulletin de Minéralogie, v. 102, p. 265-272.

Brun, J.P. and Burg, J.P.
1982: Combine thrusting and wrenching in the Ibero-Amorican arc: a corner effect during continental collision; Earth and Planetary Science Letters, v. 61, p. 319-332.

Cobbold, P.R. and Quinquis, H.
1980: Development of sheath folds in the shear regimes; Journal of Structural Geology, v. 2, p. 119-126.

Coward, M.P. and Kim, J.H.
1981: Strain within thrust sheets; Geological Society of London, Special Publication, v. 9, p. 275-292.

Coward, M.P. and Potts, G.J.
1983: Complex strain patterns developed at the frontal and lateral tips to shear zones and thrust zones; Journal of Structural Geology, v. 5, p. 383-400.

Culshaw, N.G., Davidson, A., and Nadeau, L.
1983: Structural subdivisions of the Grenville Province in the Parry Sound – Algonquin region, Ontario; in Current Research, Part B, Geological Survey of Canada, Paper 83-1B, p. 243-252.

Davidson, A.
1984: Identification of ductile shear zones in the southwestern Grenville Province of the Canadian Sheild; in Precambrian Tectonics Illustrated, ed., A. Kröner and E. Greiling; Schweitzerbart, Stuttgart, v. 17.

Davidson A., Culshaw, N.G., and Nadeau, L.
1982: A tectono-metamorphic framework for part of the Grenville Province, Parry Sound region, Ontairo; in Current Research, Part A, Geological Survey of Canada, Paper 82-1A, p. 175-190.

Davidson, A. and Morgan, W.C.
1981: Preliminary notes on the geology east of Georgian Bay, Grenville Structural Province, Ontario; in Current Research, Part A, Geological Survey of Canada, Paper 81-1A, p. 291-298.

Fischer, M.W. and Coward, M.P.
1982: Strains and folds within thrust sheets: an analysis of the Heilan Sheet, N.W. Scotland.

Hanmer, S.
1984a: Structure of the junction of three tectonic slices: Ontario Gneiss Segment, Grenville Province; in Current Research, Part B, Geological Survey of Canada, Paper 84-1B, report 13.

Hanmer, S.
1984b: The potential use of planar and elliptical inclusions as indicators of strain regime and kinematics of tectonic flow; in Current Research, Part B, Geological Survey of Canada, Paper 84-1B, report 15.

Hewitt, D.F. and James, W.
1955: Geology of Dungannon and Mayo Townships; Ontario Department of Mines, Annual Report, 65 p.

Higgins, M.W.
1971: Cataclastic Rocks; United States Geological Survey, Professional Paper, 687, 971 p.

Lister, G.S. and Price, G.P.
1978: Fabric development in a quartz-feldspar mylonite; Tectonophysics, v. 49, p. 37-78.

Lumbers, S.B.
1982: Summary of metallgeny, Renfrew county area; Ontario Geological Survey Report 212, 58 p.

Platt, J.P. and Vissers, R.L.M.
1980: Extensional structures in anisotropic rocks; Journal of Structural Geology, v. 2, p. 397-410.

Quinquis, H., Audren, Cl., Brun, J.P., and Cobbold, P.R.
1978: Intense progressive shear in Ile de Groix blueschists and compatibility with subduction or obduction; Nature, v. 273, p. 43-45.

Ramsay, J.G.
1979: Shear zones; in United States Geological Survey, Open File Report 79-1239, p. 2-35.

Ramsay, J.G. and Graham, R.H.
1970: Strain variation in shear belts; Canadian Journal of Earth Sciences, v. 7, p. 786-813.

Schwerdtner, W.M. and Lumbers, S.B.
1980: Major diapiric structures in the Superior and Grenville Provinces of the Canadian Shield; Geological Association of Canada, Special Paper 20, p. 149-180.

White, S.H., Burrows, S.E., Carreras, J., Shaw, N.D., and Humphreys, F.J.
1980: On mylonites in ductile shear zones; Journal of Structural Geology, v. 2, p. 175-187.

Wynne-Edwards, H.R.
1972: The Grenville Province; Geological Association of Canada, Special Paper 11, p. 263-334.

15.

THE POTENTIAL USE OF PLANAR AND ELLIPTICAL STRUCTURES AS INDICATORS OF STRAIN REGIME AND KINEMATICS OF TECTONIC FLOW

Project 830009

S.K. Hanmer
Precambrian Geology Division

Hanmer, S.K., The potential use of planar and elliptical structures as indicators of strain regime and kinematics of tectonic flow; in Current Research, Part B, Geological Survey of Canada, Paper 84-1B, p. 133-142, 1984.

Abstract

Heterogeneous, generally planar competent inclusions and elliptical competent inclusions with long, thin appendages (wings) commonly occur in highly strained, medium to high grade gneisses. They have been utilized as kinematic indicators of tectonic flow, although no comprehensive mechanical model has been formulated to account for their geometry. A mechanical model is proposed wherein the rotational behavior of the inclusions is a function of shape, orientation, viscosity and strain regime (strain rate ratio). An empirical analogy between certain asymmetrical pull-apart structures and experimental laboratory modelling of bulk simple shear deformation is described.

Résumé

Des gneiss très déformés à degré de métamorphisme moyen ou fort renferment couramment des inclusions compétentes généralement planes et des inclusions compétentes élliptiques, toutes deux de nature hétérogène et comportant de fins appendices allongés (ailes). Ils ont servi d'indicateurs cinématiques de l'écoulement structural, malgré l'absence d'un modèle mécanique détaillé rendant compte de leur géométrie. On propose ici un modèle mécanique dans lequel la rotation des inclusions dépend de la forme, de l'orientation, de la viscosité et du régime de déformation (rapport de taux de déformation). Les auteurs établissent un rapprochement empirique entre certaines structures boudinées d'aspect asymétrique et un modèle expérimental d'une déformation par cisaillement simple.

Introduction

This report addresses the question of the use of asymmetrical, rotated, competent inclusions in a less competent deforming matrix as indicators of strain regime and sense of differential movement. The term 'strain regime' is simply a way of expressing flow characterized by a given 'strain rate ratio' of pure shear strain rate to simple shear strain rate (Sr). In ductile deformation, a kinematic indicator is a structure which indicates the sense of flow of the progressively deforming material, at the scale of observation (e.g. Schwerdtner, 1973; Hanmer, 1982). The kinematic significance attributable to the geometry of a given structure depends entirely upon the mechanical model proposed to account for that geometry. Ghosh and Ramberg (1976) have lucidly shown that the rotational behaviour of competent inclusions is partly dependent upon strain regime. Hence, kinematic interpretation of asymmetrical inclusions is dependent upon an understanding of the strain regime. Most interpretations only consider two idealized strain regimes: ideal pure shear and ideal simple shear (Fig. 15.1). Real strain regimes are probably some intermediate combination of the two, e.g. simple shear with a component of shortening across the shear plane (i.e. a pure shear component).

Recent work in the Grenville Province (Davidson et al., 1982; Davidson, 1984) and discussions with A. Davidson have stimulated my interest in inclusions as kinematic indicators (Hanmer, 1984; Hanmer and Ciesielski, 1984). Davidson and co-workers have used rotated competent winged inclusions ('sigmoidal feldspars') to determine the sense of relative movement in highly strained tectonites deformed during the Grenville Orogeny. In my opinion, a comprehensive mechanical model for the 'sigmoidal feldspars' and several other kinematic indicators currently invoked in the Grenville (Davidson, 1984) has yet to be formulated. I will attempt to show how Ghosh and Ramberg's theoretical analysis may help to formulate such a model. I will also attempt to formulate a plausible model to account for the geometry of extended veins lying oblique to host rock foliation and will propose their potential use as kinematic and/or strain regime indicators. Many of these structures bear a geometrical resemblance to 'retort shaped feldspar augen', recently interpreted as kinematic indicators (Simpson and Schmid, 1983), to which this contribution may be pertinent.

Finally I will very briefly point out the empirical analogy between asymmetrical pull-apart structures during laboratory shearing experiments and natural examples of similar structures. Firstly, however, it is necessary to review some pertinent aspects of deformation theory which can then be applied to the field examples.

Aspects of flow

Strain regime

In any progressive deformation, the finite strain is the accumulation, over a finite period of time, of a series of instantaneous extensions and shortenings. The angular relationship between finite and instantaneous principal strain directions (axes) determines the nature of the strain regime (Fig. 15.1). Simply put, the strain regime describes the kinematic nature of the flow. In ideal pure shear, or flattening, the finite and instantaneous principal strain axes remain mutually parallel (coaxial) throughout the deformation. In ideal simple shear, however, the principal finite strain axes rotate with respect to their instantaneous

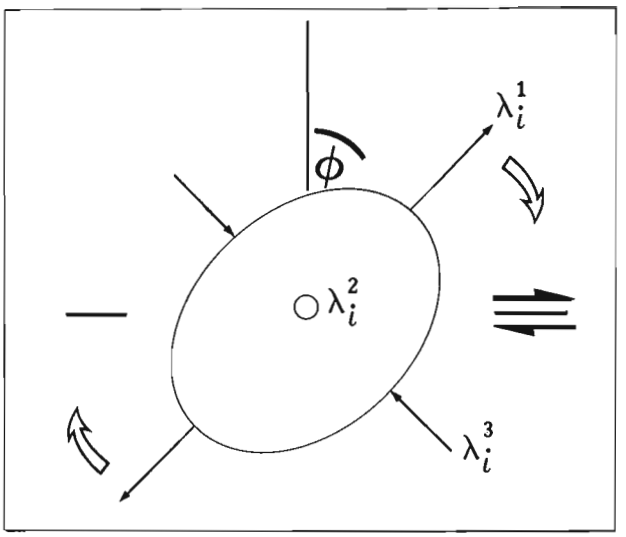

Figure 15.1. *A brief recapitulation of the principal elements of progressive ideal simple shear. The major and minor axes of the instantaneous strain ellipsoid (λ_i^1, λ_i^3) are the instantaneous principal strain or kinematic axes of the deformation. Throughout the deformation they remain fixed at 45 degrees with respect to the shear or flow plane (black arrows). All planes, real and imaginary, within the deforming material rotate (open arrows) with respect to the kinematic axes towards the shear plane. Note that all orientations (ϕ) are with respect to the normal to the shear plane and are measured in the direction of the shear.*

counterparts (Fig. 15.1). The deformation is, therefore, non-coaxial. Ideal simple shear is indeed a simple idealization of flow. Firstly, the deformation is two dimensional; no length change along λ_i^2 is considered (Fig. 15.1). Secondly, no length change occurs either within or perpendicular to the shear plane. Thirdly, the instantaneous principal strain axes (λ_i^1 and λ_i^3) remain fixed at 45 degrees to the shear plane throughout the deformation. Fourthly the deformation is volume constant. The consequence of these four boundary conditions is that the relationship between the rotation rate of the principal finite strain axes with increasing strain can be expressed as a simple mathematical equation. Similar simple expressions apply to the rotation rates of any planes and lines implicated in the deformation (see Ramsay and Graham, 1970; Schwerdtner, 1976; Means, 1976; Means et al., 1980). Using the above terminology, a kinematic indicator is a structure whose asymmetry and/or rotational behaviour during progressive deformation reflects the rotation of the finite principal strain axes with respect to the instantaneous principal strain axes and/or the shear plane.

Natural deformations are likely to deviate from this ideal simple picture (Hanmer and Ciesielski, 1984 and references therein) and a more realistic strain regime would incorporate a component of shortening across the shear plane ('transpression'). Ghosh and Ramberg (1976) have quantitatively examined the rotational behaviour of competent inclusions in a ductile matrix under various 'transpressional' strain regimes (Sr>0). However even their lucid analysis is a simplification in so far as it only considers rigid inclusions in a Newtonian viscous matrix undergoing two-dimensional deformation. The principal result of Ghosh and Ramberg's analysis which I wish to retain here is their prediction that, for a given non-zero strain rate ratio (Sr), a short, stubby inclusion of a critical aspect ratio (shape) will come to rest at a position dictated by the distribution of driving and resisting stresses set up at the matrix/inclusion interface (see below). This rest position and the critical inclusion shape both vary with the strain rate ratio (Sr). This point is illustrated in Figure 15.2 where it may be compared with the rotational behaviour of inclusions undergoing ideal simple shear. In simple shear, only inclusions of high aspect ratio or passive markers come to rest, subparallel to the shear plane (Fig. 15.2A).

From Fig. 15.2A it follows that inclusions of different aspect ratio rotate at different rates. This difference in rotation rate can be used to determine the sense shear, provided that the strain regime is known (Fernandez et al., 1983). For example, in ideal simple shear at orientations in the range $45 < \phi > 90$ degrees, stubby inclusions rotate faster than long, thin ones. A second important result of Ghosh and Ramberg's analysis is that the converse is true for transpressional deformations (Sr >> 0). The point to retain here is that 'sigmoidal feldspars' are composed of stubby central inclusions with long, thin peripheral wings. The relative orientations of these two components of the structure's geometry will depend, in part, on their relative rates of rotation which in turn are partly dependent upon the strain regime of the deformation.

Material properties

Davidson (1984) has used the rotational behaviour of extending veins which are oblique to regional foliation as indicators of the sense of shearing along the foliation. However, Ramsay (1967, p. 108-109) has shown that 'rotated' and 'sigmoid boudinage' may result from extension of veins in a matrix subjected to bulk pure shear. Both interpretations of the extensional behaviour of the respective examples suppose that the orientation of the principal strains in the vein is the same as that in the bulk of the matrix. However, until the vein is either segmented, significantly heterogeneously thinned (pinch-and-swell) or otherwise weakened, it is more competent than the matrix. Most geologists are familiar with cleavage (strain) refraction across competent members in folded multilayers. A similar phenomenon is to be expected in competent veins (see Lister and Williams, 1983). The refraction entails an external rotation of the instantaneous principal strain axes.

A vein lying at approximately 45 degrees to the shear plane in ideal simple shear will show no detectable refraction of the instantaneous principal extension direction since the latter already lies subparallel to the former. However, a vein at very slightly less than 45 degrees to the flattening plane in ideal pure shear (Fig. 15.3, vein A) will refract the instantaneous principal extension direction towards the plane of the vein i.e. the instantaneous extension undergoes 'spin' (Means et al., 1980; Lister and Williams, 1983). The early stages of extension in the pure shear and the simple shear cases outlined will be indistinguishable since the veins will form symmetrical pinch-and-swell structures in either case (Fig. 15.3, vein A). However, with initial deformation under suitable metamorphic conditions, strain rates etc., the rock forming minerals of the vein will begin to recrystallize. Such recrystallization occurs preferentially at grain margins (White, 1976). At 10-20 per cent recrystallization and grain size reduction, a drastic decrease in strength of the vein material will occur (White, 1976; Arzi, 1978). The ensuing decrease in vein competence results in a reversal of the spin of the instantaneous principal extension direction, i.e. an attenuation of strain refraction. Provided this stage is achieved early in the deformation, the further extensional behaviour of the vein will now be strain-regime dependant and will reflect the orientation of the bulk instanteous principal strains: (a) In ideal simple shear the vein will continue to extend approximately symmetrically. (b) In ideal pure shear, the behaviour of the vein will follow the asymmetric pattern of 'sigmoid boudinage'. A similar attenuation of vein strength can occur, even in the absence

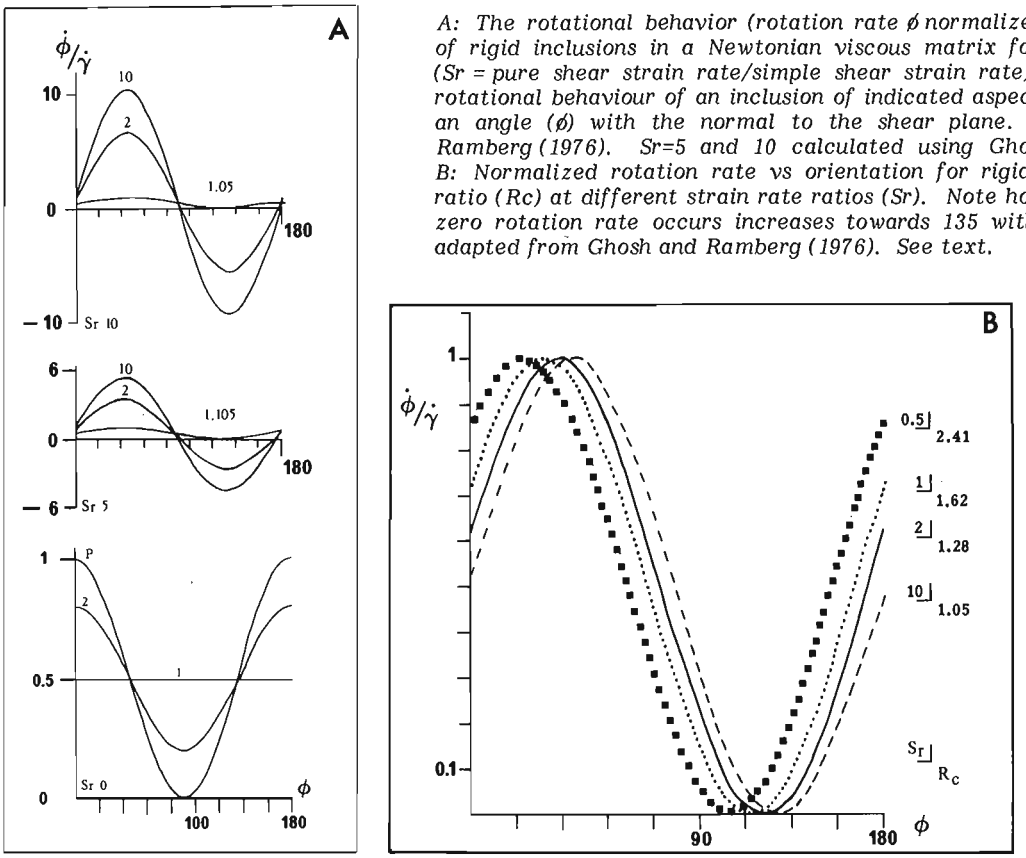

Figure 15.2

A: The rotational behavior (rotation rate ϕ normalized against shear strain rate γ) of rigid inclusions in a Newtonian viscous matrix for different strain rate ratios (Sr = pure shear strain rate/simple shear strain rate). Each curve represents the rotational behaviour of an inclusion of indicated aspect ratio whose long axis makes an angle (ϕ) with the normal to the shear plane. Sr=0 taken from Ghosh and Ramberg (1976). Sr=5 and 10 calculated using Ghosh and Ramberg's equations. B: Normalized rotation rate vs orientation for rigid inclusions of critical aspect ratio (Rc) at different strain rate ratios (Sr). Note how the orientation (ϕ) at which zero rotation rate occurs increases towards 135 with increasing Sr. Both figures adapted from Ghosh and Ramberg (1976). See text.

of significant recrystallization, if the vein boudinages. In ideal simple shear continued extension will be symmetrical whereas in pure shear 'rotated boudinage' will result.

Natural examples

'Oblique veins'

Examples are described principally from amphibolite grade gneisses of the Ontario Gneiss Segment and the northwestern boundary of the Central Metasedimentary Belt (CMB), Grenville Province. Veins of coarse grained, often isotropic quartz-feldspar ±biotite pegmatite and, less commonly, diabase/amphibolite are often observed cutting the host gneiss layering at angles of less than 45 degrees. They may occur within local shears which cut the host rock layering and have clearly influenced the vein emplacement by presenting an exploitable, more or less discrete, plane of weakness. In many other cases there is no visible evidence of a discrete pre-vein oblique structure (Fig. 15.4A). Such oblique veins are so common that their orientation in the unstrained state is unlikely to be due to random chance. The behaviour of such veins during their initial deformation is interesting: (a) The pegmatite veins extend heterogeneously (pinch-and-swell) such that poorly foliated coarse grained 'swells' alternate with thinner, finer, more highly strained tails or 'pinches'. The important point to note is that the extension is initially symmetrical along the plane of the vein (Fig. 15.4B). (b) As the vein extends, the acute angle it makes with the host gneiss layering decreases progressively (Fig. 15.4C). One possible interpretation of these two observations is that the vein in its unstrained state lies close to the approximate orientation of the instantaneous principal

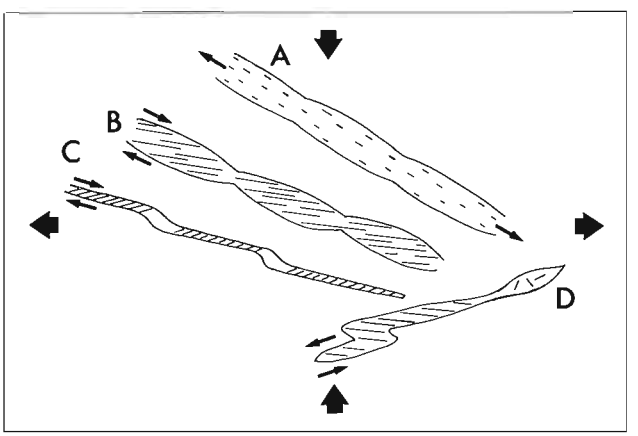

Figure 15.3. *A schematic composite of observed field relationships of moderately deformed, apparently syntectonic, pegmatite veins (from the northwest boundary of the CMB, Grenville Province) reflecting the pure shear component of deformation. A competent intact vein carries a weak, wall-parallel, internal foliation reflecting refraction (spin) of the principal instantaneous extension direction (A). As the vein boudinages and/or its internal deformation (recrystallization) increases, so the competence contrast decreases and strong internal strains reflect more closely the strain pattern in the matrix (B). As shear stresses are resolved along the vein boundaries so non-coaxial strains are manifested as oblique 'S' surfaces (cleavage), rotation of inclusions and asymmetrical folding (C,D). Note that the structures in C and D are conjugate. Arrows represent bulk principal strains.*

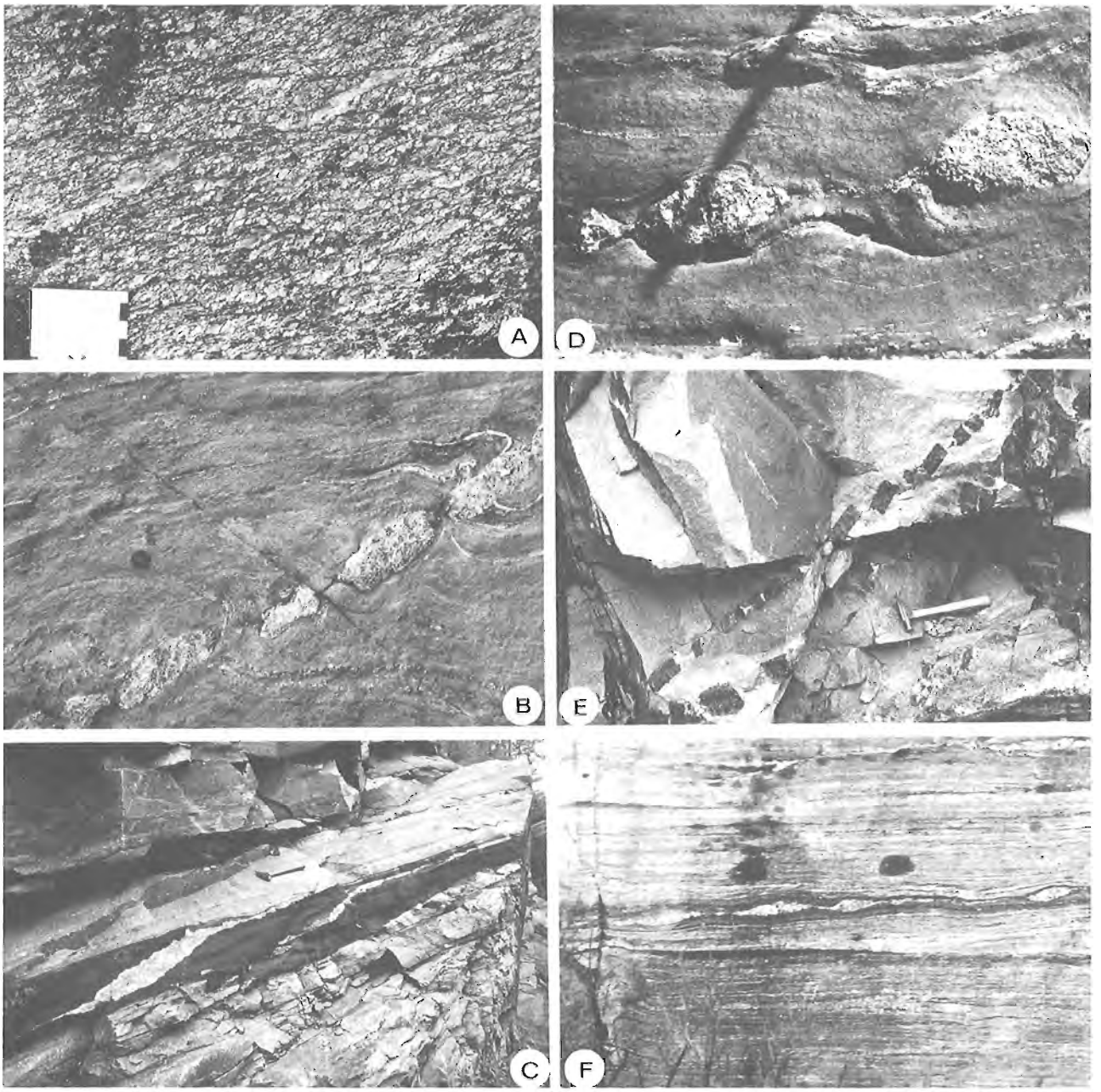

A *Sheared granite in Wopmay Fault Zone, N.W.T. (see King et al., 1983; St-Onge et al., 1984). Discrete 'C' planes dextrally off-set a coarse granite vein which is one member of an array and was emplaced parallel to the penetrative cleavage or 'S' planes. (GSC 204128-D).*

B *Symmetrical boudinage of coarse, near isotropic pegmatite. Host foliation is parallel to the shear plane. Perturbations in adjacent host are related to pegmatite extension. Parry Sound Shear Zone, Grenville Province. Picture reversed. (GSC 204128-J)*

C *Coarse, near isotropic pegmatite lies oblique to layering in competent amphibolite. Towards boundaries with less competent quartz-feldspathic gneiss, pegmatite thins, develops pinch-and-swell structure and rotates towards the layering. Northwest boundary of the CMB, Grenville Province. Picture reversed. (GSC 204105-S)*

D *Pinch-and-swell structure in pegmatite. The long axes of the low aspect ratio 'swells' make an higher angle with the foliation (shear plane) in the host gneiss than does the tail of high aspect ratio between them. Parry Sound Shear Zone, Grenville Province. Picture reversed. (GSC 204105-R).*

E *Blocky boudinage in mafic dyke lying oblique to host layering (parallel to central joint). Long axes of boudins make an higher angle with the layering than does the plane containing the boudin centres. Northwest boundary of CMB, Grenville Province. (GSC 204128-C)*

F *Pinch-and-swell structure in pegmatite in highly strained, very straight gneiss. As D. Northwest boundary of CMB, Grenville Province. (GSC 204128-S)*

Figure 15.4. *All photographs in this contribution are presented as in dextral shear (some are therefore reversed prints) and contain the extension lineation in the plane of the picture.*

flattening plane and that the host gneiss layering is the shear plane of the deformation. The direction of rotation directly indicates the sense of shear. However, this model presupposes that the kinematic framework within the vein is essentially the same as that of the matrix (but see Fig. 15.3).

Now consider the rotational behaviour of the elements of such an heterogeneously extended vein during further deformation. As mentioned above, for non-zero strain rate ratios (Sr > 0) a passive marker starts to rotate faster than its stubby counterpart as the shear plane is approached. Note that Ghosh and Ramberg (1976) showed that for aspect ratios greater than 10, an inclusion behaves much as a passive or non-material marker. This change-over in relative rotational behaviour occurs at progressively smaller angles (ϕ) as the strain rate ratio increases. I have seen evidence for this kind of behaviour in the Parry Sound Shear Zone (Davidson, 1984; Fig. 15.4D) and along the northwest boundary of the Central Metasedimentary Belt (Hanmer and Ciesielski, 1984; also Fig. 15.4E, F). These configurations do resemble 'rotated boudinage' formed under pure shear boundary conditions at this intermediate stage of their development and there is the very real risk of confusion. However, with the definition of a kinematic indicator as given above very much in mind, this intermediate geometry represents only a frozen instant in our model progressive strain history.

With yet further strain, the long thin elements (wings) of the extended vein asymptotically approach parallelism with the shear plane of the deformation (the gneissic layering in the field examples; Fig. 15.5A). In the Grenville examples this occurs while the short stubby inclusions are still markedly oblique with respect to the shear plane. The result is an 'S' or 'Z' shaped configuration depending upon the sense of shear (respectively dextral and sinistral). If flow at the scale of observation is approximately homogeneous, then the wings can not rotate through the shear plane (Fig. 15.2A).

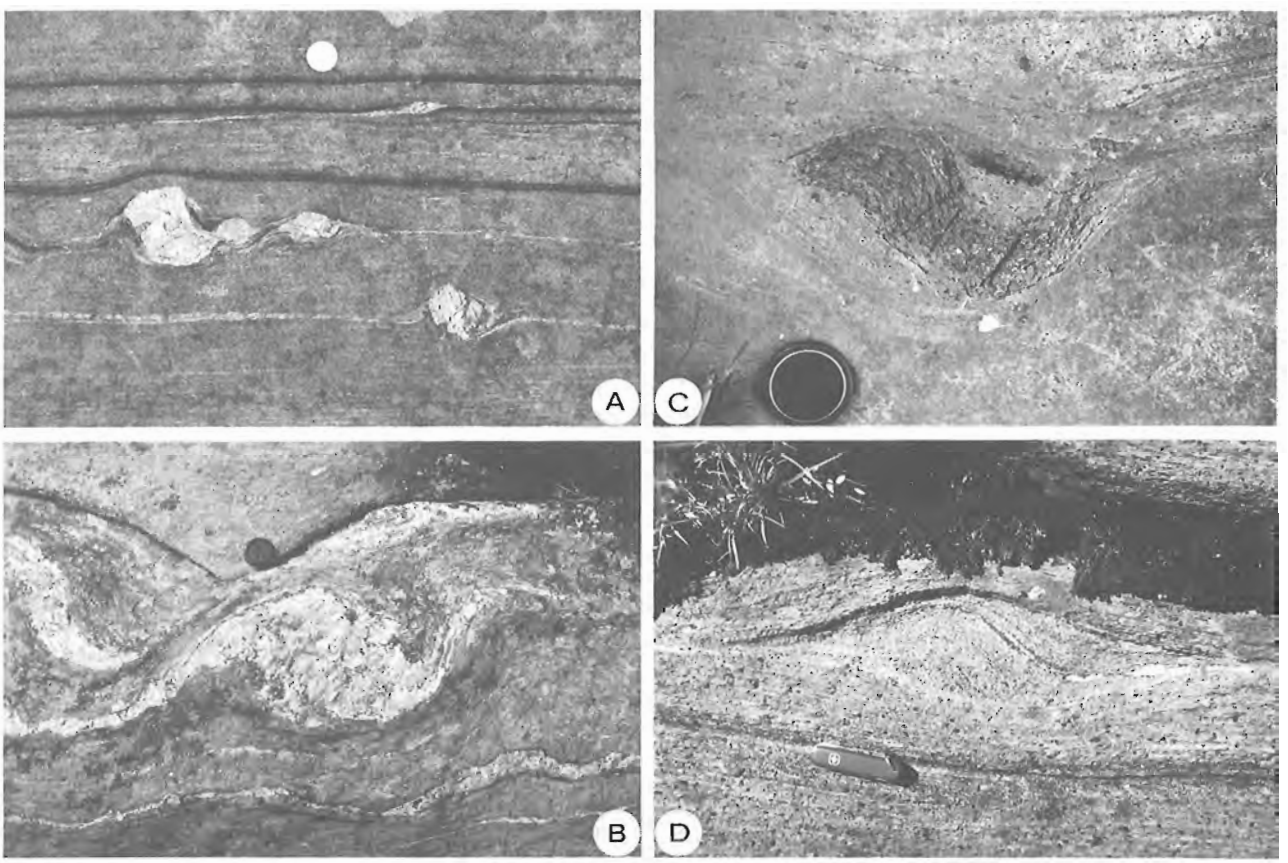

A *'Sigmoidal feldspars' of Davidson et al. (1982). Note long thin wings lie in the foliation (shear plane) while long axes of the stubbier feldspars make an angle of 135 degrees with the foliation. Note also the oblique wings to the feldspar in the upper field, geometrically very similar to 'sigmoidal boudinage' of Ramsay (1967). The long axis of the inclusion makes an higher angle with the foliation than do the wings. I interpret the upper field as an earlier stage in the evolution of the centre and lower fields. Northwest boundary of CMB, Grenville Province. (GSC 204105-Q)*

B *Pinch-and-swell structure in pegmatite. Wings lie in the foliation while the long axis of the swell lies at 135 degrees to the foliation normal. Parry Sound Shear Zone, Grenville Province. Picture reversed. (GSC 204105-U)*

C *Foliated syenite inclusion in marble mylonite. Very short wings. Central part of inclusion at 135 degrees to foliation normal. Northwest boundary of CMB, Grenville Province. Picture reversed. (GSC 204105-W)*

D *Quartzofeldspathic inclusion in quartzofeldspathic gneiss. Very short wings. Central part of inclusion at 135 degrees to main foliation. Shear zone, Ontario Gneiss Segment, Grenville Province. Picture reversed. (GSC 204105-T)*

Figure 15.5. *See Figure 15.4 for orientations. Note knicks in wings close to inclusions.*

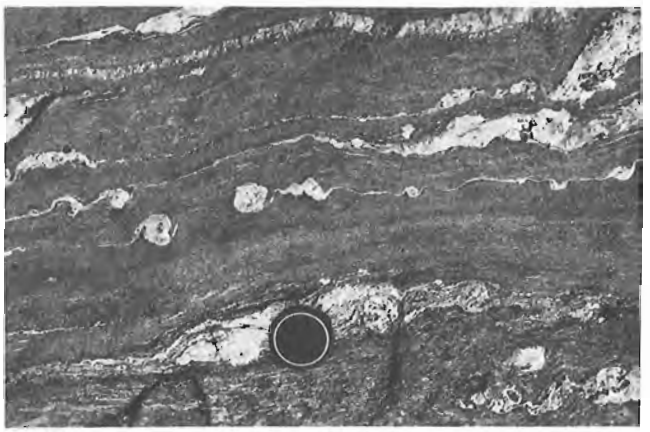

Figure 15.6. *Orientation as for Figure 15.4. Train of 'sigmoidal feldspars' (Davidson et al., 1982). Note angle of approximately 135 degrees made by the long axes of feldspars and/or by the lines joining the points of linkage between feldspars and their wings. Note knicks in wings adjacent to felspars. Grenville Front Tectonic Zone in western Québec. Picture reversed. (GSC 204128)*

The short stubby inclusion, however, continues to rotate. Its long axis approaches transient parallelism with the shear plane, at which stage the 'S' or 'Z' configurations have attenuated to concordant symmetrical planar structures.

'Competent winged inclusions'

At this point I widen the discussion to include all short stubby competent inclusions, of diverse composition and origins, to which long, thin appendages or wings are attached (Fig. 15.5B, C and D; Fig. 15.6). In the case of homogeneous (e.g., no folding) ideal simple shear, the symmetrical configuration will be a common occurrence since the rotation rates for elliptical inclusions subparallel to the shear plane are very slow (zero for long thin markers; Fig. 15.2A). In many places in the Ontario Gneiss Segment of the Grenville Province (Davidson et al., 1982; Hanmer, 1984) along the northwest boundary of the Central Metasedimentary Belt (Hanmer and Ciesielski, 1984) and along the western Grenville Front Tectonic Zone (Wynne-Edwards, 1972), I have examined stubby elliptical competent inclusions which have clearly rotated through the shear plane (defined at the scale of observation; Fig. 15.5, 15.6). Qualitatively by far the majority of inclusions are symmetrically disposed in the shear plane (ϕ=90). However, a significant proportion of inclusions make an angle (ϕ) of about 135 degrees with the shear plane (foliation) normal. Recall that this angle is measured in the direction of the shear sense in the presence of independent kinematic indicators such as 'C and S' planes and shear band foliation (Berthé et al., 1979a, 1979b; Platt and Vissers, 1980; White et al., 1980). A small proportion lie at angles (ϕ) in excess of 135 and even of 180 degrees. These I attribute (rightly or wrongly) to local heterogeneity of flow. It is the group of inclusions at ϕ=135 degrees (Fig. 15.5, 15.6) which I consider to be significant. In order to discuss this latter group of inclusions I must review the pertinent analysis of Ghosh and Ramberg concerning inclusion/matrix interface stresses. Readers who wish to skip the detailed explanation should jump to the last paragraph of the following section.

A zero rotation rate singularity

Ghosh and Ramberg (1976) give a qualitative account of the variation of the position, magnitude and nature of stresses tending to resist the rotation of a rigid inclusion, with respect to some external reference frame. These stresses are those set up at a perfectly cohesive inclusion – matrix interface. In deformations other than pure shear, the external reference frame is the shear plane of the deformation. For pure shear it is the principal flattening plane. Ghosh and Ramberg show that for an inclusion of circular section the resisting stresses, i.e. those acting to impede rotation of the inclusion with respect to its matrix, are shear stresses (Fig. 15.7A, B). For an elliptical inclusion of high aspect ratio, the resisting stresses are essentially the same as for a rectangular slab, i.e., normal stresses perpendicular to the long side of the inclusion (Fig. 15.7C). For an elliptical inclusion of moderate aspect ratio the resisting stresses are both normal and shear stresses. The resisting normal stresses increase with the half-length (distance from the centre of rotation) of the inclusion. An oar in water may be an helpful analogy. Since the resisting moment (a partial function of stress times dimension) is partly dependent on the cube of the length of the inclusion, while the driving moment is partly dependent on the simple width of the inclusion, inclusions of high aspect ratio can not rotate with respect to their adjacent matrix. They therefore behave as passive markers and their stable position in any shearing deformation is approximately in the shear plane.

For an inclusion of circular section the situation is slightly more complex since the position of the maximum resisting stresses is dependent upon the strain regime (Sr; Fig. 15.7A, B). For ease of explanation I arbitrarily choose to refer to a case of dextral shear. In ideal simple shear, the maximum resisting (sinistral) shear stress occurs at a radial angle (ϕ) of 90 degrees (Fig. 15.7A). In pure shear, maximum sinistral shear stress occurs at 135 degrees (Fig. 15.7B). In a general dextral shearing deformation the maximum resisting stresses will occur at some intermediate orientation ($90 < \phi > 135$). However, in any shearing strain, an inclusion of circular section in perfect cohesive contact with its matrix, will rotate indefinitely during deformation at a constant rate (shear strain rate/2; Fig. 15.2A).

It follows that between a circular and an approximately rectangular cross-section of high aspect ratio there is a critical inclusion aspect ratio for which infinite rotation is no longer possible in homogeneous shearing deformation. For ideal simple shear this critical ratio is that at which passive behaviour begins ($\approx$10; Fig. 15.2A). However, for more general strain regimes ($S > 0$) the critical aspect ratio is inversely proportional to the strain rate ratio (Sr; Fig. 15.2A). This means that the distribution of resisting stresses around inclusions of critical shape, under conditions of high strain rate ratio, tends to approximate that for circular sections in pure shear. The overall maximum resistance to rotation occurs when the inclusion is oriented such that the combination of shearing and normal resisting stresses is a maximum. For critical aspect ratio inclusions there is only one such position under any given set of boundary conditions (Fig. 15.2B): hence the title of this section 'zero rotation rate singularity'.

The point to note here is that in homogeneous flow under boundary conditions of significantly high strain rate ratio ($Sr \geq 5$), a mildly elliptical competent inclusion will tend to come to rest with its long axis at approximately 135 degrees to the shear plane normal (Fig. 15.2B). Contrast this with the ideal simple shear model which predicts no rest position (Fig. 15.2A). The small knicks in the wings of the competent inclusions in Figures 15.5 and 15.6 represent a drag effect in the contact strain zones (Ramsay, 1967, p. 416-417) in the adjacent matrix. Indeed, as noted by Davidson et al. (1982), it is their very presence which allows the distinction between the final 'Z' configuration of the 135 degree stage in our dextral shear case and the 'S' geometry of the earlier stages of the same deformation (Fig. 15.5A).

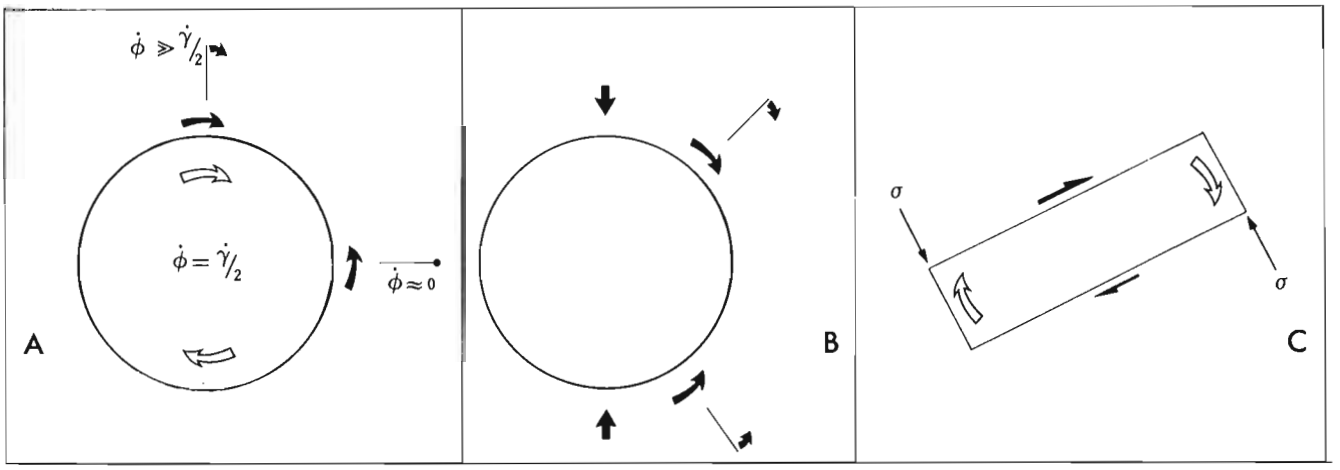

Figure 15.7. Distribution of maximum shearing and normal stresses at the perfectly cohesive contact of rigid inclusions and Newtonian viscous matrix. Short arrows: rotation rate of material lines in matrix dependent upon orientation with respect to horizontal. Long arrows: contact shearing stresses and their polarity generated by the difference in rotation rate between inclusion and matrix. Long straight arrows: normal resisting stresses (σ) generated by rotation of rectangular inclusion. Open arrows: rotation of inclusion. $\dot{\phi}$: rotation rate. $\dot{\gamma}$: shear strain rate. A: Inclusion of circular section in ideal simple shear and B: in ideal pure shear. C: Inclusion of rectangular section in shearing deformation. After Ghosh and Ramberg (1976).

'Surfs and Turfs' and 'Foliation Fish'

In the same gneisses as discussed above, as well as in the excellently exposed mylonites along the Laloche River (Reinhardt, 1969; southeast of Great Slave Lake), I have examined numerous examples of asymmetric pull-apart features, to which I have given informal names in the spirit of Lohest's (1909) culinary precedent. Furthermore, I have successfully simulated the formation of some of them in the laboratory (Fig. 15.8A, B). A full description of the field examples and of the laboratory experiments is in preparation. Only a very brief descriptive résumé is given here. Judging by associated independent kinematic indicators, when they are available, a number of these asymmetrical structures appear to have antithetically rotated to their present orientation, in the opposite sense to that of the bulk shear. These divide into two types: (a) 'Surfs' which are very obviously modified pinch-and-swell structures, some of which still contain a well developed internal foliation, developed in competent layers (Fig. 15.8D) and (b) 'Foliation Fish' (Fig. 15.8E, F) which are elliptical packets, on all scales, whose internal foliation is oblique with respect to the general foliation of the enveloping rocks. There is no necessary competence contrast across the boundaries of 'Foliation Fish'. Because (a) 'Foliation Fish' often contain internal fabrics representing qualitatively estimated high strain magnitudes similar to those of the enveloping rocks and (b) because it is frequently possible to determine the initial orientation of internal layers within both the 'Fish' and the 'Surfs', it is reasonable to suggest that they do not represent low strain pods whose long axis and/or internal foliation has not yet rotated into the bulk shear direction. The alternative explanation is that they have back-rotated during the deformation. Back-rotations of up to about 10 degrees have been recorded in the field (Fig. 15.8).

'Turfs' are derived by the imposition of an asymmetry on initially symmetrical blocky boudins developed in competent layers (Fig. 15.8C). The asymmetry is due to the development of horn-like protuberences in the top-leading and bottom-trailing corner volumes of each boudin. While short stubby boudins are observed to rotate synthetically, the centre portions of longer boudins do not turn.

While no mechanical explanation will be offered here, 'before' and 'after' illustrations of the laboratory experiment are presented for empirical comparison with the natural examples (Fig. 15.8A, B).

Concluding remarks

Natural flow in rocks is an extremely complex process which we are only beginning to comprehend in any real sense. Even Ghosh and Ramberg's analysis is two dimensional and does not allow any internal distortion (strain) within the inclusions. However, it is only through an understanding of the mechanics of progressive flow that geologists can attribute any kinematic significance to deformation structures. Formulation of a comprehensive interpretation of even a single type of structure is rarely simple and involves considering a number of variables, e.g., strain regime, shape, material properties, scale, some of which may vary through the deformation. Note that a valid kinematic indicator is demonstrably, or can be reasonably assumed to be, a frozen frame in a progressive deformation.

Interpreting the kinematic significance of an array of asymmetrical structures is dependent on the scale of the observations compared to that of the complete array. For example, it is well known that shears occur in conjugate sets in response to coaxial deformation (pure shear) and that the two sets may form in mutually exclusive spatial domains (e.g., Hoeppener, 1956; Freund, 1974). Hence the simple presence of an array of asymmetrical shears would not necessarily imply a shearing deformation. The value of an unambiguous kinematic indicator is enhanced by corroboration by another. Kinematic indicators should, therefore, be used as parts of a structural assemblage rather than as individual structures. Ambiguous kinematic indicators have no value whatsoever, whether individually or as part of an assemblage.

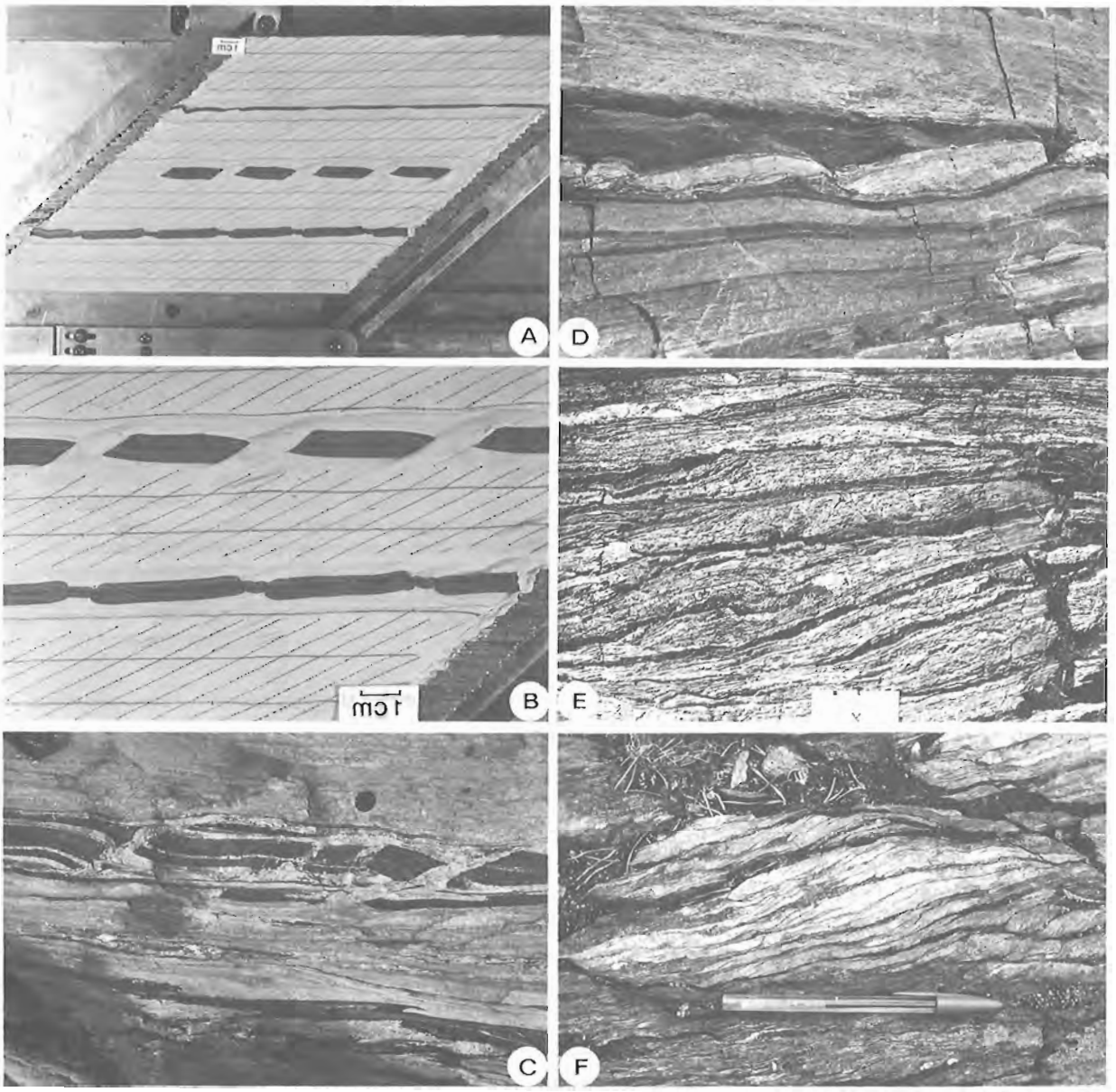

A *Experimental deformation of initially symmetrical plasticine-silicone putty blocky boudins and pinch-and-swell structure in less competent silicone putty matrix. Initially orthogonal passive grid indicates dextral shear strain of 2γ. Initial layers were parallel to the experimental shear plane. Top layer of thin pinch-and-swell behaved as passive marker except for local (initial) perturbation (left). Note inverse senses of asymmetry imposed upon blocky boudins and pinch-and-swell. Latter have clearly rotated antithetically. Picture reversed. (GSC 204105-Y)*

B *Detail of A. Note that internal layering of original blocky boudins has rotated in the top-leading and bottom-trailing corners but not in the centre parts. Picture reversed. (GSC 204128-B)*

C *'Turf' asymmetrical pull-apart structure derived by dextral shearing along amphibolite layer of initially symmetrical blocky boudins. Compare with B. Ontario Gneiss Segment, Grenville Province. Picture reversed. (GSC 204105-Z)*

D *'Surf' asymmetrical pull-apart structure. Detail of antithetically rotated 'swells' in pinch-and-swell structure developed in foliated granitoid layer. Compare with B. Northwest boundary of CMB, Grenville Province. Picture reversed. (GSC 204105-V)*

E *'Foliation Fish'. Mylonite derived from homogeneous granitoid protolith. Main or external foliation direction parallel to scale card (top and bottom). Centre field occupied by packet of mylonite making clear angle with external foliation. Note how internal foliation passes progressively into the external foliation. By comparison and analogy with B, I interpret this configuration as antithetic rotation of the internal foliation during dextral shear. LaLoche Shear Zone, NWT. (GSC 204105-V)*

F *As E except that the internal foliation (centre is a composite dextral fabric (analogous to 'C and S' but developed here in mylonite) passing out to the right into an identical fabric which is itself parallel to the main external mylonite foliation (below pen). From the continuity of individual shear ('C') planes and by analogy with B, I interpret this configuration as for E. Note that the top right corner shows another independent 'Foliation Fish'. LaLoche Shear zone, NWT. (GSC 204105-X)*

Figure 15.8. *See Figure 15.4 for orientations.*

Acknowledgments

I am indebted to Hewitt Bostock, Tony Davidson, Janet King and Marc St-Onge who generously shared with me their time, their field camps, their ideas, and who made it possible for me to visit many of their favourite outcrops which they will find illustrated herein. I am also indebted to John Dixon and John Summers of Queen's University for their generosity, technical advice and use of the experimental facilities in the Structural Geology Laboratory at the University. I thank Rein Tirrul (GSC) and Fried Schwerdtner (University of Toronto) for critically reviewing and improving an earlier draft of this note. This study obviously owes its inspiration to the work of S.K. Ghosh and H. Ramberg (1976). I am nevertheless responsible for all errors of intepretation.

References

Arzi, A.A.
1978: Critical phenomena in the rheology of partially melted rocks; Tectonophysics, v. 44, p. 173-184.

Berthé, D., Choukroune, P., and Jegouzo, P.
1979a: Orthogneiss, mylonite and non-coaxial deformation of granites: The example of South Armorican shear zone; Journal of Structural Geology, v. 1, p. 31-42.

Berthé, D. Choukroune, P., and Gapais, D.
1979b: Orientations préférentielles du quartz et orthogneissification progressive en regime cisaillant; l'exemple du cisaillement sud-armoricain; Bulletin de Minéralogie, v. 102, p. 265-272.

Choukroune, P. and Lagarde, J.L.
1977: Plans de schistosité et deformation rotationelle: L'èxemple du gneiss de Champtoceaux (Massif Armoricain); Compte Rendu de L'Academie des Sciences de Paris, v. 284, p. 2331-2334.

Coward, M.P. and Kim, J.H.
1981: Strain within thrust sheets; Geological Society of London Special Publication, v. 9, p. 275-292.

Coward, M.P. and Potts, G.J.
1983: Complex strain patterns developed at the frontal and lateral tips to shear zones and thrust zones; Journal of Structural Geology, v. 5, p. 383-400.

Davidson, A.
1984: Identification of ductile shear zones in the southwestern Grenville Province of the Canadian Shield; in Precambrian Tectonics Illustrated, A. Kroner and E. Greiling, editors, Schweizerbart, Germany, Stuttgart.

Davidson, A., Culshaw, N.G., and Nadeau, L.
1982: A tectono-metamorphic framework for part of the Grenville Province, Parry Sound region, Ontario; in Current Research, Part A, Geological Survey of Canada, Paper 82-1A, p. 175-190.

Fernandez, A., Feybesse, J.L., and Mezure, J.F.
1983: Theoretical and experimental study of fabrics developed by different shaped markers in two dimensional simple shear; Bulletin de la Societé géoloique de France, v. 25, p. 319-326.

Freund, R.
1974: The kinematics of transform and transcurrent faults; Tectonophysics, v. 21, p. 93-134.

Ghosh, S.K. and Ramberg, H.
1976: Reorientation of inclusons by combination of pure and simple shear; Tectonophysics, v. 34, p. 1-70.

Hanmer, S.
1982: Vein arrays as kinematic indicators in kinked anisotropic materials; Journal of Structural Geology, v. 4, p. 151-160.

1984: Structure of the junction of three crustal slices: Ontario Gneiss Segment, Grenville Province; Geological Survey of Canada, Paper 84-1B, Report 13.

Hanmer, S. and Ciesielski, A.
1984: A structural reconnaissance along the northwest boundary of the Central Metasedimentary Belt, Grenville Province; Geological Survey of Canada, Paper 84-1B, Report 14.

Hoeppener, R.
1956: Zum problem der Bruchbildung, Shieferung and Faltung; Geologisches Rundshau, v. 45, p. 247-283.

King, J.E., St-Onge, M.R., and Lalonde, A.E.
1983: Wopmay Fault Zone – A major mylonite and brittle fault belt, Internal Zone, Wopmay Orogen; Geological Association of Canada, Program with Abstracts, v. 8, A37.

Lohest, M.
1909: De l'origine des veines et des géodes des terranes primaires de Belgique; Societé géologique Belge Annales, v. 36B, p. 275-282.

Lister, G.S. and Price, G.P.
1978: Fabric development in a quartz-feldspar mylonite; Tectonophysics, v. 49, p. 37-78.

Lister, G.S. and Williams, P.F.
1983: The partitioning of deformation in flowing rock masses; Tectonophysics, v. 92, p. 1-33.

Means, W.D.
1976: Stress and Strain: Basic concepts in continuum mechanics for geologists; Springer-Verlag, 339 p.

Means, W.D., Hobbs, B.E., Lister, G.S., and Williams, P.F.
1980: Vorticity and non-coaxiality in progressive deformations; Journal of Structural Geology, v. 2, p. 371-378.

Platt, J.P.
1983: Short Note: Progressive refolding in ductile shear zones; Journal of Structural Geology, v. 5, p. 619-622.

Platt, J.P. and Vissers, R.L.M.
1980: Extensional structures in anisotropic rocks; Journal of Structural Geology, v. 2, p. 397-410.

Ramsay, J.G.
1967: Folding and fracturing of rocks; McGraw-Hill, 568 p.

Ramsay, J.G. and Graham, R.H.
1970: Strain variation in shear belts; Canadian Journal of Earth Sciences, v. 7, 786-813 p.

Reinhardt, E.W.
1969: Geology of the precambrian rocks of Thubin Lakes map area in relationship of the McDonald Fault System, District of Mackenzie; Geological Survey of Canada, Paper 69-21, 29 p.

St-Onge, M.R., King, J.E., and Lalonde, A.E.
1984: Deformation and Metamorphism of the Coronation Supergroup and its basement in the Hepburn Metamorphic – Plutonic Zone of Wopmay Orogen: Redrock Lake and the eastern portion of the Calder River map areas, District of MacKenzie; in Current Research, Geological Survey of Canada, Paper 84-1A, p. 171-180.

Schwerdtner, W.M.
1973: A scale problem in paleo-strain analysis; Tectonophysics, v. 16, p. 47-54.

1976: A problem of nomenclature in paleo-strain analysis; Tectonophysics, v. 30, p. T1-T2.

Simpson, C. and Schmid, S.M.
1984: An evaluation of criteria to deduce the sense of movement in sheared rocks; Geological Society of America Bulletin, v. 94, p. 1281-1288.

White, S.
1976: The effects of strain on the microstructures, fabrics and deformation mechanisms in quartzite; Philosophical Transactions of the Royal Society of London, v. A283, p. 69-86.

White, S.H., Burrows, S.E., Carreras, J., Shaw, N.D., and Humphreys, F.J.
1980: On mylonites in ductile shear zones; Journal of Structural Geology, v. 2, p. 175-187.

Wynne-Edwards, H.R.
1972: The Grenville Province; Geological Association of Canada, Special Paper 11, p. 263-334.

16.

GEOCHEMISTRY OF ARCHEAN GRANITIC ROCKS IN THE PERCHING GULL LAKES AREA, NORTHWESTERN ONTARIO

Project 820006

R.A. Stern[1]
Precambrian Geology Division

Stern, R.A., Geochemistry of Archean granitic rocks in the Perching Gull Lakes area, northwestern Ontario; in Current Research, Part B, Geological Survey of Canada, Paper 84-1B, p. 143-157, 1984.

Abstract

The Perching Gull Lakes area in the western Wawa Subprovince is intruded by two late to posttectonic granitic plutons. The older is the crescent-shaped Perching Gull Lakes Pluton, composed of hornblende diorite to quartz monzonite. The younger is leucocratic biotite granite and cuts all other rock types. The Perching Gull Lakes Pluton is characterized by high abundances of Al_2O_3, Na_2O, Ba, Sr, and light REEs, and low Ta and Ti. Major and trace element variations support a petrogenetic model in which an initial diorite magma underwent 40% fractional crystallization of plagioclase and hornblende to produce quartz monzonite. The more siliceous rocks, including quartz monzonite, have prominent microcline megacrysts and high K and Ba contents, possibly due to interaction with late-stage fluids. It is proposed that diorite of the Perching Gull Lakes Pluton originated by melting of light-REE-enriched mafic and tonalitic crust, and mixing of the melt with residual material. Late biotite granite is probably not related to its syenitic xenoliths by a simple geological process.

Résumé

La région des lacs Perching Gull située dans la sous-province ouest de Wawa est traversée par deux plutons granitiques d'origine tectonique tardive à post-tectonique. Le plus ancien, soit le pluton en forme de croissant de Perching Gull Lakes, se compose de diorite à hornblende à de la monzonite quartzique. Le plus jeune est un granite à biotite leucocrate qui traverse tous les autres types de roche. Le pluton de Perching Gull Lakes est caractérisé par de grandes abondances de Al_2O_3, de Na_2O, de Ba, de Sr et des terres rares légères, accompagnées de faibles quantités de Ta et de Ti. Les variations des éléments principaux et à l'état de traces viennent à l'appui de l'hypothèse d'un modèle pétrogénétique selon lequel le magma dioritique initial a subi une cristallisation fractionnelle de 40 % de plagioclase et de hornblende pour produire de la monzonite quartzique. Les roches les plus silicieuses, y compris la monzonite quartzique, présentent des mégacristaux proéminents de microcline et des teneurs élevées en K et Ba probablement dûs à l'interaction avec les fluides présents dans la phase finale. On suppose que la diorite du pluton de Perching Gull Lakes provient de la fusion de la croûte mafique et tonalitique riche en terres rares légères et du mélange du matériau fondu avec le matériau résiduel. Le granite à biotite tardif et ses xénolites syénitiques ne sont problablement pas associés par un simple processus géologique.

Introduction

This report presents geochemical data on plutonic rocks of the Archean Northern Light – Perching Gull Lakes plutonic terrane of northwestern Ontario. It forms part of an ongoing study of granitoid rocks in the western Wawa Subprovince by Percival (1983). Geochemical aspects of two late to posttectonic granitic bodies are summarized, and some inferences are made about their origin by a comparison with similar rocks in other well studied areas. Several features of trace element abundances of these rocks provide some new additional constraints on petrogenetic models.

Acknowledgments

This report represents the results of a B.Sc. thesis at the University of Waterloo. Thanks are extended to I.L. Gibson for his support and encouragement throughout the study. I am indebted to J.A. Percival (GSC) for the opportunity to work independently on this project. He conceived the study, introduced me to the Perching Gull Lakes area, and provided valuable guidance in the field. Discussions with I.L. Gibson, J.A. Percival, and J. Dearlove aided my attempts to interpret the geochemical data. I.L. Gibson and J. Mungle introduced me to instrumental neutron activation analysis. Critical reading by I.L. Gibson and J.A. Percival improved the manuscript. Logistical support was provided by the GSC. Scott Young provided capable field assistance.

Geological setting

The Perching Gull Lakes area is part of the Northern Light – Perching Gull Lakes plutonic terrane in the western volcanic-plutonic Wawa Subprovince of the Superior Province (Fig. 16.1). The regional geology has been summarized by Percival (1983). Detailed descriptions of field relationships and petrography are given in Percival and Stern (1984). A summary of the geology is presented here.

Bedrock in the Perching Gull Lakes (PGL) area consists of four major lithological units. From oldest to youngest these are (Fig. 16.1): 1) amphibolite grade metavolcanic rocks and derived mafic gneiss; 2) tonalitic gneiss and foliated granodiorite, the former with abundant inclusions of mafic gneiss and amphibolite; 3) massive to foliated hornblende diorite to quartz monzonite of the PGL Pluton, and various small bodies of mafic syenite; and 4) massive to foliated biotite granite. This study concerns the geochemistry of the two younger units.

The PGL Pluton is crudely zoned, with foliated hornblende diorite at the margin, grading inward to quartz monzonite (Fig. 16.2). Although exposure is limited, diorite is estimated to make up about 20% of the pluton. The body is crescent-shaped with foliation concordant to the margins. Structural studies of similar bodies in other granitoid terranes of the Superior Province indicate that the foliation

[1] Department of Earth Sciences, University of Waterloo, Waterloo, Ontario N2L 3G1

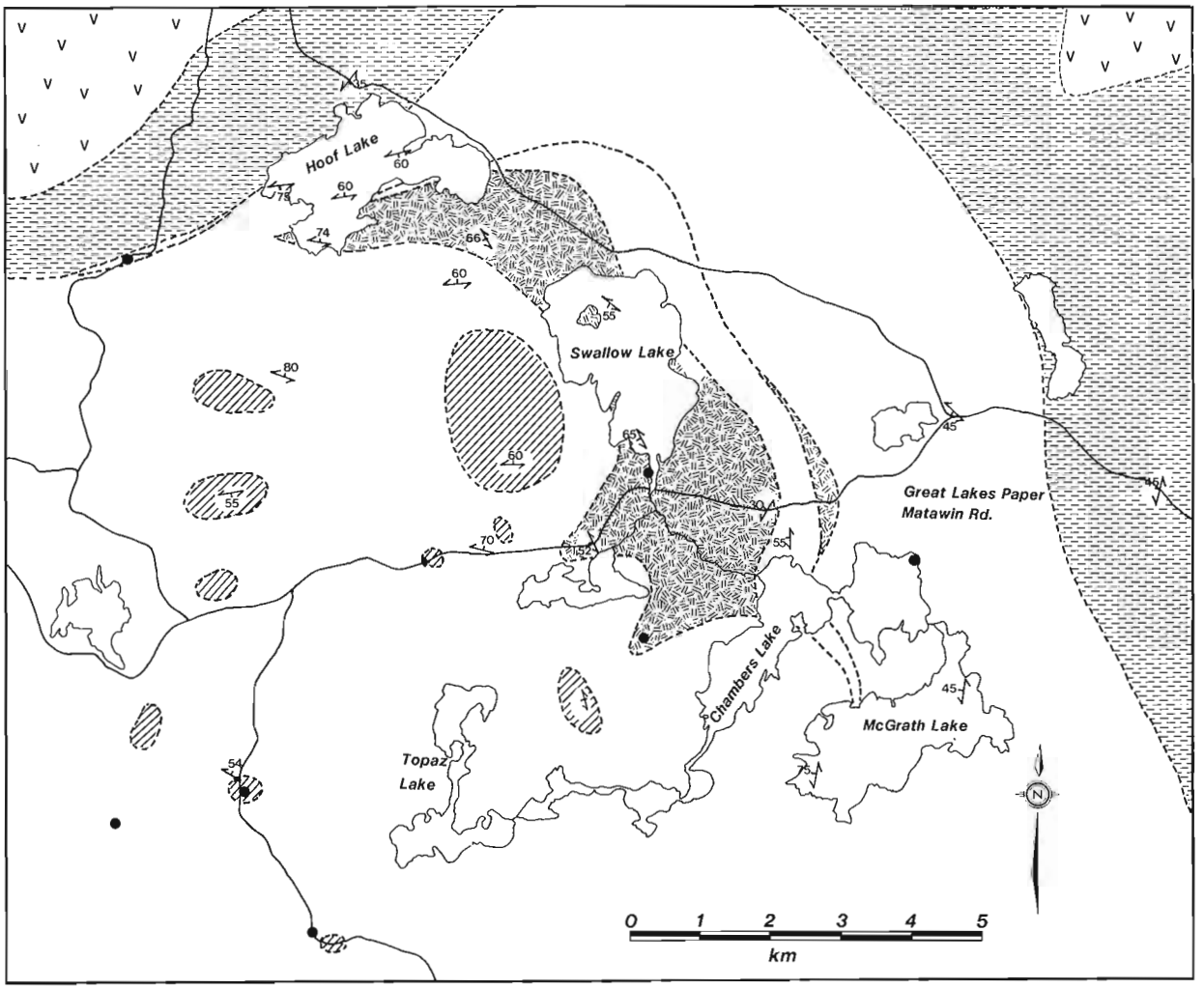

LEGEND

- massive to foliated granite
- quartz monzonite, monzodiorite, diorite
- mafic monzonite, mafic syenite
- foliated granodiorite
- tonalite gneiss
- mafic gneiss
- mafic metavolcanic rocks

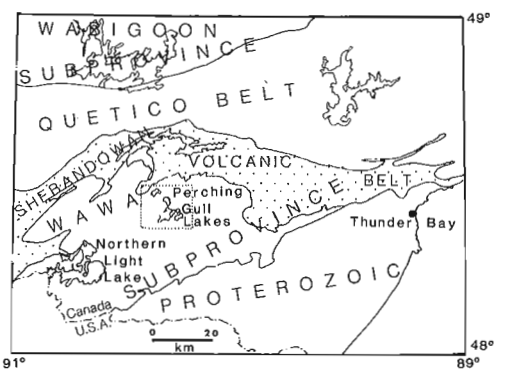

- geological contact
- strike and dip of foliation (70)

Figure 16.1. Generalized geology of the Perching Gull Lakes area. Geology by R.A. Stern and J.A. Percival.

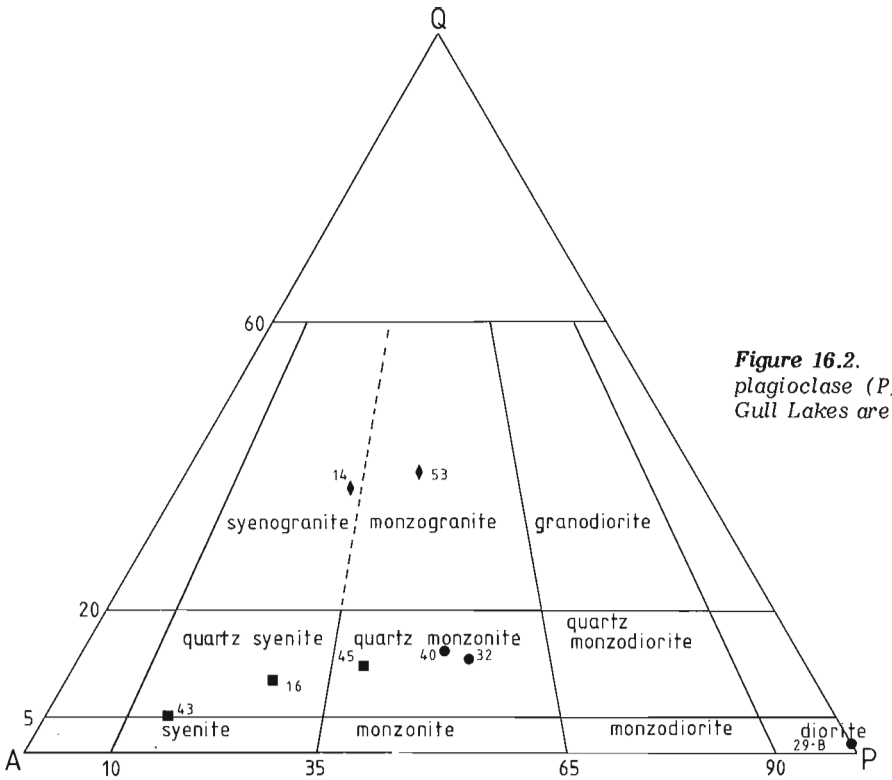

Figure 16.2. *Modal quartz (Q) – alkali feldspar (A) – plagioclase (P) diagram for granitic rocks of the Perching Gull Lakes area. Nomenclature after Streckeisen (1973).*

was acquired during intrusion (Schwerdtner et al., 1979, 1983). Xenoliths within the PGL Pluton are mafic gneiss, possibly derived from a unit on its eastern margin, and mafic monzodiorite to syenite, the latter commonly aligned in long trains of inclusions.

Isolated outcrops and patches of biotite-clinopyroxene-hornblende syenite to quartz monzonite[1] (Fig. 16.2) are present as xenoliths within late granite surrounding the PGL Pluton (Fig. 16.3). These xenoliths range from centimetre to 10 m bodies, the latter shown as black dots in Figure 16.1. They commonly have centimetre-wide biotite-rich rims in contact with granite.

Massive to foliated leucocratic biotite granite (Fig. 16.2) cuts all other rocks in the area. There are at least two ages of granite as indicated by numerous aplitic and pegmatitic dykes which cut discrete biotite granite bodies. Some granite dykes cutting the PGL Pluton contain abundant xenoliths of mafic syenite. At these locations, the granite contains hornblende rather than the more common biotite.

Perching Gull Lakes pluton

Petrography

The most mafic phase of the PGL Pluton is grey, medium grained, well-foliated diorite, mainly present at the margins of the Pluton in contact with mafic gneiss. Diorite (e.g. specimen 29-B, (Table 16.1) consists of plagioclase (70%), hornblende (15%), biotite (8%), and minor interstitial quartz (2%). Plagioclase occurs as poorly twinned, rarely bent, tabular crystals aligned in the ferromagnesian mineral foliation plane, and is partly saussuritized. Green hornblende forms ragged, subhedral crystals surrounded by flakes of brown biotite and clusters of titanite, apatite, and opaque minerals. Biotite and hornblende are only slightly alterated to chlorite and epidote.

Most of the PGL Pluton is composed of pink, medium- to coarse-grained, weakly foliated quartz monzonite, in gradational contact with diorite. Characteristics of this phase are 1.5 μm long, light pink microcline megacrysts aligned with hornblende in the foliation. Quartz monzonite (e.g. specimens 32, 40, Table 16.1) consists of quartz (10-12%), plagioclase (An_{24-33}, 35%), microcline (30 to 35%), and hornblende (10 to 12%). Plagioclase occurs as 0.5-3.0 mm long subhedral, zoned, tabular crystals with albite twinning and moderate saussurite alteration. Two ages of microcline are recognized: older, anhedral, interstitial grains, and younger megacrysts which enclose the older variety as well as small grains of plagioclase and hornblende.

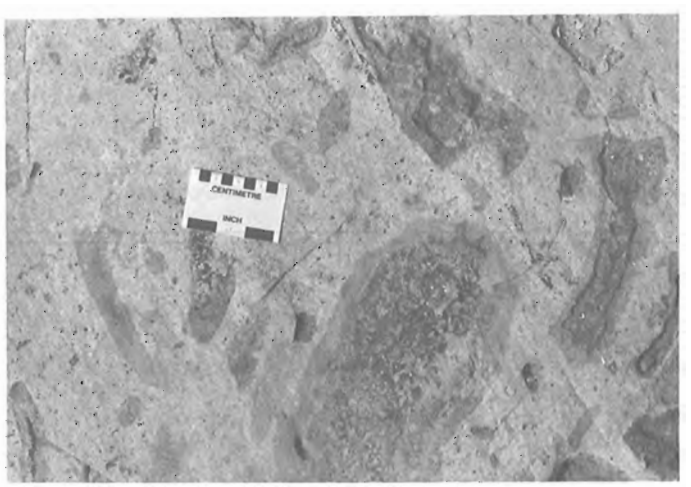

Figure 16.3. *Syenite xenoliths in late granite. Note biotite-rich rims around xenoliths, indicating that they have reacted with their host.*

[1] To avoid confusion with rocks of the PGL Pluton, these rocks are referred to as syenite, and are described as syenitic.

Table 16.1. Approximate* modal compositions of rocks from the study area.

	Perching Gull Lakes Pluton			Late granite		Syenitic xenoliths in granite		
	29B	32	40	14	53	16	43	45
Quartz	2	10	12	35	35	5	3	7
Plagioclase	70	35	35	20	25	12	8	30
(Anorthite content)	?	(33)	(24)	(28)	(33)	(38)	(30)	?
Microcline	tr	30	35	40	30	32	46	20
Hornblende	15	12	10	–	3	30	15	20
Augite	–	–	–	–	–	12	10	–
Biotite	8	tr	tr	3	–	3	10	5
Muscovite	–	–	–	1	–	–	–	–
Chlorite	tr	4	2	–	1	1	tr	2
Epidote	tr	2	1	tr	2	tr	–	2
Allanite	–	tr	–	tr	tr	–	–	–
Apatite	1	2	1	tr	1	1	2	1
Titanite (sphene)	1	2	3	tr	1	4	5	2
Zircon	tr	tr	tr	tr	1	tr	tr	tr
Fluorite	–	–	tr	–	–	–	tr	–
Carbonates	–	tr	–	–	–	–	–	–
Opaques	1-2	2	1-2	tr	tr	tr	tr	tr
IUGS rock name	diorite	quartz monzonite	quartz monzonite	syeno-granite	monzo-granite	quartz syenite	syenite	quartz monzonite

* Visual estimations of single thin sections
tr trace
– not observed

Myrmekite is common at microcline-plagioclase grain boundaries. Quartz is interstitial to the feldspars, and shows undulose extinction. Ragged, green hornblende is surrounded by chlorite and clusters of titanite and epidote. Abundant chlorite (2-4%) is interleaved with, and almost totally replaces, primary biotite. Accessory phases include apatite (1-2%), and titanite (2-3%), the latter with both rhombic cross-sections and irregular shapes. Chlorite, epidote, and minor allanite are presumed to be retrograde alteration products of primary hornblende and biotite.

Chemistry

Chemical analyses of diorite (specimen 29-B) and quartz monzonite (specimens 32 and 40) are reported in Table 16.2. Diorite is near-silica-saturated and grades into silica-oversaturated quartz monzonite (Fig. 16.4). Distinctive features of their major element chemistry are high contents of Al_2O_3 (17.2-19.6%), and K_2O/Na_2O ratios less than 0.5. Increases in SiO_2 content are accompanied by increases in alkalis (Fig. 16.5) and decreases in Al_2O_3, CaO and MgO (Table 16.2).

Trace element contents are characterized by high Ba (880-2070 ppm) and Sr (1850-2480 ppm), and low Rb (50-60 ppm) and Rb/Sr ratios (0.025-0.03). Ba increases and Sr decreases relative to increasing SiO_2 (Table 16.1).

REE patterns are light-REE-enriched [$(Ce/Yb)_n$ = 31-47], and show no Eu anomaly (Fig. 16.6). The light REE increase with increasing SiO_2, whereas heavy REE show no regular pattern.

Origin of lithological variation within the PGL Pluton

Several features characterize the transition from diorite to quartz monzonite in the PGL Pluton:

1. Contacts between diorite and quartz monzonite are gradational, and are characterized by decreasing percentages of mafic minerals (hornblende and biotite) and plagioclase, and increasing abundances of quartz and K-feldspar megacrysts (Table 16.1, Fig. 16.2).
2. Increases in SiO_2 are accompanied by increasing alkalis (Fig. 16.5) and Ba (880-2070 ppm), and decreasing Al_2O_3, CaO, MgO, and Sr (2480-1900 ppm; see Table 16.2).
3. Light REE content increases two-fold from diorite to quartz monzonite, whereas that of heavy REEs increases or decreases in different rocks (Fig. 16.6); no Eu anomaly is evident.

Table 16.2. Chemical analyses of the PGL Pluton* and rocks of similar chemistry from other areas

	29B	32	40	a	b	c
SiO_2 (wt. %)	58.3	61.1	61.8	53.97	67.74	56.6
TiO_2	0.61	0.57	0.70	0.79	0.45	0.61
Al_2O_3	19.6	17.3	17.2	16.00	15.19	19.5
Fe_2O_3	1.5	2.0	1.6	2.57	1.94	2.56
FeO	2.9	1.9	2.1	4.69	1.79	2.77
MnO	0.07	0.07	0.07	0.16	0.10	0.08
MgO	1.95	1.70	1.68	5.72	2.03	2.94
CaO	5.49	3.57	3.71	7.79	3.51	4.91
Na_2O	6.6	5.9	6.0	4.87	4.05	6.52
K_2O	1.29	2.98	2.84	1.48	3.01	2.02
H_2O (total)	0.9	0.9	0.9			0.06
CO_2	0.1	0.1	0.2			
P_2O_5	0.41	0.38	0.36	0.46	0.19	0.42
S	0.00	0.00	0.02			
loss				1.11		
Ba (ppm)	880	2070	1880		1126	1940
Rb	50	50	60	22	66	18.6
Sr	2480	1900	1850	1297	685	2039
Ni	90	80	90			
Zn	100	80	80			
Zr	260	260	250		118	
total	100.3	99.1	99.6			
Rb/Sr	0.020	0.026	0.032	0.017	0.100	0.009
Sr/Ba	2.82	0.92	0.98		0.61	1.05
K/Rb	302	710	560			901
K_2O/Na_2O	0.20	0.51	0.47	0.30	0.74	0.31
Ce (ppm)	106.9	148.3	196.9			
Nd	62.6	70.8	97.9			
Sm	10.52	10.58	14.27			
Eu	2.76	2.76	3.37			
Gd	5.76	5.20	8.08			
Tb	0.72	0.62	0.88			
Yb	0.87	0.81	1.19			
Lu	0.11	0.11	0.16			
(Ce/Yb)n	31.4	46.7	42.1			
Th	2.42	4.44	7.03			
Ta	0.21	0.13	0.47			
Hf	4.63	4.89	5.05			

29-B diorite, PGL Pluton
32 quartz monzonite, PGL Pluton
40 quartz monzonite, PGL Pluton
a hornblende diorite (76-36), Jackfish Lake-Weller Lake Pluton, Rainy Lake area (Sutcliffe and Fawcett, 1980).
b Muriel diorite-granodiorite (G1748), Kenora area (Gower et al., 1983).
c syenodiorite (32), Giants Range Batholith, Minnesota (Arth and Hanson, 1975).
* Major and trace element analyses of PGL rocks by XRF, except Fe, H_2O, CO_2, and S by rapid chemical methods, Performed at GSC Laboratories.

REE analyses of PGL rocks by INAA at University of Waterloo; analyst R. Stern. The method used is described by Gibson and Jagam (1980).

These characteristics suggest that fractional crystallization may have played an important role in the development of the PGL Pluton. In order to test the validity of this mechanism, the composition of diorite 29-B was selected as the initial melt composition in a fractional crystallization model. A mixture of 75% plagioclase (andesine) and 25% hornblende was chosen as the composition of the precipitating extract in accord with the proportions of plagioclase and mafic minerals in the diorite (Table 16.1). The removal of hornblende would deplete the melt in CaO and MgO, and, because hornblende is undersaturated in SiO_2, would also increase the SiO_2 content of the melt. Crystallization of plagioclase would deplete the melt in Al_2O_3 and Sr. No Eu anomaly results from removing about twice as much plagioclase as hornblende (Hanson, 1978).

The proposed variations in major elements have been tested using simple mass balance equations (Table 16.3), with diorite 29-B as the initial liquid composition and quartz monzonite 32 as the target liquid composition after removal of the extract of 75% plagioclase and 25% hornblende. The best fit between the calculated and observed final compositions was obtained after removal of 40% of this cumulate mixture from the initial liquid. The calculated values of Na_2O and K_2O, however, are higher and lower, respectively, than the observed values.

REEs, Ba, Rb, and Sr variations were also tested using the Rayleigh fractionation law (Table 16.4). The calculated and observed abundances of REEs and Sr agree after 40% fractional crystallization. The observed value of Ba is markedly higher than the predicted value, possibly indicating that Ba has been added, perhaps by late-stage fluids.

The disagreement between observed and calculated values of K_2O, Na_2O and Ba may be the result of incorrect assumptions in the fractional crystallization model. For example, the diorite composition chosen may be that of a cumulate rather than of an initial liquid composition. However, the fit of the other elements is good, and it is more likely that alkalis and Ba were mobile, possibly in late-stage fluids circulating through quartz monzonite. In support of this hypothesis is the presence of late microcline megacrysts which could have grown in the environment provided by these fluids. A period of metasomatism could also be the cause of corroded hornblende and biotite, and their replacement by chlorite, epidote, and traces of fluorite. Diorite, having only minor chlorite and epidote (Table 16.1), appears not to have been affected by this event. In summary, the origin of the quartz monzonites of the PGL Pluton can be explained by fractional crystallization of a dioritic magma, followed by a late-stage autometasomatic event.

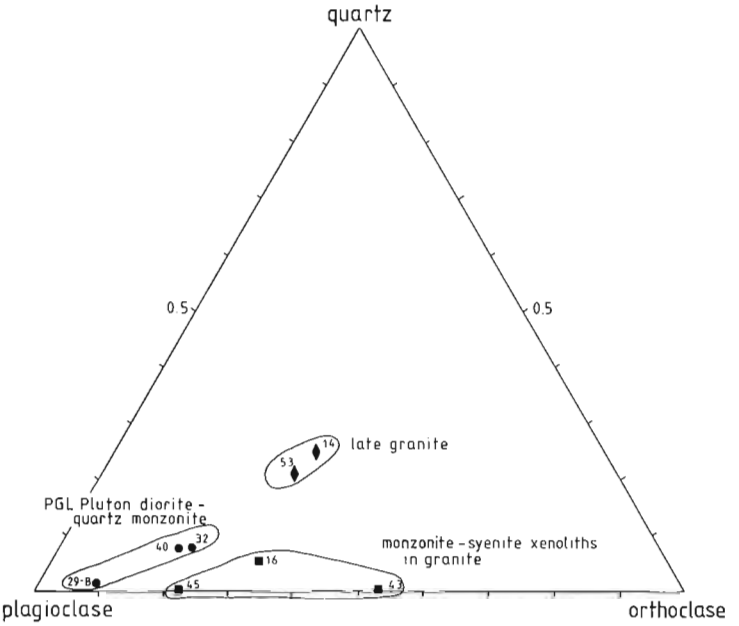

Figure 16.4. *Normative quartz-plagioclase-orthoclase diagram of granitic rocks of the study area. Nomenclature after Streckeisen (1973).*

Origin of the PGL Pluton

Late to posttectonic dioritic to syenitic plutons, such as the PGL Pluton, are common features of granitoid terranes of the Superior Province. Most of these rocks have distinct chemical characteristics, particularly high total alkalis ($Na_2O + K_2O$ = 6-9%), high Ba and Sr, low Rb, and steep, light-REE-enriched patterns. Chemical analyses of a representative group of plutons of this type in the western Superior Province are included in Table 16.2. Representative REE patterns are included in Figure 16.7, where it can be seen that all rocks are light-REE-enriched (Ce = 70-200 x chondrites) and depleted in heavy REE (Yb = 3-6 x chondrites). Investigators studying these rocks in the Rainy Lake area (Longstaffe et al., 1980, 1982; Sutcliffe and Fawcett, 1979, 1980), Kenora area (Gower et al., 1982, 1983),

Table 16.3. Calculations to show the effect of fractional crystallization on major element abundances in the PGL Pluton. All compositions in weight per cent.

oxide	initial liquid composition (C_o)=diorite sample 29B	compositions of phases removed (from Deer, Howie and Zussman, 1977)		fraction of phase removed expressed as a fraction of		calculated composition of remaining liquid (C_L); equation: $C_o=F(C_L) + X_{plag}(C_{plag}) + X_{hb}(C_{hb})$ where F=fraction melt remaining=0.60	observed composition of quartz monzonite sample 32
		plagioclase (andesine) C_{plag}	hornblende C_{hb}	X_{plag}	X_{hb}		
SiO_2	58.30	58.10	44.99	0.30	0.10	60.62	61.10
Al_2O_3	19.60	26.44	11.21	0.30	0.10	17.58	17.30
MgO	1.95	0.03	10.41	0.30	0.10	1.50	1.70
CaO	5.49	7.84	12.11	0.30	0.10	3.21	3.57
Na_2O	6.60	6.48	0.97	0.30	0.10	7.60	5.90
K_2O	1.29	1.10	0.76	0.30	0.10	1.47	2.98

and in northern Minnesota (Goldich et al., 1972; Prince and Hanson, 1972; Hanson et al., 1971; Sims and Mudrey, 1972; Geldon, 1972; Arth and Hanson, 1975; Hanson and Goldich, 1972) have described these plutons and commented upon their origin.

Two distinctly different models have emerged: (1) these rocks were derived by partial melting at crustal depths (Sutcliffe and Fawcett, 1980; Gower et al., 1983); and/or 2) the melts originated in the mantle (Longstaffe et al., 1982; Arth and Hanson, 1975). Petrogenetic models can be summarized as follows:

1. Dioritic to syenitic rocks derived from crustal processes result from partial melting of mafic crustal material and mixing of the resulting tonalitic melt with amphibolite or granulite residue. This mixture may be contaminated by later crustal melts. Associated more silica-rich rocks are derived by fractional crystallization of phases such as hornblende.

2. Dioritic to syenitic rocks derived from mantle processes result from partial melting of silica-saturated to oversaturated eclogite. Fractional crystallization may account for related, more silica-rich, rocks.

Both models are based strongly on modelling of REE. A fundamental constraint is the high abundance of light REE. It is difficult to achieve enrichment of Ce in the order of 100 times chondrite by partial melting of a basaltic composition, whether at amphibolite, eclogite, or granulite grade (see Hanson, 1981, p. 432). However, light-REE-enriched sources such as alkali basalt can provide the required abundances (Kay and Gast, 1973; Sun and Hanson, 1975; Zielinski and Frey, 1970). Hanson (1981) suggested that alkali-rich diorites to syenites share many similarities with mantle-derived alkali basalts, including high Ba, Sr, and light REE (Table 16.5).

Alkali basalts of oceanic islands may be produced by 7-15% partial melting of light-REE-enriched garnet peridotite (Sun and Hanson, 1975). Schwarzer and

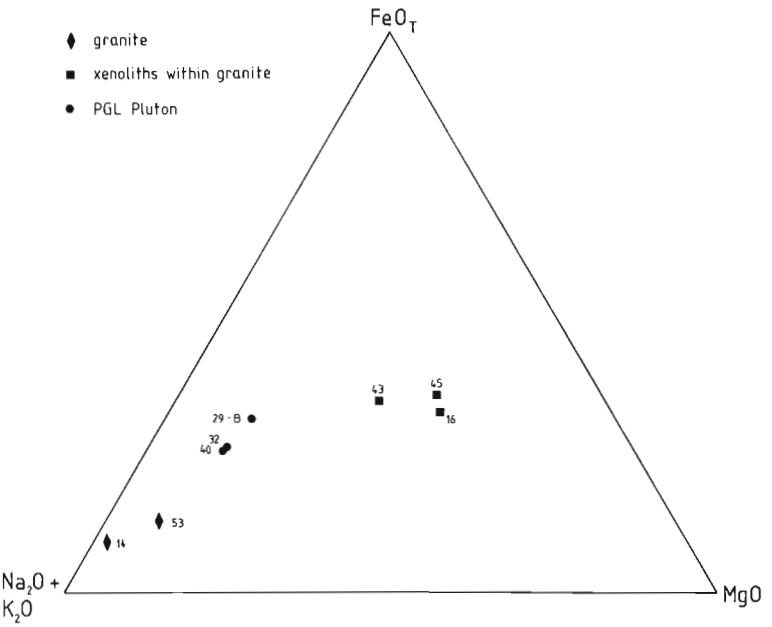

Figure 16.5. *AFM diagram for PGL granitic rocks. FeO_T = FeO + 0.8998 Fe_2O_3 in weight per cent.*

Rogers (1974) showed that alkali basalts of oceanic islands, continental regions, and island-arc environments have similar major element chemistry. They concluded that alkali basalt is a primary magma type formed in diverse settings. Other workers have shown that light-REE-enriched dioritic to syenitic rocks are genetically related to more mafic alkali basalts by fractional crystallization processes (Zielinski and Frey, 1970; Bender et al., 1979).

Table 16.4. Calculations to show the effect of fractional crystallization on REE, Ba, Rb, and Sr abundances in the PGL Pluton

element	initial liquid composition (C_o) =sample 29B (REE are chondrite-normalized)	bulk distribution coefficient (D) for a mixture of 75% plagioclase + 25% hornblende; K_d's for REE from Hanson (1981), for Rb, Sr, Ba from Arth and Hanson (1975)	calculated concentration of remaining liquid (C_L) after 40% fractional crystallization (F=0.60); equation: $\frac{C_L}{C_o} = FD-1$	observed abundance in sample 32 (REE are chondrite-normalized)
Ce	123.6	0.375	170.1	171.4
Nd	99.4	0.805	109.8	112.3
Sm	51.8	1.08	49.7	52.1
Eu	35.8	1.408	29.1	35.8
Gd	20.9	1.42	16.9	18.9
Yb	3.94	1.25	3.47	3.67
Ba	880 ppm	0.278	1273 ppm	2070 ppm
Rb	50 ppm	0.126	78 ppm	50 ppm
Sr	2480 ppm	1.488	1932 ppm	1900 ppm

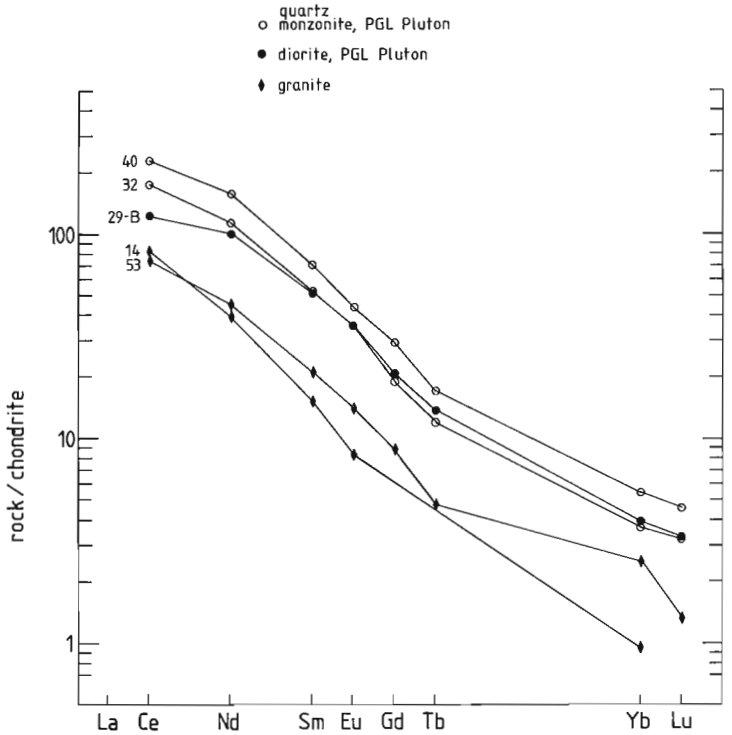

Figure 16.6

Chondrite-normalized REE patterns of the PGL Pluton (upper three curves) and late granite (lower two curves).

Figure 16.7

Chondrite-normalized REE patterns of dioritic rocks from various locations in northwestern Ontario, compared to the field for the PGL Pluton (shaded). Rock types and petrogenetic models postulated to account for the patterns are as follows:

A. *Syenodiorite* #32 from Arth and Hanson (1975; partial melting of undersaturated eclogite).

B. Muriel diorite – granodiorite (G1748) from Gower et al. (1983; partial melt of amphibole and tonalitic gneiss mixed with amphibolite or granulite residue).

C. Hornblende diorite (77-36) of the Jackfish Lake – Weller Lake Pluton, from Sutcliffe and Fawcett (1980; partial melting of a mafic crustal source to yield tonalitic melts, mixed with granulite residue).

D. Diorite #1 of the Jackfish Lake Plutonic Complex from Longstaffe et al. (1982; 10% partial melting of eclogite).

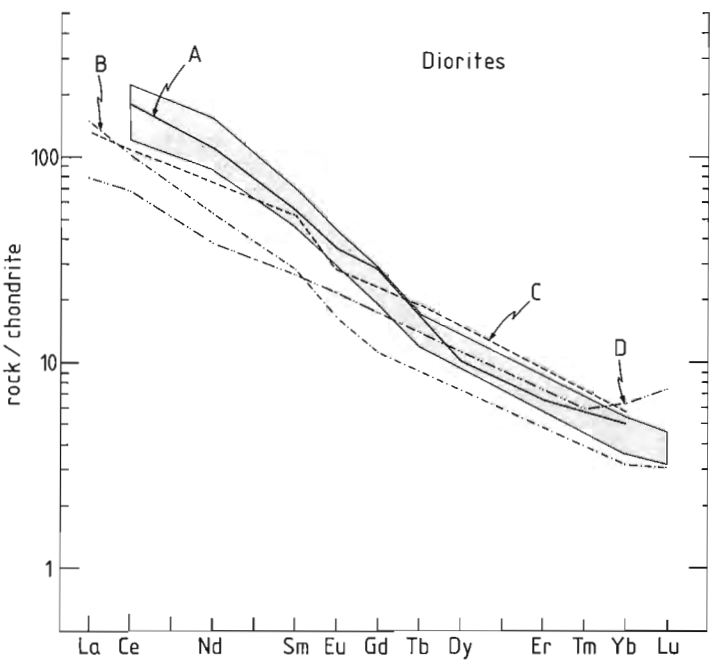

Table 16.5. Average abundances (ppm) of selected trace elements for alkali basalts (from Sun and Hanson, 1975)

K	12 500
Ba	450
Rb	31
Sr	900
Ce	90
Rb/Sr	0.034
Sr/Ba	2
K/Rb	400

Based on these studies a third possible petrogenetic model could account for dioritic to syenitic rocks similar to the PGL Pluton:

3. The melts could be derived through modification by fractional crystallization, crustal contamination, etc., of alkali basaltic melts, or partial melting of an alkali basalt source.

The application of REE in petrogenetic studies of Archean diorite-syenite suites has not led to a unique model for their genesis. For example, in the Rainy Lake area, Sutcliffe and Fawcett (1980) suggested that melting of a mafic crust had produced the Jackfish Lake – Weller Lake Pluton, whereas Longstaffe et al. (1982) concluded that the source of the same body was eclogite (Fig. 16.7). Other petrogenetic models for plutons of similar composition are also shown in Figure 16.7.

Clearly, more constraints are required to produce a unique solution. Trace element data of the PGL Pluton is presented on a chondrite-normalized incompatible element diagram (Fig. 16.8), in which a host of trace elements, including REE, are compared. The PGL rocks show distinct, negative Ta and T anomalies on this diagram. Thompson (1982) has interpreted negative TGa and Ti anomalies to indicate either fractional crystallization of Ta and Ti-rich phases, such as iron-titanium oxides, or partial melting of a source with residual phases containing Ta and Ti.

The relative concentrations of Ta and Ti with respect to other trace elements in the PGL rocks are similar to those in alkali basalts. For example, Sun and Hanson (1975) suggested that a Ti-rich residual mantle phase, such as titanoclinohumite (a Mg-nesosilicate) or ilmenite, was present during melting and production of alkali basalt. Sun (1980) has shown that high Al, calc-alkali, and alkali basalts of island arcs are characteristically low in Ta, Nb, and Ti (Fig. 16.8).

Alkali-rich basaltic rocks are present in volcanic belts of the Superior Province (Brooks et al., 1982; Shegelski, 1980; Smith and Longstaffe, 1974; Cook and Moorhouse, 1969) and lamprophyric dykes and plutons occur within granitoid terranes of the western Wawa subprovince (Sims and Mudrey, 1972; Geldon, 1972; Schulz et al., 1979, Schulz, 1982). The Shebandowan Volcanic Belt (Fig. 16.1) contains shoshonitic volcanic rocks in an area 25 km north of the study area (Shegelski, 1980). REE analyses were performed in this study on the shoshonite specimens analyzed by Shegelski (1980; see Table 16.6). These mafic (average, 53% SiO_2), alkali-rich (average, 3.8% Na_2O and 3.4% K_2O) rocks have light-REE-enriched patterns, similar to alkali basalts (Fig. 16.9). Thus, light-REE-enriched basaltic rocks occur near the study area. There is, however, no direct field evidence to suggest that they are genetically related to the PGL Pluton.

At the present scale of investigation, it is not possible to distinguish between alternatives for the origin of the PGL Pluton. In the Perching Gull Lakes area, this problem may be resolved by:

1. A detailed study of lithological variation within the PGL or other such plutons to better define their liquid line(s) or descent.
2. A careful study of mafic xenoliths, a common feature of the PGL Pluton, to determine if they represent more mafic liquid compositions or, alternatively, cognate or residual material.
3. A chemical evaluation of potential source rocks such as mafic gneiss and tonalitic gneiss, in order to outline possible light-REE-enriched and Ta and Ti-depleted sources.

Based on the information available, the best model appears to be one in which a mafic crustal source and, perhaps, tonalitic gneiss, together undergo partial melting and mixing with residual material. This hypothesis is supported by the occurrence of the PGL Pluton between mafic supracrustal rocks and tonalitic gneiss, a relationship which is characteristic of Archean diorite-syenite bodies in general. Partial melting of mafic crust at depth and incorporation of residual mafic material could result in xenolithic, dioritic melts which intrude along the structurally weak volcanic-gneiss interface. The high light REE content of the PGL Pluton may be inherited from a light-REE-enriched tonalite or mafic source. The latter could include light-REE-enriched volcanic rocks similar to the shoshonites recognized in the Shebandowan Volcanic Belt.

Late granite and syenitic enclaves

Petrography

The youngest intrusive phase in the study area is pink, fine grained, massive to weakly foliated, leucocratic granite. The mafic mineral is biotite, occurring as small flakes that locally define a weak foliation. The modal composition of biotite granite specimen 14 is given in Table 16.1. Plagioclase forms subhedral, blocky to tabular crystals which are usually zoned and display albite twins; minor saussurite occurs at the cores of some grains. Plagioclase, anhedral microcline, and interstitial quartz with undulose extinction produce a hypidiomorphic-granular texture. Ragged flakes of biotite are intergrown with minor muscovite, and both are surrounded by euhedral titanite, apatite, epidote, and magnetite.

In several areas, granite contains abundant hornblende syenite xenoliths (Fig. 16.3). At these locations, the mafic mineral in granite is hornblende. Apart from the presence of hornblende, the modal mineralogy of hornblende granite specimen 53 (Table 16.1) is the same as that of biotite granite. Hornblende granite is, however, characterized by abundant epidote, titanite, apatite, and zircon, which surround euhedral, ragged hornblende crystals or are disseminated throughout the groundmass.

Massive syenite occurs as dark grey, medium- to coarse-grained xenoliths within late granite (Fig. 16.3). A characteristic feature of these rocks is the presence of 1-5 cm long microcline megacrysts surrounded by hornblende-rich zones, which results in a "patchy" texture (Percival and Stern, 1984, Fig. 53.6). Modal analyses of three

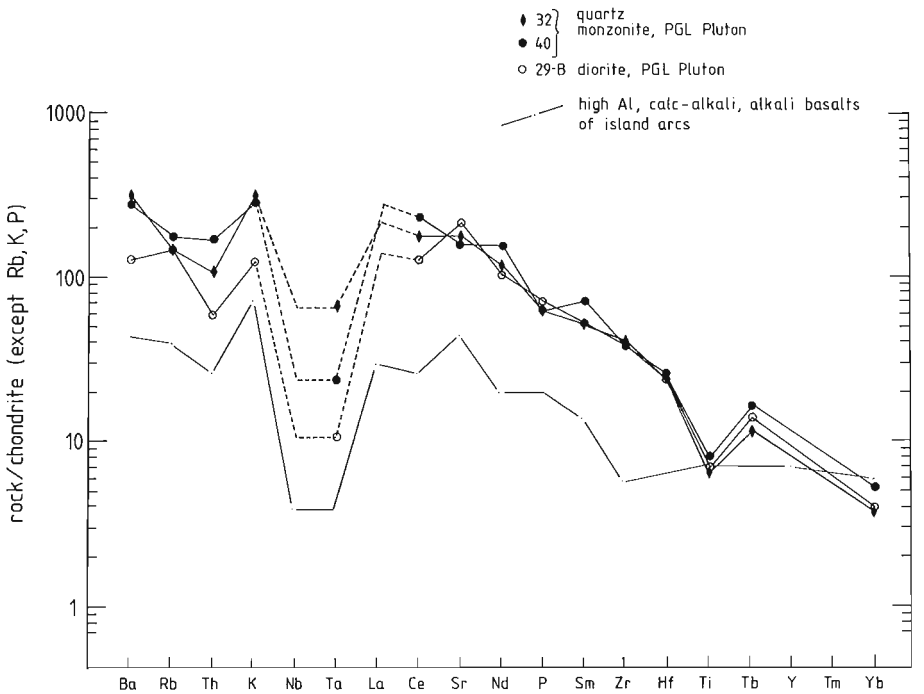

Figure 16.8. *Chondrite-normalized incompatible element diagram for the PGL Pluton. The construction procedure for the diagram is described by Thompson (1982). Rb, K, and P have been normalized to terrestrial rather than chondritic abundances. Also shown is the pattern for high Al, calc-alkali, and alkali basalts of island arc environments (Sun, 1980). Note negative Ta and Ti anomalies in PGL rocks.*

Table 16.6. REE analyses (ppm) of shoshonites from Shebandowan area. For major and other trace elements see Shegelski (1980).*

	25B-15	25B-16	4-2	22C-7
Ce	54.82	42.80	87.25	43.50
Nd	35.44	29.82	47.59	24.68
Sm	5.23	3.24	9.99	2.80
Eu	1.87	1.48	2.29	1.28
Gd	–	–	6.18	–
Tb	0.43	0.32	0.63	0.54
Yb	0.70	0.63	1.03	1.40
Lu	0.06	0.08	0.11	0.20
$(Ce/Yb)_n$	19.9	17.2	21.5	7.9
Th	2.42	2.12	10.02	1.77
Ta	2.22	1.97	0.71	0.98
Hf	4.25	3.89	4.74	2.90

* REE analyses by INAA at University of Waterloo; analyst, R. Stern. Method used is described by Gibson and Jagam (1980).

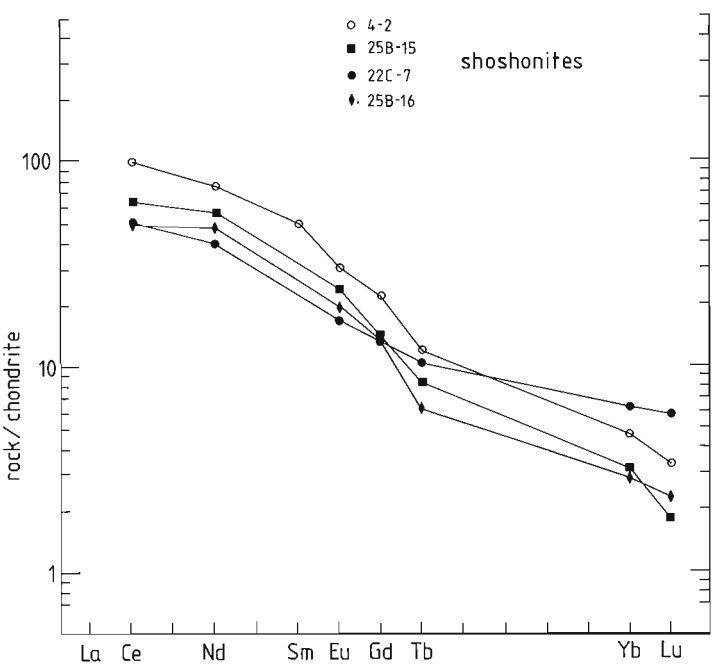

Figure 16.9. *Chondrite-normalized REE patterns for shoshonitic volcanic clasts from the Shebandowan area. These are the same samples analyzed by Shegelski (1980).*

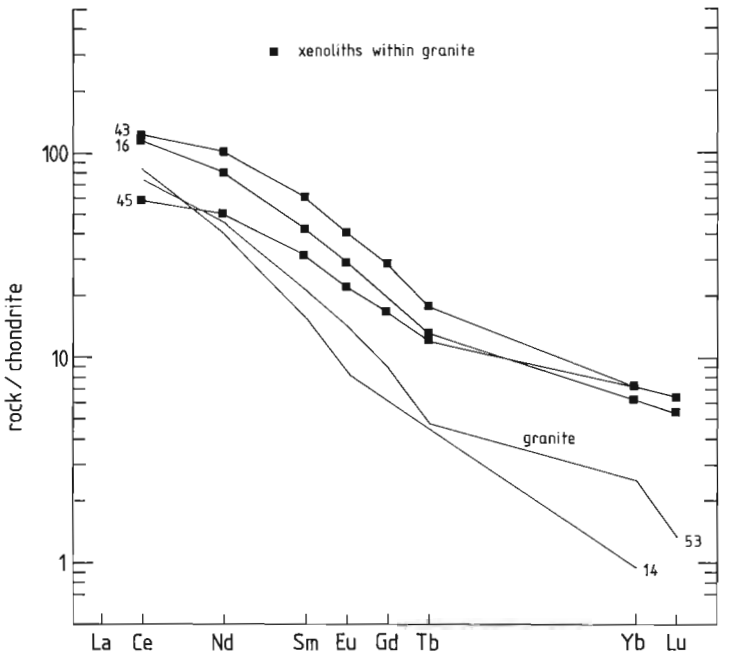

Figure 16.10. *Chondrite-normalized REE patterns for mafic quartz monzonite to syenite xenoliths within late granite. Granite patterns are shown for comparison.*

syenite specimens are given in Table 16.1. Quartz ranges from 3-7%; plagioclase (An_{30-38}), 8-30%; microcline, 20-46%; hornblende, 15-30%; augite, 10-12%; biotite, 3-10%; chlorite and apatite, 1-2%; and titanite from 2-5%. Microcline occurs as anhedral, tabular megacrysts that poikilitically enclose all other phases, and is also present as millimetre-sized grains in the groundmass. The earliest mafic mineral is 0.5-3 mm long, prismatic, green augite, mainly enclosed by microcline megacrysts. The largest augite crystals show conspicuous compositional zoning. Hornblende follows clinopyroxene in order of crystallization, and forms 0.5-5 mm twinned crystals which enclose augite cores. Hornblende is concentrated around microcline megacrysts. Biotite, the last mafic phase to crystallize, rims hornblende or clinopyroxene. Plagioclase is enclosed by microcline where it occurs as fresh, blocky to tabular crystals with albite twinning. Anhedral quartz with undulose extinction is confined to the hornblende-rich zones which surround microcline megacrysts.

Accessory minerals are abundant in the syenitic xenoliths. Euhedral titanite and apatite are concentrated around hornblende and biotite. Fluorite occurs in trace amounts as minute, purple grains interleaved with biotite. In general, the xenoliths analyzed are extremely fresh, having only small amounts of epidote and chlorite.

Chemistry

Chemical analyses of late granite are shown in Table 16.7. These rocks are metaluminous, low in TiO_2, CaO, and MgO, and have high total alkalis ($Na_2O + K_2O$ = 8.7-9.3%, Fig. 16.5), with K_2O/Na_2O ratios > 1.

Trace element contents are characterized by high Ba (1200-1580 ppm), Rb (110-150 ppm), and Rb/Sr ratios (0.11-0.38). REE patterns (Fig. 16.6) show steep negative slopes [(Ce/Yb)n = 29-86], with overall REE abundances less than those of the PGL Pluton, and no Eu anomaly.

Mafic quartz monzonite to syenite xenoliths are distinctly different from host granite in major element chemistry (Table 16.7). They are silica-saturated to oversaturated (Fig. 16.4), and are low in Al_2O_3 and high in CaO, FeO, and MgO (Fig. 16.5). In common with the granite, however, they have high Ba (980-2160 ppm), Rb (80-150 ppm), and Rb/Sr ratios (0.13). REE patterns are less fractionated than those of the granite [(Ce/Yb)n = 8-19], reflecting higher abundances of the heavy REEs (Fig. 16.10).

Relationship between granite and syenite enclaves

Mafic syenite xenoliths were collected with the view that they might be genetically related to their host granites. However, the two have significantly different compositions. For example, xenoliths are near silica-saturated in comparison to silica-oversaturated granite (Fig. 16.4). There are also large gaps between their major element trends (Fig. 16.5), which argues againt the existence of a simple liquid line of descent. Xenoliths are probably not residual or cognate material because they are highly enriched in incompatible elements such as light REE, Ba, Rb, and K_2O (2-5%). The REE patterns of the xenoliths are flatter than those of granite, and they show higher abundances of both light and heavy REE (Fig. 16.10). Based on these chemical differences, it appears that the xenoliths are not related to their host granites by any simple geological process.

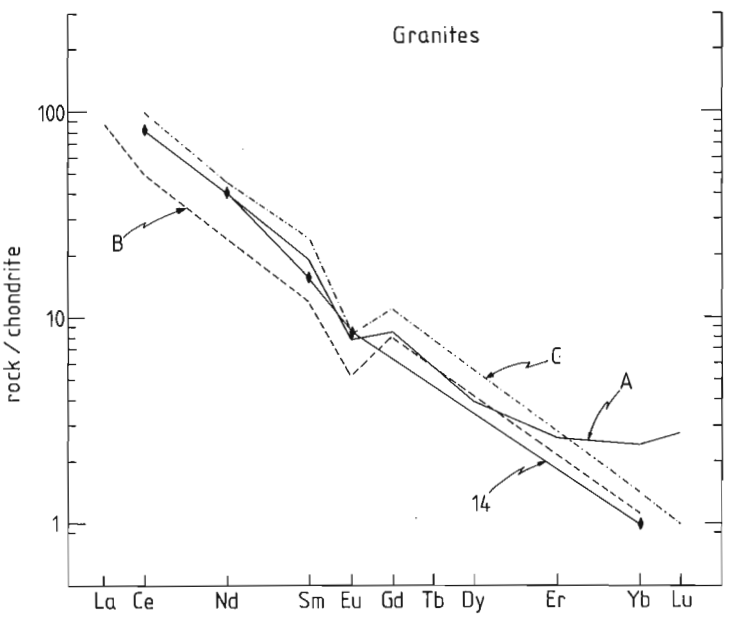

Figure 16.11. *Chondrite-normalized REE patterns for various late granites compared to late granite from the PGL area (14). Rock types and petrogenetic models postulated to account for these patterns are:*

A. Average of 7 'quartz monzonites' (numbers 25-31) from Arth and Hanson (1975; partial melting of greywacke with short crustal residence time).

B. Biotite garnite (77-36) from Sutcliffe and Fawcett (1980; partial melting of tonalite-granodiorite gneiss; the melt is mixed with residue in a 2:1 ratio).

C. Austin Granite (G1154) from Gower et al. (1983; partial melting of granodiorite).

Table 16.7. Chemical analyses of late granite of the PGL area, similar granites from other locations, and syenitic xenoliths within the PGL granite.*

	granite					mafic syenite		
	14	53	a	b	c	16	43	45
SiO_2 (wt. %)	73.3	69.7	73.2	73.82	74.27	55.2	54.2	52.7
TiO_2	0.16	0.25	0.17	0.10	0.20	0.94	0.80	0.70
Al_2O_3	14.2	14.8	14.7	14.03	13.65	12.6	12.0	13.4
Fe_2O_3	0.6	0.8	1.59	0.48	0.98	1.9	2.4	2.6
FeO	0.4	0.7		0.55	0.85	4.6	5.1	5.2
MnO	0.02	0.04	0.03	0.03	0.04	0.13	0.13	0.17
MgO	0.21	0.93	0.42	0.30	0.49	8.11	6.65	8.21
CaO	1.01	2.22	1.11	0.95	1.72	9.22	7.42	7.62
Na_2O	4.2	3.0	3.97	3.85	3.76	2.2	2.2	3.2
K_2O	5.14	4.71	4.55	5.08	3.99	3.04	5.21	2.16
H_2O (total)	0.5	0.5				1.7	1.6	2.0
CO_2	0.0	0.1				0.1	0.2	0.2
P_2O_5	0.04	0.09		0.00	0.06	0.23	0.62	0.27
S	0.00	0.02				0.01	0.03	0.02
loss				0.43				
Ba (ppm)	1200	1580	649	795	1000	1080	2160	980
Rb	150	110	170	233	104	80	150	90
Sr	400	1020	203	221	228	600	1130	670
Ni	70	80				140	180	170
Zn	50	40				80	100	130
Zr	140	150			164	100	250	100
total	100.2	99.1				100.2	99.0	98.8
Rb/Sr	0.375	0.117	0.84	1.05	0.46	0.133	0.133	0.134
Sr/Ba	0.33	0.64	0.31	0.28	0.23	0.55	0.52	0.68
K/Rb	409	468	222			455	423	291
K_2O/Na_2O	1.22	1.18	1.15	1.32	1.06	1.38	2.37	0.68
La (ppm)								
Ce	71.5	64.2				199.7	107.4	50.1
Nd	24.7	28.5				50.7	63.8	31.7
Sm	3.08	4.33				9.15	12.17	6.38
Eu	0.64	1.09				2.23	3.12	1.69
Gd	–	2.46				3.32	7.80	4.60
Tb	–	0.25				–	0.91	0.63
Yb	0.21	0.56				1.35	1.58	1.56
Lu	–	–				0.18	0.21	0.21
$(Ce/Yb)_n$	86	29.4				18.7	17.3	8.2
Th	19.07	8.67				9.63	8.98	4.22
Ta	0.10	0.30				0.07	0.07	0.17
Hf	3.28	2.98				2.80	4.83	2.64

14 biotite granite, PGL area
53 hornblende granite, PGL area
a average of 7 'quartz monzonites' (25-31), northern Minnesota (Arth and Hanson, 1975).
b biotite granite (77-36), Rainy Lake area (Sutcliffe and Fawcett, 1980); Ba value from Sutcliffe and Fawcett (1979).
c Austin granite (G1154), Kenora area (Gower et al., 1983).
16 mafic quartz syenite xenolith, PGL area.
43 mafic syenite xenolith, PGL area.
45 mafic quartz monzonite xenolith, PGL area.
* For analytical methods, see Table 16.1.

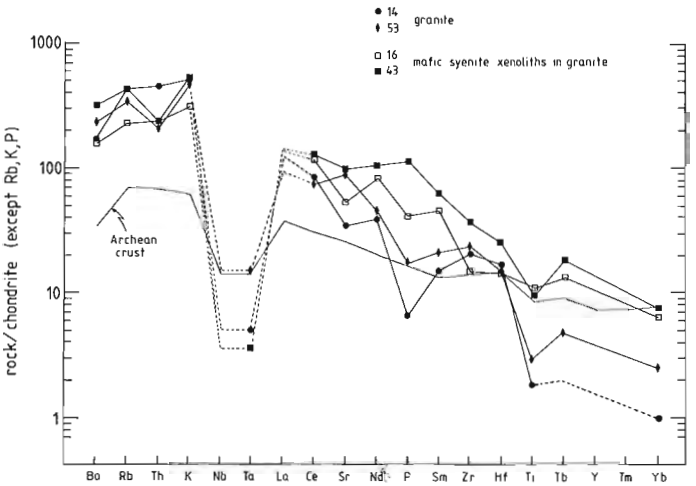

Figure 16.12. *Chondrite-normalized incompatible element diagram of late granite and mafic syenite xenoliths of the study area. Also shown is average Archean upper crust (Taylor and McLennan, 1981). Note negative Ta, P, and Ti anomalies in granite.*

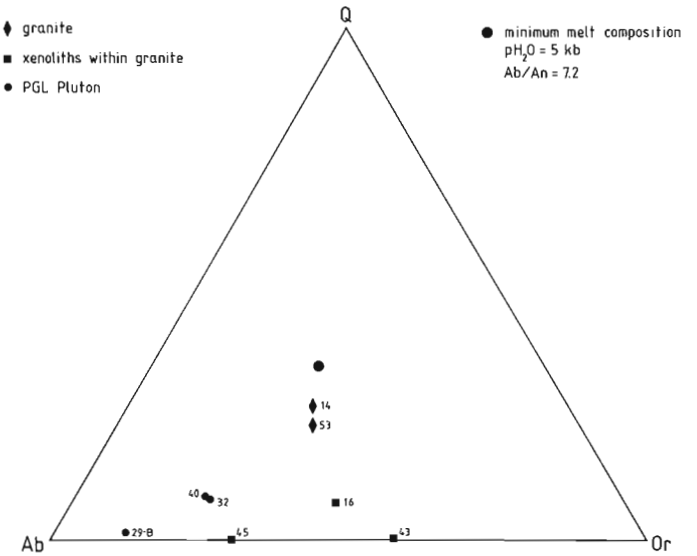

Figure 16.13. *Normative quartz (Q) – albite (Ab) – orthoclase (Or) diagram for granitic rocks of the study area. Minimum melt composition (large dot) from Winkler (1979).*

There are indications, however, that the presence of xenoliths influences the composition of granite. The REE pattern of hornblende granite specimen 53, collected from an area with abundant xenoliths, is intermediate between that of biotite granite (specimen 14) and syenite (Fig. 16.10), suggesting that the assimilation of syenite has affected the overall chemistry of the host granite. It is likely that the presence of hornblende and abundant titanite and apatite in granite specimen 53 (Table 16.1) is a result of contamination by the xenoliths, which also have an abundance of these minerals.

The common field occurrence of syenite in granite is puzzling in light of their differences in chemistry. Careful mapping of the distribution of syenite, and more detailed chemical studies of the syenite xenoliths may help to establish a genetic relationship that is not apparent at the present scale of investigation. It is possible that the granite bodies are composite, with coexisting lower mafic and upper felsic sections (I.L. Gibbons, personal communication, 1984).

Suggestions on the origin of late granite

Massive, late granite batholiths are a characteristic element of granitoid terranes of the Superior Province. They account for about 30% of exposed rocks, occurring as relatively thin sheets intruded into older gneissic rocks (Goodwin, 1978). Most petrogenetic studies have shown that these granites could be derived by partial melting of crustal rocks through a variety of mechanisms. For example, Arth and Hanson (1975) proposed that partial melting of a 'short-lived' greywacke source had produced granite in northern Minnesota. Gower et al. (1983) proposed that partial melting of granodiorite could have produced the Austin granite in the Kenora area. For granites in the Rainy Lake area, Sutcliffe and Fawcett (1980) proposed a model of 20% partial melting of tonalite-granodiorite gneiss and a mixing of the melt and residue in the ratio 2:1. This idea is in accord with the contention of White and Chappell (1977) that many granites are not liquid compositions, but rather mixes of melt and residuum.

Petrogenetic models for these granites must take into account their low initial Sr ratios ($^{87}Sr/^{86}Sr < 0.702$). This may be attributed to either a source with a short crustal residence time or a source with low Rb/Sr ratio. Peterman (1979) stressed that melting of tonalites with "geologically significant crustal residence times" still produced granites with low initial Sr-ratios because most tonalites have low Rb/Sr ratios.

Chemical analyses of granites from the areas discussed above demonstrate their similarity to late granite in the PGL area (Table 16.7). The distinctive similarities are $K_2O/Na_2O > 1$, high Ba, Rb, and Rb/Sr ratios, and high light to heavy REE ratios (average $(Ce/Yb)_n = 58$, Fig. 16.11). Late granite in the PGL area differs from the others in having no Eu anomaly. These similarities in major and trace element abundances support a crustal origin for late granite of the PGL area.

A chondrite-normalized incompatible element diagram for late granite (Fig. 16.12) shows negative Ta and Ti anomalies, like those in the PGL Pluton. In addition, it shows slightly negative P anomalies. These anomalies could result from the presence of residual phases retaining Ta, Ti, and P during melting, such as iron-titanium oxides and apatite, or from fractional crystallization of these phases. Another possibility is that low Ta, Ti, and P are inherent characteristics of the source rocks. For example, a plot of average Archean upper crust on this diagram shows it to be depleted in Nb and Ta (Fig. 16.2). This indicates that low Ta and Nb may be characteristics of the Archean upper crust. Thus, partial melts of the upper crust would also be Ta (Nb)-depleted. The upper crust can be approximated by the composition of greywacke (Taylor and McLennan, 1981), thus, partial melting of greywacke could produce Ta-depleted granitic melts. Late granite also plots near the minimum melt composition in the Q-Ab-An-Or-H_2O system (Fig. 16.13). Winkler (1979) has shown that minimum-melt compositions can be produced by partial melting of greywacke. However, greywacke is rare in the adjacent Shebandowan Volcanic Belt (Fig. 16.1) and is, therefore, not a probably source of late granite.

Partial melting of tonalitic rocks can produce granitic magma (Wyllie, 1977; Winkler, 1979), and tonalite gneiss is abundant in the area (Fig. 16.1). This tonalite is similar to the Northern Light Gneiss in Minnesota and Ontario (Goldich et al., 1972; Arth and Hanson, 1975) and tonalite-granodiorite gneiss in the Rainy Lake area (Longstaffe et al., 1980, 1982; Sutcliffe and Fawcett, 1979, 1980) which have steep, negative REE patterns. Therefore, it is probable that late granite in the PGL area was derived from melting of tonalite gneiss at crustal depths. This hypothesis would be strengthened by chemical analyses of tonalite gneiss, with particular attention to confirming its proposed light-REE-enrichment and negative Ta anomalies.

Conclusions

1. The Perching Gull Lakes (PGL) Pluton is a diorite to quartz monzonite body characterized by high abundances of Al_2O_3, Na_2O, Ba, Sr, and light REE, and low Ta and Ti.
2. Quartz monzonite of the PGL Pluton could be derived by about 40% fractional crystallization of a mixture composed of 75% plagioclase and 25% hornblende from an initial diorite magma.
3. Diorite of the PGL Pluton is possibly derived by melting of light-REE-enriched mafic and tonalitic crust, and mixing of the melt with residual material. Further study of lithological variation within the pluton, and chemical studies of its xenoliths and potential source rocks would help to establish the validity of this hypothesis.
4. Late biotite granite is characterized by K_2O/Na_2O ratios greater than 1, high Ba, Rb, and Rb/Sr ratios, and steeply negative-sloping REE patterns with no Eu anomaly.
5. Low Ta content of late granite supports the view that is was derived by melting of crustal material, perhaps tonalitic gneiss. A study of the chemistry of tonalite is necessary to test this hypothesis.
6. Based on geochemical data, mafic quartz monzonite to syenite xenoliths cannot be related to their host granites by a simple geological process.

References

Arth, J.G. and Hanson, G.N.
1975: Geochemistry and origin of the early Precambrian crust of northeastern Minnesota; Geochimica et Cosmochimica Acta, v. 39, p. 325-362.

Bender, J.F., Bence, A.E., Hanson, G.N., and Ratcliffe, N.M.
1979: The Cortlandt Complex: petrogenesis of a mafic alkalic plutonic suite; EOS, v. 60, no. 18, p. 410.

Brooks, C., Luddent, J., Pigeon, Y., and Hubregtse, J.J.M.W.
1982: Volcanism of shoshonite to high-K andesite affinity in an Archean arc environment, Oxford Lake, Manitoba; Canadian Journal of Earth Sciences, v. 19, p. 55-67.

Cook, D.L. and Moorhouse, W.W.
1969: Timiskaming volcanism in the Kirkland Lake area, Ontario, Canada; Canadian Journal of Earth Sciences, v. 6, p. 117-132.

Deer, W.A., Howie, R.A., and Zussman, J.
1977: An Introduction to the Rock Forming Minerals; Longman Group Ltd., London, 528 p.

Geldon, A.L.
1972: Petrology of the lamprophyre pluton near Dead River; in Geology of Minnesota – a Centennial Volume, ed., P.K. Sims and G.B. Morey; Minnesota Geological Survey, p. 153-159.

Gibson, I.L. and Jagam, P.
1980: Instrumental neutron activation analysis of rocks and minerals; in Short Course in Neutron Activation Analysis in the Geosciences, ed. G.K. Muecke; Mineralogical Association of Canada, Short Course Handbook, v. 5, p. 109-131.

Goldich, S.S., Hanson, G.N., Hallford, C.R., and Mudrey, M.G., Jr.
1972: Early Precambrian rocks in the Saganaga Lake-Northern Light Lake area, Minnesota-Ontario. Part I, petrology and structure; in Studies in Mineralogy and Precambrian Geology, ed. B.R. Doe and D.K. Smith; Geological Society of America, Memoir 135, p. 151-177.

Goodwin, A.M.
1978: Archean crust in the Superior Geotraverse area: geologic overview; in Proceedings of the 1978 Archean Geochemistry Conference, ed. I.E.M. Smith and J.G. Williams; University of Toronto Press, p. 73-106.

Gower, C.F., Crocket, J.H., and Kabir, A.
1983: Petrogenesis of Archean granitoid plutons from the Kenora area, English River Subprovince, northwest Ontario; Precambrian Research, v. 22, p. 245-270.

Gower, C.F., Paul, D.K., and Crocket, J.H.
1982: Protoliths and petrogenesis of Archean gneisses from the Kenora area, English River Subprovince, northwest Ontario; Precambrian Research, v. 17, p. 245-274.

Hanson, G.N.
1978: The application of trace elements to the petrogenesis of igneous rocks of granitic compositions; Earth and Planetary Science Letters, v. 38, p. 26-43.

1981: Geochemical constrains on the evolution of the early continental crust; Royal Society of London, Philosophical Transactions, Series A, v. 301, no. 1461, p. 423-442.

Hanson, G.N. and Goldich, S.S.
1972: Early Precambrian rocks in the Saganaga Lake-Northern Light Lake area, Minnesota-Ontario. Part II, petrogenesis; in Studies in Mineralogy and Precambrian Geology, ed. B.R. Doe and D.K. Smith; Geological Society of America, Memoir 135, p. 179-192.

Hanson, G.N, Goldich, S.S., Arth, J.G., and Yardley, D.H.
1971: Age of the early Precambrian rocks of the Saganaga Lake-Northern Light Lake area, Ontario-Minnesota; Canadian Journal of Earth Sciences, v. 8, p. 1110-1124.

Kay, R.W. and Gast, P.W.
1973: The rare earth contents and origin of alkali-rich basalts; Journal of Geology, v. 81, p. 653-682.

Longstaffe, F.J., McNutt, R.H., and Crocket, J.H.
1982: Rare-earth element modelling of Archean meta-igneous rocks, Lake Despair area, northwestern Ontario; Precambrian Research, v. 17, p. 275-296.

Longstaffe, F.J., McNutt, R.H., and Schwarcz, H.P.
1980: Geochemistry of Archean meta-igneous rocks, Lake Despair area, Wabigoon Subprovince, northwestern Ontario; Canadian Journal of Earth Sciences, v. 17, p. 1046-1063.

Percival, J.A.
1983: Preliminary results of geological synthesis in the western Superior Province; in Current Research, Part A, Geological Survey of Canada, Paper 83-1A, p. 125-131.

Percival, J.A. and Stern, R.A.
1984: Geological synthesis in the western Superior Province, Ontario; in Current Research, Part A, Geological Survey of Canada, Paper 84-1A, p. 397-408.

Peterman, Z.E.
1979: Strontium isotope geochemistry of Late Archean to Late Cretaceous tonalites and trondhjemites; in Trondhjemites, Dacites, and Related Rocks, ed. F. Barker; Elsevier, p. 133-147.

Prince, L.A. and Hanson, G.N.
1972: Rb-Sr isochron ages for the Giants Range Granite, northeastern Minnesota; in Studies in Mineralogy and Precambrian Geology, ed. B.R. Doe and D.K. Smith; Geological Society of America, Memoir 135, p. 217-224.

Schulz, K.J.
1982: The nature and significance of Archean alkalic magmatism, southern Superior Province; Geological Association of Canada-Mineralogical Association of Canada, Program with Abstracts, v. 7, p. 80.

Schulz, K.J., Smith, I.E.M., and Blanchard, D.P.
1979: The nature of Archean alkalic rocks from the southern portion of the Superior Province; EOS, v. 60, no. 18, p. 410.

Schulz, K.J. and Rogers, J.J.W.
1974: A worldwide comparison of alkali olivine basalts and their differentiation trends; Earth and Planetary Science Letters, v. 23, p. 286-296.

Schwerdtner, W.M., Stone, D., Osadetz, K., Morgan, J., and Stott, G.M.
1979: Granitoid complexes and the Archean tectonic record in the southern part of northwestern Ontario; Canadian Journal of Earth Sciences, v. 16, p. 1965-1977.

Schwerdtner, W.M., Scott, G.M., and Sutcliffe, R.H.
1983: Strain patterns of crescentic granitoid plutons in the Archean greenstone terrane of Ontario; Journal of Structural Geology, v. 5, p. 419-430.

Shegelski, R.J.
1980: Archean cratonization emergence and red bed development, Lake Shebandowan area, Canada; Precambrian Research, v. 12, p. 331-347.

Sims, P.K. and Mudrey, M.G., Jr.
1972: Syenitic plutons and associated lamprophyres; in Geology of Minnesota – a Centennial Volume, ed. P.K. Sims and G.B. Morey; Minnesota Geological Survey, p. 140-152.

Smith, T.E. and Longstaffe, F.J.
1974: Archean rocks of shoshonitic affinities at Bijou Point, northwestern Ontario; Canadian Journal of Earth Sciences, v. 11, p. 1407-1413.

Streckeisen, A.
1973: Plutonic rocks; Geotimes, v. 18, p. 26-30.

Sun, S.S.
1980: Lead isotopic study of young volcanic rocks from mid-ocean ridges, ocean islands and island arcs; in The Evidence for Chemical Heterogeneity in the Earth's Mantle; Royal Society of London, Philosophical Transactions, Series A, v. 297, p. 409-445.

Sun, S.S. and Hanson, G.N.
1975: Origin of Ross Island basanitoids and limitations upon the heterogeneity of mantle sources for alkali basalts and nephelinites; Contributions to Mineralogy and Petrology, v. 52, p. 77-106.

Sutcliffe, R.H. and Fawcett, J.J.
1979: Petrological and geochronological studies on the Rainy Lake granitoid complex, northwestern Ontario: a progress report; in Current Research, Part A, Geological Survey of Canada, Paper 79-1A, p. 377-380.

1980: Petrological studies on the Rainy Lake granitoid complex, northwestern Ontario: a preliminary evaluation; in Current Research, Part A, Geological Survey of Canada, Paper 80-1A, p. 335-338.

Taylor, S.R. and McLennan, S.M.
1981: The composition and evolution of the continental crust: rare earth element evidence from sedimentary rocks; Royal Society of London, Philosophical Transactions, Series A, v. 301, no. 1461, p. 381-399.

Thompson, R.N.
1982: Magmatism of the British Tertiary Volcanic Province; Scottish Journal of Geology, v. 18, p. 49-107.

White, A.J.R. and Chappell, B.W.
1977: Ultrametamorphism and granitoid genesis; in Experimental Petrology Related to Extreme Metamorphism, ed. D.H. Green; Tectonophysics, v. 43, p. 7-22.

Winkler, H.G.F.
1979: Petrogenesis of Metamorphic Rocks; 5th edition, Springer-Verlag, New York, 348 p.

Wyllie, P.J.
1977: Crustal anatexis: an experimental review; in Experimental Petrology Related to Extreme Metamorphism, ed. D.H. Green; Tectonophysics, v. 43, p. 41-71.

Zielinski, R.A. and Frey, F.A.
1970: Gough Island: evaluation of a fractional crystallization model; Contributions to Mineralogy and Petrology, v. 29, p. 242-254.

17. EARLY PROTEROZOIC AMER GROUP, BEVERLY LAKE MAP AREA, DISTRICT OF KEEWATIN

Project 820004

A.N. LeCheminant, M.J. Jackson[1], A.G. Galley,
S.L. Smith[2], and J.A. Donaldson[2]
Precambrian Geology Division

LeCheminant, A.N., Jackson, M.J., Galley, A.G., Smith, S.L., and Donaldson, J.A., Early Proterozoic Amer Group, Beverly Lake map area, District of Keewatin; in Current Research, Part B, Geological Survey of Canada, Paper 84-1B, p. 159-172, 1984.

Abstract

Two areas of deformed metasedimentary rocks in the Beverly Lake map area are assigned to the early Proterozoic Amer group. Basement to the metasedimentary rocks consists of late Archean(?) granite and felsic metavolcanic rocks. Metavolcanic rocks are largely products of subaerial ash flow eruptions. Lower greenschist/subgreenschist Amer group successions comprise orthoquartzite, turbiditic greywacke-mudstone and feldspathic siltstone and arenite. Orthoquartzite was deposited after extensive weathering of a granitoid source area. Overlying rocks reflect deposition in a deepening marine environment and subsequent rapid infilling by immature feldspar-rich detritus. Upper units are mainly intertidal and fluvial assemblages.

Undeformed Dubawnt Group acid volcanic and fluvial sedimentary rocks unconformably overlie Amer group sequences. Pitz Formation dacites include subaerial flows and subvolcanic porphyry, some of which contain evidence of mixed magma interactions. Overlying Thelon Formation strata comprise a lower unit containing debris flow deposits and an upper unit of clay-cemented sandstone and conglomerate. Phosphorous-uranium impregnations are erratically distributed in sub-Thelon saprolite and in basal Thelon Formation red sandstone and pebbly conglomerate.

Résumé

Deux zones constituées de roches métasédimentaires déformées, situées dans la région du lac Beverly, font partie du groupe protérozoïque inférieur d'Amer. Le socle des roches sédimentaires se compose de granite et de roches métavolcaniques felsiques datant de l'Archéen inférieur (?). Les roches métavolcaniques proviennent surtout d'éruptions de coulées de cendres subaériennes. Les successions inférieures de roches vertes et de sous roches vertes du groupe d'Amer sont constituées d'orthoquartzite, de grauwacke et <<mudstone>> turbiditiques, de siltstone et d'arénite feldspathiques. L'orthoquartzite a été mise en place à la suite de l'importante altération superficielle d'une zone granitoïde. Les roches sus-jacentes sont associées à une sédimentation marine progressivement plus profonde et, plus tard, à un remplissage rapide par des roches détritiques riches en feldspath encore non parvenues à maturité. Les unités supérieures se composent surtout d'assemblages intertidaux et fluviatiles.

Les roches sédimentaires non déformées de natures volcaniques acides et fluviatiles du groupe de Dubawnt reposent en discordance sur les séquences du groupe d'Amer. Les dacites de la formation de Pitz comprennent des coulées subaériennes et des porphyres subvolcaniques, dont quelques-uns renferment des preuves d'interactions de magma mixte. Les couches de la formation sus-jacente de Thelon sont constituées d'une unité inférieure contenant des débris de dépôts de coulées et d'une unité supérieure de grès et de conglomérats à ciment argileux. Des imprégnations d'uranium et de phosphore sont réparties d'une façon irrégulière dans un saprolite sous-jacent à la formation de Thelon et dans un grès rouge et un conglomérat graveleux de la partie inférieure de cette même formation.

Introduction

Donaldson (1969) briefly described several areas of deformed metasedimentary rocks within the Beverly Lake (66C) map area. In August, 1983 three weeks were spent mapping two of these metasedimentary assemblages: (1) a northeasterly trending belt in the Akiliniq Hills and (2) an inlier along the Thelon River west of Beverly Lake (Fig. 17.1). Both areas are within the Thelon Game Sanctuary.

In the Akiliniq Hills area a folded white orthoquartzite rests on a basement of leucocratic granite and felsic metavolcanic rocks. Overlying sequences of immature clastic rocks in the Akiliniq Hills and sandstone-siltstone dominated units along the Thelon River are interpreted mainly as shallow marine and fluvial deposits. Structural, lithological and stratigraphic relationships suggest that the metasedimentary rocks correlate with the Amer group which has been described by Tippett and Heywood (1978), Knox (1980), Patterson (1981) and Tella et al. (1983, 1984).

In the Beverly Lake area the metasedimentary sequences are unconformably overlain by Dubawnt Group continental volcanic and sedimentary rocks (Donaldson, 1969; Cecile, 1973). Two Dubawnt Group formations are represented. The Pitz Formation consists of rhyolitic and dacitic flows, but along the Thelon River the formation includes subvolcanic prophyry. Basal conglomerate and sandstone of the Thelon Formation overlie intensely weathered Pitz Formation and Amer group rocks.

[1] Bureau of Mineral Resources, Geology and Geophysics, Canberra, Australia
[2] Carleton University, Ottawa, Ontario, K1S 5B6

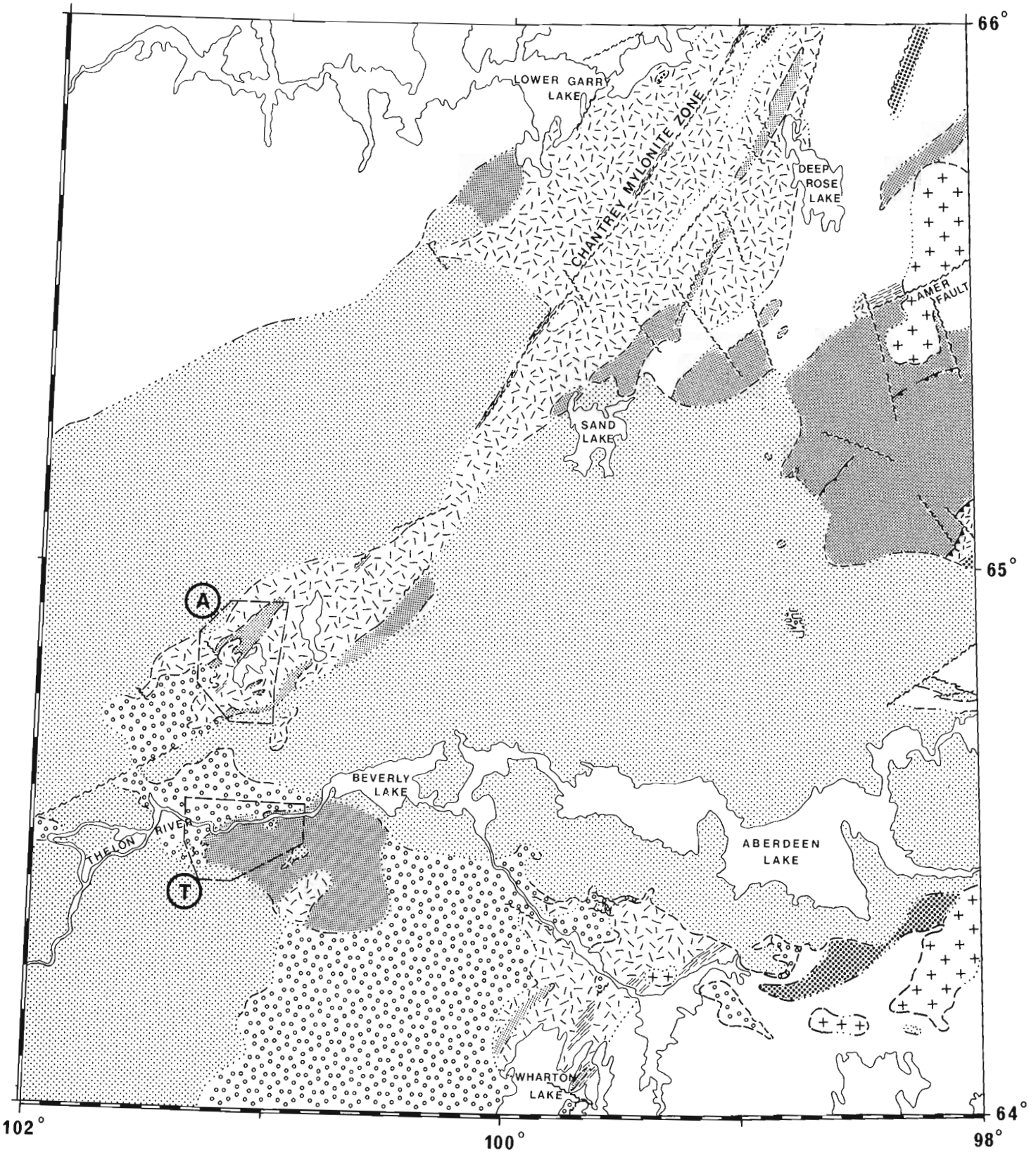
66°
LOWER GARRY LAKE
CHANTREY MYLONITE ZONE
DEEP ROSE LAKE
AMER FAULT
SAND LAKE
65°
A
BEVERLY LAKE
THELON RIVER
T
ABERDEEN LAKE
WHARTON LAKE
64°
102°
100°
98°

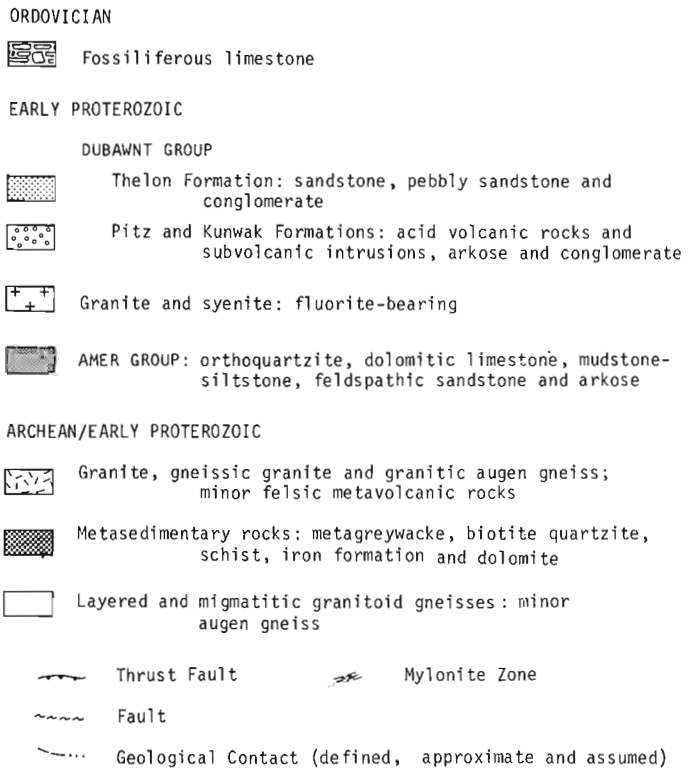

Figure 17.1. *Simplified geological map of the Beverly Lake area and adjacent map areas to the east and north. Information from Donaldson (1969), Tella et al. (1983, 1984) and LeCheminant et al. (1983). The Akiliniq Hills (A) and the Thelon River (T) areas, shown in Figure 17.2 and 17.5 are indicated by dashed outline.*

Pre-Amer group basement

Massive to weakly foliated granite and a diverse suite of felsic metavolcanic rocks dominated by ash flow tuffs underlie the Amer group in the Akiliniq Hills area (Fig. 17.2). Granite-metavolcanic contacts commonly are high strain zones with a strong foliation developed in both rock types that obscures primary relationships. However, the granite apparently is the oldest unit, because chilled margins are absent, no granitic dykes cut the metavolcanic rocks and northwest of '195 m' Lake strongly altered (weathered ?) granite is overlain by a shallow-dipping sequence of fine grained bedded tuffs and metavolcanic schists.

Granite

Granite is well exposed in the northwest part of the Akiliniq Hills map area and scattered outcrops occur south and east of '187 m' Lake (Fig. 17.2). The granite is identical to extensive plutons in the Pelly Lake and Deep Rose Lake areas to the northeast (unit 4c of Tella et al., 1984). In the Akiliniq Hills granites are homogeneous medium- to coarse-grained pink leucocratic rocks that contain 25-30% quartz and subequal proportions of plagioclase and microcline perthite. Chloritized biotite and rare hornblende constitute less than 5% of the rock. Accessory minerals are sphene, apatite, zircon and opaques. Calcite, chlorite and epidote alteration and veinlets are common. Centimetre-scale pink aplite veins, small granite pegmatite dykes and a few irregular 1-3 m wide dykes of fine- to medium-grained biotite-quartz syenite crosscut the granites. The mafic quartz syenite dykes are chilled and enclose rare granite xenoliths.

A steep dipping north-northeast- to northeast-trending foliation is present in narrow deformed zones within the granite. These zones contain extensive multiple generation quartz vein stockwork and red chert-quartz breccia up to 60 m wide. Granite within and adjacent to the quartz veins is bleached and silicified. The stockworks are best developed in the northwest part of the map area within three kilometres of the present trace of the sub-Thelon Formation unconformity. Veining and silicification was probably due to penetration of silica-rich groundwaters beneath the unconformity into faults and fractures localized within deformed zones in the granite. Chiarenzelli (1983) reported similar deep silicification beneath the Thelon Formation near Aberdeen Lake.

Felsic metavolcanic unit

Northwest of '187 m' Lake the metavolcanic unit comprises acid to intermediate quartz- and plagioclase-phyric flows with minor intercalated volcaniclastic rocks. In most outcrops primary textures are obliterated by a steep dipping north-northeast- to northeast-trending schistosity (Fig. 17.2). Bedding is measurable in a few fine grained tuffaceous rocks, but flow contacts and eutaxitic foliation are only rarely discernible in the field. Continuously exposed sections without obvious fold repetition do not exceed 500 m in thickness, although the unit has a width of up to 3 km perpendicular to the northeast-trending folds.

Most flows are crystal and crystal-lithic ash flow tuff. Distinctive lithologies include sericite, sericite-quartz and chlorite-sericite-quartz schist and more homogeneous foliated quartz, quartz-feldspar and feldspar porphyry. Schists range from light pink to white to green, with pale green hues predominant. Rhyolitic and dacitic quartz-bearing prophyry is typically red whereas less abundant andesitic plagioclase-rich porphyry is grey to grey-green.

Petrographic evidence supports a pyroclastic origin for most of these rocks. Felsic ash flows contain up to 15% broken and embayed quartz phenocrysts (1-4 mm). Broken and euhedral altered plagioclase phenocrysts (2-6 mm) are abundant throughout the unit. K-feldspar phenocrysts are relatively rare. Completely altered ferromagnesian phenocrysts (hornblende ?) are present in andesitic flows. The matrix is recrystallized to assemblages of sericite, chlorite, quartz, albite and epidote. Rarely, eutaxitic foliation can be recognized through the tectonic fabric. One very fine grained phenocryst-free sericite schist is composed of flattened devitrified bubble-wall shards indicating derivation from a glassy welded tuff. Rhyolitic and dacitic ash flows contain flattened pumice lapilli, up to about 1 cm long, recrystallized to fine quartz-sericitic-carbonate intergrowths. Microspherulites were noted in pumice lapilli from a light green dacitic crystal-lithic tuff. Dark greenish grey andesitic tuff contains abundant plagioclase phenocrysts and accidental volcanic fragments up to 2 cm across. Although primary textures in the matrix of the andesitic tuff have been destroyed by recrystallization and deformation, many siliceous fragments were unaffected: within them a eutaxitic fabric is well preserved.

The metavolcanics are interpreted as products of subaerial rhyolite-dacite ash flow eruptions with subordinate andesitic flows. Repeated units of 8-12 m thick homogeneous quartz- and feldspar-phyric schist alternating with 1-2 m thick white aphyric sericite schist suggest the presence of eruptive cycles, perhaps pyroclastic flow deposits overlain by air-fall ash. Many of the sericite schists contain abundant euhedral pyrite. One example of andesitic volcanism subsequent to more acid explosive eruptions is indicated by the presence of accidental fragments of welded dacitic tuff in crystal-rich andesitic tuff. Coarser grained red quartz- and feldspar-phyric porphyritic rocks form

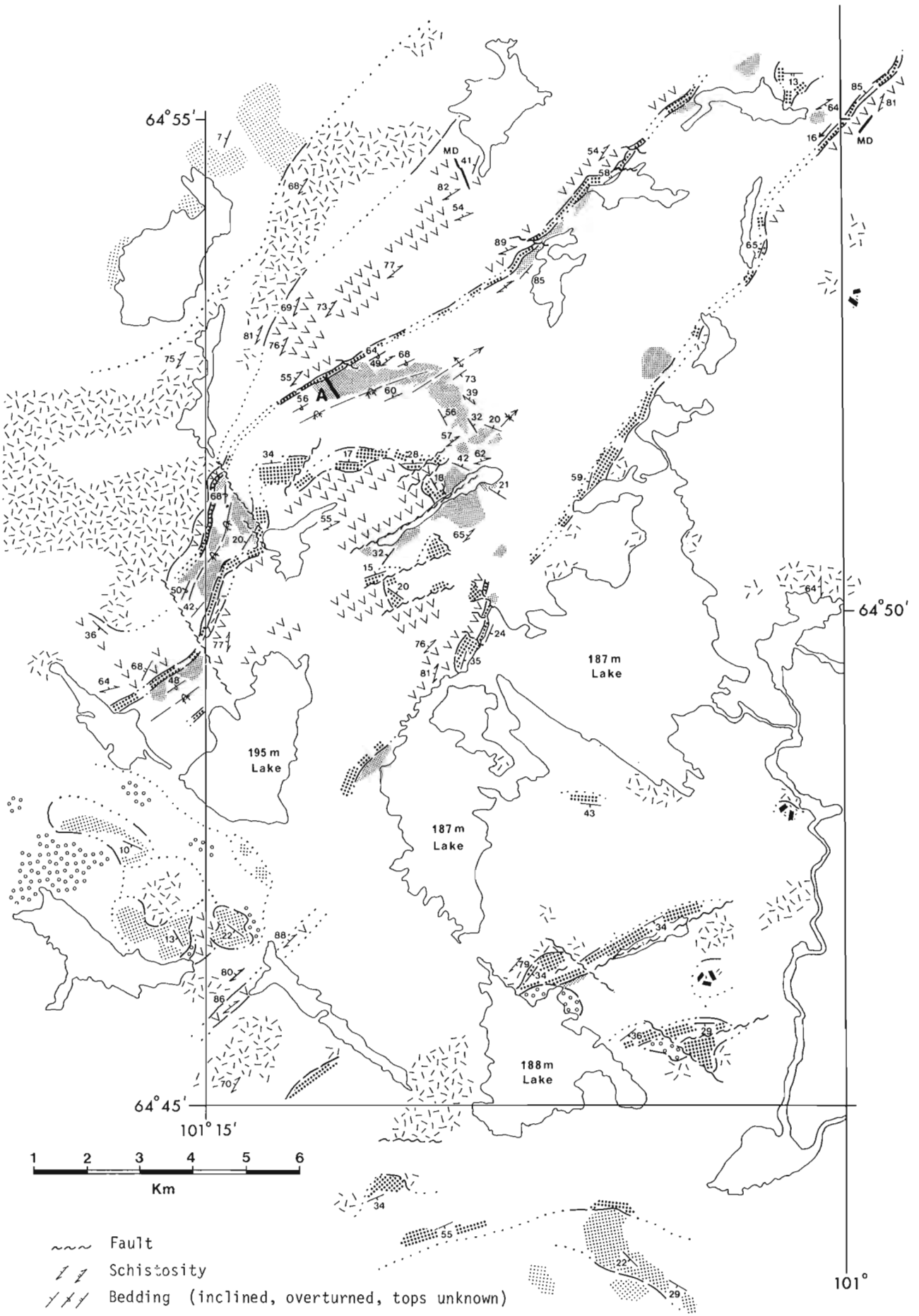
64°55′
64°50′
64°45′
101° 15′
101°
MD
MD
A
187 m Lake
195 m Lake
187 m Lake
188m Lake
1 2 3 4 5 6
Km
Fault
Schistosity
Bedding (inclined, overturned, tops unknown)
Geological Contact (defined, approximate)
Anticline
Syncline
Syncline (overturned)

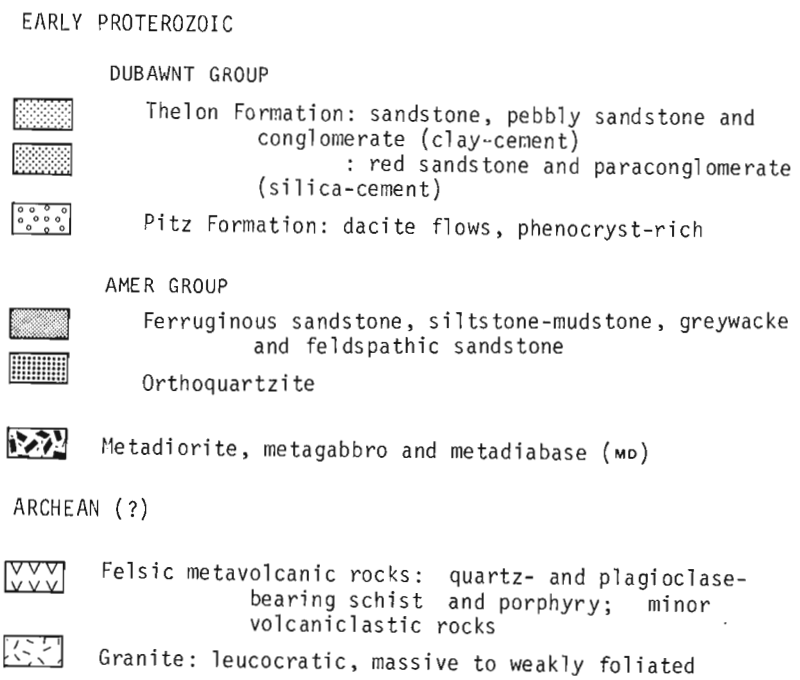

Figure 17.2

Geology of the Akiliniq Hills area. A marks the location of the measured section detailed in Figure 17.3. Patterns indicate approximate extent of outcrop and felsenmeer.

discontinuous homogeneous units 50-100 m thick. These were possibly sills or small lava domes within the pyroclastic sequence.

Age of pre-Amer group basement

Indirect evidence from adjacent map areas leads to tentative assignment of a late Archean age for both granite and felsic metavolcanic rocks in the Akiliniq Hills. Three preliminary U-Pb ages on zircons from igneous rocks unconformably overlain either by Amer group orthoquartzite or orthoquartzite-bearing sequences correlative with the Amer group cluster between 2.60 and 2.62 Ga (J.C. Roddick, personal communication, 1984). The units dated are: (1) massive leucocratic granite identical to the Akiliniq Hills granite from north of Sand Lake (Tella et al., 1984), (2) megacrystic gneissic granite from the northwest shore of Wharton Lake (LeCheminant et al., 1983) and (3) a weakly foliated quartz-feldspar porphyry similar to Akiliniq Hills porphyry from north of Pukiq Lake (LeCheminant et al., 1981). An age determination is in progress on a sample of red dacitic porphyry from the Akiliniq Hills.

Metabasic intrusions

Three small metadiorite-metagabbro bodies and two metadiabase dykes intrude pre-Amer group basement (Fig. 17.2). The only observed contact of a metagabbro exposes a fine grained, intensely fractured, carbonate-veined chilled margin against a medium grained red granite. Medium grained diabase dykes, 10-15 m wide, intrude felsic metavolcanic schists. The dykes retain well-defined chilled margins despite local development of weak to moderate foliation subparallel to country rock foliation. Gabbroic rocks and diabase have ophitic to subophitic textures. Relict cores of primary pyroxenes are only rarely preserved and plagioclase is intensely altered. The alteration assemblage consists of amphibole, chlorite, epidote, albite and sphene. Calcite-epidote-chlorite veins are abundant.

Tella et al. (1983) reported gabbro sills stratigraphically above orthoquartzite and mudstone-siltstone units of the Amer group in the Deep Rose Lake area. The degree of alteration and deformation of gabbroic rocks in the Akiliniq Hills area is consistent with post-Amer group intrusion; however, no intrusive relationships with the Amer group were observed.

Amer group – Akiliniq Hills area

In the Deep Rose Lake area, northeast of the Akiliniq Hills, the Amer group consists of a lower orthoquartzite, a transitional sequence of dolomitic limestone overlain by intercalated mudstone-siltstone, and an upper sequence of feldspathic sandstone, siltstone, mudstone and arkose (Tella et al., 1983, 1984). Abbreviated sequences exposed in the Akiliniq Hills area are thought to be part of the same clastic assemblage. Northwest of '187 m' Lake an 80-120 m thick white orthoquartzite outlines a complex northeast-trending fold structure (Fig. 17.2). The orthoquartzite is the basal unit of an otherwise largely immature clastic succession about 700 m thick. Orthoquartzite is conformably overlain by ferruginous red siliciclastic rocks, turbiditic greywacke-mudstone and feldspathic sandstone. Southeast of '187 m' Lake ridges of orthoquartzite are the only remnants of Amer group rocks. A single exception is a few metres of red ferruginous sandstone overlying orthoquartzite northeast of '188 m' Lake.

Only one section in near-continuous outcrop could be measured in rocks overlying the folded orthoquartzite northwest of '187 m' Lake (A, Fig. 17.2, 17.3). The overturned beds dip at about 60° to the northwest and are on the upper limb of an overturned syncline (Fig. 17.2). This section provides a reference for the following descriptions of major rock units.

Orthoquartzite

Ridges of massive and blocky white orthoquartzite are composed almost exclusively of fine- to medium-grained metamorphosed quartz arenite. Southeast of '187 m' Lake orthoquartzite unconformably overlies red granite. Granite within a few metres of the contact is intensely quartz veined and altered. Overlying quartzite is locally veined and brecciated suggesting some basement-cover slip during folding and/or faulting. Subparallel ridges expose 20 to 150 m thick orthoquartzite sections. Bedding consistently dips to the southeast, and all facing indications show the beds are upright.

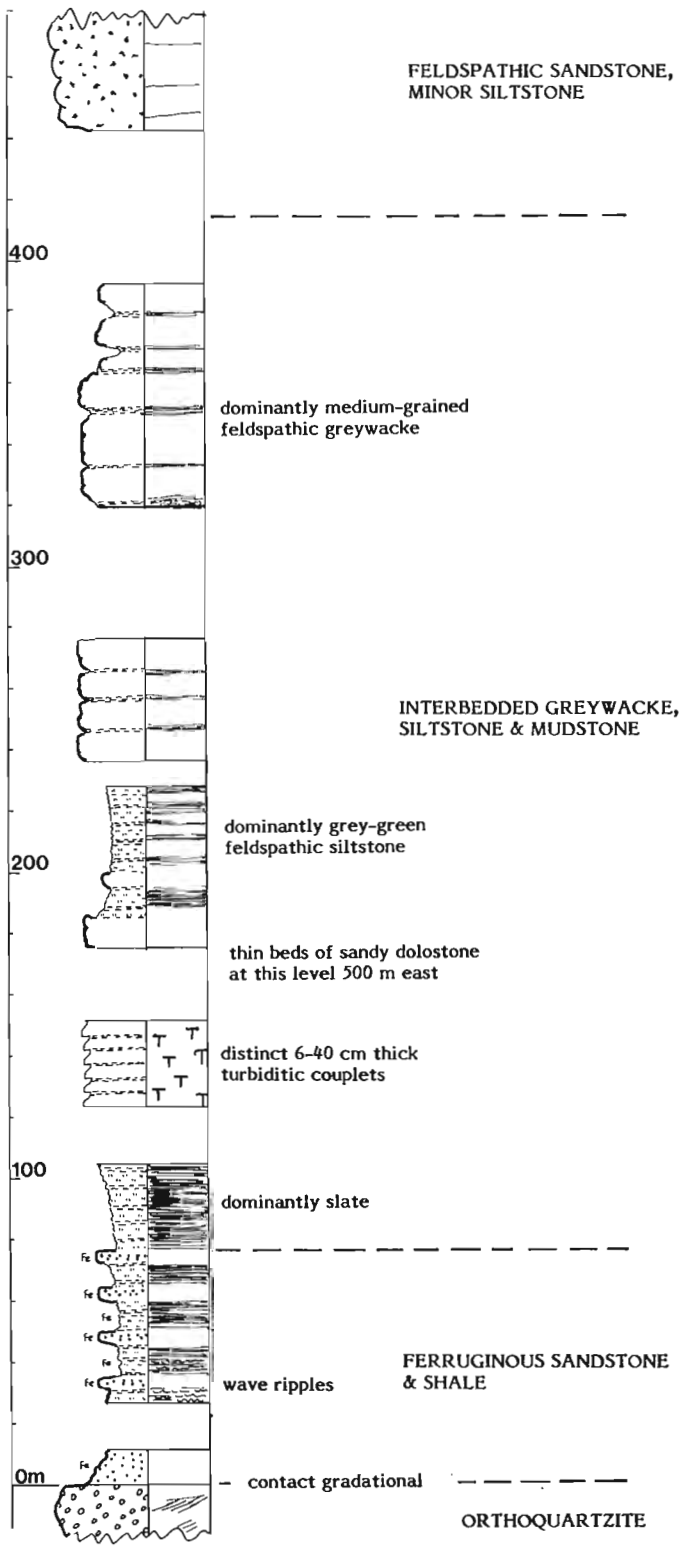

Figure 17.3. *Measured section in Amer group strata, Akiliniq Hills area (A, Fig. 17.2). Section measured by tape and 1.5 m Abney staff. Thickness in metres. Rock types - left column; sedimentary structures – right column.*

Northwest of '187 m' Lake an 80-120 m thick orthoquartzite unit is extensively folded and faulted. Contacts with underlying felsic metavolcanic schists are sharp. Intense deformation within schists adjacent to the contact and destruction of primary textures in the orthoquartzite suggest extensive basement-cover slip occurred during deformation.

Knox (1980) and Tella et al. (1983) mapped a much thicker orthoquartzite unit at the base of the Amer group in the Deep Rose Lake area and recognized a systematic variation from pink to white, grey or green in vertical sections. White orthoquartzite predominates in the Akiliniq Hills with discontinuous pink, purple and red varieties present near the base of the unit. No basal conglomerates were observed, but a few thin granule beds contain small pebbles of quartz and lithic fragments. Graded beds (0.5-2 mm grain size), low angle planar crossbedding and rippled parting surfaces provide rare evidence of stratification and facing. Asymmetric straight parallel current ripples have wavelengths of 4-6 cm and amplitudes of 1-1.5 cm. A single example of 2-10 cm scale herringbone crossbedding indicates alternating currents.

The orthoquartzite consists almost entirely of well sorted and well rounded silica-cemented quartz grains with only rare grains of zircon and opaques. More than 95% of the quartz grains are monocrystalline and many have dusty inclusion trails that are common in igneous quartz. One thin section shows bimodal sorting of well rounded quartz grains. Larger grains (average 1 mm) form a framework infilled by smaller grains (average 0.1 mm).

Regular thickness, lateral uniformity and extreme maturity of the Akiliniq Hills orthoquartzite suggests the unit was deposited after extensive weathering of a source area such as the underlying Archean(?) granite – felsic metavolcanic terrane. Sedimentary features are consistent with deposition in a shallow epicontinental sea. Bimodal sorting, considered evidence for aeolian processes by Folk (1968), may indicate nearshore environments periodically influenced by wind action.

Ferruginous siliciclastic unit

Distinctive red-brown siliciclastic rocks conformably overlie orthoquartzite and form a gradational unit between the orthoquartzite and overlying immature dark grey greywacke (Fig. 17.3). The unit is 50-80 m thick and shows a crude fining-upward trend. Current and wave rippled, fine- to medium-grained, ferruginous sandstone with thin hematitic shale partings is present near the base. Rare ripple laminations were noted near the base of overlying parallel laminated, interbedded ferruginous siltstone and mudstone. Thin sections show the sandstone is a poorly sorted, graded hematitic arkosic wacke with up to 40% feldspar.

A gradually deepening marine environment is inferred, contemporaneous with a marked change in rate of erosion in the source area. Deepening below wave base and influx of arkosic debris suggests significant contemporaneous tectonic activity. To the northeast, similar thin units of iron-rich mudstone and siltstone together with graphitic-pyritic shale overlie Amer group orthoquartzite (Knox, 1980; Patterson, 1981). These units are also thought to reflect a deepening marine depositional environment.

Turbiditic greywacke-mudstone unit

Grey to grey-green siltstone, mudstone and feldspathic greywacke comprise a poorly exposed succession about 300 m thick. Because the siltstones and mudstones tend to break along a pronounced slaty cleavage (Fig. 17.4) bedding plane features are rarely seen. The measured section shows a

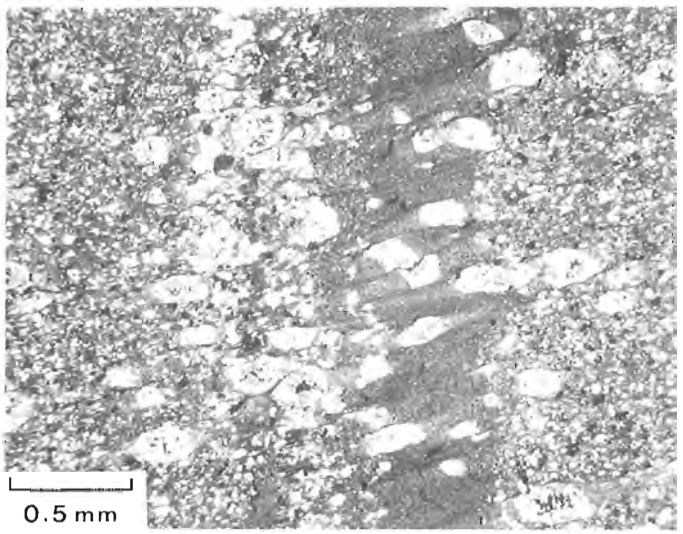

Figure 17.4. *Photomicrograph of slate from the hinge zone of a fold. Slaty cleavage is defined by narrow dark phyllosilicate-rich bands separated by quartz-rich domains. Quartz porphyroblasts (originally albite?) were rotated and offset during cleavage development.*

distinct coarsening- and thickening-upward character from deep-water thin laminated slates at the base, through various types of graded turbiditic couplets to thick-bedded medium grained feldspathic greywackes with subordinate mudstone near the top (Fig. 17.3). Although not exposed along the line of section several discontinuous 20-40 cm thick beds of massive brown-weathering sandy dolostone occur along strike at about the 180 m level.

Bouma cycles are well preserved between 120 and 150 metres. Cycles with poorly graded and ripple laminated 'B-C' subdivisions 5-20 cm thick are capped by massive 'E' subdivisions 2-40 cm thick. The lower parts of couplets are mostly fine- to medium-grained suggesting that the rhythmites are distal turbidites (Walker, 1979).

To the northeast Tella et al. (1983) and Knox (1980) also mapped a mainly siltstone-mudstone unit containing carbonates near the base at this stratigraphic level in the Amer group. Suggested thicknesses of 500 to 1000 m for the fine grained clastic rocks and up to 200 m for the carbonate are substantially greater than in the Akiliniq Hills. Knox (1980) interpreted the unit as a regressive sequence deposited in marine shelf to shallow marine and continental fluviatile settings. The slate to feldspathic turbiditic sequence in the Akiliniq Hills also suggests a shallowing marine environment which was infilled by immature detritus from a granitoid source.

Feldspathic sandstone unit

The uppermost unit in the Akiliniq Hills consists of grey, pink, and orange weathering thick-bedded feldspathic sandstone and minor siltstone. The pink- and orange-weathering beds are predominantly dolomite-cemented fine- to coarse-grained arkosic sandstone. A few beds are pyritic. A sequence about 200 m thick is poorly exposed in the core of a small northeast-plunging syncline 2 km northwest of '187 m' Lake.

In the Deep Rose Lake area the upper part of the Amer group consists of a thick siliciclastic sequence dominated by feldspathic sandstone and arkose (Tella et al., 1983). The incompletely exposed section in the Akiliniq Hills presumably correlates with the base of this upper clastic unit and probably is stratigraphically below the intertidal and fluvial assemblages in the Thelon River area, described in a subsequent section.

Metamorphism and structure

X-ray and petrographic studies of slates from the greywacke-mudstone unit northwest of '187 m' Lake indicate that the Amer group was metamorphosed to lowermost greenschist facies. Clay-sized fractions (<2 μ) separated from two slates were X-rayed to determine illite "crystallinity" (Kisch, 1983). Measured Δ 2 Θ values of 0.19 and 0.24° are within the greenschist field; the value of 0.24° is close to the anchizone-greenschist boundary of 0.25° proposed by Kubler (1968).

Slate contains the mineral assemblage quartz, iron-rich chlorite, illite, K-feldspar, albite and rutile. Silty layers contain more feldspar and less chlorite than adjacent pelitic mudstone laminae. A well developed slaty cleavage is defined by narrow (0.05 mm or less) dark phyllosilicate-rich bands separated by wider (0.25-0.3 mm) quartz-rich domains (Fig. 17.4). Small porphyroblasts (now quartz) that grew before cleavage development were rotated and offset during deformation. These porphyroblasts have an inclusion-rich core and poorly defined clearer rim. They may have formed as zoned authigenic albite during diagenesis and prograde metamorphism similar to albite porphyroblasts from pelitic schists studied by Otsuki (1980) and Eeckhout and Konert (1983).

Northwest of '187 m' Lake the basal orthoquartzite outlines a complex northwest-trending interference fold structure (Fig. 17.2). At the southwestern end of the structure a tight southeast-verging overturned first-phase syncline was refolded to expose metavolcanic schists beneath orthoquartzite in a shallow northeast-plunging anticlinal culmination. Second-phase folds have steep northwest-dipping axial surfaces. Apparent closure of the orthoquartzite to the northeast suggests a plunge reversal at the northern end of the structure. This is supported by fold mullions in orthoquartzite that plunge 16° southwest in northeasternmost outcrops.

A well-defined slaty cleavage in the mudstone-siltstone rhythmite (Fig. 17.4) was folded with the limbs of the first-phase syncline. A steep dipping weak second cleavage is locally apparent in hinge zones of second-phase folds. Later deformation produced a weak crenulation cleavage in the rhythmite unit associated with small northwest-trending open folds. Parallel northwest faults offset all units.

Major folding is not discernible in isolated orthoquartzite ridges southeast of '187 m' Lake. Upright orthoquartzite beds dip shallowly southeast and primary structures are locally well preserved. Orthoquartzite distribution is controlled by northeasterly trending faults offset by late northwesterly trending faults.

Granite is directly overlain by orthoquartzite southeast of '187 m' Lake, whereas to the northwest metavolcanic rocks generally separate the granite from folded Amer group rocks. This major change within the map area is marked by a 110 m wide flinty red quartz-feldspar-bearing tectonite with a strong vertical 050° foliation. This narrow unit occurs within a weakly foliated granite southwest of '187 m' Lake (Fig. 17.2). A volcanic protolith is indicated by quartz and feldspar crystals that have retained subhedral and embayed margins. This strongly deformed metarhyolite is on strike with the northeast trending Chantrey Mylonite Zone (Fig. 17.1) and may represent a segment of the zone. To the northeast the Chantrey Mylonite Zone has a pronounced linear aeromagnetic anomaly. Mylonite has been mapped from southwest of Sand Lake to east of Lower Garry Lake (Tella et al., 1984).

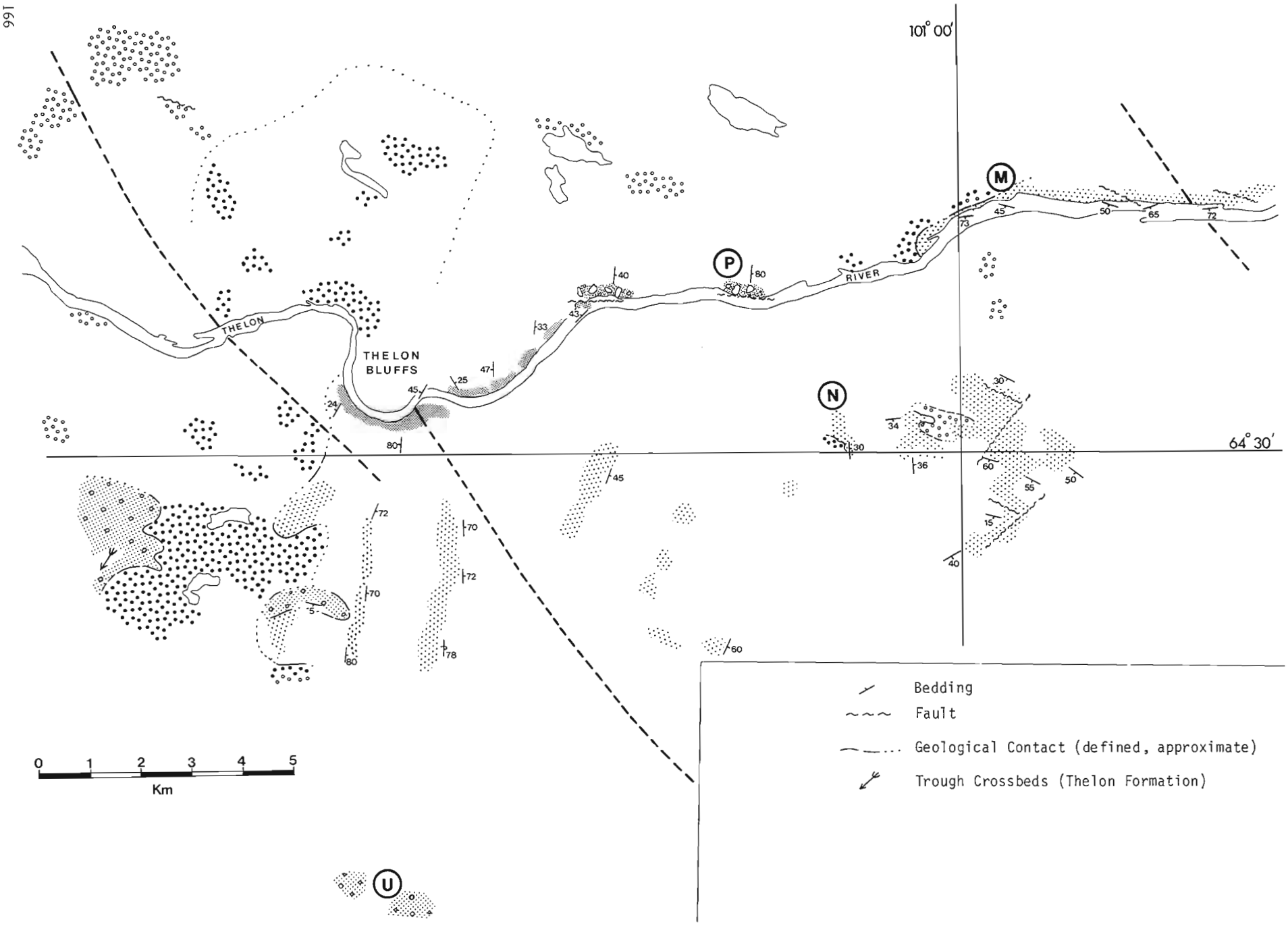
101° 00'
64° 30'
M
P
N
U
THELON
THELON BLUFFS
RIVER
0 1 2 3 4 5
Km
Bedding
Fault
Geological Contact (defined, approximate)
Trough Crossbeds (Thelon Formation)

MIDDLE PROTEROZOIC

Mackenzie Diabase (observed, aeromagnetic anomaly)

EARLY PROTEROZOIC

DUBAWNT GROUP

Thelon Formation: sandstone, pebbly sandstone and conglomerate

Pitz Formation: dacite flows, phenocryst-rich; minor rhyolite
: subvolcanic dacite porphyry

AMER GROUP

Sequence C: arkose, pebbly sandstone and conglomerate

Sequence B: feldspathic wacke, siltstone-mudstone and conglomerate

Sequence A: quartz arenite; minor conglomerate and siltstone

Figure 17.5

Geology of the Thelon River area. P and M are the locations of measured sections detailed in Figure 17.6 and 17.12. Localities N and U are mentioned in text. Patterns indicate approximate extent of outcrop and felsenmeer.

Amer group – Thelon River area

Deformed sedimentary rocks are exposed along the Thelon River west of Beverly Lake and in hills to the south (Fig. 17.5). The rocks here have better preserved primary features than Amer group units in the Akiliniq Hills, and do not contain a penetrative tectonic fabric. Illite "crystallinity" values in mudstones ($\Delta 2\theta = 0.25°, 0.27°$) indicate anchizone-grade metamorphism, just below lowermost greenschist facies conditions. A comparative study of the Thelon River metasediments and Amer group rocks in the Deep Rose Lake area suggests that only upper units of the Amer group are exposed along the river (Smith, 1984). No pre-Amer group basement occurs in the area mapped.

Despite examination of all major outcrops along the Thelon River and in hills to the south it was not possible to resolve the structure and relative stratigraphic position of the isolated and faulted successions. For convenience of description, the Amer group rocks are subdivided into three informal sequences: A, B and C.

Sequence A

Sequence A is exposed in two separate areas along the north bank of the Thelon River about 6 km east of Thelon Bluffs (Fig. 17.5). Here, the river course is probably controlled by a major east-trending fault zone. Silicified near-vertical fault and breccia zones, trending 095-115° and up to 1 m wide, cut both outcrop areas. The largest of these zones has an 18 m left lateral displacement.

A near vertical 120 m-thick section near the eastern limit of outcrop (P, Fig. 17.5) comprises mainly grey-green quartz arenite with a few thin interbeds of red-brown mudstone and siltstone (Fig. 17.6). Quartz arenite is fine- to coarse-grained and medium- to thick-bedded, but primary structures are poorly preserved in the lower 80 m due to intense silicification. Quartz arenite near the top of the section is planar crossbedded, with sets 10-40 cm thick. One large solitary set 1.5 m thick is preserved at 108 m. The quartz arenite is interbedded with 5-10 m thick intervals of reddish brown laminated or massive mudstone and siltstone. Between 98 and 108 m graded couplets of siltstone-mudstone pass upwards into a massive matrix-supported pebbly mudstone which is abruptly overlain by the large-scale crossbedded quartz arenite. The uppermost 5 m of silicified pebble-cobble conglomerate is truncated by a fault. Clasts up to 50 cm in diameter consist of white quartzite, vein quartz, brown siltstone, granite, feldspar porphyry and jasper; median size is 5-10 cm, and most clasts are well rounded.

Silicified quartz arenite and rare mudstone occur in the western outcrop area. Most rocks appear massive and stratification is difficult to discern. Small-scale cross-stratification suggests that the beds face east. Mesoscopic tight folds are indicated by Z-shaped mudstone lenses, 1-2 m thick, that pinch out laterally over a few metres.

Sedimentary features within sequence A are not sufficiently diagnostic to unambiguously define depositional environments. The thick intervals of mature quartz arenite could have been deposited in a uniform high-energy environment such as a shelf sea. However, the association of this facies with conglomerate, graded siltstone-mudstone couplets and pebbly mudstone suggests a more complex environment. A mixed fluvial regime with proximal alluvial fan, braided channel and fluvial plain subenvironments is more likely.

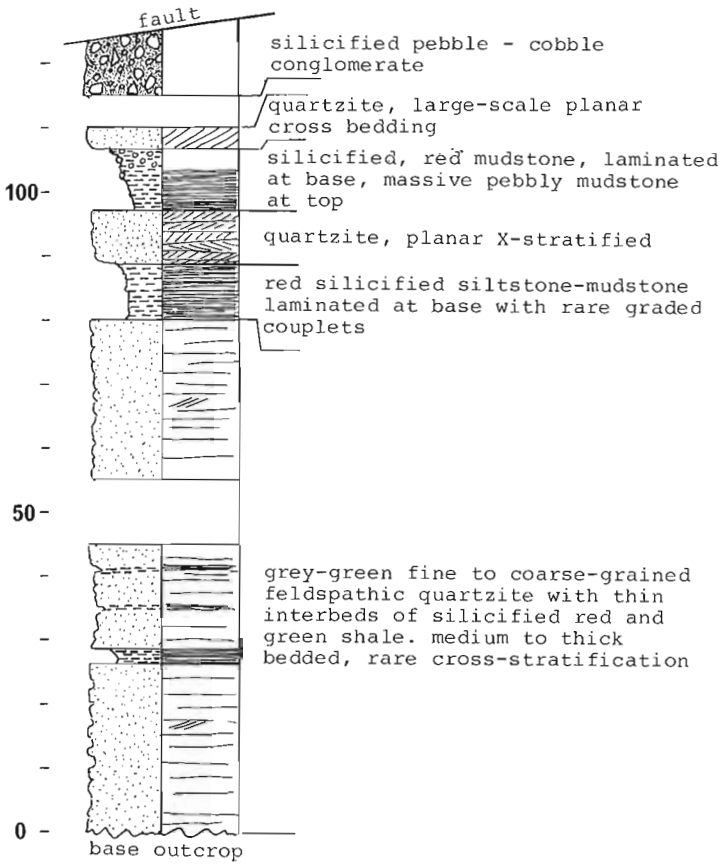

Figure 17.6. *Measured section in part of sequence A, north shore Thelon River (P, Fig. 17.5). Thickness in metres, section measured by pacing.*

Sequence B

This sequence includes the bulk of Amer group outcrops in the Thelon River area (Fig. 17.5). In the northeast river-washed exposures form an 8 km long belt of semicontinuous outcrop along the north shore of the Thelon River. Because south dipping beds strike parallel to the river only a few tens of metres of section is exposed. More extensive and continuous outcrops with at least 500 m of section are exposed on high ridges about 3 km south of the river. Bedding in this area defines a southeast-trending open syncline which has been modified by a set of northeast- and northwest-trending faults. Farther to the west steep dipping east-facing sequences outcrop on ridges and along northflowing tributaries of the Thelon River.

Sequence B consists of three dominant rock types: (1) reddish brown fine- to coarse-grained poorly sorted feldspathic wacke, (2) dark reddish brown siltstone-mudstone, and (3) pale pink, medium- to coarse-grained quartz arenite. The relative proportions of these three end members and the types of stratification vary from area to area producing four distinctive facies: (1) mudcracked rhythmite, (2) crossbedded sandstone, (3) festoon-bedded siltstone, and (4) massive facies.

Outcrops along the north bank of the Thelon River are almost entirely of mudcracked rhythmite facies. This facies consists of thinly interbedded feldspathic quartz wacke and red siltstone-mudstone. Some beds form graded couplets, indicating deposition from gradually waning traction currents, whereas others have sharp bed contacts suggesting rapid alternation of deposition from traction currents and deposition from suspension in slack water. Bedding, though

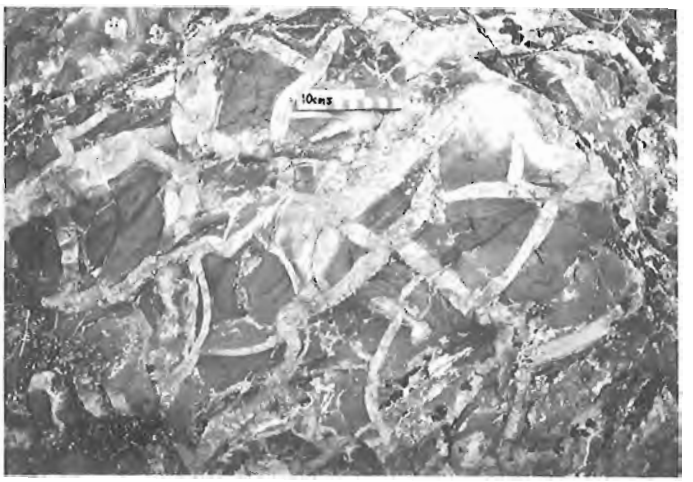

Figure 17.7. *Bedding plane surface of mudcracked rhythmite facies, sequence B, Thelon River (M, Fig. 5). Red mudstone bed (dark grey) disrupted by polygon-patterned injection of sandstone dykes. (GSC 204114-U)*

Figure 17.8. *Vertical section of rocks shown in Figure 17.7, illustrating the discontinuous stratification characteristic of this facies. (GSC 204114-T)*

mostly parallel, is noticeably wavy and discontinuous; the latter results in part from extensive sandstone injection through siltstone beds (Fig. 17.7, 17.8), but loading, desiccation (Fig. 17.9) and irregular erosion of beds is also common. Rare centimetre-scale channels and thin flaser-bedded intervals contribute to the discontinuous stratification. Some beds consist of large polygonal mudstone clasts (Fig. 17.7) separated by sandstone dykes up to 5 cm wide (Fig. 17.8).

Cross-stratification includes tabular, planar, trough and herringbone varieties; sets are commonly a few centimetres thick. Form sets (i.e. retaining original ripple morphology on upper surfaces) indicate that the cross-stratification was produced by a variety of slightly sinuous, lingoid and catenary ripples. Most ripples have wavelengths of 1-5 cm and amplitudes of 0.5-1 cm, although ripples up to 15 by 3 cm were seen. Symmetric and asymmetric ripples are equally common. Measurements from four outcrops along the river

Figure 17.9. *Section through three graded beds at locality M. Note angular desiccation and injection by sand of dark mudstone layers. Pen is 10 cm long. (GSC 204114-C)*

are shown in Fig. 17.10. Although orientations of the symmetric ripples show wide divergence, the current ripples reflect mostly west-southwest paleocurrents, with a few in the reverse direction. Interference ripples (Fig. 17.11; orientations not included in Fig. 17.10) probably formed in a shallow water environment characterized by interplay of waves and currents.

Thin and regular interbedding of coarse crossbedded sand with clay and silt indicates deposition from active migrating sandy bedforms alternating with deposition from suspension in quiet water. Discontinuous stratification, mudcracks, shale rip-ups and scours suggest a shallow water environment prone to frequent emergence and desiccation. Intertidal or fluvial environments are the most likely alternatives. A wide range in paleocurrents, local herringbone crossbedding, and an abundance of interference ripples, coupled with a lack of fining-up cycles and large channels, strongly support an intertidal – tidal flat environment.

A section measured near the western end of the outcrop belt (M, Fig. 17.5) shows large-scale cyclicity superimposed on centimetre- to decimetre-scale interbedding of fine- and coarse-grained rocks (Fig. 17.12). Larger cycles consist of mudstone-dominated intervals 1-2 m thick and thicker sandstone dominated intervals. These cycles are similar in scale and character to coarsening-up, shoaling cycles typical of prograding marginal marine clastic environments (Reading, 1978) and are tentatively interpreted as such.

In the central part of the area (N, Fig. 17.5), facies 1 rhythmites are interbedded with facies 2 sandstones. Facies 2 consists of pink quartzitic sandstone in beds 1 to 3 m thick. Internally, these beds are parallel-laminated or crosslaminated. Beds are laterally persistent, over the outcrop length of 200 m, but in places they have wavy bases channelled into the underlying facies 1 (Fig. 17.13). The sandstones probably were deposited in part from migrating sandy bedforms in shallow channels eroded into the intertidal facies. Because they lack evidence of desiccation, they probably represent slightly deeper distributary channel deposits. Paleocurrent measurements, mainly from facies 1 with a few from facies 2, display a wide range of directions at locality N (Fig. 17.14). Current ripples and cross-stratification are mostly northerly directed, in contrast to west-southwest trends along the Thelon River (Fig. 17.10).

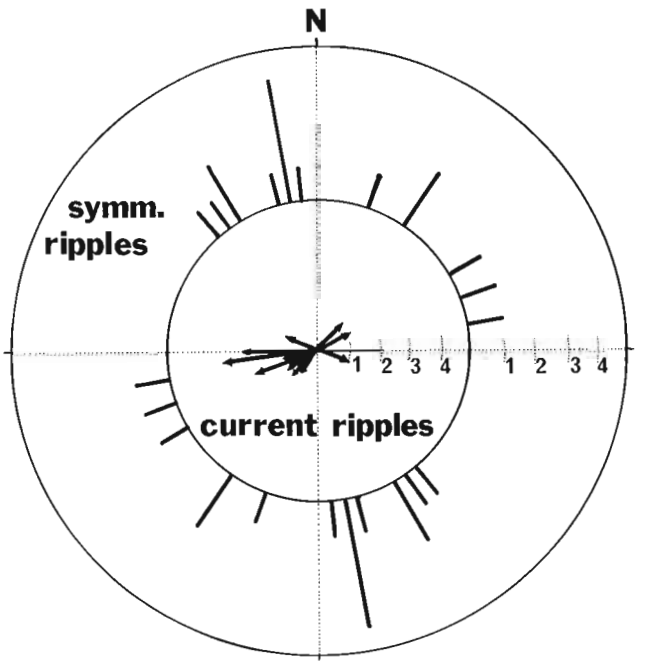

Figure 17.10. *Rose diagram of paleocurrents based on current ripples (inner circle, 15 readings) and orientations of the crests of symmetrical ripples (outer ring, 16 readings). Mudcracked rhythmite facies, sequence B, Amer group, Thelon River.*

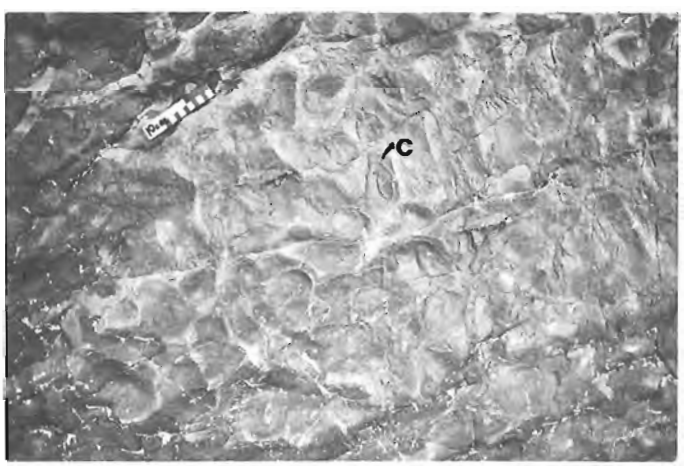

Figure 17.11. *Interference ripple marks and curved desiccation cracks ('C') on bedding surface of mudcracked rhythmite facies at locality M. (GSC 204114-V)*

Two other facies (festoon-bedded and massive) occur in the large outcrop area southeast of N. The festoon-bedded siltstone facies consists largely of reddish brown siltstone and mudstone with thin beds of fine grained sandstone. The siltstone and mudstone resemble finer interbeds in the rhythmites, but shallow water and erosional features characteristic of the intertidal facies are absent. Small-scale trough cross-stratification and vague concave-up structures (poorly preserved troughs?) were the main sedimentary structures noted. Indistinct crossbedding is visible in some thin sandstone interbeds. At two localities,

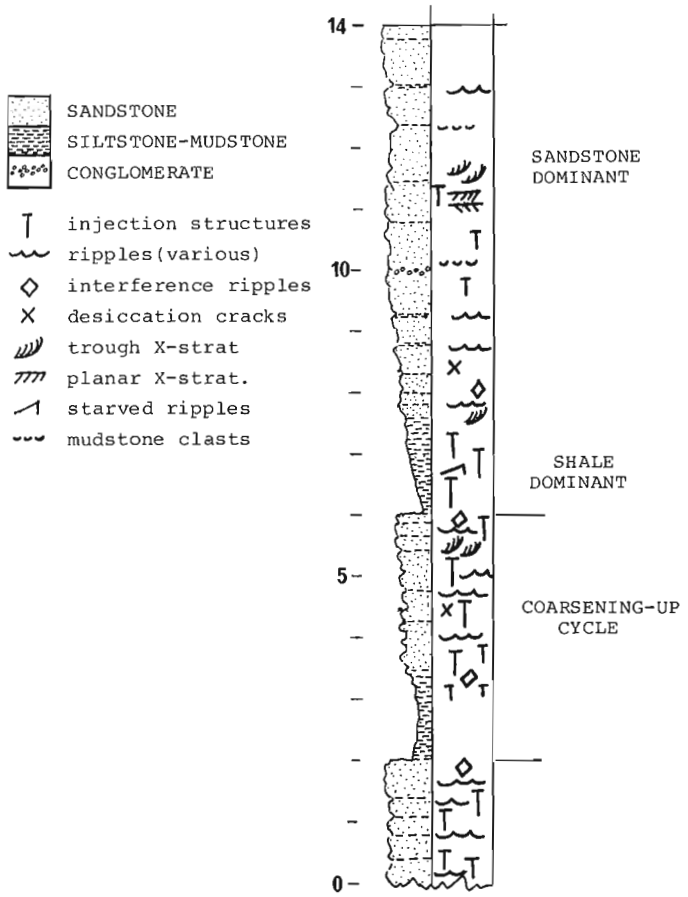

Figure 17.12. *Measured section in mudcracked rhythmite facies (M, Fig. 17.5). Thickness in metres. Section measured by 1.5 m staff and tape.*

uniform festoon crossbedded sequences of siltstone-mudstone tens of metres thick were seen. These presumably indicate continuous sedimentation from small linguoid ripples. The massive facies is formed of monotonous intervals of indistinctly bedded fine grained silty wacke or sandy siltstone. These thick sequences (to 500 m) lack obvious sedimentary structures, and even stratigraphic facing was difficult to determine.

Outcrop ridges and tributary streams southwest of locality N expose steeply dipping east-facing sequences of red-brown siltstone and mudstone, minor interbedded rippled feldspathic sandstone, and rare quartz pebble conglomerate (Fig. 17.5). Absence of desiccation and sandstone injection features indicates a correlation with rocks at locality N rather than those along the north shore of the Thelon River.

Sequence C

This unit consists mainly of red conglomeratic siliciclastics that are exposed along a 6 km stretch of the Thelon River south and east of Thelon Bluffs (Fig. 17.5). The unit is apparently faulted against sequence A; nowhere is it in contact with the fine siliciclastic rocks of sequence B. Dip reversals and variable bedding attitudes suggest that the sequence is folded, but no outcrop-scale folds were observed.

The main rock types are fine- to very coarse-grained feldspathic sandstone, arkose, pebbly sandstone and pebble to cobble conglomerate. Clasts are mostly white quartzite and red sandstone (maximum 60 cm), but small angular red mudstone clasts are also common, especially on the foresets of cross-stratification. Trough crossbedding in sets from a few centimetres up to 2 m are present, along with rare wedge-planar sets. Other sedimentary structures include graded beds, reduction spots, small-scale channels, and ripple

Figure 17.13. *Cliff section of interbedded rhythmite facies (R) and crossbedded sandstone facies (S). Geologist is 1.6 m tall. 'Massive' area above geologist is a Pitz Formation porphyry intrusion.*

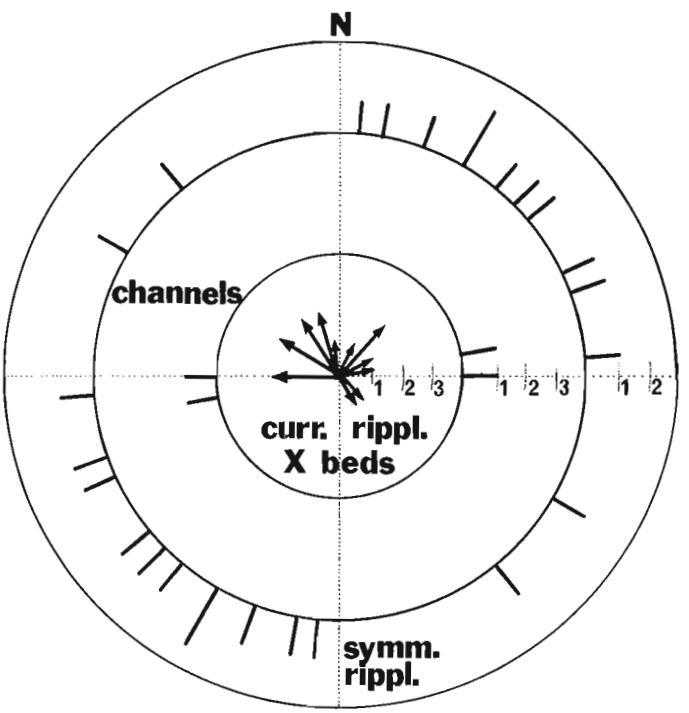

Figure 17.14. *Rose diagram of paleocurrent measurements at locality N (Fig. 17.5). Paleocurrent directions from current ripples and crossbeds (centre circle, 16 readings), channel axes (inner ring, 2 readings); and crestal trends of symmetrical ripples (outer ring, 13 readings).*

marks. Paleocurrent measurements within individual outcrops show a range of directions. Based on a few observations westerly and southerly paleocurrents appear to have prevailed.

Conglomerate beds in one well exposed 50 m thick section display a gradual up-section reduction in mean clast size from about 30 cm to about 5 cm. Contacts between conglomeratic and sandy units are mostly gradational. Thin siltstone interbeds possibly were the source of angular clasts on foresets of the crossbedded sandstone. Deposition of this sequence most likely occurred in a braided fluviatile-alluvial fan environment. The sequence closely resembles lower Dubawnt Group units deposited in similar environments, such as the Kunwak Formation (LeCheminant et al., 1981) and the South Channel and Kazan formations (Donaldson, 1965). Steep dips and apparent folding of sequence C, and the absence of volcaniclastic sediments, suggests that correlation with the upper Amer group is more likely.

Pitz Formation

Pitz Formation subaerial flows and subvolcanic porphyry intrusions in both the Akiliniq Hills and Thelon River areas are predominantly dark red-brown dacites that contain abundant feldspar phenocrysts and less than 5% small quartz eyes. Horizontal joint sets are prominently developed in the rubbly weathering outcrops. Zones of kaolinization with extensive quartz, quartz-chalcedony and calcite veins and stockworks are abundant. Sills and dykes are closely associated with flows of similar composition and phenocryst content, making distinction between intrusive and extrusive rocks locally uncertain.

The largest prophyry intrusion is a northeast-trending body approximately 4 km wide and more than 12 km long exposed north and southwest of Thelon Bluffs (Fig. 17.5). The porphyry contains 25-35% feldspar phenocrysts (to 2 cm), 3-5% altered mafic phenocysts (to 5 mm) and up to 2% quartz eyes (to 3 mm) set in a dark red-brown fine grained matrix. Rimmed and sieve-textured plagioclase phenocrysts are subordinate to ovoid and tabular red K-feldspar phenocrysts. Mafic phenocrysts are replaced by chlorite and carbonate and are spatially associated with clusters of magnetite and hollow-centred apatite needles. The matrix has a micrographic radial crystallization pattern of quartz and K-feldspar that nucleated symmetrically around small quartz eyes.

Grey calcic plagioclase megacrysts to 10 cm are sparsely distributed throughout the body. The megacrysts are commonly rimmed by K-feldspar with apatite-magnetite-mafic phenocryst clusters scattered along the core-rim interface. Similar large plagioclase megacrysts occur as xenocrysts in the Pamiutug Granite where they crystallized in ferrodioritic magma that mixed with the granitic magma (LeCheminant, 1982; Booth, 1983). Mixed magma interactions in the intrusive prophyry at Thelon Bluffs, as indicated by calcic xenocrysts, are further suggested by disequilibrium textures such as multiply rimmed feldspar phenocrysts, sieve textures and clusters of quench apatite needles.

The porphyry intrudes Amer group sandstone south of Thelon Bluffs and is flanked to the north by dacitic flows that include vesiculated crystal tuff. The pinkish brown tuff contains abundant broken and euhedral K-feldspar phenocrysts and rare quartz eyes set in an aphanitic matrix. Flattened vesicles are filled by quartz, chlorite and specularite. Devitrification recrystallization in the original glass-rich matrix crosses boundaries of poorly preserved shards.

A porphyry with flow and vesicular textures, exposed on the north shore of the Thelon River 10 km east of Thelon Bluffs, has a sheared and kaolinized intrusive contact with Amer group siltstone and mudstone. Internally the porphyry contains massive zones tens of metres wide separated by 1 to 3 m wide curved near-vertical zones of aligned phenocrysts associated with elongated vesicles that are partly filled by quartz, chalcedony and fluorite. Phenocryst proportions are identical to the Thelon Bluffs intrusion, including plagioclase megacrysts to 8 cm. One xenolith of red gneissic granite (1.3 m in diameter) and another of fine grained pink massive granite (0.7 m) suggest that a granitic basement underlies Amer group rocks in the Thelon River area.

Thelon Formation and sub-Thelon saprolite

Basal siliciclastic rocks of the Thelon Formation have been interpreted as mainly continental alluvial fan-braided fluvial deposits (Donaldson, 1969; Cecile, 1973). A distinctive map unit at the base of the Thelon Formation in the Aberdeen Lake area is inferred to have been deposited during active tectonism (LeCheminant et al., 1983). This unit is characterized by red-matrix paraconglomerate and silica-cemented lithic sandstone. In the Akiliniq Hills area, similar successions of shallow dipping red sandstone and paraconglomerate occur southwest of '187 m' Lake and southeast of '188 m' Lake (Fig. 17.2). These successions unconformably overlie silicified saprolite zones in metavolcanic schist, brecciated and quartz-veined orthoquartzite and kaolinized Pitz Formation dacite.

Sections consist of up to 20 m of red-orange extremely well indurated feldspathic and pebbly lithic sandstone capped by up to 30 m of polymictic paraconglomerate. The medium grained sandstones are thin- to medium-bedded with rare asymmetric ripples and indistinct crossbedding. Overlying massive to thick-bedded conglomerate contains clasts (maximum 35 cm, mean about 10 cm) of quartzite, Pitz Formation porphyry and sandstone set in a red sandy matrix. Massive unsorted beds contain subangular sandstone clasts similar to the basal sandstone. The unit is interpreted as alluvial fan deposits, partly of debris flow origin, associated with syndepositional faulting.

Other Thelon Formation successions exposed in the Akiliniq Hills and Thelon River areas are conglomerate and clay-cemented sandstone. Thin successions of flat-lying to gently dipping orthoconglomerate, pebbly sandstone and sandstone cap hills south and southwest of Thelon Bluffs (Fig. 17.5). The pale pink- to white-weathering beds overlie intensely hematized and clay-altered Pitz Formation and Amer group rocks. Basal units of intact framework conglomerate are less than 10 m thick. They contain well rounded orthoquartzite and vein quartz clasts to 30 cm and less abundant smaller clasts of quartz-feldspar porphyry, silcrete, and red sandstone, siltstone and mudstone. Overlying sandstone is well sorted and contains trough crossbeds in sets 1-3 m thick. Paleocurrent data display moderate dispersion about a southwesterly trend.

A well defined $\varepsilon U/K$ and $\varepsilon U/\varepsilon Th$ ratio anomaly (GSC Map 35366G) occurs 10-15 km south of Thelon Bluffs, just north of Spruce Grove Lake. The anomaly is in a flat drift-covered region containing small patches of Thelon Formation felsenmeer (U, Fig. 17.5). The felsenmeer contains numerous slabs of maroon to red U-enriched phosphatic sandstone and pebbly conglomerate. The occurrence is similar to other uranium-phosphorous associations in the Thelon Formation and underlying saprolites described by Miller (1983). Autoradiographs of mineralized sandstone and conglomerate show indistinct clouding in phosphate-cemented areas, and rare narrow rims of higher uranium content along clast boundaries. Sandstones contain up to 45% apatite and hematite interstitial to framework quartz grains. Embayed margins of these quartz grains indicate that the quartz has been partly replaced by apatite. Fine hematite selectively replaced specific framework clasts and larger hematite crystals fill interstitial voids that remained after apatite deposition.

There was some migration of phosphatic brines (Miller, 1983) into underlying Amer group sandstone. At locality N (Fig. 17.5) goyazite and white mica partly replace the matrix and altered feldspar grains in hematized facies 2 sandstone. Other phosphate occurrences are to be expected especially in structurally controlled zones where groundwaters were able to penetrate below the sub-Thelon unconformity.

Acknowledgments

The authors thank J.G. Pianosi for his cheerful and capable field assistance and G.M. LeCheminant for careful X-ray diffraction and microprobe investigations. Subhas Tella was extremely helpful and co-operative both in the field and in subsequent discussions. J.A. Donaldson received logistical support from the Geological Survey of Canada and the Geology Office, DIAND.

References

Booth, G.W.
1983: The petrology and geochemistry of the Pamiutuq Lake batholith, Northwest Terrritories; unpublished M.Sc. thesis, University of Toronto, 176 p.

Cecile, M.P.
1973: Lithofacies analysis of the Proterozoic Thelon Formation, Northwest Territories (including computer analysis of field data); unpublished M.Sc. thesis, Carleton University, 119 p.

Chiarenzelli, J.R.
1983: Mid-Proterozoic chemical weathering, regolith, and silicate in the Thelon Basin, Northwest Territories; unpublished M.Sc. thesis, Carleton University, 197 p.

Donaldson, J.A.
1965: The Dubawnt Group, Districts of Keewatin and Mackenzie; Geological Survey of Canada, Paper 64-20.

1969: Descriptive notes (with particular reference to the late Proterozoic Dubawnt Group) to accompany a geological map of central Thelon Plain, Districts of Keewatin and Mackenzie (65M, NW1/2, 66B,C,D, 75P, E1/2); Geological Survey of Canada, Paper 68-49, 4 p., Map 16-1968.

Eeckhout, B. v.d. and Konert, G.
1983: Plagioclase porphyroblast growth and its relation to deformation in the Alhamilla unit (Sierra Alhamilla, Betic Cordilleras, SE Spain); Journal of Metamorphic Geology, v. 1, p. 227-249.

Folk, R.L.
1968: Bimodal supermature sandstones. Product of the desert floor; XXIII International Geological Congress, Proceedings v. 8, p. 9-32.

Kisch, H.F.
1983: Mineralogy and petrology of burial diagenesis (burial metamorphism) and incipient metamorphism in clastic rocks; in Diagenesis in Sediments and Sedimentary Rocks, 2, ed. G. Larson and G.V. Chilingar; Developments in Sedimentology 25B, p. 289-494.

Knox, A.W.
1980: The geology and mineralization of the Aphebian Amer Group, southwest of Amer Lake, District of Keewatin, N.W.T.; unpublished M.Sc. thesis, University of Calgary, p. 207.

Kubler, B.
1968: Evaluation quantitative du métamorphisme par la cristallinité de l'illite; Bulletin du Centre de Recherches de Pau-Société Nationale des Pétroles d'Aquitaine, v. 2, p. 358-397.

LeCheminant, A.N.
1982: Magma mixing in lamprophyres and granites, central District of Keewatin; Geological Association of Canada – Mineralogical Association of Canada, Program with Abstracts, v. 7, p. 62.

LeCheminant, A.N., Iannelli, T.R., Zaitlin, B., and Miller, A.R.
1981: Geology of Tebesjuak Lake map area, District of Keewatin: A progress report; in Current Research, Part B, Geological Survey of Canada, Paper 81-1B, p. 113-128.

LeCheminant, A.N., Ashton, K.E., Chiarenzelli, J., Donaldson, J.A., Best, M.A., Tella, S., and Thompson, D.L.
1983: Geology of Aberdeen Lake map area, District of Keewatin: preliminary report; in Current Research, Part A, Geological Survey of Canada, Paper 83-1A, p. 437-448.

Miller, A.R.
1983: A progress report: uranium-phosphorus association in the Helikian Thelon Formation and sub-Thelon saprolite, central District of Keewatin; in Current Research, Part A, Geological Survey of Canada, Paper 83-1A, p. 449-456.

Otsuki, M.
1980: Notes on petrography and rock-forming mineralogy (7) zonal structure of albite porphyroblast from basic Sanbagawa schists in central Shikoku; Japanese Association of Mineralogists, Petrologists and Economic Geologists, Journal, v. 75, p. 196-202.

Patterson, J.G.
1981: Amer Lake: an Aphebian fold and thrust complex; unpublished M.Sc. thesis, University of Calgary, 106 p.

Reading, H.G.
1978: Sedimentary Environments and Facies, Oxford, Blackwell Scientific Publishers, 576 p.

Smith, S.L.
1984: Sedimentology of Amer group rocks, District of Keewatin, Northwest Territories; unpublished B.Sc. thesis, Carleton University, 60 p.

Tella, S., Ashton, K.E., Thompson, D.L., and Miller, A.R.
1983: Geology of the Deep Rose Lake map area, district of Keewatin; in Current Research, Part A, Geological Survey of Canada, Paper 83-1A, p. 403-409.

Tella, S., Thompson, D.L., and James, D.T.
1984: Geology of parts of the Deep Rose Lake and Pelly Lake map area, District of Keewatin; in Current Research, Part A, Geological Survey of Canada, Paper 84-1A, p. 313-322.

Tippett, C.R. and Heywood, W.W.
1978: Stratigraphy and structure of the northern Amer group (Aphebian), Churchill Structural Province, District of Keewatin; in Current Research, Part B, Geological Survey of Canada, Paper 78-1B, p. 7-11.

Walker, R.G.
1979: Facies model 8. Turbidites and associated coarse clastic deposits; in Facies Models, ed. R.G. Walker; Geoscience Canada, Reprint Series 1, p. 91-103.

18.

LAKE BOTTOM HEAVE IN PERMAFROST; ILLISARVIK DRAINED LAKE SITE, RICHARDS ISLAND, NORTHWEST TERRITORIES

Project 680047

J. Ross Mackay[1]
Terrain Sciences Division

Mackay, J.R., Lake bottom heave in permafrost; Illisarvik drained lake site, Richards Island, Northwest Territories; in Current Research, Part B, Geological Survey of Canada, Paper 84-1B, p. 173-177, 1984.

Abstract

In August 1978 a lake (Illisarvik Lake) was artificially drained in a co-operative experiment to study permafrost growth under full-scale natural conditions. Two components of the research are: 1) the measurement of ground temperatures at the northeastern end of the drained lake in order to study the growth of permafrost and 2) the survey of 10 and 20 m-long bench marks installed in the lake bottom to study lake bottom heave arising from permafrost growth. An examination of the first inflexion point in the temperature profile below 0°C shows that the pore water in the lake bottom sands freezes at -0.04°C. Temperature measurements combined with survey data indicate the progressive freezing of unfrozen pore water to at least -0.5°C and some freezing even below -1.0°C. The field evidence from Illisarvik indicates that in closed system freezing, heave may continue for years to decades or even centuries in warm permafrost because of the progressive freezing of unfrozen pore water.

Résumé

En août 1978, un lac (le lac Illisarvik) a été asséché de façon artificielle à l'occasion d'une expérience collaborative visant à étudier l'évolution du pergélisol dans des conditions naturelles et à échelle réelle. Les deux éléments de la recherche sont les suivants: 1) la mesure des températures au sol à l'extrémité nord-est du lac asséché afin d'étudier la croissance du pergélisol et, 2) le relevé de repères de nivellement de 10 et de 20 m de longueur installés au fond du lac pour étudier le soulèvement du fond suite à la croissance du pergélisol. Un examen du premier point d'inflexion dans le profil thermique sous 0°C indique que l'eau interstitielle dans les sables du fond du lac gèle à -0,04°C. Les mesures de la température combinées aux données du levé indiquent le gel progressif de l'eau interstitielle non gelée jusqu'à au moins -0,5°C et un peu de gel même sous -1,0°C. Les preuves recueillies sur le terrain au lac Illisarvik indiquent que dans le gel en système fermé, le soulèvement peut se poursuivre pendant des années et même pendant des décennies ou des siècles dans les zones de pergélisol chaud en raison du gel progressif de l'eau interstitielle non gelée.

Introduction

In the Tuktoyaktuk and Richards Island region, Northwest Territories, lakes cover from 20 to 40 per cent of the total area. When these lakes drain naturally – a common event – permafrost commences to aggrade downward on the exposed, drained lake bottoms. In 1978, 'Illisarvik Lake' (unofficial name), 60 km due west of Tuktoyaktuk, Northwest Territories (Fig. 18.1) was artificially drained in a co-operative research endeavor involving government and universities in order to study permafrost growth under full-scale natural conditions (Mackay, 1981). Illisarvik Lake, prior to drainage, was about 600 m long and 300 m wide. The lake was drained on 13 August 1978. A number of studies on the experimental site have already been completed (e.g. Hunter et al., 1980; Judge et al., 1980, 1981; Mackay, 1980, 1981, 1982, 1984; Scott, 1980; Burgess et al., 1982; Fransham et al., 1982; Michel and Fritz, 1982; Sinha and Stephens, 1983). This report discusses lake bottom heave in the newly formed permafrost in the northeastern end of the drained lake bottom.

Acknowledgments

The field work has been supported by the Geological Survey of Canada, the Polar Continental Shelf Project, Canada, the Natural Sciences and Engineering Research Council of Canada, and the Inuvik Scientific Resource Centre, Inuvik, Northwest Territories.

Field measurements

Lake bottom heave has been measured by precise levelling of bench marks composed of one inch (2.54 cm) diameter steel waterpipe anchored in permafrost. Ground temperatures have been measured using a precision bridge and thermistor cables inserted inside the steel waterpipes that are used as bench marks.

Bench marks

Prior to drainage of Illisarvik Lake, three deep holes were jet (water) drilled on land within several metres of the lake shore (Hunter et al., 1980; Judge et al., 1980).

[1] Department of Geography, The University of British Columbia, Vancouver, British Columbia V6T 1W5

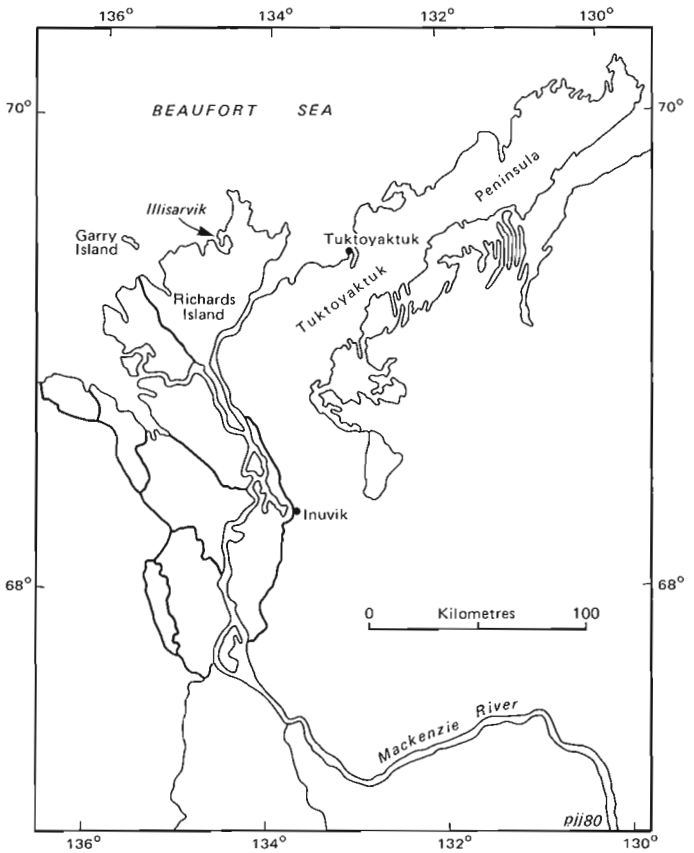

Figure 18.1. *Location map.*

The one inch (2.54 cm) diameter steel waterpipes, used for the jet drilling, were left in the holes and allowed to freeze in place. These three steel waterpipes have been used as datum bench marks, because all three after freeze-back were anchored firmly in deep permafrost and so should remain unaffected by permafrost growth in the nearby lake bottom. Bench mark 12 (BM 12) extended to a depth of 58 m below ground level, BM 14 to 65 m, and BM 15 to 53 m. The three datum bench marks formed a triangle whose sides measured about 325 m. Repetitive levelling for the 1979-1983 period showed a maximum height difference among the three datum bench marks of only 0.4 cm despite poor lake bottom conditions encountered in some of the surveys. Consequently, the datum bench marks are considered stable for the purposes of the present discussion.

In August 1978, after lake drainage, five 10 m-long bench marks (BM 16, 17, 18, 19, and 21) were installed in the lake bottom in a line perpendicular to the northeastern shore at 10 m intervals (Fig. 18.2). In 1979, five 20 m-long bench marks (BM 56, 57, 58, 59, and 60) were installed in a line parallel to, and 2 m from, the 1978 line with the bench marks also at 10 m intervals (Fig. 18.2). Therefore, BM 16 and BM 56 are 2 m apart, and so forth.

A Wild NA 2 automatic engineer's level with parallel plate micrometer reading directly to 0.01 cm and Wild GPLE 3 m invar staves with supporting struts have been used in all levelling. The invar staves have been placed directly onto the tops of the bench marks or onto steel brackets firmly clamped to the bench marks. All surveys have been closed at least once every June and August from 1979 to 1983. The heave (August surveys) for the 10 and 20 m-long bench marks are plotted in Figure 18.2.

Temperatures

The temperature measurements for the five 20 m-long bench marks and one additional bench mark (BM 61) for 10 August 1980 and 19 August 1983 are plotted in Figures 18.3 and 18.4. Ground temperature profiles for BM 60 for 11 August 1980 and 19 August 1983 are plotted in Figure 18.5. Because the 10 and 20 m-long bench marks are only 2 m apart, the temperature data in Figures 18.3-18.5 for the 20 m bench marks also apply to the adjacent 10 m bench marks.

Discussion

Illisarvik Lake had a basin-shaped talik (unfrozen zone) about 32 m deep beneath the lake centre at the time of drainage (Judge et al., 1981). The sublake-bottom permafrost surface along the line of the 10 and 20 m-long bench marks is shown in Figure 18.2. After the lake was drained, permafrost aggradation was both downwards from the exposed lake bottom and also upward from the sublake-bottom permafrost surface (Mackay, 1981). The relative importance of downward versus upward freezing has depended primarily upon the initial depth to permafrost. The temperature data show that the greater the initial depth to permafrost, the lesser has been its importance to the growth of new permafrost. The depth of downward freezing has not varied greatly across the lake bottom except for the nearshore area.

Freezing temperature for sands

The lake bottom sediments below a 1 to 2 m-thick layer of organic rich material are medium to fine grained sands. Broadly speaking, sands freeze at a temperature slightly below 0°C although appreciable amounts of unfrozen pore water may be present even at -0.5°C (Shvetsov et al., 1973). Saline pore water will, of course, depress the freezing point. A sample of Illisarvik Lake water was collected prior to lake drainage and the results were: specific conductance 277 μS/cm, calcium 22.4 mg/L, magnesium 9.8 mg/L, potassium 1.5 mg/L, sodium 18.4 mg/L, and chloride 40.0 mg/L (analyses by Environment Canada). If the pore water in the sands was similar to the surface water, salinity effects would be insignificant in depressing the freezing point.

The temperature at which pore water commences to freeze at the bottom of aggrading permafrost at Illisarvik can be estimated from the first change in thermal gradient at below 0°C. The first change in gradient or inflexion point is not at 0°C but at -0.04°C at the sites under discussion. The inflexion point shows up clearly in Figure 18.5. A further indication of the freezing point of the pore water at -0.04°C is demonstrated by the isothermal zone which persisted for three years at -0.04°C at a depth of 8 m as shown in Figure 18.5. It should be stressed that the freezing point depression at -0.04°C is specific to the sites under discussion, because at the centre of the drained lake bottom, the freezing point is much lower, presumably because of a higher pore water salinity, as measured with soil salinity cells, arising from the expulsion of solids in solution during the freezing process.

Lake bottom heave

The survey of the 10 and 20 m-long bench marks was not started until the year after the bench marks were installed in jet drilled holes in order to permit time for the bench marks to freeze solidly in place. It should be noted, therefore, that the heave of the 10 m bench marks is for the 1979-1983 period whereas that of the 20 m bench marks is for the 1980-1983 period. Consequently, there are no heave data for the first winter of 1978-1979. The heave patterns of

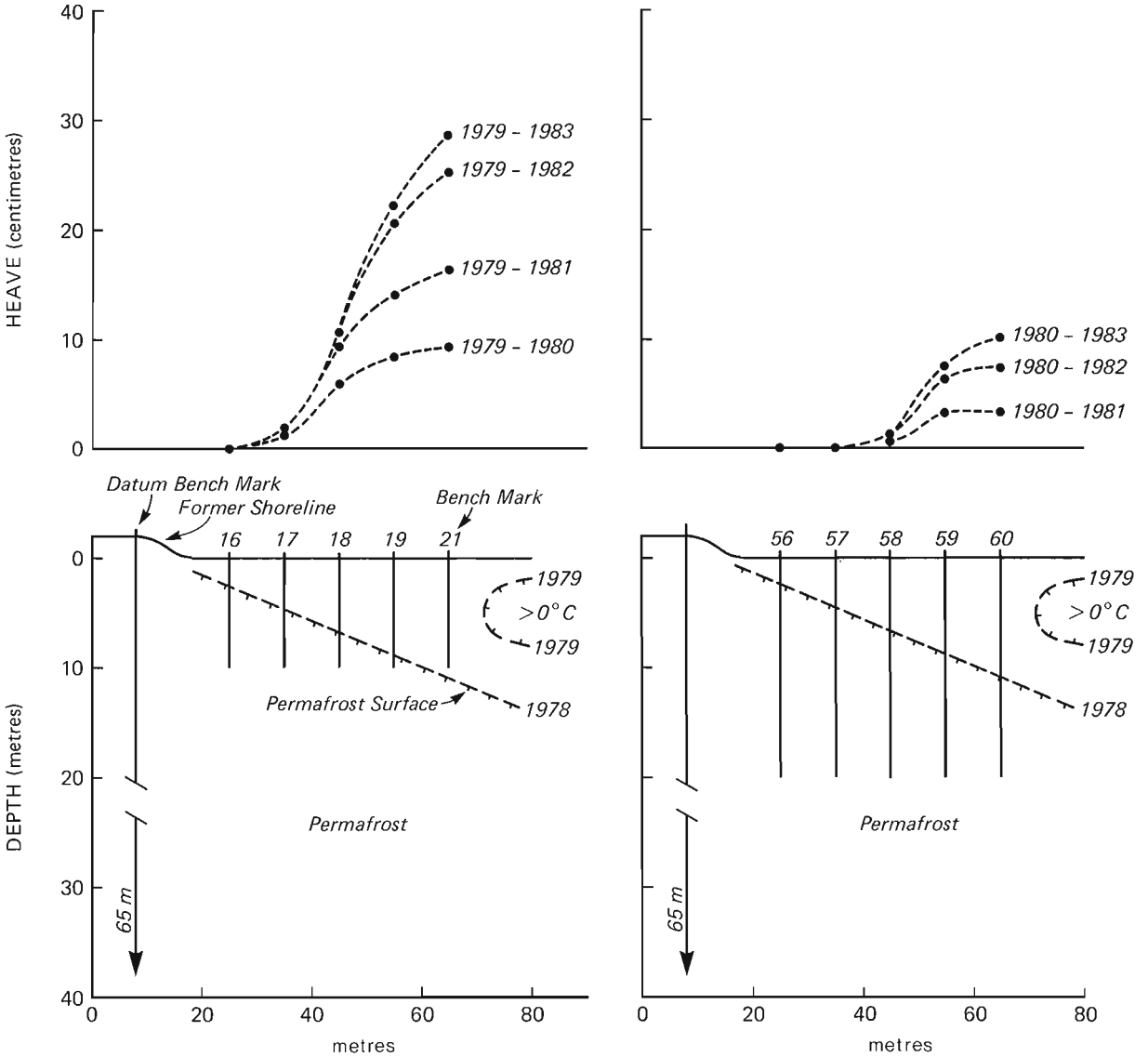

Figure 18.2. *Heave and temperature data for the northeast end of the drained lake. In August 1979, all of the 10 and 20 m-long bench marks were in ground at or below 0°C.*

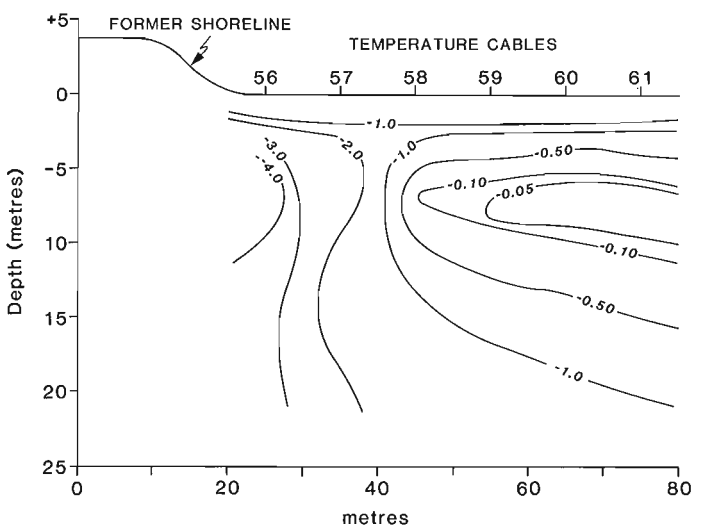

Figure 18.3. *Temperature data for 10 August 1980. Because of rapid temperature changes to a depth of about 3 m, the isotherms there are generalized.*

the bench marks show three general trends (Fig. 18.2). First, with the exception of 1981-1982, the amount of heave decreased with time, because there was progressively less unfrozen pore water remaining to be frozen as the newly formed permafrost became colder and colder (Fig. 18.3, 18.4). Second, the yearly amount of heave for the bench marks increased from the lake shore towards the lake centre. The greater lakeward heave is explained by the greater thickness of new permafrost in proceeding lakeward, so there was more unfrozen pore water to freeze. Third, the 10 m-long bench marks heaved more than the 20 m-long bench marks, because the 20 m bench marks were anchored at depth in pre-1978 permafrost (Fig. 18.2) and so were partially restrained from heaving.

A comparison of the heave data in Figure 18.2 with the ground temperature data in Figures 18.3 and 18.4 shows that measurable heave took place even though temperatures were below 0°C. The salient data are summarized in Table 18.1. To illustrate, BM 18, which is 10 m long, heaved 3.4 cm in the 1980-1981 period. The maximum temperature at depth in 1980 was -0.1°C and in 1981 it was -0.7°C. If the 3.4 cm

heave is attributed to the freezing of unfrozen pore water in the temperature range of -0.1°C to -0.7°C, then 3.4 cm represents the 9% volume expansion of the freezing of unfrozen pore water. By a similar line of reasoning, in 1981-1982 the bench mark heaved 1.2 cm with a temperature change from -0.7°C to -1.6°C, and so forth for 1982-1983 and for the other bench marks. A comparison of the heave of the 10 m-long and adjacent 20 m-long bench marks shows that the 10 m bench marks heaved, in general, about two to three times the amount of the 20 m bench marks. When the heave data of Table 18.1 are taken together, heave from the freezing of unfrozen pore water certainly occured below -0.5°C and, although small, it was detected at temperatures below -1.0°C. However, the preceding data give no indication of how much unfrozen pore water is present at any given temperature nor what is the porosity of the frozen sands. An estimate of the porosity can be derived from the heave data for BM 21. In August 1980, the -1.0°C (approximately) isotherm was at a depth of 2 m and in August 1983 the -1.0°C isotherm had descended to a depth of 6 m. In other words, the temperature curve had propagated downward about 4 m and, during this period, the ground heaved 18 cm. If the 18 cm represented the 9% volume expansion of water to ice as the temperature wave propagated down 4 m, the porosity would be about 50%, a value which is realistic, although probably slightly high. In August 1983, the zone between 6 and 19 m at the site of BM 60 was between -0.04°C and -1.0°C. In view of the heave data given in Table 18.1 for heave in this temperature range, the heave of BM 21 should be measurable for 1983-1984 and probably 1984-1985. If so, heave will have continued for at least four years (1979-1983) and possibly five or six years after the ground was at or below 0°C, the heave resulting from the progressive freezing of unfrozen pore water.

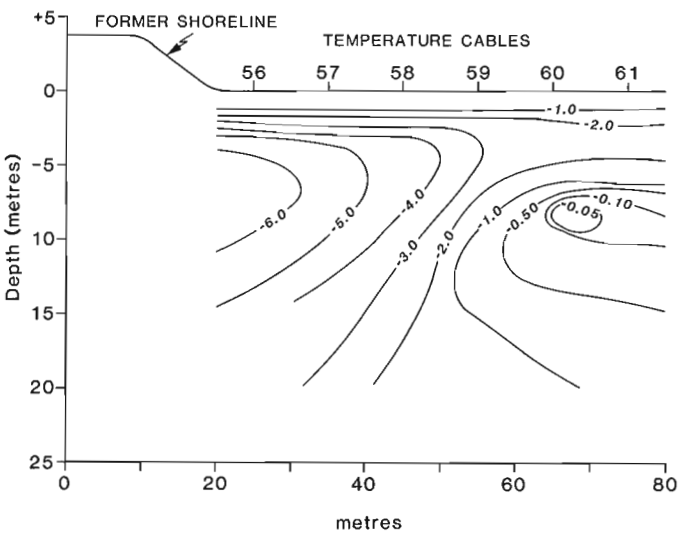

Figure 18.4. *Temperature data for 19 August 1983. Because of rapid temperature changes to a depth of about 3 m, the isotherms there are generalized.*

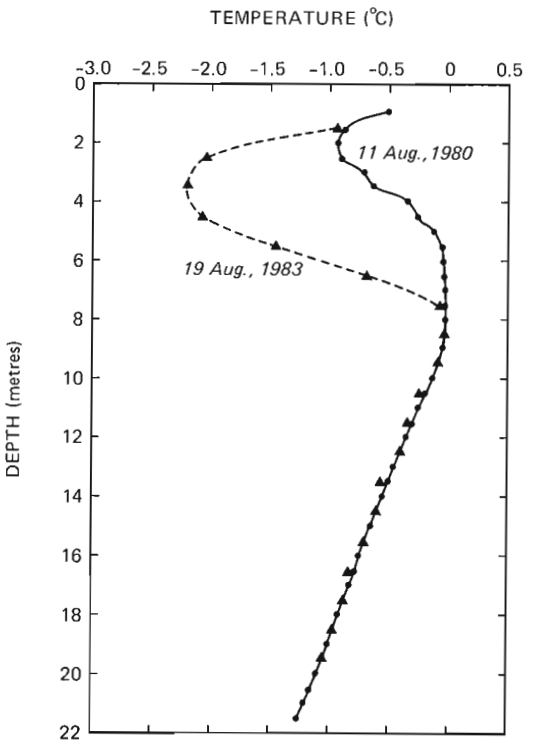

Figure 18.5. *Temperature profiles at bench mark 60 for 11 August 1980 and 19 August 1983.*

Table 18.1. Heave and ground temperature data

Bench mark number	Bench mark length (m)	Heave period (August to August)	Heave (cm)	Change in maximum temperature at depth (0°C)
18	10	1980-1981	3.4	-0.1 to -0.7
18	10	1981-1982	1.2	-0.7 to -1.6
18	10	1982-1983	0.2	-1.6 to -2.2
19	10	1980-1981	5.5	-0.04 to -0.1
19	10	1981-1982	6.6	-0.1 to -0.2
19	10	1982-1983	1.6	-0.2 to -0.9
21	10	1982-1983	2.5	-0.04 to -0.04
58	20	1980-1981	0.8	-0.1 to -0.7
58	20	1981-1982	0.4	-0.7 to -1.6
58	20	1982-1983	∿0	-1.6 to -2.2
59	20	1980-1981	3.2	-0.04 to -0.1
59	20	1981-1982	3.2	-0.1 to -0.2
59	20	1982-1983	1.5	-0.2 to -0.9
60	20	1982-1983	1.5	-0.04 to -0.04

Conclusion

Temperature measurements at the northeastern end of the drained lake bottom show that the pore water commenced to freeze at about -0.04°C. As the downward-aggrading permafrost merged with the upward-aggrading permafrost, an isothermal zone developed not at 0°C, but at -0.04°C. The isothermal zone has been thicker and has persisted for a longer period the farther the site was distant from the predrainage lake shore. At one site 50 m from the former lake shore, an isothermal zone at -0.04°C was present for at least three years. Precise levelling of 10 bench marks, when referenced to three deeply anchored bench marks, has demonstrated that appreciable heave has occurred when the ground has cooled from -0.1°C to -0.5°C, and measurable heave below -1.0°C. This heave has resulted from the progressive freezing of unfrozen pore water. At the Illisarvik drained lake experimental site, the temperature and heave data given here pertain to a maximum predrainage unfrozen zone (talik) of only 10 m. Preliminary data from the lake centre, where the predrainage depth to permafrost was 32 m, support the general principles just expressed for the area just discussed.

References

Burgess, M., Judge, A., Taylor, A., and Allen, V.
1982: Ground temperature studies of permafrost at a drained lake site, Mackenzie Delta; in Proceedings, 4th Canadian Permafrost Conference (Calgary), ed. H.M. French; National Research Council of Canada, Ottawa, p. 3-11.

Fransham, P.B., Unrau, J.D., and Reesor, S.N.
1982: Field and laboratory acoustic testing of frozen soils; in Proceedings, 4th Canadian Permafrost Conference (Calgary), ed. H.M. French; National Research Council of Canada, Ottawa, p. 274-282.

Hunter, J.A., MacAulay, H.A., Gagne, R.M., Burns, R.A., Harrison, T.E., and Hawkins, J.P.
1980: Hydraulic jet • drilling operations at Illisarvik – geological and geophysical logs; in Proceedings of a Symposium on Permafrost Geophysics (No. 5), National Research Council of Canada, Technical Memorandum No. 128, p. 5-20.

Judge, A.S., Burgess, M., Allen, V., and Taylor, A.
1980: Thermal studies at Illisarvik prior to lake drainage; in Proceedings of a Symposium on Permafrost Geophysics (No. 5), National Research Council of Canada, Technical Memorandum No. 128, p. 26-34.

Judge, A., Burgess, M., Taylor, A., and Allen, V.
1981: Ground temperature studies at an arctic drained lake site; Proceedings of the Specialty Conference on The Northern Community: A Search for a Quality Environment, ASCE/Seattle, p. 642-658.

Mackay, J.R.
1980: Illisarvik: an experiment in lake drainage; in Proceedings of a Symposium on Permafrost Geophysics (No. 5), National Research Council of Canada, Technical Memorandum No. 128, p. 1-4.

1981: An experiment in lake drainage, Richards Island, Northwest Territories: a progress report; in Current Research, Part A, Geological Survey of Canada, Paper 81-1A, p. 63-68.

1982: Active layer growth, Illisarvik experimental drained lake site, Richards Island, Northwest Territories; in Current Research, Part A, Geological Survey of Canada, Paper 82-1A, p. 123-126.

– The direction of ice-wedge cracking in permafrost: downward or upward; Canadian Journal of Earth Sciences. (in press)

Michel, F.A. and Fritz, P.
1982: Significance of isotope variations in permafrost water at Illisarvik, N.W.T; in Proceedings, 4th Canadian Permafrost Conference (Calgary), ed. H.M. French; National Research Council of Canada, p. 173-181.

Scott, W.J.
1980: D.C. soundings at Illisarvik prior to drainage; in Proceedings of a Symposium on Permafrost Geophysics (No. 5), National Research Council of Canada, Technical Memorandum No. 128, p. 21-25.

Shvetsov, P.F., Grechischev, S.Ye., and Chistotinov, L.V.
1973: Basic laws of cryogenous processes in silt-clay and sandy formation (in Russian); U.S.S.R. Contribution, Permafrost, Second International Conference (Yakutsk, U.S.S.R.), Part 3, p. 67-73; Translation, National Academy of Sciences, Washington, D.C., p. 254-261.

Sinha, A.K. and Stephens, L.E.
1983: Permafrost mapping over a drained lake by electromagnetic induction methods; in Current Research, Part A, Geological Survey of Canada, Paper 83-1A, p. 213-220.

19. GROWTH INCREMENTS OF MODERN MYA TRUNCATA L. FROM THE CANADIAN ARCTIC, GREENLAND, AND SCOTLAND[1]

Project 750063

R.A. Hewitt[2] and J.E. Dale
Terrain Sciences Division

Hewitt, R.A. and Dale, J.E., Growth increments of modern ***Mya truncata*** *L. from the Canadian Arctic, Greenland, and Scotland; in Current Research, Part B, Geological Survey of Canada, Paper 84-1B, p. 179-186, 1984.*

Abstract

A preliminary examination of modern ***Mya truncata*** *L. from numerous arctic locations in Canada and Greenland, as well as from boreal sites in Scotland, indicates that this species can live to a maximum of 40 years. These age estimates were based on counts made from thin sections. Counts made in the umbonal region of the inner shell layer and beside the ligamental pit of the chondrophore proved more reliable than estimates based on external growth ridges.*

A thin organic membrane appears to form in early spring after ice breakup and an annual translucent band is rapidly deposited during July and August in intertidal specimens. ***Mya*** *from lower tidal sites probably grow more continuously through the year and add relatively thin annual increments to the inner shell layer. Subtidal specimens are not affected by ice cover, temperature fluctuations, and tidal exposures, as are intertidal inhabitants.*

Résumé

Un examen préliminaire de ***Mya truncata*** *L. contemporain provenant de nombreuses localitiés arctiques du Canada et du Groenland ainsi que de localités boréales d'Écosse, indique que cette espèce peut vivre jusqu'à 40 ans. Ces estimations d'âge sont fondées sur des comptages faits à partir de lames minces. Les comptages faits dans la région du crochet de la couche intérieure de la coquille et à côté de la dépression ligamenteuse des chondrophores se sont révélés plus sûrs que les estimations fondées sur les crêtes extérieures de croissance.*

Une membrane mince de nature organique semble se former au début du printemps après le dégel et une bande annuelle d'apparence translucide se dépose rapidement en juillet et août dans les espèces intertidales. ***Mya****, espèce provenant des zones infratidales, croît probablement plus continuellement au cours de l'année et ajoute des pellicules annuelles relativement minces à la couche intérieure de la coquille. Les espèces infratidales ne sont pas touchées par la couverture de glace, les fluctuations de la température et les expositions à la marée, comme le sont les espèces intertidales.*

Introduction

Marine bivalves show external growth ridges that have been used to reconstruct the annual growth rate of fossil (Andrews, 1972) and modern specimens from Canada. Modern **Mya arenaria** from the Bay of Fundy grow annual ridges which show that shells with a mean length of 70 mm are 8 years old (Newcombe, 1936). Brousseau (1979) obtained values of 8 years for 80 mm-long tagged shells from Massachusetts. MacDonald and Thomas (1980) found little relationship between the number of external ridges and age in populations sampled from Bideford River, Prince Edward Island, but they observed an annual periodicity defined by alternating opaque and translucent bands within the chondrophore and inner shell layer. Using this criterion they deduced an age of 13 years for a shell with a length of 93 mm and 28 years for a shell with a length of 110 mm from the Bay of Fundy. Zolotarev (1980) used the ridges on the chondrophore and ligament pit (Fig. 19.1) to deduce an age of 42 years for an 86 mm-long **Mya japonica** from the Sea of Japan. An earlier study by Swan (1952) found that **Mya arenaria** from Washington State grew faster and had thinner shells in sand substrates than in mud or gravel.

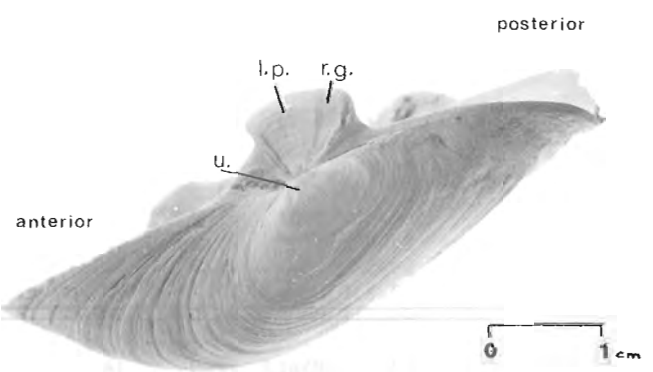

Figure 19.1. *Left valve,* ***Mya truncata****, from St. Andrews, Scotland. Dorsal view showing the umbo (u) and the poorly defined annual growth ridges on the external valve surface and the ligamental pit (l.p.) and radial groove (r.g.) of the chondrophore (c.f. Bernard, 1979). Shell length 54.6 mm, shell height 37.1 mm.*

[1] This report is contribution 18 from the Cape Herschel Project
[2] Department of Geology, McMaster University, Hamilton, Ontario
Present address: Leigh-on-Sea, Essex, England

Table 19.1. Mya truncata L. shell measurements and age estimates made with the aid of reflected (r) and transmitted light (t)

Location	Sample No.	Length mm	Height mm	Umbo Thickness mm	Pallial Myostracum	External Age Count	Internal Age Count Chondrophore r	Chondrophore t	Umbo r	Umbo t
Scotland										
Aberlady	BB84	>70	39	1.2	m	17			8	11
Arran	191	49.2	33.2	1.2	m	13			8	8
St. Andrews	117	54.6	37.1	1.2	m	12			10	
Frobisher Bay										
Apex	80-1A(JD)(L)	69.2	50.7	5.48	m	19	35	37	32	37
	80-1B(JD)(L)	56.4	45.3	2.75		16	16		16	
	80-1C(JD)(L)	28.8	19.7	–		8 or 7			7 or 8	
Tidal Pool	80-2A(JD)(L)	64.0	48.2	4.2		9			6	13
Rodgers Island	RI5A AB	76.9	51.1	3.71		16	20		19	19
	RI5A AA	95.4	–	5.17		19		22	25	24
	RI55	85.7	55.8			19				26
	RI6A AA	86.9	58.1	5.19		22		39	38	>38
	RI6B AB	72.6	51.6	4.81		17		29		30
	RI12A(L)	59.2	48.2	4.0	m	16				25
	FBJD	76.7	59.7	5.65		21	37	>23	34	37
Banks Island										
Johnson Point	BS-75-207A	55.0	45.5	2.57		17 or 29	34	>30	35	34
	BS-75-207B	53.2	41.7	2.56		22 or 25	31	32	26	33
Wellington Channel	BS-74-108	19.1	14.7	0.5		10	14			
Greenland	BS-74-4A	58.6	42.4	3.13		21 or 12	23		17	
Saunders Island	BS-74-4B	50.1	38.5	2.48		17 or 18	21	22		22
	BS-74-4C	53.9	40.0	1.91		18 or 19		23		21
	BS-74-4D	59.7	42.1	3.33		17	20	21	21	21
	BS-74-4E	52.0	38.7	2.25		18 or 14		20		19
Ellesmere Island										
Cape Storm	BS-77-299A	36.0	29.5	1.73	m	16			11	7
	BS-77-299B	40.9	30.6	2.6		8			11	
	BS-1-67	39.4	28.8	2.96		13	9	16	9	18
	BS-75-163A	37.5	27.0	2.51		14			12	
	BS-75-163B	37.7	30.5	2.09		13			12	
	BS-75-163C	32.4	25.7	1.59		14	14		14	
Rosse Bay	BS-82-46AA	33.5	25.1	1.27		14 or 9	10	11	10	9
	BS-82-46AB	31.2	22.6	1.04		16	21	13	10	13
	83-58A(JD)	24.9	18.1	1.22		6 or 7	6		6	
	83-58B(JD)	43.9	31.6	3.13		12			12	
	83-85(JD)	29.2	22.7	1.37		10			6	
	83-61(JD)	33.0	23.0	2.2	m	11	27	25	>25	>21
Alexandra Fiord	83-101(JD)(L)	22.0	14.0			5	4.5		3	
	83-102(JD)(L)	42.0	30.0	2.3		10	16	16	16	>14
	83-107(JD)	39.0	25.0	1.5	m	7	7	>7	8	

m = thick pallial myostracum >5%
L = collected live

Andrews (1972) deduced a maximum age of 17 to 20 years for fossil **Mya truncata** from the Ottawa Islands, Hudson Bay, using external ridge counts. Modern **Mya** from Canada, Greenland, and Scotland examined in this study show that these cycles of ridges and grooves correspond to alternating concave and plano-convex increments added to the internal surface of the outer shell layer. In arctic **Mya**, the concave increments forming the external grooves consist of unusually wide and translucent layers, which alternate with opaque growth bands. The resulting alternation of banded and diffuse zones of the outer shell layer corresponds to the external cycles counted by Andrews. Some contain minor increments, such as the 13 observed on the Scottish specimen 117. The amplitude of the external ridges increases near the ventral margin, where they are more difficult to count than the major growth increments added to the inner shell layer observed in thin sections. These inner growth increments define more regular growth curves than the external rings and are manifested by a variety of structures. Microstructural observations resolve difficulties posed by the relative prominence of the subannual increments discussed by Richardson et al. (1980). There do not appear to be any publications on the microstructure of arctic molluscan shells.

Collection sites

The present study compares the shell structures of modern **Mya truncata** L. from a variety of locations in Arctic Canada, Greenland, and Scotland (56°N, 03° & 05°W). Measurements of 37 of the best samples are listed in Table 19.1. The Canadian and adjacent sites are listed here in order of increasing latitude: Frobisher Bay in Baffin Island (63°43'N, 68°27' & 36'W), Johnson Point on Banks Island (72°47'N, 118°29'W), Wellington Channel (74°49'N, 93°1'W), Cape Storm on Ellesmere Island (76°20'N, 87°35'W), Saunders Island in northwest Greenland (76°30'N, 69°W), Rosse Bay in Ellesmere Island (78°37'N, 74°45'W), and Alexandra Fiord in Ellesmere Island (78°53'N, 75°45'W) (Fig. 19.2). Three of our specimens were collected live from pools in the mid-intertidal zone at Alexandra Fiord (83-101(JD), 83-102(JD), July 17, 1983) and Koojesse Inlet, Frobisher Bay (80-2A(JD), August 26, 1980). Two other specimens were collected live from sands near the low tide mark at Koojesse Inlet (80-1B(JD), August 27, 1980), and at Rodgers Island, Frobisher Bay (RI12A, August 3, 1981). The mean tidal range at Frobisher Bay is 7.8 m and the lower tidal samples were collected between 2 and 2.5 m ALLT (above lowest low tide). The other Frobisher Bay sample was collected from a gravel-floored tidal pool at 4.5 m ALLT. The large tidal range at Alexandra Fiord is approximately 4.5 m (M. Krawetz, personal communication, 1983), and the shells were collected in pools floored with fine sand and silts at 0.8 m (ALLT). The sea is frozen here from October to July. One specimen was collected from a depth of 162 m in Wellington Channel, August 1974 (Blake, 1975, p. 43).

The microstructural differences between the modern Frobisher Bay and Scottish **Mya** can be ascribed largely to the effects of winter ice cover. The exposure of the Frobisher Bay **Mya** influences growth rates by causing the retraction and closure of the siphons. Ice-free conditions occur for three months each year. Freezeup is initiated by mid-October and is characterized by repeated development and disintegration of thin ice layers, which cause temperature and salinity changes across the intertidal zone until November. Ice breakup is initiated by mid-June, with ice-free conditions by mid-July. Thus, for most of the year the lower intertidal fauna is covered by a 1.5 m-thick layer of ice subject to tidal oscillations. The upper intertidal fauna is covered by a 3 to 5 m-thick ice foot, which freezes to the substrate and does not permit them to feed. Their growth presumably resumes after the summer solstice and probably

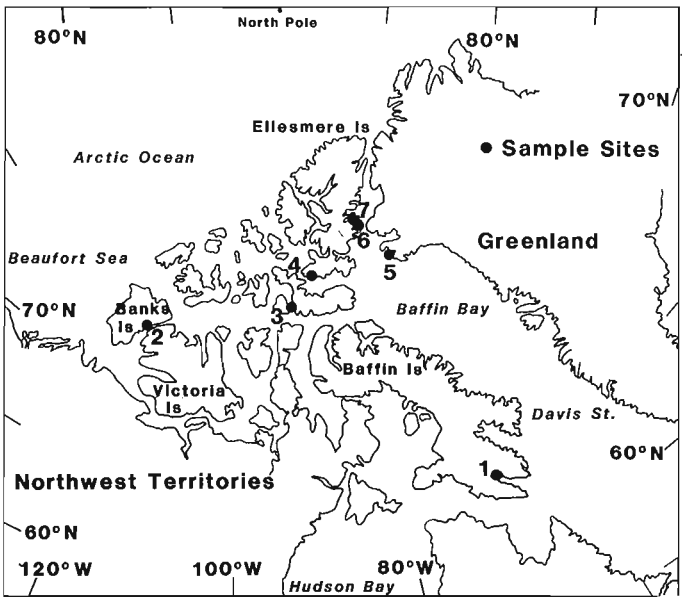

1. *Frobisher Bay,*
2. *Johnson Point,*
3. *Wellington Channel,*
4. *Cape Storm,*
5. *Saunders Island,*
6. *Rosse Bay,*
7. *Alexandra Fiord.*

Figure 19.2 *Location of* ***Mya truncata*** *samples from Arctic Canada and Greenland. See Table 19.1 for sample numbers.*

continues during the dark autumnal months before ice formation. In the lower tidal zone the growth rate may be more related to day length and temperature. Tidal oscillations enhance the ice breakup, suggesting a possible correlation between periods of exposure of the lower tidal zone and the start of growth after winter. In the upper tidal zone, the melting of the ice foot and stranding of fast ice results in an influx of fresh water during all low tides until mid-July. This influx is much reduced in the lower tidal zone.

Shell microstructure

The microstructural description of aragonitic **Mya truncata** shells given by Taylor et al. (1973, p. 275) was based on specimens from Britain. New observations were made from thin sections of Canadian and Scottish shells prepared with an ISOMET 11-1180 slow speed saw (Table 19.1). They show an apparently homogeneous outer shell layer, containing grey threads of organic matrix, which define diffuse growth increments. The middle crossed lamellar layer was only observed in the ligamental region of the chondrophore of our material (Fig. 19.3). The inner shell layer was confirmed to largely consist of alternating complex crossed lamellar and granular structures, which include a thin pallial myostracum of translucent aragonite prisms (Fig. 19.4). The annual growth bands are defined by changes in the shell structure of the inner shell layer and periodic extensions of translucent bands towards the ligamental pit on the chondrophore.

Both these regions of the Scottish chondrophores also show numerous minor growth increments, which are less apparent in the arctic material. The Scottish **Mya** are also characterized by an abundance of microborings and have thick pallial myostraca defining the boundary between the inner and outer shell layers (e.g. 13 per cent of outer layer thickness). They resemble one of the **Mya** from Johnson Point

(BS-75-207F) in having an umbonal shell thickness of only 10 mm at a shell height of about 30 mm. Their inner shell layer is largely composed of alternating growth bands. The thicker bands show zig-zag second-order lamellae, separated along the boundaries of the first order lamellae, by opaque granular crystals.

The thicker bands resemble the "cone complex crossed lamellar structure" (Carter, 1980, fig. 40) and show weak alignment of the optic axes normal to the growth bands. The alternate narrow growth bands are generally composed of an opaque homogeneous structure, but in some cases they exhibit thin prismatic layers in which the optic axes are aligned normal to the growth surface. The banding is best developed in the umbonal region where some of the thicker layers change into a coarsely crystalline, granular structure resembling neomorphic sparry calcite (Fig. 19.5). Within the chondrophore the inner shell layer changes into an "irregular complex crossed lamellar structure" (Carter, 1980, fig. 19), in which the translucent part of the growth bands at the umbo is delineated by dark brown laminated layers. Thus, the thin opaque bands seen at the umbo pass into the more translucent layers of the rather opaque crossed lamellar structure flanking the ligamental pit, before continuing through the ligament into the right valve.

Some specimens (m in Table 19.1) from Ellesmere Island and Baffin Island also exhibit a thick pallial myostracum (5 to 10 per cent of outer layer thickness) and resemble the majority of arctic specimens in having the myostracum surrounded by complex crossed lamellar structures of the inner shell layer. The distance between these pallial myostraca and the outer shell layer averages about 20 per cent of the thickness of the outer shell layer. The umbonal shell thickness typically varies from 4 to 10 per cent of the shell height in arctic samples, reaching a maximum in a specimen from Rosse Bay (83-61(JD)), which resembles the Scottish specimens in having "cone complex crossed lamellar structure" in the inner layer. The other specimens with a thick pallial myostracum have inner shell layers with granular spherulitic prismatic structure (Frobisher Bay, RI12A) or the complex crossed lamellar structure (83-107(JD), BS-77-299A).

The majority of arctic specimens have a pallial myostracum thickness of 0.3 to 2 per cent of the outer shell layer thickness. It is absent in the two shells from Johnson Point and disappears from the later growth stages of some Frobisher Bay specimens. There is a general development of translucent granules in the wider growth bands of specimens collected from tidal pools in Frobisher Bay and Alexandra Fiord. Specimens from the mid-tidal zone are characterized by discontinuous minor growth lines near the ligament in the chondrophore, and they differ from those from lower tidal zones in having relatively poorly defined annual bands in the chondrophore. In this case, it is advisable to count annual bands in the granular umbonal region of the inner shell layer,

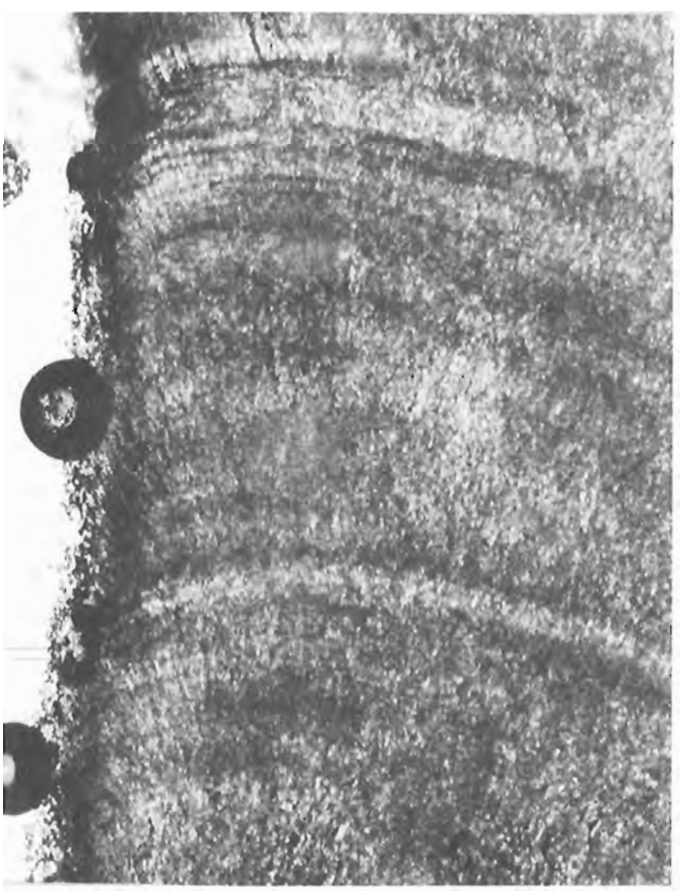

Figure 19.3. *Crossed lamellar layer in the chondrophore ligamental pit. Note the discontinuity and the small number of growth lines. Sample 80-2A(JD), magnification 55X.*

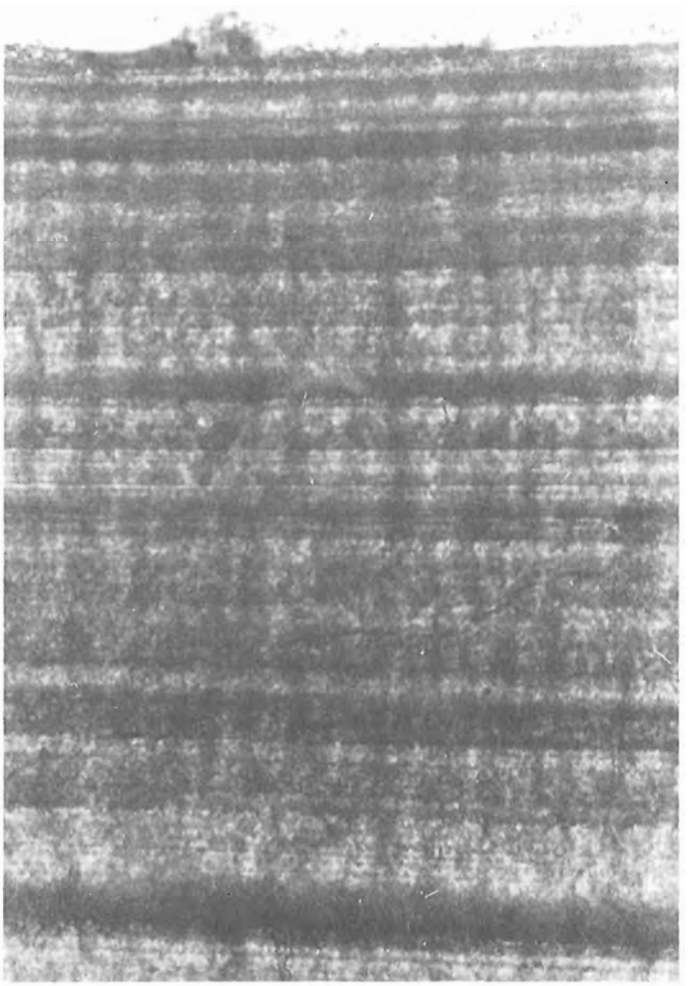

Figure 19.4. *An example of the finely banded complex crossed lamellar layer in the chondrophore. Sample 80-2A(JD), magnification 195X.*

where traces of minor growth events are destroyed (Fig. 19.6). These specimens show large myostracal prisms (see Kennedy et al. 1969, pl. 25, fig. 5) between the crossed lamellar layer of the chondrophore and the translucent bands in the umbo. Many of the larger specimens from Frobisher Bay, Saunders Island, and Johnson Point have a translucent granular structure within tubular structures in the umbonal region, which are related to irregular striated pits seen on the inside of the umbones of **Mya.** Coarse translucent calcite crystals form "nondenticular composite prismatic structure" within localized irregular zones of the inner shell layer in specimens 83-58B(JD) and RI5A-AB. These aberrations of the inner shell layer were reported from **Anadonta** from Tsingtao (Carter, 1980, Fig. 19) and form crystalline mounds on the inner surface of the **Mya** shells. Specimen 83-58B(JD) exhibits a deep uncemented hole in the inner shell layer, which suggests that these abnormalites may be related to internal parasites.

Analysis of annual growth bands

The annual banding appears similar to that described in other bivalves by Lutz (1976), Jones (1980, 1983), Lutz and Rhoads (1980), some of which are thought to have a life span over 100 years (Thompson et al., 1980). At temperate latitudes the narrower growth bands "formed by the spring probably in response to decreased winter growth rather than spawning" (MacDonald and Thomas, 1980). **Mya truncata** is a siphonate infaunal suspension feeder, that reproduces by the dispersal of small planktotrophic larvae soon after ice breakup in May to early July in the Greenland area (Thorson, 1936; Ockelmann, 1958). Two intertidal specimens were killed during growth of an opaque organic-rich 'membrane' near their umbones. This 'membrane' formed prior to July 17 in Alexandra Fiord (83-102(JD)) and prior to August 3 at Rodgers Island (RI12A) (Fig. 19.6). A smaller specimen from Alexandra Fiord (83-101(JD)) and the Koojesse Inlet specimens (80-2A(JD) and 80-1B(JD)) terminated their growth in the thicker translucent bands seen in this umbonal area. These observations suggest that the membrane formed by the end of ice breakup was rapidly covered by aragonite in July and August, with little subsequent crystalization after freezeup (November in Frobisher Bay and October in Alexandra Fiord). The opaque membranes commonly pass laterally into paired translucent bands near the ligamental pit and appear to result from a combination of retarded winter growth and early summer spawning in these intermediate-sized **Mya.** This hypothesis needs to be tested in the field.

The number of external growth ridges, internal annual bands in the crossed lamellar layer of the chondrophore, and internal annual growth bands in the inner layer of the umbonal region are compared in Table 19.1. The measurements of shell height, length, and umbonal shell thickness give an indication of the shell size and morphology. The ratio between shell height and the distance between the umbo and the ventral margin of the chondrophore (chondrophore height) is five to one. The maximum age deduced from the external growth ridges (22 years), is approximately half that deduced from well defined banding in the chondrophore. These specimens came from lower tidal

Figure 19.5. *Umbonal region of the shell showing crystalline fabric associated with thin granular layers in an annual growth band (first or second year growth). Sample 80-2A(JD), magnification 195X.*

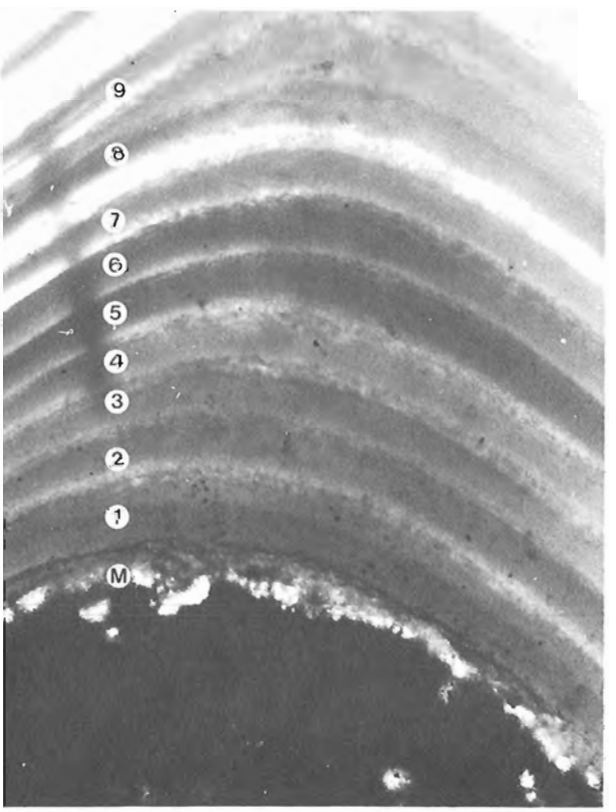

Figure 19.6. *Nine of 25 annual bands are shown for sample RI12A in the umbonal region. A thin opaque membrane (M) is also visible on the inner edge, magnification 63X.*

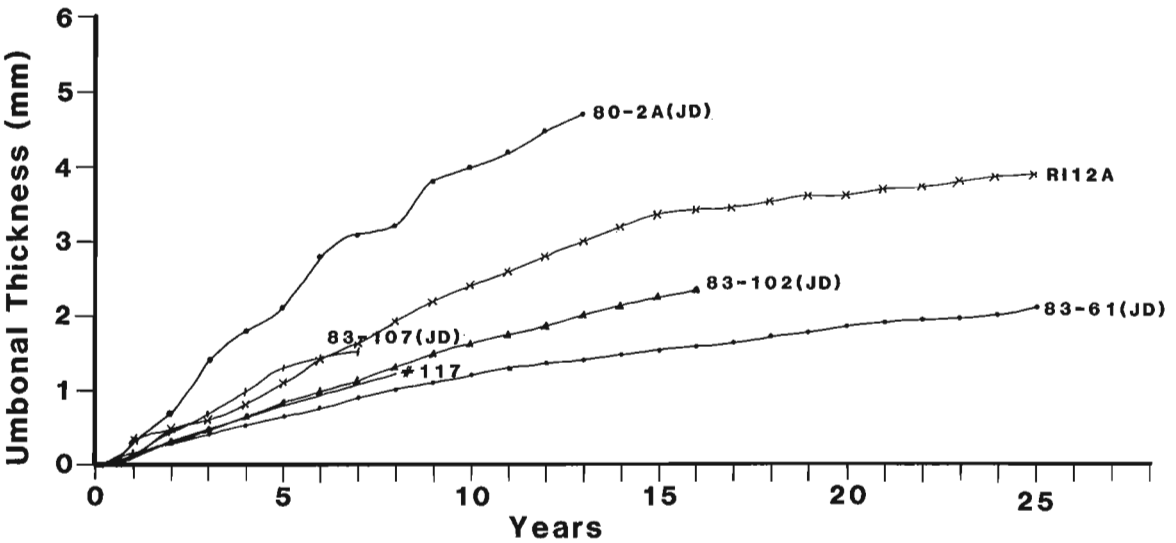

Figure 19.7. *Growth curves illustrating the annual increase of umbonal shell thickness of* ***Mya truncata*** *from the various localities listed in Table 19.1.*

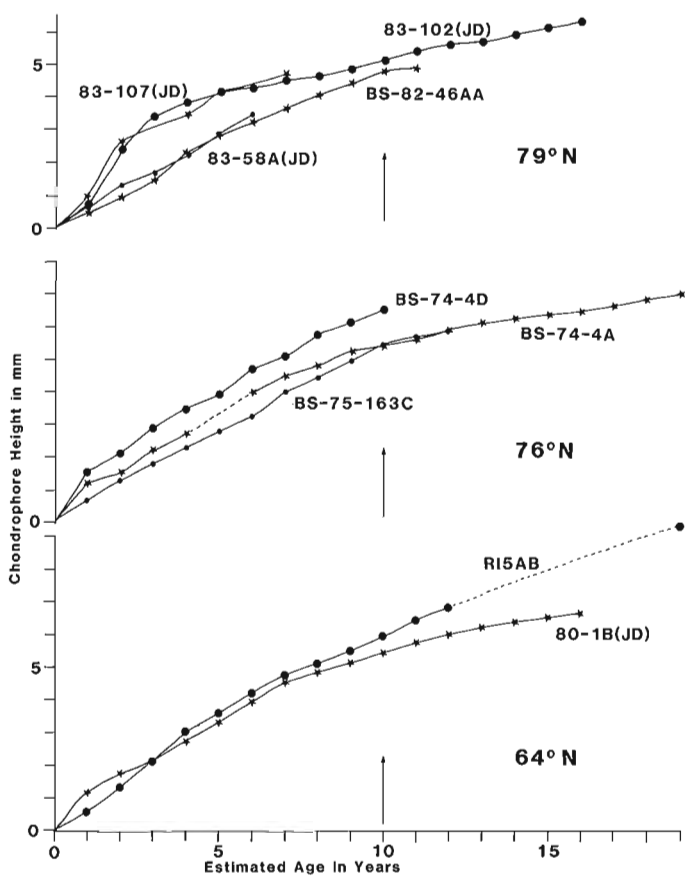

Figure 19.8. *Growth curves illustrating the annual increase in chondrophore height in young* ***Mya truncata*** *from various latitudes in Canada. The specimen numbers and localities are listed in Table 19.1 and Figure 19.2.*

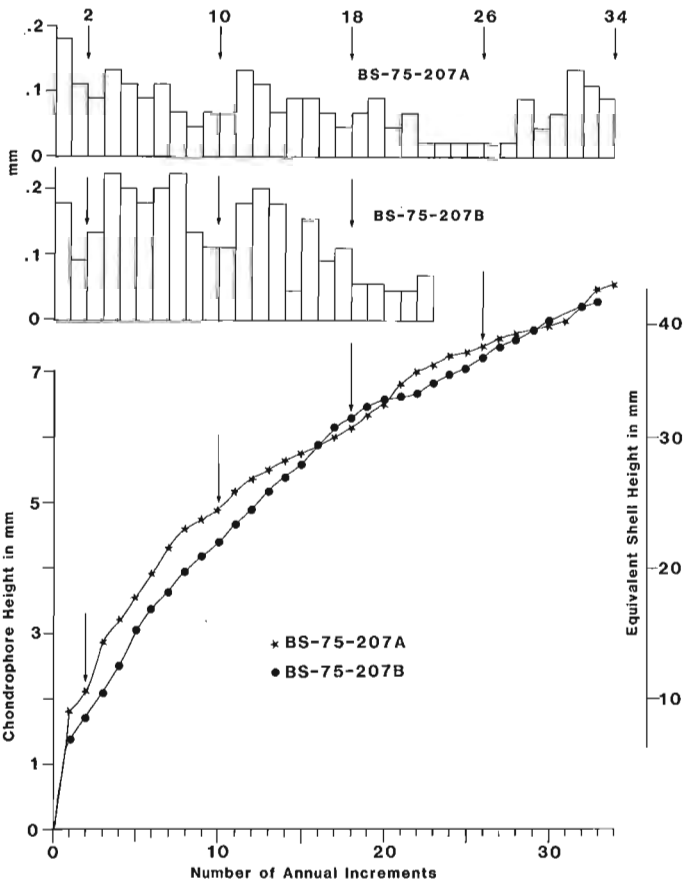

Figure 19.9. *Histograms showing the annual variation in the rate of increase of umbonal shell thickness (above) and growth curves of chondrophore height (below), in two* ***Mya truncata*** *from the storm beach at Johnson Point, eastern Banks Island (BS-75-207 A & B). Note evidence for a periodicity of about 8 years.*

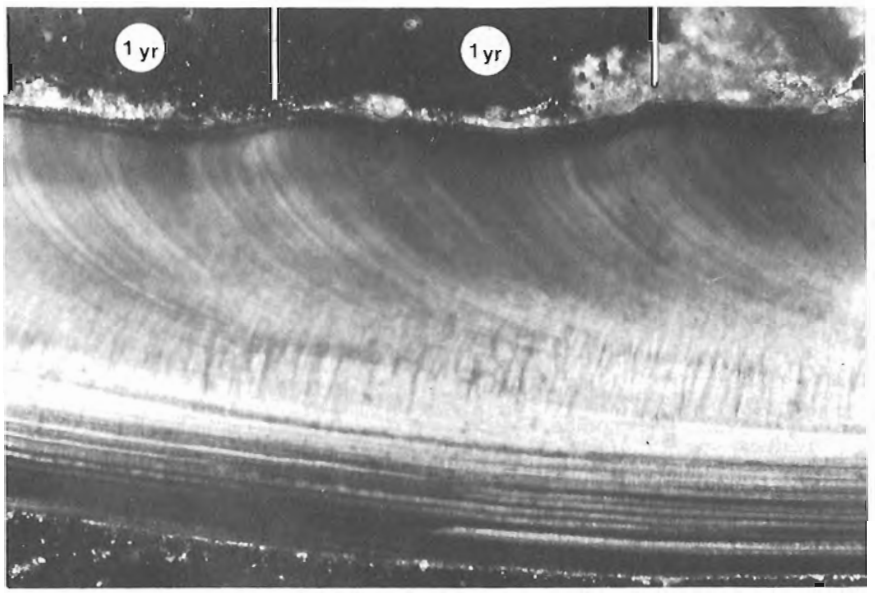

Figure 19.10

Crossed lamellar region of the inner shell layer of the chondrophore showing the regular and continuous minor lines within two of the annual bands. Sample RI12A, magnification 63X.

sites at Frobisher Bay (39 years) and the storm beach at Johnson Point, on Banks Island (34 years). Mutually consistent estimates were obtained for most of the younger specimens, such as those from Greenland and Ellesmere Island. The two specimens from tidal pools and the Scottish material show more regular growth bands under the umbo than near the ligamental pit and they had a shorter life span (8 to 13 years) than those from the lower tidal zone. The small subtidal specimen (BS-74-108) shows numerous poorly defined growth increments, some of which were counted as growth bands. Shells from northern storm beaches show a wide variation in the relative prominence of their annual bands and minor growth increments (e.g. BS-74-4C with simple bands and BS-74-4E with complex ones). It probably results from postmortem transport of subtidal specimens characterized by poorly defined annual bands.

The rate of growth declines with age and involves an unusually slow increase of umbonal shell thickness in Saunders and Banks islands (Fig. 19.7). The regularity of the growth curves supports the hypothesis that the bands represent annual cycles of growth (Fig. 19.8). The specimens from Banks Island show crude cyclic variations in the width of their two increments, with a periodicity of about 8 years (Fig. 19.9).

Preliminary studies on the maximum number of minor growth increments preserved on the umbonal margin of the chondrophore (inner shell layer) show an average of 45 increments per year in the **Mya** from a tidal pool in Frobisher Bay (Fig. 19.10). Successive annual bands showed a range of 36 to 59 increments. The finely banded region of the specimen from Arran averaged 60 increments per year, with a maximum of 114 bands in the fourth year. A specimen from the low tidal zone in Frobisher Bay (RI12A) is not so finely banded. The maximum number of increments observed in the fifteenth year of a Rodgers Island specimen (RI12A) occurred in the internal part of the crossed lamellar layer of the chondrophore (18), the umbonal margin of the chondrophore (18), and the internal edge of the outer homogeneous layer at the ventral margin (14). The four to five increments preserved in the umbonal area of the inner shell layer and the external edge of the outer shell layer were partially removed by resorption near the pallial line. The later growth bands of large arctic **Mya** generally developed a lenticular fabric near the pallial line. Specimen BS-74-4D showed more continuous bands resembling climbing-ripple lamination.

It would seem likely that the number of minor growth increments per annual band increases in lower latitude environments, due to an increase in the number of tidal cycles within the growing season and a decrease in the proportion of translucent crystals which do not preserve growth lines.

Conclusions

New evidence based on counts of the internal growth bands along the ligamental pit of the chondrophore and through the umbonal region of the inner shell layer, suggest a maximum age of 40 years for arctic and subarctic **Mya truncata** from modern intertidal zones. Their growth rate is only reduced by about 10 per cent between latitudes 64°N and 79°N in the Canadian Arctic (Fig. 19.8), the marked size reduction at Ellesmere Island being largely due to a reduction in longevity. The older shells seen in storm beaches on other northern islands are characterized by a thin inner shell layer and may have been transported from subtidal sands. In contrast, the **Mya** from the largely unfrozen seas of temperate latitudes show a more rapid linear growth rate and presumably have a shorter maximum life span. Studies of fossil bivalves from high latitudes could therefore aid the recognition of former glaciations.

It would be unwise to apply the observations from **Mya** to this problem without formulating a suitable general model for bivalve microstructures. An emphasis on periodic shell dissolution due to winter anaerobic metabolism (Lutz and Rhoads, 1980), or the effect of high temperatures and tidal exposure on organic membrane growth (Richardson et al., 1980), is only appropriate for temperate bivalves. These processes may apply to **Mya** living in gravel-floored tidal pools covered by the ice foot. However, they are not ultimately responsible for the rapid deposition of disorganized aragonite and discontinuous growth lines, which characterize this significant environment. **Mya** from lower sites probably grow more continuously through the year and paradoxically add relatively thin annual increments to the inner shell layer. Their small number of minor increments per year, the paucity of microborings, and the occurrence of partially filled cavities inside the hinge line, may be diagnostic of periodically frozen seas. Offshore, the arctic **Mya** maintain a slower and more continuous growth rate, which suggests there is little difference between high and low latitude molluscan microstructures in the deep ocean.

Acknowledgments

Thanks are extended to W. Blake, Jr. for logistical support in 1983, for providing many of the arctic bivalve samples, and his continued support and encouragement. S.B. McCann supported and supervised J.E. Dale's fieldwork in southern Baffin Island while at McMaster University. Mark Krawetz, Wilf Ruland, Janet Lambert and M.A. Whyte assisted in the collection of samples and provided information. M.A. Whyte also read the paper. Bob Bignell and Jack Whorwood provided the photographic services. R.A. Hewitt wishes to acknowledge financial support from the N.S.E.R.C. grant awarded to Professor G.E.G. Westermann at McMaster University.

References

Andrews, J.T.
1972: Recent and fossil growth rates of marine bivalves, Canadian Arctic, and Late-Quaternary Arctic marine environments; Palaeogeography, Palaeoclimatology, Palaeoecology, v. 11, p. 157-176.

Bernard, F.R.
1979: Identification of the living Mya (Bivalvia:Myoidea); Venus, v. 38, p. 185-204.

Blake, W., Jr.
1975: Radiocarbon age determinations and postglacial emergence at Cape Storm, southern Ellesmere Island, Arctic Canada; Geografiska Annaler, Series A, v. 57, p. 1-71.

Brousseau, D.J.
1979: Analysis of growth rate in Mya arenaria using the Von Bertalanffy Equation; Marine Biology, v. 51, p. 221-227.

Carter, J.G.
1980: Guide to bivalve shell microstructures; in Skeletal Growth of Aquatic Organisms, Biological Records of Environmental Change, ed. D.C. Rhoads and R.A. Lutz; Plenum Press, New York, p. 645-673.

Jones, D.S.
1980: Annual cycle of shell growth increment formation in two continental shelf bivalves and its paleoecologic significance; Paleobiology, v. 6, p. 331-340.

1983: Sclerochronology: Reading the record of the Molluscan shell; American Scientist, v. 71, p. 384-391.

Kennedy, W.J., Taylor, J.D., and Hall, A.
1969: Environmental and biological controls on bivalve shell mineralogy; Biology Review, v. 444, p. 499-529.

Lutz, R.A.
1976: Annual growth patterns in the inner shell layer of Mytilus edulis L.; Journal of the Marine Biological Association of the United Kingdom, v. 56, p. 723-731.

Lutz, R.A. and Rhoads, D.C.
1980: Growth patterns within the molluscan shell: An overview: in Skeletal Growth of Aquatic Organisms, Biological Records of Environmental Change, ed. D.C. Rhoads and R.A. Lutz; Plenum Press, New York, p. 203-254.

MacDonald, B.A. and Thomas, M.L.M.
1980: Age determination of the soft-shelled clam Mya arenaria using shell internal growth lines; Marine Biology, v. 48, p. 105-109.

Newcombe, C.L.
1936: Validity of concentric rings of Mya arenaria for determining age; Nature London, v. 137 (3457), p. 191-192.

Ockelmann, W.K.
1958: The zoology of East Greenland. Marine Lamellibranchiata; Meddelelser om Grønland, v. 122, no. 4, 256 pp., 3 pls.

Richardson, C.A., Crisp, D.J., Runham, N.W., and Gruffydd, L.D.
1980: The use of tidal growth bands in the shell of Cerastoderma edule to measure seasonal growth rates under cool temperate and sub-arctic conditions; Journal Marine Biological Association, v. 60, p. 977-989.

Swan, E.F.
1952: Growth of the clam Mya arenaria as affected by the substratum; Ecology, v. 33, p. 530-534.

Taylor, J.D., Kennedy, W.J., and Hall, A.
1973: The shell structure and mineralogy of the Bivalvia II. Lucinacea – Clavagellacea, Conclusions; Bulletin of the British Museum (Natural History) Zoology, v. 22, no. 9, pp. 255-294.

Thompson, I., Jones, D.S., and Dreibelbis, D.
1980: Annual internal growth banding and life history of the ocean quahog Arctica islandica (Mollusca:Bivalvia); Marine Biology, v. 57, p. 25-34.

Thorson, G.
1936: The larval development, growth and metabolism of Arctic marine bottom invertebrates; Meddelelser om Grønland, v. 100, no. 6, p. 1-155.

Zolotarev, V.N.
1980: The life span of bivalves from the sea of Japan and sea of Okhotsk [In Russian]; Biologiya Morya, v. 6, p. 3-12.

20.

THE BURSTING OF A SNOW DAM, TINGMISUT LAKE, MELVILLE ISLAND, NORTHWEST TERRITORIES

Project 770037

J.A. Heginbottom
Terrain Sciences Division

Heginbottom, J.A., The bursting of a snow dam, Tingmisut Lake, Melville Island, Northwest Territories; in Current Research, Part B, Geological Survey of Canada, Paper 84-1B, p. 187-192, 1984.

Abstract

In July 1979 snowmelt from the hills surrounding Tingmisut Lake, Melville Island, accumulated in the lake basin, trapped behind a dense snowdrift which blocked the valley of the outlet stream. The water level rose until it overtopped this snow dam, and the flowing water cut down rapidly through the dam, resulting in a major flood event downstream. An estimated 1.6 x 10^6 m^3 of water drained from the lake in 36 hours. The implications of such events are discussed.

Résumé

En juillet 1979, l'eau de fonte des neiges provenant des collines qui entourent le lac Tingmisut, dans l'île de Melville, s'est accumulée dans le bassin lacustre, retenue derrière un barrage de neige dense qui bloquait l'exutoire d'écoulement vers la vallée. Le niveau de l'eau s'est élevé jusqu'à ce qu'il dépasse ce barrage de neige, puis, en s'écoulant, l'eau s'est rapidement frayée un chemin à travers celui-ci, ce qui a provoqué une grave inondation en aval. En 36 heures, le lac a perdu une quantité d'eau estimée à 1,6 x 10^6 m^3. L'auteur se penche ici sur les implications de phénomènes semblables.

Introduction

This report describes the first hand observation of an event which, while it may occur quite commonly, is not often seen. In early July 1979, the small valley which drains Tingmisut Lake, Melville Island, Northwest Territories, was almost completely blocked by a dam formed by a large drift of compact, windblown snow, immediately below the outlet of the lake. As the winter's accumulation of snow in the basin surrounding Tingmisut Lake melted and ran off into the lake, the level rose until it finally overtopped the snow dam. The resulting flood event in the outlet valley can only be described as catastrophic, in relation to the small valley concerned.

The account which follows is a largely qualitative description of the breaching of the snow dam. No instruments suitable for recording hydrological parameters such as discharge or flow velocity were available in camp.

Terminology

Woo (1979, 1980) used the term "snow jam" to describe what is here called a "snow dam" – a large snowdrift which more or less completely blocks the valley of an intermittent stream and which fails by being overtopped by meltwater during the spring (Fig. 20.2A, B). In this report, the term "snow jam" is used to describe a more ephemeral obstruction caused by a pile up of large, loose blocks of snow. As described below, a "snow jam" was formed downstream of the snow dam by the failure and collapse of a snow bridge. As the water level behind the jam rises, in response to the obstruction, the blocks float, allowing some water to escape. The jam then reforms and again partially blocks the stream. This mechanism is regarded as being analogous to ice jamming on perennial rivers, and even log jams.

Flood event of 1979

When first seen on July 20, at 1800 h, the snow dam was all the way across the valley below the outlet of the lake. It extended about 500 m down the valley and ended in an almost vertical snow cliff 3-4 m in height (Fig. 20.2A). Examination of the face of the snow cliff showed that the dam was composed of layers of windblown snow with several narrow bands of dirt or dust. The snow dam formed in a valley with one steep side slope (the left bank) and one relatively gently side slope (the right bank). The snow dam apparently started as a lee-side drift on the gentle slope. This drift grew across the valley until it contacted the steep side. From this, it can be deduced that the dominant wind that built the drift was westerly. Downstream of the snow dam, the valley was walled on the east side by a rock cliff, 5-6 m in height, and on the west side by the vertical face of a large snow drift, continuous with the snow dam, and 4-5 m in height. This "gorge" section extended downstream for some 350 m where the valley opened out. Here a second, much smaller snow dam blocked the valley. Below this, the valley is open down to the sea at Weatherall Bay. The distance between the dam and the sea is about 2.5 km along the stream channel.

On July 20, the water level in Tingmisut Lake was high, as most of the snow on the surrounding hills had melted. The shores of the lake slope very gently, and the high water level had resulted in shoreline flooding, particularly at the southeast end, near the outlet (Fig. 20.1). When the upstream boundary of the dam was first seen, a little water was leaking into the snow dam and flowing onto the dam surface (Fig. 20.2B). This coalesced into a small, suprasnow stream flowing in a meandering channel, 20 to 30 cm wide and about 30 cm deep, over the surface of the dam. About half-way down the dam this stream disappeared into a "moulin", near the east side of the snow dam, reappearing at the base of the snow cliff which formed the downstream face of the dam (Fig. 20.2A). Some internal erosion may thus have been active within the dam.

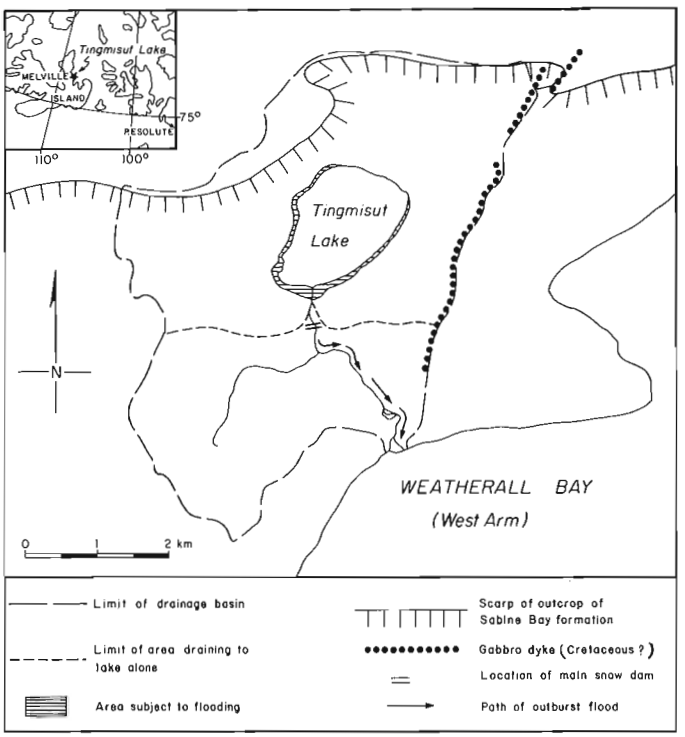

Figure 20.1. *Location map and site map for Tingmisut Lake, Melville Island, Northwest Territories.*

The sequence of events leading up to the overtopping of the snow dam on July 22 are as follows. During the previous two days, the upper edge of the dam had been eroded by wave action. On July 21 small amounts of water had begun to flow onto the dam. Most of this appeared to soak into the snow. After about midday on July 22, the weather, which had been fairly cool until then, warmed. During the afternoon the flow of water onto the dam increased until there was a continuous stream flowing as far as the moulin noted above. At about 1900 h the capacity of the moulin was exceeded and a pond began to develop on the surface of the dam (Fig. 20.3A). The rate of flow onto the upper part of the dam continued to increase as the channel across the upper part was enlarged by thermal erosion. By 2045 h this pond, now quite extensive, began to spread across the downstream part of the snow dam. Throughout this period, there was no appreciable increase in the flow of water discharged from the pipes in the face of the snow dam. The pond on the dam surface gradually spread until, at 2120 h, it spilled over the last barrier on the dam surface and, at 2125 h it began to spill down the face of the dam (Fig. 20.3B, C).

By 2300 h the stream had become a wide, fast-flowing torrent which had carved a deep notch in the face of the snow dam (Fig. 20.3D, E). Downstream of the upper dam, the water ponded behind the second dam until it was some 2 m deep, when it overtopped this dam. Farther downstream the stream continued as a torrent that completely filled the stream bed, flowing between walls of rock and snowbanks. The torrential flow continued throughout the night (Fig. 20.3F).

On the morning of July 23, the stream was still flowing across ice in the area of the upper part of the main snow dam. In the lower part of this dam, the stream had cut down to the boulders and bedrock of its normal bed (Fig. 20.4A). The increased flow of water in this section led to the sides of the "snow gorge" being undercut, by as much as 2 m in places. Periodically large blocks of snow would break away, falling into the stream (Fig. 20.4B). Farther downstream, the second dam had become a snow bridge (Fig. 20.5A). At about 1115 h this bridge collapsed, partially damming the stream again (Fig. 20.5B) and forming a "snow-jam", as discussed above. As the water level behind it rose the blocks floated, the jam failed, and some water escaped. The jam then reformed and blocked the stream again. The result was a period of pulsed flow farther downstream.

By the morning of July 24, 36 hours after the dam was first overtopped, the water level in the lake had dropped to near its normal summer level. At this stage, the level of the lake is controlled by a sill of bedrock and boulders. The flooding around the shore of the lake had retreated, and the flow of water in the stream was considerably reduced.

Estimate of 1979 flood magnitude

A rough estimate of the volume of water involved was made, based on field observations of the fall in lake level and on the area of the lake as measured on a vertical aerial photograph (Fig. 20.6). In the 36 hour period following the overtopping of the dam at 2125 h, 22 July 1979, the water level in the lake dropped approximately 80 cm.

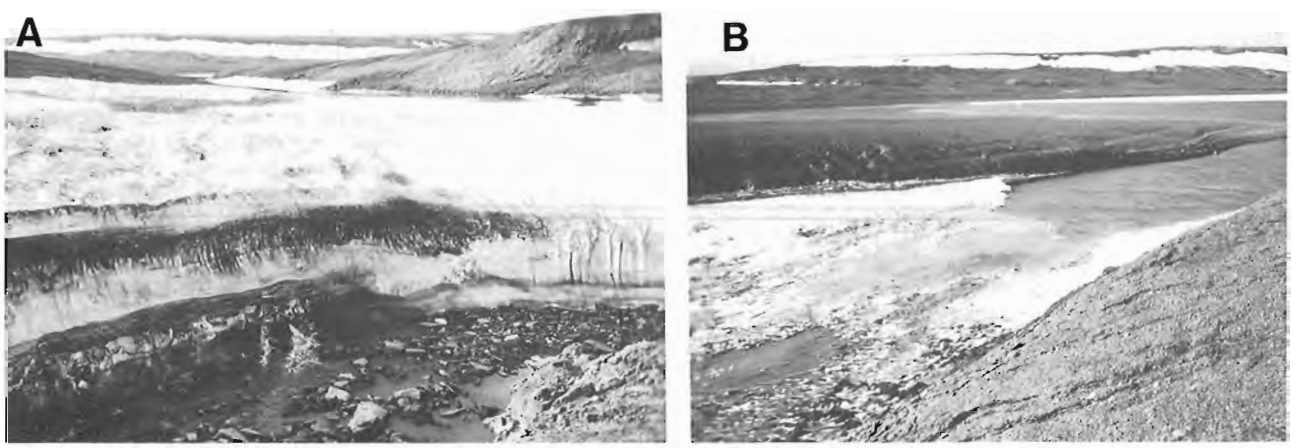

A. Downstream face of main dam; note water leaking from base of dam. (GSC 203553-V)

B. Head of dam with flooded area of Tingmisut Lake beyond. (GSC 203553-A)

Figure 20.2. *The main snow dam as first seen on 20 July 1979, at 1800 h.*

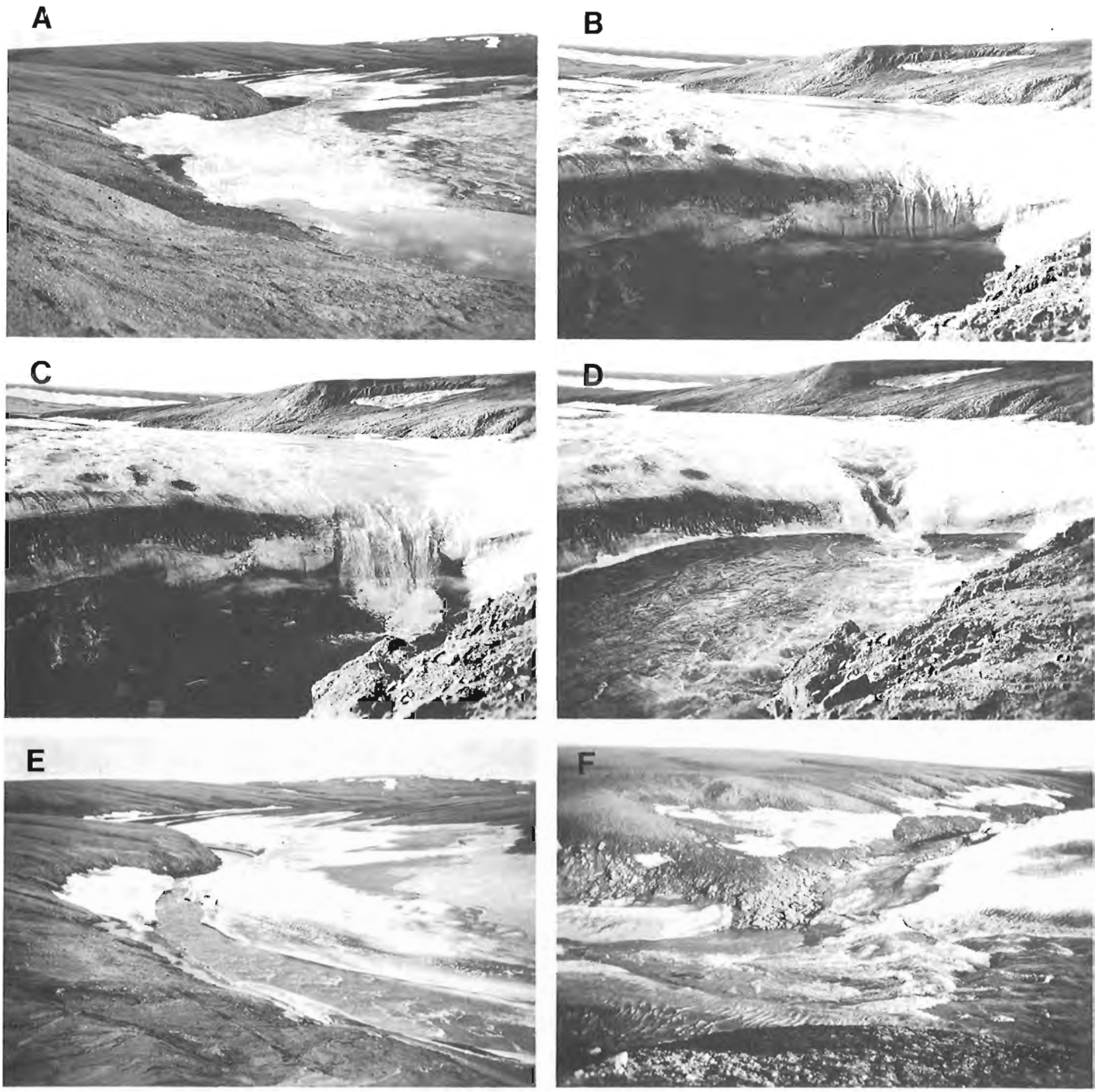

A. *1900 h: pond forming above moulin and spreading across the lower part of the main dam. (GSC 203554-T)*

B. *2120 h: water beginning to spill down face of dam. (GSC 203554-I)*

C. *2125 h: water pouring over snow dam. (GSC 203554-L)*

D. *2300 h: notch cut in main dam; water backing up due to second snow dam farther downvalley. (GSC 203553-E)*

E. *2300 h: channel cut across main snow dam (looking downstream). (GSC 203554-C)*

F. *2310 h: torrential flow in stream below the snow dams. (GSC 203553-F)*

Figure 20.3. *The failure of the main snow dam on the evening of 22 July 1979.*

The area of the lake was measured on airphoto A16763-55. By comparison with the 1:250 000 NTS map (78 H, Byam Channel), the actual scale of this photograph was determined to be 1:56 000. The area of the lake was measured at 612 mm^2 on the photograph, which equals 1.92×10^6 m^2.

Tingmusit Lake has a very gently sloping margin and at flood level is considerably more extensive than at low water. Field observations suggested that the area of dark grey, waterlogged soil evident on the airphoto (Fig. 20.6) was representative of the flooded area. The area was determined to be about 250×10^3 m^2, for a total lake area at flood level of 2.17×10^6 m^2. If this parcel of water is regarded as the frustum of a cone, with a height of 80 cm, the volume of water released is approximately 1.60×10^6 m^3.

From this volume, a rough estimate of the peak discharge was made – 102.7 $m^3 \cdot s^{-1}$ – using the empirical formula developed by Clague and Mathews (1973). Woo (1980), in studying a small lake on Cornwallis Island, also subject to flooding by the formation of a snow dam, noted the areally averaged spring flood had a value of 6.5 $m^3 \cdot s^{-1} \cdot km^{-2}$. In this example, with a drainage area of 12.9 km^2 (also measured on airphoto A16763-55) and a discharge of 102.7 $m^3 \cdot s^{-1}$, the areally averaged spring flood of Tingmisut Lake equals 6.8 $m^3 \cdot s^{-1} \cdot km^{-2}$, a very comparable value.

Previous flood events

An attempt was made to determine whether similar flood events had occurred in this valley in previous years. All available aerial photographs of the area were examined, and an attempt was made to contact all people who had visited the Tingmisut Lake area in the last few decades. In both cases the results were inconclusive. There is some evidence to suggest that floods probably occurred in 1973 and 1977, and may have occurred in 1962, 1971, and 1972. No flood occurred in 1981. Generally low snowfalls in the winter of 1981-82 resulted in a very shallow snowpack and low runoff. The dam was seen between July 5 and July 10, by which time it had not failed.

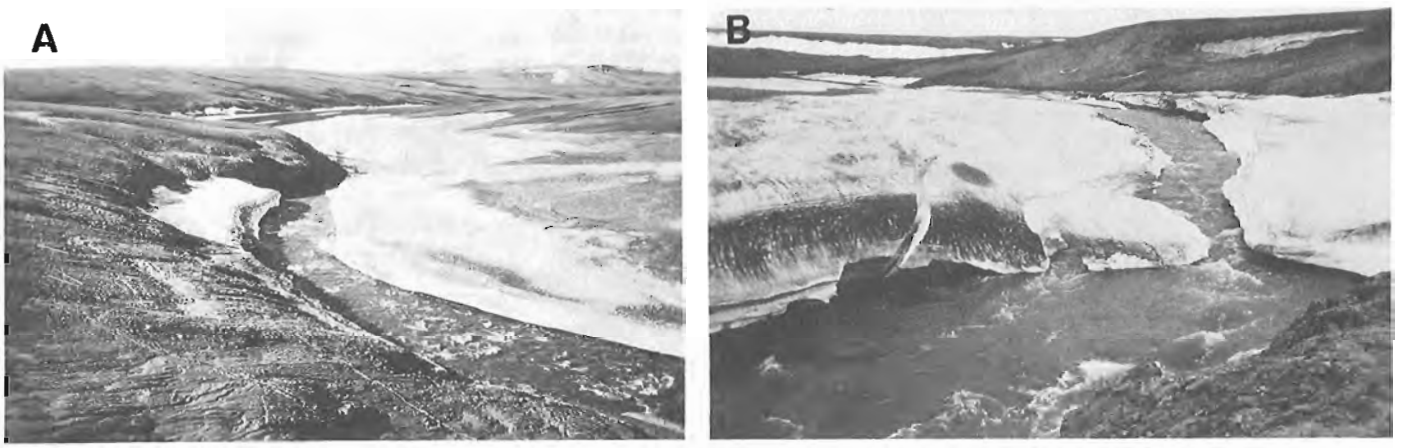

A. 0800 h: channel across main snow dam cut down to natural, rocky stream bed (compare with Fig. 20.3A and 20.3E). (GSC 203553-U)

B. 0800 h: collapsing walls of gorge, following undercutting. (GSC 203553-H)

Figure 20.4. *The remains of the snow dam on the morning of 23 July 1979.*

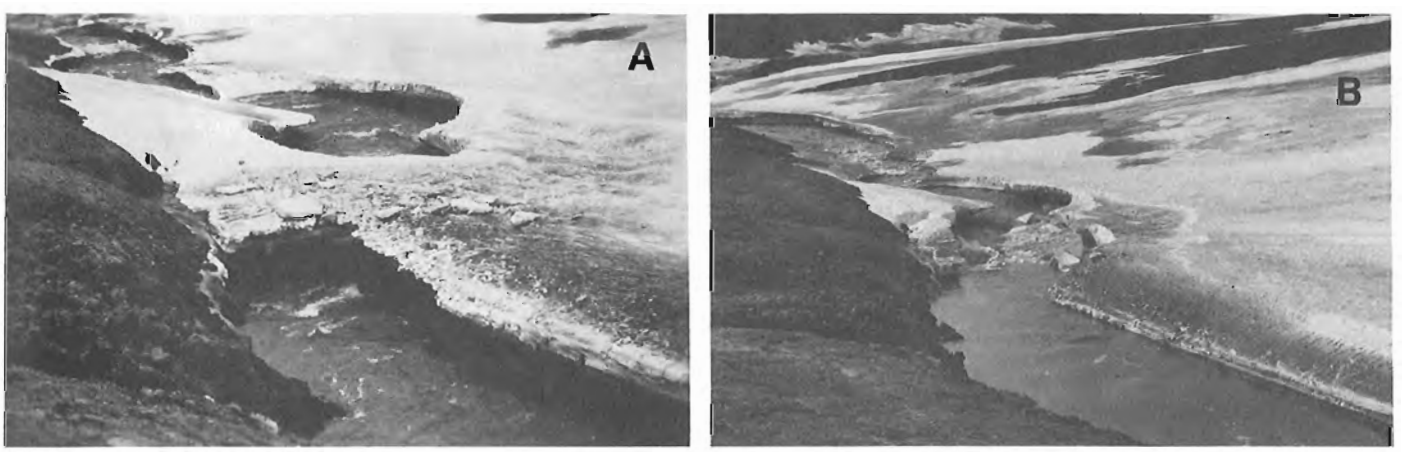

A. 1100 h: snow bridge at site of the lower snow dam. (GSC 203554-D)

B. 1115 h: collapse of the snow bridge and formation of the snow jam. (GSC 204018-H)

Figure 20.5. *Formation of the snow jam at the site of the lower snow dam on the morning of 23 July 1979.*

Figure 20.6

Vertical airphoto of Tingmisut Lake, taken in August 1950 (NAPL A16763-54). Arrow marks site of main snow dam.

Discussion

Previous report of snow dams in Arctic and Alpine environments

Similar flood events have seldom been reported in the literature. Some occurrences on eastern Bathurst Island in early July 1976 are reported by Wedel et al. (1978, p. 28), and others have been seen in central Bathurst Island by the author. An extensive description of snow dams and associated floods is presented by Woo (1979) for the period 1976 to 1978 for rivers in the vicinity of Resolute, Cornwallis Island. In a discussion of the conditions required for the development of a snow dam, Woo (1979) suggested that they are formed by compact, wind-drifted snow that has accumulated in stream valleys throughout the long arctic winter. Incised stream valleys, bordered by steep slopes are usually infilled with larger amounts of snow than more open, non-incised valleys.

A related phenomenon, the damming of an ice-marginal meltwater stream by falling glacier ice is described from Ellesmere Island by Ballantyne and McCann (1980). Burkimsher (1983) reported the damming of a subglacial steam by collapse of a tunnel within the Pasterzengletscher, Austria, in 1980. Floods due to both ice jams and snow dams have been reported from Baffin Island by Church (1972).

Distribution of snow dams

Consideration of the general conditions required for the development of snow dams suggests that they will largely be confined to Arctic regions. An open, windy landscape appears to be necessary for the redistribution of snow into drifts filling gullies and small valleys. Furthermore, wind plays a key role in the formation of dense, compact snow, such as would seem to be essential for a drift that will effectively dam a stream.

The density of newly fallen snow can vary from as low as 0.1 g/cm^3 in cold, wind-free conditions, to over 0.4 g/cm^3 for windblown snow (Mellor, 1964, p. 49). Maxwell (1980, Table 3.22) has estimated mean monthly snow cover densities for 15 stations in the Arctic Islands. His estimates range from 0.23 to 0.38 g/cm^3. Longley (1960) reported snow densities of 0.25 to 0.38, with a mean of 0.30 g/cm^3 from a site at Resolute, Cornwallis Island. Cowan (1966), working at Schefferville, Quebec, examined the differences in snow density in three different vegetation and terrain situations. He found that in well sheltered areas (closed cover forest) snow densities were less than 2.0 g/cm^3 and in some cases ran close to 0.1 g/cm^3. Within the forest edge zone densities were generally between 0.2 and 0.3 g/cm^3, but in open areas (on frozen lakes in this case) densities were as high as 0.3 to 0.4 g/cm^3. These data support the commonly held idea that arctic snow is denser and more compact than snow in other areas.

It is common to find snowbanks in Arctic regions occupying the same locations year after year. Thus it should be expected that snow dams will tend to recur in approximately the same locations in the same stream valleys; however, they may not fully block the valley each and every

year. Also, a catastrophic, dam-burst flood may not always occur. The actual occurrence of a dam or a flood will depend on the amount of snow fall, the amount of snow drift, and the pattern of snowmelt. All of these factors will vary from year to year.

Although it is concluded above that snow dams and associated floods are probably confined to Arctic regions, there are circumstances when analogous phenomena could be expected in sub-Arctic or temperate latitudes. Snow dams and floods identical to those already discussed could occur in mountainous regions, above upper timberline. They are less likely here, as snowmelt tends to progress up the mountain, and so the dam may partially melt before any significant amount of water can develop behind it.

At lower elevations, avalanche deposits could possibly block a stream, particularly early in the melt period. The ice or remoulded snow of an avalanche deposit could well be dense and compact enough to be impervious to water and so act as a dam (Haeberli, 1983). Elsewhere, in temperate and sub-Arctic regions the snow is generally too porous to dam up any significant quantity of water. Slush avalanches are a more likely result than water floods from snow dam failures (Washburn, 1980).

Implications of snow dam bursts

Snow dams and the flood events that can occur when a snow dam fails catastrophically are of more than just intrinsic interest. They have serious implications for the location and design of various forms of structures in northern regions. The greatest concern is for the design of structures, the details of sizing of which are in some manner related to the discharge of a stream or river. Chief among these are buried pipeline crossings and road crossings of streams.

In either case, if the hydrologist responsible for determining the design discharge for the stream in question visits the area in the latter part of the summer season, he may see no evidence of flooding. The snow dam remnants will have melted and the stream may look small, insignificant, and harmless. The hydrologist will probably use some form of rational formula to estimate his design discharge. If there are lakes in the system, he may well conclude that lake storage effects will give a reduced peak discharge, and design structures accordingly.

In the case of the stream draining Tingmisut Lake, this approach would yield an underestimate of the peak discharge. Here, the presence of the lake seriously aggravates the situation by providing storage space for much water before the snow dam is overtopped and destroyed. The resulting flood event is considerably larger than if the lake did not exist.

Thus in determining the design discharge for a culvert, a buried pipeline crossing, or any other structure for which stream discharge is significant, the possibility of such flood events of some considerable magnitude must be taken into consideration. In addition, the possibility of such floods must be considered in the siting of facilities beside streams which may be subject to snow damming.

Acknowledgments

S.G. Evans kindly commented on an earlier draft of this paper. Field assistance by P. Sauvé and A. Everard is appreciated.

References

Ballantyne, C.K. and McCann, S.B.
1980: Short lived damming of a high-arctic ice-marginal stream, Ellesmere Island, N.W.T., Canada; Journal of Glaciology, v. 25, no. 93, p. 487-491.

Burkimsher, M.
1983: Short term irregularities of discharge of glacial meltwater streams; Journal of Glaciology, v. 29, no. 101, p. 198-199.

Church, M.
1972: Baffin Island sandurs: a study of arctic fluvial processes; Geological Survey of Canada, Bulletin 216, 208 p.

Clague, J.J. and Mathews, W.H.
1973: The magnitude of jokülhlaups; Journal of Glaciology, v. 12, no. 66, p. 501-504.

Cowan, W.R.
1966: Snow survey of Schefferville, 1964-65; in Field Research in Labrador-Ungava, McGill Sub-Arctic Research Papers No. 21, p. 135-143; McGill University, Department of Geography, Montreal.

Haeberli, W.
1983: Frequency and characteristics of glacier floods in the Swiss Alps; Annals of Glaciology, v. 4, p. 85-90.

Longley, R.W.
1960: Snow depth and snow density at Resolute, Northwest Territories; Journal of Glaciology, v. 3, no. 28, p. 733-738.

Maxwell, J.B.
1980: The climate of the Canadian Arctic Island and adjacent waters; Environment Canada, Atmospheric Environment Service, Climatological Studies No. 30, v. 1, 532 p.

Mellor, M.
1964: Snow and ice on the Earth's surface; in Cold Regions Science and Engineering Monographs, Part III, Section A, ed. F.J. Sanger; U.S. Army, Cold Regions Research and Engineering Laboratory, 105 p.

Washburn, A.L.
1980: Geocryology; John Wiley and Sons, Halstead Press, New York, 406 p.

Wedel, J.H., Thomas, G.A., and Baracos, P.C.
1978: Site intensive hydrologic study of a small catchment on Bathurst Island: Department of Indian and Northern Affairs, Environmental and Social Committee Report No. AI-17, 122 p.

Woo, M-K.
1979: Breakup of streams in the Canadian High Arctic; Proceedings, Eastern Snow Conference, 36th Annual Meeting, Alexandria Bay, New York, p. 95-107.

1980: Hydrology of a small lake in the Canadian High Arctic; Arctic and Alpine Research, v. 12, no. 2, p. 227-235.

21.

DRILLING AND SAMPLING IN FROZEN SEABOTTOM SEDIMENTS, SOUTHERN BEAUFORT SEA

Projects 730019 and 820038

P.J. Kurfurst, K. Moran[1], and F.M. Nixon
Terrain Sciences Division

Kurfurst, P.J., Moran, K., and Nixon, F.M., Drilling and sampling in frozen seabottom sediments, southern Beaufort Sea; in Current Research, Part B, Geological Survey of Canada, Paper 84-1B, p. 193-195, 1984.

Abstract

Various drilling and sampling equipment, using different techniques, has been employed to drill and collect marginally frozen samples of seafloor sediments. Different types of corers and samplers are described and their performance is evaluated.

Résumé

Divers types d'instruments de forage et d'échantillonnage, faisant appel à des techniques différentes, ont été employés, pour forer et recueillir des échantillons marginalement gelés des sédiments du fond de la mer. Les auteurs décrivent ici différents types de carottiers et d'échantillonneurs, puis ils procèdent à l'évaluation du rendement de ces instruments.

Introduction

A two-week experimental drilling and sampling program was carried out in early April 1983, in an area of frozen seabottom sediments east of Pullen Island, near Tuktoyaktuk, Northwest Territories. Piston corers and a portable vibracorer with various sampling tools were employed from the stable, 2 m-thick landfast ice zone to drill and sample frozen sands, silts, and clays. The drilling, carried out in water depths from 5 to 13 m, penetrated the seafloor sediments to a maximum depth of 2 m.

A combination of various drilling and sampling techniques and tools was used in an attempt to compare and evaluate drilling performance (advance rate, depth penetration) and capability for the recovery of relatively undisturbed samples of marginally frozen soils.

Equipment

The equipment used includes several types of corers, drill string, and feed and hoist systems.

Piston corer

A piston corer, as described in Shepard (1973), was used with a 70 kg head weight, a 3 m-long steel core barrel, ABS plastic core liner (6.7 cm diameter), and a Benthos split piston. The corer was also tried with a bare 1.5 m length of the plastic liner and the same piston and head weight. Finger-type core catchers were used in both cases. Due to the small diameter of the ice hole and the shallow water depth, the ice platform was used to control the piston during core penetration of the seabed. Figure 21.1A is a schematic of the standard oceanographic core triggering method and Figure 21.1B shows the method used in this study.

Vibracorer

A portable, lightweight vibracorer (Archibald, 1983) was used extensively in order to evaluate its performance in frozen sediments. The system consists of a gasoline engine prime mover, flex-shaft transmission, and rod top oscillator. Power is provided by a 7 h.p., four-stroke single-cylinder gasoline engine and transmitted through a centrifugal clutch-pully and flex-shaft. This drive unit weighs about 40 kg and occupies about 0.25 m^3 of space. The oscillator, mounted on top of the drill rod string, weighs about 10 kg and vibrates at a frequency of about 200 Hz.

Drill string

The drill string used was made up of standard NQ-size diamond drill rods, about 152 cm long, adapted to a variety of sampling tools. The simplest sampling system consisted of a tapered shoe and core spring located at the end of the drill rod string just below a "side ejector" (flow-through) section of the drill string. This sampling tool recovered a nominal 5 cm-diameter sample. A 3 m-long, 10 cm diameter aluminum tube and a 1.5 m-long PVC plastic tube with finger-type core catcher and one-way valve were used for recovering large size cores. One attempt was made to drive the 3 m piston core barrel with the vibracorer for sampling a 7 cm-diameter core. Finally, a short wireline diamond drill barrel, with soil shoe and plastic inner tube 1 m long, was used for continuous sampling of 5 cm diameter core.

Feed and hoist system

The feed system for the vibracorer used the ice as a reactive force with two "deadman" rods anchored below the ice through augered holes. Small ratchet winches were connected to the anchors to maintain and control tension on the anchor wires during core penetration. These winches were, in turn, attached to the oscillator through a shock-absorbing lanyard (Fig. 21.2). The hoisting equipment used for both the piston corers and the vibracorer drill string included a light aluminum tripod and a hand winch (Fig. 21.3).

Performance

Performance of the various drilling and sampling techniques and equipment was followed closely during the program. However, the variety of sampling approaches tested during only 11 days on the ice and under moderately difficult working conditions did not allow for a detailed analysis.

[1] Atlantic Geoscience Centre, Dartmouth

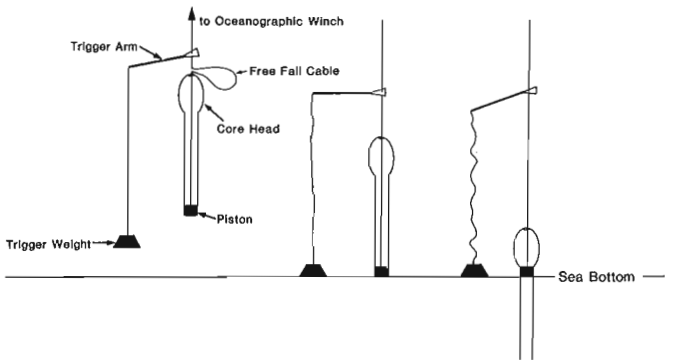

Figure 21.1A. *Schematic of a core trigger system for standard oceanographic piston corer.*

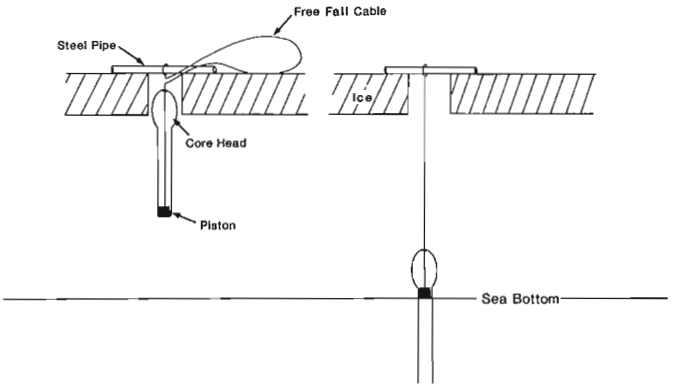

Figure 21.1B. *Schematic of a core trigger system in shallow water from an ice platform.*

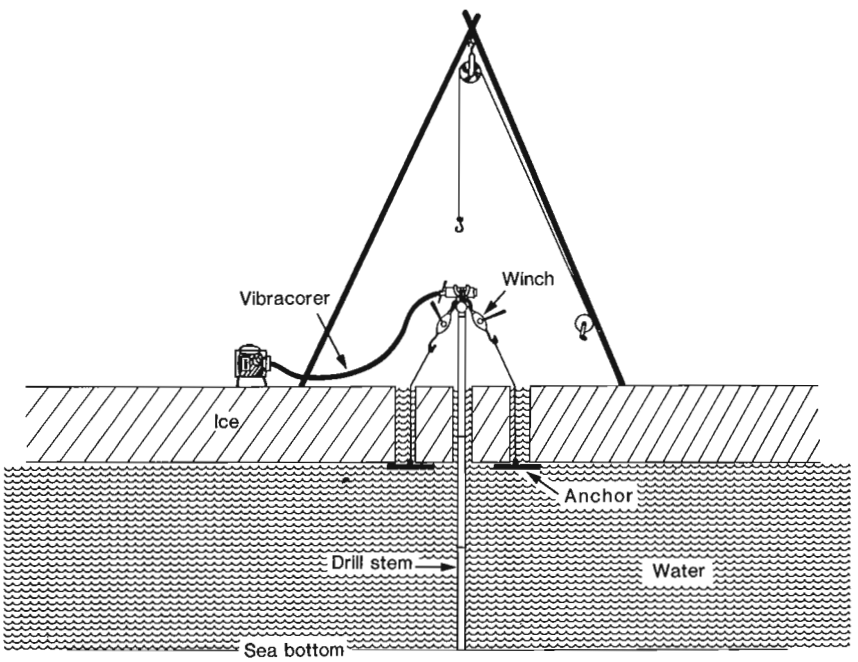

Figure 21.2

Feed and hoist system used with the vibracorer.

Piston corers

The piston corer configurations were tested and neither provided more than short (20-40 cm) core. The free-falling head weight was not massive enough to generate the force required to penetrate the high strength sediments. The weight used was restricted by the size of the hole that could be drilled through 2 m of ice in a practical length of time. Since the standard head with adjustable weight (maximum 360 kg) would not fit through the augered hole, the substitute 70 kg weight was used. Water depth varied from 5.6 m to 13.0 m including 2 m of ice. It is probable that with increased mass, increased core penetration and sample recovery would occur. However, the hoisting equipment and ice augering techniques may have to be modified for increased head weight (load) and size (ice hole diameter).

Vibracorer

All mechanical aspects of the vibracorer's functions were satisfactory and some were impressive. The engine started and ran well in temperatures ranging from -10 to -30°C with no special treatment. Vibration was transmitted effectively through the drill rod string in varying water columns to drill and sample tools of different materials, sizes, and frontal areas, which penetrated the sediments, to a shallow depth at least, with relative ease.

Large-diameter tube samples

The 3 m-long, 10 cm-diameter aluminum sample tube was used with the vibracorer and penetrated 3 m of sand in less than 10 minutes. Although hoisting was achieved without vibration, some core from the lower part of the sampler was lost and the core spring was carried up the core barrel. Only about 1 m of core was in the tube, thus suggesting that the material was significantly compacted during coring. Since no liner was used, the core was vibrated out of the barrel. Core extrusion using the oscillator was vigorous. even violent, and added to further disturbance of the sample.

This sampling tool was lost before being used in any fine sediments. A PVC sample tube with core catcher and trap valve was substituted and produced core up to

Figure 21.3. *Tripod with winch assembly.*

1.5 m long, as limited by the length of the sample tube. Rates of penetration and resistance to hoisting differed with type of sediment investigated. Penetration ranged from several metres per minute to less than 10 cm per minute. Hoisting forces of as much as one tonne were required.

Small-diameter tube samplers

The piston core barrel was adapted to the NQ-size drill rods and tested in the sandy sediments. Only 60 cm of the sediment was penetrated before the drilling advance slowed and stopped. After hoisting of the core barrel was completed, core examination showed that, despite the precautions taken, sand had seeped between the liner and the core barrel. Lack of penetration may have been due to the large frontal area of the barrel and/or to presence of large clasts in the sediment.

A similar trial using the shoe attached to the NQ-size drill rods at the same site produced good penetration to a depth of 2 m. The slowest advance without feed was at a rate of 10 cm per minute. No core spring or side ejector was used and most of the sample was lost.

Wireline

Wireline technique offers the potential for sampling long, continuous core without the stratigraphic uncertainties of the flow-through techniques. The only problems encountered were caused by material flowing between the inner and outer tubes. Although the inner tube was adjusted to near zero clearance, overdrilling caused by loss of core or by its differential distortion resulted in the sample tubes being jammed. When there was enough space in the sample tube and when sufficient feed was applied, no refusal was experienced to the depth of investigation.

A finger-type core spring worked well for sample retention in fine, stiff sediments. Saturated sands or loose mud required a different configuration. The trap-type tube head improved sample retention even in these types of sediments. The PVC inner tube sampler stood up to all stresses and temperatures and served well, when trimmed and capped, as a protective sample container.

Conclusions

Piston corers, although capable of performing the required sampling, proved inefficient due to several factors. The small weight (70 kg) generated insufficient force to penetrate the sediments to depths greater than 60 cm below seabed.

The vibracorer proved efficient with a variety of sampling tools to a depth of about 2 m, which was the maximum capacity with the feed and hoist system used. To reach a depth from 3 to 6 m, the system would require stronger feed and hoisting equipment and/or a flushing system for wireline use. Both these additions would add appreciably to the total weight and complexity of the operation, which is contrary to its main attractions of extreme portability, light weight, and simplicity.

References

Archibald, A.
1983: Portable sampling drill for exploration; The Northern Miner, April 21, p. A26.

Shepard, F.
1973: Submarine Geology; Harper and Row, New York, 517 p.

22.

PENNSYLVANIAN, PERMIAN AND TRIASSIC CONODONTS FROM THE CACHE CREEK GROUP, CACHE CREEK, SOUTHERN BRITISH COLUMBIA

Project 810028

M.J. Orchard
Cordilleran Geology Division, Vancouver

Orchard, M.J., Pennsylvanian, Permian and Triassic conodonts from the Cache Creek Group, Cache Creek, southern British Columbia; in Current Research, Part B, Geological Survey of Canada, Paper 84-1B, p. 197-206, 1984.

Abstract

Pennsylvanian, Permian and Triassic conodonts from the type area of the Cache Creek Group demonstrate that the Melange Unit of the eastern belt consists of mid- to Upper Pennsylvanian and Lower Permian limestone blocks enclosed within a younger matrix of Late Permian and Triassic age. Permian conodonts from both the blocks and the matrix have affinity with American Midcontinent faunas. In contrast, the Marble Canyon Formation of the central belt is probably wholly younger than the limestone blocks of the melange but is coeval with the melange matrix. Late Permian conodonts from the Marble Canyon Formation have affinity with Asian faunas.

Résumé

Les conodontes d'âge pennsylvanien, permien et triasique provenant de la zone du groupe de Cache Creek montrent que l'unité Mélange de la zone est constituée de blocs calcaires d'âge pennsylvanien moyen à supérieur et d'âge permien inférieur; ces blocs se trouvent à l'intérieur d'une matrice plus jeune d'âge permien supérieur et triasique. Les conondontes d'âge permien provenant des blocs et de la matrice montrent une affinité avec les faunes du << Midcontinent>> américain. Par contre, la formation de Marble Canyon de la zone centrale est probablement entièrement plus jeune que les blocs calcaires du mélange, mais elle est contemporaine de la matrice du mélange. Les conodontes d'âge permien supérieur de la formation de Marble Canyon ont une affinité avec les faunes asiatiques.

Introduction

Late Paleozoic and early Mesozoic conodonts from the type area of the Cache Creek Group are documented herein. The conodonts date many of the sediments that either lack macrofossils or contain macrofossils that are too deformed for adequate identification. The conodonts also serve as a faunal standard for the Cache Creek Terrane, a Cordilleran tectonostratigraphic package regarded as exotic in terms of North American geology because of its Late Permian fusulinacean faunas which are of 'Tethyan' aspect (e.g. Ross and Ross, 1983), that is, they closely resemble coeval faunas in regions surrounding the present Western Pacific and Himalaya.

The conodont samples (see Fig. 22.1, Table 22.1) were collected, largely by K.R. Shannon, during regional mapping of the Ashcroft area (Monger and McMillan, 1984). Three stratigraphic units, previously discussed by Shannon (1981), are covered by this study. They are the Melange Unit, the Greenstone Unit, and the Marble Canyon Formation. The first two of these are included in the eastern belt of the Cache Creek Terrane by Monger and McMillan (1984), who referred limestone of the Marble Canyon Formation to the central belt. Most of the Permian fossils previously reported from Cache Creek terrain, and regarded as characteristic of it, are from Marble Canyon Formation. Many of the conodonts reported herein came from the Melange Unit and thus provide an important supplement to the faunal picture. Within Melange Unit, a clear distinction may be made between the matrix sediments and the blocks contained within it. This study demonstrates that the blocks are consistently older than the matrix.

An earlier report (Orchard, 1981) on some Triassic conodonts from strata west of Marble Canyon, now referred to the western belt of the Cache Creek Terrane by Monger and McMillan (1984), is the only previous documentation of the conodont faunas, although they have been discussed elsewhere in a regional context (Orchard, 1983).

The conodont faunules

In general, conodonts from the Cache Creek (see Table 22.2) area are not well preserved and they are commonly fragmented. This reflects the considerable amount of shearing that has affected many of the rocks. The CAI (Colour Alteration Index) of the conodonts is generally between 4 and 5, implying post-depositional temperatures of between 200° and 300°C (Epstein et al., 1977).

The faunule interpreted to be the oldest known in the area was collected from a limestone outcrop that may be part of a large block (>1 km). The faunule (no. 2, Fig. 1, Table 22.2) comprises a three to one ratio of **Idiognathodus** aff. **I. claviformis** and **Gondolella magna** sensu lato. The former lies close to the species that occurs in Desmoinesian and Early Missourian strata in the central United States, whereas **G. magna** s. l. embraces specimens known from Desmoinesian through middle Wolfcampian strata of middle and western North America. The age of the faunule is therefore regarded as probably late Middle or early Late Pennsylvanian, Desmoinesian or Missourian. Faunules 11 and 17 may be impoverished correlatives of the Scottie Creek limestone since they both contain **Idiognathodus,** although this genus is known through most of the Pennsylvanian and lowest Permian. These two faunules were collected from

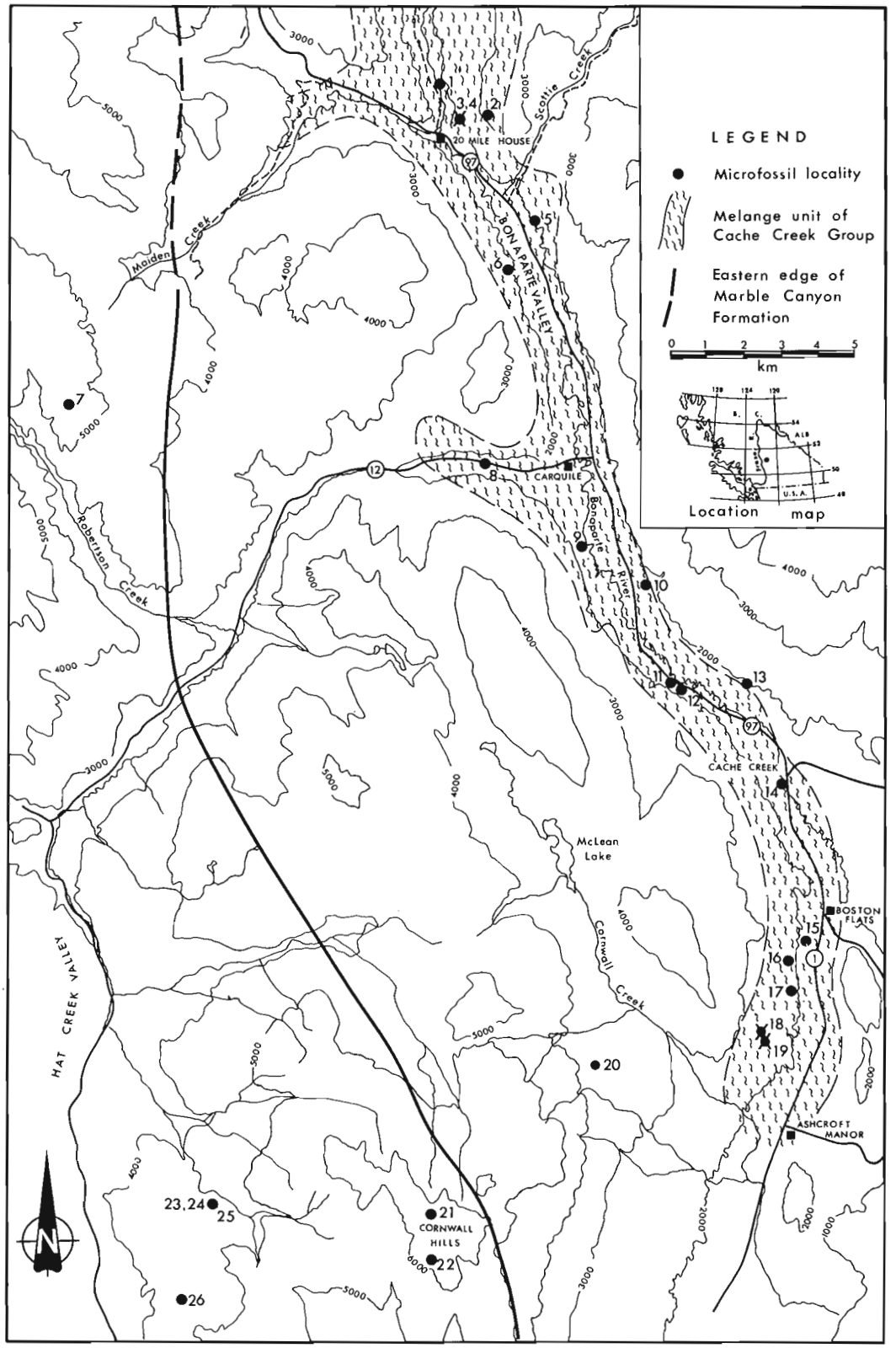

Figure 22.1. *Simplified geology and locality map of the Cache Creek area showing site of microfossil collections listed in Table 22.1*

Table 22.1. Summary of microfossil collections, GSC Locality numbers assigned, lithologic/stratigraphic description of processed sample, and age

Figure 1	GSC Loc. No.	Description	Age
1	C- 87070	grey crinoidal massive lst.	prob. Virgilian-Wolfcampian
2	C- 87067	grey crinoidal massive lst.	prob. Desmoinesian-Missourian
3	C- 87073	1 m lst. bed in phyllite	Guadalupian, Capitanian
4	C-102500	ribbon chert	Guadalupian
5	C- 87071	calcareous grit/breccia	prob. Guadalupian
6	C- 87083	interstitial lst. in pillows	indet.
7	C-102552	green chert	(M. Permian?)
8	C- 87650	grey ribbon chert	Permian (Early)
9	C- 87072	black lst. bed in phyllite	prob. Guadalupian
10	C- 87080	10 m dia. lst. block	indet.
11	C- 87068	7 m dia. lst. block	Atokan-Wolfcampian
12	C- 87084	lst. block	Wolfcampian
13	C- 87069	lst. block	Wolfcampian
14	C- 87066	2 x 3 m dia. lst. block	prob. Virgilian-Wolfcampian
15	C-102560	grey chert	indet.
16	C- 87074	lst. clasts in volcaniclastics	prob. M. to L. Permian
17	C- 87076	100 x 40 m lst. block	Atokan-Wolfcampian
18	C-102551	grey ribbon chert	Ladinian-Carnian
19	C- 87649	ribbon chert	post-Wolfcampian Permian (Early)
20	C-103592	(bio)clastic lst.	prob. Guadalupian (?Wordian)
21	C- 87078	grey limestone	Norian, Early?
22	C- 87077	black micritic lst.	Smithian
23	C- 87651	brown ribbon chert	post-Wolfcampian Permian (Leonardian?)
24	C- 87652	black chert	(Leonardian?)
25	C- 87081	black lst. in volcaniclastics	Permo-Triassic
26	C- 87079	grey crinoidal massive lst.	Early Norian
27	C- 87055	black lst. in phyllite	Dienerian
28	C- 87058	cherty lst.	Late Carnian-Early Norian

NOTE: Age shown in parenthesis for nos. 7, 8, 19, 23 and 24 are based on radiolarian faunules (B. Murchey, pers. comm., 1981). Locations are shown in Figure 22.1, except localities 27 and 28, which are shown as MaCa3 and MaCa1, respectively, in Orchard (1981, Figure 51.1).

TRIASSIC	L	NORIAN CARNIAN
	M	LADINIAN ANISIAN
	E	SPATHIAN SMITHIAN DIENERIAN GRIESBACHIAN
PERM.	L	DZULFIAN GUADALUPIAN
	E	LEONARDIAN WOLFCAMPIAN
PENN.	L	VIRGILIAN MISSOURIAN
	M	DESMOINESIAN ATOKAN
	E	MORROWAN

Figure 22.2. *Subdivision of the Late Palaeozoic and Triassic.*

recrystallized, mottled grey and white limestone blocks in a matrix of phyllite and chert. Similar limestone blocks produced faunules 10, 12, 13, 14 and probably 1. All but the first of these contain **Streptognathodus elongatus,** or a closely allied form, a species that ranges from the Late Pennsylvanian to Early Permian, Wolfcampian (Sweet, in Ziegler, 1975; Clark et al., 1979). In faunules 12 and 13, this streptognathodid is accompanied by **Neogondolella bisselli,** a late Wolfcampian index. This association has previously been recorded from the Oquirrh Formation of Utah (Larson and Clark, 1979). A specimen tentatively referred to **Neognathodus roundyi** occurs in faunule 14. Data in Lane et al. (1971), Sweet (in Ziegler, 1975), and Clark et al. (1979) collectively suggest a Morrowan through Wolfcampian age for that species. The limestone blocks, ranging in size from a few metres to several hundred metres, therefore appear to be of at least two ages: an older, probably Desmoinesian-Missourian limestone and a younger, Wolfcampian limestone. Faunules 1 and ?14 are regarded as Virgilian through Wolfcampian in age, and hence some continuity of stratigraphy may be represented by these transported limestones.

The remainder of the conodont data from the Melange Unit, and elsewhere, documents a younger history. At the moment, there is no definite conodont evidence for latest Wolfcampian through Leonardian sedimentation, an interval that is widely recognized elsewhere in the western Cordillera by species of **Sweetognathus** and **Neostreptognathodus,** genera that may have preferred shallower water, or more carbonate-rich habitats than were available at that time in the area.

Table 22.2. Numerical data on conodont faunules from the Cache Creek area (see Fig. 22.1)

	1	2	3	4	5	6	7	8	9	10	11	12	13	14	15	16	17	18	19	20	21	22	23	24	25	26
Palaeozoic conodonts:																										
Diplognathodus? sp.	-	-	1	-	-	-	-	-	-	-	-	-	-	-	-	-	-	-	-	-	-	-	-	-	-	-
Ellisonia sp.	?	-	X	-	-	-	-	-	-	-	-	-	-	-	-	-	-	-	-	?	-	-	-	-	-	-
Gondolella magna s. l.	-	16	-	-	-	-	-	-	-	-	-	-	-	-	-	-	-	-	-	-	-	-	-	-	-	-
Hindeodus spp.	1	2	2	-	-	-	-	-	1	-	-	1?	-	-	-	1	-	-	-	-	-	-	-	-	-	-
Idiognathodus aff. I. claviformis	-	45	-	-	-	-	-	-	-	-	2?	-	-	-	-	-	1?	-	-	-	-	-	-	-	-	-
Neognathodus cf. N. roundyi	-	-	-	-	-	-	-	-	-	-	-	-	-	1	-	-	-	-	-	-	-	-	-	-	-	-
Neogondolella bisselli	-	-	-	-	-	-	-	-	-	-	-	5	1?	-	-	-	-	-	-	-	-	-	-	-	-	-
N. denticulata	-	-	2	-	-	-	-	-	-	-	-	-	-	-	-	-	-	-	-	-	-	-	-	-	-	-
N. postserrata s. l.	-	-	200+	4	2	-	-	-	20	-	-	-	-	-	-	-	-	-	-	-	-	-	-	-	-	-
N. sp. A	-	-	-	-	-	-	-	-	-	-	-	-	-	-	-	-	-	-	-	9	-	-	-	-	-	-
N. sp. B	-	-	-	-	1?	-	-	-	6	-	-	-	-	-	-	-	-	-	-	-	-	-	-	-	-	-
N. sp. C	-	-	10	-	-	-	-	-	-	-	-	-	-	-	-	-	-	-	-	-	-	-	-	-	-	-
N. sp. indet.	-	-	-	-	2	-	-	1	-	-	-	-	-	-	-	-	-	-	5	-	-	-	2	-	-	-
Streptognathodus elongatus	1?	-	-	-	-	-	-	-	-	-	-	6	3?	2	-	-	-	-	-	-	-	-	-	-	-	-
Triassic conodonts:																										
Epigondolella abneptis A	-	-	-	-	-	-	-	-	-	-	-	-	-	-	-	-	(1)	-	-	-	-	-	-	-	-	3
Neogondolella cf. N. navicula	-	-	-	-	-	-	-	-	-	-	-	-	-	-	-	-	(1?)	-	-	-	5	-	-	-	-	-
Neospathodus waageni	-	-	-	-	-	-	-	-	-	-	-	-	-	-	-	-	-	-	-	-	-	2	-	-	-	-
'Paragondolella' sp(p).	-	-	-	-	-	-	-	-	-	-	-	-	-	-	-	-	-	5	-	-	1?	-	-	-	-	-
Ramiform elements	X	X	X	X	X	-	-	X	X	X	?	X	-	X	-	X	X	X	X	X	-	-	X	-	X	-
Radiolarians	-	-	-	X	-	-	X	X	-	-	-	-	-	-	X	-	-	X	X	-	-	-	X	X	-	-
Ichthyoliths	-	-	-	-	-	X	-	X	-	?	-	-	-	-	-	X	-	-	-	-	-	-	-	-	-	X

However, some radiolarian faunules from cherts of the Melange Unit (nos. 8, 19?, 23?, 24?) may be of this age (Murchey, personal communication, 1981). Sparse conodont faunas also extracted from these cherts (nos. 19, 23) may be also Leonardian in age, but they are not specifically diagnostic of that interval.

Diagnostic Late Permian, Guadalupian faunules are known from several thin limestones and from chert interbedded with phyllites and volcaniclastics of the Melange Unit. At least three species of **Neogondolella** are represented, the most common of which is referred to **N. postserrata** sensu lato. The latter species is abundant in a 1 m turbiditic limestone (faunule 3) interbedded with, and containing clasts of, chert and phyllite. This species, which also occurs in the overlying chert, has previously been recorded from Wordian and Capitanian strata of the Bell Canyon Formation in the Delaware Basin of West Texas (Behnken, 1975; Clark and Behnken, 1979), and possibly from China (Wang and Wang, 1981). A second species that occurs both in Texas and in faunule 3 is **Neogondolella denticulata,** a species that is restricted to Capitanian and Amarassian strata in the Delaware Basin (Clark and Behnken, 1979). Therefore, faunule 3 is regarded as Capitanian in age. Additional specimens referred to **N. postserrata** sensu lato occur in faunules 5 and 9, in which **N.** sp. B is associated. These too are from thin limestones interbedded with phyllite and chert; they may be a little older than faunule 3.

A fusulinid-crinoidal limestone (no. 20) mapped within the Greenstone Unit by Shannon (1981) yielded neogondolellid fragments referred to **N.** sp. A. This species resembles some specimens from the Phosphoria Formation and Gerster Limestone of Wyoming and Nevada referred to **N. rosenkrantzi** by Wardlaw and Collinson (1979). Additional specimens from faunule 3 referred to **N.** sp. C also have features in common with **N. rosenkrantzi** sensu Wardlaw and Collinson (1979), which characterizes Wordian and ?Capitanian strata in the western United States. In the Cache Creek Group, the presence of elements close to **N. rosenkrantzi** is regarded as suggestive of a Guadalupian age.

Conodonts are uncommon in the massive limestones of the Marble Canyon Formation, dated as mid- to Late Permian on the basis of their fusulinid fauna (see Trettin, 1980 for summary of fossil localities). No Permian conodonts have been found within these limestones in the Cache Creek area but the fusulinid data indicate that the limestones are in part coeval with the Permian part of the melange matrix. Farther north, at the north end of the Marble Range, several conodont faunules have been recovered from limestone. In contrast to the melange conodonts, faunules there are dominated by 'diplognathodids' and hindeodids, some of which are unknown elsewhere in North America. One species resembles **'Diplognathodus' movschovitschi** which was originally described from the lower Dzhulfian of Azerbaidzhan SSR (Kozur, 1975) and has since been tentatively recorded from Upper Permian (Kuman) strata in Japan (Igo, 1981). Hence, the Marble Canyon Formation may include the youngest Permian in North America.

Fragments that may represent **D. movschovitschi** occur also within Lower Triassic limestones interbedded with phyllites in Marble Canyon (Orchard, 1981); those strata also contain additional rare Permian elements (e.g. Plate 22.2, figures 2, 6) referred to **Sweetognathus** cf. **S. iranicus** and **Neostreptognathodus**? sp. indet. These conodonts in the Marble Canyon fauna (Orchard, 1981) imply that a strongly reduced or negative sedimentary regime prevailed thereabouts in the Late Permian and/or Early Triassic. In addition, they provide a link between the massive Permian limestones of the Marble Canyon Formation and the Lower Triassic phyllitic sediments that are now included in the western belt of the Cache Creek Group (Monger and McMillan, 1984).

More phyllites, cherts, thin limestones and volcaniclastics of Early Triassic age are seen to the south beneath Cornwall Hills where faunule 22 is dated as Smithian on the basis of **Neospathodus waageni.** This is slightly younger than the Dienerian sediments of Marble Canyon wherein **Neospathodus dieneri, N. peculiaris** and **Neogondolella carinata** are the dominant pectiniform elements. The conodonts from these Early Triassic sediments have no counterpart in the Melange Unit.

Younger Triassic conodonts have been recovered from sediments included within both the Marble Canyon Formation and the Melange Unit. In the southern part of the study area, limestones (nos. 21, 26) are dated as Late Triassic, Early Norian on the basis of **Epigondolella abneptis** subsp. A of Orchard (1983), and **Neogondolella** cf. **N. navicula.** Early Norian limestone and chert were also recognized in Marble Canyon (Orchard, 1981), also in close proximity to the Early Triassic sediments. There is at present no indication of Middle Triassic strata in the central and western belts of the Cache Creek Group.

Rare conodonts from the chert matrix of the Melange Unit are thought to be Carnian, or possible Ladinian on the basis of poorly preserved gondolelloids tentatively referred to **Paragondolella.** This age supplements that reported by Travers (1978, p. 102) on the basis of radiolarians and pelecypods from cherts nearby. The lack of post-Guadalupian, pre-Ladinian data from the Melange Unit remains an anomaly.

Conclusions

On the basis of conodonts, the matrix of the Melange Unit of the Cache Creek Group is dated as Guadalupian (Capitanian and? Wordian) and Ladinian or Carnian. Within it are older limestone blocks, of probably Desmoinesian-Missourian and Wolfcampian age. Both Pennsylvanian and Permian conodonts are like those described from Midcontinent sequences and some have yet to be found elsewhere. On the basis of a single faunule, the Greenstone Unit of Shannon (1981) is also dated as Guadalupian (?Wordian).

The Marble Canyon Formation includes Late Permian conodonts that may be as young as Dzulfian. Unlike those from the other units, the faunules characteristically include large numbers of 'diplognathodids'. Some species recovered from the Permian limestones and from overlying(?) phyllitic sediments dated as Early Triassic are known elsewhere only from Asia. However, it should be stressed that rocks of this age have been described from few areas of the world and the known distribution of Late Permian conodonts is consequently restricted. Until a direct comparison of demonstrably coeval faunules from both the Melange Unit and from the Marble Canyon Formation may be made, it is premature to conclude that the eastern and central belt of the Cache Creek Group have markedly different provinciality. Their differing lithologies may account for the observed faunal differences. Locally, the Marble Canyon Formation, as presently mapped, includes Late Triassic, Norian limestones that carry a cosmopolitan conodont fauna.

Acknowledgments

K.R. Shannon collected and processed many of the samples and hence is largely responsible for making this paper possible. E.W. Bamber, C.M. Henderson, J.W.H. Monger and J.A. Roddick suggested improvements to earlier drafts. P.T. Krauss was responsible for some of the photography, T. Oliveric for drafting and B.E. Vanlier for the typescript.

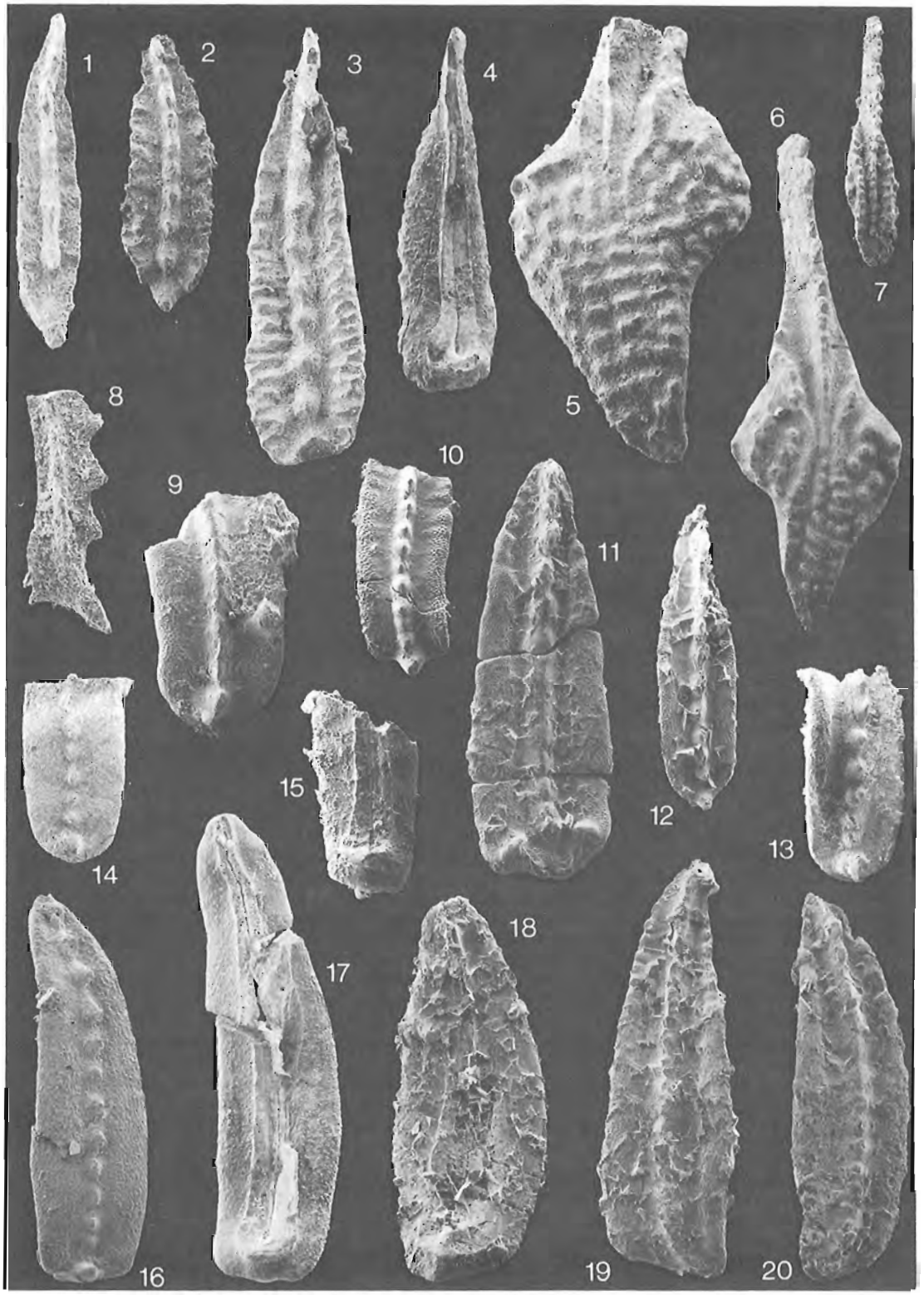
1
2
3
4
5
6
7
8
9
10
11
12
13
14
15
16
17
18
19
20

Taxonomic notes

No systematic descriptions are presented here since the material is generally not suitable. Notes are provided only for species concepts that require explanation. Figured specimens bear GSC type numbers and are deposited in the National Type Fossil Collection (Geological Survey of Canada) in Ottawa.

'Diplognathodus' movschovitschi Kozur & Pjatakova 1975?
Plate 22.2, figures 3?, 4, 8

The broad and slightly asymmetric, deep basal cup, even denticulation of the free blade and fused carina sloping down to the posterior end is characteristic. The Dzulfian holotype is too poorly illustrated to be certain that this is the same species.

Gondolella magna Stauffer & Plummer 1932 sensu lato
Plate 22.1, figures 1-4, 8

Early, medial and late growth stages are evident in the Cache Creek material. The present concept includes species that have been based on these different ontogenetic stages. As far as I can determine **G. bella** from the Early Permian is indistinguishable from Middle and Late Pennsylvanian representatives.

PLATE 22.1

Numbers in brackets refer to fossil localities in Figure 22.1 and Table 22.1. Illustrations are upper views unless stated to be otherwise.

Figures 1-4, 8. **Gondolella magna** Stauffer & Plummer sensu lato. 1. Early growth stage GSC 68992 x100. 2. Medial growth stage GSC 68993 x50. 3. Late growth stage GSC 68994 x50. 4. Lower view, GSC 68995 x50. 8. Lateral view, early growth stage GSC 68999 x100. All from (2).

Figures 5-7. **Idiognathodus** aff. **I. claviformis** Gunnell. 5. Late growth stage GSC 68996 x50. 6. Late growth stage GSC 68997 x35. 7. Early growth stage GSC 68998 x50. All from (2).

Figure 9. **Neogondolella** sp. C. Posterior fragment GSC 69000 x50, from (3).

Figures 10, 15. **Neogondolella** sp. B. Posterior fragments x50, from (9). 10. GSC 69001. 15. Lower view, GSC 69006.

Figures 11, 12, 18-20. **Neogondolella postserrata** Behnken sensu lato. 11. Posteriorly board morph GSC 69002 x50. 12. Aserrate, posteriorly symmetrical morph GSC 69003 x50. 18. Lower view, GSC 69009 x50. 19. Posteriorly asymmetrical sinistral morph GSC 69010 x50. 20. Posteriorly asymmetrical dextral morph GSC 69011 x50. All from (3).

Figure 13. **Neogondolella** sp. A. Posterior fragment GSC 69004 x50, from (20).

Figures 14, 16, 17. **Neogondolella bisselli** Clark & Behnken. 14. Posterior fragment GSC 69005 x50. 16. GSC 69007 x50. 17. Lower view, GSC 69008 x50. All from (12).

Hindeodus sp. A
Plate 22.2, figures 1, 5

A single specimen that resembles **H. typicalis** (Sweet) but differs in an abruptly terminated posterior carina and the presence of some tiny rudimentary nodes on the upper surface of the basal cup.

Idiognathodus aff. **I. claviformis** Gunnell 1931
Plate 22.1, figures 5-7

These specimens differ from the lectotype of **I. claviformis** in having a platform that is relatively longer and posteriorly pointed rather than rounded. In common with **I. claviformis,** the platform is characterized by discontinuous ridges, which appear in the Cache Creek material to develop by transverse elongation of both the medial carina and lateral ridges seen in the early growth stages (figure 7). These specimens strongly resemble the co-type of **I. claviformis** that was first illustrated by Ellison (1941, pl. 23, fig. 13), who transferred it to **I. lobatus** Gunnell, which was itself later transferred to **I. delicatus** Gunnell (Sweet, in Ziegler, 1975, p. 167, 170). The platform ornament of this co-type is characteristic of neither **I. lobatus** nor **I. delicatus** but is like that of the lectotype of **I. claviformis.**

Neogondolella postserrata Behnken 1975 sensu lato
Plate 22.1, figures 11, 12, 18-20

Neogondolellids from the matrix of the Melange Units include morphotypes of the **serrata** complex that show the posterior variation discussed by Clark and Behnken (1979, fig. 2). In addition, rare elements have broad, symmetrical posterior platforms (e.g. Plate 22.1, figure 11), but are otherwise identical to the more common morphotypes. These elements are here regarded as a part of the same platform symmetry series (see also Wardlaw and Collinson, 1979, p. 157-158). In the largest population (faunule 3) asymmetrical forms outnumber symmetrical forms by a ratio of about 2 to 1. Such a ratio is diagnostic for **N. babcocki** Clark and Behnken 1979. In a much smaller faunule (no. 9), this ratio is about 4 to 1, characteristic of **N. aserrata** Clark and Behnken 1979. Because a purely morphological basis for the differentiation of these species is uncertain, I am referring all the Cache Creek specimens to **N. postserrata** s. l.

Neogondolella sp. A
Plate 22.1, figure 13

Posterior platform fragments are terminally rounded, or less commonly subquadrate or slightly asymmetric; a prominent upright cusp is situated anterior of platform termination. The discrete carina nodes increase in size anteriorly. One large fragment has postero-lateral accessory nodes adjacent to the cusp. Anterior fragments have a low blade that rises from a point where the platform margins narrow to meet the anterior end. The lower side of the elements have a pseudokeel with distinctly raised edges. These fragments have the posterior platform outline of **N. bisselli** but have a much more developed cusp and carina. They resemble some specimens referred to **N. rosenkrantzi** by Wardlaw and Collinson (1979, pl. 2, fig. 11, 12, 26), particularly in the presence of the posterior platform brim, and progressive anterior enlargement of the carina nodes.

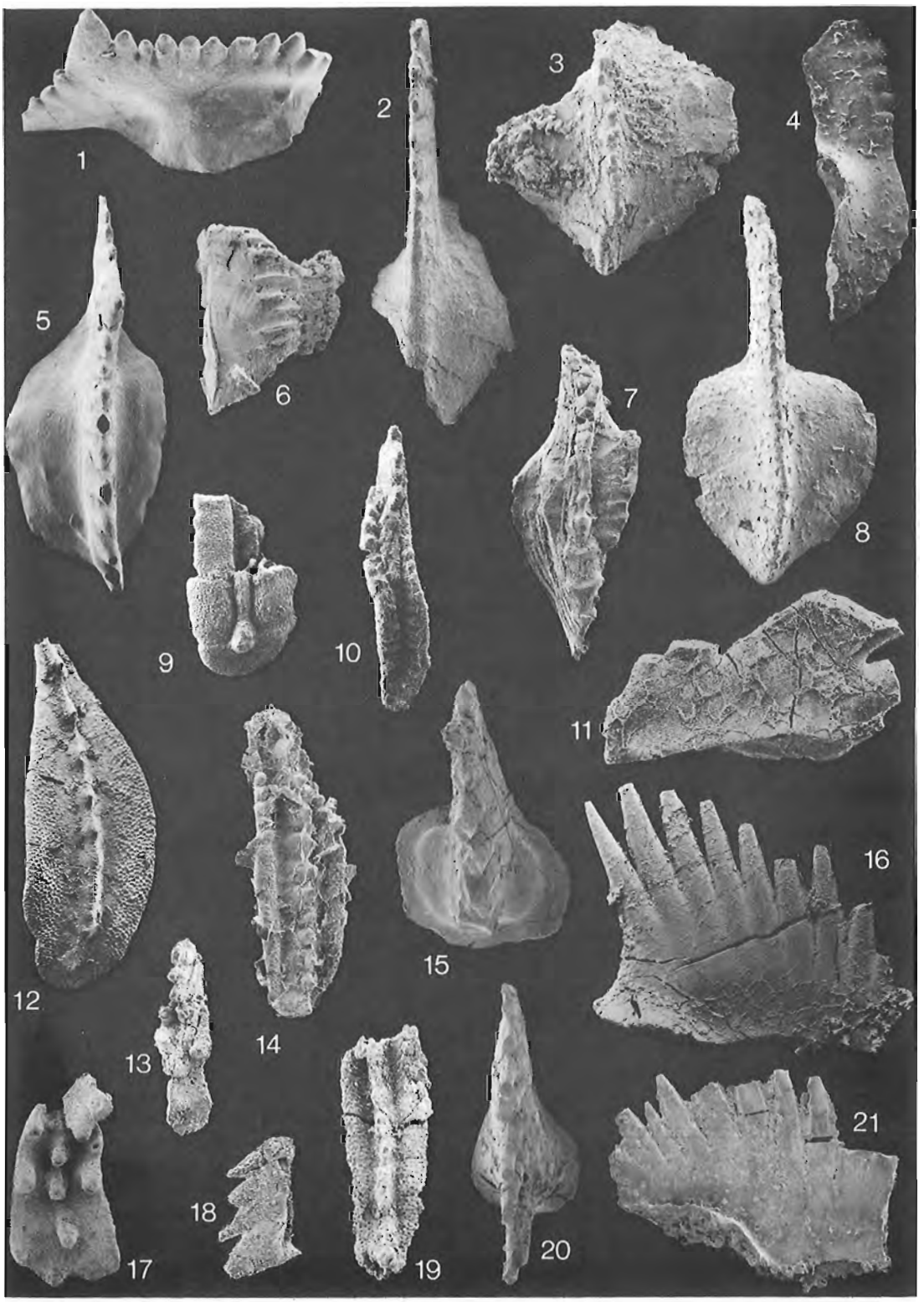
1
2
3
4
5
6
7
8
9
10
11
12
13
14
15
16
17
18
19
20
21

Neogondolella sp. B
Plate 22.1, figures 10, 15

Platform fragments with parallel margins and a quadrate posterior outline. A prominent cusp is situated medially at the posterior end and passes anteriorly into confluent carina nodes of subequal size. One fragment has faint anterior nodes. The lower surface has a pseudokeel with raised edges. These specimens resemble **N. idahoensis** but have a higher carina composed of more numerous nodes.

Neogondolella sp. C
Plate 22.1, figure 9

Neogondolellid fragments with round to subquadrate terminations and largely fused carinas. The cusp may be fused with the adjacent carina node, a feature that is characteristic of some elements referred to **N. rosenkrantzi** by Warlaw and Collinson (1979, pl. 2, fig. 21). A posterior platform brim is developed in some specimens.

PLATE 22.2

Numbers in brackets refer to fossil localities in Figure 22.1 and Table 22.1. Illustrations are upper views unless stated to be otherwise.

Figures 1, 5. **Hindeodus** sp. A. Oblique-upper and upper views, GSC 69012 x100, from (16).

Figure 2. **Sweetognathus** cf. **S. iranicus** Kozur, Mostler & Rahimi-Yazd. GSC 65951 x100, from (27g); posterior part missing.

Figures ?3, 4, 8. **'Diplognathodus' movschovitschi** Kozur & Pjatakova. 3. Posterior fragment GSC 65950 x70, from (27b). 4. Lateral view, GSC 69013 x100, from GSC Loc. No. C-87075. 8. GSC 69015 x100, from GSC Loc. No. C-87075.

Figure 6. **Neostreptognathodus**? sp. indet. Mid-platform fragment GSC 65934 x100, from (27g).

Figure 7. **Neognathodus** cf. **N. roundyi** (Gunnell). Anteriorly broken GSC 69014 x75, from (14).

Figure 9. **Neogondolella** cf. **N. navicula** (Huckriede). Posterior fragment GSC 69016 x50, from (21).

Figure 10. **Streptognathodus elongatus** Gunnell. GSC 69017 x60, from (12).

Figure 11. **Neospathodus peculiaris** Sweet. GSC 65897 x120, from (27g).

Figure 12. **Neogondolella carinata** (Clark) GSC 65880 x100, from (27g).

Figure 13. **Epigondolella** cf. **E. primitia** Mosher. Early growth stage. GSC 69018 x90, from (28c).

Figure 14. **Neogondolella denticulata** Clark & Behnken. Oblique upper view, GSC 69025 x75, from (3).

Figure 15. **Neospathodus** aff. **N. robustus** Koike. GSC 69019 x75, from (27g).

Figures 16, 20. **Neospathodus dieneri** Sweet. Lateral view, GSC 65868 x120, from (27g). 20. GSC 69023 x75, from (27h).

Figure 17. **Epigondolella abneptis** subsp. A of Orchard 1983. Anteriorly broken GSC 69020 x80, from (26).

Figures 18, 19. **Neogondolella** cf. **N. navicula** Huckriede. 18. Lateral view, GSC 69021 x90, from (28a). 19. Anteriorly broken GSC 69022 x90, from (28c).

Figure 21. **Neospathodus waageni** Sweet. Lateral view, GSC 69024 x75, from (22).

Sweetognathus cf. **S. iranicus** Zozur, Mostler and Rahimi-Yazd 1975
Plate 22.2, figure 2

A single incomplete element bearing a low blade composed of five denticles that pass posteriorly into fused denticles of the carina that broaden posteriorly and bear a pustulose micro-ornament. This element closely resembles the smaller growth stages of the species from the Abadehian of Central Iran (e.g. Kozur et al., 1975, pl. 4, fig. 2).

References

Behnken, F.H.
1975: Leonardian and Guadalupian (Permian) conodont biostratigraphy in western and southwestern United States; Journal of Paleontology, v. 49, p. 284-315.

Clark, D.L. and Behnken, F.H.
1979: Evolution and taxonomy of the North American Upper Permian **Neogondolella serrata** complex; Journal of Paleontology, v. 53, p. 263-275.

Clark, D.L., Carr, T.R., Behnken, F.H., Wardlaw, B.R., and Collinson, J.W.
1979: Permian conodont biostratigraphy in the Great Basin; Brigham Young University Geology Studies, v. 26, p. 143-149.

Ellison, S.P.
1941: Revision of the Pennsylvanian conodonts; Journal of Paleontology, v. 15, p. 107-143.

Epstein, A.G., Epstein, J.B., and Harris, L.D.
1977: Conodont Color Alteration – an Index to Organic Metamorphism; United States Geological Survey, Professional Paper 995.

Igo, H.
1981: Permian conodont biostratigraphy of Japan; Paleontological Society of Japan, Special Paper 24.

Kozur, H.
1975: Beiträge zur Conodontenfauna des Perm; Geologische-Paläontologische Mitteilungen Innsbruck, v. 5, pt. 4, p. 1-44.

Kozur, H., Mostler, H., and Rahimi-Yazd, A.
1975: Beitrage zur Mikrofauna permotriadischer Schichtfolgen Teil II: Neue Conodonten aus dem Oberperm und der basalen Trias von Nord – und Zentraliran; Geologische-Paläontologische Mitteilungen Innsbruck, v. 5, pt. 3, p. 1-23.

Lane, H.R., Merrill, G., Straka, J., and Webster, G.
1971: North American Pennsylvanian conodont biostratigraphy Geological Society of America, Memoir 127, p. 395-414.

Larson, J.A. and Clark, D.L.
1979: The Lower Permian (Sakmarian) portion of the Oquirrh Formation, Utah; Brigham Young University Geology Studies, v. 26, p. 135-142.

Monger, J.W.H. and McMillan, W.J.
1984: Ashcroft map-area; Geological Survey of Canada, Open File 980, 1:250 000 map.

Orchard, M.J.
1981: Triassic conodonts from the Cache Creek Group, Marble Canyon, Southern British Columbia; in Current Research, Part A, Geological Survey of Canada, Paper 81-1A, p. 357-359.

1983: The distribution of conodonts in tectonostratigraphic terranes of Western Canada; Geological Society of America, Abstracts with Programs, v. 15 (5), p. 385.

Ross, C.A. and Ross, J.R.P.
1983: Late Paleozoic Accreted Terranes of Western North America; in Pre-Jurassic rocks in Western North American Suspect Terranes, C.H. Stevens, ed., Society of Economic Paleontologists and Mineralogists, p. 7-22.

Shannon, K.R.
1981: The Cache Creek Group and contiguous rocks near Cache Creek, British Columbia; in Current Research, Part A, Geological Survey of Canada, Paper 81-1A, p. 217-221.

Travers, W.B.
1978: Overturned Nicola and Ashcroft strata and their relation to the Cache Creek Group, Southwestern Intermontane Belt, British Columbia; Canadian Journal of Earth Sciences, v. 15, p. 99-116.

Trettin, H.P.
1980: Permian rocks of the Cache Creek Group in the Marble Range, Clinton Area, British Columbia; Geological Survey of Canada, Paper 79-17.

Wang, C-y and Wang, Z-h
1981: Permian conodont biostratigraphy of China; Geological Society of America, Special Paper 187, p. 227-236.

Wardlaw, B.R. and Collinson, J.W.
1979: Youngest Permian Conodont Faunas from the Great Basin and Rocky Mountain Regions; Brigham Young Geology Studies, v. 26, p. 151-163.

Ziegler, W.
1975: Catalogue of Conodonts, v. 2, Stuttgart.

23.

EARLY PERMIAN CONODONTS FROM THE HARPER RANCH BEDS, KAMLOOPS AREA, SOUTHERN BRITISH COLUMBIA

Project 810028

M.J. Orchard
Cordilleran Geology Division, Vancouver

Orchard, M.J., Early Permian conodonts from the Harper Ranch beds, Kamloops area, southern British Columbia; in Current Research, Part B, Geological Survey of Canada, Paper 84-1B, p. 207-215, 1984.

Abstract

Early Permian conodonts from the "Harper Ranch beds" of southern British Columbia are referred to the Wolfcampian zone of ***Neogondolella bisselli – Sweetognathus whitei.*** *Regional and international correlation of this assemblage is presented. Some Permian taxonomic problems are discussed. One new species,* ***Adetognathus paralautus****, is described.*

Résumé

On associe les conodontes du Permien inférieur des couches de Harper Ranch de la Colombie-Britannique à la zone du Wolfcampien de ***Néogondolella bisselli – Sweetognathus whitei.*** *On présente une corrélation régionale et internationale de cet assemblage. On discute quelques problèmes taxonomiques du Permien. On décrit une nouvelle espèce:* ***Adetognathus paralautus.***

Introduction

In this paper the correlation of Early Permian conodonts from the "Harper Ranch beds" of southern British Columbia is discussed. In this, the first systematic account of Permian conodonts from the Canadian Western Cordillera, biostratigraphic and taxonomic discussion focuses on some current problems in Permian conodont studies.

Stratigraphic setting

The strata under discussion have been informally termed the Harper Ranch Group by Danner (in Smith, 1979). These Upper Paleozoic rocks are exposed along the South Thompson River in southern British Columbia (Fig. 23.1). Physiographically, they lie in the eastern Intermontane belt. They constitute the lowest recognized stratigraphic unit of Quesnellia, a tectonostratigraphic terrane bordered on the west by oceanic rocks of the 'Tethyan' Cache Creek Terrane, and on the east by the 'metamorphic welt' of the Omineca Crystalline Belt whose protolith includes rocks from along the ancient continental margin of North America.

The group has been regarded as consisting of two stratigraphic intervals separated by a major disconformity (Smith, 1979). The older package consists of mudstones and volcaniclastics with rare discontinuous limestones. Fossil control includes Late Mississippian to Middle Pennsylvanian brachiopods, corals, foraminiferids and algae (Sada and Danner, 1974; Smith, 1979). Conodont samples collected by J.W.H. Monger during regional mapping provide Late Devonian (Famennian), Early and Late Mississippian ages for this lower unit. The younger package consists of a commonly massive limestone dated as Early and Late Permian, largely on the basis of fusulinids and brachiopods (e.g. Sada and Danner, 1976). The only conodonts so far recovered from the upper unit indicate an Early Permian age, and are the subject of the present paper.

Details of the GSC Locality C-87090

The sampled section lies at the east end of the Harper Ranch at the next to highest terrace (in 1980) within the quarry of Canada Cement Lafarge Ltd. The outcrop area has been illustrated by Danner (1976, Fig. 13-14) and the local geology summarized by Sada and Danner (1974, Fig. 3). Although I collected no fusulinids from this particular outcrop, Sada and Danner (1976) have described the characteristic fauna that is found in the Harper Ranch Lower Permian. They list: **Pseudoschwagerina robusta** (Meek), **P.** sp. A, **Eoparafusulina** sp., and **Waagenophyllum** sp., an association regarded as equivalent in age to the Middle Wolfcampian fauna of Zone E in the McCloud limestone of northern California (Sada and Danner, 1976, p. 216). The precise stratigraphic relationship of this fusulinid fauna to the conodonts described below is not yet determined.

Description of the conodont faunules

The following taxa occur within the limestone beds:

Adetognathus paralautus sp. nov.
Diplognathodus sp. A.
Ellisonia conflexa (Ellison)?
Hindeodus minutus (Ellison)
Merrillina? sp. nov. A.
Neogondolella bisselli Clark & Behnken
Sweetognathus whitei (Rhodes)
S. aff. **S.** whitei (Rhodes)

The distribution of the conodonts is shown in Table 23.1. Sparse faunules collected from 2 m of fine grained, bedded limestones at the eastern edge of the outcrop are characterized by **Diplognathodus** sp. A. This species is similar to several Late Pennsylvanian and Early Permian species described from the Western U.S.A., Japan and Europe (see taxonomy), but cannot be precisely dated at present.

Limestones from the middle part of the section which is separated from the aforementioned beds by a disturbed zone of argillite and green ?tuff, are coarser grained and yield abundant faunules dominated by **Adetognathus paralautus** sp. nov., accompanied by **Sweetognathus** aff. **S. whitei** and **Neogondolella bisselli.**

The more massive beds at the west end of the outcrop, thought to be the stratigraphically highest, contain fewer conodonts. Therein **Sweetognathus whitei** is dominant, and is accompanied by **Neogondolella bisselli;** this is the **bisselli-whitei** Zone. **Ellisonia conflexa**? and **Hindeodus minutus** occur throughout the section.

The age of the conodonts: Extra-Canadian comparisons

The association of **Sweetognathus whitei** and **Neogondolella bisselli** is widespread and comparison may be made with sequences in the Great Basin of the western U.S.A., with eastern Europe, Japan, China, Spitsbergen and Columbia, South America.

In the U.S.A., a **bisselli-whitei** Assemblage Zone was originally defined on the basis of the Moorman Ranch Section in Nevada (Clark and Behnken, 1979, p. 425). There, the zone has now been identified in both the upper Riepe Springs Formation (Clark, 1974) and in the Riepetown Sandstone, below and within which rare fusulinid horizons indicate a middle and late Wolfcampian age for the fauna (Clark and Behnken, 1971).

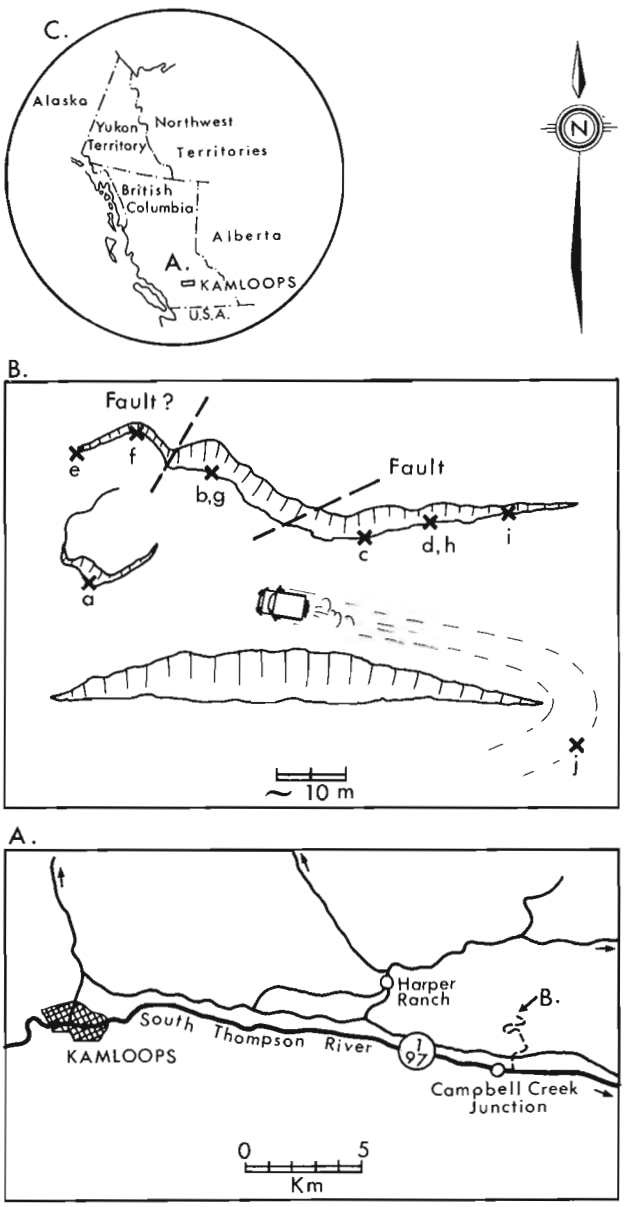

Figure 23.1. *Location of GSC Loc. C-87090 and the conodont samples a-j. Samples a through d were collected in 1980, e through j in 1981.*

Table 23.1. Numerical data on the conodont faunules from samples a through j at GSC Loc. No. C-87090

	a	e	f	g	b	h	d	i	j
Platform elements:									
Adetognathus paralautus									
left-bladed	-	-	-	51	61	-	-	-	-
right-bladed	-	-	-	44	64	-	-	-	-
indet.	-	-	-	150	200	-	-	-	-
Diplognathodus sp. A	3	-	1	?1	-	-	-	-	-
Hindeodus minutus	1	-	3	32	2	-	1	-	-
Neogondolella bisselli	-	-	-	4	13	-	-	5	-
Sweetognathus whitei	-	-	-	-	-	↑ 2	11	15	3
S. aff. S. whitei	-	1	1	44	5	↓	-	-	-
Non-platform elements:									
Ellisonia conflexa?									
Oz = ?Pb	-	-	-	-	-	-	1	-	-
Pl = ?M	-	-	-	-	-	-	4	-	-
Hi = ?Sc	-	-	-	-	-	-	-	1	1
Tr = ?Sa	1	-	-	-	1	-	-	-	-
indet. = S	-	-	-	-	-	2	2	-	-
Merrillina? n. sp. A, Pa?	-	-	-	1	-	-	-	-	-
Carminate element indet.	-	-	-	1	-	-	-	-	-
Undifferentiated ramiforms									
Pb	-	-	2	50	24	-	4	-	-
M	-	-	-	28	6	-	-	1	-
Sc	1	-	-	24	12	-	1	-	1
Sb	2	-	-	10	3	-	-	-	-
Sa	-	-	-	5	2	-	-	-	-

The phylogenetic development of **N. bisselli** and **S. whitei** was not available for documentation in Nevada where these species appear suddenly as what has been termed the 'post-crisis' fauna (Clark, 1972). 'Pre-crisis' elements (see Fauna A in Clark, 1974) are essentially Carboniferous in aspect and no overlap of the two occurs in Nevada. Some degree of overlap does occur in the Tensleep Sandstone of Wyoming (Rhodes, 1963), the type locality of **S. whitei,** and has now been documented also in the Oquirrh Formation, Utah (Larson and Clark, 1979) and in the Wahlstrom Hollow Formation, Idaho (Mytton et al., 1983).

In Kamloops, the occurrence of **Adetognathus** with **Sweetognathus** and **N. bisselli** is another example of overlap. However, the occurrence, and abundance, of **Adetognathus** also certainly reflects some specialized environmental regime and I do not regard its presence as of particular biostratigraphic significance. In common with other 'cavusgnathoids', the conditions under which **Adetognathus** flourished were probably shallow water, and possibly euryhaline and high energy (Chamblerlain and Clark, 1973; Heckel and Baesemann, 1975; Merrill and von Bitter, 1976; Larson and Clark, 1979). The presence of **Ellisonia** may reflect similar specialized conditions (von Bitter and Merrill, 1983).

Both indices of the **bisselli-whitei** Assemblage Zone range into younger strata bearing **Neostreptognathodus pequopensis** in Nevada (Behnken, 1975b). The latter species appears to be a valuable index of Leonardian strata but the overlap with the older fauna occurs within the late Wolfcampian according to Behnken (1975b), although Kozur and Mostler (1976, p. 23-24) refer these early neostreptognathodids to **N. clarki**. However, it is evidently possible in North America to differentiate a restricted **bisselli-whitei** Zone postdating an interval within both these indices occur with Carboniferous hold-overs, and predating the appearance of **Neostreptognathodus**. This restricted interval is represented by the upper part of the Kamloops section.

Eastern European Permian zonal schemes presented by Kozur (1978, 1981) and most recently updated by Bando et al. (1980) incorporate taxonomic distinctions that have yet to be fully explored in Northern American sequences (see taxonomy). Several newly differentiated species of **Sweetognathus** are employed in Early Permian zonation. The interval equivalent to the restricted **bisselli-whitei** Zone is regarded by Kozur (1981) as mid to late Artinskian (Baigendzhinian) whilst a slightly older (late Aktastinian) zone represents an overlap interval. This contrasts with the view expressed by Clark et al. (1979), who show the restricted **bisselli-whitei** Zone as correlative with the latest Sakmarian (Sterlitamakian) of the Urals. Differing taxonomic concepts apart, this age difference is problematic (see Carr and Clark, 1979).

The Permian conodont record in Japan has been summarized recently by Igo (1981), who recognized a **bisselli-whitei** Assemblage Zone that is a range-zone in scope. Thus it includes younger species of **Neostreptognathodus**, and other specimens referred to that genus that strongly resemble older species of **Streptognathodus**. Fusulinid evidence shows that this total fauna is equivalent to the middle part of the **Pseudoschwagerina** Zone of the Sakamotozowan.

Evidence for the **bisselli-whitei** Assemblage Zone elsewhere is equivocal. Wang and Wang (1981) have summarized its distribution in China where it reputedly characterizes part of the Chihsian Stage. However, at least some specimens originally referred to **S. whitei** by Wang and Wang (1981) have subsequently been described as a new species, **S. guizhouensis** Bando et al. (1980). The Chinese specimens occur with **N. pequopensis**, as do some probable **S. whitei** in the Kapp Starostin Formation of Spitsbergen (Szaniawski and Malkowski, 1979). Both these records are therefore younger than the Kamloops fauna.

Finally, Rabe (1977) described several faunules containing **Sweetognathus whitei** from the Bucaramanga region of Columbia, South America. Some of these (Rabe, 1977, probes 20, 54, 57, 74, 86-88, 92) appear to correspond to a restricted **bisselli-whitei** Zone; other are probably older (probe 70) or younger (probe 29?).

Intra-Canadian correlation

Accounts of Early Permian conodonts from western Canada are to date available only in abstract form (Orchard, 1981, 1983; Henderson and McGugan, 1983). I have previously summarized conodont distribution in that part of the Cordillera regarded as allochthonous. Therein, the only other record of the **bisselli-whitei** indices is that from the Cariboo area where poorly preserved representatives occur in association with 'pre-crisis' elements. More primitive(?) sweetognathids than **S. whitei** are known from the Chilliwack Group of southwestern British Columbia, and from unnamed carbonates in the Terrace area of west-central British Columbia and in the Stikine Valley in northern British Columbia; Carboniferous hold-overs are associated in most of these faunas too. The latter two areas lie within the tectonostratigraphic terane termed 'Stikinia'. Permian limestone is widespread therein, but most conodont faunules known to date from 'Stikinia' are characterized by **Neostreptognathodus**, and are consequently younger than the Kamloops fauna. No instance of co-occurrence of **Neostreptognathodus** and **Sweetognathus** is currently known in Western Canada.

Additional **Sweetognathus**-bearing faunules are known from the Fennel chert in the east-central British Columbia, and from an un-named chert sequence in the Nahanni map area of east-central Yukon. These faunules are dominated by **Neogondolella**, the only platform conodont that occurs in possibly contemporaneous faunules from the Cache Creek Group, to the west of Kamloops, where neither **Sweetognathus** nor **Neostreptognathodus** are recorded.

Henderson and McGugan (1983) presented a preliminary account of Early Permian conodonts from the Ishbel Group of the Telford Thrust Plate in southeastern British Columbia. There, the **bisselli-whitei** Zone is recognized in the Ross Creek Formation, which thus constitutes the only direct correlative of the Kamloops fauna within craton-bound Canadian Permian rocks. Older formations in that area possibly contain additional Early Permian conodonts, but, as in Nevada, there is apparently no overlap of 'pre-' and 'post-crisis' elements.

Systematic Paleontology

Figured specimens bear GSC type numbers and are deposited in the National Type Fossil Collection (Geological Survey of Canada) in Ottawa.

Adetognathus Lane 1967

Type species: **Cavusgnathus lautus** Gunnell 1933

Remarks: **Adetognathus** includes both left- and right-bladed forms and thus differs from Late Mississippian **Cavusgnathus**, which is exclusively right-bladed. Individual species display both Class II (e.g. A. **unicornis**, **A. flexus**) and Class IIIb (e.g. **A. spathus**, **A. lautus**) symmetry in the sense of Lane (1968). The type species, from the Kansas City Group (Missourian) of Missouri, is composed of the left-bladed **A. lautus** sensu formo and the right-bladed **A. gigantus** sensu formo. However, Baesemann (1973) found right-bladed elements morphologically comparable to both **A. gigantus** s.f. and **'A. lautus'** s.f. in the Missourian of Kansas. Right-bladed **'A. lautus'** s.f. are also known from the Leavenworth limestone (Virgilian) of the American Midcontinent (Toomey et al., 1974). From the data in Baesemann (1973) it is not possible to distinguish at which horizons right-bladed **'A. lautus'** s.f. occurs, but evidently there are either two species of **Adetognathus** present in Kansas, (specimens of **A. lautus** s.f. paired with **A. gigantus** s.f. in one, and with **'A. lautus'** s.f. in the other), or there is one species, which differs from both the type species and the Kamloops species in that the morphology of the right-bladed element is variable. However, it is assumed that Ellison's type of **A. lautus** s.f. was an example of a Class IIIb species, as it has been interpreted by others, and that a second species, like that which occurs at Kamloops, co-existed with it for a time. This second species is here referred to a new species, **A. paralautus.**

Adetognathus paralautus sp. nov.

Plate 23.1, figs. 15, 16, 20-25

?p.1973 **Adetognathus lautus** Gunnell-Baesemann, p. 697, pl. 2, figs. 31, 34, ?29, ?30.

Derivation of name: from its similarity to **A. lautus.**

Holotype: GSC 68923, figured on Plate 1, fig. 25.

Stratum typicum: Lower Permian limestone of the "Harper Ranch" beds.

Locus typicus: Canada Cement Lafarge quarry, about 20 km due east of Kamloops, southern British Columbia.

Diagnosis: A species composed of similar left- and right-bladed adetognathiform elements. The left-bladed element corresponds closely to **A. lautus** Gunnell sensu formo. The right-bladed element is similar to the left-bladed form in having relatively regular blade denticulation.

Comparisons: von Bitter (1972, p. 62-3) has provided a thorough description of the elements of **A. lautus.** The left-bladed element of the latter species strongly resembles that of **A. paralautus,** but the latter species appears to lack the strong upward convexity of the platform of **A. lautus** as seen in profile; **A. paralautus** may also have a generally longer platform. The right-bladed element differs from its counterpart in **A. lautus** in lacking the large, conspicuous denticle at the junction of the blade and outer parapet.

In terms of symmetry characteristics and blade morphology, **A. paralautus** resembles **A. flexus** von Bitter from the Shawnee Group (Virgilian) of Kansas. That species differs in possessing a rounded posterior platform termination.

Remarks: **A. paralautus** probably developed from **A. lautus** during the Late Pennsylvanian. Slight differences between sinistral and dextral elements are the same as in the older species, i.e. transverse platform ridges are unequal in length in the left-bladed form, equal in the right-bladed element. Similarly, both elements show a slight offset of the blade toward the trough.

Data in von Bitter (1972), Baesemann (1973) and Perlmutter (1975) demonstrate that the two species co-existed during both Late Pennsylvanian and Early Permian time in Kansas.

Diplognathodus Kozur & Merrill 1975

Type species: **Spathognathodus coloradoensis** Murray & Chronic, 1965.

Diplognathodus sp. A

Plate 23.1, figs. 7, 9

Description: Relatively small conodonts characterized by a short blade and wholly excavated and broadly expanded cup occupying the posterior two-thirds of the unit. The carina is largely fused and rises anteriorly into the short blade, which is composed of four or five subequal denticles that are highest at midlength. The posterior end of the carina terminates abruptly and produces a steep posterior edge to the conodont as seen in profile.

Remarks: These specimens resemble four described species from the Late Pennsylvanian – Early Permian: **D. expansus** (Perlmutter 1975); **Diplognathodus oertlii** Kozur 1975; **D. angustus** Igo 1981; **D. stevensi** Clark and Carr 1982.

Each of these species appears to embrace specimens that differ in a nonprescribed way in blade and carina profile. Some specimens have a **'Hindeodus'** like denticulation, with a large anterior denticle (e.g. Perlmutter, 1975, pl. 3, figs. 15, 16), while others (e.g. Igo, 1981, pl. 8, fig. 7), including the Kamloops specimens, do not. Illustrated specimens differ also in the degree of fusion and in the posterior profile of the carina. To what extent these variables should be regarded as intraspecific needs to be addressed before **D.** sp. A from Kamloops is confidently assigned to any one, or none, of the named species.

Perlmutter (1975) described **Diplognathodus** (formally **Ozarkodina expansa**) from the Early Permian Council Grove Group in Kansas. In general, the Kamloops specimens differ in being neither as broadly expanded nor as round in basal outline.

The early Permian diplognathids form Japan referred to **D. angustus** generally resemble the Kamloops specimens in upper view, but the blade of the holotype is different, as is also the case with **D. oertlii.** The concentric ridge near the perimeter of the basal expansion in **D. angustus** is also a feature of **D. stevensi.** In profile, the American species, from the Rib Hill Formation, Nevada, appears to have a more convex-upward, less fused carina that the Kamloops species. Both **D. stevensi** and **D. expansus** are based on multilement reconstructions, but no comparison with the ramiform elements is possible since few have been recovered.

PLATE 23.1

All collections are from GSC Loc. No. C-87090. The nine faunules are numbered a through f. Specimens are Pa elements unless stated otherwise.

Figs. 1, 2 – **Sweetognathus** aff. **S. whitei** (Rhodes). GSC Nos. 68899, x100, from f; 68900, x75 from g. Compare fig. 1 and 3; same magnification.

Figs. 3-5, 8 – **Sweetognathus whitei** (Rhodes). 3, 4. GSC Nos. 68901, x100; 68902, x75, both from i. 5, 8. GSC Nos. 68903, x75; 68904, x70, both from d.

Figs. 6, 26 – **Hindeodus minutus** (Ellison). Pa and Sa elements, GSC Nos. 68905, x50, from f; 68925, x75, from b.

Figs. 7, 9 – **Diplognathodus** sp. A. GSC Nos. 68906, 68907, both x120, from a. Anterior cup is cracked in fig. 7.

Figs. 10(?), 11, 17 – **Neogondolella bisselli** (Clark & Behnken). GSC Nos. 68908, x50, from i; 68909, 68910, both x100, from b.

Fig. 12 – Carminate element indet. GSC No. 68911, x75, from g.

Figs. 13, 14, 18, 27 – **Ellisonia conflexa** (Ellison)?. GSC Nos. 68912, x75, from d; 68913, x75, from f; 68914, x75, from d; 68915, x60, from f. "Pl" (=?M), "Hi" (=?Sc), "Oz" (=?Pb), and "Tr" (=?Sa) elements, respectively.

Figs. 15, 16, 20-25 – **Adetognathus paralautus** sp. nov. GSC Nos. 68916-68923 respectively, x50; all from b except fig. 20 (68918), from g. Fig. 25 (68923) is the holotype.

Fig. 19 – **Merrillina**? sp. A. GSC No. 68924, x75, from g.

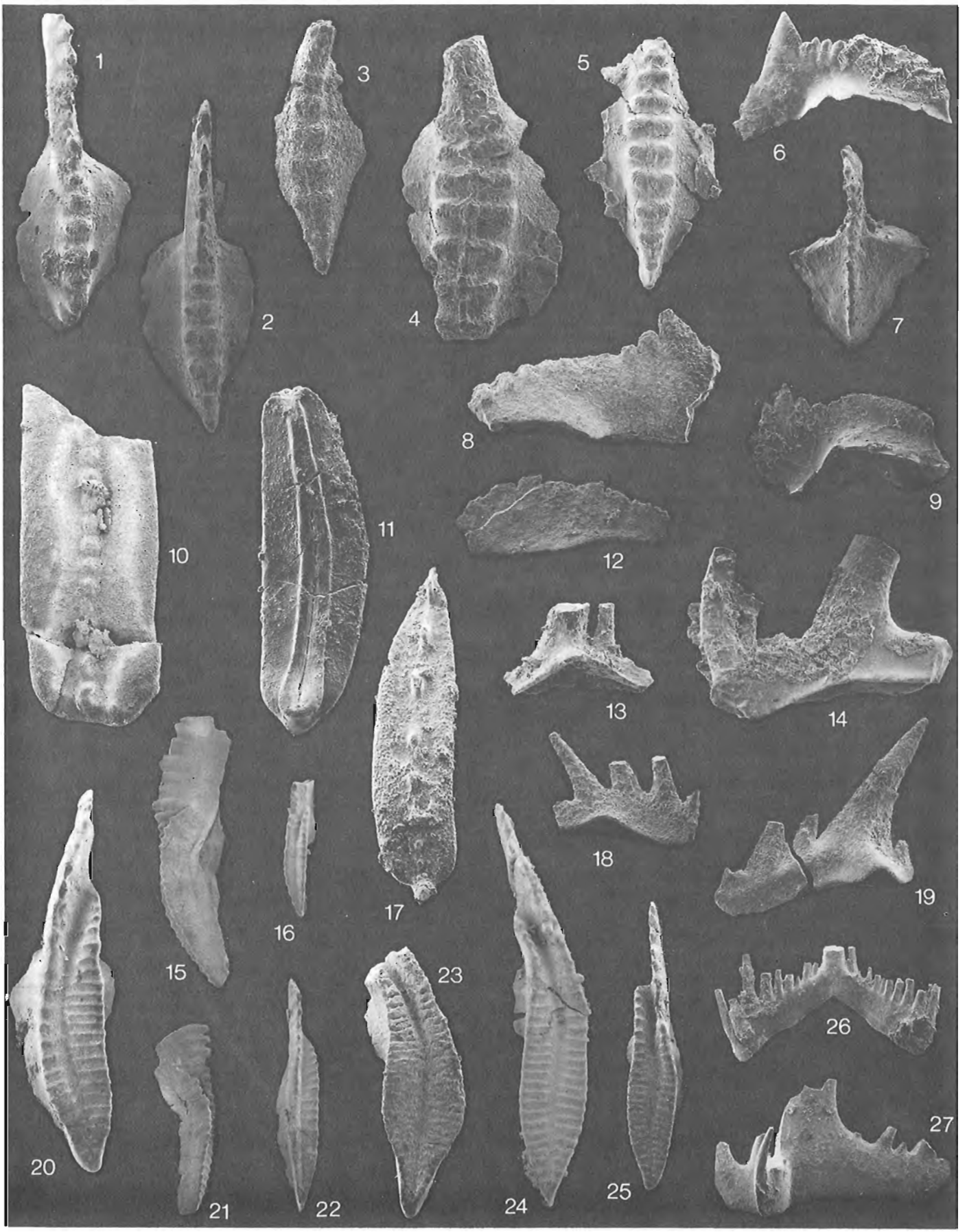
1
2
3
4
5
6
7
8
9
10
11
12
13
14
15
16
17
18
19
20
21
22
23
24
25
26
27

Ellisonia Muller 1956

Type species: **E. triassica** Muller 1956

Remarks: The ellisonids were recently reviewed by von Bitter and Merrill (1983). Two basic groups were distinguished: those with largely everted basal cavities (e.g. **E. latilaminata, E. triassica, 'Hadrodontina', 'Pachycladina'**), and those with generally open, often flaring basal cavities (**E. conflexa, E.** sp. A, **'Stepanovites'**). Both groups were included in **Ellisonia** by von Bitter and Merrill (1983) who concluded that eversion of the basal cavity was a specific variable within the evolution of the genus. von Bitter and Merrill (1983) identified five element types (termed Ne, Oz, Hi, Pl, Tr) in the Pennsylvanian. Since neither "Ne" nor "Oz" elements were identified from Permian rocks, they referred Permian representatives to **E.** sp. A.

The Kamloops fauna provides us with the first clear evidence for "Oz" (=?Pb sensu Sweet, in Clark et al., 1981) elements in Permian **Ellisonia**. Thus, **E.** sp. A of von Bitter and Merrill may be identical to **E. conflexa** (Ellison), although no "Ne" (=?Pa) has yet been identified.

Ellisonia conflexa (Ellison)?

Plate 23.1, figs. 13, 14, 18, 27

?1941 **Prioniodus? conflexus** Ellison, 1941, p. 114, pl. 20, fig. 25.

?1983 **Ellisonia conflexa** (Ellison) – von Bitter & Merrill, p. 18-20, pls. 3-11, 13 in part (see synonymy).

1983 **Ellisonia** sp. A – von Bitter & Merrill, p. 20, pl. 7, fig. 1; pl. 12, figs. 17-26; pl. 13, fig. 1, 2.

Diagnosis & Description: See von Bitter and Merrill (1983)

Remarks: Four types of elements have been found in the Kamloops fauna, although most are fragmentary and all are rare, as is generally the case (von Bitter and Merrill, 1983, p. 6). Each of the four element types compare closely with illustrated Pennsylvanian forms of **E. conflexa**, including the "Oz" (=?Pb) element (compare von Bitter and Merrill, 1983, p. 6, fig. 23; pl. 7, fig. 23). It is therefore assumed that the Pennsylvanian species ranges into the Early Permian, but because no "Ne" (=?Pa) element has been found, a question mark is attached to the name.

Hindeodus minutus (Ellison 1941)

Plate 23.1, figs. 6, 26

1941 **Spathodus minutus** n. sp. – Ellison, p. 120, pl. 20, figs. 50-52.

1973 **Spathognathodus minutus** (Ellison) – Merrill, p. 305-8, pl. 1, figs. 1-14; pl. 2, figs. 1-28 (see synonymy)

Description: See Merrill, 1973 (p. 306-7).

Remarks: Merrill (1973) provided a thorough reappraisal of the Pb element of this species, but to date the ramiform elements have not been described in detail (see Sweet, in Ziegler, 1977, p. 223). A single well preserved Sa element from the Kamloops fauna is illustrated on Plate 23.1, fig. 26. This resembles the homologous element in **H. cristulus** (Youngquist & Miller) but it has longer processes, and possibly a greater angle between them. Other elements are not well enough preserved to make meaningful comparisons at this time.

Merrillina Kozur 1975

Type species: **Spathognathodus divergens** Bender & Stoppel 1965.

Remarks: Kozur (1975) erected **Merrillina** for Middle Permian through Early Triassic angulate elements with an expanded basal cavity and a variably developed, sometimes absent, posterior process. Each of five species recognized by Kozur (1978) is further characterized by a prominent cusp and close set denticles, all of which are inclined posteriorly. Kozur (1975, p. 21) was uncertain about the multielement associatiates of **Merrillina** although he did speculate that a ramiform complex like that of **Stepanovites** = **Ellisonia** (q.v.) might be part of **Merrillina** too.

A single element from Kamloops (Pl. 23.1, fig. 19) resembles both the "Ne" (=?Pa) element of **Ellisonia conflexa** (in terms of its basal expansion and prominent cusp) and species of **Merrillina** (as described above). It may be the Pa element of the conodonts referred herein to **E. conflexa**?, in which case all of these elements should be referred to a new species of **Ellisonia**. For the present, the element is referred with question to **Merrillina.**

Merrillina? n. sp. A

Plate 23.1, fig. 19

Description: Element is arched and bears a prominent cusp rising to at least twice the height of the other denticles. The anterior process bears three denticles, the posterior process at least one. The basal cavity is deep and strongly expanded on one side beneath the cusp; it tapers to a slit distally.

Remarks: The basal configuration of this element is very similar to that of the "Oz" (=?Pb) element of **E. conflexa**?, as is the general form of the denticles. Since the two specimens do not occur in the same fauna I am reluctant to combine them as a single species although I do think it is likely that they are.

The specimen differs from other **Merrillina** species, all of which are younger, in the asymmetry of the basal cavity, although I do not know how variable this character is. The cusp is also less reclined and the processes possibly narrower. Otherwise it is similar to **M. praedivergens** (Bender & Stoppel).

Neogondolella Bender & Stoppel 1965

Type species: **Gondolella mombergensis** Tatge 1956

Remarks: The **Gondolella** versus **Neogondolella** question has been discussed at great length, most recently by Kovacs and Kozur (1980) and von Bitter and Merrill (1982). I agree with the view that, in terms of the whole spectrum of species under consideration, there is no single morphological feature that may be consistently used as a basis for separation of the two genera. However, I prefer not to submerge the distinctive Pennsylvanian **Gondolella** into the Pennsylvanian to Triassic, probably polyphyletic **Neogondolella.** Independent lineages may have given rise to neogondolellids that are not directly related to the Middle Triassic type species **N. mombergensis,** which seems to have emerged from **Neospathodus.** Only the latter stock might ultimately bear the name **Neogondolella.** Meanwhile, this nominal determination is useful in recording relatively smooth-plated Permo-Carboniferous 'gondolelloids'.

Neogondolella bisselli (Clark & Behnken 1971)

Plate 23.1, figs. 11, 17, ?10

1971 **Gondolella bisselli** n. sp. – Clark & Behnken p. 429, pl. 1, figs. 12-14.

1983 **Neogondolella bisselli** (Clark & Behnken) – Wardlaw, in Mytton et al., p. 299, fig. 12:26 (see synonymy).

p.1981 **Neogondolella bisselli** (Clark & Behnken) – Igo, p. 37, pl. 1, figs. 2, 4-9, 18 (only?).

Remarks: Wardlaw (in Mytton et al., 1983) has summarized the characteristics of this species. In addition it should be noted that the carina-blade of **N. bisselli** remains low throughout its length, and in this respect it differs from younger, otherwise similar species.

Sweetognathus Clark 1972

Type species: **Spathognathodus whitei** Rhodes 1963

Remarks: Sweet (in Ziegler, 1977) provided a review of this genus and the three Early Permian species referred to it at the time, viz. **S. whitei** (Rhodes), **S. merrilli** Kozur and **S. behnkeni** Kozur. When first described (Kozur, 1975, p. 4), **S. behnkeni** was said to be derived from **S. merrilli**, and there is also an implied relationship between the former and **S. whitei** (see Sweet, in Ziegler, 1973, p. 543). Kozur (1978) recognized two "phylomorphogenetic lines" involving sweetognathids, but neither of these mention the above relationships. The development of the sweetognathids is unlikely to be clarified until growth series and population variability is worked out for each of the species.

The youngest sweetognathids from Kamloops are referred to **S. whitei.** The larger specimens resemble **S. behnkeni** in terms of their strongly differentiated lateral nodes but there is no posterior orientation to the rows as in **S. behnkeni,** nor is the platform biconvex in upper view. In what are considered to be slightly older Kamloops specimens, lateral nodes are poorly differentiated at comparable growth stages. They appear to represent an earlier phyletic stage than **S. whitei** but their relationship to **S.** n. sp. A Kozur 1978 is unknown. Their platform nodes are similar to **S. merrilli** but in profile the postieur platform outline appears quite different. For now, the specimens are referred to **S.** aff. **S. whitei.**

Sweetognathus whitei Rhodes 1963

Plate 23.1, figs. 3-5, 8

1963 **Spathognathodus whitei** n. sp. – Rhodes, p. 404-5, pl. 47, figs. 4, 9, 10, 25, 26.

p.1971 **Sweetognathus whitei** (Rhodes) – Clark & Behnken, pl. 1, figs. 4, 6 (only).

?p.1973 **Spathognathodus whitei** (Rhodes) – Merrill, p. 310, pl. 3, figs, 8, 9 (only).

1975 **Sweetognathus whitei** (Rhodes) – Behnken (a), p. 312, pl. 1, figs. 26.

1978 **Sweetognathus whitei** (Rhodes) – Kozur, pl. 3, figs. 8, 9.

?1979 **Sweetognathus** sp. – Szaniawski & Malkowski, p. 255, pl. 5, figs. 1, 2.

1980 **Sweetognathus whitei** (Rhodes) – Ishiga & Imoto, pl. 1, fig. 4.

?p.1981 **Sweetognathus whitei** (Rhodes) – Igo, p. 44, pl. 6, figs. 21; pl. 7, figs. 2-7 (only?)

Description: See Rhodes (1963).

Remarks: The development of **Sweetognathus** in the Early Permian apparently involved a progressively earlier development of characteristics that only became manifest within the latest growth stages of the older species (recapitulation). Kozur (1975) noted this in regard to **S. behnkeni,** a species based on specimens regarded as gerontic by Igo (1981, p. 44).

It is difficult to assess many figured specimens of **S. whitei** in the literature. Even the types of **S. whitei** may not be as advanced as those subsequently referred to that species (including the Kamloops specimens), a suggestion supported by their co-occurrence with Carboniferous holdovers. Until such time as some absolute criteria are developed for distinguishing different degrees of sweetognathid phylognetic development, I refer to **S. whitei** only those specimens that have clearly differentiated lateral nodes throughout much of their growth.

Sweetognathus aff. **S. whitei** (Rhodes 1963)

Plate 23.1, figs. 1, 2

?p.1973 **Spathognathodus whitei** Rhodes – Merrill, p. 310, pl. 3, figs. 3, 7 (only).

?p.1974 **Sweetognathus whitei** (Rhodes) – Clark, pl. 2, figs. ?12, 14 (only).

?1979 **Sweetognathus whitei** (Rhodes) – Clark et al., pl. 1, fig. 15.

Description: Early growth stages have low, laterally enlarged carina denticles that show little or no tendency to become differentiated into medial and lateral parts. Such a differentiation occurs increasingly in the later growth stages but the lateral extensions of the nodes never rival the medial part in size. A medial longitudinal ridge is only weakly developed, if at all.

Remarks: These specimens differ from **S. merrilli** in that the latter has a short and anteriorly very high blade and a posterior carina with a "noticeable overhang", characteristics more typical of **Diplognathodus** species. A medial longitudinal rib is clearly developed in **S. whitei.**

carminate element indet.

Plate 23.1, fig. 12

Description: A single specimen in which only the base of denticles are preserved. Nevertheless, they can be seen to be of two different sizes, the anterior ones twice the anteroposterior width of the posterior ones. The element is also twice as high anteriorly as posteriorly due to both a progressive decline in denticle-base height and a posterior upward arching of the base. The underside of the element is broadly but shallowly expanded along its entire preserved length.

Remarks: This element may be related to Ellisonia, and/or to Merrillina? n. sp. A.

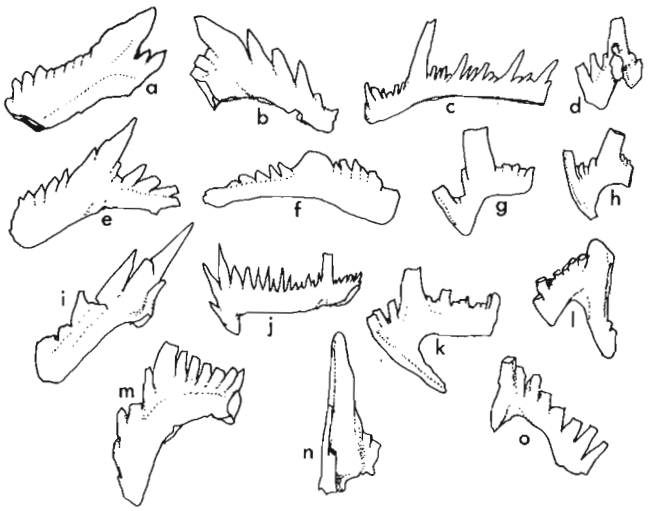

Figure 23.2. *Representative ramiform elements from the Early permian of Kamloops. The samples from which they originate are shown in brackets as follows: Pb elements = a (g), b (f), e (b), f (b), i (b), m (f); M elements = 1 (g), ?n (b), o (g); Sc elements = c (b), g (g), h (g), k (b); Sb elements = j (a); Sa elements = d (b).*

undifferentiated ramiform elements

In addition to illustrated ellisonid conodonts and the relatively well preserved Sa element of **Hindeodus,** there are a considerable number of other ramiform elements, most of which are fragmentary. For the sake of completion, I illustrate representative forms in Figure 23.2.

Acknowledgments

J.W.H. Monger introduced me to the Permian outcrops that are the subject of this paper and suggested improvements to an earlier draft, as did E.W. Bamber, C.M. Henderson and J.A. Roddick. P.T. Krauss was responsible for some of the photography, T. Oliveric for drafting Figure 23.1 and B.E. Vanlier for draft typing.

References

Baesemann, J.F.
1973: Missourian (Upper Pennsylvanian) conodonts of northeastern Kansas; Journal of Paleontology, v. 47, p. 689-710.

Bando, Y., Bhatt, D.K., Gupta, V.J., Hayashi, Sh., Kozur, H., Nakazawa, K., and Wang, Z.H.
1980: Some remarks on the conodont zonation and stratigraphy of the Permian; Recent Researches in Geology, v. 8, p. 1-53.

Behnken, F.H.
1975a: Leonardian and Guadalupian (Permian) conodont biostratigraphy in western and southwestern United States; Journal of Paleontology, v. 49, p. 284-315.

1975b: Conodonts as Permian Biostratigraphic Indices; in Permian Exploration, Boundaries, and Stratigraphy. Symposium and Field Trip, West Texas Geological Society and Permian Basin Section, Society of Economic Paleontologists and Mineralogists, No. 75-65, p. 84-90.

Bender, K.P.
1980: Lower and Middle Pennsylvanian conodonts from the Canadian Arctic Archipelago; Geological Survey of Canada, Paper 79-15, p. 1-29.

Carr, T.R. and Clark, D.L.
1979: Implications of North American Lower Permian conodont biostratigraphy; Abstracts of the 9th International Congress of Stratigraphy and Geology, p. 246.

Chamberlain, C.K. and Clark, D.L.
1973: Trace fossils and conodonts as evidence for deep-water deposits in the Oquirrh Basin of central Utah; Journal of Paleontology, v. 47, p. 663-682.

Clark, D.L.
1972: Early Permian crisis and its bearing on Permo-Triassic taxonomy; Geologica et Palaeontologica, v. 1, p. 147-158.

1974: Factors of Early Permian paleoecology in Nevada; Journal of Paleontology, v. 48, p. 710-720.

Clark, D.L. and Behnken, F.H.
1971: Conodonts and biostratigraphy of the Permian; Geological Society of America, Memoir 127, p. 415-439.

Clark, D.L. and Carr, T.R.
1982: Permian **Hindeodus** and **Diplognathodus:** Implications for Late Paleozoic conodont multi-element taxonomy: Geologica et Palaeontologica, v. 15, p. 125-138.

Clark, D.L., Carr, T.R., Behnken, F.H., Wardlaw, B.R., and Collinson, J.W.
1979: Permian conodont biostratigraphy in the Great Basin; Brigham Young University Geology Studies, v. 26, p. 143-150.

Clark, D.L., Sweet, W.C., Bergström, S.M., Klapper, G., Austin, R.L., Rhodes, F.H.T., Müller, K.J., Ziegler, W., Lindstrom, M., Miller, J.F., and Harris, A.G.
1981: Treatise on Invertebrate Paleontology, Part W, Supplement 2, Conodonta; The Geological Society of America, Inc. and The University of Kansas.

Danner, W.R.
1976: Limestone resources of southwestern British Columbia; Montana Bureau of Mines and Geology, Special Publication 74, p. 171-186.

Heckel, P.H. and Baesemann, J.F.
1975: Environmental interpretation of conodont distribution in Upper Pennsylvanian (Missourian) Megacyclothems in eastern Kansas; Bulletin of the American Association of Petroleum Geologists, v. 59, p. 486-509.

Henderson, C.M. and McGugan, A.
1983: Permian conodonts from the Canadian Rocky Mountains; Program with Abstracts, Geological Society of America, v. 15, p. 410.

Igo, H.
1981: Permian conodont biostratigraphy of Japan; Palaeontological Society of Japan, Special Paper 24, p. 1-51, 12 plates.

Ishiga, H. and Imoto, N.
1980: Some Permian radiolarians in the Tamba District, Southwest Japan; Earth Science, Journal of the Association for the Geological Collaboration in Japan, v. 34, p. 333-345.

Kovacs, S. and Kozur, H.
1980: Some remarks on Middle and Upper Triassic platform conodonts; Recent Researches in Geology, v. 6, p. 541-581.

Kozur, H.
1975: Beiträge zur Conodontenfauna des Perm; Geologisch-Paläontologische Mitteilungen Innsbruck, v. 5, p. 1-41.

1978: Beiträge zur Stratigraphie des Perms. Teil II: Die Conodontenchronologie des Perms; Freiberger Forschungsheft C 334, p. 85-161.

1981: The boundaries and subdivisions of the Permian System; Proceedings of the International Symposium on Central European Permian, Jablonna 1978, p. 401-425.

Lane, H.R.
1968: Symmetry in conodont element-pairs; Journal of Paleontology, v. 42, p. 1258-1263.

Larson, J.A. and Clark, D.L.
1979: The Lower Permian (Sakmarian) portion of the Oquirrh Formation, Utah; Brigham Young University Geology Studies, v. 26, p. 135-142.

Merrill, G.K.
1973: Pennsylvanian nonplatform conodont genera, I: **Spathognathodus**; Journal of Paleontology, v. 47, p. 289-314.

Merrill, G.K. and von Bitter, P.H.
1976: Revision of conodont biofaces nomenclature and interpretations of environmental controls in Pennsylvanian rocks of eastern and central North America; Royal Ontario Museum, Life Sciences Contribution No. 108, p. 1-46.

Mytton, J.W., Morgan, W.A., and Wardlaw, B.R.
1983: Stratigraphic relations of Permian units, Cassia Mountains, Idaho; Geological Society of America, Memoir 157, p. 281-303.

Orchard, M.J.
1981: Upper Palaeozoic conodonts from the Canadian Western Cordillera? a synopsis; Geological Association of Canada, Program with Abstracts, v. 6, p. A45.

1983: The conodont record in the terranes of Western Canada; Geological Association of Canada, Program with Abstracts, v. 8, p. A52.

Perlmutter, B.
1975: Conodonts from the uppermost Wabaunsee Group (Pennsylvanian) and the Admire and Council Grove Groups (Permian) in Kansas; Geologica et Palaeontologica, v. 9, p. 95-115.

Rabe, E.H.
1977: Zur Stratigraphie des ostandinen Raumes von Kolumbien; Giessener Geologische Schriften, no. 11, p. 1-223.

Rhodes, F.H.T.
1963: Conodonts from the topmost Tensleep sandstone of the eastern Big Horn Mountains, Wyoming; Journal of Paleontology, v. 37, p. 401-408.

Sada, K. and Danner, W.R.
1974: Early and Middle Pennsylvanian fusulinids from southern British Columbia, Canada and northwestern Washington, U.S.A.; Transactions and Proceedings of the Paleontological Society of Japan, New Series no. 93, p. 249-265.

1976: **Pseudoschwagerina** from Harper Ranch Area near Kamloops, British Columbia, Canada; Commemoration Volume of the Founding of the Faculty of Integrated Arts and Sciences, Hiroshima University, p. 213-228.

Smith, R.B.
1979: Geology of the Harper Ranch Group (Carboniferous – Permian) and Nicola Group (Upper Triassic) northeast of Kamloops, B.C.; unpublished Masters thesis, University of British Columbia, 211 p.

Szaniawski, H. and Malkowski, K.
1979: Conodonts from the Kapp Starostin Formation (Permian) of Spitsbergen; Acta Palaeontologica Polonica, v. 24, p. 231-264.

Toomey, D.F., Baesemann, J.F., and Lane, H.R.
1974: The biota of the Pennsylvanian (Virgilian) Leavenworth Limestone, Midcontinent Region, Part 5: Distribution of Miscellaneous Microfossils; Journal of Paleontology, v. 48, p. 1156-1165.

von Bitter, P.H.
1972: Environmental control of conodont distribution in the Shawnee Group (Upper Pennsylvanian) of eastern Kansas; University of Kansas Paleontological Contributions, Article 59, p. 1-105.

von Bitter, P.H. and Merrill, G.K.
1982: Naked species of **Gondolella** (Conodontophorida): Their distribution, taxonomy, and evolutionary significance; Royal Ontario Museum, Life Sciences Contributions No. 125, p. 1-49.

1983: Late Palaeozoic Species of **Ellisonia** (Conodontophorida), Evolutionary and palaeoecological significance; Royal Ontario Museum, Life Sciences Contributions No. 136, p. 1-57.

Wang, C-y. and Wang, Z-h.
1981: Permian conodont biostratigraphy of China; Geological Society of America, Special Paper 187, p. 227-236.

Ziegler, W. (ed.)
1973: Catalogue of Conodonts, v. 1. Stuttgart.

1977: Catalogue of Conodonts, v. 3. Stuttgart.

24. ESKER SEDIMENTATION MODELS, DEEP ROSE LAKE MAP AREA, DISTRICT OF KEEWATIN

Project 690095

W.W. Shilts
Terrain Sciences Division

Shilts, W.W., Esker sedimentation models, Deep Rose Lake map area, District of Keewatin; in Current Research, Part B, Geological Survey of Canada, Paper 84-1B, p. 217-222, 1984.

Abstract

Studies of the Deep Rose Lake esker system have defined three main sedimentation elements: 1) single or multiple, sharp-crested or deformed esker ridges deposited in subglacial tunnels; 2) continuous or fragmented outwash terraces deposited partially on temporary floors of glacier ice by meltwater issuing from the esker tunnel mouth in the retreating ice front; and 3) glaciolacustrine deposits, including ice-contact deltas built into proglacial lakes dammed by topographic obstructions along the esker system channel.

It is important to recognize these elements and to understand the esker depositional model in drift prospecting because erratics deposited in one sedimentation element may be related in space, but not in time or provenance to the adjacent elements.

Résumé

Des études sur les eskers du lac Deep Rose ont permis de déterminer trois principaux éléments de sédimentation: 1) eskers filiformes simples ou complexes, déformés ou à crêtes effilées déposés dans des tunnels sous-glaciaires; 2) terrasses alluviales continues ou fragmentées, déposées partiellement sur des lits temporaines de glace des glaciers par l'eau de fonte de l'exutoire du tunnel sous-glaciaire (esker), se trouvant dans le front de glace en recul; 3) dépôts glacio-lacustres, y compris les deltas morainiques formés par les lacs proglaciaires endigués par des obstacles topographiques, le long du chenal du système d'eskers.

Il est important de reconnaître ces éléments et de comprendre le modèle de dépôt des eskers dans la prospection glaciaire, car des blocs erratiques déposés dans un élément de sédimentation peuvent être associés dans l'espace, mais pas dans le temps ni dans l'origine aux éléments adjacents.

Introduction

The Deep Rose Lake map area (NTS 66 G) is located northwest of the Keewatin Ice Divide (Lee et al., 1957; Shilts, 1980). Regional ice flow and drift transportation direction in the region was 325° ± 5°, clearly indicated by orientations of long axes of lakes, fluting, and drumlin-like forms and by displacement of dolomite and orthoquartzite boulders northwestward from their outcrops. Trains of Rogen moraine, consisting of hummocks and short, arcuate ridges oriented approximately at right angles to 325°, are disposed in ribbon-like patterns trending approximately 325° over much of the region.

In the southeastern part of the Deep Rose Lake map area two segments of the Deep Rose Lake esker system were studied in detail just west of Deep Rose Lake (B.C. McDonald, unpublished data, 1968) and near "IFO[1] Lake" (Fig. 24.1). The glaciofluvial system at IFO Lake trends about 350° (± 10°) along a gentle bedrock depression, probably relict from the bedrock surface predating the last glaciation. Both glaciofluvial systems are tributary to a large esker system that starts near the Keewatin Ice Divide, about 45 km southeast of IFO Lake, and extends for more than 200 km northward to Queen Maud Gulf. The parts of the Deep Rose Lake esker system that were studied by B.C. McDonald and by the present author appear to have been deposited above the limit of marine submergence. Surface meltwater drainage followed shallow surface depressions sloping generally away from the ice front.

From his unpublished study of a 13 km-long segment of the Deep Rose Lake system about 40 km northwest of IFO Lake, McDonald compiled notes and conclusions that have been an invaluable aid in interpreting the relationships among the main elements of the glaciofluvial system at IFO Lake. A reconnaissance flight was made to the site of McDonald's study in order to compare and contrast his observations with those made at IFO Lake.

Acknowledgments

B.C. McDonald contributed copious notes, photographs, diagrams, and many hours of discussions on the Deep Rose Lake system some years ago when he was actively studying models of esker sedimentation. The report was considerably improved by comments from D.A. St-Onge on the original manuscript.

Glaciofluvial Complex

Remnants of gravel terraces were found on and adjacent to the esker ridge that extends northward from the north end of IFO Lake (Fig. 24.1). These terraces are remnants of a rather complex glaciofluvial-glaciolacustrine system typical of those that were developed during the last stages of glaciation in this part of the District of Keewatin. The IFO Lake glaciofluvial complex can be used as a model for late glacial glaciofluvial events wherever a glacier front was retreating up-gradient, allowing meltwater to flow more or less unimpeded from the ice front.

[1] IFO Lake is an informal name in common use by exploration companies working in southeastern Deep Rose Lake map area. GSC Lake is an informal name for an adjacent water body of some significance to this study. Both lakes are shown in Figure 24.1.

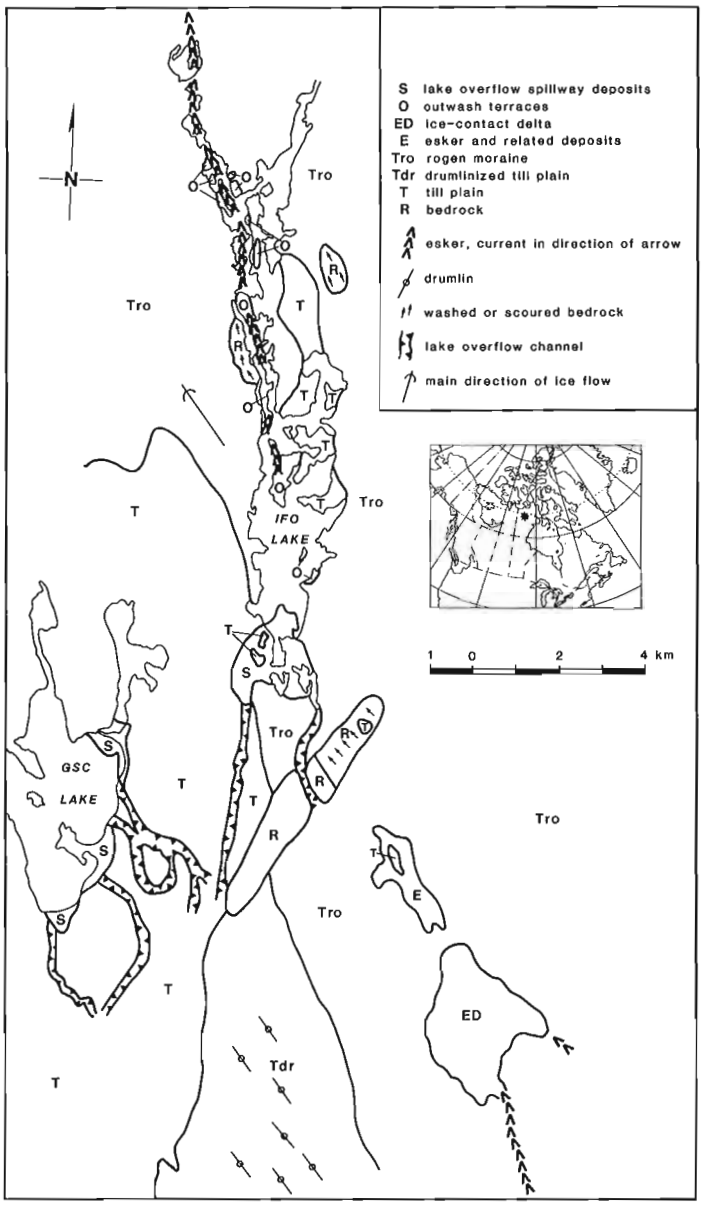

Figure 24.1. *Map of glaciofluvial system and related glacial deposits, IFO Lake area, District of Keewatin. Features were transferred from topographic maps 66 G/1, G/2, G/7, and G/8.*

The glaciofluvial-glaciolacustrine system at IFO Lake comprises several distinct elements (Fig. 24.1), most of which are time-transgressive because of their deposition in association with the steadily retreating ice front.

Esker ridge complex

The oldest component of the late glacial meltwater system at any given point is the esker ridge or ridge complex which was formed in a tunnel at or near the base of the glacier. The tunnel more or less followed the axis of a low area in the bedrock surface, but separated from its drift-bedrock floor and climbed through the ice in order to cross a transversely oriented orthoquartzite ridge at the south end of IFO lake. Where the esker sediments were deposited near the base of the ice, and were not modified by postdepositional processes, they now form a sharp-crested ridge with side slopes in excess of 25° (Fig. 24.2). Where the sediments deposited in the raised tunnel north and south of the quartzite ridge were lowered over melting ice, they formed an irregular, hummocky deposit, barely identifiable as a part of the esker.

In some places the single ridge splits into several ridges which pass downstream back into a single ridge (Fig. 24.3). This is thought to have occurred where sedimentation rates were so high, because of increased sediment supply, slope changes, slowing of ice front retreat, or other unknown factors, that the tunnel was blocked by sediment, causing formation of a bypass tunnel, which, if blocked, was bypassed again, etc.

A question of fundamental importance in developing a sedimentation model for the IFO Lake esker is, "how much of the glaciofluvial system was functioning as a tunnel at the base of the ice at any one time?" The deposits of the Deep Rose Lake and other major esker systems in the District of Keewatin reflect what appears to have been a fully integrated Horton system of tributaries and trunk streams, regularly bifurcating upstream into lower order tributaries until the deposits disappear near the Keewatin Ice Divide. This pattern may be interpreted in at least three ways: 1) The whole system may have functioned subglacially in sub-ice tunnels extending from the centre of a thin, stagnant glacier to its retreating margins, which lay at one time some 300-500 km away. Although this model has some merit, the very size of the ice sheet at the inception of esker deposition would seem to argue against it, the thicker ice near the divide being too plastic at the base to maintain open tunnels. In addition, it is hard to imagine how the Horton system could have developed so fully within a solid mass of ice; topographic irregularities at the base of the ice would have exercised greater influence on esker trends than is evident from the Horton pattern. 2) The esker may have been deposited by streams flowing in short tunnels near the margin of the glacier, continuity being maintained by up-ice migration of the heads of the tunnels by melting (St-Onge, 1984, p. 274). Although this model is more compatible with observed sedimentation features and probable dynamic conditions in the retreating ice, it does not explain well the Horton pattern of tributaries. It is hard to imagine how a subglacial tunnel would bifurcate regularly as it melted up ice without some external control. 3) The most attractive model of glacial meltwater drainage in this region is presently one in which an integrated system of drainage channels developed on the surface of the glacier, the meltwater plunging to the base of the glacier to flow in a subglacial tunnel the last few kilometres of its course before issuing from the retreating glacier front (similar to the model suggested by St-Onge, 1984, p. 273). This system would have developed quite late in the glacial cycle, when most of the glacier was below the equilibrium line. The tunnels near the ice edge would have extended themselves headward by melting, as in the preceding model, but their headward migration would have followed roughly the traces of the surface drainage, thus accounting for the regular bifurcation upstream. This hybrid model best explains both the Horton drainage pattern and the manifest evidence of subglacial origin of esker sediments.

These hypotheses cannot be tested at IFO Lake but are absolutely fundamental to interpreting both the vertical and lateral changes in provenance of the clasts that make up the esker. If the basal tunnel was only a few kilometres long (as in models 2 and 3), no clast could have been derived from bedrock, already deposited till, or the basal load of the glacier from farther upstream than the average length of the tunnel. Even so, debris may have been carried considerable distances by the glacier itself before being incorporated into the esker sediment at the head of a tunnel. If the tunnel was part of an integrated system functioning at the base of the ice everywhere at once (as in model 1), clasts at a given site

Figure 24.2. *Typical sharp-crested, single esker ridge of Deep Rose Lake esker system west of Deep Rose Lake. Note flat-topped projection of esker; outwash terraces are indicated by arrows. Depressions on either side of the esker are marginal kettles. Surveyed line of Figure 24.5 crossed esker in foreground. Photograph by B.C. McDonald, 1968.*

could have been derived from anywhere upstream to the head of the esker system. If part of the system was supraglacial and part subglacial (as in model 3), clasts could have been derived anywhere downstream from where the surface drainage plunged to the base of the ice, a point that would have shifted up ice with time.

In trying to assess the provenance of esker sediment, it should be borne in mind that the bulk of the sediment comprises clasts originally liberated from their source outcrops by glacier erosion and carried, in some cases tens or hundreds of kilometres, as a poorly sorted basal load in the glacier or deposited as till beneath the glacier. Very little esker sediment is produced by the direct effects of fluvial action on bedrock, a fact graphically illustrated on the west side of the esker north of IFO Lake by tracts of glacially rounded bedrock swept clean of drift but not modified by subglacial meltwater of the fluvial system that deposited the esker.

In the continental glacier that covered the relatively flat terrain of central District of Keewatin, the volume of debris available for transportation and erosion in any particular segment of the esker tunnel comprised mainly the sediment that was available in the basal layers of the glacier and in the subglacial till immediately underlying the tunnel down to bedrock. Lack of supraglacial deposits in this region suggests that the higher parts of the glacier were relatively free of debris. If ice was perfectly rigid, once the basal debris was carried away by meltwater, no more erosion would have occurred and consequently no more of the components in that part of the tunnel would have been available. However, since this and other eskers comprise a much greater volume of coarse debris than erosion and redistribution of the till immediately beneath their tunnels can account for, additional debris must have been brought into the esker tunnel by ice flowing into it from its sides,

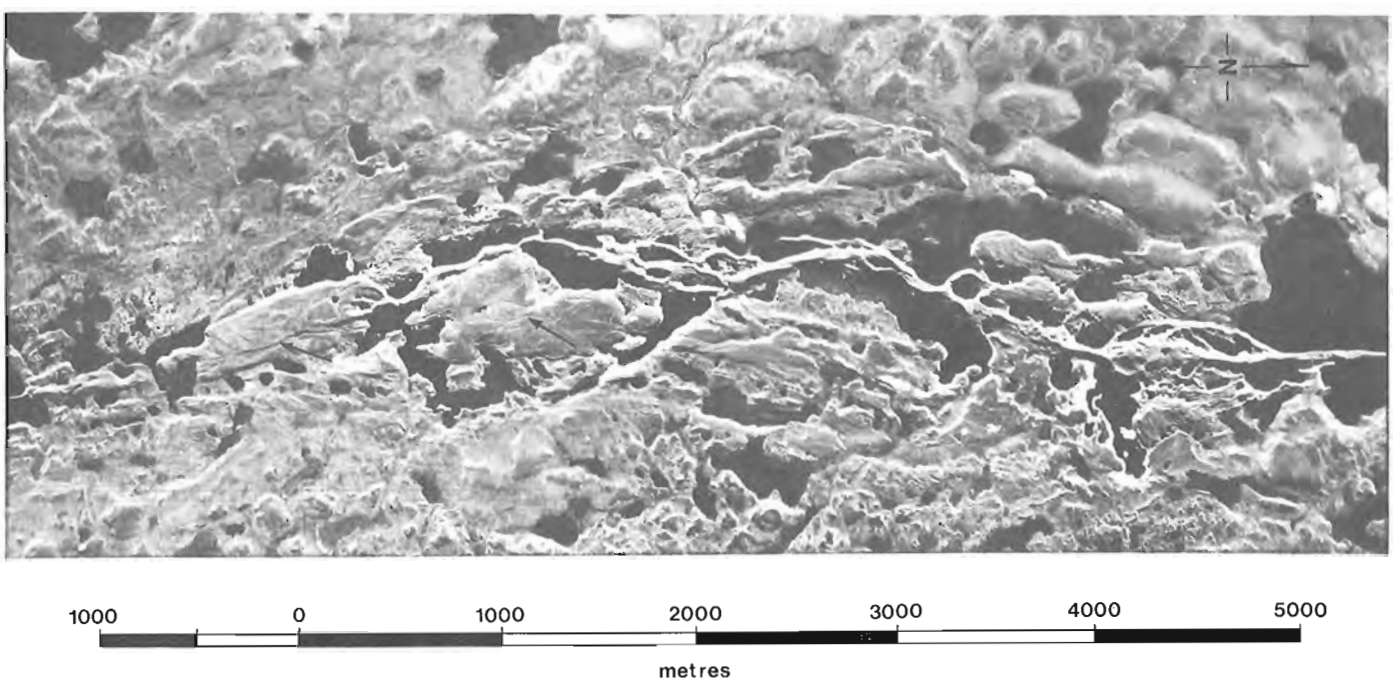

Figure 24.3. *Esker ~10 km north of IFO Lake. Note outwash terrace remnants superimposed on esker and valley sides; those in the south part of photo show scars of braided meltwater stream channels (arrows). The esker splits into multiple ridges in several places, particularly at the north end. Most lakes were filled with ice blocks when the outwash terraces were deposited. Photo enlarged from a portion of NAPL A15390-33.*

bringing debris from lateral areas into the tunnel, as shown by Repo (1954). Ice would have flowed laterally into the tunnel at a rate determined by how fast the subglacial meltwaters could melt the tunnel walls and carry away the debris entrained in them. Thus, the meltwater that formed the IFO Lake esker could have been transporting debris fluvially at 350° that had been first transported at 325° by the ice or first transported 325°, then transported 235° or 55° by lateral ice movement into the tunnel as shown schematically in Figure 24.4.

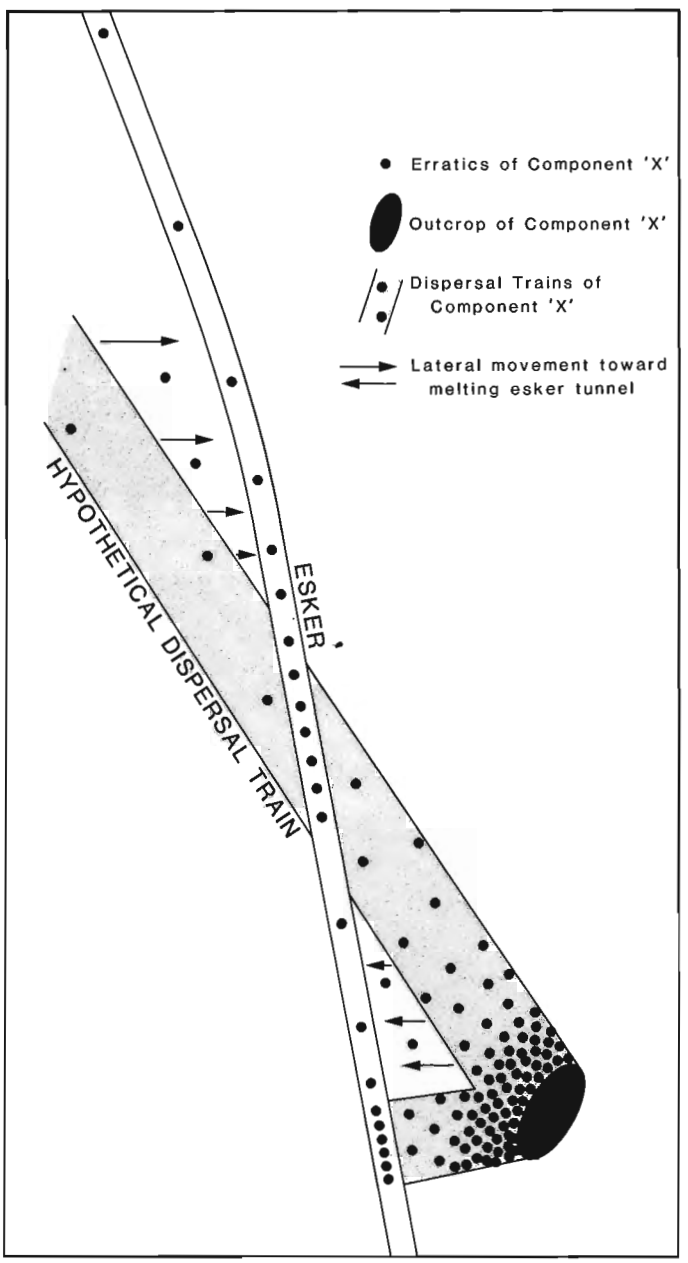

Figure 24.4. *Diagrammatic map of transportation of glacially dispersed clasts through an esker system.*

Outwash terraces and buried ice

The Deep Rose Lake esker system, like many eskers in District of Keewatin, is flanked by one or more levels of sand and gravel terraces, fragments of which are superimposed on the valley sides and on the esker ridges, themselves (Fig. 24.2, 24.3, 24.5). These terraces are remnants of sediment deposited in braided outwash streams, traces of the braided channels being preserved on many of the fragments (Fig. 24.3). The outwash streams exited from an esker tunnel mouth in the steadily retreating ice front. St-Onge (1984) described fan-shaped outwash terraces that may be similar to those described here.

The only way that fluvial outwash could have been deposited in valleys that are now interrupted by numerous lakes is if the shallow, broad valleys in this region were temporarily occupied by thin masses of remnant glacier ice, which served as temporary floors for unrestricted drainage away from the ice front. Presence of thin (< 30 m thick), persistent masses of ice in shallow depressions has been inferred by B.C. McDonald (unpublished) in his research on this system and by the author in many depressions occupied by lakes typical of the Canadian Shield (Klassen and Shilts, 1982; Shilts, 1984). St-Onge (1984) also inferred that stagnant ice of unspecified dimensions was trapped in proglacial lake waters in the Redrock Lake area, District of Mackenzie.

Observations of modern glaciers indicate that they carry significant concentrations of debris only in a zone 10-20 m above their base, the rest of the glacier generally being relatively free of debris. It is possible that, during downwasting of a largely stagnant ice sheet, such as the one visualized for this part of Keewatin, once the top of this debris-rich zone was exposed, the insulating effect of debris melting out of the ice would have retarded melting. Rapid deposition of fluvial or glaciolacustrine sediments in depressions on this surface would have further retarded melting, leaving buried glacial ice stranded in valleys and closed depressions long after well drained uplands became ice free.

As buried ice melted in its downstream reaches, lowering local base level, the upstream portions of a meltwater stream would have adjusted gradient by cutting down into both the remnant glacial ice and the superimposed glaciofluvial deposits. The end result of this controlled downcutting was the formation of a series of paired terraces throughout each valley now occupied by an esker. Although the terraces are largely depositional, where the buried esker ridge or other deposits projected through the ice, they were sometimes planed off by fluvial erosion to the level of the depositional part of the terrace or the ice floor, leaving remarkably flat-topped esker segments in places (Fig. 24.2). Like the esker ridge, the terrace deposits are in part time-transgressive, being deposited by meltwater emanating from a constantly retreating source (tunnel mouth in the ice front).

Deposits in the esker tunnel raised over the orthoquartzite ridge

There is a 5 km gap in easily identifiable esker deposits on either side of the quartzite ridge that lies at the south end of IFO lake. The ridge projected 30-40 m above the general level of the base of the retreating glacier, forming a barrier to subglacial drainage. As a result, the esker stream, which generally was flowing on or near bedrock at the base of the ice, appears to have separated from the bedrock floor, forming a tunnel that rose through the ice over the ridge and descended to the glacier's sole again in central IFO Lake. Among the most important results of decoupling of the esker stream from the glacier bed are:

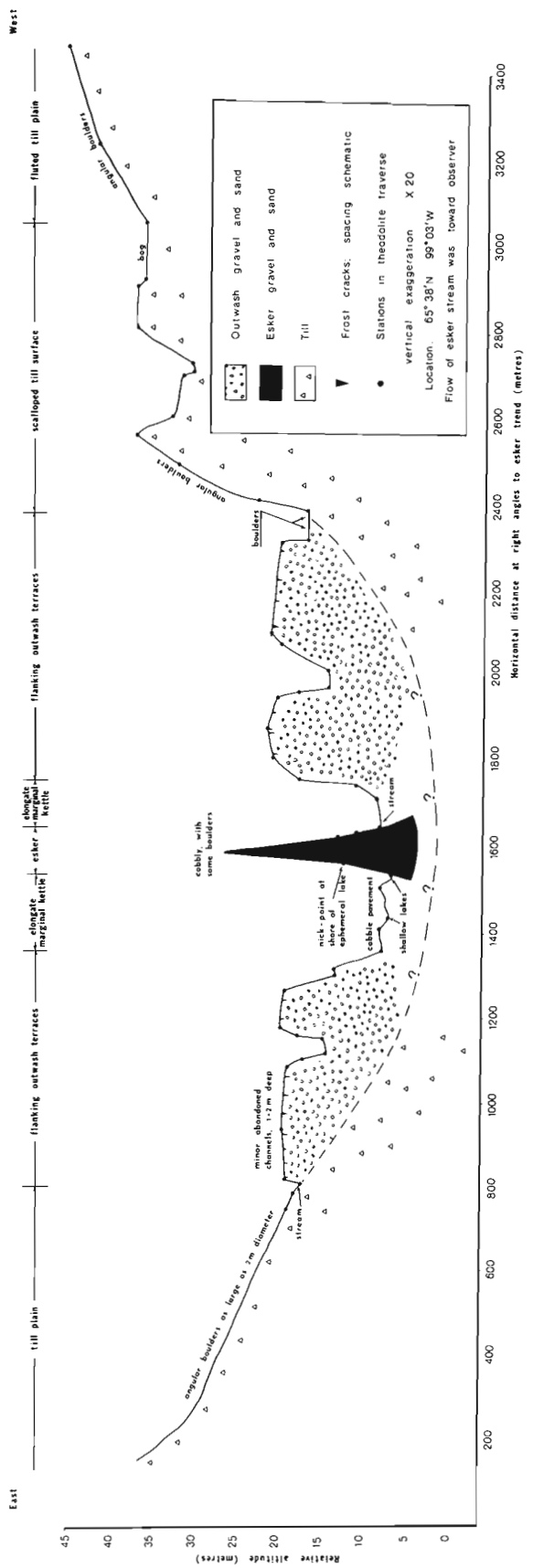

Figure 24.5. *Surveyed profile across the esker/outwash terrace system west of Deep Rose Lake, measured by B.C. McDonald, 1968. East-west traverse crosses foreground of Figure 24.2.*

1. Little sediment was derived from the segment where the decoupling took place, except at the quartzite ridge itself where one or more channels may have been cut through the quartzite by subglacial meltwater.
2. Gravel deposited in the rising esker tube south of the ridge was grossly deformed by collapse when the ice beneath the tube finally melted, lowering the deposits by as much as 40-50 m. These deformed deposits may be seen immediately south of the quartzite ridge.

Sediments of the proglacial lake south of the quartzite ridge

Once the ice front had retreated south of the quartzite ridge, meltwater issuing from the esker tunnel mouth was blocked by the ridge, forming a lake. A massive ice-contact delta, fed by two esker streams, was built at 200-210 m a.s.l. into this lake and stands now as a prominent landmark about 5 km south of IFO Lake. Water from the lake appears to have cascaded northward over the quartzite ridge at least in its earliest stages. Evidence for this drainage phase comprises the bare bedrock surface of the northeastern half of the ridge, which has been swept clean of till except for a 5-6 m-thick, teardrop-shaped remnant of till on its crest. Although the channel that was cut through the ridge lines up with and seems to be a part of the glaciofluvial system, it is physically below this washed surface and either was filled with ice or with debris, preventing drainage. Alternatively, it could have been cut by later outflow from the lake. In the latter case, the channel would have had no relationship to the subglacial fluvial system. The apparent lack of a concentration of monolithological quartzite debris at the north end of the channel suggests that it was not formed by overflow from the lake, in spite of its low elevation. The extension of the channel through drift to IFO Lake, does, however, indicate that overflow from the lake passed through it at some time.

Several clearly defined meltwater channels (Fig. 24.1) were cut by water overflowing northward from the proglacial lake when its surface stood below the crest of the quartzite ridge at about 190 to 210 m a.s.l. One of these channels was excavated in till directly south of IFO Lake and issued into IFO Lake at elevations very near to those of its present surface. The sand and gravel fractions of till eroded from the channel and from the quartzite ridge were redistributed into the lake as deltas which now form low terraces and subaqueous sand flats at its south end. These terraces can be traced directly into fluvial deposits in the abandoned meltwater channels and are not related in genesis or composition to the outwash terraces found elswhere around the lake. Meltwater discharged for a time into the large (GSC) lake a few kilometres southwest of IFO (Fig. 24.1) and built sandy deltaic deposits into it also.

Terraces and sediments relating to draining of the proglacial lake

The glacial lake ponded south of the quartzite ridge eventually drained completely. The glaciofluvial deposits south of the delta include the same types of esker tunnel sediments and ice-floored outwash trains that are found north of IFO Lake. Before the lake drained completely, however, falling lake levels caused meltwater from the south to cut into the delta, forming a series of erosional terraces on it, particularly along its southwest side. Elevated fragments of meandering channels and braided stream patterns scar the west side of the delta whereas the surface of the east side is almost wholly disrupted by kame and kettle topography, reflecting collapse of the sediment over melting ice.

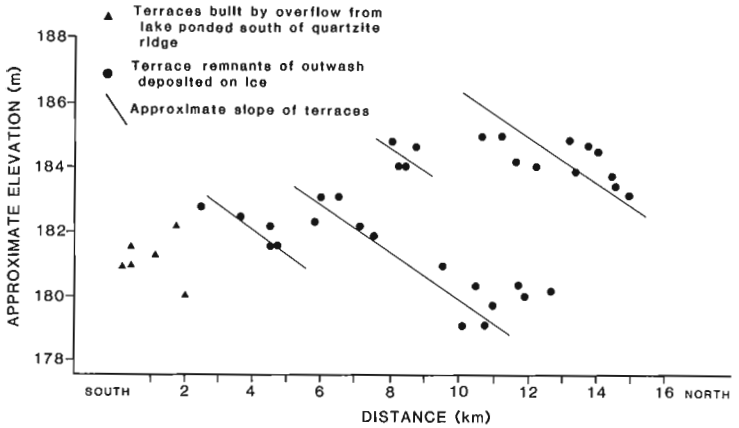

Figure 24.6. *Elevations of outwash terrace remnants of IFO Lake esker complex. Distances measured from south end of IFO Lake and elevations calculated approximately above mean sea level with absolute error of ±5 m (with respect to each other, elevations are accurate to within ±25 cm).*

Implications for drift prospecting

It is important to understand the origin of the various elements of the glaciofluvial system because, although they are related to each other in space, they are not necessarily related to each other in time. For example, the presence of economically interesting erratics on a terrace and their absence on an adjacent esker might be expected. To find the source of erratics deposited on a terrace it would be helpful to know where the ice front was and how much it retreated during formation of the terrace, since controls on esker compositions also apply to their proglacial fluvial extensions – the terraces. Only scattered fragments of terraced glaciofluvial sediment remain along the segment of the Deep Rose Lake esker studied most intensively, but the segment studied by McDonald is flanked by a single set of fairly continuous outwash terraces (Fig. 24.5).

The gradient and extent of the original terrace systems of the IFO Lake tributary can be estimated, however, by plotting elevations of terrace remnants against distance northward down the paleoslope from the south end of IFO Lake (Fig. 24.6). By connecting points representing the elevations of once contiguous terrace fragments, one can deduce the existence of a series of terrace levels, each having more or less the same gradient, and each of which can be extrapolated back approximately to the last position of the ice front before downstream melting of buried ice caused downcutting to the next lower terrace level. Areas where the source outcrops of erratics of economic importance might be located probably would have been somewhere south of an ice front deduced for a particular terrace. Source outcrops would be located within the zone traversed by the esker stream or, because of lateral ice flow into the tunnel, in the zone immediately adjacent to it.

Conclusion

The IFO Lake segment of the Deep Rose Lake esker system comprises three main sedimentation elements: 1) sharp-crested single or multiple esker ridges deposited in a tunnel(s) at the base of the ice and hummocky, rounded ridges deposited in a tunnel raised above the base of the ice. The form of the latter deposit was caused by lowering as a result of melting of underlying ice; 2) sand and gravel terraces built at one or more levels on and adjacent to esker ridges by meltwater streams issuing from the esker tunnel mouth in the retreating ice front. Only fragments may remain because the outwash trains were partially deposited on temporary floors of glacier ice that was preserved in shallow depressions. Initially, ice may have been preserved by the insulating properties of debris melted out of sediment-choked basal layers of the glacier, exposed during downwasting of the largely stagnant ice mass. As these remnant ice masses melted downstream from the tunnel mouth, local base level was lowered upstream, causing downcutting and insetting of the outwash train below the higher outwash deposits. The net result of this over-ice deposition and downcutting was the preservation of terrace remnants in the valleys now occupied by the Deep Rose Lake esker system; 3) glaciolacustrine deposits, including esker deltas and offshore, fine grained sand deposited in a lake dammed between the retreating ice front and a bedrock ridge lying athwart the depression now occupied by the esker.

With respect to mineral exploration, the provenance of sediments in the esker ridge is likely to be unrelated to that of the adjacent terrace deposits which were deposited sometime after the esker sediments were deposited. The provenance of both types of deposits depends on 1) the length of the basal tunnel functioning at one time; 2) the initial direction of transport of the basal debris eroded, sorted, and transported by the subglacial stream; and 3) the length of any segments of the esker tunnel raised above the base of the glacier, among other factors.

Although understanding of the esker sedimentation model cannot completely eliminate the element of luck in finding the source of mineralized components found on one of its elements, it can certainly make luck less of a factor in mineral exploration. Because much drift prospecting in Canada is carried out by searching for mineralized erratics on esker systems, the importance of the sedimentation model to mineral exploration cannot be overstated.

References

Klassen, R.A. and Shilts, W.W.
1982: Subbottom profiling of lakes of the Canadian Shield; in Current Research, Part A, Geological Survey of Canada, Paper 82-1A, p. 375-384.

Lee, H.A., Craig, B.G., and Fyles, J.G.
1957: Keewatin ice divide (abstract); Geological Society of America, Bulletin, no. 68, p. 1760-1761.

Repo, R.
1954: Om forhallandet mellan rafflor och asar (on the relationship between striae and eskers); Geologi, v. 6, no. 5, p. 45.

Shilts, W.W.
1980: Flow patterns in the central North American ice sheet; Nature, v. 286, p. 213-218.

1984: SONAR evidence for postglacial tectonic instability of the Canadian Shield and Appalachians; in Current Research, Part A, Geological Survey of Canada, Paper 84-1A, p. 567-579.

St-Onge, D.A.
1984: Surficial deposits of the Redrock Lake area, District of Mackenzie; in Current Research, Part A, Geological Survey of Canada, Paper 84-1A, p. 271-277.

25.

THE GEOMORPHIC EFFECTS OF THE JULY 1983 RAINSTORMS IN THE SOUTHERN CORDILLERA AND THEIR IMPACT ON TRANSPORTATION FACILITIES

Project 830016

S.G. Evans and D.R. Lister[1]
Terrain Sciences Division

Evans, S.G. and Lister, D.R., The geomorphic effects of the July 1983 rainstorms in the southern Cordillera and their impact on transportation facilities; in Current Research, Part B, Geological Survey of Canada, Paper 84-1B, p. 223-235, 1984.

Abstract

In July 1983 severe rainstorms occurred in the Hope-Chilliwack and Revelstoke-Rogers Pass areas of British Columbia. In the Hope-Chilliwack area fourteen debris torrents reached the Trans-Canada Highway, some also blocking the Canadian National Railways. The highway and railway were severed for three days. The torrents resulted from an intense rainstorm. Similar storms have an approximate return interval of ten years. In the Revelstoke-Rogers Pass area, massive floods occurred, resulting in widespread mobilization of sediment in river channels and materials in channel margins. Debris torrents were also widespread. In Illecillewaet River valley, the Trans-Canada Highway was severed by the destruction of the Woolsey Creek bridge and the Canadian Pacific Railway suffered track breaches at more than 13 locations; transportation was interrupted for approximately ten days. The floods and torrents resulted from an intense rainstorm; similar storms have an approximate return interval of 220 years.

The geomorphic responses and their impact documented in this report illustrate the effects of high magnitude rainstorm-runoff events on transportation facilities in mountainous terrain where, by necessity, these facilities have been located on, or in the vicinity of, active geomorphic surfaces in valley bottoms.

Résumé

En juillet 1983, il y a eu de grandes précipitations dans les régions de Hope-Chilliwack et du col de Revelstoke-Rogers, en Colombie-Britannique. Dans la région de Hope-Chilliwack, quatorze torrents de débris ont atteint la Transcanadienne, et certains d'entre eux ont même bloqué la voie ferrée du Canadien National. La route et la voie ferrée ont été coupées pendant trois jours. Un orage important était à l'origine de ces torrents. Des orages de cette intensité reviennent presque tous les dix ans. Dans la région du col de Revelstoke-Rogers, il y a eu des inondations étendues dont les résultats étaient une mobilisation générale des sédiments dans les chenaux des rivières et des matériaux dans les berges des chenaux. Les torrents de débris étaient aussi répandus. Dans la vallée de la rivière Illecillewaet, la Transcanadienne a été coupée à cause de la destruction du pont du ruisseau Woolsey; la voie ferrée du Canadien Pacifique s'est rompue à plus de 13 endroits. La circulation a été interrompue pendant presque 10 jours. Un orage intense est à l'origine des inondations et des torrents. Des orages de cette intensité reviennent presque tous les 220 ans.

Les conséquences géomorphiques et leurs répercussions étudiées dans le présent rapport illustrent les effets des précipitations et des eaux de ruissellement de grande envergure sur les voies de transport en montagne, où il a fallu construire ces voies, sur des surfaces géomorphiquement actives dans les fonds de vallées ou à proximité de telles surfaces.

Introduction

In July 1983 severe rainstorms occurred in the Hope-Chilliwack and Revelstoke-Rogers Pass areas, along the Trans-Canada Highway in the southern Cordillera (Fig. 25.1). This report examines the response of geomorphic systems to the two rainstorms and documents their impact on transportation facilities along a major national transportation corridor. The facilities included the Trans-Canada Highway in both areas, the Canadian National Railways in the Hope area, and the Canadian Pacific Railway in the vicinity of Revelstoke.

The first part of this report examines the effects in the Hope-Chilliwack area and is authored by D.R. Lister whilst the second part is a description of the effects in the Revelstoke-Rogers Pass area authored by S.G. Evans.

Debris torrents between Chilliwack and Hope

During the early hours of July 12, 1983, a series of debris torrents closed the Trans-Canada Highway and the Canadian National Railways main line at a number of locations within a 10 km section mid-way between Chilliwack and Hope, British Columbia (Fig. 25.2).

[1] Geotechnical and Materials Branch
British Columbia Ministry of Transportation and Highways
4A, 940 Blanshard Street
Victoria, British Columbia
V8W 3E6

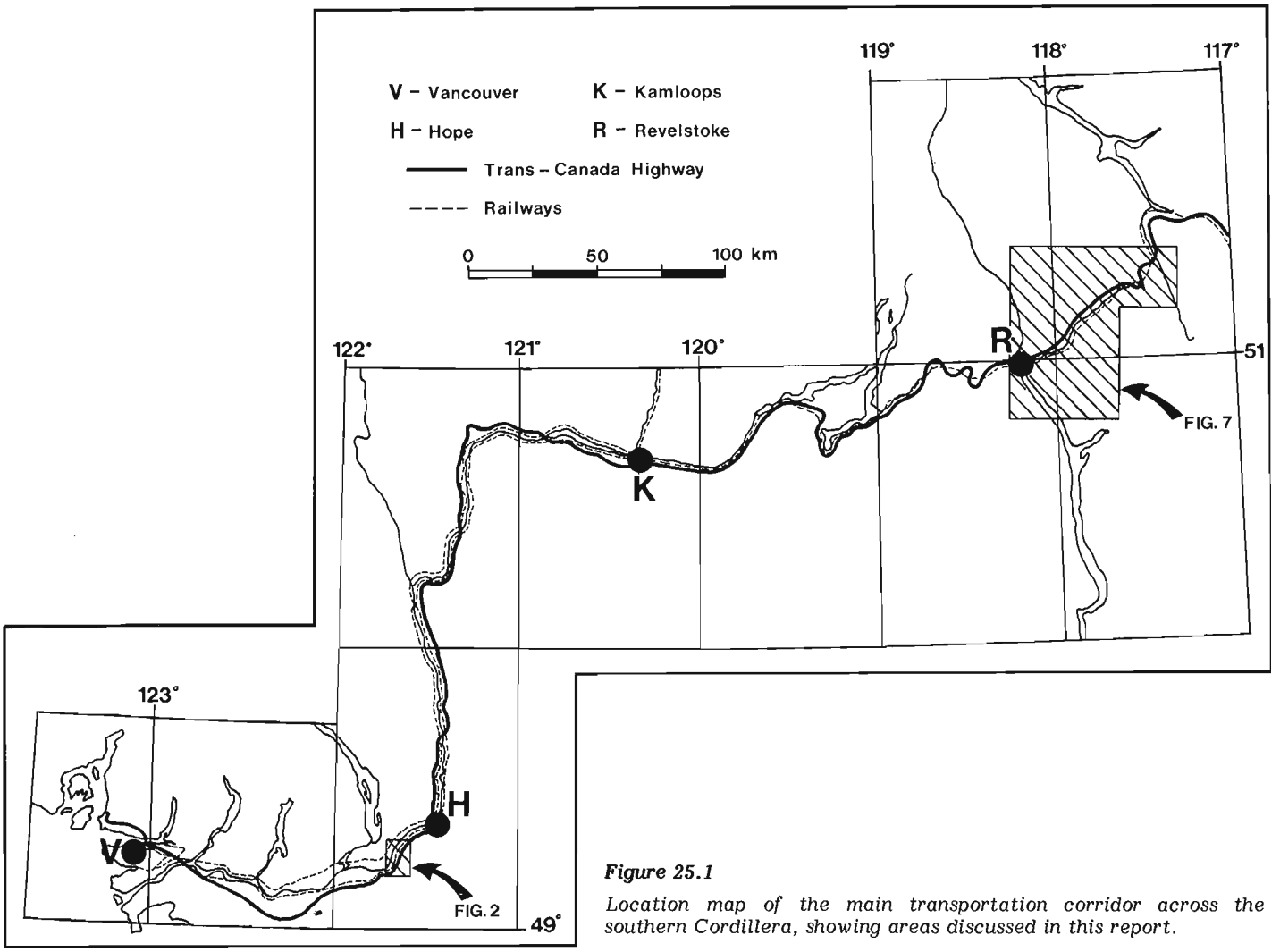

Figure 25.1

Location map of the main transportation corridor across the southern Cordillera, showing areas discussed in this report.

A debris torrent is a type of mass movement that consists of water-charged inorganic and organic material flowing rapidly down a steep confined channel. The inorganic and organic materials which comprise the debris can include rock fragments up to several metres in diameter, soil ranging from clay to gravel size, and wood ranging from mulch to logs (Thurber Consultants, 1983). Debris torrents, also known as debris flows and mud flows, are common in areas where there are creeks with steep gradients, a supply of debris and the potential for rapid runoff. Historically considered as part of a stream flood process, debris torrents have only recently been recognized as a distinct phenomenon. Takahashi (1981) has described torrents as high energy sediment gravity flows that are episodic events of relatively short duration.

At least fourteen torrents reached the highway during the July 12 event, depositing debris ranging in size from sand to boulders up to 1 m in diameter. Most of the deposition occurred between the British Columbia Hydro power line and the highway within a zone 100-200 m wide. The torrents originated on the west facing slopes of Four Brothers Mountain (elevation 1528 m) and Mount Ludwig (elevation 1396 m). Some torrents did not reach the highway and others originating on the east facing slopes terminated in Wahleach (Jones) Creek (Fig. 25.2).

The storm

For the 24 hour period, 0800 h, July 11 to 0800 h, July 12, the Agriculture Canada Research Station at Agassiz, 6 km to the west, recorded 85.4 mm of rainfall. This figure is high but not excessive, approximating to a 1 in 10 year duration for a one day storm at any time of the year (Coligado, 1982). The tight grouping of the debris torrents within a 4 km radius suggests that there was a high intensity rain cell within the storm and it is probable that precipitation within the cell far exceeded that measured at Agassiz. The preceding period of July and the month of June had been characterized by cooler than average weather. When considered with the approximate 1500 m rise in the freezing level associated with the storm, this suggests that there may have been additional runoff in the form of snowmelt.

Debris torrents

The southern part of the area is composed of quartz diorite and granodiorite rocks of the Chilliwack Pluton. North of Cheam View Station, the bedrock comprises phyllites and basaltic rocks of the Upper Pennsylvanian-Permian Chilliwack Group (Monger, 1969). Covering the bedrock is a mantle of glacial till and colluvium. The change

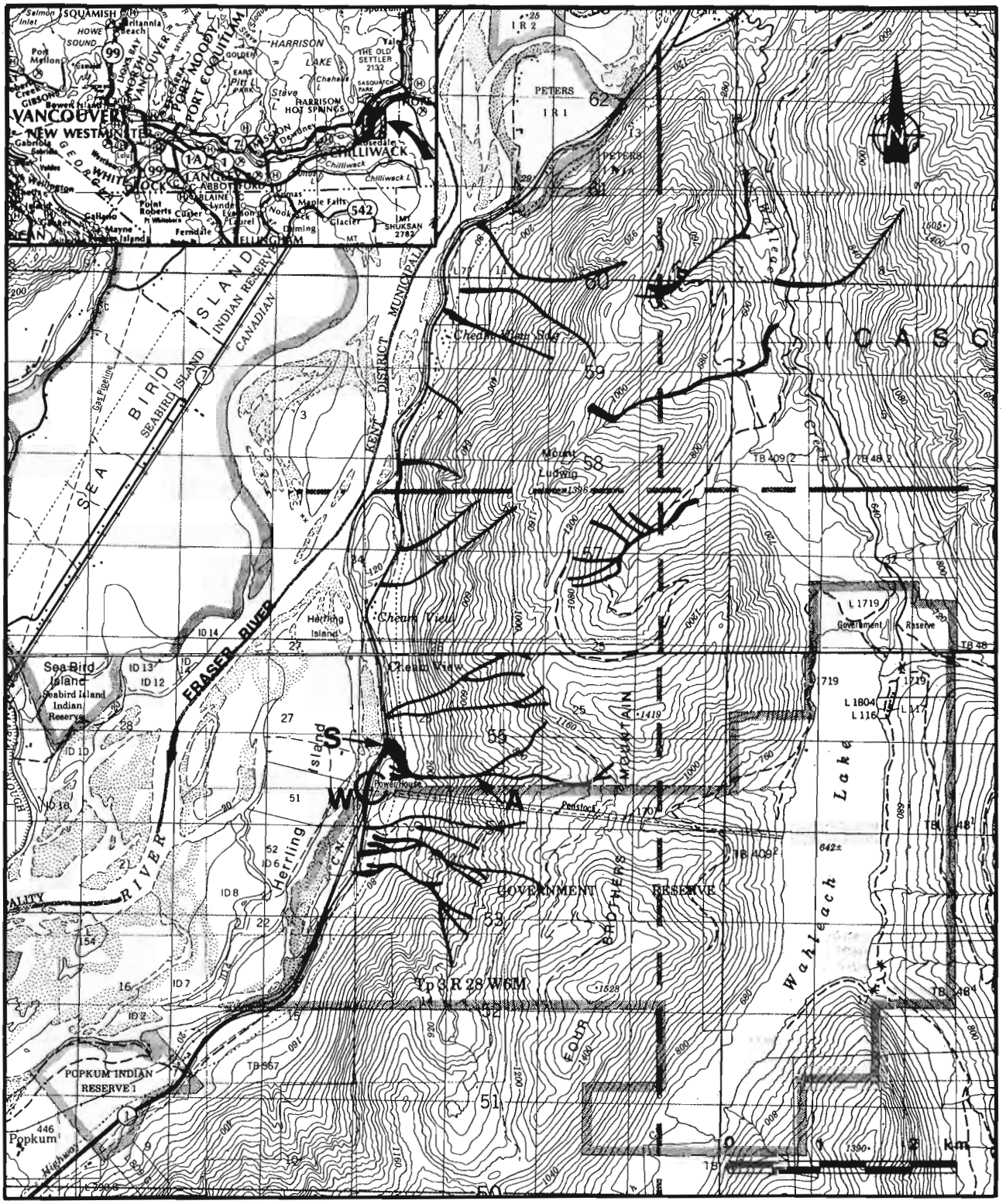
SEA BIRD ISLAND INDIAN RESERVE
SEABIRD ISLAND 2
CANADIAN
KENT DISTRICT MUNICIPALITY
Sea Pipeline
Mount Ludwig 1396
Cheam View
Herring Island
FRASER RIVER
Sea Bird Island
Seabird Island Indian Reserve
Powerhouse
Penstock
Herring Island Creek
MOUNTAIN
Wahleach Lake
GOVERNMENT RESERVE
BROTHERS
Tp 3 R 28 W6M
POPKUM INDIAN RESERVE 1
Popkum
Highway
PETERS IR 1
PETERS IR 2
CASCADE
Chilliwack River
Chilliwack Lake
Government Reserve
VANCOUVER
NEW WESTMINSTER
CHILLIWACK
HARRISON HOT SPRINGS
HARRISON LAKE
PORT MOODY
PORT COQUITLAM
SQUAMISH
LANGLEY
ABBOTSFORD
BLAINE
FERNDALE
MT SHUKSAN 2782
THE OLD SETTLER 2132
Mount Cheam 2385
Mount Slesse 2682
Mount Lady Peak 2603
Mount Redoubt 2763
Mount Baker 3285
Mount Shuksan 2782
Mount Rexford 2516
Mount Blum 2440
Mount Larrabee 2722
Mount Sefrit 2678
Mount Ballam 2678
Mount Hozameen 2468
Mount Outram 2591
Mount Spickard 2888
Mount Redan 2716
Mount Challenger 2744
Mount Logan 2821
Mount Custer 2766
Mount Fernie 2744
Mount Ida 2744
Mount Judge Howay 2744
Mount Judge Howay 2744
Mount Judge Howay

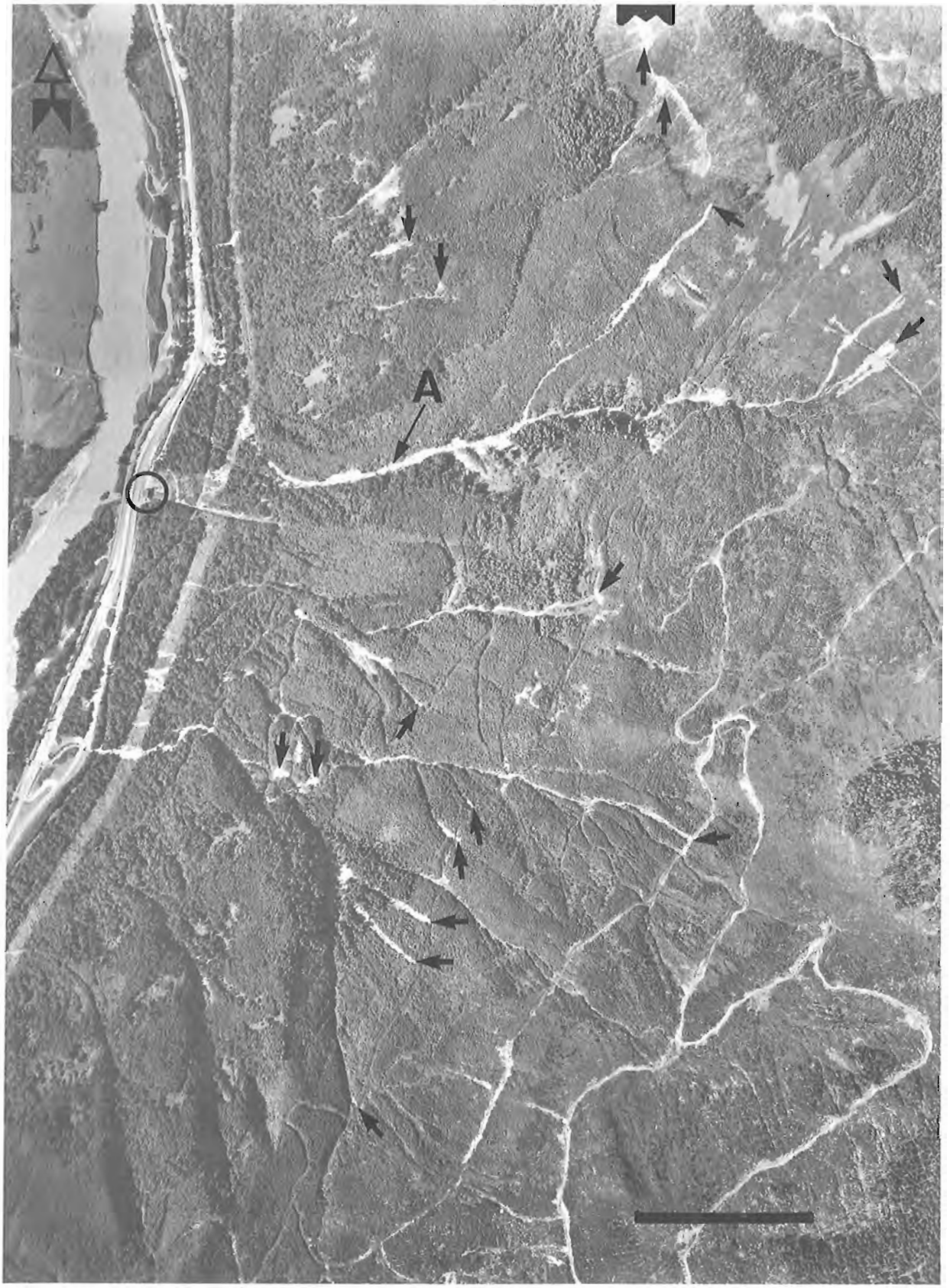

Figure 25.3. *Aerial photograph (BC 83020-104; July 30, 1983) showing debris torrents initiated by the July 11-12 storm in the vicinity of Wahleach Power Station (circled). Arrows mark initiation points of torrents. A = Torrent channel shown in Figures 25.4, 25.5, and 25.6. Bar scale is approximately 300 m.*

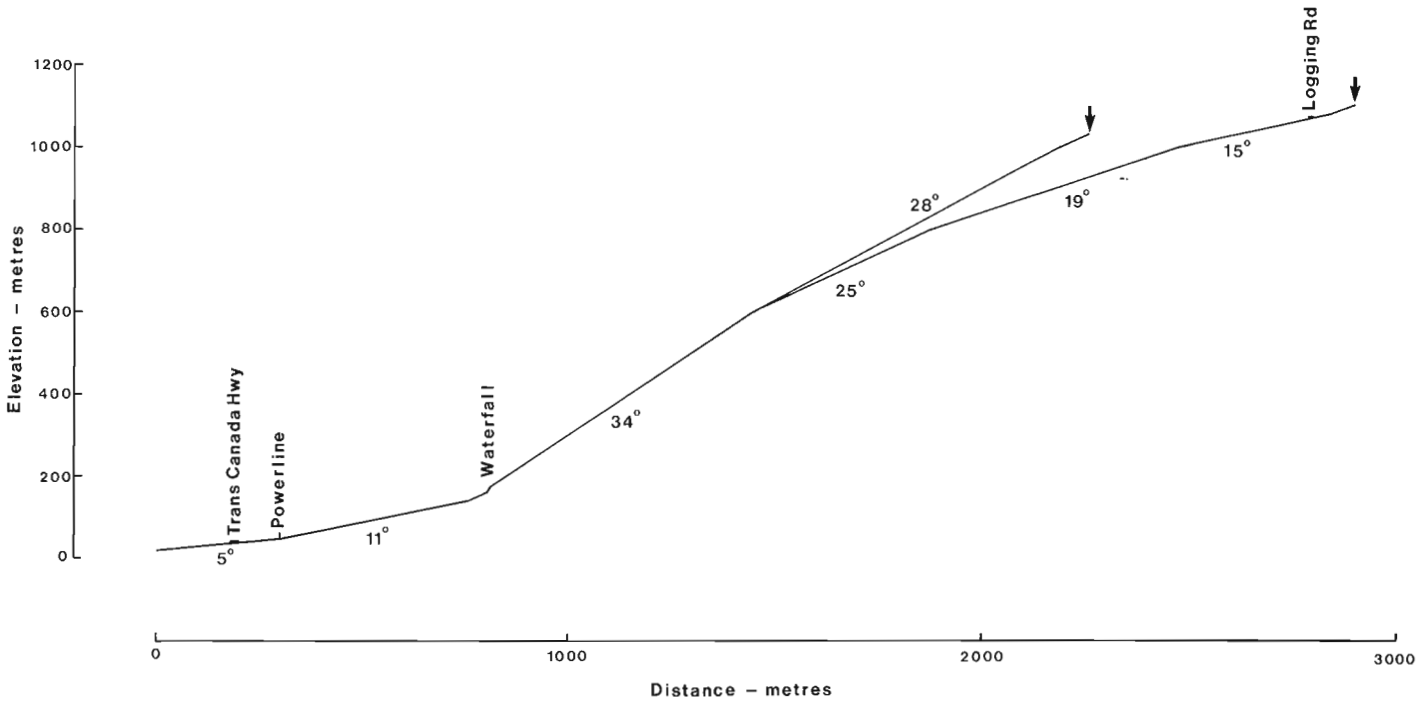

Figure 25.4 *Profile of debris torrent track immediately north of Wahleach Power Station (A in Fig. 25.3). Arrows mark initiation points.*

Figure 25.5 *(left)*

Small debris slides (outlined by white dashed line) that initiated the debris torrent immediately north of Wahleach Power Station.

Figure 25.6 *(below)*

Debris deposited north of Wahleach Power Station. Note damage to trees up to 1 m above surface of debris.

in geology is reflected in the types of debris deposited by the torrents. In the southern part, the deposits are primarily subangular to subrounded boulders of granodiorite-quartz diorite whereas north of Cheam View the debris consists of primarily angular to subangular basic volcanic rocks.

Channels subject to debris torrents can be divided into three zones, namely, initiation, erosion and transportation, and deposition (Thurber Consultants, 1983). In the initiation zone, the gradient must be steep enough (typically 25° or higher) and contain sufficient unstable debris to be mobilized. The erosion and transportation zone must remain sufficiently steep to allow the torrent to maintain its velocity. Typically such gradients are in excess of 10°. The deposition zone, with slopes normally in the range of 4-15° is where the torrent loses velocity rapidly due to the flattening out of the gradient.

In Figure 25.3, an aerial photograph taken on July 30, 1983, shows torrent channels in the vicinity of Wahleach Power Station.

The torrent channel immediately north of Wahleach Power Station (Fig. 25.3) was examined in detail. The channel, which has a catchment area of 2.26 km^2, was the site of multiple events as described below. These torrents were initiated in three locations at about 1100 m elevation (Fig. 25.3, 25.4). The two southerly trigger zones were shallow debris slides located above an old logging road in a logged off area (Fig. 25.5). The material evidently failed when oversaturated and slid into the channel. The northern initiation zone is similar to the other two, but is located in an area of dead trees. The gradients of the southern and northern initiation zones are 15° and 28°, respectively (Fig. 25.4). The 15° figure is low but is taken from a contour map; the actual slides are probably steeper. The two southern zones both reached a single channel within a hundred metres. This channel and the northern zone do not meet until 600 m elevation (Fig. 25.4). Below this elevation the channel has its steepest gradient, 34°. Below a waterfall at the 200 m elevation, the channel gradient rapidly decreases and curves to the north (Fig. 25.3). Within 50 m of the waterfall, the channel changes from scoured bedrock to one cut through previous debris torrent and alluvial deposits. At this point the channel sides are 5 m high and the gradient about 12°. At 200 m downstream from the waterfall on the south side is a small secondary channel that continues straight downslope rather than curving off to the south (Fig. 25.3). This channel was blocked off from the main channel by a wall of debris about 3 m in height. At 350 m below the waterfall, the gradient is 10° and the channel becomes an area of deposition (Fig. 25.6). Here the debris is

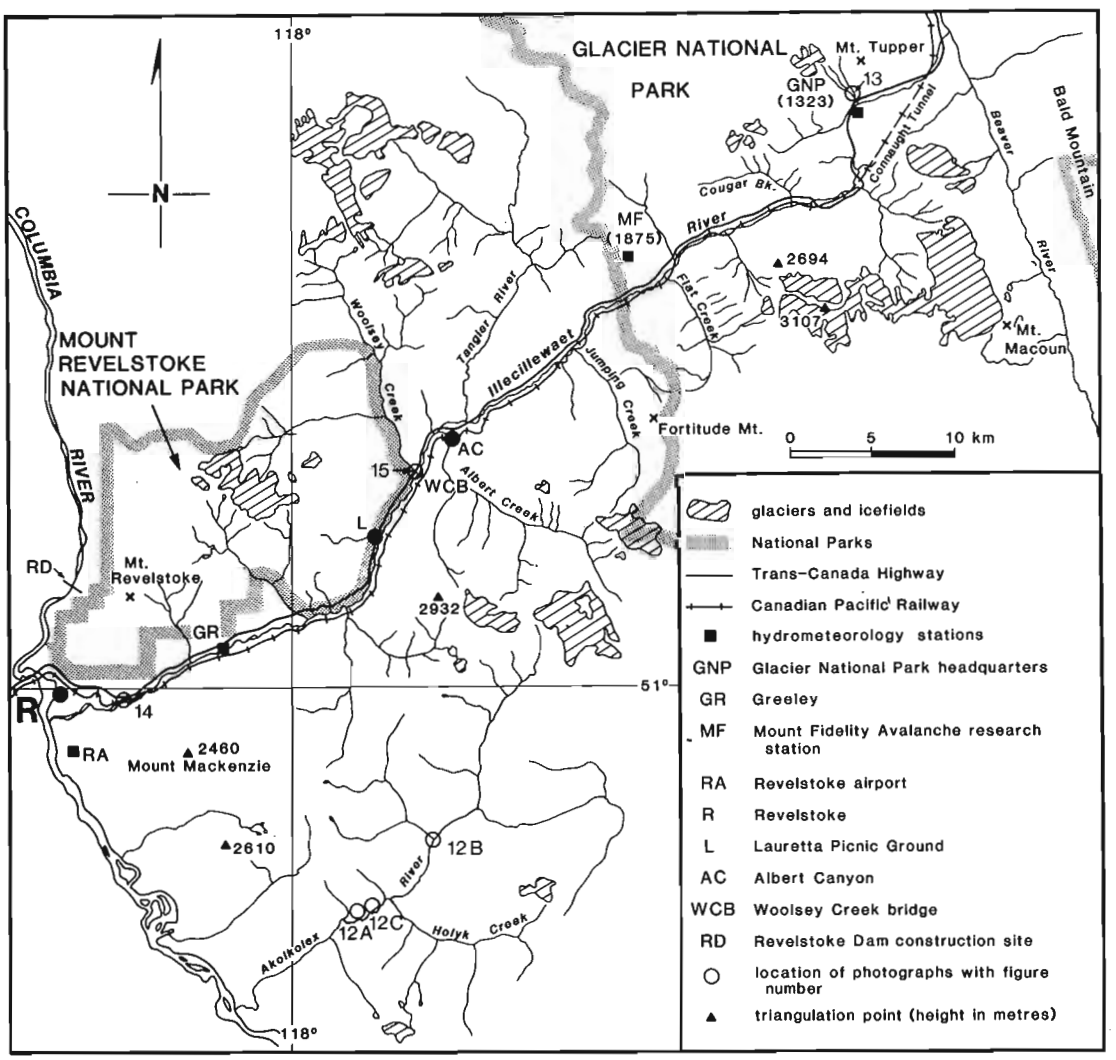

Figure 25.7. *Map of Revelstoke-Rogers Pass area showing location of hydrometeorological data stations and localities mentioned in the text.*

about 3 m thick and 35 m wide. Downstream the gradient drops to 5° between the B.C. Hydro power line and the highway, where the deposit widens to over 100 m. Close to the highway the debris piled up behind the highway embankment up to 8 m thick and behind the access road to the power station. Debris completely blocked a 3 m-high concrete box culvert causing post-torrent water flow to erode the highway fill, severing the Trans-Canada Highway and requiring the installation of a temporary metal culvert at the top of the fill.

Downstream from the small secondary channel noted above, four more debris lobes were located (Fig. 25.3). Three of these stopped only 150 m above the B.C. Hydro power station and switching yard.

Each lobe, therefore, appears to represent a separate event or surge with the most southerly lobes resulting from the initial events and the main lobe resulting from the last, or last few, surges. Approximately 60 000 m^3 of debris was deposited. Some 25 000-35 000 m^3 of this material was the result of erosion and redeposition of pre-existing debris torrent and alluvial deposits downstream of the waterfall.

Other debris torrents in the area had similar multiple initiation zones and terminated with more than one lobe. Volumes of other torrents have not been calculated, but are probably of the order of 10 000-40 000 m^3.

There was fortunately no loss of life associated with the torrents although one house was partially engulfed in the vicinity of Cheam Siding. The highway and railway were shut down for three days and the cost of repairs and remedial work has been estimated to have been in excess of $300 000.

Effects in the Revelstoke – Rogers Pass area

This part of the report examines the effects of the July 11-12 storm in the Revelstoke-Rogers Pass area of the Selkirk Mountains (Fig. 25.1). It is based on reconnaissance observations made on July 18-19 of Akolkolex River valley and the valley of Illecillewaet River between Rogers Pass and Revelstoke (Fig. 25.7).

Geomorphic setting

The Selkirk Mountains are characterized by high rugged terrain cut by steep-sided glaciated valleys which show classical U-shape form. Like many other rivers and streams in the area, the Illecillewaet River rises at the snout of a glacier (Fig. 25.7) Valley side slope processes are dominated by snow and slush avalanches during the winter (Schaerer, 1962a) and debris flows involving surficial materials during other times of the year. Debris fans are commonly found where gullies dominated by these processes debouch onto main valley floors. In addition, alluvial fans are common where smaller tributary creeks enter main valleys. The magnitude and frequency of snow avalanches in the Rogers Pass area during the winter months necessitated the construction of snow sheds at a number of locations and the implementation of a well known avalanche control program (Schaerer, 1962b).

Other elements of the process spectrum in the area include the occurrence of outburst floods from high level lake basins (e.g., in the vicinity of Mount Macoun and Fortitude Mountain) and the widespread occurrence of sackung features indicating sites of large scale slope deformation. These have been noted by Nasmith (1972) on the western slopes of both Mount Revelstoke and Mount Mackenzie in the Revelstoke area, and by the present author along the western flanks of Bald Mountain on the east side of the Beaver River (Fig. 25.7).

Both the Trans-Canada Highway and the Canadian Pacific Railway follow the narrow floor of the Illecillewaet River valley between Revelstoke and Rogers Pass (Fig. 25.7). Figure 25.8A shows typical cross-sections of the corridor. Similarly, in the Akolkolex valley logging roads also follow the valley floor (Fig. 25.8B). In the Selkirk Mountains, topographic constraints have forced transportation routes to traverse depositional zones of snow avalanches, debris flows, and tributary streams as well as maintain close proximity to major river channel margins.

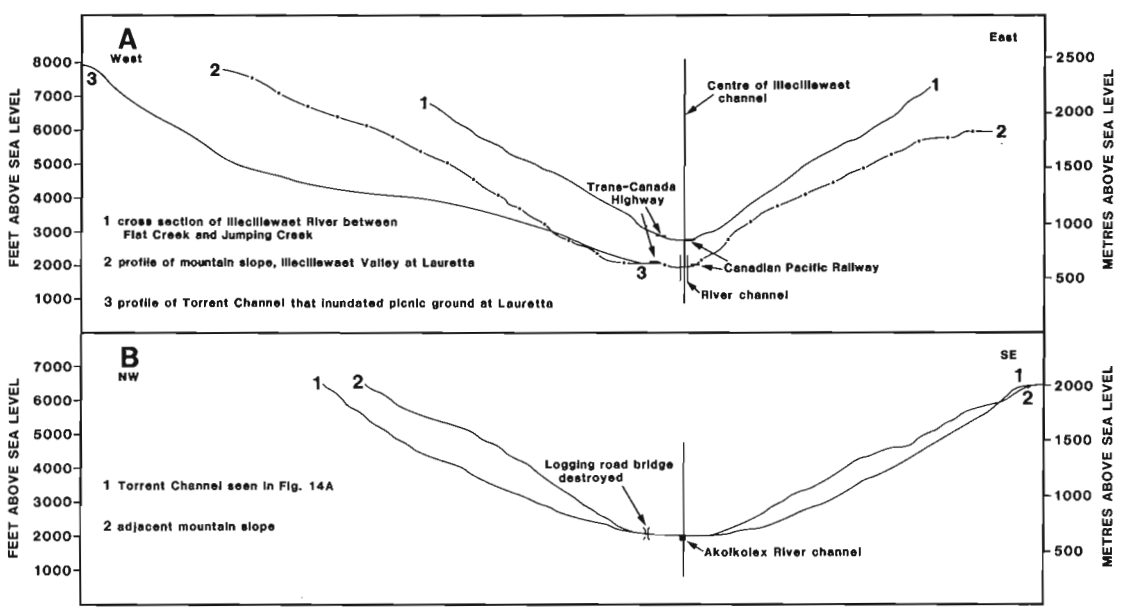

Figure 25.8. Typical cross-sections of Illecillewaet River valley (A) and Akolkolex River valley (B) showing location of river channel and transportation routes.

The storm of July 11-12, 1983

Rainfall data are available from Glacier National Park headquarters at Rogers Pass (1325 m a.s.l.), Mount Fidelity Avalanche Research Station (1875 m a.s.l.), and the Revelstoke Dam construction site (~550 m a.s.l.). These stations are shown in Figure 25.7 and the climatic data are summarized in Figure 25.9.

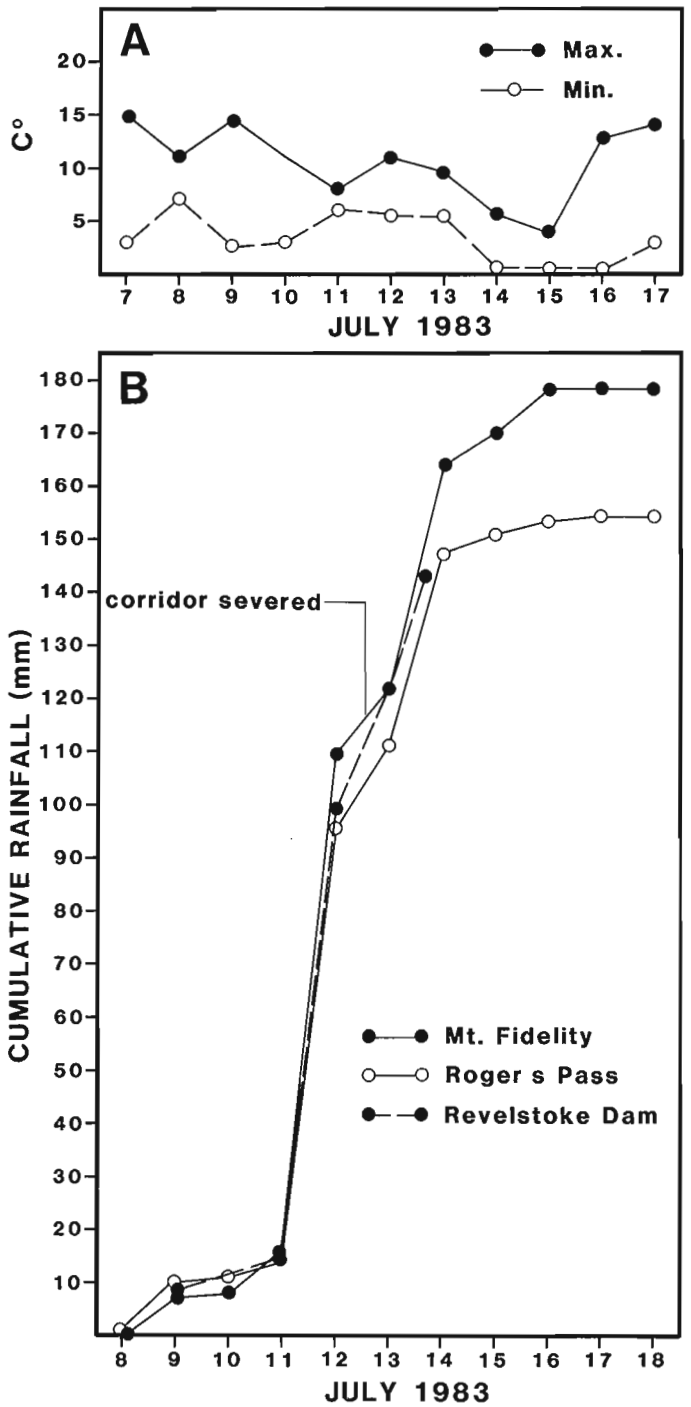

Figure 25.9. Climatic data on the July 11-12 storm in the Revelstoke-Rogers Pass area. A – maximum and minimum daily temperatures at Mount Fidelity Avalanche Research Station (1875 m a.s.l.) B – Cumulative rainfall measured at Mount Fidelity, Glacier National Park headquarters at Rogers Pass, and Revelstoke Dam construction site. Data supplied by Environment Canada and B.C. Hydro and Power Authority.

Most of the rainfall associated with the storm fell in the 24 hour period between 0700 h, July 11 and 0700 h, July 12 – the 24 hour rainfall for this period being 93.5 mm at Mount Fidelity and 82.0 mm at Glacier National Park headquarters. These amounts exceeded the previously recorded 24 hour maximums at both stations.

Based on data prepared by the Canadian Climate Centre, the 24 hour rainfall measured at Mount Fidelity represents an event with an estimated return period of approximately 220 years. This estimate is very approximate, since it is based on an analysis of only 13 years of record, but it is felt that it does give an indication of the significance of the event.

Temperatures at Mount Fidelity (Fig. 25.9) indicate that no appreciable warming took place at higher elevations during the storm. The effect of warm rain on a pregnant snow pack, however, probably contributed to runoff and it may be concluded that the total runoff-slope moisture event is in excess of a 220 year rainfall event.

It is noted that rainfall at Revelstoke Airport, located south of the city (Fig. 25.7), was not of the magnitude measured elsewhere in the area. This suggests that the boundaries of the regional rainfall event, which may have covered an area of up to 5000 km^2, were quite sharp.

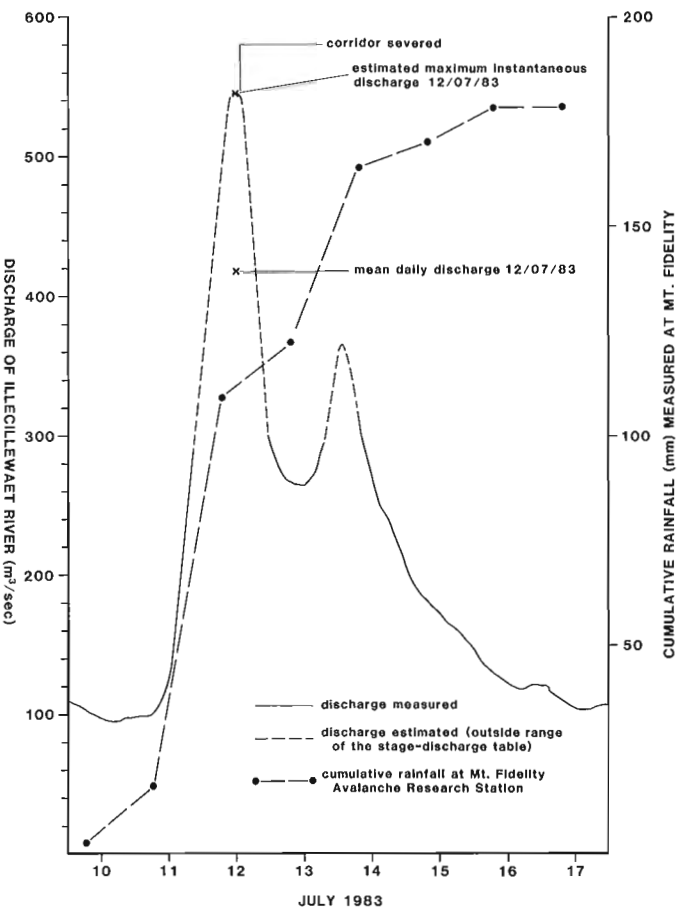

Figure 25.10. Flood hydrograph for Illecillewaet River at Greeley (for location see Fig. 25.7). Data supplied by Water Survey of Canada. Maximum instantaneous discharge is estimated only; also shown is cumulative rainfall at Mount Fidelity.

Figure 25.11. *View up the Illecillewaet at Greeley, July 12, 1983 at approximate time of maximum discharge; note the partially destroyed bridge. (Photo courtesy of C. Macdonald, Water Survey of Canada)*

Effects on geomorphic systems

The rainfall resulted in massive floods in watersheds within the area covered by the storm. As a consequence, large amounts of sediment in river channels and material in channel margins were mobilized, with resultant changes in both channel morphology and channel boundaries. Peak discharge data for streams in the area can only be estimated since in some cases Water Survey of Canada gauging stations were destroyed, whilst in other cases changes in channel geometry rendered existing rating curves obsolete.

Discharge data (Fig. 25.10) for Illecillewaet River measured at Greeley, 11 km east of Revelstoke, give an estimated maximum instantaneous discharge of 546 m^3/s on July 12, 1983. Figure 25.11 shows the partially destroyed bridge at Greeley on July 12 at the approximate time of maximum discharge.

The rainstorm also resulted in widespread mobilization of surficial materials from hillslope sites which significantly contributed to the sediment load of major rivers in the area. Debris flows were initiated on open slopes and generally flowed down gullies or alluvial channels to become torrents. These were common in steep tributary watersheds of Akolkolex and Illecillewaet rivers. Examples from the Akolkolex are shown in Figure 25.12 and it can be seen that in some cases the torrent material was deposited on existing debris fans before reaching the main river channel (Fig. 25.12C). In other cases the mass of torrent material entered the main channel resulting in extensive downstream deposition from its point of entry (Fig. 25.12A, 25.12B). An example of a debris torrent on the slopes of Mount Tupper in the Rogers Pass area is seen in Figure 25.13.

An important aspect of the material transported in the floods was the amount of logs and trees that make up the deposited debris (e.g., Fig. 25.12B). On the Columbia River log jams temporarily blocked the entrance to the diversion tunnel at the Revelstoke Dam construction site and on the Illecillewaet a massive log jam in Box Canyon (Fig. 25.14), approximately 5 km to the east of Revelstoke, temporarily dammed the river, threatening the south side of Revelstoke itself.

Effects on transportation facilities

Geomorphic events triggered by the storm inflicted massive direct damage on the transportation facilities in the area. Further, as a result of the lengthy dislocation of these transportation routes, the economy of southern British Columbia suffered substantial indirect damage.

With reference to highways and logging roads, the main effect of the storm was the destruction of bridge crossings by floods and torrents debouching into the main valleys of the Illecillewaet and Akolkolex. A major bridge crossing, constructed in 1959, on the Trans-Canada Highway at Woolsey Creek (Fig. 25.7), suffered extensive damage when it was undermined and its west abutment partially collapsed (Fig. 25.15). The collapse took place at about 1530 h on July 12, thus severing the Trans-Canada Highway. The highway remained closed for about ten days until 1200 h on July 22 when it was re-opened on a temporary crossing of Woolsey Creek.

An estimated $2 M damage was done to facilities in the Revelstoke Forest Service District. A local sawmill company suffered $1.5 M damage and lost 15 bridges on their logging operations (Revelstoke Review, July 20, 1983). In the Akolkolex River valley 8 bridges were destroyed (Fig. 25.7, 25.12).

The Canadian Pacific Railway suffered track breaks at more than 13 locations along the Illecillewaet in the 48 km between Revelstoke and the west portal of the Connaught Tunnel. Service was first interrupted some time in the afternoon of July 12 and was not re-established until 0105 h on July 19, a total closure of approximately 7 days. Further breaks in service occurred between 1600 h on July 19 and 1145 h on July 21, and between 2030 h on July 23 and 1135 h July 24. The final re-opening of the railway through Rogers Pass followed a massive repair operation by Canadian Pacific. Most of the track breaks occurred where the railway was located at, or near, the channel margin of the Illecillewaet and resulted from the erosion of the railbed. An example of the damage and reconstruction efforts is seen in Figure 25.16.

In addition to breaks due to erosion, blockages resulting from deposition also disrupted transportation on both road and railway. Debris flows and torrents debouching into the main Illecillewaet valley covered the Trans-Canada Highway at several places and covered the picnic grounds at Lauretta Creek (Fig. 25.7). Locations along the railway were also covered by deposits from debris flows and torrents.

Conclusions

This report documents the response of geomorphic systems to severe rainstorms and their impact on transportation facilities in the Hope-Chilliwack and Revelstoke-Rogers Pass areas of the southern Cordillera in July 1983. It illustrates the effect of high magnitude rainstorms and runoff events on transportation facilities in mountainous terrain where, by necessity, these facilities have been located on, or in the vicinity of, active geomorphic surfaces in valley bottoms.

The magnitude of the storm in both areas (as measured by the 24 hour rainfall) was remarkably similar. The rainfall recorded in the Hope-Chilliwack area, however, indicates a precipitation event with a 10 year return interval whilst, in contrast, the Revelstoke-Rogers Pass event had an estimated return interval of the order of 220 years. Snowmelt during the storms likely significantly contributed to runoff. Thus, the magnitude and return interval of the runoff event were in excess of that of the precipitation event.

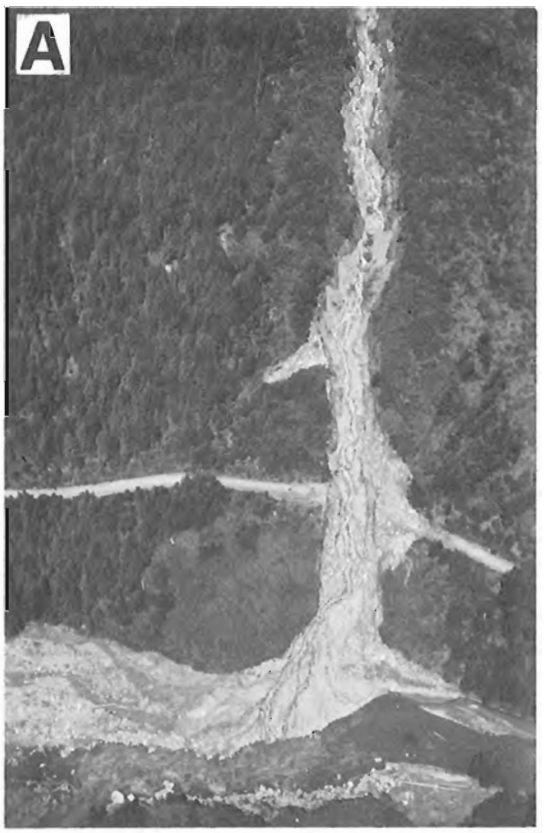

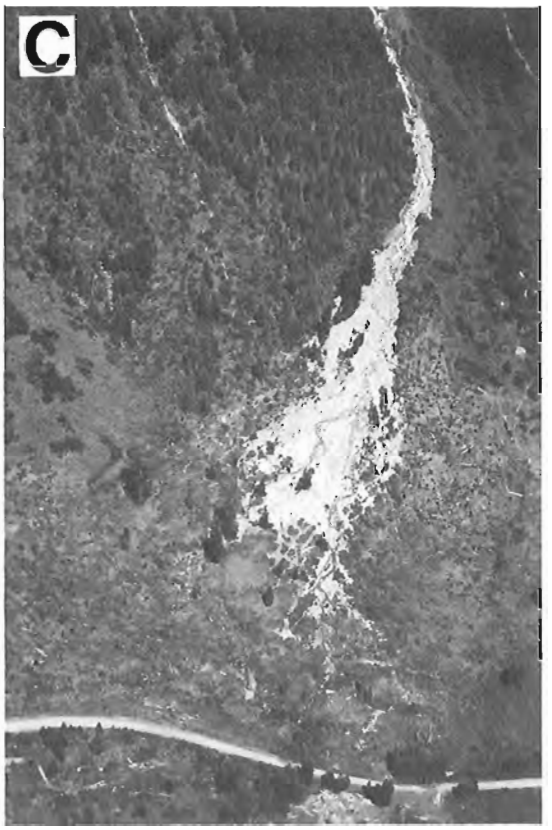

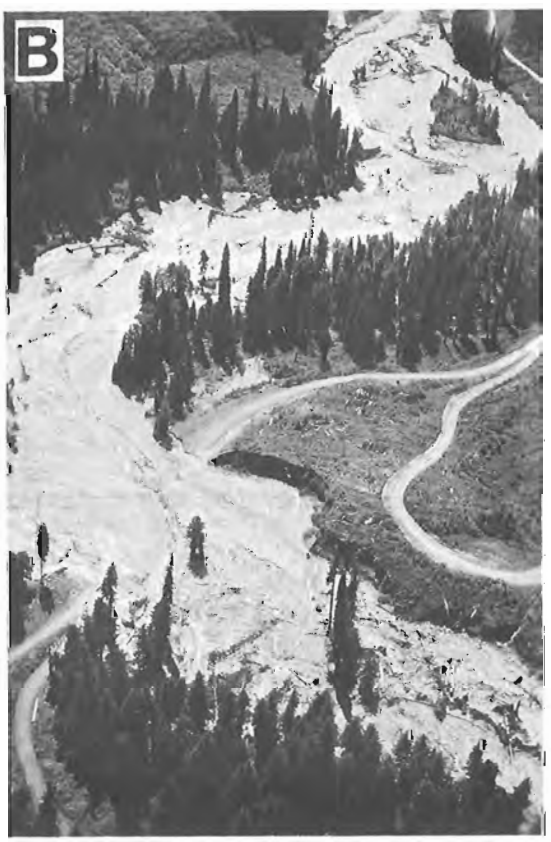

A – Torrent channel just downstream of Holyk Creek. Note severed logging road, spillage of debris over channel boundaries, and deposition of debris in main Akolkolex channel downstream of confluence. (GSC 203993-L)

B – Effects of debris torrent which emanated from Standfast Creek (lower right). Note desposition in Akolkolex channel downstream of confluence and severed logging road. (GSC 203993-O)

C – Torrent deposits on debris fan surface. (GSC 203993-N)

Figure 25.12. *Examples of debris torrents in the Akolkolex River valley, July 18, 1983.*

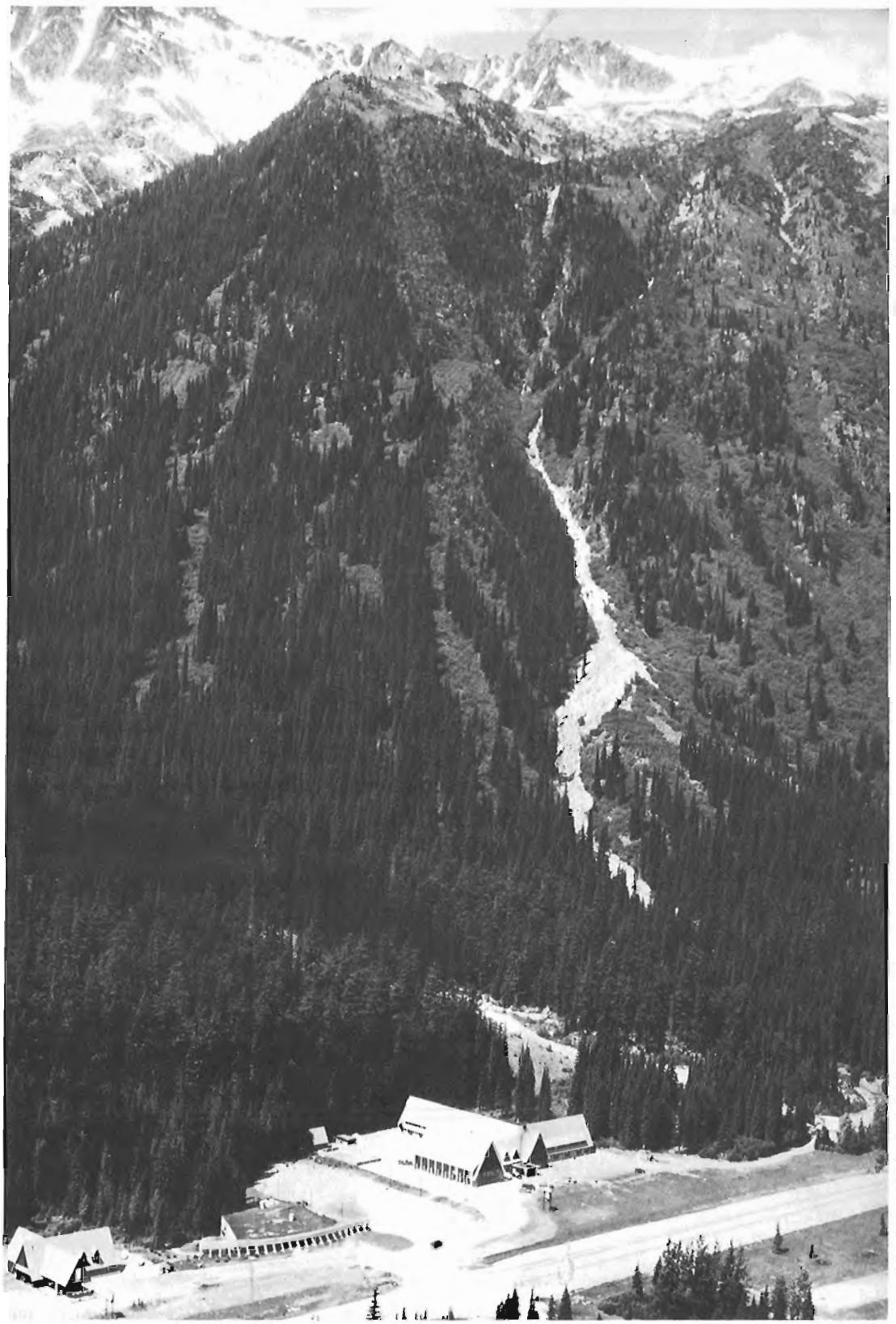

Figure 25.13. *Debris torrent on the slopes of Mount Tupper behind Glacier Park Lodge (in foreground); note spillage of debris over boundaries of channel. July 18, 1983. (GSC 204046-B)*

Figure 25.14

Log jam in Illecillewaet River at Box Canyon; the jam temporarily dammed the river on July 12, threatening the city of Revelstoke, 5 km downstream. Photograph taken July 18, 1983. (GSC 203993-U)

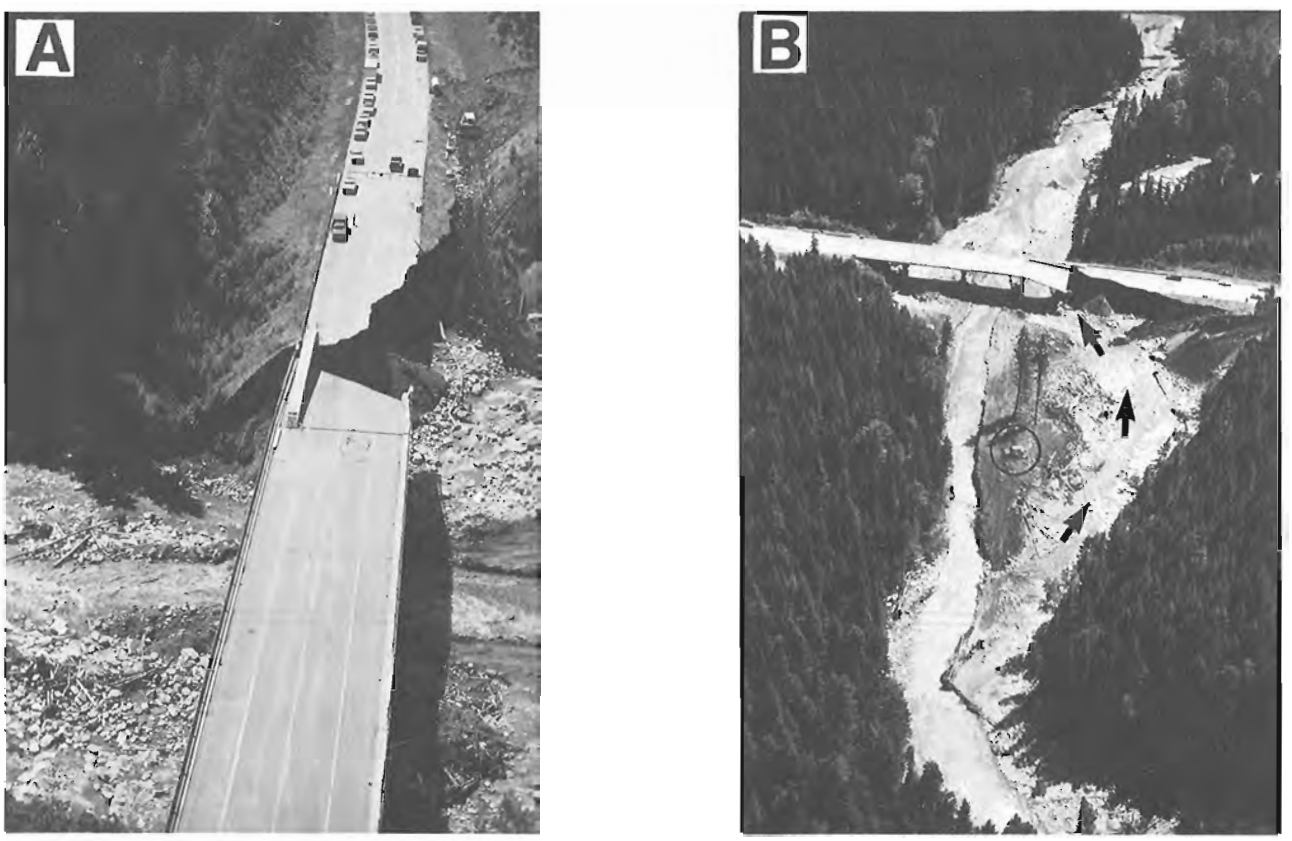

Figure 25.15. *The partially destroyed Woolsey Creek bridge, Trans-Canada Highway, July 18, 1983. A – View to the west (GSC 204045-B). B – View down Woolsey Creek showing path of river flow (arrow) that undermined the west abutment. Note attempts to control Woolsey Creek (bulldozer circled) before construction of temporary crossing. (GSC 203993-X)*

Figure 25.16. *Reconstruction of washed out Canadian Pacific Railway track in Illecillewaet River valley, July 18, 1983. Note light colour of rebuilt track bed (upper right), construction of protective riprap dykes, and rail wagons full of rockfill material (lower right). (GSC 203993-M)*

Large volumes of material were mobilized from hillslope, floodplain, and channel sites by debris flow, torrents, and floods. Erosion and deposition associated with these processes led to the severance of a major national transportation corridor for a period of three days at Hope-Chilliwack and for a total of ten days at Revelstoke-Rogers Pass.

Damage to facilities occurred due to erosional and depositional processes associated with debris flows, torrents, and floods at locations where routes cross tributary streams and follow the margins of major river channels.

Acknowledgments

Much of the hydrometeorological data presented here is preliminary in form and may be subject to revision.

S.G. Evans is indebted to Environment Canada for releasing much of the hydrometeorological information. In particular, he wishes to acknowledge the assistance of the Hydrometeorology Division, Canada Climate Centre, and the Water Survey of Canada. The British Columbia Hydro and Power Authority supplied the rainfall data from the Revelstoke Dam construction site. Mr. W.D. Gallacher, Park Superintendent, Glacier National Park, provided rainfall data and information on the closure of the Trans-Canada Highway at Woolsey Creek. The Canadian Pacific Railway supplied information on rail closures in the Illecillewaet valley. Bruce Dagg assisted in the field in the Revelstoke-Rogers Pass area. D.R. Lister particularly acknowledges the assistance of P.S. Dunn, District Highways Manager, Chilliwack, and his staff. Graham Baldwin and Laura Coughlan assisted with field measurements.

The first part of this paper is published with the approval of Mr. T.R. Johnson, Assistant Deputy Minister, British Columbia Ministry of Transportation and Highways.

References

Coligado, M.C.
1982: Multi-day extreme precipitation amounts for various return periods for selected stations on Vancouver Island and the Lower Mainland, British Columbia; British Columbia Ministry of Environment, Climatological Digest No. 2.

Monger, J.W.H.
1969: Hope map-area, west half, British Columbia; Geological Survey of Canada, Paper 69-47.

Nasmith, H.
1972: The engineering geology of the southern Cordillera of British Columbia; 24th International Geological Congress (Montreal), Guidebook, Excursion A08-C08, 34 p.

Schaerer, P.
1962a: The avalanche hazard evaluation and prediction at Rogers Pass; Division of Building Research, National Research Council, Technical Paper 142.

1962b: Avalanche defences for the Trans-Canada Highway at Rogers Pass; Division of Building Research, National Research Council, Technical Paper 141.

Takahashi, T.
1981: Debris flow; Annual Review of Fluid Mechanics, v. 13, p. 57-77.

Thurber Consultants
1983: Debris Torrent and Flooding Hazards Highway 99, Howe Sound; Report to Ministry of Transportation and Highways, British Columbia, 25 p. and Appendices.

26. PRELIMINARY ISOTOPIC AND CHEMICAL CHARACTERIZATION OF NATURAL GAS IN SEDIMENTS OF LAC HARRINGTON, QUEBEC AND GOLDEN LAKE, ONTARIO

Project 690095

T.W.D. Edwards[1] and R.A. Klassen
Terrain Sciences Division

Edwards, T.W.D. and Klassen, R.A., Preliminary isotopic and chemical characterization of natural gas in sediments of Lac Harrington, Quebec and Golden Lake, Ontario; in Current Research, Part B, Geological Survey of Canada, Paper 84-1B, p. 237-243, 1984

Abstract

Gases comprise up to 7% by volume (at 1 atmosphere) of bottom sediments in Lac Harrington, Quebec, and Golden Lake, Ontario. Stratigraphic variations in the concentration, and in the chemical and isotopic composition, of gas extracted from the bottom sediments of the two lakes are attributed to the interplay of biogenic hydrocarbon production and migrational and oxidative fractionation within the sediment columns. Nitrogen and methane constitute over 95% of the gases in ratios (N_2:CH_4) that range from 0.6:1 to greater than 19:1. Primary, unaltered methane in both lakes is considered to have a methane-$\delta^{13}C$ value of about -64‰ (PDB), although measured values range from -65.6‰ to -30.3‰ as a result of the effects of migrational depletion and oxidative enrichment, respectively.

Résumé

Les sédiments de fond du lac Harrington au Québec et du lac Golden en Ontario contiennent des gaz dont le pourcentage atteint 7 % en volume (à 1 atmosphère). Les variations stratigraphiques au regard de la concentration et des compositions chimiques et isotopiques des gaz extraits de ces sédiments sont dues aux effets combinés de la production des hydrocarbures biogéniques et au fractionnement de matières en migration et oxidantes dans les colonnes sédimentaires. L'azote et le méthane constituent plus de 95 % des gaz suivant des rapports (N_2:CH_{21}) qui se situent de 0.6:1 à plus de 9:1. En première analyse, le méthane inaltéré des deux lacs est considéré comme un méthane -$\delta^{13}C$ d'une valeur voisine de -64 ‰ (PDB), bien que les valeurs mesurées donnent une fourchette qui s'étend de -65,6 ‰ à -30,3 ‰; ceci est dû aux effets de l'épuisement par migration et à l'enrichissement de matières oxydantes.

Introduction

Zones of gas accumulation have been detected within postglacial sediment in a number of lakes in eastern Ontario and western Quebec. The gas zones characteristically appear on subbottom sonic profiles as acoustic "masks" within the sediment column that obscure the stratigraphic signature of the underlying material (Klassen and Shilts, 1982; Shilts and Farrell, 1982). The inferred presence of a gas phase in the sediments has been verified in several lakes by diving observations and coring. The gases consist primarily of nitrogen and methane, accompanied by minor amounts of carbon dioxide and C_{2+} hydrocarbons. The chemical and isotopic compositions of the gases yield information about the generation, migration, and consumption of gases within lake bottoms and pose questions about the geochemical and hydrological regime in the sediment columns.

Study Area

The locations of lakes known to contain gas zones are shown in Figure 26.1. Data from two of the lakes, Golden Lake and Lac Harrington (Lac Mousseau), are discussed.

Golden Lake lies within Ottawa valley in an area of Paleozoic carbonate and Precambrian silicate and carbonate rocks. The modern sediment in the lake is underlain by a considerable thickness (locally 20 m or more) of stratified glaciolacustrine sediment that bears evidence of collapse over buried glacial ice (Shilts and Farrell, 1982). The lake formed a natural settling basin in the ancestral Bonnechere River system, which was a major meltwater spillway during Late Wisconsinan deglaciation.

Lac Harrington is the middle of three lakes occupying a linear fault-trough in the Precambrian crystalline terrane of the Gatineau Hills, to the north of Ottawa valley. Grenville marbles outcrop around the northwest end of the lake and on several small islands, although silicate rocks predominate in the catchment area. Thin, patchy deposits of sandy till mantle the surrounding slopes. Till and stratified glaciofluvial and glaciolacustrine sediments up to several metres thick underlie a metre or more of postglacial sediment in the basin.

Both lakes lie close to or below the local limits of marine inundation by Champlain Sea, and hence some of the stratified sediments that underlie the modern lake sediment are probably of glaciomarine or estuarine origin. Cores of modern lake sediment were sampled for gas.

The lakes are dimictic and relatively productive water bodies. In August 1982 both were thermally and chemically stratified. Hypolimnetic oxygen depletion was pronounced in Lac Harrington which was almost devoid of dissolved oxygen (less than 0.4 $mg \cdot L^{-1}$) near the sediment-water interface in the deep areas. The buffering action of carbonate bedrock and drift components in both watersheds is evident in the high pH values, which ranged between 7.4 and 7.9 in the surface waters. Golden Lake is subjected to the influence of human activities associated with numerous lakeshore cottages and the effects of habitation, farming, and logging along the inflowing Bonnechere River. The lake occupies a wide, flat-bottomed basin in rolling terrain. In contrast, Lac Harrington presently sustains limited residential and recreational activity, and lies confined between bedrock ridges obliquely aligned to the direction of prevailing winds.

[1] Department of Earth Sciences, University of Waterloo, Waterloo, Ontario N3L 3G1

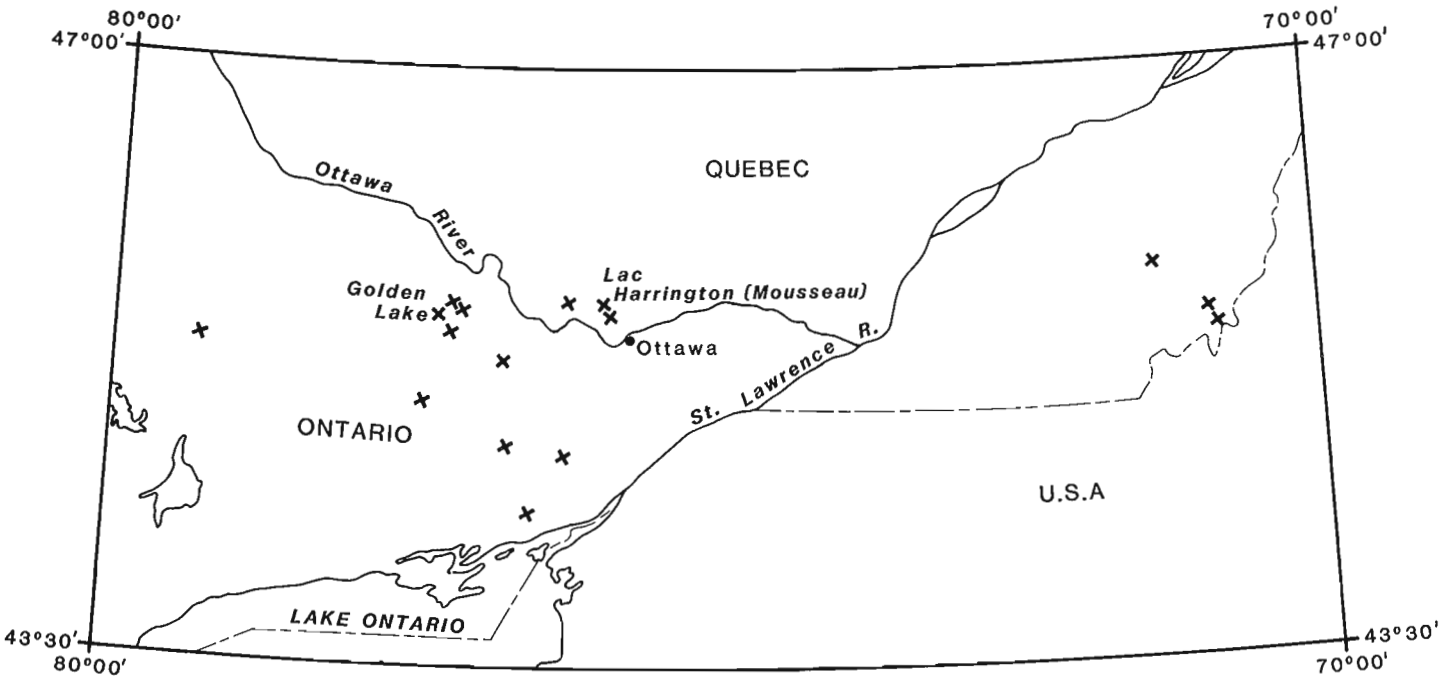

Figure 26.1. *Location (x) of lakes in eastern Ontario and western and southern Quebec in which gas zones have been detected by subbottom profiling (after W.W. Shilts, unpublished data).*

Subbottom profiles have been obtained for the basins by W.W. Shilts and co-workers (Terrain Sciences Division, Geological Survey of Canada). Selected segments of the records from each lake and discussion of their deposits have been presented previously (Klassen and Shilts, 1982; Shilts and Farrell, 1982). The subbottom profiles were used to select sites for coring and gas sampling.

Field and analytical methods

The sediment gas samples were collected from cores of undisturbed sediment obtained by divers using a modified Livingston-type piston corer. Transparent polycarbonate tubing of 4.5 or 5.3 cm inside diameter served as core barrels. Cores were extruded underwater in 10 to 25 cm increments into polyethylene sample bags; kneading the bags (underwater) caused agglomeration of the dispersed bubbles, and the gas was then transferred into inverted glass bottles filled with lake water. An additional core from Golden Lake was extruded at the lakeshore within approximately one hour of core retrieval. A core from Lac Harrington was refrigerated and extruded in the laboratory several days later. The gas samples were held with a water seal and stored in darkness at 4°C until analyzed. Duplicate cores from each site were X-rayed and stored.

Isotopic analyses were performed using the techniques described by Barker (1979) in the Isotope Laboratory, Department of Earth Sciences, University of Waterloo. This method separates the gases using a Fisher-Hamilton Model 29 gas partitioner fitted with a Porapak 'Q' absorption column. Methane is oxidized over hot cupric oxide to CO_2 and H_2O and the H_2O is subsequently reduced over hot uranium to H_2 gas. The CO_2 and H_2 gases derived from methane are isotopically analyzed for the $^{13}C/^{12}C$ and $^{2}H/^{1}H$ ratios using Micromass 903 and 602D mass spectrometers, respectively. The results are quoted as 'δ' values per mil (‰) relative to the PDB (for ^{13}C) and SMOW (for ^{2}H) standards (following international convention) (Fritz and Fontes, 1980). Reproducibility of the method on sediment gas samples is ± 0.3‰ for ^{13}C and ± 5‰ for ^{2}H.

Detailed chromatographic analyses were carried out on five samples from stratigraphic intervals in the cores, to determine the content of C_{2+} hydrocarbon gases. The chromatogram produced by the gas partitioner provided a measure of the major gas composition for the total suite of samples. The analytical results are summarized in Table 26.1.

Results

Lac Harrington core

A 1.5 m-long core from the deep (20 m) central basin in Lac Harrington yielded the stratigraphic profile of sediment gas quantity and composition shown in Figure 26.2. The core consisted of homogeneous, dark, olive-grey organic sediment lacking discernable stratigraphic variation in colour or texture. Although the bottom waters of the lake were not anoxic at the time of sampling, no oxidized sediment surface layer was present. Extruded samples, upon exposure to the atmosphere, rapidly developed the characteristic orange of oxidized iron compounds.

The sediment column can be separated into a gas-poor upper zone near the sediment-water interface and gas-rich zone below (Fig. 26.2). Abundant small bubbles (1 mm or less in diameter) were visible through the transparent core barrel throughout the lower three quarters of the core immediately upon its removal from the bottom sediment. Expansion of the existing bubbles and ebullition of additional dissolved gas displaced from less than 1 to about 7% of the sediment volume as the core equilibrated with atmospheric pressure. In situ, the gas bubbles appeared to comprise no more than about 2% of the sediment volume.

Table 26.1A. Per cent composition of sediment gases from Golden Lake and Lac Harrington determined by detailed chromatography

Sample Interval (cm below sediment surface)	CH_4	CO_2	C_2H_6	C_3H_8	C_4H_{10} (iso-)	C_4H_{10} (N-)
Golden Lake						
50 – 110	29.14	0.55	0.09	0.16	<0.02	0.41
130 – 190	30.28	0.57	< 0.03	< 0.03	<0.02	< 0.02
Lac Harrington						
29 – 69	52.66	0.88	< 0.03	< 0.03	<0.02	< 0.02
69 – 109	60.50	1.08	< 0.03	< 0.03	<0.02	< 0.02
109 – 149	56.43	0.84	< 0.03	< 0.03	<0.02	< 0.02

Table 26.1B. Sediment gas abundance and composition of per cent of total gas in Golden Lake and Lac Harrington Cores

Sample Interval (cm below sediment surface)	Gas (Volume as % of sediment)	CH_4	N_2	CO_2	C_{2+}	δ^2H (‰ SMOW)	$\delta^{13}C$ (‰ PDB)	N_2:CH_4
Golden Lake								
0 – 10	0.3	< 5	>95	<1				> 19
10 – 30	0.6	< 5	>95	<1			-34.9	> 19
30 – 50	1.2	< 5	>95	<1				> 19
50 – 70	2.4	22	77				-52.2	3.5
70 – 90	3.3	35	64	0.55	∿0.66	-198	-63.2	1.8
90 – 110	3.6	27	72			-175	-61.7	2.7
110 – 130	3.0	15	85	<1			-50.7	5.7
130 – 150	3.9	29	70				-63.5	2.4
150 – 170	4.5	30	69	0.57	<0.10	-208	-64.3	2.3
170 – 190	3.9	32	67				-64.5	2.1
190 – 200	3.6	25	75	<1			-62.0	3.0
Lac Harrington								
5 – 29	0.14	< 5	>95	<1			-30.3	> 19
29 – 69	7.1	53	43	0.88	<0.10	-223	-65.6	0.8
69 – 109	5.3	61	38	1.08	<0.10	-232	-64.6	0.6
109 – 149	4.5	56	46	0.84	<0.10	-222	-63.5	0.9

The strong zonation of the core is mirrored by the composition of the gas and the isotopic signature of the methane. The lower zone contained 50 to 60% methane having $\delta^{13}C$ values that ranged from -63.5 to -65.6‰. The methane in the upper zone comprised less than 5% of the gas and was richer in ^{13}C by more than 30‰.

Golden Lake core

The sediment gas profiles for Golden Lake were derived from a 2 m-long core of organic sediment retrieved from 26 m depth in the central part of the lake. The uppermost centimetre of sediment at the core site was orange, characteristic of oxidized iron compounds; the remainder of the core consisted of olive-grey organic sediment lacking any apparent stratification. Gas was concentrated near the base of the core, at about 160 cm below the sediment-water interface (Fig. 26.3). A regular decline in gas abundance towards the sediment-water interface is interrupted at 120 cm by a marked decrease associated with one sample.

The methane carbon-isotope and abundance profiles are strongly co-variant. Akin to the Lac Harrington core, the methane in the uppermost sediment was substantially enriched in ^{13}C compared to the gas in the underlying material. Relative isotopic enrichment also occurred in the zone of reduced gas content between 110 and 130 cm depth.

Discussion

The sediment gas samples from the two cores display a wide variety of chemical and isotopic compositions (Table 26.1). The constituents are typical of those encountered in natural gas, and the variations in their abundances and compositions provide information about the

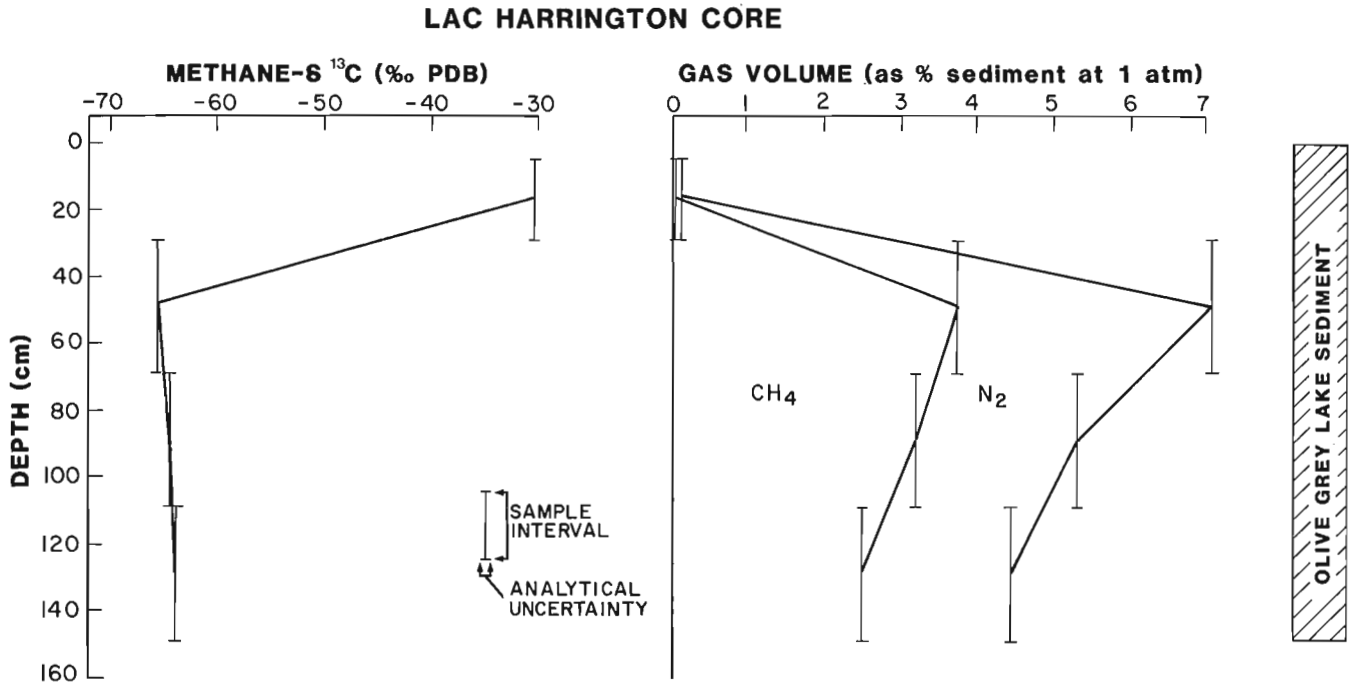

Figure 26.2. *Stratigraphic profiles of sediment gas content, composition, and methane - ^{13}C content for a sediment core from Lac Harrington, Quebec. Gas quantity is expressed as volume per cent of sediment following equilibration at atmospheric pressure.*

origin and evolution of the sediment gas. A number of generalizations can be made, based on the reported characteristics of natural gas in recent and ancient sediments (Reeburgh, 1969; Games and Hayes, 1976; Reeburgh and Heggie, 1977; Barker, 1979; Deines, 1980).

Methane forms from the breakdown of organic matter, either thermogenically, under the action of heat and pressure, or biogenically, as a metabolic product of anaerobic bacteria. Although chemically identical, thermogenic and biogenic methanes are usually distinguishable isotopically or by the levels of associated hydrocarbon gases. The presence of methane bubbles in the sediment pore waters indicates that the critical concentration of dissolved gas has been reached under the ambient conditions of temperature and pressure present. The methane sampled in this study is the gas in excess of the critical concentration at the lake surface. Because of its low solubility, essentially all the methane is retrieved by the simple sampling technique used.

Nitrogen, which is commonly associated with methane in natural gas, is a major constituent of the sediment gas analyzed in this study, and it has probably been derived from pore waters as a result of 'stripping' by methane gas. The ratio of nitrogen to methane in natural gas can provide information about their migration histories.

Carbon dioxide is a minor component of the gas sampled. It may be co-produced with biogenic methane under some conditions and it can also form from oxidation of hydrocarbon gases. Because of its high solubility and chemical reactivity, the behaviour of carbon dioxide as sampled primarily reflects the pore water chemistry and appears to yield little information about the origins of the sediment gas.

The trace quantities of C_{2+} hydrocarbons (Table 26.1) appear to be typical of the levels that form in association with biogenic methane in recent sediments and groundwater (cf. Schoell, 1980; Fig. 26.1, Table 26.1). Only the 50 to 110 cm sample from Golden Lake contains appreciable amounts of ethane, propane, and n-butane. Slightly elevated concentrations of these compounds may reflect compositional variation in the organic matter within this zone or, perhaps, enrichment from upward-migrating gas originating in underlying sediments. None of the C_{2+} gas occurred in sufficient quantities for isotopic analysis.

The isotopic compositions of thermogenic and biogenic methanes from various sources have been summarized by Schoell (1980). For methane that has not undergone partial oxidation or isotopic fractionation or exchange, δ^2H and $\delta^{13}C$ values of thermogenic and biogenic gas plot within distinct fields that are distinguished mainly by ^{13}C contents (Fig. 26.4). Thermogenic methane is relatively ^{13}C-rich generally displaying $\delta^{13}C$ values greater than -55‰; biogenic methane is relatively ^{13}C-depleted, having $\delta^{13}C$ values less than about -63‰, according to Schoell's sources. A recent survey of natural gas in groundwater places the upper limit of ^{13}C content in 'normal' biogenic methane somewhat higher, at about -60‰ (Barker and Fritz, 1981). The value attained is a function of many factors, of which the major ones are the carbon-isotope composition of the original organic matter, the bacterial assemblage responsible for methane production and (perhaps) the temperature (cf. Games and Hayes, 1976).

The deuterium (^2H) content of biogenic methane reflects the isotopic composition of the associated water during methanogenesis. Nakai et al. (1974) documented a general depletion of -160 ± 10‰ in the δ^2H values of such methane relative to water associated with it. Because of the characteristic deuterium enrichment of marine waters relative to fresh waters, the field of biogenic methane can be subdivided into marine and nonmarine fields that overlap around a δ^2H value of about -200‰ (Fig. 26.4) (Schoell, 1980). The three samples from the Lac Harrington

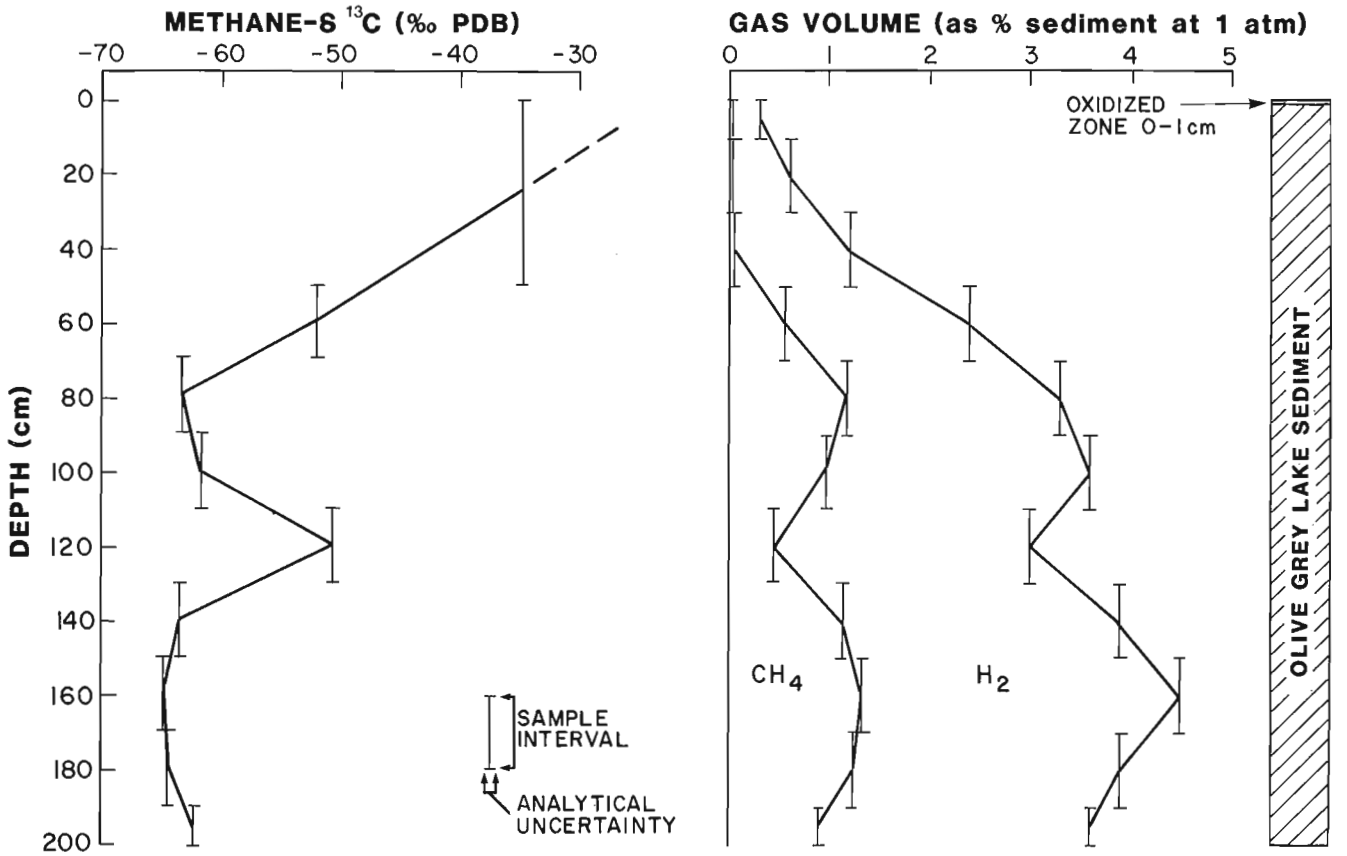

Figure 26.3. *Stratigraphic profiles of sediment gas content, composition, and methane - ^{13}C content for a sediment core from Golden Lake, Ontario. Gas quantity is expressed as volume per cent of sediment following equilibration at atmospheric pressure.*

core that were analyzed for deuterium plot, as expected, within the field of nonmarine biogenic gas (Fig. 26.4) and have methane-δ^2H values of -222 to -232‰. Modern lake water in the Ottawa area has δ^2H values of about -75‰ (unpublished data), and appears to be the source for the methane-deuterium within the core, assuming Nakai et al.'s value of -160‰ for biogenic depletion. The three samples from the Golden Lake core display δ^2H values that are higher than expected for lacustrine sediments and substantially higher than the value of -235‰ postulated above.

Stratigraphic variations in the isotopic composition of the methane may also reflect changes in the ^{13}C and ^2H contents of the associated organic matter and pore water (respectively). This effect is not considered likely to be important within the short stratigraphic intervals considered here. Production of additional methane within the sediment would moderate the fractionating effects of migration and oxidation through dilution. Because of the methane's mobility and propensity for alteration, however, the isotopic composition of the primary, unaltered gas may have to be inferred from analyses of the associated organic matter and water rather than measured directly.

Migration of methane through water-saturated sediments generally results in a depletion in the ^{13}C content of the migrating fraction. The fractionation may result from different rates of diffusion for the $^{12}CH_4$ and $^{13}CH_4$ molecules, or from stronger sorption of $^{13}CH_4$ molecules onto organic matter and consequent preferential loss of $^{12}CH_4$ (Deines, 1980). Either process can explain the effects observed in the lake sediment cores.

Consumption (oxidation) of methane by aerobic bacteria reduces the concentration of methane and enriches the residual methane in ^{13}C and ^2H. The methane that is converted to CO_2 is essentially lost to the sediment gas phase through dissolution in the pore waters. Oxidative alteration of the methane is indicated in the uppermost sediments of both cores where methane-$\delta^{13}C$ values rise sharply in concert with increases in the N_2:CH_4 ratios and decreases in total gas contents. Bacterially mediated reactions in an aerobic environment could be expected to cause more pronounced fractionation than reactions governed by molecular diffusion rates or sorption on organic matter. In other situations, however, distinguishing the effects of oxidation from those of migrational methane loss may be less clear.

Interpretation

Lac Harrington core

The gas-poor, isotopically enriched (^{13}C) upper zone of the Lac Harrington core could be due to oxidation of the methane and the thickness of the zone is probably related to the depth of oxygen penetration from lake water. The gas

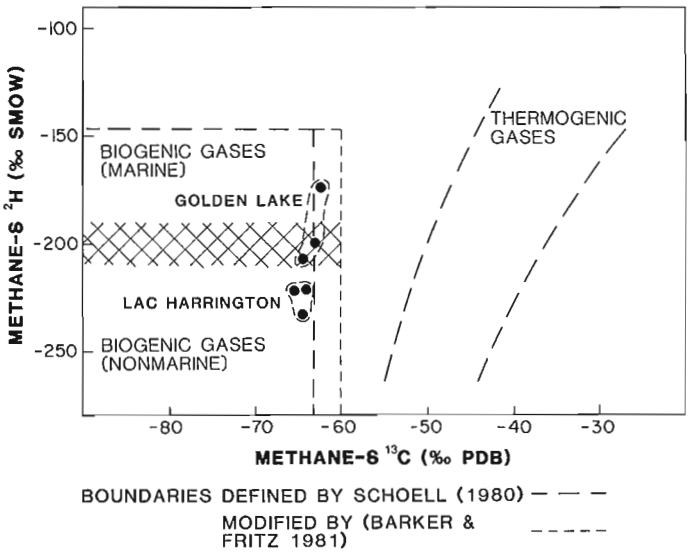

Figure 26.4. *Plot of methane $\delta^{13}C$ vs $\delta^{2}H$ for sediment gases from Lac Harrington and Golden Lake. The biogenic and thermogenic methane fields are modified after Schoell (1980). The crosshatched area represents possible overlap in the deuterium (^{2}H) composition of marine and terrestrial biogenic methanes.*

content and composition, and thickness of the oxidized layer could vary over time in response to changes in the overlying water. Large seasonal variations in the gas content of surficial sediment have been documented by acoustic records in lakes that experience severe oxygen depletion (Muller, 1977).

The slight but distinct depletion in methane-$\delta^{13}C$ values upward within the lower zone of the Lac Harrington core coincides with increasing total gas and methane contents, and suggests that methane is migrating upwards within this interval. The slight rise in the N_2:CH_4 ratio at the top of the zone indicates that some of the migrational isotopic depletion could be mitigated by the loss of ^{13}C-depleted methane to the overlying sediments. Production of methane is probably occurring throughout the zone, also helping to reduce the apparent effects of migration.

Golden Lake core

The Golden Lake profile is more complex and shows two zones of gas concentration in the intervals 130 to 190 cm and 70 to 110 cm that are characterized by lower N_2:CH_4 ratios and ^{13}C-depleted methane. The isotopic depletion is considered likely to be the result of migrational change, and the lower N_2:CH_4 ratios are possibly due to the addition of methane generated in place. In contrast, depletion of the total gas content, enrichment of methane-^{13}C, and elevated N_2:CH_4 ratios characterize the topmost interval and are attributed to methane oxidation. The 2.5‰ of the methane-^{13}C content in the sample overlying the basal gas probably represents change associated with migrational fractionation. Oxidation effects could have caused the marked isotopic enrichment (greater than 10‰) of the gas-minimum zone in the interval 110 to 130 cm, although there is no direct evidence for this.

The differences between the Lac Harrington and Golden Lake cores are consistent with the differing limnological conditions. A thicker aerobic zone in the sediments of Golden Lake is not unexpected because of greater depth of water circulation associated with its relatively exposed physiographic setting and larger surface area. In contrast, the lake basin morphology and comparatively sheltered physiographic setting of Lac Harrington promotes stable stratification of the water and restricts internal circulation. The oxygen depletion of bottom waters observed in 1982 is undoubtedly a regular summer event and the supply of oxygen to the lake sediment from bottom waters is apparently restricted. Chemical interchange between the waters and sediments in Golden Lake may also occur at a much greater rate than in Lac Harrington. The interpretation of possible aerobic activity between distinct zones characterized by anaerobic activity in the core suggests that oxygen-bearing waters may move laterally within the sediment column.

Implications for future studies

Isotopic analysis can identify compositional change within the sediment column that is likely the result of methane gas migration and aerobic consumption and can indicate the nature of chemical and physical processes operative within lake basins. For example, the distribution and areal extent of gas zones on some subbottom records of lakes in eastern Ontario and western Quebec (W.W. Shilts, unpublished data) suggest that recharging groundwater might supply gases to the sediments. Because some groundwater contains thermogenic methane or biogenic methane having distinctive isotopic characteristics (Barker and Fritz, 1981), identification of the source and influence of such recharge waters may be possible by analysis of the isotopic composition of lake sediment gases.

Migrating gas bubbles have been implicated in the movement and accumulation of trace elements in lake sediments (Cline and Upchurch, 1973). The upward movement of gases, such as postulated within the Lac Harrington core, may provide a mechanism for the accumulation of heavy metals that is commonly observed in the upper parts of lake sediment cores.

Summary and conclusions

Our model explains the profiles of gas content and composition in terms of anaerobic production and migration leading to isotopic depletion, and aerobic consumption, leading to isotopic enrichment, of the biogenically derived gas. The data for this report are few and thus the interpretations are preliminary. A gas phase, within lake sediments of Harrington and Golden lakes, occupied up to about 2% by volume of the in situ materials and from less than 1 to 7% by volume under atmospheric conditions. The gas is composed almost entirely (>95%) of nitrogen and methane in ratios that vary from about 0.6:1 to 19:1. Other minor to trace components of the gas include ethane, propane, and n-butane. The isotopic composition of the methane indicates that the gas is biogenically derived, although it is not known whether it is produced entirely within the sediments or includes a portion introduced by groundwater recharge of the lake.

Stratigraphic variations in the quantity and in the chemical and isotopic composition of the gas are attributed on a qualitative basis to fractionation associated with upward migration of gases through the sediment column and to methane oxidation. Generally, anaerobic production and migrational fractionation lead to net upward ^{13}C depletion in the lower part of the core, and aerobic consumption leads to net isotopic enrichment in the upper part. Methane near the base of cores from both lakes has methane-$\delta^{13}C$ values of about -65 to -62 ‰ (PDB), although measured values throughout the cores range from -65.6 ‰ to -30.3 ‰ due to the effects of migrational depletion and oxidative enrichment of ^{13}C.

Acknowledgments

Access to Lac Harrington was obtained through the helpful co-operation of the National Capital Commission. This study was first suggested by W.W. Shilts. Research on sediment gas in lake sediments and groundwater is being continued at the University of Waterloo by T.W.D. Edwards.

References

Barker, J.F.
1979: Methane in groundwaters – a carbon isotope geochemical study; unpublished Ph.D. thesis, University of Waterloo, Waterloo, Ontario, 310 p.

Barker, J.F. and Fritz, P.
1981: The occurrence and origin of methane in some groundwater flow systems; Canadian Journal of Earth Sciences, v. 18, p. 1802-1816.

Cline, J.T. and Upchurch, S.B.
1973: Mode of heavy metal migration in the upper strata of lake sediment; Proceedings of the 16th Conference on Great Lakes Research, International Association for Great Lakes Research, p. 349-356.

Deines, P.
1980: The isotopic composition of reduced organic carbon; in Handbook of Environmental Isotope Geochemistry, Volume 1, The Terrestrial Environment, A; ed. P. Fritz, and J.Ch. Fontes; Elsevier, New York, p. 329-406.

Fritz, P. and Fontes, J.Ch.
1980: Introduction; in Handbook of Environmental Isotope Geochemistry, Volume 1, The Terrestrial Environment, A; ed. P. Fritz and J.Ch. Fontes; Elsevier, New York, p. 1-19.

Games, L.M. and Hayes, J.M.
1976: On the mechanisms of CO_2 and CH_4 production in natural anaerobic environments; in Environmental Biogeochemistry, Volume 1; ed. J.O. Nriagu; Ann Arbor Science, Michigan, p. 51-73.

Klassen, R.A. and Shilts, W.W.
1982: Subbottom profiling of lakes of the Canadian Shield; in Current Research, Part A, Geological Survey of Canada, Paper 82-1A, p. 375-384.

Muller, H.E.
1977: Observations of interactions between water and sediment with a 30-kHz-sediment echosounder; in Interactions between sediments and freshwater, ed. H.L. Golterman; Proceedings of an International Symposium (Amsterdam), September 1976, W. Junk, B.V., p. 448-452.

Nakai, N., Yoshida, Y., and Ando, N.
1974: Isotopic studies on oil and natural gas fields in Japan; Chikyu Kagaku, v. 7/8, p. 87-98, cited in Schoell (1980).

Reeburgh, W.S.
1969: Observations of gases in Chesapeake Bay sediments; Limnology and Oceanography, v. 14, p. 368-375.

Reeburgh, W.S. and Heggie, D.T.
1977: Microbial methane consumption reactions and their effect on methane distributions in freshwater and marine environments; Limnology and Oceanography, v. 22, p. 1-9.

Schoell, M.
1980: The hydrogen and carbon isotopic composition of methane from natural gases of various origins; Geochimica et Cosmochimica Acta, v. 44, p. 649-661.

Shilts, W.W. and Farrell, L.E.
1982: Subbottom profiling of Canadian Shield lakes – implications for interpreting effects of acid rain; in Current Research, Part B, Geological Survey of Canada, Paper 82-1B, p. 209-221.

27.

UPPERMOST PRECAMBRIAN AND LOWER CAMBRIAN STRATA, NORTHERN OMINECA MOUNTAINS, NORTH-CENTRAL BRITISH COLUMBIA

Project 650024

W.H. Fritz
Institute of Sedimentary and Petroleum Geology, Ottawa

Fritz, W.H., Uppermost Precambrian and Lower Cambrian strata, northern Omineca Mountains, north-central British Columbia; in Current Research, Part B, Geological Survey of Canada, Paper 84-B, p. 245-254, 1984.

Abstract

A composite stratigraphic section through uppermost Precambrian and Lower Cambrian strata was measured in the northern Omineca Mountains, an area that has undergone moderate to strong deformation. Close similarities between the northern Omineca strata and those in the Cassiar and Cariboo mountains suggest these rocks were deposited along the depositional trend. A known disconformity near the Precambrian-Cambrian boundary in the Cassiar Mountains could not be identified in the northern Omineca Mountains, however, at or near this level in the Omineca Mountains a sharp lithological contact separates the Upper Proterozoic Stelkuz Formation from the Lower Cambrian Boya Formation. A minor Lower Cambrian disconformity between the Boya and Rosella formations in the western Cassiar Mountains extends into the northern Omineca Mountains. A dark siltstone and interbedded quartzite unit between the Rosella and Kechita formations probably represents a tectonic sliver from the underlying Boya Formation rather than part of a normal stratigraphic sequence.

Lower Cambrian strata in the Cassiar, Omineca and Cariboo mountains bear little resemblance to those in the northern Rocky Mountains. Uppermost Precambrian strata are missing in the northern Rocky Mountains because of erosion or nondeposition.

Résumé

Nous avons mesuré une coupe stratigraphique composée, effectuée dans des couches du sommet du Précambrien et du Cambrien inférieur, dans les chaînons Ominéca nord, zone qui a subi des déformations moyennes à fortes. La ressemblance frappante entre les couches d'Ominéca nord et celles des chaînes des Cassiar et des chaînons Cariboo laisse penser que ces roches se sont déposées dans la direction stratigraphique. On n'a pas pu déterminer dans les chaînons Ominéca nord une discordance connue près du contact du Précambrien et du Cambrien dans les chaînes des Cassiar; cependant, à ce niveau ou près de celui-ci dans les chaînons Ominéca, un contact lithologique bien défini sépare la formation de Stelkuz du Protérozoïque supérieur de la formation de Boya du Cambrien inférieur. Une faible discordance du Cambrien inférieur entre la formation de Boya et la formation de Rosella, dans les chaînes des Cassiar, se poursuit jusque dans les chaînons Ominéca nord. Une unité constituée de siltstone foncé et de quartzite interstratifiés, située entre la formation de Rosella et la formation de Kechita, représente probablement une bande tectonique provenant de la formation de Boya sous-jacente plutôt qu'une partie d'une séquence normale stratigraphique.

Les couches du Cambrien inférieur dans les chaînes des Cassiar et les chaînons Ominéca et de Cariboo ressemblent très peu à celles des Rocheuses septentrionales. Les couches du sommet Précambrien manquent dans les Rocheuses septentrionales à cause de l'érosion et de l'absence de sédimentation.

Introduction

During the summer of 1983, stratigraphic studies were conducted at three sites in the northern Omineca Mountains (Fig. 27.1, secs. 9C-11C) in order to piece together a representative Upper Precambrian-Lower Cambrian section. The primary objective was to collect data in order to correlate this section with equivalent strata in the Cassiar Mountains to the northwest (1C-8C), northern Rocky Mountains to the east (1R-6R), and Cariboo Mountains to the southeast.

The secondary objective was to collect fossils for several paleontologists interested in Upper Precambrian and/or Lower Cambrian paleontology of the Omineca Mountains. They are: S. Conway Morris, Cambridge, England (small shelly fossils); F. Debrenne, Institute of Paleontology, National Centre of Scientific Research, Paris (archaeocyathids); G.M. Narbonne, Queen's University, Ontario (trace fossils); and the writer (trilobites). The collection numbers and their stratigraphic horizons are given in Figures 27.2 and 27.3. A preliminary observation of the fossil material suggests that the archaeocyathids and small shelly fossils will be of scientific value, and that the trilobites and trace fossils will be of limited value because of excessive tectonic deformation.

Deformation in the northern Omineca Mountains is greater than in the Cassiar and northern Rocky mountains, and measured stratigraphic thickness presented here may differ by 20 per cent from "true" (undeformed) thickness. An unresolved structural(?) problem concerning the relationship of one stratigraphic unit to the Rosella Formation succession remains unresolved. A likely tectonic interpretation is offered for those who may wish to pursue the problem.

Acknowledgments

Section 9C was measured with the assistance of C.M. Bruce, and sections 10C and 11C with the assistance of J.A. O'Brien. Field support and general information on the location of the sections were supplied by H. Gabrielse. Drafting of illustrations was accomplished by H. McLaughlin.

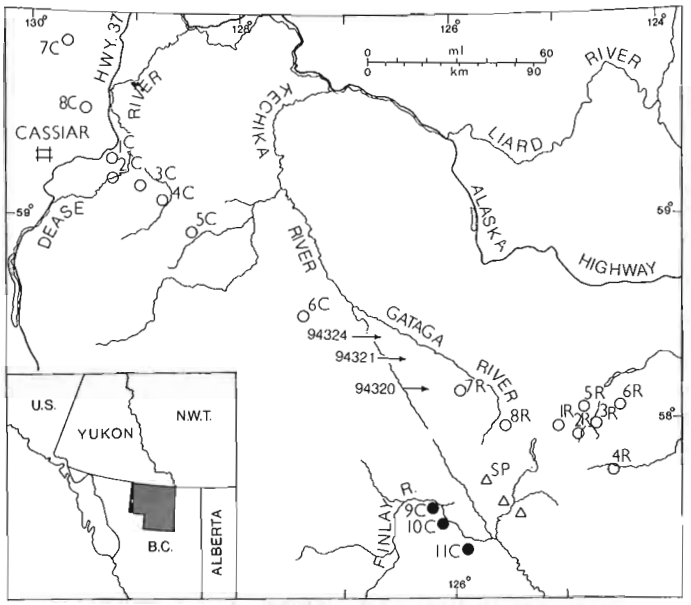

Figure 27.1. *Map showing locations of sections described in present paper (solid circles), and sections used for correlation (open circles) with Cassiar Mountains (1C-8C; Fritz, 1978, 1980a; Fritz and Crimes, 1984) and northern Rocky Mountains (1R-8R, Fritz, 1979, 1980b). Isolated Middle Cambrian fossil localities (94320, etc.; Fritz, 1980b) are located by arrows, and triangles locate large Middle Cambrian limestone buildups, such as one underlying Spectre Peak (Fritz, 1979, Pl. 13, fig. 6).*

Stelkuz Formation (1520 m+)

The uppermost Precambrian Stelkuz Formation was measured along a line of section (11C) centred 2 km north of the upper reaches of Stelkuz Creek (Pl. 27.1, fig. 2, 4). There, the underlying Espee Formation is overturned, and comprises a uniform succession of very thin-bedded (but thick parting) limestone, that is light grey to white on weathered and fresh surfaces. The contact between the Espee and Stelkuz formations was placed at the top of a thick, continuous succession of limestone, and at the base of a succession of interbedded siltstone, limestone, and dolostone that characterizes the lower member (651 m ±) of the Stelkuz Formation. From a distance, the lower member has a yellow to slightly orange weathering colour, differentiating it from the underlying light grey weathering Espee. The Espee Formation is slightly more resistant than lower Stelkuz strata and much more resistant than the middle Stelkuz member.

Nearly half of the lower member is composed of light orange weathering siltstone that is light greenish grey on fresh surfaces, and is slightly limy at various horizons. The remaining strata are composed of carbonates, consisting almost equally of Espee-like limestone, and a medium light- to medium dark-grey weathering limestone that is platy, and light orange on parting surfaces. The Espee-like limestone weathers more rapidly than the Espee Formation limestone, a quality attributed to a higher argillaceous content in the former. A small amount of thin- to thick-bedded, orange weathering dolostone is present, as are a few beds of fine- to coarse-grained quartzite. The latter beds are well within the member and are not present at the base or top.

The middle Stelkuz member (150.5 m) is composed of recessive weathering shale, nearly half of which is purple on weathered and fresh surfaces and the remainder bright green on weathered and fresh surfaces.

Light greenish grey silty shale to shaly siltstone predominates in the upper member (S3, S4, 421 m +; Fig. 27.2) of the Stelkuz Formation. Parting surfaces in these strata are light orange, yellow, or rust. Most of the clastics in the lower 258.5 m of the member are shale , and the interval from 188.5 to 218.5 m contains another Espee-like limestone, constituting the only carbonate above the lower member. In the interval from 258.5 to 421 m and higher, approximately half the clastics are shale and the remaining half siltstone and very fine grained sandstone. Between the 421 m level and the top of the formation there may be over 400 m of similar Stelkuz strata. These strata were not measured in Section 11C, however, because the tectonic thickening is probably great.

Below the Stelkuz-Boya formational contact in Section 11C the rocks consist of light orange, yellow, or rust weathering clastics, that are very fine grained or finer. Immediately above the contact is one metre of orange weathering dolostone. Above the dolostone are thick beds of white, fine- and medium-grained quartzite.

At Section 10C (Pl. 27.2, fig. 1) only the uppermost 299 m of the Stelkuz Formation are extensively exposed. Below this level the Stelkuz is recessive and heavily covered, suggesting bedrock with a high shale and siltstone content. A small outcrop below Section 10C and near the floor of Finlay River Valley (Pl. 27.2, fig. 1) exposes 5 m of limestone that is very similar to the 30 m interval of limestone in the upper member in Section 11C.

The uppermost 299 m comprises light orange to rust weathering quartzite and siltstone, interbedded in approximately equal amounts, giving the strata a higher quartzite:siltstone and/or shale ratio than that of Section 11C. The quartzite is thin- to thick-bedded and is very fine grained, except for some fine grained beds in the subinterval from 118 to 174 m below the top. Fresh surfaces of the quartzite and siltstone are medium light grey or medium light greenish grey.

At Section 10C the Stelkuz-Boya formational contact is immediately below a resistant, 86.5 m thick unit of fine grained quartzite. Below this unit the uppermost 46 m of Stelkuz are recessive and covered, suggesting that the underlying bedrock is siltstone or shale.

Boya Formation (956.5 m+)

From a distance the uniformly dark grey to dark brownish grey colour of the Boya Formation can be used to differentiate it from the underlying medium light, yellowish grey to light orange Stelkuz Formation (Pl. 27.2, fig. 1, 2). Near Section 10C a slightly more resistant topographic expression of the Boya Formation, together with the 86.5 m basal Boya quartzite unit, helps to separate the two formations. In contrast to the smooth Boya slopes near Section 10C, the Boya slopes near Section 11C are irregular (hummocky) and strewn with large, loose blocks of thick- to very thick-bedded quartzite. Time was not available to closely examine the Boya above Section 11C, but various outcrops viewed through a monocular indicate a higher (and coarser?) quartzite content there than in the lower part of the Boya at Section 10C.

The basal unit (Unit 1, 86.5 m) of the Boya Formation at Section 10C consists of thick bedded quartzite that weathers light orange to rust in the lower part, and grades through a 46 to 53 m interval into white weathering quartzite. The lower 46 m of the quartzite are very fine grained with sparse medium grains. Fresh surfaces are light grey to light brownish grey. Rust weathering, medium dark grey shale (one-third) is interbedded with the quartzite in this part of the unit. The white weathering quartzite in the upper

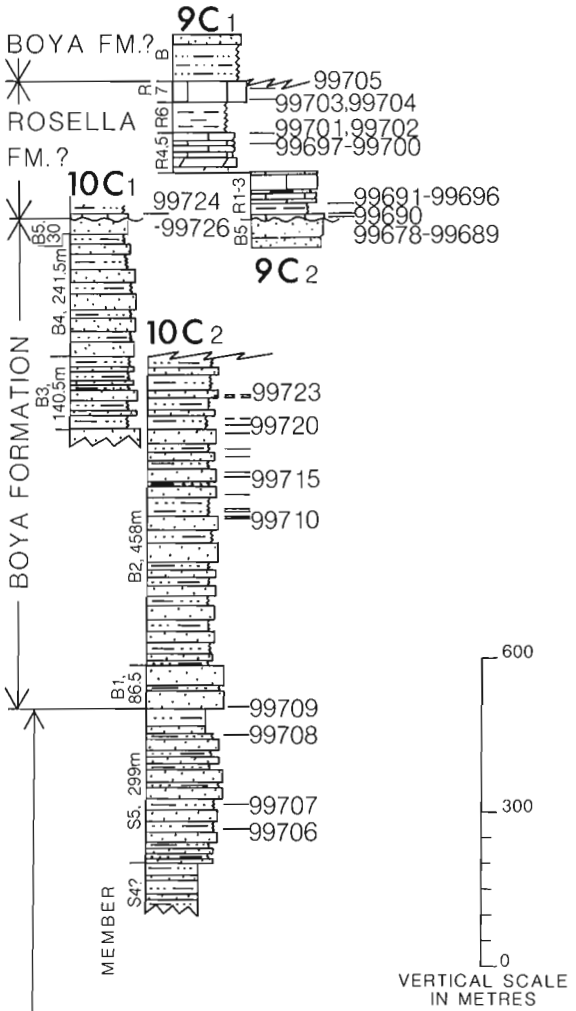

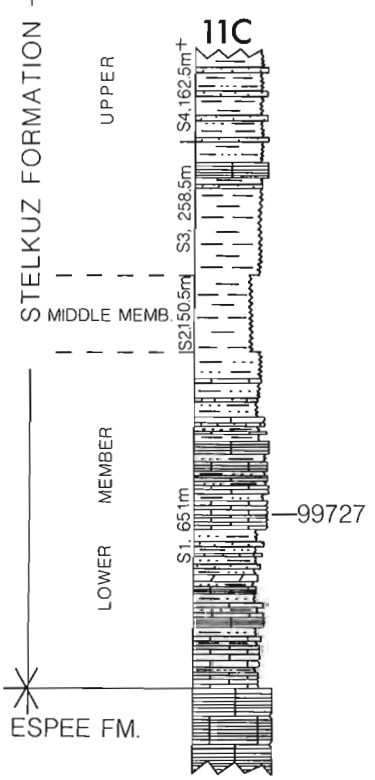

GSC LOCALITY LOCAL FLOAT ★ FLOAT ★★	DISTANCE ABOVE BASE OR TOP OF FM. IN METRES	TYPE OF FOSSIL SAMPLED ARCHAEOCYATHID (⊛), SMALL SHELLY (▽), TRILOBITE (◠), TRACE (𓂀)
ROSELLA FM.	ABOVE BASE	
99678	2.9	▽
99679	3.1	▽
99680	5.5	▽
99681 ★	6.5	▽
99682	7.2	▽
99683	7.7	▽
99684	8.0	▽
99685	9.0	⊛
99686	9.0	◠
99687	9.5	◠
99688	9.0	◠
99689 ★	10.0	◠
99690 ★★	16.5	◠
99691	26.0	◠
99692 ★	26.0-32.5	◠
99693	31.2	⊛
99694	38.0	◠
99695	40.0	⊛
99696 ★	42.0	⊛
ROSELLA FM.	BELOW TOP	
99697 ★	133.0	⊛
99698	111.5	⊛
99699 ★	110.5	⊛
99700	107.5	⊛
99701	100.5	◠
99702	95.0	◠
99703	38.0	⊛
99704	32.2	⊛
99705	3.0	⊛
STELKUZ FM.	BELOW TOP	
99706 ★	230.0	𓂀
99707 ★	184.0	𓂀
99708 ★	49.0	𓂀
BOYA FM.	ABOVE BASE	
99709	4.0-4.5	𓂀
99710 ★	374.5	𓂀
99711 ★★	376.0	𓂀
99712 ★	385.0	𓂀
99713 ★	389.5	𓂀
99714	420.5	𓂀
99715	453.5	𓂀
99716	462.5	𓂀
99717 ★	494.0	𓂀
99718 ★	510.0	𓂀
99719 ★	539.0	𓂀
99720 ★	553.0	𓂀
BOYA FM.	BELOW TOP	
99721 ★	387.5	𓂀
99722 ★	346.5	𓂀
99723 ★	345.0	𓂀
ROSELLA FM.	ABOVE BASE	
99724	0-8.0	▽
99725	0-8.0	▽
99726	0-8.0	▽
STELKUZ FM.	ABOVE BASE	
99727	337.5	▽

LEGEND

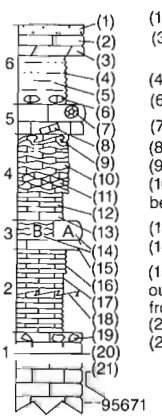

(1) Quartizite, (2) Limestone, (3) Dolostone

(4) Siltstone, (5) Shale, (6) Limestone nodule

(7) Archaeocyathid, (8) Penecontemporaneous breccia, (9) Penecontemporaneous fold, (10) Thin wavy bedded, (11) Thin nodular bedded, (12) Thin platy bedded

(13) Medium bedded, (14A) Thick bedded, (14B) Thin bedded but thick parting

(15) Resistant outcrop, (16) Recessive outcrop, (17) Covered, lithology inferred from float, (18) Fault, (19) Karst breccia, (20) Lithologic unit

(21) Fossil locality

LOCATION OF STRATIGRAPHIC SECTIONS

SECTION	LATITUDE	LONGITUDE
9C1	57°35′45″	126°14′45″
9C2	57°35′15″	126°13′30″
10C1	57°30′30″	126°06′15″
10C2	57°29′30″	126°07′15″
11C	57°20′30″	125°52′45″

Figure 27.2. *Northern Omineca Mountain stratigraphic sections measured at localities shown in Figure 27.1. Additional details for Section 9C are given in enlarged section shown in Figure 27.3. GSC localities 99721, 99722 and 99723 (marked by dashed lines) are from segment 10C, not 10C2.*

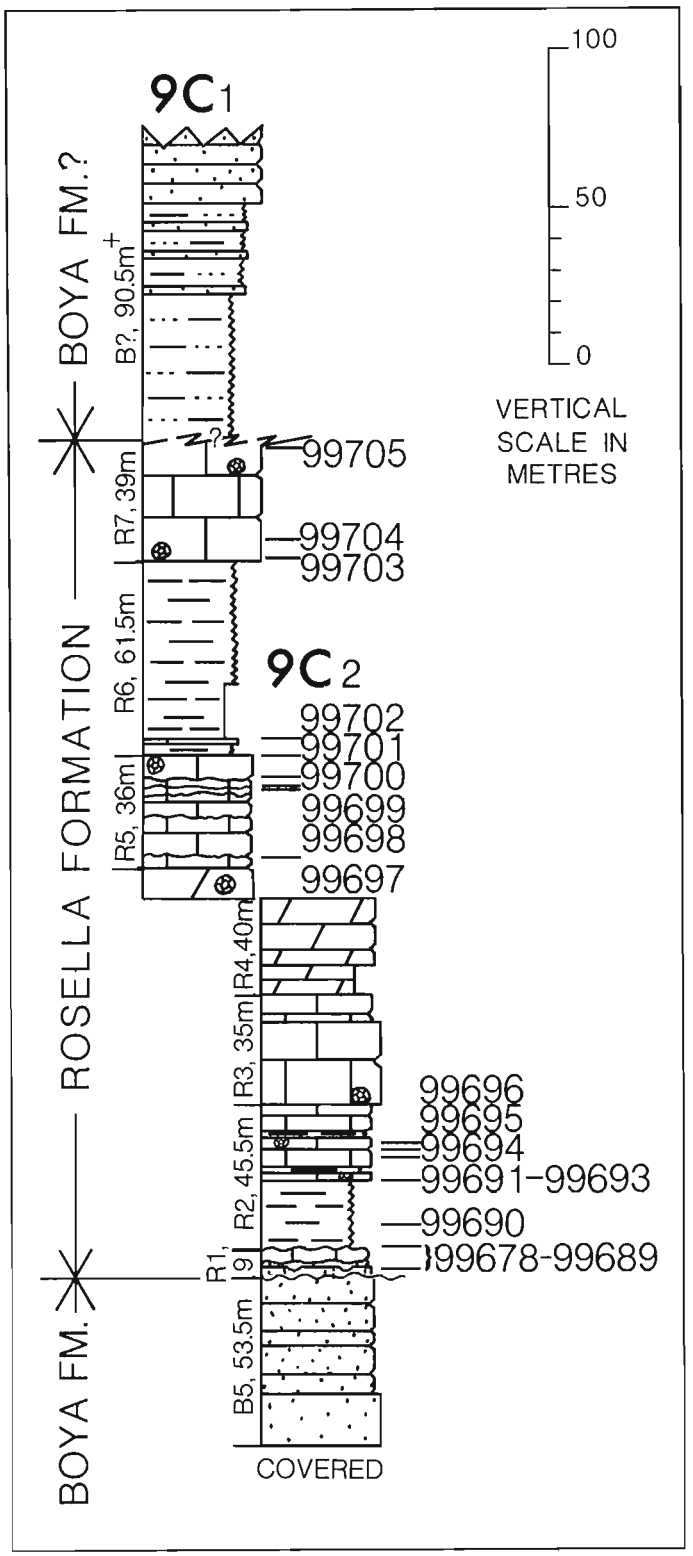

Figure 27.3. *Enlargement of northern Omineca Mountains Section 9C (also shown in Figure 27.2). Lithologies are explained in legend shown in Figure 27.2.*

part of the unit is also white on fresh surfaces and is fine grained with some medium and coarse grains near the top. Sparse, "floating", grit-sized clasts are also present in the uppermost part.

The second unit (Unit 2, 458 m) in the Boya Formation comprises very fine grained quartzite (three-fifths) in rust weathering, thin to thick beds that are very fine grained, and are light brown to medium light grey on fresh surfaces. Rust weathering siltstone (two-fifths), which is dark grey on fresh surfaces, is interbedded with the quartzite. In the basal 3 m of the unit are some (one-quarter) interbeds of white quartzite similar to those in the unit below.

The third unit (Unit 3, 140.5 m) resembles the second, except for a lower quartzite (one-third) to siltstone (two-thirds) ratio. Very light grey quartzite (one-fifth) is interbedded with siltstone in the interval 56.5 to 71.5 m above the base and fills the interval from 117 to 119 m above the base.

The fourth unit (Unit 4, 241.5 m) also resembles Unit 2, but has a different siltstone to quartzite ratio (approximately one-half of each). At 103 m above the base is a distinctive, 0.2 m thick bed of medium brown weathering limy quartzite. The uppermost 20 m of Unit 4 contains abundant (one-half) white weathering, fine grained quartzite.

PLATE 27.1 (opposite)

Figure

1. View looking east-southeast at overturned Espee and Stelkuz formations. Contact between two formations is at point "a". Espee is beyond point "a", and lower member of Stelkuz Formation is between point "a" and camera. Stelkuz Creek is at "b". Ridge shown is first ridge south of lower part of Section 11C. (GSC 204041-G)
2. View looking southwest at Stelkuz Formation in Section 11C. Photograph was taken near top of lower Stelkuz member, middle member is in deep saddle concealed from view by hill in foreground, point "a" marks limestone submember that is 188.5 to 218.5 m above base of upper member, and "b" indicates contact between upper member and overlying Boya Formation. (GSC 204041-C)
3. View looking northwest from helicopter at Section 9C on Finlay Mountain. Stratigraphic units B5 and R1 (see text – Fig. 27.3) were measured between points "a" and "b", units R2 through R4 between points "c" and "d", units R4 (remeasured) through B(?) between point "e" and "g". Contact between Rosella Formation and B(?) is at "f". (GSC 204041-I)
4. View looking northeast at overturned strata in lower member of Stelkuz Formation in Section 11C. Contact between Stelkuz and Espee formations is at "a". Photograph was taken on section and short distance northeast of place where Figure 27.2 was photographed. (GSC 203853-Y)
5. View looking northwest at contact between light coloured limestone in Rosella Formation Unit R7 and overlying dark siltstone and quartzite of Unit B(?). (GSC 204041-L)
6. View of limestone-quartzite contact within Unit 1R and 3 m above base of Rosella Formation at Section 9C. Note relief on contact between points "a" and "b". (GSC 204041-J)

1

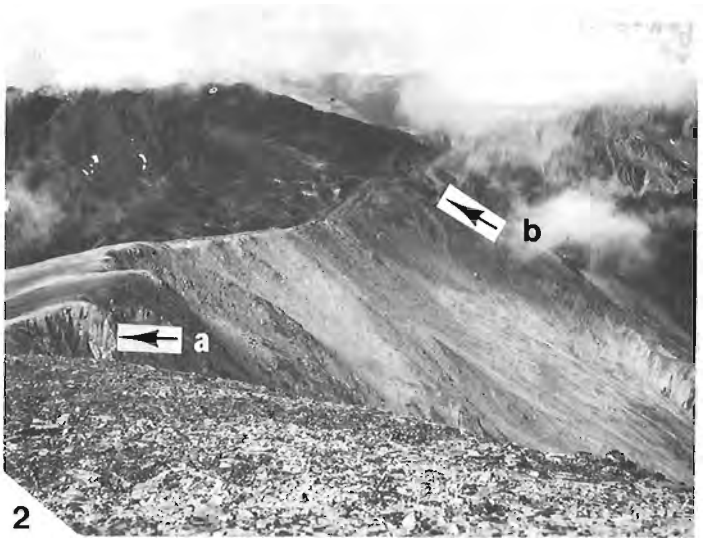

2

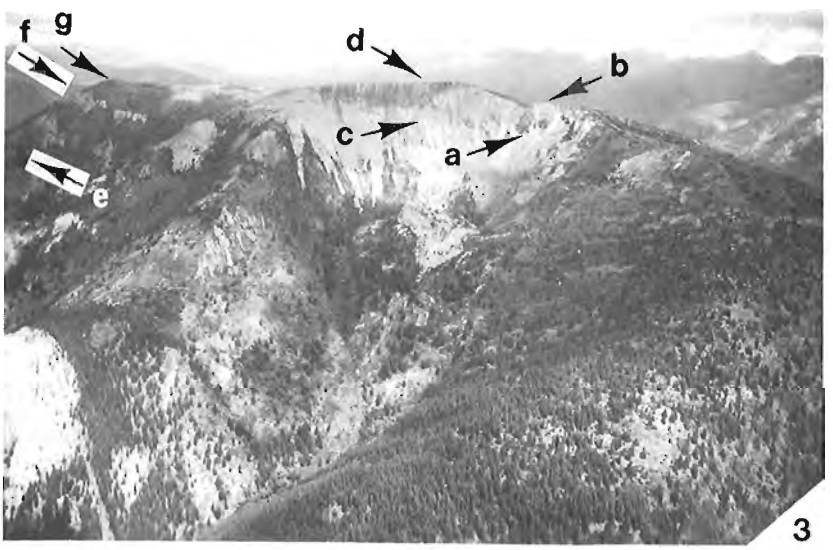

3

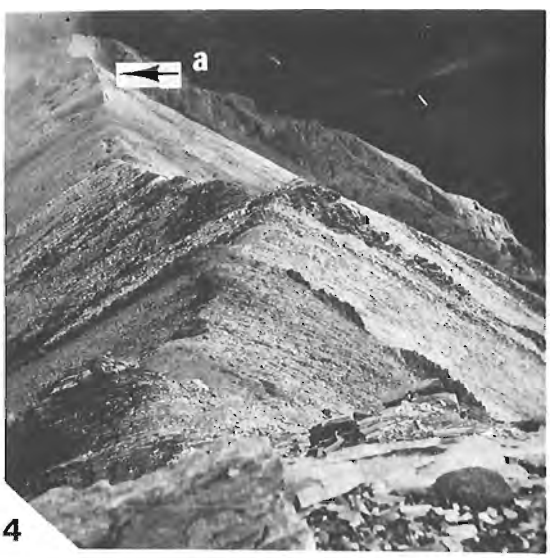

4

5

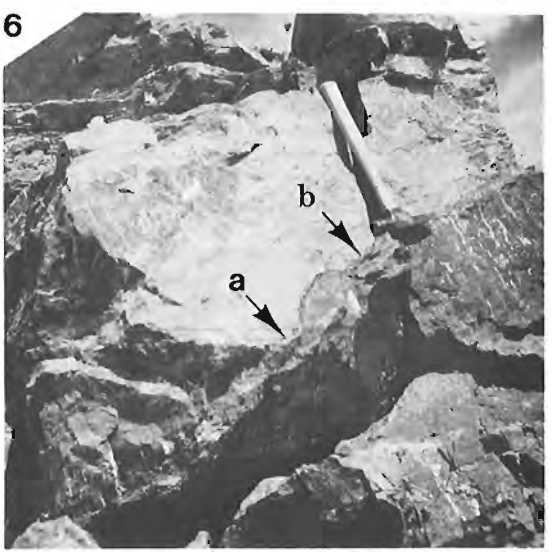

6

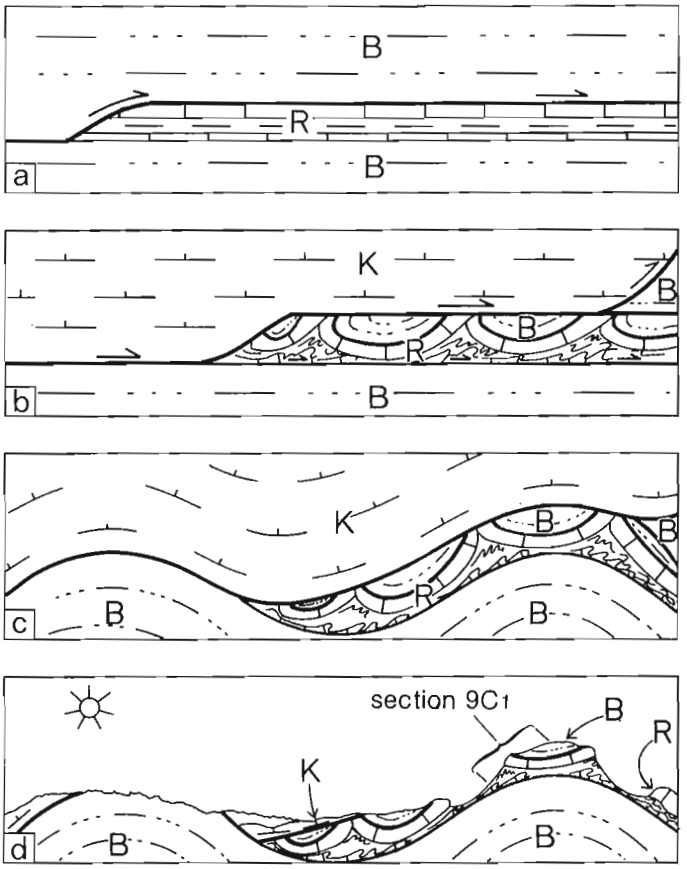

Figure 27.4. *Diagrammatic illustration of hypothesis explaining position of Boya-like strata overlying Rosella Formation at Section 9C and near Section 10C: Boya Formation is thrust over younger Boya strata and Rosella Formation ("a"); Kechika Formation moves over same thrust plane, displacing upper plate Boya and deforming Rosella Formation ("b"); broad folding is recorded along major thrust plane and secondary, sub-Rosella thrust plane ("c"); and regional uplift and erosion is accomplished ("d").*

The uppermost Boya unit (Unit 5, 30 m) in Section 10C contains white weathering, white quartzite in thick beds, which exhibit crossbedding. The quartzite is fine grained and slightly limy at some horizons. At Section 9C, Unit 5 is 53.5 m thick and is represented by a continuous succession of fine grained quartzite. The basal 16 m is light orange weathering, very thick bedded, and is light brown on fresh surfaces. The remaining 37.5 m is medium brown weathering, thin- to thick-bedded, fine grained, and in various intervals both very slightly limy and crossbedded.

Rosella Formation (266 m+)

Alternating units of light coloured limestone and shale distinguish the Rosella Formation from the dark weathering Boya and the more colourful Stelkuz clastics below. The overlying Kechika Formation is slightly darker than the Rosella and is composed of shale and limestone; the limestone is more uniformly thin bedded in the Kechika than in the Rosella. A unique, massive white limestone unit (Unit 7) bearing archaeocyathids, is the best guide to the Rosella Formation in the northern Omineca Mountains. Several similar units within the Rosella characterize the formation in the Cassiar Mountains to the northwest.

Near the base of the Rosella Formation there is a rapid increase in the amount of carbonate. At Section 10C approximately 1 m of limy, fine- to coarse-grained sandstone is present above the base.

The following description is from Section 9C where the Rosella Formation is better exposed.

The basal unit (Unit 1, 9 m) of the formation starts with 3 m of thick bedded, fine- to coarse-grained quartzite. The lowermost beds (2 m) contain sparse, irregular layers and pods of limy, recessive weathering quartzite. The calcite is more evenly distributed and highly concentrated in the upper (1 m) quartzite beds. Fresh quartzite surfaces are light brown, and the weathering colour varies from light brown to brick red, with the latter colour being more prevalent in the higher layers. Above the quartzite (3-9 m) are mainly thin- and medium-bedded limestones interbedded with some (one-fourth) light grey, orange weathering shale. The limestone in the lower layers is light grey on weathered and fresh surfaces and has a pinkish hue. Beds of this type grade

---

PLATE 27.2 (opposite)

Figure 1. View looking northwest at lower segment in Section 10C. Contact between Stelkuz Formation and overlying Boya Formation is at "b". Top of segment is at a fault ("c") located within Boya Formation. Small limestone exposure in Stelkuz Formation outcrops through cover at "a". In background is Mount Finlay, where dashed line on southeast end of mountain delineates fault between Boya (B) and Kechika (K) formations. At northwest end of mountain dashed line indicates fault lying near contact between Boya Formation and Rosella Formation (R). Point "d" shows location where units 5B and 1R were measured in Section 9C. (see Pl. 27.1, fig. 3). Composite from GSC 204041 and 204041-A.

2. View looking southeast at Stelkuz, Boya and Rosella formations from point near lower segment of Section 10C. Dashed line marks contact between Stelkuz (medium light) and Boya (dark) formations. Boya Formation in upper segment of Section 10C was measured on light coloured ridge (bleached abnormally light by waters draining from recently melted snow cover) between points "a" and "b". Rosella Formation outcrops on same ridge beyond point "b" and basal Rosella strata caps ridge in middle ground at point "c". Composite from GSC 204041-B and 204041-F.

3. View looking west-northwest from peak near top of lower segment in Section 10C. Lowest dashed line approximately delineates contact between Boya (B) and Rosella (R) formations. Middle pair dashed lines outline Unit 7 of Rosella Formation, and upper dashed line approximately indicates fault between Unit b? and Kechika Formation. Point "a" roughly indicates horizon from which small shelly fossils in GSC locality 99726 were collected. Actual locality is short distance beyond arrow and concealed behind ridge. Point "b" marks top of Rosella Unit 6, which is well exposed on other side of ridge. Points "c" and "d" in background mark outcrops of Rosella Unit R7; outcrop at "d" is on Section 9C. Composite of GSC 204041-K and 203853-W.

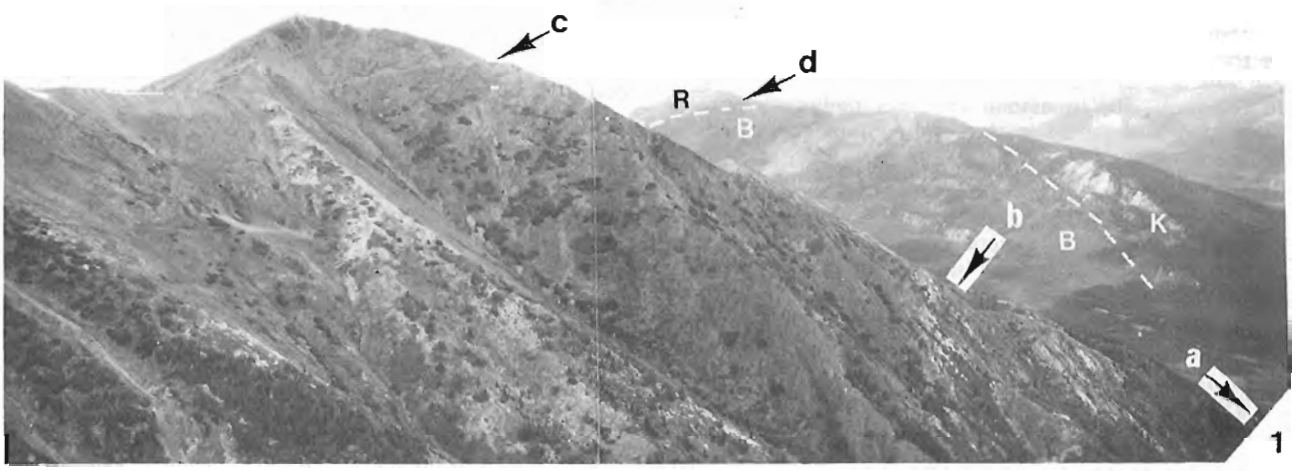

1

2

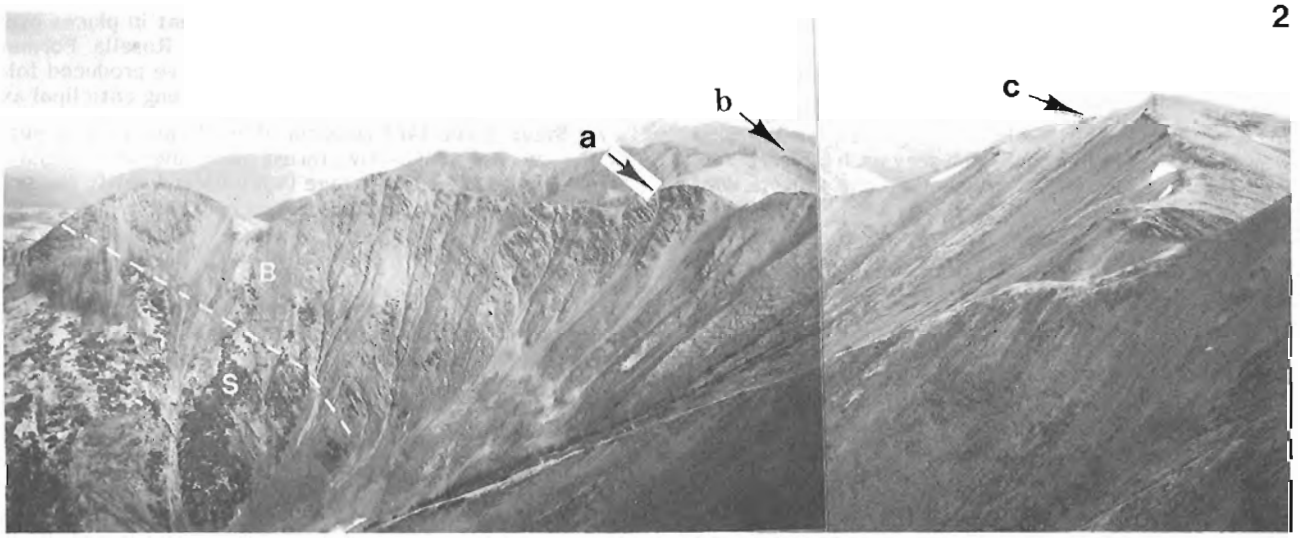

3

upward to medium grey weathering, thin and wavy beds of medium dark grey limestone at the top. The limestone-quartzite contact is irregular, and at Section 10C it exhibits at least 0.1 m of local relief (Pl. 27.1, fig. 6).

In the second unit (Unit 2, 45.5 m), light grey shale, which weathers light brown, orange and greenish grey, dominates the lower half (22 m) and is sparsely interbedded with the medium grey limestone that predominates in the upper half (23.5 m). The limestone weathers medium grey to medium blue grey and occurs in thin and medium wavy beds exhibiting fine laminae.

Unit 3 (35 m) comprises thick to massive beds of medium light grey to light blue grey limestone, which is light grey on fresh surfaces. The uppermost 5 m of this unit consist of thin and medium beds of similar limestone that is light orange on parting surfaces.

Reddish brown weathering, medium- and thick-bedded dolostone comprises the fourth unit (Unit 4, 40 m). The dolostone is finely crystalline and is dark grey on fresh surfaces. Wide (up to 0.25 m) veins of white quartz cut the unit at widespread intervals in both segments of Section 9C.

Unit 5 (36 m) contains thin- to thick-bedded limestone that weathers medium dark to medium light grey. Faint outlines of fine to coarse carbonate clasts are visible in the finely crystalline limestone. This unit contains abundant archaeocyathids, as opposed to other Rosella carbonate units where archaeocyathids are either scarce or absent.

Unit 6 (61.5 m) comprises light orange to greenish grey weathering shale that is light greenish grey on fresh surfaces. In addition to the exposure at Section 9C, the unit is well exposed near Section 10C (Pl. 27.2, fig. 3) where a thickness of 77.5 m was measured.

The uppermost unit confidently assigned to the Rosella Formation in Section 9C (Unit 7, 39 m) is the lightest coloured and has the strongest topographic expression. It is composed of massive, white weathering, finely crystalline limestone, and is light grey on fresh surfaces. The upper contact of Unit 7 (Pl. 27.1, fig. 5) is believed to be a fault contact, and the overlying dark siltstone and quartzite are tentatively assigned to the Boya Formation [B(?), see following discussion on structure].

Tectonic interpretation of Unit B(?)

The position of Unit B(?) immediately above Rosella Unit 7 at Section 9C (B(?)=90.5 m+) and above Unit 7 at a locality 2 km northwest of Section 10C (B(?) 78 m+; Pl. 27.2, fig. 3) is anomalous. At both localities the unit consists of rust weathering siltstone and interbedded very fine grained quartzite, closely resembling strata in the Boya Formation at Section 10C and in the Cassiar Mountains.

A possible structural explanation is illustrated in Figure 27.4. The first stage of deformation (4a) is the overthrusting of younger Boya and Rosella strata by older Boya strata. At least some upper Rosella beds are believed to have been removed, because archaeocyathids are present in the uppermost remaining unit (Unit 7) of the Rosella Formation, whereas in the Cassiar Mountains the highest archaeocyathids are well below the top of the Rosella (Fritz, 1978; Fig. 3.1). Repetition of Lower Cambrian strata by overthrusting is common in the northern Omineca Mountains.

The second stage of deformation (4b) is the introduction of Kechika strata along a thrust fault that in places overlies the Boya Formation and in places the Rosella Formation. Deformation related to thrusting may have produced folds in the Rosella that later broke, especially along anticlinal axes.

Stage three (4c) consists of moderate folding outlined by the major Kechika-Boya thrust plane and the Rosella-Boya thrust plane. The final stage (4d) involved uplift and erosion to the level of present exposures at Section 9C.

Age of strata

As mentioned earlier, deformation has nearly destroyed the biostratigraphic usefulness of trace fossils and trilobites in the measured sections. However, G.M. Narbonne was able to identify the trace fossil cf. **Phycodes** sp. in the collection from GSC loc. 99719, and **Paelyophycus** sp. from

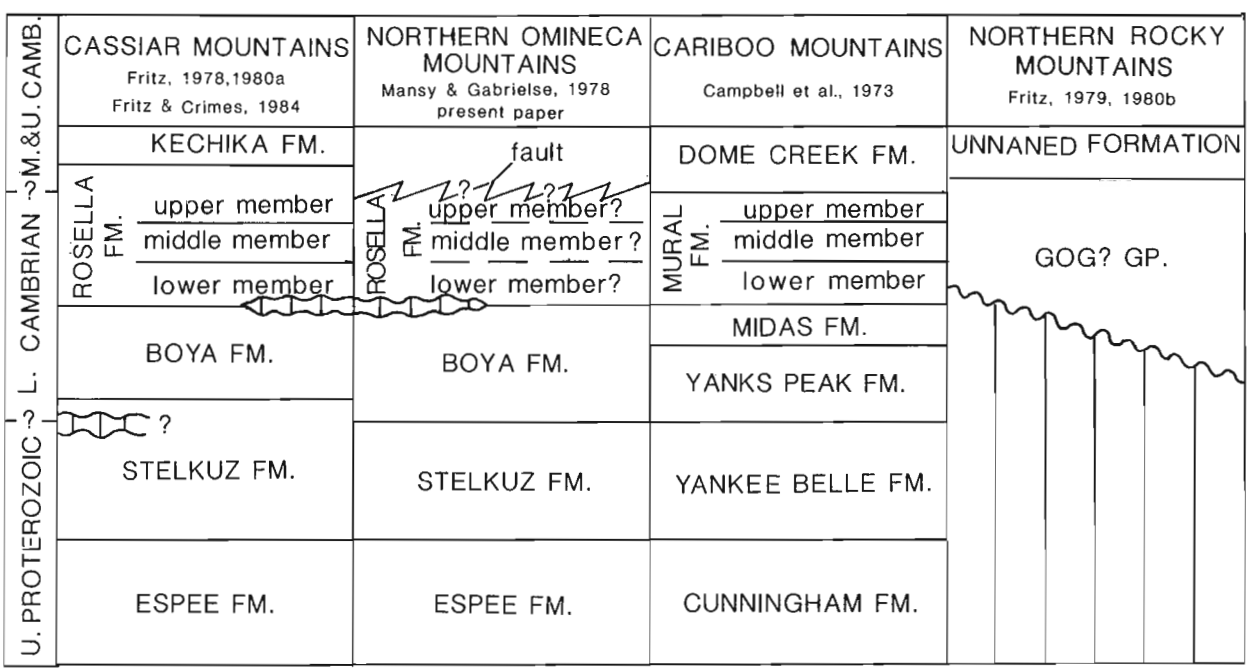

Figure 27.5. *Correlation chart for uppermost Precambrian and Lower Cambrian strata in Cassiar, northern Omineca, Cariboo, and northern Rocky mountains.*

GSC loc. 98706. These identifications indicate that the GSC loc. 99719 horizon may be within the Lower Cambrian and the GSC loc. 98706 horizon is upper Proterozoic (Vendian) or younger. Distorted trilobite fragments in collections from GSC locs. 99686 and 99688 are questionably assigned to the **Nevadella** Zone. It is hoped that studies on the small shelly fossils and archaeocyathids may improve the accuracy of the dating, but this is presently difficult, because ranges of the small shelly fossils are only now being tested, and ranges of western Canadian archaeocyathids have thus far been refined only to the stage level. The isolated sample collected for small shelly fossils (GSC loc. 99727) near the base of the Stelkuz Formation, may prove to be barren because the strata sampled may predate the evolution of skeletal material.

Correlation with Cassiar Mountains

Strata in the Cassiar Mountains correlate (Fig. 27.5) closely with those in the northern Omineca Mountains. In the following correlations, Cassiar Section 1 will be emphasized, because this section has been described in the greatest detail (Fritz, 1980a; Fritz and Crimes, 1984). One of the lowest exposed units in Section 1C is the uppermost limestone unit (44 m), locally present in the Stelkuz Formation. An attractive but speculative correlation of this unit is with the limestone outcrop below Section 10C (Pl. 27.2, fig. 1) and the youngest Stelkuz limestone (upper part of Unit 3S) in Section 11C (Pl. 27.1, fig. 2). The Cassiar limestone is slightly darker and more thickly bedded than the limestone of the Omineca exposures, but like the limestone in Section 11C, it occupies a position not far above a highly coloured shale. At Section 1C, Precambrian trace fossils were found below the limestone unit, whereas at Section 11C, trace fossils, if formerly present, have been destroyed by tectonic deformation.

The next youngest lithological change that can be widely recognized is the Stelkuz-Boya formational boundary. At Section 1C the Stelkuz-Boya boundary was placed at the base of the only prominent white quartzite unit that can be traced in the surrounding area, where exposures are poor and structurally complex. A rare outcrop below the boundary at Section 1C exposes 190 m of strata as follows (descending order): rust weathering siltstone (78.5 m); orange-brown, bioturbated sandstone (37.5 m); reddish brown weathering, crossbedded quartzite (58 m); white quartzite (14 m); and depositional breccia (2 m). The surface underlying the breccia has been interpreted as a disconformity, and was tentatively chosen to locally represent the Precambrian-Cambrian boundary (Fritz and Crimes, in press). Below the disconformity are strata that are similar to those below the Stelkuz-Boya formational contact at sections 10C and 11C.

The Stelkuz-Boya contact in the northern Omineca Mountains was examined for a disconformity, but no clear evidence was found at that level nor in closely overlying or underlying strata. At Section 10C, the 86.5 m of quartzite above the contact becomes coarser and cleaner upwards, a trend that is the reverse of what might be expected of a channel deposit overlying a disconformity. In the lower 46 m, interbedded dark grey shale is finer than the finest clastics above the 86.5 m unit or at the first exposure below. The strata immediately below the quartzite are covered at Section 10C, and for a considerable distance in any direction.

At Section 11C, 1 m of orange weathering dolomite followed by white quartzite overlie the Stelkuz-Boya boundary and provide a sharp contrast to the yellow weathering shale, siltstone, and very fine grained quartzite below.

The above observations indicate the Stelkuz-Boya contact may have been set higher in the Cassiar Mountains that at sections 10C and 11C. No evidence was found to either confirm or refute an extension of the Section 1C disconformity to sections 10C or 11C.

In the northern Omineca Mountains the Boya-Rosella boundary is probably represented by a minor disconformity. Below the contact at Section 10C, the Boya exhibits an upward increase of clean, white quartzite, suggesting a depositional environment that became more shallow. The top of the formation is believed to be an erosional surface overlain by a fine- to coarse-grained, limy sandstone. At Section 9C there is a similar Boya-Rosella contact, and archaeocyathids are found only 9 m above it. Trilobites occur at the same horizon (GSC locs. 99686, 99687) and these are tentatively placed in the **Nevadella** Zone.

The Omineca disconformity is linked with a moderate sub-Rosella disconformity reported (Fritz, 1978, p. 14) at Section 6C in the Cassiar Mountains. At this locality the basal Rosella consists of white quartzite overlain by shale containing fossils belonging to the **Bonnia-Olenellus** Zone. This moderate disconformity can be traced northwestwards in the Cassiar Mountains to other sections, such as Section 8, where a basal limy sandstone is closely overlain by limestone bearing trilobites of the **Nevadella** Zone. At Section 1C trilobites belonging to the **Fallotaspis** Zone are present a short distance above the base of the Rosella, and little or no erosion is suspected at the Boya-Rosella contact. Weak erosion at sections 9C and 10C may be approximately coeval to that at Section 8C in the Cassiar Mountains. Phosphatized small shelly fossils are present in the basal Rosella in the northern Omineca and Cassiar mountains.

Only one inter-Rosella correlation between the northern Omineca and Cassiar mountains is attempted because of the lack of fossil control. However, it should be noted here that the occurrence of archaeocyathids in the highest Rosella limestone unit (Unit R7) exposed at Section 9C and near Section 10C suggests that the upper Rosella is missing, because a considerable thickness of post-archaeocyathid Rosella limestone is present in the nearby Cassiar Mountains (Fritz, 1978, Fig. 3.1).

Correlation with northern Rocky Mountains

The best northern Rocky Mountains sections for correlation with the northern Omineca Mountains strata are sections 1R and 2R (Fritz, 1979). In these sections, strata equivalent to those in the Rosella Formation comprise clastics of the Gog(?) Group. The Gog(?) Group overlies an unconformity, below which is a thin interval containing dolomite that is in turn underlain by interbedded shale and diamictite. Eisbacher's (1981) observation that the diamictite is glacially derived can be taken as evidence of a much older age, and therefore leaves little doubt as to the great magnitude of the sub-Gog(?) unconformity. Missing at sections 1R and 2R are strata equivalent to at least part of the Boya Formation and most, if not all, of the Ingenika Group.

Farther west in the northern Rocky Mountains, sections 7R and 8R (Fritz, 1980b) exhibit upper Gog(?) Group strata that are still mainly in the clastic facies, and bear little resemblance to the equivalent Rosella Formation in the northern Omineca Mountains.

Correlation with Cariboo Mountains

The close northern Omineca-Cassiar correlations noted earlier are nearly matched by the Omineca-Cariboo correlations, suggesting the Cariboo strata were also deposited along the same depositional trend. The Espee

Formation in the Omineca Mountains is reported (Mansy and Gabrielse, 1978, Fig. 10A) to maintain its lithological character from near Section 11C through the middle and southern Omineca Mountains, and into the Cariboo Mountains, where it is referred to as the Cunningham Formation. In the Cariboo Mountains some dolomite and shallow water features are present, and on the eastern margin the Cunningham is abruptly overlain by a basal Yankee Belle (=Stelkuz) Formation sandstone (Campbell et al., 1973, p. 39).

Correlation of the Stelkuz Formation in the Omineca Mountains with the Yankee Belle Formation in the Cariboo Mountains is likewise supported by close lithological similarities. In both areas, greenish grey shale and siltstone are major components. Carbonate is common in the lower parts of the formations in both areas, extends into the middle parts, and is rare or absent in the upper parts. In the northern Omineca Mountains the upper Stelkuz boundary is sharp, but in the Cariboo Mountains it is reported to be transitional (Campbell et al., 1973, p. 40). In the Cariboo Mountains, trace fossils were noted at several upper Yankee Belle outcrops, (Campbell et al., 1973, p. 40, 41) whereas in the northern Ominecas the upper Stelkuz contains trace fossils but the lower levels could not be properly tested because of the tectonic deformation.

A stronger lateral lithological change occurs between strata assigned to the Boya Formation in the northern Omineca Mountains and the equivalent Yanks Peak and Midas formations in the Cariboo Mountains. In both areas quartzite is more abundant in the lower part of the succession. However, this is accentuated in the Cariboo Mountains where the lower quartzite (Yanks Peak Fm.) is very resistant, light coloured, and fine- to coarse-grained. It thus contrasts strongly with the overlying strata (Midas Fm.) comprising interbedded medium and dark siltstone.

At Section 9C and outcrops near Section 10C the Rosella Formation can be closely correlated with the Mural Formation in the Cariboo Mountains. This may be expected, because the Omineca outcrops are geographically between the equivalent Cariboo-Cassiar (Mural-Rosella) formations that have common lower limestone, middle siltstone, and upper limestone members (Campbell et al., 1973, p. 51; Fritz, 1978, p. 14). The middle member, which is persistent in the Cassiar Mountains (Fritz, 1978, Fig. 3.1, Unit 4), could nevertheless be confused with other, less persistent, shale members, especially when fossil control is lacking. At Section 9C, Unit R6 may represent the middle Rosella member, but no fossil confirmation is available.

Correlation between the (faulted?) top of the Rosella Formation in the northern Omineca Mountains and the top of the Mural Formation in the Cariboo Mountains is of interest. The following data are from notes taken at the type section for the Dome Creek Formation, Cariboo Mountains (see also Campbell et al., 1973, p. 55).

The rock immediately below the top of the Mural Formation (Mural-Dome Creek contact) in the western Cariboo Mountains, is white, medium and thick bedded limestone, and above (Dome Creek Unit 1, 73 m) is black shale with some interbedded dark limestone. Unit 2 (99 m) comprises highly burrowed, khaki to light greenish grey siltstone, and Unit 3 (145.5 m) contains black, silicious shale with some dark, interbedded limestone. The remainder of the Dome Creek Formation (units 4-7, 1585 m) is predominantly medium grey weathering, slightly limy shale. The Dome Creek Formation terminates at a fault contact with the Yanks Peak Formation. Fossils date Unit 1 as upper Lower Cambrian, and numerous horizons in the units 4-7 succession as Upper Cambrian. Only the second Dome Creek unit (burrowed siltstone) remotely resembles map Unit B(?) in the northern Omineca Mountains, and therefore the lateral equivalence of Dome Creek and Unit B(?) strata is considered unlikely.

References

Campbell, R.G., Mountjoy, E.W., and Young, F.G.
1973: Geology of McBridge map-area, British Columbia; Geological Survey of Canada, Paper 72-35, 104 p.

Eisbacher, G.H.
1981: The Late Precambrian Mount Lloyd George diamictites, northern British Columbia; in Earth's pre-Pleistocene glacial record; Cambridge University Press, Cambridge, p. 728-730.

Fritz, W.H.
1978: Upper (carbonate) part of Atan Group, Lower Cambrian, north-central British Columbia; in Current Research, Part A, Geological Survey of Canada, Paper 78-1A, p. 7-16.

1979: Cambrian stratigraphy in the northern Rocky Mountains, British Columbia; in Current Research, Part B, Geological Survey of Canada, Paper 79-1B, p. 99-109.

1980a: Two new formations in the Lower Cambrian Atan Group, Cassiar Mountains, north-central British Columbia; in Current Research, Part B, Geological Survey of Canada, Paper 80-1B, p. 217-225.

1980b: Two Cambrian stratigraphic sections near Gataga River, northern Rocky Mountains, British Columbia; in Current Research, Part C, Geological Survey of Canada, Paper 80-1C, p. 113-119.

Fritz, W.H. and Crimes, T.P.
1984: Lithology, trace fossils, and correlation of Precambrian-Cambrian boundary beds, Cassiar Mountains, north-central British Columbia, Canada; Geological Survey of Canada, Paper 83-13 (in press).

Mansy, J.L. and Gabrielse, H.
1978: Stratigraphy, terminology and correlation of Upper Proterozoic rocks in Omineca and Cassiar mountains, north-central British Columbia; Geological Survey of Canada, Paper 77-19, 17 p.

28.

SUPERPOSED FOLDING IN THE NORTHERN GROUNDHOG COALFIELD; EVIDENCE FOR POLYPHASE DEFORMATION IN THE NORTHEASTERN CORNER OF THE BOWSER BASIN

EMR Research Agreement 83-4081A

I.W. Moffat and R.M. Bustin[1]

Moffat, I.W. and Bustin, R.M., Superposed folding in the northern Groundhog Coalfield; evidence for polyphase deformation in the northeastern corner of the Bowser Basin; in Current Research, Part B, Geological Survey of Canada, Paper 84-1B, p. 255-261, 1984.

Abstract

In the northern part of the Groundhog Coalfield in north-central British Columbia, Mesozoic strata have been shortened by two phases of noncoaxial deformation. Both phases clearly post-date deposition of the youngest unit in the coalfield, the Devils Claw (Early Cretaceous?), and pre-date deposition of the early Eocene Brothers Peak Formation, and may pre-date deposition of the Late Cretaceous (Albian?) Tango Creek Formation. The first phase of deformation resulted in northwest-trending folds and thrusts which occur in the cores of a large suprastructural carapice consisting of an anticlinorium-synclinorium pair. The suprastructure is developed in conglomeratic units which appear to have behaved as a relatively strong beam during deformation. First phase structures are overprinted by second phase northeast-trending folds and flat-lying thrusts which deform the first phase lineations and result in telescoping of previously deformed strata in a southeasterly direction. The first phase of deformation may be related to suturing of the "Stikine terrane" with the North American craton, whereas the second phase may be related to the collision of the Stikine block with a fixed terrane as the block moved northward along a major strike-slip fault system.

Résumé

Dans la partie nord du bassin houiller de Groundhog, situé dans le centre nord de la Colombie-Britannique, des couches d'âge mésozoïque ont été raccourcies par deux phases de déformation non coaxiales. Ces deux phases ont eu lieu de façon certaine après le dépôt de l'unité la plus jeune dans le bassin houiller, unité de Devils Claw (Crétacé inférieur?) et avant le dépôt de la formation de Brothers Peak de l'Éocène inférieur; elles ont aussi probablement eu lieu avant le dépôt de la formation de Tango Creek du Crétacé supérieur (Albien?). La première phase de déformation consiste en plis et failles anormales de direction nord-ouest qui se sont produits dans le centre d'une grande carapace suprastructure formant un tandem anticlinorium-synclinorium. La suprastructure est constituée d'unités conglomératiques qui se seraient comportées lors des déformations comme une poutre relativement résistante. Les plis et les failles chevauchantes horizontales de direction nord-est de la seconde phase se superposent aux structures de la première phase dont les linéations ont été déformées et dont les couches, déformées antérieurement, se sont téléscopées dans une direction sud-est. La première phase de déformation peut être liée à la suture du <<terrain de Stikine>> avec le craton d'Amérique du Nord; alors que la seconde phase peut être associée à la collision du bloc de Stikine avec un terrain fixe, au fur et à mesure que le bloc s'avançait vers le nord le long d'un système de failles horizontales de décrochement.

Introduction

During the summers of 1982 and 1983, an area of approximately 750 square kilometres of the Groundhog Coalfield in the northeastern corner of the Bowser Basin was mapped at a scale of 1:30,000 (Fig. 28.1). This study, although concerned predominantly with the style of deformation of the coal bearing sequence and related strata, required the delineation of a mappable stratigraphy in order that detailed structural geometries could be ascertained. It is the purpose of this paper to outline the evidence for superposed deformation, compare and contrast the types of strain related to each phase, and to suggest the possible implications that these relationships have in the regional tectonics of north-central British Columbia.

Acknowledgments

This research comprises a portion of the senior author's Ph.D. thesis research. Funding was obtained from Energy, Mines and Resources Grant No. 83-4081A. Financial as well as technical support was also received from Gulf Canada Resources Incorporated. We thank Dr. D.K. Norris of the Institute of Sedimentary and Petroleum Geology for his comments on an early draft of the manuscript.

Stratigraphy

The sequence of rocks exposed in the study area is thought to be time equivalent to the Upper and Lower Bowser Lake Group and part of the Skeena Group as defined by Tipper and Richards (1976). Four mappable units have been defined in the study area, which on a gross scale are laterally continuous throughout the Groundhog Coalfield (Bustin and Moffat, in press). The details of this stratigraphic package have previously been outlined (ibid.) and hence only a brief summary is presented here (Fig. 28.2).

The age of strata exposed in the Groundhog Coalfield is uncertain because identifiable fossils have been obtained only from the Jackson and lower part of the Currier units. Such marine fossils as **Cadoceras, Trigonia, Kepplenites, Cobbanites, Pholas** (Roots in Eisbacher, 1974), and **Cardoceras** and **Buchia concentirica** (Tipper in Eisbacher, 1974) indicate that the Bowser Lake Group spans a time frame from Callovian to Oxfordian. Ammonites discovered in this study in the vicinity of the uppermost 50 m of the Jackson unit have been identified as **Amoeboceras** (P. Smith, personal communication, 1983), indicative of an upper Oxfordian age. **Amoeboceras** also occurs in the black shale facies of the Upper Bowser Lake Group (Tipper and Richards, 1976) suggesting time

[1] Department of Geological Sciences, University of British Columbia V6T 2B4

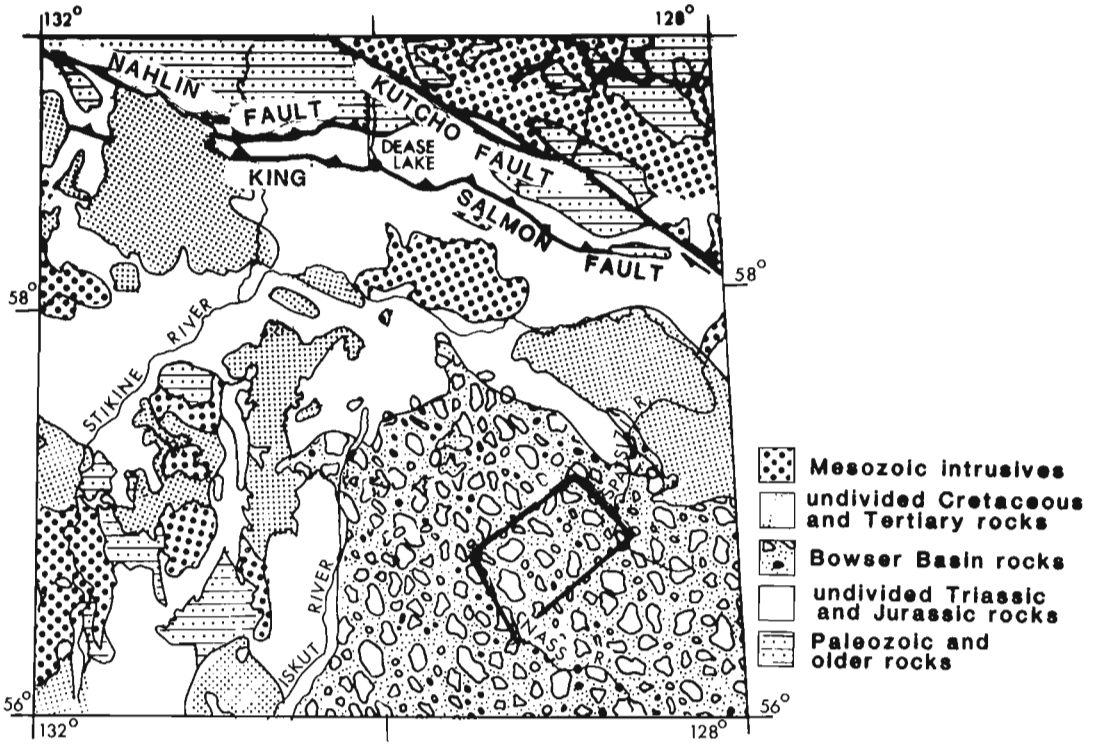

Figure 28.1. *Location of the study area. Geology modified after Tipper et al., 1981. The study area is enclosed within the area outlined between the Nass and Spatsizi rivers.*

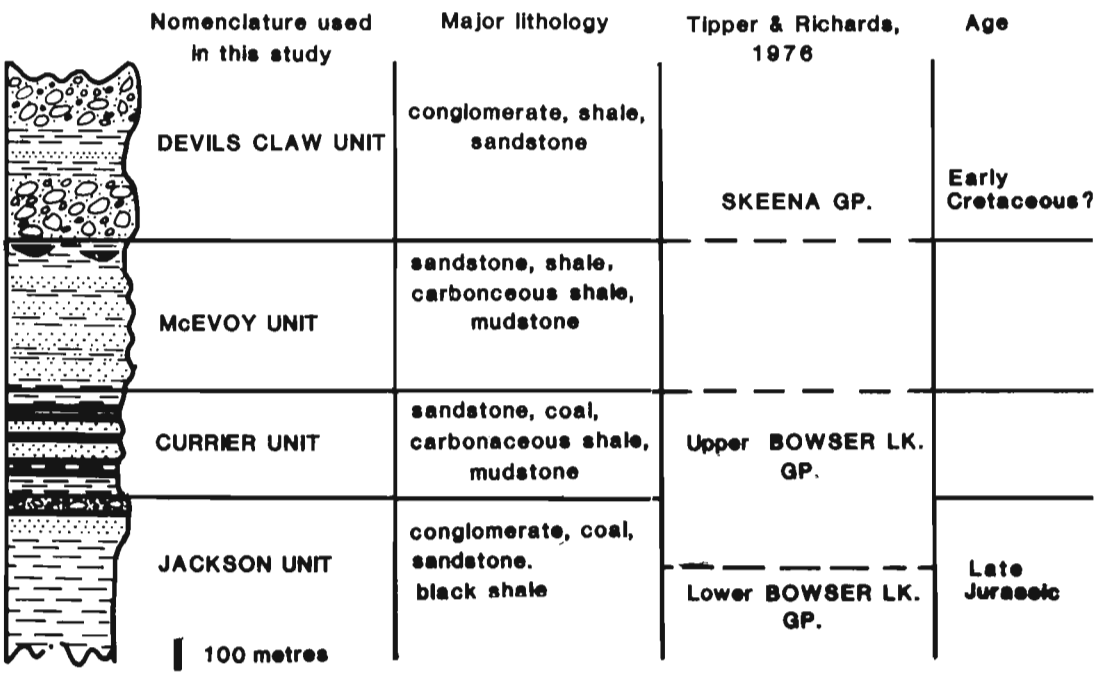

Figure 28.2. *Generalized stratigraphy of the study area illustrating possible correlation with the southern Bowser Basin (modified from Tipper and Richards, 1976; Bustin and Moffat, in press).*

equivalence of the Upper Bowser Lake Group and the upper Jackson unit. Plant fossils from coal deposits of the Currier unit in the southern portion of the coalfield indicate a Late Jurassic age (Bustin and Moffat, in press). The lack of distinctive fossils in the McEvoy and Devils Claw units makes their ages equivocable. It is possible, however, that the thick conglomerates of the Devils Claw unit are in part coeval with the Skeena Group conglomerates identified by Tipper and Richards (1976). The contact between the Skeena Group and underlying Upper Bowser Lake Group in the southern Bowser Basin is, however, unconformable (ibid.) whereas no evidence for an unconformable relationship between the Devils Claw and McEvoy units has been recognized in this study.

Structure

The study area is characterized by two phases of deformation: an early phase which resulted in northwest-trending folds and minor thrusts, and a later phase which resulted in generally broad, open, northeast-trending folds, which have rotated axial lineations of the first phase folds. Second phase thrusts appear to be less common than folds and are generally flat lying, resulting in several klippen (Fig. 28.3), with associated shortening in a southerly direction.

First phase structures

First phase structures are illustrative of the control that lithology imparts on the style of deformation in the coalfield. The overall structural geometry of the area consists of a major anticlinorium-synclinorium pair developed in large open folds in the relatively competent Devils Claw conglomeratic unit. More complicated structures are developed in weaker fine grained rocks of the McEvoy, Currier and Jackson units and are parasitic to the large scale folds. The axis of the Mount Biernes synclinorium (Richards and Gilchrist, 1979) in the study area passes through a peak

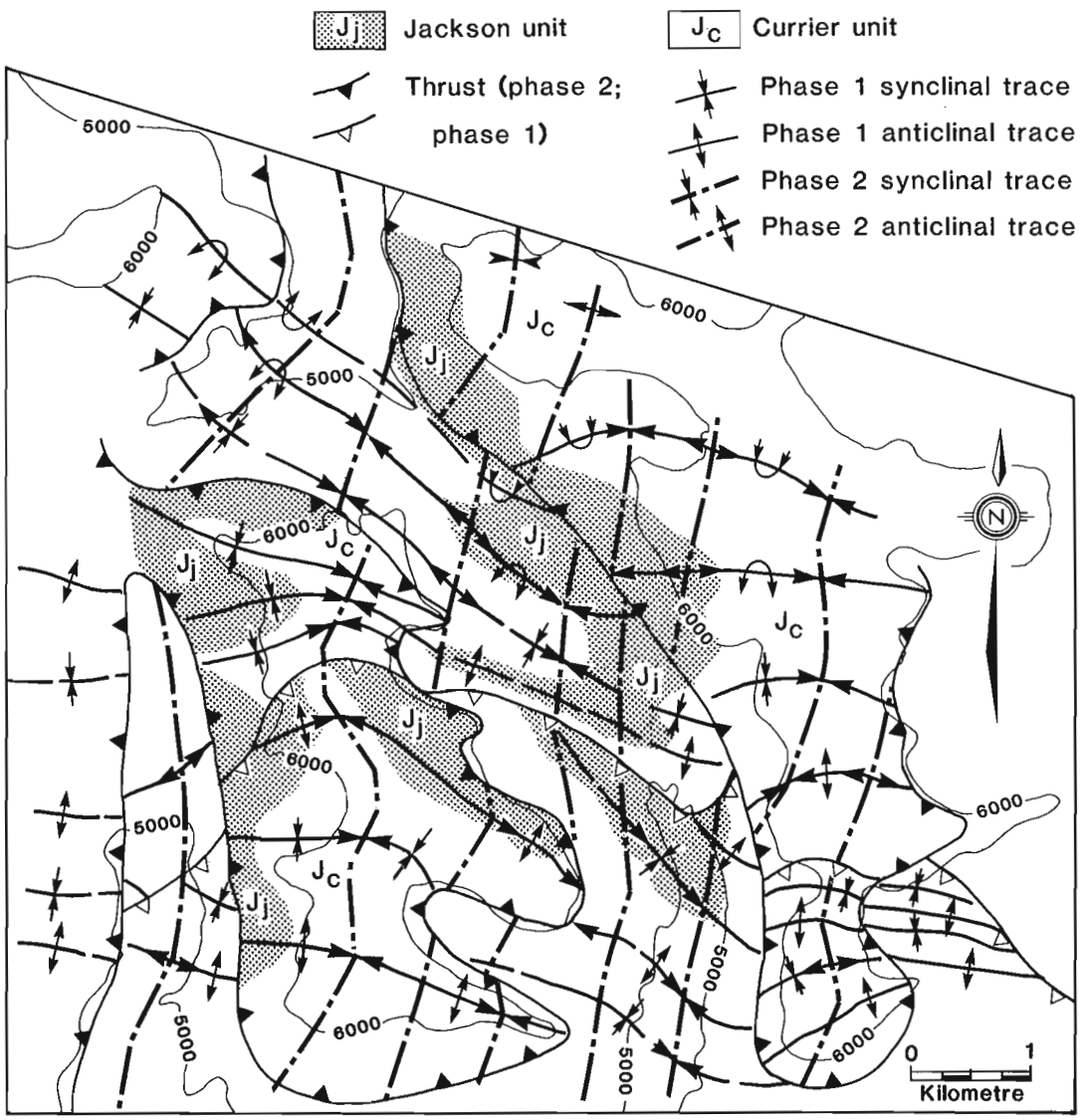

Figure 28.3. *Schematic structural map of northern portion of study area illustrating the interaction between first and second phase structures. Second phase axial traces are approximate locations only and have possibly been rotated by second phase thrusts.*

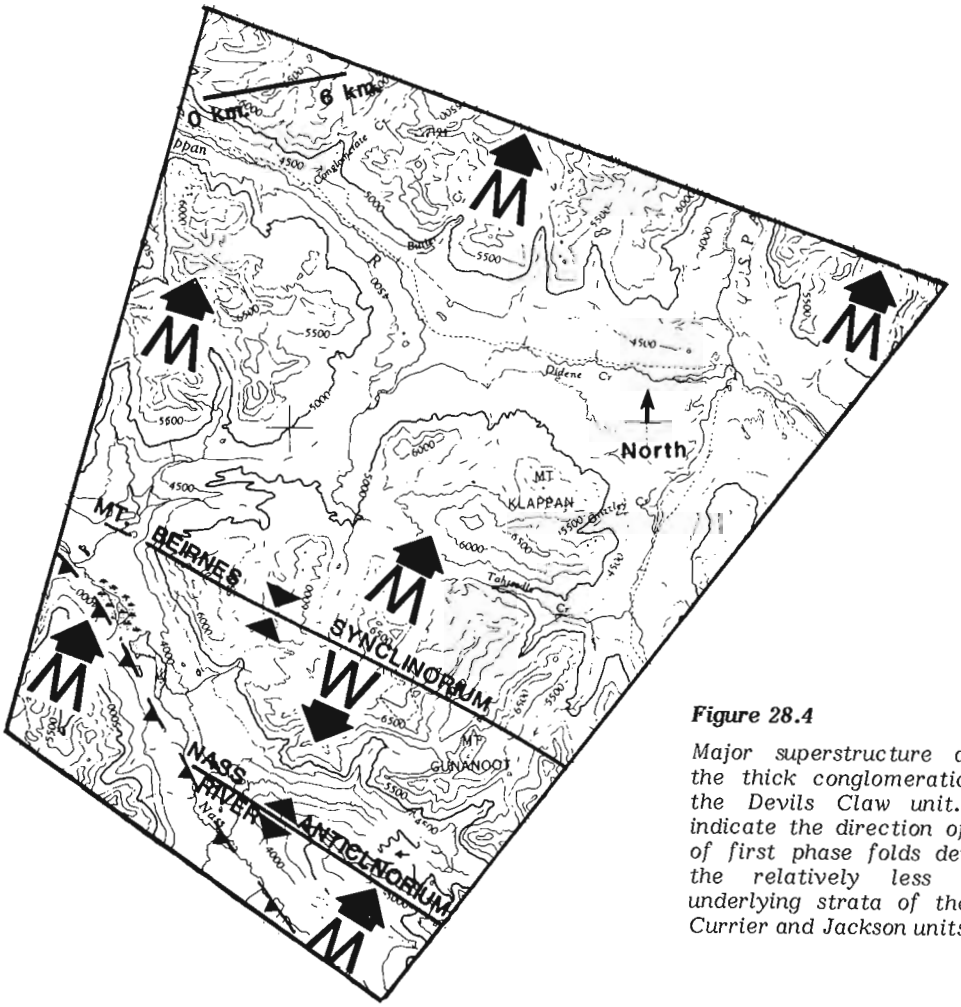

Figure 28.4

Major superstructure defined by the thick conglomeratic units of the Devils Claw unit. Arrows indicate the direction of vergence of first phase folds developed in the relatively less competent underlying strata of the McEvoy, Currier and Jackson units.

Figure 28.5. *View looking northwest at first phase folds located southeast of Conglomerate Creek, which have a megascopic kink band geometry.*

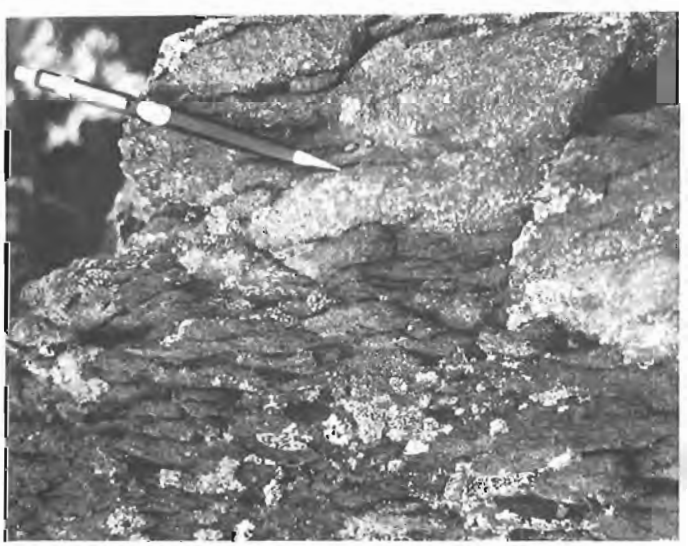

Figure 28.6. *Penetrative dissolution cleavage formed in a medium- to coarse-grained litharenite of the lower Currier unit.*

immediately east of Mount Gunanoot (Fig. 28.4). Minor folds east of the synclinorium axis verge eastwards whereas minor folds west of the axis verge westward to the valley of the Nass River (Fig. 28.4). This contrast in direction of vergence is due to the opposite sense of shear developed between units of apparent high viscosity contrast on opposite sides of the Mount Biernes synclinorium axis. On ridges west of the Nass Valley, folds in the Jackson and Currier units verge eastwards, and form the eastern limb of an anticlinorium (Fig. 28.4). The axis of this anticlinorium (here termed the Nass River anticlinorium) is exposed on a ridge immediately west of Mount Gunanoot. Whereas folds in the thick, relatively competent, thickly bedded Devils Claw and upper McEvoy units tend to be broad and open, folds developed in the weaker, thinly bedded, fine grained units of the lower McEvoy, Currier and Jackson units are assymetric to overturned, with tight hinge areas that are best described as having a megascopic kink band geometry (Fig. 28.5). Thrust faults related to the initial phase of deformation are seldom located in outcrop and, where either observed or assumed, have limited displacement (generally less than 1 km). Such thrusts are thought to have propagated through steeply dipping to overturned limbs of first phase folds. Extension faults, which trend northeast and have limited strike-slip and dip-slip displacements (hundreds of metres) are common locally. The time of formation of the extension faults is not clear although at least some dip-slip displacement is associated with the second phase of deformation.

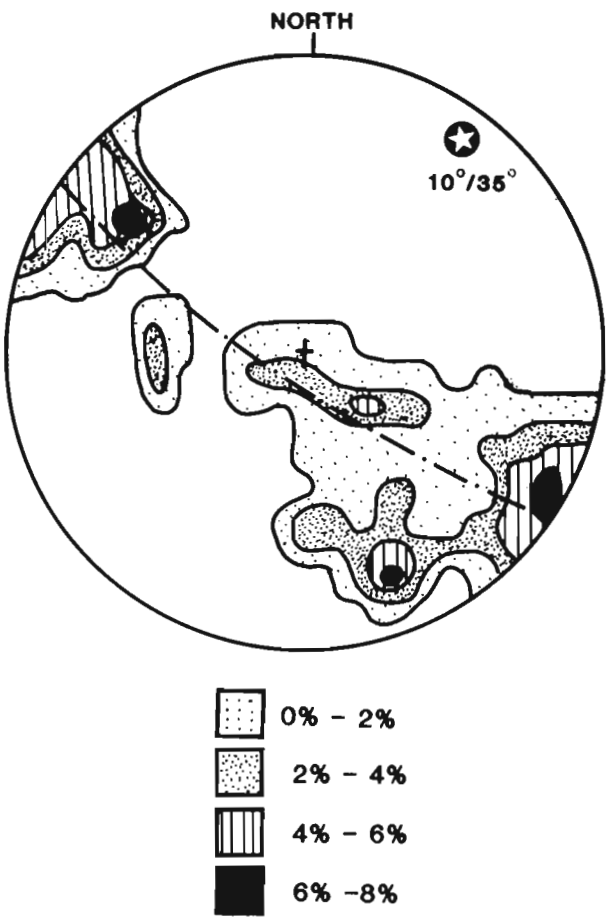

Figure 28.7 *Equal area plot of bedding to first phase cleavage intersections. Non-rigorous treatment of data suggests that the second phase was directed at approximately 90° to the first phase. Second phase fold axis approximated here by the star.*

Two types of cleavage related to the first phase of deformation are ubiquitous in the study area: a fracture cleavage (cleavage plane spacing less than 5 cm; Hancock, 1982), and a dissolution cleavage. Fracture cleavage surfaces are distinguished from dissolution surfaces in that the fractured surfaces tend to be smooth, planar and locally conjugate, whereas dissolution cleavage planes are usually sinuous to anastomosing, often rough and variably spaced to continuous in hand specimen. Fracture cleavage, oriented roughly perpendicular to layering, occurs in all units at shallower levels and in the more rigid units, which have been deeply buried. Such cleavage probably originates as closely spaced fractures formed as a result of outer arc extension during folding. This relationship is evident in several conglomerate samples, where closely spaced planar fractures traverse grain boundaries with little or no deflection. Dissolution cleavage (Fig. 28.6) fans divergently about the first phase fold axes and appears to be generally more pervasive in more argillaceous sediments deeper in the stratigraphic section than in either sediments from a higher stratigraphic level or from sediments which are relatively more competent. The divergent nature of the cleavage suggests that it formed under conditions of low buckling strain and has been further rotated during continued buckling (dissolution cleavage is considered to form generally in the plane of high normal stress; Dietrich, 1969).

Second phase structures

The second phase of deformation in the study area is characterized by broad, open, slightly asymmetric northeast-trending folds resulting in the folding of cleavage to bedding intersection lineations associated with the first phase of deformation (Fig. 28.7). The folds have a wavelength greater than first phase folds and an amplitude that is significantly smaller. Thrusts associated with the second phase of deformation are generally flat lying and are usually associated with hanging wall drag folds of second phase orientation. The second phase thrust faults offset both first phase structures as well as second phase fold axial surface traces (Fig. 28.3). Faults of this type lose displacement along bedding surfaces, in a manner similar to blind thrusts (Fig. 28.8).

Figure 28.8. *View looking northwest at second phase drag folds and thrusts (dotted lines). Thrusts follow bedding planes for large distances and may be indicative of blind thrusts. Drag fold axes trend roughly northeast.*

Figure 28.9. *View looking northeast at late stage extension faults. This fault zone occurs at the hinge line of a gentle second phase anticline.*

Several extension faults of limited displacements (no greater than 200 m) occur associated with second phase anticlinal hinge areas (Fig. 28.9). These faults probably form as a strain response to outer arc extension during the second phase of deformation. Differentiation between faults and fractures related to late extension faulting from a-c fractures[1] formed during the first phase is often tenuous except where the latter have been folded during the younger deformational event.

Penetrative cleavage related to the second phase of deformation is rare and almost solely of the fracture type, although in at least one location, approximately 6 km northeast of Mount Klappan, dissolution cleavage occurs in an orientation which is approximately axial planar to second phase folds. The apparent lack of well developed second phase pressure solution cleavage may be due either to lower values of total strain related to this phase or to the possibility that second phase deformation occurred at a higher structural level. Although no estimates on total shortening have been made it is apparent that the total strain related to the second phase of deformation is substantially less than that related to the first phase.

Discussion and conclusions

Strata in the northeastern corner of the Bowser Basin were deformed by two phases of deformation sometime between deposition of the Devils Claw unit (Early Cretaceous?) and deposition of the Brothers Peak Formation (early Eocene) east of the study area. Although the evidence is equivical, both phases of deformation may be episodic as is evident to the east of the study area in the Sustut Basin, where mildly deformed rocks of the Tango Creek Formation (Albian?) unconformably overlie more intensely deformed rocks of the Lower Bowser Lake Group (Eisbacher, 1981). In the study area the first direction of shortening is approximately northeast-southwest, followed by a later northwest-southeast compressional event which resulted in rotation of lineations and offset of thrust and folds related to the initial phase of deformation. An opposite relationship was noted in one area near Mosque Mountain in the Sustut Basin by Eisbacher (1973). Here Eisbacher describes a north-south compressional event which occurred earlier than an east-west compressional event. More detailed information on this relationship is needed, however, prior to attempting a correlation with the study area. Directly northwest of the study area, folds have been mapped in Bowser Lake Group rocks whose axial traces are similar in orientation to both first phase and second phase folds delineated in the study area (Geological Survey of Canada, 1957). The exact timing of the deformational events outside the study area is, however, not known.

Eisbacher (1981) has suggested that the northwest-trending structures in the Bowser Basin formed due to final suturing of the Stikine terrane with the North American cratonic margin. It is possible that the second phase noted in this study is related to interaction between two terranes not yet defined, as the Stikine terrane continued to move northwards along a major strike-slip fault system. Previous studies to the north (Souther, 1971; Monger, 1969; Monger et al., 1978) have noted a Mesozoic, southerly directed telescoping of strata along the King Salmon Fault near Dease Lake. It is possible that southerly directed transport related to the second phase of deformation in the study area is related to displacement along the King Salmon Fault. The minimum age of displacement (Monger et al., 1978) of the King Salmon Fault of 120 Ma ± 5 Ma is consistent with the youngest rocks in the study area (early Cretaceous?) having been deformed by the second phase of deformation. The presence of second phase 'blind thrusts' in the northern part of the Groundhog Coalfield and the apparent lack of superposed folding to the south (Bustin and Moffat, in press) suggests that strain related to the second phase dissipated in a southerly direction. This agrees well with the relationship noted by Souther (1971) in the Tulsequah map area where deformation south of the King Salmon Fault (footwall) is less intense than to the north (hanging wall). Further work is necessary to define the precise relationships between deformational events in the study area and adjacent areas.

References

Bustin, R.M. and Moffat, I.W.
– Groundhog Coalfield, Central British Columbia: Reconnaissance, stratigraphy and structure; Canadian Bulletin of Petroleum Geology. (in press)

Dietrich, H.H.
1969: Origin of cleavage in folded rocks; American Journal of Science, v. 267, p. 155-165.

Eisbacher, G.H.
1973: Tectonic framework of Sustut and Sifton Basins, British Columbia; Geological Survey of Canada, Paper 73-1, p. 24-26.

1974: Deltaic sedimentation in the northeastern Bowser Basin, British Columbia; Geological Survey of Canada, Paper 73-33, 13 p.

[1] In the notation utilized here 'a' is the direction of tectonic transport, 'c' is mutually perpendicular to 'a' as well as 'b' which is parallel to the fold axis.

Eisbacher, G.H. (cont.)
1981: Late Mesozoic – Paleogene Bowser Basin molasse and Cordilleran tectonics, Western Canada; in Sedimentation and Tectonics in Alluvial Basins, A.D. Miall (ed.); Geological Association of Canada, Special Paper 23, p. 125-151.

Geological Survey of Canada
1957: Stikine River Area, Cassiar District, British Columbia; Geological Survey of Canada, Map 9-1957.

Hancock. P.L.
1982: Distinction between cleavage and joints using fracture separation; in Atlas of Deformational and Metamorphic Rock Fabrics, G.J. Borradaile, M.B. Bayly and C. McA. Powell (eds.); Springer Verlag, 551 p.

Monger, J.W.H.
1969: Stratigraphy and structure of Upper Paleozoic rocks, northeast Dease Lake map area, British Columbia; Geological Survey of Canada, Paper 68-48, 41 p.

Monger, J.W.H., Richards, T.A., and Paterson, I.A.
1978: The Hinterland belt of Canadian Cordillera, new data from northern and central British Columbia; Canadian Journal of Earth Sciences, v. 15, p. 823-830.

Richards, T.A. and Gilchrist, R.A.
1979: Groundhog Coal Area, British Columbia; Geological Survey of Canada, Paper 79-1B, p. 411-414.

Souther, J.G.
1971: Geology and mineral deposits of Tulsequah map area, British Columbia; Geological Survey of Canada, Memoir 362, 84 p.

Tipper, H.W. and Richards, T.A.
1976: Jurassic stratigraphy and history of north-central British Columbia; Geological Survey of Canada, Bulletin 270, 73 p.

Tipper, H.W., Woodsworth, G.J., and Gabrielse, H.
1981: Tectonic assemblage map of the Canadian Cordillera and adjacent parts of the United States of America; Geological Survey of Canada, Map 1505A.

29.

PRELIMINARY OBSERVATIONS ON POCK MARKS AND FRACTURED PEBBLES IN THE UPPER CRETACEOUS AND PALEOCENE OF THE CENTRAL ALBERTA FOOTHILLS NEAR HINTON

Project 810039

T. Jerzykiewicz and D.R. Van Helden
Institute of Sedimentary and Petroleum Geology, Calgary

Jerzykiewicz, T. and Van Helden, D.R., Preliminary observations on pock marks and fractured pebbles in the Upper Cretaceous and Paleocene of the central Alberta Foothills near Hinton; in Current Research, Part B, Geological Survey of Canada, Paper 84-1B, p. 263-267, 1984.

Abstract

The Entrance and High Divide Ridge conglomerates, forming subordinate wedges within the continental Brazeau and Paskapoo formations, contain well rounded quartzose pebbles that reveal pock marks with fractures radiating from them. These features are due to the effects of tangentially oriented tectonic movements on the clast supported conglomerates. The stress was transmitted through the points of contact between the clasts, producing pock marks and tensile fractures extending across whole pebbles. The direction of the maximum compressive stress, measured as a line parallel to the major tensile fractures joining two opposite pock marks, shows a preferred orientation normal to the main NW-SE structural trend of the Rocky Mountains.

Résumé

Les conglomérats d'Entrance et de High Divide Ridge, qui forment des coins subordonnées aux formations continentales de Brazeau et de Paskapoo, contiennent des galets quartziques bien arrondis qui révèlent des cicatrices accompagnées de fractures rayonnant autour de celles-ci. Ces caractéristiques sont dues aux effets des mouvements tectoniques tangentiels aux conglomérats des terrains détritiques. La contrainte a été transmise par les points de contact entre les terrains détritiques, provoquant des cicatrices et des fractures dues à la traction s'étendant à tous les galets. La direction des contraintes à la compression maximale, mesurée selon une ligne parallèle aux fractures principales dues à la traction, en joignant deux cicatrices opposées, indique une orientation préférencielle normale à la direction structurale principale NW-SE des montagnes Rocheuses.

Introduction

Many clast supported conglomerates contain pebbles that reveal pock marks, fractures and striations produced during tectonic deformation as a result of strain in the rock mass. These so-called "tectonically significant" pebble types have been reported from many terrains that sustained long and/or repeated histories of deformation (e.g. Tanner, 1976).

The tectonically deformed pebbles discussed here were derived from the Entrance and High Divide Ridge conglomerates in the outer Foothills of the Rocky Mountains in the Athabasca River area (Fig. 29.1). These conglomerates can be considered as subordinate wedges within the Upper Cretaceous – Lower Tertiary Brazeau-Paskapoo clastic sequence. The commercially important coal-bearing Coalspur beds, straddling the Cretaceous/Tertiary boundary, occur within the Brazeau-Paskapoo sequence between the Entrance and High Divide Ridge conglomerates (Jerzykiewicz and McLean, 1980). Late Maastrichtian and mid-Paleocene ages for the Entrance and High Divide Ridge conglomerates, respectively, have been indicated by palynology (Eliuk, 1969; Sweet, personal communication, 1983).

Both the Entrance and High Divide Ridge conglomerates are composed of closely packed, well rounded quartz and quartzite pebbles. The only lithological difference between the conglomerates in question is the clast size. The diameters of the pebbles in the Entrance conglomerate average 5 to 8 cm, with maximum clast size reaching 20 cm. The clasts in High Divide Ridge conglomerate, on the other hand, are predominantly of cobble size, with maximum diameters reaching 40 cm. For the sake of simplicity the term "pebble" has been used in this paper to designate all deformed clasts.

The purpose of this article is to show the impact of compressive stress connected with the Laramide Orogeny on these pebbles.

Acknowledgments

The authors are grateful to Donald K. Norris who, as a reviewer of an earlier draft, made several comments which led to substantial improvement of the text. Palynological examinations by A.R. Sweet were invaluable in the age determination of the conglomerates. Appreciation and thanks are also extended to B.C. Rutley and W.B. Sharman for producing the photographs.

Deformation of the pebbles

Observations of the deformed pebbles were made in the Entrance quarry and in the outcrop of the High Divide Ridge conglomerate located about 8 km east of Hinton (Fig. 29.1; Pl. 29.1, fig. 1). Over 90 per cent of the pebbles in the conglomerates reveal varying signs of deformation, starting at the points of contact between pebbles (Pl. 29.1, figs. 2, 3).

Pock marks, which appear on the surface of the pebbles as numerous, light, oval spots or depressions, are the most common. Many of them are deeply indented by the intruding surfaces of neighbouring pebbles and are partly infilled with sandy matrix and powdered or recrystallized silica.

Fractures radiating from the pock marks are also common. They may die out either within the pebble (Pl. 29.1, fig. 5) or may transect the whole pebble (Pl. 29.1, fig. 8), causing varying degrees of deformation including shattering (Pl. 29.1, fig. 9).

1

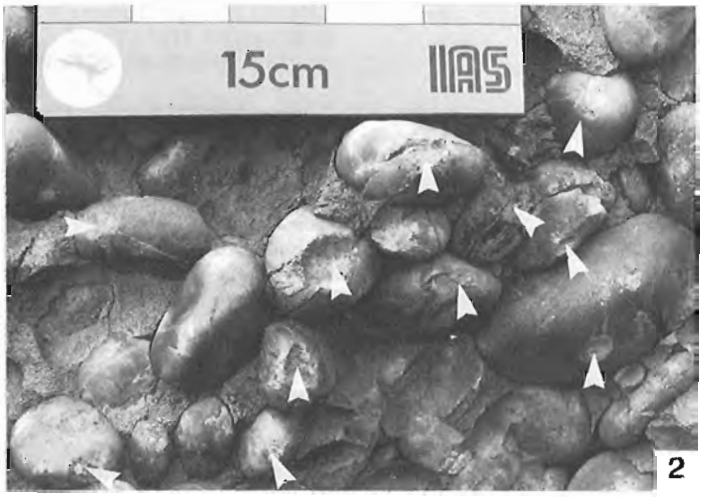

2

3

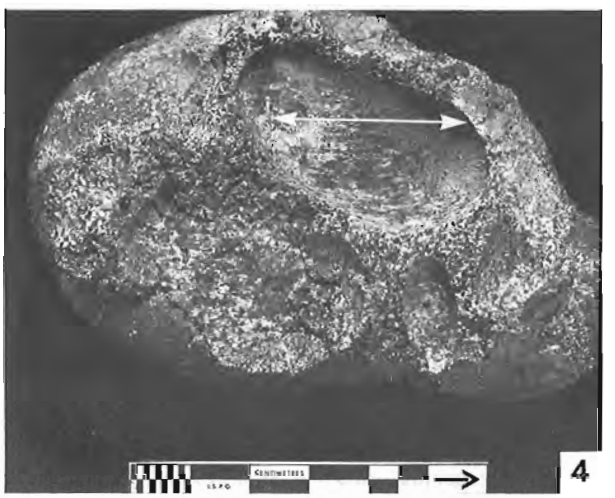

4

5

6

7

8

9

10

Many deformed pebbles have polished surfaces covered with sets of tiny parallel striations similar to those described by Clifton (1965). They are especially well developed on the large ab plane[1] of blade-shaped pebbles (Pl. 29.1, fig. 7), but similar features may also be visible around the edges of the pebbles or in the immediate vicinity of the pock marks.

Polished surfaces of a different character can be observed on the sandy infillings of some pock marks (Pl. 29.1, fig. 6) and within the conglomerate matrix on the imprints of the striated pebbles (Pl. 29.1, fig. 4). These surfaces are concave and smooth and are covered with recrystallized and parallel oriented grains of the matrix. This type of lineation is, spatially, closely related to the striations on the pebble surface and represents their counterpart, generated within the sandy matrix.

The presence of both slickensided pebbles (Pl. 29.1 fig. 10) and bedding planes has also been recorded in the Entrance and High Divide Ridge conglomerates, but their occurrence is rather sporadic.

PLATE 29.1

Examples of the main deformational features of the pebbles in the Entrance and High Divide Ridge conglomerates.

1. Part of the Entrance conglomerate quarry. The arrow indicates location of the next photograph.
2. Close-up view showing details of the deformed pebbles. The deeply indented pock marks are indicated by arrows.
3. Details of pebbles and imprints of pebbles in the same wall. The indented pock marks are designated by arrows on the pebble surface. Points of pebble contact visible inside the imprints are designated by asterisks.
4. Lineations caused by rotation of an elongate pebble visible on the pebble imprint within the sandy matrix. The white arrows indicate the direction of relative movement.
5. Fractures radiating from the pock mark (indicated by black arrow) and dying out within the pebble. The white arrows indicate direction of tiny striations visible on the polished surface of the pebble. Scale bar is 1 cm.
6. Shattered pebble with deeply indented pock mark in the middle. The concave surface of the pock mark is infilled with the sandy matrix, showing a parallel pattern of recrystallized grains. The lineation is indicated by the white arrows. Scale bar is 1 cm and stands also for the next four figures.
7. Polished ab plane of a blade-shaped pebble with the striation (indicated by the arrow) paralleling the longest axis of the pebble.
8. Fractures propagating across the pebble between two opposite pock marks visible in the section. The arrows indicate pock marks.
9. Example of shattered pebble. Deeply indented pock marks are indicated by arrows.
10. Slickensided pebble. Note the direction of movement (indicated by the black arrow) parallel to the long axis of the pebble.

Orientation of maximum strain and interpretation

The nature of some pock marks has been explained in terms of pressure solution at the points of pebble contact (Sorby, 1863; Kuenen, 1942; Klein, 1963). Some indented pock marks with fractures radiating from them, however, are believed to be produced by crushing or grinding processes during tectonic movements (Tanner, 1963, 1976).

Fractures radiating from pock marks analogous to those from the Entrance and High Divide Ridge conglomerates have been studied recently using electron microprobes and photoelastic experiments (McEwen, 1978, 1981). It has been demonstrated that a stress-controlled, low temperature, diffusional mass transfer process is responsible for the pebble pitting.

The types of fractures described by McEwen (1981), and their relationship to the maximum compressive stress affecting the pebbles, can be applied to the interpretation of the fractures that occur in the pebbles of the Entrance and High Divide Ridge conglomerates. The fractures originating from the pock marks and propagating through the pebbles to the opposing pock marks (Pl. 29.1, fig. 8) correspond to the fracture type 2a of McEwen (1981, p. 29). These fractures have been interpreted as tensile "due to approximately point loading on opposite sides of the pebble. Fractures propagate across the whole pebble because the high stress concentrations due to the point loads produce high tensile stresses in the region along their line of contact . . ." (McEwen, op. cit., p. 35).

The orientation of the local maximum stress can be measured therefore, as a line parallel to the major tensile fractures that join two opposite pock marks. Statistical data from both the Entrance and High Divide Ridge conglomerates indicate that the maximum compressive stress was transmitted in most cases through the pebble contacts approximately parallel to the bedding planes, showing a preferred orientation normal to the main NW-SE structural trend of the Rocky Mountains (Fig. 29.1). The layer-parallel orientation of the maximum compressive stress also has been concluded from measurements of the preferred orientation of extension and contraction faults in some coal mines in the eastern Cordillera (Norris, 1958).

The significance of tectonically deformed pebbles as a valuable tool for the study of deformational history has been recognized both in metamorphic and sedimentary rocks (e.g. Tanner, 1963, 1976; Hossack, 1968; Eisbacher, 1969; Gay, 1969; Thakur, 1974; Tyler, 1975; Sengupta, 1977; Roy and Gosh, 1979; McEwen, 1981). Intensively fractured and crushed pebbles from Tertiary quartzite gravels of central Alberta near Edmonton have been described by Babcock et al. (1978). These authors, however, believe that the gravels were deformed by ice-thrusting during continental glaciation.

The tectonic nature of pebble deformation presented here is not surprising. The Entrance and High Divide Ridge conglomerates were deposited and then deformed by compression during the Laramide Orogeny in the Cordillera. According to one generally accepted model of the orogenic history of the area, the Brazeau-Paskapoo sequence represents the youngest, nonmarine clastic wedge deposited during the final infilling of the foreland basin (Bally et al., 1966; Price and Mountjoy, 1970).

More comprehensive analysis of the deformational features of pebbles in the conglomerates in question is required (Jerzykiewicz, in prep.). The authors of the present article would like only to draw attention to the occurrence of pebbles deformed during the Laramide Orogeny in the Alberta Foothills.

[1] The plane containing the long (a) and intermediate (b) clast diameters

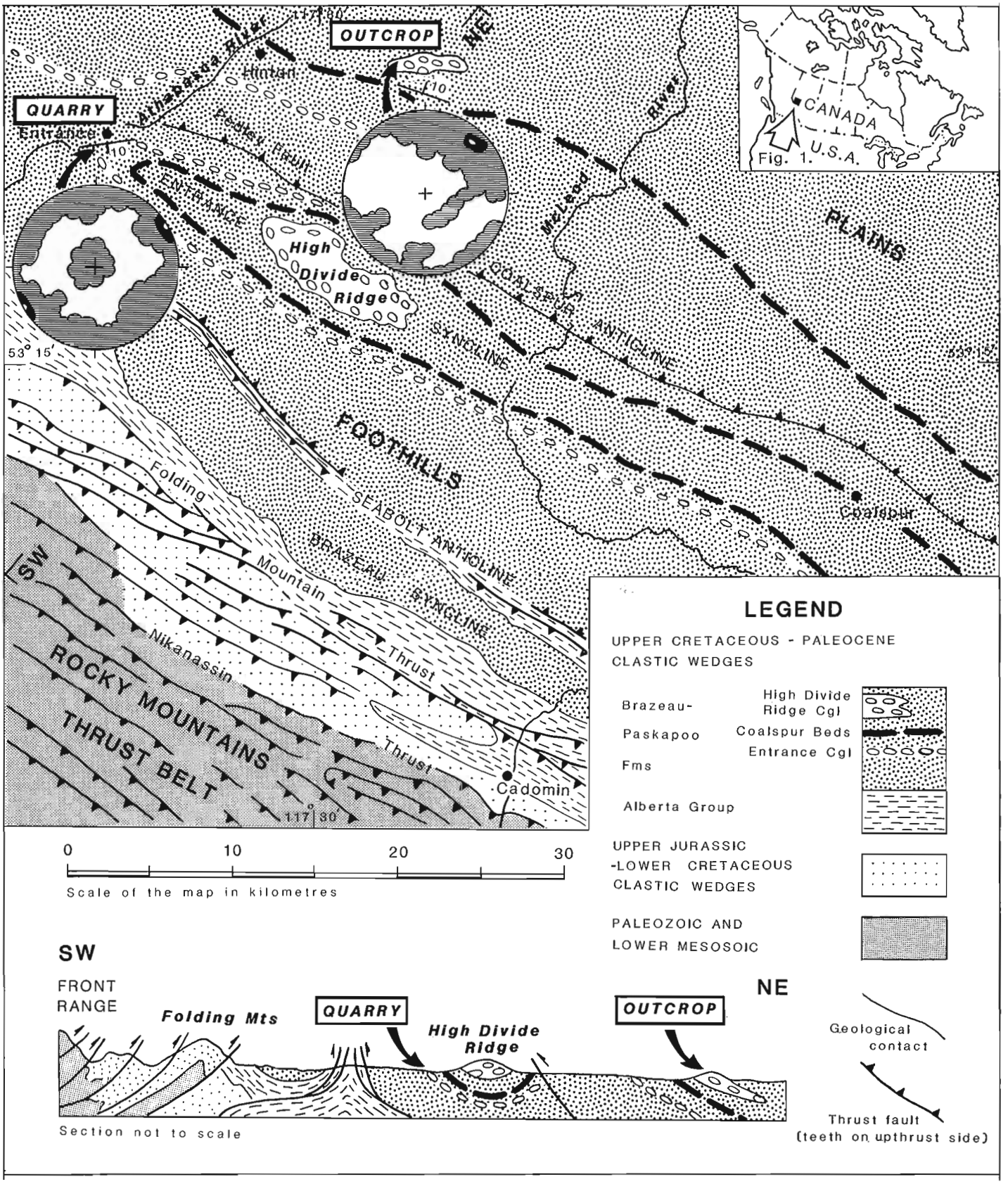

Figure 29.1. *Geological sketch map and structural section of the central Alberta Foothills between Athabasca and McLeod rivers, showing distribution of the Entrance and High Divide Ridge conglomerates and location of the outcrops. Geology simplified after Irish (1945), Lang (1945), MacKay (1929), Mountjoy (1960) and the authors' observations. INSETS: diagrams of the orientation of axes of the maximum strain in the Entrance conglomerate (100 measurements) and High Divide Ridge conglomerate (60 measurements). Schmidt Net, polar projection of the lower hemisphere. Contours: 0, 6, 10, maximum over 10 per cent.*

References

Babcock, E.A., Fenton, M.M., and Andriashek, L.D.
1978: Shear phenomena in ice-thrust gravels, central Alberta; Canadian Journal of Earth Sciences, v. 15, no. 2, p. 277-283.

Bally, A.W., Gordy, P.L., and Stewart, G.A.
1966: Structure, seismic data and orogenic evolution of southern Canadian Rocky Mountains; Bulletin of Canadian Petroleum Geology, v. 14, p. 337-381.

Clifton, H.E.
1965: Tectonic polish of pebbles; Journal of Sedimentary Petrology, v. 35, no. 4, p. 867-873.

Eisbacher, G.H.
1969: Displacement and stress field along part of the Cobequid Fault, Nova Scotia; Canadian Journal of Earth Sciences, v. 6, p. 1095-1104.

Eliuk, L.S.
1969: Correlation of the Entrance Conglomerate, Alberta, by Palynology; unpublished M.Sc. thesis, University of Alberta, Edmonton, Alberta, 143 p.

Gay, N.C.
1969: The analysis of strain in the Barberton Mountain Land, eastern Transval, using deformed pebbles; Journal of Geology, v. 77, no. 4, p. 377-396.

Hossack, J.R.
1968: Pebble deformation and thrusting in the Bygdin area (Southern Norway); Tectonophysics, v. 5, no. 4, p. 315-339.

Irish, E.J.W.
1945: Pedley map area, Alberta; Geological Survey of Canada, Paper 45-13.

Jerzykiewicz, T. and McLean, J.R.
1980: Lithostratigraphical and sedimentological framework of coal-bearing Upper Cretaceous and Lower Tertiary strata, Coal Valley area, central Alberta Foothills; Geological Survey of Canada, Paper 79-12, 47 p.

Klein, G. de V.
1963: Boulder surface markings in Quaco Formation (Upper Triassic), St. Martin's, New Brunswick, Canada; Journal of Sedimentary Petrology, v. 33, no. 1, p. 49-52.

Kuenen, Ph.H.
1942: Pitted pebbles; Leidische Geologische Mededelingen, v. 13, p. 189-201.

Lang, A.H.
1945: Entrance map area, Alberta; Geological Survey of Canada, Paper 45-11.

MacKay, B.R.
1929: Cadomin sheet; Geological Survey of Canada, Map 209A.

McEwen, T.J.
1978: Diffusional mass transfer processes in pitted pebble conglomerates; Contributions to Mineralogy and Petrology, no. 67, p. 405-415.

1981: Brittle deformation in pitted pebble conglomerates; Journal of Structural Geology, v. 3, no. 1, p. 25-37.

Mountjoy, E.W.
1960: Geology, Miette, Alberta; Geological Survey of Canada, Map 40-1959.

Norris, D.K.
1958: Structural conditions in Canadian coal mines; Geological Survey of Canada, Bulletin 44, 54 p.

Price, R.A. and Mountjoy, E.W.
1970: Geologic structure of the Canadian Rocky Mountains between Bow and Athabasca Rivers – a progress report; in Structure of the south Canadian Cordillera, J.O. Wheeler, (ed.); Geological Association of Canada, Special Paper 6, p. 7-25.

Roy, A. and Gosh, D.
1979: Study of a deformed conglomerate horizon in the Sandur Schist Belt, Bellary District, Karnataka; Journal Geological Society of India, v. 20, no. 7, p. 349-352.

Sengupta, S.
1977: Deformation of pebbles in relation to associated structures in parts of Singhbhum Shear Zone, Eastern India; Geologische Rundschau, v. 66, no. 1, p. 175-192.

Sorby, H.C.
1863: Ueber Kalkstein-Geschiebe mit Eindrucke; Neues Jahrbuch Mineralogie Abhandlung, p. 801-807.

Tanner, W.F.
1963: Crushed pebble conglomerate of southwestern Montana; Journal of Geology, v. 71, no. 5, p. 637-641.

1976: Tectonically significant pebble types: sheared, pocked and second-cycle examples; Sedimentary Geology, v. 16, no. 1, p. 69-83.

Thakur, V.C.
1974: Analysis of type of tectonic strain in polyphased deformed Molare area, Tessin, Switzerland, using deformed pebbles; Geologische Rundschau, v. 63, no. 1, p. 326-334.

Tyler, J.H.
1975: Fracture and rotation of brittle clasts in a ductile matrix; Journal of Geology, v. 83, no. 4, p. 501-510.

30.

A SULPHIDE DEPOSIT CONTAINING GALENA, IN THE LOWER DEVONIAN DISAPPOINTMENT BAY FORMATION ON BAILLIE HAMILTON ISLAND[1], CANADIAN ARCTIC ARCHIPELAGO

Project 650003

R. Thorsteinsson
Institute of Sedimentary and Petroleum Geology, Calgary

Thorsteinsson, R., A sulphide deposit containing galena, in the lower Devonian Disappointment Bay Formation on Baillie Hamilton Island, Canadian Arctic Archipelago; in Current Research, Part B, Geological Survey of Canada, Paper 84-1B, p. 269-274, 1984.

Abstract

Baillie Hamilton Island is situated in a region noted for lead and zinc deposits similar in many respects to the Mississippi Valley-type ore deposits. A sulphide deposit that includes small amounts of galena occurs in porous and vuggy dolomite of the Disappointment Bay Formation near the southwestern extremity of Baillie Hamilton Island. Mineralized deposits are rare in the Disappointment Bay Formation, and the present deposit adds further interest to this formation as a potential host for lead and zinc ore bodies. Most lead and zinc occurrences in this region of the archipelago, including that of the currently operated Polaris Mine, are replacement deposits in carbonate rocks of the Ordovician Thumb Mountain Formation that were exposed to erosion and karstification in Early Devonian time, and subsequently overlain unconformably by the Disappointment Bay Formation. Structural evidence is presented here that suggests the Disappointment Bay in southwestern Baillie Hamilton Island may lie directly on the Thumb Mountain. This in turn raises the possibility, however tenuous, that the sulphide deposit in that region indicates the presence of an ore body at depth in Thumb Mountain strata.

Résumé

L'île de Baillie Hamilton est située dans une région connue pour ses gisements de plomb et de zinc, semblables sous de nombreux aspects à ceux de la vallée du Mississippi. Un gisement de sulfure qui comprend de petites quantités de galène se trouve dans une dolomite cristallisée et poreuse de la formation de Disappointment Bay près de l'extrémité ouest de l'île Baillie Hamilton. Les gisements minéralisés sont rares dans la formation de Disappointment Bay, et ce gisement rend cette formation plus intéressante si on la considère comme pouvant contenir des gisements de plomb et de zinc. La plupart des manifestations de plomb et de zinc dans cette région de l'archipel, incluant celle de la mine de Polaris en cours d'exploitation, sont des gisements de remplacement dans des roches carbonatées de la formation ordovicienne de Thumb Mountain qui ont été mis à découvert par l'érosion et la karstification au début du Dévonien puis ont été recouverts ultérieurement, de façon non concordante, par la formation de Disappointment Bay. On présente des données structurales qui suggèrent que la formation de Disappointment Bay dans le sud-ouest de l'île Baillie Hamilton pourrait reposer directement sur la formation de Thumb Mountain. A son tour, ceci suggère la possibilité même si elle est mince, que le gisement de sulfures de la région indique la présence d'un gisement en profondeur dans les couches de Thum Mountain.

Introduction

Baillie Hamilton Island is situated about 13 km north of Cornwallis Island, in what is approximately the geographic centre of the Canadian Arctic Archipelago. Near the southwestern extremity of Baillie Hamilton Island, a small, but rather spectacular sulphide deposit, consisting mainly of pyrite and marcasite with small amounts of galena, occurs along the crest of an anticline that is exposed at the base of northwest-trending sea cliffs (Fig. 30.1, 30.2). The metallic minerals occur as infillings of pores and vugs in dolomite in the upper part of the lower member of the Lower Devonian Disappointment Bay Formation. The deposit occurs at 94°44'08"W, 75°46'16"N.

The deposit was discovered in late August of 1983 during a geological mapping traverse using a helicopter for transportation. About 10 minutes were devoted to examining the rocks at this locality. Six specimens of the mineralized rocks were collected. They have been analyzed by X-ray diffraction, and the results are summarized in Table 30.1.

Acknowledgments

I wish to record my thanks to G.D. Hobson, Director of the Polar Continental Shelf Project for logistic support during the course of field investigations; A.G. Heinrich of the Geological Survey for mineral analysis; Elspeth Snow of the Geological Survey for preparing the text figures; and Jennifer Robson who served as my field assistant in 1983.

Regional setting

Baillie Hamilton Island is part of the cratonic Boothia Uplift, a major geological province in the archipelago that extends north from Boothia Peninsula on the continental

[1] Baillie Hamilton Island was discovered in 1851 by Captain William Penny, commander of an expedition sent out by the British Admiralty to search for Sir John Franklin. Penny named the island Hamilton Island "after W.A.B. Hamilton, R.N., Secretary of the Admiralty" (Sutherland, 1952, v. 2, p. 127). However, the name of the island on the map that accompanied Sutherland's (op. cit.) narrative account of Penny's expedition was expanded to include Hamilton's commonly known christian name, and continued to appear as Baillie Hamilton Island on maps and in accounts of this region until the 1950s, after which time the name of this island has been almost invariably misspelled as Baillie-Hamilton Island.

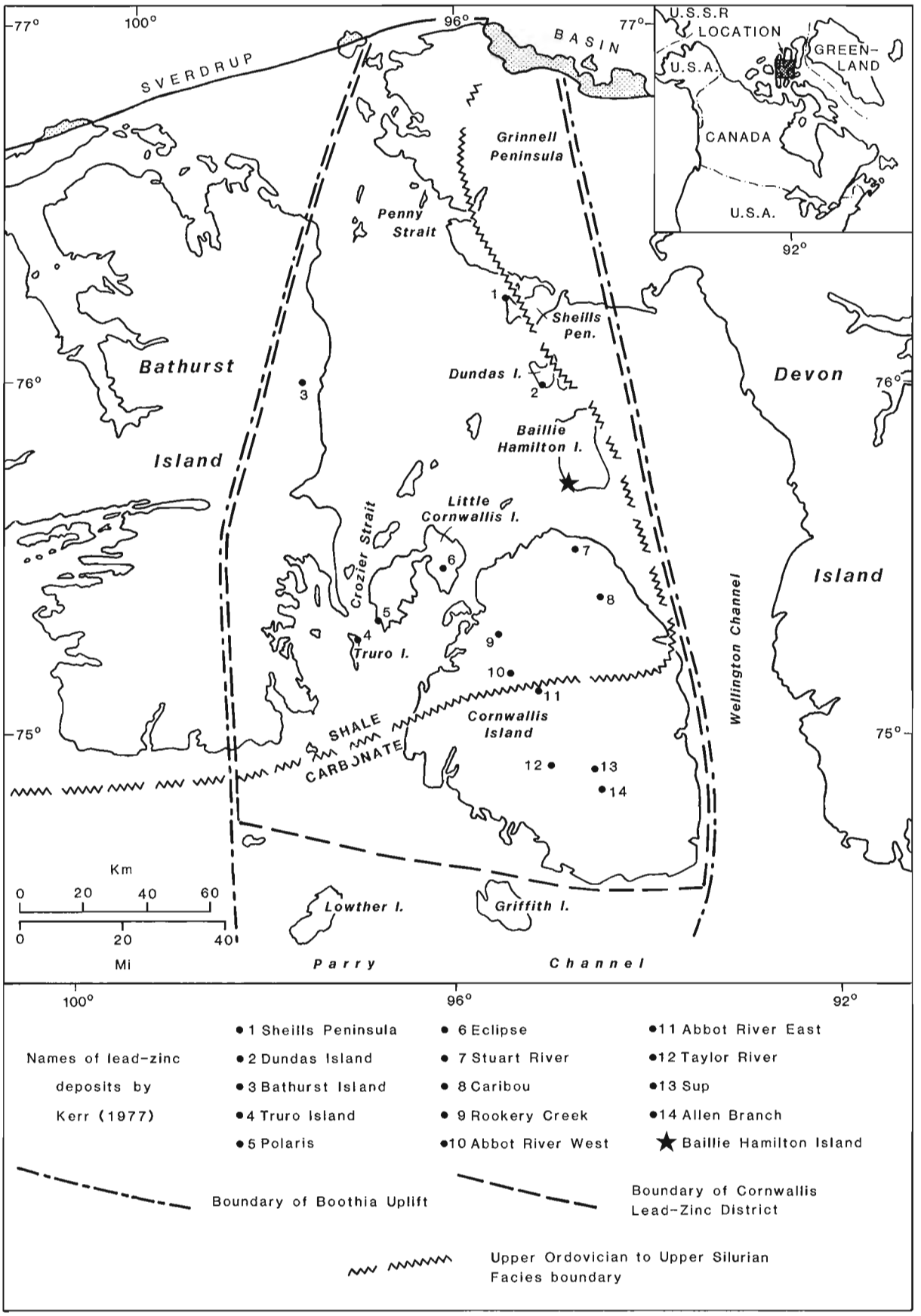

Figure 30.1. *Index map of the Cornwallis Lead-Zinc District (after Kerr, 1971).*

mainland to the north end of Grinnell Peninsula (see Thorsteinsson and Uyeno, 1981 and references contained therein). The uplift is about 800 km long and 150 km wide. South of Parry Channel, the uplift consists of Precambrian crystalline rocks and Proterozoic sediments which are flanked by mainly platform-type Cambrian to Late Silurian carbonate sediments, and Late Silurian to Early Devonian redbeds. North of the channel, the uplift includes mainly Cambrian to Lower Devonian miogeosynclinal carbonate sediments and lesser amounts of Lower Devonian redbeds. (Younger sequences of platform-type sediments that overspread this region are discussed below). The principal crustal movements by which the Boothia Uplift achieved its present areal extent and most of its present structural characteristics occurred in Late Silurian and Early Devonian times. The Late Silurian movements were limited to parts of the uplift situated south of Parry Channel, while Early Devonian movements occurred along the entire length of the uplift. The Upper Silurian and Lower Devonian redbeds mentioned above attest to these crustal movements. The structures in the Phanerozoic rocks of the uplift include mainly steeply dipping normal faults, generally broad, open synclines and more tightly folded anticlines (see for example, geological maps of the Cornwallis Island area by Thorsteinsson, 1973). The regional strike of these structures is northerly and thus aligned with the overall trend of the uplift.

North of Parry Channel, the Cambrian to Lower Devonian miogeosynclinal sediments that were deformed by the Early Devonian crustal movements are overlain unconformably by three sequences of sediments that are separated

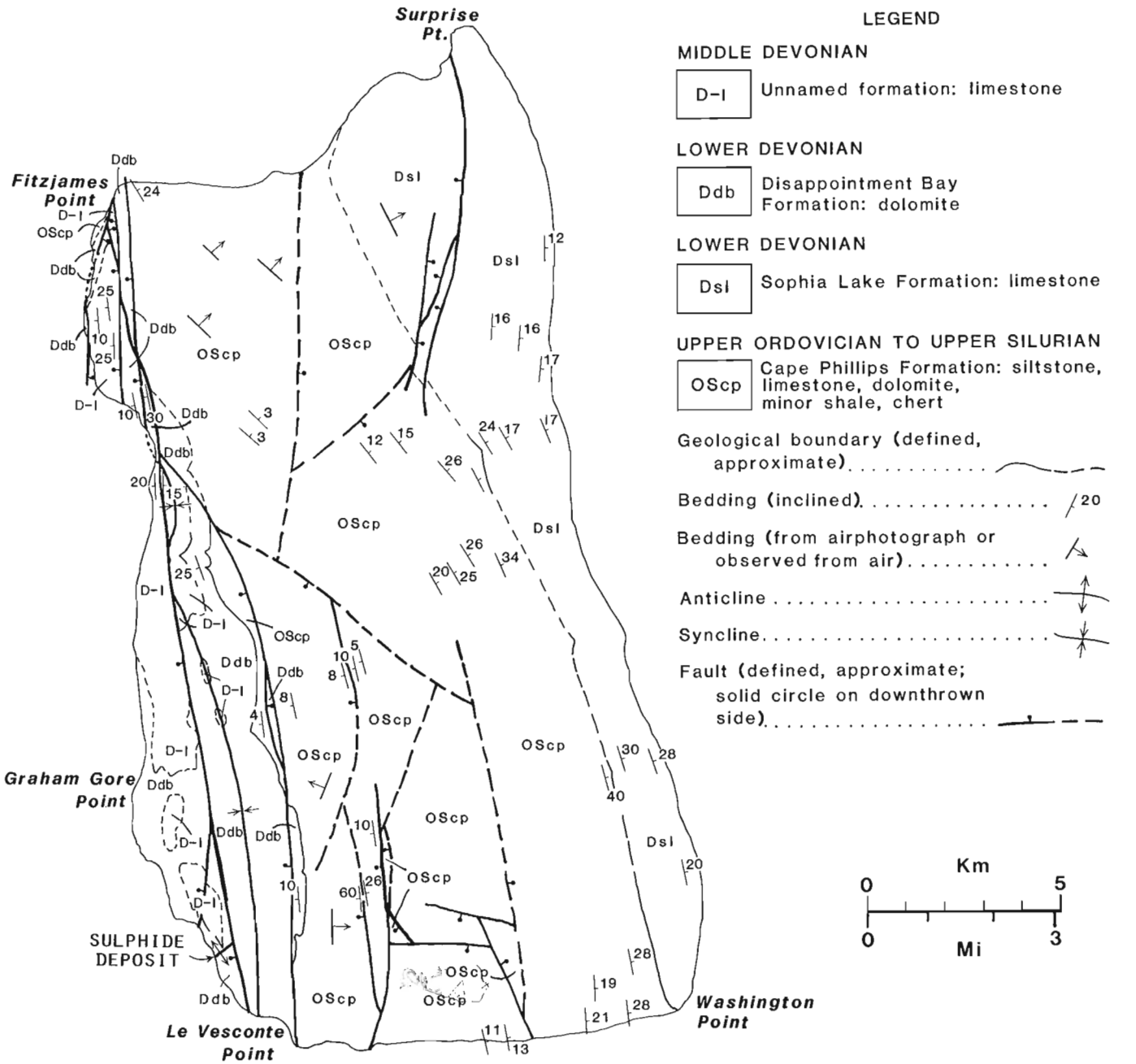

Figure 30.2. *Geological map of Baillie Hamilton Island.*

Table 30.1. Semi-quantitative X-ray diffraction analysis of samples

	#1	#2	#3	#4	#5	#6	#1	#6
Minerals	Whole-rock	Whole-rock	Whole-rock	Whole-rock	Whole-rock	Whole-rock	Metallic grain	Metallic grain
Metallic								
Galena	1.8	4.1	3.0				79.1	
Pyrite	18.3	32.0	55.5	23.2	4.7	13.7	4.1	29.9
Marcasite	20.7	57.0	27.3		4.0		4.1	
Goethite	1.8					1.3		6.9
Jarosite?		2.7	4.0					
Rock-forming								
Dolomite	1.2		10.1	71.4	81.0	82.2	2.5	56.3
Calcite	51.0			1.2	8.1			
Gypsum	2.5			1.8				2.3
Quartz	2.4			1.2				
Feldspar		4.1		1.2	2.0	2.7		
Clay							10.0	
Sulphur?								4.6

from one another by regional unconformities. These sequences occur mainly as downfaulted or downfolded outliers, and the regional trend of the folds and faults that affect them, is, like the earlier established Early Devonian trends, northerly. The sequences are described briefly from oldest to youngest as follows:

1. A conformable succession including in order upward:
   a. Disappointment Bay Formation; Lower Devonian dolomite.
   b. Unnamed formation, Middle Devonian limestone.
   c. Bird Fiord Formation; Middle Devonian sandstone and lesser amounts of limestone.
   d. Hecla Bay Formation; Middle and Upper Devonian mainly nonmarine sandstone.
2. Isachsen Formation; Lower Cretaceous nonmarine sandstone and siltstone.
3. Eureka Sound Formation; Upper Cretaceous to Lower Tertiary, mainly nonmarine sandstone and siltstone.

Stratigraphy and structural geology of Baillie Hamilton Island

The strata exposed on Baillie Hamilton Island are divisible into two structurally conformable sequences separated from one another by an angular unconformity (Fig. 30.2). The older sequence includes the Cape Phillips Formation and overlying Sophia Lake Formation. These formations outcrop in eastern parts of Baillie Hamilton Island, and together they constitute surface exposures for over more than three quarters of the island. The regional strike of these formations is northerly, and they generally dip eastward. The younger sequence is made up of the Disappointment Bay Formation and an overlying unnamed unit of limestone. These formations occupy a narrow strip of territory along the west side of the island. The regional strike and dip of these rocks is north and west, respectively. Both the older and younger sequence are cut by steeply dipping, mainly north-striking normal faults.

Cape Phillips Formation

The formation consists mainly of siltstone that is variably argillaceous, calcareous and dolomitic; limestone that is cryptocrystalline to finely crystalline and variably argillaceous, silty and dolomitic; and dolomite that is commonly finely crystalline and variably argillaceous, silty and calcareous. All of these rocks are typically dark grey, thin bedded and laminated. Also present are lesser amounts of shale and chert. Other notable features of the formation include mass-flow deposits, soft sediment deformation and abundant graptolites. The Cape Phillips ranges from Late Ordovician to Late Silurian in age. The lower part of the Cape Phillips is not exposed on Baillie Hamilton Island. However, the formation is about 3000 m thick as determined on neighbouring Cornwallis Island, and by far the greater part of it is exposed on Baillie Hamilton Island. To the east and southeast, the graptolitic beds of the Cape Phillips Formation pass laterally into a sequence of four shelf-type carbonate formations. These formations include, in upward stratigraphic order, Allen Bay, Cape Storm, Douro and Barlow Inlet (see Thorsteinsson and Uyeno, 1981). The line of facies change is shown in Figure 30.1.

Two widely distributed formations that underlie the Cape Phillips in the archipelago, though not exposed on Baillie Hamilton Island, are pertinent to the present discussions. They are the Irene Bay and Thumb Mountain formations. The Irene Bay is separated from the Cape Phillips by a sharp, yet conformable contact. It is a unit of Upper Ordovician greyish green shale with lesser amounts of limestone. It ranges in thickness from 35 to 45 m. The Irene Bay conformably overlies the Thumb Mountain Formation, which consists mainly of limestone and dolomite and subordinate amounts of shale. The Thumb Mountain is about 340 m thick on nearby Cornwallis Island, where, moreover, it appears to be variably dolomitized. In places, the formation appears to consist almost entirely of limestone; in others it is largely dolomite.

Sophia Lake Formation

The Sophia Lake Formation on Baillie Hamilton Island is represented by about 780 m of dominantly medium grey, aphanocrystalline to finely crystalline limestone. The contact of the Sophia Lake with the underlying Cape Phillips is gradational, and marked by a change from a thick unit of siltstone at the top of the latter formation to limestone in the former. The upper surface of the Sophia Lake Formation on the island is represented by the present day erosion surface so that the total thickness of the formation is unknown. The formation is dated as early Early Devonian by Thorsteinsson and Uyeno (1981).

The Sophia Lake exhibits a broad threefold subdivision on the island:

1. A lower unit, about 190 m thick, consisting mainly of thin and planar bedded limestone that passes upwards into medium bedded, nodular limestone. Minor amounts of shale and siltstone occur throughout this unit. The unit is rich in brachiopods, trilobites and conodonts.
2. A middle unit, about 140 m thick, consisting of thick-to mainly medium- and thin-bedded limestone with subordinate shale and siltstone beds. The unit is characterized by corals, stromatoporoids and brachiopods.
3. An upper unit, about 440 m thick, composed mainly of thin-bedded limestone with lesser amounts of dolomite, dolomitic limestone and siltstone. The rocks are rich in leperditicopod ostracodes. The upper 60 m or so of this unit are characterized by an increasing abundance of thin interbeds of siltstone and sandstone including a single unit of chert-pebble conglomerate about one metre thick.

Disappointment Bay Formation

The formation includes two distinctive members on Baillie Hamilton Island. The lower member is made up of resistant thin- to thick-bedded and massive dolomite that ranges from finely- to medium-crystalline, and from yellowish grey to medium grey. Porous to vuggy intervals are well developed in some sections, and are commonly impregnated with bitumen. The thickness of the member is estimated as 70 m. The upper member consists mainly of soft-weathering, variably silty and sandy dolomite that is finely crystalline, thin bedded and ranges from shades of brown to green. This member is about 140 m thick. The contact between the lower and upper members is sharply defined. The possibility that this contact may represent an unconformity is suggested by the fact that a unit of chert-pebble conglomerate, less than half a metre thick, is developed sporadically at the base of the upper member. The basal chert-pebble conglomerate that characterized the formation throughout much of the Cornwallis Island area is apparently absent on Baillie Hamilton Island. The formation has been dated as late Early Devonian on the basis of conodonts (Thorsteinsson and Uyeno, 1981).

Unnamed limestone formation

A unit of limestone, about 100 m thick, overlies the Disappointment Bay Formation with a sharp, yet conformable contact, and represents the youngest bedrock formation preserved on Baillie Hamilton Island. The top of the unit is not preserved on the island, but on neighbouring Cornwallis Island the unit is overlain by the Middle Devonian (Eifelian) Bird Fiord Formation.

The limestone unit, as developed on Baillie Hamilton Island, is typically variably silty and sandy, finely crystalline, and thin- to mainly medium-bedded. The colour of these rocks varies from shades of grey to shades of brown. Very thin interbeds of shale and greenish sandstone occur in some sections.

This unit of limestone has been referred to the Blue Fiord Formation (see for example Thorsteinsson and Kerr, 1968), but it is probably best considered as representing a new, and as yet unnamed formation. At its type section in southwestern Ellesmere Island the Blue Fiord is Early Devonian (Zlichovian to Dalejan; see Uyeno and Klapper, 1980), and therefore correlative with the Disappointment Bay Formation, whereas the limestone beds in question here are Middle Devonian (Eifelian) in age (Uyeno, personal communication). The limestone beds thus equate with the lower part of the type section of the Bird Fiord Formation, which also occurs on southwestern Ellesmere Island.

Significance of sulphide deposit

Baillie Hamilton Island is situated in the Cornwallis Lead-Zinc District, a name proposed by Kerr in 1977. The district coincides with the northern part of the Boothia Uplift (Fig. 30.1). Kerr described 14 lead-zinc deposits in the district, one of which is now in production (Polaris Mine) on the west coast of Little Cornwallis Island. According to Kerr most of these deposits are characterized by the following controls on mineralization:

1. The Middle to Upper Ordovician Thumb Mountain Formation is the host.
2. The mineralized part of this formation is brecciated dolomite.
3. The deposits occur within the distributive area of the graptolitic Cape Phillips Formation.
4. The lead-zinc deposits were at one time overlain unconformably by the Disappointment Bay Formation. Kerr has argued convincingly that the lead-zinc mineralization occurred as replacement deposits in karst caverns that developed in the Thumb Mountain Formation in places where that formation was structurally high and exposed during the Early Devonian interval of erosion marked by the unconformity at the base of the Disappointment Bay Formation.

The sulphide deposit in southwestern Baillie Hamilton Island is of interest for two reasons: 1. sulphide deposits in the Disappointment Bay Formation are rare (Kerr, 1977), and the present deposit adds further interest in this formation as a potential host for lead-zinc ore bodies in the Cornwallis district; and 2. there is a possibility, however tenuous, that the Disappointment Bay at the locality of this deposit lies directly on the Thumb Mountain Formation, and that the deposit represents the uppermost mineralized part of an ore body at depth in the latter formation. This possibility is based on the following lines of reasoning. The graptolites in the Cape Phillips indicate that all four series of the Silurian are represented in exposures of the formation, and furthermore that these series comprise north-trending belts of exposures. Thus, as one proceeds westward from any given point on the Cape Phillips-Sophia Lake contact one passes progressively, first across Pridolian beds, next across Ludlovian and Wenlockian beds, and lastly across late Llandoverian beds, which are overlain by easternmost outcrops of the Disappointment Bay Formation. This situation prompts the following conclusions:

1. It confirms that the regional dip of the Cape Phillips Formation is to the east.
2. It indicates that the normal faults transecting the formation are characterized by modest displacements.

3. It indicates that only the lower Llandoverian and Ashgillian (Upper Ordovician) parts of the Cape Phillips Formation are not exposed on Baillie Hamilton Island. The thickness of this interval of beds in nearby Dundas Island and Cornwallis Island is in the order of 200 m. On the basis of the foregoing circumstances, and the assumption that the easterly dip of Cape Phillips beds continues westward beneath the unconformable cover of the Disappointment Bay, westernmost strata of the latter formation in the environs of the sulphide deposit may well lie directly on the Thumb Mountain Formation. Such a stratigraphic-structural situation would exhibit all four of Kerr's (1977) controls for lead-zinc mineralization in this region.

References

Kerr, J.W.
1977: Cornwallis lead-zinc district; Mississippi Valley-type deposits controlled by stratigraphy and tectonics; Canadian Journal of Earth Sciences, v. 14, no. 6, p. 1402-1426.

Sutherland, P.C.
1852: Journal of a voyage in Baffin's Bay and Barrow Straits, in the year 1850-51, performed by H.M. ships **Lady Franklin** and **Sophia** under the command of William Penny; v. 1-2, Longman, Brown, Green, and Longman, London.

Thorsteinsson, R.
1973: Prince Alfred Bay (59B), Resolute (58F), Baillie Hamilton Island (58G), Lowther Island (68E) and McDougall Sound (68H) map areas, Arctic Islands; Geological Survey of Canada, Open File Report 139.

Thorsteinsson, R. and Kerr, J.W.
1968: Cornwallis and adjacent smaller islands, Canadian Arctic Archipelago; Geological Survey of Canada, Paper 67-64.

Thorsteinsson, R. and Uyeno, T.T.
1981: Stratigraphy and conodonts of Upper Silurian and Lower Devonian rocks in the environs of the Boothia Uplift, Canadian Arctic Archipelago; Geological Survey of Canada, Bulletin 292.

Uyeno, T.T. and Klapper, G.
1980: Summary of conodont biostratigraphy of the Blue Fiord formations (Lower-Middle Devonian) at the type and adjacent areas, southwestern Ellesmere Island, Canadian Arctic Archipelago; in Current Research, Part C; Geological Survey of Canada, Paper 80-1C, p. 81-93.

31. STRATIGRAPHIC SUBDIVISION OF THE ROCHE POINT, HOYLE BAY AND BARROW FORMATIONS (SCHEI POINT GROUP), WESTERN SVERDRUP BASIN, ARCTIC ISLANDS

Project 750083

Ashton F. Embry
Institute of Sedimentary and Petroleum Geology, Calgary

Embry, A.F., Stratigraphic subdivision of the Roche Point, Hoyle Bay and Barrow formations (Schei Point Group), western Sverdrup Basin, Arctic Islands; in Current Research; Part B, Geological Survey of Canada, Paper 84-1B, p. 275-283, 1984.

Abstract

In the western Sverdrup Basin the Roche Point, Hoyle Bay and Barrow formations (Schei Point Group, Middle-Upper Triassic) have been subdivided into formal members on the basis of subsurface stratigraphic analysis. Four members are recognized in the Roche Point Formation, and in ascending order are named Eldridge Bay (sandstone), Cape Caledonia (shale-siltstone), Chads Point (sandstone) and Gore Point (limestone, sandstone). The source area for the clastics of the lower three members lay to the south whereas the source for the Gore Point was to the north. The Hoyle Bay Formation is divided into two members: Eden Bay (shale, siltstone, limestone) and Cape Richards (shale, siltstone). The source area for these units was to the north. One member, the Jenness (sandstone, siltstone and shale) is recognized within the Barrow Formation, and its source area lay to the northwest.

Résumé

Une analyse stratigraphique du sous-sol nous a permis de subdiviser, dans le bassin de Sverdrup occidental, les formations de Roche Point, Hoyle Bay and Barrow (groupe de Shei Point, Trias moyen et supérieur) en membres. On a subdivisé la formation de Roche Point en quatre membres qui sont dans un ordre ascendant: Eldridge Bay (grès), Cape Caledonia (schiste argileure-siltstone), Chads Point (grès) et Gore Point (calcaire, grès). La source des roches clastiques des trois membres inférieurs se trouve au sud, alors que celle de Gore Point se trouve au nord. On subdivise la formation de Hoyle Bay en deux membres: Eden Bay (schiste argileux, siltstone, calcaire) et Cape Richards (schiste argileux, siltstone). La source de ces unités se trouve au nord. La formation de Barrow contient le membre de Jenness (grès, siltstone et schiste argileux) dont la source se trouve au nord-ouest.

Introduction

The Schei Point Group comprises Middle to Upper Triassic strata on the flanks of the Sverdrup Basin, and it contains five formations: Murray Harbour, Roche Point, Hoyle Bay, Pat Bay and Barrow (Embry, 1984). These formations are widespread in the subsurface of the western Sverdrup Basin (Fig. 31.1) and have been penetrated by 42 wells. Three of the formations – Roche Point, Hoyle Bay and Barrow – have been subdivided into members over portions of the western Sverdrup Basin.

Four members have been recognized in the Roche Point Formation, a sandstone – dominant unit of Anisian to Carnian age. These members, in ascending order, are named Eldridge Bay, Cape Caledonia, Chads Point and Gore Point. The Hoyle Bay Formation consists mainly of shale and siltstone of Carnian age and is subdivided into two members: Eden Bay (lower) and Cape Richards. One formal member, the Jenness, is recognized in the Barrow Formation, a Norian shale-siltstone unit.

These seven new members are formally defined and described in this paper. Tops for the members in selected wells in the western Sverdrup (Fig. 31.1) are listed in the Appendix. Chip samples from the type sections of the units defined may be examined at the Institute of Sedimentary and Petroleum Geology, Calgary, Alberta.

Eldridge Bay Member, Roche Point Formation

Definition

The Eldridge Bay Member consists predominantly of very fine- to medium- grained sandstone with interbeds of siltstone and shale. The type section is in the Panarctic North Sabine H-49 well (N76°48'15", W108°45'11"; spud. May 2, 1974, abandoned July 8, 1974; T.D. 3787 m, K.B. 60 m) between 3628 m (11 901 ft) and 3798 m (12 458 ft), and is 170 m thick (Fig. 31.2). The name is taken from Eldridge Bay, which is on the west coast of Sabine Peninsula, Melville Island.

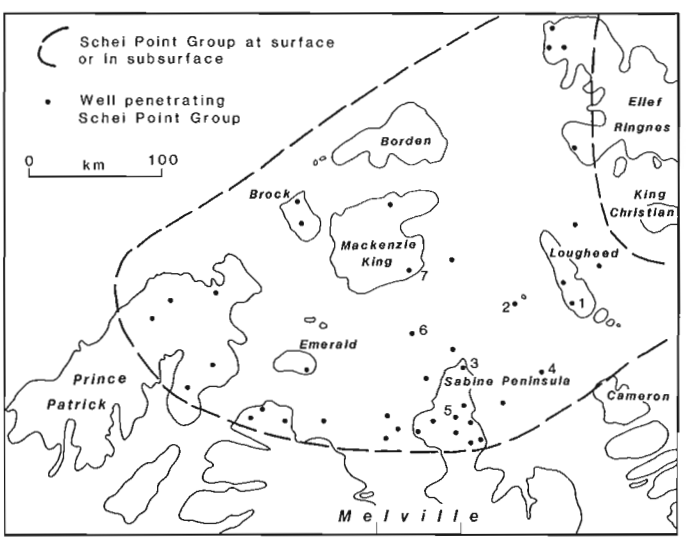

Figure 31.1. *Distribution of Schei Point Group in western Sverdrup Basin and available control points. Key to wells listed in Appendix: 1. Skybattle Bay C-15, 2. Whitefish 2H-63, 3. North Sabine H-49, 4. Desbarats B-73, 5. Drake Point D-68, 6. Hazen F-54, 7. Cape Norem A-80.*

Synonym

Bjorne Formation, Sabine Peninsula, Melville Island (Henao-Londono, 1977).

Boundaries

The Eldridge Bay Member conformably overlies the Murray Harbour Formation (shale-siltstone), with the contact placed at the base of the first sandstone unit above which sandstone is predominant. The Eldridge Bay is conformably overlain by the Cape Caledonia Member of the Roche Point Formation. This contact is placed at the top of the highest sandstone unit above which shale and siltstone become predominant (Fig. 31.2).

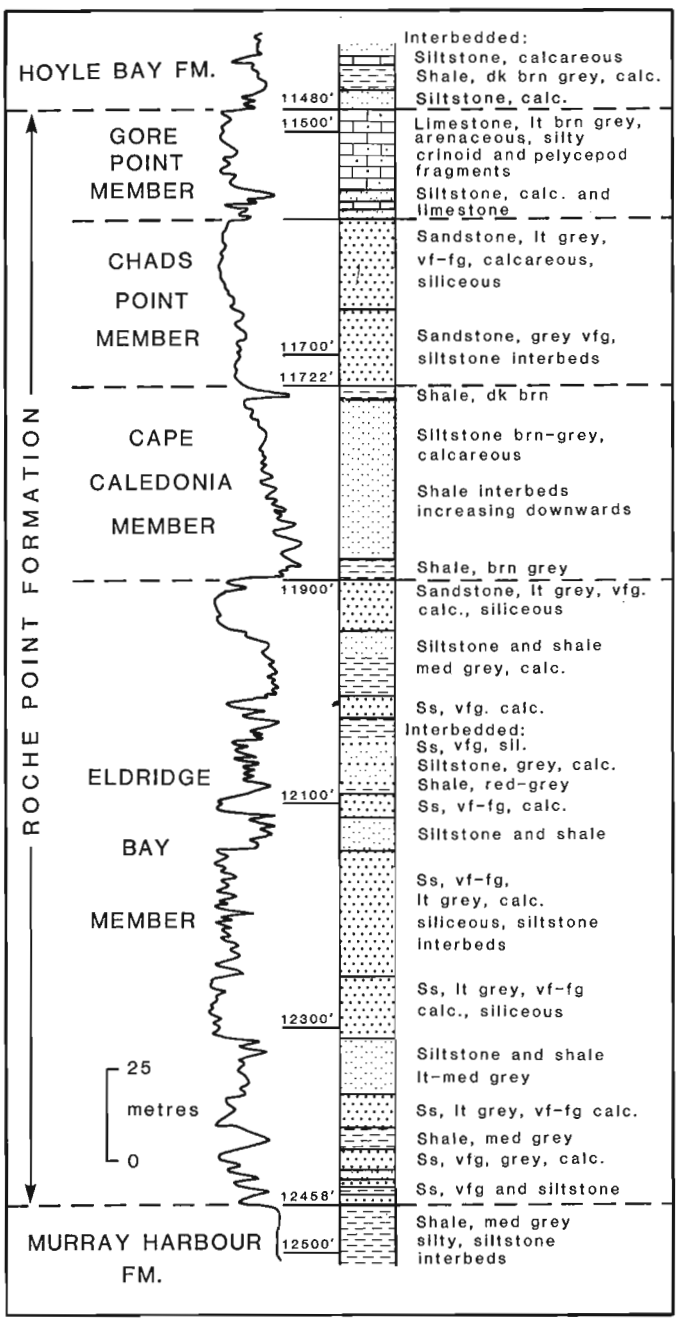

Figure 31.2. *Lithology (from samples) and gamma-ray curve for type sections of Eldridge Bay, Cape Caledonia, Chads Point and Gore Point members, Roche Point Formation; North Sabine H-49 well.*

Lithology

In the type section, the Eldridge Bay Member consists mainly of fine- to medium-grained, calcareous sandstone. Individual sandstone units may be up to 10 m thick but most of the units are 2-5 m thick. Thin units of shale and siltstone occur between the sandstones. The argillaceous lithologies are usually grey but red and green shale interbeds are present.

To the north and east of the type section shale and siltstone become more common in the Eldridge Bay, and distinct coarsening-upward cycles up to 40 m thick are present. On the southern basin margin red shale and siltstone are common in the Eldridge Bay and fining-upward cycles are indicated on gamma-ray logs.

Thickness and distribution

The Eldridge Bay Member is recognized on Sabine Peninsula, Melville Island and in the adjacent offshore areas. It disappears to the northeast due to a facies change to shale and siltstone, and is truncated by erosion (Jurassic) on the basin margin. To the west, in the Prince Patrick and Brock islands area, the Eldridge Bay is not recognized and equivalent strata are in undivided Roche Point Formation. The maximum recorded thickness of the Eldridge Bay is 170 m.

Age

The Eldridge Bay Member is interpreted to be Anisian (early Middle Triassic) in age on the basis of its correlation with the lower Murray Harbour Formation, which is well dated (Embry, 1984).

Environment of deposition

Much of the Eldridge Bay was deposited on a shallow marine shelf as is evidenced by the lithologies, fauna, cyclicity and stratigraphic relationships (Embry, 1984). On the southern basin margin, fluvial-deltaic plain strata are common within the member (red shales, fining-upward cycles).

Cape Caledonia Member, Roche Point Formation

Definition

The Cape Caledonia Member consists of shale and siltstone with minor interbeds of very fine grained sandstone. The type section is in the Panarctic North Sabine H-49 well between 3573 m (11 722 ft) and 3628 m (11 901 ft), and is 55 m thick (Fig. 31.2). The name is taken from Cape Caledonia, which is on the eastern side of Sabine Peninsula, Melville Island.

Boundaries

The Cape Caledonia Member conformably overlies the Eldridge Bay Member as described previously. The member is conformably overlain by the Chads Point Member of the Roche Point Formation with the contact placed at the base of the first sandstone unit above which sandstone is predominant (Fig. 31.2). On the basin margins, the Cape Caledonia is unconformably overlain by the Gore Point Member of the Roche Point Formation.

Lithology

The Cape Caledonia Member consists predominantly of shale and siltstone. Shale units are usually medium to dark grey, but dark brown, bituminous shale is also common in the member. Siltstone units may be up to 3 m thick and become more frequent upward in the member. Thin, very fine grained sandstone units are sometimes present in the uppermost portion of the member.

Thickness and distribution

The Cape Caledonia Member is present in the Sabine Peninsula area and the adjacent offshore. To the north and east it becomes part of the undivided Murray Harbour Formation due to the shale-out of the underlying Eldridge Bay Member (Fig. 31.3). Westward in the Prince Patrick-Brock Island area equivalent strata are sandstones of the undivided Roche Point Formation.

The maximum recorded thickness of the Cape Caledonia Member is 54 m.

Age

The Cape Caledonia is interpreted to be Anisian-Ladinian (Middle Triassic) in age on the bases of correlation with dated surface sections (Embry, 1984).

Environment of deposition

The lithologies and stratigraphic relationships of the Cape Caledonia indicate an offshore shelf environment of deposition (Embry, 1984). The common occurrence of bituminous shale in the member suggests that bottom waters were poorly oxygenated over portions of the shelf.

Chads Point Member, Roche Point Formation

Definition

The Chads Point Member consists predominantly of very fine- to medium-grained sandstone with thin interbeds of siltstone. The type section is in the Panarctic North Sabine H-49 well between 3530 m (11 578 ft) and 3574 m (11 722 ft) and is 44 m thick (Fig. 31.2). The name is taken from Chads Point, which is on the west side of Sabine Peninsula, Melville Island.

Boundaries

At the type section, the Chads Point Member conformably overlies the Cape Caledonia Member, as discussed previously. Northeast of Sabine Peninsula, where the Cape Caledonia Member is not recognized, the Chads Point Member overlies the Murray Harbour Formation, with the contact placed at the base of the first sandstone above which sandstone is predominant. The Chads Point is overlain by the Gore Point Member of the Roche Point Formation, with the contact placed at the top of the highest sandstone unit above which limestone is the predominant lithology. This contact is usually conformable, but on southern Sabine Peninsula the contact is unconformable and the Roche Point Member overlaps the Chads Point.

Lithology

The Chads Point Member consists mainly of very fine- to medium-grained sandstone with thin siltstone interbeds in the lower portion. In general the lithologies coarsen upward and, combined with the shale and siltstone of the underlying Cape Caledonia Member, form a coarsening-upward, regressive succession. The sandstone is usually light grey and characteristically contains chert (white, grey and black) grains as well as quartz. Cements include quartz, chalcedony and calcite, and porosity in the sandstone varies from near zero to 10 per cent.

Thickness and distribution

The Chads Point Member occurs in the Sabine Peninsula-Lougheed Island area of the western Sverdrup Basin. Farther northeastward the sandstones shale-out and equivalent shale and siltstone are assigned to the Murray Harbour Formation (Embry, 1984). In the Prince Patrick-Brock islands area the member is not recognized and equivalent strata are in the undivided Roche Point Formation. On southern Sabine Peninsula the Chads Point Member is truncated and overstepped by the Gore Point Member. The maximum recorded thickness for the Chads Point Member is 44 m.

Age

The Chads Point Member is interpreted to be Ladinian in age on the basis of correlation with well dated surface sections (Embry, 1984).

Environment of deposition

The lithologies and stratigraphic relationships of the Chads Point Member suggest a shallow marine shelf depositional environment for the unit.

Gore Point Member, Roche Point Formation

Definition

The Gore Point Member consists predominantly of limestone with subordinate calcareous sandstone and siltstone. The type section is in the Panarctic North Sabine H-49 well between 3499 m (11 480 ft) and 3530 m (11 578 ft) and is 31 m thick (Fig. 31.2). The name is taken from Gore Point, which is on the east side of Sabine Peninsula, Melville Island.

Synonym

Second Limestone, Schei Point Formation, (informal oil industry term).

Boundaries

As described previously, the Gore Point Member overlies the Chads Point Member. On the southern margin of the basin the Gore Point overlaps the Chads Point Member and rests unconformably on either the Cape Caledonia or Eldridge Bay Member. The Gore Point Member is conformably overlain by the Hoyle Bay Formation, with the contact placed at the base of the lowest shale-siltstone unit above which shale and siltstone are predominant.

Lithology

At the type section the Gore Point consists mainly of silty, bioclastic limestone (wackestone-packstone). Pelecypod, crinoid and possibly bryozoan fragments occur in a matrix of lime mud and quartz silt and clay. Thin, calcareous, quartz siltstone units are present and are most common in the lower portion of the member. Southward on Sabine Peninsula siltstone becomes less common and skeletal fragments are more abundant in the limestone. Northeastwards, in the Lougheed Island area, siltstone content increases and very fine grained, calcareous sandstone units up to 3 m thick occur interbedded with the limestone. In the Prince Patrick-Brock Island area the Gore Point is much like that at the type section.

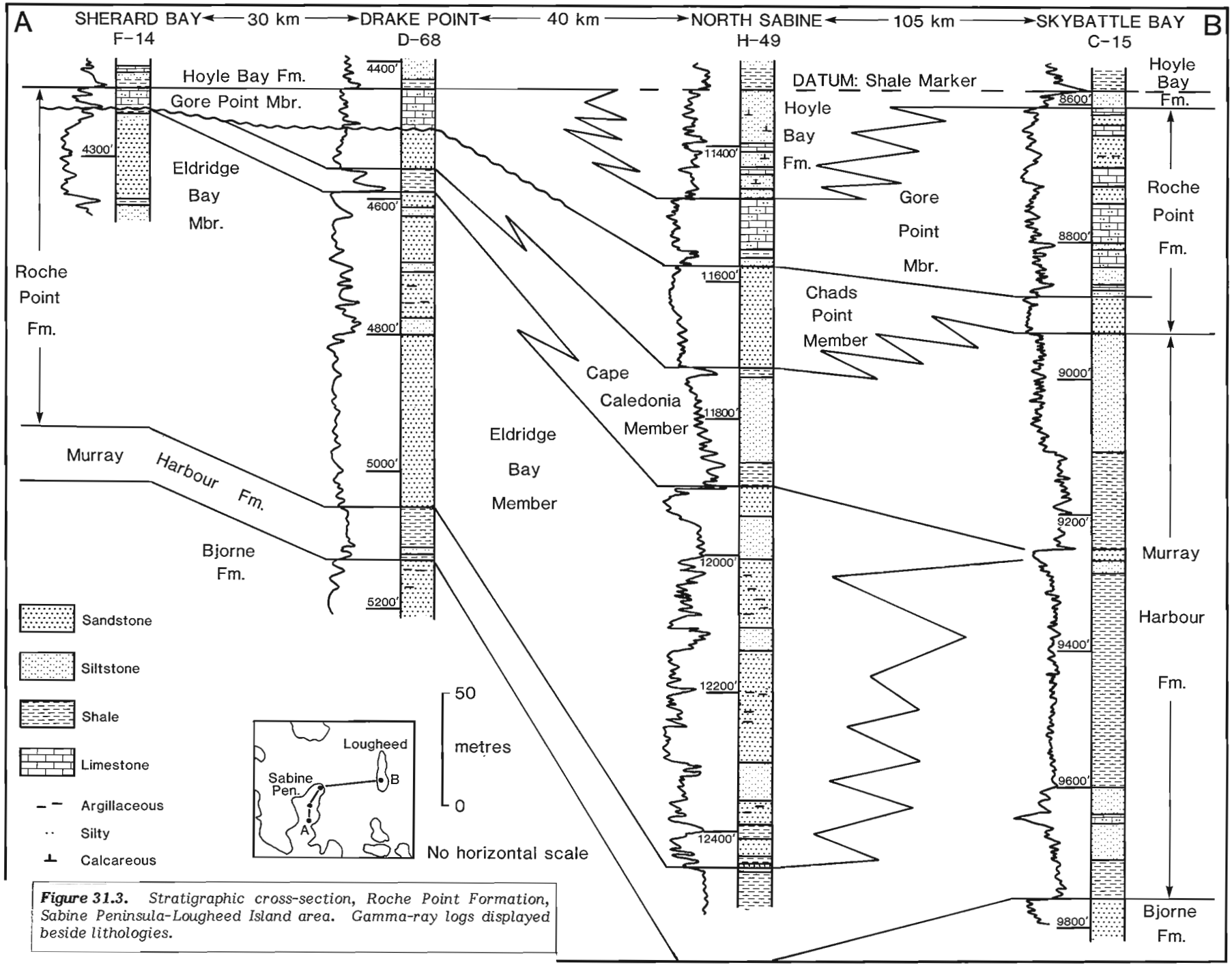

Figure 31.3. *Stratigraphic cross-section, Roche Point Formation, Sabine Peninsula-Lougheed Island area. Gamma-ray logs displayed beside lithologies.*

Thickness and distribution

The Gore Point Member is recognized over the western Sverdrup Basin (Lougheed Island and west). It disappears eastward due to a facies change to siltstone and shale of the lower Hoyle Bay Formation. The maximum thickness of the Gore Point Member is 76 m.

Age

The Gore Point is interpreted to be mainly Carnian (early Late Triassic) in age but may be as old as late Ladinian (Embry, 1984).

Environment of deposition

The lithologies, fauna and stratigraphic relationships suggest a shallow marine shelf environment of deposition for the Gore Point. The abundance of limestone in the member suggests that clastic supply to the shelf was low.

Stratigraphic relationships, Roche Point Formation

Figure 31.3 is a stratigraphic cross-section of the Roche Point Formation in the Sabine Peninsula-Lougheed Island area. The cross-section illustrates a number of important stratigraphic relationships for the Roche Point Formation and its members. These include:

1. The Eldridge Bay sandstones shale-out between Sabine Peninsula and Lougheed Island and equivalent strata form part of the Murray Harbour Formation. This relationship suggests that the source of the clastics of the Eldridge Bay Member was to the south of the Sverdrup Basin.
2. Where the Eldridge Bay Member has disappeared due to facies change to shale and siltstone, the overlying Cape Caledonia Member is no longer recognized and equivalent strata are placed in the Murray Harbour Formation.
3. The Chads Point Member is truncated by erosion on the southern margin. The shale-out edge of this unit is not shown on this cross-section but occurs to the northeast of Lougheed Island (Embry, 1984). These relationships indicate that the Chads Point and underlying Cape Caledonia Member represent a northward prograding succession derived from the south.
4. The Gore Point Member is thickest and contains considerable clastic sediment in the Lougheed Island area. The upper portion of the member changes facies to the shale and siltstone of the lower Hoyle Bay Formation towards the southwest (Sabine Peninsula). The lower portion becomes more calcareous in that direction. On Sabine Peninsula the Gore Point is almost entirely limestone and on the southern basin margin it onlaps an unconformity surface and progressively oversteps older units. These relationships indicate that the clastics of the Gore Point Member were derived mainly from the north-northeast. Little clastic input occurred along the southwestern basin margin, allowing the development of shallow water carbonates in that area.

Eden Bay Member, Hoyle Bay Formation

Definition

The Eden Bay Member consists of interbedded calcareous shale, siltstone and limestone. The type section is in the Panarctic North Sabine well between 3356 m (11 008 ft) and 3499 m (11 480 ft) and is 143 m thick (Fig. 31.4). The name is taken from Eden Bay, on the east side of Sabine Peninsula, Melville Island.

Synonym

First limestone, Schei Point Formation, (informal oil industry term).

Boundaries

The Eden Bay Member conformably overlies the Gore Point Member of the Roche Point Formation, as has been described in an earlier section. Over most of its extent the Eden Bay is conformably overlain by the Cape Richards Member of the Hoyle Bay Formation. The contact is placed at the base of a clay-rich shale unit which overlies calcareous siltstone or silty limestone of the uppermost Eden Bay. In the Lougheed Island area the Eden Bay Member is conformably overlain by the Pat Bay Formation, with the contact placed at the base of the first sandstone unit above which sandstone is predominant.

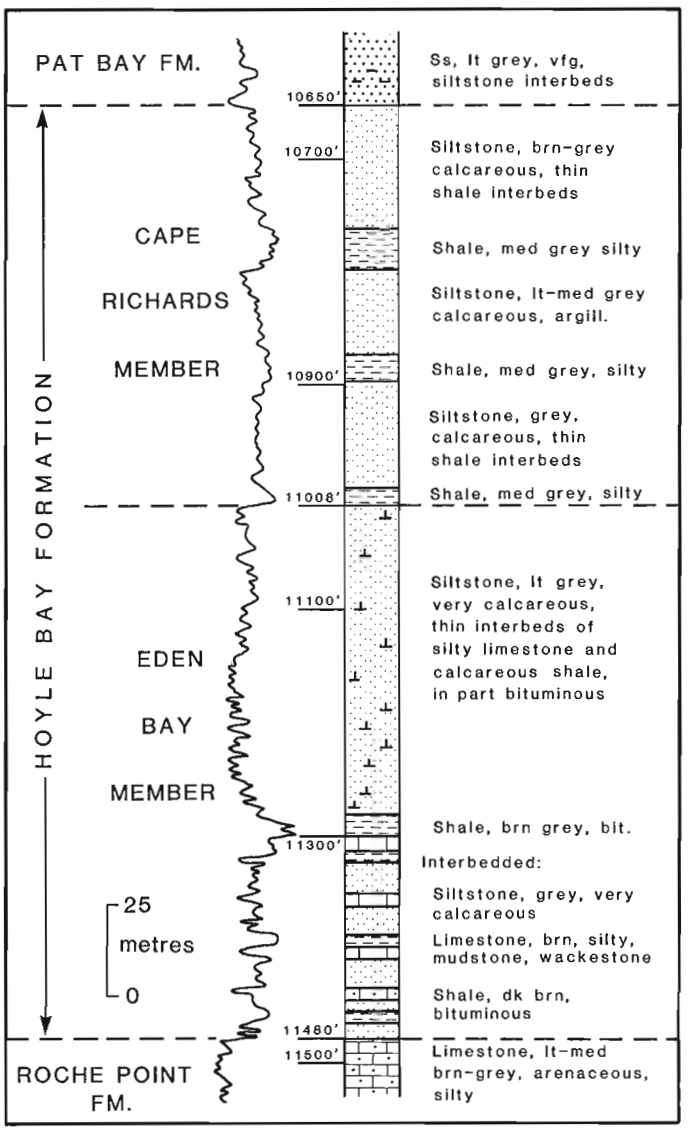

Figure 31.4. Lithology (from samples) and gamma-ray curve for type sections of Eden Bay and Cape Richards members, Hoyle Bay Formation; North Sabine H-49 well.

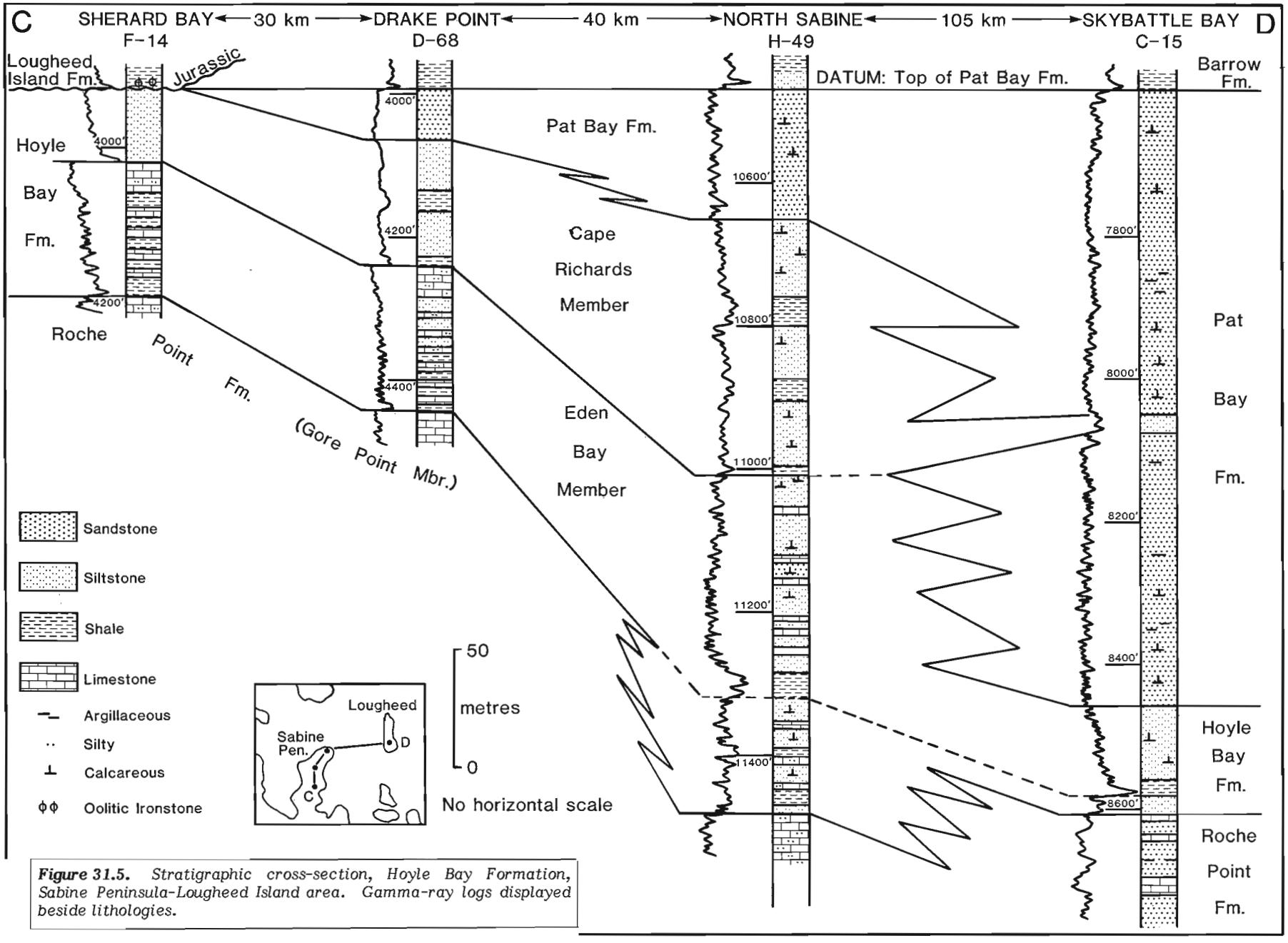

Figure 31.5. *Stratigraphic cross-section, Hoyle Bay Formation, Sabine Peninsula-Lougheed Island area. Gamma-ray logs displayed beside lithologies.*

Lithology

At the type section, the lower portion of the Eden Bay Member consists of dark grey, in part bituminous shale with thin interbeds of silty limestone (mudstone-wackestone) and calcareous siltstone. The upper portion of the member consists of calcareous siltstone with silty limestone interbeds. Southward, shale and limestone become more common in the Eden Bay at the expense of siltstone. To the northeast in the Lougheed Island area siltstone is the predominant lithology and thin interbeds of very fine grained calcareous sandstone occur in the upper portion. In the Prince Patrick Island area bituminous shale and limestone are the predominant lithologies of the Eden Bay.

Thickness and distribution

The Eden Bay Member is recognized over the western Sverdrup Basin and may be up to 175 m thick.

Age

The Eden Bay Member is Carnian in age, based on correlation with well dated surface sections (Embry, 1984).

Environment of deposition

On the basis of lithologies, fauna and stratigraphic relationships, the Eden Bay is interpreted to have been deposited in an offshore shelf environment below wave base. The common occurrence of bituminous shale within the member indicates that bottom waters on the shelf were oxygen deficient in some areas.

Cape Richards Member, Hoyle Bay Formation

Definition

The Cape Richards Member consists of interbedded calcareous siltstone and shale with minor very fine grained sandstone. The type section is in the Panarctic North Sabine H-49 well between 3246 m (10 650 ft) and 3356 m (11 008 ft) and is 110 m thick (Fig. 31.4). The name is taken from Cape George Richards on the north end of Sabine Peninsula, Melville Island.

Boundaries

As described in a previous section, the Cape Richards Member conformably overlies the Eden Bay Member. The Cape Richards Member is conformably overlain by the Pat Bay Formation, with the contact placed at the base of the first sandstone above which sandstone is predominant.

Lithology

The Cape Richards Member consists of interbedded grey, silty shale and grey, calcareous siltstone. Thin, very fine grained sandstone units commonly occur in the uppermost portion of the member. Coarsening-upward cycles (shale-coarse siltstone) are commonly present in the member and are between 20 and 40 m thick. In the Prince Patrick area, shale (in part bituminous) is the dominant lithology, with siltstone being rare. Pelecypod shell fragments are common within siltstone beds.

Thickness and distribution

The Cape Richards Member occurs over the western Sverdrup Basin except in the Lougheed Island area where equivalent strata form the middle portion of the Pat Bay Formation (Fig. 31.5). The maximum thickness of the member is 110 m.

Age

On the basis of correlation with well dated surface sections (Embry, 1984), the Cape Richards Member is Carnian in age.

Environment of deposition

The lithologies, fauna and stratigraphic relationships indicate an offshore shelf depositional environment for the Cape Richards.

Stratigraphic relationships, Hoyle Bay Formation

Figure 31.5 is a stratigraphic cross-section for the Hoyle Bay Formation and its members in the Lougheed Island-Sabine Peninsula area. Important stratigraphic relationships which are portrayed on this cross-section are:

1. The lower portion of the Eden Bay Member in the vicinity of the North Sabine H-49 well is stratigraphically equivalent to the Gore Point Member of the Roche Point Formation to both the north and the south.
2. Most of the Eden Bay Member represents the distal portion of a southwestward prograding clastic succession. Limestone and bituminous shale dominate the member along the southwestern basin margin, which was distal to the clastic source.
3. The Cape Richards Member represents the distal portion of another southwestward prograding clastic succession. Limestones did not develop along the southern basin margin at this time, suggesting that clastic influx was higher than during the deposition of the underlying Eden Bay succession in which limestones are common.
4. The Pat Bay Formation (Embry, 1984) represents the coarser, more proximal clastics of the two prograding successions and the stratigraphic relationships indicate a northerly source for the clastics during the Carnian.

Jenness Member, Barrow Formation

Definition

The Jenness Member consists of interbedded very fine- to fine-grained sandstone, siltstone and shale. The type section is in the Elf Cape Norem A-80 well (N77°29'13", W110°27'05"; spud. April 19, 1970, abandoned August 27, 1970; T.D. 2953 m, K.B. 14 m) between 1668 m (5470 ft) and 1743 m (5719 ft), and is 75 m thick (Fig. 31.6). The name is taken from Jenness Island, which lies north of Mackenzie King Island, 120 km from the Cape Norem well.

Synonym

Heiberg Formation, Brock Island (Tozer and Thorsteinsson, 1964).

Boundaries

The Jenness Member conformably overlies the Pat Bay Formation (sandstone). The contact is placed at the base of a shale unit above which shale and siltstone with interbeds of very fine- to fine-grained sandstone are the dominant lithologies (Fig. 31.6). The Jenness is conformably overlain by shale of the upper portion of the Barrow Formation. The contact is placed at the base of a clay-rich shale that rests on a calcareous siltstone unit of the uppermost Jenness.

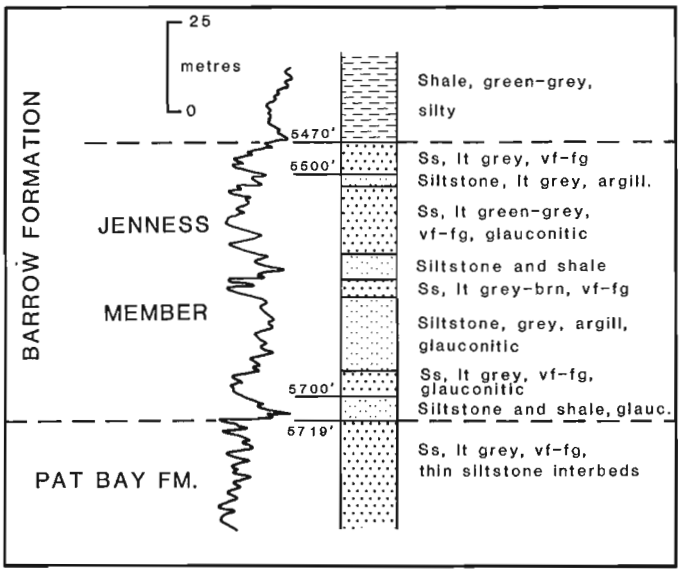

Figure 31.6. *Lithology (from samples and core) and gamma-ray curve for type section of Jenness Member, Barrow Formation; Cape Norem A-80 well.*

Lithology

The Jenness Member consists of interbedded shale, siltstone and sandstone. Individual lithological units are usually less than 2 m thick. The shale is medium grey and is commonly very silty. The siltstone varies from light grey to brown-grey and contains glauconite. The sandstone is grey to green-grey and is very fine- to fine-grained. Glauconite is common in the sandstone units. A 10 m core is available from the type section, and in the core both the sandstone and siltstone units are extensively burrowed. Pelecypods fragments and molds occur in the sandstone units.

Thickness and distribution

The Jenness Member is recognized in the Mackenzie King-Brock Island area. It is limited in extent by erosion to the northwest and by facies change to shale and siltstone of the lower Barrow Formation to the south and east. These relationships indicate that the sandstone was derived from the northwest. The maximum recorded thickness is 75 m.

Age

Pelecypod fossils recovered from core (Mackenzie King Island) and outcrop (Brock Island) date the Jenness as Norian (Tozer and Thorsteinsson, 1964; Tozer, 1973).

Environment of deposition

The lithologies, fauna and stratigraphic relationships suggest a marine shelf (below wave base) environment of deposition for the Jenness.

References

Embry, A.F.
1984: The Schei Point and Blaa Mountain Groups (Middle-Upper Triassic) Sverdrup Basin, Canadian Arctic Archipelago; in Current Research; Part B, Geological Survey of Canada, Paper 84-1B, report 31.

Henao-Londono, D.
1977: Correlation of producing formations in the Sverdrup Basin; Bulletin of Canadian Petroleum Geology, v. 25, p. 969-980.

Tozer, E.T.
1973: Triassic assemblages (macrofossils); in B.S. Norford et al., Biostratigraphic determinations of fossils from the subsurface of the Yukon Territory and the District of Franklin, Keewatin and Mackenzie; Geological Survey of Canada, Paper 72-38, p. 18-19.

Tozer, E.T. and Thorsteinsson, R.
1964: Western Queen Elizabeth Islands, Arctic Archipelago; Geological Survey of Canada, Memoir 332.

Appendix

Selected well tops for the Eldridge Bay, Cape Caledonia, Chads Point and Gore Point members of the Roche Point Formation; Eden Bay and Cape Richards members of the Hoyle Bay Formation; and Jenness Member of the Barrow Formation. Location of wells shown on Figure 31.1.

Sun Skybattle Bay C-15

Hoyle Bay Formation	
Eden Bay Member	2576 m (8452 ft)
Roche Point Formation	
Gore Point Member	2631 m (8630 ft)
Chads Point Member	2707 m (8880 ft)
Murray Harbour Formation	2723 m (8934 ft)

Panaractic Whitefish 2H-63

Hoyle Bay Formation	
Eden Bay Member	2512 m (7657 ft)
Roche Point Formation	
Gore Point Member	2600 m (7925 ft)
Chads Point Member	2663 m (8117 ft)
Murray Harbour Formation	2693 m (8208 ft)

Panarctic North Sabine H-49

Hoyle Bay Formation	
Cape Richards Member	3246 m (10 650 ft)
Eden Bay Member	3356 m (11 008 ft)
Roche Point Formation	
Gore Point Member	3499 m (11 480 ft)
Chads Point Member	3530 m (11 578 ft)
Cape Caledonia Member	3573 m (11 722 ft)
Eldridge Bay Member	3628 m (11 901 ft)
Murray Harbour Formation	3798 m (12 458 ft)

Panarctic Desbarats B-73

Hoyle Bay Formation	
Cape Richards Member	600 m (183 ft)
Eden Bay Member	685 m (209 ft)
Roche Point Formation	
Gore Point Member	765 m (233 ft)
Cape Caledonia Member	802 m (244 ft)
Eldridge Bay Member	838 m (255 ft)
Murray Harbour Formation	939 m (286 ft)

Panarctic Drake Point D-68

Hoyle Bay Formation	
Cape Richards Member	1241 m (4070 ft)
Eden Bay Member	1293 m (4240 ft)
Roche Point Formation	
Gore Point Member	1353 m (4440 ft)
Chads Point Member	1372 m (4500 ft)
Cape Caledonia Member	1390 m (4560 ft)
Eldridge Bay Member	1399 m (4590 ft)
Murray Harbour Formation	1540 m (5054 ft)

Phillips Hazen F-54

Hoyle Bay Formation	
Cape Richards Member	1502 m (4578 ft)
Eden Bay Member	1586 m (4834 ft)
Roche Point Formation	
Gore Point Member	1638 m (4993 ft)
Chads Point Member	1650 m (5029 ft)
Cape Caledonia Member	1656 m (5048 ft)
Eldridge Bay Member	1712 m (5218 ft)
Murray Harbour Formation	1748 m (5328 ft)

Elf Cape Norem A-80

Barrow Formation	
Jenness Member	1668 m (5470 ft)
Pat Bay Formation	1733 m (5719 ft)
Hoyle Bay Formation	
Cape Richards Member	1868 m (6130 ft)
Eden Bay Member	1980 m (6495 ft)
Roche Point Formation	
Gore Point Member	2159 m (7080 ft)
Roche Point sandstone undivided	2216 m (7270 ft)

32.

ORGANIC-WALLED MICROFOSSILS FROM THE LATEST PROTEROZOIC AND EARLIEST CAMBRIAN OF THE WERNECKE MOUNTAINS, YUKON

EMR Research Agreement 227/4/82

H.J. Hofmann[1]

Hofmann, H.J., Organic-walled microfossils from the latest Proterozoic and earliest Cambrian of the Wernecke Mountains, Yukon; in Current Research, Part B, Geological Survey of Canada, Paper 84-1B, p. 285-297, 1984.

Abstract

Four sections across the Precambrian-Cambrian boundary in the Wernecke Mountains have yielded a sparse and poorly preserved microbiota. Acid maceration and thin section study have allowed the identification of the acritarchs ***Leiosphaeridia*** *spp.,* ***Nucellosphaeridium*** *sp.,* ***Archaeodiscina****? sp.,* ***Eomicrhystridium****? sp.,* ***Bavlinella*** *sp., and the filamentous (nematomorph) taxa* ***Archaeotrichion*** *sp.,* ***Eomycetopsis*** *sp.,* ***Oscillatoriopsis psilata****,* ***Nostocomorpha*** *sp. and* ***Archaeorestis****? sp. Of all these taxa only* ***Leiosphaeridia*** *spp., and* ***Eomycetopsis*** *spp. are common. Also present are the rare problematic* ***Paleamorpha****? sp., three types of microdubiofossils and abundant remains of HF-insoluble organic coatings on diagenetic crystal grains. The microfossils found are long-ranging forms, and thus do not provide a good basis for drawing the Precambrian-Cambrian boundary in the Wernecke Mountains. They do, however, shed some light on diagenetic processes that modify the original morphology of the fossilized organisms.*

Résumé

Quatre coupes transversales, effectuées sur la limite du Précambrien et du Cambrien, dans les monts Wernecke, ont montré un microbiote éparpillé et mal conservé. La macération dans l'acide et l'étude en lames minces nous ont permis de déterminer des acritarches: ***Leiosphaeridia*** *spp.,* ***Nucellosphaeridium*** *sp.,* ***Archaeodiscina****? sp.,* ***Eomicrhystridium****? sp.,* ***Bavlinella*** *sp., et les taxons filamenteux (nématomorphes):* ***Archaeotrichion*** *sp.,* ***Eomycetopsis*** *sp.,* ***Oscillatoriopsis psilata****,* ***Nostocomorpha*** *sp. et* ***Archaeorestis****? sp. Parmi tous ces taxons, seuls* ***Leiosphaeridia*** *spp. et* ***Eomycetopsis*** *spp. sont communs. On trouve aussi* ***Paléamorpha****? sp., microfossile rare et problématique, trois types de microdubiofossiles et des restes abondants de revêtements organiques insolubles dans l'acide fluorhydrique sur des grains cristallins diagénétiques. Les microfossiles découverts sont des formes de longue durée et ne peuvent être alors considérés comme une bonne base pour délimiter la limite du Précambrien et du Cambrien dans les monts Wernecke. Mais ils peuvent cependant expliquer une partie des processus diagénétiques qui modifient la morphologie originale des organismes fossilisés.*

Introduction

This paper reports on the microfossils obtained from samples collected at the author's request by W.H. Fritz and G.M. Narbonne in the Wernecke Mountains during the summer of 1982, while they were studying the stratigraphy, macropaleontology, and palichnology of the Precambrian-Cambrian transition beds in the northern Cordillera. The paper follows a preliminary report on the stratigraphy and palichnology of these beds (Fritz et al., 1983) and a report on the discovery of representatives of the Ediacaran fauna in the lower part of the column (Hofmann et al., 1983). An investigation of the shelly microfossils in the sequence is under way (Nowlan, personal communication, 1983). The purpose of all these studies is to elucidate the paleontological record near the Precambrian-Cambrian boundary.

Acknowledgments

I thank G.M. Narbonne and W.H. Fritz for collecting the samples used in this study, M. Kerba-Kachaami for preparing the macerations, J.P. Bourque for making the thin sections, and G. Schonbeck for printing most of the photographs. The study was financially supported by the Department of Energy, Mines and Resources (Research Agreement EMR 227/4/82). Discussion and critical comments on the manuscript by J.D. Aitken, C.W. Allison, W.H. Fritz, R.J. Horodyski, D.J. McIntyre, G.M. Narbonne, and G. Vidal are gratefully acknowledged.

General geological setting

The general setting of the microfossil localities is described and discussed in Fritz et al. (1983) under the heading "Goz Creek Area", and the reader should consult this reference for details. Figure 32.1 summarizes the stratigraphy of the four sections from which microfossils were obtained; this figure is taken from Figures 44.1 and 44.2a of Fritz et al. (1983), slightly modified to accommodate the data on the stratigraphic distribution and composition of the microbiota.

The area is located in the Wernecke Mountains, a group of ranges in the interior of the northern Cordillera, and is covered by the reconnaissance geological report by Wheeler (1954) and an open-file report by Blusson (1974). The stratigraphic sequence in this study begins with three unnamed map units, comprising a lower sequence of siltstone and very fine grained quartzite of undetermined thickness (Unnamed siltstone unit 2), a 70-150 m thick, light grey dolostone in the middle, and a 150-230 m thick, upper siltstone and quartzite unit (Unnamed siltstone unit 1). Both unnamed siltstone units contain representatives of the Ediacaran fauna (Hofmann et al., 1983). These three formations are overlain by a 35 to 120 m thick, massive, orange weathering dolostone (Map unit 11 of Blusson, 1971), which is a distinctive marker in the northern Cordillera. Disconformably above this unit is the Vampire Formation (Fritz, 1982) which, at its base, has phosphate nodules and

[1] Department of Geology, University of Montreal, Montreal, Quebec H3C 3J7

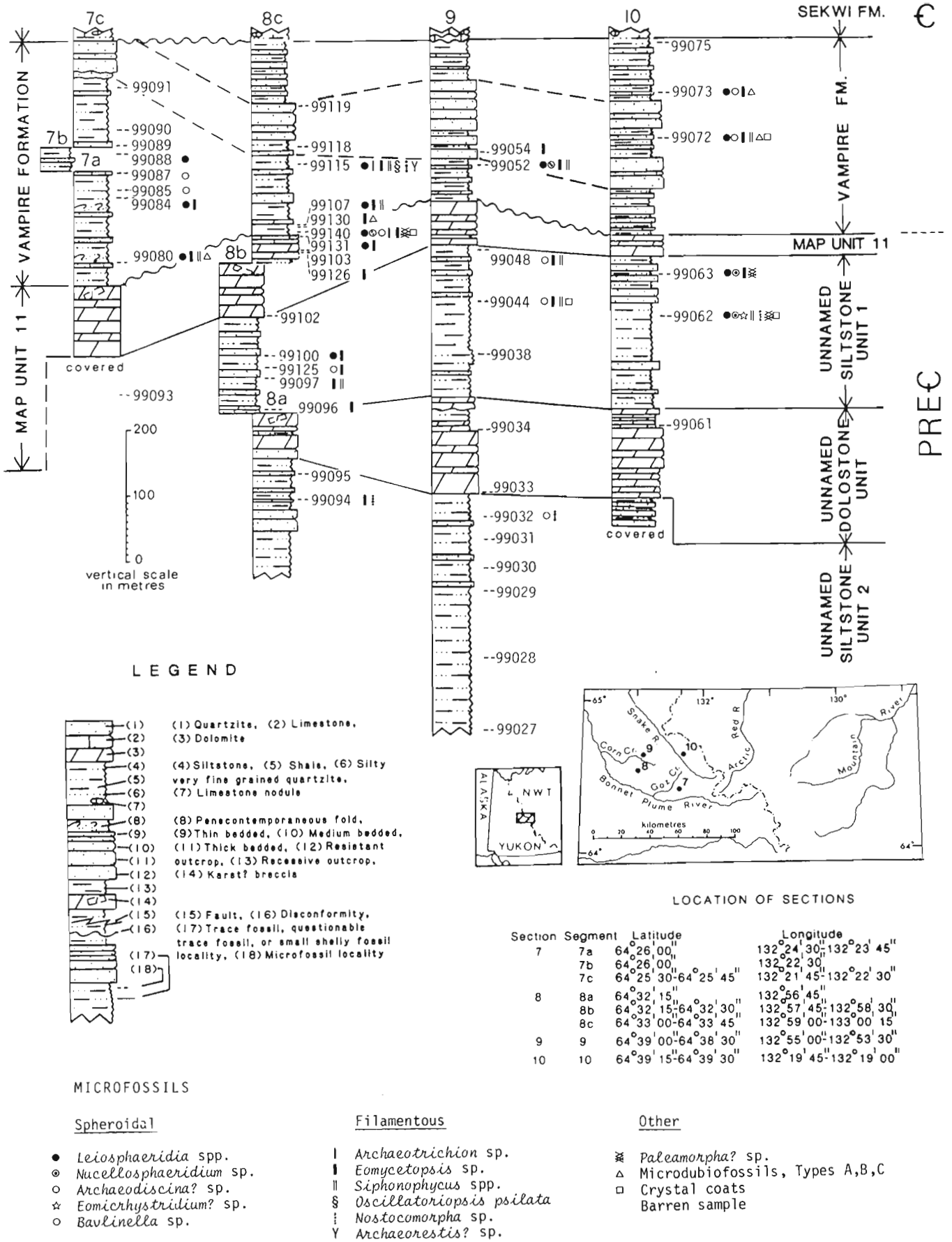

LOCATION OF SECTIONS

Section	Segment	Latitude	Longitude
7	7a	64°26'00"	132°24'30"-132°23'45"
	7b	64°26'00"	132°22'30"
	7c	64°25'30"-64°25'45"	132°21'45"-132°22'30"
8	8a	64°32'15"	132°56'45"
	8b	64°32'15"-64°32'30"	132°57'45"-132°58'30"
	8c	64°33'00-64°33'45"	132°59'00-133°00'15"
9	9	64°39'00"-64°38'30"	132°55'00"-132°53'30"
10	10	64°39'15"-64°39'30"	132°19'45"-132°19'00"

MICROFOSSILS

Spheroidal

- ● *Leiosphaeridia* spp.
- ◉ *Nucellosphaeridium* sp.
- ○ *Archaeodiscina?* sp.
- ☆ *Eomicrhystridium?* sp.
- ○ *Bavlinella* sp.

Filamentous

- | *Archaeotrichion* sp.
- ‖ *Eomycetopsis* sp.
- ‖ *Siphonophycus* spp.
- § *Oscillatoriopsis psilata*
- ⋮ *Nostocomorpha* sp.
- Y *Archaeorestis?* sp.

Other

- ⊠ *Paleamorpha?* sp.
- △ Microdubiofossils, Types A,B,C
- □ Crystal coats
- Barren sample

Figure 32.1. *Late Proterozoic and Early Cambrian sections in the Wernecke Mountains, Yukon, showing distribution of microfossils. Stratigraphic base and locality map from Fritz et al., 1983, Fig. 44.1, 44.2.*

small shelly fossils such as **Anabarites trisulcatus** Missarzhevskiy and **Protohertzina anabarica** Missarzhevskiy, as well as **Rusophycus** sp., **Cruziana** sp., and arthropod scratch marks (Fritz et al., 1983) indicative of a latest Precambrian to an earliest Cambrian age for the base of the formation at this location. The Sekwi Limestone, containing Lower Cambrian trilobites, overlies the Vampire Formation.

Sampling and preparation

The 44 samples analyzed were collected by Fritz and Narbonne on a reconnaissance basis, with collecting sites at variable spacings as shown in Figure 32.1. The samples, each between approximately 80 to 250 g in weight, are mostly from shale and siltstone beds in the sections. A 30 g portion was selected, washed, and cleaned ultrasonically and then crushed in a plastic bag into 5 to 100 mm sized chips. These were then transferred to a 400 ml pyrex beaker and treated with warm, concentrated HCl to remove carbonates. After decanting and washing with distilled water, the sample was transferred to a 400 ml propylene beaker and dissolved in concentrated HF. After rinsing with distilled water, it was treated with warm, concentrated HNO_3 to remove any sulphides. The organic residue was then washed with distilled water until neutrality was obtained, and subsequently sieved, dried, and mounted on glass slides with epoxy resin (Petropoxy 154). Other portions of some of the samples were used to prepare petrographic thin sections parallel to stratification for confirmation of the primary nature of the most commonly occurring organic remains. Thin sections also allowed some taxa to be seen as pyritized and hematized filaments, whereas the same taxa would not be observable in the maceration because of the soluble nature of the iron minerals. Some specimens from the maceration treatment were mounted for scanning electron microscope examination, but no additional useful information was thereby obtained. Of the 44 samples, 25 (or 57%) were found to contain microfossils.

Microfossils

The microfossils are generally dark brown to brownish black, indicating moderate degrees of organic metamorphism. Total abundance is not high in the samples analyzed, and there is not a great diversity of species. The best preserved and most diverse of the microfossils are from the Vampire Formation, followed by Unnamed siltstone unit 1. Map unit 11 has yielded a few sphaeromorphs and filaments. The Unnamed dolostone unit was barren, and Unnamed siltstone unit 2, which appears to be more highly metamorphosed than the overlying units, has only rare organic residues, but has some hematized filamentous remains.

The taxonomy of spheroidal and filamentous microfossils is in disorder. A treatise-like synthesis with standardized nomenclature, taxonomic keys, and superior illustrations is not yet available. Because of the less than perfect preservation, and the pending clarification of microfossil taxonomy, the identifications of the Wernecke microfossils are provisional. The fossils are amply illustrated for future comparison.

Systmatic paleontology

All slides containing specimens illustrated in this paper are deposited in the National Type-Fossil Collection of the Geological Survey of Canada, under catalogue numbers 76536-76589. Particulars are cited in the respective figure captions. Stage co-ordinates cited in the captions refer to distances, in millimeters, from the upper right reference corner formed by the intersection of the distal margin (x-axis) and right margin (y-axis) of the slide, the slide being oriented with the label to the right of the observer.

Group **Acritarcha** Downie, Evitt, and Sarjeant, 1963
Genus **Leiosphaeridia** Eisenack, 1958, emend.
Downie and Sarjeant, 1963
Leiosphaeridia spp.
Pl. 32.1, figs. P, R-U, Y?, Z; Pl. 32.2, figs. A-D

Leiosphaeridia sp. Volkova, 1964, p. 81, Pl. 1, figs. 1-11, 15-16; Pl. 2, figs. 1-4, 10-13; Pl. 3, figs. 1-12; 1974, p. 532; Pl. 9, figs. 15, 16.

Description. Compressed spheroids, diameters in the range of 6.5-115 µm, (averaging 32.0 µm, n = 45; with major mode around 20 µm and secondary mode around 85 µm); thin walled, with smooth to shagreen surface and wide folds; some diagenetically modified specimens show impressions of pyrite crystals 1-5 µm across.

Occurrence. Unnamed siltstone unit 1 (GSC locs. 99062, 99063, 99100); Map unit 11 (GSC loc. 99131); Vampire Formation (GSC locs. 99052, 99072, 99073, 99080, 99084, 99088, 99107, 99115, 99140).

Comments. Sphaeromorph acritarchs with thin, smooth walls have been described under many names. For simple spheroids, diagnostic characters are very limited, and so folds and surface textures and patterns have been used extensively to erect a large number of form taxa, a good number of which are probably degradational and preservational variants of only a few genera. Obvious diagenetic patterns are those produced by pyrite crystals, which disrupt the organic membrane or impress their crystal outlines on it, such as those illustrated in Plate 32.2, figs. B-D. Some of the degraded specimens (Pl. 32.1, figs. R-T, Z) resemble sphaeromorphs reported from the Late Proterozoic of the Avalon Peninsula of Newfoundland under the name **Trachysphaeridium** sp. (Hofmann et al., 1979, p. 90). The considerable range in size of the spheroids suggests that more than one taxon is included. Specimens in the lower size range (<55 µm) could be referred to **Protoleisphaeridium** Timofeev, a possible subgenus of **Leiosphaeridia** according to Downie and Sarjeant (1963), who, however, also suggested that it would be better treated as a synonym of **Leiosphaeridia** and rejected. The emended diagnosis of **Leiosphaeridia** given by Downie and Sarjeant (1963, p. 94-95) makes no reference to size ranges, and all the specimens from the Wernecke Mountains can thus be accommodated in this taxon.

Genus **Nucellosphaeridium** Timofeev, 1963
Nucellosphaeridium sp.
Pl. 32.1, figs. Q, V

Description. Flattened spheroids 50-90 µm across (n = 3), containing dark, round to subangulate eccentric body; surface texture smooth to granulose, morphology diagenetically modified; wrinkles and folds present.

Occurrence. Unnamed siltstone unit 1 (GSC locs. 99062, 99063).

Comments. The structures assigned to this rare form genus are regarded as probable degradational stages of spheromorph acritarchs.

Genus **Archaeodiscina** Naumova, 1960, emend. Volkova, 1968
Archaeodiscina? sp.
Pl. 32.1, fig. W

Description. Compressed spheroids, 15-20 µm across (n = 3), with dark round to subangulate inclusions 2-8 µm across.

Occurrence. Vampire Formation (GSC locs. 99052, 99140).

Comments. This fossil is a very rare component of the microbiota.

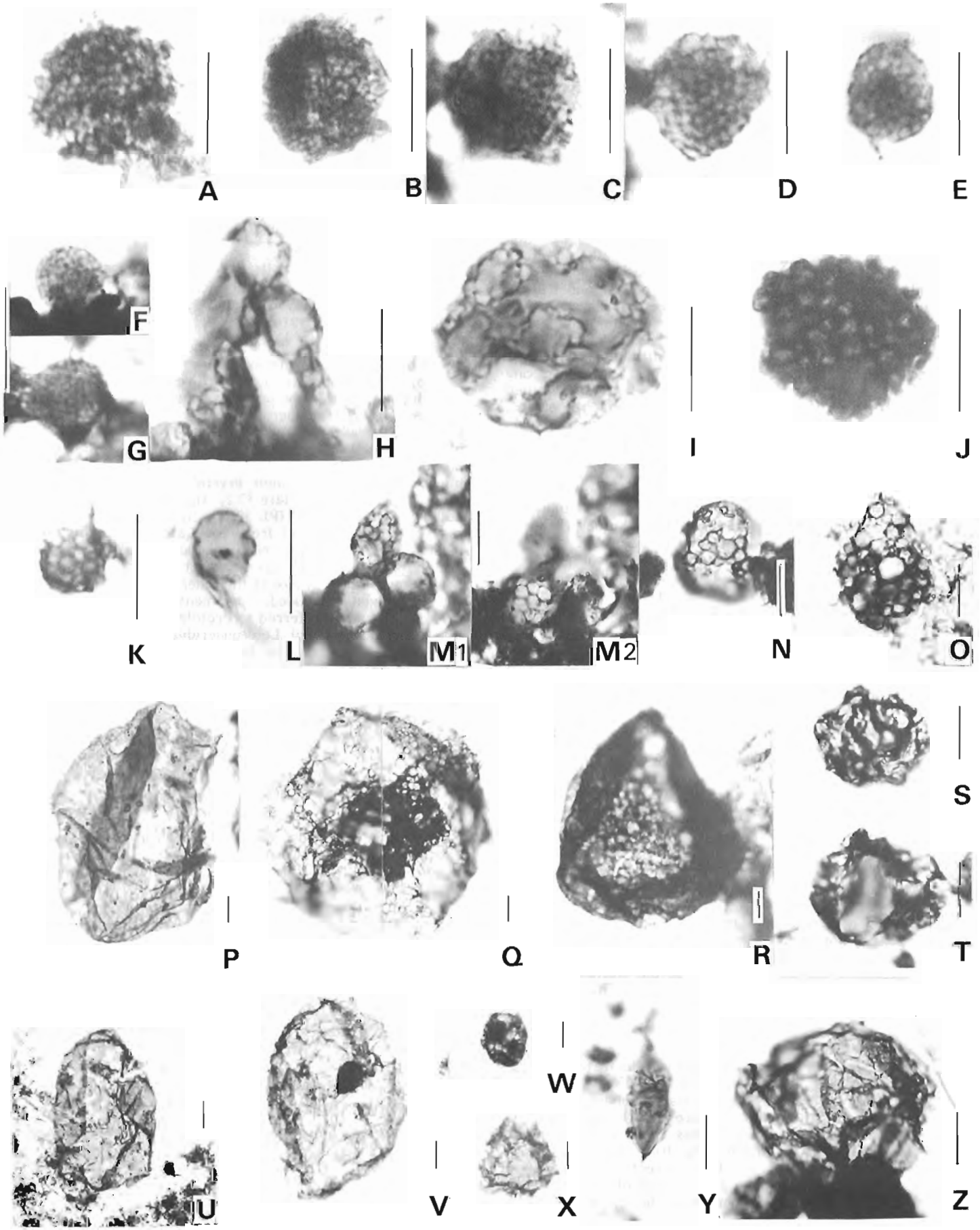
A
B
C
D
E
F
G
H
I
J
K
L
M1
M2
N
O
P
Q
R
S
T
U
V
W
X
Y
Z

Genus **Bavlinella** Shepeleva, 1962
Bavlinella sp.
Pl. 32.1, figs. A-G, H?-M?

?**Pyritosphaera barbaria** Love, 1957, p. 443, Pl. 33, figs. 3-5; Neves and Sullivan, 1964, Pl. 2, fig. 7; Volkova, 1974, p. 102, Pl. 9, fig. 4.
Bavlinella faveolatus Shepeleva, 1962, p. 456, fig. 1; Volkova, 1964, Pl. 1, figs. 13-14; 1974, p. 106, Pl. 9, figs. 1-3, 5-14.
?**Pyritosphaera barbaria** Type I Duchesne, 1963, p. B126, figs. 1-3.
Favososphaera sola Burmann, 1972, p. 405-406, Pl. 3, figs. 8-12.

PLATE 32.1

Spheriodal microfossils and microdubiofossils from Wernecke Mountains. All specimens are macerated remains photographed in transmitted light, except part J, which is in thin section in combined transmitted and partially reflected light. Length of each bar-scale is 10 μm. For localities see Figure 32.1.

		G.S.C. Locality	G.S.C. Type	Stage Coordinates
A	**Bavlinella** sp., degraded specimen	99032	76536	61.6x-7.9y
B	**Bavlinella** sp., degraded specimen	99032	76537	57.0x-12.6y
C	**Bavlinella** sp., degraded specimen	99048	76538	50.8x-13.6y
D	**Bavlinella** sp.	99087	76539	60.4x-3.3y
E	**Bavlinella** sp.	99072	76540	50.2x-4.9y
F	**Bavlinella** sp.	99125	76541	51.2x-9.8y
G	**Bavlinella** sp.	99140	76542	62.0x-7.1y
H	Microdubiofossil Type A	99080	76543	63.8x-16.4y
I	Microdubiofossil Type A	99080	76544	67.4x-9.6y
J	Pyrite framboid, thin section	99115	76545	40.3x-17.8y
K	Microdubiofossil Type A, fragment	99072	76546	51.9x-21.0y
L	Microdubiofossil Type A	99080	76547	66.7x-8.6y
M	Microdubiofossil Type A, two different focal views	99072	76548	63.1x-19.4y
N	Microdubiofossils Type B	99073	76549	40.4x-3.3y
O	Microdubiofossil Type B	99072	76550	66.6x-9.5y
P	**Leiosphaeridia** sp.	99115	76551	45.6x-4.4y
Q	**Nucellosphaeridium** sp.	99062	76552	50.4x-5.4y
R	**Leiosphaeridia** sp.	99115	76553	54.5x-13.1y
S	**Leiosphaeridia** sp.	99140	76554	55.3x-17.2y
T	**Leiosphaeridia** sp.	99140	76555	45.0x-7.7y
U	**Leiosphaeridia** sp.	99084	76556	61.1x-5.2y
V	**Nucellosphaeridium** sp.	99063	76557	48.4x-23.0y
W	**Archaeodiscina**? sp.	99052	76558	46.2x-19.9y
X	**Eomicrhystridium**? sp.	99062	76559	50.3x-5.3y
Y	**Leiosphaeridia**? sp.	99072	76560	55.5x-3.8y
Z	**Leiosphaeridia** sp.	99063	76561	36.3x-7.8y

Microsphaera faveolata Sin in Sin and Liu, 1973, Pl. 13, fig. 7.
Sphaerocongregus variabilis Moorman, 1974, p. 535, Pl. 1, figs. 1-4, 7-9; Cloud et al., 1975, p. 134-135, figs. 3-18; Chauvel and Mansuy, 1981b, p. 456, fig. 3, G, I, J, fig. 5, D-L.
Bavlinella faveolata nom. correct., emend. Vidal 1976, p. 17-18, fig. 7; Knoll et al., 1981, p. 250, Pl. 1, figs. Q, R.
Form B and Form C Chauvel and Mansuy, 1981a, p. 31, fig. 5, E-M.
Bavlinella cf. **faveolata** Lenk et al., 1982, p. 619, fig. 1f.

Description. Spheroidal aggregates of dark brown organic material, 4-16 μm across, (averaging 10.0 μm; n = 20) of tightly packed, isodiametric globular to subpolyhedral globular cell-like units 0.3-1.0 μm in diameter.

Occurrence. Unnamed siltstone unit 2 (GSC loc. 99032); Unnamed siltstone unit 1 (GSC locs. 99044, 99048, 99125); Vampire Formation (GSC locs. 99072, 99073, 99085, 99087, 99140).

Comments. **Bavlinella** is a fairly common taxon in the Wernecke microbiota. It represents somewhat problematic structures described under a variety of names. Workers dealing with Precambrian microfossils have generally referred such forms to **Bavlinella faveolata** Shepeleva, and have attributed some chronostratigraphic value to them. It is rarely mentioned (for exception see Volkova, 1974) that, when observed with the optical microscope, they appear to be indistinguishable from those first described from the Paleozoic and Mesozoic under the name **Pyritosphaera** Love, and that their chronostratigraphic value therefore has to be questioned. The genus has also been reported from the Early Proterozoic (Mikhailova, 1979, p. 126). Mansuy (personal communication, 1983) has recently studied the ultrastructure of **Bavlinella** and **Pyritosphaera** using TEM (and SEM) techniques; she has recongnized a trilaminate wall structure for **Bavlinella**, and a unilaminate one for **Pyritosphaera.**

Various affinities have been suggested for **Bavlinella.** It has been interpreted as colonies of distinctive taxa of cyanobacteria, particular morphologic stages in the life-cycle of cyanobacteria (endosporangiate structures), and pseudofossils related to framboidal pyrite formation (for which an extensive literature exists, e.g. see Kalliokoski, 1974). The current consensus among Precambrian paleontologists seems to favour the view that they are related to planktonic endosporulating cyanobacteria; their great abundance at certain levels probably being attributable to explosive blooms in a stressed habitat, such as a glacially influenced marine environment (e.g. Knoll et al., 1981; Vidal and Knoll, 1982; Mansuy and Vidal, 1983). Although they represent clusters of tightly packed, individually well defined micrometric organic spheroids, resembling certain modern chroococcalean cyanobacteria (e.g. **Gomphosphaeria, Microcystis**), they remain problematic, controversial structures and are probably polygenetic. They are common in some sediments, such as dark pelites in which formation of framboidal pyrite is favoured (perhaps biologically mediated), and in which organic matter is preserved.

Genus **Eomicrhystridium** Deflandre, 1968
Eomicrhystridium? sp.
Pl. 32.1, fig. X

Eomicrhystridium barghoorni Deflandre, 1968, p. 2387, fig. 1.
Archaeohystrichosphaeridium ianischewskyi Timofeev, Konzalová 1974, Pl. 6, figs. 1-2.
Eomicrhystridium? sp. Hofmann et al., 1979, p. 92, Pl. 12.3, figs. 16, 17.

Description. Deformed globular vesicle with simple spine-like processes and folds defining irregular polygonal fields; diameter 20-30 μm.

Occurrence. Unnamed siltstone unit 1 (GSC loc. 99062).

Comments. This fossil, which is rare, is attributed to the acanthomorph acritarchs because of the spinose nature. However, it is possible that this ornamentation is merely a preservation artifact developed on a leiosphaerid sphaeromorph, and for this reason the generic assignment is questionable.

Subgroup **Nematomorphitae** Diver and Peat, 1979
Genus **Archaeotrichion** J.W. Schopf, 1968
Archaeotrichion sp.
Pl. 32.3, figs. I, M

Archaeotrichion contortum J.W. Schopf, 1968, p. 686, Pl. 86, figs. 1, 2.

Description. Simple thread-like filaments, nonseptate, twisted, uniformly 0.3-0.5 μm wide (n = 9), up to 35 μm long, solitary, and in tangled masses.

Occurrence. Vampire Formation (GSC locs. 99115, 99140).

Comments. In the Wernecke microbiota, this is the taxon with the smallest size. It is not very common.

Genus **Eomycetopsis** J.W. Schopf, 1968, emend. Knoll and Golubic, 1979
Eomycetopsis spp.
Pl. 32.2, figs. H?, L; Pl. 32.3, figs. A, B, E?, F?, G, K?, O, P

Eomycetopsis pflugii Maithy and Shukla, 1977, p. 180, Pl. 2, fig. 16.

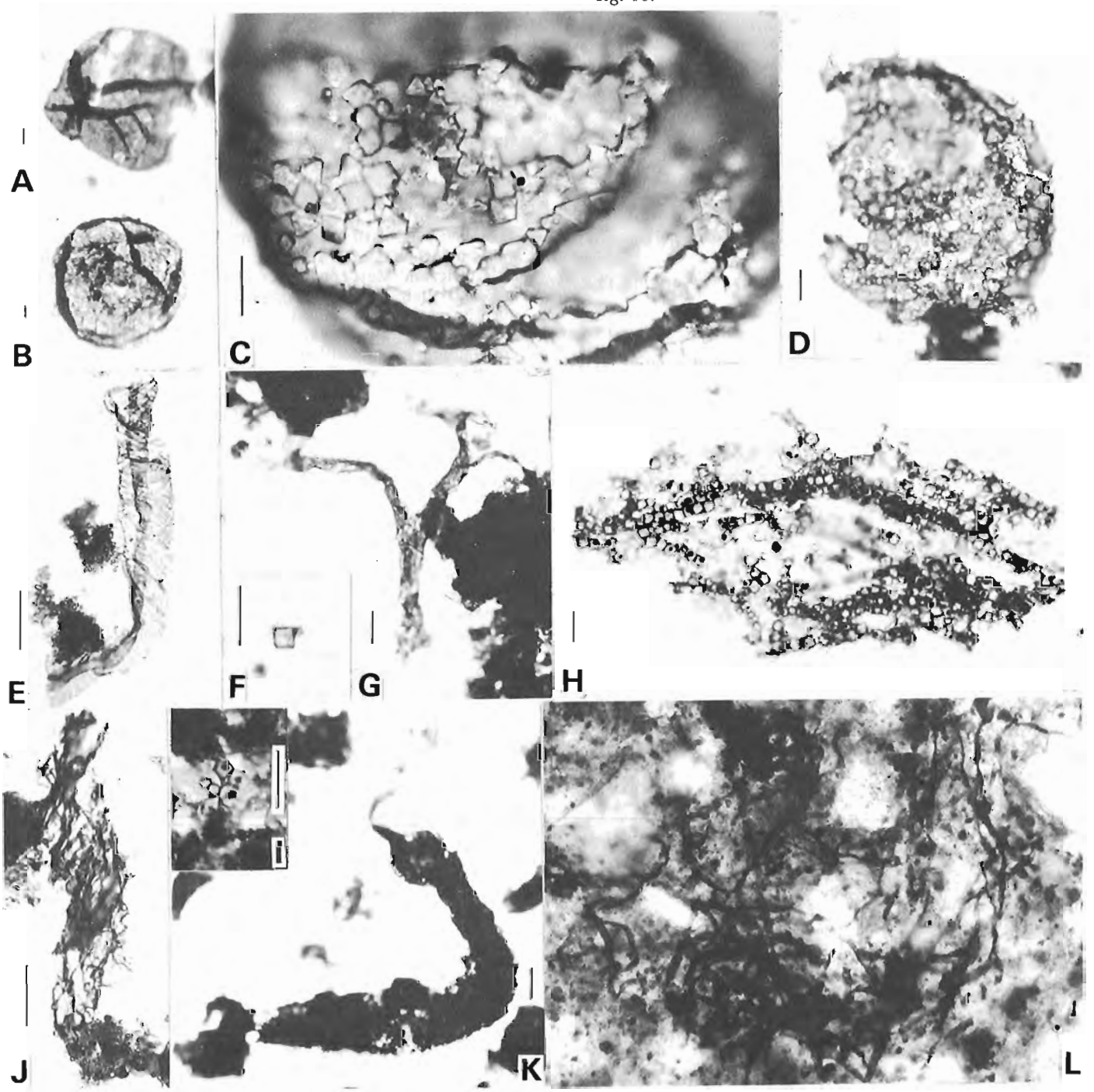

Eomycetopsis psilata Maithy and Shukla, 1977, p. 180, Pl. 2, fig. 15.
Taeniatum spp. Hofmann and Aitken, 1979, p. 156, fig. 9, A, B, C.
Siphonophycus crassiusculum Horodyski, 1980, p. 656, Pl. 1, figs. 6, 7.
Eomycetopsis crassiusculum comb. nov. Zhang, 1982, p. 455, Pl. 47, figs. 3-6, 9-13.

Description. Dark brown, simple tubular filaments, nonseptate, twisted and crushed; 1-9 μm wide, averaging 4.5 μm (n = 103), fragments up to 160 μm long; solitary and in clusters. Morphology variably modified by diagenetic pyrite crystals.

Occurrence. Unnamed siltstone unit 2 (GSC loc. 99094); Unnamed siltstone unit 1 (GSC locs. 99044, 99048, 99063, 99096, 99097, 99100, 99125); Map unit 11 (GSC locs. 99126, 99131); Vampire Formation (GSC locs. 99052, 99054, 99072, 99073, 99080, 99084, 99107, 99115, 99130, 99140).

Comments. This is the most widespread microfossil in the Wernecke biota, often forming mat-like patches of entangled tubes, seen both in thin section, and in macerations, and occurring in various diagenetically produced disguises. The degradational forms include several types modified by pyrite crystallization, which, in places, has distorted the sheath into polyhedral compartments (Pl. 32.3, figs. D, E, F, K) that bear no demonstrable relation to cells in any trichome that may originally have been present. Probably two species are represented, based on the bimodal distribution of diameters: one group in the range of 1-4 μm, the other in the range of 4.5-7 μm.

Eomycetopsis was originally diagnosed as being occasionally septate (Schopf, 1968, p. 685), but re-examination of the type material shows that the purported septa are flexures in the tubes, and that the remains are best considered to be sheaths of cyanobacterial microbes (Hofmann, 1976, p. 1052; Knoll and Golubic, 1979, p. 131).

The structures illustrated here are indistinguishable from the **Taeniatum** reported by Hofmann and Aitken (1979). Type material and the original description of **Taeniatum** have not been accessible for examination, and Wang and Luo (1982, p. 297) have reported that such filaments may be contaminants (wicks of alcohol lamp used in the preparation of slides). I therefore assign the present material, and that previously reported from the Mackenzie Mountains as **Taeniatum** spp. (see synonymy above), to **Eomycetopsis**, whose bona fide fossil nature is not in question.

PLATE 32.2

Microfossils and microdubiofossils from Wernecke Mountains. All specimens except part L are macerated remains photographed in transmitted light; filaments in L are in thin section. Length of each bar-scale is 10 μm. For localities see Figure 32.1.

		G.S.C. Locality	G.S.C. Type	Stage Coordinates
A	**Leiosphaeridia** sp.	99115	76562	53.9x-4.6y
B	**Leiosphaeridia** sp.	99062	76563	61.2x-18.0y
C	**Leiosphaeridia** sp., enlargement of lower right of specimen in B			
D	**Leiosphaeridia** sp.	99062	76564	45.3x-16.8y
E	**Paleamorpha**? sp.	99063	76565	36.5x-9.5y
F	Cubic crystal coat; compare with C, D, and H	99072	76566	56.9x-4.5y
G	**Archaeorestis**? sp.	99115	76567	54.4x-10.6y
H	Cubic crystal coats in mat of filaments (**Eomycetopsis**? sp.)	99062	76568	68.5x-13.5y
I	Crystals coats, compartments with dark inclusions	99140	76569	42.7x-13.1y
J	**Paleamorpha**? sp.	99140	76570	58.9x-13.6y
K	Microdubiofossil Type C	99130	76571	40.5x-13.7y
L	Clump of **Eomycetopsis** filaments in thin section parallel to bedding; compare with Pl. 3, O	99115	76572	21.4x-9.1y

Genus **Siphonophycus** J.W. Schopf, 1968
Siphonophycus spp.
Pl. 32.3, figs. C, D, H, J?, L

Siphonophycus spp. Hofmann and Aitken 1979, p. 156, fig. 9, E, F, H.
Siphonophycus beltensis Horodyski, 1980, p. 654-656, Pl. 1, fig. 4; Zhang, 1982, p. 456, Pl. 47, figs. 1-2.

Description. Dark brown, simple tubular filaments, 12-53 μm wide, averaging 19.6 μm (n = 17); fragments up to 310 μm long, twisted and crushed; transverse markings absent to poorly developed.

Occurrence. Unnamed siltstone unit 1 (GSC locs. 99044, 99048, 99062, 99097); Vampire Formation (GSC locs. 99052, 99072, 99080, 99107, 99115).

Comments. The tubes here assigned to **Siphonophycus** are similar to those referred to **Eomycetopsis**, but are distinguished by their greater width and the occasional presence of faint transvere marking (e.g. Pl. 32.3, H). They probably are sheaths. Judging from the wide range in tube diameter, more than one species is represented.

Genus **Oscillatoriopsis** J.W. Schopf, 1968
Oscillatoriopsis psilata
Pl. 32.3, fig. Q

Oscillatoriopsis psilata Maithy and Shukla, 1977, p. 179, Pl. 2, fig. 12.
?**Siphonophycus** sp. Hofmann and Aitken, 1979, p. 156, fig. 9, G.
Oscillatorites sp. Volkova et al., 1979, in Keller and Rozanov, ed., p. 38, Pl. 30, fig. 5.

Description. Dark brown, tubular filament, 8-10 μm wide and about 320 μm long; incomplete, twisted, characterized by well developed, regular, transverse markings whose spacing is about one-half the width of the compressed filament; transverse markings present over most of length of filament, but absent near extremities.

Occurrence. Vampire Formation (GSC loc. 99115).

Comments. Only one good specimen was observed. As with the structures reported as **Siphonophycus** sp. from the Little Dal Group of the Mackenzie Mountains (Hofmann and Aitken, 1979), the transverse markings are seen only along part of the tubes.

A
B
C
D
E
F G
H
I
J
K
L
M
N
O
P
Q

Genus **Nostocomorpha** Sin and Liu, 1978
Nostocomorpha sp.
Pl. 32.3, fig. N

Chain of cells in **Camasia spongiosa** Walcott, 1914, p. 103, 115; Pl. 20, figs. 2-4.
Filaments Gutstadt and Schopf, 1969, p. 165, figs. 1-6.
Nostocomorpha prisca Sin and Liu, Aug. 1978, p. 122-123; Pl. 7, figs. 10-12, Pl. 8, figs. 1-3.
Nostocopsis desmoides Yin and Li, Oct. 1978, p. 89-90, Pl. 8, fig. 15.

Description. Chains of spheroidal to polyhedral grains of iron oxide, or iron oxide with opaque (pyrite?) centres; diameter of elements in chain relatively uniform, ranging from 3-6 µm (n = 20); chains uniseriate, unbranched, rectilinear to strongly curved, up to 150 µm long, parallel to bedding; sometimes occurring in intertwined masses morphologically similar to tangled masses of **Eomycetopsis** and **Siphonophycus** tubes in same rock.

Occurrence. See Figure 32.1. Unnamed siltstone unit 2 (GSC locs. 99032, 99094); Unnamed siltstone unit 1 (GSC loc. 99062). Vampire Formation (GSC loc. 99115). The filaments were observed only in thin sections; they are dissolved during acid treatment, and thus not observable in macerations. Taxon probably much more widespread than indicated in Figure 32.1.

Comments. The structures are evidently the remains of filamentous organisms or sheaths such as the associated **Eomycetopsis** or **Siphonophycus**, which have been completely replaced by diagenetic iron minerals. The postulated paragenesis is: organic matter, pyrite, iron oxide. Similar structures were described by Walcott (1914) from the Newland Limestone (Belt Supergroup) of Montana. More recently, such structures, from the Sinian of China, have received the Linnéan genus designations **Nostocomorpha** and **Nostocopsis**, with the former name having priority by 2 months. Horodyski (1981) has discussed somewhat similar structures composed of apatite from the Appekunny Argillite (also Belt Supergroup in Montana), regarding them as micro-pseudofossils (pseudomicrofossils). However, there is no doubt that the Wernecke structures are the remains of completely replaced, and morphologically transformed, filamentous organisms, given their shapes, size range, disposition and orientation in the rock, and their association with organically preserved, and morphologically similar remains such as **Eomycetopsis** and **Siphonophycus** (see Pl. 32.2, fig. L; Pl. 32.3, figs. G, H, O, P, Q). Intermediate preservational stages are probably represented by **Eomycetopsis** tubes with cubic "compartments" that probably represent pyrite crystal moulds (e.g. Pl. 32.3, fig. K, from same rock sample). These elements in the tubes, or in the chains, may not necessarily have any relation to the shape or positions of original cells in the filament.

PLATE 32.3

Filamentous microfossils from the Wernecke Mountains. All remains photographed in transmitted light. All are macerations, except N and P, which are thin sections parallel to bedding. Length of all bar-scales is 10 µm. For localities see Figure 32.1.

		G.S.C. Locality	G.S.C. Type	Stage Coordinates
A	**Eomycetopsis** sp.	99097	76573	72.4x-4.6y
B	**Eomycetopsis** sp.	99094	76574	58.4x-15.0y
C	**Siphonophycus** sp.	99044	76575	56.3x-13.7y
D	**Siphonophycus** sp. with crystal coats	99062	76576	65.8x-23.7y
E	**Eomycetopsis**? sp. with crystal coats	99044	76577	52.8x-3.2y
F	**Eomycetopsis**? sp. with crystal coats	99131	76578	53.3x-8.8y
G	**Eomycetopsis** sp.	99115	76579	56.5x-7.3y
H	**Siphonophycus** sp., some faint transverse markings present	99115	76580	64.4x-7.5y
I	**Archaeotrichion** sp.	99140	76581	62.8x-6.7y
J	**Siphonophycus?** sp.	99062	76582	51.4x-8.2y
K	**Eomycetopsis?** sp. with crystal coats	99115	76583	50.5x-6.7y
L	**Siphonophycus** sp.	99080	76584	47.5x--18.3y
M	**Archaeotrichion** sp.	99140	76585	51.8x-11.6y
N	**Nostocomorpha** sp., chain of pyrite elements in thin section	99115	76586	40.0x-10.0y
O	**Eomycetopsis** sp.	99115	76587	55.3x-20.0y
P	**Eomycetopsis** sp., in thin section	99115	76588	46.4x-11.3y
Q	**Oscillatoriopsis psilata**	99115	76589	55.7x-20.0y

Genus **Archaeorestis** Barghoorn, 1965
Archaeorestis? sp.
Pl. 32.2, fig. G

Description. Incomplete, nonseptate, dichotomously branched tubular filament, about 90 µm long, twisted and distorted; filament width greatest in proximal region – 6 µm – descreasing to 4 µm distally. One branch (left of Pl. 32.2, fig. G) possibly attached to a flattened bulbose terminal structure about 20 µm across.

Occurrence. Vampire Formation (GSC loc. 99115).

Comments. Only one specimen was observed. Its taxonomic affinities remain obscure.

Incertae sedis
Genus **Paleamorpha** Sin and Liu, 1978
Paleamorpha? sp.
Pl. 32.2, figs. E, J?

Paleamorpha figurata Sin and Liu, 1978, p. 126, Pl. 10, figs. 5-6.
Tortunema eniseica Hermann, Yankauskas, 1982, p. 114-115, Pl. 38, fig. 9.

Description. One specimen (Pl. 32.2, fig. E) is a textured fragment of organic matter 5-9 µm wide, 60 µm long, with net-like pattern of closely spaced, submicrometric strands of dark, parallel to subparallel, spirally wound filaments; apparently tubular, with darker, axial portion 2-4 µm wide. A possible second specimen is a textured fragment of organic matter, 8-10 µm wide, 55 µm long, with much more irregular net-like pattern, without distinct spiraliform structure and without darker axial portion.

Occurrence. Unnamed siltstone unit 1 (GSC locs. 99062, 99063); ?basal Vampire Formation (GSC loc. 99140).

Comments. Only three specimens are known. The one in Plate 32.2, figure 3 resembles an Upper Riphean structure from Bashkiria, illustrated by Yankauskas (1982, Pl. 38, fig. 9) under **Tortunema eniseica**, which, however is larger

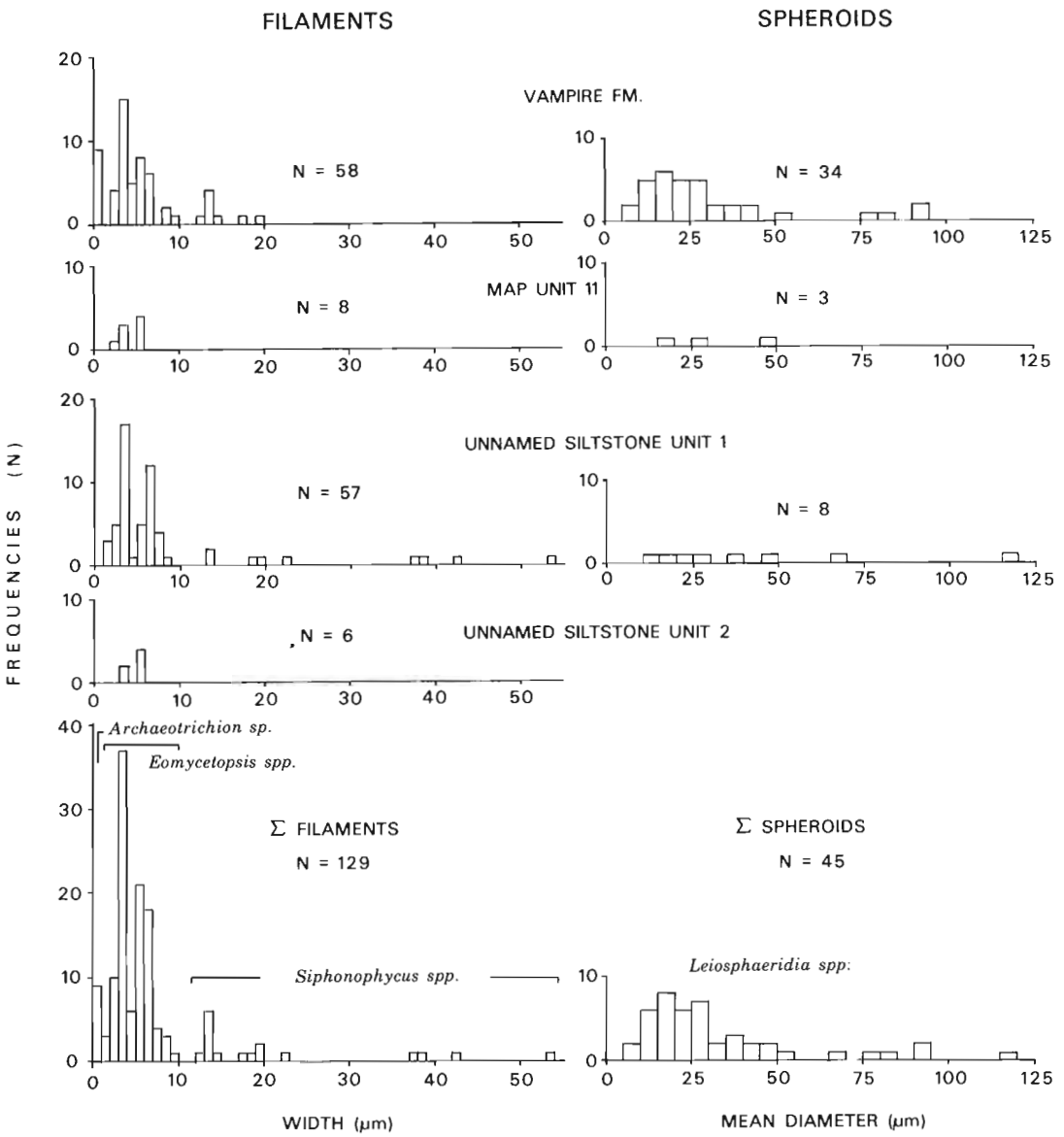

Figure 32.2. *Size ranges of selected microfossil taxa, Wernecke Mountains.*

in size. The other illustrated specimen resembles the **Paleamorpha figurata** reported by Sin and Liu (1978, p. 126, Pl. 10, figs. 5-6) from the Sinian of the Yangtse Gorge.

Microdubiofossil Type A
Pl. 32.1, figs. H, I, K-M

Description. Clumps of spheroidal aggregates of dark brown organic material with net-like pattern outlining generally regular polygons on surface; polygons of uniform size, 1.5-2.5 μm wide; spheroids in individual clumps of uniform size, 6-11 μm across; clumps containing as many as a dozen patterned spheroids; largest clump (Pl. 32.1, fig. I) 22 μm across, smallest specimen (Pl. 32.1, fig. K) a single fragmental patterned spheroid 6 μm wide. Interior of patterned spheroids apparently hollow, without structure.

Occurrence. Vampire Formation (GSC locs. 99072, 99080).

Comments. The interpretation of the structures presents some difficulty. They vaguely resemble the clumps referred to as **Pyritosphaera barbaria** Type II by Duchesne (1963) and to **Favososphaera** by Burmann (1972) and Chauvel and Mansuy (1981a, p. 37). If biologic, they may be pyritized remains of organisms such as the modern chroococcalean cyanobacteria **Microcystis** and **Gomphosphaeria.** Alternatively, they could be organic coatings on a framboidal substrate, with the shape being produced abiogenically, and thus may be related to the structures described further on under crystal coats (Pl. 32.2, figs. F, I). The patterned spheroids differ from the bodies described as microdubiofossil type B by their regular pattern of uniform, isodiametric polygonal compartments on the surface.

Microdubiofossil Type B
Pl. 32.1, figs. N, O

Description. Solitary, irregularly shaped globoids, 10-25 μm wide, with surface network of organic material outlining contiguous holes of variable size and shape, mostly angulate, and between 1 and 5 μm across.

Occurrence. Vampire Formation (GSC locs. 99072, 99073).

Comments. The cavities cause these structures to resemble the problematic acritarch **Trematosphaeridium,** but in the latter genus the outlines are not so consistently angulate, nor are they as closely spaced, and the organic matter is much denser than in the present material. The remains here reported from the Wernecke Mountains are regarded as organic spheriods which owe their ultimate morphology to the process of moulding around diagenetic pyrite crystals. These crystals are of variable size and shape, and thus differ from normal framboidal pyrite, which is characterized by the uniform size of its elements (e.g. Pl. 32.1, fig. J).

Microdubiofossil Type C
Pl. 32.2, fig. K

Description. Dense, dark brown, vesicular filamentous body, about 200 µm long, with tripartite organization. It is composed of slightly fusiform, curved cylinder 11-20 µm wide and 140 µm long, attached to a vesicular spheriod 20 µm across, to which is attached on the opposite pole a curved narrow filament 3-4 µm wide and 40 µm long.

Occurrence. Basal part of Vampire Formation (GSC loc. 99130).

Comments. Only the single specimen illustrated was observed. The affinity of this unusual form is undetermined.

Crystal coats
Pl. 32.2, figs. F, I, H; Pl. 32.3, figs. D-F, K

Description. Fragments of organic residues with single or multiple cubic and other polyhedral compartments 1-5 µm across; with and without centrally or eccentrically located opaque inclusion.

Occurrence. Unnamed siltstone unit 1 (GSC locs. 99044, 99062); Vampire Formation (GSC locs. 99072, 99140).

Comments. The remains grouped under this heading include scraps of degraded organic matter the morphology of which is quite diverse. The shape of the compartments, which are not considered to be the remains of cells, include various crystal habits of pyrite, predominantly cubes and octahedra (Pl. 32.2, figs. F, I). They appear to be of the same origin as the crystal coats developed on the more complete, identifiable taxa (Pl. 32.2, figs. C, D; Pl. 32.3, figs. D-F, K), and are most likely fragments derived from such larger specimens. The fact that they appear isolated in the macerations, as well as in identifiable microfossils, suggests that certain taxa with crystal-like outlines reported in the literature may have to be re-examined for possible reinterpretation as diagenetically produced forms, resulting from remobilization of organic matter around growing crystals (e.g. **Anguloplanina;** see also Love and Zimmerman, 1961, figs. 6-20, and Love, 1965, Pl. 14).

Discussion and summary

Organic-walled microfossils were studied from an interval that spans the Precambrian-Cambrian transition, as previously determined from shelly fossils and trace fossils. The composition of the microbiota recovered from these beds is such that no strong conclusions can be drawn concerning the placement of this boundary. The taxa are all long-ranging forms. The general absence throughout the studied interval of complex, spinose acritarchs of the baltisphaerid type, and more complex ones elsewhere typical of Cambrian deposits, is noteworthy. Sphaeromorphs are numerically more abundant in the Vampire Formation than in older units, but nematomorphs are equally common on either side of the presumed Precambrian-Cambrian boundary (Figs. 32.1, 32.2).

The presence of abundant **Bavlinella** has been used by some to suggest a Late Riphean (?) to Early Cambrian age for the containing beds (e.g. Vidal 1979a, p. 8; Lenk et al., 1982, p. 620). However, this suggestion will require further evaluation. There is obviously a need to re-examine and compare type material of the several apparently synonymous taxa erected for these raspberry-like microstructures in Early Proterozoic to Paleozoic and Mesozoic deposits. Also, it would be useful to perform further experiments that simulate diagenesis leading to organically coated framboidal pyrite and to pyritized **Microcystis**-like microfossils in fine grained sediments.

The most important results of the present study are not biostratigraphic, but deal with post-burial changes of microfossils. The great variety of diagenetic modification is remarkable, particularly the remobilization of organic matter around growing pyrite crystals and the subsequent transformation of pyrite to hematite/limonite. The post-depositional paragenesis is particularly well displayed in macerates of partially pyritized filaments and sphaeromorphs, and in some thin sections in which the reduced and oxidized remains are both present. The study thus confirms the conclusions of some previous workers (e.g. Neves and Sullivan, 1964; Volkova, 1974) regarding the great variety of degradational forms which individual taxa of shale-facies microfossils can assume during diagenesis. Such secondary morphological variability can be compared and contrasted with the various degradational stages known from individual taxa in Proterozoic stromatolitic microbiotas preserved in chert (e.g. Hofmann, 1976). The observations indicate that acritarch taxonomy and systematics continue to require reassessment.

References

Blusson, S.L.
1971: Sekwi Mountain map-area, Yukon Territory and District of Mackenzie; Geological Survey of Canada, Paper 71-22, 17 p., Map 1333A.

1974: Geological Survey of Canada, Open File Report 205; Map 106A, B, C, and 105O.

Burmann, G.
1972: Problematik aus der Lausitzer Grauwackenformation; Jahrbuch für Geologie, v. 4, p. 387-423.

Chauvel, J.J. and Mansuy, C.
1981a: Micropaléontologie du Protérozoïque du Massif Armoricain (France); Precambrian Research, v. 15, p. 25-42.

1981b: **Paleocryptidium cayeuxi:** Une Cyanophycée du Précambrien du Massif Armoricain; Bulletin Société géologique de France, sér. 7, v. 23, no. 5, p. 449-458.

Cloud, P., Moorman, M., and Pierce, D.
1975: Sporulation and ultrastructure in a Late Proterozoic cyanophyte: some implications for taxonomy and plant phylogeny; Quarterly Review of Biology, v. 50, no. 2, p. 131-150.

Deflandre, G.
1968: Sur l'existence, dès le Précambrien, d'Acritarches du type Acanthomorphitae: **Eomicrhystridium** nov. gen. Typification du genre **Palaeocryptidium** Defl. 1955; Comptes Rendus, Académie des Sciences, Paris, v. 266, sér. D, no. 26, p. 2385-2389.

Diver, W.L. and Peat, C.J.
1979: On the interpretation and classification of Precambrian organic-walled microfossils; Geology (Boulder), v. 7, p. 401-404.

Downie, C. and Sarjeant, W.A.S.
1963: On the interpretation and status of some hystrichosphere genera; Palaeontology, v. 6, pt. 2, p. 83-96.

Downie, C., Evitt, W.R., and Sarjeant, W.A.S.
1963: Dinoflagellates, hystrichospheres, and the classification of the acritarchs; Stanford University Publications, Geological Sciences, v. 7, no. 3, p. 1-16.

Duchesne, J.C.
1963: Un gisement de **Pyritosphaera barbaria** dans le Cambrien de la vallée du Bayehon (Ardennes belges); Annales, Société Géologique de Belgique, v. 86, Bulletin no. 2, p. B123-B130.

Fritz, W.H.
1982: Vampire Formation, a new Upper Precambrian(?)/Lower Cambrian formation, Mackenzie Mountains, Yukon and Northwest Territories; in Current Research, Part B, Geological Survey of Canada, Paper 82-1B, p. 83-92.

Fritz, W.H., Narbonne, G.M., and Gordey, S.P.
1983: Strata and trace fossils near the Precambrian-Cambrian boundary, Mackenzie, Selwyn, and Wernecke Mountains, Yukon and Northwest Territories; in Current Research, Part B, Geological Survey of Canada, Paper 83-1B, p. 365-375.

Gutstadt, A.M. and Schopf, J.W.
1969: Possible algal microfossils from the Late Pre-Cambrian of California; Nature, v. 223, p. 165-167.

Hofmann, H.J.
1976: Precambrian microflora, Belcher Islands, Canada: significance and systematics; Journal of Paleontology, v. 50, no. 6, p. 1040-1073.

Hofmann, H.J. and Aitken, J.D.
1979: Precambrian biota from the Little Dal Group, Mackenzie Mountains, northwestern Canada; Canadian Journal of Earth Sciences, v. 16, no. 1, p. 150-166.

Hofmann, H.J., Fritz, W.H., and Narbonne, G.M.
1983: Ediacaran (Precambrian) fossils from the Wernecke Mountains, northwestern Canada; Science, v. 221, p. 455-457.

Hofmann, H.J., Hill, J., and King, A.F.
1979: Late Precambrian microfossils, southeastern Newfoundland; in Current Research, Part B, Geological Survey of Canada, Paper 79-1B, p. 83-98.

Horodyski, R.J.
1980: Middle Proterozoic shale-facies microbiota from the lower Belt Supergroup, Little Belt Mountains, Montana; Journal of Paleontology, v. 54, no. 4, p. 649-663.

Kalliokoski, J.
1974: Pyrite framboid: animal, vegetable, or mineral?; Geology (Boulder), v. 2, no. 1, p. 26-27.

Knoll, A.H., Blick, N., and Awramik, S.M.
1981: Stratigraphic and ecologic implications of Late Precambrian microfossils; American Journal of Science, v. 281, p. 247-263.

Knoll, A.H. and Golubic, S.
1979: Anatomy and taphonomy of a Precambrian algal stromatolite; Precambrian Research, v. 10, p. 115-151.

Konzalova, M.
1974: Acritarchs from the Bohemian Precambrian (Upper Proterozoic) and Lower-Middle Cambrian; Review of Palaeobotany and Palynology, v. 18, p. 41-56.

Lenk, C., Strother, P.K., Kaye, C.A., and Barghoorn, E.S.
1982: Precambrian age of the Boston Basin: new evidence from microfossils; Science, v. 216, p. 619-620.

Love, L.G.
1957: Micro-organisms and the presence of syngenetic pyrite; Geological Society of London, Quarterly Journal, v. 113, no. 4, p. 429-437, 439-440.

1965: Micro-organic material with diagenetic pyrite from the Lower Proterozoic Mount Isa Shale and a Carboniferous shale; Proceedings of the Yorkshire Geological Society, v. 35, pt. 2, no. 9, p. 187-202.

Love, L.G. and Zimmerman, D.O.
1961: Bedded pyrite and micro-organisms from the Mount Isa Shale; Economic Geology, v. 56, p. 873-896.

Maithy, P.K. and Shukla, M.
1977: Microbiota from the Suket Shales, Rampura, Vindhyan System (Late Pre-Cambrian), Madhya Pradesh; The Palaeobotanist, v. 23, no. 2, p. 176-188.

Mansuy, C. and Vidal, G.
1983: Late Proterozoic Brioverian microfossils from France: taxonomic affinity and implications of plankton productivity; Nature, v. 302, p. 606-607.

Mikhailova, N.S.
1979: Mikrofitofossilii Udokanskoy i Bodaibinskoy serii (Microphytofossils of the Udokan and Bodaibo series); in B.S. Sokolov, ed., Paleontologiya dokembriya i rannego kembriya (Paleontology of the Precambrian and Early Cambrian); "Nauka", Leningrad, 304 p. (p. 121-128).

Moorman, M.
1974: Microbiota of the Late Proterozoic Hector Formation, southwestern Alberta, Canada; Journal of Paleontology, v. 48, no. 3, p. 524-539.

Neves, R. and Sullivan, H.J.
1964: Modification of fossil spore exines associated with the presence of pyrite crystals; Micropaleontology, v. 10, no. 4, p. 443-452.

Schopf, J.W.
1968: Microflora of the Bitter Springs Formation, Late Precambrian, central Australia; Journal of Paleontology, v. 42, p. 651-688.

Shepeleva, Ye. D.
1962: Rastitel'nye(?) ostatki neizvestnoy sistematicheskoy prinadlezhnosti iz otlozheniy bavlinskoy serii Volgo-Ural'skoy neftenosnoy provintsii [Plant (?) fossils of unknown taxonomic position from the deposits of the Bavlinskaya Series in the Volga-Urals oil province]; Doklady Akademii Nauk SSSR, v. 142, no. 2, p. 456-457 (Amer. Geol. Inst. Translation, p. 170-171).

Sin Yu-sheng and Liu Kui-chih.
1973: On Sinian microflora in Yenliao region of China and its geological significance; Acta Geologica Sinica, no. 1, p. 1-64. (In Chinese, with English abstract and diagnoses of taxa). A complete English translation is: Hsing-Yu-sheng and Liu Kuei-chih, 1975, Sinian microflora in the Yenliao region of China and its geological significance (Available from Plenum Publishing Corporation, 227 West 17th Street, New York, N.Y. 10011).

Sin Yu-sheng and Liu Kui-chih.
1978: Sinian microplant and algal fossils, p. 109-126; in "Stratigraphy and paleontology, Sinian to Permian, East Gorge Area"; Shanshia Stratigraphic Division, Hubei Geological Survey, 381 p., 113 plates.

Vidal, G.
1976: Late Precambrian microfossils from the Visingso Beds in southern Sweden; Fossils and Strata, no. 9, p. 1-57, Oslo.

1979: Acritarchs and the correlation of the Upper Proterozoic; Publications from the Institute of Mineralogy, Palaeontology and Quarternary Geology, University of Lund, Sweden, no. 219, 22 p.

Vidal, G. and Knoll, A.H.
1982: Radiations and extinctions of plankton in the Late Proterozoic and early Cambrian; Nature, v. 297, p. 57-60.

Volkova, N.A.
1964: Fitoplankton drevneyshykh otlozheniy severo-zapadnogo podmoskovya i ego znachenie dlya stratigrafii (Phytoplankton from the oldest deposits developed to the northwest of Moscow and its significance for stratigraphy); Izvestiya Akademii Nauk SSSR, Seriya Geologicheskaya; 1964, no. 4, p. 74-84.

Volkova, N.A. (cont.)
1974: Tipy povrezhdeniy obolochek dokembriyskikh i kembriyskikh akritarkh (Types of damage to the body of Precambrian and Cambrian acritarchs); Paleontologicheskiy Zhurnal, 1974, no. 9, p. 101-108 (Paleontological Journal, English translation, p. 530-536).

Volkova, N.A., Kiryanov, V.V., Piskun, L.V.,
Pashkyavichene, L.T., and Jankauskas, T.V.
1982: Mikrofossilii rifeya Yuzhnogo Urala (Microfossils of the Riphean of the South Urals); in Stratotyprifeya - paleontologiya, paleomagnetizm (Stratotype of the Riphean -- paleontology, paleomagnetism) B.M. Keller, (ed.); Akademiya Nauk SSSR, Geological Institute, Transactions, v. 368, p. 84-120.

Walcott, C.D.
1914: Cambrian geology and paleontology III, no. 2 - Pre-Cambrian Algonkian algal flora; Smithsonian Miscellaneous Collections, v. 64, no. 2, p. 77-156.

Wang, F. and Luo, Q.
1982: Precambrian Acritarcha: a cautionary note; Precambrian Research, v. 16, p. 291-302.

Wheeler, J.O.
1954: A geological reconnaissance of the northern Selwyn Mountains region, Yukon and Northwest Territories; Geological Survey of Canada, Paper 53-7, 42 p.

Yankauskas, T.V.
1979: Rastitelnye microfossilii (Microflora); in Paleontologiya verkhnedokembriiskikh i kembriiskikh otlozheniy Vostochno-Evropeiskoy platformy (Upper Precambrian and Cambrian paleontology of the East-European Platform), B.M. Keller and A. Yu. Rozanov, eds.; "Nauka", Moscow, 212 p. (p. 4-38).

Yin Leiming and Li Zaiping
1978: Precambrian microfloras of southwest China, with reference to their stratigraphical significance: Memoirs of Nanjing Institute of Geology and Paleontology, Academia Sinica, 1978, no. 10, p. 41-102. (In Chinese, with summary and diagnoses of new taxa in English).

Zhang, Z.
1982: Upper Proterozoic microfossils from the Summer Isles, N.W. Scotland; Palaeontology, v. 25, pt. 3, p. 443-460.

33.

THE WILKIE POINT GROUP (LOWER-UPPER JURASSIC), SVERDRUP BASIN, ARCTIC ISLANDS

Project 750083

Ashton F. Embry
Institute of Sedimentary and Petroleum Geology, Calgary

Embry, A.F., The Wilkie Point Group (Lower-Upper Jurassic), Sverdrup Basin, Arctic Islands; in Current Research, Part B, Geological Survey of Canada, Paper 84-1B, p. 299-308, 1984.

Abstract

The Wilkie Point Formation, a Lower-Upper Jurassic sandstone-dominant unit in the Sverdrup Basin, is herein raised to group status. Four new formations are recognized within the group. These new formations are formally defined herein and, in ascending order are: Jameson Bay, Sandy Point, McConnell Island and Hiccles Cove. The Jameson Bay and McConnell Island formations comprise mainly shale and siltstone of offshore marine shelf origin. The Sandy Point and Hiccles Cove consist predominantly of very fine- to medium-grained sandstone of nearshore to strandplain origin.

The Jameson Bay Formation is divided into three members that are formally defined herein. In ascending order these members are named Intrepid Inlet, Cape Canning and Snowpatch.

Résumé

La formation de Wilkie Point, unité à grès dominants du Jurassique inférieur et supérieur dans le bassin de Sverdrup, a été reclassée comme groupe. Quatre nouvelles formations sont reconnues dans le groupe. Ces nouvelles formations sont définies dans ce texte et elles sont par ordre ascendant: Jameson Bay, Sandy Point, McConnell Island et Hiccles Cove. Les formations de Jameson Bay et McConnell Island comprennent surtout des schistes argileux et du siltstone ayant pour origine un plateau continental marin. Les formations de Sandy Point et de Hiccles Cove comprennent surtout des grès à grains très fins à moyens provenant des plaines d'accumulation littorale.

La formation de Jameson Bay est divisée en trois membres qui sont définis dans ce texte. Par ordre ascendant ces membres sont: Intrepid Inlet, Cape Canning et Snowpatch.

Introduction

The Wilkie Point Formation was defined by Tozer (1956) as a sandstone-dominant unit of Early, Middle and Late Jurassic age that outcrops on Prince Patrick Island. Subsequent to Tozer's field studies numerous wells have been drilled on Prince Patrick and adjacent areas. Subsurface studies have led to the recognition of four distinctive lithological units in the Wilkie Point. Consequently the Wilkie Point is herein raised to group status and four component formations are formally defined.

Regional stratigraphic studies have revealed that the formations of the Wilkie Point Group are widespread in the Sverdrup Basin (Fig. 33.1). Surface sections for the formations have been measured at numerous localities in the eastern Sverdrup where Mesozoic strata are folded and faulted and exposed in mountainous terrain. In the central and western Sverdrup, where structures and the terrain have much lower relief, outcrops are confined mainly to the basin margins. Eighty-eight wells have penetrated the formations, with most of the well control occurring in the western Sverdrup (Fig. 33.1).

Previous work

Tozer (1956) recognized the Wilkie Point Formation during reconnaisance field work on Prince Patrick Island in the summer of 1954. He established a type section on the coastal exposures along the east side of Intrepid Inlet and estimated the thickness of the formation to be 200 m. The base of the formation is not exposed at the type section although at other localities Tozer (1956) found the Wilkie Point resting unconformably on Devonian strata. At the type section, the Wilkie Point is overlain by the Mould Bay Formation. The Wilkie Point is a sandstone-dominant unit and Tozer (1956) distinguished a lower member consisting of red-brown to orange weathering, fossiliferous sandstone, and an upper member of white, carbonaceous sandstone. The basal portion of the type section is recessive and not exposed.

Tozer continued his field studies of the western Sverdrup in 1958, extending the Wilkie Point Formation to Melville, Borden and Mackenzie King islands (Tozer and Thorsteinsson, 1964). The Wilkie Point on Melville is similar to that on Prince Patrick, and Tozer and Thorsteinsson (1964) recognized the same two informal members. On Mackenzie King the lower portion of the formation was found to consist of shale and siltstone, and strata similar to the upper member were not present. On Borden Island a contact of the basal shale and siltstone of the Wilkie Point with sandstone of the Borden Island Formation was established. Fossils collected from the Wilkie Point in the western Sverdrup are Early and Middle Jurassic in age (Tozer and Thorsteinsson, 1964).

The name Wilkie Point was not extended to the central and eastern Sverdrup where equivalent strata were assigned to either the Jaeger Formation or the Savik Formation. The Jaeger Formation was defined by Greiner (1963) from studies undertaken on Cornwall Island during Operation Franklin in 1955. He described the formation as consisting of 300 m of grey to red-brown, pebbly sandstone containing Lower and Middle Jurassic fossils. At the type section on eastern Cornwall Island the Jaeger is bounded by the Heiberg Formation below and the Awingak Formation above.

Also during Operation Franklin, Souther (1963) studied the Mesozoic succession of central Axel Heiberg Island. In this area, the strata between the Heiberg and Awingak formations consist of shale and siltstone. Souther (1963) named these argillaceous strata the Savik Formation, and he established a type section west of Buchanan Lake on eastern Axel Heiberg. Lower, Middle and Upper Jurassic fossils were found in the Savik during Operation Franklin (Tozer, 1963a).

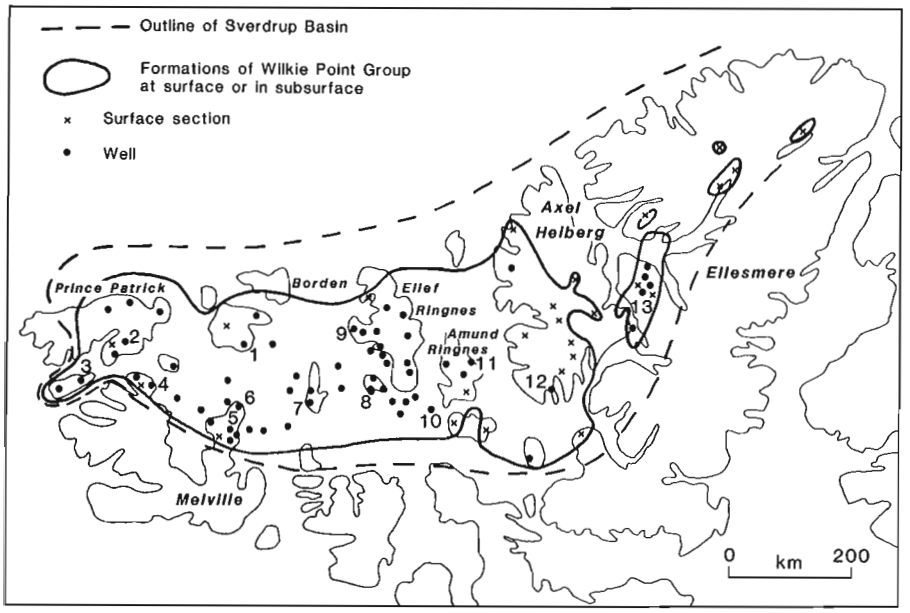

Figure 33.1. *Distribution of formations of Wilkie Point Group and control points. Key to numbered wells listed in appendix.*

1. *Cape Norem A-80,*
2. *Jameson Bay C-31,*
3. *Eglinton P-24,*
4. *Depot Island C-44,*
5. *Drake Point D-68,*
6. *North Sabine H-49,*
7. *Skybattle Bay C-15,*
8. *Sutherland O-23,*
9. *Mocklin Point D-23,*
10. *Linckens Island P-46,*
11. *East Amund M-05,*
12. *Sherwood P-37,*
13. *Romulus C-42.*

Tozer (1963b) examined Mesozoic strata on Ellesmere and Axel Heiberg islands in the late fifties and early sixties. He extended the Savik Formation over much of Axel Heiberg and western Ellesmere. On Ellesmere and southern Axel Heiberg Tozer (1963b) recognized a glauconitic sandstone unit within the Savik Formation and he referred to it as the Jaeger Member. Shales below the Jaeger Member are medium to dark green-grey and were called "Lower Savik", and those above are dark grey to black and were called "Upper Savik" (Tozer, 1963b). Tozer demonstrated that at the type section the "Upper Savik" unconformably overlies the "Lower Savik" and that Middle Jurassic strata are missing. However on western Axel Heiberg the Savik Formation includes Middle Jurassic strata (Tozer, 1963b).

Fricker (1963) mapped in detail the area surrounding Expedition Fiord on west-central Axel Heiberg and his report contains a description of three measured sections through the Savik Formation.

In 1967 Stott (1969) mapped Ellef Ringnes Island. On Reindeer Peninsula he recognized both Savik and Jaeger formations. The Savik in this area consists of 76 m of soft, greenish grey shale and contains Toarcian, Aalenian and Bathonian fossils. It overlies the Borden Island Formation and is overlain by the Jaeger, which consists of 15 m of glauconitic sandstone with Callovian fossils. The Jaeger is overlain by dark grey to black shale which Stott (1969) assigned to the Deer Bay Formation.

On northeastern Ellesmere Island Nassichuk and Christie (1969) included all strata between the Heiberg Formation and the Isachsen Formation in an informal "Jurassic-Cretaceous shales and sandstones" unit. A red weathering, glauconitic sandstone near the base of the map unit was referred to as "Jaeger equivalent".

Balkwill (1983) mapped Amund Ringnes, and Cornwall islands. He divided the Jaeger Formation of Cornwall Island into four informal members: a lower shale-siltstone (JjA), a lower sandstone (JjB), an upper shale-siltstone (JjC), and an upper sandstone (JjD). Balkwill (1983) also recognized an "Upper Savik" unit on Cornwall between the Jaeger and the Awingak. These strata consist mainly of dark grey, silty shale and contain a medial sandstone unit.

On Amund Ringnes, Balkwill (1983) mapped the Savik Formation between the Heiberg Formation and the Ringnes Formation (Upper Jurassic, dark grey shale). In subsurface sections for the area Balkwill (1983) subdivided the Savik into Lower Savik (Lower Shale), Jaeger, and Upper Savik (Upper Shale) members.

Subsurface studies of strata now included in formations of the Wilkie Point Group include those of Henao-Londono (1977) on Sabine Peninsula, Melville Island, Balkwill and Roy (1977) on King Christian Island, and Balkwill et al. (1982) on Lougheed Island. Henao-Londono (1977) subdivided the Wilkie Point interval into lower Wilkie Point (siltstone-sandstone), Savik (shale-siltstone) and upper Wilkie Point (sandstone), and indicated that both the lower contact with the Borden Island and the upper contact with the Mould Bay are unconformable.

On King Christian Island, Balkwill and Roy (1977) subdivided the Savik Formation into Lower Shale, Jaeger and Upper Shale members. Balkwill et al. (1982) did not subdivide the Savik in the Skybattle Bay C-15 well on Lougheed Island.

Macrofossil identifications from Wilkie Point Group strata are found in the above publications and also in Frebold (1958, 1960, 1961, 1964, 1975). Identifications of recent collections are in unpublished GSC paleontological reports. Palynological data from Wilkie Point strata have been published by Johnson and Hills (1973) and Davies (1983) and a considerable amount of data is also in unpublished reports. Wall (1983) described the micropaleontology from the Savik Formation of Ellesmere and Axel Heiberg islands.

Present work

Rocks now included in formations of the Wilkie Point Group comprise the strata between the sandstones of the Heiberg Formation/Group (Embry, 1983a, b) below, and the dark shales of the Ringnes Formation (Balkwill et al., 1977) above. These strata have been studied by various geologists in different parts of the Sverdrup Basin and a somewhat confusing nomenclature has evolved. For this study all subsurface sections for these strata have been examined and surface sections in the eastern, central, and western Sverdrup have been measured (Fig. 33.1). All of these sections have

been correlated, and four distinct formations have been recognized. In ascending order these four formations and their dominant lithologies are: Jameson Bay (shale-siltstone), Sandy Point (sandstone), McConnell Island (shale-siltstone), and Hiccles Cove (sandstone).

Figure 33.2 is a stratigraphic cross-section of the Wilkie Point Group between Prince Patrick and Melville islands. Notable stratigraphic relationships illustrated on this section include:

1. The Jameson Bay Formation in this area is divided into three members on the basis of the occurrence of two clay-rich shale units. In ascending order these members are named Intrepid Inlet, Cape Canning and Snowpatch. They are formally described herein.
2. The Sandy Point Formation gradationally overlies the Jameson Bay and is unconformably overlain by the McConnell Island Formation.
3. The Hiccles Cove Formation conformably overlies the McConnell Island and it gradually shales out northeastwards.
4. The contact between the Hiccles Cove and the overlying Ringnes Formation is conformable along this line of section. However, as demonstrated by Tozer and Thorsteinsson (1964), this contact becomes unconformable to the southwest of the Jameson Bay C-31 well.

Figure 33.3 illustrates the relationships between the new formations and the informal and formal nomenclature used by previous workers. "Jaeger" was used for a variety of

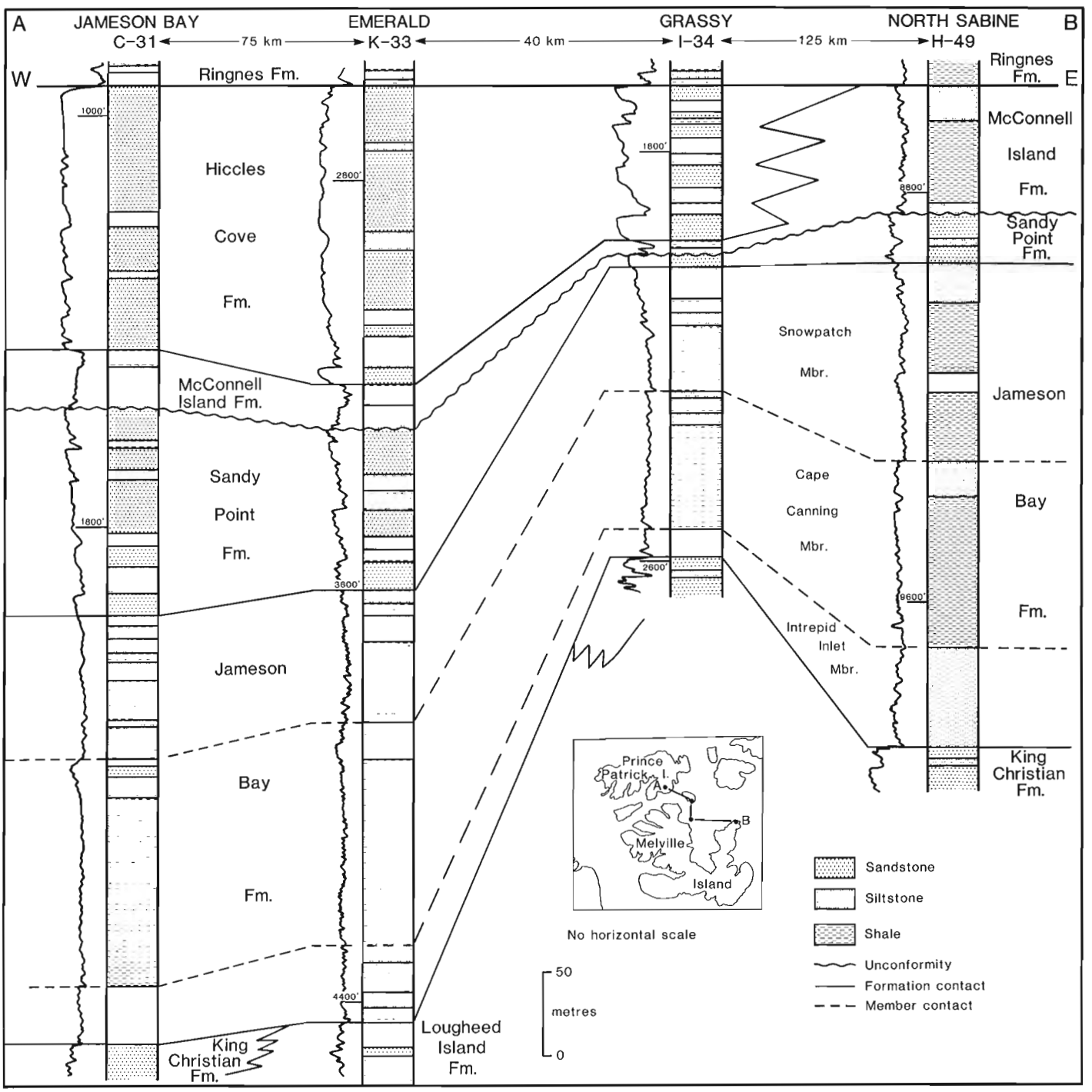

Figure 33.2. *Stratigraphic cross-section, Wilkie Point Group, western Sverdrup Basin. Gamma-ray logs displayed beside lithologies.*

stratigraphic units and consequently the term is herein abandoned. The name Wilkie Point now refers to a group and is used in basin margin areas where sandstones of the Sandy Point and Hiccles Cove formations are prominent. Strata previously assigned to the Savik Formation are now placed in the Jameson Bay, Sandy Point (thin or absent), McConnell Island and Ringnes formations. The term Savik is retained and is given group status because it is a useful mapping unit on Axel Heiberg Island where it forms a recessive interval between the resistant Heiberg and Awingak formations. Figure 33.4 is a schematic cross-section illustrating the nomenclature and stratigraphic relationships for the succession between the Heiberg and the Awingak formations.

The tops for the new formations and members from thirteen selected wells throughout the Sverdrup Basin are listed in the Appendix. Chip samples taken at three-metre intervals from the type sections of the formations and members defined in this paper can be examined at the Institute of Sedimentary and Petroleum Geology, Calgary, Alberta, Canada.

Jameson Bay Formation

Definition

The Jameson Bay Formation consists of shale and siltstone with scattered thin interbeds of very fine grained sandstone. The type section is in the Elf Jameson Bay C-31 well (76°40'12"N, 116°43'45"W; spud. March 11, 1971, abandoned May 18, 1971, T.D. 2539 m, K.B. 63 m) between 601 m (1970 ft) and 855 m (2806 ft), and is 254 m thick (Fig. 33.5). The name is taken from Jameson Bay, which is on the east coast of Prince Patrick Island.

Synonyms

1. Lower portion of Wilkie Point Formation, western Sverdrup Basin (Tozer, 1956; Tozer and Thorsteinsson, 1964).
2. Lower Savik, Savik Formation, western Ellesmere and southern Axel Heiberg (Tozer, 1963b).
3. Units 1-3, Section S1 and units 1-4, Section S2, Savik Formation, Expedition Fiord, western Axel Heiberg (Fricker, 1963).
4. Units 1-4, Savik Formation, northwestern Ellef Ringnes (Stott, 1969).
5. Member JjC, Jaeger Formation, Cornwall Island (Balkwill, 1983).
6. Lower Savik, Savik Formation, Amund Ringnes and King Christian islands (Balkwill, 1983; Balkwill and Roy, 1977).
7. Lower Wilkie Point and Savik, Sabine Peninsula (Henao-Londono, 1977).

Boundaries

In the western Sverdrup the Jameson Bay Formation overlies sandstone of the King Christian Formation. The contact is placed at the base of the lowest shale-siltstone unit above which shale and siltstone are predominant. This contact is usually conformable but is unconformable on the basin margins (Embry, 1983b). In the central and eastern Sverdrup the Jameson Bay conformably overlies the Heiberg Formation. The contact is placed at the base of the lowest shale-siltstone unit above which shale and siltstone are predominant.

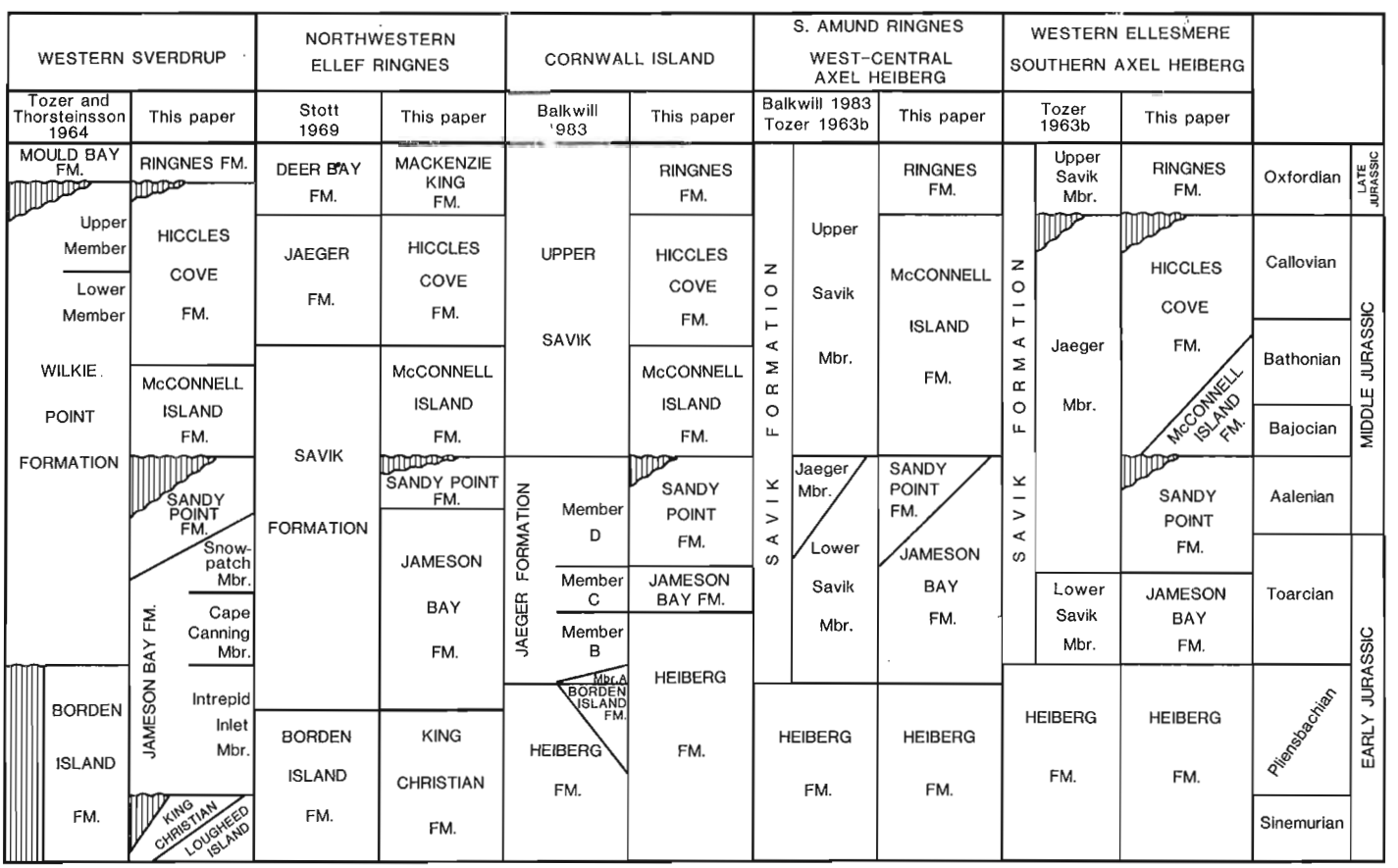

Figure 33.3. *Past and present nomenclature of Toarcian to Oxfordian strata, Sverdrup Basin.*

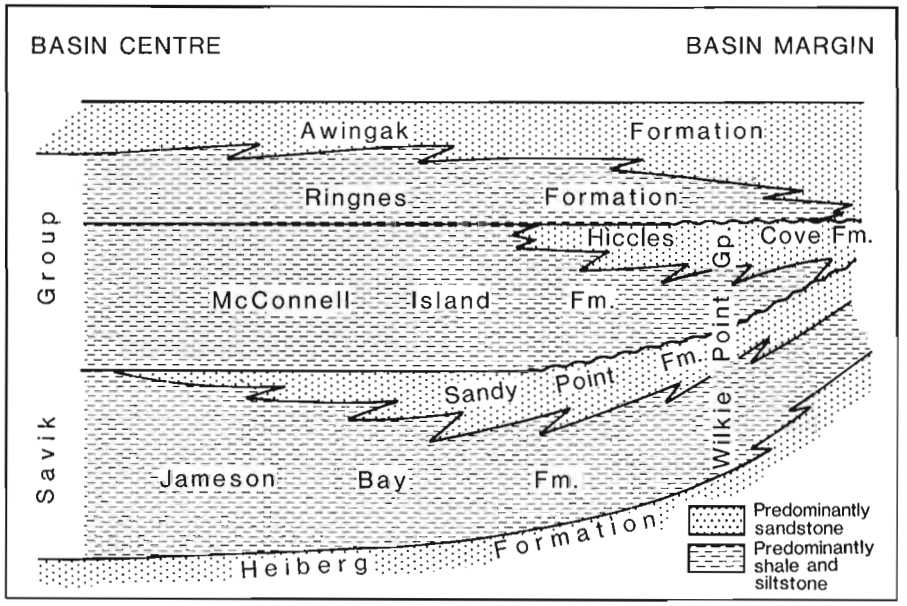

Figure 33.4

Schematic stratigraphic cross-section, Wilkie Point and Savik groups, Sverdrup basin.

Over most of the Sverdrup the Jameson Bay is conformably overlain by the Sandy Point Formation. The contact is placed at the base of the lowest sandstone unit above which sandstone is relatively common. In the basin centre the Sandy Point is absent due to facies change and the Jameson Bay is conformably overlain by the McConnell Island Formation. This contact is placed at the base of a clay-rich shale unit which overlies glauconitic siltstone of the uppermost Jameson Bay.

Lithology

The Jameson Bay consists mainly of medium to dark green-grey shale with siltstone laminae and interbeds. Very fine grained, glauconitic sandstone units up to one metre thick are also present in many sections but comprise only a small percentage of the formation. Shale units are parallel laminated to burrowed and siltstones and sandstones are usually extensively burrowed. Calcareous, dolomitic and sideritic concretions are very common throughout the Jameson Bay Formation.

Thickness and distribution

The Jameson Bay occurs over much of the Sverdrup (Fig. 33.1) and in general it thickens toward the centre of the basin. The maximum recorded thickness is 539 m (central Ellef Ringnes Island, Dumbells E-49 well).

Age

Ammonites collected from the Jameson Bay Formation on Prince Patrick, Borden, Cornwall, Axel Heiberg and Ellesmere islands have been dated as Pliensbachian, Toarcian and Aalenian (Frebold, 1960, 1975; Tozer, 1963b; Tozer and Thorsteinsson, 1964; Balkwill, 1983).

Environment of deposition

The Jameson Bay is interpreted to represent an offshore shelf deposit on the basis of lithology, fauna and stratigraphic relationships.

Intrepid Inlet Member, Jameson Bay Formation

Definition

The Intrepid Inlet Member consists of shale and siltstone with interbeds of very fine grained sandstone. The type section is in the Elf Jameson Bay C-31 well between 820 m (2690 ft) and 855 m (2806 ft) and is 35 m thick (Fig. 33.5). The name is taken from Intrepid Inlet, located on eastern Prince Patrick Island.

Synonyms

1. Glauconite unit, Borden Island Formation, Sabine Peninsula, Melville Island (Reinson, 1975).
2. Lower Wilkie Point, Sabine Peninsula (Meneley, 1977; Henao-Londono, 1977).
3. Upper portion, Borden Island Formation, Borden Island (Rahmani and Tan, 1978).
4. Unit C, Borden Island Formation, Sabine Peninsula (Douglas and Oliver, 1979).

Boundaries

The Intrepid Inlet Member overlies the King Christian Formation. The contact is placed at the base of the lowest shale-siltstone unit above which shale and siltstone are predominant. This contact varies from conformable to unconformable (Embry, 1983b). The Intrepid Inlet Member is conformably overlain by the Cape Canning Member of the Jameson Bay Formation. The contact is placed at the base of a clay-rich shale unit which rests on arenaceous siltstone of the uppermost Intrepid Inlet (Fig. 33.2, 33.5).

Lithology

The Intrepid Inlet Member consists mainly of medium grey, silty shale and light-to medium-grey siltstone. Thin, argillaceous, very fine grained sandstone beds are present in most sections. The sandstone beds are glauconitic and extensively burrowed.

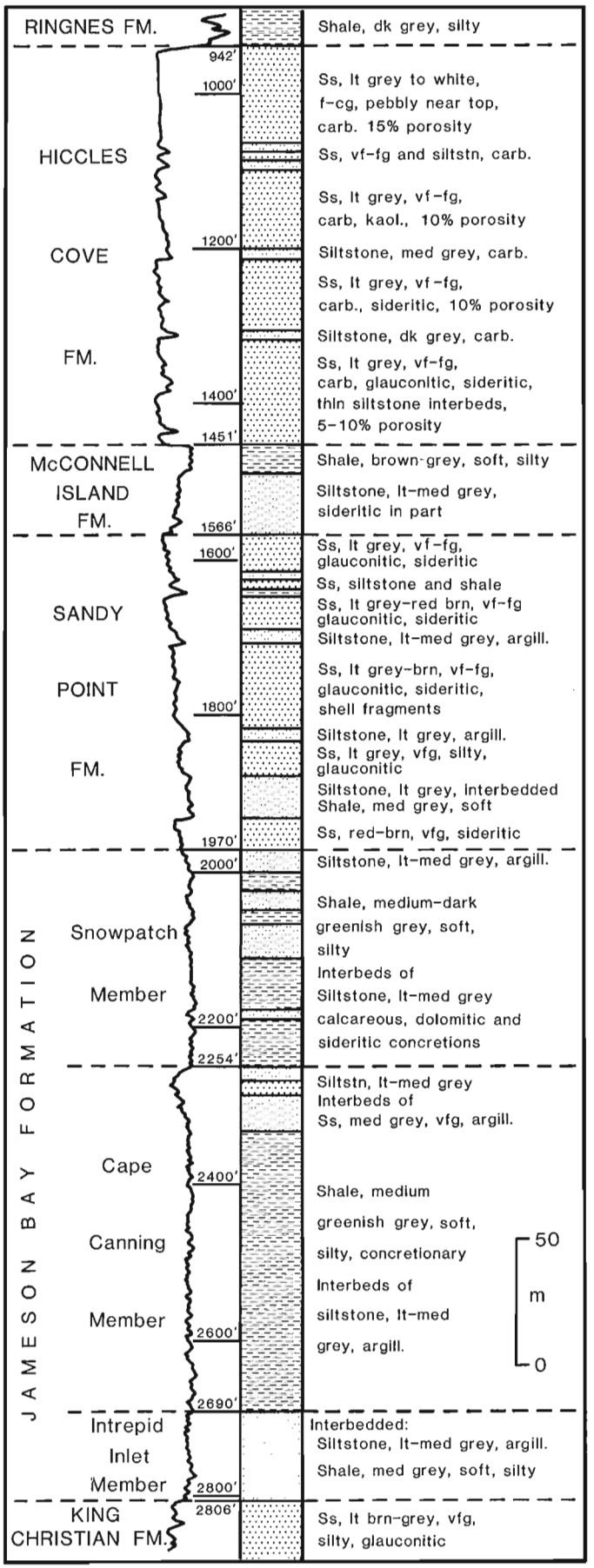

Thickness and distribution

The member is recognized in the western Sverdrup and has a maximum thickness of 81 m. East of Sabine Peninsula the Intrepid Inlet intertongues with sandstone of the King Christian Formation and the member eventually disappears due to facies change to sandstone (Embry, 1983b).

Age

The Intrepid Inlet Member is interpreted to be Pliensbachian on the basis of ammonites from Prince Patrick Island (Frebold, 1975) and stratigraphc relationships (Embry, 1983b).

Environment of deposition

The lithologies, fauna and stratigraphic relationships suggest an offshore shelf environment of deposition for the member (Embry, 1982).

Cape Canning Member, Jameson Bay Formation

Definition

The Cape Canning Member consists of shale and siltstone with thin interbeds of very fine grained sandstone in the uppermost portion. The type section is in the Elf Jameson Bay C-31 well between 687 m (2254 ft) and 820 m (2690 ft) and is 133 m thick (Fig. 33.5). The name is taken from Cape Canning, on the east coast of Intrepid Inlet, Prince Patrick Island.

Boundaries

The Cape Canning conformably overlies the Intrepid Inlet Member as described previously. The Cape Canning is conformably overlain by the Snowpatch Member of the Jameson Bay Formation. The contact is placed at the base of a clay-rich shale unit which overlies arenaceous siltstone or ironstone of the uppermost Cape Canning (Fig. 33.2, 33.5).

Lithology

The main lithologies of the Cape Canning are medium- to dark-greenish grey shale and light- to medium-grey siltstone. Shale is more common in the lower portion of the member and siltstone content gradually increases upward. In many sections thin, very fine grained sandstone units occur in the uppermost portion of the member. Along the southern margin of the basin a prominent ironstone bed forms the top of the member.

Thickness and distribution

The Cape Canning occurs in the western Sverdrup basin and may be up to 146 m thick. It is not recognized in the eastern Sverdrup. Equivalent strata are in the lower portion of the Jameson Bay Formation and the upper portion of the Remus Member of the Heiberg Formation.

Age

Ammonites collected from the Cape Canning on Borden Island indicate a Toarcian age for the member (Tozer and Thorsteinsson, 1964).

Figure 33.5. *Lithology (from samples) and gamma-ray curve for type sections of Jameson Bay, Sandy Point, McConnell Island and Hiccles Cove formations and Intrepid Inlet, Cape Canning and Snowpatch members; Jameson Bay C-31 well.*

Environment of deposition

Lithologies, fauna and stratigraphic relationships are indicative of an offshore marine shelf depositional environment for the Cape Canning Member.

Snowpatch Member, Jameson Bay Formation

Definition

The Snowpatch Member consists of interbedded shale and siltstone with minor very fine grained sandstone. The type section is in the Elf Jameson Bay C-31 well between 601 m (1970 ft) and 687 m (2254 ft) and is 86 m thick (Fig. 33.5). The name is taken from Snowpatch Point, on the west coast of Intrepid Inlet, Prince Patrick Island.

Boundaries

The Snowpatch conformably overlies the Cape Canning Member as described previously. The Snowpatch is conformably overlain by the Sandy Point Formation and the contact is placed at the base of the first sandstone unit above which sandstone is relatively common.

Lithology

Medium to dark green-grey shale and light- to medium-grey siltstone are the predominant lithologies in the Snowpatch Member. Thin units of very fine grained sandstone are locally present in the upper portion of the member. Overall the member displays a coarsening-upward trend, with siltstone content increasing upwards (Fig. 33.2, 33.5).

Thickness and distribution

The member is recognized in the western Sverdrup and may be up to 232 m thick. In the eastern Sverdrup equivalent strata are in the upper portion of the undivided Jameson Bay Formation.

Age

Ammonites collected from the member on Prince Patrick Island and stratigraphically equivalent strata are Toarcian to Aalenian in age (Tozer and Thorsteinsson, 1964).

Environment of deposition

The lithologies, fauna and stratigraphic relationships of the Snowpatch Member indicate that it was deposited in an offshore marine shelf setting.

Sandy Point Formation

Definition

The Sandy Point Formation consists of interbedded very fine- to medium-grained sandstone, siltstone and shale. The type section is in the Elf Jameson Bay C-31 well between 477 m (1566 ft) and 601 m (1970 ft) and is 124 m thick (Fig. 33.5). The name is taken from Sandy Point, on the northwestern coast of Melville Island.

Synonyms

1. Lower portion Jaeger Member, Savik Formation, western Ellesmere Island and southern Axel Heiberg Island (Tozer, 1963b).
2. Unit 4, Section S1 and Unit 5, Section S2, Savik Formation, western Axel Heiberg (Fricker, 1963).
3. Units 1-4, Wilkie Point Formation, Intrepid Inlet section, Prince Patrick Island (Tozer and Thorsteinsson, 1964).
4. Units 5 and 6, Savik Formation, northwestern Ellef Ringnes Island (Stott, 1969).
5. Upper Wilkie Point, Sabine Peninsula (Henao-Londono, 1977).
6. Jaeger Member, subsurface King Christian Island (Balkwill and Roy, 1977).
7. Member JjD, Jaeger Formation, Cornwall Island (Balkwill, 1983).
8. Jaeger Member, Savik Formation, subsurface Amund Ringnes Island (Balkwill, 1983).

Boundaries

The Sandy Point Formation conformably overlies the Jameson Bay Formation as described previously. The Sandy Point Formation is usually overlain by the McConnell Island Formation with the contact placed at the top of the highest sandstone bed above which shale and siltstone are predominant. This contact varies from conformable to unconformable. Occasionally, a thin basal conglomerate overlies the unconformity surface. This unit is included in the overlying McConnell Island Formation. In some areas along the margin of the basin the Ringnes Formation (Upper Jurassic shale-siltstone) unconformably overlies the Sandy Point.

Lithology

The Sandy Point Formation consists of interbedded sandstone, siltstone and shale. The lithologies are arranged in coarsening-upward cycles which may be up to 120 m thick. Shales are usually medium green-grey and are silty. Siltstones are light- to medium-grey and vary from very argillaceous to arenaceous. Sandstone units may be up to 30 m thick, and coarsen upward from very fine- to medium-grained. Pebbly, medium- to coarse-grained sandstone is present in the Sandy Point in basin margin sections. Sandstone units are usually extensively burrowed and glauconitic. Massive- to horizontally-bedded sandstone occurs interbedded with burrowed sandstone in some basin margin sections.

Thickness and distribution

The Sandy Point Formation is widespread in the Sverdrup Basin. Its erosional edge is shown in Figure 33.1. The formation is absent due to facies change to siltstone and shale in the central portion of the Sverdrup (east-central Ellef Ringnes, northern Amund Ringnes and west-central Axel Heiberg). The maximum recorded thickness of the formation is 162 m.

Age

Ammonites recovered from the Sandy Point on Prince Patrick, Mackenzie King, Cornwall, Axel Heiberg and Ellesmere islands are Toarcian and Aalenian in age (Tozer, 1963b; Tozer and Thorsteinsson, 1964; Balkwill, 1983).

Environment of deposition

The lithologies, sedimentary structures, fauna and stratigraphic relationships of the Sandy Point indicate a nearshore marine shelf environment of deposition.

McConnell Island Formation

Definition

The McConnell Island Formation consists of shale and siltstone with thin interbeds of very fine grained sandstone. The type section is in the Elf Jameson Bay C-31 well between 442 m (1451 ft) and 477 m (1566 ft) and is 35 m thick (Fig. 33.5). The name is taken from McConnell Island, a few kilometres west of Mackenzie King Island.

Synonyms

1. Units 6-9, Savik Formation, Strand Fiord section, western Axel Heiberg Island (Tozer, 1963b).
2. Units 5-10, Section S1 and Units 6-11, Section S2, Savik Formation, western Axel Heiberg (Fricker, 1963).
3. Unit 7, Savik Formation, northwestern Ellef Ringnes Island (Stott, 1969).
4. Lower portion Upper Savik, Cornwall Island, Amund Ringnes Island and King Christian Island (Balkwill and Roy, 1977; Balkwill, 1983).

Boundaries

As previously described, the McConnell Island Formation overlies either the Sandy Point Formation or Jameson Bay Formation. Along the margins of the basin the McConnell Island is conformably overlain by the Hiccles Cove Formation, and the contact is placed at the base of the first sandstone above which sandstone is predominant. Basinward, the Hiccles Cove passes laterally into McConnell Island shale that is conformably overlain by the Ringnes Formation. The contact is placed at the base of a dark grey to black, clay-rich shale unit, which rests on an ironstone or siltstone of the uppermost McConnell Island.

Lithology

The main lithologies of the McConnell Island are medium- to dark-grey shale and light- to medium-grey siltstone. A thin basal conglomerate is present in marginal sections, and in these areas the lower portion of the formation consists predominantly of siltstone and very fine grained sandstone. In basinal sections the basal strata are commonly highly glauconitic and siltstone content gradually increases upwards. Beds of brown-red weathering ironstone up to 0.5 m thick are common within the McConnell Island Formation, and are usually interbedded with shale.

Thickness and distribution

The McConnell Island Formation is widespread in the Sverdrup, being absent only on the extreme basin margins due to erosion and facies change, and in the northwestern portion of the basin. In the northwestern Sverdrup Basin equivalent shales and siltstones are placed in the Mackenzie King Formation, which occurs between the Sandy Point (or Jameson Bay) and the Isachsen Formation. The maximum recorded thickness of the McConnell Island Formation is 300 m (western Axel Heiberg).

Age

Bajocian, Bathonian and Callovian ammonites have been recovered from the McConnell Island Formation on Prince Patrick, Ellef Ringnes, and Axel Heiberg islands (Tozer and Thorsteinsson, 1964; Stott, 1969; Tozer, 1963b).

Environment of deposition

The lithology and fauna of the McConnell Island Formation indicate an offshore shelf environment of deposition.

Hiccles Cove Formation

Definition

The Hiccles Cove Formation consists mainly of sandstone with interbeds of shale and siltstone. The type section is in the Elf Jameson Bay C-31 well between 287 m (942 ft) and 442 m (1451 ft), and is 155 m thick (Fig. 33.5). The name is taken from Hiccles Cove, on the eastern side of Intrepid Inlet, Prince Patrick Island.

Synonyms

1. Upper portion, Jaeger Member, Savik Formation, western Ellesmere and southern Axel Heiberg (Tozer, 1963b).
2. Units 5-8, Wilkie Point Formation, Intrepid Inlet section, Prince Patrick Island (Tozer and Thorsteinsson, 1964).
3. Jaeger Formation, northwestern Ellef Ringnes Island (Stott, 1969).
4. Medial sandstone unit, Upper Savik, Cornwall Island (Balkwill, 1983).

Boundaries

The Hiccles Cove conformably overlies the McConnell Island Formation as previously described. The Hiccles Cove is overlain by the Ringnes Formation. The contact is placed at the top of the highest sandstone unit above which shale and siltstone are predominant. This contact is conformable in most areas but is unconformable at the basin margin.

Lithology

In the Prince Patrick - western Melville Island area the Hiccles Cove consists mainly of fine- to medium-grained quartzose sandstone. Thin shale and siltstone beds are present, and they become thicker and more frequent northwards and northeastwards (Fig. 33.2) as the Hiccles Cove shales out. The formation consists of stacked coarsening-upward cycles, and the sandstones are burrowed in the lower portion and massive- to horizontally-bedded in the upper portion. Thin units of coal and coaly shale occur near the top of the formation on central Prince Patrick Island. Associated sandstones are carbonaceous.

Other exposures of the Hiccles Cove along the southern, eastern and northwestern basin margins consist of extensively burrowed, argillaceous, glauconitic, very fine- to fine-grained sandstone. An exception to this is in the Lake Hazen area of northeastern Ellesmere, where massive to crossbedded fine- to medium-grained, carbonaceous sandstone dominates the formation.

Thickness and distribution

The Hiccles Cove Formation occurs only along the basin margins. The formation has been recognized in the following areas: central Prince Patrick, Eglinton, western Melville, Cornwall, southern Axel Heiberg, Fosheim Peninsula, Lake Hazen, northwestern Ellef Ringnes and northern Mackenzie King islands. Basinward the Hiccles Cove changes facies to the shale and siltstone of the McConnell Island Formation. It is truncated by the Ringnes Formation on the basin edges. The maximum thickness of the Hiccles Cove is 176 m.

Age

Ammonites collected from the Hiccles Cove on Prince Patrick and Ellef Ringnes islands are Bathonian and Callovian (Tozer and Thorsteinsson, 1964; Stott, 1969). On the basin margins the basal beds are probably as old as Bajocian based on their equivalence with dated McConnell Island strata. Uppermost strata are as young as Oxfordian according to palynological data (unpublished GSC report).

Environment of deposition

The lithologies, sedimentary structures, fauna and stratigraphic relationships of the Hiccles Cove indicate a shallow shelf to strandplain origin for the formation. Lagoonal strata are present near the top of the formation on Prince Patrick Island.

References

Balkwill, H.R.
1983: Geology of Amund Ringnes, Cornwall and Haig Thomas islands, District of Franklin; Geological Survey of Canada, Memoir 390.

Balkwill, H.R. and Roy, K.J.
1977: Geology, King Christian Island, District of Franklin; Geological Survey of Canada, Memoir 386.

Balkwill, H.R., Wilson, D.G., and Wall, J.H.
1977: Ringnes Formation (Upper Jurassic), Sverdrup Basin, Canadian Arctic Archipelago; Bulletin of Canadian Petroleum Geology, v. 25, no. 6, p. 115-144.

Balkwill, H.R., Hopkins, W.S., Jr., and Wall, J.H.
1982: Geology, Lougheed Island, District of Franklin; Geological Survey of Canada, Memoir 388.

Davies, E.H.
1983: The dinoflagellate oppel-zonation of the Jurassic-Lower Cretaceous sequence in the Sverdrup Basin, Arctic Canada; Geological Survey of Canada, Bulletin 359.

Douglas, T.R. and Oliver, T.A.
1979: Environments of deposition of the Borden Island Gas Zone in the subsurface of the Sabine Peninsula area, Melville Island, Arctic Archipelago; Bulletin of Canadian Petroleum Geology, v. 27, p. 273-313.

Embry, A.F.
1982: The Upper Triassic-Lower Jurassic Heiberg Deltaic Complex of the Sverdrup Basin; in Arctic Geology and Geophysics, ed. A.F. Embry and H.R. Balkwill; Canadian Society of Petroleum Geologists, Memoir 8, p. 189-217.

1983a: Stratigraphic subdivision of the Heiberg Formation eastern and central Sverdrup Basin, Arctic Islands; in Current Research, Part B, Geological Survey of Canada, Paper 83-1B, p. 205-213.

1983b: The Heiberg Group, western Sverdrup Basin, Arctic Islands; in Current Research, Part B, Geological Survey of Canada, Paper 83-1B, p. 381-389.

Frebold, H.
1958: Fauna, age and correlation of the Jurassic rocks of Prince Patrick Island; Geological Survey of Canada, Bulletin 41.

Frebold, H. (cont.)
1960: The Jurassic faunas of the Canadian Arctic: Lower Jurassic and lowermost Middle Jurassic ammonites; Geological Survey of Canada, Bulletin 59.

1961: The Jurassic faunas of the Canadian Arctic: Middle and Upper Jurassic ammonites; Geological Survey of Canada, Bulletin 74.

1964: The Jurassic faunas of the Canadian Arctic, Cadoceratinae; Geological Survey of Canada, Bulletin 119.

1975: The Jurassic faunas of the Canadian Arctic, Lower Jurassic ammonites, biostratigraphy and correlation; Geological Survey of Canada, Bulletin 243.

Fricker, P.E.
1963: Geology of the Expedition Fiord area, west central Axel Heiberg Island, Canadian Arctic Archipelago; McGill University, Axel Heiberg Island Research Reports, Geology no. 1.

Greiner, H.R.
1963: Jaeger River, eastern Cornwall Island; in Geology of the north-central part of the Arctic Archipelago, Northwest Territories (Operation Franklin), ed. Y.O. Fortier et al.; Geological Survey of Canada, Memoir 320, p. 533-537.

Henao-Londono, D.
1977: Correlation of producing formations in the Sverdrup Basin; Bulletin of Canadian Petroleum Geology, v. 25, p. 969-980.

Johnson, C.D. and Hills, L.V.
1973: Microplankton zones of the Savik Formation (Jurassic), Axel Heiberg and Ellesmere islands, District of Franklin; Bulletin of Canadian Petroleum Geology, v. 21, p. 178-218.

Meneley, R.
1977: Exploration Prospects in the Canadian Arctic Islands; Panarctic Oils Limited, Calgary, 16 p.

Nassichuk, W.W. and Christie, R.L.
1969: Upper Paleozoic and Mesozoic stratigraphy in the Yelverton Pass region, Ellesmere Island, District of Franklin; Geological Survey of Canada, Paper 68-31.

Rahmani, R.A. and Tan, J.T.
1978: The type section of the Lower Jurassic Borden Island Formation, Borden Island, Arctic Archipelago, Canada; in Current Research, Part A, Geological Survey of Canada, Paper 78-1A, p. 538-540.

Reinson, G.E.
1975: Lithofacies analysis of cores from the Borden Island Formation, Drake Point, Melville Island; in Report of Activities, Part B, Geological Survey of Canada, Paper 75-1B, p. 297-301.

Souther, J.G.
1963: Geological Traverse across Axel Heiberg Island from Buchanan Lake to Strand Fiord; in Geology of the north-central part of the Arctic Archipelago, Northwest Territories (Operation Franklin), ed. Y.O. Fortier et al.; Geological Survey of Canada, Memoir 320, p. 426-448.

Stott, D.F.
1969: Ellef Ringnes Island, Canadian Arctic Archipelago; Geological Survey of Canada, Paper 68-16.

Tozer, E.T.
1956: Geological reconnaissance, Prince Patrick, Eglinton and western Melville Islands, Arctic Archipelago, Northwest Territories; Geological Survey of Canada, Paper 55-5.

1963a: Mesozoic and Tertiary stratigraphy; in Geology of the north-central part of the Arctic Archipelago, Northwest Territories (Operation Franklin), ed. Y.O. Fortier et al.; Geological Survey of Canada, Memoir 320, p. 74-95.

1963b: Mesozoic and Tertiary stratigraphy, western Ellesmere Island and Axel Heiberg Island, District of Franklin; Geological Survey of Canada, Paper 63-30.

Tozer, E.T. and Thorsteinsson, R.
1964: Western Queen Elizabeth Islands, Arctic Archipelago; Geological Survey of Canada, Memoir 332.

Wall, J.H.
1983: Jurassic and Cretaceous foraminiferal biostratigraphy in the eastern Sverdrup Basin, Canadian Arctic Archipelago; Bulletin of Canadian Petroleum Geology, v. 31, p. 246-281.

Appendix

Selected well tops, formations of Wilkie Point Group, Sverdrup Basin. Location of wells shown on Figure 33.1.

Elf Cape Norem A-80

Sandy Point Formation	1009 m (3310 ft)
Jameson Bay Formation	1039 m (3409 ft)
Snowpatch Member	1039 m (3409 ft)
Cape Canning Member	1256 m (4120 ft)
Intrepid Inlet Member	1399 m (4590 ft)
Lougheed Island Formation	1467 m (4812 ft)

Elf Jameson Bay C-32

Hiccles Cove Formation	287 m (942 ft)
McConnell Island Formation	442 m (1451 ft)
Sandy Point Formation	477 m (1566 ft)
Jameson Bay Formation	601 m (1970 ft)
Snowpatch Member	601 m (1970 ft)
Cape Canning Member	687 m (2254 ft)
Intrepid Inlet Member	820 m (2690 ft)
King Christian Formation	855 m (2806 ft)

Panarctic Eglinton P-24

Hiccles Cove Formation	948 m (3110 ft)
McConnell Island Formation	1095 m (3590 ft)
Sandy Point Formation	1111 m (3645 ft)
Weatherall Formation (Devonian)	1165 m (3822 ft)

Panarctic Depot Island C-44

Hiccles Cove Formation	354 m (1160 ft)
McConnell Island Formation	457 m (1500 ft)
Sandy Point Formation	475 m (1558 ft)
Jameson Bay Formation	497 m (1630 ft)
Snowpatch Member	497 m (1630 ft)
Cape Canning Member	561 m (1840 ft)
Intrepid Inlet Member	618 m (2026 ft)
King Christian Formation	635 m (2084 ft)

Panarctic Drake Point D-68

Sandy Point Formation	945 m (3100 ft)
Jameson Bay Formation	972 m (3188 ft)
Snowpatch Member	972 m (3188 ft)
Cape Canning Member	1027 m (3368 ft)
Intrepid Inlet Member	1100 m (3607 ft)
King Christian Formation	1124 m (3687 ft)

Panarctic North Sabine H-49

McConnell Island Formation	2619 m (8590 ft)
Sandy Point Formation	2696 m (8844 ft)
Jameson Bay Formation	2726 m (8940 ft)
Snowpatch Member	2726 m (8940 ft)
Cape Canning Member	2844 m (9329 ft)
Intrepid Inlet Member	2954 m (9690 ft)
King Christian Formation	3014 m (9887 ft)

Sun Skybattle Bay C-15

McConnell Island Formation	1711 m (5612 ft)
Sandy Point Formation	1767 m (5797 ft)
Jameson Bay Formation	1784 m (5850 ft)
Snowpatch Member	1784 m (5850 ft)
Cape Canning Member	1869 m (6130 ft)
King Christian Formation	1932 m (6338 ft)

Dome Sutherland O-23

McConnell Island Formation	171 m (561 ft)
Sandy Point Formation	238 m (779 ft)
Jameson Bay Formation	252 m (826 ft)
King Christian Formation	388 m (1272 ft)

Panarctic Mocklin Point D-23

Sandy Point Formation	1192 m (3910 ft)
Jameson Bay Formation	1313 m (4308 ft)
King Christian Formation	1567 m (5140 ft)

Sun Linckens Island P-46

McConnell Island Formation	814 m (2670 ft)
Sandy Point Formation	855 m (2805 ft)
Jameson Bay Formation	870 m (2852 ft)
Heiberg Formation	980 m (3215 ft)

Imperial East Amund M-05

McConnell Island Formation	1442 m (4730 ft)
Sandy Point Formation	1602 m (5256 ft)
Jameson Bay Formation	1610 m (5280 ft)
Heiberg Formation	1701 m (5580 ft)

Imperial Sherwood P-37

Hiccles Cove Formation	363 m (1192 ft)
McConnell Island Formation	377 m (1236 ft)
Sandy Point Formation	390 m (1280 ft)
Jameson Bay Formation	407 m (1334 ft)
Thrust fault to Ringnes Formation	
Hiccles Cove Formation	502 m (1648 ft)
McConnell Island Formation	514 m (1687 ft)
Sandy Point Formation	523 m (1717 ft)
Jameson Bay Formation	540 m (1770 ft)
Heiberg Formation	631 m (2070 ft)

Panarctic Romulus C-42

Hiccles Cove Formation	1350 m (4428 ft)
Sandy Point Formation	1381 m (4530 ft)
Jameson Bay Formation	1415 m (4640 ft)
Heiberg Formation	1436 m (4711 ft)

34.

STRATIGRAPHY AND STRUCTURAL GEOLOGY OF THE REGION SURROUNDING BUNDE AND BUKKEN FIORDS, AXEL HEIBERG ISLAND, CANADIAN ARCTIC

Project 760024

Brian F.G. Fischer [1]
Institute of Sedimentary and Petroleum Geology, Calgary

Fischer, B.F.G., Stratigraphy and structural geology of the region surrounding Bunde and Bukken fiords, Axel Heiberg Island, Canadian Arctic; in Current Research, Part B, Geological Survey of Canada, Paper 84-1B, p. 309-314, 1984.

Abstract

The region surrounding Bunde and Bukken fiords on northwestern Axel Heiberg Island, in the Canadian Arctic Archipelago, is underlain by a thick (over 6000 m) succession of rocks, consisting primarily of sedimentary strata similar to those that exist elsewhere in the axial portion of the Sverdrup Basin. Included in this sequence are Cretaceous mafic volcanic flows, pyroclastic units, and lithic clastic strata. Numerous sills and dykes, presumably related to the volcanic activity, cut and thicken the sedimentary package.

Compression during the early Tertiary Eurekan Orogeny gently deformed the strata. There was an extensional event prior to this orogeny, and the resultant normal faults produced a horst, which may have affected the development of the later structures. The orogeny itself is defined as a compressional phase and resulted in the formation of three large, steeply dipping, reverse faults. The faults have opposing dips and opposing directions of vergence, and are associated with a number of folds. Horizontal shortening associated with each of these faults is estimated to be in the order of 3 km. Typically, the Permian carbonates are juxtaposed over Triassic sandstones and shales. The zone of detachment for these faults lies within the evaporites of the Otto Fiord Formation. A single normal fault which crosscuts one of the major reverse faults in the study area may represent a third deformational period.

Résumé

La région entourant les fjords Bunde et Bukken au nord-ouest de l'île Axel Heiberg, dans l'archipel canadien arctique, repose sur une épaisse succession rocheuse (6 000 m), formée principalement de strates sédimentaires semblables à celles qui existent ailleurs dans la partie axiale du bassin de Sverdrup. Cette séquence comprend des coulées volcaniques mafiques du Crétacé, des unités pyroclastiques et des strates clastiques lithiques. De nombreux sills et dykes, dus probablement aux activités volcaniques, coupent et épaississent les roches sédimentaires.

La déformation qui s'est produite pendant l'orogenèse d'Euréka du début du Tertiaire a légèrement déformé les strates. Avant cette orogenèse, s'était produit un vaste mouvement et les failles normales qui en résultaient ont soulevé un horst qui pourrait avoir modifié le développement de structures plus récentes. L'orogenèse en elle-même est définie comme une phase de compression et a eu pour résultat la formation de trois grandes failles inverses à fort pendage. Les failles ont des pendages et des directions opposés et sont associées à un certain nombre de plis. Le raccourcissement horizontal associé à chacune de ces failles est estimé être de l'ordre de 3 km. Selon un patron typique, les carbonates du Permien sont juxtaposés sur les grès et les schistes argileux triassiques. La zone de détachement de ces failles se trouve dans les évaporites de la formation d'Otto Fjord. Une seule faille normale qui traverse une des principales failles inverses dans la région étudiée, peut représenter une troisième période de déformation.

Introduction

During the 1983 field season, an area surrounding both Bunde Fiord and Bukken Fiord on northwestern Axel Heiberg Island, Canadian Arctic Archipelago, (Fig. 34.1) was mapped at a scale of 1:50 000. The study area is part of the Sverdrup Basin, an elongate, pericratonic depression comprising an esssentially conformable sequence of sedimentary and volcanic strata, ranging from Late Mississippian to Tertiary in age (see Balkwill, 1978). These strata were gently deformed during the Early Tertiary (Bustin, 1977) Eurekan Orogeny, resulting in the formation of predominantly gentle folds, steeply dipping normal faults, and a number of low angle thrust faults and high angle reverse faults.

The area of interest lies within the axial succession of the Sverdrup Basin and is structurally within the Tertiary Eurekan Sound Fold Belt (Fortier et al., 1963). N.J. McMillan conducted the first geological work in the area during his traverse of the width of northern Axel Heiberg Island (McMillan, 1963). Short visits to the area by a few members of the GSC resulted in the definition of much of the stratigraphy and delineation of the major structures (see Thorsteinsson, 1974; Thorsteinsson and Trettin, 1972; Tozer, 1963, 1967).

The field study was conducted to gather further stratigraphic data and, more importantly, to map in detail the various structures in the area, particularly the reverse faults of opposing vergence, in an attempt to determine the timing and mechanisms of the deformational events that made up the Eurekan Orogeny in this area.

Acknowledgments

I thank the Geological Survey of Canada, and especially A.F. Embry and K.G. Osadetz, for providing both the opportunity and logistic support necessary to carry out this project. The preparation of this manuscript was greatly enhanced by discussion with A.F. Embry, K.G. Osadetz, P.F. Simony, D.A. Spratt, and B. Beauchamps. I thank T.P. Poulton and J.A. Jeletzky for the fossil identifications.

[1] Department of Geology, University of Calgary, Calgary, Alberta T2L 2A7

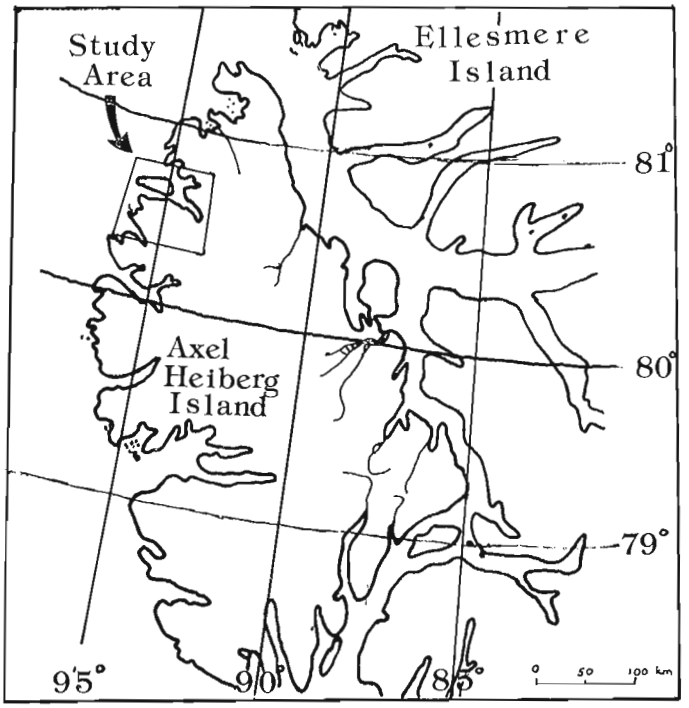

Figure 34.1. Location map.

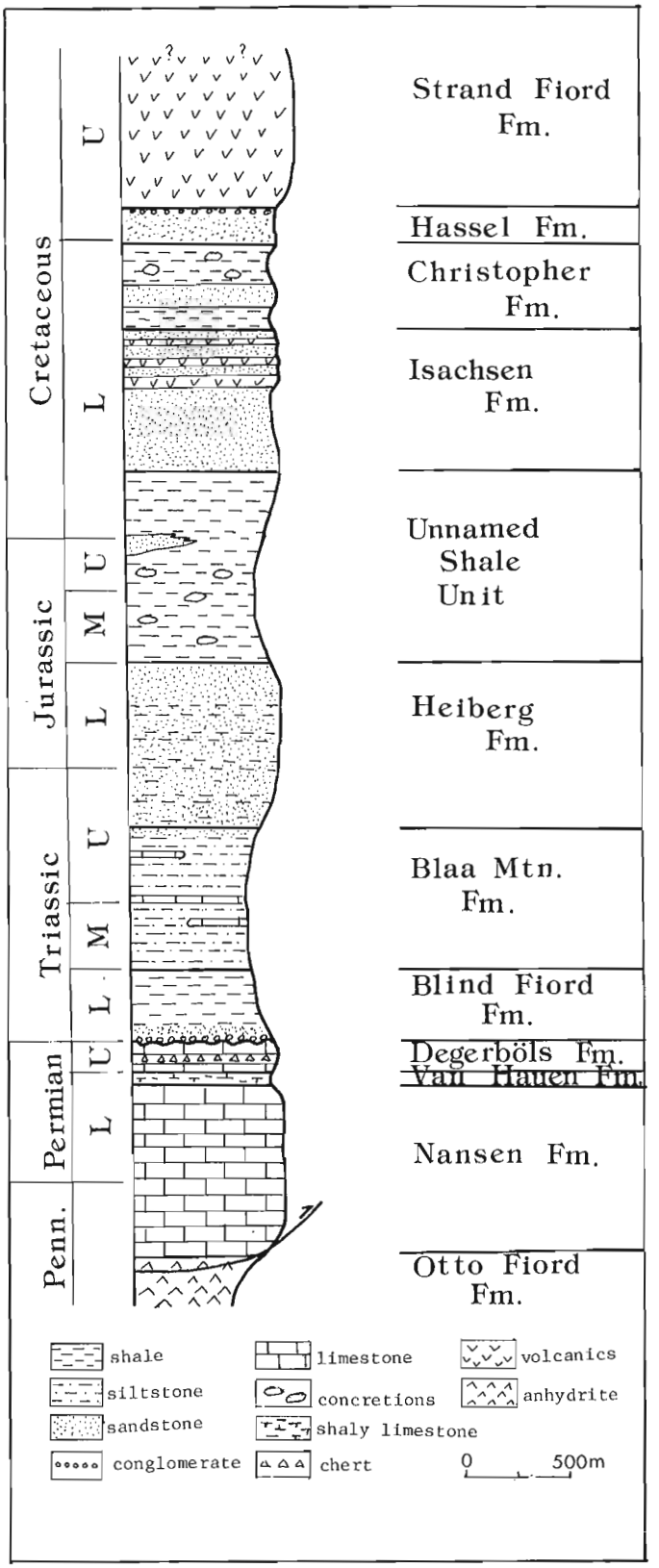

Figure 34.2. Stratigraphic column.

Stratigraphy

A thick sequence of strata, typical of that found within the axial succession of the Sverdrup Basin, is present within the study area (Fig. 34.2). The oldest rocks exposed are the anhydrites and limestones of the Upper Mississippian to Lower Pennsylvanian (Thorsteinsson, 1974) Otto Fiord Formation. These evaporites are not usually found in normal stratigraphic position here, but rather are exposed as a number of small diapiric structures located along major fault traces. The oldest strata to crop out in normal stratigraphic succession are the limestone beds of the Nansen Formation. All exposures of this formation are found in the immediate hanging wall of large reverse faults. In the study area, the Nansen Formation is approximately 830 m thick and is characterized by a cyclical pattern of light grey, fossiliferous, micritic limestones, cherty limestones, and argillaceous limestones. Algal mounds are present in a number of localities (B. Beauchamps, personal communication, 1983). The Van Hauen Formation directly overlies the Nansen Formation and comprises some 70 m of very recessive, fossiliferous, brown weathering, argillaceous limestones. Above this recessive unit are the more competent, interbedded, orange weathering, micritic limestones and dark, bedded cherts of the Degerbols Formation. This latter formation varies in thickness from some 400 m in the south to about 50 m in the north and grades into a thin, massive, white chert unit north of Bukken Fiord.

The basal bed of the overlying Blind Fiord Formation is a thin, conglomeratic band that overlies the basin-wide Permo-Triassic unconformity (Nassichuck et al., 1973). The Blind Fiord Formation is characterized by light grey-green weathering siltstones and silty shales, with a few beds of pelecypod-bearing, fine grained, brown weathering sandstones in the lower portion of the formation. A thick succession of dark grey to black shales and silty shales overlies the Blind Fiord Formation and makes up the Blaa Mountain Formation. Thin, laterally discontinuous beds of pelecypod-bearing, micritic limestones are a distinctive part of this unit.

Fine sandstones appear near the top of the formation and the upper contact is gradational with the sandstones of the lower Heiberg Formation.

The Heiberg Formation comprises approximately 800 m of interbedded fine grained sandstones, siltstones, and carbonaceous shales. The grained sandstones are typically medium bedded, locally burrowed or crossbedded, and commonly contain mud chips and lenticular bedding. The shales and silts commonly display flaser bedding. Within the upper portion of this formation, root casts and rootlets are common and suggest a marine to nonmarine progression through the formation.

A thick succession of black shales overlies the Heiberg Formation, and is characterized by the presence of large ironstone and limestone concretions in the lower portion. Ammonities found near the base of this sequence have been dated as Early Callovian (T.P. Poulton, personal communication, 1984). The upper portion of this thick shale sequence lacks the large concretions. These strata are referred to an unnamed formation that contains equivalents of the Savik, Deer Bay and Awingak formations (Thorsteinsson and Trettin, 1972). A thin, fine grained, brown sandstone unit was mapped within these shales (marked JKr in Fig. 34.3) just south of Bunde Fiord and may represent a tongue of the Awingak Formation.

The coarse grained to conglomeratic, white weathering sandstones of the Isachsen Formation are found above the unnamed formation. These sandstones display excellent trough crossbedding and ripple crosslamination. Burrowing is common. Mafic volcanic flows, commonly vesicular or amygdaloidal, are found interbedded with the sandstones of the Isachsen Formation throughout the upper third of the unit. Well preserved paleosols are commonly found at the base of these flows. A number of pyroclastic units, presumably related to this volcanic activity, are present in the upper portion of this formation.

The dark grey, concretion-bearing shales of the Christopher Formation lie above the Isachsen Formation. A very coarse grained lithic sandstone unit in the middle of the Christopher Formation is an excellent marker bed. An ammonite collected from the top of this unit has been dated

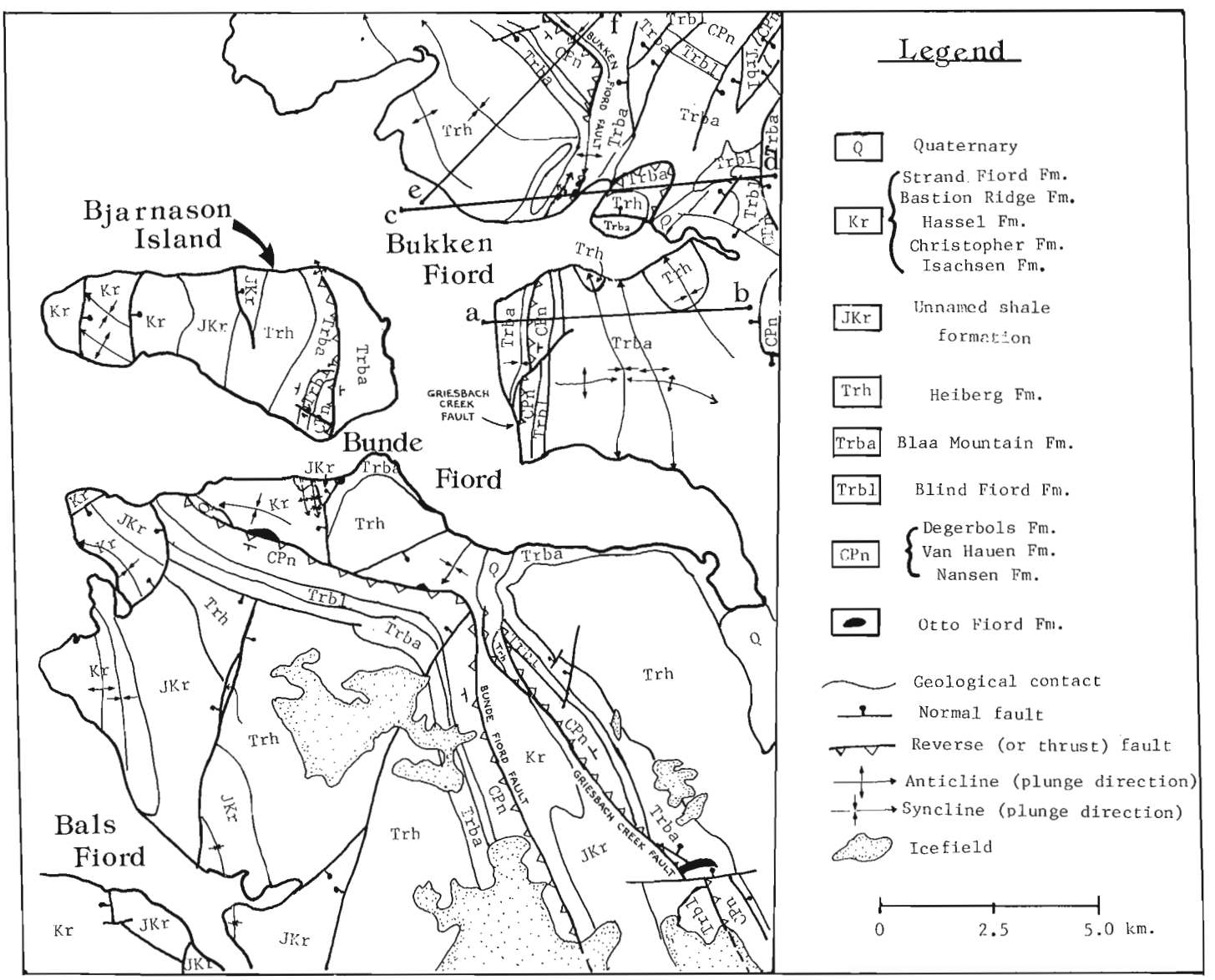

Figure 34.3. *Geology of the study area, showing location of lines of cross-section.*

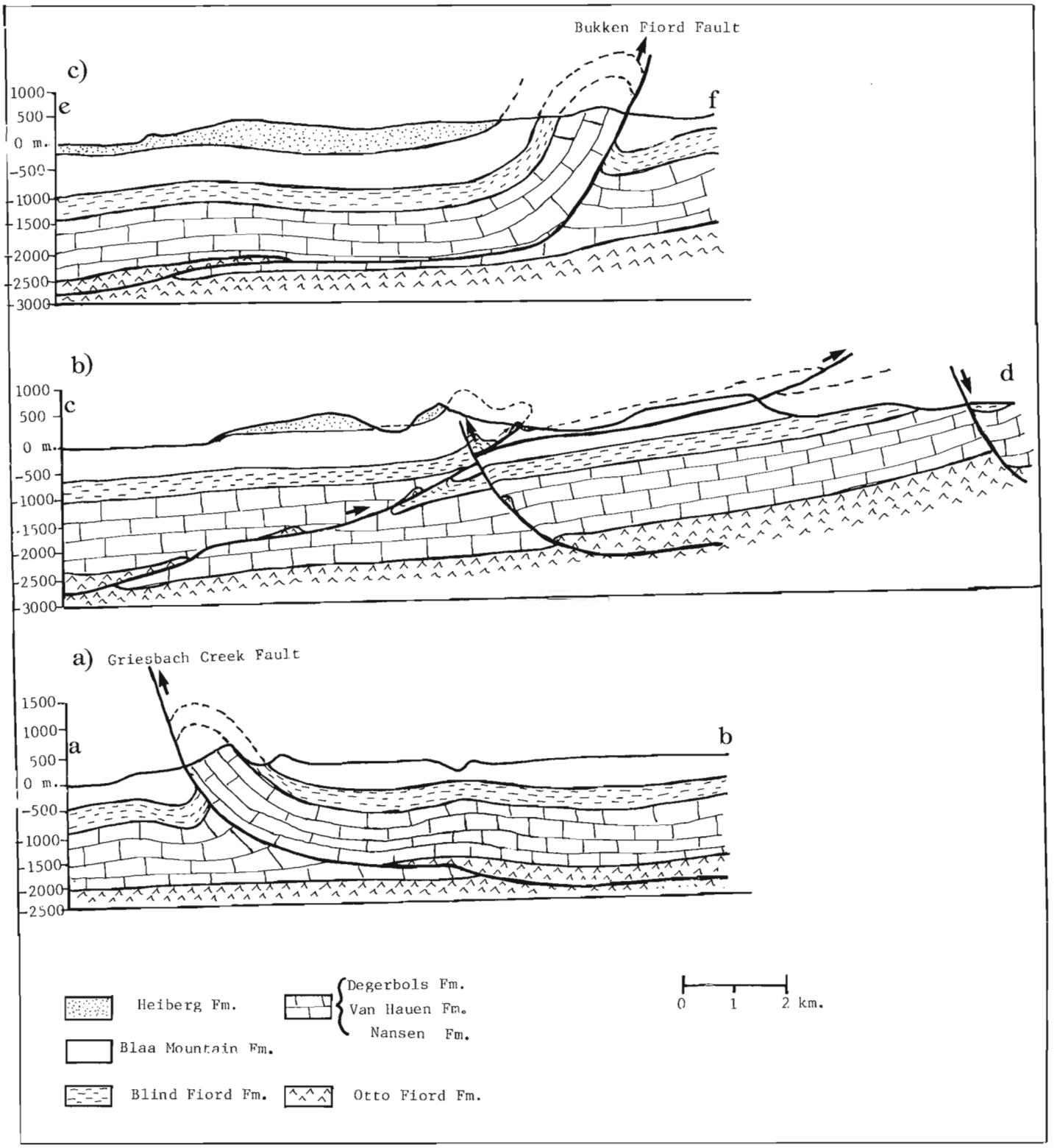

Figure 34.4. *Cross-sections through the Griesbach Creek Fault (a) and Bukken Fiord Fault (c); (b) shows the linkage between the two faults, (note that the near-horizontal thrust "slice", placing the Blaa Mountain Formation on itself, was defined by repeated sills).*

as Lower and Middle Albian (J.A. Jeletzky, personal communication, 1983). The dark brown, fine- to medium-grained sandstones of the Hassel Formation overlie the Christopher shales. The upper beds of the Hassel Formation comprise a chert-pebble conglomerate and are overlain by a thick succession of mafic volcanic flows representing the Strand Fiord Formation (K.G. Osadetz, personal communication, 1983).

The study area has a large number of diabase dykes and sills which have thickened the stratigraphic section substantially. They were noted in all formations found in the area up to the level of the Strand Fiord volcanics, and are most predominant within the less competent units, such as the unnamed formation (JKr) and the Blaa Mountain Formation. Slickensiding associated with bedding plane slip is found on these intrusive rocks, indicating that their emplacement occurred prior to deformation. It is suggested that these intrusions acted as feeder systems for the Cretaceous volcanic activity displayed in both the Isachsen and Strand Fiord formations.

Structure

The thick sequence of rocks described above was gently deformed during at least two, and possibly three, episodes (Fig. 34.3). An early extensional phase resulted in the formation of steep normal faults. This is evident on the south shore of Bunde Fiord, where two steeply dipping normal faults bring Triassic strata up against the surrounding Cretaceous rocks, forming a horst. These two faults are crosscut by the later Bunde Fiord Fault, and their continuations in the hanging wall of the latter fault have been removed by erosion.

The east and northeast verging Bunde Fiord Fault, the westerly verging Griesbach Creek Fault, and the northeast verging Bukken Fiord Fault, along with their associated folds, were formed during the Eurekan Orogeny. These steeply dipping reverse faults are the dominant structural elements within the study area. Both the Bukken Fiord Fault, and the probable northern extension of the Bunde Fiord Fault, located on Bjarnason Island, had previously been mapped as normal faults (Thorsteinsson and Trettin, 1972). However, bedding measurements taken from both the hanging walls and footwalls of these faults make it geometrically difficult to interpret them as normal faults. Further evidence supporting the reverse fault interpretation includes the apparent westerly dips of the fault planes as the fault traces cut across topography, and the fact that each fault dies out into the core of an anticline.

Away from the Bunde Fiord, Griesbach Creek and Bukken Fiord faults the strata are gently warped, with dips of 3 to 5° being common. In the vicinity of these faults, however, bedding steepens dramatically, defining the flanks of faulted, tight, asymmetric folds (Fig. 34.4a, c). Although exposures of the fault planes occur in only two locations, showing dips of around 50° for the Bunde Fiord Fault, the geometry of the large associated folds allows one to locate the fault planes in areas where they do not crop out. As each fault must cut upsection through previously undeformed or mildly deformed strata, the rocks in the hanging wall must dip at an angle that is less than, or equal to, the angle of dip of the fault plane. As a result, the dips of all the fault planes at the surface are between 50 and 70° as a minimum. A thick unit of cataclastic limestone is found along the trace of each of these three reverse faults, indicating a fault zone at least 10 m thick.

Although the exact mechanism behind the formation of these reverse faults of opposed dip has yet to be determined, linkage between these faults can be demonstrated north of Bukken Fiord (Fig. 34.3, 34.4b). At this locality, the easterly dipping Griesbach Creek Fault terminates within a northeasterly plunging anticline, and the *en echelon*, northwesterly dipping Bukken Fiord Fault terminates within the adjacent southerly plunging anticline. The difference in shortening in the interval between the two faults was compensated by the generation of these folds. This can be demonstrated by comparing shortening shown on the three structural cross-sections in Figure 34.4. The northernmost section and the southernmost section (Fig. 34.4a and c respectively) show horizontal shortening of around 3.0 km, with the central cross-section displaying the linkage between these two faults.

This central cross-section shows minor offset of the Bukken Fiord Fault by the Griesbach Creek Fault, but these two reverse faults are believed to be of the same age. The crosscutting relationship depicted in this figure is attributed to the time required for the lateral propagation of the two faults.

As drawn, the Bukken Fiord Fault, having propagated southward from its initial point of fracture, reached the location of the line of section earlier than the Griesbach Creek Fault, which presumably had a greater lateral distance to propagate northward from its initial point of fracture to the locations marked by the lines of sections C, D. The possibility then exists that farther south of the section, below Bukken Fiord, the Griesbach Creek Fault may be offset by the Bukken Fiord Fault. This would be a function of the increased southward lateral propagation distance for the Bukken Fiord Fault, along with a corresponding decrease in the northward lateral propagation of the Griesbach Creek Fault.

The gentle warping of the strata in the hanging walls of these faults is attributed to ramps on the fault surfaces in the basal portion of the Nansen Formation. Lateral ramps are also found within the study area north of Bukken Fiord along the Bukken Fiord Fault trace. It is believed that a combination of these two types of ramps result in the subtle "saddle" and "dome" structures mapped in the hanging wall of the Griesbach Creek Fault on the peninsula between Bunde and Bukken fiords.

The fault traces of these reverse faults locally show offsets, such as on the previously mentioned peninsula. These offsets however, are confined to strata in the hanging wall with no evidence of offset in the footwall rocks. It is suggested that these structures also are a result of lateral ramping. It is possible that the horst, which formed during the earlier extensional phase, could have influenced the direction of later faulting and therefore caused the deflection displayed by the Bunde Fiord Fault. The geometry of the reverse fault on Bjarnason Island remains to be analyzed.

Small anhydrite bodies are also found along the traces of these major faults. Foliations and lineations measured from the distorted, nodular, mosaic fabric of these rocks, and their position out of stratigraphic sequence, are consistent with diapiric movement of the anhydrite up along the fault zone during compression. These anhydrite bodies have been correlated, on the basis of lithology, with the evaporites of the Otto Fiord Formation. The presence of a distinctive, red, gypsiferous unit, which has also been observed by Fischer in the type section of the Otto Fiord Formation, further suggests this correlation. On the basis of the position of these diapirs along the major fault traces of the area, and because the oldest strata exposed in normal stratigraphic succession in the hanging wall of any of these reverse faults is that of the Nansen Formation, it is concluded that the zone of detachment for these faults lies within the evaporites of the Otto Fiord Formation.

In the southeast corner of the map area, a normal fault offsets the strata both above and below the Griesbach Creek Fault. This may represent a third deformation event. However, as mentioned earlier, the most probable mechanism for the formation of the reverse faults has yet to be determined, and if this second period of deformation involved a large component of shear, the possibility exists that the normal fault in the southeast corner of the map area formed syntectonically with the reverse faults (Sales, 1968).

Balkwill (1978) defines three major pulses of Eurekan orogenic activity within the Sverdrup Basin: an early phase of uplift and erosion, followed by a period dominated by compressive forces, and, lastly, a phase of renewed uplift and erosion. The most prominent structural features present in the study area are compressional features, in particular the three large reverse faults. Although in the area studied the reverse faults cut rocks as young as Late Cretaceous (and they are therefore Late Cretaceous or younger in age), they are most probably related to Balkwill's (op. cit) second pulse of orogenic activity, and as such formed between the middle Eocene and early Miocene.

As the early extensional structures in the study area also offset the Late Cretaceous Strand Fiord Formation, and as these extensional structures pre-date the reverse faults, they must be Late Cretaceous to middle Eocene in age. It is possible, therefore, that the formation of the horst south of Bunde Fiord may have been associated with Late Cretaceous to late Paleocene uplift along the Princess Margaret Arch.

Conclusions

The study area is underlain by a thick sequence of sedimentary and volcanic rocks typical of the stratigraphy found on the northwest rim of the Sverdrup Basin. Prior to deformation, the strata were thickened substantially by the intrusion of numerous diabasic dykes and sills which are presumably related to the Cretaceous volcanic flows.

The Late Cretaceous and Tertiary movements gently deformed the strata, and did so during at least two, and possibly three, deformational episodes. The first of these episodes probably occurred sometime between the Late Cretaceous to middle Eocene and was extensional in nature, causing the formation of a horst which may have affected the formation of later structures. The second episode was compressional, most likely related to the middle Eocene to early Miocene phase of the Eurekan Orogeny. This phase resulted in the formation of three large, steeply dipping reverse faults, which display opposing directions of vergence. Minimal shortening took place along these faults, and, because of the steepness of the fault zone itself, stratigraphic throw is approximately half as great as the horizontal shortening.

These faults merge into a detachment zone within the evaporites of the Otto Fiord Formation. Folding throughout the study area can be attributed to the movement along the reverse faults. Ramps, both perpendicular and parallel to the slip direction, result in the unusual map pattern of many of these folds. Most of the apparent offsets of the reverse fault traces can also be attributed to laterally discontinuous ramps. However, in at least one instance, the offset may represent normal faulting due to a third period of deformation.

References

Balkwill, H.R.
1978: Evolution of the Sverdrup Basin, Arctic Canada; American Association of Petroleum Geologists, Bulletin, v. 62, no. 6, p. 1004-1028.

Bustin, R.M.
1977: The Eureka Sound and Beaufort formations, Axel Heiberg and west-central Ellesmere Islands, District of Franklin; unpublished M.Sc. thesis, University of Calgary, 208 p.

Fortier, Y.O., Blackadar, R.G., Glenister, B.F., Greiner, H.R., McLaren, D.J., McMillan, N.J., Norris, A.W., Roots, E.F., Souther, J.G., Thorsteinsson, R., and Tozer, E.T.
1963: Geology of the north-central part of the Arctic Archipelago, Northwest Territories (Operation Franklin); Geological Survey of Canada, Memoir 320, 671 p.

McMillian, N.J.
1963: Geological Traverse from Lightfoot River to Wading River; in Fortier, Y.O. et al., Geology of the north-central part of the Arctic Archipelago, Northwest Territories (Operation Franklin); Geological Survey of Canada, Memoir 320, p. 501-512.

Nassichuk, W.W., Thorsteinsson, R., and Tozer, E.T.
1973: Permian-Triassic boundary in the Canadian Arctic Archipelago; Canadian Society of Petroleum Geologists, Memoir 2, p. 286-293.

Thorsteinsson, R.
1974: Carboniferous and Permian stratigraphy of Axel Heiberg Island and western Ellesmere Island, Canadian Arctic Archipelago; Geological Survey of Canada, Bulletin 224, 115 p.

Thorsteinsson, R. and Trettin, H.P.
1972: Geology, Bukken Fiord, District of Franklin; Geological Survey of Canada, Map 1310A.

Tozer, E.T.
1963: Mesozoic and Tertiary stratigraphy, western Ellesmere Island and Axel Heiberg Island, District of Franklin; Geological Survey of Canada, Paper 63-30, 38 p.

1967: A standard for Triassic time; Geological Survey of Canada, Bulletin 156, 103 p.

Sales, J.K.
1968: Crustal mechanics of Cordilleran foreland deformation; a regional scale model approach; American Association of Petroleum Geologists, Bulletin, v. 52, p. 2016-2044.

35. DEHISCENS ZONE CORALS FROM THE LOWER DEVONIAN OF YUKON TERRITORY

Project 680093

A.E.H. Pedder
Institute of Sedimentary and Petroleum Geology, Calgary

*Pedder, A.E.H., **Dehiscens** Zone corals from the Lower Devonian of Yukon Territory; in Current Research, Part B, Geological Survey of Canada, Paper 84-1B, p. 315-325, 1984.*

Abstract

***Ellesmerelasma expansum** sp. n., **Loyolophyllum xizangense** Yu and Liao, and **Martinophyllum altiaxis** sp. n. (holotype and three paratypes), are described from the area of Royal Creek headwaters, in beds transitional from unnamed platform limestone to the basinal Road River Formation. These are believed to be early Zlichovian corals, but there is the remote possibility that they are late Pragian.*

***Martinophyllum altiaxis** sp. n. (one paratype) and **Thoulelasma yukonanum** sp. n. are described from the early Zlichovian part of the **dehiscens** Zone in the Michelle Formation. **Thoulelasma** is removed from the Halliidae and tentively assigned to the Bethanyphyllidae.*

*The biostratigraphic values of these corals are largely unknown. However, **Martinophyllum altiaxis** is known to occur in the upper **dehiscens** Zone of Alaska, and the only other known occurrence of **Loyolophyllum xizangense** is in Tibet, in beds that are apparently either late Pragian or early Zlichovian in age.*

Résumé

*On décrit **Ellesmerelasma expansum** sp. n., **Loyolophyllum xizangense** Yu et Liao, et **Martinophyllum altiaxis** sp. n. (holotype et trois paratypes) qui proviennent des sources du ruisseau Royal, dans les couches de transition entre les calcaires de la plate-forme sans nom et la formation en forme de bassin de Road River. Ces coraux semblent appartenir au Zlichovien inférieur mais ils pourraient, ce qui est peu certain, appartenir au Pragien supérieur.*

***Martinophyllum altiaxis** sp. n. (paratype) et **Thoulelasma yukonanum** sp. n. viennent du Zlichovien inférieur partie de la zone de **dehiscens** de la formation de Michelle. On a extrait **Thoulelasma** des Halliidés et on a essayé de le mettre avec les Bethanyplyllidés.*

*Les valeurs biostratigraphiques de ces coraux sont en grande partie inconnues. Cependant, on sait que **Martionphyllum altiaxis** se trouve dans la partie supérieure de la zone de **dehiscens** de l'Alaska et le seul autre endroit où l'on trouve **Loyolophyllum xizangense** est le Tibet, dans des couches qui semblent être d'âge pragien supérieur ou zlichovien inférieur.*

Introduction

The **Polygnathus dehiscens** Zone faunas of Yukon Territory have yielded about 135 species of fossils, 16 of which are rugose corals. The present paper describes four species of rugose corals, bringing the total of formally described corals in the **dehiscens** Zone of Yukon Territory, to nine.

Royal Creek dehiscens Zone Corals

Dehiscens Zone corals from the Royal Creek headwaters area have been described or figured by Pedder (1975, and in Jackson and others, 1978) and by Pedder and McLean (1982). They occur in strata, mostly debris flows, transitional between an unnamed platform limestone and the basinal Road River Formation. The community they belong to was named the **Sieberella-Nymphorhynchia-Athyrhynchus** Community by Lenz (1976, p. 24). **Dehiscens** Zone corals of the community presently known are **Pseudamplexus** sp., **Cystiphylloides** sp. aff. **C. americanum** (Milne Edwards and Haime), **Cyttaroplasma regale** Pedder and McLean, **Gubbera congesta** Pedder and McLean, **Dohmophyllum** (broad sense) sp., **Ellesmerelasma expansum** Pedder, **Taimyrophyllum** sp., **Xystriphyllum** sp., **Fasciphyllum** sp., **Loyolophyllum xizangense** Yu and Liao and **Martinophyllum altiaxis** Pedder.

Stratigraphically controlled collections of these corals have been made from sections 3 and 7 of the Royal Creek headwaters area. Lenz (1982, Fig. 1) has located these sections on a map. In these sections, **dehiscens** Zone corals of the **Sieberella-Nymphorhynchia-Athyrhynchus** Community occur above the ranges of **Monograptus telleri** and **M. yukonensis**, and near the middle of the range of **Polygnathus dehiscens.** As such, they are probably early Zlichovian, but a late Pragian age cannot be discounted entirely. Lenz (1977, Fig. 2) questionably placed the Pragian/Zlichovian boundary almost 100 m below the occurrence of the coral assemblage in question.

Corals of the Michelle Formation

Previously, elements of the Michelle coral faunas have been made known by Pedder (1975, and in Jackson and others, 1978) and by Pedder and McLean (1982). One species, **Mesophyllum norrisi** Pedder and McLean, is a relatively deep water form known from only one locality in the northern Ogilvie Mountains. At this locality, the Michelle Formation is 116 m thick, and **M. norrisi** ranges from 42 to 87 m above the base of the formation. Since the Michelle Formation apparently entirely post-dates the last monograptids of the region, and **Polygnathus dehiscens** ranges throughout the formation (Fåhraeus, 1971), there is no doubt that known occurrences of **M. norrisi** are in early Zlichovian rocks.

Other described or figured corals from the Michelle Formation are **Pseudamplexus** sp., **Zonophyllum ludivigseni** Pedder and McLean, **Ogilvilasma discors** Pedder, **Martinophyllum altiaxis** Pedder, **Spongonaria** sp. and **Thoulelasma yukonanum** Pedder. Most, if not all of these, are

part of the **Zonophyllum-Ogilvilasma-Elythyna** Community (Pedder and McLean, 1982, p. 62) occurring in the upper beds of the formation. They underlie the Zlichovian conodont zone of **Polygnathus gronbergi**, recognized by the incoming of **P.** sp. aff. **P. perbonus**, and in one section (Section VI of Ludvigsen, 1972), overlie the Zlichovian goniatite **Teicherticeras lenzi** House.

Systematic Paleontology

Family PTENOPHYLLIDAE Wedekind, 1923
Subfamily PTENOPHYLLINAE Wedekind, 1923
Genus **Ellesmerelasma** Pedder, 1983

Ellesmerelasma Pedder, 1983, p. 343.

Type species.

Ellesmerelasma pumile Pedder, 1983, p. 343-344, Plate 42.1, figures 16-30. Bird Fiord Formation, probable Dalejan parts; southwestern Ellesmere Island, Canadian Arctic Archipelago.

Ellesmerelasma expansum sp. n.

Plate 35.1, figures 1-4

Type series. Holotype, GSC 75777 and paratype, GSC 75778, both from GSC loc. C-64149.

Diagnosis. Relatively large (maximum length and diameter at least 35 and 28 mm), turbinate species of **Ellesmerelasma** with a thick peripheral stereozone, abundant presepiments and about 20 x 2 septa at maturity.

Description. Corallum solitary, more or less erect and turbinate. Rejuvenescences prominent. The holotype is subovate in transverse section and before sectioning was about 35 mm high and 28 mm in greatest diameter. The paratype is slightly smaller and less ovate in transverse section. Before preparation, exteriors were hidden by closely adhering encrinitic matrix; in thin section, they are in part rough due to posthumous damage, and in part enveloped in a thin silicified coat of probable organic (algal or stromatoporoidal) origin. Although not exposed, it is clear from longitudinal sections that the calice would be deeply conical in shape.

Septa are greatly enlarged peripherally to form a prominent stereozone. Where a rejuvenated stereozone touches a stereozone of an old calice, the combined thickness of the two stereozones is as much as 7.5 mm. Septa, which number 20 x 2 at maturity, are flexuous and variably flanged; most are disrupted by several presepiments. The longest major septa are rhopaloid and terminate at or very close to the axis. Minor septa are as wide as major septa in the peripheral stereozone, but are reduced in length and width in the more adaxial parts of the corallum.

In early stages (diameter <10 mm) there are few or no dissepiments. At maturity, the outer dissepimentarium comprises about 7 rows of inwardly sloping presepiments; the inner dissepimentarium consists of one or two rows of almost vertically inclined plates. As in all ptenophyllinids, the transition from dissepimentarium to tabularium is abrupt. Axially depressed tabularial surfaces are formed by closely spaced, incomplete tabulae.

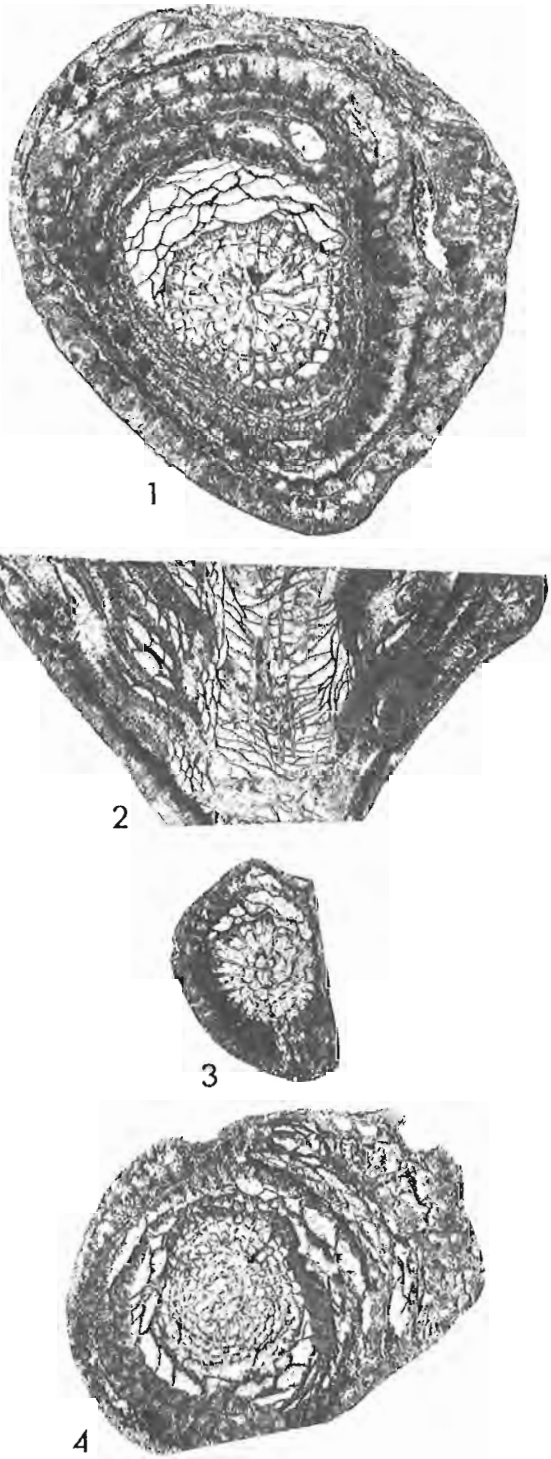

PLATE 35.1

Figures 1-4. **Ellesmerelasma expansum** sp. n.

1-3. Holotype, GSC 75777, two transverse and a longitudinal thin section, x3; GSC loc. C-64149.

4. Paratype, GSC 75778, transverse thin section, x3; GSC loc. C-64149.

Remarks. **Ellesmerelasma pumile** Pedder and **E. pinghuangshanense** (Kong) from the Longdonshui Formation (Eifelian) of southern China are the only two previously described species assigned to the genus. Both are smaller than the new species, but have as many, or more septa. Furthermore, their septa are much finer and do not form such a prominent peripheral stereozone.

Two corals, from the **Polygnathus dehiscens**-bearing Toshemka Horizon of the eastern slope of the northern Ural Mountains, have been figured by Shurygira (1977, Plate 18, figures 1a-2) as **Spongophylloides**(?) **thomasae**, Hill and Jones. Unlike the holotype of Hill and Jones' species, they appear to be solitary and have a prominent peripheral septal stereozone. They are likely to belong to an unnamed species of **Ellesmerelasma**, which would differ from **E. expansum** in having as many as 30 x 2 septa in corallites only 2 cm diameter.

The trivial name is the Latin adjective **expansus**, meaning spread out.

Family FASCIPHYLLIDAE Soshkina, 1954
Genus **Loyolophyllum** Chapman, 1914

Columnaria (Loyolophyllum) Chapman, 1914, p. 306-308.

Type species. **Columnaria (Loyolophyllum) cresswelli** Chapman, 1914, p. 306-308, Plate 51, figures 15, 16; Plate 52, figure 18, but not the specimen illustrated in Figure 17 which is a favositid species. Allochthonous lens of late Pragian limestone in the Norton Gully Sandstone; Griffiths' Quarry, 9.5 km southwest of Mansfield, Victoria, Australia.

Additional species. **Loyolophyllum savitsyi** Wu, 1980, p. 30-32, text-figures Iv, g, Plate 5, figures 3a, b. **L. xizangense** Yu and Liao, 1982.

Doubtful species. **Loyolophyllum urense** Zhmaev in Kraevskaya, 1955, p. 217, Plate 36, figures 6a, b. **L. salairicum** Ivaniya in Zheltonogova and Ivaniya, 1961, p. 373, Plate D-29, figures 6a, b. These species which occur in the Salairka (late Pragian to Zlichovian) and Shandin (Dalejan to Eifelian) Horizons of the Salair, are believed to be synonymous. They have deeply sagging tabulae, and as far as can be determined from available illustrations their septa are vepreculate. These features are characteristic of the genus **Vepresiphyllum**.

Rejected species. **Loyolophyllum cerioides** Soshkina, 1949, p. 109, Plate 4, figures 2a, b (septa reduced to ridges on the corallite wall, possibly a cystimorph coral). **L. breviseptatum** Bul'vanker, 1958, p. 159-160, Plate 77, figure 2; Plate 78, figures 1-2b (tabulate coral best referred to **Roemeripora**). **L. originale** Bul'vanker in Bul'vanker and others, 1960, p. 243, Plate 57, figures 1a, b (=**Columnaria originalis**). **L. crassispinosum** Chernychev in Bul'vanker and others, 1960, p. 244, Plate 58, figures 1a, b (=**Columnaria crassispinosa**).

Distribution. Early Pragian of Fergana (central Asia); late Pragian of southeastern Australia; late Pragian or early Zlichovian of northern Tibet (Xizang); late Pragian and Zlichovian of the northern and pripolar Urals; early Zlichovian of Yukon Territory; Zlichovian of northeastern Alaska; Dalejan or Eifelian of the northern Urals; probable Eifelian of southeastern Alaska; Givetian of Queensland and the District of Mackenzie.

Loyolophyllum xizangense Yu and Liao, 1982

Plate 35.1, figures 5-9

Loyolophyllum sp. nov., Pedder in Jackson and others, 1978, p. 41, Plate 35, figures 3-5.
Loyolophyllum sp., Pedder and McLean, 1982, p. 80.
Loyolophyllum xizangense Yu and Liao, 1982, p. 100, 101, 106, text-figures 3a, b, Plate 2, figures 1a-2b.

Material. Two figured specimens, GSC 46104 and GSC 75779, both from GSC loc. C-64149.

Diagnosis. Species of **Loyolophyllum**, most with mean corallite diameters of 2.5 to 3.0 m (maximum 3.5 mm) and 10 x 2 to 12 x 2 (maximum 14 x 2) septa. Major septa long and smooth. One or two rows of elongate dissepiments and presepiments are almost everywhere present.

Description of Yukon material. Corallum cerioid; the larger of the two specimens (GSC 46104) was about 8 cm high and 10 cm in diameter before it was sectioned. A few large corallites have a mean diameter of 3.5 mm; mature corallites typically have mean corallite diameters ranging from 2.5 to 3.0 mm. Increase is marginarial and nonparricidal. Commonly, new offsets appear singly in a corner at a narrow end of a somewhat compressed parent corallite. During ontogeny, parent corallite and offset quickly develop a communal intercorallite wall.

Intercorallite walls are uniformly well developed. Portions contributed by adjacent corallites are usually 0.1 to 0.2 mm thick between expanded septal bases, so that the thickness of the combined walls is normally not less than 0.2 to 0.4 mm; locally it may be as much as 0.55 mm. Most adult corallites have from 10 x 2 to 12 x 2 strongly differentiated septa; the maximum number observed is 14 x 2. Major septa are long, although the majority do not quite reach the axis; most of the minor septa are one quarter to one half as long as the major septa. Trabeculae appear to be absent and there is no evidence of septal carination. In the specimen registered as GSC 46104, almost all of the septa are complete, whereas in the other specimen, many of the minor and some of the major septa are disrupted by presepiments.

Locally, even in fully mature corallites, the dissepimentarium is suppressed. Usually, however, one or two rows of steeply inclined and elongate dissepiments and presepiments are present. Tabulae are commonly complete; about 15 to 20 may be counted over a vertical distance of 10 mm. Tabularial surfaces are normally slightly concave or sloping. Convex tabularial surfaces have not been observed.

Remarks. Compared with the type material from the late Pragian or early Zlichovian Daerdong Formation of Xainza, in northern Tibet, the Yukon material has slightly thicker intercorallite walls and more widely spaced tabulae. In other respects the two sets of material are remarkably similar. Indeed, one of the Yukon specimens (GSC 46104), is closer to the Tibetan holotype than it is to the other Yukon specimen.

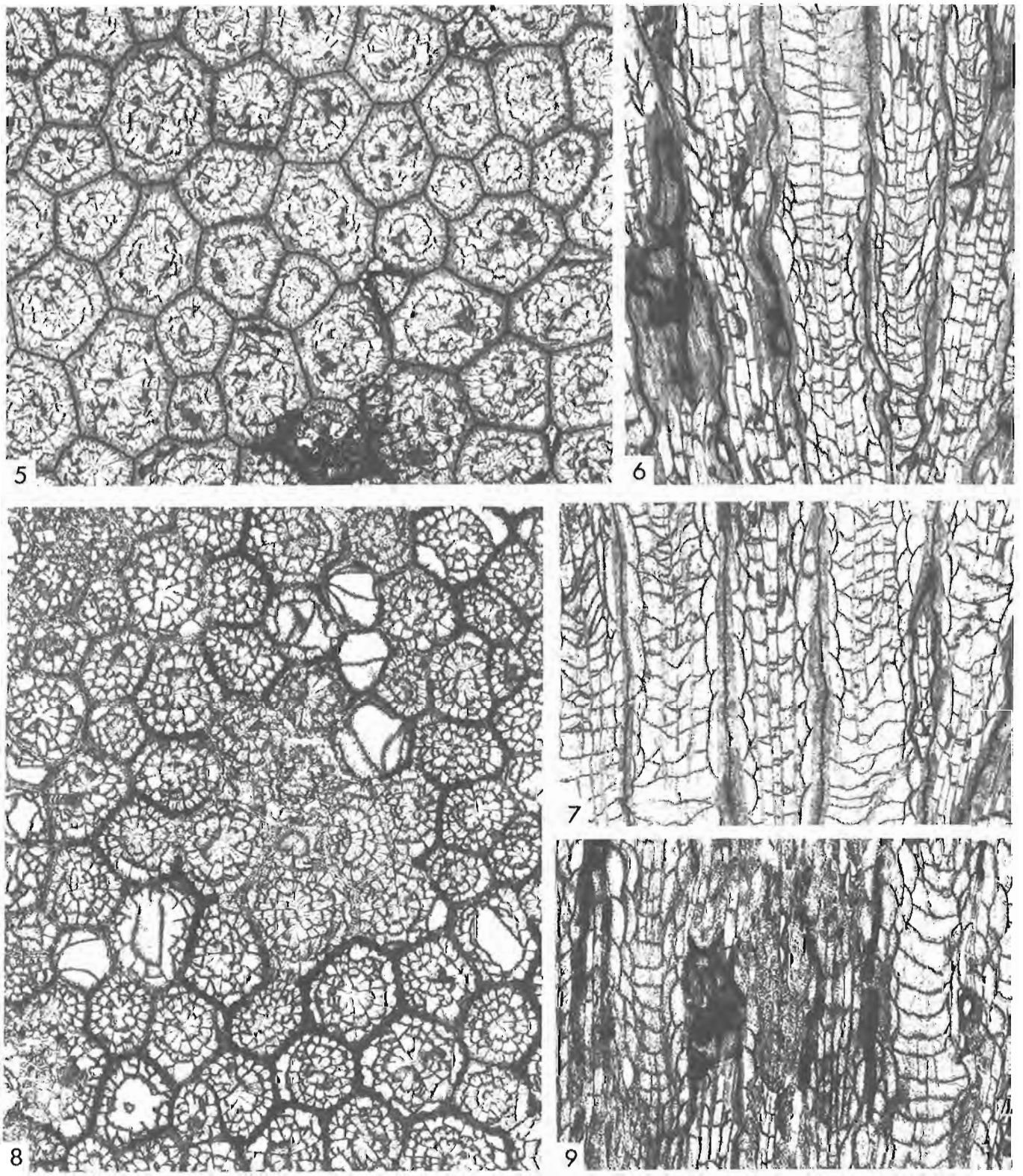

PLATE 35.1

Figures 5-9. **Loyolophyllum xizangense** Yu and Liao.

5-7. GSC 46104, transverse and two longitudinal thin sections, x6; GSC loc. C-64149.
8, 9. GSC 75779, transverse and longitudinal thin sections, x6; GSC loc. C-64149.

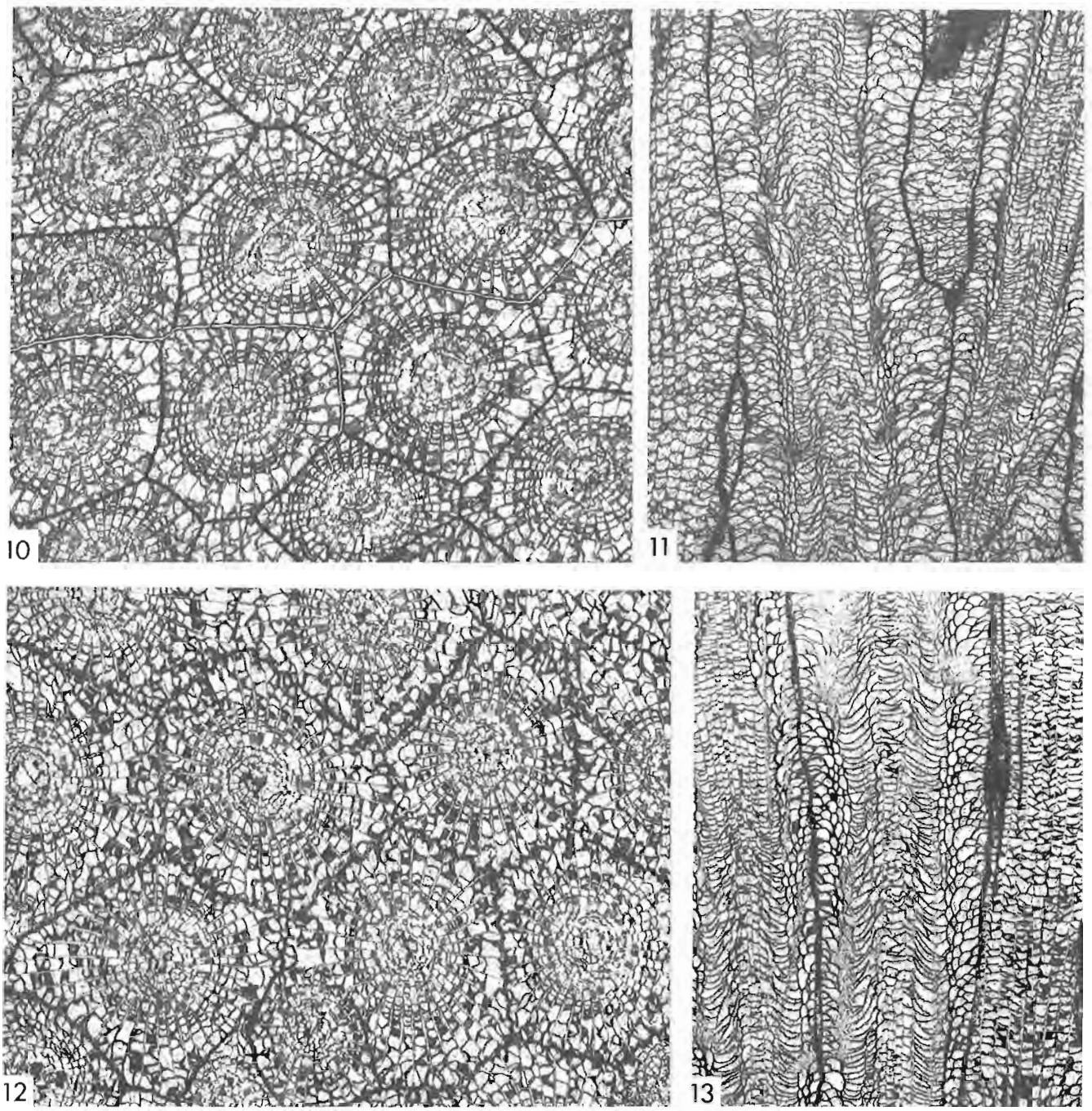

PLATE 35.1

Figures 10-13. **Martinophyllum altiaxis** sp. n.

10, 11. Holotype, GSC 75780, transverse and longitudinal thin sections, x4; GSC loc. C-12894.
12, 13. Paratype, GSC 75781, transverse and longitudinal thin sections, x4; GSC loc. C-63246.

Family COLUMNARIIDAE Nicholson, 1879
Subfamily PARADISPHYLLINAE Jell, 1969
Genus **Martinophyllum** Jell and Pedder, 1969

Martinophyllum Jell and Pedder, 1969, p. 735-736.

Type species. **Martinophyllum ornatum** Jell and Pedder, 1969, p. 736-737, text-figure 1, Plate 95, figures 4, 6-8. Martin's Well Limestone Member (Pragian) of the Broken River Formation; 1.02 km southeast of Martin's Well, 8 km east of Pandanus Creek Homestead, and 240 km northwest of Charters Towers, north Queensland.

Additional species. **Acervularia namnetensis** Barrois, 1889, p. 40-42, Plate 1, figures 1a-c. ? **A. venetensis** Barrois, 1889, p. 42-44, Plate 1, figures 2a-d. **Cyathophyllum approximans** Chapman, 1914, p. 304-305, Plate 47, figures 5, 6. **A. chalki** Chapman, 1931, p. 94. **Prismatophyllum latum** Hill, 1940, p. 153-154, Plate 2, figures 4a, b. **P. densum** Hill, 1940, p. 154, Plate 2, figures 5a, b. **Keriophylloides massivum** Vaganova in Khodalevich and others, 1959, p. 82-83, Plate 37, figures 1a-2b. **Hexagonaria approximans cribellum** Strusz, 1965, p. 544-546, text-figures 8, 9, Plate 74, figures 2a, b; Plate 75, figures 1a, b. **Keriophylloides virgatum** Cherepnina, 1970, p. 115-116, Plate 52, figures 1a, b. **K. grande** Cherepnina, 1970, p. 116, Plate 41, figures 3a, b. **Martinophyllum daerdongense** Yu and Liao, 1982, p. 103, 106, Plate 2, figure 3; Plate 3, figures 1a-2. **M. altiaxis** sp. n.

Rejected species. **Martinophyllum acerosum** Spasskiy in Spasskiy and Cherepnina, 1972, p. 83, Plate 22, figures 1a, b (=**Exilifrons** (?) **acerosa**). **M. submassivum** Cherepnina in Cherepnina and Yaroshinskaya, 1974, p. 157-158, Plate 1, figures 2a, b (=undetermined astreoid genus).

Distribution. Pragian of Tasmania, Victoria, Queensland and western France; late Pragian of Gornoy Altay and possibly Yukon Territory; late Pragian or early Zlichovian of New South Wales, Queensland and northern Tibet (Xizang); Zlichovian of Uzbekistan, western France, Yukon Territory and northeastern Alaska; Dalejan of New South Wales and northern Ural Mountains.

Martinophyllum altiaxis sp. n.

Plate 35.1, figures 10-13; Plate 35.1, figures 14-19;
Plate 35.1, figures 20, 21

Hexagonaria sp., Churkin in Churkin and Brabb, 1968, Plate 3, figures 1a, b.
Martinophyllum sp., Pedder, 1975, p. 290, figures 39, 40.
Martinophyllum sp. nov., Pedder in Jackson and others, 1978, p. 41, Plate 35, figures 4, 7, 9.
Martinophyllum sp. nov., Pedder and McLean, 1982, p. 80.

Type series. Holotype, GSC 75780, from GSC loc. C-12894. Four paratypes, GSC 46106, from GSC loc. C-12694; GSC 75781, 75782, both from GSC loc. C-63246; GSC 75783, from GSC loc. C-64149.

Diagnosis. Species of **Martinophyllum** with adult corallites that range in mean diameter from 6.5 to 10.1 mm, and have 13 x 2 to 18 x 2 septa that are neither retiform nor cavernous. Minor septa are almost as long as the long major septa. Tabularium 3.0 to 4.5 mm in diameter and strongly clisioid (that is with outer flat plates and an axial boss).

Description. Corallum cerioid; large colonies grow to a height of at least 40 cm and a diameter of at least 60 cm. In varieties with small corallites, such as the specimen figured by Churkin and Brabb (1968) from the **dehiscens** Zone of the Salmontrout Formation of Alaska, the mean diameter of adult corallites is 6.5 mm. In varieties with large corallites, such as GSC 46106 from the upper part of the **dehiscens** Zone in the Michelle Formation, the mean corallite diameter is as much as 10.1 mm. Typical specimens, including the holotype and most of the other specimens from the **dehiscens** Zone of the Royal Creek headwaters area, have mean adult corallite diameters of 7.5 to 9.0 mm. Increase is marginarial and nonparricidal, and has no visible effect on either the tabularium or innermost dissepiments. One, or as many as three offsets are produced simultaneously from the parent corallite.

Intercorallite walls are usually straight or broadly curved, but in a few specimens are locally zigzag, as viewed in transverse section. Thickness of the intercorallite walls varies from 0.05 to 0.3 mm. Walls that are partly zigzag are also partly septal in origin, and they tend to be thicker than the straight walls. Small corallite forms have a maximum of 13 x 2 to 16 x 2 septa, whereas in large corallite forms there are either 17 x 2 or 18 x 2 septa in each adult corallite. Septa vary from being slightly to distinctly fusiform, and smooth to moderately carinate. The two orders of septa are poorly differentiated. Minor septa are generally only slightly thinner and shorter than the major septa. Both orders of septa penetrate the inner tabularial boss. The apparently monacanthate tabeculae are about 0.1 to 0.15 mm in diameter, and are arranged as fans in the dissepimentarium and outer tabularium.

Dissepimentaria vary considerably. In wide parts of large corallites there are as many as 10 rows of dissepiments. In other fully developed corallites, there are locally only one or two rows of dissepiments. The innermost dissepiments are small and steeply inclined adaxially. Dissepiments in the middle and outer parts of the dissepimentarium are larger than the innermost dissepiments, and some are markedly globose. The middle and outer dissepimentarial surfaces may be more or less flat, but more commonly the inner and middle dissepimentarial surfaces are slightly to prominently arched. The tabularium, which is much less variable than the dissepimentarium, is 3.0 to 4.5 mm in diameter, and comprises two series of closely spaced plates. Plates in the outer series are mostly gently concave or sygmoidal, whereas those of the inner series are strongly convex, and collectively form a high axial boss with a more or less vertical margin. This type of tabularium was named clisioid by Hill (1939, p. 231).

PLATE 35.1 (opposite)

Figures 14-19. **Martinophyllum altiaxis** sp. n.

14-16. Large variety, paratype, GSC 46106, transverse and two longitudinal thin sections, x4; GSC loc. C-12694.
17, 18. Paratype, GSC 75783, transverse and longitudinal sections, x4; GSC loc. C-64149.
19. Paratype, GSC 75781, longitudinal thin section, x4; GSC loc. C-63246.

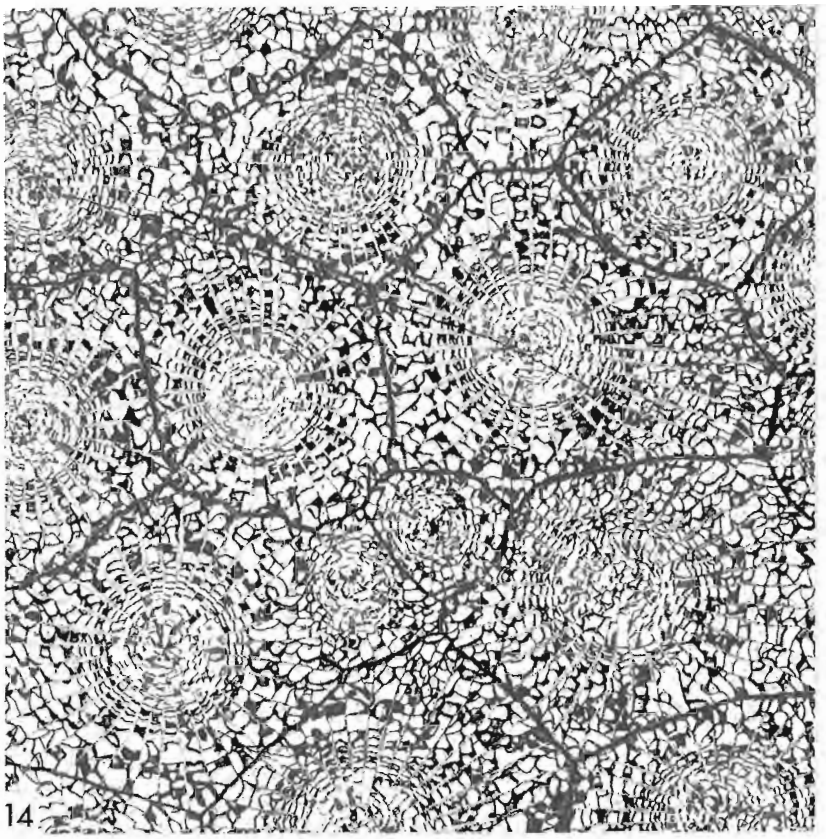

14

15

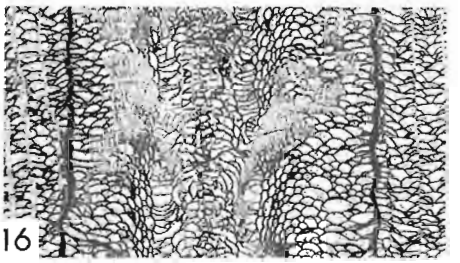

16

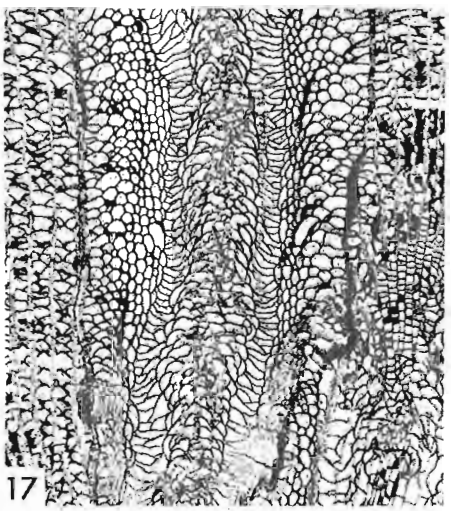

17

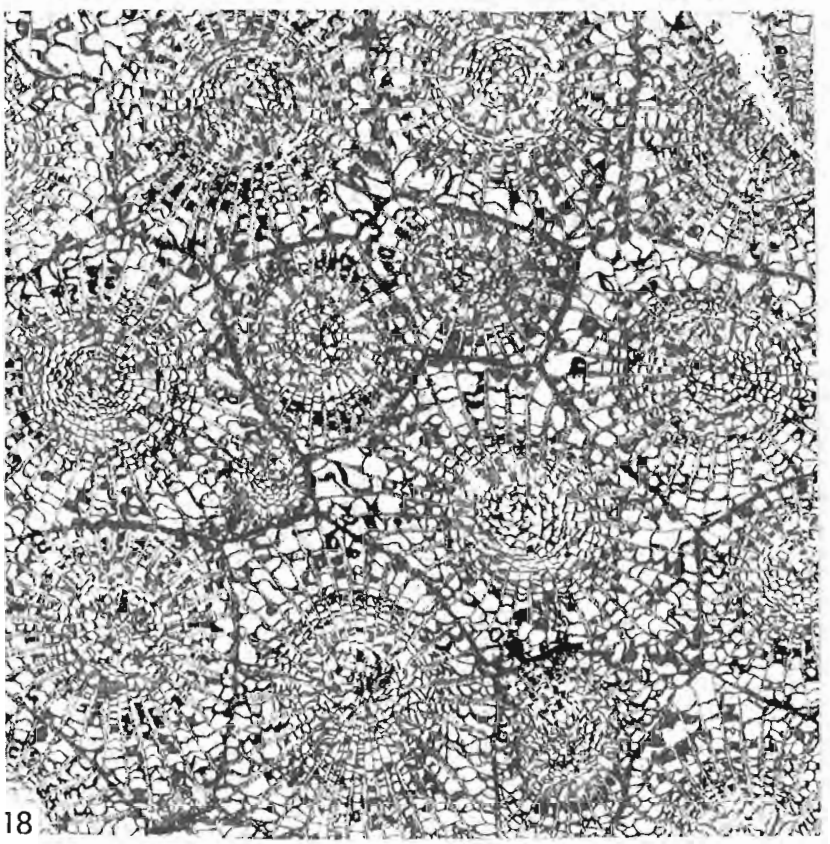

18

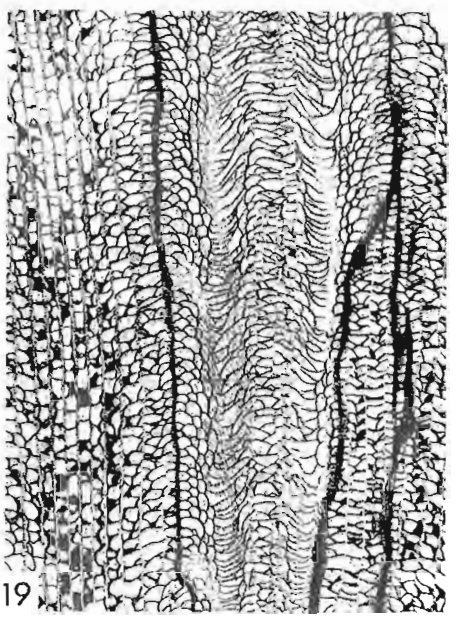

19

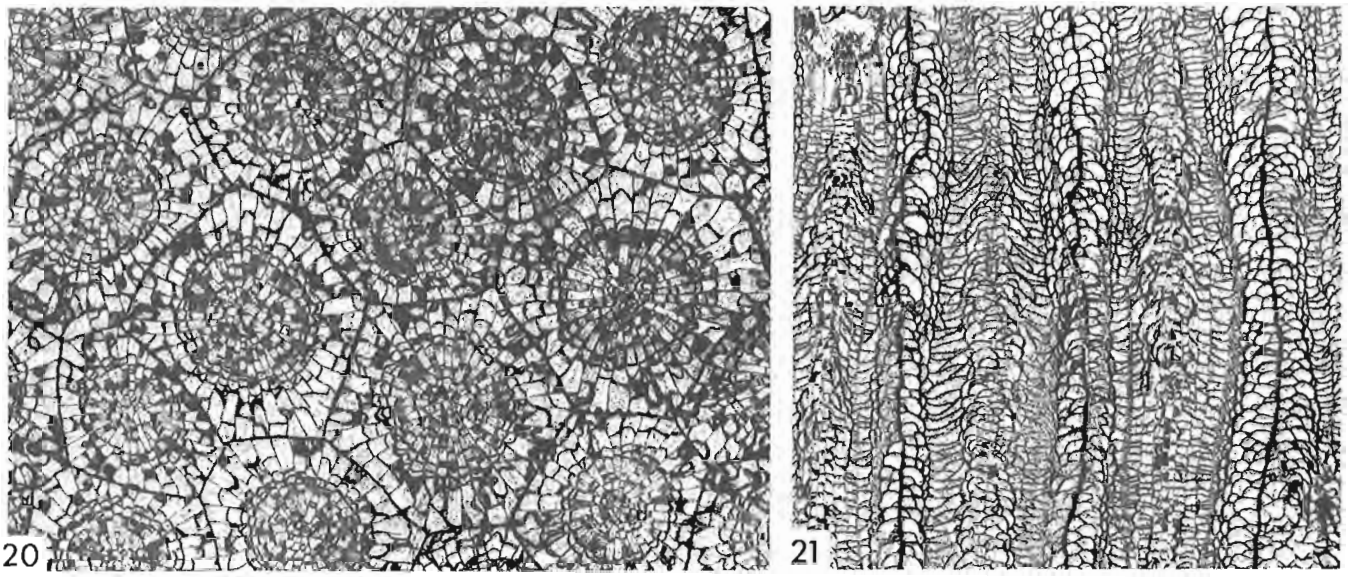

PLATE 35.1

Figures 20, 21. **Martinophyllum altiaxis** sp. n.

20, 21. Small variety, paratype, GSC 75782, transverse and longitudinal thin sections, x4; GSC loc. C-63246.

Remarks. The new species is morphologically closest to **Martinophyllum ornatum** and **M. densum**, both of which are Australian species with clisioid tabularia. Compared with **M. altiaxis, M. ornatum** is smaller (corallite and tabularium diameters 4.0 to 6.0 mm and 2.2 to 3.0 mm respectively), but has about the same number of septa (14 x 2 to 17 x 2) and has more strongly arched dissepimentaria. **M. densum** is about the same size as **M. altiaxis**, but has more septa (19 x 2 or 20 x 2). Also, its outer series of tabularial plates is narrower and less regular than that of **M. altiaxis**, and its tabularial boss is correspondingly much wider.

The trival name derives from the Latin words **altus**, meaning high, and **axis**, meaning axle.

Family BETHANYPHYLLIDAE Stumm, 1949
Genus **Thoulelasma** Pedder, 1983

Thoulelasma Pedder, 1983, p. 226-227.

Type species. **Thoulelasma loewei** Pedder, 1983, p. 227-228, Plate 26.1, figures 6-20. Blue Fiord Formation, Dalejan part; Sor Fiord section, southwestern Ellesmere Island, Canadian Arctic Archipelago.

Remarks. At the time of its proposal, only one species was known of **Thoulelasma**. It was placed in the Halliidae because its septal thickening is somewhat greater and more presistent ontogenetically in the cardinal quadrants than in the counter quadrants. In the new, but geologically older species described below, the tendency for the septa to be more dilated in the cardinal quadrants is negligible. It now seems that the overall morphology of **Thoulelasma**, especially the trabecular structure and lack of alar fossulae, relates it more to **Bethanyphyllum** than **Hallia**.

Thoulelasma yukonanum sp. n.

Plate 35.1, figures 22-30

Type series. Holotype, GSC 75784, and three paratypes, GSC 75785-75787, all from GSC loc. C-12692.

Diagnosis. Small (maximum length along the convex side of the corallum 3.2 cm; maximum diameter 2.8 cm) species of **Thoulelasma** with about 40 x 2 nonvepreculate septa at maturity. Septal dilation in cardinal and counter quadrants about equal. Dissepiments confined to no more than about eleven rows.

Description. Corallum trochoid, with no known offsets. Estimated maximum length, measured along the convex side of the corallum, 32 mm; maximum diameter 28 mm. Calicular platform narrow. The calice, which has steep sides and a moderately wide base (diameter about one half that of the corallum at the base of the calice), is 16 mm deep in the largest specimen. The outer wall is badly worn in the type series; unworn parts of the wall are from 0.1 to 0.4 mm thick.

At the earliest stage for which there is a transverse section (GSC 75787), the mean corallite diameter is 10.2 mm. This section shows a cardinal and 30 other major septa. There are probably also 30 minor septa, but the corallum is not fully preserved at the level of the section. A single row of dissepiments is present in parts of the counter quadrants. Inside the dissepiments, septa are fully dilated, leaving no interseptal space. The cardinal septum is distinguished by being narrower than other major septa, and is bounded by two minor septa that are slightly larger than the other minor septa.

As the coral exceeds a diameter of 11 to 12 mm, a cardinal fossula is formed just to one side of the most convex side of the corallum, and other interseptal spaces develop in the inner dissepimentarium and outer tabularium; a few narrow spaces may also appear in the axial region. The cardinal septum continues to be more attenuate than the adjacent major septa, and at about this stage begins to shorten. The counter septum is distinguished by being bounded by two long infra-lateral minor septa. Arrangement of the septa is bilateral about the cardinal-counter plane. At this stage, also, the minor septa become more prominent and both the major and minor septa are fusiform in the inner dissepimentarium and outer tabularium. There are 37 x 2 septa at a diameter of 18 mm.

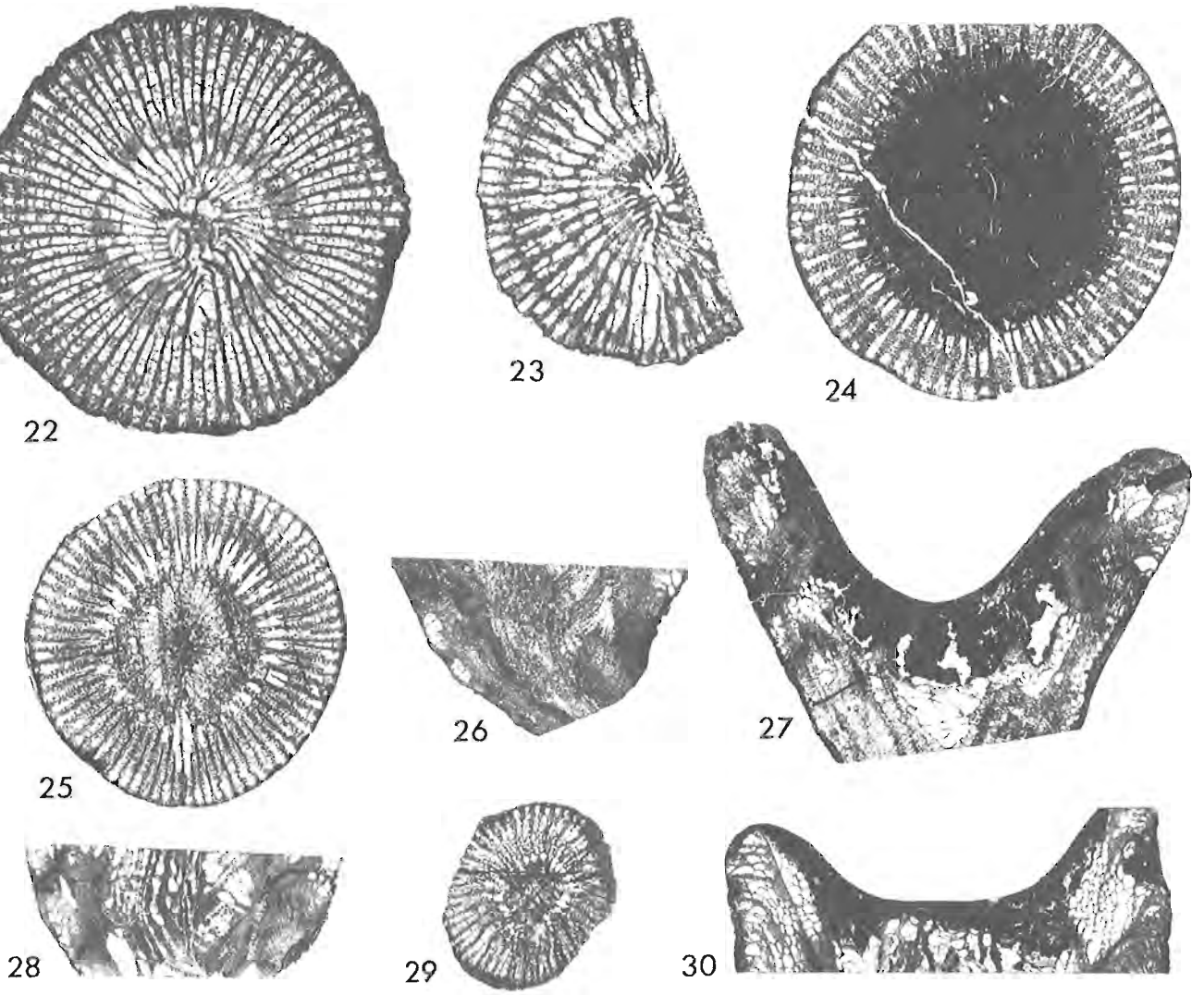

PLATE 35.1

Figures 22-30. **Thoulelasma yukonanum** sp. n.

22, 30. Paratype, GSC 75786, transverse and longitudinal thin sections, x2.5; GSC loc. C-12692.
23, 28. Paratype, GSC 75785, transverse and longitudinal thin sections, x2.5; GSC loc. C-12692.
24-26. Holotype, GSC 75784, two transverse and longitudinal thin sections, x2.5, GSC loc. C-12692.
27, 29. Paratype, GSC 75787, longitudinal and transverse thin sections, x2.5; GSC loc. C-12692.

The largest subcalicular transverse section (GSC 75786) is about 25 mm in diameter. It shows 40 x 2 septa which are still slightly bilateral in arrangement. The minor septa extend almost half the distance to the axis, and both orders of septa are less fusiform than in earlier stages. The largest calicular transverse section available (GSC 75784) is about 23 mm in diameter and has 37 x 2 septa. The cardinal septum is distinguishable as the shortest major septum; the counter septum is not differentiated from other major septa.

Just inside the outer wall, the monacanthate trabeculae are vertical or slightly outwardly directed. Further inside the wall, they become inwardly directed. Towards the axis, they at first progressively flatten, and are finally abruptly deflected upwards. The individual fibre fascicles are visible as darker regions of the septa; they do not project to form vepreculae.

The dissepimentarium first appears at a diameter of about 10 mm and comprises a single row of globular to rhomboid dissepiments. In late stages, seven to about eleven rows of dissepiments are present. The outer two or three rows tend to form flat or slightly everted dissepimentarial surfaces, whereas the inner rows are inwardly inclined. A few of the outermost dissepiments are lateral dissepiments. Because of the long axially expanded major septa, tabulae are incomplete. Tabularial surfaces are normally elevated around the margin to form a broad boss, but in one specimen (GSC 75787) are slightly depressed axially. A few tabularial surfaces are covered with stereome, typically 0.1 to 0.2 mm thick.

Remarks. **Thoulelasma loewei** is easily distinguished from the new species by its larger size (maximum length along the convex side of the corallum 9.5 cm; maximum diameter 3.9 cm), more numerous septa (as many as 54 x 2) and dissepiments (as many as 20 rows). Its septal dilation is more persistent in the cardinal quadrants, and some of its fibre fascicles project from the surface of the septum, producing incipient vepreculae.

The trivial name is coined from Yukon Territory and the suffix **-anus, -ana, -anum.**

Locality Register

GSC loc. C-12692. Michelle Formation, within upper 10 m; upper **dehiscens** Zone. Ogilvie Mountains, 1.6 km north of Ogilvie River, Yukon Territory; 65°22'30"N latitude, 138°27'00"W longitude. Collected by R. Ludvigsen, 1970. **Thoulelasma yukonanum** Pedder.

GSC loc. C-12694 and C-23538 (two numbers assigned to same collection). Michelle Formation, upper 15 m; upper **dehiscens** Zone. Ogilvie Mountain Front, about 9.7 km northwest of Hart River, Yukon Territory; 65°40'30"N latitude, 136°57'00"W longitude. Collected by R. Ludvigsen, 1971. **Pseudamplexus** sp., **Zonophyllum ludvigseni** Pedder and McLean, **Ogilvilasma discors** Pedder, **Martinophyllum altiaxis** Pedder, **Cortezorthis** sp. cf. **C. cortezensis** Johnson and Talent, **Leptaena** sp., **Megastrophia (Megastrophiella) iddingsi** (Merriam), **Desquamatia** sp., **Elythina transversa transversa** (Ludvigsen and Perry), **Nowakia acuaria** (Richter), **Panderodus** sp. (identified by T.T. Uyeno), "conodonts of the **Polygnathus dehiscens** Zone" (Ludvigsen and Perry, 1975, p. 88).

GSC loc. C-12894 (in place) and C-12895 (talus block). Isolated outcrop of strata transitional from carbonate platform to basinal Road River Formation; **dehiscens** Zone. Royal Creek headwaters, Section 4, Yukon Territory; 64°44'25"N latitude, 135°09'30"W longitude. Collected by A.E.H. Pedder, 1971. **Favosites** sp., **Cyttaroplasma regale** Pedder and McLean, **Lyrielasma** sp., **Taimyrophyllum** sp., **Xystriphyllum** sp., **Fasciphyllum** sp., **Martinophyllum altiaxis** Pedder, **Icriodus taimyricus** Kuz'min (C-12895 only, but in block with **Cyttaroplasma regale**), **Pandorinella exigua philipi** (Klapper), **Polygnathus dehiscens** Philip and Jackson, **P.** sp. cf. **P. pireneae** Boersma (C-12895 only, but in block with **Cyttaroplasma regale**). Conodonts indentified by T.T. Uyeno.

GSC loc. C-63246. Strata transitional from carbonate platform to basinal Road River Formation; **dehiscens** Zone; 55.2 to 56.4 m above base of section, 4.0 to 5.2 m below top of section. Royal Creek headwaters, Section 3, Yukon Territory; 64°45'54"N latitude, 135°09'54"W longitude. Collected by A.E.H. Pedder, 1971. **Favosites** sp., **Cyttaroplasma regale** Pedder and McLean, **Martinophyllum altiaxis** Pedder.

GSC loc. C-64149. Strata transitional from carbonate platform to basinal Road River Formation; **dehiscens** Zone; 266 to 267 m above base of section, 39 to 40 m below top of section. Royal Creek headwaters, Section 7, Yukon Territory; 64°47'30"N latitude, 135°10'00"W longitude. Collected by A.E.H. Pedder, 1976. Stromatoporoids, "**Oculipora**" with commensal **Torquaysalpinx** sp., **Pseudamplexus** sp., **Cystiphylloides** sp. aff. **C. americanum** (Milne Edwards and Haime), **Cyttaroplasma regale** Pedder and McLean, **Gubbera congesta** Pedder and McLean, **Circumtextiphyllum** sp., **Dohmophyllum** (broad sense) sp., **Ellesmerelasma expansum** Pedder, **Lyrielasma** sp., **Fasciphyllum** sp., **Loyolophyllum xizangense** Yu and Liao, **Martinophyllum altiaxis** Pedder, **Skenidioides** sp., "**Dolerorthis**" sp., **Muriferella**(?) sp., **Sieberella** sp. cf. **S. weberi** Khodalevich, **Nymphorhynchia pseudolivonica** (Barrande), "**Plectatrypa**" sp., **Spinatrypa** sp. cf. **S. echinocostata** Lenz, **Desquamatia**(?) sp., **Reticulariopsis**(?) sp., single axis crinoid ossicles, **Belodella** spp., **Panderodus** sp., **Pandorinellina exigua philipi** (Klapper). Conodonts identified by T.T. Uyeno.

References

Barrois, C.
1889: Faune du calcaire d'Erbray (Loire Inférieure); Mémoires de la Société Geologique du Nord, tome 3, p. 1-348.

Bul'vanker, E.Z.
1958: Devonskie chetyrekhluchevye korally okrani Kuznetskogo basseyna; Vsesoyuznyy Nauchno-Issledovate'skiy Geologicheskiy Institut (VSEGEI), Leningrad, text 212 p., and atlas.

Bul'vanker, E.Z., Vasilyuk, N.P., Zheltonogova, V.A., Zhizhina, M.S., Nikolaeva, T.V., Spasskiy, N.Ya., and Shchukina, V.Ya.
1960: Novye predstaveli chetyrekhluchevkh korallov SSSR; in Novye vidy drevnikh rasteniy i bespozvonochnykh SSSR, chast' 1, ed. B.P. Markovskiy; Vsesoyuznyy Nauchno-Issledovatel'skiy Geologicheskiy Institut (VSEGEI), GOSGEOLTEXIZDAT, Moskva, p. 220-254, 510-545.

Chapman, F.
1914: Newer Silurian fossils of eastern Victoria. Part III. Records of the Geological Survey of Victoria, v. 3(3), p. 301-316.

1931: A new Silurian coral from Lilydale. The Victorian Naturalist, v. 48(5), p. 94.

Cherepnina, S.K.
1970: Novye rugozy iz nizhnedevonskikh otlozheniy Gornogo Altaya; in Novye vidy paleozoiskikh mshanok i korallov, ed. G.G. Astrova and I.I. Chudinova; Izdatel'stvo "Nauka", Moskva, p. 112-116, 165.

Cherepnina, S.K. and Yaroshinskaya, A.M.
1974: Novye vidy rannedevonskikh i eifel'skikh rugoz i mshanok Gornogo Altaya; in Materialy po stratigrafii i paleontologii Zapadnoy Sibiri, ed. V.A. Ivaniya; Tomskogo Ordena Trudovogo Krasnogo Znameni Gosudarstvennogo Universiteta imeni V.V. Kuybysheva, Trudy, tom 227, p. 154-167.

Churkin, M., Jr. and Brabb, E.E.
1968: Devonian rocks of the Yukon-Porcupine Rivers area and their tectonic relation to other Devonian sequences in Alaska; in International Symposium on the Devonian System, Calgary, 1967, ed. D.H. Oswald; Alberta Society of Petroleum Geologists, Calgary, Alberta, v. II, p. 227-258.

Fåhraeus, L.E.
1971: Lower Devonian conodonts from the Michelle and Prongs Creek Formations, Yukon Territory; Journal of Paleontology, v. 45(4), p. 665-683.

Hill, D.
1939: The Devonian rugose corals of Lilydale and Loyola, Victoria; The Royal Society of Victoria, Proceedings, new ser., v. 51(2), p. 219-256.

1940: The Middle Devonian rugose corals of Queensland, II. The Silverwood-Lucky Valley area; The Royal Society of Queensland, Proceedings, v. 51(9), p. 150-168.

Jackson, D.E., Lenz, A.C., and Pedder, A.E.H.
1978: Late Silurian and Early Devonian graptolite, brachiopod and coral faunas from northeastern and arctic Canada; The Geological Association of Canada, Special Paper, no. 17, 160 p.

Jell, J.S. and Pedder, A.E.H.
1969: **Martinophyllum**, a new genus of Devonian rugose corals; Journal of Paleontology, v. 43(3), p. 735-740.

Khodalevich, A.N., Breyvel', I.A., Breyvel', M.G., Vaganova, T.I., Torbakova, A.F., and Yanet, F.E.
1959: Brakiopody i Korally iz eifel'skikh boksitonosnykh otlozheniy vostochnogo sklona srednego i severnogo Urala; GOSGEOLTEKHIZDAT, Moskva, 286 p.

Kraevskaya, L.N.
1955: Podklass Zoantharia. Otryad tetracoralla ili rugosa. Tetrakorally (nizhniy i sredniy devon); in Atlas rukovadyashchikh form iskopaemykh fauny i flory zapadnoy Sibiri. Tom 1, ed. L.L. Khalfin; Gosudarstvennoe Nauchno-Tekhnicheskoe Izdatel'stvo Literatury po Geologii i Okhrane Nedr, Moskva, p. 206-228.

Lenz, A.C.
1976: Lower Devonian brachiopod communities of the northern Canadian Cordillera; Lethaia, v. 9(1), p. 19-27.

1977: Upper Silurian and Lower Devonian brachiopods of Royal Creek, Yukon, Canada. Part 1. Orthoida, Strophomenida, Pentamerida, Rhynchonellida; Palaeontographica, Abt. A, Band 159, p. 37-109.

1982: New data on Late Silurian and Early Devonian brachiopods from the Royal Creek area, Yukon Territory; Canadian Journal of Earth Sciences, v. 19(2), p. 364-375.

1972: Late Early Devonian dacryoconarid tentaculites, northern Yukon Territory; Canadian Journal of Earth Sciences, v. 9(3), p. 297-318.

Ludvigsen, R. and Perry, D.G.
1975: The brachiopod **Warrenella** in the Lower Devonian and Middle Devonian formations of northwestern Canada; in Contributions to Canadian Paleontology, Geological Survey of Canada, Bulletin 235, p. 59-107.

Pedder, A.E.H.
1975: Sequence and relationships of three Lower Devonian coral faunas from Yukon Territory; in Report of Activities, Part B, Geological Survey of Canada, Paper 75-1B, p. 285-295.

1983: New Dalejan (Early Devonian) rugose corals from the Blue Fiord Formation of southwestern Ellesmere Island, Northwest Territories; in Current Research, Part B, Geological Survey of Canada, Paper 83-1B, p. 233-236.

Pedder, A.E.H. and McLean, R.A.
1982: Lower Devonian cystiphyllid corals from North America and eastern Australia with notes on the genus **Utaratuia**; Geologica et Palaeontologica, 16, p. 57-110.

Shurygina, M.V.
1977: Rogozy; in Biostratigrafiya i fauna rannego devona vostochnogo sklona Urala, ed. E.S. Sycheva and L.N. Shimanova; Ural'skoe Territorial'noe Geologicheskoe Upravlenie, Moskva, "Nedra", p. 43-51, 161-163.

Soshkina, E.D.
1949: Devonskie korally Rugosa Urala; Akademiya Nauk SSSR, Paleontologicheskogo Instituta, Trudy, tom 15, vyp. 4, 160 p.

Spasskiy, N. Ya. and Chereprina, S.K.
1972: Novye devonskie tetrakorally SSSR; in Novye vidy drevnikh rasteniy i bespozvonochnykh SSSR, ed. I.E. Zanina; Izdatel'stvo "Nauka", Moskva, p. 82-86, 348-349.

Strusz, D.L.
1965: Disphyllidae and Phacellophyllidae from the Devonian Garra Formation of New South Wales; Palaeontology, v. 8(3), p. 518-571.

Wu (Vu) Din-li.
1980: Novye vidy rugoz iz verkhnesiluriyskikh i devonskikh otlozheniy severo-vostochnoy Fergany; Paleontologicheskiy Zhurnal, 1980(3), p. 28-33.

Yu Chang-min and Liao Wei-hua.
1982: Discovery of Early Devonian tetracorals from Xainza, northern Xizang (Tibet) (Chinese with English abstract); Acta Palaeontologica Sinica, v. 21(1), p. 96-107.

Zheltonogova, V.A. and Ivaniya, V.A.
1961: Devonskaya Sistema. Podklass Tetracoralla (Rugosa). Tetrakorally; in Biostratigrafiya paleozoya Sayano-Altayskoy gornoy oblasti. Tom II. Sredniy paleozoy, ed. L.L. Khalfin; Sibirskogo Nauchno-Issledovatel'skogo Instituta Geologii, Geofiziki i Mineral'nogo Syr'ya (SNIGGIMS), Trudy, vyp. 20, p. 266-280, 368-408 (imprint 1960).

36. # THE SCHEI POINT AND BLAA MOUNTAIN GROUPS (MIDDLE-UPPER TRIASSIC), SVERDRUP BASIN, CANADIAN ARCTIC ARCHIPELAGO

Project 750083

Ashton F. Embry
Institute of Sedimentary and Petroleum Geology, Calgary

Embry, A.F., The Schei Point and Blaa Mountain groups (Middle-Upper Triassic), Sverdrup Basin, Canadian Arctic Archipelago; in Current Research, Part B, Geological Survey of Canada, Paper 84-1B, p. 327-336, 1984.

Abstract

The Schei Point Formation, a Middle-Upper Triassic clastic unit in the Sverdrup Basin of Arctic Canada, is herein raised to group status, and five new formations are recognized within the group. These new formations are formally defined herein and, in ascending order, are: Murray Harbour, Roche Point, Hoyle Bay, Pat Bay and Barrow. The Roche Point and Pat Bay formations consist mainly of nearshore marine sandstones and are present only on the basin margins. The Murray Harbour, Hoyle Bay and Barrow formations consist of shale and siltstone of offshore shelf to slope origin, and these formations extend across the basin. Within the basin the Murray Harbour, Hoyle Bay and Barrow comprise strata formerly assigned to the Blaa Mountain Formation. Consequently the Blaa Mountain is also given group status.

Résumé

Dans la présente étude, on élève au rang du groupe la formation de Schei Point, unité clastique du Trias moyen et supérieur du bassin de Sverdrup de l'Arctique canadien. On subdivise ce groupe en cinq nouvelles formations qu'on définit ici dans un ordre ascendant: Murray Harbour, Roche Point, Hoyle Bay, Pat Bay et Barrow. Les formations de Roche Point et de Pat Bay sont surtout constituées de grès marins littoraux; on ne les trouve que sur les bordures du bassin. Les formations de Murray Harbour, de Hoyle Bay et de Barrow sont constituées de schiste argileux et de siltstone de faciès plateaux à talus continentaux; elles occupent l'étendue du bassin. A l'intérieur du bassin les formations de Murray Harbour, de Hoyle Bay et de Barrow contiennent des couches qui appartenaient antérieurement à la formation de Blaa Mountain; nous élevons aussi au rang de groupe cette dernière formation.

Introduction

Regional stratigraphic studies combining both surface and subsurface information on the Mesozoic succession of the Sverdrup Basin have led to the recognition of numerous new stratigraphic units (Embry, 1983a, b). Five new formations have been delineated in strata formerly assigned to either the Schei Point Formation or the Blaa Mountain Formation (Middle-Upper Triassic). Accordingly, both the Schei Point and Blaa Mountain are now given group status, and the five newly recognized formations are described herein.

The Schei Point and Blaa Mountain groups comprise Middle to Upper Triassic (Anisian-Norian) strata in the Sverdrup Basin. The Schei Point encompasses strata deposited on the basin margins, and comprises sandstone and bioclastic limestone along with shale and siltstone. The Blaa Mountain is composed of equivalent strata deposited in the basin and characterized by shale and siltstone with few coarse grained interbeds.

The strata are present at the surface and in the subsurface over much of the basin (Fig. 36.1). Outcrops are plentiful in the eastern Sverdrup, occurring both on the margins and well within the basin. In the western Sverdrup, scattered, poorly exposed outcrops occur on the southern and northern basin margins. However, subsurface control is relatively plentiful for the western Sverdrup as opposed to the eastern Sverdrup, where only a few wells penetrate the strata (Fig. 36.1).

Previous work

The Schei Point Formation was defined by Tozer (1963a) as a result of work completed on Operation Franklin in 1955. He established a type section on Bjorne Peninsula, southwestern Ellesmere Island, where the formation is 600 m thick. At this locality, the Schei Point consists of interbedded calcareous sandstone, siltstone and shale, and lies between two major sandstone units, the Bjorne Formation below, and the Heiberg Formation above. Subsequent fieldwork by Tozer in the late fifties and early sixties led to the recognition of the Schei Point along the eastern and southern margins of the Sverdrup Basin (Tozer, 1961, 1963b; Tozer and Thorsteinsson, 1964). Tozer and Thorsteinsson (1964) also mapped the Schei Point on the northwestern margin of the basin on Borden Island.

In sections of the Schei Point on Ellesmere Island, Tozer (1961, 1963b) recognized four distinct units: a lower shale, a lower sandstone, an upper shale-siltstone and an upper sandstone ("Gryphea bed"). He also noted (Tozer, 1963b, p. 9) that a covered interval occurs between the upper sandstone and the Heiberg Formation. This interval may represent a thin shale unit at the top of the Schei Point.

Subsurface occurrences of the Schei Point were first described by Henao-Londono (1977), who briefly described the formation in the Sabine Peninsula area of Melville Island. Balkwill et al. (1982) described the Schei Point encountered in the Sun Skybattle C-15 well on southern Lougheed Island. In both these areas the Schei Point consists of interbedded calcareous sandstone, siltstone, shale and limestone. Both Henao-Londono (1977) and Balkwill et al. (1982) recognized a distinctive shale unit between the uppermost sandstone unit of the Schei Point and strata of the Heiberg Group. They assigned this shale unit to the Blaa Mountain Formation rather than the Schei Point Formation.

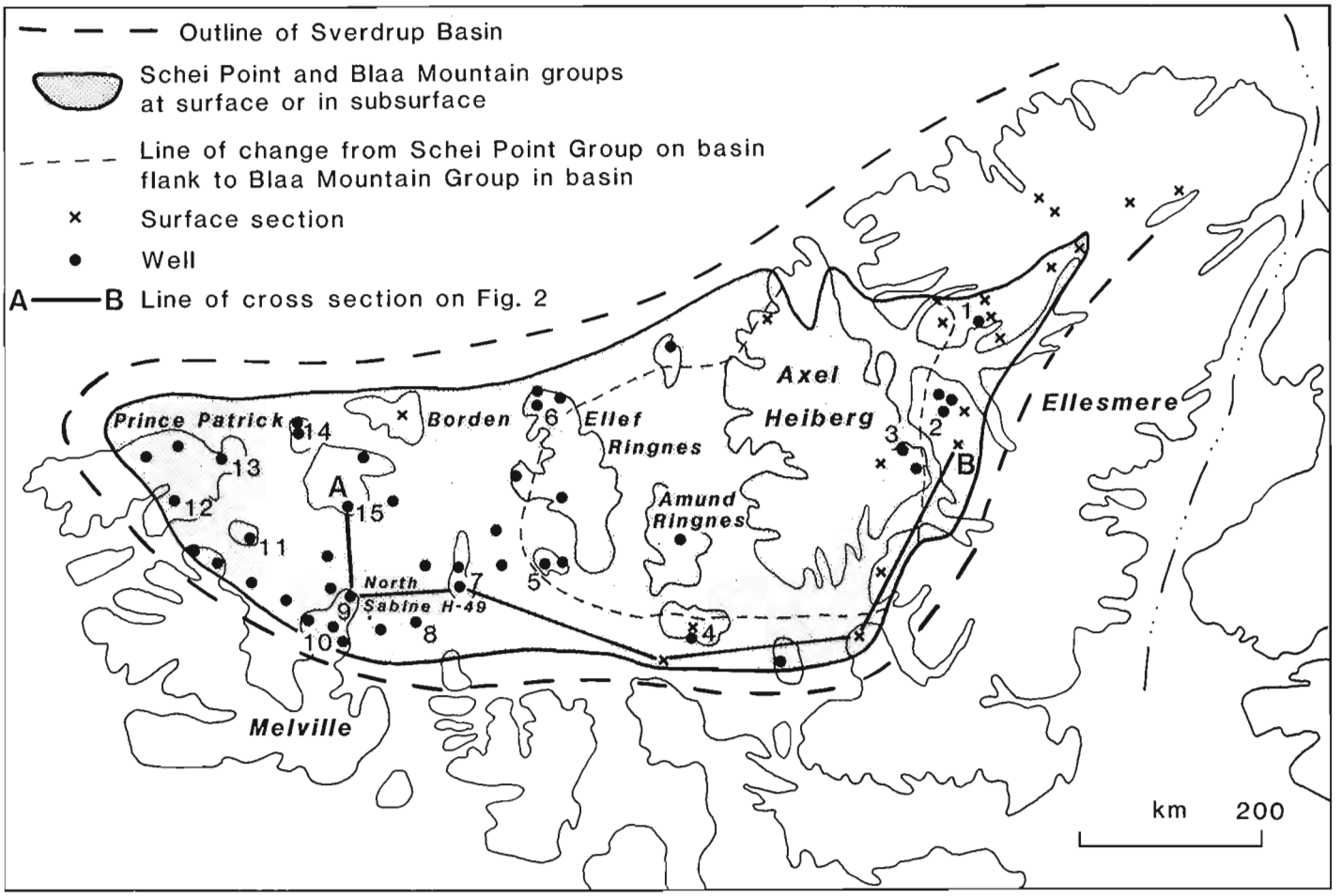

Figure 36.1. *Distribution of Schei Point and Blaa Mountain groups in Sverdrup Basin, and available control points. Key to wells listed in Appendix: 1. Neil O-15, 2. Romulus C-42, 3. Mokka A-02, 4. Cornwall O-30, 5. Sutherland O-23, 6. Pollux G-60, 7. Skybattle C-15, 8. Desbarats B-73, 9. North Sabine H-49, 10. Drake Point D-68, 11. Emerald K-33, 12. Jameson Bay C-31, 13. Satellite F-68, 14. Brock C-50, 15. Cape Norem A-80.*

The Blaa Mountain Formation was defined by Troelsen (1950) after reconnaissance work on Ellesmere Island. He established a type section on northern Ellesmere, but he did not define the boundaries of the formation. Subsequent stratigraphic work by Tozer (1961, 1963b, c) and Souther (1963) refined the definition of the formation and established it as a widespread unit of interbedded dark grey to black shale, calcareous siltstone and silty limestone, which lies between the Blind Fiord Formation and the Heiberg Formation. The Blaa Mountain is up to 2500 m thick, and in most sections Tozer (1961, 1963b) recognized a five-fold division: a lower shale, a lower calcareous siltstone, a middle shale, an upper calcareous siltstone and an upper shale.

Tozer's surface investigations on Ellesmere and Axel Heiberg islands demonstrated that the Blaa Mountain Formation is stratigraphically equivalent to the Schei Point Formation. He showed that the two sandstone units recognized in the Schei Point change facies basinward into the calcareous siltstone units of the Blaa Mountain, and that the three shale units of the Blaa Mountain extend into the Schei Point. Tozer (1970), in a review of the Mesozoic stratigraphy of the Arctic Islands, provided an excellent summary of the lithologies and stratigraphic relationships of the Middle and Upper Triassic strata in the Sverdrup Basin.

Present work

Since the pioneering stratigraphic studies of Tozer, over one hundred wells have penetrated Mesozoic strata in the Sverdrup Basin, and many of the wells encountered Middle-Upper Triassic strata (Fig. 36.1). In subsurface sections of the Schei Point the same five-fold lithological subdivision recognized by Tozer in outcrop – lower shale, lower sandstone, middle shale, upper sandstone and upper shale – is apparent (Fig. 36.2). Because these distinct lithological units are so widespread, and because each has economic importance as a potential hydrocarbon reservoir, source, or seal, they are given formation status. They have been named, in ascending order: Murray Harbour, Roche Point, Hoyle Bay, Pat Bay and Barrow formations. The relationships of these units with previously designated units are shown in Figure 36.3.

The sandstone-dominant Roche Point and Pat Bay formations are recognizable only on the basin margins, due to basinward facies change to siltstone and shale (Fig. 36.1). However, the shale-siltstone units – Murray Harbour, Hoyle Bay and Barrow – can be extended across the basin, and comprise the Blaa Mountain Group within the basin centre. Figure 36.4 is a schematic stratigraphic cross-section that

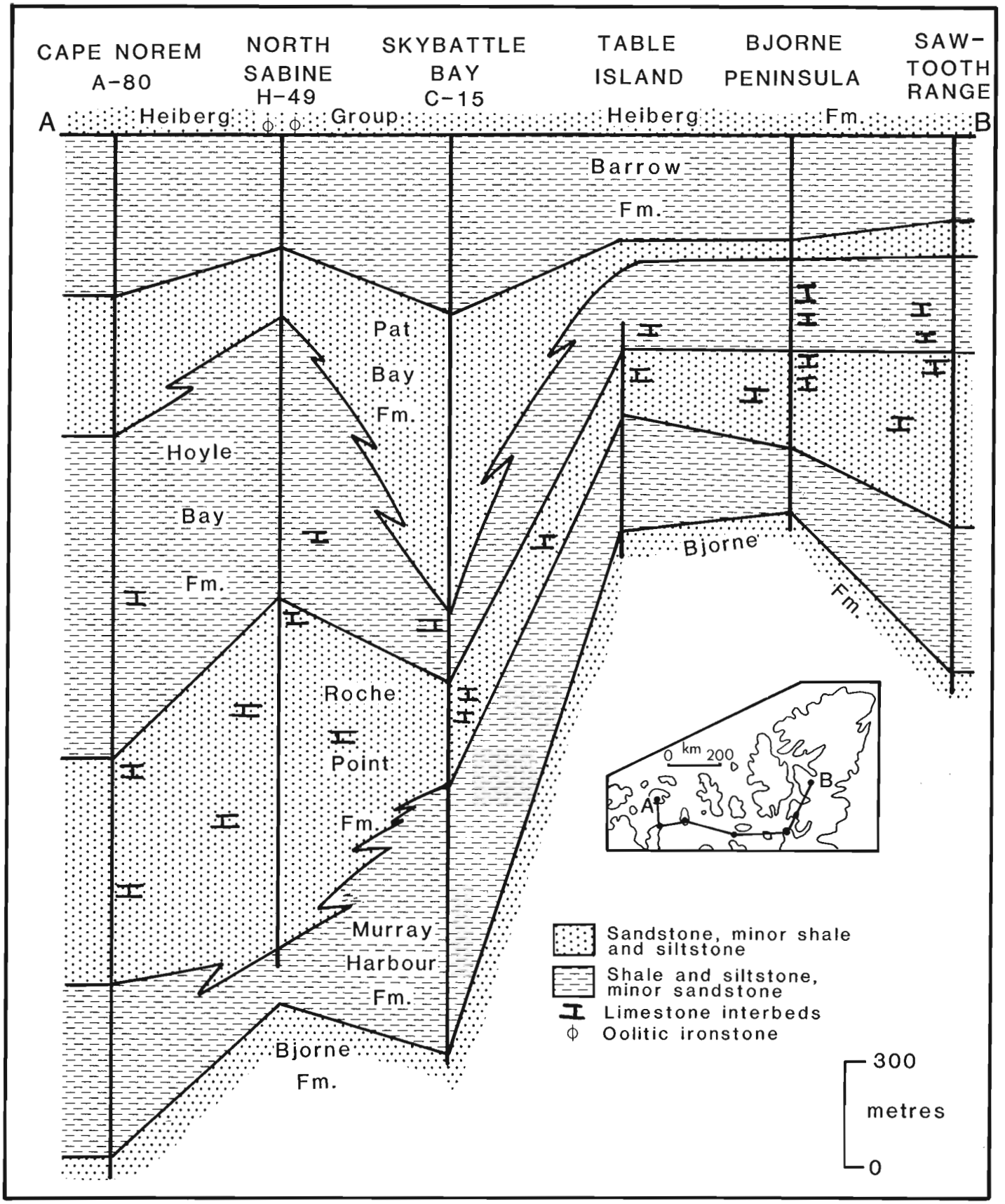

Figure 36.2. *Stratigraphic cross-section, Schei Point Group.*

		BASINAL AREA Tozer 1961, 1963a	BASINAL AREA This paper	BASIN FLANKS Tozer 1961, 1963a	BASIN FLANKS This paper
		Heiberg Fm.	Heiberg Fm.	Heiberg Fm.	Heiberg Fm.
Late Triassic	Norian	Blaa Mountain Formation: Upper Shale	Barrow Fm.	Schei Point Formation: Covered Interval	Barrow Fm.
	Carnian	Upper Calcareous	Hoyle Bay Fm.	Gryphea Bed	Pat Bay Fm.
		Middle Shale		Undivided	Hoyle Bay Fm.
Middle Triassic	Ladinian	Lower Calcareous	Murray Harbour Fm.		Roche Point Fm.
	Anisian	Lower Shale			Murray Harbour Fm.
Early Triassic	Spathian	Blind Fiord Fm.	Blind Fiord Fm.	Bjorne Fm.	Bjorne Fm.

Blaa Mountain Group; Schei Point Group

Figure 36.3. *Past and present nomenclature, Middle-Upper Triassic strata, Sverdrup Basin.*

illustrates the main lithological subdivisions and facies changes for the Middle-Upper Triassic strata of the Sverdrup Basin and the new stratigraphic nomenclature proposed in this paper. The tops, for units within the Schei Point and Blaa Mountain groups in fifteen selected wells (Fig. 36.1) in the Sverdrup Basin, are listed in the Appendix.

Murray Harbour Formation

Definition

The Murray Harbour Formation consists of shale and calcareous siltstone with thin interbeds of very fine grained, calcareous sandstone in the upper portion. The type section is in the Desbarats B-73 well (N 76°42'13", W 105°57'07"; spud. February 18, 1979, abandoned March 27, 1979; T.D. 1085 m; K.B. 4.9 m) between 939 m and 977 m, and is 38 m thick (Fig. 36.5). Chip samples taken at three-metre intervals from these strata, and from the type sections of the other formations defined in this paper, can be examined at the Institute of Sedimentary and Petroleum Geology, in Calgary, Alberta. The formation name is taken from Murray Harbour, an inlet on the northern end of Sabine Peninsula, Melville Island.

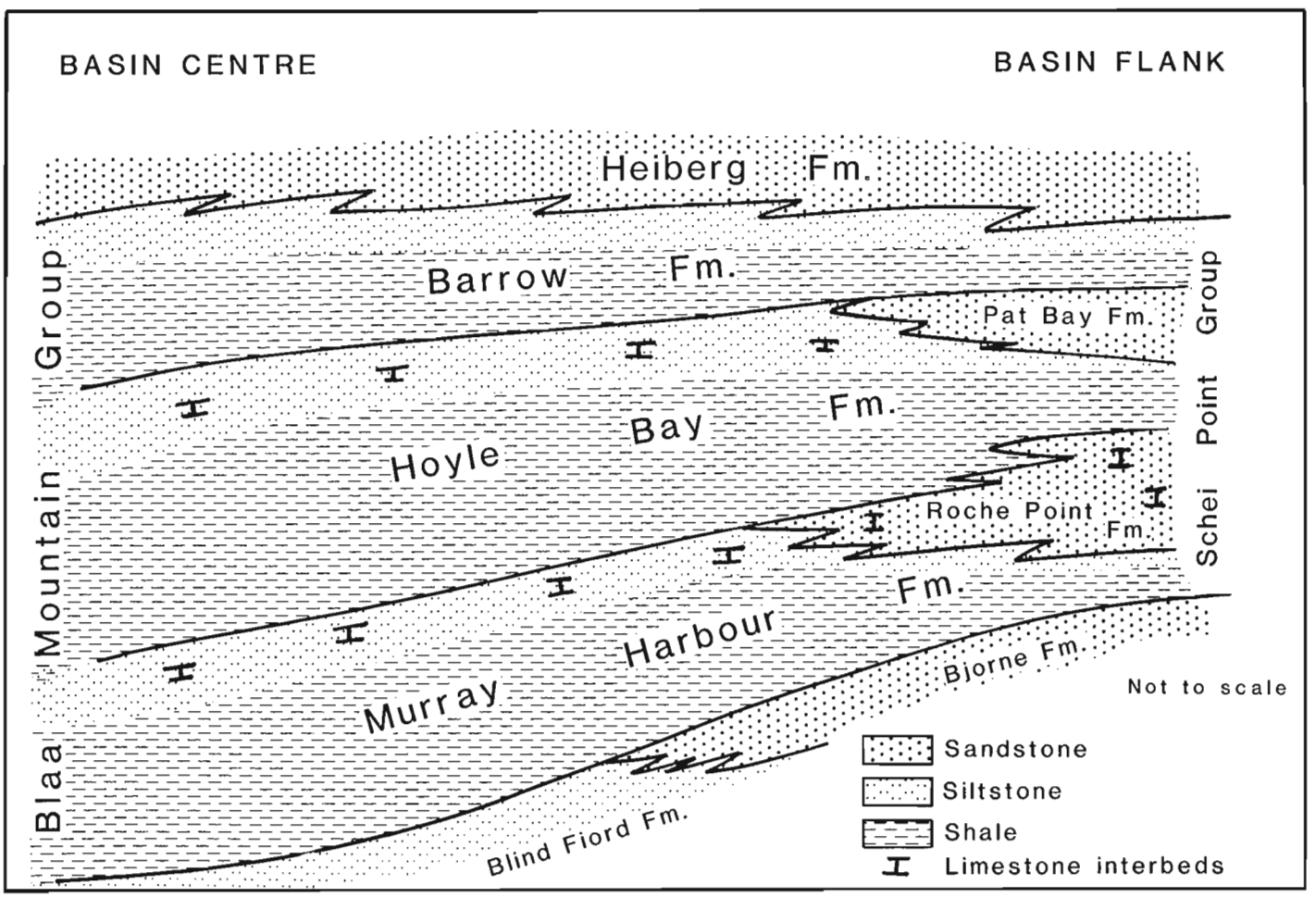

Figure 36.4. *Schematic stratigraphic cross-section, Middle-Upper Triassic strata, Sverdrup Basin.*

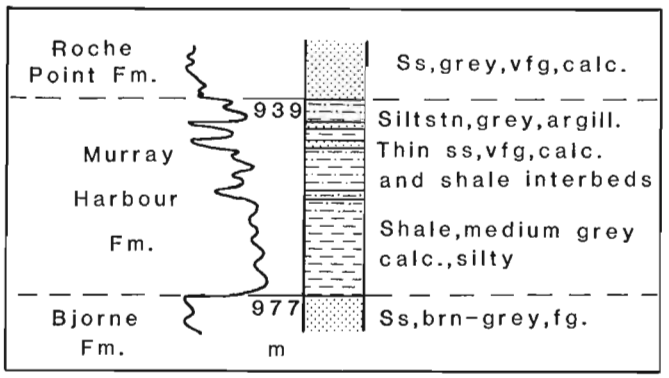

Figure 36.5. *Lithology (from samples) and gamma ray curve for type section of Murray Harbour Formation; Desbarats B-73 well.*

Synonyms

1. Units 2 and 3, Schei Point Formation, Table and Exmouth islands composite section (Tozer, 1961)
2. Units 2 and 3, Schei Point Formation, Bay Fiord - Vesle Fiord composite section (Tozer, 1961)
3. Units 1 and 2, Blaa Mountain Formation, Nansen Sound section (Tozer, 1961)
4. Units 1-4, Schei Point Formation, Bjorne Peninsula (Tozer, 1963b)
5. Unit 1, Blaa Mountain Formation, Oobloyah Bay section (Tozer, 1963b)
6. Units 1 and 2, Blaa Mountain Formation, Hare Fiord section (Tozer, 1963b)
7. Lower shale and lower calcareous members, Blaa Mountain Formation, Ellesmere Island (Tozer, 1963b)

Boundaries

On the basin margins, the Murray Harbour Formation overlies sandstone of the Bjorne Formation. The contact is placed at the base of the lowest shale-siltstone unit, above which shale and siltstone are predominant, and varies from conformable to unconformable. Within the basin the contact is placed at the base of a dark grey to black, calcareous shale unit, which rests conformably on grey-green siltstone of the Blind Fiord Formation.

The Murray Harbour Formation is conformably overlain by the Roche Point Formation. The contact is placed at the base of the first sandstone or bioclastic limestone (packstone-grainstone) above which sandstone and limestone are the predominant lithologies. In basinal areas, where the Roche Point Formation is no longer present, the Murray Harbour Formation is conformably overlain by the Hoyle Bay Formation. This contact is placed at the base of a clay-rich shale unit, which overlies calcareous siltstone of the uppermost Murray Harbour.

Lithology

At the type section, the Murray Harbour consists of medium to dark-grey shale, which coarsens upward to grey, calcareous siltstone with thin interbeds of very fine grained, calcareous siltstone (Fig. 36.5). This general description is applicable to the formation over most of its area of occurrence. In some sections, silty limestone (mudstone-wackestone) is common in the upper part of the formation. Shale colour varies from dark grey to black in the basin, to medium grey and green, and even red, on the basin margins. Siltstone and limestone units are usually highly burrowed. Pelecypods and rare ammonites are the main fossil fauna of the Murray Harbour.

Thickness and distribution

The formation is present throughout the area of distribution of the Schei Point and Blaa Mountain groups, except on the extreme margins of the basin where it is overstepped by younger units of the Schei Point Group. The maximum recorded thickness is 670 m on Axel Heiberg Island near the basin centre.

Age

Ammonite and pelecypod fossils from the Murray Harbour Formation on Ellesmere, Axel Heiberg and Table islands indicate an Anisian to Ladinian age (Middle Triassic) for the unit (Tozer, 1961, 1963b).

Environment of deposition

The argillaceous nature of the formation, the occurrence of marine fossils and the stratigraphic relationships of the formation suggest an outer shelf to slope environment of deposition for the Murray Harbour.

Roche Point Formation

Definition

The Roche Point Formation consists of interbedded calcareous sandstone and arenaceous, bioclastic limestone (packestone-grainstone) with subsidiary interbeds of shale and siltstone. The type section is in the Panarctic North Sabine H-49 well (N 76°48'15", W 108°45'11"; spud. May 2, 1974, abandoned July 8, 1974; T.D. 3810 m, K.B. 60 m) between 3499 m (11 480 ft) and 3797 m (12 458 ft), and is 298 m thick (Fig. 36.6). The name is taken from Roche Point, on the northwestern side of Sabine Peninsula, Melville Island.

Synonyms

1. Unit 4, Schei Point Formation, Table and Exmouth islands composite section (Tozer, 1961)
2. Unit 4, Schei Point Formation, Bay Fiord-Vesle Fiord composite section (Tozer, 1961)
3. Unit 5, Schei Point Formation, Bjorne Peninsula section (Tozer, 1963b)
4. Unit 2, Blaa Mountain Formation, Oobloyah Bay section (Tozer, 1963b)

Boundaries

The Roche Point Formation conformably overlies the Murray Harbour Formation as described above. The Roche Point Formation is conformably overlain by the Hoyle Bay Formation. The upper contact is placed at the top of the highest sandstone or limestone unit, above which shale and siltstone are predominant.

Lithology

In the type section (Fig. 36.6), the Roche Point Formation consists mainly of very fine- to medium-grained, calcareous sandstone and bioclastic limestone (packestone) with lesser amounts of calcareous siltstone and shale. Over much of the western Sverdrup Basin the Roche Point is divided into four formal members which, in ascending order, are: Eldridge Bay (sandstone), Cape Caledonia (shale-siltstone), Chads Point (sandstone), and Gore Point (limestone). The members were defined and described by Embry (1984).

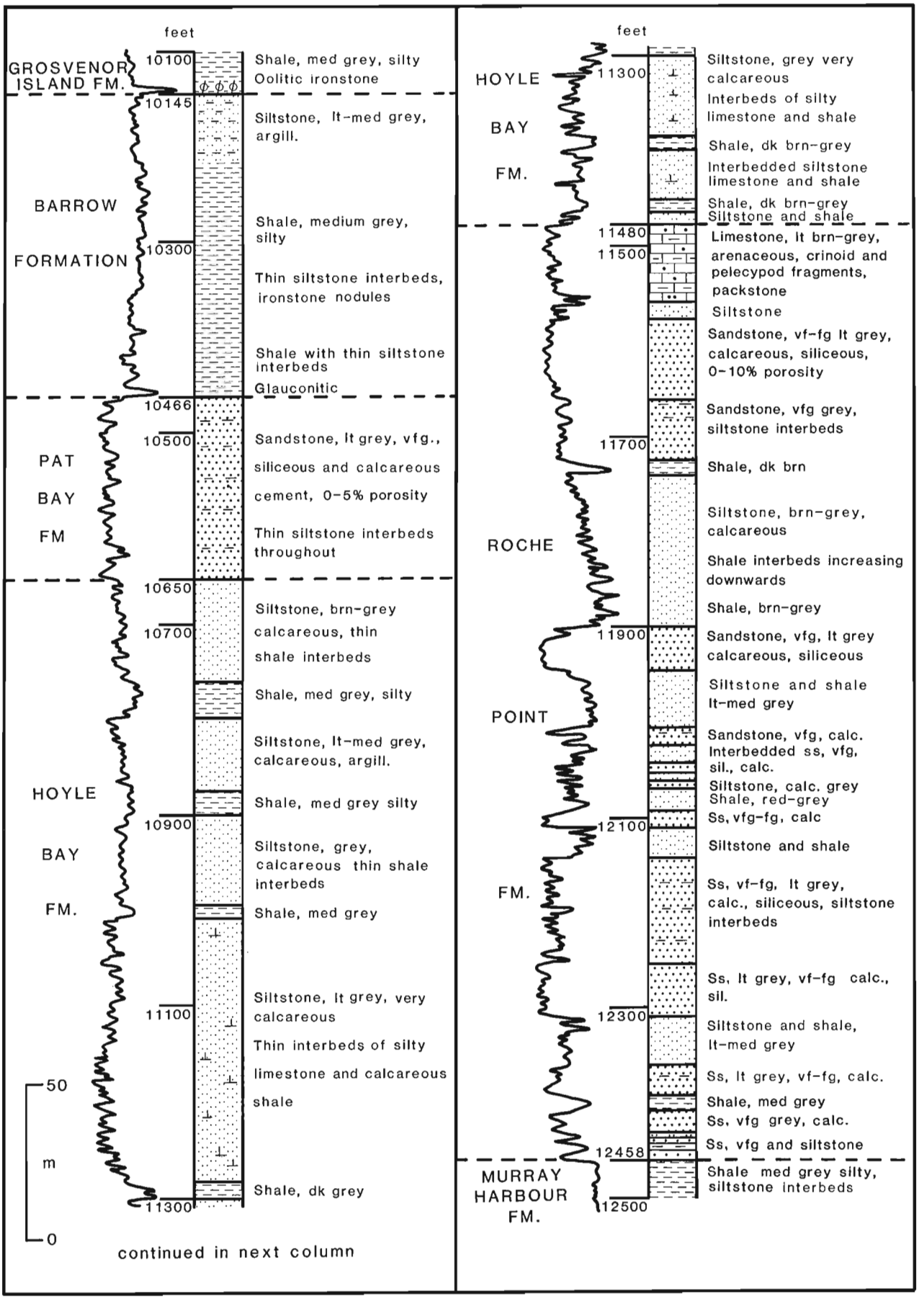

Figure 36.6. *Lithology (from samples) and gamma ray curve for type sections of Roche Point, Hoyle Bay, Pat Bay and Barrow formations; North Sabine H-49 well.*

In the eastern Sverdrup, the Roche Point has not been formally subdivided, and consists mainly of interbedded very fine- to coarse-grained, calcareous sandstone and arenaceous, bioclastic limestone. Both lithologies commonly contain abundant pelecypod shells and are extensively burrowed.

Shales and siltstones within the Roche Point are usually medium- to dark-grey and are calcareous. Red and green shale and siltstone are present in the Eldridge Bay Member along the southwestern margin of the basin.

Thickness and distribution

The Roche Point Formation occurs over much of the western Sverdrup Basin and along the southern and eastern margins of the basin (Fig. 36.1). The formation may be up to 250 m thick. It thins toward the basin centre and eventually disappears due to facies change to the shale and siltstone of the Murray Harbour Formation.

Age

Ammonite and pelecypod fossils collected from the Roche Point Formation on Ellesmere and Table islands range in age from Ladinian to Karnian (Tozer, 1961, 1963b). Along the basin margin the lower part of the formation is probably as old as Anisian, a conclusion reached on the basis of its intertonguing relationship with the Murray Harbour Formation, which contains Anisian ammonites.

Environment of deposition

The lithologies, sedimentary structures, and fauna of the Roche Point indicate a shallow marine shelf environment for the formation, below normal wave-base.

Hoyle Bay Formation

Definition

The Hoyle Bay Formation consists primarily of interbedded medium- to dark-grey shale, calcareous siltstone and silty limestone. The type section is in the Panarctic North Sabine well between 3246 m (10 650 ft) and 3499 m (11 480 ft), and is 253 m thick (Fig. 36.6). The name is taken from Hoyle Bay, which is on the western side of Sabine Peninsula, Melville Island.

Synonyms

1. Unit 5, Schei Point Formation, Table and Exmouth islands composite section (Tozer, 1961)
2. Unit 5, Schei Point Formation, Bay Fiord and Vesle Fiord, composite section (Tozer, 1961)
3. Units 3, 4, Blaa Mountain Formation, Nansen Sound section (Tozer, 1961)
4. Units 6-11, Schei Point Formation, Bjorne Peninsula section (Tozer, 1963b)
5. Units 3-9, Blaa Mountain Formation, Oobloyah Bay section (Tozer, 1963b)
6. Middle shale and upper calcareous members, Blaa Mountain Formation, Ellesmere Island (Tozer, 1963b)

Boundaries

The Hoyle Bay overlies either the Roche Point or Murray Harbour Formation, as has been described above. Along the basin margins the Hoyle Bay is conformably overlain by the Pat Bay Formation. The contact is placed at the base of the first sandstone unit, above which sandstone is predominant. Basinward, the Hoyle Bay Formation is conformably overlain by the Barrow Formation. This contact is placed at the base of a clay-rich shale unit that rests on calcareous siltstone of the uppermost Hoyle Bay.

Lithology

At the type section, the Hoyle Bay Formation consists of interbedded shale, siltstone and silty limestone (Fig. 36.6). The highly serrated nature of the gamma ray curve (Fig. 36.6) suggests that individual lithological units are usually less than 2 m thick. Overall, calcareous siltstone is the predominant lithology.

Over much of the western Sverdrup Basin the Hoyle Bay Formation has been divided into two formal members, the Eden Bay and the Cape Richards (Embry, 1984). The lower of the two, the Eden Bay Member, is distinguished by the presence of numerous limestone units with bituminous shale interbeds. Embry (1984) described the two members as they occur in the western Sverdrup.

In the eastern Sverdrup, the Hoyle Bay Formation is not formally subdivided. In this area the formation also consists mainly of shale and calcareous siltstone, and along the basin margin is characterized by units of arenaceous, bioclastic limestone and calcareous sandstone that may be up to 8 m thick. Basinward, these coarser grained units change facies and the Hoyle Bay consists entirely of shale and siltstone.

Thickness and distribution

The Hoyle Bay is present over the extent of the Schei Point and Blaa Mountain groups. The formation thickens toward the basin centre, with the maximum recorded thickness being 1300 m at Buchanan Lake on eastern Axel Heiberg Island.

Age

Ammonite and pelecypod fossils from the Hoyle Bay on Ellesmere, Axel Heiberg and Table islands are indicative of a Carnian age (Tozer, 1961, 1963b).

Environment of deposition

The lithologies and fauna of the Hoyle Bay suggest an outer shelf to slope environment of deposition for the formation.

Pat Bay Formation

Definition

The Pat Bay Formation consists of very fine- to fine-grained, calcareous sandstone with subordinate siltstone and shale. The type section is in the Panarctic North Sabine H-49 well between 3190 m (10 466 ft) and 3246 m (10 650 ft), and is 56 m thick (Fig. 36.6). The name is taken from Pat Bay, on the western side of Lougheed Island.

Synonyms

1. Unit 6, Schei Point Formation, Bay Fiord - Vesle Fiord composite section (Tozer, 1961)
2. Units 10-16, Blaa Mountain Formation, Oobloyah Bay section (Tozer, 1963b)
3. Unit 3, Blaa Mountain Formation, Hare Fiord section (Tozer, 1963b)
4. "**Gryphea** bed", Ellesmere Island (Tozer, 1963b)
5. Schei Point Formation, Borden Island (Tozer and Thorsteinsson, 1964)
6. Pollux sand, western Sverdrup Basin (Henao-Londono, 1977)

Boundaries

The Pat Bay Formation conformably overlies the Hoyle Bay Formation as described previously. The Pat Bay is conformably overlain by the Barrow Formation. The upper contact is placed at the top of the highest sandstone unit, above which shale and siltstone are predominant.

Lithology

At the type section, the Pat Bay Formation consists of very fine- to fine-grained, calcareous sandstone with thin interbeds of siltstone. This description applies to the formation over much of its extent. In outcrop, sandstone units are commonly massive to highly burrowed, and contain pelecypod shells. There is usually a coarsening-upward trend in the formation, with the thickest and coarsest grained units in its upper portion.

Thickness and distribution

The Pat Bay Formation occurs over much of the western Sverdrup and along the basin margins in the eastern Sverdrup (Fig. 36.1). In the western Sverdrup, the Pat Bay thins from north to south due to facies change to the siltstone and shale of the Hoyle Bay Formation. The maximum recorded thickness in this area is 262 m. In the east, the Pat Bay forms a narrow band of sandstone along the basin margins, with a thickness of about 20 m.

Age

On the basis of pelecypod fossils collected on Ellesmere and Border islands (Tozer, 1961, 1963b), and its intertonguing relationship with the well-dated Hoyle Bay Formation, the Pat Bay Formation is considered to be Carnian in age.

Environment of deposition

The lithologies, sedimentary structures and fauna in the Pat Bay Formation suggest a nearshore marine shelf environment of deposition.

Barrow Formation

Definition

The Barrow Formation consists of shale and siltstone with minor interbeds of very fine grained sandstone. The type section is in the North Sabine H-49 well between 3092 m (10 145 ft) and 3190 m (10 466 ft), and is 98 m thick (Fig. 36.6). The formation is named after Barrow Harbour, an inlet on the northern end of Sabine Peninsula, Melville Island.

Synonyms

1. Unit 5, Blaa Mountain Formation, Nansen Sound area, Ellesmere Island (Tozer, 1961)
2. Units 17, 18, Blaa Mountain Formation, Oobloyah Bay section (Tozer, 1963b)
3. Unit 4, Blaa Mountain Formation, Hare Fiord section (Tozer, 1963b)
4. Upper shale member, Blaa Mountain Formation, Ellesmere and Axel Heiberg islands (Tozer, 1961, 1963b)
5. Upper Blaa Mountain, western Sverdrup Basin (Henao-Londono, 1977)
6. Blaa Mountain Formation, Lougheed Island (Balkwill et al., 1982)
7. Blaa Mountain Formation, Cornwall Island (Balkwill, 1983)

Boundaries

Over much of its extent, the Barrow Formation conformably overlies either the Pat Bay or Hoyle Bay Formation, as described previously. On northeastern Ellesmere Island the Barrow Formation oversteps the Pat Bay Formation and rests on various formations, ranging in age from Devonian to Triassic.

In the western Sverdrup, the Barrow Formation is overlain by either the Skybattle Formation (contact placed at base of lowest sandstone unit) or the Grosvenor Island Formation (contact placed at the base of a widespread oolitic ironstone unit; Embry, 1983a). This contact is conformable, except on the basin margin where the Grosvenor Island unconformably overlies the Barrow. In the eastern Sverdrup the Barrow is conformably overlain by the Heiberg Formation. The contact is placed at the base of the first sandstone unit >4 m thick and above which sandstone is relatively common (Embry, 1983b).

Lithology

The Barrow Formation at its type section, and over its entire extent, consists of medium grey, silty shale and siltstone with minor interbeds of very fine grained sandstone. The lithologies commonly display parallel lamination, although burrows and ripple crosslamination are almost as common. Sandstone units usually occur near the top of the formation, heralding the presence of the overlying Heiberg or Skybattle formations. An exception to this is the occurrence of very fine grained, glauconitic sandstone units in the lower part of the formation on Mackenzie King Island. These sandstones form the Jenness Member of the Barrow Formation (Embry, 1984).

Thickness and distribution

The Barrow Formation is present over the extent of the Schei Point and Blaa Mountain groups. In the western Sverdrup, and along the basin margins, it is usually less than a few hundred metres thick. It thickens rapidly toward the basin centre where it may be up to 1000 m thick.

Age

The Barrow is dated as Norian (Late Triassic) on the basis of pelecypod fossils collected from Cornwall and Brock islands (Tozer, 1973; Balkwill, 1983) and palynomorphs (Balkwill et al., 1982).

Environment of deposition

The Barrow Formation is of prodelta and offshore marine shelf origin (Embry, 1982).

References

Balkwill, H.R.
1983: Geology of Amund Ringnes, Cornwall and Haig-Thomas islands, District of Franklin; Geological Survey of Canada, Memoir 390.

Balkwill, H.R., Hopkins, W.S. Jr., and Wall, J.H.
1982: Geology, Lougheed Island, District of Franklin; Geological Survey of Canada, Memoir 388.

Embry, A.F.
1982: The Upper Triassic - Lower Jurassic Heiberg Deltaic Complex of the Sverdrup Basin; in Arctic Geology and Geophysics, ed. A.F. Embry and H.R. Balkwill; Canadian Society of Petroleum Geologists, Memoir 8, p. 189-217.

Embry, A.F. (cont.)
1983a: The Heiberg Group, western Sverdrup Basin; in Current Research, Part B; Geological Survey of Canada, Paper 83-1B, p. 381-389.

1983b: Stratigraphic subdivision of the Heiberg Formation, eastern and central Sverdrup Basin; in Current Research, Part B; Geological Survey of Canada, Paper 83-1B, p. 205-213.

1984: Stratigraphic subdivision of the Roche Point, Hoyle Bay and Barrow formations, (Schei Point Group) western Sverdrup Basin, Arctic Islands; in Current Research, Part B; Geological Survey of Canada, Paper 84-1B, report 31.

Henao-Londono, D.
1977: Correlation of producing formations in the Sverdrup Basin; Bulletin of Canadian Petroleum Geology, v. 25, p. 969-980.

Souther, J.G.
1963: Geological traverse across Axel Heiberg Island from Buchanan Lake to Strand Fiord; in Y.O. Fortier et al., Geology of the north central part of the Arctic Archipelago, Northwest Territories (Operation Franklin); Geological Survey of Canada, Memoir 320, p. 426-448.

Tozer, E.T.
1961: Triassic stratigraphy and faunas, Queen Elizabeth Islands, Arctic Archipelago; Geological Survey of Canada, Memoir 316.

1963a: Northwestern Bjorne Peninsula; in Y.O. Fortier et al., Geology of the north-central part of the Arctic Archipelago, Northwest Territories (Operation Franklin); Geological Survey of Canada, Memoir 320, p. 363-370.

Tozer, E.T. (cont.)
1963b: Mesozoic and Tertiary stratigraphy, western Ellesmere Island and Axel Heiberg Island, District of Franklin; Geological Survey of Canada, Paper 63-30.

1963c: Mesozoic and Tertiary stratigraphy; in Y.O. Fortier et al., Geology of the north-central part of the Arctic Archipelago, Northwest Territories (Operation Franklin); Geological Survey of Canada, Memoir 320, p. 74-94.

1970: Geology of the Arctic Archipelago, Mesozoic; in Geology and Economic Minerals of Canada, ed. R.J.W. Douglas; Geological Survey of Canada, Economic Geology Report 1, p. 574-583.

1973: Triassic assemblages (macrofossils); in B.S. Norford et al., Biostrati-graphic determinations of fossils from the subsurface of the Yukon Territory and the District of Franklin, Keewatin and Mackenzie; Geological Survey of Canada, Paper 72-38, p. 18-19.

Tozer, E.T. and Thorsteinsson, R.
1964: Western Queen Elizabeth Islands, Arctic Archipelago; Geological Survey of Canada, Memoir 332.

Troelsen, J.
1950: Contributions to the geology of northwest Greenland, Ellesmere Island and Axel Heiberg Island; Meddelelser om Grønland, v. 149, n. 7.

Appendix

Selected well tops, Schei Point and Blaa Mountain groups, Sverdrup Basin. Location of wells shown on Figure 36.1.

Gulf Neil 0-15

Barrow Formation	609 m (1997 ft)
Pat Bay Formation	747 m (2450 ft)
Hoyle Bay Formation	759 m (2490 ft)
Roche Point Formation	1018 m (3339 ft)
Murray Harbour Formation	1029 m (3375 ft)
Bjorne Formation	1098 m (3602 ft)

Panarctic Romulus C-42

Barrow Formation	2400 m (7870 ft)
Hoyle Bay Formation	2510 m (8234 ft)
Roche Point Formation	2740 m (8990 ft)
Murray Harbour Formation	2843 m (9328 ft)
Bjorne Formation	2922 m (9585 ft)

Imperial Mokka A-02

Barrow Formation	330 m (1084 ft)
Hoyle Bay Formation	842 m (2762 ft)
Murray Harbour Formation	2507 m (8226 ft)

Mobil Cornwall 0-30

Barrow Formation	spud
Hoyle Bay Formation	151 m (495 ft)
Roche Point Formation	446 m (1463 ft)
Murray Harbour Formation	487 m (1598 ft)
Bjorne Formation	797 m (2615 ft)

Dome Sutherland 0-23

Barrow Formation	804 m (2637 ft)
Hoyle Bay Formation	1200 m (3938 ft)
Murray Harbour Formation	1707 m (5600 ft)
Blind Fiord Formation	1981 m (6498 ft)

Panarctic Pollux G-60

Barrow Formation	501 m (1645 ft)
Pat Bay Formation	860 m (2820 ft)
Hoyle Bay Formation	997 m (3272 ft)
Roche Point Formation	1039 m (3410 ft)
Murray Harbour Formation	1089 m (3572 ft)
Blind Fiord Formation	1420 m (4658 ft)

Sun Skybattle C-15

Barrow Formation	2159 m (7082 ft)
Pat Bay Formation	2314 m (7592 ft)
Hoyle Bay Formation	2576 m (8452 ft)
Roche Point Formation	2630 m (8630 ft)
Murray Harbour Formation	2723 m (8934 ft)
Bjorne Formation	2974 m (9758 ft)

Panarctic Desbarats B-73

Barrow Formation	567 m (1860 ft)
Hoyle Bay Formation	600 m (1969 ft)
Roche Point Formation	765 m (2510 ft)
Murray Harbour Formation	939 m (3081 ft)
Bjorne Formation	977 m (3205 ft)

Panarctic North Sabine H-49

Barrow Formation	3092 m (10 145 ft)
Pat Bay Formation	3190 m (10 466 ft)
Hoyle Bay Formation	3246 m (10 650 ft)
Roche Point Formation	3499 m (11 480 ft)
Murray Harbour Formation	3797 m (12 458 ft)

Panarctic Drake Point D-68

Barrow Formation	1166 m (3827 ft)
Pat Bay Formation	1218 m (3995 ft)
Hoyle Bay Formation	1241 m (4070 ft)
Roche Point Formation	1353 m (4440 ft)
Murray Harbour Formation	1540 m (5054 ft)
Bjorne Formation	1563 m (5128 ft)

BP Emerald K-33

Barrow Formation	1461 m (4793 ft)
Hoyle Bay Formation	1521 m (4990 ft)
Roche Point Formation	1600 m (5250 ft)
Murray Harbour Formation	1747 m (5739 ft)
Bjorne Formation	1762 m (5780 ft)

Elf Jameson Bay C-31

Barrow Formation	992 m (3255 ft)
Hoyle Bay Formation	1032 m (3386 ft)
Roche Point Formation	1140 m (3740 ft)
Murray Harbour Formation	1258 m (4126 ft)
Bjorne Formation	1271 m (4171 ft)

BP Satellite F-68

Barrow Formation	588 m (1930 ft)
Hoyle Bay Formation	688 m (2258 ft)
Roche Point Formation	892 m (2928 ft)
Murray Harbour Formation	1125 m (3691 ft)
Bjorne Formation	1170 m (3840 ft)

Panarctic Brock C-50

Hoyle Bay Formation	spud
Roche Point Formation	168 m (550 ft)
Murray Harbour Formation	431 m (1414 ft)
Bjorne Formation	446 m (1462 ft)

Elf Cape Norem A-80

Barrow Formation	1599 m (5246 ft)
Pat Bay Formation	1743 m (5719 ft)
Hoyle Bay Formation	1868 m (6130 ft)
Roche Point Formation	2156 m (7075 ft)
Murray Harbour Formation	2402 m (7880 ft)
Bjorne Formation	2499 m (8200 ft)

37. CORRELATION BETWEEN UPPER DEVONIAN SURFACE AND SUBSURFACE MAP UNITS IN WEST-CENTRAL ALBERTA

Project 810017

N.C. Meijer Drees and H.H.J. Geldsetzer
Institute of Sedimentary and Petroleum Geology, Calgary

Meijer Drees, N.C. and Geldsetzer, H.H.J., Correlation between Upper Devonian surface and subsurface map units in west-central Alberta; in Current Research, Part B, Geological Survey of Canada, Paper 84-1B, p. 337-349, 1984.

Abstract

The Upper Devonian surface geology of Jasper National Park and the subsurface geology of central Alberta were extended northwestward and westward respectively into the Kakwa River area of west-central Alberta. Relatively closely spaced sections suggest good surface to subsurface correlations. For example, the Flume may be correlated with the Beaverhill Lake, the Maligne with most of the strongly radioactive Duvernay, the Perdrix with the Ireton, the Mount Hawk with a relatively thin Nisku, the Simla with a Graminia carbonate, and the Palliser with the Wabamun.

Regional northwesterly trends observed in the mountains as well as in the subsurface are:

- *the reduction of the limestone component in the lower parts of the Nisku and MountHawk formations.*
- *the disappearance of the Calmar and of a similar recessive siltstone above the Nisku and Mount Hawk formations.*
- *the disappearance of clastics at the base of the Palliser-Wabamun interval, i.e. the Sassenach Formation and the "siltstone marker" of the Graminia Formation are absent in the Kakwa River area.*

Biostratigraphic control is needed for more precise correlation.

Résumé

La géologie de surface du Dévonien supérieur du parc national de Jasper et la géologie des roches profondes du centre de l'Alberta s'étendent vers le nord-ouest et vers l'ouest respectivement dans la région de la rivière Kakwa située dans le centre-ouest de l'Alberta. Des profils relativement proches suggèrent que les corrélations entre la surface et le sous-sol sont bonnes. Par exemple, la formation de Flume peut être liée à celle de la Beaverhill Lake, celle de Maligne avec la plupart des parties fortement radioactive de la formation de Duvernay, celle de Perdix avec celle de Ireton, celle de Mount Hawk avec les parties relativement mince de la formation de Nisku, celle de Simla avec la partie carbonatée de la formation de Graminia et celle de Palliser avec celle de Wabamum.

Les tendances régionales vers le nord-ouest observées dans les montagnes ainsi que sous terre sont:

- *la réduction de l'élément calcaire dans les parties inférieures des formations de Mount Nisku et Hawk.*
- *la disparition de la formation de Calmar et des siltstones en voie de disparition semblables au-dessus des formations de Mount Nisku et de Hawk.*
- *la disparition de roches clastiques à la base de l'intervalle Palliser-Wabamum, c'est-à-dire la formation Sassenach et le "marqueur de siltstone" de la formation de Graminia sont absents dans la région de la rivière Kakwa.*

Un contrôle biostratigraphique est nécessaire pour une corrélation plus précise.

Introduction

During the past ten years, the petroleum industry in Alberta has focused its attention on the gas potential of the Mesozoic and Paleozoic rocks in west-central Alberta, and many new wells have been drilled in the area between the Athabasca and Wapiti rivers. A small number of deep wells tested the potential of the Devonian carbonates. Information derived from these wells makes possible more precise comparison and correlation of the Devonian oil and gas bearing carbonates in the subsurface of the Interior Plains with equivalent strata exposed in the Rocky Mountains.

The following description of the Devonian succession in the subsurface is based on a study of drill cuttings and cores from 12 deep wells located at relatively short distances (between 22 and 135 km) from the surface sections in the Rocky Mountains measured and described by Geldsetzer (1982). The Devonian sections in the 12 wells were correlated by means of borehole logs and lithology logs of Canadian Stratigraphic Service Ltd., with Devonian sections from more than a hundred wells located in the Gold Creek, Simonette, Sturgeon Lake, Ante Creek, Big Stone, Pine Creek, Snipe Lake and Bigoray pools of west-central Alberta. These correlations made it possible to select an additional number of cores for those intervals not represented by core in the 12 wells studied.

The correlations proposed and the stratigraphical nomenclature used in this report are of a preliminary nature. It is anticipated that information resulting from the study of microfossils, for which samples were collected, will refine and change some of the lithostratigraphical correlations used here.

Acknowledgments

Field assistance was given by David Van Everdingen in 1979, and by Brian Fischer and Torsten Geldsetzer in 1981. Hal Tetz (Highland Helicopters Ltd.) and John Bell (Trans North Air) showed their skills as pilots in very rugged terrain. Photographs were taken by B.C. Rutley and printed by W.B Sharman. A.W. Norris critically read and improved the manuscript.

Geological setting

Figure 37.1 indicates the locations of the deep wells and the surface sections in relation to the major geological provinces (Price et al., 1977; Tipper et al., 1979). All wells are located on the Interior Platform near the western edge of the Alberta Syncline except for one (Sec. 4 of Fig. 37.1), which is located in the Foothills Belt of the Cordilleran Orogen. The surface sections are all situated in the Rocky Mountains Thrust Belt.

On the Interior Platform, the sedimentary rock succession is relatively undisturbed, and correlations between well sections are straightforward. In the Cordilleran Orogen, the sedimentary rock succession is folded, and cut by thrust faults. Because borehole sections in the Foothills Belt are rarely perpendicular to the bedding and may also include minor thrust faults, the thickness of a particular rock unit, as measured in the borehole, usually does not represent the true stratigraphic thickness. For this reason, the steep structural dip of subsurface Section 4 (see Fig. 37.2) has been corrected by an appropriate increase in vertical scale.

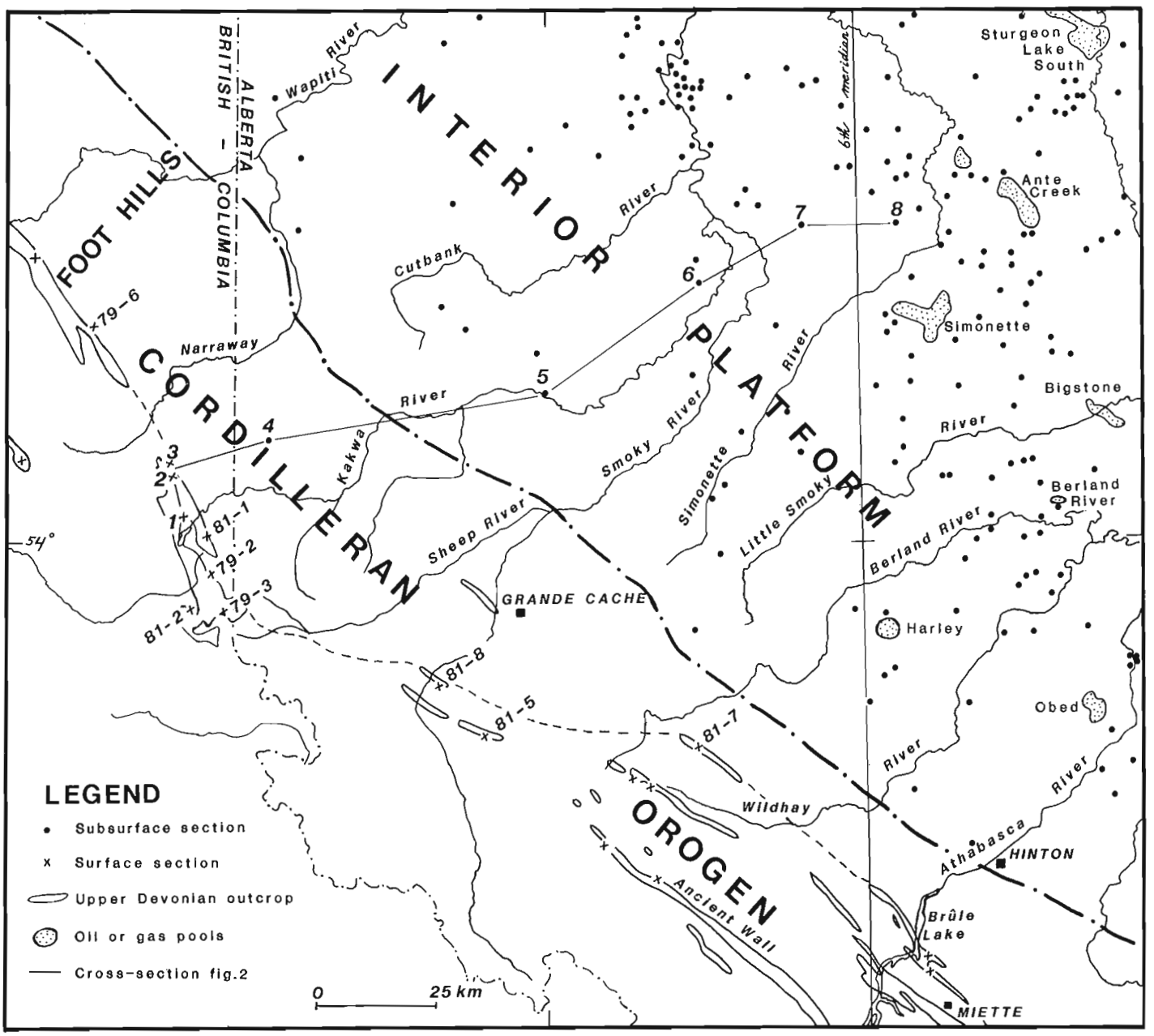

Figure 37.1. *Map including the main geographical and geological features and the location of surface and subsurface sections.*

Stratigraphy

The subdivision of the Devonian rock succession in west-central Alberta is based on previously established map units. Rock units in the Cordilleran region are differentiated on the basis of lithology, weathering character and fossil content. Map units established in the Interior Plains are segregated on the basis of lithology, geophysical log character and fossil content.

In the initial stage of geological mapping, diagenetic changes (limestone to dolostone) and the more subtle differences in lithology were not considered to be important. Fossil collections were only made in the Cordilleran region. In the selection of boundaries between surface map units, the emphasis was on the differences in weathering character. Boundaries between the subsurface map units were defined with the aid of borehole logs.

The differences in approach as to what constitutes a useful map unit, and the need to quickly establish a stratigraphic framework in the Interior Plains after the discovery of oil in the Devonian succession, led to the introduction of two stratigraphic nomenclatures. One terminology applies to the Cordilleran region, the other to the Interior Plains.

Cordilleran region

Beach (1943) subdivided the Devonian succession in the Moose Mountain and Morley map area, west of Calgary, into a lower Fairholme Formation and an upper Palliser Formation. Both the Fairholme and the Palliser formations are composed of carbonates.

This two-fold division of the Devonian carbonates was extended northward into the Sunwapta Pass area by Sverson (1950) and Fox (1951). DeWit and McLaren (1950) expanded the two-fold framework with the addition of the Alexo Formation and a redefinition of the upper contact of the Fairholme Formation. The redefined Fairholme Formation was subsequently raised to group status by the introduction of the Cairn and Southesk formations (McLaren, 1955).

In the area north of Jasper, the Devonian succession below the Palliser Formation includes a thick sequence of basal carbonate, shale and argillaceous limestone. These beds, earlier described by Raymond (1930) from Roche Miette, were subdivided by DeWit and McLaren (1950) into the Flume, Perdrix and Mount Hawk formations. A transitional unit, the Maligne Formation, was later added between the Flume and Perdrix formations (Taylor, 1957). The Alexo Formation at this locality was subdivided into two parts. The upper part, containing Famennian fossils, was named the Sassenach Formation; the lower part, containing Frasnian fossils, was named the Ronde Member of the Southesk Formation (McLaren and Mountjoy, 1962).

The clastic facies of the Perdrix and Mount Hawk formations were recognized as "off-reef" or "basinal" sediments that were deposited around organic buildups known as the Fairholme, Cairn-Southesk, Miette and Ancient Wall carbonate complexes. Carbonate banks (Grotto, Arcs and Ronde members of the Southesk Formation) cap these carbonate buildups and extend into and across the surrounding clastic facies. The precise correlation of the buildups, the basin-filling clastics and the carbonate banks is still a matter of discussion (Mountjoy, 1980).

There is a marked facies change to the northwest of the Ancient Wall carbonate complex. The clastic facies predominates and is consistently capped by a carbonate bank (Simla Formation). As well, the Sassenach Formation thins against the southwest margin of the Ancient Wall buildup and is entirely absent farther to the northwest where the Palliser Formation rests directly on the carbonate bank (Geldsetzer, 1982).

Throughout Jasper National Park the Fairholme group overlies Lower Paleozoic sediments. This trend continues northwestward into the area south and northwest of Grande Cache but is restricted to the northeasternmost thrust sheet of the Rocky Mountains Thrust Belt. In adjacent thrust sheets to the southwest the Fairholme Group rests on two Devonian carbonate-dominated units, the Dunedin Formation of probable Givetian age (late middle Devonian), and the Stone Formation, tentatively assigned to the Emsian (late early Devonian). Both units thicken to several hundred metres to the northwest but are consistently absent in the northeasternmost thrust sheet (Geldsetzer, 1982).

Because of the limited scope of this report, only those rock units present on the cross-section will be described. The map units of the Kakwa River area are, in ascending order: the Flume, Maligne, Perdrix, Mount Hawk, Simla and Palliser formations.

Flume Formation

The name Flume Formation was introduced by Raymond (1930) to describe the carbonates which underlie the shaly beds of the Perdrix Formation and overlie the sub-Devonian unconformity in the Jasper area. DeWit and McLaren (1950) selected the type section and defined the upper boundary. Taylor (1957) elevated the upper member of the Flume to formational status, introduced the name Maligne Formation, and redefined the upper boundary of the Flume below the Maligne. At the type section, the carbonates of the Flume Formation overlie unfossiliferous dolostone of the Cambrian Lynx Formation (Mountjoy and Geldsetzer, 1981).

In the area west of Grande Cache, the Flume Formation overlies the Middle Devonian Dunedin Formation or the Ordovician Skoki Formation (Geldsetzer, 1982). It includes three units: a lower unit of interbedded calcareous shale and limestone with a thin basal, crossbedded, quartzose sandstone; a thick middle unit composed of dark grey stromatoporoidal limestone; and, an upper unit of grey to light grey fossiliferous limestone. Both the lower and upper units carry abundant brachiopods suggesting a correlation with the Calumet and Moberly members of the Waterways Formation (A.W. Norris, personal communication). The stromatoporoidal biostrome unit varies considerably in thickness, increasing from 13 m at Mount St. Andrews (Sec. 1), to 49 m at Wallbridge Mountain (Sec. 79-2), and to 111 m at Mount Buchanan (Sec. 81-2), over a distance of 17 km (Fig. 37.1).

Maligne Formation

The Maligne Formation was defined by Taylor (1957) as a unit of nodular, interbedded, argillaceous limestone and shale, rich in brachiopods and crinoidal debris. It overlies the Flume Formation and underlies the dark shales of the Perdrix Formation. The Maligne Formation thickens considerably toward carbonate buildups, reaching 40 m at the Miette complex (Mountjoy, 1965), and 92 m at the Ancient Wall complex. Away from these complexes, the unit thins to only a few metres. Brachiopod assemblages suggest a post-Waterways Frasnian age (A.W. Norris, personal communication). The formation weathers recessively and is rarely exposed.

The best exposed section in the Kakwa River area occurs at Mount Ruth (Fig. 37.1, Sec. 81-1), where 21 m of the Maligne Formation occur below the Perdrix Formation.

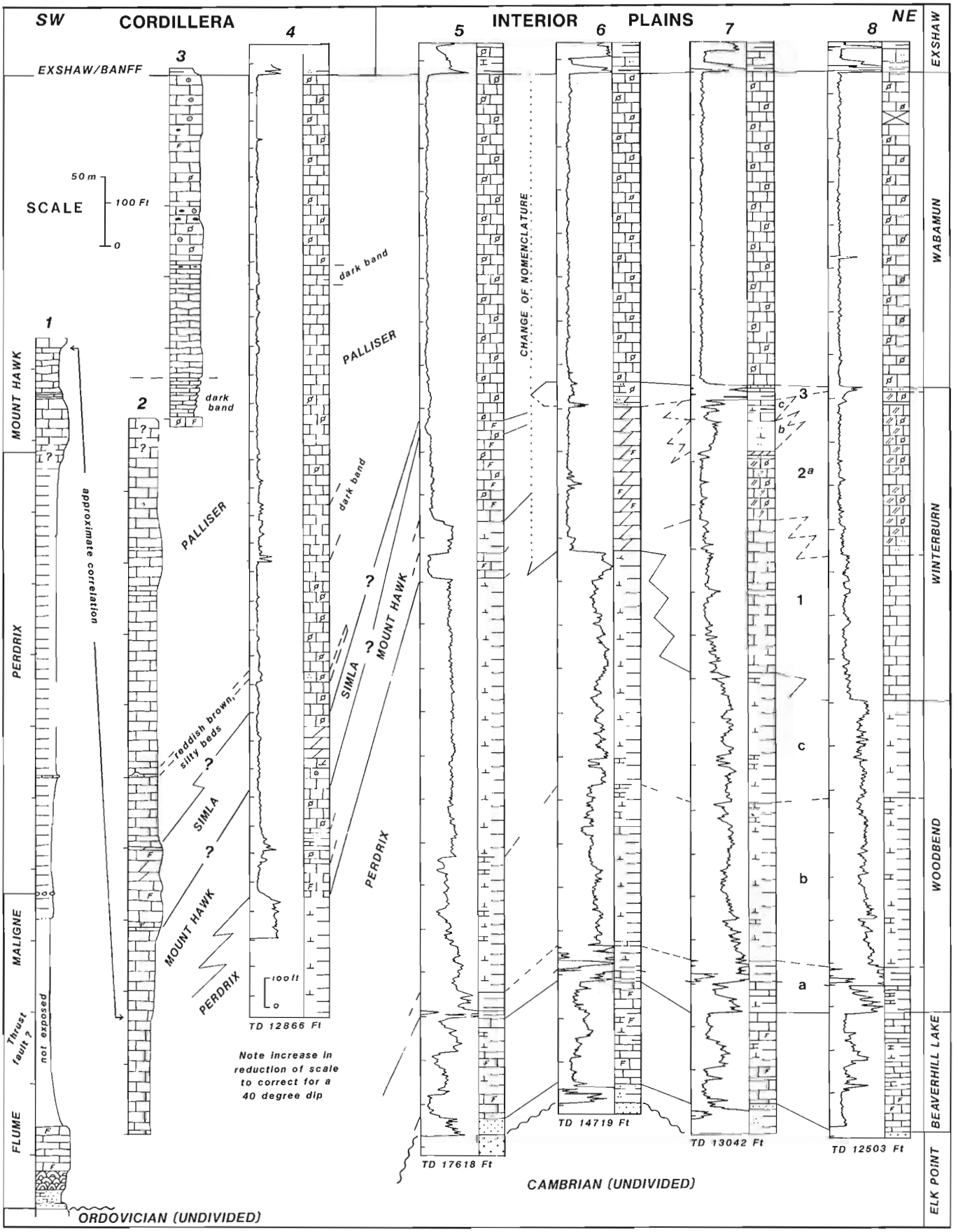
SW
CORDILLERA
INTERIOR PLAINS
NE
1
2
3
4
5
6
7
8
EXSHAW/BANFF
50 m
SCALE
100 Ft
0
dark band
PALLISER
CHANGE OF NOMENCLATURE
MOUNT HAWK
PERDRIX
SIMLA
Teddish brown, silty beds
approximate correlation
Thrust fault ?
not exposed
FLUME
MALIGNE
PERDRIX
MOUNT HAWK
WINTERBURN
WOODBEND
BEAVERHILL LAKE
ELK POINT
EXSHAW
WABAMUN
100 ft
0
TD 12866 Ft
TD 17618 Ft
TD 14719 Ft
TD 13042 Ft
TD 12503 Ft
Note increase in reduction of scale to correct for a 40 degree dip
CAMBRIAN (UNDIVIDED)
ORDOVICIAN (UNDIVIDED)

The unit is in thrust contact with the Ordovician Skoki Formation, but it is believed that this fault contact is close to the depositional contact with the underlying Flume Formation. The Maligne Formation consists of thin and wavy bedded, grey limestone with argillaceous interbeds and an abundance of well preserved brachiopods. Some bedding planes include many burrow-like structures. A thin interval of very dark, micritic limestone separates the fossiliferous limestone from the overlying, very dark, calcareous shale of the Perdrix Formation.

Perdrix Formation

The term Perdrix Formation was introduced by Raymond (1930) for the thick succession of Upper Devonian shale exposed in the Rocky Mountains east and west of the Athabasca River. The type section is on Roche Miette, where about 110 m of very dark bituminous pyritic shale and calcareous shale with limestone layers or nodules are exposed. The boundary with the Maligne Formation is fairly sharp. The boundary with the overlying Mount Hawk Formation can be transitional over more than 30 m (Mountjoy and Geldsetzer, 1981) and the criteria used in its selection differ from place to place (see McLaren, 1955, p. 10 and Mountjoy and Mackenzie, 1973, p. 15).

Due to the incompetent nature of the Perdrix Formation, thrust faults are common. Furthermore, the recessive nature of the Perdrix causes large parts of the unit to be covered by talus debris. The only unfaulted and fully exposed sections were measured along the southwest margin of the Ancient Wall complex, where the Perdrix Formation is 175 m thick.

In the Kakwa River area, the Perdrix Formation is at least 184 m thick at Bastille Mountain (Fig. 37.1, Sec. 79-3), thickens to 306 m at Mount St. Andrews (Fig. 37.2, Sec. 1) and thins again to 120 m at Mount Ruth (Fig. 37.1, Sec. 81-1).

The lower part of the formation consists of dark grey to black shales with rare interbeds of yellowish or rusty brown weathering, micritic limestone. There is a change to greenish grey silty shales in the upper part, but dark grey to black shale sections can reoccur. For example, in the Bastille Mountain section (Fig. 37.1, Sec. 79-3), a 9 m section of dark grey to black shale is found 15 to 24 m below the Perdrix - Mount Hawk contact. The top 20 to 30 m show an increasing number of very thin, evenly bedded interbeds of yellowish weathering biomud – and biopackstones. This interbedded unit grades over a few metres into the thin and nodular bedded, argillaceous and highly fossiliferous limestone of the Mount Hawk Formation.

A series of very thin oolitic beds form very consistent markers that occur 30 to 40 m below the Perdrix-Mount Hawk contact. They do not occur south of the Kakwa River area; individual beds increase in thickness from a few centimetres up to 15 cm in a northwesterly direction.

The upper part of the Perdrix Formation was penetrated by the Michigan Wisconsin LRI Torrens well (located in Lsd. 6-21-60-13W6) between depths 12 435 and 12 861 feet (3790.1 and 3920.0 m). In this well (Fig. 37.2, Sec. 4), the lithology is a greenish grey to dark greenish grey, slightly calcareous to calcareous, silty shale with interbeds of very silty limestone. According to the Continuous Dipmeter log, dips in the shale range from 10 to 80°, with more reliable measurements ranging from 14 to 50°. The boundary between the Perdrix and Mount Hawk formations in the borehole is transitional over an interval of about 20 feet (9.1 m). The stratigraphic thickness of the transitional interval is estimated to be about 13 feet (3.9 m).

Mount Hawk Formation

The Mount Hawk Formation was introduced by DeWit and McLaren (1950) and redefined by McLaren (1955). It overlies the Perdrix Formation with a transitional boundary and is overlain by the Sassenach Formation. Mountjoy (1980; Figure 4) shows the Mount Hawk as being laterally equivalent to, and partly overlain by, the upper part of the Peechee, Grotto, Arcs and Ronde members of the Southesk Formation. Thus, the upper boundary of the Mount Hawk Formation lies at different stratigraphic levels. In the mountains south and west of Grande Cache, Geldsetzer (1982) applied the name Mount Hawk Formation to a unit underlying the Simla Formation and composed of thin and nodular bedded, argillaceous limestone, medium- to thick-bedded fossiliferous limestone, and cryptalgal laminite. Geldsetzer's Mount Hawk Formation is equivalent to the upper argillaceous limestone of the Mount Hawk Formation of McLaren (1955). The interbedded calcareous shales and shaly limestones of the lower Mount Hawk at the type section change facies by a significant decrease of the limestone component adjacent to, and to the northwest of, the Ancient Wall carbonate complex. In that way, the lower part of the Mount Hawk Formation of McLaren (ibid.) loses its character as a mappable unit, and was thus added to the Perdrix Formation (Geldsetzer, 1982).

In the sections at Mount St. Andrews and Mount Hanington (see Fig. 37.2, secs. 1, 2), the Mount Hawk Formation consists of grey to dark grey, nodular bedded, fossiliferous limestone with minor shaly interbeds. The unit weathers moderately recessively, but locally includes some fairly resistant, very fossiliferous limestone beds. Fossils include solitary corals, gastropods, brachiopods, amphiporids and crinoidal debris (see Fig. 37.3c, d). The lower contact is exposed at Bastille Mountain (Fig. 37.1, Sec. 79-3); the upper contact, exposed at Mount Hanington, is transitional and is

---

Figure 37.2 *(opposite). Stratigraphic cross-section of Devonian succession in Kakwa River area. Section locations are:*

1. *Mount Saint Andrews, Section 79GCA1; 54°3'15"N, 120°9'40"W.*
2. *Mount Hanington, Section 79GCA4; 54°7'54"N, 120°12'16"W.*
3. *North of Mount Hanington, Section 79GCA5; 54°9'19"N, 120°12'30"W.*
4. *Michigan Wisconsin Torrens 6-21-60-13W6.*
5. *Seafort et al. Kakwa 2-20-61-7W6.*
6. *Pan Am et al. Kakwa 7-34-63-4W6.*
7. *R.O. Sinclair Karr 12-1-65-2W6.*
8. *Triad CDP Amerada Mer 10-4-65-26W5.*

LEGEND

limestone
dolostone
shale, calcareous
shale with limestone beds
shale, silty
shale, sandy
siltstone
sandstone
anhydritic
calcareous nodule
cherty
echinoderm debris
peloidal
F fossiliferous
stromatoporoidal biostrome
3 "Siltstone Marker"
2 Graminia equiv.
1 Nisku equiv.
c upper Ireton equiv.
b lower Ireton equiv.
a Duvernay equiv.

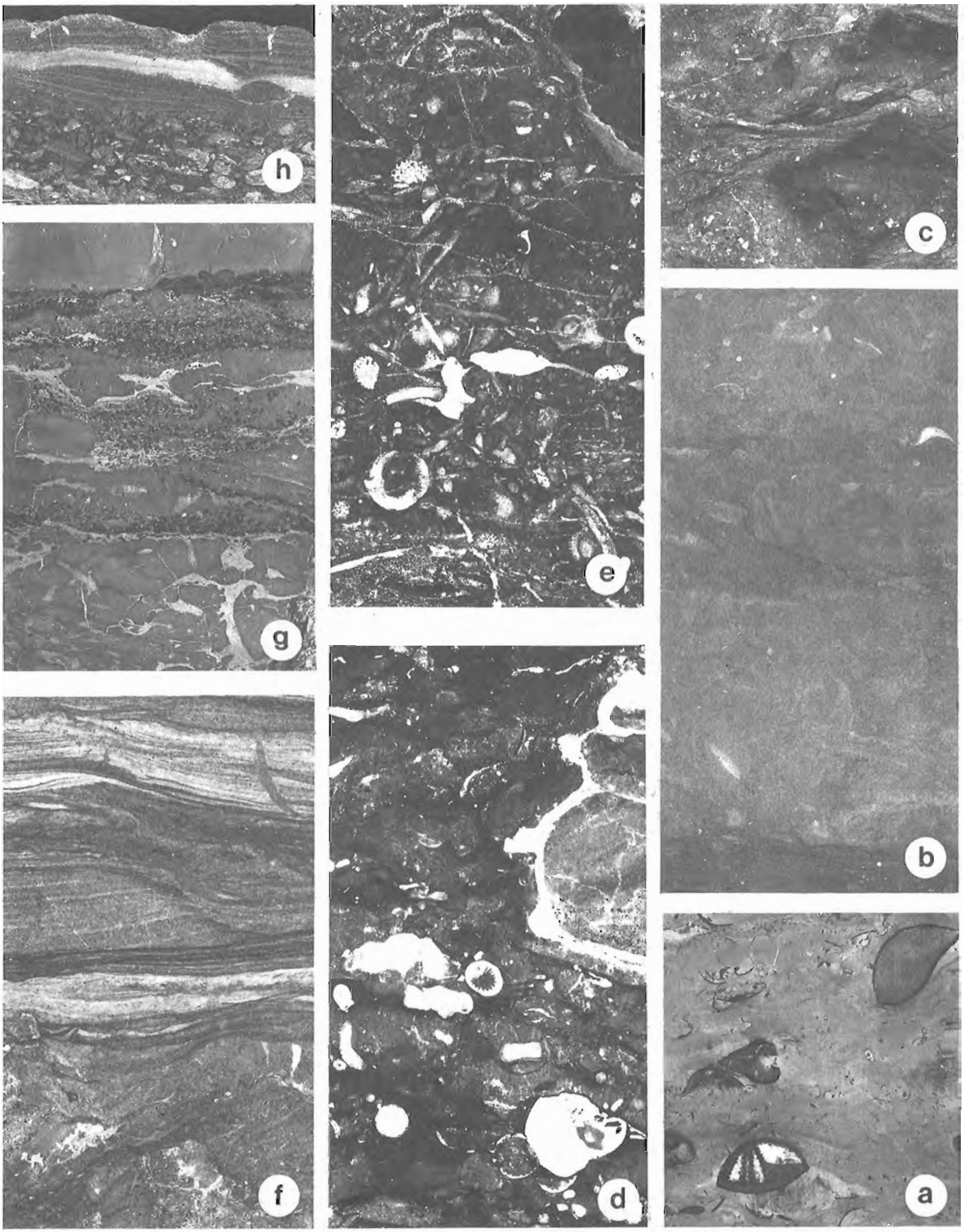
h
e
c
g
b
f
d
a

placed at the level where the colour of the exposures changes from dark grey to light grey and/or the first appearance of silicified stromatoporoids and other fossil debris.

In the Michigan Wisconsin LRI Torrens well (located in Lsd. 6-21-60-13W6; see Fig. 37.2, Sec. 4), the Mount Hawk Formation, in the sense of Geldsetzer (1982), is present between depths 12 075 and 12 435 feet (3680.4 and 3790.1 m). The lower part of this interval is composed of a light and dark grey mottled, micritic limestone, with scattered crinoidal debris and fragments of other, larger fossils. The middle part of this interval includes dark greyish brown micritic limestone, dark- to very dark-grey, argillaceous limestone and very dark grey shale. The upper part consists of mottled light and dark greyish brown, somewhat argillaceous, micritic and fine grained peloidal wackestone and packstone. The lower contact with the Perdrix Formation is transitional; the upper contact is also transitional and is selected at the base of light coloured, fossiliferous limestone.

Simla Formation

The term Simla Member was introduced by McLaren and Mountjoy (1962) and was applied to the upper part of the Southesk Formation in the area of the "Ancient Wall carbonate complex". It includes a lower unit, 12.4 m thick, composed of recessive weathering, argillaceous siltstone, and an upper unit, 67.3 m thick, composed of resistant limestone and dolostone. The upper unit includes, in the lower part, dolomitic limestone and dolostone beds with a distinctive fauna of corals and brachiopods; in the uppermost part, it includes thick bedded, cliff forming, medium to coarse, nonskeletal calcarenites with amphiporids. The entire upper resistant part forms a distinctive, light coloured unit in the Ancient Wall area.

The Simla Formation can be traced from the Ancient Wall area into the Monkman Pass area west of Grande Prairie. The contact with the overlying Palliser Formation is sharp but relatively easy to recognize, because it is based on a subtle lithological change from a light grey, amphiporid-bearing limestone below to a brownish grey pellet-intraclast limestone above. The lower contact with the Mount Hawk Formation is obvious as long as the basal recessive unit of reddish brown shales and siltstones is present. Unfortunately, this marker horizon is gradually lost to the northwest of Winnifred Pass (Fig. 37.1, Sec. 81-5). In the Kakwa River area the recessive basal unit thins to 4 m of grey, nodular, shaly limestone at Bastille Mountain (Fig. 37.1, Sec. 79-3), and it is absent at Mount Hanington (Fig. 37.2, Sec. 2).

The Simla Formation is remarkably consistent in thickness, normally ranging from 60 to 85 m; an anomalously thin section of only 30 m occurs at Belcourt Mountain (Fig. 37.1, Sec. 79-6).

At Mount Hanington (Fig. 37.2, Sec. 2), the Simla Formation forms a distinctive, light coloured band, 60 m thick. The lower part is a light grey, massive limestone containing corals and gastropod fossils; the upper part is composed of interbedded yellowish grey weathering dolostone and light grey, fossiliferous limestone. The fossils are commonly silicified.

In the Michigan Wisconsin LRI Torrens well (Fig. 37.2, Sec. 4), the Simla Formation is present between depths from 11 800 to 12 075 feet (3596.6 and 3682.4 m). Here, it includes three units. The lower unit is composed of light and dark greyish brown mottled, aphanitic or fine grained peloidal limestone, in places very finely recrystallized and containing crinoidal debris and macrofossils. The middle unit is a very light grey to grey, fine- to medium-crystalline dolostone with poor intercrystalline porosity. The upper unit consists of very light grey and greyish brown limestone with interbeds of dolostone: a partly dolomitized fine, or fine-to-medium peloidal grainstone. In the Torrens well, both the upper and lower boundaries of the Simla Formation are transitional, and the formation does not form a distinctive unit on borehole logs.

Palliser Formation

The term Palliser Formation was first used by Beach (1943) to describe the upper part of the Upper Devonian succession in the Rocky Mountains west of Calgary. The formation was traced northwestward into the Jasper area by DeWit and McLaren (1950), Sverson (1950) and Fox (1951). DeWit and McLaren (1950) redefined the base of the Palliser Formation above a unit composed of grey, greenish grey and reddish brown, well bedded and laminated, argillaceous siltstone and silty dolostone (the Sassenach Formation). The top of the Palliser Formation is distinct and is marked by the overlying shales of the Exshaw and Banff formations, which are dark coloured and weather very recessively.

In the northern part of Jasper National Park, the Sassenach Formation is locally thin or absent (McLaren and Mountjoy, 1962), and farther north, in the area west of Grande Cache, the Sassenach Formation is consistently absent. Here, the base of the Palliser is placed at the top of the Simla Formation (Geldsetzer, 1982). The top of the Palliser lies below the Exshaw Formation or, in places where the Exshaw Formation is absent, below the Banff Formation.

Figure 37.3 *(opposite). True-to-scale photographs of core and outcrop samples.*

a. Bioturbated calcareous and silty claystone with scattered crinoidal debris and brachiopods. B.A. Kakwa 6-15-64-4W6 well, 14 126 feet (4305.6 m); Beaverhill Lake.

b. Interbedded very argillaceous limestone and dark marl. Beds have bioturbated appearance and include crinoidal and shelly debris. Amoco et al. Nose 8-19-66-12W6 well, 16 888 feet (5147.5 m); Ireton.

c. Nodular bioturbated argillaceous limestone with crinoidal debris, Belcourt Mountain; Section 79GCA6; basal Mount Hawk.

d. Nodular, bedded limestone with corals, gastropods, digital stromatoporoids and crinoidal debris, Belcourt Mountain; Section 79GCA6; 23 m above the base of Mount Hawk.

e. In part vuggy dolostone with corals, bulbous and digital stromoporoids and crinoidal debris, Amoco Nose 8-19-66-12W6 well, 16 888 feet (5147.4 m); Mount Hawk.

f. Silty, finely peloidal limestone including shells of ostracodes and brachiopods, overlain by laminated and crosslaminated, sandy and peloidal limestone with scattered burrows. B.P. Baseline 10-25-65-27W5 well, 3382.3 m; Winterburn, unit 3.

g. Nodular, bedded, greyish brown limestone with irregular silt-filled cracks and burrows. Irregular layers consists of dark grey or reddish brown coated, medium- to coarse-peloids and mudstone pebbles. Belcourt Mountain; Section 79GCA6; basal Palliser.

h. Finely peloidal, silty limestone with dark or reddish brown coated pebbles overlain by laminated, very silty limestone and siltstone beds. Belcourt Mountain; Section 79GCA6; basal Palliser.

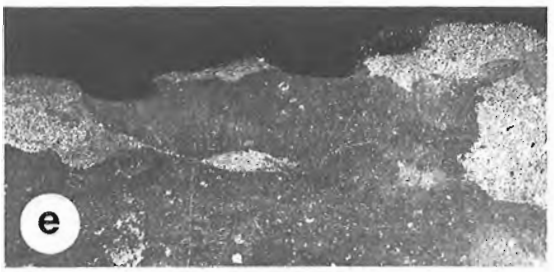
e

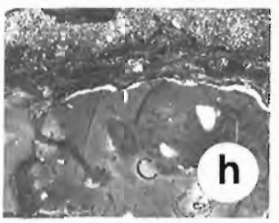
h

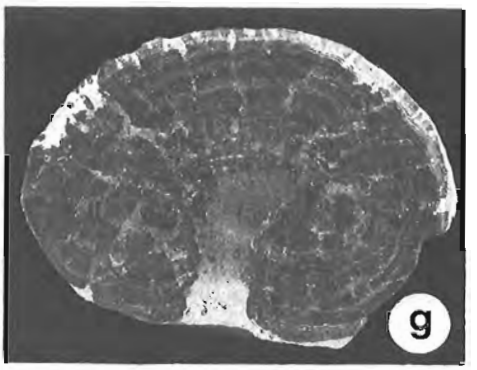
g

d

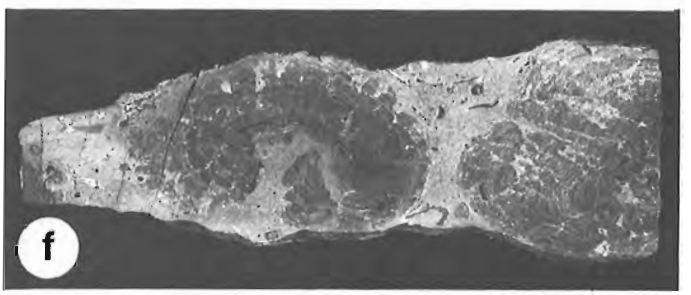
f

c

b

a

In the area west of Grande Cache, the Palliser Formation is a resistant unit composed of thick bedded, nodular, light greyish brown or greyish brown limestone. In most sections, the limestone is a mudstone or a fine grained peloidal wackestone, packstone or grainstone, containing scattered fragments of crinoids, ostracodes and brachiopods. The limestone is bioturbated and locally includes chert nodules, commonly in the form of silicified burrows.

In the sections at Mount Hanington (Fig. 37.2, Sec. 2) and Belcourt Mountain (Fig. 37.1, Sec. 79-6), the basal part of the Palliser Formation includes several reddish brown weathering, peloidal or micritic limestone beds that include thin, flat-pebble conglomerates and considerable quartz silt (see Fig. 37.3g, h). These reddish brown, silty beds are also present in the Michigan Wisconsin LRI Torrens well (Fig. 37.2, Sec. 4) and they may form a useful stratigraphic marker.

In the Mount Hanington, North Mount Hanington and Belcourt Mountain sections (see Fig. 37.1, secs. 2, 3 and 79-6), the Palliser Formation includes in its upper half a dark coloured, recessive unit of thin- and very thin-bedded micrite. The base of this dark interval was used to correlate the Mount Hanington and North Mount Hanington sections on Figure 37.2. Geldsetzer (1982) used it to subdivide the Palliser Formation into lower and upper members. One would assume that this unit is also a useful marker in the subsurface. The presence of two dark intervals in the anomalously thick borehole section of the Palliser Formation in the Michigan Wisconsin LRI Torrens well (Fig. 37.2, Sec. 4), may thus indicate a repetition in the succession due to a thrust fault. However, it is not clear where the thrust fault (or thrust faults) cut the section.

If one assumes that the borehole section in the Michigan Wisconsin LRI Torrens well is not complicated by faulting, the conclusion is that at this locality the Palliser Formation includes two dark intervals. Neither one seems to correlate with the dark coloured interval present in the surface sections.

In the North Mount Hanington section (Fig. 37.2, Sec. 3) the Palliser is sharply overlain by a recessive-weathering shale that resembles the Exshaw. Here, the uppermost Palliser beds include scattered brachiopods. In the sections at Planet Creek (Fig. 37.1, Sec. 81-7), and at Kvass Mountain (Fig. 37.1, Sec. 81-8), the Palliser limestone is sharply overlain by rusty weathering, sandy and silty beds of the Banff Formation (see Fig. 37.4d, h). Just below the upper contact the Palliser limestone includes sand filled burrows, and pyrite in the limestone is locally oxidized to hematite. The sand above the contact occurs in the form of horizontal burrows in the basal part of an argillaceous siltstone (see Fig. 37.3e). At Planet Creek the siltstone includes crinoidal debris, brachiopods and oncolites (see Fig. 37.3f, g).

In the Michigan Wisconsin LRI Torrens well, the Palliser is overlain by siltstone and sandstone beds that are probably part of the Banff Formation.

Figure 37.4 *(opposite). Photographs of exposures and true-to-scale outcrop and core samples.*

a. Nodular interbedded marl and finely peloidal limestone including shell fragments of brachiopods, gastropods and ostracodes, calcispheres and coated peloids. The oncolith contains a shell fragment. White patches are dolomite: BP Baseline 10-25-25-65-27W5 well, 3388.8 m; Winterburn, unit 2c.

b. Contact between Wabamun and Exshaw formations. Lower part of photo shows a very pyritic, nodular, finely fragmental limestone including much crinoidal debris. Overlying a sharp and irregular contact is a thin, very pyritic, fine- to medium-grained layer composed of siltstone granules, quartz grains and (?)phosphate grains in a matrix of dark shale. Upper part of photo is dark, noncalcareous, pyritic shale with scattered fine and medium quartz and chert grains. Home et al. Beaverlodge 4-23-72-10W6 well, 11 712 feet (3569.8 m).

c. Bedding surfaces in bioturbated nodular limestone, upper Palliser, Planet Creek, Section 81GCA7.

d. Pencil rests with flat end on contact between Palliser and Banff formations. Palliser is nodular limestone. Banff is calcareous sandstone grading upward into siltstone with scattered limestone oncoliths. Planet Creek, section 81GCA7.

e. Detail of contact in "d". Limestone is crinoidal wackestone with calcareous sand filled burrows. Some flattened, horizontal burrows are located at the contact.

f, g. Detail of limestone oncoliths of "d" in matrix of fossiliferous siltstone. Two oncoliths include a brachiopod shell in their central parts.

h. Detail of contact similar to the one shown in "e". A lime-mudstone with gastropod shell fragments is overlain by an 80 cm thick bed of calcareous sandstone composed of crinoidal debris, dark limestone pebbles and silicified concretions. Kvass Fire Lookout; Section 81GCA8.

Interior Plains

The subdivision of the Upper Devonian succession in the subsurface of the Interior Plains in the Edmonton area was introduced by the geological staff of Imperial Oil Ltd. (1950). The subdivision is based on differences in lithology, and originally included four lithostratigraphic units. They are, in ascending order: the Beaverhill Lake, Woodbend and Winterburn groups and the Wabamun Formation. For each of the four units, cored type sections were selected for future reference. In the type sections members were named and described. This subdivision was accepted by the petroleum industry in Alberta and is still being used with some minor alterations. Some groups are now regarded as formations and some members as formations (see Belyea, 1964). Several new map units of member and formational rank were introduced in the area west of Edmonton.

In the following description, the groups and formations will be described in ascending order.

Beaverhill Lake Group

In central Alberta, the Beaverhill Lake Group includes the Fort Vermilion, Slave Point, Waterways and Swan Hills formations.

The Fort Vermilion Formation is the basal unit of the group. It consists of thinly interbedded anhydrites and carbonates with minor amounts of shale, and reaches a thickness of about 12 m in the northern part of the Swan Hills area. It grades north and westward into the basal Devonian, clastic sediments that overlie the Peace River Arch and Western Alberta Ridge (Leavitt and Fischbuch, 1968; Jansa and Fischbuch, 1974). In some areas, the Fort Vermilion Formation is so thin that it is regarded as a member of the overlying Slave Point Formation, and eastward at the fifth meridian, it is shown to wedge out below carbonates of the Slave Point Formation (Hemphill et al., 1970). The contact with the underlying sandy and shaly beds of the Elk Point Group is transitional.

On the crests of paleotopographic highs the Slave Point Formation overlies the basal Devonian clastics with a transitional boundary. The Slave Point Formation consists of carbonates and ranges in thickness from 3 to 38 m. It contains a sparse fauna that is generally thought to represent the late Givetian.

The Slave Point Formation is overlain by the Waterways Formation, a unit composed of interbedded limestone, argillaceous limestone and shale. The Waterways Formation is fossiliferous, and includes an early Frasnian fauna of brachiopods, ostracodes and conodonts (McLaren, 1962; Norris, 1963; McGill, 1963; Uyeno, 1974; Norris and Uyeno, 1981). According to a 1982 resolution of the Devonian Subcommission, the Givetian-Frasnian boundary would fall into the Calumet Member of the Waterways Formation (A.W. Norris, personal communication). The thickness of the formation ranges from 9 to 152 m.

In central Alberta, the Slave Point and the lower part of the Waterways Formation change laterally into the Swan Hills Formation, a stromatoporoidal limestone or dolostone of highly variable thickness that forms large, flat-topped, biohermal and biostromal mounds (Fong, 1960; Murray, 1965; Fischbuch, 1968; Leavitt, 1968; Jenik and Lerbekmo, 1968; Jansa and Fischbuch, 1974). These biohermal and biostromal mounds form the reservoir rock in the Swan Hills, Virginia Hills, Carson Creek, Judy Creek, Snipe Lake, Goose River, Ante Creek and Kaybob oil pools, (see Wallace-Dudley, 1981). The thickness ranges from 15 to 152 m.

In the subsurface of west-central Alberta, the lack of biostratigraphic control does not allow for the subdivision of the Beaverhill Lake Group into formations. When compared with the equivalent section in central Alberta, the rocks are generally darker coloured and the succession is relatively thin (less than 90 m). The Beaverhill Lake Group overlies a regional paleotopographic high, the Western Alberta Ridge, and the Fort Vermilion Formation is absent. The probable equivalent of the Slave Point Formation overlies an interbedded shale and sandstone unit, which is commonly referred to as the Gilwood Sandstone. The upper part of the Beaverhill Lake Group is a succession of fossiliferous limestone and thinly interbedded argillaceous limestone and calcareous shale with crinoidal debris and brachiopods (see Fig. 37.3a). The boundary with the overlying Woodbend Group is selected at the contact between dark bituminous shale (above) and greyish brown, fragmental or micritic limestone (below). This boundary is a distinct marker on borehole logs (see Fig. 37.2, Sec. 5-8).

Woodbend Group

In central Alberta, the Woodbend Group includes a basal carbonate unit, the Cooking Lake Formation. The Cooking Lake Formation is overlain either by a carbonate facies or a shale facies. The carbonate facies is named the Leduc Formation and it consists of fossiliferous, biohermal, biostromal or biofragmental limestone or dolostone. In many sections, the carbonate facies of the Swan Hills Formation grades upward into the Leduc Formation without the presence of the Waterways Formation. Examples of such sections are present in the Gold Creek, Sturgeon Lake, Marlboro, Obed and Bigstone oil pools. In these sections, it is difficult or impossible to define the base of the Leduc Formation.

The shale facies includes, in ascending order: the Duvernay and Ireton formations. The Duvernay Formation is a dark coloured, very bituminous, somewhat argillaceous limestone that is laterally equivalent to the lower part of the Leduc Formation. The Ireton Formation is a greenish grey, calcareous or dolomitic shale with scattered interbeds of silty and argillaceous limestone or dolostone. The lower part of the Duvernay abuts the upper part of the Leduc Formation and the upper part of the Ireton overlies the Leduc Formation. However, there are sections in the Sturgeon Lake oilfield and in the area southwest of Simonette oilfield where the Ireton Formation is absent. Here, the carbonates of the Leduc Formation are transitionally overlain by carbonates of the lower Winterburn Group.

In the area west of Edmonton, the Cooking Lake and the overlying Leduc Formation are absent. Dark shales similar to the Duvernay Formation directly overlie the Beaverhill Lake Group and are overlain by the Ireton Formation (see Stoakes, 1980, Fig. 4; Leavitt and Fischbuch, 1968, figs. 3 and 4; Fischbuch, 1968). These dark shales show up as a prominent radioactive unit on the gamma ray logs, and have been traced westward as Unit a of the Woodbend Group (see Fig. 37.2, Sec. 5-8). This radioactive unit is about 33 m thick and includes in cuttings very dark grey, pyritic shale, minor calcareous siltstone and, in the lower part, a subunit of greyish brown, very argillaceous limestone. This limestone subunit appears to thin out to a zero edge in a westward direction (Fig 37.2). The upper shale subunit is overlain with a fairly sharp contact by the Ireton Formation (Fig. 37.2, Woodbend Group, units b and c).

In the subsurface near Grande Cache, the Ireton is a thick, interbedded succession of dark greenish grey, calcareous to very calcareous shale; dark grey, fissile shale; and minor greyish brown, argillaceous limestone. It ranges in thickness from 102 to 275 m and can be subdivided into two parts (units b and c on Fig. 37.2). The upper contact of the Ireton with the argillaceous limestone or limestone of the Winterburn Group is transitional.

Winterburn Group

In the area south of Edmonton, the Winterburn includes, in ascending order: the Nisku, Calmar and Graminia formations (Geological Staff, Imperial Oil, 1950). After the discovery of oil in the Graminia and Nisku formations, these formations were further subdivided into members by Choquette (1955) and the Exploration Staff of Chevron Standard Ltd. (1979). A transitional contact separates the Winterburn Group from the underlying Ireton Formation: the base of the Winterburn was selected at the boundary between greyish brown dolostone (above) and greenish grey, argillaceous dolostone or dolomitic shale (below). The Nisku Formation consists of fossiliferous dolostone or limestone, dolomitic siltstone, argillaceous siltstone, calcareous silty shale and silty limestone. The Calmar Formation is a red and green mottled, dolomitic, in part anhydritic siltstone. The Graminia Formation is a silty and anhydritic dolostone or anhydrite, which grades upwards into a greenish grey, dolomitic siltstone bed. This siltstone bed forms a prominent marker and is between 3 and 4 m thick. The boundary between the Winterburn Group and the Wabamun Formation was selected as the top of this siltstone bed.

When one traces the Winterburn Group westward from central to west-central Alberta, the Calmar Formation becomes an argillaceous carbonate and cannot be mapped as a separate unit in the area southwest of Sturgeon Lake (Sec. 5-8, Fig. 37.2). Another facies change affects the lower part of the Nisku Formation. The interbedded succession of carbonates and argillaceous carbonates in the lower part of the Nisku Formation changes westward into a calcareous shale facies similar to that of the Ireton Formation. This facies change is schematically shown between sections 6 and 7 on Figure 37.2. An identical facies change occurs in the lower part of the Mount Hawk Formation when traced northwestward from its type section. This change prompted Geldsetzer (1982) to include the lower Mount Hawk Formation in the Perdrix Formation. A third facies change

occurs in the area west of the sixth meridian. The anhydritic carbonates in the Graminia Formation, the upper part of the Winterburn Group, change westward into carbonates, and the siltstone bed at the top ceases to be a mappable unit (see Fig. 37.2, Sec. 5, 6). A similar facies change within the Graminia Formation was discussed by Choquette (1955). South of Lesser Slave Lake and west of the fifth meridian a silty and anhydritic Graminia changes northwestward into a massive dolostone with silty beds. Choquette (ibid.) named this massive carbonate the Blue Ridge Member.

The facies changes are well documented in sections 5 to 8 in Figure 37.2. In Section 8 the Winterburn Group includes three distinct units: a lower unit consisting of argillaceous and nonargillaceous, bioclastic carbonates correlating with the Nisku Formation; a middle unit composed of anhydrite, and anhydritic, commonly peloidal carbonates representing the bulk of the Graminia Formation; and a thin upper unit composed of calcareous siltstone or dark grey shale, the "siltstone marker" in the upper part of the Graminia Formation. In Section 7, the Winterburn Group has been subdivided into informal units 1, 2a, 2b, 2c and 3. Unit 1, the Nisku equivalent, remains unchanged, whereas the Graminia equivalent changes considerably. The anhydritic carbonates (Unit 2a) are overlain by a green and reddish brown mottled, pyritic and silty shale or siltstone unit (Unit 2b), which is in turn overlain by an interbedded unit of laminated, very silty limestone, fossiliferous and peloidal limestone, and dark grey calcareous shale (Unit 2c, Fig. 37.4a). This interbedded unit is overlain by the "siltstone marker" (Unit 3, Fig. 37.3f). In sections 5 and 6 the Nisku equivalent (Unit 1) has largely graded westward into the upper part of the Ireton Formation (Woodbend unit c). Most of the Graminia equivalent (units 2a, b, c) changes into a bioclastic dolostone in Section 6 and into a fossiliferous, micritic limestone, with minor amounts of quartz silt and clay, in Section 5. The upper "siltstone marker" (Unit 3) changes southwestward into an interbedded succession of peloidal limestone, argillaceous limestone and siltstone and can no longer be identified in sections 4 or 5.

Wabamun Formation

The Wabamun Formation was not subdivided into smaller units by the Geological Staff of Imperial Oil (1950). In the type section, located southwest of Edmonton, the formation consists of interbedded limestone and dolostone. In the area south of Edmonton, the lower part of the formation includes anhydrite interbeds and the upper part is mainly a dolostone. The contact between the Wabamun Formation and the underlying siltstone marker of the Graminia Formation is relatively sharp. The Wabamun is overlain by the Exshaw Formation, in which case the contact is sharp, or is erosionally overlain by Cretaceous strata.

The formation can be traced westward into the study area with little change in lithology. In west-central Alberta, it is a greyish brown limestone, in part dolomitized or including dolostone interbeds. The limestone includes micritic mudstone and fine-to medium-peloidal wackestone, packstone and grainstones. It has a nodular appearance and is poorly bedded, and commonly includes crinoidal debris, brachiopods and Famennian ostracodes (Lethiers, 1981). In the area where the siltstone marker at the top of the Winterburn Formation is present, it is easy to establish the base of the formation. In the region just east of the Foothills Belt, the "siltstone marker" is absent and there is no log indicator between the Wabamun and Winterburn equivalents (see Fig. 37.2, Sec. 5).

The top of the Wabamun Formation forms a distinct marker below the dark shales of the Exshaw Formation (see Fig. 37.2, 37.4b).

Correlation between Cordilleran and Plains stratigraphy

There have been numerous attempts to correlate the Devonian of the surface and the subsurface. Virtually all of them were based on lithostratigraphic data. One of the more recent correlation charts for west-central Alberta is illustrated in Geldsetzer et al. (1982, Fig. 5). All lithostratigraphic correlations suffer from the same handicap – a lack of sufficient well control in the Foothills Belt and, if such wells are available, faults and folds that render them unreliable.

Excellent exposures in the Rocky Mountains Thrust Belt more than offset the stratigraphic fragmentation in that area by the thrust faults, and a good lithostratigraphic framework has been established. Problems do exist (Mountjoy, 1980), and the recognition of several unconformity-bounded sequences (Workum, 1983) has added another degree of complexity to the Devonian story.

The Devonian stratigraphic framework is equally well established in the Interior Platform. The major subdivisions of the Beaverhill Lake, Woodbend, Winterburn and Wabamun can easily be traced to the Foothills Belt of west-central Alberta. However, geophysical logs have their limitations and are subject to ambiguous interpretations when smaller stratigraphic units, such as formations or members, are traced. The interpretation of erosional truncation, depositional thinning, or facies change is not always easy in surface geology and even less so in the subsurface.

The sections selected for this report are reasonably spaced and allow a good correlation of the Cordilleran and Plains' frameworks.

The Flume Formation correlates well with the Beaverhill Lake Group. The Flume of the Kakwa River area contains faunal assemblages found in the Waterways Formation, but Slave Point equivalent sediments wedge out eastward against the West Alberta Ridge and last occur at Mount Buchanan (Fig. 37.1, Sec. 81-2). A similar, probably westward, thinning of the Slave Point against the same ridge has not yet been documented in the subsurface of west-central Alberta.

The Maligne Formation appears to correlate with the lower argillaceous limestone of the radioactive Unit a, the Duvernay equivalent of the Woodbend Group, whereas the upper, dark, pyritic shales of Unit a are probably represented by the basal part of the Perdrix Formation.

It has been shown that both the Perdrix and the Ireton formations expand upsection in a westerly direction at the expense of the Mount Hawk and Nisku formations respectively. Both cases are caused by a substantial reduction of the carbonate component in the lower parts of the overlying units.

The Mount Hawk Formation of the Kakwa River area is a distinct carbonate unit and is most likely equivalent to Unit 1, the Nisku equivalent of the Winterburn Group. The difficulty of recognizing the upper contacts is again the result of a regional westerly trend. In the mountains, it is caused by the northwesterly disappearance of the recessive siltstones at the base of the overlying Simla Formation, between Winnifred Pass (Fig. 37.1, Sec. 81-5) and the Kakwa River area; in the subsurface, it is the westerly wedging out of the silty Calmar Formation east of the sixth meridian. Whereas in the mountains a change in colour and subtle lithological differences make it possible to trace the upper contact of the Mount Hawk Formation, there is no log expression for the upper Nisku contact in the subsurface west of the sixth meridian.

It has been argued that the base of the Calmar Formation represents an unconformity (Workum, 1983). Minor brecciation, silicification and iron oxidation occur at the top of the Mount Hawk Formation in some mountain sections, and below the recessive siltstones at the base of the Simla Formation. These features support the presence of an unconformity. The absence of the Calmar between the sixth meridian and the Kakwa River area may simply be due to a gentle topographic high, which was not onlapped by the initial clastic sediments of the Calmar-Graminia sequence (Sequence D of Workum, 1983).

The Simla Formation forms a very resistant and massive light coloured band in the mountains and appears to correlate well with the massive carbonate unit which grades eastward into units 2a, b, and c, of the Graminia Formation.

The Palliser and Wabamun formations are obvious correlatives. The lack of a log expression makes it difficult to identify the basal contact in subsurface sections 4 and 5. The contact is quite evident farther east where the "siltstone marker" appears at the top of the Graminia Formation. If this "siltstone marker" can be shown to contain Famennian fossils it would be a Sassenach equivalent and could be regarded as a basal clastic unit of the Wabamun depositional episode.

It is clear that more precise correlations between the Cordilleran and Plains' successions depend upon biostratigraphic data. Only then will it be possible to accurately document basin-filling events, unconformities and carbonate platform development. Biostratigraphic control is also needed to document the "progradational model" applied to the Upper Devonian succession in the Interior platform (Oliver and Cowper, 1963; Stoakes, 1980; Cutler, 1983). How far west can this progradational model be applied?

The main thrust of the second phase of this surface-subsurface correlation project will be to superimpose a biostratigraphic zonation on the lithostratigraphic frameworks.

References

Beach, H.H.
1943: Moose Mountain and Morley map-areas, Alberta; Geological Survey of Canada, Memoir 236.

Belyea, H.R.
1964: Upper Devonian, Chapter 6, part 2; in Geological History of Western Canada, ed. R.G. McCrossan and R.P. Glaister; Alberta Society of Petroleum Geologists, Calgary, Alberta.

Choquette, A.L.
1955: The Blue Ridge member of the Graminia Formation; Journal of the Alberta Society of Petroleum Geologists, v. 3, p. 70-73.

Cutler, W.G.
1983: Stratigraphy and sedimentology of the Upper Devonian Grosmount Formation, northern Alberta; Bulletin of Canadian Petroleum Geology, v. 31, p. 282-325.

DeWit, R. and McLaren, D.J.
1950: Devonian sections in the Rocky Mountains between Crowsnest Pass and Jasper, Alberta; Geological Survey of Canada, Paper 50-23.

Exploration Staff, Chevron Standard Ltd.
1979 The geology, geophysics and significance of the Nisku reef discoveries, west Pembina area, Alberta, Canada; Bulletin of Canadian Petroleum Geology, v. 27, p. 326-359.

Fischbuch, N.R.
1968: Stratigraphy, Devonian Swan Hills reef complexes of central Alberta; Bulletin of Canadian Petroleum Geology, v. 16, p. 446-587.

Fong, G.
1960: Geology of Devonian Beaverhill Lake Formation, Swan Hills area; Bulletin of the American Association of Petroleum Geologists, v. 44, p. 159-209.

Fox, F.G.
1951: Devonian stratigraphy of Rocky Mountains and Foothills between Crowsnest Pass and Athabasca River, Alberta, Canada; Bulletin of the American Association of Petroleum Geologists, v. 35, p. 822-843.

Geldsetzer, H.H.J.
1982: Depositional history of the Devonian succession in the Rocky Mountains southwest of the Peace River Arch; in Current Research, Part C, Geological Survey of Canada, Paper 82-1C, p. 54-64.

Geldsetzer, H.H.J., Mountjoy, E.W., Tebbutt, G.E., and Burrows, O.G.
1982: Upper Devonian stratigraphy and sedimentology, southern Alberta Rocky Mountains; International Association of Sedimentologists, Eleventh International Congress on Sedimentology, McMaster University, Hamilton, Ontario, Canada, Field Excursion Guidebook 28.

Geological Staff, Imperial Oil Ltd.
1950: Devonian nomenclature in Edmonton area; Bulletin of the American Association of Petroleum Geologists, v. 34, p. 1807-1825.

Hemphill, C.R., Smith, R.I., and Szabo, F.
1970: Geology of Beaverhill Lake reefs, Swan Hills area, Alberta; in Geology of giant petroleum fields; American Association of Petroleum Geologists, Memoir No. 14, p. 50-90.

Jansa, L.F. and Fischbuch, N.R.
1974: Evolution of a Middle and Upper Devonian sequence from a clastic coastal plain – deltaic complex into overlying carbonate reef complexes and banks, Sturgeon-Mitsue area, Alberta; Geological Survey of Canada, Bulletin 234.

Jenik, A.J.. and Lerbekmo, J.F.
1968: Facies and geometry of Swan Hills Reef member of Beaverhill Lake Formation (Upper Devonian), Goose River Field, Alberta, Canada; Bulletin of the American Association of Petroleum Geologists, v. 52, p. 21-56.

Leavitt, E.M.
1968: Petrology, palaeontology, Carson Creek North reef complex, Alberta; Bulletin of Canadian Petroleum Geology, v. 16, p. 298-413.

Leavitt, E.M. and Fischbuch, N.R.
1968: Devonian nomenclatural changes, Swan Hills area, Alberta, Canada; Bulletin of Canadian Petroleum Geology, v. 16, p. 288-297.

Lethiers, F.
1981: Ostracodes du Devonien terminal de l'ouest du Canada: Systématique, biostratigraphie et paléoécologie; Geobios, mémoire spécial 5, édition de l'Université Claude Bernard, Lyon.

McGill, P.
1963: Upper and Middle Devonian ostracodes from the Beaverhill Lake Formation, Alberta, Canada; Bulletin of Canadian Petroleum Geology, v. 11, p. 1-26.

McLaren, D.J.
1955: Devonian formations in the Alberta Rocky Mountains between Bow and Athabasca Rivers; Geological Survey of Canada, Bulletin 35.

McLaren, D.J.
1962: Middle and Early Upper Devonian Rhynchonellid brachiopods from western Canada; Geological Survey of Canada, Bulletin 86.

McLaren, D.J. and Mountjoy, E.W.
1962: Alexo equivalents in the Jasper region, Alberta; Geological Survey of Canada, Paper 62-23.

Mountjoy, E.W.
1965: Stratigraphy of the Devonian Miette Reef Complex and associated strata, eastern Jasper National Park, Alberta; Geological Survey of Canada, Bulletin 110.

1980: Some questions about the development of Upper Devonian carbonate buildups (reefs), Western Canada; Bulletin of Canadian Petroleum Geology, v. 28, p. 315-344.

Mountjoy, E.W. and Geldsetzer, H.H.J.
1981: Devonian stratigraphy and sedimentation, southern Rocky Mountains; in Field guide to geology and mineral deposits: Calgary '81 annual meeting, ed. R.I. Thompson, D.G. Cook [Calgary?]: GAC; Mineralogical Association of Canada; Canadian Geophysical Union, [1981], p. 195-224.

Mountjoy, E.W. and Mackenzie, W.S.
1973: Stratigraphy of the southern part of the Devonian Ancient Wall Carbonate Complex, Jasper National Park, Alberta; Geological Survey of Canada, Paper 72-20.

Murray, J.W.
1965: Stratigraphy and carbonate petrology of the Waterways Formation, Judy Creek, Alberta, Canada; Bulletin of Canadian Petroleum Geology, v. 13, p. 303-326.

Norris, A.W.
1963: Devonian stratigraphy of northeastern Alberta and northwestern Saskatchewan; Geological Survey of Canada, Memoir 313.

Norris, A.W. and Uyeno, T.T.
1981: Stratigraphy and paleontology of the lowermost Upper Devonian Slave Point Formation on Lake Claire and the lower Upper Devonian Waterways Formation on Birch River, northeastern Alberta; Geological Survey of Canada, Bulletin 334.

Oliver, T.A. and Cowper, N.W.
1963: Depositional environments of the Ireton Formation, central Alberta; Bulletin of Canadian Petroleum Geology, v. 11, p. 183-202.

Price, R.A., Stott, D.F., Cambell, R.B., Mountjoy, E.W., and Ollerenshaw, N.C.
1977: Athabasca River Sheet 83; Geological Survey of Canada, Geological Atlas scale 1:1 000 000, Map 1339A.

Raymond, P.E.
1930: The Paleozoic Formations in Jasper Park, Alberta; American Journal of Science, 5th Ser., v. 20.

Sverson, J.L.
1950: Devonian stratigraphy, Sunwapta Pass area, Alberta, Canada; Bulletin of the American Association of Petroleum Geologists, v. 34, p. 1826-1849.

Stoakes, F.A.
1980: Nature and control of shale basin fill and its effect on reef growth and termination: Upper Devonian Duvernay and Ireton Formations of Alberta, Canada; Bulletin of Canadian Petroleum Geology, v. 28, p. 345-410.

Taylor, P.W.
1957: Revision of Devonian nomenclature in the Rocky Mountains; Journal of the Alberta Society of Petroleum Geologists, v. 5, p. 183-195.

Tipper, H.W., Campbell, R.B., Taylor, G.C., and Stott, D.F.
1979: Parsnip River Sheet 93; Geological Survey of Canada, Geological Atlas, scale 1:1000,000 Map 1424A.

Uyeno, T.T.
1974: Conodonts of the Waterways Formation (Upper Devonian) of northeastern and central Alberta; Geological Survey of Canada, Bulletin 232.

Wallace-Dudley, K.E.
1981: Oil Pools of Western Canada; Geological Survey of Canada, Map 1559A.

Workum, R.H.
1983: Patterns within the Devonian of the Alberta Rocky Mountains as analogs to the subsurface; Canadian Society of Petroleum Geologists, short course, Calgary, Alberta.

NOTE ON OPTIMAL COMPOSITE SAMPLE SIZE SELECTION

Projects 750094 and 790004

C.F. Chung [1] and Robert G. Garrett [2]

Chung, C.F. and Garrett, R.G., Note on optimal composite sample size selection; in Current Research, Part B, Geological Survey of Canada, Paper 84-1B, p. 351-354, 1984.

Abstract

Statistical models are developed to describe the distribution of composite sample data. The effects of forming composite samples by diluting a single geochemically anomalous or mineralized sample unit with background or barren units of similar size is studied for both the independent and autocorrelated situations.

Résumé

On élabore des modèles statistiques décrivant la répartition de données d'échantillons composés. On étudie les effets de la formation d'échantillons composés par dilution d'un seul échantillon minéralisé ou comportant une anomalie géochimique avec des échantillons de référence ou stériles de même taille dans des situations indépendantes et dans des situations autocorrélées.

Introduction

In some geological surveys involving physical sampling it is possible to collect far more material than it is feasible to study. For example, in overburden and soil geochemical surveys involving surface sampling by hand, rather than overburden drilling, it is relatively inexpensive to collect material at 10 or 20 m intervals rather than at 30 m intervals. The cost controlling factors are those involved in getting the sampler to the survey area which is to be traversed, the incremental cost of collecting additional material is small. Similarly, continuous sampling or recovery is usually possible in drilling programs. A question of concern is, how long should the sections submitted for analysis or assay be? Presumeably some multiple of a measurement unit, but 1, 2, 3 or how many metres long? Clearly geological and other considerations influence decisions on sample density in surveys, and section lengths in drilling programs. However, one common objective is to obtain maximum relevant information at minimum cost. If samples can be composited, or longer sections submitted for analysis, and the features sought still be recognized this is to advantage in reducing overall costs.

In this note we investigate the effects of increasing the size of composite samples by diluting a single geochemically anomalous or mineralized sample unit with background or barren units of similar size. In instances where physical samples are collected from close to one another, or adjacently, one cannot ignore the effects of spatial correlation. It is well established that in many instances measured properties in adjacent samples are correlated. As the distance increases between samples this correlation decreases until one reaches a distance beyond which the properties are essentially uncorrelated, and the variations in the data may be considered random and independent.

Specifically we develop a model for drill hole samples where sampling units are adjacent, rather than at discrete intervals along a traverse. However, the results may be extrapolated to the traverse situation with generality, and it may be that in some instances where the discrete sample sites are sufficiently separated the effects of spatial correlation may be ignored.

Model

Data are perceived to represent discrete segments drawn from either a background population, X, or an anomalous population, Y, both with known, but different, distribution functions. However, which segment is from which population is unknown, and the individual segments are simply considered as random variables, Z_i, with known distribution functions. In order to simplify the problem from a statistical point of view, the distributions of background, X, and anomalous, Y, data are assumed to be normal, or can be transformed to normality through an appropriate transformation, e.g., logarithmic.

A composite sample, C_n, composed of n discrete segments along a line, see Figure 1, is defined as:

$$C_n = \frac{1}{n} \sum_{i=1}^{n} Z_i \qquad (1)$$

In this note such a composite will be referred to as a composite of size n in a discrete model where the Z_i represents either a background segment, X_i, or an anomalous segment, Y_i.

Let $C_{n,m}$ denote a composite sample of size n with n-m background, X_i, segments and m anomalous, Y_i, segments at locations j1, . . . ,jm as shown in Figure 2. Then for the composite of size n we have:

$$C_{n,m} = \frac{1}{n} \left(\sum_{i=1}^{n-m} X_i + \sum_{j=1}^{m} Y_j \right) \qquad (2)$$

[1] Economic Geology and Mineralogy Division
[2] Resource Geophysics and Geochemistry Division

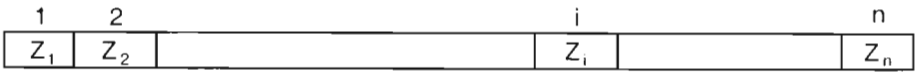

Figure 1

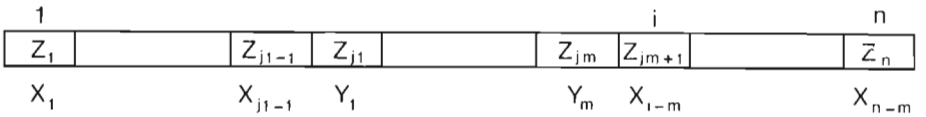

Figure 2

If the distribution functions of X and Y are known, then by comparing $C_{n,o}$ with $C_{n,m}$ ($m \neq 0$) we can distinguish between composites drawn from only the background populations ($m = 0$) and composites containing one or more anomalous segments ($m \geq 1$).

Model development continues along two paths beyond this point. Firstly, the special case of spatial independence of samples in the composite is addressed, then secondly, the more general case of some stated spatial dependence, i.e., correlation, is studied.

Spatial Independence

The background and anomalous populations are both assumed to be independently, identically distributed (iid) normal random variables. The means and variances of these two populations are respectively a, b^2 and c, d^2. Thus we have:

$$X \sim N(a, b^2), \text{ and}$$
$$Y \sim N(c, d^2) \tag{3}$$

Consider a composite of size n containing n-m discrete segments drawn from the background population X, and m discrete segments drawn from the anomalous population Y. The composite sample $C_{n,m}$ is drawn from a normal distribution with mean, e, and variance, f^2, assuming that X and Y are in fact independent:

$$C_{n,m} \sim N(e, f^2)$$

where:

$$e = ((n-m)a + mc)/n, \text{ and} \tag{4}$$
$$f^2 = ((n-m)b^2 + md^2)/n^2$$

Since the exact distribution of $C_{n,m}$ is known, all the probabilities related to the composite sample $C_{n,m}$ may be computed by specifying the necessary parameters.

For example, for a given threshold level, t, the probability that the composite sample $C_{n,m}$ is lower in content than t is given by:

$$P(C_{n,m} < t) = \Phi((t-e)/f) \tag{5}$$

where:

$$\Phi(x) = \frac{1}{\sqrt{2\pi}} \int_{-\infty}^{x} \exp(-0.5y^2)\,dy \tag{6}$$

is the cumulative normal distribution function whose values may easily be computed (Abramowitz and Stegun, 1970; IMSL, 1982).

Similarly, the probability that the composite sample $C_{n,m}$ containing no anomalous segments drawn from population Y, i.e., $m = 0$, is greater than t is obtained from:

$$P(C_{n,o} > t) = 1 - \Phi\left(\frac{\sqrt{n}(t-a)}{b}\right) \tag{7}$$

where Φ is as defined in equation (6)

Inversely, given some probability level p_o that the composite is greater than the threshold level t, i.e., p_o is the probability that the composite containing m anomalous segments is greater than t, the optimal composite size n can be obtained by solving the equation:

$$\frac{nt - (n-m)a - mc}{((n-m)b^2 + md^2)^{1/2}} = \Phi^{-1}(1-p_o) \tag{8}$$

If we let $\delta_o = \Phi^{-1}(1 - p_o)$ we have:

$$(t-a)^2 n^2 - \delta_o^2 b^2 n + 2m(t-a)(a-c) + \delta_o^2 mb^2 - \delta_o^2 md^2 + m^2(a-c)^2 = 0 \tag{9}$$

Similarly, comparing the distribution functions $C_{n,m}$ and $C_{n,o}$ in (4), we can look at several different combinations of the problem, which can then be solved as has been done in Garrett and Sinding-Larsen (in press).

Spatial Dependence

As discussed in the Introduction it is not reasonable to assume spatial independence when the separate samples being composited are close or adjacent to each other. Let us suppose that individuals drawn from the background population, X, are identically distributed normal variates, but are not independent. A set of such individuals is shown in Figure 3. Suppose that the correlation between two adjacent background samples X_i and X_{i+1}, regardless of the position of i is q, i.e.;

$$\text{Cov}(X_i X_{i+1}) = qb^2 \tag{10}$$

where a and b are as defined in (1). Then, under the Markovian assumption, the correlation between X_i and X_{i+h}, as illustrated in Figure 3 is simply q^h:

$$\text{Cov}(X_i X_{i+h}) = q^h b^2 \tag{11}$$

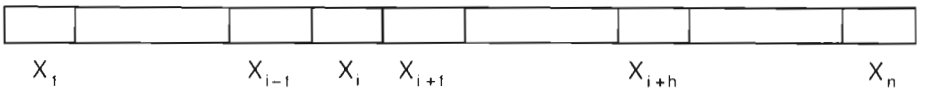

Figure 3

As the size of X_i becomes smaller, the correlation q will monotonically increase towards 1. On the other hand, as the size of X_i becomes larger, q will monotonically decrease to 0. In other words, q is a function of the size of the segment. When q = 0 the problem will be identical to that presented in the previous section, i.e., spatial independence.

As assumed in the previous section the background, X, and anomalous, Y, populations are assumed to be independent of each other. The implication is that we accept that at a detailed scale the anomalous samples are not related to the background. This is not a serious constraint as it is commonly accepted that the processes leading to the formation of mineral deposits are locally independent of those forming their hosts, except in the case of certain areally extensive syngenetic deposits. In the case of such large deposits the need for compositing does not arise in the same manner due to geometric probability concerns in the sampling design (see Garrett and Sinding-Larsen, in press). Additionally, we assume that there is no periodicity in the background population, X, i.e., there is no systematic layering occurring at constant interval.

The locations of the anomalous segments, Y, in a composite play a significant role in estimating the distribution of $C_{n,m}$, as opposed to the case of spatial independence in the previous section.

First, we consider the variance of $C_{n,o}$:

$$\begin{aligned}
\mathrm{Var}(C_{n,o}) &= \frac{1}{n^2}\,\mathrm{Var}\left(\sum_{i=1}^{n} X_i\right) \\
&= \frac{1}{n^2}\left(nb^2 + 2b^2 \sum_{i=1}^{h-1}\sum_{j=i+1}^{h} \mathrm{Cov}(X_i X_j)\right) \\
&= \frac{b^2}{n^2}\left(n + 2\sum_{i=1}^{n-1}\sum_{j=i+1}^{n} q^{j-i}\right) \\
&= \frac{b^2}{n^2}\left(n + 2\sum_{j=2}^{n}(n-(j-1))q^{j-1}\right) \\
&= \frac{b^2}{n^2}\left(n + 2\sum_{j=1}^{n-1}(n-j)q^{j}\right) \\
&= \frac{b^2}{n}\left(1 + F_n(q)\right)
\end{aligned} \tag{12}$$

where:

$$F_n(q) = \frac{2}{n}\sum_{j=1}^{n-1}(n-j)q^j \tag{13}$$

Hence, the composite $C_{n,o}$ is distributed as:

$$C_{n,o} \sim N\left(a, \frac{b^2}{n}\left(1 + F_n(q)\right)\right) \tag{14}$$

instead of $N(a, \frac{b^2}{n})$ for the spatially independent case when m = o in (4). Spatial dependence effectively increases the variance. In the independent case each individual segment of the composite contributes unique information, however, with spatial dependence the individuals are correlated, the information no longer unique, and the effective sample size is less than the n physical segments.

Now let us consider the variance of the composite $C_{n,m}$ (jl, . . . ,jm) as described in (2). Then:

$$\begin{aligned}
\mathrm{Var}(C_{n,m}) &= \mathrm{Var}(C_{n,o}) - \frac{b^2}{n^2}\sum_{k=1}^{m}\left(1 + \delta_{jk} - \frac{d^2}{b^2}\right) \\
&= \frac{b^2}{n} + \frac{b^2}{n}F_n(q) - \frac{mb^2}{n^2} + \frac{md^2}{n^2} - \frac{b^2}{n^2}\sum_{k=1}^{m}\delta_{jk} \\
&\text{where: } \delta_u = 2\left(\sum_{i=1}^{u-1} q^i + \sum_{i=1}^{n-u} q^i\right)
\end{aligned} \tag{15}$$

If q = 0 equation (15) reduces to:

$$\begin{aligned}
\mathrm{Var}(C_{n,m}, q=0) &= \frac{b^2}{n} - \frac{mb^2}{n^2} + \frac{md^2}{n^2} \\
&= \frac{(n-m)b^2}{n^2} + \frac{md^2}{n^2}
\end{aligned} \tag{16}$$

which is seen to be identical to (4), indicating the special nature of spatial independence.

Therefore, the distribution of composites in the case of spatial dependence, i.e., autocorrelation q, is:

$$C_{n,m}(jl, \ldots, jm), q \sim N(g, h^2)$$

where: (17)

$$g = \frac{(n-m)a + mc}{n}, \text{ and}$$

$$h^2 = \frac{b^2}{n} + \frac{b^2}{n}F_n(q) - \frac{mb^2}{n^2} + \frac{md^2}{n^2} - \frac{b^2}{n^2}\sum_{k=1}^{m}\delta_{jk}$$

Using (14) and (17) we can compare $C_{n,o}$ and $C_{n,m}$ for any autocorrelation, q. The worst case scenario of only one segment drawn from the anomalous population, Y, i.e., m = 1, and that segment being at the end of the composited sequence, i.e., jl = 1, so leading to maximum variance was investigated by Garrett and Sinding-Larsen (in press). The performance of $F_n(q)$ was graphed over composite sizes from 2 to 100 for autocorrelations from 0 to 1. Additionally, the inverse problem was studied, as for the independent case, in order to determine optimal composite sample sizes for stated background and anomalous conditions and the limiting situation of q = 1.

Remarks

To date we have not fully explored the generalized one-dimensional distribution function (17). It is planned to do so by the preparation of a range of graphic displays. We believe that these will provide additional insight into the determination of optimal segment lengths for analysis, or compositing, under varying conditions of spatial dependence and anomalous segment location. This sensitivity study will also reveal those practical conditions under which the simpler spatially independent model may be used.

To date our study has been restricted to the one-dimensional discrete autocorrelation case. The two-dimensional case is of interest and importance in remote sensing sensitivity studies. In such cases the finite area pixels are implicit composites of sub-pixel sized units all contributing to the remotely sensed response. The topic of interest is, what areal extent and how much contrast should a sub-pixel sized feature have before it can be recognized in the overall pixel response? To fully generalize our study it is also necessary to permit continuous autocorrelation, rather than the discrete case used here.

References

Abramowitz, M. and Stegun, I.A.
1970: Handbook of mathematical functions with formulas, graphs and mathematical tables; National Bureau of Standards Applied Mathematics Series 55, Washington, D.C., Ninth printing, 1046 p.

IMSL
1982: Reference Manual, Edition 9, MDNOR and MDNRIS; International Mathematical and Statistical Libraries, Inc., Houston, Texas, v. 3.

Garrett, R.G. and Sinding-Larsen, R.
– Optimal composite sample size selection, applications in geochemistry and remote sensing; in Exploration Geochemistry 1983, ed. A. Bjorklund; Journal of Geochemical Exploration, v. 21. (in press)

GEOLOGY OF THE WELDON BAY-FAY LAKE AREA, MANITOBA

Project 800007

E. Froese
Precambrian Geology Division

Froese, E., Geology of the Weldon Bay-Fay Lake area, Manitoba; in Current Research, Part B, Geological Survey of Canada, Paper 84-1B, p. 355-358, 1984.

Abstract

The subdivision of the Kisseynew gneisses into micaceous gneisses of the Nokomis Group and quartz-rich gneisses of the Sherridon Group, as established elsewhere in the Kisseynew gneiss belt, has been extended to the Weldon Bay-Fay Lake area. The boundary between the Flin Flon volcanic belt and the Kisseynew gneiss belt follows the lithological contact of Amisk Group volcanic rocks with Nokomis and Sherridon gneisses. The Amisk-Nokomis contact is obscured by the development of mylonite. The Amisk-Sherridon contact probably is an unconformity. Several occurrences of garnet-anthophyllite rocks in felsic volcanic rocks of the Amisk Group are thought to represent metamorphosed hydrothermally altered rocks; however, these rocks are not associated with sulphide mineralization. Some subeconomic sulphide deposits with minor amounts of chalcopyrite and sphalerite are present near a contact of Amisk mafic and felsic rocks.

Résumé

On a prolongé jusqu'à la région de Weldon Bay – Fay Lake la subdivision des gneiss de Kisseynew en gneiss micassés du groupe de Nokomis et en gneiss riches en quartz du groupe de Sherridon comme établi ailleurs dans la zone des gneiss de Kisseynew. La limite entre la zone volcanique de Flin Flon et la zone des gneiss de Kisseynew suit le contact lithologique des roches volcaniques du groupe d'Amisk et des gneiss de Nokomis et de Sherridon. Le contact Amisk-Nokomis est caché par la formation de mylonites. Le contact Amisk-Sherridon se fait probablement par discordance. Plusieurs manifestations de roches à grenat et anthophyllite à l'intérieur de roches volcaniques felsiques du groupe d'Amisk semblent être des roches métamorphiques ayant subi une altération hydrothermale; cependant, ces roches ne sont pas associées à une minéralisation en sulfures. Certains gisements de sulfures relativement économiques, contenant de petites quantités de chalcopyrite et de sphalérite, sont présents près du contact des roches mafiques et acides d'Amisk.

Introduction and previous work

In southern Churchill Province, the Flin Flon volcanic belt is flanked on the north by the Kisseynew sedimentary gneiss belt. The transition zone between the two belts and the relationship of the Kisseynew gneisses to the supracrustal rocks of the volcanic belt have been subjects of considerable study and varied interpretation. In an attempt to further the understanding of this geological problem, an area straddling the boundary has been investigated in greater detail.

A sketch map of the regional geology (Fig. 1) is based mainly on the compilation of Bailes (1971) and on maps produced by Byers and Dahlstrom (1954) and Byers et al. (1965). Some modifications were made in the light of more recent mapping (Froese and Gall, 1981; Froese and Goetz, 1981; James, 1983; McRitchie, 1980; Parslow and Gaskarth, 1981; Tuckwell, 1979; Zwanzig, 1983) and as a consequence of the present study. The basic stratigraphic subdivision of supracrustal rocks of the Flin Flon belt into the predominantly volcanic Amisk Group and sedimentary Missi Group is essentially the one established by Bruce (1918). The only significant change, made by Wright (1933), was the inclusion of some sedimentary rocks, mainly greywackes, in the Amisk Group, whereas Bruce (1918) had assigned all sedimentary rocks to the Missi Group.

In the earliest mapping by Bruce (1918) and Wright (1931), the Kisseynew gneisses were regarded as a separate stratigraphic unit between the Amisk Group and Missi Group. However, Wright and Stockwell (1935) mapped the gneisses north of Annabel Lake as metamorphosed Amisk and Missi rocks. Bateman and Harrison (1945) regarded the gneisses at Kisseynew Lake as metamorphosed Missi rocks. Harrison (1951a, b) and Kalliokoski (1952, 1953) proposed a major fault between the two belts but this interpretation was questioned by Robertson (1951) and not accepted by Byers and Dahlstrom (1954) for the Annabel Lake area; they agreed with the earlier interpretation of Wright and Stockwell (1935).

Roberston (1953) proposed a subdivision of the Kisseynew gneisses into the Nokomis Group consisting of relatively micaceous gneisses and Sherridon Group consisting mainly of quartz-rich gneisses. He accepted the previous definition of Sherridon Group by Bateman and Harrison (1946) who noted a similarity between Sherridon Group and Missi Group. More recently, Bailes (1971) suggested a correlation of Nokomis Group with Amisk Group sediments. Tuckwell (1979) proposed a transitional group between the Nokomis and Sherridon groups; however, the lithology is similar to that of the Sherridon Group. Robertson (1953) included migmatites and granitoid gneisses in the Nokomis Group; however, it is advisable to assign these rocks to a separate map unit because they are orthogneisses (Zwanzig, 1983). These divisions have not yet been extended to all areas of Kisseynew gneisses.

Geology of the Weldon Bay-Fay area

The Weldon Bay-Fay Lake area, (Fig. 2) straddles the junction of four one-mile map areas (Bateman and Harrison, 1946; McGlynn, 1959; Kalliokoski, 1952; Frarey, 1961). Mapping was begun in 1980 (Froese and Gall, 1981) and completed in 1982 and 1983. The main rock type of the Amisk Group is a fine grained amphibolite, derived from volcanic flow rocks. A lenticular unit of fine grained biotite-garnet schist probably is a metamorphosed felsic volcanic rocks because a few fragments are locally preserved. A few lenses of garnet-anthophyllite rock, probably representing metamorphosed hydrothermally altered rocks, are interlayered with the biotite-garnet schist. South of Weldon Bay,

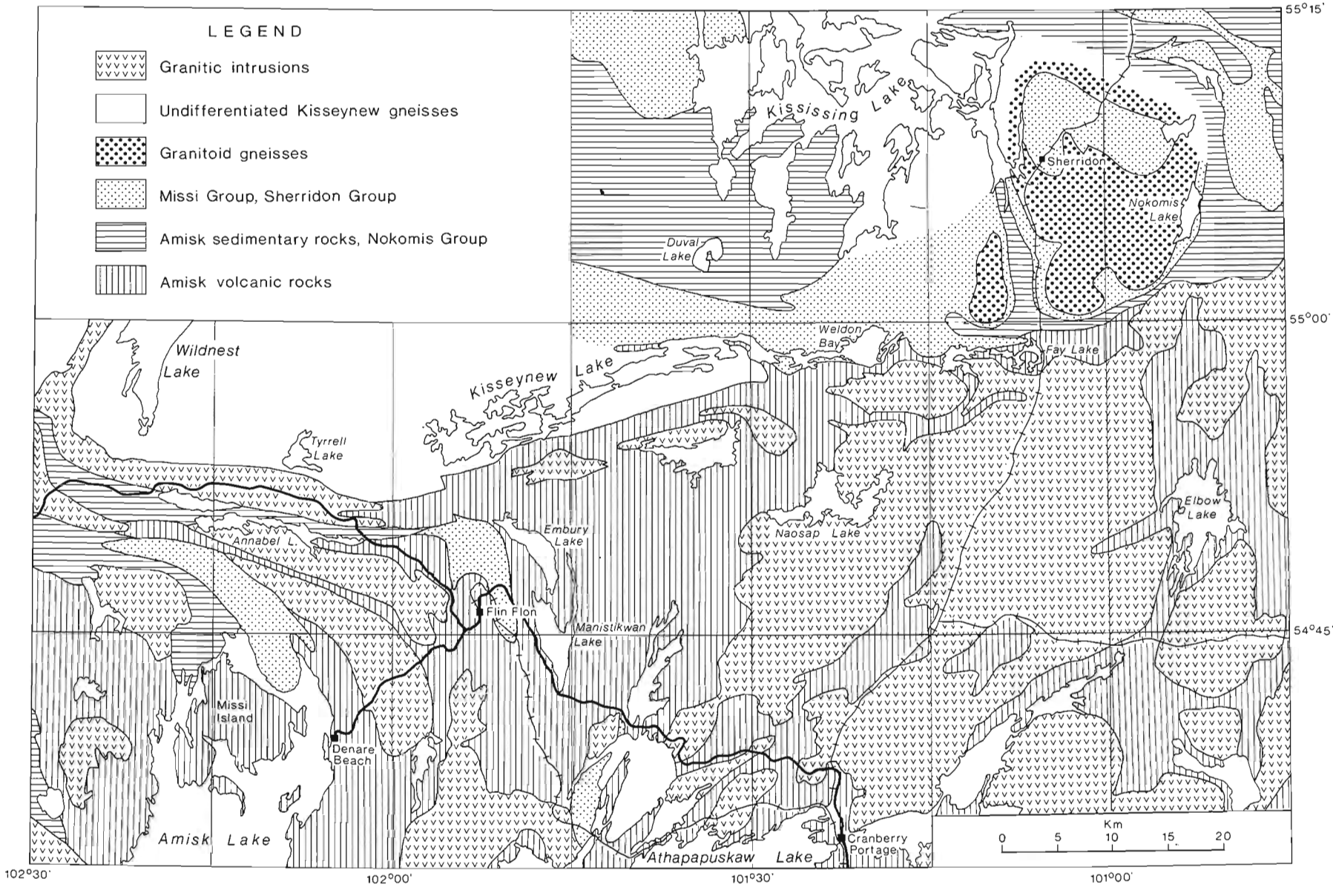

Figure 1. *Regional geology of the Amisk Lake-Sherridon area, Saskatchewan and Manitoba.*

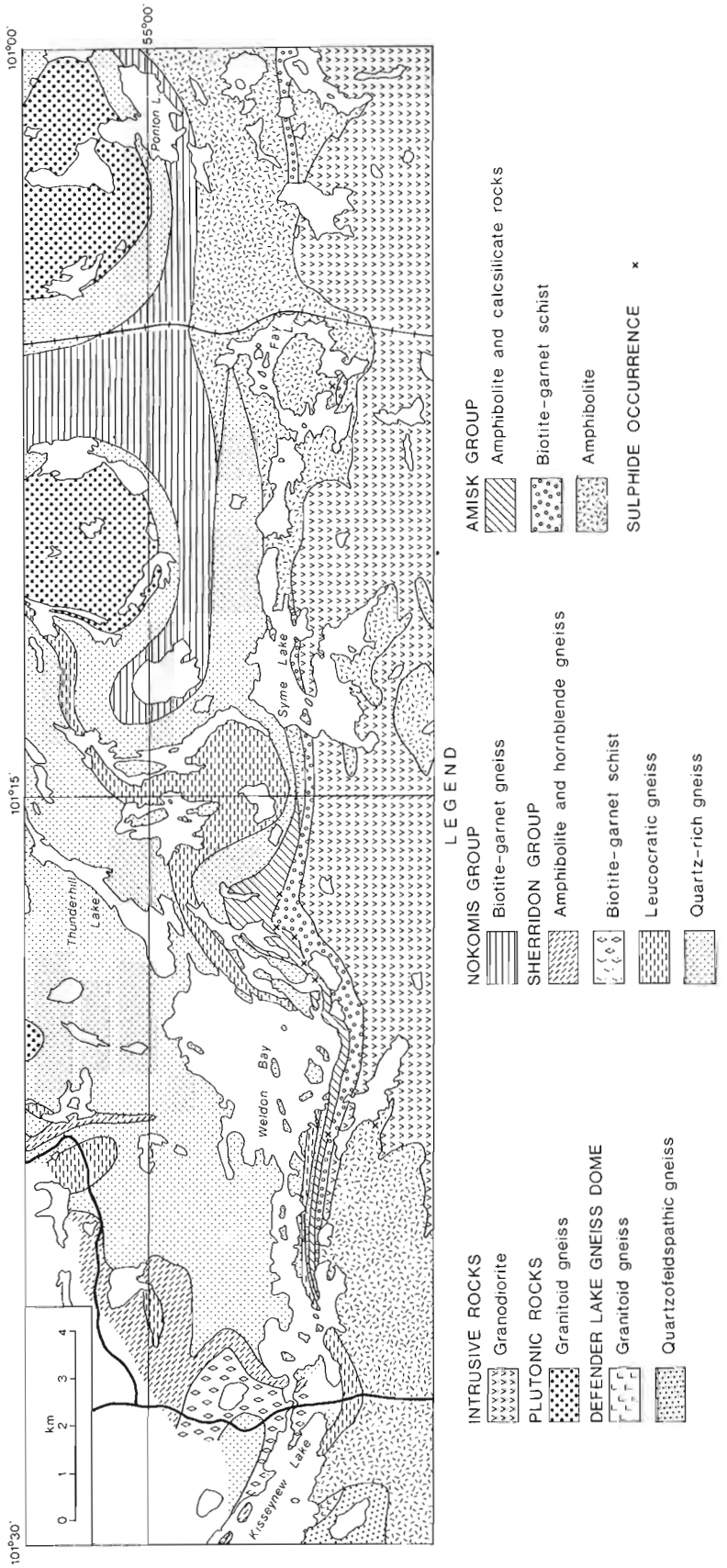

Figure 2. *Geological sketch map of the Weldon Bay-Fay Lake area, Manitoba.*

a layer of fine grained to coarse grained amphibolite contains some lenses of calc-silicate rock. Possibly this unit represents mafic volcaniclastic rocks. The rocks of the Amisk Group are intruded by medium grained granodiorite, including a few small bodies of diorite.

North of Fay Lake, the Amisk Group is in sharp contact with the Nokomis Group. However, the nature of the contact is obscured by extreme flattening of rocks and the development of mylonite, particularly in layers of felsic to intermediate rocks within the predominantly mafic volcanic rocks. The biotite-garnet gneiss of the Nokomis Group probably represents metamorphosed greywacke.

The main rock type of the Sherridon Group in a grey, medium grained, quartz-rich gneiss, probably derived from lithic arenite. Conglomerate composed of felsic to mafic fragments, including some magnetite-chert pebbles, occurs in some places. Within the gneiss, there is a unit of a fine grained leucocratic rock with a great stratigraphic persistence. Froese and Gall (1981) suggested a sedimentary origin for this rock. However, James (1983) thought that the chemical composition indicated derivation from felsic volcanic rocks. Such interpretation is supported by the local presence of quartz eyes and feldspar phenocrysts (Zwanzig, 1983). Northwest of Weldon Bay, some biotite-garnet schist has been included in the Sherridon Group because it is interlayered with quartz-rich gneisses and amphibolites of the Sherridon Group. However, Zwanzig (1983) assigned this unit to the Nokomis Group because of lithological similarity. Northwest of Weldon Bay, amphibolites and hornblende gneisses of sedimentary origin are common in the Sherridon Group. The lithological similarity of the Sherridon Group to the Missi Group, including the presence of conglomerate, suggests that it unconformably overlies rocks of the Amisk Group. The contact relationship between Sherridon Group and Nokomis Group is uncertain. The change in sedimentation products from greywackes to lithic arenites might indicate a disconformity.

The quartzofeldspathic gneisses of the Defender Lake gneiss dome were considered to be metamorphosed Missi rocks by Bateman and Harrison (1945). Froese and Gall (1981) had some doubts about this correlation but still regarded the gneisses as derived from some supracrustal rocks. Zwanzig (1983) regarded these rocks as orthogneisses. Within the quartz-rich Sherridon gneisses, there are domal bodies of granitoid orthogneisses. It is possible that they represent remobilized rocks, older than the Sherridon Group.

In the Weldon Bay-Fay Lake area, all rocks have been metamorphosed to about the same grade of metamorphism. One occurrence of well-preserved staurolite at Syme Lake was noted, but commonly

staurolite is present as relics in sillimanite-bearing biotite-garnet schist. Therefore, metamorphic conditions were near those corresponding to the decomposition of staurolite in the presence of muscovite.

Sulphide occurrences

Subeconomic occurrences of sulphides have been known in the area for some time (Wright, 1931; Kalliokoski, 1952; McGlynn, 1959). East of Weldon Bay, disseminated sulphides are present along the contact of biotite-garnet schist and amphibolite. Massive bodies of iron sulphides, up to 6 m wide, with disseminated chalcopyrite occur in amphibolite at the south end of Fay Lake. South of Weldon Bay a narrow layer of quartz-sericite-pyrite schist, interlayered with biotite-garnet schist contains sphalerite (Gale, 1980).

Acknowledgments

I was ably assisted in the field by T.D. Peterson in 1982 and L.B. McIntyre in 1983. Discussion in the field with E.W. Brown, J.R. Pickell, D.P. Price, and H.V. Zwanzig were found very helpful during the course of this work.

References

Bailes, A.H.
1971: Preliminary compilation of the geology of the Snow Lake – Flin Flon-Sherridon area; Manitoba Mines Branch, Geological Paper 1/71.

Bateman, J.D. and Harrison, J.M.
1945: Mikanagan Lake, Manitoba; Geological Survey of Canada, Map 832A with descriptive notes.

1946: Sherridon, Manitoba, Geological Survey of Canada, Map 862A with descriptive notes.

Bruce, E.L.
1918: Amisk-Athapapuskow Lake district; Geological Survey of Canada, Memoir 105.

Byers, A.R. and Dahlstrom, C.D.A.
1954: Geology and mineral deposits of the Amisk-Wildnest Lakes area, Saskatchewan; Saskatchewan Department of Mineral Resources, Report 14.

Byers, A.R., Kirkland, S.J.T. and Pearson, W.J.
1965: Geology and mineral deposits of the Flin Flon area, Saskatchewan; Saskatchewan Department of Mineral Resources, Report 62.

Frarey, M.J.
1961: Collins Point, Manitoba; Geological Survey of Canada, Map 1068A with descriptive notes.

Froese, E. and Gall, Q.
1981: Geology of the eastern vicinity of Kisseynew Lake, Manitoba; in Current Research, Part A, Geological Survey of Canada, Paper 81-1A, p. 311-313.

Froese, E. and Goetz, P.A.
1981: Geology of the Sherridon Group in the vicinity of Sherridon, Manitoba; Geological Survey of Canada, Paper 80-21.

Gale, G.H.
1980: Mineral deposit studies – Flin Flon/Kisseynew; Manitoba Mineral Resources Division, Report of Field Activities 1980, p. 51-64.

Harrison, J.M.
1951a: Possible major structural control of ore deposits, Flin Flon-Snow Lake mineral belt, Manitoba; Canadian Mining and Metallurgy Institute, Transactions, v. 54, p. 4-8.

1951b: Precambrian correlation and nomenclature, and problems of the Kisseynew gneisses, in Manitoba; Geological Survey of Canada, Bulletin 20.

James, D.T.
1983: Origin and metamorphism of the Kisseynew gneisses, Kisseynew Lake – Cacholotte Lake area, Manitoba; M.Sc. Thesis, Carleton University, Ottawa.

Kalliokoski, J.
1952: Weldon Bay map-area, Manitoba; Geological Survey of Canada, Memoir 270.

1953: Interpretations of the structural geology of the Sherridon-Flin Flon region, Manitoba; Geological Survey of Canada, Bulletin 25.

McGlynn, J.C.
1959: Elbow-Heming Lakes area, Manitoba; Geological Survey of Canada, Memoir 305.

McRitchie, W.D.
1980: Cacholotte Lake (parts of 63K/13,14 and 63N/3,4); Manitoba Mineral Resources Division, Report of Field Activities 1980, p. 65-69.

Parslow, G.R. and Gaskarth, W.J.
1981: Flin Flon base metals project: Annabel Lake area; Saskatchewan Geological Survey, Summary of Investigation 1981, p. 101-104.

Robertson, D.S.
1951: The Kisseynew lineament, northern Manitoba; The Precambrian, v. 24, p. 8-11, 13, 23.

1953: Batty Lake map-area, Manitoba; Geological Survey of Canada, Memoir 271.

Tuckwell, K.
1979: Stratigraphy and mineral deposits of the Sherridon area; Manitoba Mineral Resources Division, Report of Field Activities 1979, p. 42-45.

Wright, J.F.
1931: Geology and mineral deposits of a part of north-western Manitoba; Geological Survey of Canada, Summary Report 1930, Part C, p. 1-124.

1933: Amisk Lake area, Saskatchewan; Geological Survey of Canada, Summary Report 1932, Part C, p. 73-110.

Wright, J.F. and Stockwell, C.H.
1935: Amisk Lake, Saskatchewan; Geological Survey of Canada, Map 314A with descriptive notes.

Zwanzig, H.V.
1983: Kisseynew project: Lobstick Narrows (parts of 63K/13,14 and 63N/3,4); Manitoba Mineral Resources Division, Report of Field Activities 1983, p. 15-22.

PALEONTOLOGICAL EVIDENCE RELATING TO THE DISTRIBUTION AND PALEOENVIRONMENTS OF THE EUREKA SOUND AND BEAUFORT FORMATIONS, NORTHEASTERN BANKS ISLAND, ARCTIC CANADA

Project 650003

Mary R. Dawson[1], Robert M. West[1], and Leo J. Hickey[2]

Dawson, M.R., West, R.M., and Hickey, L.J., Paleontological evidence relating to the distribution and paleoenvironments of the Eureka Sound and Beaufort formations, northeastern Banks Island, Arctic Canada; in Current Research, Part B, Geological Survey of Canada, Paper 84-1B, p. 359-361, 1984.

Abstract

Recent discoveries of vertebrate, invertebrate and plant fossils near Nangmagvik Lake, northeastern Banks Island, N.W.T., confirm the presence of marine strata in the local Paleogene Eureka Sound Formation and indicate a wider distribution of the Neogene Beaufort Formation than previously believed.

Résumé

Les récentes découvertes de vertébrés, invertébrés et plantes fossiles près du lac Nangmagvik, au nord-est de l'île Banks, (T.N.-O.), confirment la présence de strates marines dans la formation locale paléogène d'Euréka Sound et indiquent une distribution plus large de la formation néogène de Beaufort que celle que l'on avait supposé auparavant.

Introduction

In the course of a continuing paleontological investigation of upper Cretaceous and Tertiary terrestrial deposits of the Canadian Arctic Archipelago, field research was conducted on Banks Island in July 1982. This work was undertaken to follow up on recent indications from mapping and sedimentological analyses (Miall, 1979) that northern Banks Island would be an appropriate region for the discovery of remains of terrestrial organisms in the upper Cretaceous and Paleogene Eureka Sound Formation. This formation has yielded a significant vertebrate fossil record on Ellesmere Island (Dawson et al., 1976; West and Dawson, 1978). Work in one area in the northeastern parts of Banks Island led to some reinterpretations of formational distributions and of habitats represented.

Acknowledgments

R. Thorsteinsson has encouraged us in all aspects of our investigations of the late Cretaceous and Tertiary fossil record of the Arctic Archipelago. Sincere thanks are extended to him, to David Bardack for identifications of sharks, to William Zinsmeister for identifications of invertebrates, and to Polar Continental Shelf Project and the Committee on Research and Exploration, National Geographic Society, for making this work possible.

Results

The area examined is in the vicinity of Nangmagvik Lake and north of Desert Creek (between approximately 74°07' to 74°12' north latitude and 119°55' to 120°25' west longitude; see Fig. 1). Exposures referred by Miall (1979, p. 44-48) to an upper, cyclic member of the Eureka Sound Formation were examined on both sides of Nangmagvik Lake (Fig. 1, sites A and B). Fossil wood occurs, both in lignite deposits and in sideritic lenses, as does other plant debris, including some leaves. West of Nangmagvik Lake (Fig. 1, B), a thin band of unconsolidated brownish grey sand, no more than 3 m thick and extending about 20 m along strike, yielded shark teeth and steinkerns of pelecypods and gastropods. Some of the teeth retain delicate basal cusps, indicating that they were preserved with little, if any, reworking. The sharks were odontaspids, bottom-feeding marine forms having a stratigraphic range of late Cretaceous to Recent. The invertebrates include both gastropods and pelecypods. One snail species, a naticid, is abundant. The clams found include a large venerid, a tellenid-like species, and a corbiculid. These four species together suggest a slightly brackish, shallow water marine situation.

Although earlier workers (Troelson, 1950; Tozer, 1963, p. 92-95; West et al., 1975) generally regarded the Eureka Sound Formation as a largely nonmarine unit, recent, more detailed studies (West et al., 1981) have demonstrated the presence of considerable thicknesses of marine rocks in the formation. The mollusc and shark fossils in the upper part of the Eureka Sound Formation near Nangmagvik Lake confirm this conclusion.

Farther west (Fig. 1, C), deposits referred by Miall (1979) to the cyclic member of the Eureka Sound Formation consist largely of unconsolidated sand, both massive and well bedded, with finer silt beds. As Miall noted for the cyclic member, plant rootlets and other plant debris occur at numerous levels within these deposits. However, one of their most characteristic features is the presence of large, apparently unaltered logs and pieces of wood (Fig. 2). The deposits also yielded a well preserved cone of **Picea banksii** (Fig. 3), a positive indicator of the Neogene Beaufort Formation (Hills and Ogilvie, 1970). The preservation of this delicate cone shows that it was found in place and had not been reworked. The deposits containing the cone and the logs, which also are characteristic of the Beaufort Formation, occur topographically at between 190 and 280 m elevation and are higher stratigraphically than rocks clearly belonging to the cyclic member of the Eureka Sound Formation on both sides of Nangmagvik Lake.

[1] Carnegie Museum of Natural History, Carnegie Institute, Pittsburgh, PA 15213
[2] Peabody Museum of Natural History, Yale University, New Haven, CT 06520

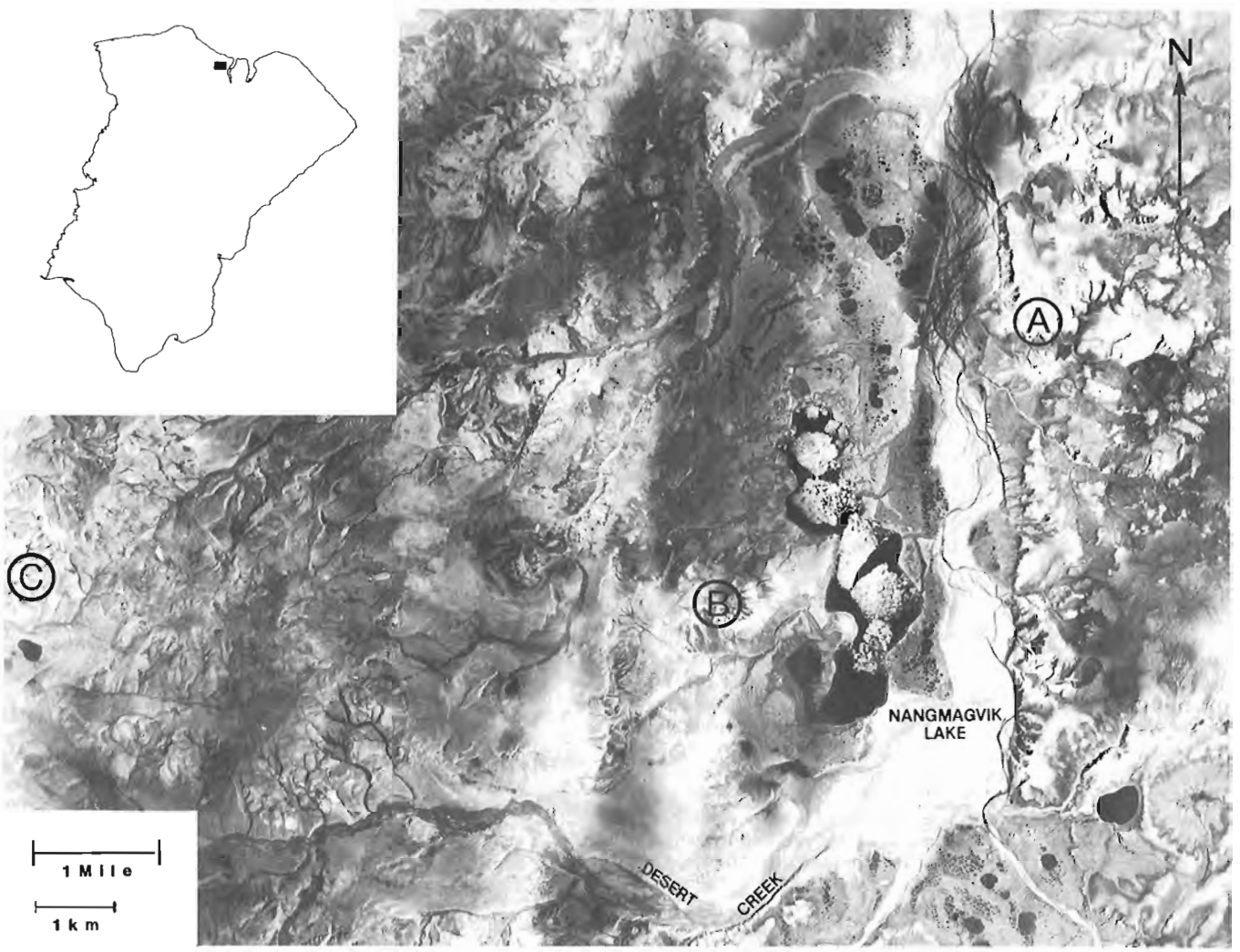

Figure 1. *Aerial photograph of Nangmagvik Lake — Desert Creek area, northeastern Banks Island. Reproduced from Department of Energy, Mines and Resources Aerial Photograph A-17379-26. Insert shows location of photographed area on Banks Island. A, site with fossil plants in cyclic member, Eureka Sound Formation; B, site with molluscs and vertebrates, Eureka Sound Formtion; C, site with plants in Neogene deposits.*

The stratotype of the Beaufort Formation on Prince Patrick Island (Tozer, 1956) consists of about 80 m of unconsolidated, monotonous sandstone. Our paleontological investigations near Desert Creek and Nangmagvik Lake suggest an outcrop thickness for the Beaufort Formation there of about 90 m, similar to thicknesses reached by the formation in northwestern Banks Island (Miall, 1979, p. 55).

The local contact between the Beaufort Formation and the Eureka Sound Formation was not seen; it apparently occurs in a flat, tundra-covered area west of Nangmagvik Lake. Thus, the formation assignments made here are based on lithology, fossil content and relative stratigraphic position.

The thick Beaufort Formation section noted in 1982 lies directly upon the north-northeast trending axis of the synclinal structure marking the axis of the Northern Banks Basin (Miall, 1979). It therefore appears that this structure plays a major role in preserving more of the Beaufort Formation than was appreciated previously.

References

Dawson, M.R., West, R.M., Langston, W., and Hutchison, J.H. 1976: Paleogene terrestrial vertebrates: northernmost occurrence, Ellesmere Island, Canada; Science, v. 192, p. 781-782.

Hills, L.V. and Ogilvie, R.T. 1970: **Picea banksii** n. sp. Beaufort Formation (Tertiary), northwestern Banks Island, Arctic Canada; Canadian Journal of Botany, v. 48, no. 3, p. 457-464.

Miall, A.D. 1979: Mesozoic and Tertiary geology of Banks Island, Arctic Canada: the history of an unstable craton margin; Geological Survey of Canada, Memoir 387, p. 1-235.

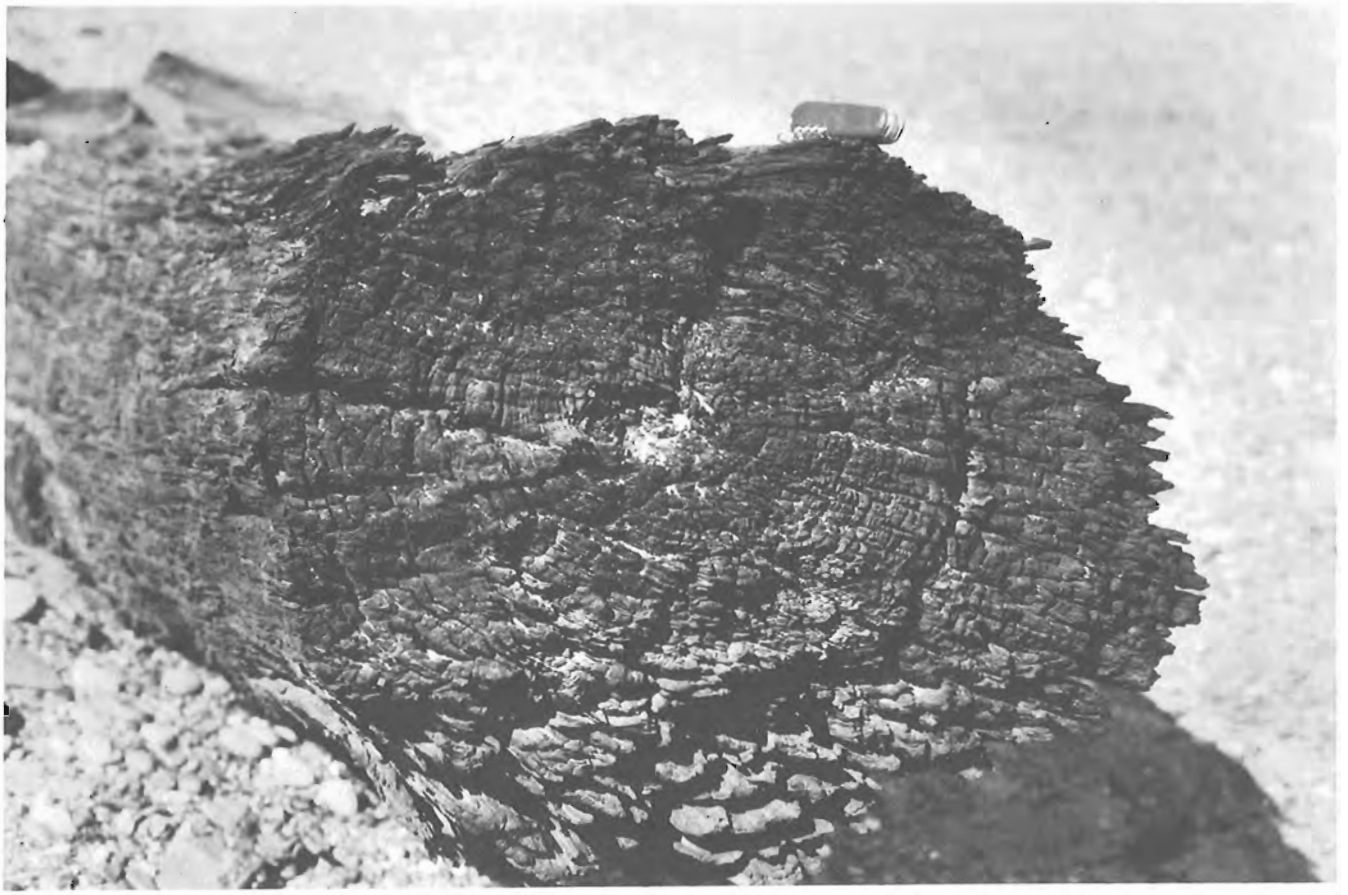

Figure 2. *Closeup of log eroding out of Neogene deposits, Locality C. Pocket knife for scale.*

Figure 3. ***Picea banksii*** *cone found at Locality C.*

Tozer, E.T.
1956: Geological reconaissance, Prince Patrick, Eglinton and western Melville Islands, Arctic Archipelago; Geological Survey of Canada, Paper 60-5.

1963: Mesozoic and Tertiary stratigraphy; in Geology of the north-central part of the Arctic Archipelago, Northwest Territories (Operation Franklin); Geological Survey of Canada, Memoir 320, p. 74-95.

Troelson, J.C.
1950: Contributions to the geology of northwest Greenland, Ellesmere and Axel Heiberg islands; Meddelelser om Grønland, v. 149, no. 7, 85 p.

West, R.M. and Dawson, M.R.
1978: Vertebrate paleontology and Cenozoic history of the North Atlantic region; Polarforschung, v. 48, no. 1/2, p. 103-119.

West, R.M., Dawson, M.R., Hickey, L.J., and Miall, A.D.
1981: Upper Cretaceous and Paleogene sedimentary rocks, eastern Canadian Arctic and related North Atlantic areas; in Geology of the North Atlantic Borderlands, J.M. Kerr and A.J. Ferguson (eds.); Canadian Society of Petroleum Geologists, Memoir 7, p. 279-298.

West, R.M., Dawson, M.R., Hutchison, J.H., and Ramackers, P.
1975: Paleontologic evidence of marine sediments in the Eureka Sound Formation of Ellesmere Island, Arctic Archipelago, N.W.T., Canada; Canadian Journal of Earth Sciences, v. 12, p. 574-579.

CONTINUED HEADWALL RETREAT OF A RETROGRESSIVE THAW FLOW SLIDE, EASTERN MELVILLE ISLAND, NORTHWEST TERRITORIES

Project 770037

J.A. Heginbottom
Terrain Sciences Division

Heginbottom, J.A., Continued headwall retreat of a retrogressive thaw flow slide, eastern Melville Island, Northwest Territories; in Current Research, Part B, Geological Survey of Canada, Paper 84-1B, p. 363-365, 1984.

Abstract

The mean rate of headwall retreat of a retrogressive thaw flow slide near Tingmisut Lake, eastern Melville Island, decreased each year from 57 cm/100 h (1977) to 29 cm/100 h (1978), 28 cm/100 h (1979), to practically nil in 1981. By 1982 the headwall was reduced to a rubbly slope. Both the mean and maximum amounts of retreat correlate well with the thawing index, in Celsius degree-days, from Rea Point (r = 0.73 and 0.94, respectively).

Résumé

La vitesse moyenne de recul du front d'une coulée de dégel rétrogressif à proximité du lac Tingmisut, dans l'est de l'île de Melville, a diminué tous les ans, passant de 57 cm/100 h (1977) à 29 cm/100 h (1978), 28 cm/100 h (1979), jusqu'à être pratiquement nulle en 1981. En 1982, le front était réduit à une pente pierrailleuse. Les valeurs moyennes et maximales du recul se corrèlent bien toutes deux avec l'indice de dégel en degrés-jours Celsius, à partir de Rea Point (r = 0,73 et 0,94, respectivement).

Introduction

This note reports on the continued retreat of the headwall of a retrogressive thaw flow slide near Tingmisut Lake, eastern Melville Island, first seen in July 1977 (Heginbottom, 1978). When the slide was first visited, on 17 July 1977, a set of marker pegs was installed around the uphill edge of the slide area, and the distances from the pegs to the edge of the slide area were measured, along the slope of the ground, using a steel tape measure. The distances were measured to the nearest centimetre; the accuracy of the remeasurement is estimated to be ±2 cm. Four days later the slide was visited again and the distances measured. The amount of headwall retreat in a 100 hour period was found to range from 40 to 80 cm, with a mean of 57 cm. Additional measurements were made in July 1978 (3 sets), July-August 1979 (3 sets), June 1981 (2 sets), and a final set in July 1982. All data are presented in Table 1; retreat distances and retreat rates (in m/100 h) are presented in Table 2. The plan position of the network of pegs and the position of the headwall at each survey are shown in Figure 1.

Table 1. Successive Positions of the Headwall (cf. Table 1)

Date and time of survey	P	Q	Line R	S	T
17 July 1977, 1200 h	28.67	26.61	25.00	23.59	24.12
21 July 1977, 1615 h	27.94	26.13	24.22	23.18	23.69
11 July 1978, 1400 h	26.12	23.54	19.83	19.03	20.93
18 July 1978, 1830 h	25.94	23.45	18.88	18.05	20.92
24 July 1978, 1300 h	23.47	23.47	17.78	17.25	20.95
20 July 1979, 1700 h	25.24	22.95	16.52	15.26	21.10
24 July 1979, 2100 h	25.23	22.71	16.20	14.59	21.10
6 Aug 1979, 1500 h	25.22	21.01	15.09	12.78	21.00
20 June 1981, 0830 h	24.73	20.84	13.02	11.16	21.00
24 June 1981, 1230 h	24.74	20.90	13.02	11.16	21.00

The pattern of headwall retreat

In 1977, when first seen, the flow slide was quite active. The headwall was retreating rapidly and at the foot was a mass of liquid mud with free water on the surface. This mud was moving slowly downhill, draining and drying as it did so. Headwall retreat was mainly by melting of the exposed massive ground ice and the continual falling away of the thawed soil above. The flow slide is situated on the northeast side of the valley, in slumped and frost riven material of the Canyon Fiord Formation, about 1.5 km from Tingmisut Lake and an equal distance from the sea at Weatherall Bay (Heginbottom, 1978). The exposed ice mass appeared to be in the form of a large lens, about 40 m wide and at least 20 m in extent up and down the slope. The origin of the ice body could not be determined.

The slide was visited in 1978 by W.D. Roggensack and Kurt Stangl of EBA Engineering Ltd. (Edmonton). Roggensack (personal communication, 1978) reported that, although the general situation was the same as in 1977, the thickness of ice exposed in the headwall was only about 1 m. When L.D. Dyke, then with Geological Survey of Canada, visited the site in 1978, the rate of headwall retreat was less

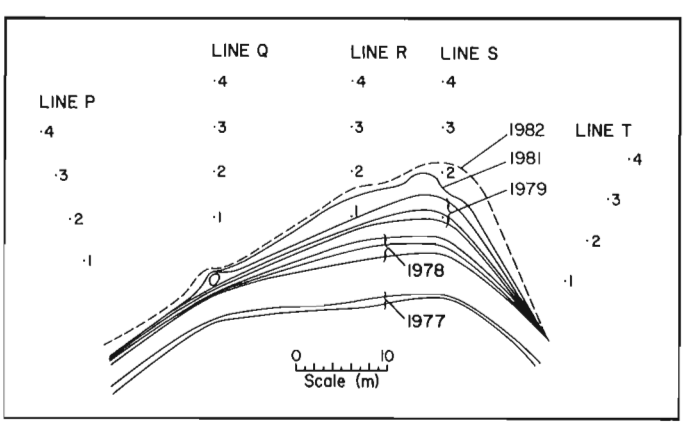

Figure 1. *Successive positions of headwall, 1977-1982.*

Table 2. Amount and Rate of Headwall Retreat

Survey dates	Elapsed time (days)	Amount of retreat (cm) *Rate of retreat (m/100 h)*[1] Line P	Line Q	Line R	Line S	Line T	Average	Thawing index (DDC) (at Rea Point)
1977 17 July-	4	0.73	0.48	0.78	0.41	0.43	0.57	21
21 July		*0.73*	*0.48*	*0.78*	*0.41*	*0.43*	*0.57*	
1978 11 July-	7	0.18	0.09	0.95	0.98	0.01	0.44	32
18 July		*0.10*	*0.05*	*0.55*	*0.57*	*0.00*	*0.25*	
18 July-	6	0.47	+0.02	1.10	0.80	+0.03	0.46	35.5
24 July		*0.34*	*0.01*	*0.79*	*0.58*	*+0.01*	*0.34*	
1979 20 July-	4	0.01	0.24	0.32	0.67	0.00	0.25	30.5
24 July		*0.01*	*0.24*	*0.32*	*0.67*	*0.00*	*0.25*	
24 July-	13	0.01	1.70	1.11	1.81	0.10	0.95	56
6 August		*0.00*	*0.56*	*0.36*	*0.59*	*0.03*	*0.31*	
1981 20 June-	4	+0.1	+0.06	0.00	0.00	0.00	+0.01	--
24 June		*+0.01*	*+0.06*	*0.00*	*0.00*	*0.00*	*+0.01*	

[1]Maximum values are underlined

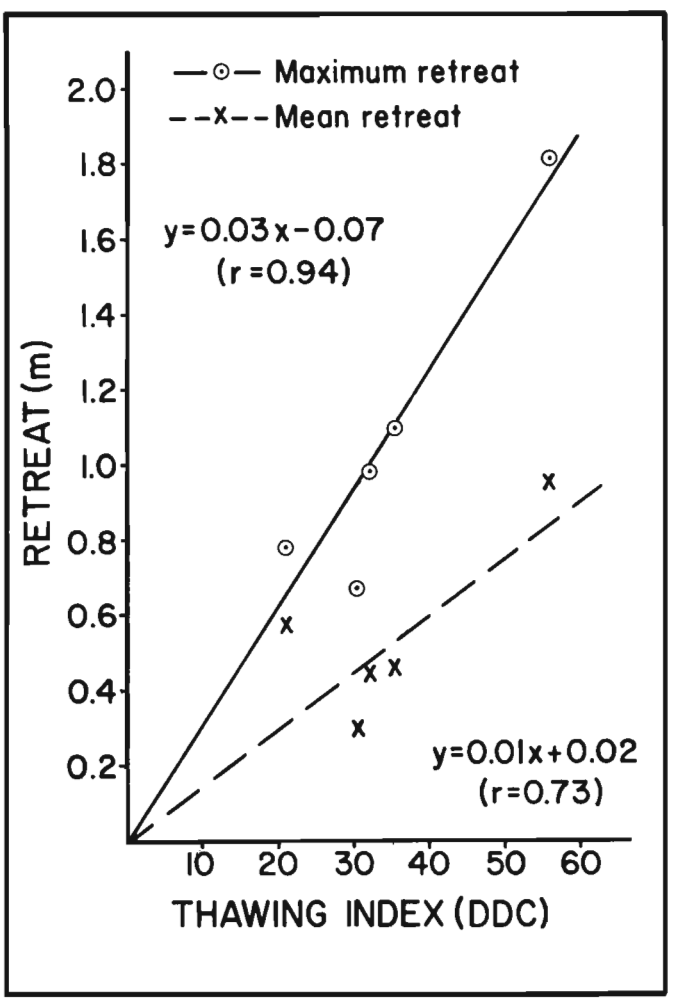

Figure 2. *Comparison of rate of headwall retreat with thawing index for Rea Point, 1977-1979.*

than that in 1977, ranging from 1 to 66 cm per 100 hours, with a mean of 29 cm. The amount of retreat since the previous year ranged from 1.82 m to 4.39 m.

Three visits were made to the site in 1979. The headwall had continued to retreat to the extent that one of the front pegs was only 20 cm from the scarp. Additional pegs were installed farther upslope on each line. All the distances reported in Table 1 are referred to these additional pegs. Much less ground ice was exposed in the headwall; ice was visible only in one 3 m-wide segment and to a thickness of 50 cm. The floor of the basin was stepped, in two levels, with the upper level approximately 50 cm higher than the lower level. The line of the step or rampart was approximately along the line of the headwall as seen in 1977. The rate of retreat in 1979 ranged from 0 to 61 cm per 100 hours, and the amount of retreat since 1978 ranged from -0.15 m (due to extension of the ground surface?) to 1.99 m.

During the second visit in 1979, it was noted that a large boulder was exposed in the face of the headwall at Line Q (see Fig. 1). By the third visit, this boulder had tipped forward, leaving a re-entrant in the headscarp. The measurements were made to the tip of this re-entrant, about 1 m behind the general line of the scarp.

The site was not visited in 1980, but two visits were made in 1981. Although the headwall had continued to retreat, the rate was much reduced, the lower part of the headscarp had degenerated into a rubbly slope and no ground ice was exposed. The relatively smooth curve of the headwall, as first seen in 1977, had also begun to degenerate, first with the re-entrant behind the boulder (noted above) and now with the development of an embayment in the headwall between lines Q and R. At this location the headwall had retreated about 2 m farther than the sections either side of it.

On 5 July 1982, the headscarp had degenerated even further, and was now just a rubbly slope of about 45°. The sharp crest of the scarp had now become a rough curve of crumbling soil blocks, such that no obvious measurement points were available. It appears that this particular thaw flow slide is no longer active, although the scar may well remain visible for many years to come.

Relation to temperature

An attempt has been made to relate the rate of headwall retreat to climatic parameters. **A priori** consideration suggested that the thawing index would be the most appropriate parameter for this purpose. The test was done for the period 1977 to 1979, when the headscarp was most active. The closest climatological station to the site is Rea Point, on southeast Melville Island, although it is 85 km away and in a very different topographic setting. No other reliable temperature data were available from nearby points. Accordingly, the climatic data for the summers of 1977, 1978, and 1979 for Rea Point, Melville Island, were obtained, and the thawing indexes calculated (the data are included in Table 2).

Five time periods were used for the comparison, one for 1977 and two each for 1978 and 1979. The periods ranged from four to thirteen days. Comparisons were made for the average and maximum rate of headwall retreat for each of the periods. Linear regression coefficients were calculated for each comparison, as shown in Figure 2. The regression coefficients are high for both comparisons, but noticeably higher for the maximum retreat data: 0.94 as opposed to 0.73 for the average retreat data.

Summary

An active retrogressive thaw flow slide, near Tingmisut Lake, eastern Melville Island, discovered in 1977, was observed periodically until 1982 when the activity had apparently ceased. When first seen, some 2 m of massive ground ice was exposed in the headwall of the feature and the headwall continued to retreat, but the thickness of ground ice exposed was less and less until, by 1981, no ice was visible. After 1981, the rate of retreat of the headwall slowed and the scarp itself degenerated into a rubbly slope. For the active period (1977 to 1979), rate of headwall retreat shows a high correlation with the thawing index as calculated for Rea Point, 85 km to the southeast.

Acknowledgments

Provision of field data for 1978 by W.D. Roggensack, K.O. Stangl, and L.D. Dyke is gratefully acknowledged. Field assistance by G. McMurachy, W. Weatherall, P. Sauvé, A. Everard, J. Perrot, M. Coire, and L. Légère is appreciated.

Reference

Heginbottom, J.A.
1978: An active retrogressive thaw flow slide on eastern Melville Island, District of Franklin; in Current Research, Part A, Geological Survey of Canada, Paper 78-1A, p. 525-526.

REGIONAL DISTRIBUTION OF MARINE MOLLUSCA (GASTROPODS AND PELECYPODS) IN EASTERN CANADA

Project 800038

F.J.E. Wagner
Atlantic Geoscience Centre, Dartmouth

Wagner, F.J.E., Regional distribution of marine mollusca (gastropods and pelecypods) in eastern Canada; in Current Research, Part B, Geological Survey of Canada, Paper 84-1B, p. 367, 1984.

Abstract

An index collection of Recent molluscan populations in Eastern Canada, including late glacial specimens from Scotian Shelf, has been established at the Bedford Institute of Oceanography. Distribution data are contained in a file, and specimens identified from Atlantic Geoscience Centre cruise collections are incorporated in a System 2000 database.

Résumé

On a établi à l'Institut océanographique Bedford, une collection stratigraphique des populations récentes de mollusques du Canada de l'Est. Cette collection comprend les espèces du plateau continental Scotian de la fin de l'époque glaciaire. Les données sur la distribution sont contenues dans un fichier, et les espèces identifiées, provenant des collections de la mission du Centre géoscientifique de l'Atlantique, sont intégrés dans une base de données, Système 2000.

The primary objective of this project was to set up a molluscan index collection to illustrate the known regional distribution of species in Eastern Canada. A file detailing the distribution of species with available ecological data was prepared to accompany the collection. In addition, distribution data for molluscs identified from AGC cruise collections were incorporated in a System 2000 computer data base. One phase of the project was the preparation of a volume on Champlain Sea fossils (Wagner, 1984a) requested by the Royal Ontario Museum for their "Fossils of Ontario" series.

The index collection now contains 598 lots of molluscs from the following areas: Beaufort Sea, Labrador Shelf, Bay of Fundy, Gulf of Maine, Miramichi estuary, Strait of Canso, Baie des Chaleurs, Exeter Bay (off Baffin Island), Emerald Basin, Hubbards, Nova Scotia and Lewisporte, Newfoundland. All species in the collection are represented in the ecological file. The file also covers all other species reported from Atlantic Canadian waters.

An illustrated catalogue covering the first 571 lots of molluscs placed in the index collection has been completed (Wagner, 1984b). In Part I of the catalogue, the species are listed by accession number and locality. Part II gives the original reference for each species and, where applicable, a synonymy. Illustrations are included as an aid for persons not having ready access to the collection. The illustrated specimens are part of the Geological Survey of Canada type collection but will be retained in the index collection at the Bedford Institute of Oceanography.

Although the collection was intended to have representatives of Recent populations only, late glacial specimens from the Scotian Shelf have also been included. To be of maximum value the collection should represent molluscs from the Late Quaternary and all geographic areas for which core samples, currently stored at AGC, are available.

Representation in the index collection is sparse from the Labrador Shelf and arctic waters and lacking from most of the Scotian Shelf, Gulf of St. Lawrence, Grand Banks and Hudson Strait. Also, much of the shallow inshore environment of these areas is unrepresented. To be of greatest value, the collection should be as comprehensive as possible. That means that an effort should be made to fill the existing gaps.

Data for all collections on hand from Beaufort Sea (cruise number 69-050, AC-71, Rich-70, Przo-70, Przo-71, Przo-72), Baie des Chaleurs (74-013), Bay of Fundy and Gulf of Maine (71-014, 73-003, 75-028), Emerald Basin (75-007), Labrador Shelf (77-021), St. Pierre Bank (81-044), Verrill Canyon area (82-004), Lake Melville (79-018), Chedabucto Bay (73-003), Chignecto Bay (78-025, 79-004), Strait of Canso (73-022) and Miramichi (75-048) have been prepared for the System 2000 data base. As data become available from future cruises they should be compiled and added to the System 2000 file.

References

Wagner, F.J.E.

1984a: Molluscs: in Macroinvertebrates and Vertebrates of the Champlain Sea; Royal Ontario Museum, Life Sciences Miscellaneous Publication.

1984b: Illustrated Catalogue of the Mollusca (Gastropodia and Bivalvia) in the Atlantic Geoscience Centre Index Collection; Geological Survey of Canada Catalogue, 80 p.

A NOTE ON THE SOLUBILITY OF QUARTZ IN SUPERCRITICAL WATER

Project 680071

K.L. Currie
Precambrian Geology Division

Currie, K.L., A note on the solubility of quartz in supercritical water; in Current Research, Part B, Geological Survey of Canada, Paper 84-1B, p. 369-372, 1984

Abstract

A preferred data set for the solubility of quartz in supercritical water can be fitted by the equation

$$m = \exp(-0.031+0.0152\ T+4.415E\text{-}6\ T^2-2.172\ \ln V)$$

where m is in ppm, T in kelvins, and V the specific volume of water in cm^3/gm. The root mean square error is 3.21 per cent, and the maximum error 9.01 per cent, both well within experimental accuracy limits. Equations with more than four adjustable constants must be overfitted, and their successful fitting of experimental data gives no support to their theoretical correctness.

Résumé

Un ensemble de données choisies sur la solubilité du quartz dans l'eau dans des conditions supercritiques peut être représenté par l'équation

$$m = \exp(-0,031+0,0152\ T+4,415E\text{-}6\ T^2-2,172\ \ln V)$$

où m est en ppm et T en degrés Kelvin, et V est le volume massique de l'eau en cm^3/g. L'erreur quadratique moyenne est de 3,21 % et l'erreur maximale de 9,01 %, les deux valeurs se situant dans les limites de la précision expérimentale. Lorsqu'il y a plus de quatre paramètres ajustables, on doit surajuster les équations et le fait qu'elles permettent un bon lissage des données expérimentales ne garantit pas leur justesse théorique.

Introduction

Recent models involving topics as diverse as the origin of ore deposits (Helgeson, 1982), mechanisms of metasomatism (Weare et al., 1976) and the structural regime around crystallizing plutons (Knapp and Norton, 1981) assume that the composition of the aqueous fluid in equilibrium with solid or liquid silicates can be adequately described. Considering that the amount of experimental data on the solubility of silicates under geologically plausible conditions is sparse and of doubtful quality, this assumption obviously involves a high degree of confidence in theoretical solution models. Comparison of available solubility data for quartz with solution models suggests that this confidence may be unwarranted.

Reasonably complete solubility data for silicates in supercritical water have been obtained only for quartz. Some data exist for feldspar (Currie, 1968; Davis, 1972; Adams, 1968; Spengler, 1965) and scattered measurements for leucite, nepheline, hornblende, diopside, olivine and orthopyroxene (Morey and Hesselgesser, 1951; Adcock, 1980), but none of these data sets are sufficient to test a solution model. Such models therefore depend heavily on the data for quartz, as is made quite explicit by Walther and Helgeson (1977). Since the models are designed to predict solubility under conditions where no experimental data exist (extrapolation), they must not only reproduce the existing data base with some acceptable degree of precision, but must also exhibit the correct functional dependence on intensive parameters such as pressure and temperature. The model must not be overfitted. Overfitted models will certainly produce the existing data set with ever increasing precision as the number of variables is increased, but extrapolation of overfitted models rarely produces reliable quantitative estimates, and even the direction of change may be erroneously predicted.

In order to test the applicability of current models, I have adopted a data set for quartz solubility, taking into account the experimental uncertainties indicated by reproducibility within and between data sets, and then determined the number of parameters needed to reproduce the adopted data set within the prescribed errors. Finally, the number of parameters thus determined is compared with the number of adjustable constants in current solution models.

Selection of data

Determinations of quartz solubility abound in the literature. Fournier and Potter (1982) list 16 experimental studies considered to be significant, while Walther and Helgeson (1977) list an even larger selection. However in the supercritical range relevant to most geological applications the list is much shorter. The most systematic studies are those of Anderson and Burnham (1965) and Weill and Fyfe (1964), supplemented by older partial results of Kennedy (1950) and Morey and Hesselgesser (1951). I have not used the results of Khitarov (1956) and Semenova and Tsiklis (1970) because they fall much below the results of other investigators in the same range. If they were included, the conclusions drawn would be strengthened even further.

When the above data sets are tabulated, it is apparent that determinations of solubility vary substantially both within and between data sets. Weill and Fyfe (1964) report 8 determination at 625°C, 1000 bars. Rejecting the two lowest values as due to lack of equilibration, the remaining 6 vary by about 7 per cent for no obvious reasons. Anderson and Burnham (1965) report two runs at 700°C, 1500 bars which gave essentially identical results, but two duplicates at 700°, 2000 bars which differ by 11 per cent. When different studies are compared the differences

become even larger. Thus at 500°, 2000 bars, Anderson and Burnham (1965), Weill and Fyfe (1964), and Morey and Hesselgesser (1951) obtained respectively 0.41, 0.456, and 0.499 weight per cent SiO_2, a total difference of over 20 per cent. The differences are not systematic, since at 500°, 1000 bars all three groups, as well as Kennedy (1950), determined values between 0.23 and 0.24 weight per cent SiO_2. Anderson and Burhnam (1965) noted that at solubilities of several weight per cent SiO_2, reproducibility was poor, possibly due to the determinative method used by them (weight loss of weighed plates). Some of the differences quoted are undoubtedly due to differences in experimental technique (weight loss of plates, periodic sampling, continuous flow) and to determinative methods (weight loss, gravimetric determination, colorimetric determination), but the effects of these factors are poorly known. Walther and Helgeson (1977) imply that dynamic methods, such as that used by Morey and Hesselgesser (1951) give results which are too low, but these results are consistently higher in the supercritical range than those given by weight loss methods. The latter are well known to encounter difficulties at high concentrations due to precipitation problems.

Considering these points, the solubility data clearly must be used with a certain degree of caution. I adopted the solubility values in column A of Table 1. These values have the following characteristics. (i) Each value falls inside the range given by the referenced experimental work. (ii) The error attached to each value covers the range of experimental values, and (iii) subject to the above constraints, the values fall on smooth curves when isobars are plotted against temperature and isotherms against pressure. A minimum error value of 4 per cent was attached to each data point, since literature data and many years of experience in my laboratory suggest that this it the maximum precision attainable by the experimental and analytical methods used. The maximum error values are about 10 per cent.

Treatment of experimental data

The preferred data set in Table 1 was fitted to a solution equation by a semi-empirical process. The isothermal pressure dependence of the solubility has long been known to be roughly linear in V, the mol volume of the solvent (Franck, 1956). Marshall (1972) has shown that this relation holds for a great variety of solids. In order to test the adequacy of a single parameter to model the pressure dependance, the eight isothermal data sets of Table 1 were fitted by nonlinear least squares to the form

$$m = \exp(a+b \ln V)$$

where m is the solubility in parts per million, and a and b constants to be determined. The values of b so derived varied from -2.10 to -2.54 with standard errors of estimate ranging from 0.02 to 0.18. The solubilities predicted all lay within 9 per cent of tabulated values with root mean square errors in the range 2.5 to 4 per cent.

When a and b are plotted against T, the values form an almost perfectly linear array, while the values of b form a somewhat irregular U-shaped curve. This plot suggests two possibilities: (a) the pressure dependence is correct, but the temperature dependance is not linear, as it appears, or (b) the temperature dependance is linear, as it appears, but the parameter b is a function of temperature.

Assuming the dependence on V to be correctly expressed, the dependence on T can always be expressed in terms a power series in T, although there is no a priori way of telling how many terms may be necessary to achieve a satisfactory fit. Since initial fitting showed that the dependence of m on T must be at least linear, I began with the expression

$$m = \exp(a+bT+c \ln V)$$

Fitting for a, b, and c by nonlinear least squares gave values of 4.626, 0.00728 and -1.288. The predicted values of solubility differed from the tabulated values by up to 40 per cent, with a root mean square error of 11 per cent.

Table 1. Preferred data set for quartz solubility compared to predicted values

P(kb)	673°K			723°K			773°K			823°K		
	A	B	C	A	B	C	A	B	C	A	B	C
1.00	1800	1939	1805	2160	2365	2193	2450	2702	2498	2700	2959	2710
1.25	2000	2146	2008	2500	2741	2569	3000	3300	3108	3500	3806	3590
1.50	2150	2306	2164	2900	3036	2863	3650	3788	3609	4400	4541	4359
1.75	2300	2441	2290	3200	3280	3107	4100	4199	4030	5000	5178	5029
2.00	2450	2563	2414	3450	3494	3320	4450	4556	4397	5530	5741	5620
2.25	2550	2677	2525	3650	3688	3515	4750	4878	4727	6100	6246	6153
2.50	2650	2785	2630	3850	3870	3696	5050	5173	5031	6600	6710	6641
2.75	2750	2888	2731	4050	4041	3867	5350	5449	5314	7000	7140	7093
3.00	2850	2987	2827	4250	4204	4029	5650	5709	5580	7400	7542	7517
3.25	2950	3081	2918	4350	4358	4183	5900	5954	5831	7800	7921	7915
3.50	3020	3171	3005	4495	4505	4329	6150	6186	6069	8200	8278	8289
4.00	3150	3337	3166	4775	4776	4598	6650	6613	6506	9000	8933	8977
5.00	(3390)	3627	3447	(5225)	5246	5065	7400	7350	7259	(10200)	10058	10155
6.00	(3630)	3879	3690	(5535)	5651	5466	8100	7983	7903	(11200)	11022	11161
7.00	(3870)	4105	3908	(5815)	6015	5825	8700	8552	8482	(12000)	11891	12067
8.00	(4110)	4313	4107	(6095)	6349	6155	9200	9078	9015	(12800)	12699	12905
9.00	(4350)	4513	4298	(6375)	6672	6473	9600	9587	9530	(13600)	13483	13718
10.00	(4590)	4708	4486	(6655)	6991	6786	(10000)	10096	10044	(14400)	14277	14537
Isotherm error	9			8			5			5		

Experimental data smoothed on plots against P and T. Quoted errors cover the discrepancies between referenced experimental data. Figures in parentheses are graphical extrapolations only, and have not been used for fitting. Column A: - preferred value for solubility of quartz in ppm. Column B: - predicted solubility from 8-constant equation of Fournier and Potter (1982), Column C: - predicted solubility from 4-constant equation.

This expression clearly was inadequate to reproduce the experimental data within the adopted error limits. I therefore proceded to the next step,

$$m = \exp (a+bT+cT^2+d \ln V)$$

Fitting for a, b, c, and d by nonlinear least squares gave values of -0.0311 ± 0.154, 0.0152 ± 0.000357, 4.415E-6 ± 2.236E-7, and -2.172 ± 0.019, where the error ranges quoted are 1 standard error. The predicted values of solubility given by this expression are shown in column C of Table 1. Compared to the experimental data, the root mean square discrepancy is 3.21 per cent, and the maximum discrepancy 9.01 per cent. Compared to the error limits in Table 1, this expression clearly predicts the solubility of quartz in supercritical water to within experimental accuracy, and no further fitting is justified.

No claim can be made that this expression is the correct theoretical expression for expressing the solubility of quartz. Indeed it can readily be shown that other four parameter models will give comparable accuracy, for example

$$m = \exp (a+bT+c \ln V+d \ln P)$$

with values a = 1.857, b = 0.00652, c = 1.507, d = 0.259. The significant point is that no more than four adjustable constants are required to reproduce the experimental data within experimental error. The theoretical significance of these constants cannot be derived from empirical equations (although this was attempted by earlier workers, such as Mosebach (1957)), but theoretical equations with more than four constants must either be overfitted or exhibit some kind of inter-dependence among the constants.

Discussion

Walther and Helgeson (1977), basing themselves on a theoretical solubility equation developed by Helgeson and Kirkham (1976), fitted silica solubility using seven adjustable constants. These data included not only the solubility of quartz in supercritical water, but also data on quartz solubility in the two phase region, and data on the solubility of cristobalite, tridymite and amorphous silica. Walther and Helgeson (1977) reported agreement between calculated and observed values within about 0.05 in molality, although it is evident from the discrepancies within and between data sets, as discussed above, that such agreement could be reached in the supercritical region only for a selected data set. This data set is not quoted explicitly by Walther and Helgeson (1977). Fournier and Potter (1982) analyzed empirically roughly the same experimental data considered by Walther and Helgeson (1977), and give a regression equation with eight constants, said to reproduce the data with an average discrepancy of 0.016 molal, and a standard deviation of 0.089. Again such precision requires selection of data, and Fournier and Potter (1982) discussed criteria for selection at some length, including such factors as surface damage due to excessive grinding. However, both studies accept the results of Morey and Hesselgesser (1951), Anderson and Burnham (1965) and Weill and Fyfe (1964), and claim good agreement between their predicted values and experimental values, even though these experimental values vary by 10 to 20 per cent within and between the studies.

It might be argued that more than four adjustable parameters may be justified in the solubility equations of Walther and Helgeson (1977) and Fournier and Potter (1982) because these equations cover a much larger range than that covered by the present analysis. However extrapolation suggests that the improvement in precision obtained with the extra adjustable coefficients is less than might be anticipated. Thus at 298°K, 1 bar the solubility predicted by the four-constant models ranges from 6 to 66 ppm, depending on choice of constants, as against the (rather dubious) experimental values of 4-6 ppm (Walther and Helgeson, 1977). There appears at first sight to be a large discrepancy between maximum and minimum values, but because of the convention of reporting molality, it amounts to a discrepancy of only $7.5{:}10^{-4}$ molal and hence lies well

Table 1. (cont.)

P(kb)	873°K			973°K			1073°K			1173°K			Isobar error
	A	B	C	A	B	C	A	B	C	A	B	C	
1.00	2900	3179	2856	(3000)	3517	2913	(3500)	4698	3532	(4200)	6650	4349	8
1.25	4000	4281	4012	(4800)	5338	4785	(5700)	6958	5712	(7300)	9756	7010	8
1.50	5150	5300	5093	6650	7008	6546	(8300)	9430	8168	(10400)	13312	10154	8
1.75	5900	6221	6076	8200	8643	8288	(10500)	11986	10747	(13500)	17094	13550	6
2.00	7200	7053	6966	10000	10204	9961	13100	14547	13348	17100	21001	17080	6
2.25	7900	7809	7776	11600	11682	11548	15500	17066	15912	20700	24971	10672	5
2.50	8600	8506	8523	13100	13076	13046	17500	1921	18411	24300	28968	24283	5
2.75	9300	9153	9216	14500	14394	14461	20000	21903	20832	27900	32966	27885	4
3.00	10000	9757	9863	15800	15639	15797	23000	24206	23168	31500	36945	31455	4
3.25	10550	10326	10471	17000	16819	17060	25500	26426	25414	35000	40882	34971	4
3.50	11100	10860	11043	18100	17935	18254	28000	28562	27567	38400	44754	38414	5
4.00	12000	11842	12091	20100	19995	20451	31000	32572	31593	45000	52224	45004	5
5.00	13800	13522	13880	23000	23540	24213	37000	39622	38610	55100	65731	56757	7
6.00	15400	14959	15404	26000	26582	27421	43000	45654	44647	66100	77529	66854	7
7.00	16800	16261	16781	29500	29368	30341	49000	51441	50193	76000	88465	76080	8
8.00	18000	17476	18061	33000	31997	33081	55000	56890	55459	86000	99128	84959	8
9.00	19000	18660	19303	36000	34552	35730	60000	62197	60544	95000	109793	93732	9
10.00	19800	19865	20565	39000	37151	38410	65000	67544	65627	(103000)	120830	102703	9
Isotherm error	4			4			5			5			

Values calculated using mol volumes for water from Burnham et al. (1969).

within the error limits of both Walther and Helgeson (1977) and Fournier and Potter (1982). Since the four-constant equation gives smooth curves joining this value with those in the supercritical range, and gives results within about 5 per cent of Fournier and Potter (1982) in the supercritical range (Table 1), the advantage of the latter is not obvious. Subcritical data were not considered in this study because relative experimental discrepancies within and between studies are much larger than those in the supercritical region.

Fournier (1983) has shown that the solubility of quartz in NaCl brines can be calculated from solubility equations in pure water by correctly calculating the density, (inversely proportional to the mol volume of the solvent). This simple consideration suggsts that the complex theoretical calculations of Walther and Helgeson (1977) may be unnecessary, even for ionized solvents.

In summary, no need has yet been demonstrated for more then four adjustable constants in solubility equations for quartz, and by extension for other silicates (compare Currie, 1968). Equations with more constants should be regarded with suspicion as probably overfitted. Since they are overfitted, good predictions of experimental results do not justify the models. Considering that few, if any, measurements of solubility of silicates in the supercritical range can be considered to be precise to better than ± 5 per cent, and that speciation is unknown for any silicate solution in this range, the composition of aqueous solutions in equilibrium with geological materials can only be considered known in semiquantitative fashion at best, and calculations involving the composition and mass transport qualities of such fluids should be treated as illustrative and qualitative only.

References

Adams, J.B.
1968: Differential solubility of plagioclase in supercritical water; American Mineralogist, v. 53, p. 1603-1613.

Adcock, S.W.
1980: The solubility of silicate minerals in supercritical water; unpublished M.Sc. thesis, Victoria University of Manchester.

Anderson, G.M. and Burnham, S.W.
1965: The solubility of quartz in supercritical water; American Journal of Science, v. 263, p. 495-511.

Burnham, C.W., Holloway, J.R., and Davis, N.F.
1969: Thermodynamic properties of water to 1000°C and 10,000 bars; Geological Society of America, Special Paper 132.

Currie, K.L.
1968: On the solubility of albite in supercritical water in the range 400 to 600°C and 750 to 3500 bars; American Journal of Science, v. 266, p. 321-341.

Davis, N.F.
1972: Experimental studies in the system sodium-alumina trisilicate-water: part I: The apparent solubility of albite in supercritical water; unpublished Ph.D. thesis, The Pennsylvania State University.

Fournier, R.D.
1983: A method of calculating quartz solubilities in aqueous sodium chloride solutions; Geochimica et Cosmochimica Acta, v. 47, p. 579-586.

Fournier, R.D. and Potter, R.W.
1982: An equation correlating the solubility of quartz in water from 25°C to 900°C at pressures up to 10 000 bars; Geochimica et Cosmochimica Acta, v. 46, p. 1969-1973.

Franck, E.U.
1956: Zur Loslichkeit fester Stoffe in verdichten Gasen; Zeitschrift fur physikalische Chemie, v. 6, p. 345-355.

Helgeson, H.C.
1982: Prediction of the thermodynamic properties of electrolytes at high pressures and temperatures; Physics and Chemistry of the Earth, v. 13/14, p. 133-177.

Helgeson, H.C. and Kirkham, D.H.
1976: Theoretical prediction of the thermodynamic properties of electrolytes at high pressures and temperatures. III Equation of state for aqueous species at infinite dilution; American Journal of Science, v. 276, p. 97-240.

Kennedy, G.C.
1950: A portion of the system silica-water; Economic Geology, v. 45, p. 629-653.

Khitarov, N.I.
1956: The 400° isotherm for the system H_2O-SiO_2 at pressures up to 2000 kg/cm^2; Geochemistry, v. 1, p. 55-61.

Knapp, R.B. and Norton, D.
1981: Preliminary numerical analysis of processes related to magma crystallization and stress evolution in cooling pluton environments; American Journal of Science, v. 281, p. 35-68.

Marshall, W.L.
1972: Predictions of the geochemical behaviour of aqueous electrolytes at high temperatures and pressures; Chemical Geology, v. 10, p. 59-68.

Morey, G.W. and Hesselgesser, J.M.
1951: The solubility of quartz and some other substances in superheated steam at high pressures; American Society of Mechanical Engineers, Transactions, v. 73.

Mosebach, R.
1957: Thermodynamic behaviour of quartz and other forms of silica in pure water at elevated temperatures and pressure with conclusions on their mechanism of solution; Journal of Geology, v. 65, p. 347-363.

Semenova, A.I. and Tsiklis, D.S.
1970: Solubilily of silicon dioxide in water vapour at high pressures and high temperatures; Fizikalish Khimie, v. 44, p. 2505-2508.

Spengler, C.J.
1965: The upper three phase region in a portion of the system $KAlSi_2O_6$-SiO_2-H_2O at water pressures from two to seven kilobars; unpublished Ph.D. thesis, The Pennsylvania State University.

Walther, J.V. and Helgeson, H.C.
1977: Calculation of the thermodynamic properties of aqueous silica and the solubility of quartz and its polymorphs at high pressures and temperatures; American Journal of Science, v. 277, p. 1315-1351.

Weare, J.H., Stephens, J.R., and Eugster, H.P.
1976: Diffusion metasomatism and mineral reaction zones: general principles and applications to feldspar alteration; American Journal of Science, v. 276, p. 767-816.

Weill, D.F. and Fyfe, W.S.
1964: The solubility of quartz in the range 1000-4000 bars and 400-550°C; Geochimica et Cosmochimica Acta, v. 28, p. 1243-1255.

NEW DEVELOPMENTS IN THE GSC BOREHOLE GEOPHYSICS TEST AREA AND CALIBRATION FACILITIES

Projects 740085 and 820021

P.G. Killeen, G.R. Bernius, L. Schock, and C.J. Mwenifumbo
Resource Geophysics and Geochemistry Division

Killeen, P.G., Bernius, G.R., Schock, L., and Mwenifumbo, C.J., New developments in the GSC borehole geophysics test area and calibration facilities; in Current Research, Part B, Geological Survey of Canada, Paper 84-1B, p. 373-374, 1984.

Abstract

Two new developments are briefly described, which relate to the calibration and testing of borehole geophysical equipment. These include additional deep test holes recently drilled at the geophysics test area at Bells Corners near Ottawa, and a new model borehole constructed in Ottawa as a preliminary to developing field calibration facilities in Eastern and Western Canada.

Résumé

Les auteurs décrivent brièvement deux nouveaux progrès concernant calibration et l'essai du matériel géophysique de sondage. Il s'agit notamment de sondages profonds supplémentaires récemment forés sur les lieux de la station d'essais géophysique à Bells Corners près d'Ottawa ainsi que d'un nouveau trou de sondage modèle construit à Ottawa dans le cadre d'un programme visant à perfectionner des installations de calibration sur le terrain dans l'Est et dans l'Ouest du Canada.

New deep test holes at Bells Corners

The Geological Survey of Canada has completed 730 m of new diamond drilling at the borehole geophysics test area at Bells Corners near Ottawa. This is part of an on-going program to provide facilities for testing and evaluating borehole logging instrumentation and development of new borehole geophysical techniques (Killeen, 1978; Killeen and Conaway, 1978). The new holes are offset (Fig. 1) from the previously drilled line of holes described by Bernius (1981), to allow an expanded range of hole-to-hole measurements to be used and thereby develop methods to produce a three dimensional picture of the geology and structure.

The drilling consisted of deepening borehole BC 81/4 from 120 m to 300 m, as well as drilling two new holes, BC 84/5 (250 m depth) and BC 84/6 (300 m depth). Figure 1 shows the locations of the boreholes which form a triangular pattern. A triangle with 30 m sides is formed by BC 81/1, BC 81/3, and BC 84/5. A triangle with 100 m sides is formed by BC 81-1, 81-4, and BC 84-6. Over 99% of the core was recovered from all of the vertically drilled NQ size boreholes. The geology is similar to that described for the first set of holes (Bernius, 1981). The top 65 m is Upper Cambrian Nepean sandstone which is separated from the underlying Precambrian mixed granite and gneiss at an unconformity marked by a 17 m thick alteration zone of Precambrian rocks. Detailed geological logs are being prepared and will be available to users of the test area. This will make it possible to correlate the geophysical data with structural, petrological and lithological information. There is presently considerable interest in the development of hole-to-hole acoustic and electrical methods for the mapping of fractures and faults between boreholes. For this reason the geological log includes descriptions of fractures, faults and joints.

New multiple-zone calibration facility in Ottawa

A multiple-zone model borehole has been designed for calibration of logging probes, and for testing and evaluation of the calibration zones to be used in future field calibration models. The new calibration facility, located in Ottawa, consists of a series of zones in the form of concrete cylinders placed in contact with each other in a configuration as shown in Figure 2. Each cylinder represents a 'zone' with specific known physical properties for which the logging tool response can be evaluated. The horizontal model borehole produced by the alignment of the axial holes in the individual zones, will be used to calibrate logging tools as they are pulled through the successive zones.

Initial construction of the calibration facility includes a series of calibration zones with different densities as shown in Figure 3. These zones, when tested for homogeneity and accurately measured for density, will be shipped to field calibration facilities to be established in western and eastern Canada for coal logging. The field calibration facilities will

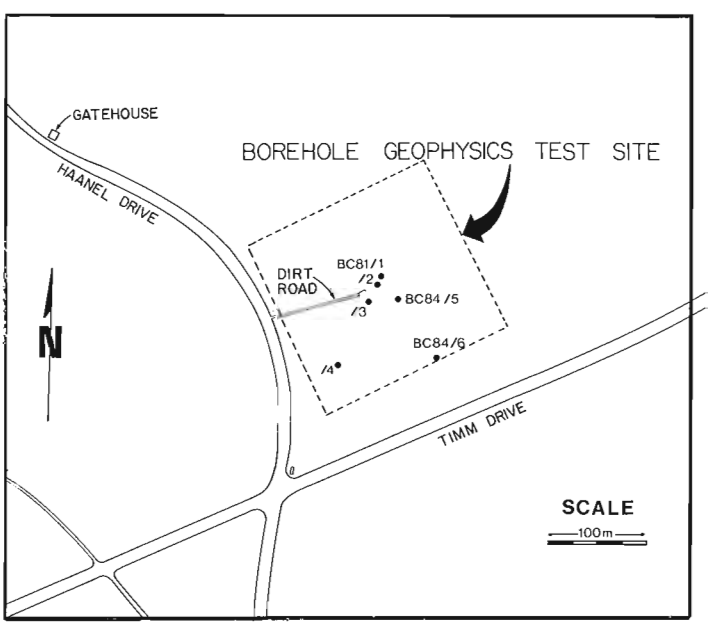

Figure 1. *Location of boreholes near Ottawa for testing and evaluating borehole logging instrumentation. The borehole geophysics test area, at the intersection of Haanel Drive and Timm Drive is near the entrance to the CANMET Mining Research Laboratories, Bells Corners complex (note gatehouse).*

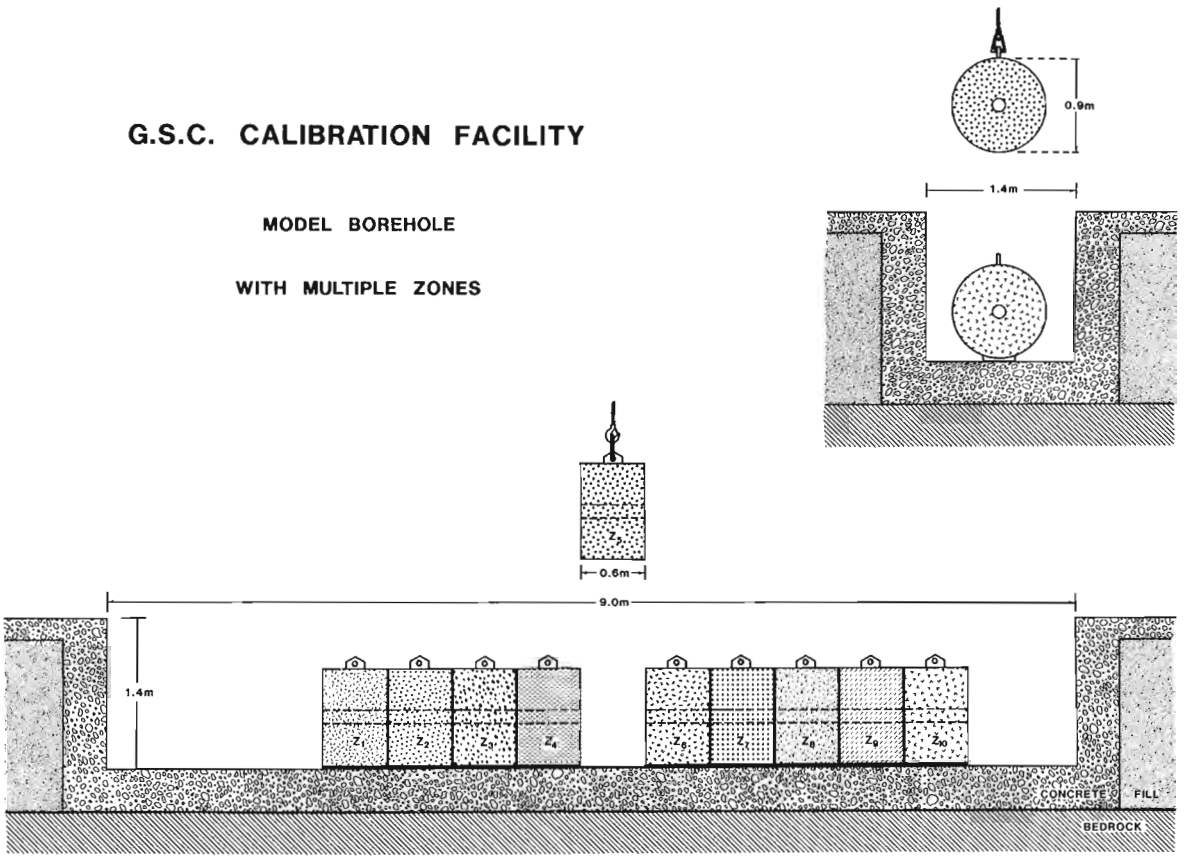

Figure 2. *Configuration of cylindrical concrete zones used for calibration of borehole logging probes. Each zone will have specific known physical properties. The horizontal configuration makes it easy to interchange zones using an overhead crane assembly. Some calibration zones will be shipped to other areas in Canada to establish field calibration model boreholes.*

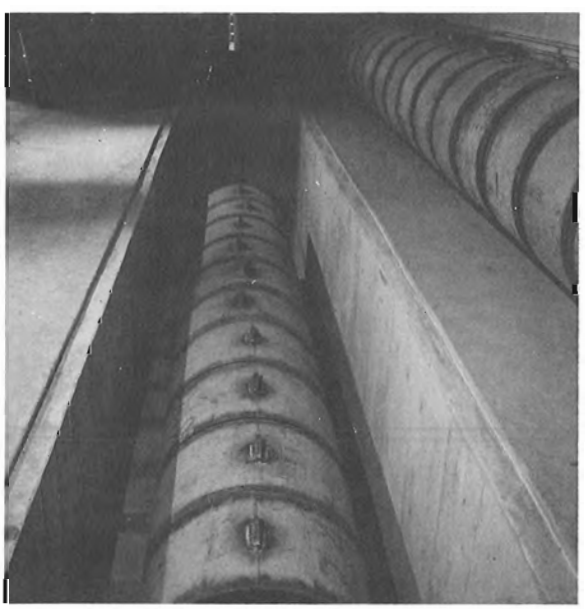

Figure 3. *The multiple-zone horizontal model borehole in its below-ground tank, located in the Borehole Geophysics Laboratory at Aberdeen Street, Ottawa. (GSC 204145-B)*

be model boreholes consisting of a vertical stack of calibration zones, contained in an appropriate below-ground tank.

Both the Ottawa primary facility and the two field calibration facilities will have provision for saturating the model borehole with water to simulate most field conditions. The horizontal configuration of the Ottawa model borehole makes it a versatile facility allowing removal and insertion of different calibration zones during testing and evaluation as shown in Figure 2.

It is expected that the Ottawa facility will be used to develop standardized calibration zones for other physical properties such as porosity, or magnetic susceptibility. These will be added to the field calibration facilities as they become available.

References

Bernius, G.R.
1981: Boreholes near Ottawa for the development and testing of borehole logging equipment – a preliminary report; in Current Research, Part C, Geological Survey of Canada, Paper 81-1C, p. 51-53.

Killeen, P.G.
1978: Gamma-ray spectrometric calibration facilities – a preliminary report; in Current Research, Part A, Geological Survey of Canada, Paper 78-1A, p. 243-247.

Killeen, P.G. and Conaway, J.G.
1978: New facilities for calibrating gamma-ray spectrometric logging and surface exploration equipment; Canadian Institute of Mining and Metallurgical Bulletin, 793, p. 84-87.

COMPUTER PROGRAMS FOR PRODUCTION OF SHADED RELIEF AND STEREO SHADED RELIEF MAPS

Project 820027

D. Teskey and J. Broome
Resource Geophysics and Geochemistry Division

Teskey, D. and Broome, J., Computer programs for production of shaded relief and stereo shaded relief maps; in Current Research, Part B, Geological Survey of Canada, Paper 84-1B, p. 375-389, 1984.

Abstract

Shaded relief and stereo shaded relief maps which emphasize small amplitude features can be produced from grids of magnetic field data. Two computer programs are provided with which the reflectance grids representing these maps can be calculated from a magnetic field grid and a third program plots these reflectance grids on an Applicon plotter.

Résumé

On peut produire des cartes de relief par estompage normales et à trois dimensions qui font ressortir des traits de faible amplitude, à partir de grilles de données du champ magnétique. Deux programmes d'ordinateur pouvant servir à calculer les grilles de réflectance représentant ces cartes à partir d'une grille du champ magnétique sont fourni; un troisième programme restitue ces grilles de réflectance sur un restituteur Applicon.

Shaded magnetic relief maps

Shaded magnetic relief maps have proved to be a useful method for the enhancement of small amplitude features in magnetic field data. In many cases small amplitude features which are invisible on conventional contour maps and colour plotted maps are clearly visible on shaded relief images. These synthetic images are created using a simplified model based on the reflectance of the magnetic surface as defined by the angle between the normal to a local surface element and a supposed sun angle. Examples of shaded magnetic relief maps for the Lockhart River Sheet, IMW NP 12/13 are given in Figure 1a and b at 30° inclination and 45° and 135° declination respectively. The principles and application of these techniques are described in more detail in Dods et al. (1984).

Directional features in the data can be enhanced by carefully choosing the incident light directions since features striking perpendicular to the incident light direction will be emphasized. Thus pairs of shaded relief images with perpendicular illumination directions are useful for general interpretation.

Stereo shaded relief maps

Despite the above-mentioned advantage of shaded relief maps the amplitude information on the original magnetic anomaly map is lost. This amplitude information can be recovered by producing a second offset shaded relief image with a parallax based on the amplitude of the magnetic field and viewing the offset and original images as a stereo pair. This technique is a simplified form of a method developed at the Canada Centre for Remote Sensing for analyzing satellite image data (Simard, 1982) which has been successfully applied to magnetic data[1]. The stereo pair of images are plotted superimposed on the same sheet in two different colours; the original shaded relief image in cyan and the offset image in magenta. By viewing the resulting double image using glasses with an appropriate filter over each eye the correct three-dimensional image can be perceived.

This three-dimensional image exhibits an apparent relief corresponding to the amplitude of the magnetic field with the shaded relief image superimposed. Considerably more information can be seen using this method than using either normal shaded relief maps or conventional colour maps.

Three programs; SHADE, STEREO and SHDPLT, are presented in the Appendix which allow shaded relief images and stereo shaded relief images to be calculated from an input grid of magnetic field data and plotted on an Applicon ink-jet plotter. Of the three programs only SHDPLT is specific to the Applicon plotter. These programs are all written in Fortran IV and are presently in use at the Computer Science Centre of the Department of Energy, Mines and Resources in Ottawa.

Program : SHADE

From an input grid of magnetic field data the program SHADE calculates an output grid of reflectance values. The input grid format is one integer record containing the number of grid rows and columns followed by real grid data written column by column from left to right.

Incident light direction is entered by the user as degrees of inclination from the horizontal and as degrees of declination measured clockwise from north. A scale factor is also entered to allow control over the vertical relief of the calculated image. The cosine of the angle between the incident light direction and the local surface normal is then calculated. This value varies between zero for a surface with no illumination and one for a fully illuminated surface. This simplified model does not consider cast shadows.

A histogram is plotted in the output showing the percentage of pixels in the seventeen grey levels plotted by program SHDPLT. If an appropriate scale factor is used the pixels will be distributed among a number of grey levels while too large a scale factor will cause all the pixels to cluster in one or two levels causing the resulting map to have low contrast.

Program : STEREO

Input to STEREO is the magnetic field grid and the reflectance grid calculated by program SHADE.

[1] A paper discussing the application of these techniques to geological problems is under preparation.

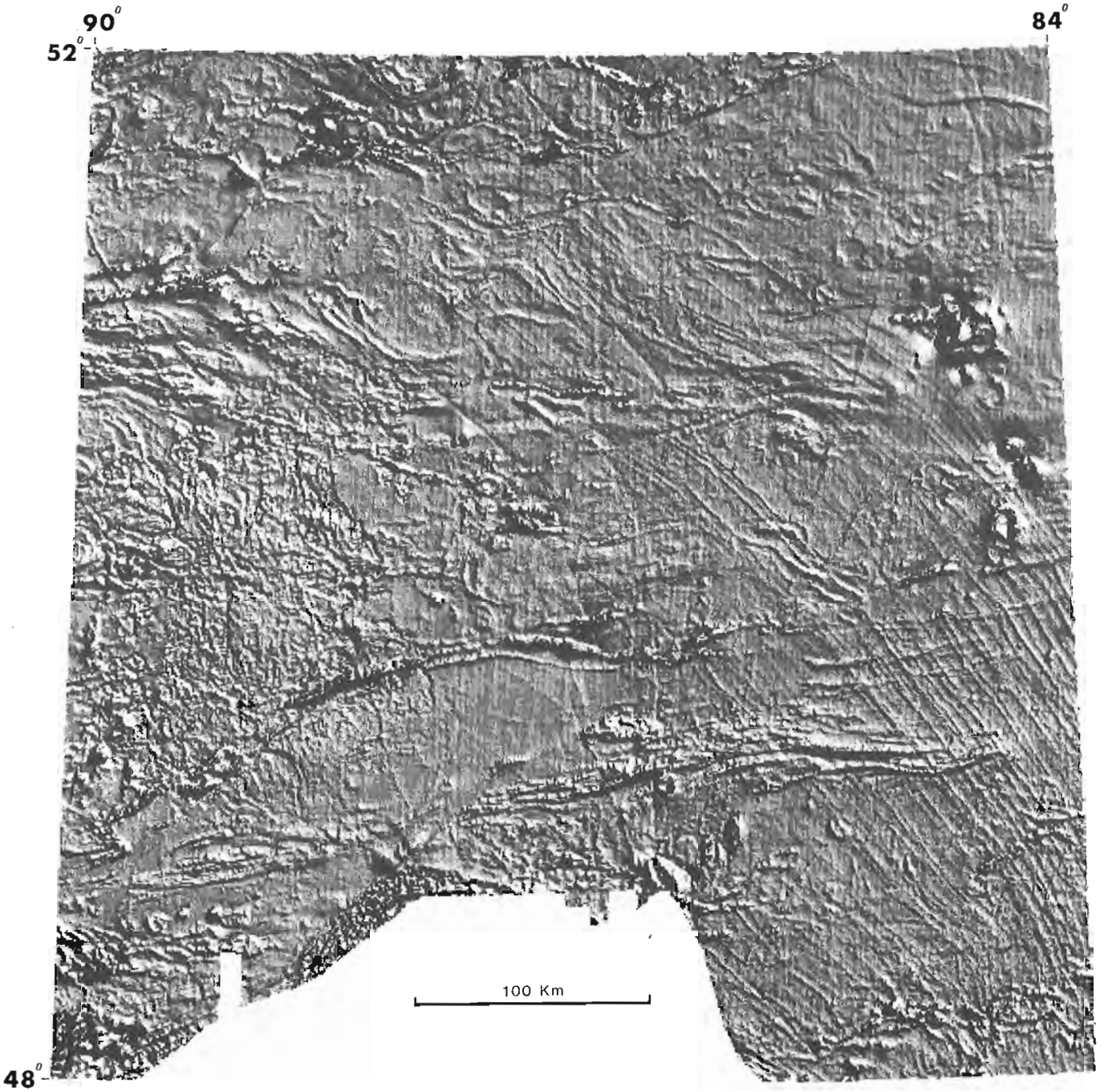

Figure 1a. *Shaded magnetic relief map IMW NM 16. Inclination = 40°; declination = 45°*

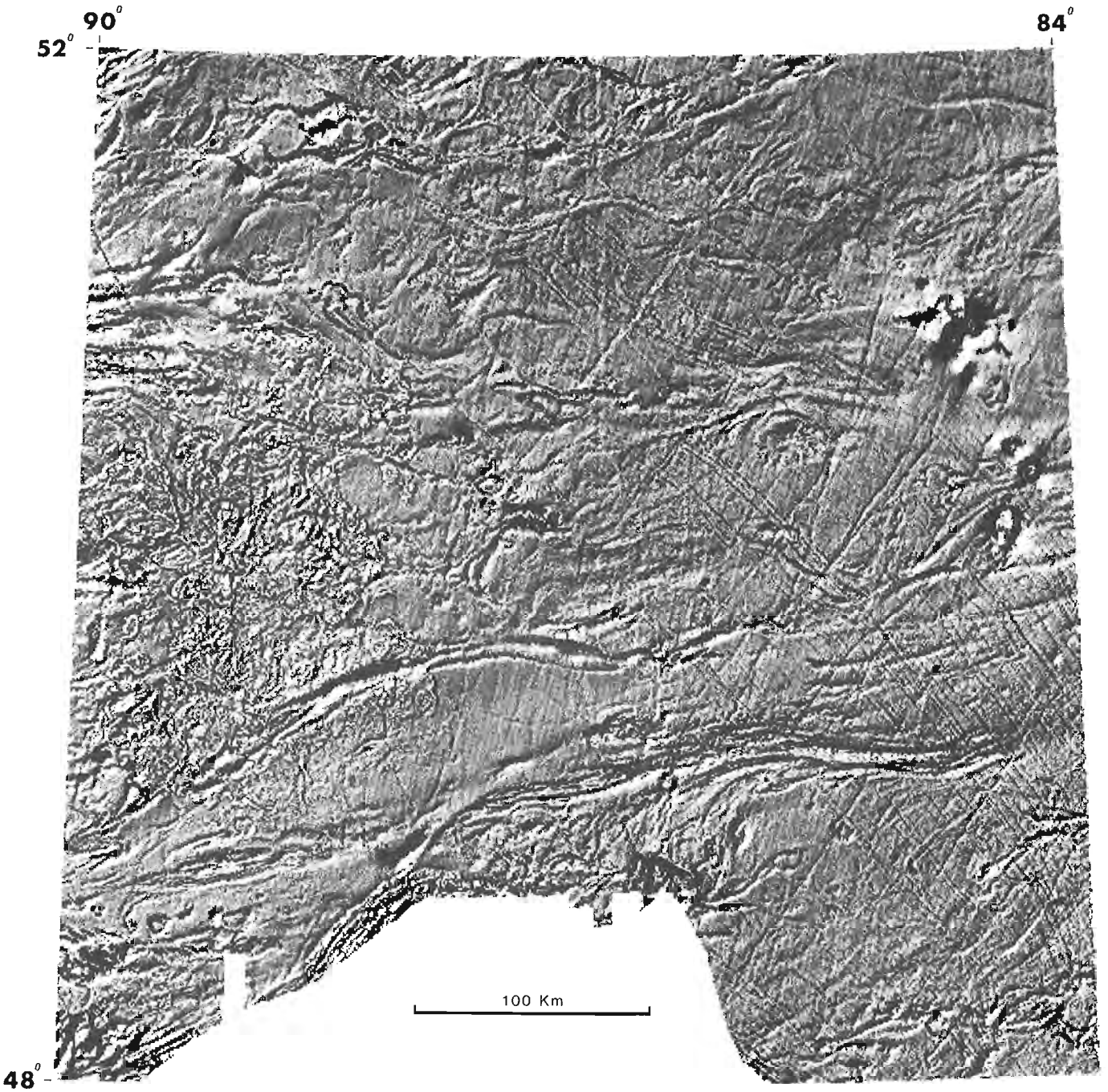

Figure 1b. *Shaded magnetic relief map IMW NM 16. Inclination = 40°; declination = 135°.*

An offset reflectance grid is calculated by applying a parallax determined by the magnetic field amplitude to the normal reflectance grid. The user enters a background magnetic value which serves as the base value and a scaling factor which determines the amount of parallax in the offset image. The background magnetic value is calculated automatically if the user enters a value of zero. The amount of offset is then proportional to the difference between the magnetic field amplitude and the background at each pixel.

Program : SHDPLT

SHDPLT creates a plot tape specifically for an Applicon ink-jet plotter from the grids created by SHADE and STEREO. Calls to Applicon "COLOR" software are used to create the plot file; however, calls to other software packages could be substituted to allow the use of other types of raster display devices. Values from the grids are mapped onto 17 colour intensity levels. A reflectance value of zero representing a completely shaded surface would be set to maximum intensity level 17.

One of two modes of operation: "stereo" or "shade" must be specified by the user. For a normal shaded relief plot only the output from program SHADE is input and the mode of operation set to "shade". In this mode the intensities of the three ink colours used on the plotter are set equal resulting in a grey-tone image. A alternate method of presentation can be seen on the published 1:1 000 000 scale "Magnetic shadowgram" of the Lockhart River sheet (Geological Survey of Canada, 1983). In this method the reflectance values of zero to one are mapped onto twenty colours ranging from deep purple for a completely shaded surface to bright yellow for a completely illuminated surface.

For a stereo shaded relief plot both the outputs from program SHADE and STEREO are input. Both images are plotted superimposed on the same sheet with the original reflectance grid in cyan and the offset reflectance grid in magenta. The reflectance values are mapped onto the 17 colour intensity levels using the same method as the normal shaded relief plot. An alternate method would be to produce a stereo pair of normal shaded relief plots and to view them using a stereo viewer. This could be done by plotting the output grids from programs SHADE and STEREO separately using SHDPLT in the "shade" mode.

References

Geological Survey of Canada
1983: Magnetic shadowgram of Lockhart River Northwest Territories (1:1 000 000); Geological Survey of Canada Map 1586A (inclination 40°, declination 45°), Map 1587A (inclination 40°, declination 135°).

Dods, S.D., Teskey, D.J., and Hood, P.J.
1984: The new 1:1 000 000 magnetic anomaly map series of the Geological Survey of Canada – compilation techniques and interpretation; in Society of Exploration Geophysicists Publication on the Utility of Regional Gravity and Magnetic Maps.

Simard, R.
1982: Improved Spatial and Alternative Information from Spot Composite Imagery; Proceedings of the last Symposium on Remote Sensing of Environment Second Thematic Conference "Remote Sensing for Exploration Geology"; Forth Worth Texas, v. 1, p. 433-444.

```
C ***************************************************************************
C
C PROGRAM : SHADE
C
C REVISION : 1.4 , FEB.29 , 1984.
C
C PURPOSE : THIS PROGRAM CALCULATES REFLECTANCE VALUES FOR EACH GRID
C           CELL ON A TOTAL FIELD MAGNETIC GRID FOR A USER SPECIFIED
C           INCIDENT SUN DIRECTION.
C
C DESCRIPTION :A GRID OF TOTAL FIELD MAGNETIC DATA IS INPUT AND A
C           EQUAL SIZE GRID OF REFLECTANCE VALUES IS OUTPUT.
C           REFLECTANCE IS CALCULATED BY TAKING THE DOT PRODUCT
C           OF THE UNIT VECTORS REPRESENTING THE LOCAL NORMAL TO
C           THE MAGNETIC SURFACE AND THE INCIDENT LIGHT DIRECTION.
C           THE REFLECTANCE VALUES VARY FROM 0 TO 1 WITH 0 REPRESENTING
C           A SURFACE COMPLETELY IN SHADOW. A USER SUPPLIED SCALE FACTOR
C           IS USED TO CONTROL VERTICAL EXAGGERATION.
C           A HISTOGRAM IS PLOTTED OF THE OUTPUT GRAY LEVELS.
C            MAXIMUM NUMBER OF GRID ROWS ON INPUT IS 1000.
C
C FILES : TAPE5 - INPUT AND CONTROL
C         TAPE6 - OUTPUT LISTING
C         TAPE9 - INPUT MAGNETIC GRID WRITTEN COLUMN BY COLUMN
C                 FROM LEFT TO RIGHT.
C         TAPE11- OUTPUT REFLECTANCE GRID IN THE SAME FORMAT AS TAPE9
C
C DATA INPUT : ONE RECORD ; 3F10.0 FORMAT.
C              SI - SUN INCLINATION IN DEGREES FROM HORIZONTAL
C              SD - SUN DECLINATION IN DEGREES CLOCKWISE FROM NORTH
C              SCFACT - SCALE FACTOR FOR VERTICAL EXAGGERATION
C
C WRITTEN BY: D. TESKEY AND J. BROOME
C             REGIONAL GEOPHYSICS SUBDIVISION
C             RESOURCE GEOPHYSICS AND GEOCHEMISTRY DIVISION
C             GEOLOGICAL SURVEY OF CANADA
C             ENERGY MINES AND RESOURCES
C
C ***************************************************************************
C
      PROGRAM SHADE(INPUT,OUTPUT,TAPE5=INPUT,TAPE6=OUTPUT,TAPE9,TAPE11)
      REAL L1,M1,N1,L2,M2,N2,LS,MS,NS,LN,MN,NN,MG
      DIMENSION MG(1000),RG(1000),NCNT(17),VAL(18)
C
      DATA INPUT/5/,IOUT/6/,IMG/9/,IRG/11/
      DATA BNDVAL/-9999.0/,NINT/17/
C
C
C READ HEADER FROM INPUT GRID;NR=NO. OF ROWS IN GRID
C                             NC=NO. OF COLUMNS IN GRID
C
      READ(IMG)NR,NC
C
C CHECK IF INPUT GRID EXCEEDS SIZE LIMIT OF 1000*1000
C
      IF(NR.LE.1000.AND.NC.LE.1000) GO TO 10
      WRITE(IOUT,1002)NR,NC
1002  FORMAT(1H1,*ERROR ! ,INPUT GRID SIZE (NR,NC) OF*,
     *2I6,* EXCEEDS 1000 BY 1000 LIMIT !*)
      GO TO 999
C
10    WRITE(IOUT,1005)NR,NC
1005  FORMAT(1H1,* INPUT GRID NR,NC = *,2I8)
      NRM1=NR-1
      NCM1=NC-1
C
```

```
C WRITE HEADER TO OUTPUT GRID FILE.
C
      WRITE(IRG)NR,NC
C
C READ SUN INCLINATION,SUN DECLINATION, AND VERTICAL SCALE FACTOR
C  FROM INPUT
C
      READ(INPUT,1010)SI,SD,SCFACT
1010  FORMAT(2F10.0,F13.3)
      WRITE(IOUT,1015)SI,SD,SCFACT
1015  FORMAT(1H ,* SUN INCLINATION ENTERED = *,F10.0,/,
     +* SUN DECLINATION ENTERED = *,F10.0,/,
     +* VERTICAL SCALE FACTOR ENTERED = *,F15.5)
C
C INITIALIZE BUFFER AND SET VALUE LIMITS FOR HISTOGRAM
C
      DO 100 KK=1 , NINT
       NCNT(KK) = 0
       VAL(KK+1) = 0.0589 * FLOAT(KK)
100   CONTINUE
      VAL(1) = 0.0
C
C CALCULATE UNIT VECTOR FOR INCIDENT LIGHT DIRECTION
C
      PI=3.14159/180.
      LS=COS(SI*PI)*SIN(SD*PI)
      MS=COS(SI*PI)*COS(SD*PI)
      NS=SIN(SI*PI)
C
C READ IN FIRST COLUMN FROM INPUT GRID
C
      READ(IMG)(MG(K),K=1,NR)
C
C FOR EACH COLUMN ON THE INPUT GRID
C
      DO 500 ICOL=1,NCM1
C
C USE OUTPUT COLUMN BUFFER TO STORE LAST INPUT COLUMN TEMPORARILY
C
      DO 20 IPIX=1,NR
       RG(IPIX) = MG(IPIX)
20    CONTINUE
C
C READ IN NEXT COLUMN FROM INPUT GRID
C
      READ(IMG)(MG(J),J=1,NR)
C
C FOR EACH POINT IN THE GRID COLUMN
C ***************************************************************
C
      DO 510 IPIX=1,NRM1
C
C IF GRID CELL IS IN BOUNDRY AREA SKIP IT AND SET OUTPUT = BNDVAL
C
      IF(MG(IPIX).EQ.BNDVAL) GO TO 509
      IF(MG(IPIX+1).EQ.BNDVAL) GO TO 509
      IF(RG(IPIX).EQ.BNDVAL) GO TO 509
      IF(RG(IPIX+1).EQ.BNDVAL) GO TO 509
C
C CALCULATE UNIT VECTOR NORMAL TO MAGNETIC SURFACE
C
50    D1=(RG(IPIX)-MG(IPIX))/SCFACT
      R1=SQRT(1.+D1**2)
      L1=1./R1
      M1=0.
      N1=D1/R1
      D2=(MG(IPIX)-MG(IPIX+1))/SCFACT
      R2=SQRT(1.+D2**2)
      L2=0.
```

```
      M2=1./R2
      N2=D2/R2
      LN=M1*N2-N1*M2
      LN=-LN
      MN=N1*L2-L1*N2
      MN=-MN
      NN=L1*M2-M1*L2
C
C CALCULATE THE COSINE OF THE ANGLE BETWEEN THE TWO UNIT VECTORS
C  OR DOT PRODUCT
C
      CSI=LN*LS+MN*MS+NN*NS
      CSI=CSI/SQRT(LS**2+MS**2+NS**2)/SQRT(LN**2+MN**2+NN**2)
      IF(CSI.LT.0.0) CSI=C.C
      IF(CSI.GT.1.0) CSI=1.0
C
C DETERMINE SHADING LEVEL AND INCREMENT APPROPRIATE COUNTER
C
      INT = 17 - IFIX(CSI/0.0589)
      NCNT(INT) = NCNT(INT) + 1
C
C SET OUTPUT GRID VALUE EQUAL TO DOT PRODUCT (REFLECTANCE)
C
      RG(IPIX)=CSI
C
      GO TO 510
5C9   RG(IPIX) = BNDVAL
C
510   CONTINUE
C
C WRITE COLUMN OF REFLECTANCE VALUES TO OUTPUT GRID FILE.
C
      RG(NR)=RG(NR-1)
      WRITE(IRG)(RG(J),J=1,NR)
C
5CC   CONTINUE

C
C WRITE LAST COLUMN TO OUTPUT  GRID AGAIN TO COMPLETE OUTPUT
C
      WRITE(IRG)(RG(J),J=1,NR)
      ENDFILE IRG
C
C CALL SUBROUTINE TO PLOT HISTOGRAM OF GRAY LEVELS
C
      WRITE(IOUT,1050)
1050  FORMAT(1H0,*HISTOGRAM SHOWING POPULATIONS OF THE 17 GRAY LEVELS*)
       CALL HISTO(NINT,NCNT,VAL,IOUT)
C
999   STOP
      END


       SUBROUTINE HISTO (N,NY,VAL,IOUT)
 C
 C ***************************************************************************
 C SUBROUTINE - HISTO
 C
 C REVISION - 1.0 , FEB 27/84 , BROOME
 C
 C PURPOSE - TO PLOT A HISTOGRAM OF "N" INTERVALS WITH "NY"EVENTS
 C           IN EACH INTERVAL ON A 132 COLUMN LINE PRINTER
 C
 C INPUT VARIABLES - N - NUMBER OF INTERVALS(MAX. = 200)
 C                   NY - NUMBER OF EVENTS IN  EACH INTERVAL
 C                   YVAL - RANGE OF INTERVAL(EG. FOR N=1 ,
 C                            RANGE IS FROM VAL(1) TO VAL(2))
 C                   IOUT - DEVICE NUMBER FOR PRINTER
```

```
C
C ***********************************************************************
C
      DIMENSION NY(200),VAL(200),H(10),A(11),Y(200)
C
      DATA A/10H          ,
     +       10HX         ,
     +       10HXX        ,
     +       10HXXX       ,
     +       10HXXXX      ,
     +       10HXXXX5     ,
     +       10HXXXX5X    ,
     +       10HXXXX5XX   ,
     +       10HXXXX5XXX  ,
     +       10HXXXX5XXXX ,
     +       10HXXXX5XXXX0/
C
C PRINT HEADER
C
      WRITE(IOUT,1001)
1001  FORMAT(1HO,*   SUBROUTINE HISTO 1.0*,/
     +*    ---------------------*,//,
     +*   I  EVENTS(I)      RANGE(I)          PERCENTAGE OF TOTAL*,
     +* (1 CHARACTER PER %)*,/)
C
C CALCULATE PERCENTAGE FOR EACH INTERVAL
C
      TOTN = 0.0
      DO 200 J=1 ,N
      Y(J) = FLOAT(NY(J))
      TOTN = TOTN + Y(J)
200   CONTINUE
C
C FOR EACH INTERVAL
C
      DO 300 J=1, N
C
C BLANK OUT PLOT ARRAY "H"
C
      DO 310 K= 1 , 10
      H(K) = A(1)
310   CONTINUE
C
C CALCULATE PERCENTAGE
C
      PER = Y(J) * 100.0 / TOTN
C
C SET UP PLOT
C
      NA = IFIX((PER+ .5)/ 10.0)
      NREM = IFIX(PER+ .5) - NA*10
      DO 320 L=1, NA
      H(L) = A(11)
320   CONTINUE
C
      H(NA+1) = A(NREM+1)
C
C PRINT OUTPUT FOR INTERVAL "J"
C
      WRITE(IOUT,1002)J,NY(J),VAL(J),VAL(J+1),H
1002  FORMAT(1H ,I3,I8,F9.2,* -*,F9.2,2X,10A10)
C
300   CONTINUE
C
      WRITE(IOUT,1003)
1003  FORMAT(1HO,*... END OF SUBROUTINE HISTO*)
      RETURN
      END
```

```
C ***************************************************************************
C
C PROGRAM : STEREO
C
C REVISION : 1.5 , MAR. 7 1984
C
C PURPOSE : THIS PROGRAM PRODUCES A GRID TAPE THAT CONTAINS AN
C           IMAGE OFFSET FROM THE INPUT REFLECTANCE GRID. THIS
C           GRID CAN BE PLOTTED TOGETHER WITH THE ORIGIONAL
C           REFLECTANCE GRID AS A STEREO PAIR.
C
C DESCRIPTION : A GRID OF MAGNETIC FIELD DATA AND A REFLECTANCE
C           GRID FOR THE SAME AREA ARE INPUT. BY OFFSETTING THE GRID
C           VALUES ON THE REFLECTANCE GRID TO THE LEFT A DISTANCE
C           DETERMINED FROM THE AMPLITUDE OF THE FIELD, A SECOND OUTPUT
C           REFLECTANCE GRID IS CALCULATED. A BACKGROUND VALUE IS
C           CALCULATED TO SET THE MINIMUM FIELD VALUE NEAR ZERO OR
C           A USER SELECTED BACKGROUND MAY BE USED.
C           A PARALLAX SCALING FACTOR MUST BE ENTERED AS WELL TO
C           DETERMINE THE EXTENT OF THE OFFSET.
C
C FILES  : TAPE5 - INPUT AND CONTROL
C          TAPE6 - OUTPUT LISTING
C          TAPE9 - INPUT MAGNETIC FIELD GRID WRITTEN COLUMN BY COLUMN
C                  FROM LEFT TO RIGHT.
C          TAPE11- INPUT REFLECTANCE GRID,SAME FORMAT AS TAPE9
C                  ( OUTPUT FROM PROGRAM SHADE )
C          TAPE13- OUTPUT OFFSET REFLECTANCE GRID,SAME FORMAT AS TAPE9
C
C DATA INPUT : ONE RECORD , 2F10.2 FORMAT
C          PARSF - PARALLAX SCALING FACTOR
C          BCKMAG - MAG. BACKGROUND VALUE (0 FOR AUTOMATIC)
C
C WRITTEN BY : D. TESKEY AND J. BROOME
C              REGIONAL GEOPHYSICS SUBDIVISION
C              RESOURCE GEOPHYSICS AND GEOCHEMISTRY DIVISION
C              GEOLOGICAL SURVEY OF CANADA
C              ENERGY , MINES AND RESOURCES
C
C ***************************************************************************
C
      PROGRAM STEREO(INPUT,OUTPUT,TAPE5=INPUT,TAPE6=OUTPUT,TAPE9,
     *TAPE11,TAPE13)
C
      REAL MG
      DIMENSION MG(1000),ORG(18,1000),KC(18)
      DATA IMG/9/,IRG/11/,IORG/13/,INPUT/5/,IOUT/6/,BNDVAL/-9999./
      DATA BCKMAG/99999./
C
C READ IN INPUT GRID HEADERS AND STOP IF UNEQUAL
C
      READ(IMG)NR,NC
      READ(IRG)NRRG,NCRG
      IF(NR.EQ.NRRG.AND.NC.EQ.NCRG) GO TO 10
C
      WRITE(IOUT,1005)NR,NC,NRRG,NCRG
1005  FORMAT(1H1,* ERROR, INPUT GRID SIZES UNEQUAL ! *,/,
     *** TOTAL FIELD GRID ; NR,NC = *,2I8,/,
     ** REFLECTANCE GRID ; NR,NC = *,2I8)
      GO TO 999
C
C CHECK IF INPUT GRID EXCEEDS 1000 ROW LIMIT
C
10    IF(NR.LE.1000) GO TO 20
      WRITE(IOUT,1008)NR,NC
1008  FORMAT(1H1,*ERROR !,INPUT GRID SIZE(NR,NC) OF *,2I6,
     ** EXCEEDS 1000 ROW LIMIT*)
      GO TO 999
C
C PRINT OUT GRID SIZE AND WRITE TO OUTPUT
C
20    WRITE(IOUT,1010)NR,NC
```

```
1010  FORMAT(1H1,* INPUT GRID SIZE ; NR,NC = *,2I8)
      WRITE(IORG)NR,NC
C
C READ IN PARALLAX SCALING FACTOR AND MAG. BACKGROUND
C
      READ(INPUT,1015)PARSF,BCKMAG
1015  FORMAT(2F10.2)
      IF(BCKMAG.NE.0.0) GO TO 90
C
C SEARCH INPUT MAG. FIELD GRID FOR MINIMUM VALUE IF REQUIRED
      BCKMAG = 9999999.9
      DO 80 KCOL=1,NC
       READ(IMG)(MG(I),I=1,NR)
C
       DO 70 IPIX=1 , NR
        IF(MG(IPIX).EQ.BNDVAL) GO TO 70
        IF(MG(IPIX).LT.BCKMAG) BCKMAG= MG(IPIX)
70     CONTINUE
80    CONTINUE
      BCKMAG = (-1) * BCKMAG
      REWIND IMG
      READ(IMG)IDUM,IDUM,IDUM,IDUM
      READ(IMG)NR,NC
C
C
90    WRITE(IOUT,1020)BCKMAG,PARSF
1020  FORMAT(1H ,*MAGNETIC BACKGROUND VALUE = *,F10.2,/,
     +* OFFSET SCALING FACTOR = *,F10.2)
C
      IOFFSUM = IOFFCNT = IERROR = 0
      CNTTOT = OFFTOT = 0.0
      IOFFLIM = 18
C
C FOR THE FIRST 18 COLUMNS ON THE INPUT GRIDS
C ********************************************
C
      DO 100 LCOL=1,18
C
C READ ONE COLUMN FROM EACH INPUT GRID
C
       READ(IRG)(ORG(LCOL,I),I=1,NR)
       READ(IMG)(MG(I),I=1,NR)
C
C FOR EACH PIXEL IN CURRENT COLUMN CALCULATE OFFSET
C
       DO 110 IPIX=1,NR
        IF(MG(IPIX).EQ.BNDVAL) GO TO 110
        IF(ORG(LCOL,IPIX).EQ.BNDVAL) GO TO 110
        IOFF=(MG(IPIX)+BCKMAG)/PARSF
C
        IOFFSUM = IOFFSUM + IOFF
        IOFFCNT = IOFFCNT + 1
        IF(IOFF.GT.IOFFLIM) IOFF = IOFFLIM
        IFCOL=LCOL-IOFF
        IF (IFCOL.GT.17) IFCOL=17
C
C  PUT REFLECTANCE VALUES IN OFFSET POSITION IN OUTPUT BUFFER
C
        LCOLM1 = LCOL -1
        DO 120 ICOL=IFCOL , LCOLM1
         ORG(ICOL,IPIX) = ORG(LCOL,IPIX)
120     CONTINUE
C
110   CONTINUE
C
C CALL SUBROUTINE TO CALCULATE OFFSET LIMIT AND PRINT DIAGNOSTICS
C
      IF(IOFFCNT.EQ.0) GO TO 101
      CALL OFFSET(LCOL,IOFFSUM,IOFFCNT,OFFTOT,CNTTOT,IOFFLIM,IERROR)
```

```
      IF(IERROR.EQ.1) GO TO 999
C
101   KC(LCOL) = LCOL
100   CONTINUE
C
C FOR COLUMNS 19 TO THE LAST COLUMN ON THE INPUT GRIDS
C ***************************************************
C
      DO 200 LCOL = 19 , NC
C
C SHIFT COUNTERS IN 18 COLUMN BUFFER OVER 1 COLUMN
C
      NEWC = KC(1)
      DO 210 K=1 , 17
       KC(K) = KC(K+1)
210   CONTINUE
      KC(18) = NEWC
C
C OUTPUT COLUMN 1 FROM 18 COLUMN BUFFER
C
      WRITE(IORG)(ORG(NEWC,I),I=1,NR)
C
C READ IN ONE COLUMN FROM BOTH INPUT GRIDS
C
      READ(IRG)(ORG(NEWC,I),I=1,NR)
      READ(IMG)(MG(I),I=1,NR)
C
C CALCULATE OFFSET FOR EACH PIXEL IN CURRENT COLUMN
C
      DO 230 IPIX=1 , NR
       IF(ORG(NEWC,IPIX).EQ.BNDVAL) GO TO 230
       IF(MG(IPIX).EQ.BNDVAL) GO TO 230
       IOFF = (MG(IPIX)+BCKMAG)/PARSF
       IOFFSUM = IOFFSUM + IOFF
       IOFFCNT = IOFFCNT + 1
       IF(IOFF.GT.IOFFLIM) IOFF = IOFFLIM
       IFCOL = 18 - IOFF
       IF(IFCOL.GT.17) IFCOL = 17
C
C
C WRITE  REFLECTANCE VALUES TO OFFSET POSITIONS IN OUTPUT BUFFER
C
       DO 234 ICOL=IFCOL , 17
        ORG(KC(ICOL),IPIX) = ORG(NEWC,IPIX)
234    CONTINUE
230   CONTINUE
C
C CALL SUBROUTINE TO CALCULATE OFFSET LIMIT AND PRINT DIAGNOSTICS
C
      IF(IOFFCNT.EQ.0) GO TO 200
      CALL OFFSET(LCOL,IOFFSUM,IOFFCNT,OFFTOT,CNTTOT,IOFFLIM,IERROR)
      IF(IERROR.EQ.1) GO TO 999
200   CONTINUE
C
C ON COMPLETION OUTPUT THE 18 COLUMNS REMAINING IN THE BUFFER
C
      DO 300 JCOL=1 , 18
       WRITE(IORG)(ORG(KC(JCOL),IPIX),IPIX=1,NR)
300   CONTINUE
      ENDFILE IORG
C
C CALCULATE AVERAGE OFFSET FOR THE WHOLE GRID AND PRINT OUT
C
      AVGTOT = OFFTOT/CNTTOT
      WRITE(IOUT,1025)AVGTOT
1025  FORMAT(1HO,'AVERAGE PARALLAX OFFSET FOR WHOLE GRID = ',F6.2)
C
C PRINT MESSAGE TO RECOMMEND BACKGROUND AND PARALLAX FACTOR ADJUSTMENT
C
```

```
      IF(IERROR.NE.-1) GO TO 999
      WRITE(IOUT,1030)
1030  FORMAT(1HO,*AVERAGE OFFSETS ON SOME LINES ARE HIGH.AS A RESULT*
     +,/,*THE PARALLAX FOR SOME PIXELS MAY BE TRUNCATED. THE PLOT WILL*
     +,/,* PROBABLY BE ACCEPTABLE BUT A LOWER BACKGROUND VALUE OR *
     +,/,* LARGER PARALLAX SCALE FACTOR IS ADVISABLE*)
C
999   STOP
      END


      SUBROUTINE OFFSET(ICOL,IOFFS,IOFFN,TOTO,TOTN,IOFFL,IERROR)
C
C ***************************************************************
C
C SUBROUTINE - OFFSET
C
C PURPOSE - TO CALCULATE THE CURRENT OFFSET LIMIT FOR STEREO AND
C           PRINT DIAGNOSTICS
C
C INPUT VARIABLES -          ICOL = CURRENT COLUMN NUMBER
C
C INPUT/OUTPUT VARIABLES -   IOFFS = SUM OF OFFSETS FOR COLUMN
C                            IOFFN = NUMBER OF OFFSET POINTS IN COLUMN
C                            TOTO  = RUNNING TOTAL OF OFFSETS
C                            TOTN  = RUNNING TOTAL OF OFFSET POINTS
C                            IOFFL = OFFSET LIMIT FOR NEXT COLUMN
C
C OUTPUT VARIABLES -         IERROR = FLAG TO STOP PROGRAM FOR ERRORS
C
C ***************************************************************
C
      DATA IOUT/6/
C
      AVG = FLOAT(IOFFS)/FLOAT(IOFFN) +.5
      IOFFAVG = IFIX(AVG)
      IOFFL = IOFFAVG + 6
      IF(IOFFL.GT.17) IOFFL = 17
C
      IF(IOFFAVG.LT.17) GO TO 10
      WRITE(IOUT,1001)ICOL,IOFFAVG
1001  FORMAT(1H+,*ERROR ! ,AVERAGE OFFSET IN COLUMN *,I6,* EQUALS *,
     +I8,/,*A DESIRABLE VALUE IS LESS THAN 10 AND THE MAXIMUM IS 17.*,
     +/,* TO REDUCE THE OFFSET EITHER DECREASE THE MAGNETIC BACKGROUND*,
     +/,* OR INCREASE THE PARRALLAX SCALING FACTOR.*)
      IERROR = 1
      GO TO 999
C
10    IF(IOFFAVG.LT.12) GO TO 20
      WRITE(IOUT,1002)ICOL,IOFFAVG
1002  FORMAT(1H ,*WARNING ! ,AVERAGE OFFSET IN COLUMN *,I5,* EQUALS*,
     +I8,*OFFSET MAY BE TRUNCATED.*)
      IERROR = -1
C
20    TOTO = TOTO + FLOAT(IOFFS)
      TOTN = TOTN + FLOAT(IOFFN)
C
      IOFFN = IOFFS = 0
C
999   RETURN
      END
```

```
C ***************************************************************
C
C PROGRAM NAME: SHOPLT
C
C REVISION: 1.4 , APR. 11 , 1984
C
C PURPOSE : THIS PROGRAM PRODUCES A PLOT TAPE TO ALLOW A
C           STEREO OR REGULAR PLOT OF SHADED RELIEF DATA ON
C           AN APPLICON PLOTTER.
C
C DESCRIPTION : THE APPLICON PLOT TAPE IS CREATED BY CALLS TO
C           SUBROUTINES IN THE APPLICON "COLOR" SOFTWARE.
C           TWO MODES OF OPERATION ARE DEFINED ; STEREO OR SHADE.
C            SHADE : FOR THE PRODUCTION OF NORMAL SHADED RELIEF
C                    PLOTS THE REFLECTANCE GRID VALUES OF FROM 0
C                    TO 1 ARE MAPPED ONTO COLOUR INTENSITIES OF 16
C                    TO 0. ALL THREE COLOURS ARE SET TO THE SAME
C                    INTENSITY PRODUCING A GRAY TONE PLOT.
C            STEREO : FOR THE PRODUCTION OF STEREO SHADED RELIEF
C                    PLOTS THE ORIGIONAL REFLECTANCE GRID IS PLOTTED
C                    IN THE SAME MANNER AS IN THE "SHADE" MODE BUT
C                    ONLY IN THE COLOUR CYAN(BLUE). THE OFFSET
C                    REFLECTANCE GRID (STEREO OUTPUT) IS THEN MAPPED
C                    ONTO THE MAGENTA (RED) COLOUR IN  THE SAME MANNER.
C
C INPUT : TAPE5 - INPUT
C         TAPE6 - OUTPUT
C         TAPE11 - REFLECTANCE OR "SHADED RELIEF" GRID OF AREA
C                  (SHADE OUTPUT)
C         TAPE13 - OFFSET REFLECTANCE MAP GRID
C                  (STEREO OUTPUT)
C         TAPE25 - PICTURE STORAGE FOR COLOR
C         TAPE28 - DIRECTORY OF PAGES ON TAPE 25
C         TAPE29 - FOR PICTURE WHEN COPIED TO TAPE
C
C DATA INPUT : RECORD ONE ; FORMAT : A6
C               TYPE - "SHADE" OR "STEREO"
C              RECORD TWO ; FORMAT : 4I10
C               NRF,NRL,NCF,NCL ; FIRST AND LAST ROWS AND COLUMNS
C               TO BE PLOTTED : MAX. NO. ROWS = 690
C                               MAX. NO. COLUMNS = 1050
C
C WRITTEN BY : J. BROOME AND D. TESKEY
C              REGIONAL GEOPHYSICS SUBDIVISION
C              RESOURCE GEOPHYSICS AND GEOCHEMISTRY DIVISION
C              GEOLOGICAL SURVEY OF CANADA
C
C ***************************************************************
C
      PROGRAM SHOPLT(INPUT,OUTPUT,TAPE5=INPUT,TAPE6=OUTPUT,TAPE11,
     *TAPE13,TAPE25,TAPE28,TAPE29)
C
      DIMENSION IVECT4(3,690),RG(1000),ORG(1000)
C
      DATA INPUT/5/,IOUT/6/,IRG/11/,IORG/13/,BNDVAL/-9999./
      DATA XORIG/C.C/,YORIG/0.0/,NCELL/1/
C
C CALL "COLOR" ROUTINES TO SET MODE OF OPERATION
C
      IPAR = 1
      CALL IPAGB
      CALL ISTART(2)
      CALL ISCAN4(2,IVECT4)
C
C READ TYPE AND AREA TO BE PLOTTED
C
      READ(INPUT,1005)TYPE
1005  FORMAT(A6)
      READ(INPUT,1007)NRF,NRL,NCF,NCL
1007  FORMAT(4I10)
C
C READ HEADER FROM INPUT GRID OR GRIDS AND CHECK
```

```
C
      READ(IRG)NRR,NCR
C
      IF(TYPE.EQ.EMSPACE ) GO TO 90
C
      READ(IORG)NRO,NCO
C
      IF(NRR.EQ.NRO.AND.NCR.EQ.NCO) GO TO 90
C
      WRITE(IOUT,1010)NRR,NCR,NRO,NCO
1010  FORMAT(1H1,* ERROR IN INPUT GRID SIZES !*,/,
     +* REFLECTANCE GRID (TAPE11); NR,NC = *,2I8,/,
     +* SIMULATED REF. GRID (TAPE13); NR,NC = *,2I8)
      GO TO 999
C
C CHECK IF "NR" ON INPUT GRID(S) EXCEEDS CURRENT MAXIMUM (1000)
C
90    IF(NRR.LE.1000) GO TO 100
      WRITE(IOUT,1008)NRR
1008  FORMAT(1H1,*ERROR !,SIZE OF NR ON INPUT GRID = *,I8,
     +* MAXIMUM IS CURRENTLY 1000*)
      GO TO 999
C
C CALCULATE SIZE OF PLOT AREA (NR,NC)
C
100   IF(NRL.GT.NRR) NRL = NRR
      IF(NCL.GT.NCR) NCL = NCR
      NR = NRL - NRF + 1
      NC = NCL - NCF + 1
C
      IF(NC.LE.1050) GO TO 110
      WRITE(IOUT,1015)NC
1015  FORMAT(1H1,* ERROR ! ,NC = *,I8,* MAXIMUM FOR PLOT = 1050*)
      GO TO 999
C
110   IF(NR.LE.690) GO TO 120
      WRITE(IOUT,1020)NR
1020  FORMAT(1H1,* ERROR ! ,NR = *,I8,* MAXIMUM FOR PLOT = 690*)
      GO TO 999
C
120   WRITE(IOUT,1025)TYPE,NRR,NCR,NRF,NRL,NR,NCF,NCL,NC
1025  FORMAT(1H1,* TYPE = *,A6,/
     +* INPUT GRID SIZE; NR,NC = *,2I7,/
     +* FIRST AND LAST PLOT ROWS ARE    : *,2I7,* ,NR PLOTTED = *,I7
     +* FIRST AND LAST PLOT COLUMNS ARE : *,2I7,* ,NC PLOTTED = *,I7
C
C READ IN COLUMNS OF DATA FROM INPUT GRIDS ,UP TO FIRST PLOTTED
C
      DO 200 ICOL=1,NCF
       READ(IRG)(RG(J),J=1,NRR)
       IF(TYPE.NE.6HSTEREO) GO TO 200
       READ(IORG)(ORG(J),J=1,NRR)
200   CONTINUE
C
C
C FOR EACH COLUMN TO BE PLOTTED
C ******************************
C
      DO 500 ICOL =1 , NC
C
C BLANK OUT "IVECT4" COLOUR ARRAY TO 0
C
       DO 510 N=1 , 690
        IVECT4(1,N) = 0
        IVECT4(2,N) = 0
        IVECT4(3,N) = 0
510    CONTINUE
C
C CALCULATE COLOUR INTENSITIES FOR NORMAL SHADED RELIEF PLOT
```

```
C
      DO 520 KPIX=1,NR
       IPIX = NRF - 1 + KPIX
       IF(RG(IPIX).EQ.BNOVAL) GO TO 520
       INT = 16-IFIX(RG(IPIX)/0.0589)
       IVECT4(1,KPIX) = INT
       IVECT4(2,KPIX) = INT
       IVECT4(3,KPIX)=INT
C
C IF TYPE = SHADE , PLOT IVECT4
C
       IF(TYPE.EQ.6HSHADE ) GO TO 520
C
C CALCULATE COLOUR INTENSITY LEVELS FOR TYPE=STEREO PLOT
C
       IF(ORG(IPIX).LT.C.0) ORG(IPIX)=0.0
       IF(ORG(IPIX).GT.1.0) ORG(IPIX)=1.0
       INT = 16-IFIX(ORG(IPIX)/.0589)
C
C SET YELLOW COLOUR INTENSITY TO 0 AND MAGENTA TO INTENSITY CALCULAT
C   FROM SIMULATED REF. GRID.
C
       IVECT4(1,KPIX) = C
       IVECT4(2,KPIX) = INT
520    CONTINUE
C
C IF LAST COLUMN SET IPAR=3 TO CLOSE PLOT
C
       IF(ICOL.GE.NC) IPAR=3
C
C CALL "COLOR" ROUTINE TO PLOT CURRENT GRID COLUMN
C
       CALL ISCAN4(IPAR,IVECT4)
C
C READ IN ONE COLUMN FROM REFLECTANCE GRID AND IF TYPE=STEREO
C  ONE COLUMN FROM SIMULATED REF. GRID.
C
       IF(I.EQ.NC) GO TO 500
       READ(IRG)(RG(J),J=1,NRR)
       IF(TYPE.EQ.6HSHADE ) GO TO 500
       READ(IORG)(ORG(J),J=1,NRR)
C
500    CONTINUE
C
       CALL ICLB
999    STOP
       END
```

DISCUSSIONS AND COMMUNICATIONS
DISCUSSIONS ET COMMUNICATIONS

DISCUSSION DE "NOTES ON THE DEGLACIATION OF SOUTHEASTERN QUEBEC"

Jean-Marie Dubois, Armand Larocque, Paul Boissonnault, Clément Dubé, André Poulin, Q.H.J Gwyn, Gérard Larocque, et Anne Morissette

Département de géographie
Université de Sherbrooke
Sherbrooke, Québec J1K 2R1

Introduction

Gadd (1983) propose une version revisée du modèle de déglaciation du sud-est du Québec (Gadd, McDonald and Shilts, 1972). Cette revision s'appuie sur des travaux de reconnaissance de la géologie du Quaternaire de cette région. Cependant, Gadd manque non seulement de données détaillées pour bien établir son nouveau modèle, mais il n'utilise pas assez l'analyse géographique qui allie les données géomorphologiques aux données stratigraphiques. Cette méthode est particulièrement efficace dans les régions accidentées de stagnation glaciaire et de lacs proglaciaires.

Le modèle de Gadd (1983) repose sur l'isolement d'importantes masses de glace localisées le long du Piedmont appalachien, ce qui modifierait d'une facon appréciable les concepts antérieurs expliquant la chronologie et l'évolution de la déglaciation du sud du Québec. Ces masses résiduelles auraient eu des conséquences importantes sur le drainage proglaciaire des Cantons de l'Est et sur l'invasion du Piedmont par la mer de Champlain. Ce nouveau modèle semble en fait répondre aux interrogations soulevées en conclusion d'un livret-guide d'excursion dans la région de Drummondville (La Salle, David et Bouchard, 1982).

Notre contribution démontre que le modèle de déglaciation proposé par Gadd (1983) présente des déficiences sérieuses et que plusieurs conclusions sont prématurées. Les données et les interprétations que nous avancons dans notre discussion concernent la région située a l'est de l'axe des monts Sutton et Orford (fig. 1 de Gadd, 1983). Les données sont basées sur des levés de terrain régulièrement compilés (Dubois, 1972-83).

Discussion

Les problèmes majeurs du schéma de déglacement de Gadd sont liés autant au manque de données précises sur le synchronisme des fronts morainiques que sur l'évolution des lacs proglaciaires. Les fronts glaciaires sont nettement diachroniques (surtout sur les figures 2 et 3 de Gadd). Lorsque les constructions morainiques sont très éloignées les unes des autres, le meilleur moyen de les corréler est de les relier à l'évolution du drainage proglaciaire. C'est ce que démontrent les études de Parent (1978), de Boissonnault, Gwyn et Morin (1981), Boissonnault et Gwyn (1980, 1983), Larocque, A., Gwyn et Poulin (1983), Larocque, G., Gwyn et Poulin (1983), Dubé (1983) et Clément (1982).

Les fronts morainiques et le drainage proglaciaire près de la frontière canado-américaine

Les tracés des positions glaciaires de Gadd (1983), pour la région du mont Mégantic, semblent être basés sur Gadd, McDonald and Shilts (1972). Des travaux récents (Larocque, A. et Gwyn, 1981; Larocque, Larocque, Poulin et Gwyn, 1982; Larocque, A., Gwyn et Poulin, 1983), ont révisé l'emplacement de ces diverses positions. D'autres études permettent déjà de croire que plusieurs corrections devront être apportées sur le trace du front glaciaire situé entre le mont Mégantic et la rivière Coaticook (Morissette, en prép.; Larocque, en prép.).

Les figures 2 et 3 du texte de Gadd (1983) laissent croire que les écoulements proglaciaires vers le sud se sont faits à peu près en même temps. Larocque et Gwyn (1981) et Larocque, A., Gwyn et Poulin (1983) ont plutôt établi que ces écoulements proglaciaires se sont effectués par l'intermédiaire de cols longeant la frontière Québec – U.S.A. a des moments différents. Selon ces études, le drainage s'est d'abord fait vers la rivière Cupsuptic puis vers les rivières Kennebago, Dead, Magalloway et enfin vers la rivière Connecticut.

Le déglacement de la vallée de la Coaticook et de l'est du lac Memphrémagog

La section sur l'évolution lacustre précoce de la vallée de la Coaticook de Gadd (1983) est exacte et avait déjà été discutée dans Clément et Parent (1977). Par contre, la section sur l'évolution tardive du drainage proglaciaire et des lacs de cette même vallée présente des erreurs d'interprétation.

D'abord, le niveau lacustre de 370 m dans le bassin de la Coaticook n'est pas relié à l'utilisation du chenal juxtaglaciaire de Hatley (figure 3 de Gadd, 1983). Le lac confiné dans le bassin de la Coaticook se déversait plutôt par un chenal situé immédiatement à l'ouest de Coaticook (Boissonnault, 1983). Ce chenal se termine à l'ouest par un delta à 365 m d'altitude qui est associé aux formes littorales d'une des phases du lac proglaciaire Memphremagog (Boissonnault, Gwyn et Morin, 1981). La position frontale associée à ce plan à l'ouest de l'interfluve Coaticook-Memphrémagog rejoint la frontière Québec-Vermont à l'est de Stanstead Plain et non à Beebe Plain.

Tel que Gadd (1983, p. 404) le mentionne, le chenal proglaciaire de Hatley est effectivement lié au plan d'eau de 300 m. Cependant, il débouche sur un delta de type emboîte qui correspond aussi au niveau intermédiaire de 320 m. Pour chacune de ces deux phases glacio-lacustres, Boissonnault et Gwyn (1983) ont pu tracer des positions frontales distinctes sur le versant est du bassin du lac Memphrémagog. Lors de la phase de 320 m, le front glaciaire forme un lobe à l'est du lac Memphrémagog et jusqu'à une moraine cartographiée par Stewart et MacClintock (1970) aux environs de Newport au Vermont. Par la suite, il remonte au nord-ouest jusqu'à

De: Discussion et Communications dans Recherche en cours, partie B; CGC Etude 84-1B.

Bolton Centre (figure 4 de Gadd, 1983). Lors de la phase de 300 m, le lobe glaciaire s'est rétrécit et sa pointe sud coincide avec le delta de Beebe Plain sis à 305 m d'altitude (Boissonnault, Gwyn et Morin, 1981). Plusieurs deltas et lignes de rivages témoignent aussi de l'importance de ce lac proglaciaire qui se drainait vers le sud par le col d'Eligo Pond au Vermont (Stewart et MacClintock, 1969).

En deuxième lieu, Gadd (1983, p. 407) affirme qu'il existe immédiatement au nord de Coaticook, des systèmes d'épandange proglaciaire vers et sous 200 m d'altitude, avec un écoulement des eaux vers le sud. Gadd semble associer ce système à des déversoirs utilisés par des lacs proglaciaires contrôlés par une masse de glace située au nord de Sherbrooke. Au nord de Coaticook, il existe effectivement une terrasse entaillée dans des matériaux fluvioglaciaires situés dans le prolongement d'un esker à environ 220 m d'altitude. Cette terrasse est plutôt le résultat de l'érosion fluviale d'une portion de l'esker alors que les paléocourants observes correspondent à la période de mise en place de l'esker (Morissette, en prép.). Quant aux autres terrasses observées, elles constituent des niveaux inférieurs mis en place par les eaux s'écoulant vers le nord et formant la plaine alluviale de la rivière Coaticook. De plus, pour qu'il y ait un écoulement proglaciaire vers le sud par la vallée de la Coaticook, tel que présenté sur la figure 4 de Gadd (1983), il aurait fallu que le plan d'eau soit à une altitude de plus de 290 m et non vers 200 m. En effet, tout le secteur nord de la vallée de la Coaticook serait contrôlé par un seuil rocheux situé à l'entrée sud de la gorge localisée dans la ville de Coaticook, à une altitude de 290 m.

Le déglacement des vallées du lac Memphrémagog et de la rivière Missisquoi

À partir des figures 4 et 5, Gadd (1983) amène le concept d'une vaste masse résiduelle de glace stagnante. Un concept comportant une certaine similitude a déjà été établie dans la région par Dubois (1974), Fortin (1974) et Landry (1974) mais pour des masses d'échelle locale et non régionale. Leur modèle met en valeur le rôle du relief dans les modalités de fusion glaciaire.

La présence de masses glaciaires résiduelles ne cadre cependant pas avec l'évolution du retrait glaciaire observé dans la région. Dans le bassin du lac Memphrémagog par exemple, cette hypothèse vient contredire les données de Boissonnault (1983), Dubé (1983) et Boissonnault et Gwyn (1980 et 1983). En effet, ces études montrent que le lac proglaciaire Memphrémagog a évolué en une succession de huit phases différentes entre 365 et 165 m d'altitude. Ces phases sont très bien identifiées par des deltas, des lignes de rivage et des champs de blocs. Cette reconstitution montre que le front glaciaire reculait sous forme d'un lobe sur l'interfluve est du lac actuel à cause de l'influence locale du relief et du lac proglaciaire. De plus, la présence d'une grande masse de glace stagnante aurait favorisé la formation de plusieurs lacs proglaciaires d'altitudes différentes de part et d'autres alors qu'il est prouvé que plusieurs phases glaciolacustres ont occupé simultanément les deux versants du bassin du Memphrémagog.

Sur la figure 4, Gadd (1983) montre que la masse de glace a barré un lac près de Beebe Plain. Cette hypothèse contredit les résultats de Boissonnault, Gwyn et Morin (1981) puis de Boissonnault et Gwyn (1983) qui avaient bien démontré que les formes associées à ce lac sont antérieures a l'évènement présenté par Gadd (1983). De plus, Gadd (1983) n'a pas indiqué le lac proglaciaire qui ennoyait la vallée de la Saint-Francois près de Sherbrooke à ce moment-là. Pourtant, les travaux de McDonald (1967), de Parent (1978, fig. 25), de Boissonnault, Gwyn et Morin (1981) et de Boissonnault et Gwyn (1983) démontrent que cette vallée était alors inondée par le lac proglaciaire Memphrémagog; ce lac proglaciaire était contrôlé par l'exutoire du lac Nick, situé sur le côté ouest du lac actuel et donc contemporain de l'évènement présenté sur la figure 4 de Gadd (1983).

Sur cette figure 4, Gadd (1983) présente aussi ce qui semble être la position de la glace, lors de la construction de la moraine de la rivière aux Cerises (Cherry River Moraine). Ce tracé est une adaptation de celui qui avait été présenté par McDonald (1967) puis par Gadd, McDonald and Shilts (1972). Selon Gadd (1983), cette moraine aurait été mise en place par de la glace stagnante. Les travaux de Boissonnault (1983) et de Boissonnault et Gwyn (1983) montrent plutôt le contraire. En plus de redéfinir l'ancien tracé, leurs travaux corroborent plutôt la présence d'une récurrence du front glaciaire ainsi que McDonald (1967) le soupçonnait. Des drumlins et des crêtes morainiques ont été mis en place entre Magog et le lac Lovering, lors de cette dernière récurrence. McDonald (1967) a aussi observé une autre surface modelée par l'action glaciaire à environ 6 km au nord de Magog. La présence de ces formes est peu compatible avec des processus liés à une stagnation de la glace. De plus, Clément et Poulin (1975), Parent (1978) et Larocque, G. (en prép.) ont aussi observé des phénomènes de récurrence glaciaire dans les environs de Sherbrooke.

Enfin, Gadd (1983, p. 407) associe la mise en place du système morainique des Hautes-Terres (Highland Front Morainic System) et de la moraine de la rivière aux Cerises (Cherry River Moraine) au tracé du front glaciaire présenté sur sa figure 4. Le manque de précision du texte nous force à nous demander si Gadd (1983) propose ou non que ces deux évènements soient possiblement contemporains.

Sur la figure 4, Gadd (1983) indique deux chenaux proglaciaires vers l'ouest allant du bassin du lac Memphrémagog vers le bassin de la Missisquoi. Le chenal du lac Nick, connu depuis longtemps (McDonald, 1967), est exact mais l'orientation de l'écoulement de celui du ruisseau Castle, situé au sud du mont Orford, est erronée (figure 5 de Gadd, 1983). Toutes les preuves de terrain l'orientent vers l'est, comme McDonald (1967) l'avait indiqué: marques d'écoulement dans les sables du complexe kame-esker qui borde le côté nord du chenal et surtout la présence d'un épandage au nord-ouest du lac Memphrémagog, à une altitude de 245 m. Cet épandage se termine par un delta lacustre dont les apports sédimentaires provenaient d'un chenal du ruisseau Castle. Sur la même figure 4, Gadd (1983) indique une masse de glace stagnante dans le bassin du Massawippi alors que sur la figure précédente ce bassin était libre de glace. N'aurait-il pas fallu une glace active pour permettre une telle récurrence?

Le déglacement du bassin de la rivière Missisquoi

La déglaciation de la vallée de la rivière Missisquoi est caractérisée par la construction d'une plaine d'épandage proglaciaire bien développée (McDonald, 1967, p. 51; Dubé, 1983; Dubé, Dubois et Provencher, sous presse). Gadd (1983, fig. 4 et 5) mentionne que la tête de cet épandage, localisé à Lawrenceville, est associé au système morainique des Hautes-Terres. Il n'apporte cependant aucune preuve qui viendrait confirmer cette hypothèse.

Plus loin, Gadd (1983) mentionne la présence, à Mansonville, d'un esker interdigité avec des silts rouges-bruns glaciolacustres, qui le recouvrent partiellement et qui occupent une plaine argileuse à 190 m d'altitude et plus. Cet esker serait, selon lui, un segment précoce du système décrit précédemment. Cette forme n'est pas un esker mais plutôt le vestige d'une plaine d'épandage dont l'échine convexe et effilée traverse la vallée d'est en ouest (Dubé, 1983).

Enfin, sur la figure 6, Gadd (1983) a indiqué que le système d'épandage de la vallée de la Missisquoi était encore en fonction. Il serait assez surprenant qu'il en soit ainsi car à

l'époque où l'on se place, la Missiquoi avait repris son cours fluvial normal (Dubé, 1983) et qu'il ne bénéficiait d'aucun apport provenant de la fusion de la glace.

Conclusion

Gadd (1983) n'arrive pas à nous convaincre de la présence d'une immense masse de glace stagnante localisée sur le Piedmont appalachien, ni de l'exactitude des fronts glaciaires qu'il présente. Le schéma de la déglaciation du sud-est du Québec est beaucoup plus complexe et dynamique que celui que Gadd (1983) présente. Il doit faire appel à des données précises et continues de terrain accompagnées d'analyses très fouillées à l'échelle locale avant d'arriver à une reconstitution détaillée des évènements tant dans l'espace que dans le temps. L'analyse stratigraphique doit se doubler d'une analyse géographique soignée.

Comme le démontre notre critique, le modèle doit définir avec toutes les nuances requises les bordures glacio-lacustres et les fronts glaciaires sous un système cohérent. Malheureusement, la présence d'erreurs d'observation et l'absence de justification de plusieurs hypothèses diminuent la portée du modèle de Gadd (1983).

Remerciements

Nous remercions le ministère de l'Éducation du Québec (F.C.A.C.) et le Bureau de la recherche de l'Université de Sherbrooke qui ont financés nos études depuis le début, ainsi que le C.R.S.N.G.

Références

Boissonnault, P.
1983: Géomorphologie et lithostratigraphie à l'est du lac Memphrémagog; mémoire de M.Sc., Université de Sherbrooke, 150 p.

Boissonnault, P. et Gwyn, Q.H.J.
1980: Évolution du lac glaciaire Memphrémagog; annales de l'ACFAS, vol. 47, p. 113.

1983: Le lac proglaciaire Memphrémagog, sud du Québec, Géographie physique et Quaternaire, vol. 37, nº 2, p. 197-204.

Boissonnault, P., Gwyn, Q.H.J., et Morin, B.
1981: Le lac proglaciaire Memphrémagog: géologie, géomorphologie, archéologie; Département de géographie, Université de Sherbrooke, bulletin de recherche nº 55, 40 p.

Clément, P.
1982: Cartes géomorphologiques des Cantons de l'Est: régions de Dudswell, Scotstown, Sherbrooke, La Patrie, Coaticook et Malvina. Département de géographie, Université de Sherbrooke, bulletin de recherche nº 61, 22 p.

Clément, P. et Parent, M.
1977: Contribution à l'étude de la déglaciation wisconsinienne dans le centre des Cantons de l'Est, Québec; Géographie physique et Quaternaire, vol. 31, nºs 3-4, p. 217-228.

Clément, P. et Poulin, A.
1975: La fossilisation des réseaux de vallées aux environs de Sherbrooke. Revue de géographie de Montréal, vol. 29, nº 2, p. 167-171.

Dubé, C.
1983: Géomorphologie quaternaire et déglaciation à l'ouest du lac Memphrémagog; mémoire de M.Sc., Université de Sherbrooke, 139 p.

Dubé, C. et Gwyn, Q.H.J.
1983: La déglaciation de la rivière Missisquoi-Nord et la corrélation entre les lacs proglaciaires Memphrémagog et Vermont; annales de l'ACFAS, vol. 50, p. 121.

Dubé, C., Dubois, J.M.M., et Provencher, L.
– Les plaines d'épandage proglaciaires: un exemple synthèse dans la vallée de la rivière Missisquoi-Nord au Québec. Photo-interprétation. (sous presse)

Dubois, J.M.M.
1972-
1983: Bibliographie sur les caractéristiques physiques des Cantons de l'Est, province de Québec, Canada; Département de géographie, Université de Sherbrooke, bulletins de recherche nº 3 (1972), nº 12 (1973), nº 24 (1975), nº 29 (1976), nº 43-44 (1979), nº 59-60 (1981) et nº 69 (1983).

1974: Phases et formes de déglaciation du bassin du Bury, Estrie, Québec; Rev. géogr. Montréal, vol. 28, nº 4, p. 389-406.

Fortin, N.
1974: Étude morpho-sédimentologique du bassin de la rivière Clifton; mémoire de maîtrise, Université de Sherbrooke, 182 p.

Gadd, N.R.
1983: Notes on the deglaciation of southeastern Quebec; in Current Research, Part B, Geological Survey of Canada, Paper 83-1B, p. 403-412.

Gadd, N.R., McDonald, B.C., et Shilts, N.W.
1972: Deglaciation on southern Quebec; Geological Survey of Canada, Paper 71-47, 19 p.

Landry, B.
1974: Étude morpho-sédimentologique du bassin de la rivière Eaton supérieure; mémoire de maîtrise, Université de Sherbrooke, 110 p.

Larocque, A.
– La dynamique glaciaire lors de la déglaciation du haut Saint-Francois, Québec. Thèse de doctorat, Université de Montréal en collaboration avec l'Université de Sherbrooke. (en prép.)

Larocque, G.
– Déglaciation de la région de Sherbrooke. Thèse de doctorat, Université de Montréal en collaboration avec l'Université de Sherbrooke. (en prép.)

Larocque, A. et Gwyn, Q.H.J.
1981: Évolution du drainage des lacs proglaciaires et les positions frontales associées, hautes vallées de la Saint-Francois et de la Chaudière; annales de l'ACFAS, vol. 48, p. 103.

Larocque, A., Gwyn, Q.H.J., et Poulin, A.
1983: Développement des lacs proglaciaires et déglaciation des hauts-bassins des rivière au Saumon et Chaudière, sud du Québec; Géographie physique et Quaternaire, vol. 37, nº 1, p. 93-105.

Larocque, G., Gwyn, Q.H.J., et Poulin, A.
1983: Évolution des lacs proglaciaires et déglaciation de la haute-vallée de la Saint-Francois, sud du Québec; Géographie physique et Quaternaire, vol. 37, nº 1, p. 85-92.

Larocque, A., Larocque, G., Poulin, A., et Gwyn, Q.H.J.
1982: Modèle de déglaciation de la vallée de la rivière au Saumon, Cantons de l'Est, Québec; annales de l'ACFAS, vol. 49, p. 129.

LaSalle, P., David, P.P., and Bouchard, M.A.
1982: Friends of the Pleistocene Guidebook: 45th Annual Meeting, Drummondville-St-Hyacinthe, Quebec, Canada; ministère de l'Énergie et des Ressources du Québec, 57 p.

McDonald, B.C.
1967: Pleistocene events and chronology in the Appalachian region of southeastern Quebec, Canada; unpublished Ph.D. thesis, Yale University, 161 p.

Morissette, A.
– Géomorphologie et géologie quaternaires de la région de Coaticook; mémoire de M.Sc., Université de Sherbrooke. (en prép.)

Parent, M.
1978: Géomorphologie quaternaire de la région de Stoke-Watopeka, Québec; mémoire de M.Sc., Département de géographie, Université de Sherbrooke, 206 p.

Stewart, D.P. and MacClintock, P.
1969: The superficial geology and Pleistocene history of Vermont; Vermont Geological Survey, Bulletin 31, 251 p.

1970: Surficial geologic map of Vermont; Vermont Geological Survey, 1:250 000.

NOTES ON THE DEGLACIATION OF SOUTHEASTERN QUEBEC: DISCUSSION

Michel Parent
Department of Geology
The University of Western Ontario
London, Ontario N6A 5B7

Introduction

A salient point of Gadd's (1983) report is to draw attention to new observations which make it possible to envisage a deglacial history that would be reconcilable with the idea that an extensive body of "Laurentide" ice became isolated on the south shore of the Champlain Sea (Gadd, 1980). This interpretation may seem attractive since it has broad similarities to deglaciation models that have been tentatively proposed for nearby areas (Gauthier, 1975; Lortie, 1976; Shilts, 1976, 1981; Thomas, 1977; LaSalle et al., 1977). It is not my intention of disrupting Dr. Gadd's claim that new observations can be "used to demonstrate a need to modify some previous interpretations" (Gadd, 1983, p. 403). Indeed it is with that objective in mind that I carried out fieldwork in the Asbestos-Valcourt region for my Ph.D. thesis (Quaternary stratigraphy and events of the Asbestos-Valcourt region, southeastern Québec, in preparation). This discussion will be restricted to points which indicate that Dr. Gadd's deglacial history is incorrect.

Discussion

On the basis of rather scattered field evidence, Dr. Gadd proposes a model which may be divided into two parts:

1. The southeastern margin of large remnant ice masses generally retreated northwestward in the Appalachian uplands of southeastern Québec.
2. Large masses of stagnant ice were left stranded in vast areas in the vicinity of Monts Sutton and in areas farther east.

I could agree at least with the broad aspects of the first part of his model. However, some key evidence, other than hotly debated ^{14}C dates (Hillaire-Marcel, 1981; Karrow, 1981; Gadd, 1981), is urgently needed before accepting his idea that large ice masses formed parts of the south shore of the Champlain Sea for a period of about 2000 years – this being a minimum period of time if his third "tentative" conclusion (p. 411) is to be accepted together with his previous assertion (Gadd, 1980, p. 1441) that marine waters were present in Ottawa valley somewhat before 12 500 BP. For example, one might reasonably expect to find at least some field data indicating that glaciofluvial sediments near the northern margin of the postulated remnant ice masses were deposited by meltwater which flowed northward, that is towards the supposedly adjacent marine basin. I have searched for such data in several glaciofluvial sediment bodies in the appropriate areas of the Appalachian piedmont and uplands and, so far, I have found no convincing evidence of northward meltwater flow, nor can such evidence be found in the pertinent literature.

As for the northwestward deglaciation pattern depicted in his Figures 2, 3, and 4, it is correct but only in very broad terms. A persistent problem is that it does not take into account the diachronous nature of the observed ice-marginal features as this has been evidenced in the literature (Clément and Parent, 1977; Parent, 1978; Prichonnet et al., 1982). I must emphasize however that this diachronism has more importance from a methodological point of view than it has for recognizing regional deglaciation patterns. His reportedly new observations of deglacial features near Lac Lindsay, Dixville, Coaticook, Stanstead, and Way Mills (his Fig. 2 and 3) were reported, discussed, and mapped in a previous paper (Clément and Parent, 1977; Fig. 2, 6). Further work by Boissonnault (Boissonnault and Gwyn, 1983 and references therein) confirmed our preliminary interpretation.

Westward flow in a meltwater channel at the southern toe of Mont Orford is a determining point for Dr. Gadd's interpretation of the deglaciation history of the Lac Memphrémagog basin and of Missisquoi River valley (his Fig. 4). I believe that his interpretation of the field evidence is incorrect. Observed paloecurrent indicators (ripple-drift lamination and pebble imbrication) show that ice-contact sediments within the col south of Mont Orford, near Delaire, were deposited by meltwater flowing eastward. Unfortunately, primary structures could not be observed within outwash gravels lying on the floor of the adjacent Delaire meltwater channel as they lie below the water table underneath a 1 m-thick layer of peat. However, the Delaire meltwater channel grades down to a large outwash deposit at its eastern exit (as mapped by McDonald, 1967a); and the gravel outwash grades in turn to a pair of deltas (as mapped by McDonald, 1967a) within which I have measured ripple-drift trains trending eastward, i.e., towards the Lac Memphrémagog basin. McDonald (1967b) already noted that these delta sediments showed no evidence of collapse due to buried ice blocks or of other ice-contact features, and I have not noted any either; he also established that the deltas were formed during the Sherbrooke phase of glacial Lake Memphrémagog (McDonald, 1968). Furthermore there are no glaciofluvial sediments near Lac Orford at the western exit of the Delaire meltwater channel. Deglacial features near Mont Orford do not show any evidence of westward meltwater flow, and they cannot be used to support Dr. Gadd's concept of a large stagnant ice mass in the Lac Memphrémagog basin. Furthermore, discontinuous shoreline features on the slopes of the lake basin are associated with receding levels of glacial Lake Memphrémagog (Boissonnault and Gwyn, 1983). This coherent body of field data makes highly unlikely Dr. Gadd's concept (as shown in his Fig. 4) that a large mass of stagnant ice occupied the Lac Memphrémagog basin and that it existed at a time when glacial retreat had uncovered the Rivière Missisquoi-Nord valley as far north as Lawrenceville.

Partly on the basis of McDonald's (1967b, Fig. 12) work, Dr. Gadd postulates that a mass of stagnant ice also occupied a vast area centred about Windsor (his Fig. 4 and 5). He certainly is aware that McDonald did not reiterate that idea after an extensive sedimentological analysis of the Windsor esker revealed that it formed at the interface of a backwasting ice front and a deep proglacial lake, and that the esker segments formed diachronously (Banerjee and McDonald, 1975). Similarly, sedimentological and geomorphic evidence indicates that the neighbouring Saint-Claude esker was also emplaced diachronously (Parent, 1978).

Furthermore, abundant shoreline features as well as other glaciolacustrine sediments, including varves at several localities, indicate that this part of the Rivière Saint-François valley was submerged by high level (approximately 260 and 225 m) ice-dammed lakes (McDonald, 1967b; Parent, 1978). There is, however, field evidence indicating that only small bodies of buried stagnant ice remained here and there during the Sherbrooke phase of glacial Lake Memphrémagog and during subsequent glaciolacustrine phases. Recent measurements of shoreline features (Parent, 1978; Prichonnet, 1982a, 1982b) strongly suggest that the western margin of the Appalachian uplands was occupied by an extensive ice-dammed lake. Upwarped shoreline indicators now stand at elevations varying from about 230 m near Asbestos, Durham-Sud, and Mont Shefford

From: Discussions and Communications in Current Research, Part B; Geol. Surv. Can., Paper 84-1B.

to about 215 m near Sherbrooke and Cowansville. Related ice-contact deltas and kame terraces indicate that this proglacial lake expanded northwestward as the receding ice margin uncovered the Appalachian valleys and piedmont (Prichonnet et al., 1982). Despite its diachronism, the water plane thus defined constitutes a promising geological marker for deglacial events which predate the Champlain Sea in southeastern Québec. At the very least. these abundant shoreline features clearly indicate that stagnant ice masses did not have regional extent, as it has been postulated by Dr. Gadd (his Fig. 4 and 5).

Dr. Gadd presents very little field evidence to support the existence of an 80 km-long system of outwash channels between Richmond and Abercorn, as indicated in his Figure 5. Not only would such a major outwash system require meltwater to flow upslope in numerous localities, but detailed field surveys show no conclusive evidence of its existence (McDonald, 1967b; Prichonnet et al., 1982). Perhaps he meant that the 80 km-long system served as a general meltwater pathway during successive phases of ice retreat. If such is the case, his Figure 5 as well as its caption are misleading. Perhaps more importantly, Dr. Gadd's interpretation of deglacial events fails to account for the presence of numerous glaciolacustine shoreline features reported within this region (McDonald, 1967b; Prichonnet, 1982a).

There is ample field evidence supporting Dr. Gadd's observation that a large outwash system was formed in the valley between Lawrenceville and Eastman (his Fig. 4, 5, and 6). But it must also be stressed that glaciofluvial sediments near Lawrenceville are mainly esker sediments rather than outwash sediments associated with a "valley train" (p. 407). The high elevation (approximately 260-265 m) of the highest exposed glaciofluvial sediments, as well as that of the meltwater channel entrenched through them (slightly above 250 m), makes it very unlikely that the outwash channel remained active as late as the deglaciation phase tentatively depicted in his Figure 6.

In the abstract of Dr. Gadd's paper, it is implied that a remnant ice mass occupied a large area on the south shore of the Champlain Sea and he states (p. 411) that "marine invasion there took place, apparently, only after a considerable amount of isostatic uplift had occurred and after the **Mya** biotic phase of Champlain Sea had developed". His conclusions seem largely based on two lines of evidence:

1. The first one is derived from his observations of unfossiliferous ice-contact sediments below marine limit in the vicinity of Granby. I may agree that ice-contact features are somewhat uncommon below marine limit, but it must be stressed that their presence does not "preclude the existence of seawater at those places and elevations" (p. 411). I can readily think of two localities where this can be demonstrated: near Danville, fossiliferous marine delta sediments, ^{14}C dated at 11 370 ± 200 BP (UQ-290, unpublished)[1], show ice-contact features so abundant that Gadd et al. (1972) identified them as "ice-front accumulations" associated with the formation of the Highland Front Moraine Complex. Secondly, in the vicinity of St-André-Avellin, some 60 km northeast of Ottawa, many kettle lakes, some of which are bordered by unfossiliferous ice-contact sediments, occur within areas which are generally underlain by a thick layer of marine silt and clay and which are well below the local marine limit.
2. His second line of evidence is related to the absence of marine submergence prior to the **Mya** biotic phase in the vicinity of Granby and to "young" ^{14}C dates (10 700 ± 100 BP, GSC-3574; and 10 300 ± 90 BP, GSC-3539) associated with the **Mya** phase. His interpretation squarely contradicts published data from the same region: Prichonnet (1982a, p. 232) reported a series of ^{14}C dates on Champlain Sea fossils which includes UQ-29 (11 360 ± 110 BP) on **Macoma balthica** shells collected near Adamsville just a few kilometres east of the site of GSC-3574. Furthermore, Prichonnet (1982a, Fig. 29.6; 1982b, Fig. 3) reported evidence of marine shorelines at elevations up to 190 m; whether or not his higher shorelines are to be accepted as marine does not have much importance here, because those features at elevations up to about 150 m could hardly be anything other than marine.

Conclusion

Although Dr. Gadd presented his interpretations and conclusions as tentative ones, it is important to point out that a large body of field evidence does not lend support to several key interpretations embodied in his assessment of the last deglacial events. Consequently, it would be premature to consider that his "Figures 2 to 6, depict a pattern and a chronological sequence of events in the deglaciation of southeastern Quebec, *regardless* (my italics) of the age of those events" (p. 411). Nevertheless, the paper has brought forward valuable observations towards resolving some of the difficulties pertaining to the mode of introduction of the Champlain Sea in St. Lawrence valley and to its relationships to deglacial events in the Appalachian uplands of southeastern Quebec.

References

Banerjee, I. and McDonald, B.C.
1975: Nature of esker sedimentation; in Glaciofluvial and glaciolacustrine sedimentation, ed. A.V. Jopling and B.C. McDonald; Society of Economic Paleontologists and Mineralogists, Special Publication 23, p. 132-154.

Boissonnault, P. et Gwyn, Q.H.J.
1983: L'évolution du lac proglaciaire Memphrémagog, sud du Québec; Géographie physique et Quaternaire, vol. 37, p. 199-204.

Clément, P. et Parent, M.
1977: Contribution à l'étude de la déglaciation wisconsinienne dans le centre des Cantons de l'Est, Québec; Géographie physique et Quaternaire, vol. 31, p. 217-228.

Gadd, N.R.
1980: Late-glacial regional ice-flow patterns in eastern Ontario; Canadian Journal of Earth Sciences, v. 17, p. 1439-1453.

1981: Late-glacial regional ice-flow patterns in eastern Ontario: Reply; Canadian Journal of Earth Sciences, v. 18, p. 1390-1393.

1983: Notes on the deglaciation of southeast Quebec; in Current Research, Part B, Geological Survey of Canada, Paper 83-1B, p. 403-412.

Gadd, N.R., McDonald, B.C., and Shilts, W.W.
1972: Deglaciation of southern Québec; Geological Survey of Canada, Paper 71-47, 19 p.

Gauthier, R.C.
1975: Déglaciation d'un secteur des rivières Chaudière et Etchemin, Québec; mémoire de M.Sc., inédit, McGill University, 180 p.

[1] UQ-290 was obtained from **Macoma balthica** shells collected by the author. Shells were in growth position in the foreset beds of a delta whose surface stands at 153 m a.s.l.

Hillaire-Marcel, C.
1981: Late-glacial regional ice-flow patterns in eastern Ontario: Discussion; Canadian Journal of Earth Sciences, v. 18, p. 1385-1386.

Karrow, P.F.
1981: Late-glacial regional ice-flow patterns in eastern Ontario: Discussion; Canadian Journal of Earth Sciences, v. 18, p. 1386-1390.

LaSalle, P., Martineau, G., et Chauvin, L.
1977: Morphologie, stratigraphie et déglaciation dans la région de Beauce-Monts Notre-Dame – Parc des Laurentides, Québec; Ministère des Richesses naturelles, DPV-516, 74 p.

Lortie, G.
1976: Les écoulements glaciaires wisconsiniens dans les Cantons de l'Est et la Beauce, Québec; mémoire de M.Sc. inédit, McGill University, 219 p.

McDonald, B.C.
1967a: Surficial geology, Sherbrooke-Orford-Memphrémagog, Québec; Geological Survey of Canada, Map 5-1966.

1967b: Pleistocene events and chronology in the Appalachian region of southeastern Québec, Canada; unpublished Ph.D. dissertation, Yale University, 161 p.

1968: Deglaciation and differential postglacial rebound in the Appalachian region of southeastern Québec; Journal of Geology, v. 76, p. 664-677.

Parent, M.
1978: Géomorphologie quaternaire de la région de Stoke-Watopéka, Québec; mémoire de M.Sc., inédit, Université de Sherbrooks, 206 p.

Prichonnet, G.
1982a: Quelques données nouvelles sur les dépôts quaternaires du Wisconsinien et de l'Holocène dans le piedmont appalachien, Granby, Québec; Recherches en cours, Partie B, Commission géologique du Canada, Étude 82-1B, p. 225-238.

1982b: Résultats préliminaires sur la géologie quaternaire de la région de Cowansville, Québec; Recherches en cours, Partie B, Commission géologique du Canada, Étude 82-1B, p. 297-300.

Prichonnet, G., Doiron, A., et Cloutier, M.
1982: Le mode de retrait glaciaire tardiwisconsinien sur la bordure appalachienne au sud du Québec; Géographie physique et Quaternaire, vol. 36, p. 125-137.

Shilts, W.W.
1976: Glacial events in southern Quebec-northern New England, a reappraisal (Abstract); Geological Society of America, Abstracts with Program, v. 8, no. 2.

1981: Surficial geology of the Lac-Mégantic area, Québec; Geological Survey of Canada, Memoir 397, 102 p.

Thomas, R.H.
1977: Calving bay dynamics and ice-sheet retreat up the St. Lawrence Valley system; Géographie physique et Quaternaire, v. 31, p. 347-356.

NOTES ON THE DEGLACIATION OF SOUTHEASTERN QUEBEC: REPLY

Nelson R. Gadd
Terrain Sciences Division

Dubois et coll. (1984) et Parent (1984), dans des textes séparés, ont remis sérieusement en question mon court rapport (Gadd, 1983), ce qui appelle une réponse. Comme on pourra le constater, quand je parle de certaines observations nouvelles, il s'agit en réalité de nouvelles données de terrain qui n'auraient pas encore été enregistrées tandis que d'autres sont des observations concernant le sens de données de terrain déjà connues, mais maintenant considérées sous un jour légèrement différent par rapport aux travaux originaux.

Dubois et coll. (1984) revèlent un certain nombre de détails dont je n'ai pas tenu compte dans mon hypothèse de travail (Gadd, 1983) concernant la déglaciation du sud du Québec. Comme l'usage le veut dans ce genre de discussion, on a peut-être trop insisté sur le repérage précis des traits tracés sur mes diagrammes (et non pas des cartes géologiques) dont j'ai nettement établi la nature hypothétique. Il n'y a aucun doute que des études approfondies comme celles qui ont été mentionnées par Dubois et coll. (1984), ainsi que des travaux semblables encore à venir, pourront confirmer que les limites glaciaires véritables ressemblaient très peu aux configurations que j'ai indiquées.

Il semble que ma désignation des figures et que la formulation du texte aient permis à Dubois et à ses collègues de comprendre à partir de ma figure 6 (Gadd, 1983, p. 410) que ce système Missisquoi appartenait à une phase d'épandage fluvio-glaciaire à une époque où la marge glaciaire est indiquée à une certaine distance à l'ouest du système. Je les remercie de me signaler une erreur commise par inadvertance. Cependant, une lecture un peu plus généreuse du texte et des figures démontrerait que nos opinions respectives ne divergent en rien; ainsi, nous sommes d'accord que la vallée du Missisquoi a déjà été occupée dans des sédiments de contact glaciaire, d'épandage fluvio-glaciaire et lacustre au cours d'une phase glaciaire et que le système a par la suite été érodé jusqu'à son état actuel, dans des conditions non glaciaires.

Toutefois, je dois souligner qu'une mise en place abondante des sédiments glaciaires en question a eu lieu dans la vallée de la rivière Missisquoi, mais non dans la vallée du lac Memphrémagog qui est à la fois parallèle et plus grande. Il s'agit là d'un élément d'information capital que parvient à dissimuler la discussion plutôt longue concernant certains détails qui n'interviennent pas dans le problème beaucoup plus pertinent en question. Ma note (Gadd, 1983) postule et fait allusion à la preuve évidente sur le terrain, voulant que le bassin du lac Memphrémagog doive avoir été rempli par une masse stagnante de glace pendant la période qu'il a fallu pour remplir presque complètement la vallée de la rivière Missisquoi par des sédiments d'origine glaciaire. La publication presque simultanée de l'étude de Boissonnault et Gwyn (1983) retraçant l'évolution du lac glaciaire Memphrémagog n'exclut pas cette anomalie apparente dans la sédimentation glaciaire, et c'est pourquoi j'en ai donc parlé ailleurs (Gadd, sous presse).

Parent (1984) has stated that certain of my observations are not new, and that some are incorrect or unfounded; these statements I must treat more directly.

In the first few paragraphs of his discussion, Parent calls for key evidence of the sea in contact with the northern margin of the remnant ice mass that I have postulated in the Quebec areas north of Lake Champlain. Admittedly, I have left this question hanging, for this is an area in which we have relatively little recent information. I recall, however, on a field trip many years ago, wondering about the structure of an esker-like ridge we called the Ste. Philomène ridge (on the plain south of Montreal). In it stream flow produced structures dipping northward and containing some marine shells. Although the ridge has been heavily exploited for sand and gravel, the features were still visible only a few years ago. Other evidence of northward stream flow from a stagnating ice mass south of Champlain Sea and within the zone of late, northward ice flow, may be found in a short esker near Saint-Jacques-de-Leeds (Gadd, 1978, p. 5). The evidence is sparse, however, because the bulk of such features must have formed on the flat plain of St. Lawrence Lowland and easily could have been destroyed by wave action in the Champlain Sea after the temporarily protective ice mass had melted. Many such features may exist today as fossiliferous boulder and gravel deposits on ridges within the marine plain – an idea worth investigating further, perhaps.

The above-mentioned northward flow of ice from the Appalachians towards the St. Lawrence (Lamarche, 1971) is clear evidence that drawdown was occurring and that ultimately a lead of marine water, a calving bay (Thomas, 1977) for example, may have separated ice masses north and south of the modern St. Lawrence.

With due apology to Clément and Parent (1977) for lack of reference to their previous work, I suggest that my observations are new in that they indicate that in certain areas the ponded sediments are confined to the valley walls, and do not occur as erosional remnants on the adjacent valley floor. I deduce from such evidence that high level lakes may have been localized by ice lobes in the valleys. Such features are not necessarily to be correlated with similar features farther north, or in adjacent valleys, unless synchroneity and continuity can be established on a good basis. As Parent states, many of the phenomena we look at are diachronous and therefore must be dealt with cautiously. Both lakes and ice masses, with their characteristic deposits, situated in isolated basins may have quite discordant (diachronous) histories – a feature that I have attempted to illustrate in my Figures 4 and 5 (Gadd, 1983, p. 408, 409) by showing an active (?) ice margin on one side of the Sutton Mountains and stagnant ice masses (McDonald, 1967) on the other. I maintain, however, that even where ice masses may be separated from the main ice sheet and described as "stagnation zones", there may be a residual ice flow within such isolated masses that depends upon their physical dimensions in relation to the physics of the ice.

Parent notes that "sediments within the col south of Mont Orford, near Delaire, were deposited by meltwater flowing eastward", and no doubt this is true; I, too, have seen these. But these were not the deposits that I observed showing westward dips in coarse ice-contact sediments. These latter are at considerably higher elevation and, therefore, are probably older and more clearly related to the immediate presence of ice in the Memphrémagog basin. The meltwater carried by channels referred to by Parent may have been produced by ice that was several miles distant.

There is a later, somewhat misleading reference to "outwash channels between Richmond and Abercorn, as reported in his figure 5". The figure does not show a connection with Saint-François valley in the highland at Richmond, but rather that the system extends along the toe of the highland escarpment from a point between Richmond and Ulverton. The ice margin is shown at a known Highland Front morainic feature at Ulverton. From there, over much of the distance to Abercorn there is a broad channel with, in places, ice-contact deposits on the northwest side and fluvial terraces on the other (perhaps it would have been better to describe the system in the legend as ice-marginal drainage,

From: Discussions and Communications in Current Research, Part B; Geol. Surv. Can., Paper 84-1B.

rather than an outwash channel system). The detailed maps referred to in this part of the comment do not cover all of the area in question, thus I have made new, unrecorded, observations not known to the authors cited, and I have seen the area through different eyes and in the context of rather different regional concepts.

The sediments near Danville (Ms p. 5), which Parent identifies as "fossiliferous marine delta sediments", as he says, were earlier identified by Gadd et al. (1972) as "ice-front accumulations associated with the Highland Front Moraine Complex". I am sure, had I mentioned the marine sediments, I would have interpreted them to be shoreline features, such as beach bar or spit, that were superposed on the older glacial feature. There is no suggestion in my statement that the sea and the ice were in contact. What was described in the note under discussion here was nothing like the Danville situation. I identify an open-water fluvial system with associated glacial lakes and ice marginal features. The well preserved open water system could not have existed below marine limit without being inundated and in some way modified by subsequent marine erosion and deposition, as in the Danville case given in Parent's example. It therefore seems axiomatic to me that the marine waters, at the time of the formation of ice-marginal channels, were excluded by a mass of ice situated to the northwest and that subsequently, when the ice melted, marine limit had to lie below the unmodified features. Comparison of radiocarbon dates from the areas near the channels in question with those in other areas of the Champlain Sea, where glacial features have been modified, is a pertinent part of my interpretation.

The dates in the area around Adamsville and Granby cluster around 11 000 BP, whereas those of other parts of St. Lawrence Lowland, including the Danville area, approach or exceed 12 000 BP. There is no clear time established for the **Mya** phase of the Champlain Sea, but the assemblage probably represents a late phase of the sea; it occurs in the area in question and has yielded dates that also represent late Champlain Sea time. I have found no higher fossil assemblages or evidence of marine action in the channelled areas. The earlier interpretation of higher marine levels (Goldthwait, 1913) is based, in my opinion, on an interpretation of beach-like forms that I now claim may be interpreted as kame terraces. Further evidence of control of marine inundation, by glacial ice, is in the fact that the abandoned channel systems described show evidence of flow towards the south and south-southwest, whereas unrestricted modern drainage trends north, northwest, and northeast. Thus, it is my conclusion that over a period of time when marine sediments were being deposited in other parts of the region at and below the elevation of the abandoned channels, in the area east of Cowansville, along the lower northwest-facing flanks of Sutton Mountains, the direction of flow and orientation of meltwater channels were being controlled by the presence of a significant mass of glacier ice.

Needless to say, I do not feel that the comments of either Dubois et al. (1984) and of Parent (1984) have in any way diminished the usefulness of the working hypotheses I have presented. On the other hand, I thank them for their interest, and hope that we may all one day examine the field evidence together.

References

Boissonnault, P. et Gwyn, Q.H.J.
1983: L'évolution du lac proglaciaire Memphrémagog, sud du Québec; Géographie physique et Quaternaire, vol. 37, p. 197-204.

Clément, P. and Parent, M.
1977: Contribution à l'étude de la déglaciation wisconsinienne dans le centre des Cantons de l'Est, Québec; Géographie physique et Quaternaire, vol. 31, no. 3-4, p. 217-228.

Dubois, J-M., Larocque, A., Boissonnault, P., Dubé, C., Poulin, A., Gwyn, Q.H.J., Larocque, G., et Morissette, A.
1984: Discussion de "Notes on the deglaciation of southeastern Quebec"; dans Recherches en cours, Partie B, Commission géologique du Canada, Étude 84-1B.

Gadd, N.R.
1978: Surficial geology of Saint-Sylvestre map-area, Quebec; Geological Survey of Canada, Paper 77-16.

1983: Notes on the deglaciation of southeastern Quebec; in Current Research, Part B, Geological Survey of Canada, Paper 83-1B, p. 403-412.

– L'évolution du lac proglaciaire Memphrémagog, sud du Québec: Comment: Géographie physique et Quaternaire. (sous presse)

Gadd, N.R., McDonald, B.C., and Shilts, W.W.
1972: Deglaciation of southern Quebec; Geological Survey of Canada, Paper 71-47, 19 p.

Goldthwait, J.W.
1913: Quebec and vicinity: physiographic notes; 12th International Geological Congress (Canada), Guide-book No. 1, Part 1, p. 48-51.

Lamarche, R.
1971: Northward moving ice in the Thetford Mines area of southern Quebec; American Journal of Science, v. 271, no. 4, p. 383-388.

McDonald, B.C.
1967: Pleistocene events and chronology in the Appalachian region of southeastern Quebec, Canada; unpublished Ph.D. dissertation, Yale University.

Parent, M.
1984: Notes on the deglaciation of southeastern Quebec: Discussion; in Current Research, Part B, Geological Survey of Canada, Paper 84-1B.

Thomas, R.H.
1977: Calving bay dynamics and ice sheet retreat up the St. Lawrence Valley system; Géographie physique et Quaternaire, v. 31, no. 3-4, p. 347-356.

STRATA AND TRACE FOSSILS NEAR THE PRECAMBRIAN – CAMBRIAN BOUNDARY, MACKENZIE, SELWYN AND WERNECKE MOUNTAINS, YUKON AND NORTHWEST TERRITORIES: DISCUSSION

J.D. Aitken
Institute of Sedimentary and Petroleum Geology, Calgary

Introduction

The recent paper by Fritz, Narbonne, and Gordey (1983) is an important contribution, both to the resolution of stratigraphic relationships near the Precambrian-Cambrian boundary in the northwestern Cordillera, and to the question of paleobiological criteria for that boundary, worldwide. My independent study of a number of the areas and sections reported on by Fritz and co-workers largely confirms their data and supports their interpretations. The purpose of this note is to draw attention to additional data, to comment on some implications of these data and to point out two instances in which our data and our interpretations are at variance.

Physical Stratigraphy

The contribution of Fritz et al. (1983) can be enhanced by establishing a tie between their informal lithostratigraphic units and the underlying, formally named formations. Such a tie will be made briefly here.

Corn Creek area

Because one formation of dark-coloured, deep-water mudrocks is much like another (except for its biota), the lithostratigraphic correlation of such mudrock units in the Mackenzie and Wernecke mountains depends on correlation of the intervening, mainly carbonate units. Fortunately, three lithologically distinct carbonate units punctuate the uppermost Proterozoic stratigraphic column of the region. These are, in downward succession: 1. Map unit 11 of Blusson (1971) – dolomite and minor sandstone of mainly shallow-water character; 2. a distinctive carbonate unit of which both deep water and platformal facies are known, bearing a facies relationship to the upper beds of the Sheepbed Formation (middle part of Map unit 10b of Blusson, 1971; "Sheepbed carbonate" of Aitken, 1982); and 3. the extensive and easily recognized Keele Formation (Gabrielse et al., 1973; Eisbacher, 1978, 1981).

Localities at which I have studied the Sheepbed Formation (Gabrielse et al., 1973) are identified in Figure 1; these are coded to identify the sections in which downward stratigraphic continuity with the Keele Formation and/or upward continuity with Map unit 11 are observable.

A key section is my section "A" (Fig. 1), in southeastern Nadaleen River map area. This section, my section "B", and Section 9 of Fritz et al. (1983) are all in the same structural panel, over a strike length of 20 km (Fig. 2). At "A", the Keele Formation, mapped by Eisbacher (1981), is thin but clearly recognizable; its lower part is quartz-pebble conglomerate and quartzite, and its upper part is the distinctive "teepee dolostone". By definition, the formation of dark mudrocks conformably overlying the Keele is the Sheepbed. At "A", the Sheepbed shale is overlain by ribbon-bedded dolomite with a few matrix-supported breccias (debris-flows), and in the upper few metres, a few beds of ex-grainstone and a horizon of metre-high, domal stromatolites. This is a typical expression of the "Sheepbed carbonate" of Aitken (1982). Pockets and sedimentary sills of fine grained sandstone testify to a karstic erosion surface atop the unit.

At "A", the "Sheepbed carbonate" is overlain immediately by "peach-coloured weathering", largely thick-bedded dolomites that are in part ex-grainstones, interrupted by beds of quartz sandstone and quartz-pebble conglomerate. Recognition of this unit as Map unit 11 is supported by its bipartite character; two units of mainly dolomite are separated by a poorly exposed, medial, recessive-weathering unit containing rusty weathering, shaly strata. The same bipartite character is displayed by Map unit 11 in the Sekwi Brook and June Lake areas of Sekwi Mountain map area ("E" and "F", Fig. 1).

The succession at Section A has been traced southward, by helicopter traverse, in virtual continuity to Section B, only 7 km north of Section 9 of Fritz et al. (1983). I believe that structural complications will prevent the "flying-out" of units between the latter two sections, but both are in the same major structural unit, and each one contains at its top the unmistakable clastic formation, consisting of two coarsening-upward cycles with Cambrian trace fossils, that Fritz et al. assigned to the Vampire Formation. Significant changes are observable along the traverse from Section A to Section 9 (Fig. 2). A few kilometres south of "A", a unit of recessive-weathering, clastic strata appears between the "Sheepbed carbonate" and the overlying Map unit 11. This clastic unit thickens southward to 190 m at "B" and about 240 m (Fritz et al., 1983, Fig. 44.2) at Section 9. At their Section 9, Fritz et al. recognized as Map unit 11 the carbonate unit disconformably underlying the Vampire Formation. Map unit 11 overlies a unit of fine grained clastic strata, termed by them "Siltstone unit 1". "Siltstone unit 1" overlies another carbonate unit, termed by Fritz et al. "Unnamed dolostone unit". This lower carbonate unit is, on the basis of its lithology and stratigraphic position, the "Sheepbed carbonate" (Fig. 2); it is in gradational contact with underlying dark mudrocks of the Sheepbed Formation proper ("Siltstone unit 2" of Fritz et al., 1983).

Section B brings to light a significant regional variation in facies of "Siltstone unit 1". There, "Siltstone unit 1" consists of mudrocks, partly purple-red, and quartzites of shallow-water aspect, with sun cracks, shale-pebble (rip-clast) conglomerates, and some trough crosslamination. A one metre thick bed of chert- and quartzite-pebble conglomerate is 23 m above the base. No trace nor body fossils were found at Section B. In contrast, near Sekwi Brook ("E", Fig. 1) and south of June Lake ("F", Fig. 1) in Sekwi Mountain map area, the homotaxial unit between the "Sheepbed carbonate" and Map unit 11 consists of dark mudrocks with subordinate turbiditic sandstone and minor turbiditic limestone. Small, simple trace fossils (**Torrowangea** sp., **Planolites** sp.) occur throughout, and at Sekwi Brook, Ediacaran fossils (to those reported by Hofmann, 1981, can be added a specimen of **Pteridinium** sp., GSC Loc. C-94062, collected by Jon Jones and identified by M. Fedonkin).

Sekwi Brook - southern June Lake area

The uppermost Proterozoic and basal Cambrian section in the overturned structural panel passing through June Lake, in Sekwi Mountain map area, is better exposed and more complete downward at Fritz's (1979) Section 35 ("F", Fig. 1) than his Section 33 (11, Fig. 1), 20 km to the north, near June Lake. The southern section can be summarized from top to bottom as follows (Fig. 3):

7. A recessive-weathering formation of mainly siltstone and mudstone; dark grey, micaceous, weathering dark brown; minor, similar, shaly sandstone; minor, thin and medium beds of quartzite, brownish grey, very fine grained; about 273 m thick (*fide* Fritz, 1979, Fig. 3). This is the Vampire Formation (Fritz, 1982).

From: Discussions and Communications in Current Research, Part B; Geol. Surv. Can., Paper 84-1B.

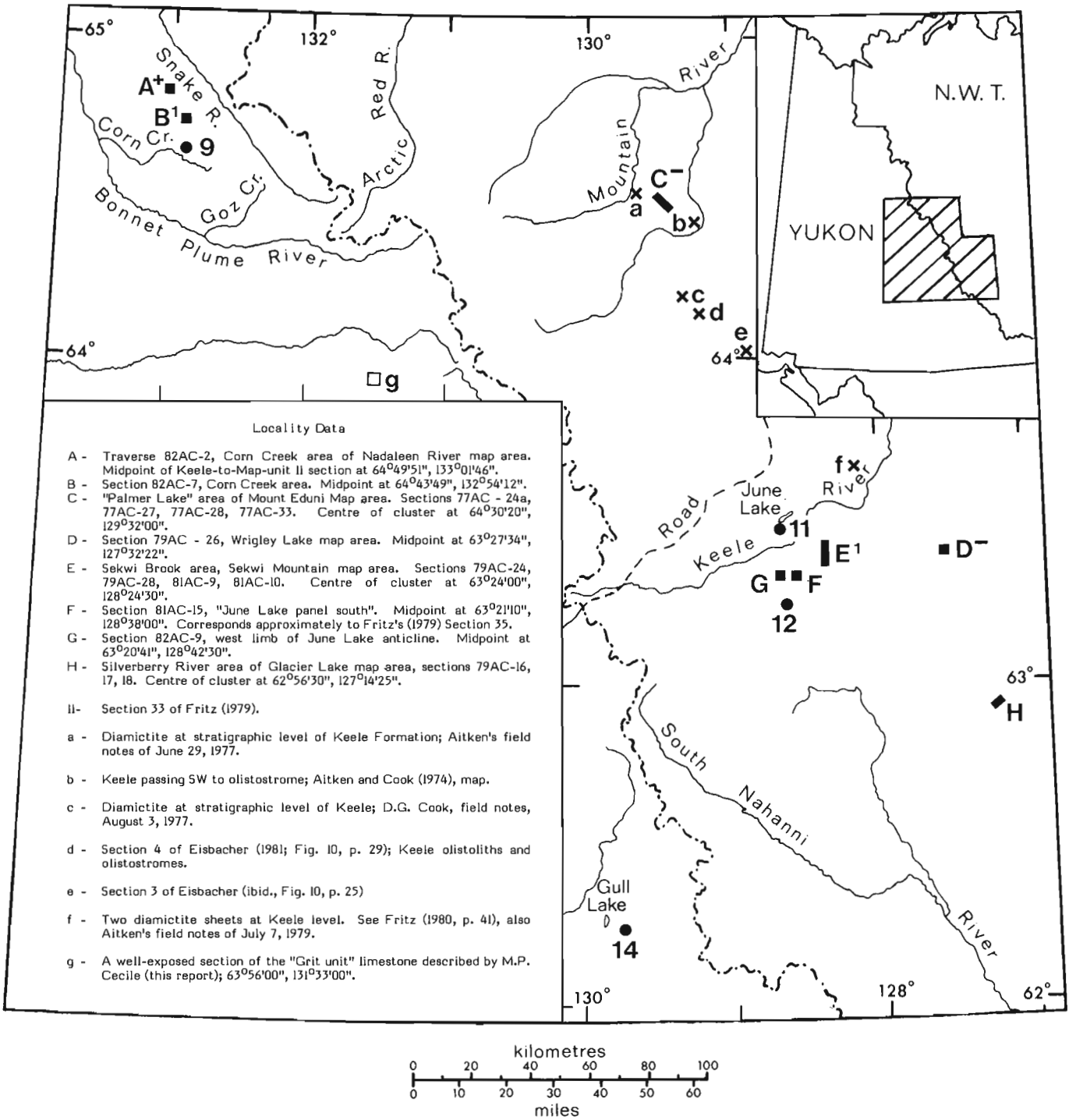

Locality Data

A - Traverse 82AC-2, Corn Creek area of Nadaleen River map area. Midpoint of Keele-to-Map-unit II section at 64°49'51", 133°01'46".

B - Section 82AC-7, Corn Creek area. Midpoint at 64°43'49", 132°54'12".

C - "Palmer Lake" area of Mount Eduni Map area. Sections 77AC - 24a, 77AC-27, 77AC-28, 77AC-33. Centre of cluster at 64°30'20", 129°32'00".

D - Section 79AC - 26, Wrigley Lake map area. Midpoint at 63°27'34", 127°32'22".

E - Sekwi Brook area, Sekwi Mountain map area. Sections 79AC-24, 79AC-28, 81AC-9, 81AC-10. Centre of cluster at 63°24'00", 128°24'30".

F - Section 81AC-15, "June Lake panel south". Midpoint at 63°21'10", 128°38'00". Corresponds approximately to Fritz's (1979) Section 35.

G - Section 82AC-9, west limb of June Lake anticline. Midpoint at 63°20'41", 128°42'30".

H - Silverberry River area of Glacier Lake map area, sections 79AC-16, 17, 18. Centre of cluster at 62°56'30", 127°14'25".

II- Section 33 of Fritz (1979).

a - Diamictite at stratigraphic level of Keele Formation; Aitken's field notes of June 29, 1977.

b - Keele passing SW to olistostrome; Aitken and Cook (1974), map.

c - Diamictite at stratigraphic level of Keele; D.G. Cook, field notes, August 3, 1977.

d - Section 4 of Eisbacher (1981; Fig. 10, p. 29); Keele olistoliths and olistostromes.

e - Section 3 of Eisbacher (ibid., Fig. 10, p. 25)

f - Two diamictite sheets at Keele level. See Fritz (1980, p. 41), also Aitken's field notes of July 7, 1979.

g - A well-exposed section of the "Grit unit" limestone described by M.P. Cecile (this report); 63°56'00", 131°33'00".

● Sections of Fritz et al.(1983) to which reference is made.

■ Sections (areas) studied by the writer and cited here, coded for content as follows: C^-: Sheepbed and Keele Formations in same section; C^1: Sheepbed and Map unit II in same section; C^+: Sheepbed, Keele and Map unit II in same section; X: locality at which Keele or equivalent is in olistostrome or diamictite facies.

Figure 1. *Map of localities.*

6. A resistant-weathering formation dominated by sandstone and quartzite that are mainly whitish (pale brown near the base), of fine sand to granule grade, and in large part thickly bedded. There are several conspicuous units of shale and mudstone, largely khaki, dark grey toward the base, partly silty, sandy and/or micaceous. A unit of limestone and dolomite, 6.5 m thick, occurs 82 m above the base. Simple non-diagnostic trace fossils occur at intervals throughout. This formation, 637 m thick, is the "Upper submember" of Blusson's (1971) Map unit 12, a correlative of part or possibly all of the Backbone Ranges Formation. Its base here is erosional, with a quartzite filled channel 4.5 m deep.

5. A moderately resistant formation dominated by carbonate rocks, as follows:
   - c. (24 m): Grey limestone, and pale orange dolomite; stacked biostromes of columnar-branching stromatolites.
   - b. (7.5 m): 80 per cent sandstone, partly calcareous and dolomitic, very fine grained, very well sorted, medium and thin bedded, mostly plane-parallel laminated; 20 per cent limestone, as in Unit a.
   - a. (7.5 m): Limestone, dolomitic, siliceous, nodular thin bedded, scaly to massive; mostly pale-pellet grainstone, with limestone intraclasts in the basal bed.

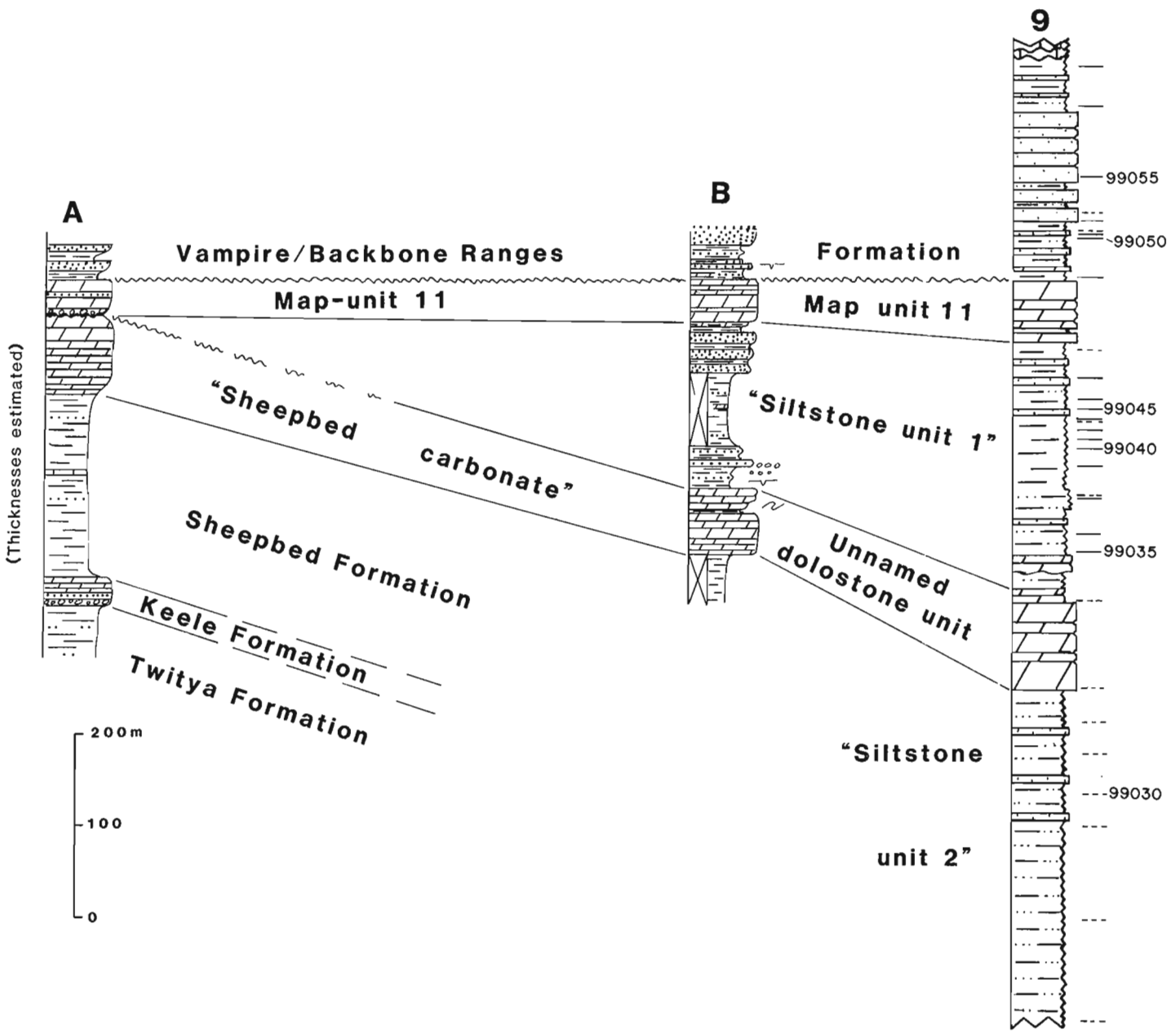

Figure 2. Correlations between sections "A" and "B" (this paper, Fig. 1) and Section 9 of Fritz et al. (1983). The correlations are by Aitken. Nomenclature at "9" is that of Fritz et al.

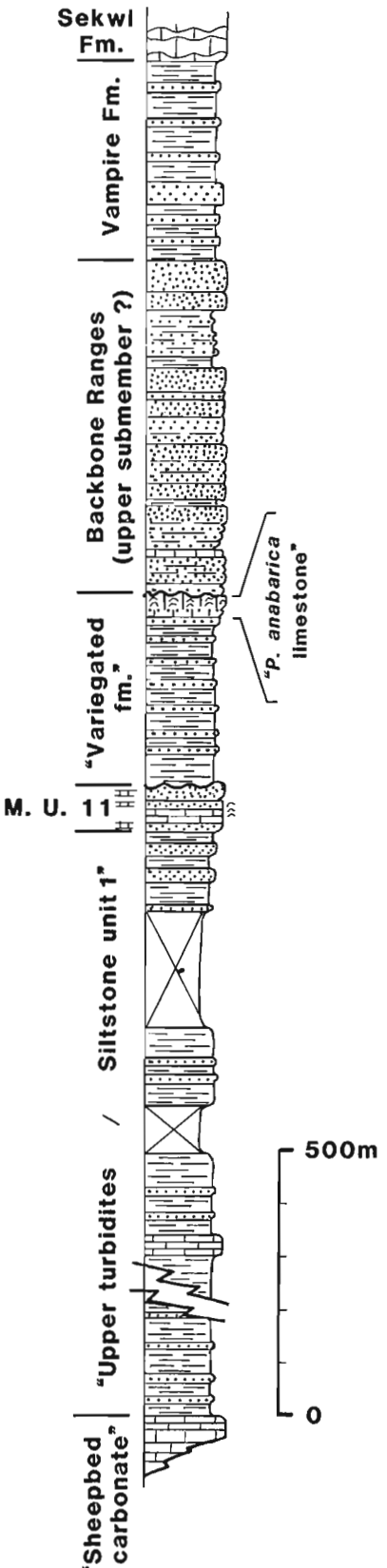

Figure 3. Stratigraphic column straddling the Precambrian – Cambrian boundary, 20 km south of June Lake ("F", Fig. 1).

This formation (Unit 5) has no lithostratigraphically recognizable equivalent in either the Sekwi Brook area ("E", Fig. 1), or in the Corn Creek area ("A", "B", Fig. 1). The same carbonate unit, 12 m thick, is shown in Fritz's (1979) Section 33, about 320 m above the base of Map unit 12. Fritz (ibid.) identified it in his Section 35 as Map unit 11, but, in view of the presence of Map unit 11 lower in the same section (see below), that is now interpreted as a miscorrelation. This point is extremely important, because the specimen of **Protohertzina** cf. **anabarica** (GSC loc. 94597), reported by Conway Morris and Fritz (1980) was recovered from the limestone formation just described. This unit, to which I will refer informally as the "**P. anabarica** limestone", is only 4 m thick on the next spur south of the line of Section F, and at Section 12 of Fritz et al. (1983) it is unreported. These observations indicate that its top represents a significant unconformity.

4. A moderately resistant formation of mainly interbedded shaly siltstone and sandstone. The formation is characterized by the colour of the mudrocks – dominantly green – with subordinate units that are purple-red. Diagnostic evidence of shallow water deposition is lacking. Trace fossils are abundant and well preserved, but non-diagnostic of age. H.J. Hofmann and Guy Narbonne report the following (pers. comm., 1982):

   Planolites sp., GSC locs. C-94060, C-94099, C-94090
   Scolicia senso lato, GSC loc. C-94090
   "**Neonereites**-like trails" cf. Brasier and Hewitt (1979), GSC loc. C-94090
   grooves connected to pits, GSC loc. C-94090
   bilobate impressions; may be related to **Scolicia** (above), GSC loc. C-94090
   Cochlichnus serpens Webby, 1970, GSC loc. C-94086
   cf. **Harlanielle podolica** in Palii et al. (1976), GSC loc. C-94088

   This formation, 256 m thick, is the "lower submember of Map unit 12" of Fritz et al. (1983). I will refer to it informally as the "variegated formation", and will include with it the "**P. anabarica** limestone" at its top, as an informal member. It thins westward to 220 m in the west limb of the June Lake anticline (plus 5 m of sandy limestone at its top).

   The base of the "variegated formation" is erosional. The contact with the underlying carbonate rocks has 25 cm of local relief that is not constructional. Pockets and veins of mudstone, presumably introduced downward at a karstic erosion surface, extend to 2.1 m below the contact. Pronounced variation in the regional thickness of the carbonate interval above the medial, shaly "break" of the underlying formation suggests that this is a significant unconformity.

3. A resistant formation characterized by carbonate rocks, including limestone that is mainly sandy (quartz sand) and in part crossbedded and dolomitic, stromatolitic dolomite (simple domes), and sandstone that is dolomitic and calcareous in part. A medial, recessive-weathering unit consists of sandstone and dark grey shale, and contains the simple trace fossil ?**Torrowangea** sp., (GSC loc. C-89434). The basal contact is interbedded with the underlying clastic rocks. This carbonate-bearing formation is Map unit 11; correlation with the unit identified by both Fritz and myself at Fritz's (1979) Section 33 as Map unit 11 is straightforward.

   Map unit 11 thins and pinches out westward, from the Sekwi Brook area ("E", Fig. 1), where it is up to 167 m thick, to the vicinity of Fritz's (1979) Section 35 ("F", Fig. 1) where it is 84 to 97 m thick; it is missing in the west limb of the anticline, opposite Section 35 ("G", Fig. 1).

2. A recessive-weathering formation, characterized by dark-coloured mudrocks with minor turbiditic sandstone beds and rare turbiditic limestone beds. Toward the top, sandstone beds are cleaner and thicker, in a shallowing-upward progression to the interbedded contact with Map unit 11. This formation, from its position between Map unit 11 and the "Sheepbed carbonate", corresponds to "Siltstone unit 1" of Fritz et al. (1983). It is referred to as the "Upper turbidites" in Baudet et al. (ms). It is characterized almost throughout by abundant, small, simple trace fossils, mainly **Torrowangea** sp. and **Planolites** sp.
(GSC locs. C-94094, C-94097-99, C-94101). Up to 408 m thick near Sekwi Brook ("E", Fig. 1), "Siltstone unit 1" thickens westward, to over 1000 m in the west limb of the June Lake anticline ("G", Fig. 1).

1. Forming the tight, faulted core of June Lake anticline, a formation of medium bedded and ribbon bedded lime mudstone with thick beds of debris-flow breccia. This is clearly the "Sheepbed carbonate", here undolomitized (unlike exposures farther platform-ward). The exposed thickness is at least 30 m, and the exposed part appears to be structurally detached from lower strata. The contact with the overlying clastics is faulted in the east limb, but depositional in the west limb.

Biostratigraphy

An important biostratigraphic point arises out of the preceding description of the lithostratigraphy in Sekwi Mountain map area. The only reported skeletal fossils reported from Map unit 11 or older formations are the **Protohertzina** cf. **P. anabarica** and problematic associates (GSC loc. 94597) reported from Fritz's (1979) Section 35 (Conway Morris and Fritz, 1980), but as shown above, these fossils are from a younger stratigraphic unit, the "**P. anabarica** limestone". This correction is important, because the critical fossil's stratigraphic position is above, rather than below, the karstic erosion surface, recognized by Fritz et al. (1983) and by myself, that overlies Map unit 11 and may be the widely recognized "sub-Cambrian unconformity".

A second report of highly significant fossils should be treated with caution until very carefully confirmed; this is the report of Ediacaran fossils from a loose block whose source is reported to be "Siltstone unit 2" (Fritz et al., 1983, p. 375; Hofmann, Fritz and Narbonne, 1983). I advocate caution, simply because this occurrence contradicts my experience in the region. I have found trace fossils with relative ease in the turbiditic facies of "Siltstone unit 1", where I have examined it, but in searching with equal zeal for fossils in the Sheepbed Formation ("Siltstone unit 2") at five well-exposed sections (A, C, D, E, H, Fig. 1) have found not a single trace nor body fossil. At some localities, the Sheepbed is of a turbiditic facies identical with fossiliferous facies of "Siltstone unit 1". Near Sekwi Brook, the lowest trace fossils appear immediately above the "Sheepbed carbonate" and are abundant at their first appearance.

Correlation of the "Grit unit" Limestone

Fritz et al. (1983, p. 373) made a tentative correlation between Map unit 11 of Blusson (1971) and a thin limestone at the top of the lower subunit of the regional "Grit unit" (Gabrielse, 1967, p. 275) near Gull Lake ("14", Fig. 1). As documented above, Map unit 11 thins westward, and pinches out between the east and west limbs of the June Lake anticline (between "F" and "G", Fig. 1). The repetitive pattern of erosional thinning of Upper Proterozoic units in the region is one of eastward thinning and truncation, therefore, the westward disappearance of Map unit 11 is more probably a downslope depositional pinchout. It is therefore unlikely that Map unit 11 persists west of the June Lake anticline or reappears as far west as Gull Lake.

If correlation of the "Grit unit" limestone with Map unit 11 as suggested by Fritz et al. (ibid.) is incorrect, it is worthwhile to examine such other platformal carbonate units in the region that might have basinal, carbonate equivalents near Gull Lake. The first of these is the Keele Formation. The Keele is most unlikely to have as its basinal equivalent bedded carbonates, because, where seen at its most southwesterly exposures, it is passing, or has passed, into diamictites and olistostromal breccias (see locs. "a" to "f", Fig. 1). These fragmental rocks have clastic matrices, indicating an overall basinward facies change to clastic strata at the level of the Keele.

The next higher Upper Proterozoic carbonate unit is the "Sheepbed carbonate". It is up to 326 m thick and displays remarkable consistency in lithic character, both along and across the depositional strike (Fig. 1). All of the more southwestward sections are of slope or basinal facies, regularly thin- and partly medium-bedded dolomites (limestones at F, Fig. 1), with internal, millimetre lamination. Medium and thick, massive beds and lenses of debris-flow breccia are sparse but characteristic signatures of the formation. In the absence of other plausible candidates, the "Sheepbed carbonate" is the most likely candidate as the shelfward equivalent of the limestones exposed near Gull Lake ("14", Fig. 1).

Northwest of Gull Lake, at "g" (Fig. 1), Proterozoic to Cambrian argillites contain a distinct carbonate formation that may be equivalent to the "Grit unit" limestone and the "Sheepbed carbonate". M.P. Cecile provides the following remarks about the limestones found in the vicinity of "g" (personal communication, 1982):

> "The 'uppermost' Proterozoic stratigraphy of the northwestern 105-O (Niddery Lake) map area and, based on direct physical correlation to the maps of Blusson (1974), the southwestern part of the 106-B (Bonnet Plume Lake) and southern 106 C map areas, includes a prominent 200 m thick succession of grey, generally unfossiliferous limestone. This limestone is mappable at a 1:250 000 scale, and it can be divided into two members of equal thickness – an upper resistant succession of thick bedded grey limestone and a lower recessive succession of thin bedded, dark grey, shaly limestone. The contact between the two members is gradational over a few metres.
>
> The upper member consists of fine to medium crystalline limestone with patchy traces of dolomite spar, and in many sections a metre or more of zebra dolostone. Typically, the limestone beds in this unit are internally massive but in the upper part of this unit pisolite grainstones, limestone conglomerates, or beds with planar or festoon cross stratification (usually the more arenaceous limestones) were frequently observed. This upper member also features a number of minor rock types: thin, brown weathering, green argillite beds; arenaceous limestone; and, in the upper few metres, abundant arenaceous or silty, yellow-weathering, limestone-clast para- and ortho-conglomerates.
>
> The lower member consists of dark grey, finely crystalline, shaly limestone beds that are internally massive. Minor rock types found with this unit are thin beds of rusty black shale, and in the basal few metres, limestone-clast para- and ortho-conglomerates.
>
> Although this limestone has been traversed extensively in the northwestern 105-O map area it is unfossiliferous, with the exception of one locality where

a thick bed of limestone features low amplitude, laterally-linked hemispherical stromatolite laminae with a low degree of vertical inheritance.

This prominent limestone unit is abruptly overlain by a 600 m thick succession of dark grey, grey and green argillites that are unfossiliferous and contain minor beds of quartzite, quartz-pebble conglomerate, and yellow weathering silty to arenaceous limestone. This argillite is in turn overlain by 200 m of maroon to apple green and green argillite with similar minor rock types and abundant trace fossils (see Hofmann and Cecile, 1981) which place it close to the Proterozoic/Cambrian boundary. Gordey (1978) has found archeocyathid-bearing limestone debris-flow units directly overlying this unit. During the 1983 field season additional trace fossils were found, including a back-filling burrower which has yet to be identified.

The limestone is abruptly underlain by more than 200 m of interstratified quartzite, arenaceous limestone to limy quartzite, and green to dark grey calcareous and non-calcareous argillite. Most bedding units are thick and massive and dominantly weather yellow or grey.

In the west central 105-O map area the limestone unit thins dramatically and argillite and quartzite make up more than 50 per cent of the succession. In addition, the underlying quartzite, limestone and argillite unit becomes extensively interstratified with maroon and apple green argillites that are unfossiliferous."

It remains to be demonstrated by careful geological mapping whether the thick limestone formation at "g" is the same unit as the thin limestone unit at Gull Lake ("14"), or a completely different one.

The final candidate for a platformal limestone equivalent to the "Grit unit" limestone at Gull Lake ("14") is the **"P. anabarica"** limestone at the top of the "variegated formation" of June Lake anticline. This possibility is enhanced by the presence of maroon shales below the "grit" limestone at one section reported by Fritz et al. (1983), although it was emphasized that such an occurrence is rare. I observed that, between the east and west limbs of the June Lake anticline, 20 km south of June Lake ("F", "G", Fig. 1), the "**P. anabarica**" limestone thins from 39 to only 5 m, and becomes largely sandy (quartz sand). Parallel westward changes in Map unit 11 are precursory to its westward pinchout, and for this reason, the "**P. anabarica**" limestone is unlikely to persist much farther west.

In summary, if it be assumed that:

a. the limestone in the "Grit unit" at Gull Lake ("14") and at "g" (Fig. 1) are one and the same formation, and

b. if this limestone has a carbonate equivalent in the platform-ward sections at the northeast margin of Selwyn Basin, then the most probable correlative is the "Sheepbed carbonate". This correlation is supported by the succession of rock units upward from the limestone to the Precambrian – Cambrian boundary in Selwyn Basin, as described by Cecile above (and given the evidence for the westward pinchout of the Map unit 11 and "**P. anabarica**" carbonates). On the other hand, given the cluster of unconformities in the vicinity of the Precambrian – Cambrian boundary on the platform, the limestones in the "Grit unit" need have no preserved platformal equivalent to the northeast.

Vampire Formation versus Backbone Ranges Formation, Corn Creek area

Fritz et al. (1983), have elected to assign basal Cambrian clastic strata in the Corn Creek – Goz Creek areas of Nadaleen map area to the Vampire Formation (Fritz, 1982). This is certainly one of the two acceptable options. The rocks are not, however, of characteristic subtidal and deeper-water Vampire facies. They make up two classical coarsening-upward cycles, from fossiliferous, subtidal, dark coloured mudrocks with minor sandstone at the base, to thick bedded, crossbedded, littoral sandstones at the top. To the writer, they are more easily seen as Backbone Ranges Formation, even though they may be younger than the type Backbone. Fritz (1982) has documented the diachronous top of the Backbone/Map unit 12 sandstones. Some other geologists also may find it more meaningful to view this unit, as little as 30 m thick, as Backbone Ranges, greatly thinned by onlap onto a recurrent Late Precambrian – Early Cambrian "high".

References

Aitken, J.D.
1982: Precambrian of the Mackenzie Fold Belt – a stratigraphic and tectonic overview, in Precambrian Sulphide Deposits, ed. R.D. Hutchinson, C.D. Spence and J.M. Franklin; Geological Survey of Canada, Special Paper 25, p. 149-161.

Aitken, J.D. and Cook, D.G.
1974: Geology of parts of Mount Eduni (106A) and Bonnet Plume Lake (106B) map-areas, District of Mackenzie; Geological Survey of Canada, Open File 221.

Blusson, S.L.
1971: Sekwi Mountain map-area, Yukon Territory and District of Mackenzie (with Map 1333A); Geological Survey of Canada, Paper 71-22.

Conway Morris, S. and Fritz, W.H.
1980: Shelly microfossils near the Precambrian – Cambrian boundary, Mackenzie Mountains, northwestern Canada; Nature, v. 286, no. 5771, p. 381-384.

Eisbacher, G.H.
1978: Re-definition and subdivision of the Rapitan Group, Mackenzie Mountains; Geological Survey of Canada, Paper 77-35.

1981: Sedimentary tectonics and glacial record in the Windermere Supergroup, Mackenzie Mountains, northwestern Canada; Geological Survey of Canada, Paper 80-27.

Fritz, W.H.
1979: Eleven stratigraphic sections from the Lower Cambrian of the Mackenzie Mountains, northwestern Canada; Geological Survey of Canada, Paper 78-23.

1980: International Precambrian-Cambrian Boundary Working Group's 1979 field study to Mackenzie Mountains, Northwest Territories, Canada; in Current Research, Part A, Geological Survey of Canada, Paper 80-1A, p. 41-45.

1982: Vampire Formation, a new Upper Precambrian(?)/Lower Cambrian Formation, Mackenzie Mountains, Yukon and Northwest Territories; in Current Research, Part B, Geological Survey of Canada, Paper 82-1B, p. 83-92.

Fritz, W.H., Narbonne, G.M., and Gordey, S.P.
1983: Strata and trace fossils near the Precambrian – Cambrian boundary, Mackenzie, Selwyn and Wernecke mountains, Yukon and Northwest Territories; in Current Research, Part B, Geological Survey of Canada, Paper 83-1B, p. 365-375.

Gabrielse, H.
1967: Tectonic evolution of the northern Canadian Cordillera; Canadian Journal of Earth Sciences, v. 4, p. 271-298.

Gabrielse, H., Blusson, S.L., and Roddick, J.A.
1973: Geology of Flat River, Glacier Lake and Wrigley Lake map-areas, District of Mackenzie and Yukon Territory; Geological Survey of Canada, Memoir 366.

Gordey, S.P.
1978: Stratigraphy and structure of the Summit Lake area, Yukon and Northwest Territories; in Current Research, Part A, Geological Survey of Canada, Paper 78-1A, p. 43-48.

Hofmann, H.J.
1981: First record of a Late Proterozoic faunal assemblage in the North American Cordillera; Lethaia, v. 14, p. 303-310.

Hofmann, H.J. and Cecile, M.P.
1981: Occurrence of **Oldhamia** and other trace fossils in Lower Cambrian(?) argillites, Niddery Lake map-area, Selwyn Mountains, Yukon Territory; in Current Research, Part A, Geological Survey of Canada, Paper 81-1A, p. 281-290.

Hofmann, H.J., Fritz, W.H., and Narbonne, G.M.
1983: Ediacaran (Precambrian) fossils from the Wernecke Mountains, northwestern Canada; Science, v. 221, p. 455-457.

STRATA AND TRACE FOSSILS NEAR THE PRECAMBRIAN-CAMBRIAN BOUNDARY, MACKENZIE, SELWYN, AND WERNECKE MOUNTAINS, YUKON AND NORTHWEST TERRITORIES: REPLY

W.H. Fritz, G.M. Narbonne[1], and S.P. Gordey[2]
Institute of Sedimentary and Petroleum Geology, Ottawa

Introduction

In the preceding discussion, Aitken has suggested refinements and some alternatives to our stratigraphic correlations for strata near the Precambrian-Cambrian boundary in Mackenzie, Selwyn and Wernecke mountains. Of particular importance is the Sekwi Brook – southern June Lake area studied by Aitken (see Aitken, Fig. 3) and the authors (Fritz et al., 1983, secs. 11 and 12). There, many of the significant stratigraphic relationships are best illustrated and provide a common ground for Aitken's and our descriptions and correlations. The following discussion, therefore, deals first with suggested terminology and correlation in the Sekwi Brook – southern June Lake area (see also Handfield, 1968; Blusson, 1971) followed by the Goz Creek (Aitken's Corn Creek discussion answered here) and Gull Lake areas.

Sekwi Brook – southern June Lake area
(see Aitken, Fig. 1, locs. 11, 12, E-G)

For this area Aitken has introduced four informal stratigraphic terms, and has used the name "Backbone Ranges Formation" in correlation with the type section. He also emphasizes the importance of two "significant" unconformities. These points are discussed below.

In his reference section, Aitken (Fig. 3) shows the Sekwi and Vampire formations in positions that agree with our stratigraphy (Fritz et al., 1983, secs. 11, 12). Between the base of the Vampire and the top of Map unit 11 he divides strata previously assigned by Blusson (1971) to Map unit 12, and divided by us unto an upper and lower submember, into three map units. In place of the upper submember Aitken has used the name "Backbone Ranges Formation" and suggests that it is the "correlative of part or possibly all of the [type] Backbone Ranges Formation". No mention is made of the previous correlation of all of Map unit 12 to the upper member of the type Backbone Ranges (Fritz, 1982, Fig. 12.4).

Underlying the Backbone Ranges in Aitken's reference section is his "**P. anabarica** limestone", informally named for the protoconodont **Protoherzina anabarica**. It is 39 m thick at the reference section, 4 m thick on the next ridge to the south, and 3 m thick at our (Fritz et al., 1983) Section 12 located 15 km farther south. At Aitken's Section 11, located 11 km to the north (see also Fritz, 1979, Sec. 33), the formation is 14 m thick. There, Fritz and Aitken sampled the formation for small shelly fossils (GSC locs. C-70293, C-70294) without success. We (WHF, GMN) sampled the formation at Section 12 where it was also found to be barren. Aitken does not mention having found **P. anabarica** or any other small shelly fossils in the "**P. anabarica** limestone" at his reference section or elsewhere. He does, however, say that the single specimen of **P.** cf. **anabarica** reported by Conway Morris and Fritz (1980) came from his "**P. anabarica** limestone", and that their reference to the specimen as having come from Map unit 11 is in error. We agree that Aitken may be correct, but have been unable to return to the section to sample and otherwise test the level of occurrence. To date the only unquestionably located specimen of **P. anabarica** known to us from the Sekwi Brook – southern June Lake area is a single specimen that can be reported as coming from an outcrop 7 m above the top of Map unit 11 near Section 11 (Fritz et al., 1983, Fig. 44.2b, Sec. 11, GSC loc. 99169).

Aitken states that the top of the "**P. anabarica** limestone" represents a "significant unconformity", citing a rapid lateral change in the thickness as evidence. Given only these data, we find no compelling reason to so emphasize this surface. There are numerous other horizons in the Upper Precambrian/Lower Cambrian strata in the area that exhibit rapid lateral changes and bear evidence of channeling. If significant erosion had taken place, we think the latest Precambrian species **P. anabarica** probably would have been removed from the section.

Below the "**P. anabarica** limestone" are strata that Aitken has informally named the "variegated formation". The "**P. anabarica** limestone", which was earlier described as a formation, is here placed within the "variegated formation". We surmise the introduction of the name "variegated formation" was deemed necessary to emphasize the maroon and green interbedded shale and siltstone that typify this unit. We believe the unit's lithology bears a close resemblance to the upper "grit unit" in the Gull Lake area 140 km to the south-southwest. In our correlations (Fritz et al., 1983, Fig. 44.3) the lower part of Map unit 12 ("variegated formation") is coeval with the lower part of the upper "grit unit". We suggest that the lower submember of Map unit 12 could be an eastward directed tongue of the lower part of the upper "grit unit". These and related correlations are presently being written into a manuscript (SPG). The resulting publication will include a formal description of new formations to replace the lower "grit unit" and upper "grit unit". The type section for what is now regarded as the upper "grit unit" will be in the Gull Lake area. It is our hope that by formally naming these colourful shales in the Gull Lake area where they are fully developed, the relationship between this unit and its various tongues (as in southern June Lake subarea?) will be appreciated and complex nomenclature will have been avoided.

Underlying the "variegated formation" is the second of Aitken's "significant" unconformities. Evidence cited is 25 cm of local relief, 2.1 m of karstic erosion, and a pronounced variation in regional thickness in the upper part of underlying Map unit 11. Although the first two items are associated elsewhere with variable amounts of erosion, the latter item deserves careful consideration. The regional thickness of Map unit 11 can be checked by examining this unit in the four sections in Aitken's discussion (Figs. 2, 3), eight sections in our paper (Fritz et al., 1983), and one section in Hofmann's (1981) paper. These sections document a remarkably thin (averaging 70 m), laterally extensive unit that could be expected to vary much more in its off-craton setting without postdepositional erosion. A marked increase in thickness (382 m) is present on the North Nahanni River (Fritz et al., 1983, Sec. 13). There, Map unit 11 includes a great amount of quartz sand that may correlate with the quartzites in the upper part of Blusson's (1971) Map unit 10B.

The reasons for Aitken's having introduced informal names for the next two underlying "formations" and how they are to be applied is not clear. The upper of the two, the "Upper turbidites" has an unfortunate environmental interpretation, which has prevented Aitken from using it in the Corn Creek area (Aitken, Fig. 2).

[1] Department of Geological Sciences, Queen's University, Kingston, Ontario K7L 3N6
[2] Cordilleran Geology Division, Vancouver

From: Discussions and Communications in Current Research, Part B; Geol. Surv. Can., Paper 84-1B.

The introduction of the other formation, the "Sheepbed carbonate", is particularly obscure. In the Sekwi Brook – southern June Lake area dark siliciclastic strata closely resembling those in the type Sheepbed, plus minor dark limestone have previously been referred to Map unit 10B. A considerable thickness of these strata contains earliest trace fossils. Because the type Sheepbed lies closer to the craton and is terminated at its upper limit by an unconformity below which no trace fossils have been found, it is older than most of Map unit 10B. No lithology similar to Aitken's "Sheepbed carbonate" is present in the type Sheepbed.

The basinward correlation (i.e., into Sekwi Brook – southern June Lake area) of the Sheepbed Formation is clearly a difficult problem. If the formation is introduced into the area, and if a diachronous upper contact is accepted, the top of the dark siliciclastic succession (immediately below Map unit 11) would be an attractive upper limit. In dealing with the Precambrian/Cambrian relationships in the Mackenzie Mountains, Aitken (1982, p. 159) both expresses an opinion on the problem and makes the only other previous mention of the "Sheepbed carbonate". Here he implies that the "Sheepbed carbonate" is part of the Sheepbed Formation, that the "Sheepbed carbonate" has a regional unconformity at its top, and that this unconformity is overlain by the Lower Cambrian Backbone Ranges and Sekwi formations. Although these relationships may exist elsewhere, they do not seem to exist at Aitken's reference section (see Fig. 3). Here no unconformity is drawn at the top of the "Sheepbed carbonate", and between this horizon and his selected base of the Backbone Ranges Formation are shown three (four with "**P. anabarica** limestone") formations. Obviously there are a number of horizons where the top of the Sheepbed could be drawn in this section, and we believe this is a problem that should receive high priority.

In summary, we feel Aitken's new nomenclature adds little to the understanding of the stratigraphy in the Sekwi Brook – southern June Lake area, that the base of Backbone Ranges Formation has been misplaced, and that two "significant" unconformities need more documentation before they are accepted.

Goz Creek area
(see Aitken, Fig. 1, south of locs. A, B)

The Goz Creek area is a name we have used to describe the area surrounding our four stratigraphic sections on the south flank of the Wernecke Mountains (Fritz et al., 1983). In his discussion, Aitken drops this usage (except in his last paragraph) and has erected a Corn Creek area that slightly overlaps our Goz Creek area to the north. Section 9 (see Aitken, Fig. 1) is in the overlapping zone and therefore is within both areas. Aitken (Fig. 2) has helpfully shown that from Section 9 northward, Map unit 11 and our dolostone unit (identified by Aitken as "Sheepbed carbonate") converge in the Corn Creek area at the expense of our siltstone unit 1 (correlated by Aitken to his "Upper turbidites"). Convergence of the same two dolostone units is shown on Blusson's (1974) map.

It is at Section 9 that Aitken purports to have "enhanced" our paper by correlating our lowest strata with the Sheepbed Formation. However, we have already pointed out in a photo and explanation (Fritz et al., 1983, Pl. 44.2, fig. 5) that at and near Section 9 Blusson (1974) and Eisbacher (1981) have recognized the Sheepbed. We show their upper Sheepbed contact, and have respected this contact by making it coincide with the top of our siltstone unit 2. Sheepbed-equivalent strata in or below our other three sections were not covered by Eisbacher. At the latter three sections Blusson did not recognize the Sheepbed, but gave several other designations – probably because of a lateral change in lithology. Since these strata are stratigraphically below the main focus of our paper, and because Blusson's designation vary, we opted to refer to these strata throughout the Goz Creek area as siltstone unit 2.

Although emphasizing the importance of recognizing the Sheepbed Formation in the Corn Creek and Goz Creek areas, Aitken is not clear as to where he would define the formation's upper contact. He correlates two Sheepbed map units into Section 9 (Aitken, Fig. 2). One is the Sheepbed Formation with an upper contact coinciding with that mentioned above, and the second is his newly introduced "Sheepbed carbonate" (our dolostone unit). Given these two map units with nearly identical names and within the same section, we ask "Are we to have a Sheepbed Formation below and a 'Sheepbed carbonate' above that together comprise a Sheepbed Group?". Or, "Are we to have a Sheepbed Formation with a 'Sheepbed carbonate' member at the top?". Both of these approaches require, with an appropriate explanation, raising the top of the Sheepbed from the level previously used. Finally, Aitken might intend having a Sheepbed Formation as used in the past overlain by a "Sheepbed carbonate" (formation), the latter formation to receive a different (formal) name in the future.

Although suggesting at one point in his discussion that the "Sheepbed carbonate" be correlated into our Goz Creek area, Aitken at another point raises an obstacle to this idea. The obstacle is that Hofmann et al. (1983) have reported Ediacaran fossils below our dolostone unit (Aitken's "Sheepbed carbonate"), and Aitken has not found Ediacaran fossils (or trace fossils) to range below the "Sheepbed carbonate" elsewhere. Despite the fossil problem, Aitken presses ahead with his "Sheepbed carbonate" correlation by suggesting that the Ediacaran fossils in the Goz Creek area actually have come from above the dolostone unit, and not below as reported. He favours this latter position by showing an unquestioned correlation of the "Sheepbed carbonate" from the Corn Creek area into our Goz Creek area (see Aitken, Fig. 2).

In the description of the Ediacaran fossils in the Goz Creek area (Hofmann et al., 1983, p. 455, Fig. 1, 2), it is stated that two of us (WHF, GMN) found Ediacaran fossils at three localities, two of which are below the dolostone unit. One locality (GSC loc. 99093) is unquestionably below the dolostone unit. It was found in an unusually large (1 m x 1/3 m x 2 cm) sandstone plate 200 m below the base of the formation. The plate closely resembles those in the adjacent outcrop. No remotely similar plates were seen above the dolostone unit in the vicinity surrounding this locality. The second occurrence (GSC loc. 99095) is 25.8 km from the first. The fossil impressions are on a locally derived quartzite block found 22.5 m below the dolostone unit. The block matches the local lithology, it is from a ridge section, and it is separated from younger siliciclastic strata by an extensive, resistant outcrop of the dolostone unit.

Overlying the dolostone unit in the Goz Creek area is siltstone unit 1. This unit may have been reported by Aitken as only "homotaxial" with his "Upper turbidites" formation because no turbiditic features were noted in the adjacent Corn Creek area. In the Corn Creek area these strata are left unnamed in Aitken's Figure 2. In the same figure and text Aitken agrees with our recognition of the next overlying unit, Map unit 11.

The uppermost map unit to be discussed in the Goz Creek area is the Vampire Formation. Our recognition of this formation is judged by Aitken to be "one of the two acceptable options". However, after a brief description of these strata, he adds, "To the writer, they [the strata] are more easily seen as Backbone Ranges Formation, even though they may be younger than the type Backbone". Aitken provides no reason as to why the Vampire in the Goz Creek

area should be younger than the type Backbone Ranges, nor does he mention our report (Fritz et al., 1983, p. 371) of the small shelly fossils **Anabarites trisulcatus** and **Protohertzina anabarica** from the base of the Vampire there. He does, however, attach considerable significance to the presence of **Protohertzina anabarica** in the Sekwi Brook – southern June Lake area. A correlation of **P. anabarica** from the base of the Vampire Formation in the Goz Creek area to our **P. anabaric**a locality well below the horizon where Aitken drew the base of the Backbone Ranges Formation in the Sekwi Brook – southern June Lake area contradicts the age relationship that Aitken has suggested. This correlation enhances the earlier concept (Fritz, 1982) that the Vampire Formation laterally interfingers with the upper member of the Backbone Ranges Formation.

After a detailed study of the mentioned and additional small shelly fossils from the Goz Creek area, G.S. Nowlan (oral communication) believes that the basal Vampire strata correlate with the **Anabarites-Circotheca-Protohertzina** Assemblage Zone in the type Meishucun Stage, China. The top of this zone in China was chosen by the Precambrian-Cambrian Boundary Working Group in January, 1983 to serve as the international Precambrian-Cambrian boundary and the Group has submitted this proposal to the International Commission on Stratigraphy for official approval. If accepted, we will then favour a Precambrian-Cambrian boundary correlation that would show the boundary as being within the Vampire in the Goz Creek area and at the type Vampire section, within Map unit 12 in the Sekwi Brook – southern June Lake area, and probably within the upper member of the Backbone Ranges Formation at the type section.

The above discussion is within the context of Aitken's having sanctioned the use of the Vampire in the Goz Creek area as "one of the two acceptable options". The second option, which he favours, is recommended to others by his statement that "some other geologists also may find it more meaningful to view this unit [Vampire Formation], as little as 30 m thick, as Backbone Ranges, greatly thinned by onlap onto a recurrent Late Precambrian-Early Cambrian 'high'". We have already shown these strata (as Vampire Fm.) thinning onto a high (Fritz et al., 1983, Fig. 44.3), and the high has long been known as the Yukon Stable Block (Jeletzky, 1961, Fig. 24; 1962, Fig. 2). We would argue that these strata more closely match those of the Vampire Formation than those of the Backbone Ranges Formation. For readers wishing to have a visual overview of the disputed strata, we suggest first inspecting photos of the thick bedded, light coloured Backbone Ranges quartzite at the type and nearby section (Fritz, 1982, Pl. 12.3). Contrast these photos with those of the Vampire Formation at the type and nearby section (op. cit., Pls. 12.1, 12.2). Note the Vampire's much darker colour and lesser resistance, reflecting a higher proportion of dark grey shale, siltstone and very fine grained quartzite. Then turn to photos of the Vampire in the Goz Creek area (Fritz et al., 1983, Pl. 44.2) and note the same dark colour and the even slightly more recessive nature of the outcrops. The proportion of dark shale, siltstone and quartzite closely matches that at the type Vampire section.

Gull Lake area
(see Aitken, Fig. 1, Loc. 14)

Aitken directs a considerable amount of discussion toward our tentative correlation (Fritz et al., 1983, Fig. 44.3) of a widespread but thin succession of limestone beds in this area with Map unit 11 in the Sekwi Brook – southern June Lake area. We show the limestone beds as comprising the uppermost part of the lower "grit unit", and show trace fossil localities a short distance above and below these beds (op. cit., Fig. 44.2b, Sec. 14). Current studies of the fossils (GMN) indicate those in the interval 0 to 20 m above the limestone beds (GSC locs. 99023-99025) are **Gordia**?, **Palaeophycus**, and **Planolites**. In the interval 0 to 45.5 m below (GSC loc. 99022) is **Planolites** sp. Most of the strata below the limestone beds are generally unfavourable for trace fossil preservation.

In his discussion, Aitken suggests that our tentative correlation between the two carbonate units may be incorrect, and that it is "worthwhile" to consider a correlation of the Keele Formation (older than the "Sheepbed carbonate"), "Sheepbed carbonate", and "**P. anabarica** limestone" with the Gull Lake limestone beds. We find the first two of these considerations inconsistent with Aitken's statements in which he indicates a strong doubt that trace fossils extend below his "Sheepbed carbonate". We see no reason to consider the Keele Formation because of its position well below the known range of trace fossils. Aitken's observation that trace fossils extend down to the top of the "Sheepbed carbonate" in the Sekwi Brook – southern June Lake area at least puts their range immediately over that unit, and thus leaves some argument open as to the "Sheepbed carbonate" – Gull Lake limestone beds correlation on the grounds of a slightly lower range in the Gull Lake area. However, the known range of early trace fossils across both Map unit 11 and the Gull Lake limestone beds in the mentioned two areas greatly favours our tentative correlation of these two carbonate units.

Aitken acknowledges that the "**P. anabarica** limestone"-Gull Lake limestone beds correlation is unlikely, but does draw a parallel between the position of the "**P. anabarica** limestone" above a maroon and green siltstone (his "variegated fm.") and the similar position of the Gull Lake limestone beds above local maroon shale. We feel the local maroon shale in the Gull Lake area has been overemphasized. A more obvious parallel between carbonate units and maroon shale units can be drawn between Map unit 11 and the overlying maroon and green siltstone ("variegated fm.") in the southern June Lake subarea, and the Gull Lake limestone beds overlain by the thick, widespread maroon and green shales of the upper "grit unit". This latter parallel strengthens our tentative correlation between Map unit 11 and the Gull Lake limestone beds that was drawn on the basis of trace fossils.

Aitken has expressed doubt that Map unit 11 extends into the Gull Lake area because this unit rapidly thins westward (basinward) from his reference section in the Sekwi Brook – southern June Lake area. A glance at Aitken's map, however, shows the Gull Lake area to be 140 km south-southwest (not west) of his reference section (see Aitken, Fig. 1, locs. F, 14). Given this distance and the lack of detailed mapping available between the two areas, it is presently uncertain as to where the basinward limit of Map unit 11 lies relative to the Gull Lake area.

Aitken also discusses a correlation between the Gull Lake limestone beds and a limestone unit located in an isolated section 200 km to the north-northwest at point "g" (see Aitken, Fig. 1). The lithologies in the section were communicated to Aitken by M.P. Cecile, who also reported the limestone unit to be mappable on a regional scale. We note that Aitken states that his suggested correlation between the Gull Lake limestone beds and the limestone unit at "g" "remains to be demonstrated", and that the correlation between the unit at "g" and his "Sheepbed carbonate" is highly conditional. Given only these data, we fail to see how the quotation from Cecile's work either strengthens or weakens Aitken's correlation of his "Sheepbed carbonate" to the Gull Lake area or elsewhere.

References

Aitken, J.D.
1982: Precambrian of the Mackenzie Fold Belt – a stratigraphic and tectonic overview; Geological Association of Canada, Special Paper 25, p. 149-161.

Blusson, S.L.
1971: Sekwi Mountain map-area, Yukon Territory and District of Mackenzie; Geological Survey of Canada, Paper 71-22, 17 p.

1974: Geology, northern Selwyn Basin (Operation Stewart), Yukon and Northwest Territories; Geological Survey of Canada, Open File 205.

Conway Morris, S. and Fritz, W.H.
1980: Shelly microfossils near the Precambrian-Cambrian boundary, Mackenzie Mountains, northwestern Canada; Nature, v. 286, no. 5771, p. 381-384.

Eisbacher, G.H.
1981: Sedimentary tectonics and glacial record in the Windermere Supergroup, Mackenzie Mountains, northwestern Canada; Geological Survey of Canada, Paper 80-27, 40 p.

Fritz, W.H.
1979: Eleven stratigraphic sections from the lower Cambrian of the Mackenzie Mountains, northwestern Canada; Geological Survey of Canada, Paper 78-23, 19 p.

1982: Vampire Formation, a new Upper Precambrian(?)/Lower Cambrian formation, Mackenzie Mountains, Yukon and Northwest Territories; in Current Research, Part B, Geological Survey of Canada, Paper 82-1B, p. 83-92.

Fritz, W.H., Narbonne, G.M., and Gordey, S.P.
1983: Strata and trace fossils near the Precambrian-Cambrian boundary, Mackenzie, Selwyn, and Wernecke mountains, Yukon and Northwest Territories; in Current Research, Part B, Geological Survey of Canada, Paper 83-1B, p. 365-375.

Handfield, R.C.
1968: Sekwi Formation, a new Lower Cambrian Formation in the southern Mackenzie Mountains, District of Mackenzie (95L, 105I, 105); Geological Survey of Canada, Paper 68-47, 23 p.

Hofmann, H.J.
1981: First record of Late Proterozoic faunal assemblage in the North American Cordillera; Lethaia, v. 14, p. 303-310.

Hofmann, H.J., Fritz, W.H., and Narbonne, G.M.
1983: Ediacaran (Precambrian) fossils from Wernecke Mountains, northwestern Canada; Science, v. 221, p. 445-457.

Jeletzky, J.A.
1961: Eastern slope, Richardson Mountains: Cretaceous and Tertiary structural history and regional significance; in Geology of the Arctic; Proceedings of the First International Symposium on Arctic Geology, v. 1, University of Toronto Press, p. 532-583.

1962: Pre-Cretaceous Richardson Mountains Trough: its place in the tectonic framework of Arctic Canada and its bearing on some geosynclinal concepts; The Royal Society of Canada, Transactions, v. 56, ser. III, Sec. III, p. 55-84.

CANADA-NEWFOUNDLAND CO-OPERATIVE MINERAL PROGRAM 1982-84

CANADA-TERRE-NEUVE: PROGRAMME CO-OPERATIF SUR LES MINERAUX 1982-84

CONTENTS/TABLES DES MATIÈRES

G.A.G. NUNN, N. NOEL, N.G. CULSHAW:

Geology of the Atikonak Lake area, Grenville Province, western Labrador [1,2]

---

[1] Project carried by Geological Survey of Canada

[2] Text and figures as published by:

Mineral Development Division, Department of Mines and Energy, Government of Newfoundland and Labrador, Current Research, Report 84-1, p. 30-41.

GEOLOGY OF THE ATIKONAK LAKE AREA, GRENVILLE PROVINCE, WESTERN LABRADOR

by

G.A.G. Nunn, N. Noel[2] and N.G. Culshaw[2]
Newfoundland Department of Mines and Energy

Also *in* Current Research, Part B, Geological Survey of Canada, Paper 84-1B.

Abstract

The map area lies within the Grenville Province in southwestern Labrador and an adjacent part of Quebec. High grade pelitic to semipelitic gneiss is predominant and is intercalated with minor basic paragneiss. The paragneiss is intruded by a basic plutonic suite and a younger acidic plutonic suite. Anorthositic rocks outcrop in the southeast part of the map area; the age and contact relationships of the anorthositic suite are unknown.

Age dating of probably related, and in some cases equivalent, rock units to the north and northeast indicate a polyorogenic history for the map area. The paragneiss was affected by an older event that was separated from a younger orogenic event by the emplacement of the basic and acidic plutonic suites. Probable equivalents of the acidic suite yield ages of circa 1654 Ma. The paragneiss and the plutonic suites were later affected by a series of tectonic episodes, which locally attained granulite facies pressures and temperatures, dated at circa 1646 Ma and termed here the Labradorian orogeny.

The effect of the Grenville Orogeny in this part of the Grenville Province is presumed to consist of low grade thermal features and brittle deformation, possibly with considerably higher grade events in localized ductile shear zones.

Introduction

This report summarizes the results of 1:100,000 scale geological mapping carried out during 1983 in N.T.S. map areas 23A/9, 10, 15 and 16 (Figure 1).

The area centers around Atikonak Lake, which occupies a broad, shallow, drift-blanketed depression at an elevation of 550 to 600 m, from which the land rises to the east and northwest to a better exposed, deeply dissected peneplain at about 770 m. Atikonak Lake and many other large lakes allow float plane access to most of the lowlands, but large tracts of swamp and the mountains are mostly accessible only by helicopter.

Previous Work

Pyke (1956) reported the preliminary results of exploration by BRINEX throughout the area, which included geological reconnaissance in 1953, airborne geophysics in 1954 and ground prospecting in 1956. BRINEX found widespread but minor occurrences of Fe, Ti and Cu mineralization.

Stevenson (1968) mapped the area at 1:250,000 scale and determined it to be largely underlain by quartzofeldspathic, sillimanite-bearing paragneisses with minor amounts of gabbroid, granitoid and anorthositic rocks. He noted the particularly complex structure of the gneisses and the higher grade of those underlying the upland regions in this area. Stevenson's map was incorporated into the regional geological compilation of Labrador at 1:1,000,000 scale by Greene (1972).

The area has traditionally been regarded as lying well south of the Grenville Front zone and, by inference, as underlain by high grade Grenvillian gneisses (Stevenson, 1968; Greene, 1974; Smyth and Greene, 1976; Nunn and Christopher, 1983). Mapping carried out during 1982 established a polydeformational history for the paragneiss in the area to the north (Nunn and Christopher, 1983). Effects of the early episodes, which were tentatively assigned to the Hudsonian Orogeny and are recorded in the paragneiss as a folded gneissosity, are separated from the effects of later orogenies by the

[1] Department of Earth Sciences, Memorial University of Newfoundland, St. John's, Newfoundland A1B 3X5

[2] Geological Survey of Canada, Precambrian Geology Division, 601 Booth Street, Ottawa, Ontario K1A 0E8

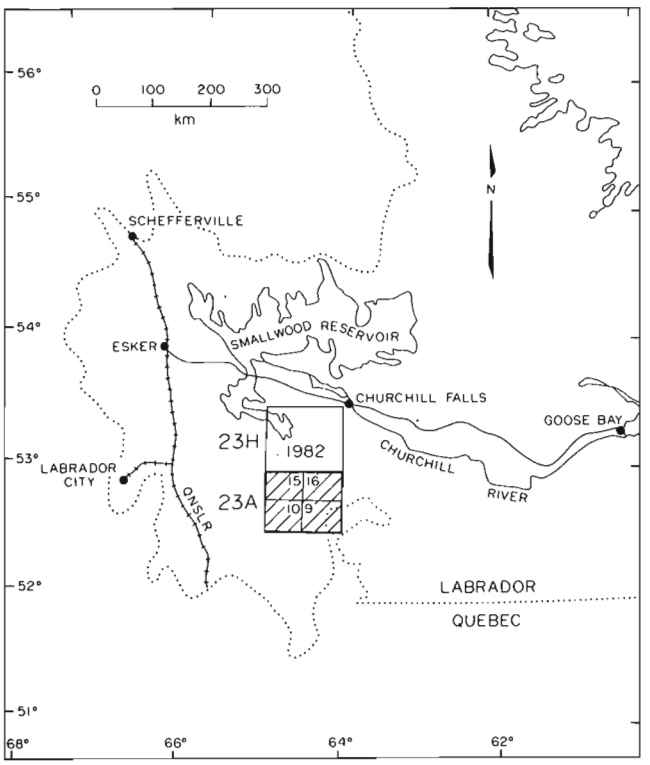

Figure 1. *Location map of the Atikonak Lake area, western Labrador.*

emplacement of granitoid and gabbroid plutonic suites. The later events, which were thought to reflect the Grenvillian Orogeny by Nunn and Christopher (1983), are manifested by further migmatization, a pervasive mineral recrystallization and several deformational episodes. These later events affected all the rock types in the area of Nunn and Christopher (1982 in Figure 1).

General Geology

Most of the map area (Figure 2) is underlain by sillimanite-bearing, quartzofeldspathic, pelitic to semipelitic paragneiss (unit 1) of three main subfacies. The differences between the subfacies are structural and textural, not compositional, and are considered to reflect a relationship between the structural development of the paragneiss and the grade and timing of peak metamorphism. The metamorphic grade is determined from the associated plutonic suites (units 2 and 3) in each subfacies area. The central and southwestern lowland areas are underlain by upper amphibolite facies rocks (subfacies 1a) whereas the eastern and northwestern upland areas are underlain by granulite facies rocks (subfacies 1b and 1c, respectively). The boundaries between the subfacies are approximate and appear transitional. In previous work to the north, the boundaries were inferred to be thrust zones (Nunn and Christopher, 1983). The northwestern granulite facies paragneiss is structurally more like the amphibolite facies rocks than its eastern counterpart, and appears to have undergone peak metamorphism at a later stage than the eastern granulites.

Banded, supracrustal metabasic rocks and minor quartzite (unit 1d) form widespread but minor intercalations in the paragneiss. They are particularly abundant in the northwestern map area (23A/10). Throughout the Atikonak Lake area, these basic gneisses contain both orthopyroxene and clinopyroxene, and appear to consist of granulite facies assemblages even in the parts of the map area believed to be in the amphibolite facies.

The paragneiss is intruded by a gabbroid suite (unit 2) and a predominantly K-feldspar megacrystic granitoid suite (unit 3). The former is more abundant in the granulite facies parts of the map area, and the latter is more abundant in the poorly exposed amphibolite facies terrane. To the west of the area in map sheet 13D/12 (Thomas et al., 1984 (this volume)), charnockitic varieties of the granitoid unit (3b) are associated with and intrusive into noritic rocks (unit 2). This relationship has also been recognized to the northeast of this area in the Red Wine Mountains (Emslie et al., 1978). It is not known whether the generally weaker fabric development in the charnockitic rocks (unit 3b), in contrast to the basic plutonic suite (unit 2), reflects a different response to deformation or a structural event separating the two plutonic suites.

A rock equivalent to the unit 3b granitoid rocks from just north of the western part of the map area has given a U-Pb zircon core age of 1672 Ma (Krogh, written communication, 1983). Based upon continuity (Thomas et al., 1981; Wardle and Britton, 1981; Nunn and Christopher, 1983) and mineralogical composition and texture (Nunn and Christopher, 1983), the dated rock has been correlated by Nunn and Christopher (1983) with units to the north and northeast of the map area (e.g. North Pole Brook Intrusive Suite, Thomas and Hibbs, 1980; Michikamau plutonic suite, Nunn and Noel, 1982). These units have yielded ages ranging from circa 1700 Ma to 1576 Ma with a distinct cluster at approximately 1650 ± 20 Ma (e.g. Fryer, 1983; Krogh et al., in preparation). These data suggest an age of about 1670 Ma for the emplacement of the plutonic granitoid suite, and freezing of the U-Pb and Rb-Sr geochronological systems due to regional cooling following low grade to granulite grade metamorphism at around 1650 Ma.

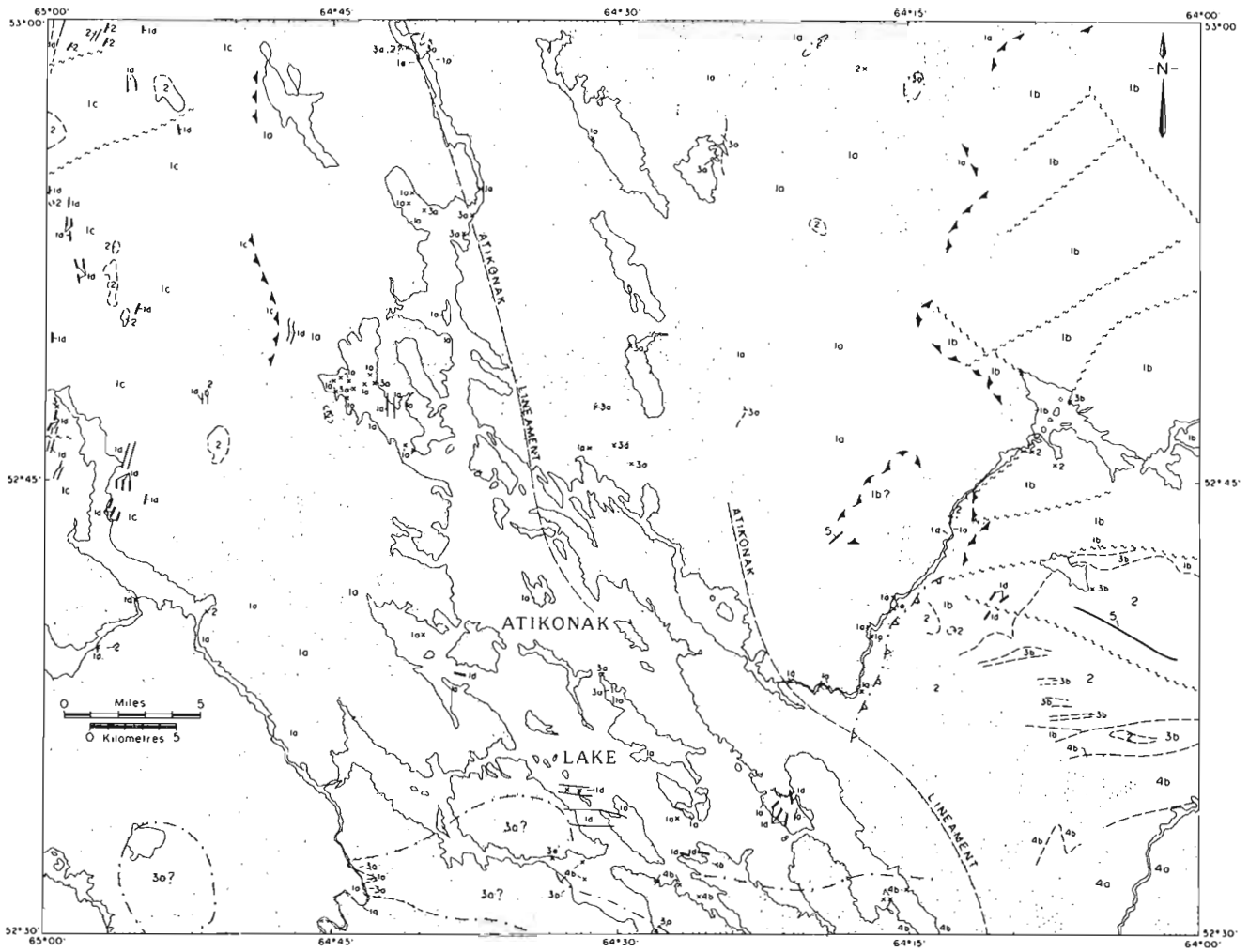

Figure 2: *Geology of the Atikonak Lake area.*

SYMBOLS

Thin layers and sheets, schematic (exaggerated)

Isolated outcrops or outcrop groups

Geological boundary (approximate, inferred)

Interpretative aeromagnetic boundary (geological, thrust)

Faults and lineaments (inferred)

Thrust, teeth on upthrust block (inferred)

Atikonak lineament

Legend for Figure 2

LEGEND

HELIKIAN or younger

5 *Diabase dykes.*

HELIKIAN

4 **Anorthosite suite:** *possibly approximately synchronous with Unit 2.*
4a - *anorthosite and noritic anorthosite.*
4b - *leuconorite.*

PALEOHELIKIAN

3 **Orthogneiss and foliated granitoid rocks:** *possible equivalents of the North Pole Brook Intrusive Suite (Thomas and Hibbs, 1980).*
3a - *K-feldspar megacrystic granodiorite and quartz monzonite and strongly deformed porphyroclastic equivalents; minor non-megacrystic granodiorite.*
3b - *opdalite and farsundite equivalents of* **3a.**

2 **Basic plutonic suite:** *possible equivalents of the Ptarmigan Complex (Emslie et al., 1978). Primary or metamorphic textured gabbro to norite; partial to complete plagioclase-hornblende-biotite replacement in amphibolite facies areas.*

APHEBIAN

1 **Paragneiss:**
1a - *migmatite-banded pelitic to semipelitic amphibolite facies metasedimentary gneisses in central lowlands.*
1b - *granulite grade equivalents of* **1a** *in the east.*
1c - *granulite grade equivalents of* **1a** *in the west.*
1d - *metabasic gneisses with minor metasedimentary paragneiss layers and rare quartzite.*

The major metamorphic events which affected units 2 and 3 have been dated. The granulite facies metamorphism recorded in the same equivalent of the unit 3b granitoid rock (see above) has yielded U-Pb zircon concordia ages of 1645 and 1647 Ma (Krogh, written communication, 1983). Furthermore, U-Pb dating on sphene (Krogh et al., in preparation) from granitoid units throughout the Grenville Front Tectonic Zone to the north and the northeast of the map area has demonstrated fairly conclusively that the main upper amphibolite to granulite facies metamorphism occurred around or before 1650 Ma rather than during the Grenville Orogeny as previously thought. Tectonic features attributed to this Paleohelikian event, though not necessarily assigned thus by the authors at the time, are widespread in central Labrador and range from greenschist facies foliations to migmatites and gneissic fabrics. These structures are not confined to the high grade gneisses and migmatites of previous mapping (Thomas and Wood, 1983; Nunn and Christopher, 1983) and the Red Wine Mountains (Emslie et al., 1978) but extend farther north into lower grade rocks of the Trans-Labrador batholith (Ryan, 1980; Thomas and Hibbs, 1980; Nunn, 1981; Thomas et al., 1981; Nunn and Noel, 1982; Ryan et al., 1982). We have tentatively termed these events the Labradorian orogeny.

Equivalents of the plutonic suites yielding similar ages are known from a long belt subparallel to the northern margin of the Grenville Province, stretching from Scandinavia through Labrador to Mexico. In Labrador, these have been collectively termed the Trans-Labrador batholith (Wardle and staff, 1982); elsewhere, they include the Smaland-Varmland granitoid terrane in Sweden (Gower and Owen, in preparation) and the Mazatzal Belt in the United States (Van Schmus and Bickford, 1981). The only tectonic events of this age known to the authors are from the Mazatzal orogeny in the southwestern United States and from the American midwest (Van Schmus and Bickford, 1981). Along the southeastern margin of Laurentia the Labradorian orogeny may be only one of a series of localized to extensive "... repeated overprinting or overlapping of successive tectonic events ..." (Baragar, 1981). However, as more dates become available, in particular those from methods capable of seeing through the Grenvillian resetting, the orogeny may take on more than local significance.

Unit 4 consists of anorthosite (unit 4a) and leuconorite (unit 4b), and occurs only in the southeastern corner of the map area. The age of the anorthositic rocks is unknown, as is their position in the chronological sequence. The major shear zone which affects the northern margin of unit 4 could be Labradorian or Grenvillian in age.

Unit 1: Supracrustal Gneisses

Unit 1a consists of upper amphibolite facies metasedimentary paragneiss, and units 1b and 1c consist of equivalent granulite facies paragneiss. The hand specimen mineralogy of these paragneisses is typical of both facies, and their distinction relies on the mineralogy of the spatially associated plutonic rocks and their neosomes, and the structural morphology of the paragneisses.

The paragneisses are predominantly a monotonous sequence of pelitic to semi-pelitic migmatites. They consist of quartz + feldspar + biotite ± magnetite ± garnet migmatitic neosomes and sillimanite + biotite + opaque oxides ± plagioclase ± garnet restites. The early neosomes form a concordant layering which is cut across by later generations of similar material. Either the restite or the neosome may form disrupted layers within the other. Patches and dikes, up to 5 m thick, of diatexite containing small patches of restite indicate coalescing melt and local mobility of the neosome phase.

Homogeneous, nonmigmatitic, paleosome layers and thin, psammitic layers are uncommon relicts of the primary layering.

The quartzofeldspathic minerals commonly display a mineral fabric or static recrystallization textures. The restites always contain a mineral fabric, though this may be dynamic or mimetic.

Despite the monotonous compositional character of unit 1, it can commonly be subdivided on a structural basis. Unit 1a is composed mostly of tight, straight belttype structures. Unit 1b is characterized by more areas of irregular fabric, thicker, wavy layering and open folding and, in contrast to unit 1a, fewer zones of regular, attenuated, straight fabrics and tight folds. Structures in unit 1c are like those of 1a but the melt layering in the straight zones commonly exhibits porphyroclastic textures whereas that in units 1a and 1b is commonly annealed.

The basic gneisses (unit 1d) intercalated with the paragneiss are homogeneous to layered, plagioclase - two-pyroxene rocks with minor biotite and a quartz segregation banding. The basic gneisses appear to retain a granulite facies mineralogy in the lowlands around Atikonak Lake where other lithologies suggest amphibolite facies conditions. The granulite facies assemblages may be metastable and inherited from earlier, possibly more widespread, granulite facies metamorphism. The basic gneisses are intimately associated with tonalitic to granodioritic, concordant and discordant sheets and net veins which do not occur in the paragneiss sequence. Garnet ± biotite are common in these granitoid sheets and at metabasite/paragneiss contacts; an alternative ferromagnesian mineralogy in these sheets at granulite facies is orthopyroxene ± biotite. Rare, quartzite layers also occur with the metabasites. They are clean, medium grained, recrystallized, thin to medium bedded rocks with up to 10 percent diopside or garnet + magnetite ± biotite. The thinner bedded quartzites usually contain the diopside or have a calcareous matrix. A large boulder of interlayered quartzite, granulite facies metabasite and pink marble was found and is believed to have been locally derived. The rocks of unit 1d are believed to represent a basic volcanic - quartzite or chert - carbonate association, and the metasedimentary paragneiss to have a graywacke protolith.

Unit 2: Basic Plutonic Suite

Members of this suite range from noritic through gabbronoritic to gabbroic, and are dominated by leucocratic lithologies. They vary from massive, medium to very coarse grained, seriate intergranular rocks preserving primary or pseudomorphed igneous textures, to isotropic to foliated (rarely gneissic) fine to medium grained granoblastic metamorphic rocks with coarser grained sweats. In the first type, primary pyroxene phenocrysts and groundmass plates are abundant whereas plagioclase is usually recrystallized, but may contain rare relict cores. Olivine and biotite may be present and Fe-Ti oxides are abundant. Compositional variations are common but layering is rare. With increased recrystallization and deformation, these rocks grade into the metamorphic members of the suite in which they are locally preserved as strain augen. Olivine is absent in the recrystallized rocks, but biotite is more abundant and the clinopyroxene may be diopside rather than augite. These rocks are generally massive with weak pyroxene and plagioclase mineral fabrics, and they may contain coarser grained noritic or granitic material in irregular patches and net veins or as an incipient layering. A strong fabric is present in the granitic veins. Rare, folded layering in the basic plutonic rocks may represent an earlier metamorphic fabric or relict primary layering.

In the areas metamorphosed to amphibolite facies, there is partial replacement of the pyroxenes by hornblende and biotite. Corona textures were not noted in any of the basic plutonic suite lithologies (*cf.* unit 3, Nunn and Christopher, 1983).

Unit 3: Orthogneiss and Foliated Granitoid Rocks

Unit 3a consists of moderately to strongly foliated, weakly migmatitic, megacrystic granodiorite, adamellite and quartz monzonite with minor nonmegacrystic lithotypes. The megacrysts are up to 5 cm across and the groundmass is composed of recrystallized quartz, feldspar, biotite and magnetite. The megacrysts are usually partially rounded and variably replaced by

polygonal microcline. A strongly deformed variety of this rock contains rounded and oval, medium to coarse grained (less than 1.5 cm across) K-feldspar relicts in a fine grained groundmass. The megacrystic rocks are weakly migmatitic and contain an incipient layering or patchy development of granitic melt which is in contrast to the less abundant nonmegacrystic rocks that are generally well layered.

Unit 3b consists of orthopyroxene-bearing varieties, chiefly farsundite (quartz monzonite to adamellite) and opdalite (granodiorite), and is closely associated with the eastern occurrences of the gabbronorite suite. These rocks of charnockitic affinity are weakly foliated and megacrystic, weathering to a rusty buff color. About half of the feldspar fraction consists of centimetric K-feldspar megacrysts in a matrix of medium grained, recrystallized plagioclase and quartz. Orthopyroxene, opaque oxides, and fine felted biotite possibly replacing orthopyroxene, comprise up to 10 percent of the rock.

Unit 4: Anorthosite Suite

This unit consists of massive anorthosite and noritic anorthosite (4a) with a northern (?marginal) anorthositic norite phase (4b). The plagioclase in both units is a dark gray or reddish color and varies from coarse to very coarse grained. The color index ranges from 5 to 20 in unit 4a and from 20 to 35 in unit 4b. The matrix is composed of orthopyroxene and Fe-Ti oxides ± olivine, and pyrite is a common accessory. The pyroxene and olivine are commonly partly or completely replaced by corona minerals. The overall texture appears intergranular to subophitic, but layering and igneous lamination observed in rocks to the south of the map area suggest that the body is of cumulate origin.

Parts of this unit have been strongly deformed and the plagioclase has recrystallized to form polygonal white aggregates with or without relicts of the gray and red feldspar. In the eastern part of the unit 4 outcrop area, the mafic minerals are recrystallized to fine grained, equigranular orthopyroxene, whereas farther west they are replaced by polygonal hornblende aggregates. Locally, the rocks become fine grained, flaggy white gneisses. Corona textures generally have been destroyed wherever deformation and recrystallization are well developed.

Unit 5: Diabase dikes

Diabase dikes are widespread and are most common in the western uplands. They are very variable in orientation and seem post-tectonic, although one dike was observed to contain a fabric. The dikes are fine grained and generally less than 50 cm wide; two coarser grained dikes, approximately 40 m and more than 100 m wide, are shown in map sheet 23A/9. The former is traceable for more than 6 km.

Mineralization

The intercalated metabasic volcanic rocks and paragneisses contain numerous rusty weathering zones whereas the paragneisses away from this association are not known to contain such zones. Malachite showings are present in all the major rock types in the northwestern part of the map area (23A/15) and may be associated with north trending ductile structures or lineaments, or the basic rocks (units 1d and 2). The granitoid, gabbroid and paragneiss units are all rich in magnetite and poor in sulfides. No gemstone quality laboradorite occurrences were found in the anorthositic suite, but these rocks contain abundant magnetite and disseminated pyrite, and similar anorthosites in nearby Quebec are a major source of titanium.

Lake sediment geochemistry is now available for the area (Geological Survey of Canada, 1982).

Structure and Metamorphism

The structural and metamorphic history of the area has been summarized in Table 1, and a structural and metamorphic facies map has been reproduced in Figure 3.

The oldest structures in the area are the migmatitic layering in the metasedimentary units (1a,b,c), and a quartz segregation fabric in the metabasic unit (1d) of the paragneisses. The former structure occurs in very rare inclusions of paragneiss within unit 3 and elsewhere is cut across by dikes of unit 2. Folding of the layering in the inclusions is not necessarily a record of polydeformation prior to inclusion (*cf.* Nunn and Christopher, 1983). However, the inclusions are evidence of a gneiss-forming event prior to the emplacement of the plutonic suites (units 2 and 3) in the Paleohelikian, and this event is assumed to be Hudsonian or early Paleohelikian (HPD) in age.

The deformation sequence is divided by the emplacement of units 2 and 3 in this map area. Regionally, either intrusion of unit 3 or the younger Labradorian events might be diachronous, or a part of unit 3 might be syntectonic, since there is such close agreement between the ages of emplacement of the North Pole Brook Intru-

Table 1: *Summary of structural and metamorphic events.* *

UNIT	EVENTS	FOLDING, FAULTING	FABRICS	MIGMATIZATION	METAMORPHIC GRADE
1	Deposition Basic dykes HPD_1	–	HPS_1, Location fabric** in (1)	HPM_1, major	uA+
	HPD_2	HPF_2, rare isoclines in (1a)	–		?
2	Intrusion				
3	Intrusion				
	LD_1	–	LS_1, rare location fabric in (3)	LM_1, possible range in (1)	uA(1a, 1c), G(1b)
	LD_2 - early	LF_2, tight to isoclinal in (1, 3)	LS_2, major, mineral and shape fabrics in (1, 2, 3)	LM_2, minor + late to post-tectonic sweats	uA(1a,), G(1b, 1c)
	- late	Thrusting, possible range or regeneration	Mylonite, shear zones and straight belts		uA
	LD_3 ***	LF_3, moderate to tight in (1)	–	–	A
	Basic dykes			2-mica and muscovite-bearing granite dykes	mA?
	LD_4	LF_4, open to tight, regional map scale	–	–	mA?
				2-mica and muscovite-bearing granite dykes	mA?
4	Intrusion				
	GD_1, or LD_2 - late to pre-LD_4	Major ductile shear zone	transposition in (1b), mineral fabric in (2, 3), mineral and shape fabrics in (4)	–	mA?
	GD_2, or LD_4, or later	Atikonak lineament	–	–	?
	D	Faulting			Gs

* *Adapted from Nunn and Christopher, 1983. Numbers in parentheses refer to legend and text. A, amphibolite facies; u, upper; m, middle; G, granulite facies; Gs, greenschist facies; + denotes "or higher".*

** *Arrangement of fabric elements in layers (three dimensional).*

*** *This event is not equivalent to that labelled GD_3 in the table of Nunn and Christopher (1983); an equivalent of this event should be inserted between GD_3 and GD_4 of their table.*

sive Suite and ages of the peak metamorphism of the Labradorian events.

Structures that postdate the granitoid and gabbroid plutonic suites are assigned to the Labradorian deformation (LD). Early Labradorian deformation (LD_1) is represented by a major discordant migmatization in unit 1 and by a migmatitic layering in parts of unit 3. Its effect on units 2 and 4 is unknown. In order to account for the subsequently more rigid behavior of the paragneisses of subfacies 1b, we suggest that this domain was metamorphosed to granulite facies at LD_1 time, and thence behaved as a relatively dehydrated block, whereas the other paragneiss areas reached only upper amphibolite grade (*cf.* units 1b to 1a and 1c). However, we cannot exclude possibilities of older (HPD) or younger Labradorian ages of granulite facies metamorphism.

LD_2 was the peak metamorphic event of the Labradorian orogeny. Earlier migmatite or primary fabrics were tightly to isoclinally folded, major recrystallization occurred, and axial planar fabrics were developed in units 1, 2 and 3. Further migmatization was restricted to the formation of isolated axial-plane-parallel pegmatites and diatexites. Metamorphism reached upper amphibolite facies in the lowland regions and granulite facies in the areas underlain by subfacies 1b and 1c, the two upland portions of the map area. Late LD_2 events include the thrusting of the western upland granulite terrane into its present position overlying amphibolite facies paragneiss, and a posttectonic, static recrystallization which destroyed many of the LS_2 mineral fabrics. The eastern upland granulite block may also have been thrust into place at that time.

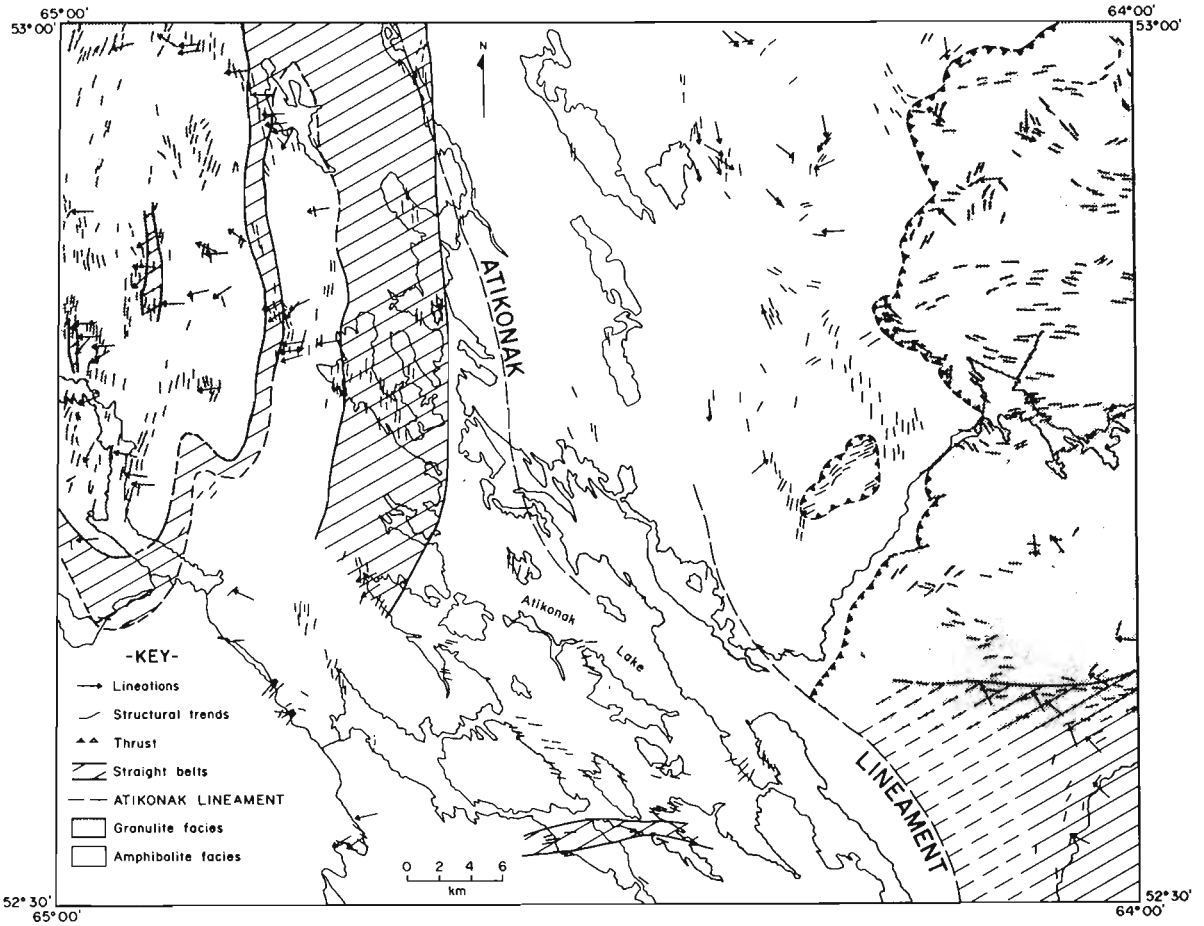

Figure 3: *Structural and metamorphic facies map.*

The mineral and migmatite fabrics were moderately to tightly folded during LD_3 and openly to tightly folded during LD_4. No new mineral fabrics were developed with these deformations.

LD_1, 2 and 3 structures have an overall easterly but variable strike in the eastern upland region of the map area, and the lineations are variable except along the southern margin of the granulite facies area where a high strain zone (late LD_2?) tightens all the earlier structures and the lineation becomes consistently steeply plunging to the north-northwest. In the other regions of the map area, these structures are oriented with a northerly strike controlled by the limbs of LD_4 folds. In the western uplands where the LD_4 deformation is tight, and apparently colinear with LD_2, the northerly strike is very consistent and the lineations are strong and moderately plunging to the west. Throughout the lowland regions, the structures are less regular and LD_4 hinge zones are common perturbations on the regional strike pattern. The lineation is still fairly consistently toward the west. Most of the lineations are more or less down-dip regardless of the strike of the LS_2 fabric.

The high strain zones and metamorphic facies boundaries are principally late LD_2 events. The one surrounding the eastern upland has not been seen except in the south where it appears to be truncated by the Atikonak lineament. There is, however, a strong discordance of fabric at the base of the small inferred klippe in the southern part of map sheet 23A/16. The western boundary is a transition zone marked by a number of straight belts. Fabrics within these straight belts may be glassy and submylonitic and are conformable with the "normal" LD_2 structures outside the shear zones, a feature that is also common north of the map area (Nunn and Christopher, 1983). The substitution of biotite-rich restites for the more common sillimanite - Fe-Ti oxide - biotite restite is best developed in these straight belts and is clearly related to deformation.

These high strain zone fabrics are also moderately to tightly folded by LD_4 folds in the western areas.

The LF_4 axial traces in the map area and related fold axes to the north and northeast (Figure 4) form a divergent fan in the less competent upper amphibolite facies gneisses around the northwestern corner of the eastern granulite terrane which appears to be acting as a rigid block. This fanning of the fold axes indicates that the eastern upland thrust block was in place at that time and that thrust-emplacement occurred at a time similar to that of the western granulite terrane (i.e. late LD_2).* The last generation of granitic intrusion consists of dikes of muscovite granite, commonly tourmaline-bearing, which were emplaced both before and after the LD_4 folding. The LD_4 folding is responsible for the regional map pattern.

Though the sequence of events from LD_2 to LD_4 apparently represents the waning stages of an orogenic cycle, there are no age constraints on post-LD_2 structures, and subsequent events might be Grenvillian.

In the southeastern part of the map area, a major shear zone occurs principally in the anorthositic rocks (unit 4). The zone strikes approximately 090°, dips steeply to the north and has a down-dip lineation. The sense of movement on the shear zone is not known.

The Atikonak lineament (Figure 3) is based primarily on aeromagnetic interpret-

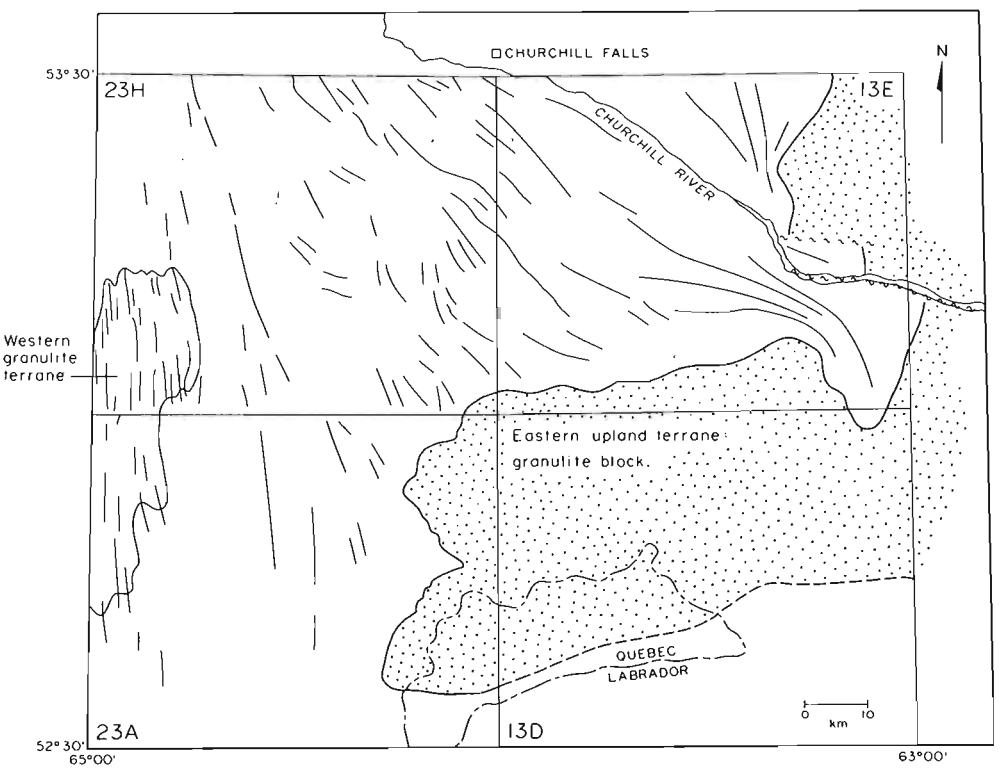

Figure 4: *Schematic representation of late fold traces, mostly LF_4 and equivalents, to show fanning of LD_4 structures around the eastern granulite facies block. Data from the present study (23A), and adapted from Nunn and Christopher, 1983 (23H), Thomas and Wood, 1983 (13E) and Thomas et al., 1984 (this volume) (13D).*

** In the Wabush area of western Labrador, 140 km to the west-northwest, northwesterly trending structures similar to, and possibly synchronous with, the LD_4 folds occurred late in a Grenvillian deformation sequence that was initially characterized by northwesterly directed thrusting (T. Rivers, 1983). The LD_4 folds, therefore, might be Grenvillian structures and the thrust-emplacement of the eastern upland terrane might be late Labradorian or early Grenvillian.*

ation. The feature truncates other trends on the aeromagnetic map (Geological Survey of Canada, 1978), appears to deflect the shear zone fabric in unit 4, and may have a sinistral displacement. The lineament may have reactivated older strain zones in the northern part of the map area. The post-unit 4 structures may be Labradorian or Grenvillian in age.

Summary

Field mapping undertaken during 1983, combined with recent geochronological results (Krogh, written communications, 1983) on the whole project area, suggests, in agreement with previous work, that:

(i) the paragneisses were derived from a slope or basinal sequence, probably largely of graywacke-shale composition, with minor intercalations of basic volcanic rocks and either quartzite or chert horizons. In previous work (e.g. Nunn and Christopher, 1983; Rivers and Nunn, 1983), this sequence has been tentatively proposed as an equivalent to the deeper water parts of the Labrador Trough succession, located 100 km northwest of the area. However, reconnaissance mapping conducted in 1983 indicates that these paragneisses and the metasediments of the Labrador Trough are probably separated by major thrusts, and it may be premature or invalid to correlate the two;

(ii) the paragneisses record a polyorogenic history with a preplutonic and a postplutonic component. The early component was probably pre-1670 Ma but is otherwise constrained only by the probable Aphebian age of the sedimentary protolith. Units 2 and 3 comprise the plutonic interval;

(iii) a major granitoid plutonic event probably occurred within the time interval 1670-1650 Ma, possibly in association with the intrusion of the gabbroid suite. Pregranitoid gabbroid suites are spatially and complexly associated with the granitoid rocks throughout the Trans-Labrador batholith (Emslie et al., 1978; Wardle and Britton, 1981; Nunn and Noel, 1982; Gower and Owen, in preparation).

However, contrary to previous work, it is concluded that:

(i) the main dynamothermal events in the area were mid-Paleohelikian (circa 1650 Ma), not Grenvillian, and are here termed the Labradorian orogeny;

(ii) the basic plutonic suite predates the granitoid plutonic suite and the correlation by Nunn and Christopher (1983) with the Shabogamo Intrusive Suite of western Labrador (Rivers, 1980) is probably no longer valid;

(iii) structures of apparent Grenville age consist of shear and thrust zones which in places separate huge tracts of older gneisses;

(iv) the Grenvillian metamorphic grade probably does not exceed lower amphibolite facies throughout the northern 120 km of the Grenville Province.

The structural history of the Labradorian orogeny is complex and its effects were heterogeneous. Because of this structural heterogeneity, separation of younger (post-LD_2) Labradorian from Grenvillian structures is locally difficult, and considerable uncertainty still exists regarding the effects of the Grenvillian Orogeny versus those of earlier events. The uncertainty is presently most marked for the anorthosite suite, since the ages of both the anorthosite suite and the structures in it are not known.

Acknowledgements

We thank the members of base camps 544 and 546 and Lakeland Helicopters, the Churchill Falls (Labrador) Corporation, Charra Limited and W. Tuttle and K. O'Quinn for field assistance. We also wish to thank T.E. Krogh for permission to use his unpublished sphene data. The manuscript benefited from discussion with A. Thomas and C.F. Gower and was greatly improved by reviewers R.J. Wardle and W.L. Dickson.

References

Baragar, W.R.A.
1981: Tectonic and regional relationships of the Seal Lake and Bruce River magmatic provinces. Geological Survey of Canada, Bulletin 314, page 47.

Emslie, R.F., Hulbert, L.J., Brett, C.P. and Garson, D.F.
1978: Geology of the Red Wind Mountains, Labrador: the Ptarmigan Complex. *In* Current Research, Part A, Geological Survey of Canada, Paper 78-1A, pages 129-134.

Fryer, B.J.
1983: Report on geochronology - Labrador mapping. Newfoundland Department of Mines and Energy, Mineral Development Division, unpublished report, 35 pages.

Geological Survey of Canada
1978: Aeromagnetic map of Lac Joseph, Map 7381G, 1:250,000 scale.

1982: National geochemical reconnaissance data, Map 55-1982. Geological Survey of Canada, Open File Report 902 and Newfoundland Department of Mines and Energy, Mineral Development Division, Open File Report Lab 613.

Gower, C.F. and Owen, V.
in preparation: Pre-Grenvillian and Grenvillian lithotectonic regions in eastern Labrador - correlations with the Sveconorwegian Orogenic Belt in Sweden.

Greene, B.A.
1972: Geological map of Labrador, 1:1,000,000. Newfoundland Department of Mines, Agriculture and Resources, Mineral Resources Division.

1974: An outline of the geology of Labrador. Newfoundland Department of Mines and Energy, Mineral Development Division, Information Circular 15, 64 pages.

Krogh, T.E., Nunn, G.A.G., Thomas, A. and Wardle, R.J.
in preparation: A circa 1650 Ma metamorphic-plutonic belt in the Grenville Province of Labrador: new U-Pb data.

Nunn, G.A.G.
1981: Regional geology of the Michikamau Lake map area, central Labrador. *In* Current Research, Newfoundland Department of Mines and Energy, Mineral Development Division, Report 81-1, pages 138-148.

Nunn, G.A.G. and Christopher, A.
1983: Geology of the Atikonak River area, Grenville Province, western Labrador. *In* Current Research, Part A, Geological Survey of Canada, Paper 83-1A, pages 363-370.

Nunn, G.A.G. and Noel, N.
1982: Regional geology east of Michikamau Lake, central Labrador. *In* Current Research, Newfoundland Department of Mines and Energy, Mineral Development Division, Report 82-1, pages 149-167.

Pyke, M.W.
1956: Report on exploration in areas G and K, Labrador, 1956. Unpublished assessment report, BRINEX G56015, (on file at Newfoundland Department of Mines and Energy, St. John's), 13 pages.

Rivers, C.T.E.
1980: Revised stratigraphic nomenclature for Aphebian and other rock units, southern Labrador Trough, Grenville Province. Canadian Journal of Earth Sciences, Volume 17, pages 668-670.

1983: The northern margin of the Grenville Province in western Labrador - anatomy of an ancient orogenic front. Precambrian Research, Volume 22, pages 41-73.

Rivers, C.T.E. and Nunn, G.A.G.
1983: Grenvillian reworking of Lower Proterozoic basement rocks in central and western Labrador. Geological Association of Canada, Program with Abstracts, Volume 8, page A58.

Ryan, A.B.
1980: Preliminary reconnaissance of the northern Grenville Province, Naskaupi River area, Labrador. *In* Current Research, Newfoundland Department of Mines and Energy, Mineral Development Division, Report 80-1, pages 147-153.

Ryan, A.B., Neale, T. and McGuire, J.
1982: Descriptive notes to accompany geological maps of the Grand Lake area, Labrador, 13F/10, 11, 14 and 15. Newfoundland Department of Mines and Energy, Mineral Development Division, Maps 82-64, 65, 66 and 67 with descriptive notes.

Smyth, W.R. and Greene, B.A.
1976: Isotopic age map of Labrador. Newfoundland Department of Mines and Energy, Mineral Development Division, Map 76-04.

Stevenson, I.M.
1968: Geology of the Lac Joseph map area, Newfoundland and Quebec. Geological Survey of Canada, Paper 67-62.

Thomas, A., Culshaw, N., Mannard, G. and Whelan, G.
1984: Geology of the Lac Ghyvelde - Lac Long area, Grenville Province, Labrador and Quebec. *In* Current Research, Part A, Geological Survey of Canada, Paper 84-1A. Also in this volume.

Thomas, A. and Hibbs, D.
1980: Geology of the southwestern margin of the Central Mineral Belt. *In* Current Research, Newfoundland Department of Mines and Energy, Mineral Development Division, Report 80-1, pages 166-176.

Thomas, A., Jackson, V. and Finn, G.
1981: Geology of the Red Wine Mountains and surrounding area, central Labrador. *In* Current Research, Newfoundland Department of Mines and Energy, Mineral Development Division, Report 81-1, pages 111-120.

Thomas, A. and Wood, D.
1983: Geology of the Winokapau Lake area, Grenville Province, central Labrador. *In* Current Research, Part A, Geological Survey of Canada, Paper 83-1A, pages 305-312.

Van Schmus, W.R. and Bickford, M.E.
1981: Proterozoic chronology and evolution of the midcontinent region, North America. *In* Precambrian plate tectonics. *Edited by* A. Kroner, Elsevier, Amsterdam, pages 261-296.

Wardle, R.J. and Britton, J.M.
1981: The geology of the Churchill Falls area, Labrador. *In* Current Research, Newfoundland Department of Mines and Energy, Mineral Development Division, Report 81-1, pages 130-137.

Wardle, R.J. and staff
1982: The Trans-Labrador Batholith; a major pre-Grenvillian feature of the eastern Grenville Province. Friends of the Grenville Workshop, Program with Abstracts, Rideau Ferry Inn, February, 1982, page 11.

Author Index

	Page
Aitken, J.D.	401
Bernius, G.R.	373
Blaise, B.	85
Boissonnault, P.	391
Bristow, Q.	41, 101
Broome, J.	375
Bustin, R.M.	255
Chung, C.F.	351
Ciesielski, A.	1, 121
Conaway, J.G.	101
Culshaw, N.G.	414
Currie, K.L.	369
Dale, J.E.	179
Dawson, M.R.	359
Donaldson, J.A.	53, 159
Dubé, C.	391
Dubois, J-M.	391
Dyck, W.	41
Edwards, T.W.D.	237
Ejeckam, R.B.	75
Embry, A.F.	275, 299, 327
Evans, S.G.	223
Fischer, B.F.G.	309
Flindall, R.	75
Forbes, D.L.	11
Fritz, W.H.	245, 409
Frobel, D.	25
Froese, E.	355
Gadd, N.R.	399
Galley, A.G.	159
Gandhi, S.S.	33
Garrett, R.G.	351
Geldsetzer, H.H.J.	337
Gordey, S.P.	409
Gwyn, Q.H.J.	391
Hanmer, S.K.	109, 121, 133
Heffler, D.E.	47
Heginbottom, J.A.	187, 363
Hewitt, R.A.	179
Hickey, L.J.	359
Hofmann, H.J.	285
Jackson, M.J.	53, 159
Jerzykiewicz, T.	263
Kamineni, D.C.	75
Keen, C.E.	93
Keen, M.J.	93
Killeen, P.G.	373
Klassen, R.A.	237
Kurfurst, P.J.	193
Larocque, A.	391
Laroque, G.	391
LeCheminant, A.N.	159
Lister, D.R.	223
MacDonald, M.A.	65
Mackay, J.R.	173
McCrank, G.F.	75
Meijer Drees, N.C.	337
Mercier, E.	85
Moffat, I.W.	255
Moran, K.	193
Morissette, A.	391
Mwenifumbo, C.J.	373
Narbonne, G.M.	409
Nixon, F.M.	193
Noel, N.	414
Nunn, G.A.G.	414
Orchard, M.J.	197, 207
Parent, M.	395
Pedder, A.E.H.	315
Pianosi, J.G.	53
Poulin, A.	391
Rogers, P.J.	65
Schock, L.	373
Shilts, W.W.	217
Sikorsky, R.	75
Smith, S.L.	159
Stern, R.A.	143
Stone, D.	75
Taylor, R.B.	25
Teskey, D.	375
Thorsteinsson, R.	269
Van Helden, D.R.	263
Wagner, F.J.E.	367
West, R.M.	359
Wright, J.A.	93

NOTE TO CONTRIBUTORS

Submissions to the *Discussion* section of *Current Research* are welcome from both the staff of the Geological Survey and from the public. Discussions are limited to 6 double-spaced typewritten pages (about 1500 words) and are subject to review by the Chief Scientific Editor. Discussions are restricted to the scientific content of Geological Survey reports. General discussions concerning branch or government policy will not be accepted. Illustrations will be accepted only if, in the opinion of the editor, they are considered essential. In any case no redrafting will be undertaken and reproducible copy must accompany the original submissions. Discussion is limited to recent reports (not more than 2 years old) and may be in either English or French. Every effort is made to include both *Discussion* and *Reply* in the same issue. *Current Research* is published in January and July. Submissions for these issues should be received not later than 1 November and 1 May respectively. Submissions should be sent to the Chief Scientific Editor, Geological Survey of Canada, 601 Booth Street, Ottawa, Canada, K1A 0E8.

AVIS AUX AUTEURS D'ARTICLES

Nous encourageons tant le personnel de la Commission géologique que le grand public à nous faire parvenir des articles destinés à la section discussion *de la publication* Recherches en cours. *Le texte doit comprendre au plus six pages dactylographiées à double interligne (environ 1500 mots), texte qui peut faire l'objet d'un réexamen par le rédacteur en chef scientifique. Les discussions doivent se limiter au contenu scientifique des rapports de la Commission géologique. Les discussions générales sur la Direction ou les politiques gouvernementales ne seront pas acceptées. Les illustrations ne seront acceptées que dans la mesure où, selon l'opinion du rédacteur, elles seront considérées comme essentielles. Aucune retouche ne sera faite aux textes et dans tous les cas, une copie qui puisse être reproduite doit accompagner les textes originaux. Les discussions en français ou en anglais doivent se limiter aux rapports récents (au plus de 2 ans). On s'efforcera de faire coincider les articles destinés aux rubriques* discussions et reponses *dans le même numéro. La publication* Recherches en cours *paraît en janvier et en juillet. Les articles pour ces numéros doivent être reçus au plus tard le 1er novembre et le 1er mai respectivement. Les articles doivent être renvoyés au rédacteur en chef scientifique: Commission géologique du Canada, 601, rue Booth, Ottawa, Canada, K1A 0E8.*

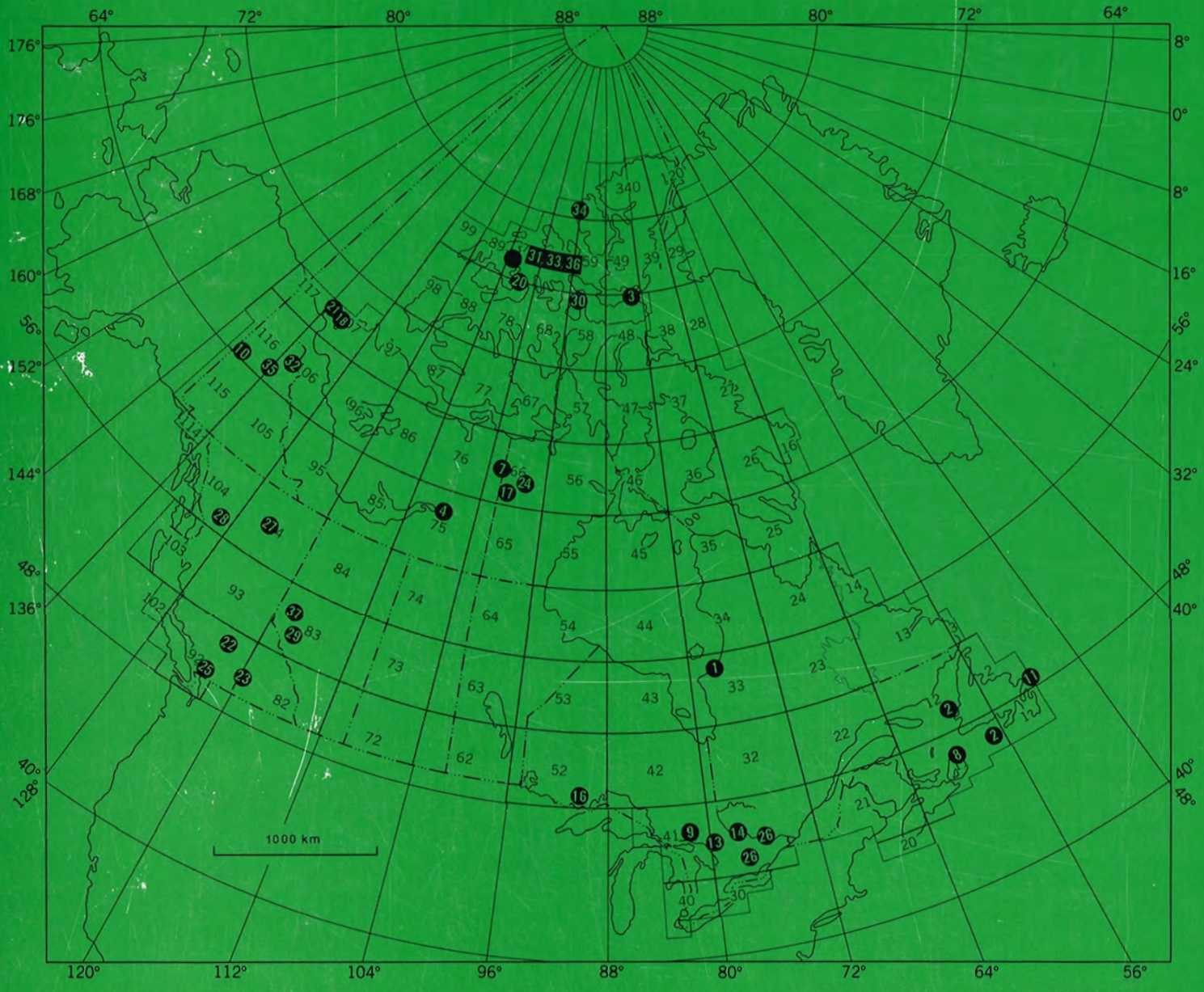

Energy, Mines and Resources Canada

Énergie, Mines et Ressources Canada